

Ervin B. Podgoršak

Compendium to Radiation Physics for Medical Physicists

300 Problems and Solutions

 Springer

Compendium to Radiation Physics for Medical Physicists

Ervin B. Podgoršak

with contribution by Wamied Abdel-Rahman

Compendium to Radiation Physics for Medical Physicists

300 Problems and Solutions

With 266 Figures

 Springer

Ervin B. Podgoršak, Ph.D., FCCPM, FCOMP,
FAAMP, FACMP, DABMP
Professor Emeritus
Faculty of Medicine, Department
of Oncology and Medical Physics Unit
McGill University
Montreal
Québec, Canada

ISBN 978-3-642-20185-1

ISBN 978-3-642-20186-8 (eBook)

DOI 10.1007/978-3-642-20186-8

Springer Heidelberg New York Dordrecht London

Library of Congress Control Number: 2013946032

© Springer-Verlag Berlin Heidelberg 2014

This work is subject to copyright. All rights are reserved by the Publisher, whether the whole or part of the material is concerned, specifically the rights of translation, reprinting, reuse of illustrations, recitation, broadcasting, reproduction on microfilms or in any other physical way, and transmission or information storage and retrieval, electronic adaptation, computer software, or by similar or dissimilar methodology now known or hereafter developed. Exempted from this legal reservation are brief excerpts in connection with reviews or scholarly analysis or material supplied specifically for the purpose of being entered and executed on a computer system, for exclusive use by the purchaser of the work. Duplication of this publication or parts thereof is permitted only under the provisions of the Copyright Law of the Publisher's location, in its current version, and permission for use must always be obtained from Springer. Permissions for use may be obtained through RightsLink at the Copyright Clearance Center. Violations are liable to prosecution under the respective Copyright Law.

The use of general descriptive names, registered names, trademarks, service marks, etc. in this publication does not imply, even in the absence of a specific statement, that such names are exempt from the relevant protective laws and regulations and therefore free for general use.

While the advice and information in this book are believed to be true and accurate at the date of publication, neither the authors nor the editors nor the publisher can accept any legal responsibility for any errors or omissions that may be made. The publisher makes no warranty, express or implied, with respect to the material contained herein.

Printed on acid-free paper

Springer is part of Springer Science+Business Media (www.springer.com)

*To my teachers of medical physics
John R. Cameron and Paul R. Moran
from the University of Wisconsin,
Harold E. Johns and John R. Cunningham
from the University of Toronto,
and
to medical physics students everywhere*

Preface

This book is intended as a supplementary textbook for a radiation physics course in academic medical physics and biomedical engineering graduate programs as well as a reference book for candidates preparing for certification examinations in medical physics subspecialties. The book may also be of interest to graduate students in physics, chemistry, and various branches of engineering wishing to improve their knowledge and understanding of modern physics and its intimate relationship with radiation physics applied to medicine.

The book contains 129 specific sections grouped into 14 chapters. Each section contains one or more long questions that consist of several shorter questions related to the subject material of the specific section. The chapters and sections of this textbook follow the layout of the textbook: “*Radiation Physics for Medical Physicists*” published by Springer in 2010 and the 300 solved problems presented in this book are intended to provide supplementary information to the radiation physics textbook through examples relevant to the topics discussed in individual sections of the textbook. Of course, this book can also stand on its own as a radiation physics textbook serving as a tool for learning radiation physics through perusing a series of solved radiation physics problems.

Many of the problems in this textbook are based on notes and written as well as oral examinations that I used over the past 35 years of teaching radiation physics to M.Sc. and Ph.D. students in medical physics at McGill University in Montreal. I am indebted to the many students who contributed to radiation physics classes with probing questions and who, through their performance on examinations, highlighted difficulties with certain concepts in radiation physics either because I did not explain them well enough in class or because they are truly difficult to grasp. A set of solved problems in these areas is bound to be of interest and benefit to medical physics students, to candidates in medical physics certification examinations as well as to professionals who wish to review and improve their understanding of radiation physics.

The material covered in this textbook does not deal with intricacies of medical physics subspecialties: radiation oncology physics, diagnostic radiology physics, and nuclear medicine physics. Many well-established textbooks are already available for this purpose. Rather, this textbook highlights the basic knowledge of modern radiation physics that a medical physicist must possess to be able to function as a professional on a multidisciplinary medical team that uses ionizing radiation for imaging and treatment of human disease.

Special thanks are due to my colleague Dr. Wamied Abdel-Rahman from King Fahad Specialist Hospital in Dammam, Saudi Arabia for his skillful drawing of figures presented in the textbook, for contributing several problems to the set, and for many helpful discussions and advice on individual questions.

Finally, I gratefully acknowledge that completion of this textbook could not have been accomplished without the support, encouragement, and patience of my spouse Mariana.

Montréal, Canada

Ervin B. Podgoršak

General Notes About The Book

- (1) This book contains 300 problems on modern physics with emphasis on the radiation physics component of medical physics. The problems are grouped into 129 sections spread over 14 chapters and typically consist of several questions identified with (a), (b), (c), etc.
- (2) The chapters and sections of this textbook follow the layout of the textbook *Radiation Physics for Medical Physicists* published by Springer in 2010.
- (3) The text of problems is printed on grey background and each problem is identified with two labels; the right hand label gives the problem serial number (between 1 and 300) and the left hand label identifies the Section of the textbook and the problem number for the given section.
- (4) Detailed solutions to questions on individual problems allow the reader to follow the path from the formulation of the question to final numerical solution or to a descriptive answer. Where applicable, the numerical solution for a given physical quantity is displayed on a graph to show how the solution fits with the general behavior of the physical quantity under study.
- (5) Equations that appear in this book are referenced by stating the equation number and chapter number of their location. Thus, for example, (8.112) stands for a reference to equation 112 in Chap. 8 of this book.
- (6) Equations that appear in the textbook: “Radiation Physics for Medical Physicists” (2nd edition, Springer 2010) are referenced in this book by stating their equation number and chapter number in the textbook preceded by T for textbook. Thus, for example, notation (T12.89) in this book refers to equation 89 in Chap. 12 of the radiation physics textbook.
- (7) Many graphs displaying important physical quantities are plotted with curves representing the functional relationship between the dependent and independent physical variable and, in addition, also show some easy to remember anchor points superimposed onto the curves. This is done to remind students of the importance of knowing the general functional trends governing the behavior of important physical quantities studied in this book.

Contents

1	Introduction to Modern Physics	1
1.1	Fundamental Physical Constants	2
1.2	Derived Physical Constants and Relationships	4
1.3	Milestones in Modern Physics and Medical Physics	6
1.4	Physical Quantities and Units	7
1.5	Classification of Forces in Nature	11
1.6	Classification of Fundamental Particles	13
1.7	Classification of Radiation	14
1.8	Classification of Ionizing Radiation	16
1.9	Classification of Directly Ionizing Radiation	17
1.10	Classification of Indirectly Ionizing Photon Radiation	19
1.11	Radiation Quantities and Units	20
1.12	Dose Distribution in Water for Various Radiation Beams	21
1.13	Basic Definitions for Atomic Structure	24
1.14	Basic Definitions for Nuclear Structure	27
1.15	Nuclear Binding Energies	28
1.16	Nuclear Models	31
1.17	Physics of Small Dimensions and Large Velocities	32
1.18	Planck Energy Quantization	34
1.19	Quantization of Electromagnetic Radiation	40
1.20	Special Theory of Relativity	43
1.21	Important Relativistic Relations	50
1.22	Particle-Wave Duality	69
1.23	Matter Waves	80
1.24	Uncertainty Principle	87
1.25	Complementarity Principle	88
1.26	Emission of Electrons from Material Surface: Work Function	89
1.27	Thermionic Emission	92
1.28	Tunneling	98
1.29	Maxwell Equations	107
1.30	Poynting Theorem and Poynting Vector	110
1.31	Normal Probability Distribution	112

2	Coulomb Scattering	117
2.1	General Aspects of Coulomb Scattering	118
2.2	Geiger-Marsden Experiment	122
2.3	Rutherford Scattering	128
2.4	Cross Sections for Rutherford Scattering	145
2.5	Mott Scattering	152
2.6	General Aspects of Elastic Scattering of Charged Particles	165
2.7	Molière Multiple Elastic Scattering	171
3	Rutherford–Bohr Atomic Model	177
3.1	Bohr Model of Hydrogen Atom	178
3.2	Multi-electron Atoms	208
3.3	Experimental Confirmation of the Bohr Atomic Model	213
3.4	Schrödinger Equation for Hydrogen Atom	222
4	Production of X Rays	225
4.1	X-Ray Line Spectra	226
4.2	Emission of Radiation by Accelerated Charged Particle (Bremsstrahlung Production)	242
4.3	Synchrotron Radiation	256
4.4	Čerenkov Radiation	258
5	Two-Particle Collisions	267
5.1	Collisions of Two Particles: General Aspects	268
5.2	Nuclear Reactions	272
5.3	Two-Particle Elastic Scattering: Energy Transfer	281
6	Interaction of Charged Particles with Matter	299
6.1	General Aspects of Energy Transfer from Charged Particle to Medium	300
6.2	General Aspects of Stopping Power	303
6.3	Radiation Stopping Power	306
6.4	Collision (Electronic) Stopping Power for Heavy Charged Particles	309
6.5	Collision Stopping Power for Light Charged Particles	335
6.6	Total Mass Stopping Power	343
6.7	Radiation Yield	350
6.8	Range of Charged Particles	356
6.9	Mean Stopping Power	363
6.10	Restricted Collision Stopping Power	367
6.11	Bremsstrahlung Targets	376
7	Interaction of Photons with Matter	387
7.1	General Aspects of Photon Interactions with Absorbers	388
7.2	Thomson Scattering	402
7.3	Incoherent Scattering (Compton Effect)	408
7.4	Incoherent (Rayleigh) Scattering	455
7.5	Photoelectric Effect	465

7.6	Pair Production	483
7.7	Photonuclear Reactions	499
8	Energy Transfer and Energy Absorption in Photon Interaction with Matter	515
8.1	Macroscopic Attenuation Coefficient	516
8.2	Energy Transfer from Photons to Charged Particles in Absorber	520
8.3	Energy Transfer and Energy Absorption	532
8.4	Coefficients of Compounds and Mixtures	548
8.5	Effects Following Photon Interactions with Absorber	553
8.6	Summary of Photon Interactions with Absorbers	557
8.7	Sample Calculations	567
9	Interaction of Neutrons with Matter	581
9.1	General Aspects of Neutron Interactions with Absorbers	582
9.2	Neutron Interactions with Nuclei of the Absorber	589
9.3	Neutron Kerma	601
9.4	Neutron Kerma Factor	605
9.5	Neutron Dose Deposition in Tissue	611
9.6	Neutron Beams in Medicine	621
10	Kinetics of Radioactive Decay	637
10.1	General Aspects of Radioactivity	638
10.2	Decay of Radioactive Parent into a Stable Daughter	640
10.3	Radioactive Series Decay	646
10.4	General Form of Daughter Activity	663
10.5	Equilibria in Parent-Daughter Activities	666
10.6	Bateman Equations for Radioactive Decay Chain	671
10.7	Mixture of Two or More Independently Decaying Radionuclides in a Sample	682
10.8	Branching Decay and Branching Fraction	685
11	Modes of Radioactive Decay	693
11.1	Introduction to Radioactive Decay Processes	694
11.2	Alpha Decay	696
11.3	Beta Decay	703
11.4	Beta Minus Decay	708
11.5	Beta Plus Decay	717
11.6	Electron Capture	727
11.7	Gamma Decay	737
11.8	Internal Conversion	741
11.9	Spontaneous Fission	746
11.10	Proton Emission Decay	748
11.11	Neutron Emission Decay	755
11.12	Chart of Nuclides	759
11.13	Summary of Radioactive Decay Modes	773

12	Production of Radionuclides	787
12.1	Origin of Radioactive Elements (Radionuclides)	788
12.2	Naturally Occurring Radionuclides	795
12.3	Man-Made (Artificial) Radionuclides	798
12.4	Radionuclides in the Environment	801
12.5	General Aspects of Nuclear Activation	805
12.6	Nuclear Activation with Neutrons	809
12.7	Nuclear Fission Induced by Neutron Bombardment	890
12.8	Nuclear Chain Reaction	901
12.9	Production of Radionuclides with Radionuclide Generator	914
12.10	Nuclear Activation with Protons and Heavier Charged Particles	931
13	Waveguide Theory	941
13.1	Microwave Propagation in Uniform Waveguide	942
13.2	Boundary Conditions	945
13.3	Differential Wave Equation	950
13.4	Electric and Magnetic Fields in Uniform Waveguides	970
13.5	General Conditions for Particle Acceleration	976
13.6	Dispersion Relationship	980
13.7	Transverse Magnetic TM_{01} Mode	999
13.8	Acceleration Waveguide Compared to Transmission Waveguide	1008
13.9	Relationship Between Velocity of Energy Flow and Group Velocity in Uniform Waveguide	1014
13.10	Disk-Loaded Waveguide	1023
13.11	Capture Condition	1028
14	Particle Accelerators in Medicine	1041
14.1	Basic Characteristics of Particle Accelerators	1042
14.2	Practical Use of X Rays	1045
14.3	Practical Considerations in Production of X Rays	1048
14.4	Traditional Sources of X Rays	1051
14.5	Circular Accelerators	1061
14.6	Clinical Linear Accelerator	1075
Appendix A Main Attributes of Nuclides Presented in This Book		1101
Appendix B Roman Letter Symbols		1107
Appendix C Greek Letter Symbols		1117
Appendix D Electronic Databases of Interest in Nuclear Physics and Medical Physics		1121
Bibliography		1127
Index		1129

Chapter 1 consists of **59 problems** that are spread over 31 sections providing an introduction to modern physics by addressing the basic elements of atomic, nuclear, relativistic, and quantum physics as well as electromagnetic theory. Medical physics has its origin in Wilhelm Röntgen's discovery of x rays in 1895, Antoine-Henri Becquerel's discovery of natural radioactivity in 1896 and discovery of radium by Marie Skłodowska-Curie and Pierre Curie in 1898. Just as knowledge of basic physics was important to physicists working with physicians on the early uses of ionizing radiation in medicine, so is knowledge of basic physics and modern physics of great importance to contemporary medical physicists.

After introducing the basic physical constants and the derived physical constants of importance in modern physics and medical physics, this chapter deals with rules that govern physical quantities and units and the classification of natural forces, fundamental particles, and ionizing radiation. It also addresses the basic definitions for atomic and nuclear structure, concepts of physics of small dimensions (quantum physics) and concepts of physics of large velocities (relativistic physics). Problems at the end of Chap. 1 deal with wave-particle duality, basic wave mechanics, Maxwell equations, and normal probability distribution.

Medical physics is a perfect and long-standing example of translational research where basic experimental and theoretical discoveries are rapidly implemented into benefiting humanity through improved diagnostic and therapeutic procedures based on ionizing radiation. This chapter provides the background knowledge that is required for a study of radiation physics as well as for working as medical physicist on a medical team dealing with patients in diagnostic radiology, nuclear medicine, and radiotherapy.

1.1 Fundamental Physical Constants

1.1.Q1

(1)

- (a) The use of prefixes (decimal based multipliers) in conjunction with units of physical quantities is a common method for avoiding very large and very small numbers when describing the magnitude of physical quantities. The prefix precedes a fundamental unit of measure to indicate a decimal multiple or decimal fraction of the physical unit. Give the names and symbols for the following two groups of prefixes:
- (1) Factors > 1 : $10^1, 10^2, 10^3, 10^6, 10^9, 10^{12}, 10^{15}, 10^{18}, 10^{21}, 10^{24}$.
 - (2) Factors < 1 : $10^{-1}, 10^{-2}, 10^{-3}, 10^{-6}, 10^{-9}, 10^{-12}, 10^{-15}, 10^{-18}, 10^{-21}, 10^{-24}$.
- (b) Complete Table 1.1A on fundamental physical constants. The entries should be rounded off to four significant figures and based on the 2006 CODATA set of values available from the website supported by the National Institute of Science and Technology (NIST) in Washington, D.C., USA (<http://physics.nist.gov/cuu/Constants/>).

Table 1.1A Selected physical constants of importance to modern physics and radiation physics

	Physical constant	Value
1	Speed of light in vacuum	$c =$
2	Avogadro constant	$N_A =$
3	Electron charge	$e =$
4	Electron rest mass	$m_e =$
5	Proton rest mass	$m_p =$
6	Neutron rest mass	$m_n =$
7	Electric constant	$\epsilon_0 =$
8	Magnetic constant	$\mu_0 =$
9	Ratio proton to electron rest mass	$m_p/m_e =$

SOLUTION:

(a) Standard prefixes for physical quantities are used to form decimal multiples of fundamental and derived units with special names. Currently 20 agreed upon prefixes are in use; 10 for multipliers larger than 1 and 10 for multipliers smaller than 1. Most of the prefixes are based on Greek and Latin language; however, a few can also be traced to Dutch, Norwegian and Italian languages.

- (1) For multipliers exceeding 1 the 10 agreed upon prefixes are as follows: 10^2 deca (da); 10^2 hecto (h); 10^3 kilo (k); 10^6 mega (M); 10^9 giga (G); 10^{12} tera (T); 10^{15} peta (P); 10^{18} exa (E); 10^{21} zetta (Z); and 10^{24} yotta (Y).
- (2) For multipliers smaller than 1 the 10 agreed upon prefixes are as follows: 10^{-1} deci (d); 10^{-2} centi (c); 10^{-3} milli (m); 10^{-6} micro (μ); 10^{-9} nano (n); 10^{-12} pico (p); 10^{-15} femto (f); 10^{-18} atto (a); 10^{-21} zepto (z); 10^{-24} yocto (y).

(b) Values of selected physical constants of importance to modern physics and medical physics are given in Table 1.1B.

Table 1.1B Selected physical constants of importance to modern physics and radiation physics

	Physical constant	Value	
1	Speed of light in vacuum	$c = 2.998 \times 10^8 \text{ m/s} \approx 3 \times 10^8 \text{ m/s}$	(1.1)
2	Avogadro constant	$N_A = 6.022 \times 10^{23} \text{ mol}^{-1}$	(1.2)
3	Electron charge	$e = 1.602 \times 10^{-19} \text{ C}$	(1.3)
4	Electron rest mass	$m_e = 0.5110 \text{ MeV}$	(1.4)
5	Proton rest mass	$m_p = 938.3 \text{ MeV}$	(1.5)
6	Neutron rest mass	$m_n = 939.6 \text{ MeV}$	(1.6)
7	Electric constant	$\epsilon_0 = 8.854 \times 10^{-12} \text{ C}/(\text{V} \cdot \text{m})$	(1.7)
8	Magnetic constant	$\mu_0 = 4\pi \times 10^{-7} \text{ (V} \cdot \text{s)} / (\text{A} \cdot \text{m})$	(1.8)
9	Ratio of proton to electron rest mass	$m_p/m_e = 1836$	(1.9)

1.2 Derived Physical Constants and Relationships

1.2.Q1

(2)

Complete Table 1.2A of important derived physical constants and provide the value of the derived constants to four significant figures as well as appropriate units.

Table 1.2A Selected derived physical constants

(a) Speed of light in vacuum

$$c =$$

(b) Reduced Planck constant \times speed of light in vacuum

$$\hbar c =$$

(c) Bohr radius constant

$$a_0 =$$

(d) Fine structure constant

$$\alpha =$$

(e) Rydberg energy

$$E_R =$$

(f) Rydberg constant

$$R_\infty =$$

(g) Classical electron radius

$$r_e =$$

(h) Compton wavelength of the electron

$$\lambda_C =$$

(i) Thomson classical cross section

$$\sigma_{\text{Th}} =$$

SOLUTION:**Table 1.2B** Selected derived physical constants

- (a) Speed of light in vacuum

$$c = \frac{1}{\sqrt{\epsilon_0 \mu_0}} = 2.998 \times 10^8 \text{ m/s} \approx \mathbf{3 \times 10^8 \text{ m/s}} \quad (1.10)$$

- (b) Reduced Planck constant
- \times
- speed of light in vacuum

$$\hbar c = \frac{h}{2\pi} c = 197.3 \text{ MeV} \cdot \text{fm} = \mathbf{197.3 \text{ eV} \cdot \text{nm}} \approx 200 \text{ MeV} \cdot \text{fm} \quad (1.11)$$

- (c) Bohr radius constant

$$a_0 = \frac{4\pi\epsilon_0 (\hbar c)^2}{e^2 m_e c^2} = \mathbf{0.5292 \text{ \AA}} \quad (1.12)$$

- (d) Fine structure constant

$$\alpha = \frac{e^2}{4\pi\epsilon_0 \hbar c} = \frac{\hbar c}{a_0 m_e c^2} = 7.297 \times 10^{-3} \approx \mathbf{\frac{1}{137}} \quad (1.13)$$

- (e) Rydberg energy

$$E_R = \frac{1}{2} m_e c^2 \alpha^2 = \frac{1}{2} \left[\frac{e^2}{4\pi\epsilon_0} \right] \frac{m_e c^2}{(\hbar c)^2} = \mathbf{13.61 \text{ eV}} \quad (1.14)$$

- (f) Rydberg constant

$$R_\infty = \frac{E_R}{2\pi \hbar c} = \frac{m_e c^2 \alpha^2}{4\pi \hbar c} = \frac{1}{4\pi} \left[\frac{e^2}{4\pi\epsilon_0} \right] \frac{m_e c^2}{(\hbar c)^2} = \mathbf{109737 \text{ cm}^{-1}} \quad (1.15)$$

- (g) Classical electron radius

$$r_e = \frac{e^2}{4\pi\epsilon_0 m_e c^2} = \mathbf{2.818 \text{ fm}} \quad (1.16)$$

- (h) Compton wavelength of the electron

$$\lambda_C = \frac{h}{m_e c} = \frac{2\pi \hbar c}{m_e c^2} = \mathbf{0.02426 \text{ \AA}} \quad (1.17)$$

- (i) Thomson classical cross section

$$\sigma_{\text{Th}} = \frac{8\pi}{3} r_e^2 = \mathbf{0.6653 \text{ b}} = 0.6653 \times 10^{-24} \text{ cm}^2 \quad (1.18)$$

1.3 Milestones in Modern Physics and Medical Physics

1.3.Q1

(3)

Complete Table 1.3A related to major discoveries in modern physics and medical physics. Provide the name of the discoverer and the year of discovery.

Table 1.3A Major discoveries of importance to modern physics and medical physics

	Discovery	Discoverer	Year
1	X rays		
2	Natural radioactivity		
3	Electron		
4	Radium-226		
5	Special theory of relativity		
6	Photoelectric effect		
7	Thermionic emission		
8	Model of hydrogen atom		
9	Coolidge x-ray tube		
10	Proton		
11	Incoherent (Compton) scattering		
12	Cyclotron		
13	Neutron		
14	Positron		
15	Artificial radioactivity		
16	Uranium fission		
17	Cobalt-60 teletherapy machine		
18	GammaKnife		
19	CT scanner		
20	Magnetic resonance scanner		
21	Positron emission tomography		

SOLUTION:**Table 1.3B** Major discoveries of importance to modern physics and radiation physics

	Discovery	Discoverer	Year
1	X rays	Wilhelm Konrad Röntgen	1895
2	Natural radioactivity	Antoine-Henri Becquerel	1896
3	Electron	Joseph John Thomson	1897
4	Radium-226	Pierre Curie , Marie Curie-Skłodowska	1898
5	Special theory of relativity	Albert Einstein	1905
6	Photoelectric effect	Albert Einstein	1905
7	Thermionic emission	Owen W. Richardson	1911
8	Model of hydrogen atom	Niels Bohr	1913
9	Coolidge x-ray tube	William D. Coolidge	1914
10	Proton	Ernest Rutherford	1919
11	Incoherent (Compton) scattering	Arthur H. Compton	1922
12	Cyclotron	Ernest O. Lawrence	1931
13	Neutron	James Chadwick	1932
14	Positron	Carl D. Anderson	1932
15	Artificial radioactivity	Irène Joliot-Curie , Frédéric Joliot	1934
16	Uranium fission	Lise Meitner , Otto Frisch , Otto Hahn , Friedrich Strassmann	1939
17	Cobalt-60 teletherapy machine	Harold E. Johns	1951
18	GammaKnife	Lars Leksell	1968
19	CT scanner	Godfrey Hounsfield , Alan Cormack	1971
20	Magnetic resonance scanner	Paul C. Lauterbur , Peter Mansfield	1973
21	Positron emission tomography	Michael Phelps	1973

1.4 Physical Quantities and Units**1.4.Q1****(4)**

The text presented below with five bullets appears like a standard scientific text but contains several errors in style commonly found in scientific texts and scientific presentations. Correct the text following the common rules used in scientific publishing. The corrected text is presented on next page, with footnotes identifying the mistakes and providing an explanation for each error.

- Exposure X is related to the ability of photons to ionize air. Its unit Röntgen (R) is defined as charge of $2.58 \cdot 10^{-4} \text{C}$ produced per kilogram of air.
- Kerma K is defined for indirectly ionizing radiations (photons and neutrons) as the energy transferred to charged particles per unit mass of the absorber. Its SI unit gray (Gy) is defined as 1 J of energy absorbed per kilogram of medium, i.e., $1 \text{ Gy} = 1 \text{ J kg}^{-1}$.
- Dose, D , is defined as the energy absorbed per unit mass of medium. Its SI unit gray (Gy) is defined as 1 J of energy absorbed per kilogram of medium, i.e., $1 \text{ Gy} = 1 \text{ J/kg}$. The old unit of dose is rad where $1 \text{ Gy} = 100 \text{ cGy} = 100 \text{ rad} = 100,000 \text{ mrad}$.
- Equivalent dose H is defined as the dose multiplied by a radiation-weighting factor w_R . The SI unit of equivalent dose is sievert (Sv), the old unit is rem where $1 \text{ Sv} = 100 \text{ rem}$.
- Activity \mathcal{A} of a radioactive substance is defined as the number of nuclear decays per unit time. Its SI unit is becquerel (Bq) corresponding to one decay per second or $1 \text{ Bq} = 1 \text{ s}^{-1}$.

SOLUTION:

The correct text should read as follows:

- Exposure X is related to the ability of photons to ionize air. Its unit röntgen (R) is defined as charge of $2.58 \times 10^{-4} \text{ C}$ produced per kilogram of air.
- Kerma K is defined for indirectly ionizing radiations (photons and neutrons) as the energy transferred to charged particles per unit mass of the absorber. Its SI unit gray (Gy) is defined as 1 J of energy absorbed per kilogram of medium, i.e., $1 \text{ Gy} = 1 \text{ J} \cdot \text{kg}^{-1}$.
- Dose D is defined as the energy absorbed per unit mass of medium. Its SI unit gray (Gy) is defined as 1 J of energy absorbed per kilogram of medium, i.e., $1 \text{ Gy} = 1 \text{ J/kg}$. The old unit of dose is rad where $1 \text{ Gy} = 100 \text{ cGy} = 100 \text{ rad} = 100000 \text{ mrad}$.
- Equivalent dose H is defined as the dose multiplied by a radiation-weighting factor w_R . The SI unit of equivalent dose is sievert (Sv), the old unit is rem where $1 \text{ Sv} = 100 \text{ rem}$.
- Activity \mathcal{A} of a radioactive substance is defined as the number of nuclear decays per unit time. Its SI unit is becquerel (Bq) corresponding to one decay per second or $1 \text{ Bq} = 1 \text{ s}^{-1}$.

The errors are highlighted as follows and explained with footnotes (a) through (i) below:

- Exposure $X^{(a)}$ is related to the ability of photons to ionize air. Its unit Roentgen^(b) (R) is defined as charge of $2.58 \cdot 10^{-4} \text{ C}^{(c)}$ produced per kilogram of air.

- Kerma K is defined for indirectly ionizing radiations (photons and neutrons) as the energy transferred to charged particles per unit mass of the absorber. Its SI unit gray (Gy) is defined as 1 J of energy absorbed per kilogram of medium, i.e., $1 \text{ Gy} = 1 \text{ J kg}^{-1}$ ^(d).
- Dose, D , ^(e) is defined as the energy absorbed per unit mass of medium. Its SI unit gray (Gy) is defined as $1 \text{ J}^{(f)}$ of energy absorbed per kilogram of medium, i.e., $1 \text{ Gy} = 1 \text{ J/kg}^{(f)}$. The old unit of dose is rad where $1 \text{ Gy} = 100,^{(g)} 000 \text{ mrad} = 100 \text{ rad} = 100 \text{ cGy}$.
- Equivalent dose H is defined as the dose multiplied by a radiation-weighting factor w_R ^(h). The SI unit of equivalent dose is sievert (Sv), the old unit is rem where $1 \text{ Sv} = 100 \text{ rem}$.
- Activity \mathcal{A} of a radioactive substance is defined as the number of nuclear decays per time. Its SI unit is becquerel (Bq) corresponding to one decay per second or $1^{(i)} \text{ Bq} = 1^{(i)} \text{ s}^{-1}$.

Footnotes

- Exposure is a physical quantity and its symbol should be written in italic font. Therefore, “X” should read: “*X*”.
- Full names of physical units, even when they originate from a surname of a person, are customarily spelled out with initial letter in low case. Thus, “Röntgen” designating the unit of exposure should read: “röntgen”. However, abbreviations for physical units linked to surnames are commonly spelled out with initial capital letter. Thus, the symbol for the unit “röntgen” is “R”, for “volt” it is “V”, for “gray” it is “Gy”, and so on.
- Multiplication of numbers with powers of 10 is usually indicated with the multiplication sign “ \times ” rather than with a period “.” or a half-high dot “ \cdot ”. Thus the corrected version of “ $2.58 \cdot 10^{-4}$ ” should read: “ 2.58×10^{-4} ”.
- Multiplication of physical units, on the other hand, is usually designated with blank space between the units or, preferably, with a half-high dot “ \cdot ” separating the units. Thus, “ J kg^{-1} ” should read: “ J kg^{-1} ” or, preferably, “ $\text{J} \cdot \text{kg}^{-1}$ ”. Another example: “ $1 \text{ N} = 1 \text{ kg} \cdot \text{m} \cdot \text{s}^{-2}$ ” and NOT “ $1 \text{ N} = 1 \text{ kgms}^{-2}$ ”.
Note: “ms” stands for millisecond and NOT “meter \times second”.
- In many texts symbols for physical units are placed between commas. This unnecessary use of commas is generally not used in current scientific texts. Thus, we say: “Dose D is defined. . .” rather than: “Dose, D , is defined. . .”
- While physical quantities are designated with italic symbols, units of physical quantities are designated with roman type font. Thus, we have “1 J” and NOT “1 *J*”, and “ $1 \text{ Gy} = 1 \text{ J/kg}$ ” is corrected to “ $1 \text{ Gy} = 1 \text{ J/kg}$ ”.
- While banks and economic texts often use commas to identify thousands in large numbers, this practice is not acceptable in science. In many countries comma is actually used to designate the decimal point; thus to avoid confusion between the “decimal” comma and a comma designating groups of thousands, the latter is not allowed in scientific literature. Thus, “100,000 mrad”

in the text has been corrected to read: “100000 mrad”. If thousands must be grouped together, the use of blank space is allowed in scientific literature. Thus, “100000 mrad” can also be written as: “100 000 mrad” for better clarity.

- (h) Subscripts and superscripts used with physical quantities are in italic type if they represent variables, physical quantities, or running numbers; they are in roman type if they are descriptive. Thus, “ w_R ” is corrected to read: “ w_R ”, since “R” is descriptive representing radiation. However, the exposure calibration coefficient is written as “ N_X ” with italic “X” and NOT “ N_X ” with roman “X”, since X represents the quantity exposure.
- (i) Physical quantities have a numerical value and physical unit. The two MUST be separated with one blank space. We thus have: “ $E = 6 \text{ MeV}$ ” and NOT “ $E = 6\text{MeV}$ ”. The text reading: “ $1\text{Bq} = 1\text{s}^{-1}$ ” has therefore been corrected to read: “ $1 \text{ Bq} = 1 \text{ s}^{-1}$ ”.

1.4.Q2

(5)

In Table 1.4A list the seven basic physical quantities and their units in the international system (SI) of units. Also list a few non-SI units for the basic physical quantities that are used in radiation physics and medical physics.

Table 1.4A The seven basic physical quantities and their units in the SI system of units

	Basic physical quantity	SI unit	Other units
1			
2			
3			
4			
5			
6			
7			

SOLUTION:

Table 1.4B The seven basic physical quantities and their units in the SI system of units

	Basic physical quantity	SI unit	Other units
1	Length ℓ	meter (m)	nm, Å, fm
2	Mass m	kilogram (kg)	g, mg, µg, eV/c ² , keV/c ² , MeV/c ²
3	Time t	second (s)	a, h, ms, µs, ns, ps (“a” stands for “year”)
4	Electric current I	ampere (A)	mA, µA, nA, pA
5	Temperature T	kelvin (K)	°C
6	Amount of substance	mole (mol)	mmol, µmol
7	Luminous intensity	candela (cd)	

1.5 Classification of Forces in Nature

1.5.Q1

(6)

In Table 1.5A list the four distinct forces acting between various particles in decreasing order of magnitude. For each force also list its source, transmitted particle, and relative strength.

Table 1.5A The four fundamental forces in nature, their source, their transmitted particle, and their relative strength normalized to 1 for the strong force

	Natural force	Source of force	Transmitted particle	Relative strength
1				
2				
3				
4				

SOLUTION:

Four distinct forces, listed in Table 1.5B are observed in the interaction between various types of particles. These forces, in decreasing order of strength, are the strong force, electromagnetic (EM) force, weak force, and gravitational force, with relative strengths of 1, $1/137$, 10^{-6} , and 10^{-39} , respectively. As far as the range of the four fundamental forces is concerned, the forces are divided into two groups: two are infinite range force (electromagnetic force and gravitational force) and two are very short-range force (strong force and weak force).

Each force results from a particular intrinsic property of the particles, such as strong charge for the strong force, electric charge for the EM force, weak charge for the weak force, and energy for the gravitational force:

Table 1.5B The four fundamental forces in nature, their source, their transmitted particle, and their relative strength normalized to 1 for the strong force

	Natural force	Source of force	Transmitted particle	Relative strength
1	Strong	Strong charge	Gluon	1
2	Electromagnetic	Electric charge	Photon	$1/137$
3	Weak	Weak charge	W^+ , W^- , Z^0	10^{-6}
4	Gravitational	Energy	Graviton	10^{-39}

1.5.Q2

(7)

For proton-electron system determine:

- (a) Gravitational force constant $Gm_p m_e$, where G is the gravitational constant $G = 6.67 \times 10^{-11} \text{ m}^3 \cdot \text{kg}^{-1} \cdot \text{s}^{-2}$.
- (b) Electromagnetic (EM) force constant $e^2/(4\pi\epsilon_0)$.
- (c) Ratio between the gravitational force constant of (a) and the EM force constant of (b).

SOLUTION:**(a) Gravitational force constant for proton-electron system:**

Mass of proton:

$$\begin{aligned} m_p &= 938.3 \times 10^6 \text{ eV}/c^2 = \frac{938.3 \times 10^6 \text{ eV}}{(3 \times 10^8 \text{ m/s})^2} \times (1.602 \times 10^{-19} \text{ J/eV}) \\ &= 1.67 \times 10^{-27} \text{ kg}. \end{aligned} \quad (1.19)$$

Mass of electron:

$$\begin{aligned} m_e &= 0.511 \times 10^6 \text{ eV}/c^2 = \frac{0.511 \times 10^6 \text{ eV}}{(3 \times 10^8 \text{ m/s})^2} \times (1.602 \times 10^{-19} \text{ J/eV}) \\ &= 9.11 \times 10^{-31} \text{ kg}. \end{aligned} \quad (1.20)$$

Charge of proton and electron: $e = 1.602 \times 10^{-19} \text{ C}$

$$\begin{aligned} Gm_p m_e &= (6.67 \times 10^{-11} \text{ m}^3 \cdot \text{kg}^{-1} \cdot \text{s}^{-2}) \times \frac{938.3 \times 10^6 \text{ eV}}{(3 \times 10^8 \text{ m} \cdot \text{s}^{-1})^2} \frac{0.511 \times 10^6 \text{ eV}}{(3 \times 10^8 \text{ m} \cdot \text{s}^{-1})^2} \\ &\quad \times (1.602 \times 10^{-19} \text{ J/eV})^2 \\ &= 1.01 \times 10^{-67} \text{ J} \cdot \text{m} = 6.32 \times 10^{-39} \text{ eV} \cdot \text{\AA}. \end{aligned} \quad (1.21)$$

(b) Electromagnetic force constant for proton-electron system:

Electric constant of vacuum: $\epsilon_0 = 8.85 \times 10^{-12} \text{ C}/(\text{V} \cdot \text{m})$

Charge of proton and electron: $e = 1.602 \times 10^{-19} \text{ C}$

$$\frac{e^2}{4\pi\epsilon_0} = \frac{(1.6 \times 10^{-19} \text{ C})^2}{4\pi \times [8.85 \times 10^{-12} \text{ C}/(\text{V} \cdot \text{m})]} = 2.3 \times 10^{-28} \text{ J} \cdot \text{m} = 14.4 \text{ eV} \cdot \text{\AA}. \quad (1.22)$$

(c) **Ratio** of gravitational force constant $Gm_p m_e$ for proton-electron system to electromagnetic force constant $e^2/(4\pi\epsilon_0)$ for proton-electron system

$$\frac{Gm_p m_e}{e^2 / (4\pi \epsilon_0)} = \frac{1.01 \times 10^{-67} \text{ J} \cdot \text{m}}{2.3 \times 10^{-28} \text{ J} \cdot \text{m}} = \frac{6.32 \times 10^{-39} \text{ eV} \cdot \text{\AA}}{14.4 \text{ eV} \cdot \text{\AA}} = 4.39 \times 10^{-40}. \quad (1.23)$$

1.6 Classification of Fundamental Particles

1.6.Q1

(8)

Complete the block diagram of Fig. 1.1A dealing with the basic classification of fundamental particles.

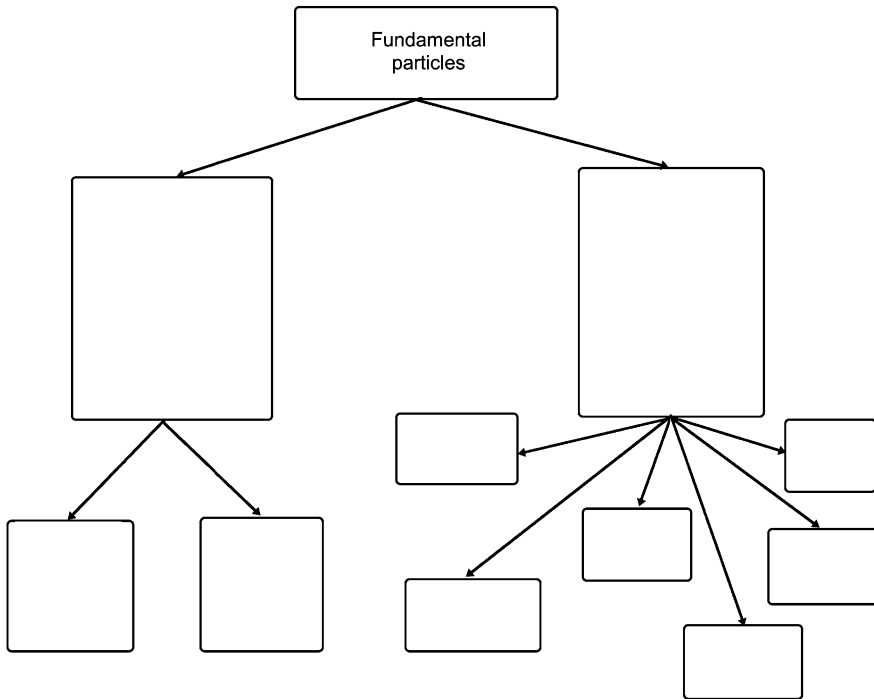
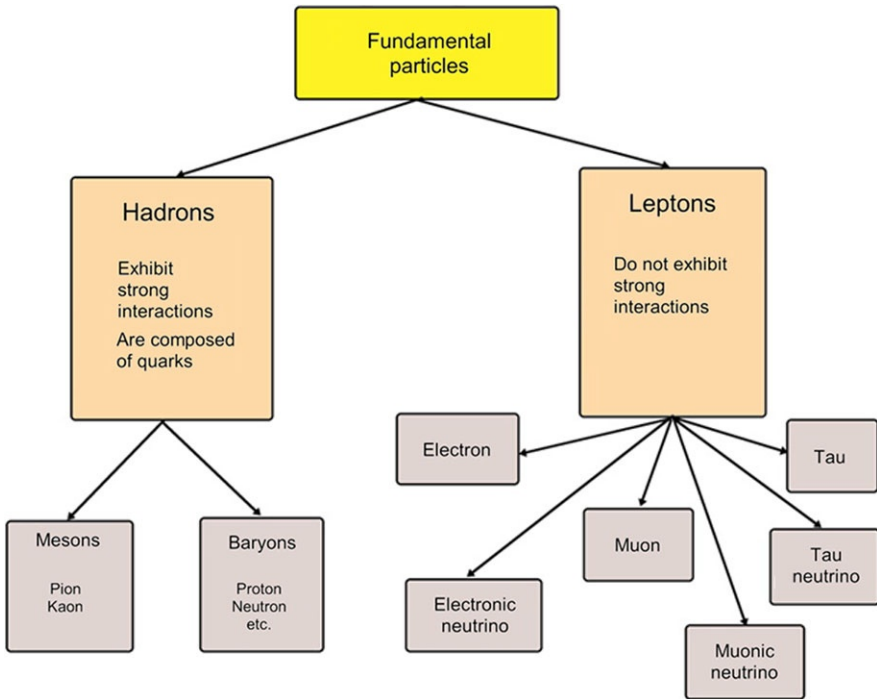


Fig. 1.1A Classification of fundamental particles

SOLUTION:**Fig. 1.1B** Classification of fundamental particles**1.7 Classification of Radiation**

1.7.Q1

(9)

Radiation is classified into two main categories: non-ionizing and ionizing, depending on its ability to ionize matter. The ionization potential of atoms, i.e., the minimum energy required for ionizing an atom, ranges from a few electron volts for alkali elements to 24.6 eV for helium (noble gas). Ionization potentials of all other atoms are between these two extremes.

Complete the block diagram of Fig. 1.2A dealing with classification of radiation.

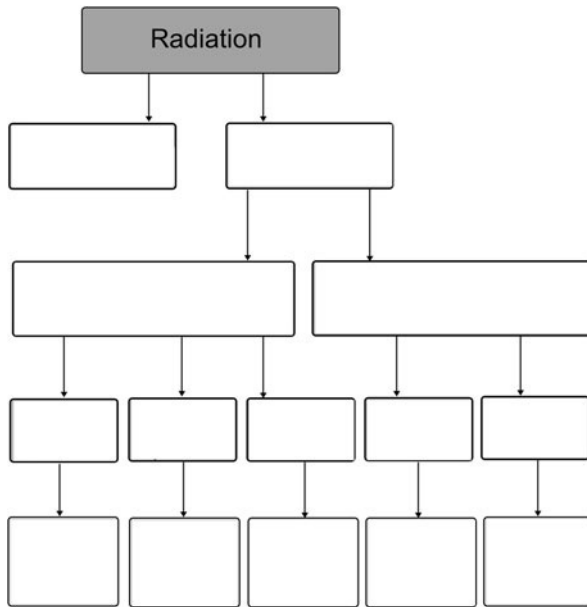


Fig. 1.2A Classification of radiation

SOLUTION:

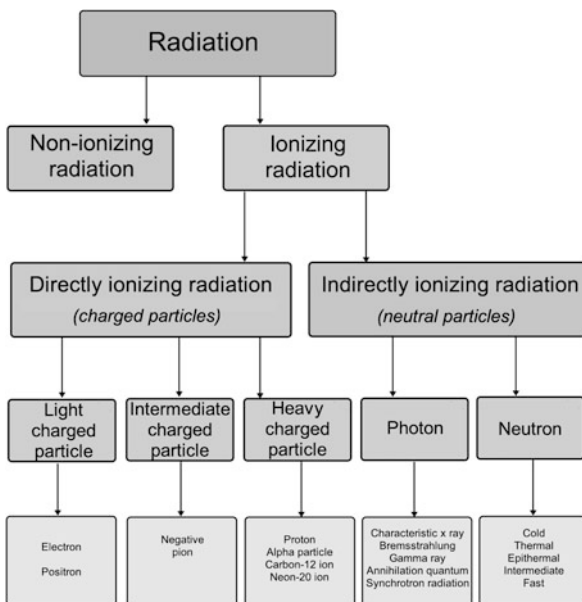


Fig. 1.2B Classification of radiation

1.8 Classification of Ionizing Radiation

1.8.Q1

(10)

Complete Table 1.6A listing areas of modern life in which ionizing radiation is used.

Table 1.6A Use of ionizing radiation in science and industry

Use of ionizing radiation	Brief description of the particular use
1	
2	
3	
4	
5	
6	
7	
8	
9	
10	

SOLUTION:

Table 1.6B Use of ionizing radiation in science and industry

Use of ionizing radiation	Brief description of the particular use
1 Medicine	Diagnostic radiology. Nuclear medicine. Radiotherapy.
2 Nuclear reactor	Basic research. Production of radionuclides. Electric power.
3 Industrial radiography	Nondestructive inspection of welds in airplanes and pipelines.
4 Well logging	Inspection of geologic and recoverable hydrocarbon zones.
5 Insect pest control	For pest sterilization in insect pest eradication.
6 Security services	Screening of cargo and luggage. Sanitation of mail (antrax).
7 Food production	Killing of bacteria and viruses in food. Slowing ripening process.
8 Waste management	Killing of pathogenic microorganisms and harmful bacteria.
9 Chemical industry	Production of polymers and vulcanized tires.
10 Production of weapons	Military production of weapons of mass destruction.

1.9 Classification of Directly Ionizing Radiation

1.9.Q1

(11)

Directly ionizing radiation consists of charged particles and for use in medical physics falls into two categories: light charged particles (electrons and positrons) and heavy charged particles such as protons, etc. In the table below list the most common sources of electrons as well as the specific names of the electrons that the sources emit.

Table 1.7A Common sources of electrons and nomenclature for electrons produced

	Source of electrons	Name of electron that the source produces
1		
2		
3		
4		
5		
6		
7		
8		
9		
10		
11		

SOLUTION:

Table 1.7B Common sources of electrons and nomenclature for electrons produced

	Source of electrons	Name of electron that the source produces
1	Photoelectric effect	Photoelectron
2	Compton effect	Compton recoil electron
3	Nuclear pair production	Pair production electron
4	Triplet production	Pair production electron
5	Beta minus nuclear decay	Beta particle (electron)
6	Internal conversion	Internal conversion electron
7	Linac, betatron, microtron	Megavoltage electron
8	Auger effect	Auger electron, Coster-Kronig electron
9	Charged particle collision	Delta ray electron
10	Thermionic emission	Thermion
11	Exoelectron emission	Exoelectron

1.9.Q2

(12)

In Table 1.8A list the first five lowest-mass heavy charged particles. List their designation, such as “hydrogen-1”, their symbol, as well as the name for the nucleus and the associated atom.

Table 1.8A Basic properties of common heavy charged particles used in nuclear physics and medicine

	Designation	Symbol	Name of nucleus	Protons	Neutrons	Nuclear stability	Name of atom
1							
2							
3							
4							
5							

SOLUTION:

According to the mode of ionization, ionizing radiation is classified into two distinct categories: *directly ionizing radiation* and *indirectly ionizing radiation*. Directly ionizing radiation comprises charged particles that deposit energy in the absorber through a direct one-step process involving Coulomb interactions between the directly ionizing charged particle and orbital electrons of the atoms of the absorber.

For use in radiotherapy heavy charged particles are defined as particles such as a proton and heavier ions with mass exceeding that of the electron. The first five lowest-mass heavy charged particles of importance in nuclear physics and also potentially useful in medicine for treatment of disease are listed in Table 1.8B.

Table 1.8B Basic properties of common heavy charged particles used in nuclear physics and medicine

	Designation	Symbol	Name of nucleus	Protons	Neutrons	Nuclear stability	Name of atom
1	Hydrogen-1	${}^1_1\text{H}$	Proton	1	0	Stable	Protium
2	Hydrogen-2	${}^2_1\text{H}$	Deuteron	1	1	Stable	Deuterium
3	Hydrogen-3	${}^3_1\text{H}$	Triton	1	2	Radioactive	Tritium
4	Helium-3	${}^3_2\text{He}$	Helion	2	1	Stable	Helium-3
5	Helium-4	${}^4_2\text{He}$	Alpha particle	2	2	Stable	Helium-4

1.10 Classification of Indirectly Ionizing Photon Radiation

1.10.Q1

(13)

In addition to ultraviolet radiation there are five other types of indirectly ionizing photon radiation. In Table 1.9A provide a list of the five types of indirectly ionizing photon radiation used in medical imaging and radiotherapy. Also provide the source of each radiation type.

Table 1.9A Classification of indirectly ionizing photon radiation

Indirectly ionizing photon radiation	Origin of radiation
1	
2	
3	
4	
5	

SOLUTION:

Indirectly ionizing radiation comprises neutral particles (photons and neutrons) that deposit energy in the absorber through a two-step process with the first step releasing charged particles (photons release either electrons or electron/positron pairs; neutrons release protons or heavier ions) and the second step the released charged particles deposit a portion of their energy in the absorber through direct Coulomb interactions with orbital electrons of the atoms of the absorber.

Indirectly ionizing photon radiation consists of three categories of photon: ultraviolet (uv), x ray, and gamma ray. While ultraviolet photons are of some limited use in medicine, imaging and treatment of disease with radiation are carried out with photons of higher energy than that of uv photons. With regard to their origin, these higher energy photons fall into five categories as listed in Table 1.9B:

Table 1.9B Classification of indirectly ionizing photon radiation

	Indirectly ionizing photon radiation	Origin of radiation
1	Gamma rays	Result from nuclear transitions in excited radionuclides referred to as gamma decay.
2	Annihilation quanta	Result from positron-electron annihilation, be it with stationary positron or an energetic positron.
3	Characteristic (fluorescence) x rays	Result from electron transitions between atomic shells in an excited atom.
4	Bremsstrahlung x rays	Result from interactions between an energetic electron and a nucleus of absorber.
5	Synchrotron radiation	Results from electrons moving in circular orbits in a magnetic field (storage ring).

1.11 Radiation Quantities and Units

1.11.Q1

(14)

Several quantities and units are used for quantifying radiation. In Table 1.10A list at least five of these quantities, their definition, their unit in the SI system, their traditional old unit, and the relationship between their SI unit and the old unit.

Table 1.10A Basic physical quantities and their units used in radiation measurement

	Quantity	Definition	SI unit	Old unit	Conversion
1					
2					
3					
4					
5					

SOLUTION:**Table 1.10B** Basic physical quantities and their units used in radiation measurement

Quantity	Definition	SI unit	Old unit	Conversion
1 Exposure X	$X = \frac{\Delta Q}{\Delta m_{\text{air}}}$	$2.58 \times \frac{10^{-4} \text{C}}{\text{kg air}}$	$1 \text{ R} = \frac{1 \text{ esu}}{\text{cm}^2 \text{ air}_{\text{STP}}}$	$1 \text{ R} = 2.58 \times \frac{10^{-4} \text{C}}{\text{kg air}}$
2 Kerma K	$K = \frac{\Delta E_{\text{tr}}}{\Delta m}$	$1 \text{ Gy} = 1 \frac{\text{J}}{\text{kg}}$	–	–
3 Dose D	$D = \frac{\Delta E_{\text{ab}}}{\Delta m}$	$1 \text{ Gy} = 1 \frac{\text{J}}{\text{kg}}$	$1 \text{ rad} = 100 \frac{\text{erg}}{\text{g}}$	$1 \text{ Gy} = 100 \text{ rad}$
4 Equivalent dose H	$H = D w_R$	1 Sv	1 rem	$1 \text{ Sv} = 100 \text{ rem}$
5 Activity \mathcal{A}	$\mathcal{A} = \lambda N$	$1 \text{ Bq} = 1 \text{ s}^{-1}$	$1 \text{ Ci} = 3.7 \times 10^{10} \text{ s}^{-1}$	$1 \text{ Bq} = \frac{1 \text{ Ci}}{3.7 \times 10^{10}}$

1.12 Dose Distribution in Water for Various Radiation Beams**1.12.Q1****(15)**

Dose deposition in water is one of the most important characteristics of the interaction of radiation beams with matter. This is true in general radiation physics and even more so in medical physics, where the dose deposition properties in tissue govern both the diagnosis of disease with radiation (*imaging physics*) as well as treatment of disease with radiation (*radiotherapy physics*).

Imaging with ionizing radiation is limited to the use of x-ray beams in *diagnostic radiology* and gamma ray beams in *nuclear medicine*, while in *radiotherapy* the use of radiation is broader and covers essentially all ionizing radiation types ranging from x rays and gamma rays through electrons to neutrons, protons and heavier charged particles. For a given radiation beam, its dose deposition in water is usually depicted in the form of percentage depth dose (PDD) curve that plots the radiation dose (normalized to 100 % at the depth of dose maximum) against depth z in water.

Diagrams in Fig. 1.3 depict percentage depth doses (PDD) against depth in water z for various directly and indirectly ionizing radiation beams used in radiotherapy. For PDD curves in (A), (B), (C), and (D) identify:

- Mode of radiation (directly or indirectly ionizing).
- Type of radiation (photon, electron, etc.).
- Beam energy (80 kVp, 18 MV, 10 MeV, etc.)

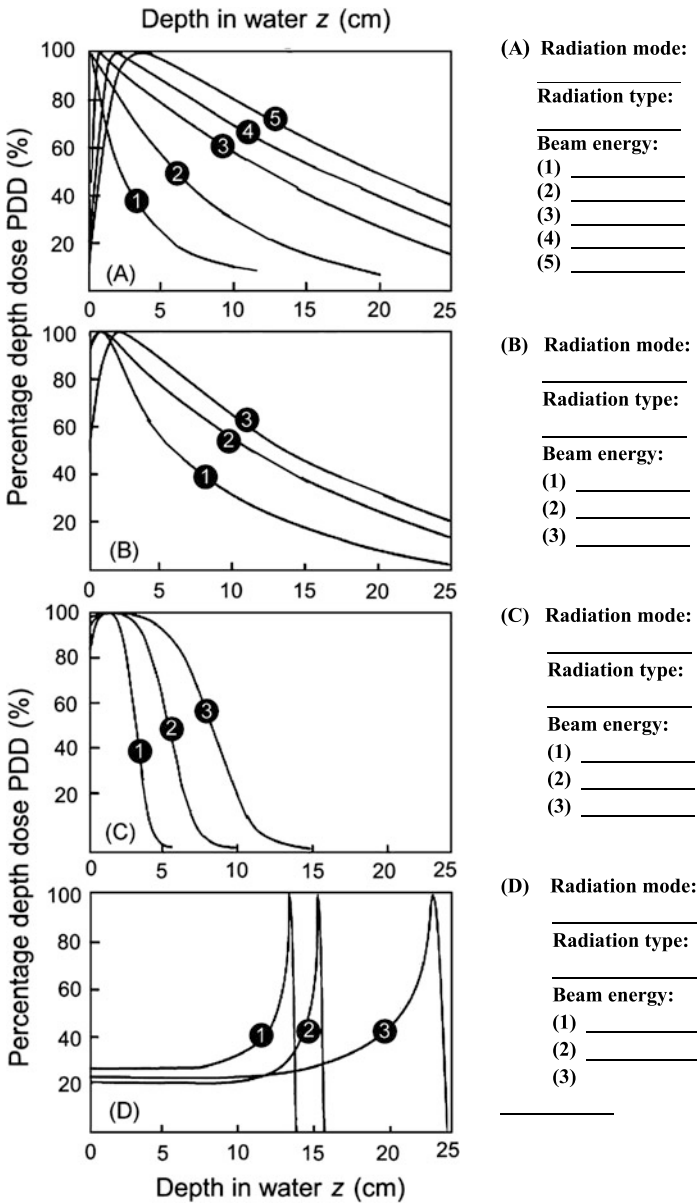
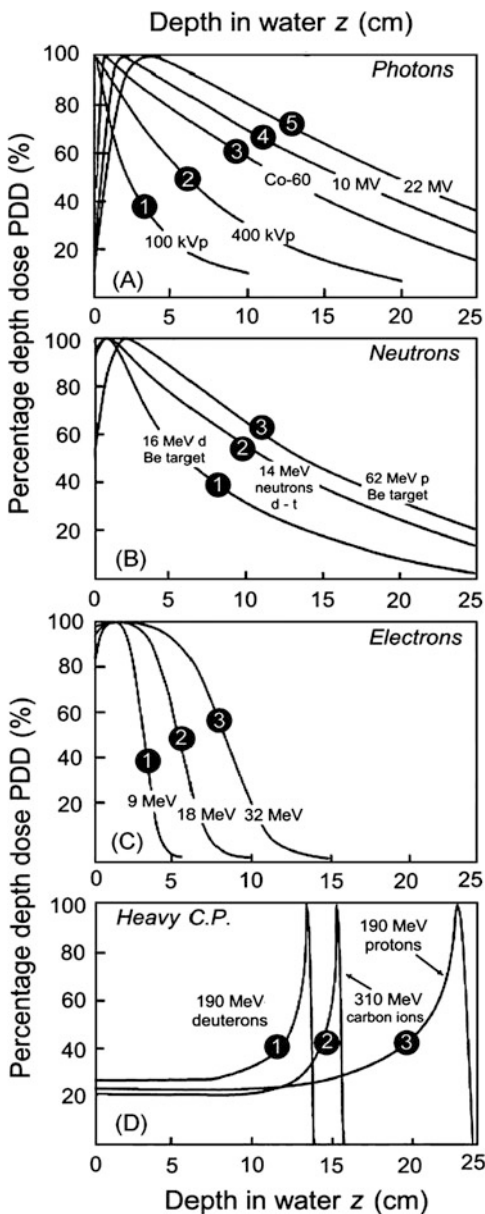


Fig. 1.3 Percentage depth dose (PDD) against depth z in water for radiation beams of various modes, types and energies

SOLUTION:

Figure 1.4 depicts percentage depth doses (PDD) against depth z in water for radiation beams of various modes, types and energies.



(A) **Radiation mode:**
Indirectly ionizing

Radiation type:
Photon beams

- Beam energy:**
 (1) 100 kVp
 (2) 400 kVp
 (3) Cobalt-60
 (4) 10 MV
 (5) 22 MV

(B) **Radiation mode:**
Indirectly ionizing

Radiation type
Neutron beams

- Beam energy:**
 (1) 16 MeV d – Be target
 (2) (d-t) 14 MeV neutrons
 (3) 62 MeV p – Be target

(C) **Radiation mode:**
Directly ionizing

Radiation type:
Electron beams

- Beam energy:**
 (1) 9 MeV
 (2) 18 MeV
 (3) 32 MeV

(D) **Radiation mode:**
Directly ionizing

Radiation type:
Heavy C.P. beams

- Beam energy:**
 (1) d (190 MeV)
 (2) C (310 MeV)
 (3) p (190 MeV)

Fig. 1.4 Percentage depth dose (PDD) against depth z in water for radiation beams of various modes, types and energies. (A) and (B) are for indirectly ionizing radiation (photons and neutrons, respectively); (C) and (D) are for directly ionizing radiation (electrons and heavy charged particles, respectively). C.P. = charged particle, d = deuteron, t = triton, C = carbon ion, p = proton

Of the four beam categories of Fig. 1.4, photon beams in the indirectly ionizing radiation category and electron beams in the directly ionizing radiation category are considered conventional beams, well understood, and readily available for radiotherapy in all major medical institutions around the world. On the other hand, neutron beams in the indirectly ionizing radiation category and heavy ions including protons in the directly ionizing radiation category remain in the category of special beams, available in only a limited number of institutions around the world, despite having been in use for the past 5 decades. These beams offer some advantages in treatment of certain malignant diseases; however, in comparison with conventional beams, they are significantly more complicated to use as well as to maintain and their infrastructure and operating costs are also significantly higher, currently precluding a widespread clinical use.

Special beams (neutrons and protons) provide certain advantages when used in treatment of selected tumor types; however, their choice and prescribed dose must account not only for the physical beam characteristics but also for the biological effects associated with radiation beams: the relative biological effectiveness (RBE) and the oxygen enhancement ratio (OER). The RBE is defined by the ratio between dose of test radiation to dose of standard radiation (250 kVp x rays) to produce the same biological effect. The OER is defined by the ratio of doses without and with molecular oxygen (hypoxic versus well oxygenated cells) to produce the same biological effect.

1.13 Basic Definitions for Atomic Structure

1.13.Q1

(16)

Complete Table 1.11A dealing with basic constituents of nuclides of importance to medical physics.

Table 1.11A Basic characteristics of selected nuclides of importance to medical physics

Physical quantity	Symbol	^1_1H	$^{12}_6\text{C}$	$^{60}_{27}\text{Co}$	$^{137}_{55}\text{Cs}$	$^{192}_{77}\text{Ir}$	$^{207}_{82}\text{Pb}$	$^{226}_{88}\text{Ra}$	$^{235}_{92}\text{U}$
1 Atomic number		1	6	27	55	77	82	88	92
2 Number of protons		1	6	27	55	77	82	88	92
3 Number of electrons		1	6	27	55	77	82	88	92
4 Atomic mass number		1	12	60	137	192	207	226	235
5 Number of nucleons		1	12	60	137	192	207	226	235
6 Number of neutrons		0	6	33	82	115	125	138	143

SOLUTION:**Table 1.11B** Basic characteristics of selected nuclides of importance to medical physics

Physical quantity	Symbol	${}^1_1\text{H}$	${}^{12}_6\text{C}$	${}^{60}_{27}\text{Co}$	${}^{137}_{55}\text{Cs}$	${}^{192}_{77}\text{Ir}$	${}^{207}_{82}\text{Pb}$	${}^{226}_{88}\text{Ra}$	${}^{235}_{92}\text{U}$
1 Atomic number	Z	1	6	27	55	77	82	88	235
2 Number of protons	Z	1	6	27	55	77	82	88	235
3 Number of electrons	Z	1	6	27	55	77	82	88	235
4 Atomic mass number	A	1	12	60	137	192	207	226	92
5 Number of nucleons	A	1	12	60	137	192	207	226	92
6 Number of neutrons	$A-Z$	0	6	33	82	115	125	138	143

1.13.Q2**(17)**

Lithium borate with chemical formula $\text{Li}_2\text{B}_4\text{O}_7$ is used as ingredient in production of glass and ceramics. It is also used as a sensitive phosphor in thermoluminescence dosimetry (TLD). Determine the mean molecular mass of lithium borate, having the following atomic constituents: lithium Li, boron B, and oxygen O. Also determine the mean rest energy of a lithium borate molecule.

SOLUTION:

From the NIST (<http://physics.nist.gov/PhysRefData/Compositions/index.html>) we obtain the isotopic composition and atomic masses for the stable isotopes of the constituent nuclides: Li, B, and O. The relevant data are shown in the table below:

Table 1.12 Basic atomic data for constituents of lithium borate ($\text{Li}_2\text{B}_4\text{O}_7$) according to the NIST

Nuclide	Atomic number	Stable isotopes	Abundance (%)	Isotopic atomic mass
Li	3	Li-6	7.59	6.0151223
		Li-7	92.41	7.0160041
B	5	B-10	20	10.012937
		B-11	80	11.009306
O	8	O-16	99.76	15.994915
		O-17	0.04	16.999132
		O-18	0.20	17.999161

Using the data given in Table 1.12 we now calculate the mean atomic masses for the three atoms comprising lithium borate as follows:

$$\bar{M}(\text{Li}) = 0.0759 \times 6.0151223 \text{ u} + 0.9241 \times 7.0160041 \text{ u} = 6.941 \text{ u}, \quad (1.24)$$

$$\bar{M}(\text{B}) = 0.20 \times 10.012937 \text{ u} + 0.80 \times 11.0093055 \text{ u} = 10.811 \text{ u}, \quad (1.25)$$

$$\begin{aligned} \bar{M}(\text{O}) &= 0.9976 \times 15.994915 \text{ u} + 0.0004 \times 16.9991315 \text{ u} \\ &\quad + 0.0020 \times 17.999161 \text{ u} \\ &= 15.9994 \text{ u}. \end{aligned} \quad (1.26)$$

Mean molecular mass of $\text{Li}_2\text{B}_4\text{O}_7$ is determined by adding the weighted mean atomic masses of the individual constituents to get

$$\begin{aligned} \bar{M}(\text{Li}_2\text{B}_4\text{O}_7) &= 2\bar{M}(\text{Li}) + 4\bar{M}(\text{B}) + 7\bar{M}(\text{O}) \\ &= 2 \times 6.941 \text{ u} + 4 \times 10.811 \text{ u} + 7 \times 15.9994 \text{ u} = 169.12 \text{ u}. \end{aligned} \quad (1.27)$$

Finally, the mean rest energy of a lithium borate molecule is

$$\begin{aligned} \bar{M}(\text{Li}_2\text{B}_4\text{O}_7)c^2 &= \bar{M}(\text{Li}_2\text{B}_4\text{O}_7, \text{u}) \times 931.494028 \text{ MeV/u} \\ &= (169.12 \text{ u}) \times 931.494028 \text{ MeV/u} = 157\,534.27 \text{ MeV}. \end{aligned} \quad (1.28)$$

1.13.Q3

(18)

Cells in human body use sugar (glucose: $\text{C}_6\text{H}_{12}\text{O}_6$) as their major source of energy. Blood circulating in the body delivers glucose to cells and the blood sugar concentration (also referred to as blood glucose level) is controlled through various negative feedback mechanisms and kept within a relatively narrow range.

The blood sugar concentration is specified either in mmol/ℓ representing molar concentration of sugar per liter of blood or in $\text{mg}/\text{d}\ell$ representing mass concentration of sugar per deciliter of blood.

Determine the relationship between mmol/ℓ and $\text{mg}/\text{d}\ell$ in measurement of blood glucose.

SOLUTION:

To find the relationship between mmol/ℓ and $\text{mg}/\text{d}\ell$ we first determine the mean molecular mass (standard molecular weight) \mathcal{M} of glucose $\text{C}_6\text{H}_{12}\text{O}_6$ using the following standard molecular weight of carbon C, hydrogen H, and oxygen O

(see T1.22 and T1.23)

$$\mathcal{M}(\text{C}) = 12.0107 \text{ u},$$

$$\mathcal{M}(\text{H}) = 1.00794 \text{ u},$$

$$\mathcal{M}(\text{O}) = 15.9994 \text{ u}$$

to get the following result for the mean molecular mass (standard molecular weight) of glucose

$$\mathcal{M}(\text{C}_6\text{H}_{12}\text{O}_6) = 6 \times 12.0107 \text{ u} + 12 \times 1.00794 \text{ u} + 6 \times 15.9994 \text{ u} = 180.12 \text{ u}. \quad (1.29)$$

Thus,

1 mole of glucose corresponds to 180.12 g of glucose,

1 mmol/l corresponds to 180.12 mg/l or 18.012 mg/dl, usually approximated to 18 mg/dl.

The normal fasting glucose level in human blood is about 4.5 mmol/l to 5.6 mmol/l or 80 mg/dl to 100 mg/l.

1.14 Basic Definitions for Nuclear Structure

1.14.Q1

(19)

For all stable nuclides listed in Table A.1 of Appendix A prepare a Cartesian diagram plotting their atomic number Z on the ordinate (y) axis and atomic mass number A on the abscissa (x) axis. On the same diagram also plot the function

$$Z(A) = \frac{A}{2 + 0.0155A^{2/3}}, \quad (1.30)$$

which has been proposed empirically as a reasonable approximation linking Z and A for all stable nuclides.

SOLUTION:

A plot of atomic number Z against atomic mass number A for the stable isotopes listed in Table A.1 is given in Fig. 1.5.

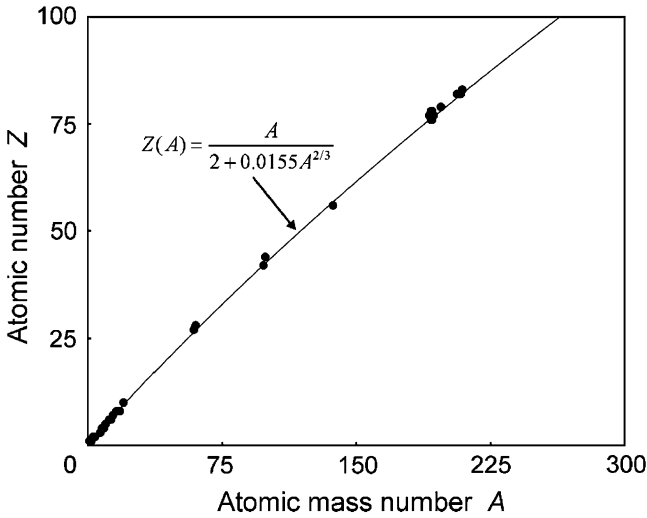


Fig. 1.5 Plot of (1.30) shown with *solid line* and data from Table A.1 of Appendix A for all stable nuclides shown with *data points*. Atomic mass number A is plotted on the abscissa (x) axis and atomic number Z on the ordinate (y) axis. The agreement between the data points and (1.30) is excellent

1.15 Nuclear Binding Energies

1.15.Q1

(20)

The sum of masses of the individual components of a nucleus that contains Z protons and $(A-Z)$ neutrons is larger than the actual mass of the nucleus. This difference in mass is called the mass defect (mass deficit) Δm and its energy equivalent Δmc^2 is called the total binding energy E_B of the nucleus. The binding energy per nucleon (E_B/A) in a nucleus (i.e., the total binding energy of a nucleus divided by the number of nucleons) varies with the number of nucleons A and is of the order of ~ 8 MeV/nucleon.

- (a) Determine the binding energy per nucleon $E_B/A = \Delta mc^2/A$, where A is the atomic mass number, for the following nuclei: (1) deuteron (${}^2_1\text{H}$), (2) alpha particle (${}^4_2\text{He}$), (3) boron (${}^{10}_5\text{B}$), (4) oxygen-16 (${}^{16}_8\text{O}$), (5) cobalt-60 (${}^{60}_{27}\text{Co}$), (6) cesium-137 (${}^{137}_{55}\text{Cs}$), (7) lead-208 (${}^{208}_{82}\text{Pb}$), and (8) uranium-235 (${}^{235}_{92}\text{U}$).
- (b) Plot E_B/A against A for nuclides listed in (a).

- (c) The peculiar shape of the E_B/A curve against A suggests two methods for converting mass into energy: fusion of nuclei at low A and fission of nuclei at large A . Briefly discuss the principles of: (1) Fusion and (2) Fission.

SOLUTION:

- (a) Binding energy per nucleon E_B/A is given as follows

$$\frac{E_B}{A} = \frac{\Delta mc^2}{A} = \frac{Zm_p c^2 + (A - Z)m_n c^2 - Mc^2}{A}, \quad (1.31)$$

where

Z and A are the nuclide atomic number and atomic mass number, respectively.

$m_p c^2$ is the proton rest energy (938.272013 MeV).

$m_n c^2$ is the neutron rest energy (939.565346 MeV).

Mc^2 is the nuclear rest energy that may be obtained directly from nuclear data tables or from atomic mass $\mathcal{M}(u)$ available from the NIST with the following expression

$$\begin{aligned} Mc^2 &= \mathcal{M}(u)c^2 - Zm_e c^2 \\ &= \mathcal{M}(u) \times 931.494028 \text{ MeV/u} - Z \times 0.510999 \text{ MeV}, \end{aligned} \quad (1.32)$$

with $m_e c^2$ the electron rest mass (0.510999 MeV).

By way of example, we calculate E_B/A for the ${}^4_2\text{He}$ nucleus using the following steps:

- (1) According to the NIST (<http://physics.nist.gov/PhysRefData/Compositions/index.html>) the atomic mass of ${}^4_2\text{He}$ is 4.002603 u.
- (2) According to (1.32) the nuclear rest energy of ${}^4_2\text{He}$ is

$$\begin{aligned} Mc^2 &= (4.002603 \text{ u}) \times (931.494028 \text{ MeV/u}) - 2 \times 0.510999 \text{ MeV} \\ &= 3728.4009 \text{ MeV} - 1.0220 \text{ MeV} = 3727.3791 \text{ MeV}. \end{aligned} \quad (1.33)$$

- (3) Using (1.31) we now calculate E_B/A for ${}^4_2\text{He}$ and get

$$\begin{aligned} \frac{E_B}{A} &= \frac{2 \times (938.272013 \text{ MeV}) + 2 \times (939.565346 \text{ MeV}) - (3727.3791 \text{ MeV})}{4} \\ &= 7.0739 \text{ MeV}. \end{aligned} \quad (1.34)$$

Binding energies per nucleon for the other nuclei of part (a) were calculated with the same technique as the one used for the helium-4 nucleus and the final results are tabulated in Table 1.13 and plotted in Fig. 1.6.

Table 1.13 Atomic mass $\mathcal{M}(u)$, nuclear rest energy Mc^2 , nuclear binding energy E_B , and binding energy per nucleon E_B/A for selected nuclides. Data are available in Table A.1 of Appendix A

	Nucleus	Atomic mass $\mathcal{M}(u)$	Nuclear rest energy Mc^2 (MeV)	Binding energy E_B (MeV)	Binding energy per nucleon E_B/A (MeV)
1	${}^1_2\text{H}$	2.014102	1875.6128	2.22458	1.1123
2	${}^4_4\text{He}$	4.002603	3727.3791	28.29569	7.0739
3	${}^{10}_5\text{B}$	10.012937	9324.4362	64.75071	6.4751
4	${}^{16}_8\text{O}$	15.994915	14895.0796	127.61927	7.9762
5	${}^{60}_{27}\text{Co}$	59.933822	55814.2014	524.80028	8.7467
6	${}^{137}_{55}\text{Cs}$	136.907084	127500.0283	1149.29287	8.3890
7	${}^{208}_{82}\text{Pb}$	207.976636	193687.0956	1636.44573	7.8675
8	${}^{235}_{92}\text{U}$	235.043923	218895.0023	1783.87084	7.5909

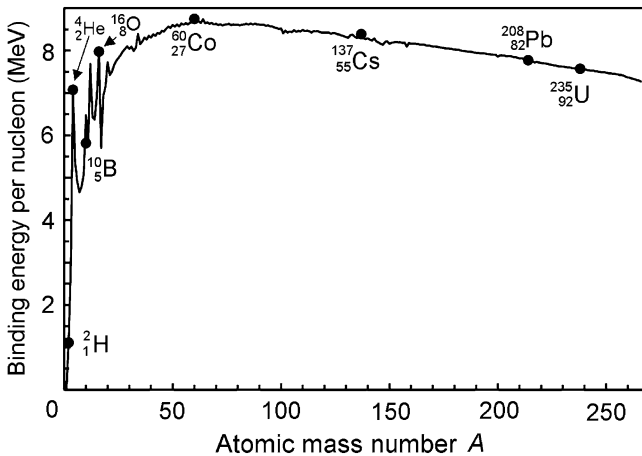


Fig. 1.6 Binding energy per nucleon E_B/A in MeV/nucleon against atomic mass number A for all known nuclides shown with solid curve and for the nuclides of Table 1.13 shown with data points

(b) Plot of E_B/A data of Table 1.13 against the atomic mass number A is shown in Fig. 1.6.

(c) Nuclear fusion and fission are practical examples of converting mass into energy. Nuclear energy is contained within the atomic nucleus that consists of protons and neutrons held together by a strong force. The larger the binding energy per nucleon of an atom, the more stable is the atom. As shown in Fig. 1.6, atoms with atomic mass number $A \approx 60$ are the most stable in nature. Therefore, fusing light nuclei into a heavier nucleus or splitting a heavy nucleus into lighter fragments both

result in nuclei with stronger binding energy per nucleon and, consequently, conversion of a fraction of nuclear mass into energy.

(1) *Fusion* of two nuclei of very small mass, e.g., ${}^2_1\text{H} + {}^3_1\text{H} \rightarrow {}^4_2\text{He} + \text{n}$, creates a more massive nucleus and releases a certain amount of energy. Experiments using controlled nuclear fusion for production of energy have so far not been successful; however, steady progress in fusion research is being made in various laboratories around the world, so it is reasonable to expect that in the future controlled fusion will become possible and will result in a relatively clean and abundant means for sustainable power generation.

(2) *Fission* of elements of large mass, e.g., ${}^{235}_{92}\text{U} + \text{n}$, creates two smaller mass and more stable nuclei with release of energy in the form of heat and radiation. Nuclear fission was observed first in 1934 by Enrico Fermi and described correctly by Otto Hahn, Friedrich Strassmann, Lise Meitner, and Otto Frisch in 1939. In 1942 at the University of Chicago Enrico Fermi and colleagues carried out the first controlled chain reaction based on nuclear fission.

1.16 Nuclear Models

1.16.Q1

(21)

Use the Weizsäcker binding energy formula to determine the binding energy of the following three nuclei: **(a)** Boron-10 (B-10); **(b)** Cobalt-60 (Co-60); and **(c)** Uranium-235 (U-235).

SOLUTION:

The liquid drop nuclear model assumes that nuclei resemble a very dense incompressible spherical liquid drop. The Weizsäcker empirical binding energy formula

$$E_B\left(\frac{A}{Z}\text{X}\right) \approx C_1 A - C_2 A^{2/3} - C_3 \frac{Z^2}{A^{1/3}} - C_4 \frac{(A - 2Z)^2}{A}, \quad (1.35)$$

where Z and A are the atomic number and atomic mass number, respectively, of nucleus X , accounts for the nuclear volume effect (C_1), nuclear surface effect (C_2), Coulomb repulsion of protons (C_3), and excess of neutrons over protons in the nucleus (C_4). Constants C_1 , C_2 , C_3 , and C_4 were determined empirically and equal to 15.75 MeV, 17.8 MeV, 0.711 MeV, and 23.7 MeV, respectively.

Using Weizsäcker equation we get the following results for the binding energies of ${}^{10}_5\text{B}$, ${}^{60}_{27}\text{Co}$, and ${}^{235}_{92}\text{U}$:

(a)

$$\begin{aligned}
 E_B(^{10}_5\text{B}) &= 15.75 \times 10 \text{ MeV} - 17.8 \times 10^{2/3} \text{ MeV} \\
 &\quad - 0.711 \times \frac{5^2}{10^{1/3}} \text{ MeV} - 23.7 \times \frac{(10 - 2 \times 5)^2}{10} \text{ MeV} \\
 &= 66.6 \text{ MeV},
 \end{aligned} \tag{1.36}$$

deviating from the actual value of 64.8 MeV determined in Prob. 20 by 2.8 %.

(b)

$$\begin{aligned}
 E_B(^{60}_{27}\text{Co}) &= 15.75 \times 60 \text{ MeV} - 17.8 \times 60^{2/3} \text{ MeV} \\
 &\quad - 0.711 \times \frac{27^2}{60^{1/3}} \text{ MeV} - 23.7 \times \frac{(60 - 2 \times 27)^2}{60} \text{ MeV} \\
 &= 525 \text{ MeV},
 \end{aligned} \tag{1.37}$$

deviating from the actual value of 524.8 MeV determined in Prob. 20 by 0.04 %.

(c)

$$\begin{aligned}
 E_B(^{235}_{92}\text{U}) &= 15.75 \times 235 \text{ MeV} - 17.8 \times 235^{2/3} \text{ MeV} \\
 &\quad - 0.711 \times \frac{92^2}{235^{1/3}} \text{ MeV} - 23.7 \times \frac{(235 - 2 \times 92)^2}{235} \text{ MeV} \\
 &= 1782.9 \text{ MeV},
 \end{aligned} \tag{1.38}$$

deviating from the actual value of 1783.9 MeV determined in Prob. 20 by -0.06 %.

1.17 Physics of Small Dimensions and Large Velocities

1.17.Q1

(22)

At the end of the 19-th century physics was considered a completed discipline within which most of the natural physical phenomena were satisfactorily explained. However, as physicists broadened their interests and refined their experimental techniques, it became apparent that classical physics suffered severe limitations in two areas: (i) dealing with dimensions comparable to small atomic dimensions and (ii) dealing with velocities comparable to speed

of light. Modern physics handles these limitations in two distinct, yet related, specialties: quantum physics and relativistic physics, respectively.

State or calculate typical dimensions of:

- (a) Rutherford-Bohr atomic model (radii of nucleus and atom) for hydrogen-1 (H-1 protium) atom and for uranium-235 atom.
- (b) Copernican heliocentric planetary celestial model (radii of Sun and Earth's orbit) for the Earth and Sun planetary system.
- (c) Normalize both models to the same scale and determine which model exhibits larger radius and by what factor?

SOLUTION:

(a) Rutherford-Bohr atomic model: Electrons are in planetary motion about the stationary nucleus. Most of the atomic mass is concentrated in the nucleus that is some five orders of magnitude smaller than the atomic radius.

Nuclear radius R is estimated with the following expression

$$R = R_0 \sqrt[3]{A}, \quad (1.39)$$

where R_0 is the nuclear radius constant (1.25 fm) and A is the atomic mass number of a given nuclide.

Using (1.39) we get the following nuclear radii for the hydrogen-1 (protium) atom and for the uranium-235 atom, respectively

$$R({}_1^1\text{H}) = R_0 \approx 1.25 \text{ fm} \quad \text{and} \quad R({}_{92}^{235}\text{U}) = (1.25 \text{ fm}) \times \sqrt[3]{235} \approx 7.7 \text{ fm}. \quad (1.40)$$

Atomic radius of the Rutherford-Bohr atomic model is defined well for one-electron structures such as the hydrogen atom for which one can determine the atomic Bohr radius a_0 from first principles as

$$a_0 = a_{\text{H}} = \frac{4\pi\epsilon_0 (\hbar c)^2}{e^2 m_e c^2} \approx 0.53 \text{ \AA}. \quad (1.41)$$

Contrary to the impression that a high atomic number Z atom is much larger than the hydrogen atom, measurements have shown that the outer shell radius of a high Z atom such as uranium ($Z = 92$) exceeds the hydrogen atomic radius by only a factor of ~ 2 . We thus estimate the radius of the uranium atom to be about 1 Å.

(b) Heliocentric Copernican planetary system: Planets revolve about the stationary Sun in or close to the ecliptic plane.

Solar radius r_{S} is used as unit of length suitable for expressing the size of stars and is estimated to be $1 r_{\text{S}} = 6.955 \times 10^8 \text{ m} \approx 7 \times 10^8 \text{ m}$.

Mean distance between the Earth and the Sun (mean radius of Earth's orbit around the Sun) is used as unit of length suitable for expressing the distance between a planet and the Sun in the Solar system. The unit is called the astronomical unit (au) and has the following magnitude $1 \text{ au} = 149.6 \times 10^{11} \text{ m} = 215 r_S \approx 150 \times 10^6 \text{ km}$.

(c) **Ratios:**

$$\frac{\text{Earth's orbit}}{\text{Solar radius}} \approx \frac{150 \times 10^9 \text{ m}}{7 \times 10^8 \text{ m}} = 215 \quad (1.42)$$

$$\frac{\text{Hydrogen radius}}{\text{Proton radius}} \approx \frac{0.53 \times 10^{-10} \text{ m}}{1.25 \times 10^{-15} \text{ m}} = 42400 \quad (1.43)$$

$$\frac{\text{Uranium radius}}{\text{Radius of U-235 nucleus}} \approx \frac{1.5 \times 10^{-10} \text{ m}}{7.7 \times 10^{-15} \text{ m}} = 19500 \quad (1.44)$$

Thus, when the Sun and the atomic nucleus are normalized to the same size, the Rutherford-Bohr atom has a radius at least two orders of magnitude larger (range: factor of ~ 90 for the uranium-235 atom to ~ 200 for the hydrogen-1 atom) than the Sun-Earth planetary system. The amount of empty space in an atom is truly staggering and can be explained only by the enormous mass density of the nucleus which amounts to $\sim 1.5 \times 10^{15} \text{ g/cm}^3$.

1.18 Planck Energy Quantization

1.18.Q1

(23)

Quantum physics was born in 1900 when Max Planck presented his revolutionary idea of energy quantization of physical systems that undergo simple harmonic oscillations. Planck energy ε quantization is expressed as $\varepsilon = nh\nu$, where n is the quantum number ($n = 0, 1, 2, 3, \dots$), h is a universal constant referred to as the Planck constant, and ν is the frequency of oscillation.

- (a) Define the process of quantization.
- (b) Give at least five examples of quantization in daily life.
- (c) Provide at least five examples of quantization in modern physics.
- (d) Describe Planck postulate and briefly discuss Planck's pioneering use of the quantization idea in 1900.

SOLUTION:

(a) Quantization is a process of constraining a quantity from a set of continuous values to a set of discrete values. The process is applied in various domains resulting in audio quantization, video and image quantization, and color quantization. It is

also applied in mathematics and modern physics where it is used to develop quantum field theory from the classical field theory.

(b) Examples of quantization in daily life are:

Height quantization using steps in stairwells or rungs on ladders.

Quantization of currency and prices of goods and services.

Quantization of time.

Quantization of person's age.

(c) Examples of quantization in modern physics are:

Planck's quantization of oscillators in emission of blackbody radiation in 1900.

Einstein's quantization of light quanta in photoelectric effect in 1905.

Einstein's quantization of atomic vibrations in theory of specific heat in 1907.

Millikan's elementary charge quantization in 1910.

Bohr's quantization of angular momentum and energy in 1913.

Hydrogen emission spectrum and derivation of Rydberg constant in 1913.

(d) Classical physics predicts that the relationship between $d\rho(T)/d\nu$, the spectral energy density (energy per volume per frequency), and frequency ν of the emitted radiation is given by the Rayleigh-Jeans law as follows

$$\frac{d\rho(T)}{d\nu} = \frac{8\pi kT}{c^3} \nu^2, \quad (1.45)$$

with

T absolute temperature of the blackbody.

k Boltzmann constant.

c speed of light in vacuum.

Rayleigh-Jeans law predicts that energy density $\rho_\nu(T)$ increases as the square of frequency ν , approaching ∞ as $\nu \rightarrow \infty$, as shown with dashed curves in Fig. 1.7. This phenomenon, termed the ultraviolet catastrophe, is not borne out by experiments which show that blackbody emitters have clear maxima in their emission spectra with $\rho_\nu(T) \rightarrow 0$ as $\nu \rightarrow \infty$, as shown schematically with the solid curves in Fig. 1.7.

To solve the discrepancy between the classical theory and experiment Planck modeled a blackbody as a collection of oscillators that can only take on discrete, quantized energies described as

$$\varepsilon_n = nh\nu, \quad (1.46)$$

where n is an integer ($0, 1, 2, \dots$); ν is the frequency of emitted radiation; and h is a constant, now referred to as the Planck constant.

Based on oscillator energy quantization, Planck's alternative to Rayleigh-Jeans classical law for spectral energy density $\rho_\nu(T)$ is called the Planck law of blackbody

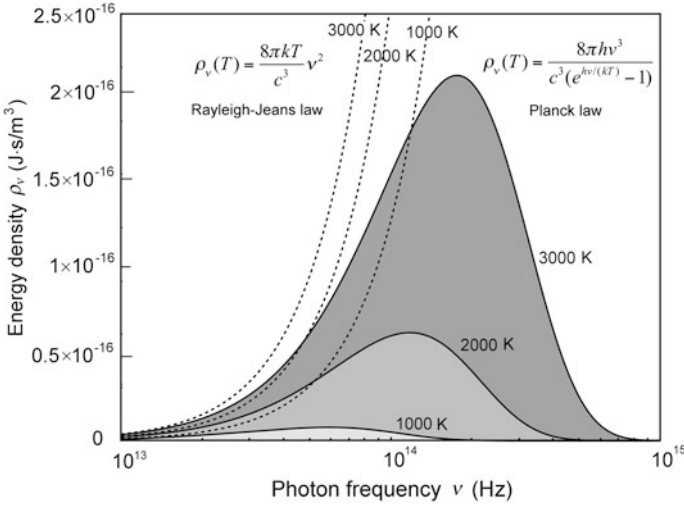


Fig. 1.7 Spectral energy density $d\rho(T)/d\nu$ against photon frequency ν in black body radiation for three temperatures: 1000 K, 2000 K, and 3000 K. *Dashed lines* are for Rayleigh-Jeans theory, *solid lines* for Planck theory. Note the shift of the peak in $d\rho(T)/d\nu$ toward higher frequencies with an increase in temperature T (see Prob. 24)

radiation and reads as follows

$$\frac{d\rho(T)}{d\nu} = \frac{8\pi h\nu^3}{c^3(e^{\frac{h\nu}{kT}} - 1)}. \quad (1.47)$$

The Planck law accurately predicts experimental data and, as shown in Fig. 1.7, exhibits a maximum; approaches 0 at low and high frequencies ν and, furthermore, at low frequencies transforms into Rayleigh-Jeans law, making the energy spectrum of each oscillator effectively continuous. However, at high frequencies the use of energy quantization is required in order to reach agreement between theory and experiment avoiding the ultraviolet catastrophe.

At low frequencies ν we can expand the exponential function of (1.47) as follows

$$\left\{e^{\frac{h\nu}{kT}} - 1\right\} \approx 1 + \frac{h\nu}{kT} + \dots - 1 \quad (1.48)$$

and (1.47) transforms into Rayleigh-Jeans equation given in (1.45).

Planck's use of the simple oscillator energy quantization $\varepsilon_n = nh\nu$ in theory of blackbody radiation ushered in the quantum physics which subsequently made use of several other quantization processes, listed in (c). For example, in 1905 Einstein took the quantization idea a step further and explained the surface photoelectric effect by introducing the "photon quantum hypothesis" whereby an electron is ejected from metallic surface by the impact of a particle of light (photon). The relationship between the photon frequency ν and the kinetic energy of the emitted electron E_K

is given as

$$h\nu = E_K + e\phi, \quad (1.49)$$

where $e\phi$ is the work function, characteristic of the particular metal.

1.18.Q2

(24)

In Prob. 23 the Planck law of blackbody radiation expressing the spectral density of a blackbody emitter was written in the frequency ν domain as

$$\frac{d\rho(T)}{d\nu} = \frac{8\pi h\nu^3}{c^3(e^{\frac{h\nu}{kT}} - 1)}. \quad (1.50)$$

The spectral energy density can also be written in the wavelength λ domain and is usually designated as $d\rho(T)/d\lambda$. A plot of $d\rho(T)/d\lambda$ against λ , similarly to a plot of $d\rho(T)/d\nu$ against ν (see Fig. 1.7), exhibits a peak λ_{\max} which is proportional to temperature T ; however, its position shifts toward shorter λ as the temperature increases, in contrast to the behavior of the $d\rho(T)/d\nu$ against ν graphs where ν_{\max} shifts toward higher frequencies ν as the temperature increases.

-
- (a) Derive an expression for $d\rho(T)/d\lambda$ from $d\rho(T)/d\nu$ given in (1.50).
 (b) Show that the maximum in $d\rho(T)/d\nu$ which occurs at frequency ν_{\max} is proportional to temperature T (Wien displacement law in frequency domain).
 (c) Show that the maximum in $d\rho(T)/d\lambda$ which occurs at wavelength λ_{\max} is inversely proportional to temperature T (Wien displacement law in wavelength domain).

SOLUTION:

- (a) The spectral energy density in the wavelength domain $d\rho(T)/d\lambda$ is given as

$$\frac{d\rho(T)}{d\lambda} = \frac{d\rho(T)}{d\nu} \left| \frac{d\nu}{d\lambda} \right| = \frac{8\pi h\nu^3}{c^3(e^{\frac{h\nu}{kT}} - 1)} \frac{c}{\lambda^2} = \frac{8\pi hc}{\lambda^5(e^{\frac{hc}{\lambda kT}} - 1)}. \quad (1.51)$$

Equation (1.51) is plotted in Fig. 1.8 for three temperatures (2000 K, 2500 K, and 3000 K), while Fig. 1.9 displays (1.50) for the same three temperatures. The shifts in ν_{\max} and λ_{\max} with temperature T are clearly noticeable with ν_{\max} proportional to T and λ_{\max} inversely proportional to T .

- (b) The Wien displacement law in the frequency domain states that ν_{\max} is proportional to temperature T of the blackbody emitter, i.e., $\nu_{\max} = C_\nu T$ (see Fig. 1.9). The constant C_ν is obtained from the Planck law by setting the second derivative

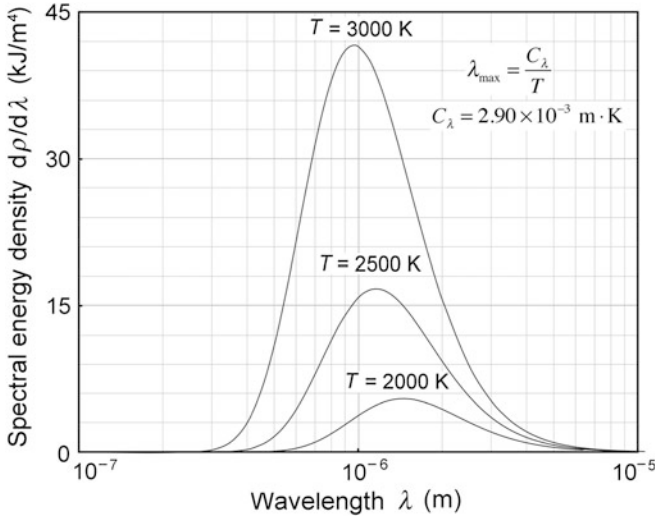


Fig. 1.8 Spectral energy density in the wavelength domain, $d\rho(T)/d\lambda$, against wavelength λ . Note the shift of λ_{\max} to lower wavelengths with increasing temperature T of the blackbody emitter

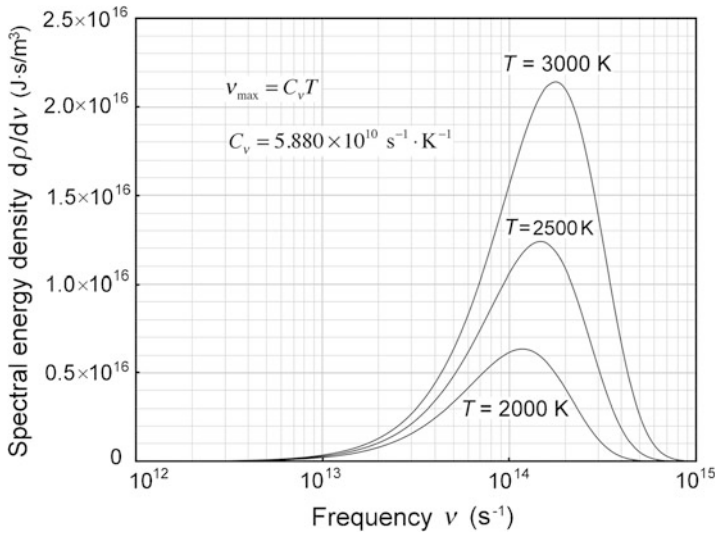


Fig. 1.9 Spectral energy density in the frequency domain, $d\rho(T)/d\nu$, against frequency ν . Note the shift of ν_{\max} to higher frequencies with increasing temperature T of the blackbody emitter

$d^2\rho(T)/d\nu^2|_{\nu=\nu_{\max}}$ equal to zero to find the relationship between ν_{\max} and T as follows

$$\frac{d^2\rho(T)}{d\nu^2}\bigg|_{\nu=\nu_{\max}} = \frac{24\pi h\nu^2 c^3 (e^{\frac{h\nu_{\max}}{kT}} - 1) - 8\pi h\nu^3 c^3 \frac{h}{kT} e^{\frac{h\nu_{\max}}{kT}}}{c^6 (e^{\frac{h\nu_{\max}}{kT}} - 1)^2} = 0 \quad (1.52)$$

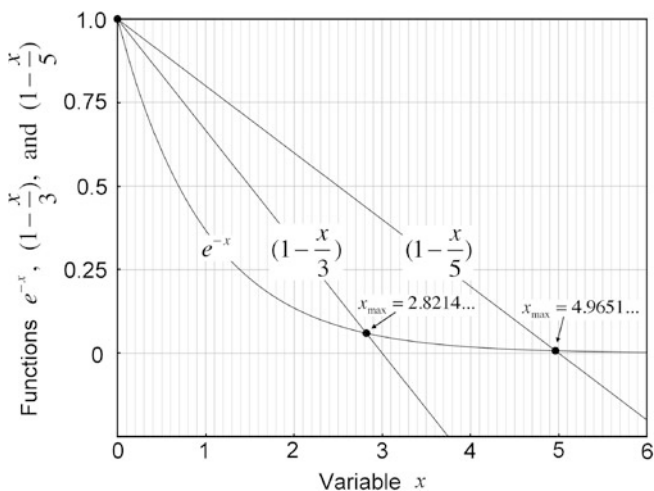


Fig. 1.10 Functions e^{-x} , $1 - \frac{1}{3}x$, and $1 - \frac{1}{5}x$ plotted against variable x and used in graphical solution of transcendental equations (1.54) and (1.58)

or

$$3\left(e^{\frac{h\nu_{\max}}{kT}} - 1\right) - \frac{h\nu}{kT} e^{\frac{h\nu_{\max}}{kT}} = 0. \tag{1.53}$$

Introducing a new variable $x_{\max} = h\nu_{\max}/(kT)$ into (1.53) we get a transcendental equation

$$3\left(e^{x_{\max}} - 1\right) - x_{\max} e^{x_{\max}} = 0 \quad \text{or} \quad 1 - \frac{x_{\max}}{3} = e^{-x_{\max}} \tag{1.54}$$

that cannot be solved in a closed form; however, we can solve it numerically or graphically by plotting its two functions: e^{-x} and $1 - \frac{1}{3}x$ and finding solutions to (1.54) through determining the intercepts between the two functions occurring at $x = x_{\max}$. As shown in Fig. 1.10, the two functions have two intercepts that provide two solutions: a trivial solution at $x_{\max} = 0$ and a physical solution at $x_{\max} = 2.8214$. The frequency ν_{\max} where $d\rho(T)/d\nu$ attains its maximum value at a given T is now determined as follows

$$\begin{aligned} \nu_{\max} &= x_{\max} \frac{k}{h} T = \frac{2.8214 \times 1.38 \times 10^{-23} \text{ J} \cdot \text{K}^{-1}}{6.626 \times 10^{-34} \text{ J} \cdot \text{s}} T = C_{\nu} T \\ &= (5.880 \times 10^{10} \text{ s}^{-1}/\text{K}) \times T. \end{aligned} \tag{1.55}$$

The Wien displacement constant in the frequency domain is given as $C_{\nu} = 5.880 \times 10^{10} \text{ s}^{-1}/\text{K}$.

(c) The Wien displacement law in the wavelength domain states that λ_{\max} is inversely proportional to the temperature T of the blackbody emitter, i.e., $\lambda_{\max} = C_{\lambda}/T$ (see Fig. 1.8). The constant C_{λ} is obtained by setting the second derivative

$d^2\rho_\lambda(T)/d\lambda^2|_{\lambda=\lambda_{\max}}$ equal to zero to find the relationship between λ_{\max} and T as follows

$$\left. \frac{d^2\rho_\lambda(T)}{d\lambda^2} \right|_{\lambda=\lambda_{\max}} = \frac{-8\pi hc [5\lambda^4 (e^{\frac{hc}{kT\lambda_{\max}}} - 1) - \lambda_{\max}^5 \frac{hc}{kT\lambda_{\max}^2} e^{\frac{hc}{kT\lambda_{\max}}}] }{\lambda^{10} (e^{\frac{hc}{kT\lambda_{\max}}} - 1)^2} = 0 \quad (1.56)$$

or

$$5(e^{\frac{hc}{kT\lambda_{\max}}} - 1) - \frac{hc}{kT\lambda_{\max}} e^{\frac{hc}{kT\lambda_{\max}}} = 0. \quad (1.57)$$

Introducing a new variable $x_{\max} = hc/(kT\lambda_{\max})$ into (1.57) we get a transcendental equation

$$5(e^{x_{\max}} - 1) - x_{\max} e^{x_{\max}} = 0 \quad \text{or} \quad 1 - \frac{x}{5} = e^{-x_{\max}} \quad (1.58)$$

that like (1.54) cannot be solved in a closed form; however, we can solve it numerically or graphically by plotting its two functions: e^{-x} and $(1 - \frac{1}{5}x)$ and finding solutions to (1.58) through determining the intercepts between the two functions occurring at $x = x_{\max}$. As shown in Fig. 1.10, the two functions have two intercepts that provide two solutions: a trivial solution at $x_{\max} = 0$ and a physical solution at $x_{\max} = 4.9651$. The wavelength λ_{\max} where $d\rho(T)/d\lambda$ attains its maximum value at a given T is now determined as follows

$$\begin{aligned} \lambda_{\max} &= \frac{hc}{x_{\max} kT} = \frac{(6.626 \times 10^{-34} \text{ J} \cdot \text{s}) \times (3 \times 10^8 \text{ m} \cdot \text{s}^{-1})}{4.9651 \times 1.381 \times 10^{-23} \text{ J} \cdot \text{K}^{-1}} \frac{1}{T} \\ &= \frac{C_\lambda}{T} = \frac{2.90 \times 10^{-3} \text{ m} \cdot \text{K}}{T}. \end{aligned} \quad (1.59)$$

The Wien displacement constant in the wavelength domain is given as $C_\lambda = 2.90 \times 10^{-3} \text{ m} \cdot \text{K}$.

1.19 Quantization of Electromagnetic Radiation

1.19.Q1

(25)

- (a) Show that photon energy E_ν is related to photon wavelength λ through the following relationship

$$E_\nu = \frac{12.4 \times 10^3 \text{ eV} \cdot \text{\AA}}{\lambda} = \frac{1.24 \times 10^{-6} \text{ eV} \cdot \text{m}}{\lambda}. \quad (1.60)$$

- (b) Show that photon momentum p_ν is related to photon wavelength λ through the following relationship

$$p_\nu = \frac{0.6613 \times 10^{-33} \text{ kg} \cdot \text{m}^2 \cdot \text{s}^{-1}}{\lambda}. \quad (1.61)$$

- (c) In Table 1.14A list the major components of the electromagnetic spectrum and for each component indicate the range in wavelength λ , frequency ν , and energy E_ν .

Table 1.14A Main characteristics of the electromagnetic (EM) spectrum

	Component of EM spectrum	Wavelength λ (m)	Frequency ν (Hz) $\nu =$	Energy E_ν (eV) $E_\nu =$
1		To	From	From
		↑	↓	↓
		From	To	To
2		To	From	From
		↑	↓	↓
		From	To	To
3		To	From	From
		↑	↓	↓
		From	To	To
4	Visible	To	From	From
		↑	↓	↓
		From	To	To
5		To	From	From
		↑	↓	↓
		From	To	To
6		To	From	From
		↑	↓	↓
		From	To	To

SOLUTION:

The oscillator energy quantization that Max Planck proposed for solving the black-body emission spectrum problem introduced the notion that energy of electromagnetic radiation can only be released in packets of energy called quanta. These quanta have subsequently been named photons. Photon is characterized with its wavelength λ , frequency ν , energy E_ν , and momentum p_ν . Furthermore, the photon has

no mass, possesses no charge, does not decay in empty space, and moves in vacuum with speed $c = 3 \times 10^8$ m/s that is a universal constant independent of the motion of the source. The following basic relationships apply for photons:

$$(a) \quad c = \lambda \nu \quad (1.62)$$

$$E_\nu = h\nu = h \frac{c}{\lambda} = \frac{2\pi \hbar c}{\lambda} = \frac{2\pi \times 197.3 \text{ MeV} \cdot \text{fm}}{\lambda} = \frac{1.24 \times 10^{-6} \text{ eV} \cdot \text{m}}{\lambda} \quad (1.63)$$

$$(b) \quad p_\nu = \frac{E_\nu}{c} = \frac{h}{\lambda} = \frac{1.24 \times 10^{-6} \text{ eV} \cdot \text{m}}{(3 \times 10^8 \text{ m} \cdot \text{s}^{-1}) \times \lambda} \\ = \frac{(1.24 \times 10^{-6} \text{ eV} \cdot \text{m}) \times (1.6 \times 10^{-19} \text{ N} \cdot \text{m})}{(3 \times 10^8 \text{ m} \cdot \text{s}^{-1}) \times \lambda} \\ = \frac{0.6613 \times 10^{-33} \text{ kg} \cdot \text{m}^2 \cdot \text{s}^{-1}}{\lambda} \quad (1.64)$$

(c) Major components of the electromagnetic spectrum are listed in Table 1.14B.

Table 1.14B Main characteristics of the electromagnetic (EM) spectrum

Component of EM spectrum	Wavelength λ (m)		Frequency ν (Hz) $\nu = c/\lambda$		Energy E_ν (eV) $E_\nu = 1.24 \times 10^{-6} \text{ eV} \cdot \text{m}$	
1 Radio waves	To	10^3	From	3×10^5	From	1.24×10^{-9}
	↑		↓		↓	
	From	10^{-1}	To	3×10^9	To	1.24×10^{-5}
	<hr/>					
2 Microwaves	To	10^{-1}	From	3×10^9	From	1.24×10^{-5}
	↑		↓		↓	
	From	10^{-3}	To	3×10^{11}	To	1.24×10^{-3}
	<hr/>					
3 Infrared radiation	To	10^{-3}	From	3×10^{11}	From	1.24×10^{-3}
	↑		↓		↓	
	From	7×10^{-7}	To	0.43×10^{15}	To	1.77
	<hr/>					
4 Visible light	To	7×10^{-7}	From	0.43×10^{15}	From	1.77
	↑		↓		↓	
	From	4×10^{-7}	To	0.75×10^{15}	To	3.10
	<hr/>					
5 Ultraviolet radiation	To	4×10^{-7}	From	0.75×10^{15}	From	3.10
	↑		↓		↓	
	From	10^{-8}	To	3×10^{16}	To	124
	<hr/>					
6 X rays and γ rays	To	10^{-8}	From	3×10^{16}	From	124
	↑		↓		↓	
	From	10^{-15}	To	3×10^{23}	To	1.24×10^9

1.20 Special Theory of Relativity

1.20.Q1

(26)

Lorentzian transformations relate the spatial and temporal coordinates x , y , z , and t in a stationary frame F to spatial and temporal coordinates x' , y' , z' , and t' in a reference frame F' moving with uniform velocity v in the direction of the abscissa (x) axis. The two frames are parallel to one another, i.e., the x' axis is parallel to the x axis, the y' axis is parallel to the y axis, and the z' axis is parallel to the z axis. Equations for the forward Lorentzian transformation are as follows: $x' = \gamma(x - vt)$; $y' = y$; $z' = z$; and $t' = \gamma[t - vx/(c^2)]$, where γ is the standard Lorentz factor $\gamma = (1 - v^2/c^2)^{-1/2}$.

Determine the relationships that govern the inverse Lorentzian transformation.

SOLUTION:

Expressions for $y' = y$ and $z' = z$ remain the same in the inverse transformation; expressions for x and t we determine by solving expressions for x' and t' in the forward transformation. We first derive the expression for x using expressions for x' and t' as follows

$$x' = \gamma(x - vt) \quad \text{or} \quad x = \frac{1}{\gamma}x' + vt, \quad (1.65)$$

$$t' = \gamma\left(t - \frac{v}{c^2}x\right) \quad \text{or} \quad t = \frac{1}{\gamma}t' + \frac{v}{c^2}x. \quad (1.66)$$

Inserting (1.66) into (1.65) we get

$$x = \frac{1}{\gamma}x' + \frac{v}{\gamma}t' + \frac{v^2}{c^2}x \quad \text{or} \quad x\left(1 - \frac{v^2}{c^2}\right) = \frac{1}{\gamma}(x' + vt'). \quad (1.67)$$

Since $(1 - v^2/c^2) = 1/\gamma^2$, we get the following expression for x

$$x = \gamma(x' + vt'). \quad (1.68)$$

We now derive the expression for t using expressions for x' and t' as follows

Inserting (1.65) into (1.66) we get

$$t = \frac{1}{\gamma}t' + \frac{1}{\gamma}\frac{v}{c^2}x' + \frac{v^2}{c^2}t \quad \text{or} \quad t\left(1 - \frac{v^2}{c^2}\right) = \frac{1}{\gamma}\left(t' + \frac{v}{c^2}x'\right). \quad (1.69)$$

Since $(1 - v^2/c^2) = 1/\gamma^2$, we get the following expression for t

$$t = \gamma\left(t' + \frac{v}{c^2}x'\right). \quad (1.70)$$

Equations for the inverse Lorentzian transformation

$$x = \gamma(x' + vt'); \quad y = y'; \quad z = z'; \quad \text{and} \quad t = \gamma[t' + vx'/(c^2)] \quad (1.71)$$

are equivalent to equations governing the forward Lorentzian transformation, except that the velocity of the moving frame is $-v$ in the inverse transformation as opposed to $+v$ in the forward transformation.

1.20.Q2

(27)

(a) Show that the wave equation

$$\frac{\partial \phi}{\partial x^2} + \frac{\partial \phi}{\partial y^2} + \frac{\partial \phi}{\partial z^2} = \frac{1}{c^2} \frac{\partial \phi}{\partial t^2} \quad (1.72)$$

is invariant under Lorentzian transformation.

(b) What is the effect of this invariance on Maxwell equations?

SOLUTION:

(a) The Lorentzian transformation for two inertial frames, F and F' , with parallel corresponding axes, with x and x' axes being common, and with frame F' moving along the x axis with velocity v relative to frame F , is expressed as follows

$$x' = \gamma(x - vt); \quad y' = y; \quad z' = z; \quad \text{and} \quad t' = \gamma\left(t - \frac{v}{c^2}x\right) \quad (1.73)$$

where γ is the standard Lorentz factor $\gamma = (1 - v^2/c^2)^{-1/2}$ and the following derivatives should be noted

$$\frac{\partial x'}{\partial x} = \gamma, \quad \frac{\partial x'}{\partial t} = -\gamma v, \quad \frac{\partial t'}{\partial t} = \gamma, \quad \text{and} \quad \frac{\partial t'}{\partial x} = -\gamma \frac{v}{c^2}. \quad (1.74)$$

The space derivatives are expressed as follows

$$\frac{\partial \phi}{\partial x} = \frac{\partial \phi}{\partial x'} \frac{\partial x'}{\partial x} + \frac{\partial \phi}{\partial t'} \frac{\partial t'}{\partial x} = \frac{\partial \phi}{\partial x'} \gamma - \frac{\partial \phi}{\partial t'} \gamma \frac{v}{c^2}, \quad (1.75)$$

$$\begin{aligned} \frac{\partial^2 \phi}{\partial x^2} &= \frac{\partial}{\partial x'} \left[\frac{\partial \phi}{\partial x'} \right] \frac{\partial x'}{\partial x} \gamma + \frac{\partial}{\partial t'} \left[\frac{\partial \phi}{\partial x'} \right] \frac{\partial t'}{\partial x} \gamma - \frac{\partial}{\partial x'} \left[\frac{\partial \phi}{\partial t'} \right] \frac{\partial x'}{\partial x} \gamma \frac{v}{c^2} \\ &\quad - \frac{\partial}{\partial t'} \left[\frac{\partial \phi}{\partial t'} \right] \frac{\partial t'}{\partial x} \gamma \frac{v}{c^2} \\ &= \gamma^2 \frac{\partial^2 \phi}{\partial x'^2} - \gamma^2 \frac{v}{c^2} \frac{\partial^2 \phi}{\partial x' \partial t'} - \gamma^2 \frac{v}{c^2} \frac{\partial^2 \phi}{\partial x' \partial t'} + \gamma^2 \frac{v^2}{c^4} \frac{\partial^2 \phi}{\partial t'^2} \\ &= \gamma^2 \frac{\partial^2 \phi}{\partial x'^2} + \gamma^2 \frac{v^2}{c^4} \frac{\partial^2 \phi}{\partial t'^2} - 2\gamma^2 \frac{v}{c^2} \frac{\partial^2 \phi}{\partial x' \partial t'}, \end{aligned} \quad (1.76)$$

$$\frac{\partial^2 \phi}{\partial y^2} = \frac{\partial^2 \phi}{\partial y'^2}, \quad (1.77)$$

$$\frac{\partial^2 \phi}{\partial z^2} = \frac{\partial^2 \phi}{\partial z'^2}. \quad (1.78)$$

The time derivatives are

$$\frac{\partial \phi}{\partial t} = \frac{\partial \phi}{\partial t'} \frac{\partial t'}{\partial t} + \frac{\partial \phi}{\partial x'} \frac{\partial x'}{\partial t} = \frac{\partial \phi}{\partial t'} \gamma - \frac{\partial \phi}{\partial x'} \gamma v, \quad (1.79)$$

$$\begin{aligned} \frac{\partial^2 \phi}{\partial t^2} &= \frac{\partial}{\partial t'} \left[\frac{\partial \phi}{\partial t'} \right] \frac{\partial t'}{\partial t} \gamma + \frac{\partial}{\partial x'} \left[\frac{\partial \phi}{\partial t'} \right] \frac{\partial x'}{\partial t} \gamma - \frac{\partial}{\partial t'} \left[\frac{\partial \phi}{\partial x'} \right] \frac{\partial t'}{\partial t} \gamma v - \frac{\partial}{\partial x'} \left[\frac{\partial \phi}{\partial x'} \right] \frac{\partial x'}{\partial t} \gamma v \\ &= \gamma^2 \frac{\partial^2 \phi}{\partial t'^2} - \gamma^2 v \frac{\partial^2 \phi}{\partial x' \partial t'} - \gamma^2 v \frac{\partial^2 \phi}{\partial x' \partial t'} - \gamma^2 v^2 \frac{\partial^2 \phi}{\partial x'^2} \\ &= \gamma^2 \frac{\partial^2 \phi}{\partial t'^2} + \gamma^2 v^2 \frac{\partial^2 \phi}{\partial x'^2} - 2\gamma^2 v \frac{\partial^2 \phi}{\partial x' \partial t'}. \end{aligned} \quad (1.80)$$

The components of the wave equation can now be expressed as follows

$$\frac{\partial^2 \phi}{\partial x^2} + \frac{\partial^2 \phi}{\partial y^2} + \frac{\partial^2 \phi}{\partial z^2} = \gamma^2 \frac{\partial^2 \phi}{\partial x'^2} + \gamma^2 \frac{v^2}{c^4} \frac{\partial^2 \phi}{\partial t'^2} - 2\gamma^2 \frac{v}{c^2} \frac{\partial^2 \phi}{\partial x' \partial t'} + \frac{\partial^2 \phi}{\partial y'^2} + \frac{\partial^2 \phi}{\partial z'^2} \quad (1.81)$$

and

$$\frac{1}{c^2} \frac{\partial^2 \phi}{\partial t'^2} = \frac{\gamma^2}{c^2} \frac{\partial^2 \phi}{\partial t'^2} + \gamma^2 \frac{v^2}{c^2} \frac{\partial^2 \phi}{\partial x'^2} - 2\gamma^2 \frac{v}{c^2} \frac{\partial^2 \phi}{\partial x' \partial t'}, \quad (1.82)$$

resulting in the following expression for the wave equation

$$\gamma^2 \left(1 - \frac{v^2}{c^2} \right) \frac{\partial^2 \phi}{\partial x'^2} + \frac{\partial^2 \phi}{\partial y'^2} + \frac{\partial^2 \phi}{\partial z'^2} = \gamma^2 \frac{1}{c^2} \left(1 - \frac{v^2}{c^2} \right) \frac{\partial^2 \phi}{\partial t'^2}. \quad (1.83)$$

Recognizing that $\gamma^2(1 - v^2/c^2) = \gamma^2(1 - \beta^2) = 1$ we finally get the following expression for the wave equation in the inertial frame F'

$$\frac{\partial^2 \phi}{\partial x'^2} + \frac{\partial^2 \phi}{\partial y'^2} + \frac{\partial^2 \phi}{\partial z'^2} = \frac{1}{c^2} \frac{\partial^2 \phi}{\partial t'^2}, \quad (1.84)$$

showing that equation $\partial^2 \phi / \partial x'^2 + \partial^2 \phi / \partial y'^2 + \partial^2 \phi / \partial z'^2 = (1/c^2) \partial^2 \phi / \partial t'^2$ is invariant under Lorentzian transformation.

(b) The form of the wave equation in a frame F' moving with uniform velocity v is identical to the form of the wave equation in fixed inertial frame F . A result of this invariance is the invariance of Maxwell equations governing the electric and magnetic fields produced by a charge moving with uniform velocity v .

1.20.Q3

(28)

Theory of relativity has several consequences, some of them quite dramatic, counter-intuitive, and irreconcilable with classical physics. Three important phenomena in this category are: (i) length contraction, (ii) time dilation, and (iii) mass increase with velocity, all three phenomena governed by the Lorentz factor $\gamma = [1 - \beta^2]^{-1/2} = [1 - (v/c)^2]^{-1/2}$ which becomes significant when the speed v of an object or particle is an appreciable fraction of the speed of light c in vacuum.

Use the Lorentzian transformation between two inertial frames, one stationary and the other moving with velocity v with respect to the stationary frame, to show that

- (a) Length contraction is inversely proportional to γ , i.e., $L = \frac{L_0}{\gamma}$.
- (b) Time dilation is proportional to γ as $\Delta t = \gamma \Delta t_0$. In equations for L and Δt , L_0 and Δt_0 are the proper length and the proper time interval, respectively, measured by an observer moving with the object, while L and Δt are the length and time interval, respectively, measured by an observer in the stationary frame.
- (c) The increase in relativistic mass $m(v)$ of a particle as a function of its velocity v makes the speed of light c in vacuum the upper limit of speed in the universe. Calculate the velocity relative to speed of light c of a particle at which the relativistic mass of the particle exceeds its rest mass m_0 by 2 %, 10 %, 50 %, a factor of 10, and a factor of 100.

SOLUTION:

(a) Length contraction. The measured length of an object depends on the relative velocity of the object and observer. The largest length of an object is measured in a frame in which the object is at rest. This length is referred to as the proper or rest length L_0 .

Assume that we have a rod placed along the x' axis in the moving frame F' . The length L_0 measured by an observer at rest with respect to the moving frame F' is given as $L_0 = x'_2 - x'_1$. The length of the rod L measured in the fixed reference frame F is $L = x_2 - x_1$ with the coordinates x_1 and x_2 related to coordinates x'_1 and x'_2 , respectively, through the Lorentzian transformation. We can thus express L_0 as follows

$$L_0 = x'_2 - x'_1 = \gamma(x_2 - vt_2) - \gamma(x_1 - vt_1). \quad (1.85)$$

Since the two measurements made in the fixed frame F were made simultaneously, we have $t_1 = t_2$ and (1.85) is simplified to read

$$L_0 = \gamma(x_2 - x_1) = \gamma L \quad \text{and} \quad L = \frac{1}{\gamma} L_0. \quad (1.86)$$

Length L of an object that is moving with velocity v relative to the observer is inversely proportional to Lorentz factor γ and is smaller than or equal to the proper length L_0 , since $\gamma \geq 1$. This phenomenon is referred to as the length contraction.

(b) Time dilation. The shortest time interval is measured in a frame in which the clock is at rest. The time interval so measured is referred to as the proper or rest time interval Δt_0 . We now assume that we are measuring a time interval Δt_0 in the moving frame F' where $\Delta t_0 = t'_2 - t'_1$. The time interval Δt measured for the same event in the fixed frame F is given as

$$\Delta t = t_2 - t_1 = \gamma \left(t'_2 + \frac{v}{c^2} x'_2 \right) - \gamma \left(t'_1 + \frac{v}{c^2} x'_1 \right). \quad (1.87)$$

Since the two measurements made in F' are made at the same location, we have $x'_1 = x'_2$ and (1.87) simplifies to read $\Delta t = \gamma(t'_2 - t'_1) = \gamma \Delta t_0$. This phenomenon is referred to as time dilation.

(c) Relativistic mass. Particle mass m depends on particle velocity v through the following relationship

$$m(v) = \gamma m_0 = \frac{m_0}{\sqrt{1 - \beta^2}} = \frac{m_0}{\sqrt{1 - \frac{v^2}{c^2}}} \quad \text{or} \quad (1.88)$$

$$\frac{m(v)}{m_0} = \gamma = \frac{1}{\sqrt{1 - \beta^2}} = \frac{1}{\sqrt{1 - \frac{v^2}{c^2}}}$$

where m_0 is the particle mass at rest at $v = 0$ referred to as the particle rest mass or invariant mass and γ is the Lorentz factor. The relativistic mass of a particle becomes infinite as the velocity of the particle approaches the speed of light c .

Solving (1.88) for $\beta = v/c$ against $\gamma = m(v)/m_0$ results in the following relationship

$$\beta = \frac{v}{c} = \frac{\sqrt{\gamma^2 - 1}}{\gamma} = \sqrt{1 - \frac{1}{\gamma^2}}. \quad (1.89)$$

Results for β with various values of $\gamma = m(v)/m_0$ are shown in Table 1.15.

Table 1.15 Speed v of particle normalized to speed of light c against Lorentz factor $\gamma = m(v)/m_0$

$\gamma = m(v)/m_0$	1.01	1.02	1.10	1.50	10	100
$\beta = v/c$	0.140	0.197	0.417	0.745	0.995	0.99995

1.20.Q4

(29)

Pions π also called π mesons belong to a group of short-lived subatomic particles called mesons. They are either neutral (π^0) or come with positive (π^+) or negative (π^-) electron charge and their rest mass is about $273m_e$ where $m_e = 0.511$ MeV is the rest mass of the electron. Pions do not exist in free state in nature; they reside inside the nuclei of atoms and, based on their mass, were identified as the quanta of the strong interaction. They can be ejected from the nucleus in nuclear reactions by bombarding target nuclei with energetic electrons or protons. Mean lifetime of a free negative pion (π^-) and positive pion π^+ in its own reference frame (proper or rest mean lifetime) is 2.6×10^{-8} s and they decay through weak interaction.

Of the three pion types negative pions have been used for radiotherapy, since by virtue of their negative charge, they produce the so-called “pion stars” in irradiated nuclei. They showed great promise for use in radiotherapy; however, during recent years pions, because of their complexity and cost, were largely abandoned in favor of heavy charged particles such as protons and heavier ions.

If the pion travels with velocity of $0.99c$ where c is the speed of light in vacuum, determine:

- Mean lifetime of the pion when measured by a stationary observer on earth.
- Mean distance the pion travels before it decays, as measured by a stationary observer on earth.

SOLUTION:

First we determine the Lorentz factor γ for $\beta = 0.99c$

$$\gamma = \frac{1}{\sqrt{1 - \beta^2}} = \frac{1}{\sqrt{1 - 0.99^2}} = 7.09. \quad (1.90)$$

- Mean lifetime $\bar{\tau}$ of the pion as measured on earth is longer than the proper (rest) mean lifetime $\bar{\tau}_0$ because of the relativistic time dilation effect. The following relationship between $\bar{\tau}$ and $\bar{\tau}_0$ applies (see Prob. 28)

$$\bar{\tau} = \gamma \bar{\tau}_0 = 7.09 \times 2.6 \times 10^{-8} \text{ s} = 18.4 \times 10^{-8} \text{ s} = 0.184 \text{ ms}. \quad (1.91)$$

- Mean distance $\bar{\ell}$ that the pion with velocity of $0.99c$ travels is calculated by multiplying the pion's mean lifetime $\bar{\tau}$ with its velocity to get

$$\bar{\ell} = \bar{\tau} v = (0.184 \times 10^{-6} \text{ s}) \times (0.99 \times 3 \times 10^8 \text{ m/s}) = 54.6 \text{ m}. \quad (1.92)$$

1.20.Q5

(30)

- (a) A meter stick moving in the direction parallel to its long dimension appears to be only 80 cm long to a stationary observer. Calculate the speed of the stick.
- (b) Estimate the length L of an acceleration waveguide of a linear accelerator (linac) as seen by an accelerated electron, if the length L_0 of the accelerator waveguide is 1.5 m, the accelerator gun voltage is 100 kV, and the linac nominal energy is 25 MV.

SOLUTION:

(a) The proper (rest) length of the stick is $L_0 = 100$ cm. Since, as a result of the relativistic length contraction, the stick appears shorter ($L = 80$ cm), it must be moving with significant speed that can be determined from the length contraction expression, given in Prob. 28 as

$$L = \frac{L_0}{\gamma} = L_0 \sqrt{1 - \beta^2} = L_0 \sqrt{1 - \frac{v^2}{c^2}}, \quad (1.93)$$

where γ is the Lorentz factor.

Solving (1.93) for the normalized velocity $\beta = v/c$ we get

$$\beta = \sqrt{1 - \frac{1}{\gamma^2}} = \sqrt{1 - \frac{L^2}{L_0^2}} = 0.6 \quad \text{or} \quad v = 0.6c = 1.8 \times 10^8 \text{ m/s}. \quad (1.94)$$

(b) The proper (rest) length of a linac waveguide measured in the reference frame of the linac is L_0 and the length of the waveguide as it appears to an observer traveling with the accelerated electron is L . The two lengths L and L_0 are related through relativistic length contraction (see Prob. 28) as follows

$$L = \frac{L_0}{\gamma} = L_0 \sqrt{1 - \beta^2} \quad \text{or} \quad dz' = \frac{dz}{\gamma} = dz \sqrt{1 - \beta^2}, \quad (1.95)$$

where dz is an element of accelerated electron's path in the linac reference frame and dz' is an element of path in the rest frame.

Since the total energy E of the electron is related to the rest energy E_0 of the electron through the Lorentz factor γ as $E = \gamma E_0$ we note that $\gamma = E/E_0$ and (1.95) becomes

$$dz' = \frac{dz}{\gamma} = dz \sqrt{1 - \beta^2} = \frac{E_0}{E} dz = \frac{E_0}{E_i + eE_z z} dz = \frac{E_0}{E_0 + (E_K)_i + eE_z z} dz, \quad (1.96)$$

where the total energy E as a function of z along the waveguide axis is given as the sum of the total energy E_i of the electrons injected from the electron gun into

the accelerator waveguide and energy $e\mathcal{E}_z z$ gained by the electron in the electric field \mathcal{E}_z used for electron acceleration in the waveguide. The total energy E_i of the injected electron is the sum of electron rest energy E_0 and its kinetic energy $(E_K)_i$ at the time of injection into the waveguide. We thus have

$$E = E_i + e\mathcal{E}_z z = E_0 + (E_K)_i. \quad (1.97)$$

Next, we integrate (1.96) over z from 0 to L_0 and over z' from 0 to L to get

$$\int_0^L dz' = \int_0^{L_0} \frac{E_0}{E_0 + (E_K)_i + e\mathcal{E}_z z} dz = \frac{E_0}{e\mathcal{E}_z} \int_0^{L_0} \frac{d(E_0 + (E_K)_i + e\mathcal{E}_z z)}{E_0 + (E_K)_i + e\mathcal{E}_z z} \quad (1.98)$$

leading to

$$L = \frac{E_0}{e\mathcal{E}_z} \left\{ \ln[E_0 + (E_K)_i + e\mathcal{E}_z z] \right\}_0^{L_0} = \frac{E_0}{e\mathcal{E}_z} \ln \frac{E_f}{E_0 + (E_K)_i}, \quad (1.99)$$

where we recognize that $E_0 + (E_K)_i + e\mathcal{E}_z L_0$ is the final total energy E_f of the electron as it exits the acceleration waveguide.

Equation (1.99) is the general equation for estimating the waveguide contraction of an acceleration waveguide and we now use this equation to solve our specific problem given with the following parameters: $L_0 = 1.5$ m, $E_0 = 0.511$ MeV, $E_f = 25$ MeV, and $(E_K)_i = 100$ keV. The electric field \mathcal{E}_z is estimated from the capture condition for a linac waveguide (T13.110) to be ~ 8 MV/m for electron gun voltage of 100 kV.

The apparent length L of the waveguide is from (1.99) given as follows

$$L = \frac{E_0}{e\mathcal{E}_z} \ln \frac{E_f}{E_0 + (E_K)_i} = \frac{0.511 \text{ MeV}}{e \times (8 \text{ MV/m})} \ln \frac{25 \text{ MeV}}{(0.511 + 0.100) \text{ MeV}} = 0.24 \text{ m} \quad (1.100)$$

compared to a waveguide length of 1.5 m in the linear accelerator frame.

1.21 Important Relativistic Relations

1.21.Q1

(31)

Determine the speed of a particle (as fraction of the speed of light in vacuum c) at which the particle mass $m(v)$ becomes:

- (a) Twice its rest mass m_0 ,
- (b) Three times its rest mass m_0 ,
- (c) Four times its rest mass m_0 .

SOLUTION:

(a) Using the basic Einstein expression that states that the ratio between particle's relativistic mass $m(v)$ and rest mass m_0 equals to particle's Lorentz factor γ , i.e., $m(v)/m_0 = \gamma$ we set

$$\frac{m(v)}{m_0} = 2 = \gamma = \frac{1}{\sqrt{1 - \beta^2}} = \frac{1}{\sqrt{1 - \frac{v^2}{c^2}}} \quad (1.101)$$

and solve for v/c to get

$$\frac{v}{c} = \sqrt{1 - \frac{1}{\left[\frac{m(v)}{m_0}\right]^2}} = \sqrt{\frac{3}{4}} = 0.866 \quad (1.102)$$

corresponding to $v = 0.866c = 2.60 \times 10^8$ m/s.

(b) For $m(v) = 3m_0$ we get

$$\frac{v}{c} = \sqrt{1 - \frac{1}{\left[\frac{m(v)}{m_0}\right]^2}} = \sqrt{\frac{8}{9}} = 0.943 \quad (1.103)$$

corresponding to $v = 0.943c = 2.83 \times 10^8$ m/s.

(c) For $m(v) = 4m_0$ we get

$$\frac{v}{c} = \sqrt{1 - \frac{1}{\left[\frac{m(v)}{m_0}\right]^2}} = \sqrt{\frac{15}{16}} = 0.968 \quad (1.104)$$

corresponding to $v = 0.968c = 2.90 \times 10^8$ m/s. Figure 1.11 is a plot of γ against β for a particle of rest mass m_0 , where

β is the particle velocity v normalized to speed of light c in vacuum, i.e., $\beta = v/c$.

γ is the so called Lorentz factor defined as:

- (i) $\gamma = 1/\sqrt{1 - v^2/c^2}$.
- (ii) $\gamma = m(v)/m_0$ with $m(v)$ particle mass m at velocity v and m_0 particle rest mass.
- (iii) $\gamma = E/E_0 = (E_K + E_0)/E_0 = 1 + E_K/E_0$ with E particle total energy, E_K particle kinetic energy, and E_0 particle rest energy.

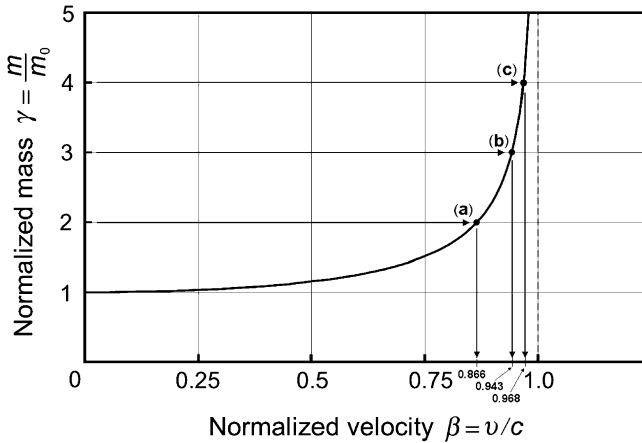


Fig. 1.11 Particle normalized mass $m(v)/m_0$ against its normalized velocity $\beta = v/c$. Data points represent results of (a), (b), and (c)

1.21.Q2

(32)

The standard expression of special relativity

$$E^2 = p^2c^2 + E_0^2 \quad (1.105)$$

linking particle's total energy E with its momentum p and rest energy E_0 is universally valid for all particles ($m_0 \neq 0$) as well as for photons ($m_0 = 0$).

- Derive (1.105) from the basic Einstein expression for relativistic mass m as a function of velocity v , i.e., from $m(v) = \gamma m_0$ where m is the particle's relativistic mass depending on particle's velocity v and m_0 is the particle's rest mass.
- Show that the expression $E^2 = p^2c^2 + E_0^2$ can also be derived directly from the two basic relativistic expressions: $E = \gamma E_0$ and $p = m v$ with γ the Lorentz factor given as $\gamma = [1 - v^2/c^2]^{-1/2}$ and $\beta = v/c$ the velocity v normalized to speed of light c .
- Show that a massless particle ($m_0 = 0$) always travels at the speed of light c .
- Show that a particle that travels with speed of light c possesses no rest energy ($E_0 = 0$) and no rest mass ($m_0 = 0$).

SOLUTION:

(a) The derivation of (1.105) from the basic Einstein relationship for relativistic mass proceeds as

(1) Start with the basic equation

$$m = \frac{m_0}{\sqrt{1 - \frac{v^2}{c^2}}}. \quad (1.106)$$

(2) Square (1.106), multiply the result by c^4 , and rearrange the terms to obtain

$$m^2 c^4 - m^2 c^2 v^2 = m_0^2 c^4. \quad (1.107)$$

(3) Equation (1.107) can be written as

$$E^2 - p^2 c^2 = E_0^2 \quad \text{or} \quad E = \sqrt{E_0^2 + p^2 c^2}, \quad (1.108)$$

incorporating into (1.107) the common relativistic relationships for total energy $E = mc^2$, rest energy $E_0 = m_0 c^2$, and momentum $p = mv$.

(b) Particle momentum $p = mv$ may be expressed as $p = mv = \gamma E_0 \beta / c$ using the standard relationships for γ and E_0 . Multiplying the expression for p with c , squaring the result, and recognizing that $\beta^2 = 1 - \gamma^{-2}$ gives

$$p^2 c^2 = \gamma^2 E_0^2 \beta^2 = E^2 \left[1 - \frac{1}{\gamma^2} \right] = E^2 - \frac{E^2}{\gamma^2} = E^2 - E_0^2 \quad (1.109)$$

or

$$E^2 = p^2 c^2 + E_0^2. \quad (1.110)$$

(c) From (1.110) we get

$$E^2 = E_0^2 + p^2 c^2 = 0 + p^2 c^2 \quad \text{or} \quad E = pc. \quad (1.111)$$

Equation (1.111) gives the following relationship for particle speed v , total energy E , and momentum p

$$\frac{v}{c} = \beta = \frac{pc}{E} \quad \text{or} \quad E = \frac{pc}{\beta}. \quad (1.112)$$

Equations (1.109) and (1.110) can hold simultaneously only for $\beta = 1$, i.e., $v = c$.

(d) From (1.111) we have $v/c = pc/E = 1$ or $E = pc$. From (1.110) we get the following expression for the rest energy E_0

$$E^2 = E_0^2 + p^2 c^2 \quad \text{or} \quad E_0 = \sqrt{E^2 - p^2 c^2} = 0. \quad (1.113)$$

Thus, when the total energy E equals pc , the rest energy E_0 is zero and the particle's rest mass m_0 is zero.

1.21.Q3

(33)

An electron is accelerated in a 10 MV linear accelerator (linac) and strikes an x-ray target. For the electron determine:

- (a) Kinetic energy E_K .
- (b) Total energy E .
- (c) Lorentz factor γ .
- (d) Velocity v .
- (e) Mass m .

SOLUTION:

(a) By definition a 10 MV linac produces a 10 MV x-ray beam whereby electrons of kinetic energy of 10 MeV strike the x-ray target and produce a 10 MV spectral distribution. Kinetic energy of the electron when it strikes the target is thus $E_K = 10 \text{ MeV}$. It is customary to describe an electron with its kinetic energy, so that a label “10 MeV electron” implies that kinetic energy of the electron is 10 MeV.

(b) Total energy E of an electron with kinetic energy $E_K = 10 \text{ MeV}$ is given as the sum of electron’s kinetic energy E_K and its rest energy $E_0 = 0.511 \text{ MeV}$.

$$E = E_K + E_0 = 10 \text{ MeV} + 0.511 \text{ MeV} = 10.511 \text{ MeV}. \quad (1.114)$$

(c) Lorentz factor γ is given as $\gamma = (1 - v^2/c^2)^{-1/2}$ and depends, in addition to velocity v , also indirectly on electron kinetic energy E_K

$$E_K = (\gamma - 1)E_0. \quad (1.115)$$

Solving (1.115) for γ results in the following expression

$$\gamma = 1 + \frac{E_K}{E_0} = 1 + \frac{10 \text{ MeV}}{0.511 \text{ MeV}} = 20.57. \quad (1.116)$$

The Lorentz factor γ can also be calculated from the basic definitions that implicitly state the following relationships

$$E = mc^2 = \gamma E_0 = \gamma m_0 c^2 \quad \text{or} \quad \gamma = \frac{E}{E_0} = \frac{10.511 \text{ MeV}}{0.511 \text{ MeV}} = 20.57. \quad (1.117)$$

A plot of the Lorentz factor γ against velocity v normalized to speed of light c in vacuum of Fig. 1.12 shows that an electron with $\gamma = 20.57$ is highly relativistic and travels with a velocity close to speed of light c in vacuum.

(d) Now that we have the Lorentz factor γ for a 10 MeV electron, we can calculate the normalized electron velocity v/c . Solving $\gamma = (1 - v^2/c^2)^{-1/2}$ for v/c results

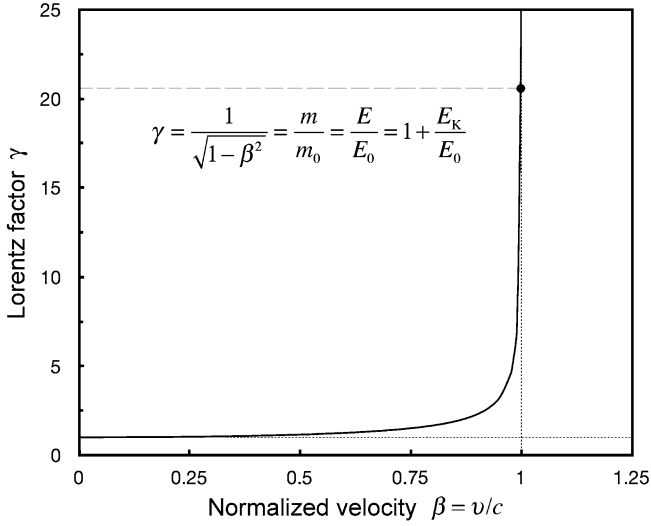


Fig. 1.12 Lorentz factor γ against normalized velocity β for electron. The *solid dot* on the curve indicates the Lorentz factor γ of 20.57 for a 10 MeV electron ($E_K = 10$ MeV) with normalized velocity $\beta = 0.999$

in the following expression

$$\frac{v}{c} = \sqrt{1 - \frac{1}{\gamma^2}} = \sqrt{1 - \frac{1}{20.57^2}} = 0.999. \quad (1.118)$$

We can also get v/c of a 10 MeV electron using the general expression for kinetic energy E_K given in (T1.58) as

$$E_K = (\gamma - 1)E_0 = \left(\frac{1}{\sqrt{1 - \frac{v^2}{c^2}}} - 1 \right) E_0. \quad (1.119)$$

Solving (1.119) for v/c we get the following result of the normalized electron velocity

$$\frac{v}{c} = \sqrt{1 - \frac{1}{\left(1 + \frac{E_K}{E_0}\right)^2}} = \sqrt{1 - \frac{1}{\left(1 + \frac{10 \text{ MeV}}{0.511 \text{ MeV}}\right)^2}} = 0.999. \quad (1.120)$$

(e) Mass m of the electron is calculated from the basic Einstein relationship as follows

$$m = \gamma m_0 = 20.57 \times 0.511 \text{ MeV}/c^2 = 10.511 \text{ MeV}/c^2. \quad (1.121)$$

1.21.Q4

(34)

- (a) Present at least three methods for calculation of momentum p of a relativistic particle.
- (b) Show that for particle velocity v much less than speed of light c all expressions presented in (a) transform into classical relationship for momentum given as $p = m_0v$.
- (c) Use methods presented in (a) to determine momentum p of a 10 MeV electron. Express momentum in units of MeV/c^2 .
- (d) Use methods presented in (a) to determine momentum p of a 10 MeV proton. Express momentum in units of MeV/c^2 .
- (e) Express the common unit of momentum MeV/c^2 in SI units.

SOLUTION:

(a) Several expressions are available for calculation of momentum p in relativistic physics. The methods are, of course, all related and the choice of which one to use at a given time depends on the available input data. Four related methods are presented below:

- (1) The most general relationship for momentum p is the product of relativistic mass m and particle velocity v

$$p = mv = mc \frac{v}{c} = \frac{mc^2}{c} \beta = \frac{E\beta}{c} = mc\beta = \gamma m_0 v = \frac{m_0 v}{\sqrt{1 - \beta^2}} = \frac{E_0 \beta}{c \sqrt{1 - \beta^2}} \quad (1.122)$$

where m is the particle's relativistic mass, E is its total energy, m_0 is its rest mass, E_0 is its rest energy, v is its velocity, and γ is the Lorentz factor given as $\sqrt{1 - \beta^2}$ with $\beta = v/c$.

- (2) Momentum can also be determined from the basic expression for relativistic total energy E of a particle

$$E^2 = p^2 c^2 + E_0^2. \quad (1.123)$$

Solving (1.123) for p we get the general expression for relativistic momentum p

$$\begin{aligned} p &= \frac{1}{c} \sqrt{E^2 - E_0^2} = \frac{1}{c} \sqrt{(E_K + E_0)^2 - E_0^2} = \frac{1}{c} \sqrt{E_K^2 + 2E_K E_0} \\ &= \frac{E_K}{c} \sqrt{1 + \frac{2E_0}{E_K}}, \end{aligned} \quad (1.124)$$

where E_K is its kinetic energy of the particle.

- (3) From the basic expression (1.122) for momentum p we get the following expression

$$p = m\mathbf{v} = \gamma m_0 \mathbf{v} = \gamma m_0 c^2 \frac{\mathbf{v}}{c^2} = \frac{E\boldsymbol{\beta}}{c}. \quad (1.125)$$

- (4) Momentum p can also be calculated expanding (1.125) to read

$$p = m\mathbf{v} = \gamma m_0 \mathbf{v} = \gamma m_0 c^2 \frac{\boldsymbol{\beta}}{c} = \frac{E_0 \gamma \boldsymbol{\beta}}{c} = \frac{E_0}{c} \sqrt{\gamma^2 - 1}, \quad (1.126)$$

since, as can easily be shown, the product $\gamma\boldsymbol{\beta}$ is given as $\gamma\boldsymbol{\beta} = \boldsymbol{\beta}/\sqrt{1 - \beta^2} = \sqrt{\gamma^2 - 1}$.

(b) All four relativistic expressions for momentum p introduced in **(a)** transform into classical expression for momentum that reads $p = m_0 \mathbf{v}$ for $v/c = \beta \rightarrow 0$ as follows:

- (1) From (1.122) given as $p = m_0 \mathbf{v}/\sqrt{1 - \beta^2}$ we get the following classical limit

$$\begin{aligned} \lim_{\beta \rightarrow 0} p &= \lim_{\beta \rightarrow 0} \frac{m_0 \mathbf{v}}{\sqrt{1 - \beta^2}} = \lim_{\beta \rightarrow 0} m_0 c \boldsymbol{\beta} (1 - \beta^2)^{-1/2} \approx \lim_{\beta \rightarrow 0} m_0 c \boldsymbol{\beta} \left(1 + \frac{1}{2} \beta^2\right) \\ &\approx m_0 c \boldsymbol{\beta} = m_0 \mathbf{v}. \end{aligned} \quad (1.127)$$

- (2) From (1.124) given as $p = (E_K^2/c)\sqrt{1 + 2E_0/E_K}$ we get the following classical limit for $E_K \ll E_0$

$$\begin{aligned} \lim_{\beta \rightarrow 0} p &= \lim_{\beta \rightarrow 0} \frac{E_K^2}{c} \sqrt{1 + \frac{2E_0}{E_K}} \approx \lim_{E_K \ll E_0} \frac{E_K^2}{c} \sqrt{\frac{2E_0}{E_K}} = \frac{1}{c} \sqrt{2E_K m_0 c^2} \\ &= \sqrt{2 \frac{m_0 v^2}{2} m_0} = m_0 \mathbf{v}. \end{aligned} \quad (1.128)$$

- (3) From (1.125) given as $p = E\boldsymbol{\beta}/c$ we get the following classical limit for $E_K \ll E_0$

$$\lim_{\beta \rightarrow 0} p = \lim_{\beta \rightarrow 0} \frac{E\boldsymbol{\beta}}{c} = \lim_{E_K \ll E_0} \frac{(E_K + E_0)\boldsymbol{\beta}}{c} \approx \frac{E_0 \boldsymbol{\beta}}{c} = \frac{m_0 c^2 \mathbf{v}}{c^2} = m_0 \mathbf{v}. \quad (1.129)$$

- (4) From (1.126) given as $p = (E_0/c)\sqrt{\gamma^2 - 1}$ we get the following classical limit as $E_K \ll E_0$

$$\begin{aligned} \lim_{\beta \rightarrow 0} p &= \lim_{\beta \rightarrow 0} \frac{E_0}{c} \sqrt{\gamma^2 - 1} = \lim_{\beta \rightarrow 0} \frac{E_0}{c} \boldsymbol{\beta} (1 - \beta^2)^{-1/2} \approx \lim_{\beta \rightarrow 0} m_0 c \boldsymbol{\beta} \left(1 + \frac{1}{2} \beta^2\right) \\ &\approx m_0 c \boldsymbol{\beta} = m_0 \mathbf{v}. \end{aligned} \quad (1.130)$$

(c) By way of example, the expressions for relativistic momentum p that were presented in (a) will be used to calculate momentum p of a 10 MeV electron. By definition a label “10 MeV electron” designates an electron with kinetic energy of 10 MeV. Characteristics of a 10 MeV electron are: $E_K = 10$ MeV; $E_0 = 0.511$ MeV; and $E = E_K + E_0 = 10$ MeV + 0.511 MeV = 10.511 MeV.

Lorentz factor γ of a 10 MeV electron is determined as

$$\gamma = \frac{E}{E_0} = \frac{E_0 + E_K}{E_0} = 1 + \frac{E_K}{E_0} = 1 + \frac{10}{0.511} = 20.569. \quad (1.131)$$

Normalized velocity $\beta = v/c$ of a 10 MeV electron is calculated either from kinetic energy E_K as

$$E_K = E - E_0 = (\gamma - 1)E_0 = \left(\frac{1}{\sqrt{1 - \beta^2}} - 1 \right) E_0 \quad (1.132)$$

leading to

$$\beta = \sqrt{1 - \frac{1}{\left(1 + \frac{E_K}{E_0}\right)^2}} = \sqrt{1 - \frac{1}{\left(1 + \frac{10}{0.511}\right)^2}} = \sqrt{1 - \frac{1}{20.569^2}} = 0.9988 \quad (1.133)$$

or from the Lorentz factor γ of 20.569 given in (1.131)

$$\gamma = \frac{1}{\sqrt{1 - \beta^2}} \quad \rightarrow \quad \beta = \frac{\sqrt{\gamma^2 - 1}}{\gamma} = \frac{\sqrt{20.569^2 - 1}}{20.569} = 0.9988. \quad (1.134)$$

Based on the information above we now determine the momentum of a 10 MeV electron:

(1)

$$p = \frac{E_0 \beta}{c \sqrt{1 - \beta^2}} = \frac{(0.511 \text{ MeV}) \times 0.9988}{c \sqrt{1 - 0.9988^2}} = 10.42 \text{ MeV}/c^2. \quad (1.135)$$

(2)

$$p = \frac{E_K}{c} \sqrt{1 + \frac{2E_0}{E_K}} = \frac{(10 \text{ MeV})}{c} \sqrt{1 + \frac{2 \times 0.511}{10}} = 10.5 \text{ MeV}/c. \quad (1.136)$$

(3)

$$p = \frac{E\beta}{c} = \frac{E_K + E_0}{c} \beta = \frac{10 \text{ MeV} + 0.511 \text{ MeV}}{c} \times 0.999 = 10.50 \text{ MeV}/c. \quad (1.137)$$

(4)

$$p = \frac{E_0}{c} \sqrt{\gamma^2 - 1} = \frac{0.511 \text{ MeV}}{c} \sqrt{20.569^2 - 1} = 10.5 \text{ MeV}/c. \quad (1.138)$$

As shown by (1.135) through (1.138), all methods of momentum calculation for a 10 MeV electron give essentially identical results with some minor discrepancies arising from rounding errors.

(d) Momentum of a 10 MeV proton. By definition a label “10 MeV proton” designates a proton with kinetic energy of 10 MeV. Characteristics of a 10 MeV proton are as follows: $E_K = 10$ MeV; $E_0 = 938.3$ MeV; and $E = E_K + E_0 = 10$ MeV + 938.3 MeV = 948.3 MeV.

Lorentz factor γ of a 10 MeV proton is determined as follows

$$\gamma = \frac{E}{E_0} = \frac{E_0 + E_K}{E_0} = 1 + \frac{E_K}{E_0} = 1 + \frac{10}{938.3} = 1.0107, \quad (1.139)$$

making the proton almost classical but not quite.

Normalized velocity $\beta = v/c$ of a 10 MeV proton is calculated (i) either from kinetic energy E_K as

$$E_K = E - E_0 = (\gamma - 1)E_0 = \left(\frac{1}{\sqrt{1 - \beta^2}} - 1 \right) E_0 \quad (1.140)$$

leading to

$$\beta = \sqrt{1 - \frac{1}{\left(1 + \frac{E_K}{E_0}\right)^2}} = \sqrt{1 - \frac{1}{\left(1 + \frac{10}{938.3}\right)^2}} = \sqrt{1 - \frac{1}{1.0107^2}} = 0.145 \quad (1.141)$$

or (ii) from the Lorentz factor γ of 1.10107 given in (1.139)

$$\gamma = \frac{1}{\sqrt{1 - \beta^2}} \rightarrow \beta = \frac{\sqrt{\gamma^2 - 1}}{\gamma} = \frac{\sqrt{1.0107^2 - 1}}{1.0107} = 0.145. \quad (1.142)$$

Based on the information above we now determine the momentum of a 10 MeV proton:

(1)

$$p = \frac{E_0 \beta}{c \sqrt{1 - \beta^2}} = \frac{(938.3 \text{ MeV}) \times 0.145}{c \sqrt{1 - 0.145^2}} = 137.5 \text{ MeV}/c^2. \quad (1.143)$$

(2)

$$p = \frac{E_K}{c} \sqrt{1 + \frac{2E_0}{E_K}} = \frac{(10 \text{ MeV})}{c} \sqrt{1 + \frac{2 \times 938.3}{10}} = 137.4 \text{ MeV}/c. \quad (1.144)$$

(3)

$$p = \frac{E\beta}{c} = \frac{E_K + E_0}{c} \beta = \frac{10 \text{ MeV} + 938.3 \text{ MeV}}{c} \times 0.145 = 137.5 \text{ MeV}/c. \quad (1.145)$$

(4)

$$p = \frac{E_0}{c} \sqrt{\gamma^2 - 1} = \frac{938.3 \text{ MeV}}{c} \sqrt{1.0107^2 - 1} = 137.6 \text{ MeV}/c. \quad (1.146)$$

As shown by (1.142) through (1.146), all methods of momentum calculation for a 10 MeV proton give essentially identical results with some minor discrepancies arising from rounding errors.

(e) The units of momentum in (1.135) through (1.138) for 10 MeV electron and from (1.143) through (1.146) for 10 MeV proton are given in MeV/c. This is a common and convenient unit of momentum used in nuclear, medical, and relativistic physics, especially since momentum, despite being a very important physical quantity, does not have an assigned special unit in contrast to other physical quantities, such as force with newton N, energy with joule J, and power with watt W, etc., that do.

The SI derived unit of momentum is $\text{kg} \cdot \text{m} \cdot \text{s}^{-1}$ or $\text{N} \cdot \text{s}$ and the relationship between $1 \text{ MeV}/c$ and $\text{kg} \cdot \text{m} \cdot \text{s}^{-1}$ is given as follows

$$\begin{aligned} \frac{1 \text{ MeV}}{c} &= \frac{(10^6 \text{ eV}) \times (1.602 \times 10^{-19} \text{ J/eV})}{3 \times 10^8 \text{ m} \cdot \text{s}^{-1}} = 5.34 \times 10^{-22} \text{ N} \cdot \text{s} \\ &= 5.34 \times 10^{-22} \text{ kg} \cdot \text{m} \cdot \text{s}^{-1} \end{aligned} \quad (1.147)$$

or for $1 \text{ eV}/c$

$$\begin{aligned} \frac{1 \text{ eV}}{c} &= \frac{(1 \text{ eV}) \times (1.602 \times 10^{-19} \text{ J/eV})}{3 \times 10^8 \text{ m} \cdot \text{s}^{-1}} = 5.34 \times 10^{-16} \text{ N} \cdot \text{s} \\ &= 5.34 \times 10^{-16} \text{ kg} \cdot \text{m} \cdot \text{s}^{-1}. \end{aligned} \quad (1.148)$$

Momentum of a 10 MeV electron, expressed as $10.5 \text{ MeV}/c$ in (c), is in the SI system of units given as

$$p = 10.5 \text{ MeV}/c = 10.5 \times (5.34 \times 10^{-22} \text{ kg} \cdot \text{m} \cdot \text{s}^{-1}) = 5.61 \times 10^{-21} \text{ kg} \cdot \text{m} \cdot \text{s}^{-1}. \quad (1.149)$$

Momentum of a 10 MeV proton, expressed as $137.5 \text{ MeV}/c$ in (c), is in the SI system of units given as

$$p = 137.5 \text{ MeV}/c = 137.5 \times (5.34 \times 10^{-22} \text{ kg} \cdot \text{m} \cdot \text{s}^{-1}) = 7.343 \times 10^{-20} \text{ kg} \cdot \text{m} \cdot \text{s}^{-1}. \quad (1.150)$$

1.21.Q5

(35)

The standard Newton second law $\mathbf{F} = m\mathbf{a}$ stating that force \mathbf{F} is proportional to acceleration \mathbf{a} with mass m the proportionality constant does not hold in relativistic mechanics where mass m of an object moving with velocity \mathbf{v} is not constant and depends on velocity \mathbf{v} .

- (a) Express the Newton second law in relativistic form accounting for the variation in mass m with velocity \mathbf{v} .
- (b) Show that for $\mathbf{v} \rightarrow 0$ the relativistic form of Newton second law derived in (a) transforms into the standard classical Newton second law.
- (c) A particle with charge q moves along a straight path in a uniform electric field \mathcal{E} with velocity \mathbf{v} . The two vectors \mathcal{E} and \mathbf{v} are parallel. Calculate the relativistic acceleration \mathbf{a} of the charged particle and show that for relativistic particles the acceleration depends on velocity \mathbf{v} .
- (d) If particle in (c) starts its motion at rest at position $x = 0$ and time $t = 0$, calculate its speed $v(t)$ and its position $x(t)$ at time t . Also, calculate the classical limits of $v(t)$ and $x(t)$.
- (e) Lorentz force \mathbf{F}_L on a charged particle q of rest mass m_0 moving with velocity \mathbf{v} in magnetic field \mathcal{B} is given as $\mathbf{F}_L = q\mathbf{v} \times \mathcal{B}$. Use Newton second law in relativistic form derived in (a) to show that the angular “cyclotron frequency” ω_{cyc} of the relativistic particle is given as $\omega_{\text{cyc}} = q\mathcal{B}/(\gamma m_0)$.

SOLUTION:

(a) Relativistic force \mathbf{F} with mass m a function of particle velocity $|\mathbf{v}| = v$ is in general given as follows

$$\mathbf{F} = \frac{d\mathbf{p}}{dt} = \frac{dm\mathbf{v}}{dt} = m \frac{d\mathbf{v}}{dt} + \mathbf{v} \frac{dm}{dt} = \gamma m_0 \frac{d\mathbf{v}}{dt} + m_0 \mathbf{v} \frac{d\gamma}{dt} \quad (1.151)$$

with \mathbf{p} the particle momentum, m_0 the particle rest mass, and γ the Lorentz factor of the particle: $\gamma = (1 - v^2/c^2)^{-1/2}$. Force \mathbf{F} as expressed in (1.151) depends on $d\gamma/dt$ that can be expanded to read as follows

$$\frac{d\gamma}{dt} = \frac{d\gamma}{d\mathbf{v}} \frac{d\mathbf{v}}{dt} = \frac{d}{d\mathbf{v}} \frac{1}{\sqrt{1 - \frac{v^2}{c^2}}} \cdot \frac{d\mathbf{v}}{dt} = \left[1 - \frac{v^2}{c^2}\right]^{-\frac{3}{2}} \frac{\mathbf{v}}{c^2} \cdot \frac{d\mathbf{v}}{dt} = \gamma^3 \frac{\mathbf{v}}{c^2} \cdot \frac{d\mathbf{v}}{dt}. \quad (1.152)$$

After inserting (1.152) into (1.151) we get the following expression for \mathbf{F}

$$\mathbf{F} = \gamma m_0 \frac{d\mathbf{v}}{dt} + m_0 \mathbf{v} \frac{d\gamma}{dt} = \gamma m_0 \frac{d\mathbf{v}}{dt} + \gamma^3 m_0 \left[\frac{\mathbf{v}}{c} \left(\frac{\mathbf{v}}{c} \cdot \frac{d\mathbf{v}}{dt} \right) \right]. \quad (1.153)$$

A scalar product of \mathbf{F} and \mathbf{v} will be of help in expanding (1.153) further

$$\mathbf{F} \cdot \mathbf{v} = \gamma m_0 \mathbf{v} \cdot \frac{d\mathbf{v}}{dt} + \gamma^3 \beta^2 m_0 \mathbf{v} \cdot \frac{d\mathbf{v}}{dt} = \gamma^3 m_0 \mathbf{v} \cdot \frac{d\mathbf{v}}{dt}, \quad (1.154)$$

recalling that $\frac{v}{c} \cdot \frac{v}{c} = \beta^2$ and $\beta^2 \gamma^2 = \gamma^2 - 1$.

Force (1.153) incorporating (1.154) is now expressed as follows

$$\mathbf{F} = \gamma m_0 \frac{d\mathbf{v}}{dt} + (\mathbf{F} \cdot \boldsymbol{\beta}) \boldsymbol{\beta}, \quad (1.155)$$

and leads directly to a relativistic expression relating force \mathbf{F} and acceleration $\mathbf{a} = d\mathbf{v}/dt$, allowing us to express acceleration \mathbf{a} as

$$\mathbf{a} = \frac{d\mathbf{v}}{dt} = \frac{1}{\gamma m_0} [\mathbf{F} - (\mathbf{F} \cdot \boldsymbol{\beta}) \boldsymbol{\beta}]. \quad (1.156)$$

(b) As shown in (1.156), acceleration \mathbf{a} is not parallel to force \mathbf{F} at large velocities because a particle velocity cannot exceed the speed of light c in vacuum. However, for velocities $v \ll c$, where $\beta \rightarrow 0$ and $\gamma \rightarrow 1$, the relativistic expression for acceleration \mathbf{a} given in (1.156) transforms into Newton's classical result $\mathbf{a} = d\mathbf{v}/dt = \mathbf{F}/m_0$, with \mathbf{a} parallel to \mathbf{F} .

(c) Since force \mathbf{F} is given as $\mathbf{F} = q\boldsymbol{\mathcal{E}}$ and $\boldsymbol{\mathcal{E}}$ is parallel to \mathbf{v} , we can express (1.156) in scalar form to get

$$a = \frac{dv}{dt} = \frac{F - F\beta^2}{\gamma m_0} = \frac{F}{\gamma m_0} (1 - \beta^2) = \frac{q\mathcal{E}}{m_0} (1 - \beta^2)^{\frac{3}{2}} = \frac{q\mathcal{E}}{m_0} \frac{1}{\gamma^3}. \quad (1.157)$$

The relativistic expression for acceleration a shows that a depends on velocity v through the Lorentz factor γ . The following conditions apply in the limits: (1) as $v \rightarrow c$ and (2) as $v \rightarrow 0$.

- (1) As v increases into the highly relativistic region ($v \approx c$), acceleration a decreases reaching 0 as the velocity approaches c , irrespective of the magnitude of force F .
- (2) For $v \ll c$ that results in $\beta \rightarrow 0$ and $\gamma \rightarrow 1$ the relativistic expression (1.157) transforms into the classical relationship $a = q\mathcal{E}/m_0$ that is independent of velocity of the particle v .

(d) The speed $v(t)$ of a particle with charge q and rest mass m_0 moving in a uniform electric field parallel to the particle's velocity can be obtained using (1.157). We rearrange (1.157) to read

$$\gamma^3 dv = \frac{dv}{\left(1 - \frac{v^2}{c^2}\right)^{\frac{3}{2}}} = \frac{q\mathcal{E}}{m_0} dt. \quad (1.158)$$

For a particle at rest at time $t = 0$, the speed of the particle v at time t is obtained by integration of (1.158) in velocity v from 0 to $v(t)$ and in time t from 0 to t

$$\int_0^{v(t)} \frac{dv}{\left(1 - \frac{v^2}{c^2}\right)^{3/2}} = \frac{q\mathcal{E}}{m_0} \int_0^t dt = \frac{q\mathcal{E}}{m_0} t = a_E t, \quad (1.159)$$

where $a_E = q\mathcal{E}/m_0$ is the classical acceleration limit under the influence of electric field.

We solve the first integral of (1.159) with the help of the substitution $v = c \sin u$ and $dv = c \cos u du$ to get

$$\begin{aligned} \int_0^{v(t)} \frac{dv}{\left(1 - \frac{v^2}{c^2}\right)^{3/2}} &= c \int \frac{\cos u du}{\left(1 - \sin^2 u\right)^{3/2}} = c \int \frac{du}{\cos^2 u} = c \tan u \\ &= c \frac{\sin u}{\sqrt{1 - \sin^2 u}} = \left[\frac{v}{\sqrt{1 - \frac{v^2}{c^2}}} \right]_0^{v(t)}. \end{aligned} \quad (1.160)$$

Merging (1.159) and (1.160) we get a simple expression relating velocity v and acceleration a_E as follows

$$\frac{v}{\sqrt{1 - \frac{v^2}{c^2}}} = \gamma v = a_E t. \quad (1.161)$$

Finally, solving (1.161) for $v(t)$ yields the relativistic relationship between velocity $v(t)$ and acceleration a_E

$$v(t) = \frac{a_E t}{\sqrt{1 + (c^{-1} a_E t)^2}}. \quad (1.162)$$

The classical limit of velocity $v(t)$ from the general expression given in (1.162) is obtained for small time t such that $a_E t \ll c$ or $a_E t \ll 1$. For such conditions, velocity v is expressed as

$$v(t) \approx a_E t, \quad (1.163)$$

the well-known non-relativistic (classical) velocity of a particle undergoing constant acceleration.

If the initial position of the particle is $x(t = 0) = 0$, the position $x(t)$ of the particle at time t is

$$\begin{aligned} x(t) &= \int_0^t v(t) dt = \int_0^t \frac{a_E t}{\sqrt{1 + (a_E t/c)^2}} dt \\ &= \frac{c^2}{2a_E} \int_0^t \left[1 + (a_E t/c)^2\right]^{-1/2} d\left[1 + (a_E t/c)^2\right] \\ &= \frac{c^2}{a_E} \left[\sqrt{1 + (a_E t/c)^2} \right]_0^t = \frac{[\sqrt{1 + (a_E t/c)^2} - 1]c^2}{a_E}. \end{aligned} \quad (1.164)$$

To calculate the classical limit of (1.164), we express (1.164) using Taylor's expansion to get

$$x(t) = \frac{c^2}{a_E} \left[\sqrt{1 + \frac{a_E^2 t^2}{c^2}} - 1 \right] \approx \frac{c^2}{a_E} \left[1 + \frac{1}{2} \frac{a_E^2 t^2}{c^2} + \dots - 1 \right]. \quad (1.165)$$

For $a_E t \ll c$ or $a_E t/c \ll 1$, (1.165) becomes

$$x(t) \approx \frac{1}{2} a_E t^2 \quad (1.166)$$

that is the non-relativistic position of a particle undergoing a constant acceleration.

(e) Equation (1.156) gives the general expression for relativistic acceleration \mathbf{a} . In our case of charged particle q motion in magnetic field \mathcal{B} under the influence of the Lorentz force \mathbf{F}_L , the particle velocity \mathbf{v} is perpendicular to magnetic field \mathcal{B} as well as to Lorentz force \mathbf{F}_L , so we write the Lorentz force $F_L = qv\mathcal{B}$ and acceleration from (1.156) as $a = F/(\gamma m_0)$ using $|\mathbf{v} \times \mathcal{B}| = v\mathcal{B}$ and $\mathbf{F} \cdot \boldsymbol{\beta} = 0$. Since $a = v^2/r = \omega_{\text{cyc}}^2 r$ we get the following expression for the two forces that are in equilibrium

$$F = \gamma m_0 a = \gamma m_0 \omega_{\text{cyc}}^2 r = qv\mathcal{B} = q\omega_{\text{cyc}} r \mathcal{B}. \quad (1.167)$$

From (1.167) the cyclotron angular frequency is expressed as follows

$$\omega_{\text{cyc}} = \frac{q\mathcal{B}}{\gamma m_0} = \frac{q\mathcal{B}}{m_0} \sqrt{1 - \beta^2} = \frac{q\mathcal{B}}{m_0} \sqrt{1 - \frac{v^2}{c^2}}. \quad (1.168)$$

For $v \ll c$ that results in $\beta \rightarrow 0$ and $\gamma \rightarrow 1$ the relativistic expression (1.168) for the angular cyclotron frequency transforms into the classical cyclotron angular frequency given as

$$\omega_{\text{cyc}} = \frac{q\mathcal{B}}{m_0}. \quad (1.169)$$

1.21.Q6

(36)

An electron has velocity v_e of $0.95c$. Calculate velocity of a proton that has:

- (a) Same kinetic energy $(E_K)_p$ as the electron; i.e., $(E_K)_p = (E_K)_e$.
- (b) Same momentum p_p as the electron; i.e., $p_p = p_e$.

SOLUTION:

We first calculate the kinetic energy $(E_K)_e$ and momentum p_e of an electron with velocity $v_e = 0.95c$ corresponding to $\beta_e = 0.95$ and $\gamma_e = [1 - \beta_e^2]^{-1/2} = 3.2$. Electron kinetic energy $(E_K)_e$ is calculated using (1.115) as follows

$$\begin{aligned}
 (E_K)_e &= (\gamma_e - 1)(E_0)_e = \left[\frac{1}{\sqrt{1 - \beta_e^2}} - 1 \right] (E_0)_e \\
 &= (3.2 - 1) \times 0.511 \text{ MeV} = 1.124 \text{ MeV}. \quad (1.170)
 \end{aligned}$$

Electron momentum p_e is calculated using (T1.67) as follows

$$p_e = \frac{(E_0)_e}{c} \sqrt{\gamma_e^2 - 1} = 0.511 \text{ (MeV}/c) \times \sqrt{3.2^2 - 1} = 1.55 \text{ MeV}/c. \quad (1.171)$$

Now we can address the two questions dealing with protons, first question **(a)** with protons of kinetic energy $(E_K)_p = 1.124 \text{ MeV}$ and then question **(b)** with protons of momentum $p_p = 1.55 \text{ MeV}/c$.

(a) Kinetic energy of the proton $(E_K)_p$ equals kinetic energy of the electron $(E_K)_e$; i.e., $(E_K)_p = (E_K)_e = 1.124 \text{ MeV}$.

We again use (1.115) and express $(E_K)_p$ as follows

$$(E_K)_p = (\gamma_p - 1)(E_0)_p = 1.124 \text{ MeV}, \quad (1.172)$$

then solve this relationship for γ_p to get

$$\gamma_p = 1 + \frac{(E_K)_p}{(E_0)_p} = 1 + \frac{1.124 \text{ MeV}}{938.3 \text{ MeV}} = 1.0012. \quad (1.173)$$

Next we calculate β_p using the standard definition of Lorentz factor $\gamma_p = [1 - \beta_p^2]^{-1/2}$ to get

$$\beta_p = \sqrt{1 - \frac{1}{\gamma_p^2}} = \sqrt{1 - \frac{1}{1.0012^2}} = 0.049 \quad (1.174)$$

or

$$v_p = \beta_p c = 0.049 \times (3 \times 10^8 \text{ m/s}) = 1.47 \times 10^7 \text{ m/s}. \quad (1.175)$$

Thus, a proton with kinetic energy $(E_K)_p$ of 1.124 MeV has a velocity v_p equal to about 5 % of the speed of light in vacuum c , while an electron with same kinetic energy $(E_K)_e = 1.124 \text{ MeV}$ travels at 95 % of c . A proton with kinetic energy of the order of 1 MeV can be treated as a classical particle, an electron of same kinetic energy is highly relativistic as result of the significant difference in the rest masses of the two particles with $m_p/m_e = 1836$.

(b) Proton momentum p_p equals electron momentum p_e , i.e., $p_p = p_e = 1.55 \text{ MeV}/c$. We now again use (1.171), write the proton momentum p_p as follows

$$p_p = \frac{(E_0)_p}{c} \sqrt{\gamma_p^2 - 1} = 1.55 \text{ MeV}/c, \quad (1.176)$$

and then solve this expression for γ_p^2 to get

$$\gamma_p^2 = 1 + \frac{p_p^2}{(E_0)_p^2/c^2} = \frac{1}{1 - \beta_p^2} = 1.00000273. \quad (1.177)$$

Next, we solve (1.177) for β_p and get

$$\beta_p = \sqrt{1 - \frac{1}{\gamma_p^2}} = \sqrt{1 - \frac{1}{1.00000273^2}} = 2.34 \times 10^{-3} \quad (1.178)$$

or

$$v_p = \beta_p c = 7.02 \times 10^5 \text{ m/s}. \quad (1.179)$$

Thus, a proton with momentum p_p of 1.55 MeV/c has a velocity of about 0.23 % of the speed of light in vacuum c , while an electron of this momentum has a velocity of 95 % of c . Proton of momentum $p_p = 1.55 \text{ MeV}/c$ is a classical particle, while an electron of same momentum is clearly a relativistic particle.

1.21.Q7

(37)

Determine the energy required to accelerate an electron:

- (a) From a velocity of $0.25c$ to velocity of $0.75c$.
- (b) From a velocity of $0.95c$ to velocity of $0.99c$.

SOLUTION:

We determine the rise in kinetic energy E_K of the electron using the following standard relationship for kinetic energy

$$\begin{aligned} \Delta E_K &= c^2 \int_{m(v_1)}^{m(v_2)} dm = m(v_2) - m(v_1) \\ &= m_e c^2 \left[\frac{1}{\sqrt{1 - \frac{v_2^2}{c^2}}} - \frac{1}{\sqrt{1 - \frac{v_1^2}{c^2}}} \right] = E_0 \left[\frac{1}{\sqrt{1 - \beta_2^2}} - \frac{1}{\sqrt{1 - \beta_1^2}} \right] \\ &= E_0(\gamma_2 - \gamma_1), \end{aligned} \quad (1.180)$$

where γ is the Lorentz factor of an electron with velocity v : $\gamma = (1 - \beta^2)^{-\frac{1}{2}} = (1 - v^2/c^2)^{-\frac{1}{2}}$.

(a) We now calculate ΔE_K for a velocity increase from $v_1 = 0.25c$ to $v_2 = 0.75c$ corresponding to an increase in γ from $\gamma_1 = 1.033$ to $\gamma_2 = 1.512$ as follows

$$\Delta E_K = (\gamma_2 - \gamma_1) E_0 = (1.512 - 1.033) \times 0.511 \text{ MeV} = 0.245 \text{ MeV}. \quad (1.181)$$

It takes energy of 0.245 MeV to accelerate an electron from velocity of $0.25c$ to velocity of $0.75c$.

(b) Energy ΔE_K for velocity increase from $v_1 = 0.95c$ to $v_2 = 0.99c$ corresponding to an increase in γ from $\gamma_1 = 3.203$ to $\gamma_2 = 31.623$ is calculated as follows

$$\Delta E_K = (\gamma_2 - \gamma_1)E_0 = (31.623 - 3.203) \times 0.511 \text{ MeV} = 14.52 \text{ MeV}. \quad (1.182)$$

It takes energy of 14.52 MeV to accelerate an electron from velocity of $0.95c$ to velocity of $0.99c$.

A conclusion can be made from **(a)** and **(b)** that in the vicinity of the speed of light c much more energy is required to increase the velocity of a particle than at relatively low particle velocities.

1.21.Q8

(38)

The relativistic red and blue Doppler shifts play an important role in astrophysics, as they allow the determination of the motion of distant galaxies relative to Earth. A blue shift suggests that the source is moving toward the observer, a red shift that the source is moving away from the observer.

- (a)** Derive the basic expression for the relativistic Doppler shift using Lorentz transformations on energy and momentum.
- (b)** Plot the ratio $\lambda_{\text{observed}}/\lambda_{\text{source}}$ for the red and blue shift against β , the normalized velocity v of the photon source.

SOLUTION:

The simplest and fastest method for deriving the relativistic Doppler equation is through the use of Lorentz transformations relating total energy E and momentum p of a particle in two inertial reference frames F and F' . Assume that frame F' moves with uniform velocity v along the abscissa (x) axis of frame F and that a particle of interest moves in frame F' also along the abscissa axis.

The general Lorentz transformations for E and p of the particle are given as follows

$$E' = \gamma(E - \beta cp) \quad \text{and} \quad p' = \gamma\left(p - \frac{v}{c^2}E\right), \quad (1.183)$$

where γ is the Lorentz factor $\gamma = (1 - \beta^2)^{-1/2}$ and β is the relative velocity v normalized to speed of light c in vacuum. Note that energy E transform takes the form of the x coordinate Lorentz transformation and momentum p transform takes the form of the transformation for time t coordinate, as given in Prob. 26.

For a particle with zero rest mass, such as photon, energy $E = h\nu$ is directly proportional to momentum $p = E/c = h\nu/c = h/\lambda$ and the Lorentz transformation

of (1.183) for a photon source moving away from the observer simplifies to read

$$E' = hv' = \gamma(E - \beta E) = \gamma E(1 - \beta) = \gamma hv(1 - \beta). \quad (1.184)$$

We can obtain the same result using the momentum transformation

$$\frac{hv'}{c} = \gamma \left(\frac{hv}{c} - \frac{v}{c^2} hv \right) = \gamma \frac{hv}{c} (1 - \beta). \quad (1.185)$$

The ratio of photon energies hv'/hv coincides with the ratio of photon frequencies ν'/ν found in the relativistic Doppler shift usually expressed as

$$\frac{\nu'}{\nu} = \frac{\nu_{\text{observed}}}{\nu_{\text{source}}} = \gamma(1 - \beta) = \frac{\sqrt{1 - \beta} \sqrt{1 - \beta}}{\sqrt{1 - \beta^2}} = \sqrt{\frac{1 - \beta}{1 + \beta}}. \quad (1.186)$$

This result for $\nu_{\text{observed}}/\nu_{\text{source}}$ translates into the following expression for the ratio of wavelengths $\lambda_{\text{observed}}/\lambda_{\text{source}}$

$$\frac{\lambda'}{\lambda} = \frac{\lambda_{\text{observed}}}{\lambda_{\text{source}}} = \sqrt{\frac{1 + \beta}{1 - \beta}} > 1. \quad (1.187)$$

For the case of photon source moving away from the observer, $\lambda_{\text{observed}}/\lambda_{\text{source}} > 1$ and the increase in wavelength of the observed photon emission is referred to as the *red shift*.

If the photon wavelength is measured in a frame that moves toward the photon source, the velocity v is negative and the measured energy E' is expressed as

$$E' = hv' = \gamma(E + \beta E) = \gamma E(1 + \beta) = \gamma hv(1 + \beta). \quad (1.188)$$

The ratio of photon energies E'/E corresponds to the ratio of photon frequencies

$$\frac{E'}{E} = \frac{\nu'}{\nu} = \frac{\nu_{\text{observed}}}{\nu_{\text{source}}} = \frac{\sqrt{1 + \beta} \sqrt{1 + \beta}}{\sqrt{1 - \beta^2}} = \sqrt{\frac{1 + \beta}{1 - \beta}} \quad (1.189)$$

and translates into the following wavelength ratio

$$\frac{\lambda'}{\lambda} = \frac{\lambda_{\text{observed}}}{\lambda_{\text{source}}} = \sqrt{\frac{1 - \beta}{1 + \beta}} < 1. \quad (1.190)$$

Since $\lambda_{\text{observed}}/\lambda_{\text{source}} < 1$, the decrease in wavelength λ with the source approaching the observer is referred to as the *blue shift*.

The speed of light c is the same in all reference frames; however, photon energy $h\nu$, frequency ν , and wavelength λ all depend on the relative velocity v between the source and observer. The following conclusions apply:

- (1) With the source moving away from the observer, the frequency ratio and photon energy ratio decrease, the ratio of wavelengths increases, the velocity v in the Lorentz transformation is positive, and the effect is referred to as the red Doppler shift.
- (2) With the source moving toward the observer, the frequency ratio and photon energy ratio increase, the ratio of wavelengths decreases, the velocity v in the Lorentz transformation is negative, and the effect is referred to as the blue Doppler shift.

(b) A plot of $\lambda_{\text{observed}}/\lambda_{\text{source}}$ is shown in Fig. 1.13.

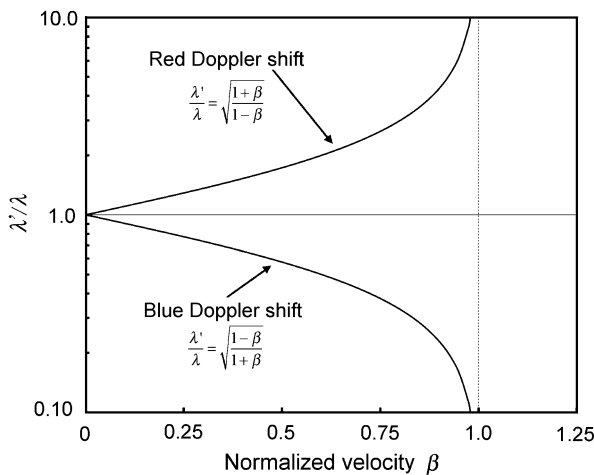


Fig. 1.13 Red and blue Doppler shifts ($\lambda/\lambda' = \lambda_{\text{observed}}/\lambda_{\text{source}}$) against normalized velocity $\beta = v/c$. For the red shift the source is approaching the observer and $\lambda/\lambda' > 1$, while for the blue shift the source is moving away from the observer and $\lambda/\lambda' < 1$

1.22 Particle-Wave Duality

1.22.Q1

(39)

Calculate the de Broglie wavelength λ of the following:

- (a) Electron with velocity of $0.01c$.
- (b) Electron with kinetic energy of 100 eV.
- (c) Electron with kinetic energy of 200 MeV.
- (d) Proton with kinetic energy of 10 MeV.
- (e) Marble of mass 100 g moving with velocity of 50 m/s.

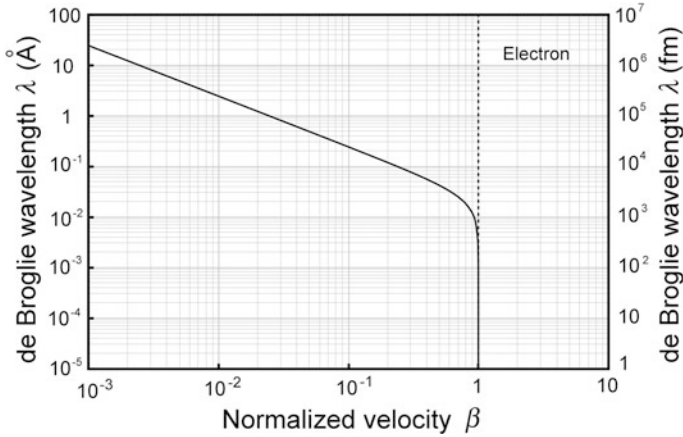


Fig. 1.14 De Broglie wavelength λ against normalized velocity β for electrons in the range of β from 10^{-3} to 1

Figure 1.14 plots the de Broglie wavelength λ against normalized velocity β (T1.79) of electrons in the range $10^{-3} \leq \beta \leq 10$, while Fig. 1.15 plots the de Broglie wavelength λ against kinetic energy E_K for both electrons as well as protons in the kinetic energy range $10^{-5} \text{ MeV} \leq E_K \leq 10^3 \text{ MeV}$.

- (f) Verify your data calculated in (a), (b), and (c) for electrons by superimposing them as data points on Fig. 1.14 and Fig. 1.15.
- (g) Verify the de Broglie wavelength calculated in (d) for protons by superimposing the point on the diagram of Fig. 1.15.
- (h) Energetic electrons and protons can serve as excellent probes in studies of atomic and nuclear structure. Can the particles of (a) through (d) be of any use in atomic and nuclear physics?

SOLUTION:

De Broglie wavelength λ of an object or particle is defined as $\lambda = h/p$, where h is the Planck constant and p is the momentum of the object or particle. As shown in Prob. 34, momentum is in general expressed as

$$p = mv = \gamma m_0 \beta c \equiv \frac{m_0 c^2}{c} \frac{\beta}{\sqrt{1 - \beta^2}} \equiv \frac{E_0}{c} \frac{\beta}{\sqrt{1 - \beta^2}} = \frac{E_K}{c} \sqrt{1 + \frac{2E_0}{E_K}}, \quad (1.191)$$

where γ is the Lorentz factor, m_0 is the rest mass of the object or particle, and E_0 is the rest energy of the object or particle. It is easy to show that for $v \ll c$

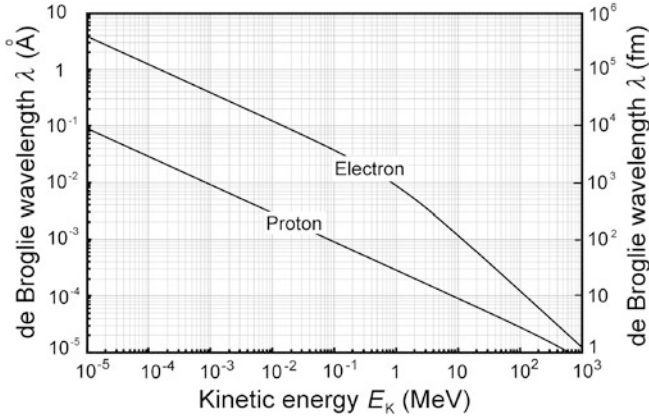


Fig. 1.15 De Broglie wavelength λ against kinetic energy E_K for electrons and protons in kinetic energy range from 10 eV to 1000 MeV

where $E_K \ll E_0$ the general relationship for the momentum reduces to the classical expression $p = m_0 v = \sqrt{2m_0 E_K}$, while in the extreme relativistic region with $v \approx c$ where $E_K \gg E_0$ the general relationship for the momentum p simplifies to read $p \approx E_K/c$.

(a) Electron travelling with velocity $v = 0.01c$ equivalent to $\beta = 0.01$.

According to (1.115) an electron with β of 0.01 possesses kinetic energy E_K of 25.6 eV. Since $\beta \ll 1$, the classical expression $E_K = \frac{1}{2}m_0 v^2 = \frac{1}{2}m_0 c^2 \beta^2$ gives the same result (25.6 eV). The de Broglie wavelength λ is calculated as follows

$$\lambda = \frac{h}{p} = \frac{h}{\gamma m_0 v} = \frac{2\pi \hbar c \sqrt{1 - \beta^2}}{\beta m_0 c^2} = \frac{2\pi (197.3 \text{ MeV} \cdot \text{fm}) \times \sqrt{1 - 0.01^2}}{0.01 \times 0.511 \text{ MeV}} = 2.42 \text{ \AA}. \quad (1.192)$$

(b) Electron with kinetic energy $E_K = 100 \text{ eV}$, i.e., 100 eV electron.

According to classical and relativistic expressions an electron with kinetic energy E_K of 100 eV travels with velocity of $0.02c$. Since $\beta \ll 1$, the classical expression $v = \sqrt{2E_K/m_e}$ gives the same result as the relativistic one. The de Broglie wavelength λ is calculated as follows

$$\begin{aligned} \lambda &= \frac{h}{p} = \frac{2\pi \hbar c}{E_K \sqrt{1 + \frac{2E_0}{E_K}}} \approx \frac{2\pi \hbar c}{\sqrt{2m_e c^2 E_K}} = \frac{2\pi \times (197.3 \times 10^6 \text{ eV} \cdot \text{fm})}{\sqrt{2 \times (0.511 \times 10^6 \text{ eV}) \times (10^2 \text{ eV})}} \\ &= 1.2 \times 10^5 \text{ fm} = 1.2 \text{ \AA}, \end{aligned} \quad (1.193)$$

where we used (1.128) to calculate momentum p of the 100 eV electron in (1.193).

(c) Electron with kinetic energy $E_K = 200 \text{ MeV}$, i.e., 200 MeV electron.

According to (1.115) an electron with kinetic energy E_K of 200 MeV travels with velocity of $0.99999675c$ and is thus highly relativistic. In the case of β for

highly relativistic particles we have no choice but to use the value of β with many significant figures, since we are in a region of extremely rapid change of E_K with β . The de Broglie wavelength λ is calculated with the standard de Broglie expression $\lambda = h/p$ expressing p with (1.124) or (1.126) (both expressions should give the same result)

$$\begin{aligned}\lambda &= \frac{h}{p} = \frac{2\pi\hbar c}{E_K\sqrt{1 + \frac{2E_0}{E_K}}} = \frac{2\pi \times (197.3 \text{ MeV} \cdot \text{fm})}{(200 \text{ MeV}) \times \sqrt{1 + \frac{2 \times 0.511 \text{ MeV}}{200 \text{ MeV}}}} \\ &= 6.17 \text{ fm} = 6.17 \times 10^{-15} \text{ m}\end{aligned}\quad (1.194)$$

or

$$\begin{aligned}\lambda &= \frac{h}{p} = \frac{2\pi\hbar c}{E_0} \frac{\sqrt{1 - \beta^2}}{\beta} = \frac{2\pi \times (197.3 \text{ MeV} \cdot \text{fm})}{0.511 \text{ MeV}} \times \frac{\sqrt{1 - 0.99999675^2}}{0.99999675} \\ &= 6.17 \text{ fm} = 6.17 \times 10^{-15} \text{ m}.\end{aligned}\quad (1.195)$$

(d) Proton with kinetic energy $E_K = 10 \text{ MeV}$, i.e., 10 MeV proton. A proton with kinetic energy E_K of 10 MeV travels with classical velocity of $0.146c$. Since $\beta \ll 1$, the classical expression $v = \sqrt{2E_K/m_P}$ can be used in calculation of v_P . The de Broglie wavelength λ is calculated as follows

$$\begin{aligned}\lambda &= \frac{h}{p} = \frac{2\pi\hbar c}{E_K\sqrt{1 + \frac{2E_0}{E_K}}} = \frac{2\pi \times (197.3 \text{ MeV} \cdot \text{fm})}{(10 \text{ MeV}) \times \sqrt{1 + \frac{2 \times (938.3 \text{ MeV})}{10 \text{ MeV}}}} \\ &= 9.02 \text{ fm} = 9.02 \times 10^{-15} \text{ m}.\end{aligned}\quad (1.196)$$

(e) Marble of mass $m = 100 \text{ g}$ travelling with velocity $v = 50 \text{ m/s}$. The de Broglie wavelength λ is calculated as follows

$$\begin{aligned}\lambda &= \frac{h}{p} = \frac{h}{m_0 v} = \frac{2\pi\hbar c}{m_0 v c} \\ &= \frac{2\pi \times (197.3 \times 10^6 \text{ eV} \cdot \text{fm}) \times (1.6 \times 10^{-19} \text{ J/eV}) \times (10^{-15} \text{ m/fm})}{(10^{-1} \text{ kg}) \times (3 \times 10^8 \text{ m/s}) \times (50 \text{ m/s})} \\ &= 1.32 \times 10^{-34} \text{ m} = 1.32 \times 10^{-19} \text{ fm}.\end{aligned}\quad (1.197)$$

(f) Figure 1.16 plots the de Broglie wavelength λ for electrons against the normalized velocity β . Data points calculated in (a), (b), and (c) for electrons are shown superposed onto the de Broglie wavelength λ curve.

(g) Figure 1.17 plots the de Broglie wavelength λ for electrons and protons against kinetic energy E_K . Data points calculated in (a), (b), and (c) for electrons and in (d) for protons are shown superposed onto appropriate de Broglie wavelength λ curves.

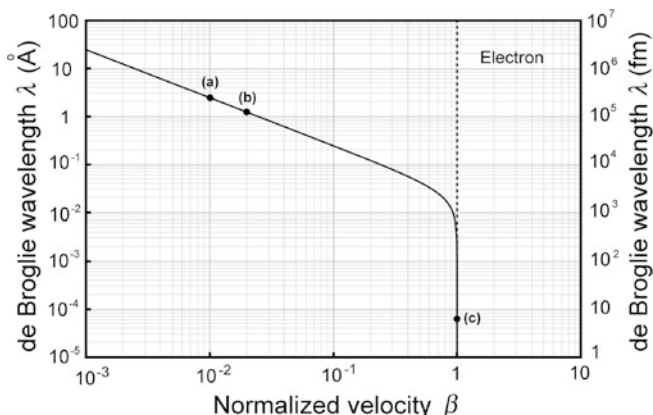


Fig. 1.16 De Broglie wavelength λ against normalized velocity $\beta = v/c$ for electron. The data points (a), (b), and (c) correspond to results calculated in (a), (b), and (c), respectively

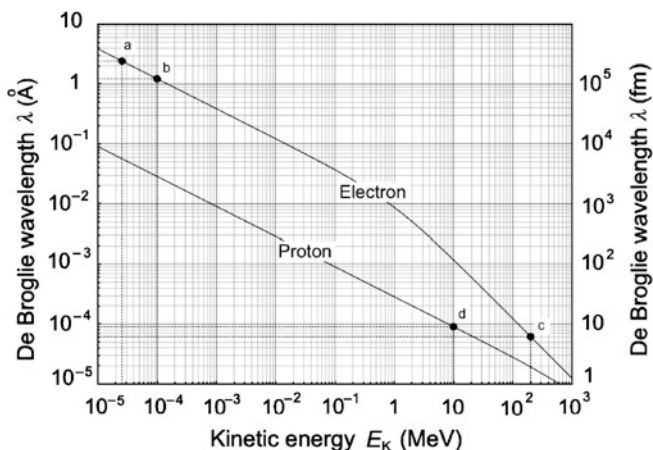


Fig. 1.17 De Broglie wavelength λ against kinetic energy E_K for electron and proton. Data points (a), (b), (c), and (d) correspond to results calculated in (a), (b), (c), and (d), respectively

(h) To be useful as a probe in scattering experiments a particle must have the de Broglie wavelength λ of the order of the dimension of the investigated target: few angstroms for atoms and few fermis (femtometers) for nuclei.

Electrons in (a) and (b) with kinetic energy of 25.6 eV and 100 eV, respectively, and de Broglie wavelengths λ of 2.4 Å and 1.2 Å, respectively, would be suitable for scattering experiments on atoms, while electrons of (c) with kinetic energy of 200 MeV corresponding to λ of 6.2 fm and protons of (d) with kinetic energy of 10 MeV corresponding to a wavelength λ of 9 fm would be suitable as nuclear probes.

1.22.Q2

(40)

In 1927 Clinton J. Davisson and Lester H. Germer confirmed experimentally the wave nature of electrons by bombarding a nickel target with electrons and measuring the intensity of electrons scattered from the target. The target was in the form of a regular crystalline alloy that was formed through a special annealing process. The beam of electrons was produced by thermionic emission from a heated tungsten filament. The electrons were accelerated through a relatively low variable potential difference U that enabled the selection of the electron kinetic energy E_K incident onto the nickel crystal. Electrons scattered from the crystal were collected with a Faraday cup and their intensity was measured with a galvanometer.

In a Davisson-Germer experiment electrons (rest energy $m_e = 0.511$ MeV and charge $e = 1.602 \times 10^{-19}$ C) are accelerated through a potential difference U of the order of 100 V and scattered on nickel crystals with crystalline plane separation of the order of 2 \AA . Show that the non-relativistic de Broglie wavelength λ_{clas} of electrons in Davisson-Germer experiment has the following characteristics:

- (a) Is inversely proportional to \sqrt{U} .
- (b) Can be expressed as $\lambda = (12.26 \text{ \AA} / \sqrt{U})$ when U is given in volts.
- (c) Is equal to 1.73 \AA for $U = 50$ V.
- (d) Requires a correction factor $C = \frac{1}{\sqrt{1+eU/(2m_e c^2)}}$ for relativistic electrons.

SOLUTION:

- (a) Momentum p for non-relativistic electron.

Recalling that kinetic energy E_K of charge q accelerated through potential difference U is given as a product qU , we can use the classical relationship $E_K = \frac{1}{2}p^2/m_0$ to express momentum p as $p = \sqrt{2m_e E_K} = \sqrt{2m_e eU}$ and get the following classical expression for de Broglie wavelength λ .

$$\lambda_{\text{class}} = \frac{h}{p} = \frac{2\pi \hbar c}{\sqrt{2m_e c^2 E_K}} = \frac{2\pi \hbar c}{\sqrt{2m_e c^2 eU}} \propto \frac{1}{\sqrt{U}}. \quad (1.198)$$

- (b) Equation (1.198) shows that the non-relativistic relationship for the de Broglie wavelength λ is inversely proportional to \sqrt{U} and the proportionality constant when U is given in volts is

$$\lambda_{\text{class}} = \frac{h}{p} = \frac{2\pi \hbar c}{\sqrt{2m_e c^2 eU}} = \frac{2\pi \cdot 1973 \text{ eV} \cdot \text{\AA}}{\sqrt{2 \times 0.511 \times 10^6 \text{ e}^2 \text{V}^2 U (\text{in V})}} = \frac{12.26 \text{ \AA}}{\sqrt{U (\text{in V})}}. \quad (1.199)$$

(c) We use (1.199) to determine λ_{clas} for $U = 50$ V and get

$$\lambda_{\text{clas}} = \frac{h}{p} = \frac{12.26 \text{ \AA}}{\sqrt{50}} = 1.73 \text{ \AA}. \quad (1.200)$$

(d) Momentum p for relativistic electron is calculated from the basic expression for the relativistic total energy $E = \sqrt{p^2c^2 + E_0^2}$ where E_0 is the particle rest mass

$$\begin{aligned} p &= \frac{1}{c} \sqrt{E^2 - E_0^2} = \frac{1}{c} \sqrt{E_{\text{K}}^2 - 2E_0E_{\text{K}}} = \frac{1}{c} \sqrt{(eU)^2 + 2m_0c^2eU} \\ &= \sqrt{2m_e eU \left(1 + \frac{eU}{2m_e c^2}\right)}. \end{aligned} \quad (1.201)$$

Equation (1.201) gives the following de Broglie wavelength λ_{rel} for a relativistic electron

$$\lambda_{\text{rel}} = \frac{h}{p} = \frac{2\pi \hbar c}{\sqrt{2m_e c^2 eU} \sqrt{1 + \frac{eU}{2m_e c^2}}} = \frac{\lambda_{\text{clas}}}{\sqrt{1 + \frac{eU}{2m_e c^2}}} = C \lambda_{\text{clas}}, \quad (1.202)$$

where λ_{clas} is the classical de Broglie wavelength of (1.198) and the constant C is given as

$$C = \frac{1}{\sqrt{1 + \frac{eU}{2m_e c^2}}}. \quad (1.203)$$

1.22.Q3

(41)

Neutron diffraction is a powerful tool for studying the structure of crystals, especially organic hydrogen-rich crystals. In a Davisson-Germer type diffraction experiment with monochromatic neutrons on an organic sample with plane separation $d = 1.85 \text{ \AA}$, the resulting diffraction pattern exhibited a maximum at an angle $\varphi = 50^\circ$. Calculate the kinetic energy E_{K} of the monochromatic neutrons that were used in the experiment.

SOLUTION:

The diffraction pattern with its specific intensity maximum results from the wave nature of neutrons. Similarly to the behavior of light and sound, we assume that neutrons also exhibit wavelike behavior that is governed by: (1) the Bragg diffraction law expressed as

$$m\lambda = 2d \sin \varphi, \quad (1.204)$$

with m an integer, φ the Bragg angle measured between the incident beam direction and the crystal surface, and d atomic lattice spacing as well as (2) the de Broglie particle-wave duality hypothesis expressed with the de Broglie wavelength λ as

$$\lambda = \frac{h}{m_n v}, \quad (1.205)$$

where v is the velocity of the neutron and m_n is the neutron rest mass.

We first calculate the neutron de Broglie wavelength λ from Bragg law for $m = 1$ and get

$$\lambda = 2d \sin \varphi = 2 \times (1.85 \text{ \AA}) \times \sin 50^\circ = 2.8 \text{ \AA} \quad (1.206)$$

and next we calculate the kinetic energy E_K of neutrons with de Broglie wavelength λ of 2.8 Å from the following basic de Broglie expression

$$\lambda = \frac{h}{m_n v} = \frac{h}{\sqrt{2m_n E_K}} \quad (1.207)$$

to get

$$E_K = \frac{h^2}{2m_n \lambda^2} = \frac{(2\pi)^2 (\hbar c)^2}{2m_n c^2 \lambda^2} = \frac{(2\pi)^2 \times (1973 \text{ eV} \cdot \text{\AA})^2}{2 \times (939.5 \times 10^6 \text{ eV}) \times (2.8 \text{ \AA})^2} = 0.01 \text{ eV}. \quad (1.208)$$

Neutrons with kinetic energy E_K of 0.01 eV fall into the upper level of so-called cold neutrons but they can also be classified as thermal neutrons that are defined as having energy of about 0.025 eV.

1.22.Q4

(42)

A beam of thermal neutrons with kinetic energy E_K of 0.04 eV is used in a scattering experiment on a crystal of sodium chloride with a lattice separation $d = 2.8 \text{ \AA}$. Calculate:

- (a) The Bragg angle φ at which the first order ($m = 1$) Bragg reflection occurs.
- (b) Energy $h\nu$ of monoenergetic x rays that would undergo first order Bragg reflection on sodium chloride crystal at the same Bragg angle φ .

SOLUTION:

(a) Equation $m\lambda = 2d \sin \varphi$ illustrates the Bragg condition for constructive interference between waves scattered from two planes with separation d , with m the order of the Bragg reflection, λ the wavelength of the incident radiation or matter wave, and φ the angle of incidence.

Thermal neutrons with $E_K = 0.04$ eV are characterized with the following de Broglie wavelength λ , as given by (1.193) or its classical approximation for $E_K \ll E_0$

$$\begin{aligned}\lambda &= \frac{h}{p} = \frac{2\pi\hbar c}{E_K\sqrt{1 + \frac{2E_0}{E_K}}} \approx \frac{2\pi\hbar c}{\sqrt{2E_0E_K}} = \frac{2\pi \times (197.3 \text{ MeV} \cdot \text{fm}) \times (10^{-5} \text{ \AA}/\text{fm})}{\sqrt{2 \times (939.6 \text{ MeV}) \times (4 \times 10^{-8} \text{ MeV})}} \\ &= 1.43 \text{ \AA},\end{aligned}\quad (1.209)$$

where h is the Planck constant; \hbar is the reduced Planck constant ($\hbar = h/(2\pi)$); p is momentum of the neutron; c is speed of light in vacuum; and E_0 is rest energy of the neutron (939.6 MeV).

According to (1.209) the de Broglie wavelength λ of a 0.04 MeV thermal neutron is 1.43 Å resulting in the following angle of incidence φ for the first order Bragg reflection

$$\sin\varphi = \frac{\lambda}{2d} = \frac{1.43 \text{ \AA}}{2 \times 2.8 \text{ \AA}} = 0.255 \quad \text{corresponding to } \varphi = 14.8^\circ. \quad (1.210)$$

(b) A mono-energetic x-ray photon that would experience first order reflection at the same angle of incidence ($\varphi = 14.8^\circ$) as the thermal neutron beam, would have a wavelength λ equal to the de Broglie wavelength λ of the thermal neutron beam. The energy of the mono-energetic x-ray photons is calculated using the Planck law

$$h\nu = h\frac{c}{\lambda} = \frac{2\pi\hbar c}{\lambda} = \frac{2\pi \times (1973 \text{ eV} \cdot \text{\AA})}{1.43 \text{ \AA}} = 8.67 \text{ eV}. \quad (1.211)$$

1.22.Q5

(43)

Based on experimental nuclear data:

- (a) Evaluate the feasibility of a nuclear model in which atomic electrons are confined within the atomic nucleus.
- (b) Compare the results with those for the model in which protons are confined within the atomic nucleus.

SOLUTION:

(a) Nuclear radius is given as $R(A) = R_0\sqrt[3]{A}$ where R_0 is the nuclear radius constant (1.25 fm) and A is the atomic mass number or number of nucleons in the nucleus. This defines the range of nuclear diameters between 2 fm for low- A nuclei and 20 fm for high- A nuclei, and stipulates that an electron residing in the nucleus would have a de Broglie wavelength λ below ~ 20 fm.

Equation (1.193) gives the following relationship between de Broglie wavelength λ and kinetic energy E_K of a particle

$$\lambda = \frac{h}{p} = \frac{2\pi\hbar c}{E_K \sqrt{1 + \frac{2E_0}{E_K}}} = \frac{2\pi\hbar c}{\sqrt{E_K^2 + 2E_0 E_K}}, \quad (1.212)$$

where E_0 is the rest energy of the particle.

Squaring (1.212) results in a quadratic equation for E_K with the following general solution

$$E_K = \frac{-2E_0 \pm \sqrt{4E_0^2 + 4\frac{(2\pi\hbar c)^2}{\lambda^2}}}{2} = E_0 \left[\sqrt{1 + \left(\frac{2\pi\hbar c}{\lambda E_0}\right)^2} - 1 \right], \quad (1.213)$$

with the + sign in the \pm option providing a physically relevant solution.

In the non-relativistic (classical) region where $2\pi\hbar c \ll \lambda E_0$ we simplify (1.213) to read

$$E_K = E_0 \left[1 + \frac{1}{2} \left(\frac{2\pi\hbar c}{\lambda E_0}\right)^2 + \dots - 1 \right] \approx \frac{2\pi^2}{E_0} \left(\frac{\hbar c}{\lambda}\right)^2 \quad (1.214)$$

and in the extreme relativistic region where $2\pi\hbar c \gg \lambda E_0$ we simplify (1.213) to

$$E_K \approx \frac{2\pi\hbar c}{\lambda}. \quad (1.215)$$

Inserting $\lambda = 20$ fm and $E_0 = 0.511$ MeV into (1.213) or just $\lambda = 20$ fm into (1.215) we obtain kinetic energy $E_K = 62$ MeV for the electron and establish that λ of less than 20 fm corresponds to electron kinetic energy E_K of more than 62 MeV.

Even if we take the reduced de Broglie wavelength $\tilde{\lambda}$ that is defined as $\lambda/(2\pi)$ and compare it to a nuclear diameter of 20 fm, we note that $\tilde{\lambda}$ of 20 fm corresponds to electron kinetic energy E_K of ~ 9.8 MeV. Since kinetic energies of 10 MeV have never been observed experimentally for electrons emitted from the nucleus in any of the nuclear processes such as beta decay, we conclude that a nuclear model housing electrons in addition to protons is not feasible.

Actually, electrons emitted from nuclei have maximum kinetic energies at least an order of magnitude smaller than 10 MeV and amount to only about 1 MeV corresponding to de Broglie wavelengths λ of about 900 fm or reduced de Broglie wavelengths $\tilde{\lambda}$ of ~ 150 fm, significantly larger than the nuclear diameter that is of the order of 10 fm.

(b) A similar look at protons confined to the nucleus shows that this model of proton confinement in the nucleus is feasible because of the much larger mass of the proton m_p compared to that of the electron m_e ($m_p/m_e = 1836$). Inserting $\lambda = 20$ fm and $E_0 = 938.3$ MeV into (1.213) we get the following result for the proton

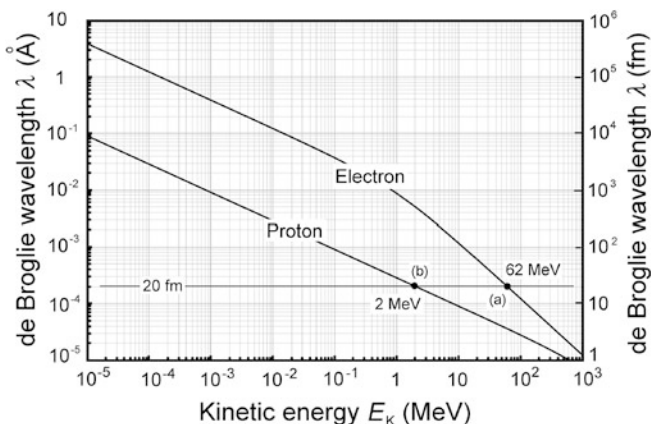


Fig. 1.18 De Broglie wavelength λ for electron and proton against kinetic energy E_K in the range from 10^{-5} MeV to 10^3 MeV. Points **(a)** and **(b)** correspond to kinetic energy of electron of 62 MeV and of proton of 2 MeV for de Broglie wavelength λ of 20 fm, determined in **(a)** and **(b)**, respectively, and estimated as the upper limit on the size of the nucleus for high atomic mass elements

kinetic energy E_K

$$E_K = (938.3 \text{ MeV}) \times \left[\sqrt{1 + \left(\frac{2\pi \times (197.3 \text{ MeV} \cdot \text{fm})}{(20 \text{ fm}) \times (938.3 \text{ MeV})} \right)^2} - 1 \right] \approx 2 \text{ MeV}. \quad (1.216)$$

The estimated proton kinetic energy E_K of 2 MeV is well within the binding energy per nucleon E_B/A that is of the order of 8 MeV/nucleon and ranges from 1.2 MeV/nucleon for deuterium to the highest value at slightly less than 9 MeV/nucleon. The estimated proton kinetic energy is also of the same order of magnitude as the energy of protons emitted from the nuclei in proton emission decay.

Figure 1.18 plots the de Broglie wavelengths of proton and electron against kinetic energy E_K . In **(a)** we established 20 fm as the upper limit on the size of the nucleus for high atomic mass elements and this provides us with an order of magnitude for de Broglie wavelength λ of electron and proton residing in the nucleus. From the two curves in Fig. 1.18 we note that for $\lambda = 20$ fm kinetic energy of the electron would exceed 62 MeV, while it exceeds 2 MeV for a proton. Since electrons emitted from nuclei have kinetic energies of the order of 1 MeV, it is clear that a nuclear model incorporating electrons in the atomic nucleus would not be practical.

We thus conclude that, based upon the de Broglie hypothesis of matter waves, electrons cannot reside within the nucleus while the protons can.

1.23 Matter Waves

1.23.Q1

(44)

Write the one-dimensional time-dependent Schrödinger wave equation for a free electron and show that a plane wave function is a solution to the wave equation.

SOLUTION:

The 1-dimensional time-dependent Schrödinger wave equation is written as follows

$$-\frac{\hbar^2}{2m_0} \frac{\partial^2 \Psi(z, t)}{\partial z^2} + V(z, t) \Psi(z, t) = i\hbar \frac{\partial \Psi(z, t)}{\partial t}, \quad (1.217)$$

where

$\Psi(z, t)$ is the wave function containing the information about the given particle.

$V(z, t)$ is the potential energy operator governing the motion of the particle.

m_0 is the particle rest mass.

\hbar is the reduced Planck constant.

A free electron is an electron subject to no force ($V(z, t) = 0$) and the Schrödinger equation (1.217) for a free electron in one dimension simplifies to

$$-\frac{\hbar^2}{2m_0} \frac{\partial^2 \Psi(z, t)}{\partial z^2} = i\hbar \frac{\partial \Psi(z, t)}{\partial t}, \quad (1.218)$$

with $\Psi(z, t)$ a simple plane wave of the form

$$\Psi(z, t) = C e^{i\varphi} = C e^{i(kz - \omega t)} = C e^{ikz} e^{-i\omega t}, \quad (1.219)$$

where

$\varphi = kz - \omega t$ is the phase of the plane wave and

k is the wave number ($k = 2\pi/\lambda$).

ω is the angular frequency ($\omega = 2\pi\nu$, with ν the frequency).

C is the normalization constant and here it is also the amplitude of the oscillation.

Using the Planck-Einstein quantum hypothesis $E = h\nu = \hbar\omega$ and the de Broglie particle-wave hypothesis $\lambda = h/p = 2\pi/k$ in conjunction with the classical relationship $E_K = p_e^2/(2m_e)$, we note that $\omega = E/\hbar$ and $\Psi(z, t)$ is a solution to the time-dependent Schrödinger equation (1.218) separable as a product of two functions: $\psi(z) = C e^{ikz}$ that is a function of the spatial coordinate z only and $T(t) = e^{-i\omega t}$ that is a function of the temporal coordinate t only.

The equation for the space function $\psi(z)$ is the so-called time-independent Schrödinger equation, given for a free particle as follows

$$-\frac{\hbar^2}{2m_0} \frac{d^2\psi(z)}{dz^2} = E\psi(z), \quad (1.220)$$

with solution $\psi(z) = Ce^{ikz}$ and energy $E = p^2/(2m_0) = \hbar^2k^2/(2m_0)$. Thus, the total energy E equals the kinetic energy.

The general solution to the Schrödinger equation for a free electron (1.218) is thus given as

$$\Psi(z, t) = Ce^{ikz}e^{-i\frac{E}{\hbar}t}. \quad (1.221)$$

For a free particle the energy is not quantized; the wave number k can take any value and the same holds for energy E . Thus, the states of k and E form a continuum.

To verify that (1.221) is indeed a viable solution to (1.218) we evaluate the derivatives $\partial^2\Psi/\partial z^2$ and $\partial\Psi/\partial t$

$$\frac{\partial\Psi(z, t)}{\partial z} = ikCe^{ikz}e^{-i\omega t} = ik\Psi(z, t), \quad (1.222)$$

$$\frac{\partial^2\Psi(z, t)}{\partial z^2} = -k^2Ce^{ikz}e^{-i\omega t} = -k^2\Psi(z, t), \quad (1.223)$$

$$\frac{\partial\Psi(z, t)}{\partial t} = -i\omega Ce^{ikz}e^{-i\omega t} = -i\omega\Psi(z, t). \quad (1.224)$$

Insert the appropriate derivatives into (1.218) and get

$$-\frac{\hbar^2}{2m_0} \frac{\partial^2\Psi(z, t)}{\partial z^2} = -\frac{\hbar^2}{2m_0} k^2\Psi(z, t) \quad (1.225)$$

and

$$i\hbar \frac{\partial\Psi(z, t)}{\partial t} = \hbar\omega\Psi(z, t). \quad (1.226)$$

Wave function $\Psi(z, t) = C \exp[i(kz - \omega t)]$ (in quantum physics referred to as an eigenfunction) satisfies (1.218) provided that $\hbar^2k^2/(2m_0)$ from (1.223) equals to $\hbar\omega$ from (1.226). This condition holds since the following three conditions apply:

- (i) $\hbar\omega = E$ according to the Planck-Einstein quantum hypothesis.
- (ii) $k = p/\hbar$ according to the de Broglie particle-wave hypothesis.
- (iii) $E_K = p^2/(2m_0)$ according to the classical kinetic energy-momentum relationship.

Energy E is the total energy of the particle; energy E_K is its kinetic energy. For a free particle, the potential energy $V(z, t)$ is zero, so that the total energy E equals the kinetic energy E_K .

1.23.Q2

(45)

As shown in Prob. 32, in special relativity the relationship between total energy E and momentum p of a free particle of rest mass m_0 is given by

$$E^2 = p^2 c^2 + m_0^2 c^4. \quad (1.227)$$

- (a) Use the quantum operators for total energy $E \rightarrow i\hbar\partial/\partial t$ and momentum $p \rightarrow -i\hbar\nabla$ to derive the relativistic Klein-Gordon equation for a free particle.
- (b) Show that the Klein-Gordon equation for a free particle transforms into the common wave equation when the free particle is a photon. (Note: photon has zero rest mass).
- (c) Show that inserting operators for E and p of (a) into the classical expression $E = p^2/2m_0$ results in the 3-dimensional time-dependent Schrödinger equation for a free particle.

SOLUTION:

- (a) Insert $E \rightarrow i\hbar\frac{\partial}{\partial t}$ and $p \rightarrow -i\hbar\nabla$ into $E^2 = p^2 c^2 + m_0^2 c^4$ and get

$$-\hbar^2 \frac{\partial^2 \Psi}{\partial t^2} = -\hbar^2 c^2 \nabla^2 \Psi + m_0^2 c^4 \Psi \quad \text{or} \quad \left(\nabla^2 - \frac{1}{c^2} \frac{\partial^2}{\partial t^2} \right) \Psi = \frac{m_0^2 c^4}{\hbar^2} \Psi. \quad (1.228)$$

Equation (1.228) is known as the Klein-Gordon wave equation and it correctly describes the propagation of relativistic particles of rest mass m_0 .

- (b) Insert $m_0 = 0$ into the Klein-Gordon equation (1.228) and the result will be the standard wave equation governing EM waves expressed as

$$\nabla^2 \Psi = \frac{1}{c^2} \frac{\partial^2 \Psi}{\partial t^2}. \quad (1.229)$$

- (c) Insert $E \rightarrow i\hbar\frac{\partial}{\partial t}$ and $p \rightarrow -i\hbar\nabla$ into the classical relationship for kinetic energy $E = p^2/2m_0$ to get

$$i\hbar \frac{\partial \Psi}{\partial t} = -\frac{\hbar^2}{2m_0} \nabla^2 \Psi \quad \text{or} \quad -\frac{\hbar^2}{2m_0} \nabla^2 \Psi = i\hbar \frac{\partial \Psi}{\partial t}. \quad (1.230)$$

Equation (1.230) is the non-relativistic 3-dimensional time-dependent Schrödinger equation for a free particle.

1.23.Q3

(46)

For a free electron with a spatial wave function $\psi(z) = Ce^{i(7.5 \text{ \AA}^{-1})z}$.

- (a) Write the spatial component of the Schrödinger equation.
- (b) Determine the wave number k of the electron.
- (c) Calculate the de Broglie wavelength λ of the electron
- (d) Calculate the momentum p_e of the electron
- (e) Calculate the kinetic energy E_K^e of the electron.
- (f) Calculate the velocity v_e of the electron.

SOLUTION:

(a) The general wave equation for the free electron is given as

$$-\frac{\hbar^2}{2m_e}\nabla^2\psi(z) = E\psi(z), \quad (1.231)$$

where E is the total energy of the free electron and $\psi(z)$ is the time-independent wave function.

(b) Wave number of the free electron with a spatial wave function $\psi(z) = Ce^{i(7.5 \text{ \AA}^{-1})z}$ is obtained directly from the wave function as $k = 7.5 \text{ \AA}^{-1} = 7.5 \times 10^{-10} \text{ m}^{-1}$.

(c) De Broglie wavelength λ of the free electron with a spatial wave function $\psi(z) = Ce^{i(7.5 \text{ \AA}^{-1})z}$ is calculated from the definition for the wave number expressed as $k = 2\pi/\lambda$

$$\lambda = \frac{2\pi}{k} = \frac{2\pi}{7.5} \text{ \AA} = 0.84 \text{ \AA} = 0.84 \times 10^{-10} \text{ m}. \quad (1.232)$$

(d) Momentum p of free electron with a spatial wave function $\psi(z) = Ce^{i(7.5 \text{ \AA}^{-1})z}$ is calculated as

$$\begin{aligned} p &= \hbar k = (\hbar c) \frac{k}{c} = (1973 \text{ eV} \cdot \text{\AA}) \times \frac{7.5 \text{ \AA}^{-1}}{c} = 1.48 \times 10^4 \text{ eV}/c = 14.8 \text{ keV}/c \\ &= \frac{(1.48 \times 10^4 \text{ eV}) \times (1.602 \times 10^{-19} \text{ kg} \cdot \text{m}^2 \cdot \text{s}^{-1}/\text{eV})}{3 \times 10^8 \text{ m} \cdot \text{s}^{-1}} \\ &= 7.9 \times 10^{-24} \text{ kg} \cdot \text{m} \cdot \text{s}^{-1}. \end{aligned} \quad (1.233)$$

(e) Kinetic energy E_K of the free electron with a spatial wave function $\psi(z) = Ce^{i(7.5 \text{ \AA}^{-1})z}$ is calculated from: (1) classical relationship, (2) de Broglie wavelength λ , and (3) general relativistic expression. The three calculations are expected to give same results.

- (1) From classical expression for kinetic energy
- E_K

$$E_K = \frac{1}{2}m_e v^2 = \frac{p^2}{2m_e} = \frac{(pc)^2}{2m_e c^2} = \frac{(1.48 \times 10^4 \text{ eV})^2}{2 \times 0.511 \times 10^6 \text{ eV}} = 214.3 \text{ eV}. \quad (1.234)$$

- (2) From de Broglie wavelength
- λ
- of 0.84 Å corresponding to wave number
- k
- of 7.5 Å
- ⁻¹

$$E_K = \frac{\hbar^2 k^2}{2m_e} = \frac{(\hbar c)^2 k^2}{2m_e c^2} = \frac{(1973 \text{ eV} \cdot \text{Å})^2 \times (7.5 \text{ Å}^{-1})^2}{2 \times 0.511 \times 10^6 \text{ eV}} = 214.3 \text{ eV}. \quad (1.235)$$

- (3) From the basic relativistic relationship for total energy
- $E = \sqrt{p^2 c^2 + E_e^2} = E_K + E_e$

$$\begin{aligned} E_K &= E - E_e = \sqrt{E_e^2 + p^2 c^2} - E_e = E_e \left(\sqrt{1 + \frac{p^2 c^2}{E_e^2}} - 1 \right) \\ &\approx E_e \left(1 + \frac{1}{2} \frac{p^2 c^2}{E_e^2} + \dots - 1 \right) \\ &\approx \frac{p^2 c^2}{2E_e} = \frac{(1.48 \times 10^4 \text{ eV})^2}{1.022 \times 10^6 \text{ eV}} = 214.3 \text{ eV}. \end{aligned} \quad (1.236)$$

(f) Velocity v_e of the electron can be calculated: (1) from momentum p_e of the electron in **(d)** or (2) from kinetic energy E_K^e of the electron in **(e)**. We use here the relativistic expressions for momentum and kinetic energy to highlight the general relativistic case even though the electron in this problem can also be treated classically

- (1) Using momentum
- $p_e = 14.8 \text{ keV}/c$
- and the relativistic expression for momentum we get

$$p_e = \gamma m_e v_e = \gamma \beta m_e c = \frac{\beta}{\sqrt{1 - \beta^2}} m_e c \quad (1.237)$$

where γ is the Lorentz factor and m_e is the rest mass of the electron.

Solving (1.237) for β we obtain the following result for the electron velocity v_e

$$\beta = \frac{v_e}{c} = \frac{\frac{p_e}{m_e c}}{\sqrt{1 + \left[\frac{p_e}{m_e c} \right]^2}} = \frac{\frac{14.8 \text{ keV}/c}{0.511 \times 10^3 \text{ keV}/c}}{\sqrt{1 + \left[\frac{14.8 \text{ keV}/c}{0.511 \times 10^3 \text{ keV}/c} \right]^2}} = 0.029. \quad (1.238)$$

- (2) As expected, using the standard relationship (see T2.7) between particle velocity
- v
- and its kinetic energy
- E_K
- , we get the same result as in (1.238) for the

electron velocity v_e

$$\beta = \frac{v_e}{c} = \sqrt{1 - \frac{1}{\left(1 + \frac{E_K^e}{m_e c^2}\right)^2}} = \sqrt{1 - \frac{1}{\left(1 + \frac{214.3}{0.511 \times 10^6}\right)^2}} = 0.029. \quad (1.239)$$

1.23.Q4**(47)**

A particle has the following one-dimensional, time independent wave function $\psi(z) = C e^{-\frac{1}{2}\alpha^2 z^2}$. Calculate:

- (a) Normalization constant C of the particle wave function $\psi(z)$.
- (b) Average or expectation value \bar{z} of particle position z .
- (c) Average or expectation value $\bar{z^2}$ of z^2 of the particle.
- (d) Quantum uncertainty Δz in particle position z .

SOLUTION:

(a) The normalization condition for wave function $\psi(z)$ is given as

$$\int_{-\infty}^{\infty} |\psi(z)|^2 dz = \int_{-\infty}^{\infty} \psi^*(z)\psi(z) dz = C^2 \int_{-\infty}^{\infty} e^{-\alpha^2 z^2} dz = 1, \quad (1.240)$$

resulting in the following expression for the normalization constant C

$$C = \left\{ \int_{-\infty}^{\infty} e^{-\alpha^2 z^2} dz \right\}^{-\frac{1}{2}}. \quad (1.241)$$

In standard *Tables of Integrals* we find the following definite integral

$$\int_{-\infty}^{\infty} e^{-az^2} dz = \sqrt{\frac{\pi}{a}}. \quad (1.242)$$

Inserting $a = \alpha^2$ into (1.242) we obtain the following value for the constant C

$$C = \frac{1}{\sqrt{\int_{-\infty}^{\infty} e^{-\alpha^2 z^2} dz}} = \frac{\sqrt{\alpha}}{\sqrt[4]{\pi}}. \quad (1.243)$$

The wave function of our particle is thus given as

$$\psi(z) = \frac{\sqrt{\alpha}}{\sqrt[4]{\pi}} e^{-\frac{1}{2}\alpha^2 z^2}, \quad (1.244)$$

and, when inserted into the normalization condition (1.240), the result is 1, as expected.

(b) The mean (average) or expectation value \bar{z} of particle position z is calculated as follows

$$\bar{z} = \int_{-\infty}^{\infty} z |\psi(z)|^2 dz = C^2 \int_{-\infty}^{\infty} z e^{-\alpha^2 z^2} dz = \frac{\alpha}{\sqrt{\pi}} \int_{-\infty}^{\infty} z e^{-\alpha^2 z^2} dz. \quad (1.245)$$

In standard *Tables of Integrals* we find the following definite integral

$$\int_{-\infty}^{\infty} z e^{-a(z-b)^2} dz = b \sqrt{\frac{\pi}{a}}. \quad (1.246)$$

Since in our example the constant b equals zero, the value of the definite integral (1.246) is zero, which is to be expected, since the wave function is essentially Gaussian as well as even and centered at $z = 0$. We thus conclude that the mean or expectation value of position z is equal to zero, i.e., $\bar{z} = 0$.

(c) The (mean) average or expectation value $\overline{z^2}$ is calculated as follows

$$\overline{z^2} = \int_{-\infty}^{\infty} z^2 |\psi(z)|^2 dz = C^2 \int_{-\infty}^{\infty} z^2 e^{-\alpha^2 z^2} dz = \frac{\alpha}{\sqrt{\pi}} \int_{-\infty}^{\infty} z^2 e^{-\alpha^2 z^2} dz. \quad (1.247)$$

In standard *Tables of Integrals* we find the following definite integral

$$\int_{-\infty}^{\infty} z^2 e^{-az^2} dz = \frac{1}{2} \sqrt{\frac{\pi}{a^3}}. \quad (1.248)$$

Inserting (1.248) with $a = \alpha^2$ into (1.247) we get the following result for $\overline{z^2}$

$$\overline{z^2} = \frac{1}{2\alpha^2}. \quad (1.249)$$

(d) Δz , the quantum uncertainty in position z , is given as

$$\Delta z = \sqrt{\overline{z^2} - (\bar{z})^2}. \quad (1.250)$$

Inserting $\bar{z} = 0$ from (1.246) and $\overline{z^2} = 1/(2\alpha^2)$ from (1.249) into (1.250) we obtain the following result for the quantum uncertainty Δz

$$\Delta z = \sqrt{\frac{1}{2\alpha^2} - 0} = \frac{1}{\alpha\sqrt{2}} = \frac{0.707}{\alpha}. \quad (1.251)$$

1.24 Uncertainty Principle

1.24.Q1

(48)

Take the radius a and momentum p of the electron occupying the innermost orbit (shell) of the hydrogen atom and show that the two quantities satisfy the *Heisenberg uncertainty principle* $\Delta z \Delta p \geq \frac{1}{2} \hbar$. Assume that maximum uncertainties in position z and momentum p are equal to a and p , respectively, of the $n = 1$ hydrogen orbit.

SOLUTION:

The innermost electronic shell in a hydrogen atom is characterized with $n = 1$ and $Z = 1$, where n is the principal quantum number and Z is the atomic number of hydrogen.

The innermost electron orbit in hydrogen atom has the following radius: $r_1 = a_0 = 0.53 \text{ \AA} = 0.53 \times 10^{-5} \text{ fm}$, where a_0 is a constant called the Bohr radius constant. The maximum uncertainty in position is then $\Delta z \approx a_0 = 0.53 \times 10^{-5} \text{ fm}$.

The velocity of the electron in the first orbit of the hydrogen atom is given as: $v_1 = \alpha c = (1/137)c$, where α is the fine structure constant and c is the speed of light in vacuum. Since $v_1 \ll c$, we can use the classical expression for the electron momentum p as follows

$$p = m_e v_1 = \frac{m_e c^2}{c} \frac{v_1}{c} = \frac{m_e c^2}{c} \alpha = 0.511 \frac{\text{MeV}}{c} \times \frac{1}{137} = 3.73 \times 10^{-3} \frac{\text{MeV}}{c}, \quad (1.252)$$

resulting in maximum uncertainty in momentum p of $\Delta p \approx 3.73 \times 10^{-3} \text{ MeV}/c$.

Next we determine the product $\Delta z \Delta p$ and get

$$\Delta z \Delta p \approx a_0 m_e v_1 = (0.53 \times 10^{-5} \text{ fm}) \times 3.73 \times 10^{-3} \frac{\text{MeV}}{c} = 197.7 \frac{\text{MeV} \cdot \text{fm}}{c} \quad (1.253)$$

and evaluate $\frac{1}{2} \hbar$ to get

$$\frac{1}{2} \hbar = \frac{\hbar c}{2c} = \frac{197.3}{2c} \text{ MeV} \cdot \text{fm} = 98.7 \frac{\text{MeV} \cdot \text{fm}}{c}. \quad (1.254)$$

A comparison of (1.253) to (1.254) shows that the Heisenberg uncertainty principle stating that $\Delta z \Delta p \geq \frac{1}{2} \hbar$ is satisfied for the electron in the innermost shell of the hydrogen atom, since

$$\Delta z \Delta p = 197.7 \frac{\text{MeV} \cdot \text{fm}}{c} \geq \frac{1}{2} \hbar = 98.7 \frac{\text{MeV} \cdot \text{fm}}{c}. \quad (1.255)$$

1.25 Complementarity Principle

1.25.Q1

(49)

- (a) Define the “*Principle of Complementarity*” in quantum physics.
- (b) List a few examples for which the principle of complementarity applies.

SOLUTION:

(a) Introduced in 1927 by Niels Bohr, the principle of complementarity in quantum physics, also known as wave–particle duality, stipulates that the complete description of a phenomenon in physics of nano-dimensions relies on two contradictory, yet complementary, models. One or the other model alone cannot fully explain a particular phenomenon; complete understanding of a given phenomenon is only obtained if both models are combined in a complementary fashion.

In a narrower sense the principle of complementarity states that a quantum mechanical phenomenon behaves either as particle (corpuscle) or as wave but not as particle and wave simultaneously. A stronger emphasis on the wave nature diminishes the particle nature and vice-versa. This links the Bohr principle of complementarity, which stipulates that the particle and wave models complement rather than contradict one another, with the Heisenberg principle of uncertainty which sets a limit to the precision with which two conjugate physical quantities, such as particle’s position and momentum or its energy and duration of energy measurement, can be determined.

(b) There are several phenomena in quantum physics where the particle-wave duality is apparent. In the broadest sense we can say that both radiation as well as matter exhibit the particle–wave duality to which the Bohr principle of complementarity applies. Results of a particular experiment with radiation or matter will be explained with only one of the two models and never with both; however, for a complete understanding of radiation and matter both models must be invoked. For example:

- (1) Aspects of radiation explained by corpuscular nature: (i) photoelectric effect and (ii) Compton effect.
- (2) Aspects of radiation explained by wave nature: (i) diffraction of x rays (Bragg law); (ii) diffraction of visible light (single slit, double slit (Young experiment), diffraction grating, circular aperture, (iii) wave equations for electric and magnetic fields for EM radiation (Maxwell equations).
- (3) Aspects of matter explained by corpuscular nature: (i) electron ionization track in ionization chamber and bubble chamber, (ii) neutron track in neutron bubble detector, (iii) electron in Rutherford-Bohr atom (particle model).

- (4) Aspects of matter explained by wave nature: (i) Bragg diffraction of electrons and neutrons on crystals with de Broglie wavelength λ much shorter than the separation d of crystallographic planes, (ii) electron in Rutherford-Bohr atom (electron wave functions).

1.26 Emission of Electrons from Material Surface: Work Function

1.26.Q1

(50)

In a surface photoelectric experiment the surface of sodium metal is exposed to incident monochromatic light of various wavelengths λ . The measured retarding potentials U_0^{ret} required to stop completely the emitted photoelectron current at a given λ are listed in Table 1.16.

Table 1.16 Retarding potential U_0^{ret} required for stopping photoelectron current against λ

Photon wavelength $\lambda(\text{\AA})$	5051	4475	4100	3591	3193	2723
Retarding potential $U_0^{\text{ret}}(\text{V})$	0.15	0.37	0.71	1.23	1.61	2.17

From a graphical presentation of appropriate data determine:

- Ratio h/e where h is the Planck constant and e the electron charge.
- Planck constant assuming that we know the electron charge ($e = 1.602 \times 10^{-19} \text{ C}$).
- Work function $e\phi$ for sodium metal.

SOLUTION:

The surface photoelectric experiment consists of measuring the number of photoelectrons emitted and their kinetic energies as functions of intensity I and wavelength λ of monochromatic incident visible or ultraviolet light. Experimental apparatus allows application of retarding $U^{\text{ret}} < 0$ or accelerating $U^{\text{accel}} > 0$ electric field to the emitted photoelectrons. For $U^{\text{accel}} > 0$, all emitted electrons strike the collecting electrode and the current is essentially independent of the applied voltage. For $U^{\text{ret}} < 0$, the retarding potential prevents lower energy electrons from reaching the collecting electrode, so the current decreases with increasing negative potential

until at U_0^{ret} no photoelectrons can overcome the retarding potential and the current drops to 0. For a given material of the emitting electrode, U_0^{ret} is constant and independent of light intensity I , a finding that cannot be explained with classical theory. This peculiar result caused significant difficulties for physicists at the beginning of the 20-th century and it was Albert Einstein who in 1905 explained the experimental data by introducing the idea of the photon quantum and the corpuscular nature of the photon.

According to Einstein, the kinetic energy E_K of the emitted photoelectron is given by

$$E_K = h\nu - e\phi, \quad (1.256)$$

where $h\nu$ is the energy of the incident photon quantum and $e\phi$ is the work function representing the minimum energy the photon must possess to be able to eject an electron from the surface of the electrode material.

The retarding potential U^{ret} decreases the measured electron current I at a given photon energy $h\nu = hc/\lambda$ and at U_0^{ret} completely stops the photoelectron current such that the kinetic energy E_K of the photoelectron equals to eU_0^{ret} . We now modify (1.256) to accommodate the measured data as follows

$$E_K = U_0^{\text{ret}} = \frac{h}{e}\nu - \frac{e\phi}{e}, \quad (1.257)$$

calculate frequencies ν from wavelengths λ using $\nu = c/\lambda$, and plot U_0^{ret} against the calculated frequencies ν based on the following frequency ν and U_0^{ret} data:

Table 1.17 Photon frequency for wavelength λ data of Table 1.16

	(1)	(2)	(3)	(4)	(5)	(6)
Photon wavelength $\lambda(\text{\AA})$	5051	4475	4100	3591	3193	2723
Photon frequency $\nu(\text{s}^{-1}) = c/\lambda$	5.94×10^{14}	6.70×10^{14}	7.32×10^{14}	8.35×10^{14}	10.6×10^{14}	11.0×10^{14}
Retarding potential $U_0^{\text{ret}}(\text{V})$	0.15	0.37	0.71	1.23	1.61	2.17

(a) As shown in Fig. 1.19, the (ν, U_0^{ret}) plot is linear and allows us to determine the h/e ratio of (1.257) from the slope of the straight line obtained through the least squares fit to measured data. The slope is $4.12 \times 10^{-15} \text{ V} \cdot \text{s}$ which means that $h/e = 4.12 \times 10^{-15} \text{ V} \cdot \text{s}$.

(b) We can now determine the Planck constant h from the h/e ratio of **(a)** using the known value of the electron charge $e = 1.602 \times 10^{-19} \text{ C}$ as follows

$$\begin{aligned} h &= \frac{h}{e}e = (4.12 \times 10^{-15} \text{ V} \cdot \text{s}) \times e = 4.12 \times 10^{-15} \text{ V} \cdot \text{s} \\ &= (4.12 \times 10^{-15} \text{ eV} \cdot \text{s}) \times (1.602 \times 10^{-19} \text{ J/eV}) = 6.60 \times 10^{-34} \text{ J} \cdot \text{s}, \end{aligned} \quad (1.258)$$

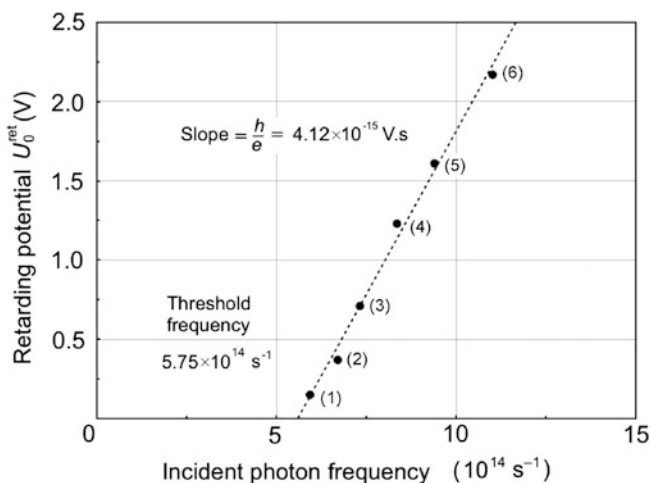


Fig. 1.19 Measured retarding potential U_0^{ret} against photon frequency ν . The slope of the linear plot obtained with the least squares fit to measured data is equal to h/e with h the Planck constant and e the electron charge. Data points (1) through (6) represent data presented in Table 1.17

that compares reasonably well with the currently accepted value of the Planck constant quoted as $h = 6.626 \times 10^{-34} \text{ J} \cdot \text{s}$.

(c) The work function $e\phi$ of sodium will be determined from the intercept of the linear (ν, U_0^{ret}) plot with the abscissa (ν) axis ($U_0^{\text{ret}} = 0$) which yields $\nu_0 = 5.75 \times 10^{14} \text{ s}^{-1}$. We then get the following value for the work function $e\phi$ of sodium

$$e\phi = h\nu_0 = \frac{(6.60 \times 10^{-34} \text{ J} \cdot \text{s}) \times (5.75 \times 10^{14} \text{ s}^{-1})}{1.602 \times 10^{-19} \text{ J/eV}} = 2.37 \text{ eV}, \quad (1.259)$$

in good agreement with currently used value of 2.36 eV for the photoelectric work function $e\phi$ of sodium.

1.26.Q2

(51)

In a surface photoelectric experiment photons with a wavelength λ are incident on the photo-cathode and eject photoelectrons with kinetic energy $E_K(\lambda)$ of 2.5 eV. When photons with a wavelength $\frac{1}{2}\lambda$ are incident on the photocathode, they eject photoelectrons with kinetic energy $E_K(\frac{1}{2}\lambda)$ of 9.25 eV. The threshold frequency ν_0 of the photocathode is $1.03 \times 10^{15} \text{ s}^{-1}$. Calculate:

- Photoelectric work function $e\phi$.
- Wavelength λ of the incident photons.

SOLUTION:

(a) The photoelectric work function $e\phi$ is calculated from the threshold frequency ν_0

$$e\phi = h\nu_0 = \frac{2\pi\hbar c}{c}\nu_0 = \frac{2\pi \times (1973 \text{ eV} \cdot \text{\AA}) \times (1.03 \times 10^{15} \text{ s}^{-1})}{3 \times 10^{18} \text{ \AA} \cdot \text{s}^{-1}} = 4.25 \text{ eV}. \quad (1.260)$$

(b) We now express mathematically the two sets of experimental data for photoelectron kinetic energies: $E_K(\lambda)$ and $E_K(\frac{1}{2}\lambda)$ using the Einstein photoelectric equation linking the photoelectron kinetic energy E_K with photon energy $h\nu$ and the photocathode photoelectric work function $e\phi$

$$E_K = h\nu - e\phi = \frac{2\pi\hbar c}{\lambda} - e\phi. \quad (1.261)$$

For the two wavelengths λ and $\frac{1}{2}\lambda$ we get the following expressions

$$E_K(\lambda) = \frac{2\pi\hbar c}{\lambda} - e\phi \quad (1.262)$$

and

$$E_K\left(\frac{1}{2}\lambda\right) = \frac{4\pi\hbar c}{\lambda} - e\phi. \quad (1.263)$$

Subtracting (1.262) from (1.263) one obtains

$$E_K\left(\frac{1}{2}\lambda\right) - E_K(\lambda) = \frac{4\pi\hbar c}{\lambda} - \frac{2\pi\hbar c}{\lambda} = \frac{2\pi\hbar c}{\lambda} = 9.25 \text{ eV} - 2.25 \text{ eV} = 6.75 \text{ eV} \quad (1.264)$$

or

$$\lambda = \frac{2\pi \times (1973 \text{ eV} \cdot \text{\AA})}{6.75 \text{ eV}} = 1836 \text{ \AA}. \quad (1.265)$$

Photoelectric work function $e\phi$ is 4.25 eV and wavelength λ of the incident photons is 1836 Å.

1.27 Thermionic Emission**1.27.Q1****(52)**

The thermionic technique was used for measurement of the work function $e\phi$ of tungsten and the data listed in Table 1.18 were measured:

Table 1.18 Data for measurement of work function $e\phi$ with the thermionic technique

T (K)	1250	1500	1750	2000	2250	2500
j (A/m ²)	6.62×10^{-7}	1.03×10^{-3}	0.345	14.9	220	3.05×10^3

Plot the data in an Arrhenius-type graph using the Richardson-Dushman equation (T1.132) and from the graph determine:

- Richardson constant A_R for tungsten.
- Thermionic work function $e\phi$ for tungsten.

SOLUTION:

The Richardson-Dushman equation expresses the thermionic current density j in A/m² as a function of the temperature T in degree K of a heated metallic emitter as follows

$$j = A_R T^2 e^{-\frac{e\phi}{kT}}, \quad (1.266)$$

where k is the Boltzmann constant (8.617×10^{-5} eV · K⁻¹) and A_R is the Richardson constant for a given emitter material. Equation (1.266) can be written in the form of Arrhenius-type equation as follows

$$\ln \frac{j}{T^2} = -\frac{e\phi}{k} \frac{1}{T} + \ln A_R, \quad (1.267)$$

to get a linear relationship of the form $y = Kx + b$ which, if borne out by experimental data, enables the determination of the work function $e\phi$ and constant A_R for a given thermionic emitter.

Thermionic data of Table 1.18 for tungsten were expanded to make them useful for Arrhenius diagram and are plotted in Fig. 1.20 with $\ln(j/kT)$ on the ordinate (y) axis against $10^4/T$ on the abscissa (x) axis.

The Arrhenius diagram of Fig. 1.20 for tungsten results in a straight line which:

- When extrapolated to $T \rightarrow \infty$, i.e., $1/T \rightarrow 0$, results in $\ln(j/kT) = \ln A_R = 13.4$ or $A_R = 0.6 \times 10^6$ A/(m² · K²).

Table 1.19 Expanded Table 1.18 to make data measured with the thermionic technique suitable for determination of Richardson constant A_R and work function $e\phi$ of tungsten

	(1)	(2)	(3)	(4)	(5)	(6)
T (K)	1250	1500	1750	2000	2250	2500
$10^4/T$ (K ⁻¹)	8	6.67	5.71	5.00	4.44	4.00
j (A/m ²)	6.62×10^{-7}	1.03×10^{-3}	0.345	14.9	220	3.05×10^3
$\ln(j/T^2)$	-28.49	-21.51	-16.00	-12.50	-10.04	-7.63

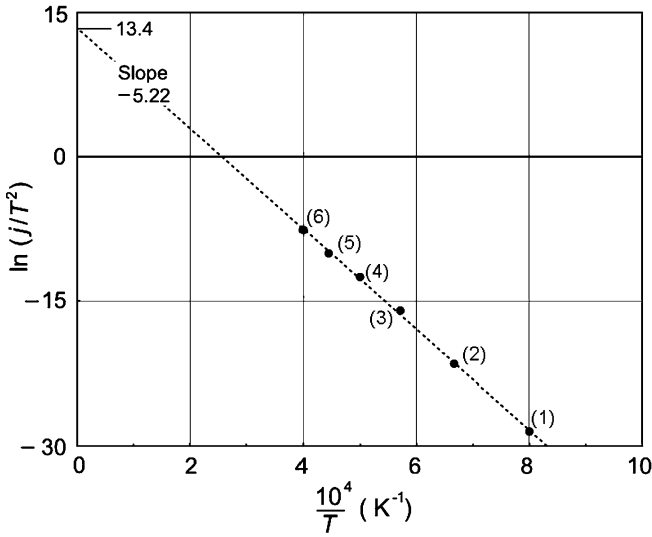


Fig. 1.20 Experimental data of Table 1.19 for tungsten plotted in the form $\ln(j/T^2)$ against $(10^4/T)$ to find solution to the Richardson-Dushman equation (1.266)

- (b) Exhibits a slope of $e\phi/k = -5.22 \times 10^4 \text{ K}^{-1}$ yielding a work function for tungsten $e\phi = 4.5 \text{ eV}$.

Thus, the Richardson constant for tungsten is $A_R = 0.6 \times 10^6 \text{ A}/(\text{m}^2 \cdot \text{K}^2)$ and its work function is $e\phi = 4.5 \text{ eV}$. *Note:* the photoelectric work function and thermionic work function are assumed to be the same for the same emitter material.

1.27.Q2 (53)

Thermionic emission is a phenomenon in which an electronic current with density j evaporates from a metallic surface heated to temperature T in the absence of an external electric field. The current density j is given by the Richardson-Dushman equation

$$j = A_R T^2 e^{-\frac{e\phi}{kT}}, \tag{1.268}$$

where $e\phi$ is the work function of the metal, A_R is the theoretical Richardson constant [$A_R \approx 0.6 \times 10^6 \text{ A}/(\text{m}^2 \cdot \text{K}^2)$] and k is the Boltzmann constant ($k = 8.617 \times 10^{-5} \text{ eV} \cdot \text{K}^{-1}$).

When the surface of a heated metallic cathode is immersed in an electric field, the field enhances the thermionic emission of the cathode by lowering the cathode’s work function $e\phi$ by $e\Delta\phi$ and this results in a correction to the Richardson-Dushman equation.

The effect and the corrected equation are called the Schottky effect and the Schottky equation, respectively, in honor of German physicist Walter H. Schottky who discovered and explained the effect classically in 1914.

Based on the Richardson-Dushman equation (1.268), the current density j for the Schottky effect is written as

$$j = A_{\text{R}} T^2 e^{-\left[\frac{\phi}{kT} - \frac{e\Delta\phi}{kT}\right]} = A_{\text{R}} T^2 e^{-\frac{e}{kT}[\phi - \Delta\phi]}, \quad (1.269)$$

where $e\Delta\phi$ represents the work function reduction because of the influence of the external electric field \mathcal{E} on the work function $e\phi$.

- (a) Sketch the work function $e\phi$ of a typical metal showing the potential energy E_{P} of an electron as a function of electron's distance x from the surface of the metal. On the same graph sketch the Schottky barrier that arises when external electric field \mathcal{E} is applied to the metal. Indicate all parameters of interest in studies of the Schottky barrier.
- (b) Show that $e\Delta\phi$, the decrease in work function $e\phi$ in Schottky effect is proportional to $\alpha\sqrt{\mathcal{E}}$, where \mathcal{E} is the external electric field and $\alpha = -\sqrt{e^3/(4\pi\epsilon_0)}$ is the proportionality constant.
- (c) Determine the magnitude of the external electric field \mathcal{E} required to reduce the work function of tungsten by 1%. The work function $e\phi$ of tungsten is 4.52 eV.
- (d) Determine the relative change in the thermionic emission current density j for a tungsten filament at temperature $T = 2300$ K, if the temperature T increases by 1% and the work function $e\phi$ decreases by 1%.

SOLUTION:

(a) Figure 1.21 shows a sketch of potential energy E_{P} of an electron against its distance x from the surface of a metal. The dotted curve is for metal with no external electric field \mathcal{E} applied, the dashed curve shows the potential $-e\mathcal{E}x$ of the applied external electric field \mathcal{E} , and the solid curve shows the combined potential energy forming the Schottky potential barrier as a result of the applied external electric field \mathcal{E} . Also indicated are x_{S} , the location of the maximum potential energy E_{P} of the Schottky barrier and the reduction of the work function $e\phi$ as a result of the applied external electric field \mathcal{E} .

Using the electrostatic method of images, the Coulomb force exerted on an electron with charge $-e$ at a distance x from a metallic emitter (cathode) is the same as the Coulomb force of attraction between the electron and its image with positive charge $+e$ separated by a distance $2x$. Coulomb force on the electron is thus expressed as

$$F_{\text{Coul}} = -\frac{e^2}{4\pi\epsilon_0(2x)^2} = -\frac{e^2}{16\pi\epsilon_0x^2}, \quad (1.270)$$

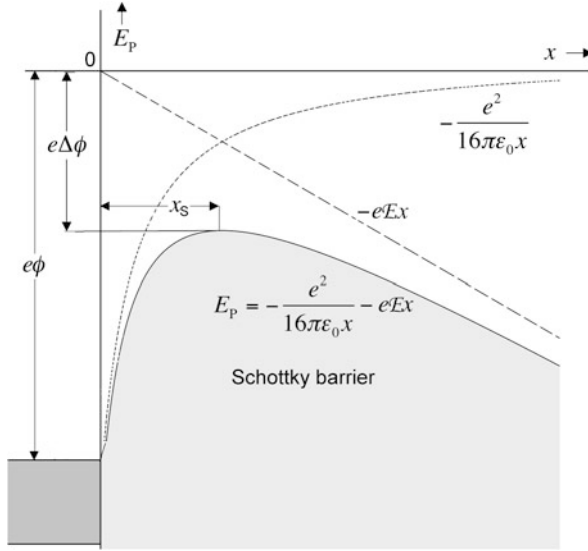


Fig. 1.21 Schematic representation of the Schottky barrier in thermionic emission enhanced by external electric field \mathcal{E} showing the potential energy E_P of an electron as a function of its distance x from the surface of a metal. The *dotted curve* is for metal with no external electric field \mathcal{E} applied, the *dashed curve* shows the potential $-e\mathcal{E}x$ of the applied external electric field \mathcal{E} , and the *solid curve* shows the combined potential energy forming the Schottky potential barrier as a result of the applied external electric field \mathcal{E}

resulting in potential energy $E_P(x, \mathcal{E} = 0)$

$$E_P(x, \mathcal{E} = 0) = \int_x^\infty F_{\text{Coul}} dx = -\frac{e^2}{16\pi\epsilon_0} \int_x^\infty \frac{dx}{x^2} = \frac{e^2}{16\pi\epsilon_0} \left[\frac{1}{x} \right]_x^\infty = -\frac{e^2}{16\pi\epsilon_0 x} \tag{1.271}$$

associated with the Coulomb force F_{Coul} given in (1.270).

(b) If an external electric field \mathcal{E} is applied, there is an additional contribution $-e\mathcal{E}x$ to the potential energy $E_P(x, \mathcal{E} = 0)$ of the electron resulting in total potential energy $E_P(x, \mathcal{E})$ expressed as

$$E_P(x, \mathcal{E}) = -\frac{e^2}{16\pi\epsilon_0 x} - e\mathcal{E}x. \tag{1.272}$$

The extra potential energy term generated by the external electric field \mathcal{E} causes a lowering of the work function $e\phi$ by a small amount $e\Delta\phi$ and an effective work function $(e\phi)_{\text{eff}} = e\phi - e\Delta\phi$ (Schottky effect). Because of the presence of electric field \mathcal{E} , potential energy E_P exhibits not only a maximum but also has the shape of a potential barrier that is referred to as the Schottky barrier. As shown in Fig. 1.21, for a given electric field \mathcal{E} the work function reduction $e\Delta\phi$ occurs at position x_S where E_P exhibits a maximum, in contrast to the behavior of E_P for $\mathcal{E} = 0$ where maximum of E_P occurs at $x = \infty$.

We find x_S by setting $dE_P/dx|_{x=x_S} = 0$ and get

$$\frac{dE_P(x = x_S, \mathcal{E})}{dx} = \frac{d}{dx} \left[-\frac{e^2}{16\pi\epsilon_0 x} - e\mathcal{E}x \right] \Big|_{x=x_S} = \frac{e^2}{16\pi\epsilon_0 x_S^2} - e\mathcal{E} = 0. \quad (1.273)$$

Solving (1.273) for x_S , we get the following expression for the position of the maximum x_S of the Schottky barrier

$$x_S = \sqrt{\frac{e}{16\pi\epsilon_0\mathcal{E}}} = \frac{1}{2} \sqrt{\frac{e}{4\pi\epsilon_0\mathcal{E}}}. \quad (1.274)$$

Since by definition $E_P(x = x_S, \mathcal{E}) = e\Delta\phi$, we insert x_S of (1.274) into (1.273) and get the following expression for the reduction in the Schottky work function $e\Delta\phi$

$$\begin{aligned} e\Delta\phi &= -\frac{e^2}{16\pi\epsilon_0 x_S} - e\mathcal{E}x_S = -\frac{e^2}{16\pi\epsilon_0} \sqrt{\frac{16\pi\epsilon_0\mathcal{E}}{e}} - e\mathcal{E} \sqrt{\frac{e}{16\pi\epsilon_0\mathcal{E}}} \\ &= -e \sqrt{\frac{e}{4\pi\epsilon_0}} \sqrt{\mathcal{E}} = -e \sqrt{\frac{1.602 \times 10^{-19} \text{ A} \cdot \text{s}}{4\pi \times 8.85 \times 10^{-12} \text{ A} \cdot \text{s}/(\text{V} \cdot \text{m})}} \sqrt{\mathcal{E}} \\ &= -(e\sqrt{0.144 \times 10^{-8} \text{ V} \cdot \text{m}}) \sqrt{\mathcal{E}} = \alpha \sqrt{\mathcal{E}}. \end{aligned} \quad (1.275)$$

According to (1.275) the magnitude of the Schottky work function reduction $e\Delta\phi$ is proportional to $\sqrt{\mathcal{E}}$, the square root of the external electric field \mathcal{E} , and the proportionality constant α is equal to $-e\sqrt{0.144 \times 10^{-8} \text{ V} \cdot \text{m}}$.

(c) To calculate to magnitude of the external field required to reduce the work function of tungsten by 1 % we use (1.275) with $e\Delta\phi = -0.01 \times (4.52 \text{ eV}) = -0.0452 \text{ eV}$. Rearranging (1.275) we get

$$\mathcal{E} = \frac{(e\Delta\phi)^2}{e^2(0.144 \times 10^{-8} \text{ V} \cdot \text{m})} = \frac{(-0.0452 \text{ eV})^2}{e^2(0.144 \times 10^{-8} \text{ V} \cdot \text{m})} = 3.14 \times 10^7 \text{ V/m}. \quad (1.276)$$

Thus, it takes a very strong external electric field \mathcal{E} to reduce the work function of tungsten by a relatively small amount of 1 %.

(d) The current density j , temperature T , and work function $e\phi$ in thermionic emission are related to one another by the Richardson-Dushman equation stated in (1.268). The change in the current density Δj can be expressed in terms of the change in temperature ΔT and the change in work function $\Delta(e\phi)$ as

$$\Delta j = \frac{\partial j}{\partial T} \Delta T + \frac{\partial j}{\partial(e\phi)} \Delta(e\phi) \quad \text{or} \quad \frac{\Delta j}{j} = \frac{1}{j} \left[\frac{\partial j}{\partial T} \Delta T + \frac{\partial j}{\partial(e\phi)} \Delta(e\phi) \right], \quad (1.277)$$

where $\Delta j/j$ represents the relative change in the current density, i.e., the relative change in the number of electrons emitted from the surface of the metal.

Using the Richardson-Dushman equation (1.268) we evaluate the partial derivatives $\partial j/\partial T$ and $\partial j/\partial(e\phi)$, respectively, as

$$\frac{\partial j}{\partial T} = 2A_{\text{R}}T e^{-\frac{e\phi}{kT}} + A_{\text{R}}T^2 \left(\frac{e\phi}{kT^2} \right) e^{-\frac{e\phi}{kT}} = \frac{2kT + e\phi}{kT^2} j \quad (1.278)$$

and

$$\frac{\partial j}{\partial(e\phi)} = -A_{\text{R}}T^2 \left(\frac{1}{kT} \right) e^{-\frac{e\phi}{kT}} = -\frac{1}{kT} j. \quad (1.279)$$

Inserting (1.278) and (1.279) into (1.277) we get the following expression for the relative change $\Delta j/j$

$$\frac{\Delta j}{j} = \frac{2kT + e\phi}{kT} \left(\frac{DT}{T} \right) - \frac{e\phi}{kT} \left(\frac{eD\phi}{e\phi} \right). \quad (1.280)$$

For tungsten filament ($e\phi = 4.52$ eV) at temperature $T = 2300$ K the product kT amounts to $kT = (0.8617 \times 10^{-4} \text{ eV} \cdot \text{K}^{-1}) \times (2300 \text{ K}) = 0.1982 \text{ eV} \approx 0.2 \text{ eV}$ and the relative change in thermionic current density $\Delta j/j$ for a relative change in temperature of $\Delta T/T = 0.01$ and a relative change in the work function of $\Delta(e\phi)/e\phi = -0.01$ is from (1.280) calculated as

$$\begin{aligned} \frac{\Delta j}{j} &= \frac{2 \times (0.2 \text{ eV}) + (4.52 \text{ eV})}{0.2 \text{ eV}} \times 0.01 + \frac{(4.52 \text{ eV})}{0.2 \text{ eV}} \times 0.01 \\ &= 0.246 + 0.226 = 0.472. \end{aligned} \quad (1.281)$$

The result of (1.281) shows that at $T = 2300$ K a 1 % increase in temperature T has roughly the same effect as a 1 % decrease in tungsten work function $e\phi$ (as a result of Schottky effect), both effects working together to increase the number of electrons emitted from the surface of the tungsten metal.

1.28 Tunneling

1.28.Q1

(54)

A general model for alpha decay tunneling and alpha barrier penetration is shown schematically in Fig. 1.22 for nucleus with atomic number Z and atomic mass number A .

For the α decay of radium-226 into radon-222 with a half-life $t_{1/2}$ of 1602 years and α -particle kinetic energy E_{K} of 4.78 MeV, define, calculate or estimate the following pertinent parameters of α decay:

- (a) R_{sep} ; (b) $D_{\text{C}}(r)$; (c) $U(R_{\text{sep}})$; (d) $D_{\alpha\text{-N}}$; (e) w ; (f) v_{α} ; (g) t_0 , and (h) ν
 (i) Summarize your calculated answers in a figure similar to Fig. 1.22.

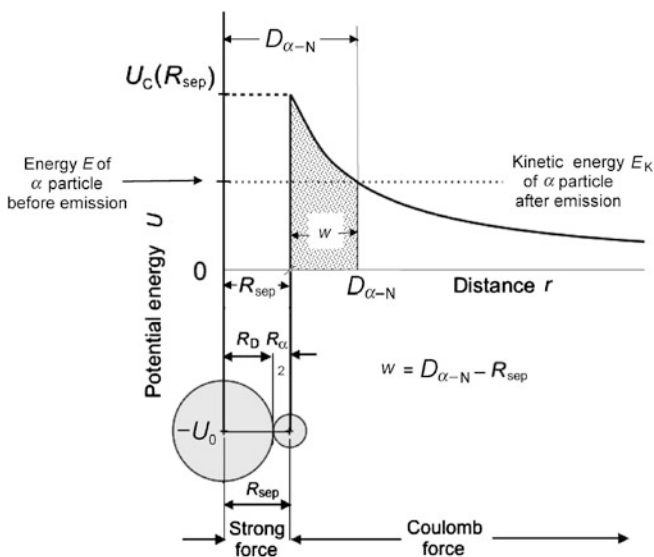


Fig. 1.22 Schematic representation of parameters in alpha decay tunneling

SOLUTION:

The parameters of α decay are defined as follows:

- R_{sep} is the separation distance between the centers of the daughter nucleus D with radius R_{A-4} and the α particle with radius R_α when they are just touching one another.
- $U(r)$ is the Coulomb repulsion potential between the daughter nucleus D and the α particle as a function of distance r for $r \geq R_{\text{sep}}$.
- $U(R_{\text{sep}})$ is the Coulomb repulsion potential between daughter nucleus D and α particle at distance $r = R_{\text{sep}}$.
- $D_{\alpha-N}$ is the distance r at which the Coulomb potential $U(r)$ equals the kinetic energy of the emitted α -particle, i.e., $U(r_0) = E_K(\alpha)$.
- w is the width of the barrier at the level $U(r_0)$.
- v_α is the velocity of the α -particle with kinetic energy E_K .
- \bar{t}_α is the mean time for traversal of a nucleus by α particle.
- ν_α is the frequency of the α particle hitting the barrier wall inside the nucleus.

- (a) Separation distance R_{sep} between $^{222}_{86}\text{Rn}$ nucleus and α particle, is determined with the standard relationship between the nuclear radius R and atomic mass number A given as $R(A) = R_0 \sqrt[3]{A}$, where R_0 is the nuclear radius constant (1.25 fm)

$$\begin{aligned}
 R_{\text{sep}} &= R_D + R_\alpha = R_0(\sqrt[3]{A-4} + \sqrt[3]{A_\alpha}) = (1.25 \text{ fm}) \times (\sqrt[3]{222} + \sqrt[3]{4}) \\
 &= 7.57 \text{ fm} + 1.98 \text{ fm} = 9.55 \text{ fm}.
 \end{aligned}
 \tag{1.282}$$

- (b) Coulomb potential energy $U_C(r)$ between the daughter nucleus D and the α particle is

$$U_C(r) = \frac{2(Z-2)e^2}{4\pi\epsilon_0 r}. \quad (1.283)$$

- (c) Height $U_C(R_{\text{sep}})$ of the Coulomb barrier $U_C(r)$ at $r = R_{\text{sep}}$ is given as

$$\begin{aligned} U_C(R_{\text{sep}}) &= \frac{2(Z-2)e^2}{4\pi\epsilon_0 R_{\text{sep}}} \\ &= \frac{2 \times 86e \times (1.602 \times 10^{-19} \text{ A} \cdot \text{s})}{4\pi \times (8.85 \times 10^{-12} \text{ A} \cdot \text{s} \cdot \text{V}^{-1} \cdot \text{m}^{-1}) \times (9.6 \times 10^{-15} \text{ m})} \\ &= 25.81 \text{ MeV}. \end{aligned} \quad (1.284)$$

- (d) Distance $D_{\alpha-N}$ is the distance at which the Coulomb potential $U_C(r)$ equals the kinetic energy E_K attained by the α particle at very large distance from the nucleus. In α -particle scattering this distance is known as the distance of closest approach in a head-on collision between the α particle and the nucleus. For a nucleus with atomic number $Z-2$ distance $D_{\alpha-N}$ is expressed as follows

$$\begin{aligned} D_{\alpha-N} &= \frac{2(Z-2)e^2}{4\pi\epsilon_0 E_K} \\ &= \frac{2 \times 86e \times (1.602 \times 10^{-19} \text{ A} \cdot \text{s})}{4\pi \times (8.85 \times 10^{-12} \text{ A} \cdot \text{s} \cdot \text{V}^{-1} \cdot \text{m}^{-1}) \times (4.78 \times 10^6 \text{ eV})} \\ &= 5.2 \times 10^{-14} \text{ m} = 52 \text{ fm}. \end{aligned} \quad (1.285)$$

- (e) Width w of the potential barrier at $U_C(r_0) = E_K$ is

$$w = D_{\alpha-N} - R_{\text{sep}} = 52 \text{ fm} - 9.6 \text{ fm} = 42.4 \text{ fm}. \quad (1.286)$$

- (f) Velocity v_α of the α particle is calculated using the relativistic expression (T1.58) and (T2.7) to get

$$\begin{aligned} v_\alpha &= c \sqrt{1 - \frac{1}{(1 + \frac{E_K}{m_\alpha c^2})^2}} = c \sqrt{1 - \frac{1}{(1 + \frac{4.78 \text{ MeV}}{3727 \text{ MeV}})^2}} = 0.05c \\ &= 1.52 \times 10^7 \text{ m/s}, \end{aligned} \quad (1.287)$$

where $m_\alpha c^2$ is the rest energy of the α particle (3727.3 MeV).

- (g) Average time \bar{t}_α for the α particle to traverse the nucleus

$$\bar{t}_\alpha = \frac{2R_{\text{sep}}}{v_\alpha} = \frac{2 \times (9.55 \times 10^{-15} \text{ m})}{1.52 \times 10^7 \text{ m/s}} = 1.26 \times 10^{-21} \text{ s}. \quad (1.288)$$

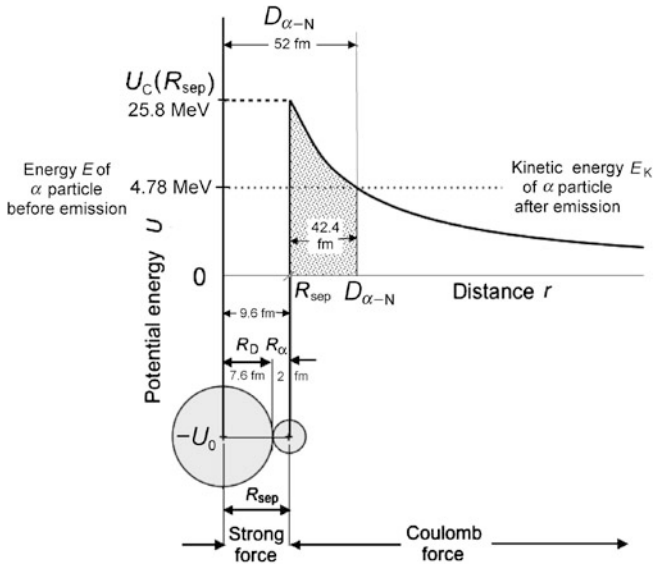


Fig. 1.23 Summary of results for tunneling of alpha particles in alpha decay of radium-226 into radon-222 (a) Separation distance: $R_{\text{sep}} = 9.6 \text{ fm}$; (b) Coulomb potential energy: $U_C(r) = 2(Z - 2)e^2/(4\pi\epsilon_0 r)$; (c) Height of Coulomb barrier at separation distance: $U_C(R_{\text{sep}}) = 25.8 \text{ MeV}$; (d) Distance $D_{\alpha-N}$ at which Coulomb potential equals kinetic energy of α particle: $D_{\alpha-N} = 52 \text{ fm}$; (e) Width w of the potential barrier at the level of tunneling: $w = 42.4 \text{ fm}$; (f) Velocity v_α of the α particle: $v_\alpha = 0.05c$; (g) Mean time \bar{t}_α for the α particle to traverse the nucleus: $\bar{t}_\alpha = 1.3 \times 10^{-21} \text{ s}$; and (h) Frequency ν_α of α particle hitting the potential barrier: $\nu_\alpha = 8 \times 10^{20} \text{ s}^{-1}$

(h) Frequency ν_α of hitting the potential barrier wall inside the nucleus

$$\nu_\alpha = \frac{1}{t_0} = \frac{v}{2R_{\text{sep}}} = \frac{1.52 \times 10^7 \text{ m} \cdot \text{s}^{-1}}{2 \times 9.55 \times 10^{-15} \text{ m}} = 7.96 \times 10^{20} \text{ s}^{-1}. \quad (1.289)$$

(i) Summary of results (a) through (h) is given in Fig. 1.23.

1.28.Q2

(55)

In classical physics, a particle striking a potential barrier will only be repelled by the barrier; in quantum physics, however, the particle striking a potential barrier may be repelled by the barrier or transmitted through the barrier in a peculiar phenomenon referred to as quantum tunneling.

The tunneling transmission factor T is used to describe the probability of a particle tunneling through a potential barrier. It is given as the ratio of the

transmitted probability current density j_{trans} to the incident probability current density j_{inc} and approximated as

$$T = \frac{j_{\text{trans}}}{j_{\text{inc}}} \approx \exp \left\{ -\frac{2\sqrt{2m}}{\hbar} \int_a^b \sqrt{U(z) - E} dz \right\}, \quad (1.290)$$

where E , m , and $U(z)$ are the particle energy, particle mass, and barrier potential, respectively, and the integration limits a and b represent the classical limits of the potential barrier. Inside the barrier the following condition applies: $E < U(z)$.

The barrier transmission coefficient T_α for α decay is given by the Gamow expression

$$\ln T_\alpha = -4\pi(Z-2)\sqrt{\frac{E_G}{E_K}} + 8\sqrt{\frac{(Z-2)R_{\text{sep}}}{a_G}}, \quad (1.291)$$

where

$$a_G = \frac{4\pi\epsilon_0}{e^2} \frac{\hbar^2 c^2}{m_\alpha c^2} = 7.256 \text{ fm}$$

and

$$E_G = \frac{1}{2} \left(\frac{e^2}{4\pi\epsilon_0} \right)^2 \frac{m_\alpha c^2}{\hbar^2 c^2} = 0.09927 \text{ MeV}.$$

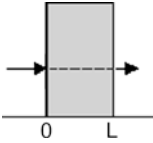
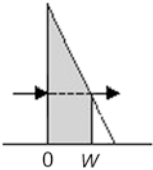
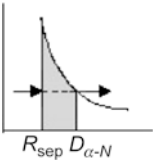
-
- (a) List and sketch at least three examples of a quantum potential barrier, provide expressions for $U(z)$ for each barrier, and state the classical limit a and b for each barrier.
- (b) Use the general approximation for potential barrier transmission coefficient T given as

$$T = \exp \left\{ -\frac{2\sqrt{2m_\alpha}}{\hbar} \int \sqrt{U(z) - E} dz \right\} \quad (1.292)$$

to derive the general expression for the Gamow potential barrier transmission coefficient T_α in α decay. General parameters of α decay of importance to calculation of the barrier transmission factor are given in Fig. 1.22.

- (c) Use (1.291) to calculate potential barrier transmission coefficient T_α for radium-226 (Ra-226) α decay into radon-222 (Rn-222). Relevant parameters for Ra-226 α decay were determined in Prob. 54.
- (d) Use T_α determined in (b) to calculate the decay constant λ and half-life $t_{1/2}$ for α decay of Ra-226.

Table 1.20 Various tunneling phenomena in physics with their associated charged particle, functional shape of potential energy, and classical limits

Tunneling potential	Tunneling particle	Potential diagram	Potential $U(z)$	Classical limits a and b
Square potential	Arbitrary charge q		$U(z) = qV$ constant (1.293)	0 and L
Field emission	Electron charge e		$U(z) = eEz$ linear (1.294)	0 and w
Alpha decay	Alpha particle charge $2e$		$U(z) = \frac{2(Z-2)e^2}{4\pi\epsilon_0 z}$ (1.295)	R_{sep} and r_0 [see Prob. 54(b)]

SOLUTION:

(a) Examples of quantum potential barrier are provided in Table 1.20 that provides for each example the tunneling particle, sketch of the potential barrier, mathematical expression for the potential barrier, and classical limits for each barrier function.

(b) The transmission coefficient T_α for α -particle tunneling through the nuclear potential barrier is approximated with the so-called Gamow formula as follows (see Prob. 54)

$$\begin{aligned} \ln T_\alpha &\approx -\frac{2\sqrt{2m_\alpha c^2}}{\hbar c} \int_{R_{\text{sep}}}^{D_{\alpha-N}} \sqrt{\left(\frac{2(Z-2)e^2}{4\pi\epsilon_0 r} - E_K\right)} dr \\ &= -\frac{2\sqrt{2m_\alpha c^2 E_K}}{\hbar c} \int_{R_{\text{sep}}}^{D_{\alpha-N}} \sqrt{\left(\frac{D_{\alpha-N}}{r} - 1\right)} dr, \end{aligned} \tag{1.296}$$

where Z is the atomic number of the parent nucleus and $m_\alpha c^2$ is the rest energy of the α particle (3727.3 MeV).

As indicated in Fig. 1.23, the two classical distances which set the upper and lower limit in the barrier transmission integral are: $D_{\alpha-N}$, the distance of closest approach in head-on collision α -particle scattering on daughter nucleus with atomic number $(Z - 2)$ and R_{sep} , the separation between the daughter nucleus and the α -particle when the two nuclei are just touching each other. $D_{\alpha-N}$ is given as: $D_{\alpha-N} = 2(Z - 2)e^2 / (4\pi\epsilon_0 E_K)$ with E_K the kinetic energy of the α particle.

To simplify the integral in (1.296) we now introduce a new variable: $u = r/D_{\alpha-N}$, recognize that $dr = D_{\alpha-N} du$ and get

$$\ln T_{\alpha} = -\frac{2\sqrt{2m_{\alpha}c^2 E_K}}{\hbar c} D_{\alpha-N} \int_{R_{\text{sep}}/D_{\alpha-N}}^1 \sqrt{\left(\frac{1}{u} - 1\right)} du. \quad (1.297)$$

To solve the integral in (1.297) we introduce the following new variable $u = \sin^2 \theta$, recognize that $du = 2 \sin \theta \cos \theta d\theta$, and obtain the following solution

$$\int_{R_{\text{sep}}/D_{\alpha-N}}^1 \sqrt{\left(\frac{1}{u} - 1\right)} du = 2 \int_{\sqrt{R_{\text{sep}}/D_{\alpha-N}}}^{\pi/2} \cos^2 \theta d\theta = [\sin \theta \cos \theta + \theta]_{\sqrt{R_{\text{sep}}/D_{\alpha-N}}}^{\pi/2}, \quad (1.298)$$

with the upper integration limit equal to $\frac{1}{2}\pi$ and the lower integration limit approximated to read $\sqrt{R_{\text{sep}}/D_{\alpha-N}}$ based on an assumption that $R_{\text{sep}}/D_{\alpha-N}$ is very small, allowing the use of the approximation $\sin \theta \approx \theta$.

Inserting the upper and lower integration limits into (1.298) we get the following solution

$$\int_{R_{\text{sep}}/D_{\alpha-N}}^1 \sqrt{\left(\frac{1}{u} - 1\right)} du = \{\sin \theta \cos \theta + \theta\}_{\sqrt{R_{\text{sep}}/D_{\alpha-N}}}^{\pi/2} = \frac{\pi}{2} - 2\sqrt{\frac{R_{\text{sep}}}{D_{\alpha-N}}}. \quad (1.299)$$

Inserting (1.299) into (1.297) results in the following general expression for transmission of the nuclear potential barrier in α decay

$$\begin{aligned} \ln T_{\alpha} &= -\frac{2\sqrt{2m_{\alpha}c^2 E_K}}{\hbar c} D_{\alpha-N} \left(\frac{\pi}{2} - 2\sqrt{\frac{R_{\text{sep}}}{D_{\alpha-N}}} \right) \\ &= -4\pi(Z-2) \sqrt{\frac{1}{2} \left(\frac{e^2}{4\pi\epsilon_0} \right)^2 \frac{m_{\alpha}c^2}{E_K}} + 8\sqrt{\frac{m_{\alpha}c^2}{\hbar^2 c^2} \frac{e^2}{4\pi\epsilon_0} (Z-2) R_{\text{sep}}} \\ &= -4\pi(Z-2) \sqrt{\frac{E_G}{E_K}} + 8\sqrt{\frac{(Z-2)R_{\text{sep}}}{a_G}}, \end{aligned} \quad (1.300)$$

where we introduced two constants: a_G and E_G relevant to α decay. The two constants are modeled after the well-known atomic constants: the Bohr radius constant $a_0 = 0.5292 \text{ \AA}$ and the Rydberg energy $E_R = 13.61 \text{ eV}$, except that the electron mass m_e in the Bohr radius constant and in the Rydberg energy is replaced by the mass of the α particle m_{α} . The two nuclear constants are thus expressed as follows

$$a_G = \frac{4\pi\epsilon_0}{e^2} \frac{\hbar^2 c^2}{m_{\alpha}c^2} = a_0 \frac{m_e c^2}{m_{\alpha}c^2} = (0.5292 \text{ \AA}) \times \frac{0.511}{3727} = 7.256 \text{ fm} \quad (1.301)$$

and

$$E_G = \frac{1}{2} \left(\frac{e^2}{4\pi\epsilon_0} \right)^2 \frac{m_\alpha c^2}{\hbar^2 c^2} = E_R \frac{m_\alpha c^2}{m_e c^2} = (13.61 \text{ eV}) \times \frac{3727.3}{0.511} = 0.09927 \text{ MeV}. \quad (1.302)$$

(c) From Prob. 54 we get the following relevant parameters for the radium-226 decay: $Z = 88$, $E_K = 4.78 \text{ MeV}$ and $R_{\text{sep}} = 9.55 \text{ fm}$. Inserting these parameters into the general expression for T_α results in the following barrier transmission factor T_α for Ra-226 α decay

$$\begin{aligned} T_\alpha &= \exp \left\{ -4\pi \times 86 \sqrt{\frac{0.09927 \text{ MeV}}{4.78 \text{ MeV}}} + 8 \sqrt{86 \frac{9.55 \text{ fm}}{7.256 \text{ fm}}} \right\} \\ &= \exp\{-155.74 + 85.1\} = 2.1 \times 10^{-31}. \end{aligned} \quad (1.303)$$

(d) The barrier transmission coefficient T_α is the probability for the α particle to tunnel through the potential barrier upon striking the barrier. In Prob. 54 we calculated the frequency (repetition rate) ν_α of the α particle striking the potential barrier and obtained $\nu_\alpha = 7.96 \times 10^{20} \text{ s}^{-1}$ for the α decay of Ra-226. The α decay constant λ_α of Ra-226 can be expressed as the product of the barrier transmission coefficient T_α as well as the repetition rate ν_α and the half-life $t_{1/2}$ is then given as

$$t_{1/2} = \frac{\ln 2}{\lambda_\alpha} = \frac{\ln 2}{T_\alpha \nu_\alpha} = \frac{\ln 2}{(2.1 \times 10^{-31}) \times (7.96 \times 10^{20} \text{ s}^{-1})} = 4.15 \times 10^9 \text{ s} = 131.5 \text{ a}. \quad (1.304)$$

This result is more than an order of magnitude smaller than the measured half-life of 1602 years for radium-226. However, the estimate is satisfactory, considering the series of approximations that were involved in the derivation of the tunneling transmission coefficient T_α . Moreover, T_α depends heavily on kinetic energy E_K of the α particle as well as on the initial separation R_{sep} between the α particle and the daughter nucleus and a minute change in one or both of these parameters results in a large change in T_α , since both parameters appear in the exponential.

1.28.Q3

(56)

Thermionic emission (TE) and field emission (FE) are physical phenomena of importance not only in theoretical physics but also in practical production of x rays.

- (a) In point form compare thermionic emission (TE) from a metal with field emission (FE) from a metal.
- (b) Provide schematic diagrams for potential energy of electron against its distance from metal surface for thermionic emission and field emission.

SOLUTION:

(a) In both the thermionic emission (TE) and field emission (FE) electrons are emitted from the surface of a metal. On a microscopic scale, however, the two effects are different:

- (1) In TE electrons surmount the potential barrier, while in FE electrons tunnel through the potential barrier.
- (2) In TE the temperature T of the metal increases the energy of electrons to allow them to surmount the potential barrier; in FE a strong external electric field \mathcal{E} narrows the potential barrier to make the tunneling of electrons through the barrier possible.
- (3) In TE the work function remains constant with temperature but the kinetic energy of electrons rises with metal temperature, allowing electrons to escape from the metal. In FE the barrier thickness diminishes with an increasing applied electric field, making it easier for electrons to tunnel through the barrier.
- (4) The higher the temperature T of the metal, the stronger is the emission of electrons in TE; the stronger is the external electric field \mathcal{E} , the stronger is the emission of electrons in FE.
- (5) TE is of importance in the fields of electronics and communications in general. In medical physics TE plays an important role in hot cathode x-ray tubes (Coolidge tubes) and electron guns in linear accelerators. FE shows promise in the development of cold cathode x-ray tubes.
- (6) The form of the functional dependence of electron current density j on T in TE is the same as that on \mathcal{E} in FE.
- (7) In TE the electron current density $j(T)$ is expressed by the Richardson-Dushman equation as follows

$$j_{\text{RD}}(T) = A_{\text{R}} T^2 e^{-\frac{e\phi}{kT}}, \quad (1.305)$$

where A_{R} is the Richardson constant of the electron-emitting metal; k is the Boltzmann constant; and $e\phi$ is the work function of the metal (of the order of 2 eV to 5 eV). The Richardson-Dushman plot of Arrhenius diagram requires plotting $\ln(j/T^2)$ against $1/T$ and results in a straight line with slope $e\phi/k$ allowing determination of the work function $e\phi$ and ordinate intercept $\ln A$ allowing determination of the Richardson constant A .

- (8) In FE the electron current density $j(\mathcal{E})$ is expressed by the Fowler-Nordheim equation as follows

$$j_{\text{FN}}(\mathcal{E}) = \alpha \mathcal{E}^2 e^{-\frac{\beta}{\mathcal{E}}}, \quad (1.306)$$

where α and β are constants specific to the metallic electron emitter. The Fowler-Nordheim plot of Arrhenius diagram requires plotting $\ln(j/\mathcal{E}^2)$ against $1/\mathcal{E}$ and results in a straight line with slope β and ordinate intercept $\ln \alpha$ allowing determination of α .

- (9) FE is in principle similar to the Schottky effect; however, it is generally accepted that Schottky effect influences electron emission from metallic surfaces

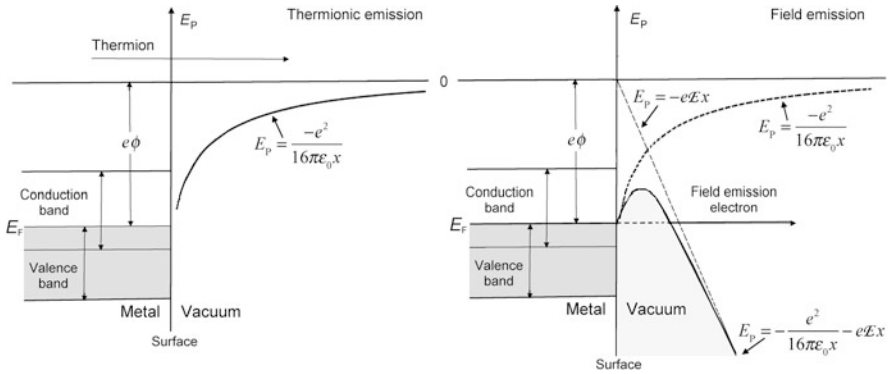


Fig. 1.24 Schematic diagram for thermionic emission (TE) on the left and field emission (TE) tunneling of electrons through the surface potential barrier on the right

at relatively low electric fields and field emission deals with extremely high electric fields.

(b) Schematic diagrams for potential energy E_p of electron against its distance from surface of the metal emitter for thermionic emission (left side) and field emission (right side) are depicted in Fig. 1.24.

1.29 Maxwell Equations

1.29.Q1

(57)

All electromagnetic phenomena are governed by Maxwell equations which form a set of four partial differential equations that are invariant with respect to Lorentz transformation (see Prob. 26) and relate the electric field \mathcal{E} as well as the magnetic field \mathcal{B} to their source: the charge density ρ and current density \mathbf{j} , respectively.

- (a) State the four Maxwell equations for vacuum in the differential form and in the integral form. Define the physical quantities pertaining to each of the four Maxwell equations and state their units in the SI system. For each of the four equations, in addition to Maxwell, give the name of the physicist who is associated with the given equation.
- (b) State the two theorems that link the Maxwell equations in the differential form with Maxwell equations in the integral form and indicate how the two theorems are used to modify the Maxwell equations from the differential into integral form.
- (c) Modify the general Maxwell equations in (a) for use in evacuated waveguides.

SOLUTION:

(a) The four general Maxwell equations are as follows:

Table 1.21 The four general Maxwell equations in differential and integral form

Equation	Differential form	Integral form	
1 Maxwell <i>Gauss law for electricity</i>	$\nabla \cdot \mathbf{E} = \frac{\rho}{\epsilon_0}$	$\oiint_S \mathbf{E} \cdot d\mathbf{S} = \frac{q}{\epsilon_0}$	(1.307)
2 Maxwell <i>Gauss law for magnetism</i>	$\nabla \cdot \mathbf{B} = 0$	$\oiint_S \mathbf{B} \cdot d\mathbf{S} = 0$	(1.308)
3 Maxwell <i>Faraday law of induction</i>	$\nabla \times \mathbf{E} = -\frac{\partial \mathbf{B}}{\partial t}$	$\oint \mathbf{E} \cdot d\boldsymbol{\ell} = -\frac{\partial}{\partial t} \iint \mathbf{B} \cdot d\mathbf{S}$	(1.309)
4 Maxwell <i>Ampère law</i> extended by Maxwell	$\nabla \times \mathbf{B} = \mu_0 \mathbf{j} + \frac{1}{c^2} \frac{\partial \mathbf{E}}{\partial t}$	$\oint \mathbf{B} \cdot d\boldsymbol{\ell} = \mu_0 I + \frac{1}{c^2} \frac{\partial}{\partial t} \iint \mathbf{E} \cdot d\mathbf{S}$	(1.310)

where

\mathcal{E} is electric field in V/m.

\mathcal{B} is magnetic field in tesla (1 T = 1 V · s/m²).

ρ is total charge density in C/m³.

q is total charge in volume \mathcal{V} given in C.

\mathbf{j} is current density in A/m².

I is current in A.

$d\mathbf{S}$ is differential vector element of surface area S with direction normal to the surface.

$d\boldsymbol{\ell}$ is differential vector element of path length tangential to the path.

ϵ_0 is the electric constant (8.85×10^{-12} A · s · V⁻¹ · m⁻¹).

μ_0 is the magnetic constant ($4\pi \times 10^{-7}$ V · s · A⁻¹ · m⁻¹).

(b) The two theorems are the Stokes-Kelvin curl theorem and the Gauss-Ostrogradski divergence theorem:

Stokes-Kelvin curl theorem:

$$\iint_S (\nabla \times \mathbf{A}) \cdot d\mathbf{S} = \iint_S \text{curl } \mathbf{A} \cdot d\mathbf{S} = \oint_{\ell} \mathbf{A} \cdot d\boldsymbol{\ell} \quad (1.311)$$

relates the surface integral of the curl ($\nabla \times$) of a vector field \mathbf{A} over surface S to the closed loop line integral of the vector field \mathbf{A} over the boundary of the surface S given by closed loop ℓ .

Gauss-Ostrogradski divergence theorem:

$$\iiint_{\mathcal{V}} \nabla \cdot \mathbf{A} d\mathcal{V} = \iiint_{\mathcal{V}} \text{div } \mathbf{A} d\mathcal{V} = \oiint_S \mathbf{A} \cdot d\mathbf{S} \quad (1.312)$$

relates the volume integral of the divergence ($\nabla \cdot$) of a vector field \mathbf{A} over volume \mathcal{V} to the closed surface integral of the vector field \mathbf{A} over the boundary of the volume \mathcal{V} given by closed surface S .

Maxwell equation #1 ($\nabla \cdot \mathbf{E} = \rho/\epsilon_0$) is also known as the *Gauss law of electrostatics* and can be expressed in integral form through application of the Gauss divergence theorem as follows

$$\iiint_{\mathcal{V}} \nabla \cdot \mathbf{E} \, d\mathcal{V} = \oiint_S \mathbf{E} \cdot d\mathbf{S} = \frac{1}{\epsilon_0} \iiint_{\mathcal{V}} \rho \, d\mathcal{V} = \frac{q}{\epsilon_0}. \quad (1.313)$$

The Gauss law states that the electric flux $\oiint_S \mathbf{E} \cdot d\mathbf{S}$ through any closed surface S is proportional to the total charge q enclosed in volume \mathcal{V} by the closed surface S .

Maxwell equation #2 ($\nabla \cdot \mathbf{B} = 0$) is also known as the *Gauss law of magnetism* and can be expressed in integral form through application of the Gauss divergence theorem

$$\iiint_{\mathcal{V}} \nabla \cdot \mathbf{B} \, d\mathcal{V} = \oiint_S \mathbf{B} \cdot d\mathbf{S} = 0. \quad (1.314)$$

The Gauss law states that the magnetic flux $\oiint_S \mathbf{B} \cdot d\mathbf{S}$ through any closed surface S is equal to zero implying that there are no magnetic monopoles.

Maxwell equation #3 ($\nabla \times \mathbf{E} = -\partial \mathbf{B} / \partial t$) is also known as the *Faraday law of induction*. It can be expressed in integral form through application of the Stokes curl theorem

$$\iint_S (\nabla \times \mathbf{E}) \cdot d\mathbf{S} = \oint_{\ell} \mathbf{E} \cdot d\boldsymbol{\ell} = -\frac{\partial}{\partial t} \iint_S \mathbf{B} \cdot d\mathbf{S} = -\frac{\partial \phi_B}{\partial t} = U_{\text{ind}}, \quad (1.315)$$

where $\phi_B = \iint_S \mathbf{B} \cdot d\mathbf{S}$ is the magnetic flux and U_{ind} is the induced voltage.

The Faraday law of induction states that the line integral of the electric field \mathcal{E} over a closed loop ℓ is equal to the negative of the rate of change of the magnetic flux ϕ_B through the area enclosed by the closed loop ℓ .

Maxwell equation #4 ($\nabla \times \mathbf{B} = \mu_0 \mathbf{j} + c^{-2} \partial \mathbf{E} / \partial t$) is also known as the *Ampère law* extended by Maxwell. It can be expressed in integral form through application of the Stokes curl theorem

$$\iint_S (\nabla \times \mathbf{B}) \cdot d\mathbf{S} = \oint_{\ell} \mathbf{B} \cdot d\boldsymbol{\ell} = \mu_0 \iint_S \mathbf{j} \cdot d\mathbf{S} + \frac{1}{c^2} \frac{\partial}{\partial t} \iint_S \mathbf{E} \cdot d\mathbf{S} = \mu_0 I + \frac{1}{c^2} \frac{\partial \phi_E}{\partial t}, \quad (1.316)$$

where $\phi_E = \iint_S \mathbf{E} \cdot d\mathbf{S}$ is the electric flux and I is the current.

The Ampère law states that the line integral of the magnetic field \mathcal{B} over a closed loop ℓ is equal to sum of the net free current $I = \iint_S \mathbf{j} \cdot d\mathbf{S}$ passing through the surface enclosed by the closed loop ℓ and the rate of change of the electric flux ϕ_E through the same surface.

(c) Based on Maxwell equations in (a) above and assuming that there are no electric currents or charges present in vacuum, Maxwell equations are simplified to read, as shown in Table 1.17.

Table 1.22 The four Maxwell equations for free space in differential and integral form

Equation	Differential form	Integral form	
1 Maxwell <i>Gauss law for electricity</i>	$\nabla \cdot \mathbf{E} = 0$	$\oiint_S \mathbf{E} \cdot d\mathbf{S} = 0$	(1.317)
2 Maxwell <i>Gauss law for magnetism</i>	$\nabla \cdot \mathbf{B} = 0$	$\oiint_S \mathbf{B} \cdot d\mathbf{S} = 0$	(1.318)
3 Maxwell <i>Faraday law of induction</i>	$\nabla \times \mathbf{E} = -\frac{\partial \mathbf{B}}{\partial t}$	$\oint_{\ell} \mathbf{E} \cdot d\boldsymbol{\ell} = -\frac{\partial}{\partial t} \iint_S \mathbf{B} \cdot d\mathbf{S} = -\frac{\partial \Phi_M}{\partial t}$	(1.319)
4 Maxwell <i>Ampère law</i> extended by Maxwell	$\nabla \times \mathbf{B} = \frac{1}{c^2} \frac{\partial \mathbf{E}}{\partial t}$	$\oint_{\ell} \mathbf{B} \cdot d\boldsymbol{\ell} = \frac{1}{c^2} \frac{\partial}{\partial t} \iint_S \mathbf{E} \cdot d\mathbf{S} = \frac{1}{c^2} \frac{\partial \Phi_E}{\partial t}$	(1.320)

1.30 Poynting Theorem and Poynting Vector

1.30.Q1

(58)

In 1884 English physicist John Henry Poynting used the Lorentz equation for a moving charge in an electromagnetic (EM) field and Maxwell equations for electromagnetism to derive a theorem that expresses the conservation of energy for EM fields. The theorem relates the rate of change of the energy u stored in the EM field and energy flow expressed by the Poynting vector \mathbf{S} . The Poynting vector \mathbf{S} points in the direction of motion of the EM wave, coincides with the direction of energy flow, and is generally expressed as

$$\mathbf{S} = \frac{\mathbf{E} \times \mathbf{B}}{\mu_0} = \varepsilon_0 c^2 \mathbf{E} \times \mathbf{B} \quad (1.321)$$

where c , the speed of light in vacuum, is given by the standard expression $c = 1/\sqrt{\varepsilon_0 \mu_0}$

- Express the Poynting vector \mathbf{S} of (1.321) for electromagnetic radiation.
- Determine the intensity I of electromagnetic radiation.
- Pressure p_{rad} that EM radiation exerts on an absorbing target.

Note: Both I and p_{rad} are related to the mean Poynting vector $\overline{|\mathbf{S}|} = \bar{S}$ of the EM radiation.

SOLUTION:

(a) The magnitude of the Poynting vector $|\mathbf{S}| = S$ equals to the power per unit area crossing a surface normal to the direction of \mathbf{S} . Electric field \mathbf{E} and magnetic field \mathbf{B} are perpendicular to one another as well as to the direction of wave propagation and expressed generically as

$$\mathbf{E} = \mathbf{E}_0 f(\mathbf{k} \cdot \mathbf{r} - \omega t) \quad \text{and} \quad \mathbf{B} = \mathbf{B}_0 f(\mathbf{k} \cdot \mathbf{r} - \omega t), \quad (1.322)$$

where

- \mathbf{k} is the wave vector in direction of wave propagation.
- ω is the angular frequency of the plane wave.
- \mathcal{E}_0 is the constant amplitude vector for the electric field \mathcal{E} .
- \mathcal{B}_0 is the constant amplitude vector for the magnetic field \mathcal{B} .

In (1.322) function f satisfies the wave equation $\nabla^2 f = c^{-2} \partial^2 f / \partial t^2$ that is derived from the four Maxwell equations for free space (see Prob. 58). For electric field \mathcal{E} and magnetic field \mathcal{B} function f is usually given as

$$\mathcal{E} = \mathcal{E}_0 e^{i(\mathbf{k} \cdot \mathbf{r} - \omega t)} \quad \text{and} \quad \mathcal{B} = \mathcal{B}_0 e^{i(\mathbf{k} \cdot \mathbf{r} - \omega t)} \quad (1.323)$$

or

$$\mathcal{E} = \mathcal{E}_0 \cos(\mathbf{k} \cdot \mathbf{r} - \omega t) \quad \text{and} \quad \mathcal{B} = \mathcal{B}_0 \cos(\mathbf{k} \cdot \mathbf{r} - \omega t). \quad (1.324)$$

The Poynting vector (1.321) can thus be expressed as follows

$$\mathbf{S} = \frac{\mathcal{E} \times \mathcal{B}}{\mu_0} = \varepsilon_0 c^2 \mathcal{E} \times \mathcal{B} = \varepsilon_0 c^2 \mathcal{E}_0 \times \mathcal{B}_0 \cos^2(\mathbf{k} \cdot \mathbf{r} - \omega t). \quad (1.325)$$

(b) In practice S varies at exceedingly large frequencies, making it more practical to use the mean value of S averaged over one period of oscillation or over a multiple integer number of periods. The mean value of S over one period is thus the mean power per unit area in the wave and is expressed as

$$\bar{S} = \overline{|\mathbf{S}|} = \varepsilon_0 c^2 |\mathcal{E}_0 \times \mathcal{B}_0| \overline{\cos^2(\mathbf{k} \cdot \mathbf{r} - \omega t)}. \quad (1.326)$$

The mean value of $\cos^2(\mathbf{k} \cdot \mathbf{r} - \omega t)$ is evaluated as follows

$$\begin{aligned} \overline{\cos^2 x} &= \frac{1}{2\pi} \int_0^{2\pi} \cos^2 x \, dx = \frac{1}{4\pi} \int_0^{2\pi} \cos 2x \, dx + \frac{1}{4\pi} \int_0^{2\pi} dx \\ &= \frac{1}{8\pi} [\sin 2x + 2x]_0^{2\pi} = \frac{1}{2}, \end{aligned} \quad (1.327)$$

providing the following expression for the mean Poynting vector $\bar{\mathbf{S}}$ that is also referred to as the EM intensity or irradiance I

$$\bar{S} = I = \frac{1}{2} \varepsilon_0 c^2 \mathcal{E}_0 \mathcal{B}_0 = \frac{1}{2} \varepsilon_0 c \mathcal{E}_0^2 = \frac{1}{2} \frac{c}{\mu_0} \mathcal{B}_0^2, \quad (1.328)$$

where we used the following equality: $\mathcal{E}_0 = c \mathcal{B}_0$. A plot of $\cos^2 x$ against x is given in Fig. 1.25 which also shows that $\overline{\cos^2 x}$ equals to 0.5 for one period or integer number of periods.

(c) Electromagnetic radiation pressure p_{rad} results from the momentum carried by radiation and is defined as the force per unit area exerted by an EM wave upon

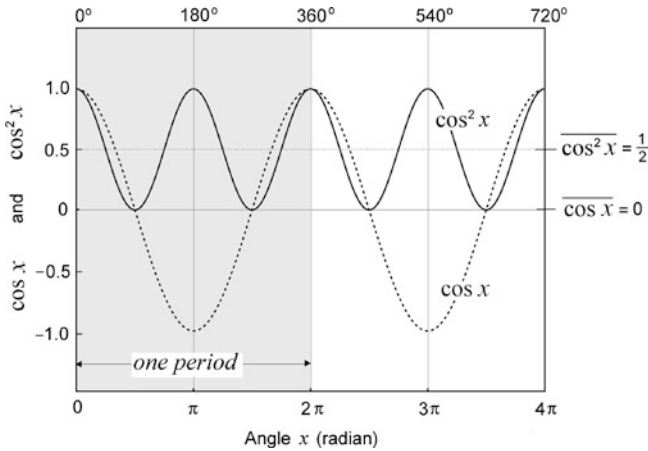


Fig. 1.25 Trigonometric functions $\cos x$ (dotted curve) and $\cos^2 x$ (solid curve) against angle x . For one period or for an integer number of periods $\overline{\cos x} = 0$ and $\overline{\cos^2 x} = 0.5$

the surface of a target exposed to EM radiation or energy per unit volume (energy density) carried by radiation. It acts in the direction of the Poynting vector \mathbf{S} .

Since the mean Poynting vector \bar{S} is the mean power per unit area A in the wave, we can say that the power P in the wave is $P = \bar{S}A$ and the force F of the wave when it hits a target is power P over velocity c of the wave, i.e., $F = \bar{S}A/c$. Therefore, the radiation pressure p_{rad} is given as

$$p_{\text{rad}} = \frac{F}{A} = \frac{\bar{S}}{c} \tag{1.329}$$

when the target fully absorbs the incident radiation and $p_{\text{rad}} = 2\bar{S}/c$ when the target fully reflects the incident radiation. Radiation pressure is thus proportional to the EM intensity I (mean Poynting vector \bar{S}) and inversely proportional to the speed of light c in vacuum

$$p_{\text{rad}} = \frac{I}{c} = \frac{1}{2} \epsilon_0 E_0^2 = \frac{1}{2\mu_0} B_0^2. \tag{1.330}$$

1.31 Normal Probability Distribution

1.31.Q1

(59)

Random variation in natural processes most commonly follows the probability distribution generally known in mathematics as the normal probability distribution but also referred to as Gaussian distribution in physics and “bell

curve” in social science. The function describing the normal distribution has a long tradition in mathematics and physics. De Moivre used it in 18th century as an approximation to the binomial distribution, Laplace used it to study measurement errors, and Gauss used it in his analysis of astronomical data.

For the probability density function

$$P(x) = \frac{1}{\sigma\sqrt{2\pi}} e^{-\frac{x^2}{2\sigma^2}}, \quad (1.331)$$

with the mean value $\bar{x} = 0$ (also referred to as the expectation value $\bar{x} = 0$) and for the following values of standard deviation $\sigma = 0.5; 1; 2; 3; 5; \text{ and } 10$:

- (a) Plot $P(x)$ for the following values of σ : 0.5; 1; 2; 3; 5; and 10.
- (b) Show that $\int_{-\infty}^{\infty} P(x) dx = 1$ for all σ .
- (c) Determine $P(0)$ as a function of σ .
- (d) Determine $P(\sigma)$ as a function of σ .
- (e) Determine the general expression for the full-width-at-half-maximum (FWHM) as a function of σ .
- (f) Summarize your results of (a) through (e) in Table 1.23A.

Table 1.23A Summary of results (a) through (e)

1	σ	0.5	1.0	2.0	3.0	5.0	10.0
2	$P(0) =$						
3	$P(\sigma) =$						
4	FWHM =						

SOLUTION:

(a) A plot of the probability density function $P(x)$ against x for various values of the standard deviation σ is given in Fig. 1.26; a plot of $\sigma P(x)$ against x/σ is shown in Fig. 1.27.

(b)

$$\begin{aligned} \int_{-\infty}^{\infty} P(x) dx &= \frac{1}{\sigma\sqrt{2\pi}} \int_{-\infty}^{\infty} e^{-\frac{x^2}{2\sigma^2}} dx = \frac{2\sigma\sqrt{2}}{\sigma\sqrt{2\pi}} \int_0^{\infty} e^{-\frac{x^2}{2\sigma^2}} \frac{dx}{\sigma\sqrt{2}} \\ &= \frac{2}{\sqrt{\pi}} \int_0^{\infty} e^{-u^2} du = \text{erf}(\infty) = 1. \end{aligned} \quad (1.332)$$

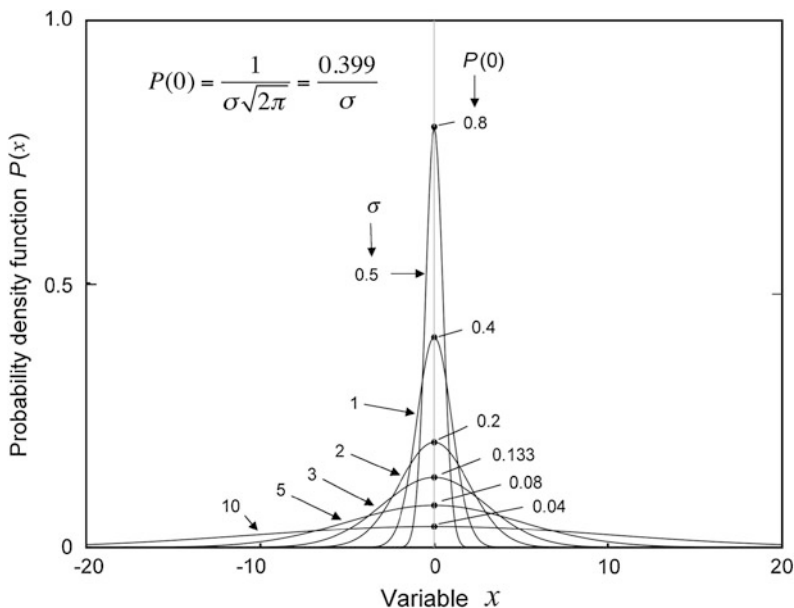


Fig. 1.26 Probability density function $P(x)$ against coordinate x for various values of the standard deviation σ in the range from $\sigma = 0.5$ to $\sigma = 10$

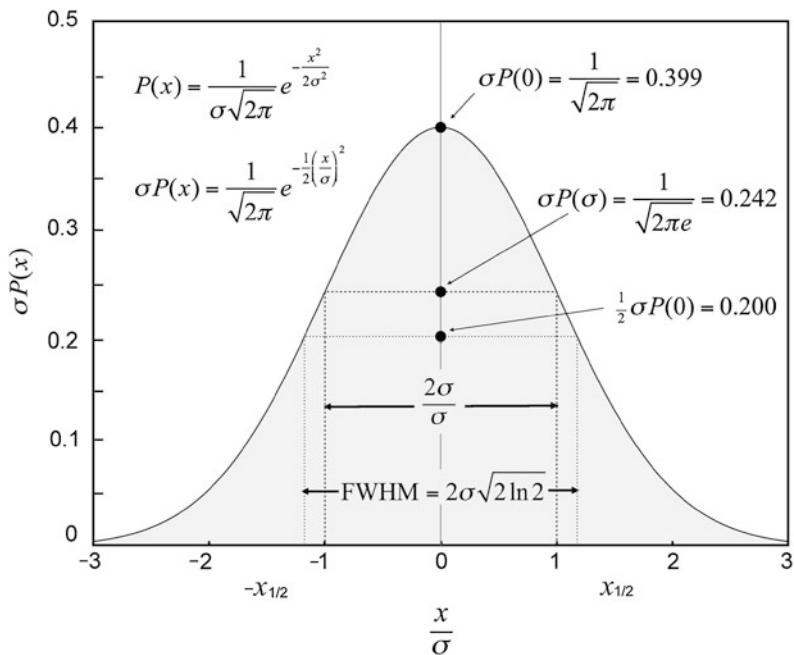


Fig. 1.27 Plot of $\sigma P(x)$, the probability density function $P(x)$ multiplied by standard deviation $P(x)$ against x/σ , the coordinate x divided by σ

Values for the error function $\operatorname{erf}(x) = \frac{2}{\sqrt{\pi}} \int_0^x e^{-u^2} du$ are available in standard mathematical tables and for $x = \infty$ we get $\operatorname{erf}(\infty) = 1$. Thus, integral $\int_{-\infty}^{\infty} P(x) dx = 1$ for all σ .

(c)

$$P(0) = \frac{1}{\sigma\sqrt{2\pi}} e^{-\frac{x^2}{2\sigma^2}} \Big|_{x=0} = \frac{1}{\sigma\sqrt{2\pi}} = \frac{0.399}{\sigma}. \tag{1.333}$$

(d)

$$\begin{aligned} P(\sigma) &= \frac{1}{\sigma\sqrt{2\pi}} e^{-\frac{x^2}{2\sigma^2}} \Big|_{x=\sigma} = \frac{1}{\sigma\sqrt{2\pi}} e^{-\frac{1}{2}} = \frac{1}{\sigma\sqrt{2\pi e}} = \frac{0.242}{\sigma} \\ &= \frac{P(0)}{\sqrt{e}} = 0.6065 P(0). \end{aligned} \tag{1.334}$$

(e) The maximum in $P(x)$ occurs at $x = 0$ and the value of $P(0)$ is given in (c) above. The full-width-at-half-maximum (FWHM) occurs at $x = \pm x_{1/2}$ where

$$P(x_{1/2}) = \frac{1}{2} P(0) = \frac{1}{2\sigma\sqrt{2\pi}} = \frac{1}{\sigma\sqrt{2\pi}} e^{-\frac{x_{1/2}^2}{2\sigma^2}} \tag{1.335}$$

or

$$\ln \frac{1}{2} = -\frac{x_{1/2}^2}{2\sigma^2} \quad \text{and} \quad x_{1/2} = \sigma\sqrt{2\ln 2} = 1.177\sigma. \tag{1.336}$$

Since by definition the full-width-at-half-maximum (FWHM) equals to $2x_{1/2}$, we get

$$\text{FWHM} = 2x_{1/2} = 2\sigma\sqrt{2\ln 2} = 2.355\sigma. \tag{1.337}$$

(f) Results of (a) through (e) are summarized in Table 1.23B.

Table 1.23B Summary table for Prob. 59

1	σ	0.5	1.0	2.0	3.0	5.0	10.0
2	$P(0) = \frac{0.399}{\sigma}$	0.800	0.400	0.200	0.133	0.080	0.040
3	$P(\sigma) = \frac{0.242}{\sigma}$	0.484	0.242	0.121	0.081	0.048	0.024
4	$\text{FWHM} = 2.355\sigma$	1.178	2.355	4.710	7.064	11.77	23.55

Chapter 2 consists of **23 problems** that cover 7 sections dealing with various types of elastic scattering interactions that heavy and light charged particles can have with atoms of an absorber. The problems address the general category of Coulomb elastic scattering covering the practical and theoretical aspects of Coulomb scattering ranging from the seminal Geiger and Marsden experiment and Rutherford theory of alpha particle scattering on metallic foils through Mott scattering of electrons on nuclei of absorber to practical aspects of Molière multiple scattering.

The concepts addressed in this chapter are of great importance to modern physics because much of the current knowledge in atomic, nuclear, and particle physics has been derived from various Coulomb scattering experiments. Based on the unexpected angular distribution of scattered alpha particles, measured by Geiger and Marsden, Rutherford in 1912 proposed the current atomic model in which the atomic mass and the positive atomic charge are concentrated in the atomic nucleus that is at least four orders of magnitude smaller than the size of the atom.

Section 2.1 covers the basic characteristics of Coulomb scattering and the problem in Sect. 2.2 deals with the Geiger–Marsden experiment and introduces a comparison between the Thomson and Rutherford model of the atom. Problems of Sect. 2.3 deal with various aspects of Rutherford scattering, while Sect. 2.4 addresses the differential and total cross sections for Rutherford scattering. The problems of Sect. 2.5 concentrate on Mott scattering of electrons on nuclei of absorber and the problems of Sect. 2.6 cover the general aspects of Coulomb elastic scattering including characteristic scattering distance, minimum and maximum scattering angle, mean square scattering angle for single scattering. The last two problems of this chapter concentrate on mass scattering power (Sect. 2.6) and root mean square scattering angle for multiple scattering (Sect. 2.7).

2.1 General Aspects of Coulomb Scattering

2.1.Q1

(60)

Coulomb scattering is a general term used to describe elastic Coulomb interaction between two charged particles: an energetic projectile and a stationary target.

- (a) In Table 2.1A provide a list of at least 5 elastic Coulomb scattering interactions and for each interaction give the projectile and the target.
- (b) Define Molière scattering.

Table 2.1A Five most common elastic Coulomb scattering interactions

	Coulomb scattering interaction	Projectile	Target
1			
2			
3			
4			
5			

SOLUTION:

(a) Five most common elastic Coulomb scattering interactions are presented in Table 2.1B.

Table 2.1B Five most common elastic Coulomb scattering interactions

	Coulomb scattering interaction	Projectile	Target
1	Rutherford scattering	Alpha particle	Nucleus
2	Ramsauer scattering	Electron (non-relativistic)	Atom or molecule
3	Mott scattering	Electron (relativistic)	Atomic nucleus
4	Møller scattering	Electron	Atomic orbital electron
5	Bhabha scattering	Positron	Atomic orbital electron

(b) Molière scattering is defined as multiple scattering involving any one of the scattering interactions listed in Table 2.1B.

2.1.Q2

(61)

Much of the information on the structure and charge distribution of nuclei has been gathered through elastic Coulomb scattering experiments.

Discuss the two most important characteristics that a particle must possess when used as nuclear probe in elastic scattering experiments.

SOLUTION:

The two most important characteristics that a particle must possess when used as nuclear probe in elastic scattering experiments are: (1) de Broglie wavelength λ of the particle and (2) charge q of the particle.

(1) The particle serving as nuclear probe must have a de Broglie wavelength λ of the order of the size of the nucleus or smaller. The radius R of the nucleus (i.e., size of the nucleus) is estimated from $R = R_0 \sqrt[3]{A}$, where R_0 is the nuclear radius constant (1.25 fm) and A is the atomic mass number of the nucleus.

The de Broglie wavelength of the nuclear probe projectile is calculated from the standard de Broglie expression $\lambda = h/p$, where p is the particle momentum derived in Prob. 34 as

$$p = \frac{E_0}{c} \beta \gamma = \frac{E_0}{c} \frac{\beta}{\sqrt{1 - \beta^2}} \quad \text{or} \quad p = \frac{1}{c} \sqrt{E^2 - E_0^2} = \frac{E_0}{c} \sqrt{1 + \frac{2E_0}{E_K}} \quad (2.1)$$

with

E total energy of the particle.

E_K kinetic energy of the particle ($E_K = E - E_0$).

E_0 rest energy of the particle.

γ Lorentz factor of the particle.

β velocity of the particle normalized to the speed of light c in vacuum.

The de Broglie wavelength of the particle is thus given as

$$\lambda = \frac{h}{p} = \frac{2\pi \hbar c}{E_0} \frac{\sqrt{1 - \beta^2}}{\beta} = \frac{2\pi \hbar c}{E_K \sqrt{1 + \frac{2E_0}{E_K}}} \quad (2.2)$$

(2) The particle serving as nuclear probe must possess charge to enable an elastic Coulomb interaction between the nuclear probe (projectile) and the nucleus (target). Charge is also important in accelerating the particle to sufficiently high kinetic energy for the de Broglie wavelength λ to become of the order of, or smaller than, the size of the nucleus.

2.1.Q3

(62)

The distance of closest approach $D_{\alpha-N}$ in a head-on collision between an α particle of kinetic energy E_K and an atomic nucleus is calculated from conservation of energy considerations whereby we equate the α particle kinetic energy E_K at large (∞) distance from the nucleus with repulsive Coulomb potential energy E_P when the α particle is at a distance $D_{\alpha-N}$ from the nucleus. $D_{\alpha-N}$ is then given as follows

$$D_{\alpha-N} = \frac{zZe^2}{4\pi\epsilon_0 E_K} = C_{\alpha-N} \frac{Z}{E_K}. \quad (2.3)$$

- (a) Determine the constant $C_{\alpha-N}$ for alpha (α) particle scattering and use it to calculate $D_{\alpha-N}$ for scattering of 5.5 MeV α particles ($z = 2$) on gold nucleus ($Z = 79$, $A = 197$).
- (b) Plot $D_{\alpha-N}$ against E_K for α particle scattering on gold nuclei in the kinetic energy E_K range from 1 MeV to 40 MeV.
- (c) Compare $D_{\alpha-N}$ of (a) with the radius R_{Au} of the gold nucleus and determine at what kinetic energy E_K would the α particle just penetrate the gold nucleus.

SOLUTION:

- (a) Constant $C_{\alpha-N}$ for α particle scattering is calculated from (2.3) as follows

$$\begin{aligned} C_{\alpha-N} &= \frac{ze^2}{4\pi\epsilon_0} = \frac{2e \times (1.602 \times 10^{-19} \text{ A} \cdot \text{s})}{4\pi \times (8.85 \times 10^{-12} \text{ A} \cdot \text{s} \cdot \text{V}^{-1} \cdot \text{m}^{-1})} = 2.88 \times 10^{-9} \text{ eV} \cdot \text{m} \\ &= 2.88 \text{ MeV} \cdot \text{fm} \end{aligned} \quad (2.4)$$

and $D_{\alpha-N}$ in terms of $C_{\alpha-N}$ for scattering of 5.5 MeV α particle on gold nucleus is given as

$$D_{\alpha-N} = C_{\alpha-N} \frac{Z}{E_K} = \frac{(2.88 \text{ MeV} \cdot \text{fm}) \times 79}{5.5 \text{ MeV}} = 41.4 \text{ fm}. \quad (2.5)$$

To see whether or not the α particle of initial kinetic energy $(E_K)_i = 5.5 \text{ MeV}$ can penetrate the gold nucleus we estimate the radius R_{Au} of the gold nucleus with the following relationship

$$R(A) = R_{Au} = R_0 \sqrt[3]{A} = (1.25 \text{ fm}) \times \sqrt[3]{197} = 7.3 \text{ fm}, \quad (2.6)$$

where R_0 is the nuclear radius constant (T1.26). Since R_{Au} of (2.6) is significantly smaller than $D_{\alpha-N}$ of (2.5), we conclude that $(E_K)_i = 5.5 \text{ MeV}$ α particle does not penetrate the gold nucleus.

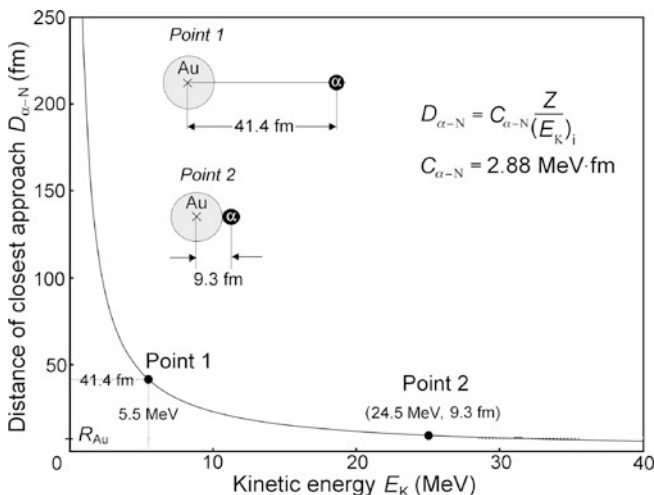


Fig. 2.1 Distance of closest approach $D_{\alpha-N}$ against kinetic energy E_K of the α particle in a direct-hit ($\theta = \pi$) collision between α particle and gold nucleus ($Z = 79$). Point 1 on the curve represents $D_{\alpha-N}$ of 41.4 fm for $(E_K)_i$ of 5.5 MeV; point 2 represents $(E_K)_i$ of 24.5 MeV for $D_{\alpha-N}$ of 9.3 fm

(b) Figure 2.1 shows a plot of the distance of closest approach $D_{\alpha-N}$ in a direct-hit collision of an α particle with a gold nucleus in the initial kinetic energy $(E_K)_i$ range from 1 MeV to 40 MeV. As shown in (2.5), $D_{\alpha-N}$ in general is linearly proportional to the atomic number Z of the absorber and inversely proportional to the kinetic energy $(E_K)_i$ of the α particle, and constant $C_{\alpha-N}$ is equal to 2.88 MeV \cdot fm, as determined in (2.4) for all absorbers Z .

(c) In (a) we showed that the distance of closest approach $D_{\alpha-N}$ for a 5.5 MeV α particle in a head-on collision with gold nucleus is 41.4 fm, while the radius R_{Au} of gold nucleus is 7.3 fm. We assume that at point of initial penetration of the gold nucleus the distance $D_{\alpha-N}$ between the center of the gold nucleus and the center of the α particle is simply the sum of their radii, i.e., $D_{\alpha-N} = R_\alpha + R_{Au} = 9.3$ fm where we used $R_\alpha = R_0 \sqrt[3]{A} = (1.25 \text{ fm}) \times \sqrt[3]{4} \approx 2$ fm for radius of α particle.

We now rearrange (2.5) to calculate the initial kinetic energy $(E_K)_i$ that an α particle must possess to attain a distance of closest approach $D_{\alpha-N}$ of 9.3 fm in a head-on collision

$$E_K = \frac{C_{\alpha-N} Z}{D_{\alpha-N}} = \frac{C_{\alpha-N} Z}{R_\alpha + R_{Au}} = \frac{(2.88 \text{ MeV} \cdot \text{fm}) \times 79}{9.3 \text{ fm}} = 24.5 \text{ MeV}. \quad (2.7)$$

Points 1 and 2 in Fig. 2.1 represent two direct-hit collisions of α particle with gold nucleus. In Point 1, $(E_K)_i = 5.5$ MeV resulting in $D_{\alpha-N} = 41.4$ fm, as determined in (2.5) and in point 2, $D_{\alpha-N} = 9.3$ fm resulting in $(E_K)_i = 24.5$ MeV, as determined in (2.7).

2.2 Geiger-Marsden Experiment

2.2.Q1

(63)

- (a) Write short notes on: (1) Thomson “plum pudding” model of the atom and (2) Rutherford nuclear model of the atom and for each model present a sketch.
- (b) Discuss the expected angular distribution of α particles in Geiger-Marsden scattering experiment assuming the validity of Thomson “plum-pudding” model of the atom.
- (c) Discuss the expected angular distribution of α particles in Geiger-Marsden scattering experiment assuming the validity of Rutherford nuclear model of the atom.
- (d) A collimated beam of α particles emitted from a Po-210 source ($E_K = 5.4$ MeV) strikes a $2.5 \mu\text{m}$ gold foil ($Z = 79$, $A = 197$ g/mol, and $\rho = 19.3$ g/cm³). Calculate the probability of an α particle to be scattered at angles between $\Theta_1 = 10^\circ$ and $\Theta_2 = 12^\circ$ according to: (1) Thomson “plum pudding” model of the atom and (2) Rutherford nuclear model of the atom.

SOLUTION:

(a) In 1898 Joseph J. Thomson, who is also credited with the discovery of the electron in 1897, proposed an atomic model in which the mass of the atom is distributed uniformly over the volume of the atom that has a radius of the order of 1 \AA and negatively charged electrons are dispersed uniformly within a continuous spherical distribution of positive charge. Thus, positive charges and the negative (electron) charges of an atom are distributed uniformly over the atomic volume (“plum pudding” model) to make the atom neutral on the outside [see Fig. 2.2(A)].

Based on α scattering results that Geiger and Marsden carried out with gold foils, Ernest Rutherford in 1911 proposed a completely new atomic model that was much better suited than Thomson model to explain the peculiar α scattering experimental results obtained by Geiger and Marsden. In the Rutherford nuclear model, essentially all atomic mass is concentrated in a small nucleus with the size of the order of few femtometers and the negatively charged electrons revolve about the nucleus in a cloud, the radius of which is of the order of 1 \AA [see Fig. 2.2(B)].

(b) Thomson model

The Thomson “plum pudding” model of the atom results in a Gaussian distribution of α particles about the incident pencil beam direction expressed as follows

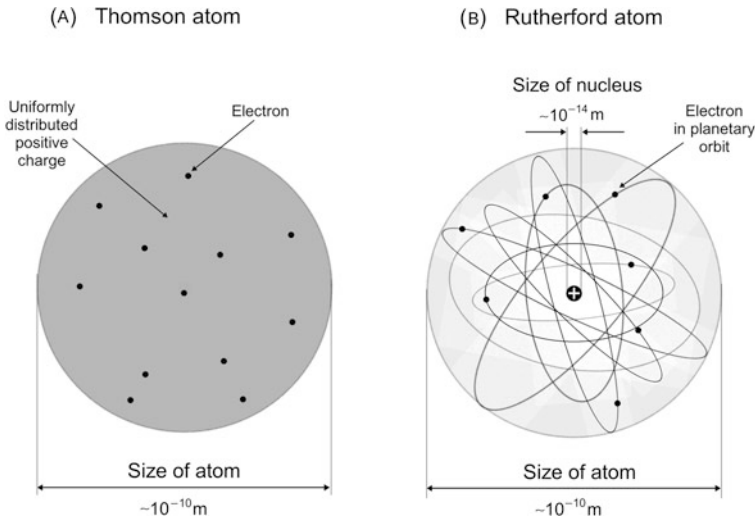


Fig. 2.2 Schematic diagram of two atomic models: (A) Thomson model and (B) Rutherford model

$$\frac{N(\Theta) d\Theta}{N_0} = \frac{2\Theta}{\Theta^2} e^{-\frac{\Theta^2}{\Theta^2}} d\Theta = e^{-\frac{\Theta^2}{\Theta^2}} d\left(\frac{\Theta^2}{\Theta^2}\right), \tag{2.8}$$

where

N_0 is the incident number of α particles, i.e., the number of α particles striking the gold foil.

Θ is the scattering angle of the α particle after it passes through the gold foil.

$N(\Theta) d\Theta$ is the number of α particles scattered within the angular range of Θ and $\Theta + d\Theta$, i.e., scattered between angles Θ and $\Theta + d\Theta$.

$\overline{\Theta^2}$ is the mean square net deflection experimentally determined to be of the order of $3 \times 10^{-4} \text{ rad}^2$ giving $\sqrt{\overline{\Theta^2}} \approx 1^\circ$.

(c) Rutherford model

The distribution of scattered α particles assuming the validity of the Rutherford nuclear model is given as follows

$$\frac{N(\Theta) d\Theta}{N_0} = \frac{\pi}{8} \rho \frac{N_A}{A} t D_{\alpha-N}^2 \frac{\sin \Theta d\Theta}{\sin^4(\frac{1}{2}\Theta)} = \frac{\pi}{2} \rho \frac{N_A}{A} t D_{\alpha-N}^2 \frac{d \sin(\frac{1}{2}\Theta)}{\sin^3(\frac{1}{2}\Theta)}. \tag{2.9}$$

The distribution in (2.9) can be derived as follows. In general, the number N of scattering events is proportional to the incident particle beam intensity N_0 as well as to the number n of atoms (nuclei) per unit area. The proportionality constant is defined as the cross section σ for the scattering event and N is then expressed as

$$N = \sigma N_0 n. \tag{2.10}$$

In (2.10) the absorber (scattering foil) is assumed to be thin enough to ensure that the incident particles have only one or no scattering events as they traverse the absorber. The probability of scattering into scattering angles from θ to $\theta + d\theta$ is given by

$$dN = N(\theta) d\theta = d\sigma_{\text{Ruth}} N_0 n = \frac{d\sigma_{\text{Ruth}}}{d\Omega} N_0 n d\Omega, \quad (2.11)$$

where θ is the scattering angle in a single scattering event in contrast to Θ which is the combined scattering angle for α particle traversal of the gold foil, Ω is the solid angle, and $d\sigma_{\text{Ruth}}/d\Omega$ is the Rutherford differential cross section given as (T2.38)

$$\frac{d\sigma_{\text{Ruth}}}{d\Omega} = \frac{D_{\alpha-N}^2}{16} \frac{1}{\sin^4(\frac{1}{2}\theta)}, \quad (2.12)$$

with $D_{\alpha-N}$ the distance of closest approach in a direct hit (head-on) collision where $\theta = \pi$.

The number of atoms \mathcal{N}_a per area S of the absorber (scattering foil) is given as follows

$$n = \frac{\mathcal{N}_a}{S} = \frac{\mathcal{N}_a}{\mathcal{V}} t = \rho \frac{\mathcal{N}_a}{m} t = \rho \frac{N_A}{A} t, \quad (2.13)$$

where t , \mathcal{V} , m , and ρ are the thickness, volume, mass, and density, respectively, of the absorber foil; N_A is the Avogadro number, and A is the atomic mass of the scattering foil.

The number of α particles scattered into an angular range of θ to $\theta + d\theta$ normalized to the number of incident α particles N_0 is determined from (2.11) as follows

$$\begin{aligned} \frac{N(\theta) d\theta}{N_0} &= n \frac{d\sigma_{\text{Ruth}}}{d\Omega} d\Omega = \rho \frac{N_A}{A} t \frac{d\sigma_{\text{Ruth}}}{d\Omega} d\Omega = \rho \frac{N_A}{A} t \frac{D_{\alpha-N}^2}{16} \frac{1}{\sin^4(\frac{1}{2}\theta)} 2\pi \sin\theta d\theta \\ &= \frac{\pi}{8} \rho \frac{N_A}{A} t D_{\alpha-N}^2 \frac{\sin\theta d\theta}{\sin^4(\frac{1}{2}\theta)} = \frac{\pi}{2} \rho \frac{N_A}{A} t D_{\alpha-N}^2 \frac{d\sin(\frac{1}{2}\theta)}{\sin^3(\frac{1}{2}\theta)}. \end{aligned} \quad (2.14)$$

Since the vast majority of α particles experience only one Rutherford interaction while traversing the foil, the probability for multiple Rutherford interactions is very low and one can replace the single scattering angle θ in (2.14) with angle Θ to get the following distribution for α particles traversing the foil

$$\frac{N(\Theta) d\Theta}{N_0} = \frac{\pi}{8} \rho \frac{N_A}{A} t D_{\alpha-N}^2 \frac{\sin\Theta d\Theta}{\sin^4(\frac{1}{2}\Theta)} = \frac{\pi}{2} \rho \frac{N_A}{A} t D_{\alpha-N}^2 \frac{d\sin(\frac{1}{2}\Theta)}{\sin^3(\frac{1}{2}\Theta)}. \quad (2.15)$$

$N(\theta) d\theta/N_0$ can be considered the probability that incident particles will be scattered into the angular range from θ to $\theta + d\theta$ corresponding to impact parameter range from b to $b - db$.

(d) In the early 20th century physicists had two competing models of the atom: (1) Thomson “plum pudding” model and (2) Rutherford nuclear model, each model predicting significantly different α -particle scattering probabilities from the other model. The Rutherford model eventually prevailed based on unequivocal support from experimental results and today the Rutherford model is considered the universally accepted model of the atom.

(1) According to the Thompson model of the atom the probability of an α particle to be scattered between angle Θ and $\Theta + d\Theta$ is given by (2.8). To get the probability of an α particle to be scattered between angles Θ_1 and Θ_2 we integrate (2.8) and get

$$P_{\text{Th}}(\Theta_2 \geq \Theta \geq \Theta_1) = \frac{1}{N_0} \int_{\Theta_1}^{\Theta_2} N(\Theta) d\Theta = \int_{\Theta_1}^{\Theta_2} e^{-\frac{\Theta^2}{\Theta_1^2}} d\left(\frac{\Theta^2}{\Theta_1^2}\right) = e^{-\frac{\Theta_2^2}{\Theta_1^2}} - e^{-\frac{\Theta_1^2}{\Theta_1^2}}. \quad (2.16)$$

Inserting $\overline{\Theta^2} \approx 1^\circ$, $\Theta_1 = 10^\circ$, and $\Theta_2 = 12^\circ$ into (2.16), we get

$$P_{\text{Th}}(10^\circ \geq \Theta \geq 12^\circ) = e^{-10^2} - e^{-12^2} \approx 10^{-100 \times \log_{10} e} = 10^{-43}. \quad (2.17)$$

(2) The probability of an α particle to be scattered between angle Θ and $\Theta + d\Theta$ according to the Rutherford nuclear model of the atom is given by (2.9). The probability of an α particle to be scattered between angle Θ_1 and Θ_2 according to Rutherford nuclear model of the atom is obtained by integrating (2.9) from Θ_1 to Θ_2 to get

$$\begin{aligned} P_{\text{Ruth}}(\Theta_2 \geq \Theta \geq \Theta_1) &= \frac{1}{N_0} \int_{\Theta_1}^{\Theta_2} N(\Theta) d\Theta = \frac{\pi}{2} \rho \frac{N_A}{A} t D_{\alpha-N}^2 \int_{\Theta_1}^{\Theta_2} \frac{d \sin(\frac{1}{2}\Theta)}{\sin^3(\frac{1}{2}\Theta)} \\ &= \frac{\pi}{4} \rho \frac{N_A}{A} t D_{\alpha-N}^2 \left[\frac{1}{\sin^2(\frac{1}{2}\Theta)} \right]_{\Theta_1}^{\Theta_2} \\ &= \frac{\pi}{4} \rho \frac{N_A}{A} t D_{\alpha-N}^2 \left[\frac{\sin^2(\frac{1}{2}\Theta_2) - \sin^2(\frac{1}{2}\Theta_1)}{\sin^2(\frac{1}{2}\Theta_1) \sin^2(\frac{1}{2}\Theta_2)} \right]. \end{aligned} \quad (2.18)$$

We now use (2.18) to determine the probability of an α particle to be scattered with scattering angle Θ between $\Theta_1 = 10^\circ$ and $\Theta_2 = 12^\circ$ but, before embarking on the calculation, we must determine the distance of closest approach $D_{\alpha-N}$ for a head-on collision between a 5.4 MeV α particle and a gold nucleus (T2.12)

$$D_{\alpha-N} = \frac{zZe^2}{4\pi\epsilon_0} \frac{1}{E_K} = \frac{zZhc\alpha}{E_K} = \frac{2 \times 79 \times (197.3 \text{ MeV} \cdot \text{fm})}{137 \times (5.4 \text{ MeV})} = 42.1 \text{ fm}. \quad (2.19)$$

For a 2.5 μm thick gold foil, the probability of an α particle to be scattered between angles $\Theta_1 = 10^\circ$ and $\Theta_2 = 12^\circ$ is based on (2.19) given as follows

$$\begin{aligned}
 P_{\text{Ruth}}(10^\circ \geq \Theta \geq 12^\circ) &= \frac{\pi \times (19.3 \times 10^6 \text{ g} \cdot \text{m}^{-3}) \times (6.022 \times 10^{23} \text{ mol}^{-1}) \times (2.5 \times 10^{-6} \text{ m}) \times (42.1 \times 10^{-15} \text{ m})^2}{4 \times (197 \text{ g} \cdot \text{mol}^{-1})} \\
 &\times \left[\frac{\sin^2(10^\circ) - \sin^2(12^\circ)}{\sin^2(10^\circ) \times \sin^2(12^\circ)} \right] \\
 &= 8.2 \times 10^{-3}. \tag{2.20}
 \end{aligned}$$

Comparing (2.17) and (2.20), the probability of an α particle to be scattered between angle $\Theta_1 = 10^\circ$ and $\Theta_2 = 12^\circ$ according to the Rutherford nuclear model of the atom is substantially greater than that predicted by the Thomson model of the atom. Extensive experimental work has confirmed the validity of the Rutherford nuclear model of the atom in comparison with the Thomson model of the atom.

2.2.Q2

(64)

Using the general results of Prob. 63 for Rutherford scattering on the Thomson and Rutherford models of the atom, determine, for the Geiger-Marsden experiment with α particles of kinetic energy E_K striking a gold foil of thickness t , the fractional number of α particles scattered with angle Θ_0 or larger assuming the validity of:

- Thomson “plum pudding” model.
- Thomson “plum pudding” model and $t = 1 \mu\text{m}$ and $\Theta_0 = \frac{1}{2}\pi$.
- Rutherford nuclear model.
- Rutherford nuclear model and $t = 1 \mu\text{m}$, $\Theta_0 = \frac{1}{2}\pi$, and $E_K = 5.5 \text{ MeV}$.

SOLUTION:

(a) In conjunction with the **Thomson model** the number of α particles scattered by a foil of thickness t with an angle equal to or larger than Θ_0 is from (2.8) given as

$$\begin{aligned}
 \frac{N(\Theta \geq \Theta_0)}{N_0} &= \frac{1}{N_0} \int_{\Theta_0}^{\pi} N(\Theta) d\Theta = \int_{\Theta_0}^{\pi} e^{-\frac{\Theta^2}{\Theta^2}} d\left(\frac{\Theta^2}{\Theta^2}\right) \\
 &= -e^{-\frac{\Theta^2}{\Theta^2}} \Big|_{\Theta_0}^{\pi} = e^{-\frac{\Theta_0^2}{\Theta^2}} - e^{-\frac{\pi^2}{\Theta^2}}. \tag{2.21}
 \end{aligned}$$

(b) For the **Thomson model** the number of α particles scattered by a foil of thickness t of $1 \mu\text{m}$ with an angle equal to or larger than $\Theta_0 = \frac{1}{2}\pi = 90^\circ$ is from (2.21) given as

$$\begin{aligned}
\frac{N(\Theta \geq \Theta_0)}{N_0} &= \frac{1}{N_0} \int_{\frac{\pi}{2}}^{\pi} N(\Theta) d\Theta = \int_{\frac{\pi}{2}}^{\pi} e^{-\frac{\Theta^2}{\Theta^2}} d\left(\frac{\Theta^2}{\Theta^2}\right) \\
&= -e^{-\frac{\Theta^2}{\Theta^2}} \Big|_{\frac{\pi}{2}}^{\pi} = e^{-\left(\frac{90^\circ}{1^\circ}\right)^2} - e^{-\left(\frac{180^\circ}{1^\circ}\right)^2} \approx e^{-\left(\frac{90^\circ}{1^\circ}\right)^2} \approx 10^{-3500},
\end{aligned} \tag{2.22}$$

where we used the experimentally determined value of $\sim 1^\circ$ for the root mean square angle $\sqrt{\overline{\Theta^2}}$.

(c) In conjunction with the **Rutherford model** of the atom the number of α particles scattered by a foil of thickness t with an angle equal to or larger than Θ_0 is from (2.15) given as

$$\begin{aligned}
\frac{N(\Theta \geq \Theta_0)}{N_0} &= \frac{1}{N_0} \int_{\Theta_0}^{\pi} N(\Theta) d\Theta = \frac{\pi}{2} \rho t \frac{N_A}{A} D_{\alpha-N}^2 \int_{\Theta_0}^{\pi} \frac{d \sin(\frac{1}{2}\Theta)}{\sin^3(\frac{1}{2}\Theta)} \\
&= -\frac{\pi}{4} \rho t \frac{N_A}{A} D_{\alpha-N}^2 \left[\frac{1}{\sin^2(\frac{1}{2}\Theta)} \right]_{\Theta_0}^{\pi} \\
&= \frac{\pi}{4} \rho t \frac{N_A}{A} D_{\alpha-N}^2 \left[\frac{1}{\sin^2(\frac{1}{2}\Theta_0)} - 1 \right] \\
&= \frac{\pi}{4} \rho t \frac{N_A}{A} D_{\alpha-N}^2 \cot^2\left(\frac{1}{2}\Theta_0\right) = C(A, t) \cot^2\left(\frac{1}{2}\Theta_0\right), \tag{2.23}
\end{aligned}$$

where $C(A, t)$ is a constant depending on the atomic mass A and thickness t of the target. For a given target material and thickness the fractional number of α particles scattered with a scattering angle exceeding Θ_0 increases rapidly with decreasing Θ_0 , as shown in Fig. 2.3.

(d) For the Rutherford atomic model, the fractional number of α particles scattered by a gold scattering foil of thickness $t = 1 \mu\text{m}$ with a scattering angle Θ equal to $\Theta_0 = \frac{1}{2}\pi$ or larger is calculated from (2.23) after inserting appropriate values for the pertinent parameters: $\rho_{\text{Au}} = 19.3 \text{ g/cm}^{-3}$; $A = 197 \text{ g/mol}$; $N_A = 6.022 \times 10^{23} \text{ mol}^{-1}$; and $D_{\alpha-N} = 41 \text{ fm}$. The value of 41.4 fm for $D_{\alpha-N}$ is obtained from Prob. 62 which plots $D_{\alpha-N}$, the distance of closest approach in a head-on α particle collision with a gold nucleus, against kinetic energy E_K of α particles. With these values the fraction $N(\Theta \geq \Theta_0 = \frac{1}{2}\pi)/N_0$ is given as

$$\begin{aligned}
\frac{N(\Theta \geq \Theta_0 = \frac{1}{2}\pi)}{N_0} &= C(A, t) \cot^2 \frac{\pi}{4} = \frac{\pi}{4} \times (19.3 \text{ g} \cdot \text{cm}^{-3}) \times (10^{-4} \text{ cm}) \\
&\quad \times \frac{(6.022 \times 10^{23} \text{ mol}^{-1})}{(197 \text{ g} \cdot \text{mol}^{-1})} \\
&\quad \times (41.4 \times 10^{13} \text{ cm})^2 \times \cot^2 \frac{\pi}{4} \\
&= 7.8 \times 10^{-5} \cot^2 \frac{\pi}{4} \approx 10^{-4}. \tag{2.24}
\end{aligned}$$

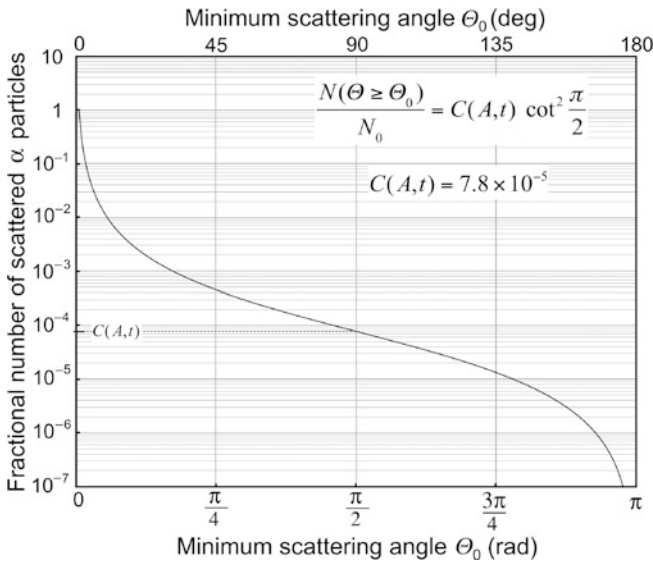


Fig. 2.3 Fractional number of scattered α particles against the minimum scattering angle θ_0 for α particles scattered on gold nucleus

This result, stating a probability of about 10^{-4} for scattering of α particles with an angle larger than 90° on $1 \mu\text{m}$ thick gold foil, confirms the validity of the Rutherford model of the atom. Moreover, it agrees very well with experimental results that Geiger and Marsden obtained in their historic experiment which showed that roughly one in 10^4 α particles was scattered with scattering angles larger than 90° . While relatively small, this probability is nonetheless enormous compared to the probability 10^{-3500} calculated with the Thomson model in (b).

2.3 Rutherford Scattering

2.3.Q1

(65)

Many approaches have been developed for the derivation of the Rutherford α -particle scattering formula. The fastest and most elegant approach is based on the derivation of the momentum transfer Δp from the α particle to the nucleus.

- (a) Plot a schematic diagram of the α particle scattering on a gold nucleus and clearly label all parameters that play a role in the scattering process.
- (b) Derive the relationship between the impact parameter b and the scattering angle θ using the momentum transfer Δp approach.

(c) Show that the impact parameter b that is usually expressed as

$$b = \frac{1}{2} D_{\alpha-N} \cot \frac{\theta}{2} \tag{2.25}$$

can also be expressed as

$$b = \frac{1}{2} D_{\alpha-N} \sqrt{\frac{1 + \cos \theta}{1 - \cos \theta}}. \tag{2.26}$$

SOLUTION:

(a) The schematic diagram of the scattering process is presented in Fig. 2.4. The nucleus of mass M and atomic number Z is in the outer focus of the hyperbola because of the repulsive interaction between the α particle and the nucleus and the assumption is made that $M \gg m_\alpha$ with m_α the mass of the α particle. The other parameters of Fig. 2.4 are defined as follows:

- r is the distance between the α particle and the nucleus (outer focus).
- r' is the distance between the α particle and the inner focus.
- a is the distance between the vertex V and the center C of the hyperbola.
- b is the impact parameter.
- ε is the eccentricity of the hyperbola.
- θ is the scattering angle.
- F_{Coul} is the Coulomb force between the α particle and the nucleus.
- $F_{\Delta p}$ is the projection of F_{Coul} onto the axis of symmetry of the hyperbola.

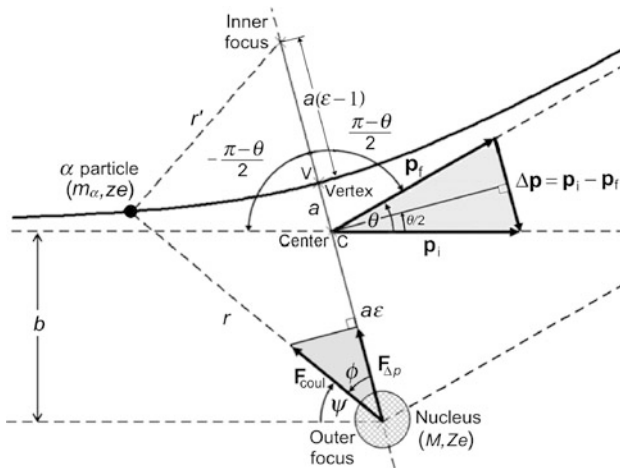


Fig. 2.4 Schematic diagram of α particle scattering

(b) The relationship between the impact parameter b and the scattering angle θ is derived as follows:

The momentum transfer Δp from the α particle to the nucleus can be treated as an impulse that is equal to the change in momentum of the α particle and defined as the integral of force F with respect to time t . As shown in Fig. 2.3, the momentum transfer is along a line that bisects the angle $\pi - \theta$. The magnitude of the Coulomb force acting on the α particle is given by

$$F_{\text{Coul}} = \frac{zeZe}{4\pi\epsilon_0} \frac{1}{r^2}, \quad (2.27)$$

where

r is the distance between the α particle and the nucleus of mass M , atomic number Z , and atomic mass number A .

z is the atomic number of the α particle.

The component of the Coulomb force F_{Coul} in the direction of the momentum transfer is $F_{\Delta p} = F_{\text{Coul}} \cos \phi$ so that the momentum transfer (impulse) Δp can be written as the time integral of the force component $F_{\Delta p}$

$$\begin{aligned} \Delta p &= \int_{-\infty}^{\infty} F_{\Delta p} dt = \int_{-\infty}^{\infty} F_{\text{Coul}} \cos \phi dt = \frac{zZe^2}{4\pi\epsilon_0} \int_{-\frac{\pi-\theta}{2}}^{\frac{\pi-\theta}{2}} \frac{\cos \phi}{r^2} \frac{dt}{d\phi} d\phi \\ &= \frac{zZe^2}{4\pi\epsilon_0} \int_{-\frac{\pi-\theta}{2}}^{\frac{\pi-\theta}{2}} \frac{\cos \phi}{r^2 \omega} d\phi, \end{aligned} \quad (2.28)$$

where

ϕ is the angle between the radius vector \mathbf{r} and the bisector.

$dt/d\phi$ is the inverse of the angular frequency ω .

We now use the conservation of angular momentum L for the α -scattering process to obtain a relationship between the angular frequency ω and impact parameter b . For the α particle at a very large distance ($r = \infty$) from the nucleus, L is given as $L = m_\alpha v_i b$ with m_α and v_i the mass and initial velocity of the α particle. For the α particle in the vertex of the hyperbolic trajectory, on the other hand, we get $L = m_\alpha \omega r^2$. Thus

$$L = |\mathbf{L}| = |\mathbf{r} \times \mathbf{p}| = |\mathbf{r} \times m_\alpha \mathbf{v}| = m_\alpha v_i b = m_\alpha \omega r^2 \quad \text{and} \quad \frac{1}{\omega} = \frac{r^2}{v_i b}. \quad (2.29)$$

Inserting (2.29) into (2.28) the momentum transfer is now expressed as

$$\Delta p = \frac{zZe^2}{4\pi\epsilon_0} \frac{1}{v_i b} \int_{-\frac{\pi-\theta}{2}}^{\frac{\pi-\theta}{2}} \cos \pi d\phi = 2 \frac{zZe^2}{4\pi\epsilon_0} \frac{1}{v_i b} \cos \frac{\theta}{2}. \quad (2.30)$$

The momentum vector diagram of Fig. 2.4 shows that Δp can also be expressed as follows

$$\Delta p = 2m_{\alpha}v_i \sin \frac{\theta}{2} \quad (2.31)$$

and this expression combined with (2.30) results in the following relationship between the impact parameter b and scattering angle θ

$$b = \frac{zZe^2}{4\pi\epsilon_0m_{\alpha}v_i^2} \cot \frac{\theta}{2} = \frac{1}{2}D_{\alpha-N} \cot \frac{\theta}{2} = \frac{1}{2}D_{\alpha-N} \sqrt{\frac{1+\cos\theta}{1-\cos\theta}}, \quad (2.32)$$

where $D_{\alpha-N}$ is the distance of closest approach in a direct-hit collision between an α particle and the nucleus (T2.12).

(c) We show that

$$b = \frac{1}{2}D_{\alpha-N} \cot \frac{\theta}{2} = \frac{1}{2}D_{\alpha-N} \sqrt{\frac{1+\cos\theta}{1-\cos\theta}} \quad (2.33)$$

by recalling the well known trigonometric expression $\cos\theta = \cos^2\frac{1}{2}\theta - \sin^2\frac{1}{2}\theta$ in conjunction with the following trigonometric identity $\sin^2\frac{1}{2}\theta + \cos^2\frac{1}{2}\theta = 1$ to get

$$\cot \frac{\theta}{2} = \frac{\cos\frac{1}{2}\theta}{\sin\frac{1}{2}\theta} = \sqrt{\frac{\cos^2\frac{1}{2}\theta}{\sin^2\frac{1}{2}\theta}} = \sqrt{\frac{1+\cos\theta}{1-\cos\theta}}. \quad (2.34)$$

2.3.Q2

(66)

A lithium ion Li^{+++} ($Z = 3$, $A = 6$ g/mol) with incident kinetic energy $(E_K)_i = 7.5$ MeV is scattered on a gold nucleus ($Z = 79$, $A = 197$ g/mol) through an angle θ of 10° . Assume that the mass of the alpha particle is much smaller than the mass of the lithium ion and calculate:

- Impact parameter b .
- Distance of closest approach $R_{\alpha-N}$.
- Eccentricity of the hyperbolic trajectory of the Li^{+++} ion.
- Distance a between the vertex V and the center C of the hyperbolic trajectory.

SOLUTION:

Before calculating the individual parameters of the specific scattering interaction, we calculate the distance of closest approach in a head-on elastic collision between the Li^{+++} ion and gold nucleus using (T2.12)

$$\begin{aligned}
 D_{\alpha-N} &= \frac{zZe^2}{4\pi\epsilon_0(E_K)_i} \\
 &= \frac{3 \times 79 \times e \times (1.6 \times 10^{-19} \text{ A} \cdot \text{s})}{4\pi \times (8.85 \times 10^{-12} \text{ A} \cdot \text{s} \cdot \text{V}^{-1} \cdot \text{m}^{-1}) \times (7.5 \times 10^6 \text{ eV})} \\
 &= 4.55 \times 10^{-14} \text{ m} = 45.5 \text{ fm}.
 \end{aligned} \tag{2.35}$$

(a) Impact parameter b is calculated from (T2.23) as

$$b = \frac{1}{2} D_{\alpha-N} \cot \frac{\theta}{2} = \frac{1}{2} \times (45.5 \text{ fm}) = 260 \text{ fm}. \tag{2.36}$$

(b) Distance of closest approach is calculated from (T2.31) as follows

$$R_{\alpha-N} = \frac{1}{2} D_{\alpha-N} \left(1 + \frac{1}{\sin \frac{\theta}{2}} \right) = \frac{(45.5 \text{ fm})}{2} \times \left(1 + \frac{1}{\sin 5^\circ} \right) = 283.8 \text{ fm}. \tag{2.37}$$

(c) Eccentricity ε of the trajectory is calculated from (T2.28) as follows

$$\varepsilon = \frac{1}{\sin \frac{\theta}{2}} = \frac{1}{\sin 5^\circ} = 11.5. \tag{2.38}$$

(d) Distance a between the vertex V and the center C of the hyperbolic trajectory is calculated using (T2.30)

$$a = \frac{1}{2} D_{\alpha-N} = 22.8 \text{ fm}. \tag{2.39}$$

2.3.Q3

(67)

An α particle interacts with a silver nucleus (atomic number $Z = 47$, atomic mass $A = 108$, and rest mass $Mc^2 = 100455 \text{ MeV}$) and undergoes Rutherford scattering with scattering angle θ of 45° resulting in a distance of closest approach $R_{\alpha-N}$ of 32.2 fm. For this Rutherford scattering event:

- Calculate impact parameter b .
- Calculate kinetic energy E_K of the incident α particle.
- Calculate momentum p_α of the incident α particle.
- Calculate recoil momentum Δp of the nucleus.
- Calculate recoil energy ΔE_K of the nucleus.
- Calculate eccentricity ε of the hyperbolic trajectory of the α particle.
- Draw a schematic diagram of the scattering event and clearly show all given and calculated parameters.

SOLUTION:

(a) The impact parameter b is calculated using (T2.31) to get

$$b = R_{\alpha-N} \frac{1 - \sin \frac{\theta}{2}}{\cos \frac{\theta}{2}} = (32.2 \text{ fm}) \times \frac{1 - \sin 22.5^\circ}{\cos 22.5^\circ} = 21.5 \text{ fm}. \quad (2.40)$$

(b) Kinetic energy E_K of the incident α particle is calculated using (T2.12) which contains $D_{\alpha-N}$, the distance of closest approach in a head-on collision ($\theta = \pi$, $b = 0$), calculated using (T2.23) as follows

$$D_{\alpha-N} = 2b \tan \frac{\theta}{2} = 2 \times (21.5 \text{ fm}) \times \tan 22.5^\circ = 17.8 \text{ fm}. \quad (2.41)$$

According to (T2.12) E_K is given as follows

$$E_K = \frac{2zZe^2}{4\pi\epsilon_0} \frac{1}{D_{\alpha-N}} = \frac{2 \times 47 \times (1.602 \times 10^{-19} \text{ A} \cdot \text{s}) \times e}{4\pi \times [8.85 \times 10^{-12} \text{ A} \cdot \text{s}/(\text{V} \cdot \text{m})] \times (17.8 \times 10^{-15} \text{ m})} \\ = 7.6 \text{ MeV}. \quad (2.42)$$

(c) Momentum of the incident α particle is calculated using the standard p vs E_K relativistic expression given in (T1.64) as follows

$$p_\alpha = \frac{E_K}{c} \sqrt{1 + \frac{2m_\alpha c^2}{E_K}} = \left(7.6 \frac{\text{MeV}}{c}\right) \times \sqrt{1 + \frac{2 \times (3727.3 \text{ MeV})}{7.6 \text{ MeV}}} \\ = 238.1 \text{ MeV}/c. \quad (2.43)$$

(d) Recoil momentum Δp of the nucleus is calculated using (T2.22) to get

$$\Delta p = 2p_\alpha \sin \frac{\theta}{2} = 2 \times (238.1 \text{ MeV}/c) \times \sin 22.5^\circ = 182.2 \text{ MeV}/c. \quad (2.44)$$

(e) Recoil energy ΔE_K of the nucleus is determined from the standard relativistic equation for kinetic energy as follows

$$\Delta E_K = \sqrt{(\Delta p_{\text{Ag}})^2 c^2 + (M_{\text{Ag}} c^2)^2} - M_{\text{Ag}} c^2 \\ = \sqrt{(182.2 \text{ MeV})^2 + (100455 \text{ MeV})^2} - (100455 \text{ MeV}) = 0.165 \text{ MeV}. \quad (2.45)$$

(f) Eccentricity ε of the α particle trajectory is determined from (T2.28) to get

$$\varepsilon = \frac{1}{\sin \frac{\theta}{2}} = \frac{1}{\sin 22.5^\circ} = 2.61. \quad (2.46)$$

(g) Schematic diagram of the scattering process is shown in Fig. 2.5.

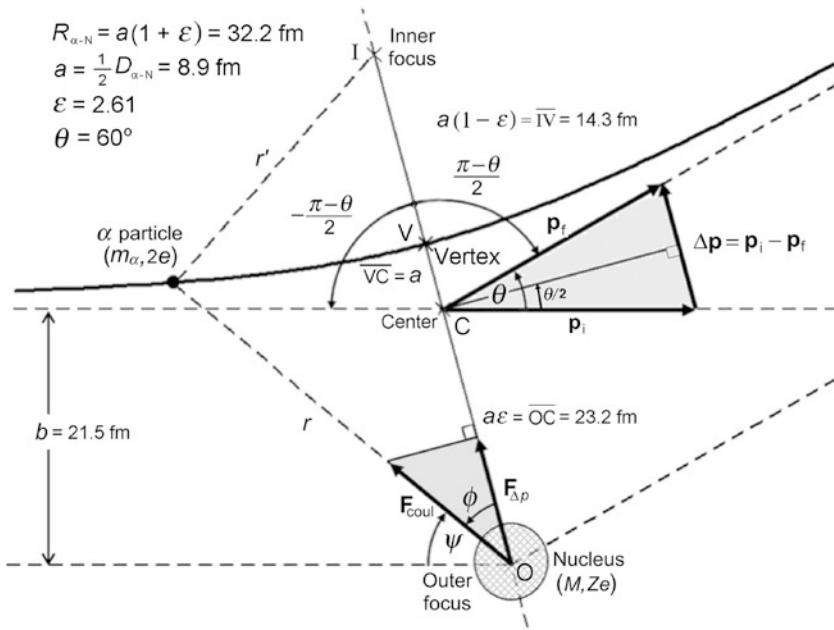


Fig. 2.5 Schematic diagram of the Rutherford scattering process with scattering angle $\theta = 45^\circ$ and the distance of closest approach $R_{\alpha-N} = 32.2 \text{ fm}$ defined as the distance between the outer focus and vertex of the hyperbolic trajectory

2.3.Q4

(68)

An α particle with initial kinetic energy $(E_K)_i$ of 5.5 MeV and initial velocity v_i undergoes a direct-hit Rutherford scattering (head-on collision) on a gold nucleus.

- Derive and plot the general relationship for v_x/v_i against $x/D_{\alpha-N}$ for the α particle with x the α particle distance from the center of the nucleus, v_x the velocity of the α particle at x , and $D_{\alpha-N}$ the distance of closest approach in a direct-hit collision of the α particle with the nucleus.
- Calculate the initial velocity of the 5.5 MeV α particle.
- Determine v_x/v_i of the α particle when the particle is a distance $x = 2D_{\alpha-N}$ from the nucleus. For a 5.5 MeV α particle $D_{\alpha-N}$ was determined as 41.3 fm in Prob. 62.
- Calculate the distance x at which the α particle velocity v_x is at 50 % of its initial velocity v_i .
- Calculate the distance x at which the α particle velocity v_x is at 90 % of its initial velocity v_i .

SOLUTION:

(a) In a direct-hit elastic collision between an α particle and a nucleus (scattering angle $\theta = \pi$ and impact parameter $b = 0$) the following expression holds in general for the conservation of energy of the α particle.

$$(E_K)_i = \frac{m_\alpha v_i^2}{2} = \frac{m_\alpha v_x^2}{2} + \frac{zZe^2}{4\pi\epsilon_0} \frac{1}{x} = 0 + \frac{zZe^2}{4\pi\epsilon_0} \frac{1}{D_{\alpha-N}}, \quad (2.47)$$

where

- x is the distance between the α particle and the nucleus in a direct-hit collision
- v_i is the initial velocity of the α particle (at $x = \infty$).
- $(E_K)_i$ is the initial kinetic energy of the α particle (at $x = \infty$).
- $E_K(x)$ is the kinetic energy at x .
- $E_P(x)$ is the potential energy at x .
- $D_{\alpha-N}$ is the distance of closest approach in a direct-hit collision ($\theta = \pi$) between the α particle and the nucleus.
- v_x is the velocity of the α particle at a distance x from the nucleus for $D_{\alpha-N} \leq x \leq \infty$.

Equation (2.47) states that at any point x of the α particle trajectory the total α particle energy which is the sum of kinetic energy $E_K(x) = \frac{1}{2}m_\alpha v_x^2$ and potential energy $E_P(x) = zZe^2/(4\pi\epsilon_0 x)$ is equal to initial kinetic energy $(E_K)_i$ of the α particle. We thus have

$$E_K(x = \infty) = (E_K)_i \quad \text{and} \quad E_K(x = D_{\alpha-N}) = 0 \quad (2.48)$$

as well as

$$E_P(x = \infty) = 0 \quad \text{and} \quad E_P(x = D_{\alpha-N}) = \frac{zZe^2}{4\pi\epsilon_0 D_{\alpha-N}} = (E_K)_i. \quad (2.49)$$

To derive a general expression for normalized velocity v_x/v_i as a function of normalized distance $x/D_{\alpha-N}$ we insert (2.49) into (2.47) and get

$$\frac{m_\alpha v_i^2}{2} = \frac{m_\alpha v_x^2}{2} + \frac{(E_K)_i}{(x/D_{\alpha-N})} = \frac{m_\alpha v_x^2}{2} + \frac{m_\alpha v_i^2}{2(x/D_{\alpha-N})} \quad (2.50)$$

Solving (2.50) for v_x/v_i gives the following result

$$\frac{v_x}{v_i} = \sqrt{1 - \frac{1}{(x/D_{\alpha-N})}}. \quad (2.51)$$

A plot of normalized velocity v_x/v_i against the normalized distance $x/D_{\alpha-N}$ is given in Fig. 2.6. The plot is valid for all classical α particles irrespective of the kinetic energy of the α particle. Points (c), (d), and (e) on the graph represent solutions for problem sections (c), (d), and (e) below.

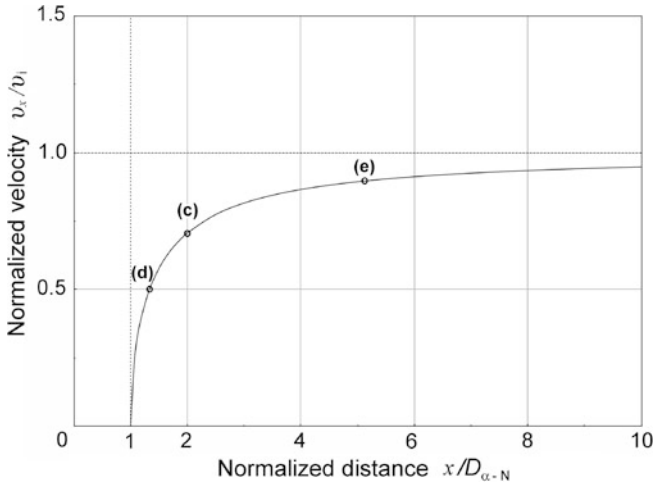


Fig. 2.6 Normalized velocity v_x/v_i against normalized distance $x/D_{\alpha-N}$ for classical direct-hit α particle Rutherford scattering. Points labeled (c), (d), and (e) correspond to results obtained in sections (c), (d), and (e)

(b) Velocity of 5.5 MeV α particle is calculated in (T2.5) classically and in (T2.7) relativistically as follows

$$\frac{v_i}{c} = \sqrt{\frac{2E_K}{m_\alpha c^2}} = \sqrt{1 - \frac{1}{\left(1 + \frac{(E_K)_i}{m_\alpha c^2}\right)^2}} = 0.0543. \quad (2.52)$$

The first square-root in (2.52) follows from the classical expression for kinetic energy while the second comes from relativistic considerations. Both give the same result, since the initial kinetic energy of the α particle is much smaller than its rest energy, allowing us to use the classical expression for $E_K(x)$ in (2.47).

(c) Our specific problem calls for determination of the ratio v_x/v_i for $x = 2D_{\alpha-N}$. Inserting $x/D_{\alpha-N} = 2$ into (2.51) we obtain the following result

$$\frac{v_x^2}{v_i^2} = \frac{1}{2} \quad \text{or} \quad \frac{v_x}{v_i} = \frac{1}{\sqrt{2}} = 0.707. \quad (2.53)$$

(d) To calculate the distance at which the α particle velocity v_x is 50 % of its initial velocity v_i we use (2.51) and solve for $x/D_{\alpha-N}$ to get

$$\frac{x}{D_{\alpha-N}} = \frac{1}{1 - \frac{v_x^2}{v_i^2}} = \frac{1}{1 - 0.25} = 1.33. \quad (2.54)$$

(e) To calculate the distance at which the α particle velocity v_x is 90 % of its initial velocity v_i we use (2.54) and get

$$\frac{x}{D_{\alpha-N}} = \frac{1}{1 - \frac{v_x^2}{v_i^2}} = \frac{1}{1 - 0.81} = 5.26. \quad (2.55)$$

2.3.Q5

(69)

A hyperbola consists of two disconnected open curves called the arms or branches of the hyperbola. The distance of closest approach between the two branches defines the vertices of the hyperbola, one vertex V for each branch. A straight line through the two vertices defines the transverse axis of the hyperbola, and the midpoint between the two vertices on the transverse axis is the center C of the hyperbola.

Show that the two expressions [(T2.27) and (T2.32), respectively]

$$r(\phi) = \frac{a(\varepsilon^2 - 1)}{\varepsilon \cos \phi - 1} \quad (2.56)$$

and

$$\frac{1}{r(\psi)} = \frac{1}{b} \sin \psi + \frac{a}{b^2} (\cos \psi - 1) \quad (2.57)$$

given in polar coordinates for the trajectory of an α particle undergoing Rutherford elastic scattering on a high atomic number nucleus are equivalent. The trajectory is a hyperbola and the polar coordinate system is centered at the outer focus F_O of the hyperbola. The angles θ , ϕ , and ψ are defined in Fig. 2.7 and

- ε is the eccentricity of the hyperbola.
- a is the distance between the vertex V and the center C of the hyperbola.
- b is the impact parameter of Rutherford elastic scattering.

SOLUTION:

From Fig. 2.7 we recognize the following relationship among angles θ , ϕ , and ψ

$$\psi + \phi = \frac{\pi - \theta}{2} \quad \text{or} \quad \phi = \frac{\pi}{2} - \frac{\theta}{2} - \psi. \quad (2.58)$$

The cosine of angle ϕ is then expressed as follows

$$\cos \phi = \cos \left[\left(\frac{\pi}{2} - \frac{\theta}{2} \right) - \psi \right] = \cos \left(\frac{\pi}{2} - \frac{\theta}{2} \right) \cos \psi + \sin \left(\frac{\pi}{2} - \frac{\theta}{2} \right) \sin \psi$$

we change (2.60) to read

$$\frac{1}{r} = \frac{\cos \psi + \cot \frac{\theta}{2} \sin \psi - 1}{a \cot^2 \frac{\theta}{2}}. \quad (2.64)$$

Furthermore, as shown in (T2.23) and (T2.30), $b = a \cot(\frac{1}{2}\theta)$ resulting in the following expression for (2.64)

$$\frac{1}{r} = \frac{\cos \psi + \frac{b}{a} \sin \psi - 1}{a \frac{b^2}{a^2}} = \frac{1}{b} \sin \psi + \frac{a}{b^2} (\cos \psi - 1) \quad (2.65)$$

and showing that in polar coordinates $1/r$ can be expressed in two ways

$$\frac{1}{r} = \frac{1}{b} \sin \psi + \frac{a}{b^2} (\cos \psi - 1) \quad \text{and} \quad r(\phi) = \frac{a(\varepsilon^2 - 1)}{\varepsilon \cos \phi - 1}. \quad (2.66)$$

To test the validity of (2.56) and (2.57) we measure the appropriate parameters for point P in Fig. 2.7 and insert the measured values into the two equations. The measured parameters are as follows:

$$r = 146 \text{ fm}, \quad \psi = 22^\circ, \quad (2.67)$$

$$r' = 105 \text{ fm}, \quad \psi = 46^\circ, \quad (2.68)$$

$$a = \frac{1}{2}(r - r') = \frac{1}{2}D_{\alpha-N} = 20.5 \text{ fm}, \quad \frac{\theta}{2} = 22^\circ = \frac{\pi}{2} - (\psi + \phi), \quad (2.69)$$

$$b = 50 \text{ fm}, \quad \varepsilon = \frac{1}{\sin \frac{\theta}{2}} = 2.67. \quad (2.70)$$

Insertion of these parameters into (2.56) and (2.57) gives the following results

$$r(\phi) = \frac{a(\varepsilon^2 - 1)}{\varepsilon \cos \phi - 1} = \frac{(20.5 \text{ fm}) \times 6.13}{0.855} = 147 \text{ fm} \quad (2.71)$$

and

$$\frac{1}{r(\psi)} = \frac{\sin \psi}{b} + \frac{a}{b^2} (\cos \psi - 1) = \frac{0.375}{50 \text{ fm}} + \frac{20.5}{2500 \text{ fm}} (-0.0728) = 0.0069 \quad (2.72)$$

or

$$r(\psi) = 145 \text{ fm}.$$

Equations (2.71) and (2.72) do not agree perfectly with the measured radius r of 146 fm because of rounding errors and measurement inaccuracy; however, they serve as reasonable proof that (2.56) and (2.57) provide identical results in polar coordinates.

2.3.Q6

(70)

Figure 2.8 shows a trajectory of an α particle scattered on a platinum ($Z = 78$) nucleus. The interaction between the α particle and the nucleus is assumed to be Coulomb scattering of the Rutherford type where the nuclear mass is much larger than the α particle mass. The nucleus is located at the outer focus of the hyperbolic trajectory coinciding with the origin $(0, 0)$ of the Cartesian coordinate system and the α particle trajectory is symmetrical about the ordinate (y) axis. The distances on the coordinate system are given in femtometers (fm). Based on data in Fig. 2.8 determine:

- Distance of closest approach $R_{\alpha-N}$, defined as the distance between the platinum nucleus and the vertex V of the hyperbolic trajectory.
- Eccentricity ε of the hyperbolic trajectory and the distance a between the vertex V and center C of the hyperbola.
- Coordinates of the center $C(x_C, y_C)$ of the hyperbolic trajectory.
- Scattering angle θ and distance of closest approach $D_{\alpha-N}$ in direct-hit scattering.
- Impact parameter b .
- Initial kinetic energy $(E_K)_i$ of the α particle.

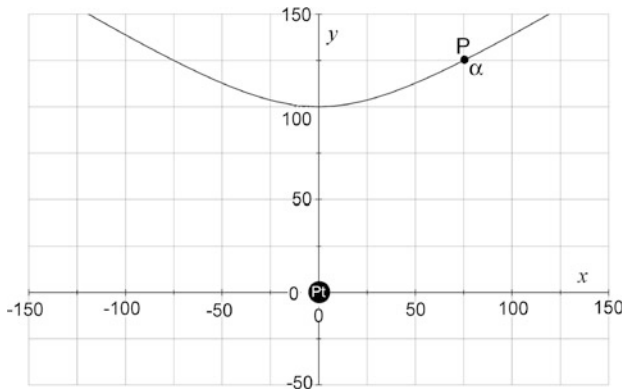


Fig. 2.8 Trajectory of an α particle having a Coulomb interaction of Rutherford type on a platinum nucleus. The nucleus is located in the outer focus of the hyperbolic trajectory. Distances on the Cartesian coordinate system are in femtometers. ($1 \text{ fm} = 10^{-5} \text{ \AA}$). Point P is an arbitrary point on the hyperbola

SOLUTION:

- Distance of closest approach $R_{\alpha-N}$ between the α particle and platinum nucleus can be read directly from the graph in Fig. 2.8 and amounts to $R_{\alpha-N} = 100 \text{ fm}$.

(b) We determine ε and a as follows: The equation for the hyperbola is in polar coordinates (r, ϕ) given as [see (T2.27)]

$$r(\phi) = \frac{a(\varepsilon^2 - 1)}{\varepsilon \cos \phi - 1}, \quad (2.73)$$

where

$r(\phi)$ is the magnitude of the radius vector \mathbf{r} directed from point OF(0, 0) to any arbitrary point P on the hyperbola.

ϕ is the angle between the ordinate (y) axis and the radius vector \mathbf{r} .

a is the distance between the vertex V and center C of the hyperbola.

ε is the eccentricity of the hyperbola.

Next, we choose an arbitrary point P on the hyperbola, for example at $x_P = 75$ fm and $y_P = 125$ fm (see Fig. 2.8), and determine the polar coordinates r_P and ϕ_P for point P as

$$r_P = \sqrt{x_P^2 + y_P^2} = \sqrt{(75 \text{ fm})^2 + (125 \text{ fm})^2} = 145.8 \text{ fm} \quad (2.74)$$

and

$$\cos \phi_P = \frac{y_P}{r_P} = \frac{125.0}{145.8} = 0.857 \quad \text{or} \quad \phi_P = \cos^{-1} \frac{y_P}{r_P} = \cos^{-1} 0.857 = 31^\circ. \quad (2.75)$$

We now express (2.73) for two points on the hyperbola: [point V($r = y_P = R_{\alpha-N}$, $\phi = 0$) and arbitrary point P($r_P = 145.8$ fm, $\phi_P = 31^\circ$)] and get two equations for two unknowns (a and ε) reading as follows

$$r(\phi = 0) = R_{\alpha-N} = \frac{a(\varepsilon^2 - 1)}{\varepsilon - 1} = a(\varepsilon + 1) \quad (2.76)$$

and

$$r(\phi = \phi_P) = r_P = \frac{a(\varepsilon^2 - 1)}{\varepsilon \cos \phi_P - 1}. \quad (2.77)$$

Inserting $a = R_{\alpha-N}/(\varepsilon + 1)$ from (2.76) into (2.77) results in the following values for the eccentricity ε and distance a between vertex V and center C of the hyperbolic trajectory

$$\varepsilon = \frac{r_P - R_{\alpha-N}}{r_P \cos \phi_P - R_{\alpha-N}} = \frac{145.8 - 100.0}{145.8 \times 0.857 - 100.0} = 1.835 \quad (2.78)$$

and

$$a = \frac{R_{\alpha-N}}{\varepsilon + 1} = \frac{100 \text{ fm}}{1.835 + 1} = 35.3 \text{ fm}. \quad (2.79)$$

(c) The distance between the outer focus OF and the center C of the hyperbola is equal to $a\varepsilon$. The coordinates x_C and y_C for center point C of the hyperbolic

trajectory are thus given as

$$x_C = 0 \quad \text{and} \quad y_C = a\varepsilon = (35.3 \text{ fm}) \times 1.835 = 64.7 \text{ fm}. \quad (2.80)$$

(d) Since, as shown in (T2.28), $\varepsilon = 1/\sin(\frac{1}{2}\theta)$, we calculate the scattering angle θ as

$$\theta = 2 \sin^{-1} \frac{1}{\varepsilon} = 66.2^\circ, \quad (2.81)$$

while, as shown in (T2.30), the distance of closest approach $D_{\alpha-N}$ for a direct-hit collision equals $2a$ in general and thus is 70.6 fm in the example studied here.

(e) The impact parameter b is calculated from the standard Rutherford scattering expression linking b and θ [see (T2.23)]

$$b = \frac{D_{\alpha-N}}{2} \cot \frac{\theta}{2} = \frac{70.6 \text{ fm}}{2} \cot 33.1^\circ = 54.2 \text{ fm}. \quad (2.82)$$

(f) Finally, the relationship between $D_{\alpha-N}$ and initial kinetic energy E_K is shown in (T2.12) as

$$D_{\alpha-N} = \frac{zZe^2}{4\pi\varepsilon_0(E_K)_i}, \quad (2.83)$$

giving the following expression for E_K

$$\begin{aligned} E_K &= \frac{zZe^2}{4\pi\varepsilon_0 D_{\alpha-N}} \\ &= \frac{2 \times 78 \times (1.6 \times 10^{-19} \text{ A} \cdot \text{s})e}{4\pi \times [8.85 \times 10^{-12} \text{ A} \cdot \text{s}/(\text{V} \cdot \text{m})] \times (70.6 \times 10^{-15} \text{ m})} \\ &= 3.18 \text{ MeV}. \end{aligned} \quad (2.84)$$

Solutions **(a)** through **(f)** are illustrated graphically in Fig. 2.9 and summarized as follows:

- (a)** Distance of closest approach for the α particle $R_{\alpha-N} = 100$ fm.
- (b)** Eccentricity $\varepsilon = 1.835$ and distance vertex-center $a = 35.3$ fm.
- (c)** Coordinates of hyperbola center C(x_C, y_C): $x_C = 0$; $y_C = 64.7$ fm.
- (d)** Scattering angle $\theta = 66.2^\circ$ and direct-hit distance of closest approach $D_{\alpha-N} = 70.6$ fm.
- (e)** Impact parameter $b = 54.2$ fm.
- (f)** Initial kinetic energy of the α particle $(E_K)_i = 3.18$ MeV.

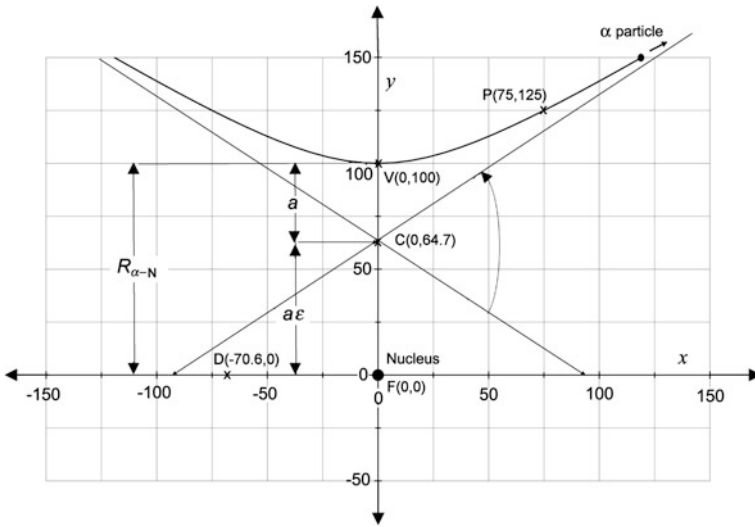


Fig. 2.9 Graphical representation of results calculated in (a) through (f). C designates the center C of the hyperbola, V designates the vertex of the hyperbola. P is an arbitrary point on the hyperbola with coordinates $x = 75$ and $y = 125$

2.3.Q7

(71)

For Rutherford scattering, derive an expression for the distance of closest approach $R_{\alpha-N}$ as a function of the initial kinetic energy $(E_K)_i$ and impact parameter b of the α particle.

SOLUTION:

In Rutherford scattering the total energy $E(r)$ of the α particle is conserved and equal to the initial kinetic energy $E_K(r)$ of the α particle at $r = \infty$. For $r < \infty$, total energy $E(r)$ is the sum of the kinetic energy $E_K(r)$ and potential energy $E_P(r)$

$$E(r) = (E_K)_i = E_K(r) + E_P(r) = \frac{m_\alpha v_\alpha^2}{2} + \frac{zZe^2}{4\pi\epsilon_0 r}, \quad (2.85)$$

where

- z is the atomic number of the projectile (α particle: $z = 2$).
- Z is the atomic number of the absorber.
- m_α is the mass of the α particle.
- v_α is the velocity of the α particle.
- v_i is the initial velocity of the α particle.

The α particle attains $R_{\alpha-N}$, its distance of closest approach to the nucleus, when it reaches the vertex V of the hyperbolic trajectory. Conservation of angular momentum L at point V can be expressed as

$$|\vec{L}| = L = m_{\alpha} v_i b = m_{\alpha} v_{\alpha} R_{\alpha-N} \quad \text{or} \quad v_{\alpha} = \frac{v_i b}{R_{\alpha-N}}, \quad (2.86)$$

where b is the impact parameter. Inserting the expression for v_{α} of (2.86) into (2.85) and rearranging the terms results in the following quadratic equation for $R_{\alpha-N}$

$$R_{\alpha-N}^2 - \frac{zZe^2}{4\pi\epsilon_0(E_K)_i} R_{\alpha-N} - b^2 = R_{\alpha-N}^2 - D_{\alpha-N} R_{\alpha-N} - b^2 = 0, \quad (2.87)$$

where $D_{\alpha-N}$ is the distance of closest approach in a direct-hit ($b = 0$) interaction between the α particle and the nucleus.

The quadratic equation (2.87) has the following simple and physically relevant solution

$$R_{\alpha-N} = \frac{D_{\alpha-N} + \sqrt{D_{\alpha-N}^2 + 4b^2}}{2} = \frac{D_{\alpha-N}}{2} \left\{ 1 + \sqrt{1 + \left[\frac{2b}{D_{\alpha-N}} \right]^2} \right\}. \quad (2.88)$$

In a direct-hit collision $b = 0$ and the distance of closest approach $R_{\alpha-N}$ given in (2.88) transforms into the well-known relationship which follows directly from the conservation of energy in a Rutherford scattering interaction

$$R_{\alpha-N}(b = 0) = D_{\alpha-N} = \frac{zZe^2}{4\pi\epsilon_0(E_K)_i}. \quad (2.89)$$

Using the well-known Rutherford expression that relates the impact parameter b with the scattering angle θ given in (T2.23) as

$$b = \frac{1}{2} D_{\alpha-N} \cot \frac{\theta}{2} \quad \text{or} \quad 1 + \left[\frac{2b}{D_{\alpha-N}} \right]^2 = 1 + \cot^2 \frac{\theta}{2} = \frac{1}{\sin^2 \frac{\theta}{2}}, \quad (2.90)$$

we can write (2.88) for $R_{\alpha-N}$ as

$$R_{\alpha-N} = \frac{D_{\alpha-N}}{2} \left\{ 1 + \frac{1}{\sin \frac{\theta}{2}} \right\} \quad (2.91)$$

in agreement with the derivation of (T2.31).

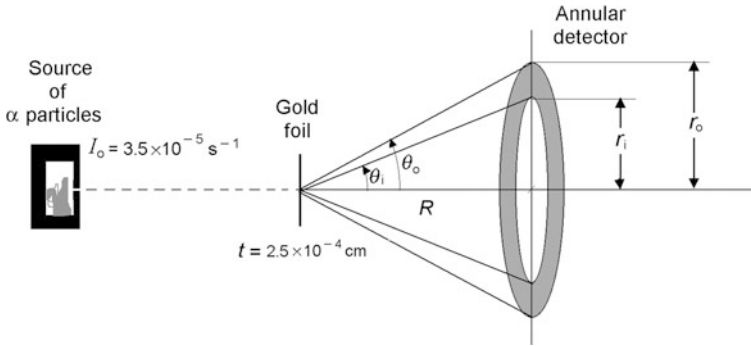


Fig. 2.10 Schematic diagram of the scattering experiment

2.4 Cross Sections for Rutherford Scattering

2.4.Q1

(72)

A beam of α particles with kinetic energy E_K of 6.5 MeV and intensity I_0 of $3.5 \times 10^6 \text{ s}^{-1}$ is incident normally onto a gold foil ($\rho = 19.3 \text{ g} \cdot \text{cm}^{-3}$, $A = 197 \text{ g} \cdot \text{mol}^{-1}$) of thickness $t = 2.5 \times 10^{-5} \text{ cm}$.

An α particle counter in the shape of an annular ring is placed downstream, concentrically with the beam direction and with its center at a distance R of 5 cm from the center of the gold foil. The inner radius r_i of the ring detector is 7.5 mm; the outer radius r_o is 10 mm. The ring width thus is 2.5 mm.

- Draw a schematic diagram of the scattering experiment.
- Determine the intensity of α particles striking the detector.

SOLUTION:

(a) A schematic diagram of the scattering experiment is shown in Fig. 2.10 and contains the following main components:

- Source of α particles.
- Gold foil of thickness $t = 2.5 \times 10^{-5} \text{ cm}$.
- Annular (ring) detector.

(b) The experiment described above is a typical example of Rutherford scattering experiment involving α particle scattering on atomic nuclei. The differential cross section for Rutherford scattering is given as (T2.38)

$$\frac{d\sigma_{\text{Ruth}}}{d\Omega} = \left(\frac{D_{\alpha-N}}{4} \right)^2 \frac{1}{\sin^4 \frac{\theta}{2}}, \quad (2.92)$$

where θ is the scattering angle and $D_{\alpha-N}$ is the distance of closest approach in a head-on collision given as (T2.12)

$$\begin{aligned} D_{\alpha-N} &= \frac{zZe^2}{4\pi\epsilon_0 E_K} \\ &= \frac{2 \times 79e \times (1.6 \times 10^{-19} \text{ C})}{4\pi \times (8.85 \times 10^{-12} \text{ C} \cdot \text{V}^{-1} \cdot \text{m}^{-1}) \times (6.5 \times 10^6 \text{ eV})} \\ &= 35 \text{ fm}, \end{aligned} \quad (2.93)$$

with z and Z the atomic number of the α particle ($z = 2$) and gold atom ($Z = 79$), respectively.

To define the sensitive scattering area of the annular (ring) detector we now introduce two scattering angles θ : θ_i and θ_o , the inner scattering angle and the outer scattering angle, respectively. With the help of the schematic diagram of the experiment, given in (a), we find the following values for θ_i and θ_o

$$\tan \theta_i = \frac{r_i}{R} = \frac{7.5}{50} = 0.15 \quad \text{or} \quad \theta_i = 0.149 = 8.5^\circ \quad (2.94)$$

and

$$\tan \theta_o = \frac{r_o}{R} = \frac{10}{50} = 0.2 \quad \text{or} \quad \theta_o = 0.197 = 11.3^\circ. \quad (2.95)$$

To determine the probability $\sigma|_{\theta_i}^{\theta_o}$ for α particle scattering with scattering angle θ between θ_i and θ_o (i.e., $\theta_i \leq \theta \leq \theta_o$) we integrate (2.92) between the two angular limits assuming azimuthal symmetry with $d\Omega = 2\pi \sin \theta d\theta$

$$\begin{aligned} \sigma|_{\theta_i}^{\theta_o} &= \int_{\theta_i}^{\theta_o} \frac{d\sigma_{\text{Ruth}}}{d\Omega} d\Omega = 2\pi \left(\frac{D_{\alpha-N}}{4} \right)^2 \int_{\theta_i}^{\theta_o} \frac{\sin \theta}{\sin^4 \frac{\theta}{2}} d\theta = \frac{\pi D_{\alpha-N}^2}{2} \int_{\theta_i}^{\theta_o} \frac{d \sin \frac{\theta}{2}}{\sin^3 \frac{\theta}{2}} \\ &= -\frac{\pi}{4} \frac{D_{\alpha-N}^2}{\sin^2 \frac{\theta}{2}} \Big|_{\theta_i}^{\theta_o} = -\frac{\pi}{4} \times (35 \times 10^{-13} \text{ cm})^2 \left[\frac{1}{\sin^2 0.0985} - \frac{1}{\sin^2 0.0745} \right] \\ &= 7.42 \times 10^{-22} \text{ cm}^2. \end{aligned} \quad (2.96)$$

To complete the calculation we must still determine the number of gold targets per unit area N_a/S and multiply this number by the incident beam intensity I_0 and the probability $\sigma|_{\theta_i}^{\theta_o}$ for scattering into the annual detector.

Number of atoms N_a per volume \mathcal{V} of gold is given as

$$\frac{N_a}{\mathcal{V}} = \rho \frac{N_a}{m} = \rho \frac{N_A}{A} = \frac{(19.3 \text{ g} \cdot \text{cm}^{-3}) \times (6.022 \times 10^{23} \text{ mol}^{-1})}{(197 \text{ g} \cdot \text{mol}^{-1})} = 5.9 \times 10^{22} \text{ cm}^{-3}. \quad (2.97)$$

Number of atoms (targets) per area S of gold is

$$\frac{N_a}{S} = \frac{N_a}{\mathcal{V}} t = (5.9 \times 10^{22} \text{ cm}^{-3}) \times (2 \times 10^{-5} \text{ cm}) = 1.18 \times 10^{18} \text{ cm}^{-2}. \quad (2.98)$$

The rate (intensity) I of α particles reaching the annular detector is now given as

$$\begin{aligned} I &= \frac{N_a}{S} I_0 \sigma |_{\theta_1}^{\theta_2} = (1.18 \times 10^{18} \text{ cm}^{-2}) \times (3.5 \times 10^6 \text{ s}^{-1}) \times (7.42 \times 10^{-22} \text{ cm}^2) \\ &= 3.06 \times 10^3 \text{ s}^{-1}. \end{aligned} \quad (2.99)$$

2.4.Q2**(73)**

A beam of α particles with kinetic energy E_K of 5.5 MeV and intensity I_0 of $2 \times 10^4 \text{ s}^{-1}$ is incident normally on a gold foil ($\rho = 19.3 \text{ g} \cdot \text{cm}^{-3}$; $A = 197 \text{ g/mol}$) of thickness $t = 1.5 \times 10^{-5} \text{ cm}$. An α particle counter of area S_{det} of 1 cm^2 is placed at a distance R of 12 cm from the center of the foil.

Determine the number of counts per hour measured by the detector placed with its center at a scattering angle Θ of (a) 15° and (b) 45° .

SOLUTION:

In Prob. 63 (2.15) we calculated the following expression for the probability $P(\Theta) d\Theta$ of α particle scattering into an angular range from Θ to $\Theta + d\Theta$

$$P(\Theta) d\Theta = \frac{\pi}{8} \rho \frac{N_A}{A} t D_{\alpha-N}^2 \frac{\sin \Theta d\Theta}{\sin^4(\frac{1}{2}\Theta)}. \quad (2.100)$$

Since the detector is placed at a distance $R = 12 \text{ cm}$ from the center of the foil, we apply a correction factor f_{corr} to account for the difference between the scattering area S_{scat} and the detector sensitive area S_{det} where $S_{\text{det}} < S_{\text{scat}}$, as shown in Fig. 2.11. The scattering area S_{scat} encompassed between scattering angles Θ and $\Theta + d\Theta$ is expressed as

$$S_{\text{scat}} = (2\pi R \sin \Theta) \times (R d\Theta) = 2\pi R^2 \sin \Theta d\Theta, \quad (2.101)$$

and the correction factor f_{corr} is thus given as

$$f_{\text{corr}} = \frac{S_{\text{det}}}{S_{\text{scat}}} = \frac{S_{\text{det}}}{2\pi R^2 \sin \Theta d\Theta}. \quad (2.102)$$

The signal intensity (number of particles per hour) $dN/dt|_{\text{det}}$ measured by the detector is estimated as follows accounting for:

- (1) Scattering probability $P(\Theta) d\Theta$ into angular range between Θ and $\Theta + d\Theta$ covered by the detector.
- (2) Fraction of all α particles scattered into angular range between Θ and $\Theta + d\Theta$ that the detector of area S_{det} actually detects

$$dN/dt|_{\text{det}} = I_0 \times \{P(\Theta) d\Theta\} \times f_{\text{corr}}$$

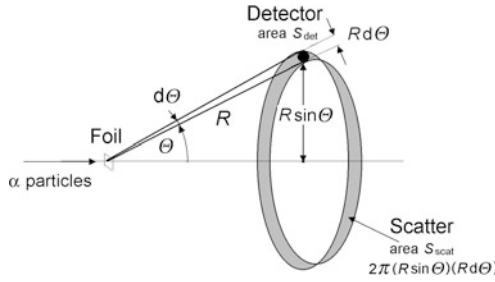


Fig. 2.11 Schematic diagram of the scattering experiment. The detector sensitive area is smaller than the scattering area

$$\begin{aligned}
 &= \frac{S_{\text{det}}}{2\pi R^2 \sin \theta d\theta} I_0 \frac{\pi}{8} \rho \frac{N_A}{A} t D_{\alpha-N}^2 \frac{\sin \theta d\theta}{\sin^4(\frac{1}{2}\theta)} \\
 &= \rho \frac{N_A}{A} t D_{\alpha-N}^2 I_0 \frac{S_{\text{det}}}{16R^2 \sin^4(\frac{1}{2}\theta)} = C_1 \frac{I_0}{\sin^4(\frac{1}{2}\theta)}, \quad (2.103)
 \end{aligned}$$

where C is a constant dependent on physical properties of the scattering foil (ρ , A , t and $D_{\alpha-N}$) as well as the geometry of the scattering experiment (R and S_{det}) but independent of the scattering angle θ and the intensity I_0 of the incident α particle beam.

For our gold foil experiment we calculate the following (unit-less) C_1

$$\begin{aligned}
 C_1 &= \rho \frac{N_A}{A} t D_{\alpha-N}^2 \frac{S_{\text{det}}}{16R^2} = \left[19.3 \frac{\text{g}}{\text{cm}^3} \right] \times \left[\frac{6.022 \times 10^{23} \text{ mol}^{-1}}{197 \text{ g}} \right] \\
 &\quad \times [1.5 \times 10^{-5} \text{ cm}] \times [41.4 \times 10^{-13} \text{ cm}]^2 \times \frac{[1 \text{ cm}^2]}{16 \times [12 \text{ cm}]^2} = 6.58 \times 10^{-9}, \quad (2.104)
 \end{aligned}$$

with $D_{\alpha-N}$ calculated in (2.5) for $E_K = 5.5 \text{ MeV}$ α particle scattering on gold nucleus as

$$D_{\alpha-N} = \frac{C_{\alpha-N} Z}{E_K} = \frac{zZe^2}{4\pi\epsilon_0 E_K} = 41.4 \text{ fm}. \quad (2.105)$$

(a) Scattering angle $\theta = 15^\circ$

Equation (2.103) gives the general result for particle intensity measured by the detector for a given incident intensity I_0 and a given scattering angle θ . Inserting $I_0 = 2 \times 10^4 \text{ s}^{-1}$ and $\theta = 15^\circ$ into (2.103) we get the following result for particle intensity measured by the detector

$$\left. \frac{dN}{dt} \right|_{\text{det}} = C_1 \frac{I_0}{\sin^4(\frac{1}{2}\theta)} = 6.58 \times 10^{-9} \times \frac{2 \times 10^4 \text{ s}^{-1}}{\sin^4 7.5^\circ} = 1632 \text{ h}^{-1}. \quad (2.106)$$

(b) Scattering angle $\Theta = 45^\circ$

Inserting $I_0 = 2 \times 10^4 \text{ s}^{-1}$ and $\Theta = 45^\circ$ into (2.103) results in

$$\left. \frac{dN}{dt} \right|_{\text{det}} = C_1 \frac{I_0}{\sin^4(\frac{1}{2}\theta)} = 6.58 \times 10^{-9} \times \frac{2 \times 10^4 \text{ s}^{-1}}{\sin^4 22.5^\circ} = 6.14 \times 10^{-3} \text{ s}^{-1} = 22.1 \text{ h}^{-1}. \quad (2.107)$$

2.4.Q3

(74)

Several special angles have been defined in conjunction with experiments and theory of elastic particle scattering, such as θ , Θ , θ_{\min} , θ_{\max} , $\sqrt{\theta^2}$, and $\sqrt{\Theta^2}$, where

- θ is the scattering angle for single scattering.
- Θ is the scattering angle for multiple scattering.
- θ_{\min} is a cut-off angle used to account for nuclear Coulomb shielding by atomic orbital electrons.
- θ_{\max} is a cut-off angle used to account for the finite size of the nucleus.
- $\sqrt{\theta^2}$ is the root-mean-square (RMS) angle for single scattering.
- $\sqrt{\Theta^2}$ is the root-mean-square (RMS) scattering angle for multiple scattering.

For Rutherford scattering of particles with kinetic energy $E_K = 5.5 \text{ MeV}$ on a silver foil of thickness $t = 10^{-5} \text{ cm}$ calculate:

- (a) Cut-off angles θ_{\min} and θ_{\max} as well as ratio $\theta_{\max}/\theta_{\min}$. Verify the calculated θ_{\min} and θ_{\max} on a graph showing the two angles for silver against kinetic energy E_K of the α particle.
- (b) Total Rutherford cross-section σ_{Ruth} .
- (c) Mean square scattering angle θ^2 and the root-mean-square scattering angle $\sqrt{\theta^2}$ for single scattering.
- (d) Mean square scattering angle Θ^2 and root-mean-square scattering angle $\sqrt{\Theta^2}$ for multiple Rutherford scattering.

The following data for silver may be useful: mass density $\rho = 10.5 \text{ g/cm}^3$; atomic number $Z = 47$; atomic weight $A = 107.87 \text{ g/mol}$.

SOLUTION:

All relationships used for solving this problem are derived in Sect. T2.4 and summarized in Table T2.3. Before delving into the individual sections of the problem we calculate $D_{\alpha-N}$, the distance of closest approach in a head-on collision between

α particle and silver nucleus (T2.12)

$$\begin{aligned} D_{\alpha-N} &= \frac{zZe^2}{4\pi\epsilon_0 E_K} = \frac{2 \times 47 \times e \times (1.6 \times 10^{-19} \text{ A} \cdot \text{s})}{4\pi \times (8.85 \times 10^{-12} \text{ A} \cdot \text{s} \cdot \text{V}^{-1} \cdot \text{m}^{-1}) \times 5.5 \times 10^6 \text{ eV}} \\ &= 24.6 \text{ fm}. \end{aligned} \quad (2.108)$$

(a) Cut-off angles θ_{\min} and θ_{\max} are given as [(T2.57) and (T2.69), respectively]

$$\begin{aligned} \theta_{\min} &= \frac{\hbar}{pa_{\text{TF}}} = \frac{\hbar c \sqrt[3]{Z}}{a_0 \sqrt{E_K(E_K + 2E_\alpha)}} \\ &= \frac{(197.3 \text{ MeV} \cdot \text{fm}) \times \sqrt[3]{47}}{(0.529 \times 10^5 \text{ fm}) \times \sqrt{(5.5 \text{ MeV}) \times (5.5 \text{ MeV} + 3727 \text{ MeV})}} \\ &= 6.64 \times 10^{-5} \text{ rad} \end{aligned} \quad (2.109)$$

and

$$\begin{aligned} \theta_{\max} &= \frac{\hbar}{pR} = \frac{\hbar c}{R_0 \sqrt[3]{AZ} \sqrt{E_K(E_K + 2E_\alpha)}} \\ &= \frac{(197.3 \text{ MeV} \cdot \text{fm})}{(1.25 \text{ fm}) \times \sqrt[3]{107.87} \sqrt{(5.5 \text{ MeV}) \times (5.5 \text{ MeV} + 3727 \text{ MeV})}} = 0.164 \text{ rad}. \end{aligned} \quad (2.110)$$

Angles calculated in (2.109) and (2.110) are superimposed onto the graph in Fig. 2.12 plotting cutoff angles θ_{\min} and θ_{\max} against kinetic energy E_K for electrons and α particles scattered on various materials. The calculated data for 5.5 MeV α particles fit nicely onto the curve for silver.

Ratio $\theta_{\max}/\theta_{\min}$ is thus given as

$$\frac{\theta_{\max}}{\theta_{\min}} = \frac{a_0}{R_0 \sqrt[3]{AZ}} = \frac{0.529 \times 10^5 \text{ fm}}{1.25 \text{ fm}) \times \sqrt[3]{107.87 \times 47}} = \frac{0.164}{6.64 \times 10^{-5}} = 2470. \quad (2.111)$$

(b) Total Rutherford cross section is given in (T2.79) as

$$\sigma_{\text{Ruth}} = \frac{\pi D_{\alpha-N}^2}{\theta_{\min}^2} = \frac{\pi \times (24.6 \text{ fm})^2}{(6.64 \times 10^5 \text{ rad})^2} = 4.31 \times 10^9 \text{ b}. \quad (2.112)$$

(c) Mean square scattering angle $\overline{\theta^2}$ and root-mean-square scattering angle $\sqrt{\overline{\theta^2}}$ for single scattering are given as [see (T2.84) and (T2.86)]:

$$\overline{\theta^2} \approx 2\theta_{\min}^2 \ln \frac{\theta_{\max}}{\theta_{\min}} = 2 \times (6.64 \times 10^{-5} \text{ rad})^2 \times \ln 2470 = 6.89 \times 10^{-8} (\text{rad})^2 \quad (2.113)$$

and

$$\sqrt{\overline{\theta^2}} = \sqrt{6.89 \times 10^{-8}} \text{ rad} = 2.6 \times 10^{-4} \text{ rad} = 0.015^\circ. \quad (2.114)$$

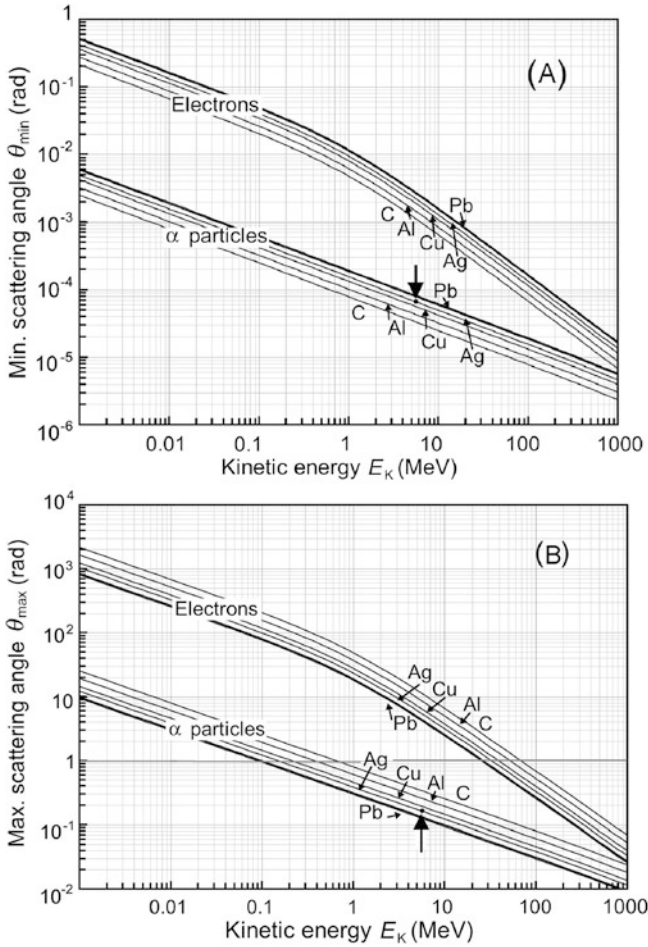


Fig. 2.12 Minimum scattering angle θ_{\min} in (A) and maximum scattering angle θ_{\max} in (B) against kinetic energy E_K for electrons and α particles scattered on carbon, aluminum, copper, silver, gold, and lead. The data points calculated in (a) for α particles of $E_K = 5.5$ MeV scattered on silver are indicated with heavy arrows

(d) Cumulative mean square scattering angle $\overline{\Theta^2}$ and root-mean-square scattering angle $\sqrt{\overline{\Theta^2}}$ for multiple scattering are given as [see (T2.91) and (T2.92)]

$$\overline{\Theta^2} = 2\pi\rho \frac{N_A}{A} t D_{\alpha-N}^2 \ln \frac{\theta_{\max}}{\theta_{\min}} = n\overline{\theta^2}, \tag{2.115}$$

where n is the number of scattering events expressed as (T2.88)

$$n = \rho \frac{N_A}{A} \sigma_{\text{Ruth}} t$$

$$\begin{aligned}
 &= (10.5 \text{ g/cm}^3) \times \frac{6.022 \times 10^{23} \text{ mol}^{-1}}{107.87 \text{ g} \cdot \text{mol}^{-1}} \times (4.31 \times 10^{-15} \text{ cm}^2) \\
 &\quad \times (10^{-5} \text{ cm}) = 2526. \tag{2.116}
 \end{aligned}$$

After inserting (2.116) into (2.115) we get $\overline{\Theta^2} = 1.74 \times 10^{-4} \text{ (rad)}^2$ and $\sqrt{\overline{\Theta^2}} = 0.13 \text{ rad} = 0.7^\circ$.

2.5 Mott Scattering

2.5.Q1

(75)

An electron with kinetic energy E_K is scattered elastically off a nucleus of rest mass Mc^2 . In addition to the scattering angle θ , the following parameters govern the interaction: rest energy $m_e c^2$, momentum \mathbf{p} , and kinetic energy E'_K of the incident electron; rest energy $m_e c^2$, momentum \mathbf{p}' , and kinetic energy E'_K of the scattered electron; rest energy Mc^2 , recoil momentum $\Delta\mathbf{p}$, and recoil kinetic energy ΔE_K of the nucleus.

- Plot a vector diagram of the scattering process and derive a general expression for momentum transfer Δp (recoil momentum of the nucleus) as a function of θ , E_K , and E'_K .
- Derive a relativistic expression for energy transfer ΔE_K from the incident electron to the nucleus (recoil energy of the nucleus) as a function of θ , E_K , E'_K , and Mc^2 .
- Derive a relativistic expression for kinetic energy E'_K of scattered electron as a function of θ , E_K , and Mc^2 .
- Equation, derived in (c) for kinetic energy of the scattered electron, is well known and of great importance in another area of radiation physics. Name that area and briefly explain how the equation is used there.
- Based on result of (c) show that, as $E_K \rightarrow \infty$, maximum kinetic energy E'_K of an electron scattered with an angle $\theta = \frac{1}{2}\pi$ is $E'_K = Mc^2$.
- Based on result of (c) show that, as $E_K \rightarrow \infty$, maximum kinetic energy E'_K of an electron scattered with a scattering angle $\theta = \pi$ is $E'_K = \frac{1}{2}Mc^2$.

SOLUTION:

(a) A schematic diagram of the scattering process is shown in Fig. 2.13. An incident electron of momentum \mathbf{p} and kinetic energy E_K is scattered elastically by nucleus of rest energy Mc^2 through a scattering angle θ to end with momentum \mathbf{p}' and kinetic energy E'_K .

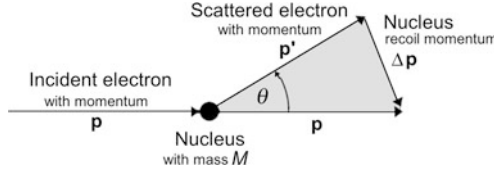


Fig. 2.13 Schematic representation of electron–nucleus scattering (Mott scattering)

Momentum transfer to nucleus (nuclear recoil momentum) Δp

Conservation of momentum for the elastic scattering process is expressed as follows

$$\mathbf{p} = \mathbf{p}' + \Delta \mathbf{p}, \quad (2.117)$$

where \mathbf{p} and \mathbf{p}' are momenta of the incident and scattered electron, respectively, and $\Delta \mathbf{p}$ is the momentum transferred from the incident electron to the nucleus (also called recoil momentum of the nucleus). We use the law of cosines on the momentum triangle of Fig. 2.13 to get

$$\begin{aligned} |\Delta \mathbf{p}|^2 &= (\Delta p)^2 = |\mathbf{p}|^2 + |\mathbf{p}'|^2 - 2|\mathbf{p}||\mathbf{p}'| \cos \theta = p^2 + p'^2 - 2pp' \cos \theta \\ &= \frac{E_K^2}{c^2} \left(1 + \frac{2m_e c^2}{E_K}\right) + \frac{E_K'^2}{c^2} \left(1 + \frac{2m_e c^2}{E_K'}\right) \\ &\quad - 2 \frac{E_K E_K'}{c^2} \sqrt{\left(1 + \frac{2m_e c^2}{E_K}\right) \left(1 + \frac{2m_e c^2}{E_K'}\right)} \cos \theta, \end{aligned} \quad (2.118)$$

where we used the well known expression for electron momenta p and p' as a function of kinetic energy E_K from (T1.64)

$$p = \frac{E_K}{c} \sqrt{\left(1 + \frac{2m_e c^2}{E_K}\right)} \quad \text{and} \quad p' = \frac{E_K'}{c} \sqrt{\left(1 + \frac{2m_e c^2}{E_K'}\right)}. \quad (2.119)$$

(b) Energy transfer to nucleus (nuclear recoil energy) ΔE_K

Conservation of energy for the scattering process is expressed as follows

$$E_K + m_e c^2 + M c^2 = E_K' + m_e c^2 + \Delta E_K + M c^2 \quad \text{or} \quad E_K = E_K' + \Delta E_K, \quad (2.120)$$

where ΔE_K is the energy transfer from the incident electron of rest energy $m_e c^2$ to the nucleus of rest energy $M c^2$ (i.e., recoil energy of the nucleus) expressed in relativistic form as

$$\begin{aligned} \Delta E_K &= E_K - E_K' = \sqrt{(\Delta p)^2 c^2 + (M c^2)^2} - M c^2 \\ &= \sqrt{E_K^2 + E_K'^2 - 2E_K E_K' \cos \theta + (M c^2)^2} - M c^2. \end{aligned} \quad (2.121)$$

(c) Kinetic energy of the scattered electron E'_K

From (2.121) we can obtain another expression for $(\Delta p)^2$, the square of the momentum transfer from incident electron to the nucleus, as a function of kinetic energies E_K and E'_K and nuclear rest energy Mc^2 . We first rearrange (2.121) to get

$$\Delta E_K + Mc^2 \equiv E_K - E'_K + Mc^2 = \sqrt{(\Delta p)^2 c^2 + (Mc^2)^2} \quad (2.122)$$

and then we square (2.122) to get the following expression for $(\Delta p)^2$

$$(\Delta p)^2 = \frac{1}{c^2} (E_K - E'_K)^2 + 2(E_K - E'_K)Mc^2. \quad (2.123)$$

Now we have two expressions for $(\Delta p)^2$ given in (2.118) and (2.123). Equating the two expressions we obtain the following expression linking θ , E_K , E'_K , and Mc^2

$$\begin{aligned} E_K^2 + 2E_K m_e c^2 + E_K'^2 + 2E'_K m_e c^2 - 2E_K E'_K \sqrt{\left(1 + \frac{2m_e c^2}{E_K}\right) \left(1 + \frac{2m_e c^2}{E'}\right)} \cos \theta \\ = E_K^2 - 2E_K E'_K + E_K'^2 + 2E_K Mc^2 - 2E'_K Mc^2. \end{aligned} \quad (2.124)$$

The quadratic terms in (2.124) cancel out and since $E'_K \approx E_K$ we can simplify the square root expression in (2.124) to read

$$\sqrt{\left(1 + \frac{2m_e c^2}{E_K}\right) \left(1 + \frac{2m_e c^2}{E'}\right)} \approx \left(1 + \frac{2m_e c^2}{E_K}\right) \quad (2.125)$$

resulting in the following solution for the kinetic energy of the scattered electron E'_K

$$\begin{aligned} E'_K &= E_K \frac{1}{1 + \frac{m_e c^2}{Mc^2} + \frac{E_K}{Mc^2} \left(1 + \frac{2m_e c^2}{E_K}\right) (1 - \cos \theta)} \\ &= E_K \frac{1}{1 + \frac{m_e c^2}{Mc^2} + \frac{E_K}{Mc^2} (1 - \cos \theta) + \frac{2m_e c^2}{Mc^2} (1 - \cos \theta)}. \end{aligned} \quad (2.126)$$

A closer look at (2.126) shows that the expression for E'_K can be simplified by recognizing that $m_e c^2 \ll Mc^2$ even for the lightest nuclei such as the proton or deuteron to obtain a much simpler expression for E'_K now expressed as follows

$$E'_K = E_K \frac{1}{1 + \frac{E_K}{Mc^2} (1 - \cos \theta)}. \quad (2.127)$$

Energy transfer from incident electron to the nucleus ΔE_K can then, using (2.121) in conjunction with (2.127), be expressed as follows

$$\Delta E_K = E_K - E'_K = E_K \left(1 - \frac{1}{1 + \frac{E_K}{Mc^2}(1 - \cos \theta)} \right) = E_K \frac{\frac{E_K}{Mc^2}(1 - \cos \theta)}{1 + \frac{E_K}{Mc^2}(1 - \cos \theta)}. \quad (2.128)$$

(d) Equation (2.128) is of exactly the same form as the equation for scattered photon energy $h\nu'$ as a function of incident photon energy $h\nu$ and scattering angle θ in Compton effect. A comparison between the two effects is given in Table 2.2.

Table 2.2 Comparison between relationship for electron–nucleus Mott scattering and relationship for photon–free electron Compton scattering

Incident electron kinetic energy E_K	Incident photon energy $h\nu$
Nuclear rest energy Mc^2	Electron rest energy $m_e c^2$
Scattered electron kinetic energy E'_K	Scattered photon energy $h\nu'$
$E'_K = E_K \frac{1}{1 + \frac{E_K}{Mc^2}(1 - \cos \theta)} \quad (2.129)$	$h\nu' = h\nu \frac{1}{1 + \frac{h\nu}{m_e c^2}(1 - \cos \theta)} \quad (2.130)$
Recoil nucleus kinetic energy ΔE_K	Recoil (Compton) electron kinetic energy E_K
$\Delta E_K = E_K \frac{\frac{E_K}{Mc^2}(1 - \cos \theta)}{1 + \frac{E_K}{Mc^2}(1 - \cos \theta)} \quad (2.131)$	$E_K = h\nu \frac{\frac{h\nu}{m_e c^2}(1 - \cos \theta)}{1 + \frac{h\nu}{m_e c^2}(1 - \cos \theta)} \quad (2.132)$

(e) To determine the upper limit in E'_K as $E_K \rightarrow \infty$ and $\theta = \frac{1}{2}\pi$, we rearrange (2.127) to get

$$\begin{aligned} \lim_{\substack{E_K \rightarrow \infty \\ \theta = \frac{1}{2}\pi}} E'_K &= \lim_{\substack{E_K \rightarrow \infty \\ \theta = \frac{1}{2}\pi}} \frac{E_K}{1 + \frac{E_K}{Mc^2}(1 - \cos \theta)} \\ &= \lim_{\substack{E_K \rightarrow \infty \\ \theta = \frac{1}{2}\pi}} \frac{1}{\frac{1}{E_K} + \frac{1}{Mc^2}(1 - \cos \frac{1}{2}\pi)} \\ &= Mc^2. \end{aligned} \quad (2.133)$$

Thus, no matter how high is the incident electron kinetic energy E_K , the side scattered ($\theta = \frac{1}{2}\pi$) electron kinetic energy E'_K cannot exceed Mc^2 where Mc^2 is the rest energy of the scattering nucleus.

(f) To determine the upper limit in E'_K as $E_K \rightarrow \infty$ and $\theta = \pi$, we rearrange (2.127) to get

$$\begin{aligned} \lim_{\substack{E_K \rightarrow \infty \\ \theta = \pi}} E'_K &= \lim_{\substack{E_K \rightarrow \infty \\ \theta = \pi}} \frac{E_K}{1 + \frac{E_K}{Mc^2}(1 - \cos \theta)} \\ &= \lim_{\substack{E_K \rightarrow \infty \\ \theta = \pi}} \frac{1}{\frac{1}{E_K} + \frac{1}{Mc^2}(1 - \cos \pi)} \\ &= \frac{1}{2} Mc^2. \end{aligned} \quad (2.134)$$

Thus, no matter how high is the incident electron kinetic energy E_K , the backscattered ($\theta = \pi$) electron kinetic energy E'_K cannot exceed $\frac{1}{2}Mc^2$ where Mc^2 is the rest energy of the scattering nucleus.

2.5.Q2

(76)

An electron with kinetic energy E_K of 20 MeV is scattered elastically by gold nucleus ($Z = 79Mc^2 = 183433$ MeV). The scattering angle is 60° . For the scattering process calculate:

- Momentum p of the incident electron.
- Kinetic energy E'_K of the scattered electron.
- Recoil energy ΔE_K of the gold nucleus.
- Recoil momentum Δp of the nucleus.
- Momentum p' of the scattered electron.
- Assume that incident electron kinetic energy is $E_K = 2$ GeV, that the scattering nucleus is a proton ($M_p c^2 = 938.3$ MeV) and that scattering angle $\theta = \frac{1}{2}\pi$. Determine E'_K and verify the result with Fig. 2.14.

SOLUTION:

(a) **Momentum p of the incident electron** is calculated using the standard relationship (T1.64) to get

$$p = \frac{E_K}{c} \sqrt{1 + \frac{2m_e c^2}{E_K}} = \frac{(20 \text{ MeV})}{c} \sqrt{1 + \frac{2 \times 0.5110}{20}} = 20.5046 \text{ MeV}/c. \quad (2.135)$$

(b) **Kinetic energy E'_K of the scattered electron** is calculated using (2.127) as follows (see Point B in Fig. 2.14)

$$E'_K = E_K \frac{1}{1 + \frac{E_K}{Mc^2}(1 - \cos \theta)} = \frac{20 \text{ MeV}}{1 + \frac{20}{183433}(1 - \cos 60^\circ)} = 19.99891 \text{ MeV}. \quad (2.136)$$

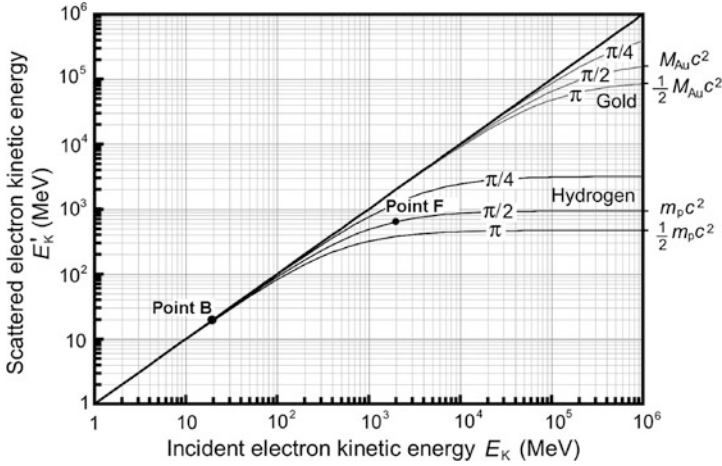


Fig. 2.14 Scattered electron kinetic energy E'_K against the incident electron kinetic energy for Mott scattering on hydrogen and gold nuclei for four scattering angles θ (0 , $\frac{1}{4}\pi$, $\frac{1}{2}\pi$, and π). Points **B** and **F** represent solutions reached in (b) and (f)

(c) **Recoil energy ΔE_K of the gold nucleus** is calculated from (2.128) as follows

$$\begin{aligned} \Delta E_K &= E_K \frac{\frac{E_K}{Mc^2}(1 - \cos\theta)}{1 + \frac{E_K}{Mc^2}(1 - \cos\theta)} \\ &= (20 \text{ MeV}) \times \frac{\frac{20}{183433}(1 - \cos 60^\circ)}{1 + \frac{20}{183433}(1 - \cos 60^\circ)} \\ &= 1.0903 \times 10^{-3} \text{ MeV}. \end{aligned} \quad (2.137)$$

(d) **Recoil momentum Δp of the nucleus** is determined using (2.118) as follows

$$\begin{aligned} \Delta p &= \frac{1}{c} \left\{ E_K^2 + 2E_K m_e c^2 + E'_K{}^2 + 2E'_K m_e c^2 \right. \\ &\quad \left. - 2E_K E'_K \sqrt{\left(1 + \frac{2m_e c^2}{E_K}\right) \left(1 + \frac{2m_e c^2}{E'_K}\right) \cos\theta} \right\}^{\frac{1}{2}} \\ &= \left\{ 20^2 + 2 \times 20 \times 0.511 + 19.99891^2 + 2 \times 19.99891 \times 0.511 - 2 \times 20 \right. \\ &\quad \left. \times 19.99891 \times \sqrt{\left(1 + \frac{2 \times 0.511}{20}\right) \times \left(1 + \frac{2 \times 0.511}{19.99891}\right) \cos 60^\circ} \right\}^{\frac{1}{2}} \text{ MeV}/c \\ &= 20.5041 \text{ MeV}/c. \end{aligned} \quad (2.138)$$

(e) **Momentum p' of the scattered electron** is calculated using the standard relationship given in (2.136) and (T1.64) to get

$$p' = \frac{E'_K}{c} \sqrt{1 + \frac{2m_e c^2}{E_K}} = \frac{(19.99891 \text{ MeV})}{c} \sqrt{1 + \frac{2 \times 0.5110}{19.99891}} = 20.5035 \text{ MeV}/c. \quad (2.139)$$

(f) **Kinetic energy E'_K of the scattered electron** is calculated using (2.127) as follows (see Point F in Fig. 2.14)

$$E'_K = E_K \frac{1}{1 + \frac{E_K}{Mc^2} (1 - \cos \theta)} = \frac{2 \times 10^3 \text{ MeV}}{1 + \frac{2 \times 10^3}{938.3} (1 - \cos 90^\circ)} = 638.7 \text{ MeV}. \quad (2.140)$$

Table 2.3A Determination of the nuclear recoil correction factor f_{recoil}

Element		Hydrogen	Silver	Gold
Z		1	47	79
A		1	107	197
Mc^2 (MeV)		938.3	100455	183433
E_K	θ	$\theta = \frac{1}{4}\pi = 45^\circ$	$\theta = \frac{1}{2}\pi = 90^\circ$	$\theta = \pi = 180^\circ$
≤ 10 MeV		$x \leq$ $f_{\text{recoil}} =$	$x \leq$ $f_{\text{recoil}} =$	$x \leq$ $f_{\text{recoil}} =$
100 MeV		$x =$ $f_{\text{recoil}} =$	$x =$ $f_{\text{recoil}} =$	$x =$ $f_{\text{recoil}} =$
1 GeV		$x =$ $f_{\text{recoil}} =$	$x =$ $f_{\text{recoil}} =$	$x =$ $f_{\text{recoil}} =$
10 GeV		$x =$ $f_{\text{recoil}} =$	$x =$ $f_{\text{recoil}} =$	$x =$ $f_{\text{recoil}} =$
100 GeV		$x =$ $f_{\text{recoil}} =$	$x =$ $f_{\text{recoil}} =$	$x =$ $f_{\text{recoil}} =$
1000 GeV		$x =$ $f_{\text{recoil}} =$	$x =$ $f_{\text{recoil}} =$	$x =$ $f_{\text{recoil}} =$

2.5.Q3

(77)

Nuclear recoil correction factor f_{recoil} is one of several factors used to correct the Rutherford scattering cross section for relativistic and quantum effects in studies of electron scattering on nuclei. The f_{recoil} correction factor is defined as the ratio of the scattered electron kinetic energy E'_K to incident electron kinetic energy E_K and, as derived in Prob. 76, can be expressed as follows

$$f_{\text{recoil}} = \frac{E'_K}{E_K} = \frac{1}{1 + \frac{E_K}{Mc^2}(1 - \cos \theta)}, \quad (2.141)$$

where Mc^2 is the rest energy of the target nucleus and θ is the scattering angle of the electron.

- (a) Discuss the dynamic range of f_{recoil} with respect to E_K , Mc^2 , and θ .
- (b) Plot f_{recoil} against variable x for scattering angles $\theta = 0, \frac{1}{4}\pi, \frac{1}{2}\pi, \frac{3}{4}\pi$, and π , where x is defined as $x = E_K/(Mc^2)$.
- (c) With the help of the graph prepared in (b) determine f_{recoil} for hydrogen, silver, and gold at various electron kinetic energies E_K and scattering angles θ , as indicated in Table 2.3A.

SOLUTION:

(a) As evident from (2.141), the nuclear recoil correction factor f_{recoil} depends upon three parameters: E_K , Mc^2 , and θ . The major trends in f_{recoil} behavior are as follows:

- (1) The dynamic range of f_{recoil} is from 0 to 1, i.e., $0 \leq f_{\text{recoil}} \leq 1$.
- (2) For $\theta = 0$, $f_{\text{recoil}} = 1$ irrespective of E_K .
- (3) For constant E_K and Mc^2 , f_{recoil} decreases with increasing θ .
- (4) For constant Mc^2 and $\theta > 0$, f_{recoil} decreases with increasing E_K .
- (5) For constant E_K and θ , f_{recoil} increases with increasing Mc^2 .

(b) Energy dependence of f_{recoil} can be compressed into one graph by plotting f_{recoil} against variable $x = E_K/(Mc^2)$, as shown in Fig. 2.15.

(c) Determination of the nuclear recoil correction factor f_{recoil} of (2.141) for electron scattering on nuclei of hydrogen ($\theta = 45^\circ$), silver ($\theta = 90^\circ$), and gold ($\theta = 180^\circ$) for electron kinetic energies E_K of 10 MeV, 100 MeV, 1 GeV, 10 GeV, 100 GeV, and 1000 GeV. For each scattering material we first determine parameter $x = E_K/(Mc^2)$ and then use the graph (f_{recoil}, x) of Fig. 2.15 to determine f_{recoil} for a given x .

By way of example, we now determine f_{recoil} for scattering of 100 GeV electrons on silver nucleus: Parameter $x = (10^5 \text{ MeV})/(100455 \text{ MeV}) = 0.995$ and from Fig. 2.15 we read $f_{\text{recoil}}(x = 0.995) \approx 0.5$. This result and results for all other required combinations of electron kinetic energy E_K , scattering angle θ , and scattering material were entered into Table 2.3B.

From Table 2.3B it is obvious that the nuclear recoil correction factor f_{recoil} is only of theoretical interest to medical physics, since for electron energies below 100 MeV it is equal to 1. However, at electron kinetic energies above 100 MeV the recoil correction becomes progressively more important in the theory of Mott scattering.

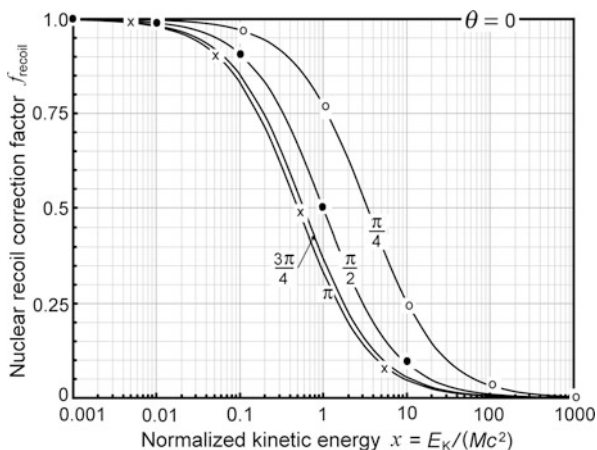


Fig. 2.15 Nuclear recoil correction factor f_{recoil} against normalized kinetic energy $x = E_K/(Mc^2)$ with Mc^2 the rest energy of the target nucleus for scattering angles θ between 0° , 45° , 90° , 135° , and 180°

Table 2.3B Nuclear recoil correction factor f_{recoil} determined with the graph of (f_{recoil}, x) where x is the normalized kinetic energy E_K of the electron [$x = E_K/(Mc^2)$]. The graph was determined with (2.141) and is provided in Fig. 2.15

Element	Hydrogen	Silver	Gold	
Z	1	47	79	
A	1	107	197	
Mc^2 (MeV)	938.3	100455	183433	
E_K	θ	$\theta = \frac{1}{4}\pi$	$\theta = \frac{1}{2}\pi$	$\theta = \pi$
≤ 10 MeV	$x \leq 0.0107$ $f_{\text{recoil}} \approx 1$	$x \leq 0.0001$ $f_{\text{recoil}} = 1$	$x \leq 0.000055$ $f_{\text{recoil}} = 1$	
100 MeV	$x = 0.107$ $f_{\text{recoil}} = 0.97$	$x = 0.001$ $f_{\text{recoil}} \approx 1$	$x = 0.00055$ $f_{\text{recoil}} \approx 1$	
1 GeV	$x = 1.07$ $f_{\text{recoil}} = 0.76$	$x = 0.01$ $f_{\text{recoil}} = 0.99$	$x = 0.0055$ $f_{\text{recoil}} = 0.99$	
10 GeV	$x = 10.7$ $f_{\text{recoil}} = 0.24$	$x = 0.1$ $f_{\text{recoil}} = 0.91$	$x = 0.055$ $f_{\text{recoil}} = 0.90$	
100 GeV	$x = 107$ $f_{\text{recoil}} = 0.03$	$x = 1$ $f_{\text{recoil}} = 0.5$	$x = 0.55$ $f_{\text{recoil}} = 0.48$	
1000 GeV	$x = 1070$ $f_{\text{recoil}} \approx 0$	$x = 10$ $f_{\text{recoil}} = 0.09$	$x = 5.5$ $f_{\text{recoil}} = 0.08$	

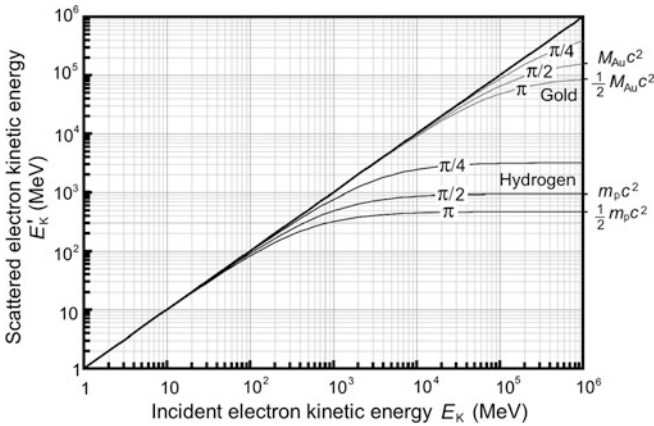


Fig. 2.16 Scattered electron kinetic energy $E'_K = f_{\text{recoil}} E_K$ against incident electron kinetic energy E_K for Mott elastic scattering of electrons on hydrogen and gold nuclei for four scattering angles θ

2.5.Q4

(78)

For Mott elastic scattering of electrons with kinetic energy E_K of 10 GeV on protons at rest determine:

- (a) Kinetic energy E'_K of electron scattered at scattering angles $\theta = 0, \frac{1}{12}\pi, \frac{1}{4}\pi, \frac{1}{2}\pi, \frac{3}{4}\pi, \text{ and } \pi$.
- (b) Recoil energy ΔE_K of proton for scattering angles $\theta = 0, \frac{1}{12}\pi, \frac{1}{4}\pi, \frac{1}{2}\pi, \frac{3}{4}\pi, \text{ and } \pi$.
- (c) Nuclear recoil correction factor f_{recoil} for scattering angles $\theta = 0, \frac{1}{12}\pi, \frac{1}{4}\pi, \frac{1}{2}\pi, \frac{3}{4}\pi, \text{ and } \pi$.
- (d) Enter the results calculated in (a) onto appropriate curves in Fig. 2.16 that plots E'_K against incident electron energy E_K for hydrogen and gold nuclei for various scattering angles θ .
- (e) Sketch kinetic energy E'_K of scattered electron and recoil energy ΔE_K of the nucleus against scattering angle θ .
- (f) Sketch the nuclear recoil correction factor f_{recoil} against scattering angle θ .

SOLUTION:

To solve this problem we use expressions derived in Prob. 76 for E'_K , ΔE_K , and f_{recoil} in Mott elastic scattering of electrons on atomic nuclei and show below a sample calculation for scattering angle $\theta = \frac{1}{4}\pi$.

Table 2.4 Kinetic energy E'_K of scattered electron, proton recoil energy ΔE_K , and recoil correction factor f_{recoil} for various scattering angles θ in Mott elastic scattering of electrons on protons at rest. Kinetic energy E_K of incident electrons is 10 GeV

(1)	Scattering angle θ	0	$\frac{\pi}{12} = 15^\circ$	$\frac{\pi}{4} = 45^\circ$	$\frac{\pi}{2} = 90^\circ$	$\frac{3\pi}{4} = 135^\circ$	$\pi = 180^\circ$
(2)	$\cos \theta$	1	0.966	0.707	0	-0.707	-1
(3)	E'_K (GeV)	10	7.34	2.43	0.86	0.52	0.45
(4)	ΔE_K (GeV)	0	2.66	7.57	9.14	9.48	9.55
(5)	f_{recoil}	1	0.734	0.243	0.086	0.052	0.045

- (a) **Kinetic energy E'_K of the scattered electron** is in (2.127) given as function of scattering angle θ and incident electron kinetic energy E_K (see point A in Fig. 2.18)

$$E'_K = \frac{E_K}{1 + \frac{E_K}{M_p c^2} (1 - \cos \theta)} = \frac{10 \text{ GeV}}{1 + \frac{10}{0.9383} (1 - \cos 45^\circ)} = 2.43 \text{ GeV}. \quad (2.142)$$

- (b) **Recoil kinetic energy ΔE_K of the nucleus** is in (2.128) also given as function of scattering angle θ and incident electron kinetic energy E_K and expressed as follows (see point B in Fig. 2.18)

$$\begin{aligned} \Delta E_K &= E_K \frac{\frac{E_K}{M_p c^2} (1 - \cos \theta)}{1 + \frac{E_K}{M_p c^2} (1 - \cos \theta)} \\ &= (10 \text{ GeV}) \frac{\frac{10}{0.9383} (1 - \cos 45^\circ)}{1 + \frac{10}{0.9383} (1 - \cos 45^\circ)} \\ &= 7.57 \text{ GeV}. \end{aligned} \quad (2.143)$$

- (c) **Recoil correction factor f_{recoil}** is in (2.141) given as (see point C in Fig. 2.19)

$$\begin{aligned} f_{\text{recoil}} &= \frac{E'_K}{E_K} = \frac{2.43}{10} = 0.243 \equiv \frac{E_K - \Delta E_K}{E_K} = 1 - \frac{\Delta E_K}{E_K} \\ &= 1 - \frac{7.57}{10} = 0.243. \end{aligned} \quad (2.144)$$

Results of calculations in (a), (b), and (c) as well as of corresponding calculations for several other scattering angles θ are presented in Table 2.4 and in Figs. 2.18 and 2.19.

- (d) **Kinetic energy E'_K of the scattered electron** calculated with (2.142) and listed in row (3) of Table 2.4 is entered with solid circle data points in Fig. 2.17 superimposed on curves plotting E'_K against incident electron kinetic energy E_K for $\theta = 0, \frac{1}{4}\pi, \frac{1}{2}\pi$, and π in the E_K range from 1 MeV to 10^6 MeV.

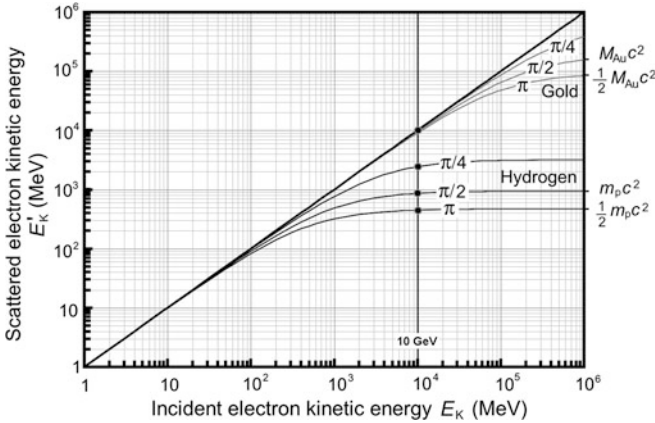


Fig. 2.17 Scattered electron kinetic energy $E'_K = f_{\text{recoil}} E_K$ against incident electron kinetic energy E_K for Mott elastic scattering of electrons on hydrogen and gold nuclei for four scattering angles θ . Results of calculations in (a) for 10 GeV electrons are entered on E'_K vs. E_K curves by solid circle data points

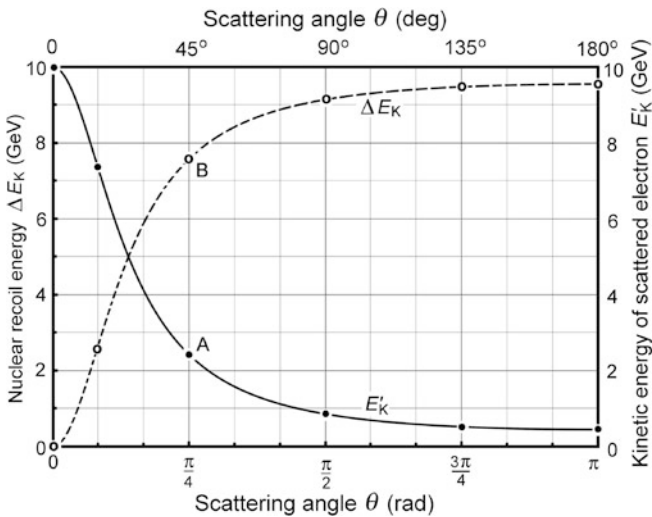


Fig. 2.18 Nuclear recoil energy ΔE_K and kinetic energy of the scattered electron E'_K against scattering angle θ for $0 \leq \theta \leq \pi$ for electrons of kinetic energy E_K of 10 GeV scattered on protons at rest. Points A and B represent results of sample calculations for $\theta = 45^\circ$ in (a) and (b), respectively

Several interesting points can be made based on Fig. 2.17:

- (1) $E'_K = E_K$ at relatively low E_K , irrespective of nuclear mass M and scattering angle θ .
- (2) At high E_K , on the other hand, E'_K saturates at $(E'_K)_{\text{max}}$ that is proportional to M and inversely proportional to θ .

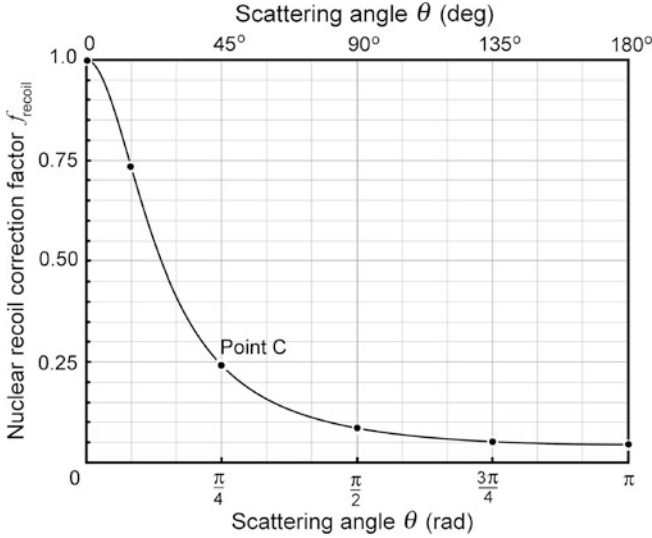


Fig. 2.19 Nuclear recoil correction factor f_{recoil} against electron scattering angle θ for $0 \leq \theta \leq \pi$ for electrons of kinetic energy E_K of 10 GeV scattered on protons at rest. Point C represents the result of the sample calculation of f_{recoil} at $\theta = 45^\circ$ in (c)

- (3) For a given M and θ the maximum E'_K is determined from (2.142) as follows

$$\begin{aligned}
 (E'_K)_{\max} &= \lim_{E_K \rightarrow \infty} \frac{E_K}{1 + \frac{E_K}{Mc^2}(1 - \cos \theta)} \\
 &= \lim_{E_K \rightarrow \infty} \frac{1}{\frac{1}{E_K} + \frac{1}{Mc^2}(1 - \cos \theta)} \\
 &= \frac{Mc^2}{1 - \cos \theta}. \tag{2.145}
 \end{aligned}$$

- (4) Equation (2.145) gives $(E'_K)_{\max}$ in general and provides the following results for special angles: forward scattering at $\theta = 0$, side scattering at $\theta = \frac{1}{2}\pi$, and backscattering at $\theta = \pi$, respectively

$$(E'_K)_{\max} = E_K, \tag{2.146}$$

$$(E'_K)_{\max} = Mc^2, \tag{2.147}$$

$$(E'_K)_{\max} = \frac{1}{2}Mc^2, \tag{2.148}$$

where M stands for the mass of the particle upon which electrons are scattered.

(5) Equations (2.142) through (2.148) for Mott scattering on nuclei have exactly the same structure as equations used for describing Compton scattering of photon on free electron, if we replace E_K of (2.142) with incident photon energy $h\nu$, $M_p c^2$ of (2.142) with rest energy $m_e c^2$ of electron, and ΔE_K of (2.142) with recoil energy E_K of electron (see (7.41)).

(e) Kinetic energy E'_K of the scattered electron and recoil energy ΔE_K of the nucleus for Mott elastic scattering of electrons of incident kinetic energy E_K on protons at rest are calculated with (2.142) and (2.143), respectively, for scattering angles $\theta = 0, \frac{1}{4}\pi, \frac{1}{2}\pi, \frac{3}{4}\pi, \text{ and } \pi$, listed in rows (3) and (4), respectively, of Table 2.4, and plotted with solid circle data points and open circle data points, respectively, in Fig. 2.18. Points A and B in Fig. 2.18 represent results of the calculations of scattered electron kinetic energy E'_K and nuclear recoil energy ΔE_K in (a) and (b), respectively, for 10 GeV electrons scattered at $\theta = 45^\circ$.

(f) Nuclear recoil correction factor f_{recoil} is calculated for scattering angles $\theta = 0, \frac{1}{4}\pi, \frac{1}{2}\pi, \frac{3}{4}\pi, \text{ and } \pi$ with (2.144), listed in row (5) of Table 2.4, and plotted with solid circle data points in Fig. 2.19. Point C on the plot represents the result of f_{recoil} calculation in (c) for 10 GeV electrons scattered at $\theta = 45^\circ$.

2.6 General Aspects of Elastic Scattering of Charged Particles

2.6.Q1

(79)

Each elastic scattering event between two particles (projectile and target) can be characterized by a scattering parameter referred to as the characteristic scattering distance D . This distance depends on the nature of the specific scattering event as well as on various physical properties of the projectile and the target.

(a) Determine the general expression for the characteristic scattering distance D as a function of incident particle's normalized kinetic energy τ where $\tau = E_K/m_0c^2$ with E_K the particle's incident kinetic energy and m_0c^2 its rest energy.

Determine expressions for characteristic scattering distance D for four standard examples of Coulomb elastic scattering and summarize the results in a table:

- (b) Rutherford scattering: α particle–nucleus (α -N).
- (c) Mott scattering: electron–nucleus (e-N).
- (d) Møller scattering: electron–orbital electron (e-e).
- (e) Electron–atom (e-a) scattering.

SOLUTION:

(a) The following expression defines the characteristic scattering distance D for any type of Coulomb scattering

$$D = \frac{zZe^2}{4\pi\epsilon_0\frac{mv^2}{2}}, \quad (2.149)$$

where z , m , and v are the atomic number, relativistic mass, and relativistic velocity, respectively, of the incident charged particle and Z is the atomic number of the target. The relativistic mass m of the projectile is given as $m = m_0/\sqrt{1-\beta^2}$ with β the velocity v of the particle normalized to speed of light c in vacuum ($\beta = v/c$). Inserting expressions for m and β into (2.149) we now get the following general expression for D

$$D = \frac{2zZe^2}{4\pi\epsilon_0m_0c^2} \frac{\sqrt{1-\beta^2}}{\beta^2}. \quad (2.150)$$

We now relate $\sqrt{1-\beta^2}/\beta^2$ with particle's normalized kinetic energy $\tau = E_K/(m_0c^2)$. Following the standard definition of relativistic kinetic energy E_K we have

$$\tau = \frac{E_K}{m_0c^2} = \frac{1}{\sqrt{1-\beta^2}} - 1 \quad \text{or} \quad \tau + 1 = \frac{1}{\sqrt{1-\beta^2}}, \quad (2.151)$$

which gives

$$\sqrt{1-\beta^2} = \frac{1}{\tau+1} \quad \text{and} \quad \frac{1}{\beta^2} = \frac{(\tau+1)^2}{(\tau+1)^2-1} = \frac{(\tau+1)^2}{\tau(\tau+2)}. \quad (2.152)$$

From (2.152) we now get

$$\frac{\sqrt{1-\beta^2}}{\beta^2} = \frac{\tau+1}{\tau(\tau+2)}, \quad (2.153)$$

and finally express (2.149) as a function of τ

$$D = \frac{zZe^2}{4\pi\epsilon_0\frac{mv^2}{2}} = \frac{2zZe^2}{4\pi\epsilon_0m_0c^2} \frac{\sqrt{1-\beta^2}}{\beta^2} = \frac{2zZe^2}{4\pi\epsilon_0m_0c^2} \frac{\tau+1}{\tau(\tau+2)} = \frac{2zZe^2}{4\pi\epsilon_0E_K} \frac{\tau+1}{(\tau+2)}. \quad (2.154)$$

Note: For very large kinetic energies where the kinetic energy is much larger than the rest energy of the scattered particle ($E_K \gg m_0c^2$) we can make the following approximation

$$\frac{\sqrt{1-\beta^2}}{\beta^2} = \frac{\tau+1}{\tau(\tau+2)} \approx \frac{1}{\tau}, \quad (2.155)$$

Table 2.5 Characteristic scattering distances D for four elastic Coulomb scattering types

Type of scattering	Projectile vs. Target	Atomic number		Effective charge	Characteristic scattering distance D
		Projectile	Target		
Rutherford scattering	α particle vs. nucleus	2	Z	$2Ze^2$	$\frac{2Ze^2}{4\pi\epsilon_0(E_K)_\alpha}$
Mott scattering	Electron vs. nucleus	1	Z	Ze^2	$2Zr_e \frac{\sqrt{1-\beta^2}}{\beta^2}$
Moller scattering	Electron vs. orbital electron	1	1	e^2	$2r_e \frac{\sqrt{1-\beta^2}}{\beta^2}$
Electron-atom scattering	Electron vs. whole atom	–	–	$\sqrt{Z(Z+1)}e^2$	$2r_e\sqrt{Z(Z+1)} \frac{\sqrt{1-\beta^2}}{\beta^2}$

suggesting that for $E_K \gg m_0c^2$, the characteristic scattering distance becomes inversely proportional to kinetic energy E_K of the incident charged particle.

Equation (2.154) provides a general expression of the characteristic scattering distance D as a function of various physical properties of the projectile (charged particle) and absorber (target). We now use the general relationship (2.154) to express the characteristic scattering distance D for the four most common scattering types, each characterized by specific atomic number of projectile and target, as summarized in Table 2.5.

(b) Characteristic scattering distance $D_{\alpha-N}$ for Rutherford α particle–nucleus scattering:

$$D_{\alpha-N} = \frac{2zZe^2}{4\pi\epsilon_0m_\alpha c^2} \frac{\tau+1}{\tau(\tau+2)} = \frac{4Ze^2}{4\pi\epsilon_0(E_K)_\alpha} \frac{\tau+1}{\tau+2} = \frac{2Ze^2}{4\pi\epsilon_0(E_K)_\alpha}, \quad (2.156)$$

since

$$m_\alpha c^2 \tau = (E_K)_\alpha \quad \text{and} \quad \frac{\tau+1}{\tau+2} = \frac{\frac{(E_K)_\alpha}{m_\alpha c^2} + 1}{\frac{(E_K)_\alpha}{m_\alpha c^2} + 2} = \frac{\frac{3727.3 \text{ MeV}}{3727.3 \text{ MeV}} + 1}{\frac{(E_K)_\alpha}{3727.3 \text{ MeV}} + 2} \approx \frac{1}{2}. \quad (2.157)$$

(c) Characteristic scattering distance D_{e-N} for Mott electron–nucleus scattering:

$$D_{e-N} = \frac{2zZe^2}{4\pi\epsilon_0m_e c^2} \frac{\tau+1}{\tau(\tau+2)} = 2Zr_e \frac{\sqrt{1-\beta^2}}{\beta^2} = 2Zr_e \frac{\tau+1}{\tau(\tau+2)}, \quad (2.158)$$

after recognizing that $r_e = \frac{e^2}{4\pi\epsilon_0m_e c^2} = 2.818 \text{ fm}$.

(d) Characteristic scattering distance D_{e-N} for Moller electron–orbital electron scattering:

$$D_{e-N} = \frac{2zZe^2}{4\pi\epsilon_0m_e c^2} \frac{\tau+1}{\tau(\tau+2)} = 2r_e \frac{\sqrt{1-\beta^2}}{\beta^2} = 2r_e \frac{\tau+1}{\tau(\tau+2)}. \quad (2.159)$$

(e) Characteristic scattering distance D_{e-a} for electron–atom scattering:

$$D_{e-a} = \sqrt{D_{e-N}^2 + ZD_{e-e}^2} = 2r_e \sqrt{Z(Z+1)} \frac{\sqrt{1-\beta^2}}{\beta^2} = 2r_e \sqrt{Z(Z+1)} \frac{\tau+1}{\tau(\tau+2)}. \quad (2.160)$$

2.6.Q2

(80)

Minimum and maximum scattering angles (θ_{\min} and θ_{\max} , respectively) were introduced into particle scattering theories to account for deviations of the effective nuclear potential from the simple Coulomb point-source potential that forms the basis of scattering theories.

- (a) Briefly discuss definitions of minimum scattering angle θ_{\min} and maximum scattering angle θ_{\max} . Express the two characteristic angles as a function of physical characteristics of the absorber and the scattered particle; and describe how these characteristics affect θ_{\min} and θ_{\max} .
- (b) θ_{\min} and θ_{\max} can be determined for any charged particle used as projectile and for any absorbing material used as target. Calculate θ_{\min} and θ_{\max} for 6 MeV and 100 MeV α particles and for 6 MeV and 100 MeV electrons. Despite the two particles having the same kinetic energy, their characteristic angles differ significantly. Explain.

SOLUTION:

(a) Scattering theories are generally based on the Coulomb point-source potential and predict cross sections that contain the Rutherford component as the sole component (in Rutherford α particle–nucleus scattering) or major component (in Mott electron–nucleus and Moller electron–electron scattering). While the Rutherford derivation predicts result for the differential cross-sections for α particle scattering on nuclei in reasonable agreement with measured data, problems arise as scattering angle θ approaches 0 (singularity at $\theta = 0$) as well as for large scattering angles θ .

At small scattering angles θ (i.e., at large impact parameters b) atomic orbital electrons screen the nuclear potential, effectively causing the nuclear potential to falloff faster than the $1/r$ Coulomb point-source potential. This effect becomes pronounced for scattering angles θ smaller than a characteristic angle referred to as the minimum cutoff angle θ_{\min} or the Born screening angle. With the use of Fermi second golden rule, in conjunction with Born approximation, Thomas-Fermi atomic model, and Heisenberg uncertainty principle, one obtains the following expression

for θ_{\min} (see (T2.57))

$$\begin{aligned}\theta_{\min} &= \frac{\hbar}{p a_{\text{TF}}} = \frac{\hbar c \sqrt[3]{Z}}{a_0 E_K \sqrt{1 + \frac{2E_0}{E_K}}} \approx \frac{(197.3 \text{ MeV} \cdot \text{fm}) \times \sqrt[3]{Z}}{(0.5292 \times 10^5 \text{ fm})} \\ &\approx \frac{(3.723 \times 10^{-3} \text{ MeV}) \times \sqrt[3]{Z}}{E_K \sqrt{1 + \frac{2E_0}{E_K}}}. \end{aligned} \quad (2.161)$$

where

p is the incident momentum of the incident particle.

E_K is the kinetic energy of the incident particle.

E_0 is the rest energy of the incident particle.

a_0 is the Bohr radius (0.53 Å).

a_{TF} is the Thomas-Fermi atomic radius given as: $a_{\text{TF}} = a_0 / \sqrt[3]{Z}$ with a_0 the Bohr radius.

Z is the atomic number of the absorber atom.

At large scattering angles θ (i.e., small impact parameters b) the finite size of the nucleus affects the measured scattering cross sections. A characteristic angle θ , referred to as the maximum cutoff angle θ_{\max} , is defined beyond which the deviation between point-source calculation and measurement becomes significant. θ_{\max} is usually expressed as follows (T2.69)

$$\begin{aligned}\theta_{\max} &= \frac{\hbar}{p R} = \frac{\hbar c}{R_0 \sqrt[3]{A} E_K \sqrt{1 + \frac{2E_0}{E_K}}} \\ &\approx \frac{(197.3 \text{ MeV} \cdot \text{fm})}{(1.25 \text{ fm}) \times \sqrt[3]{A} E_K \sqrt{1 + \frac{2E_0}{E_K}}} \approx \frac{157.8 \text{ MeV}}{\sqrt[3]{A} E_K \sqrt{1 + \frac{2E_0}{E_K}}}, \end{aligned} \quad (2.162)$$

where

R is the nuclear radius given as $R = R_0 \sqrt[3]{A}$ with R_0 the nuclear radius constant (1.25 fm).

A is the atomic mass number of the absorber atom.

The minimum and maximum scattering angles θ_{\min} and θ_{\max} , respectively, have the following properties, as shown in Fig. 2.20:

- (1) In general, θ_{\min} and θ_{\max} depend on kinetic energy E_K and rest energy E_0 of the scattered projectile as well as the atomic number Z and atomic mass number A of the target. However, the ratio $\theta_{\max}/\theta_{\min}$ is independent of the incident particle physical properties and depends only on the atomic number Z and atomic mass number A of the target as follows

$$\frac{\theta_{\max}}{\theta_{\min}} = \frac{a_{\text{TF}}}{R} = \frac{a_0}{R_0 \sqrt[3]{Z A}} = \frac{0.5292 \times 10^5 \text{ fm}}{(1.25 \text{ fm}) \times \sqrt[3]{Z A}} = \frac{0.423 \times 10^5}{\sqrt[3]{Z A}}. \quad (2.163)$$

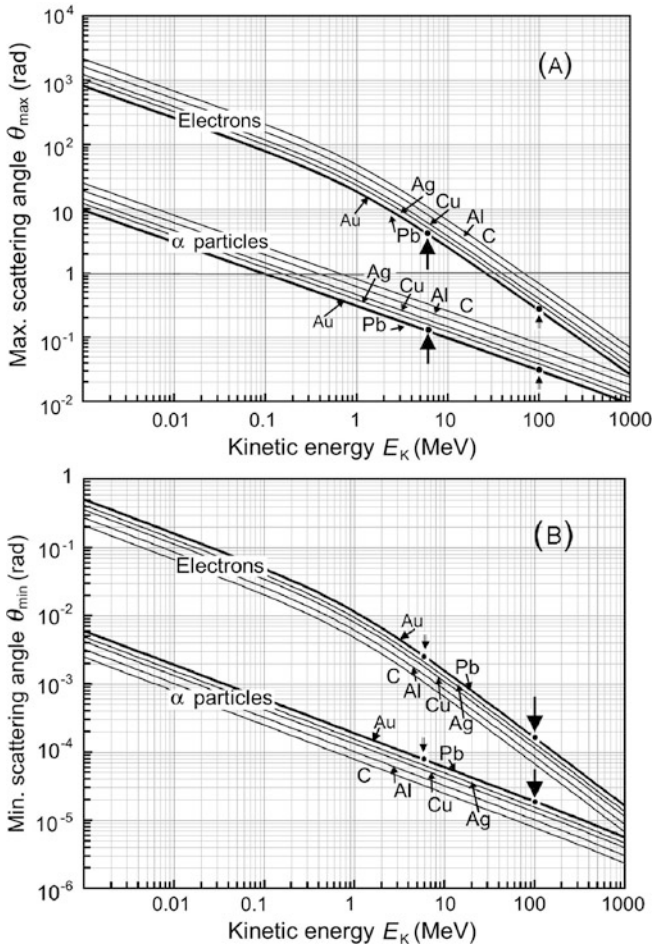


Fig. 2.20 Maximum scattering angle θ_{\max} in (A) and minimum scattering angle θ_{\min} in (B) against kinetic energy E_K for electrons and α particles scattered on carbon, aluminum, copper, silver, gold and lead. The data points indicate calculations for scattering of electrons and α particles on gold of part (b) of this problem, as summarized in Table 2.6

Thus, $\theta_{\max}/\theta_{\min} \propto (ZA)^{-1/3}$ where $(ZA)^{-1/3}$ ranges from 1 for hydrogen to ~ 0.035 for very high atomic number elements.

- (2) For a given E_K and E_0 the maximum scattering angle θ_{\max} is inversely proportional to $Z^{-1/3}$ since $\theta_{\max} \propto A^{-1/3}$ and $A \approx 2Z$. The minimum scattering angle θ_{\min} is proportional to $Z^{1/3}$.
- (3) For kinetic energies E_K of the projectile much smaller than its rest energy E_0 both θ_{\min} and θ_{\max} for a given target are proportional to $1/\sqrt{E_K}$, while for kinetic energies E_K of the projectile much larger than its rest energy E_0 both θ_{\min} and θ_{\max} for a given target are proportional to $1/E_K$, as shown in Fig. 2.20.

Table 2.6 Minimum and maximum cutoff angles θ_{\min} and θ_{\max} , respectively, for electrons and α particles with kinetic energies E_K of 6 MeV and 100 MeV scattered by gold nucleus. θ_{\min} is calculated with (2.161), θ_{\max} with (2.162)

Kinetic energy E_K	6 MeV		100 MeV	
	θ_{\min}	θ_{\max}	θ_{\min}	θ_{\max}
Electron $E_0 = 0.511$ MeV	2.46×10^{-3}	0.644	1.59×10^{-4}	0.270
α particle $E_0 = 3727.3$ MeV	7.55×10^{-5}	0.128	1.84×10^{-5}	0.0312

(b) For calculation of θ_{\min} and θ_{\max} we use (2.161) and (2.162), respectively, and summarize the results in Table 2.6. The target is gold with $Z = 79$ and $A = 197$. The projectiles are either α particles with rest energy $E_0 = 3727.3$ MeV or electrons with rest energy $E_0 = 0.511$ MeV. Kinetic energy E_K of particles is either 6 MeV or 100 MeV. The calculated results are also shown with data points in Fig. 2.20 displaying excellent agreement between data calculated for Table 2.6 and published data plotted in Fig. 2.20 in kinetic energy range from 0.001 MeV to 1000 MeV.

Since θ_{\min} and θ_{\max} depend not only on kinetic energy E_K of the scattered charged particle but also on its rest energy E_0 , we note that charged particles with the same kinetic energies but different rest masses E_0 may have significantly different θ_{\min} and θ_{\max} ; the larger is E_0 , the smaller are θ_{\min} and θ_{\max} , because, as evident from (2.161) and (2.162), the cutoff angles are inversely proportional to $\sqrt{1 + 2E_0/E_K}$.

2.7 Molière Multiple Elastic Scattering

2.7.Q1

(81)

Multiple or compound Coulomb scattering, also known as Molière scattering, results from a large number of single scattering events that a charged particle experiences as it moves through an absorber. Mean square scattering angle $\overline{\Theta^2}$, radiation length X_0 , and mass scattering power T/ρ are physical parameters that govern multiple scattering.

- Define radiation length X_0 .
- Determine radiation length X_0 for electrons in water.
- Determine radiation length X_0 for electrons in air.
- For bremsstrahlung loss of a high-energy electron beam determine the mean energy of electrons after penetrating into an absorber to depths of $0.5X_0$, X_0 , and $2X_0$.

SOLUTION:

(a) Radiation length X_0 in g/cm^2 is a physical quantity used to measure the thickness of absorber traversed by beams of high-energy charged particles or high-energy photons. Specifically, X_0 depends on the mass of the charged particle and the atomic number Z of the absorber and is defined as follows:

- (1) For charged particles as the mean distance a relativistic charged particle travels in an absorber while its energy, as a result of bremsstrahlung losses, decreases to $1/e$ ($\sim 36.8\%$) of its initial value.
- (2) For photons as $7/9$ fraction (78%) of the mean free path for pair production by a high-energy photon traversing the absorber.

As stated in (T2.137), X_0 is given by the following expression

$$\begin{aligned} X_0 &= \left[4\alpha \frac{N_A}{A} Z(Z+1)r_e^2 \ln(183Z^{-1/3}) \right]^{-1} \\ &= (716.2 \text{ g/cm}^2) \times \frac{A}{Z(Z+1) \ln(183Z^{-1/3})} \end{aligned} \quad (2.164)$$

where

α is the fine structure constant ($\alpha = 1/137$).

N_A is the Avogadro constant ($N_A = 6.022 \times 10^{23} \text{ mol}^{-1}$).

A is the atomic mass of the absorber.

Z is the atomic number of the absorber.

r_e is the classical radius of the electron [$r_e = e^2/(4\pi\epsilon_0 m_e c^2) = 2.818 \text{ fm}$].

(b) Radiation length for electrons in water X_0 (H_2O) will be determined by using the Bragg additivity rule for chemical compounds. We therefore first determine X_0 for hydrogen H and oxygen O using (2.164) and get

$$X_0(\text{H}) = \frac{716.2 \times 1.008}{1 \times 2 \times \ln(183 \times 1)} = 69.3 \text{ g/cm}^2 \quad (2.165)$$

and

$$X_0(\text{O}) = \frac{716.2 \times 15.994}{8 \times 9 \times \ln(183 \times 8^{-1/3})} = 35.2 \text{ g/cm}^2. \quad (2.166)$$

Radiation length for water X_0 (H_2O) will now be determined using the Bragg additivity rule for chemical compounds as follows

$$\begin{aligned} \frac{1}{X_0(\text{H}_2\text{O})} &= \frac{2}{18} \times \frac{1}{X_0(\text{H})} + \frac{16}{18} \times \frac{1}{X_0(\text{O})} \\ &= \frac{2 \text{ cm}^2/\text{g}}{18 \times 69.3} + \frac{16 \text{ cm}^2/\text{g}}{18 \times 35.2} = 0.0253 \text{ cm}^2/\text{g} \end{aligned} \quad (2.167)$$

Table 2.7 Radiation lengths X_0 for constituents of water and air

Element	Atomic number Z	Atomic mass A (g/mol)	Radiation length X_0 (g/cm ²)
Hydrogen H	1	1.008	69.3
Nitrogen N	7	14.007	39.3
Oxygen O	8	15.994	35.2
Argon Ar	18	39.948	19.7

or

$$X_0(\text{H}_2\text{O}) = 39.6 \text{ g/cm}^2 = 39.6 \text{ cm.} \quad (2.168)$$

(c) Radiation length for electrons in air $X_0(\text{air})$ will be determined by using the Bragg additivity rule for gas mixtures such as air: nitrogen N 75.5 %; oxygen O 23.2 % and argon Ar 1.3 %. We therefore first determine X_0 for nitrogen, oxygen [already calculated in (b)], and argon using (2.164) and get

$$X_0(\text{H}) = \frac{716.2 \times 14.007}{7 \times 8 \times \ln(183 \times 7^{-1/3})} = 39.3 \text{ g/cm}^2 \quad (2.169)$$

and

$$X_0(\text{Ar}) = \frac{716.2 \times 39.948}{18 \times 19 \times \ln(183 \times 18^{-1/3})} = 19.7 \text{ g/cm}^2. \quad (2.170)$$

Radiation length for air $X_0(\text{air})$ will now be determined using the Bragg additivity rule for gas mixtures as follows

$$\begin{aligned} \frac{1}{X_0(\text{air})} &= \frac{0.755}{X_0(\text{N})} + \frac{0.232}{X_0(\text{O})} + \frac{0.013}{X_0(\text{Ar})} \\ &= \frac{0.755 \text{ cm}^2/\text{g}}{39.3} + \frac{0.232 \text{ cm}^2/\text{g}}{35.2} + \frac{0.013 \text{ cm}^2/\text{g}}{19.7} \\ &= 0.0265 \text{ cm}^2/\text{g} \end{aligned} \quad (2.171)$$

or

$$X_0(\text{air}) = 37.8 \text{ g/cm}^2 = 29234 \text{ cm@STP.} \quad (2.172)$$

Radiation lengths for components of water and air are summarized in Table 2.7.

(d) Mean rate of energy loss per cm of path length due to bremsstrahlung is directly proportional to particle energy

$$\frac{dE}{\rho dx} = -\frac{E}{X_0} \quad \text{or} \quad \frac{dE}{E} = \frac{\rho dx}{X_0} \quad (2.173)$$

and

$$\int_{E_0}^E \frac{dE}{E} = -\frac{\rho}{X_0} \int_0^x dx \quad \text{or} \quad E(x) = E_0 e^{-\frac{\rho}{X_0} x}. \quad (2.174)$$

Therefore, $E(x)/E_0$ for $\rho x = 0.5X_0$, $\rho x = X_0$, and $\rho x = 2X_0$ equals to 0.607, 0.368, and 0.135, respectively.

2.7.Q2

(82)

For scattering of electrons with kinetic energy E_K of 25 MeV on a silver foil of thickness $t = 10^{-4}$ cm calculate:

- Maximum scattering angle θ_{\max} for single scattering.
- Minimum scattering angle (Born screening angle) θ_{\min} .
- Radiation length X_0 .
- Mean square scattering angle $\overline{\Theta^2}$ and root-mean-square scattering angle $\sqrt{\overline{\Theta^2}}$ for multiple scattering.
- Mass scattering power T/ρ .

The following data for silver may prove useful in the calculation: density $\rho = 10.5 \text{ g/cm}^3$; atomic number $Z = 47$; atomic mass $A = 107.87 \text{ g/mol}$.

SOLUTION:

(a) The maximum scattering angle θ_{\max} for electron scattering on silver nucleus is calculated from (T2.147) as follows

$$\begin{aligned} \theta_{\max} &= \frac{\hbar}{p_e R} = \frac{\hbar c A^{-1/3}}{R_0 \sqrt{E_K(E_K + 2m_e c^2)}} = \frac{\hbar c A^{-1/3}}{R_0 m_e c^2 \sqrt{\tau(\tau + 2)}} \\ &\approx \frac{309 A^{-1/3}}{\sqrt{\tau(\tau + 2)}} = \frac{309}{\sqrt[3]{107.87} \sqrt{48.92(48.92 + 2)}} \\ &= 1.3 \text{ rad} = 74.6^\circ, \end{aligned} \quad (2.175)$$

where

R_0 is the nuclear radius constant ($R_0 = 1.25 \text{ fm}$).

A is the atomic mass of the silver absorber.

$m_e c^2$ is the rest energy of the electron ($m_e c^2 = 0.511 \text{ MeV}$).

τ is the kinetic energy of the electron normalized to its rest energy

$$\tau = \frac{E_K}{m_e c^2} = \frac{25 \text{ MeV}}{0.5211 \text{ MeV}} = 48.92. \quad (2.176)$$

Note: Since the calculated θ_{\max} exceeds one radian (1 rad), it is customary to use 1 rad for the maximum scattering angle θ_{\max} .

(b) The minimum scattering angle (Born screening angle) θ_{\min} for electron scattering on silver nucleus is calculated from (T2.148) as follows

$$\begin{aligned}\theta_{\min} &= \frac{\hbar}{pe^{aTF}} = \frac{\hbar c \sqrt[3]{Z}}{a_0 \sqrt{E_K(E_K + 2m_e c^2)}} = \frac{\hbar c \sqrt[3]{Z}}{a_0 m_e c^2 \sqrt{\tau(\tau + 2)}} = \frac{\alpha \sqrt[3]{Z}}{\sqrt{\tau(\tau + 2)}} \\ &\approx \frac{\sqrt[3]{Z}}{137 \sqrt{\tau(\tau + 2)}} = \frac{\sqrt[3]{47}}{137 \sqrt{48.92(48.92 + 2)}} = 5.3 \times 10^{-4} \text{ rad} = 0.03^\circ.\end{aligned}\quad (2.177)$$

Note: In contrast to individual θ_{\max} and θ_{\min} the ratio $\theta_{\max}/\theta_{\min}$ is independent of electron energy and depends only on the atomic number Z and atomic mass A as follows

$$\frac{\theta_{\max}}{\theta_{\min}} = \frac{309 \times 137}{\sqrt[3]{AZ}} = \frac{0.423 \times 10^5}{\sqrt[3]{107.87 \times 47}} = \frac{1.3}{2.58 \times 10^{-4}} = 2462, \quad (2.178)$$

however, since we use 1 rad for θ_{\max} we get for $\theta_{\max}/\theta_{\min}$ ratio a value of ~ 1900 .

(c) Radiation length X_0 for 25 MeV electrons in silver is calculated from (T2.137) as

$$\begin{aligned}X_0 &= \left[4\alpha \frac{N_A}{A} Z(Z+1) r_e^2 \ln(183Z^{-1/3}) \right]^{-1} \\ &= (716.2 \text{ g/cm}^2) \times \frac{A}{Z(Z+1) \ln(183Z^{-1/3})} \\ &= \frac{(716.2 \text{ g/cm}^2) \times 107.87}{47 \times 48 \times \ln(183 \times 47^{-1/3})} = 8.72 \text{ g/cm}^2 = 0.83 \text{ cm}.\end{aligned}\quad (2.179)$$

(d) Mean square scattering angle $\overline{\Theta^2}$ for 25 MeV electrons in silver is calculated from (T2.135) as follows

$$\begin{aligned}\overline{\Theta^2} &= 16\pi\rho \frac{N_A r_e^2 Z(Z+1)}{A\gamma^2\beta^4} \{ \ln[183Z^{-1/3}] \} t = \frac{4\pi\rho t}{\alpha X_0 \gamma^2 \beta^4} = \frac{4\pi\rho t}{\alpha X_0} \left[\frac{\tau+1}{\tau(\tau+2)} \right]^2 \\ &= \frac{4\pi \times 137 \times (10.5 \text{ g/cm}^3) \times (10^{-4} \text{ cm})}{(8.72 \text{ g/cm}^2)} \left[\frac{48.92+1}{48.92(48.92+2)} \right]^2 \\ &= 8.32 \times 10^{-5} \text{ rad}^2\end{aligned}\quad (2.180)$$

yielding the following result for the root-mean-square scattering angle $\sqrt{\overline{\Theta^2}}$

$$\sqrt{\overline{\Theta^2}} = \sqrt{8.32 \times 10^{-5}} \text{ rad} = 9.1 \times 10^{-3} \text{ rad} = 0.52^\circ. \quad (2.181)$$

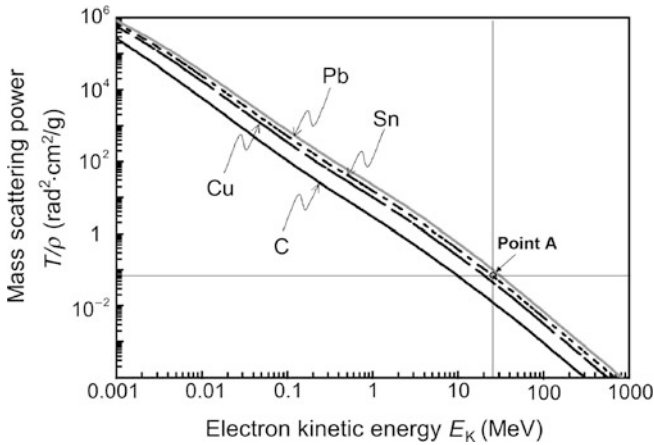


Fig. 2.21 Mass scattering power T/ρ against electron kinetic energy E_K for various materials of interest in medical physics. Point A represents the result of T/ρ calculation (2.82) for 25 MeV electrons in silver

(e) Mass scattering power T/ρ is calculated using (T2.145) to get

$$\begin{aligned} \frac{T}{\rho} &= \frac{\overline{\Theta^2}}{\rho t} = \frac{4\pi}{\alpha X_0} \left[\frac{\tau + 1}{\tau(\tau + 2)} \right]^2 = \frac{8.32 \times 10^{-5}}{(10.5 \text{ g/cm}^3) \times (10^{-4} \text{ cm})} \\ &= 0.079 \text{ rad}^2 \cdot \text{cm}^2/\text{g}. \end{aligned} \quad (2.182)$$

The calculated scattering power $T/\rho = 0.079 \text{ rad}^2 \cdot \text{cm}^2/\text{g}$ for 25 MeV electrons in silver fits nicely on the graph as point A in Fig. 2.21 showing T/ρ against electron kinetic energy E_K for various materials ranging in atomic number Z from 6 (carbon) to 82 (lead).

Chapter 3 consists of **21 problems** that cover 4 sections devoted to the Rutherford-Bohr model of the atom that Bohr introduced in 1913. Bohr combined Rutherford's concept of the nuclear atom with Planck's idea of quantized nature of the radiation process and developed from first principles an atomic model that successfully deals with one-electron structures, such as the hydrogen atom. The model is based on four postulates that combine classical mechanics with the concept of angular momentum quantization.

The problems of this chapter concentrate on concepts that Bohr enunciated 100 years ago for one-electron structures to predict accurately the radius of electron orbits, velocity of electron in allowed orbit, binding energy of electron while in allowed orbit, as well as photon spectra emitted by excited one-electron atoms. At the end of the chapter, problems also address issues related to multi-electron atoms and experimental confirmation of the Bohr atomic theory.

The set of problems in Sect. 3.1 covers one-electron structures in detail and deals not only with hydrogen but also with other one-electron structures, such as one-electron ions and more exotic Bohr-like atomic structures such as positronium, muonium, antihydrogen, etc. Problems in this group also address the corrections to Bohr theory resulting from the finite mass of the nucleus. Problems of Sect. 3.2 deal with multi-electron atoms and issues related to periodic properties of elements, spectra of characteristic radiation emitted by multi-electron atoms, and the Hartree approximation.

Problems of Sect. 3.3 cover the three experiments that serve as experimental confirmation of Bohr theory: (1) atomic emission and absorption spectra, (2) Moseley experiment on characteristic lines from metallic x-ray targets, and (3) Franck–Hertz experiment. The last question of this chapter deals with the atomic radius calculated using the Schrödinger equation for hydrogen atom (Sect. 3.4).

3.1 Bohr Model of Hydrogen Atom

3.1.Q1

(83)

Larmor classical electromagnetic (EM) theory states that when a charged particle is accelerated or decelerated part of its kinetic energy is emitted in the form of EM radiation (photons). Using classical physics (Larmor law) estimate the time of collapse of the Bohr orbit for hydrogen atom in the ground state.

SOLUTION:

At first glance the Rutherford-Bohr atomic model is analogous to the Kepler-Newton planetary model except that in the latter the Newton gravitational attraction between the sun and the planet plays the role of the centripetal force, while in the former the centripetal force is provided by the Coulomb electrostatic attraction between the positively charged nucleus and the negative electron. However, the difficulty with the Rutherford-Bohr model is that the electron is charged and, by revolving about the nucleus, it is also constantly accelerated. Therefore, by virtue of its charge, the electron should be losing part of its energy in the form of photons and, according to classical physics, spiral into the nucleus.

In Rutherford-Bohr theory of the hydrogen atom the Coulomb force F_{Coul} provides the centripetal force F_{cent} and is expressed as follows

$$F_{\text{cent}} = F_{\text{Coul}} = \frac{1}{4\pi\epsilon_0} \frac{e^2}{r^2}. \quad (3.1)$$

The magnitude of the electron centripetal (radial) acceleration a_r and kinetic energy E_K , respectively, of the electron are classically given as

$$a_r = \frac{v^2}{r} = \frac{F_{\text{Coul}}}{m_e} = \frac{e^2}{4\pi\epsilon_0 m_e r^2} \quad \text{and} \quad E_K = \frac{m_e v^2}{2} = \frac{1}{2} \frac{e^2}{4\pi\epsilon_0} \frac{1}{r}, \quad (3.2)$$

with e , v , and m_e the charge, velocity, and mass of the electron, respectively, ϵ_0 the electric constant, and r the distance between the electron and the nucleus (proton).

Total energy E of the electron in the ground state of hydrogen is given as (T3.7)

$$E = E_K + E_P = \frac{1}{2} \frac{e^2}{4\pi\epsilon_0} \frac{1}{r} + \int_{\infty}^r \frac{e^2}{4\pi\epsilon_0} \frac{dr}{r^2} = -\frac{1}{2} \frac{e^2}{4\pi\epsilon_0} \frac{1}{r}. \quad (3.3)$$

Inserting $1/r$ from (3.3) into (3.2) yields the following expression for acceleration a

$$a = \frac{v^2}{r} = \frac{e^2}{4\pi\epsilon_0 m_e} \frac{1}{r^2} = \frac{e^2}{4\pi\epsilon_0 m_e} \left(-\frac{8\pi\epsilon_0}{e^2} \right)^2 E^2 = -\frac{16\pi\epsilon_0}{m_e e^2} E^2. \quad (3.4)$$

According to the classical Larmor expression (T4.18) the power emitted by an accelerated particle of charge e is given as

$$P = -\frac{dE}{dt} = \frac{e^2 a^2}{6\pi \epsilon_0 c^3}, \quad (3.5)$$

which, after inserting (3.4), reads

$$-\frac{dE}{dt} = \frac{128\pi \epsilon_0}{3m_e^2 c^3 e^2} E^4 = bE^4, \quad (3.6)$$

where b is a constant given as

$$\begin{aligned} b &= \frac{128\pi \epsilon_0 c}{3(m_e c^2)^2 e^2} = \frac{128\pi \times [8.85 \times 10^{-12} \text{ A} \cdot \text{s}/(\text{V} \cdot \text{m})] \times (3 \times 10^8 \text{ m/s})}{3 \times (0.511 \times 10^6 \text{ eV})^2 \times e \times (1.6 \times 10^{-19} \text{ A} \cdot \text{s})} \\ &= 8.51 \times 10^6 \text{ (eV)}^{-3} \cdot \text{s}^{-1}. \end{aligned} \quad (3.7)$$

The differential equation (3.6) will now be rearranged to read

$$\int_{E_1}^E \frac{dE}{E^4} = -b \int_0^t dt, \quad (3.8)$$

resulting in the following general solution

$$-\frac{3}{E^3} + \frac{3}{E_1^3} = -bt. \quad (3.9)$$

To determine the time of orbit collapse we carry out the integration in (3.8) in energy E from $E_1 = -13.61 \text{ eV}$ (ground state of hydrogen atom) to $-\infty$ (energy level for $r \rightarrow 0$) and in time t from the initial time ($t = 0$) to the time of orbit collapse at $t = t_{\text{coll}}$. The time of orbit collapse is thus given as

$$t_{\text{coll}} = -\frac{3}{bE_1^3} = -\frac{3}{(8.51 \times 10^6 \text{ eV}^{-3} \cdot \text{s}^{-1}) \times (-13.61 \text{ eV})^3} = 1.4 \times 10^{-10} \text{ s}. \quad (3.10)$$

3.1.Q2

(84)

A hypothetical excited one-electron atom (NOT hydrogen) releases a visible photon of wavelength $\lambda = 5500 \text{ \AA}$. Assume that

- (1) Atom follows the Bohr atomic model.
- (2) Nuclear mass is infinitely large in comparison with the mass of the orbital electron.

- (3) Photon originated from an $n = 3 \rightarrow n = 2$ (also known as M–L) electronic transition.

Determine:

- (a) Ionization potential (IP) of this hypothetical atom.
 (b) Energy level diagram (first 5 energy levels) of this hypothetical atom.
 (c) Minimum excitation potential of the hypothetical one-electron atom.

SOLUTION:

Five energy levels in addition to the $n = \infty$ level are plotted in the energy level diagram for the hypothetical excited one-electron atom shown in Fig. 3.1. The ionization potential of the atom is designated by x and the M–L transition is also indicated.

- (a) We first determine the energy $h\nu$ of the photon emitted with a wavelength $\lambda = 5500 \text{ \AA}$ and get

$$\begin{aligned} h\nu &= \frac{hc}{\lambda} = \frac{2\pi\hbar c}{\lambda} = \frac{2\pi \times (197.3 \text{ MeV} \cdot \text{fm})}{5500 \text{ \AA}} \\ &= \frac{2\pi \times (197.3 \times 10^6 \text{ eV} \cdot \text{fm})}{5500 \times 10^5 \text{ fm}} = 2.25 \text{ eV}. \end{aligned} \quad (3.11)$$

Next, we calculate the ionization potential x by setting the emitted photon energy $h\nu = 2.25 \text{ eV}$ equal to the difference between energy level M ($n = 3$; energy level $= -x/3^2$) and energy level L ($n = 2$; energy level $= -x/2^2$) as follows

$$\left(-\frac{x}{3^2}\right) - \left(-\frac{x}{2^2}\right) = x\left(\frac{1}{4} - \frac{1}{9}\right) = h\nu = 2.25 \text{ eV}, \quad (3.12)$$

resulting in

$$x = E_M - E_L = \frac{2.25 \text{ eV}}{\frac{1}{4} - \frac{1}{9}} = 16.2 \text{ eV}. \quad (3.13)$$

Thus, the ionization potential of our hypothetical one-electron atom is $+16.2 \text{ eV}$ and the ground state energy level ($n = 1$) is at $E(n = 1) = E_1 = -16.2 \text{ eV}$.

- (b) The energy levels for the ground state ($n = 1$) and first four excited states ($n > 1$) of our one-electron hypothetical atom are plotted schematically in Fig. 3.1 and given as follows

$$\begin{aligned} E_1 &= -16.2 \text{ eV}; & E_2 &= -4.05 \text{ eV}; & E_3 &= -1.80 \text{ eV}; \\ E_4 &= -1.01 \text{ eV}; & E_5 &= -0.64 \text{ eV}. \end{aligned}$$

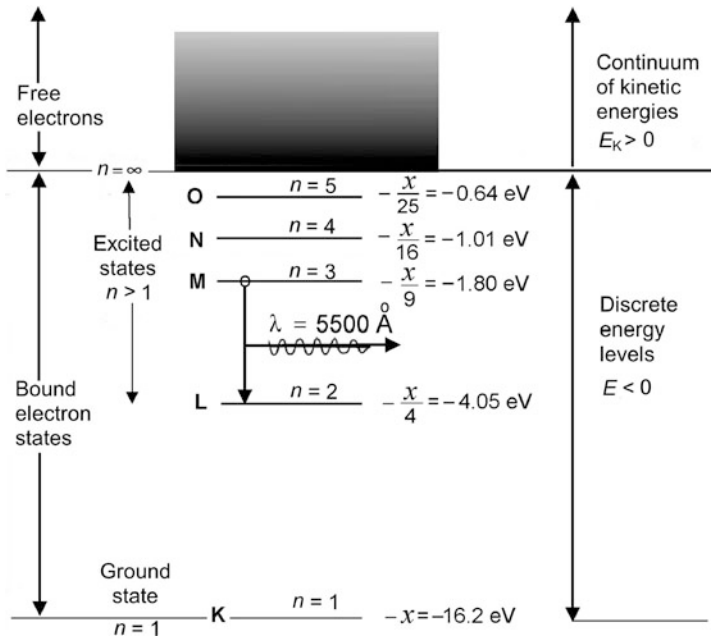


Fig. 3.1 Atomic energy level diagram for the hypothetical one-electron atom of Prob. 84

(c) The minimum excitation potential of the hypothetical one-electron atom is the energy required to transfer the orbital electron from the ground state ($n = 1$) to the first excited state ($n = 2$). This energy is equal to $|E_K - E_L| = |-16.2 \text{ eV} - 4.05 \text{ eV}| = 12.15 \text{ eV}$.

3.1.Q3

(85)

A single-electron ion emits a photon of wavelength $\lambda = 1170 \text{ \AA}$ when its electron makes a transition from the $n = 4$ to the $n = 3$ atomic energy level. Assume that the nuclear mass is infinite in comparison with the electron mass.

- (a) Determine momentum p_ν and energy E_ν of the emitted photon.
- (b) Determine the atomic number Z of the nucleus.
- (c) Determine the binding energy $E_B(K)$ of the electron when it is in the K shell.
- (d) Draw an atomic energy level diagram of the ion for $n = 1$ to $n = 5$ energy levels and indicate the electronic transition from $n = 4$ to $n = 3$.
- (e) Determine the wavelength λ of the photon emitted by the ion when its electron undergoes a transition from the $n = 5$ energy level to ground state. Indicate the electronic transition on diagram plotted in (d).

SOLUTION:

(a) Photon momentum p_ν is calculated from the general relativistic expression for total energy E of any particle (including a photon) with rest energy E_0

$$E = \sqrt{E_0^2 + p^2 c^2} \quad \text{or} \quad p = \frac{1}{c} \sqrt{E^2 - E_0^2}. \quad (3.14)$$

For a photon rest energy $E_0 = E_\nu = 0$ and from (3.14) we get the following expression for the photon momentum

$$p_\nu = \frac{E_\nu}{c} = \frac{h\nu}{c} = \frac{h}{\lambda} = \frac{2\pi\hbar}{\lambda} = \frac{2\pi\hbar c}{\lambda c} = \frac{2\pi \times (1973 \text{ eV} \cdot \text{\AA})}{(1170 \text{ \AA}) \times c} = 10.6 \text{ eV}/c. \quad (3.15)$$

A photon with wavelength $\lambda = 1170 \text{ \AA}$ possesses energy E_ν according to Planck law

$$E_\nu = h\nu = \frac{hc}{\lambda} = \frac{2\pi\hbar c}{\lambda} = \frac{2\pi \times (1973 \text{ eV} \cdot \text{\AA})}{1170} = 10.6 \text{ eV}. \quad (3.16)$$

We can obtain the result of (3.16) faster by using the photon momentum p_ν of (3.15), since

$$E_\nu = p_\nu c = (10.6 \text{ eV}/c) \times c = 10.6 \text{ eV}. \quad (3.17)$$

(b) Atomic number Z of the ion will be determined through the following steps:

- (1) We know that ΔE_{4-3} , the energy difference between $n = 4$ and $n = 3$ atomic energy levels is equal to the emitted photon energy $E_\nu = 10.6 \text{ eV}$, as determined in (a).
- (2) The $n = 4$ and $n = 3$ atomic energy levels are, respectively, given as

$$E_4 = -E_R \frac{Z^2}{4^2} \quad \text{and} \quad E_3 = -E_R \frac{Z^2}{3^2}. \quad (3.18)$$

- (3) We thus have

$$\Delta E_{4-3} = E_\nu = E_4 - E_3 = -E_R Z^2 \left(\frac{1}{4^2} - \frac{1}{3^2} \right) = 0.04861 E_R Z^2 \quad (3.19)$$

or

$$Z = \sqrt{\frac{E_\nu}{0.04861 E_R}} = \sqrt{\frac{10.6 \text{ eV}}{0.04861 \times (13.61 \text{ eV})}} \approx \sqrt{16} = 4. \quad (3.20)$$

Looking at the periodic table of elements we find that the element with $Z = 4$ is beryllium. The one-electron ion that we are dealing with in this problem is therefore a triply-ionized beryllium atom Be^{+++} .

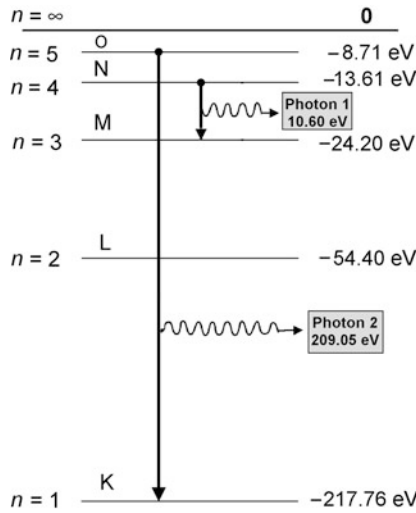


Fig. 3.2 Atomic energy level diagram for one-electron structure Be^{+++} ion

(c) To determine the binding energy $E_B(\text{K})$ of the electron in the K shell (also known as the $n = 1$ shell) of Be^{+++} we now find the energy E_1 of the ground state. Since, in general, the energy levels E_n are given by

$$E_n = -E_R \frac{Z^2}{n^2}, \quad (3.21)$$

and the ground state energy E_1 is thus given as

$$E_1 = -E_R Z^2 = -16E_R = -16 \times (13.61 \text{ eV}) = -217.76 \text{ eV}. \quad (3.22)$$

The binding energy $E_B(\text{K})$ of the K shell electron in Be^{+++} ion is thus $+217.76 \text{ eV}$. *Note:* By convention, in contrast to the positive binding energy $E_B(\text{K})$, the K shell energy level of Be^{+++} is negative at $E_1 = -217.76 \text{ eV}$.

(d) Energy levels for the first five values of n are calculated from (3.22) and plotted in Fig. 3.2

$$E_1 = -\frac{E_R Z^2}{n^2} = -\frac{217.76 \text{ eV}}{1} = -217.76 \text{ eV}, \quad (3.23)$$

$$E_2 = -\frac{E_R Z^2}{n^2} = -\frac{217.76 \text{ eV}}{4} = -54.44 \text{ eV}, \quad (3.24)$$

$$E_3 = -\frac{E_R Z^2}{n^2} = -\frac{217.76 \text{ eV}}{9} = -24.20 \text{ eV}, \quad (3.25)$$

$$E_4 = -\frac{E_R Z^2}{n^2} = -\frac{217.76 \text{ eV}}{16} = -13.61 \text{ eV}, \quad (3.26)$$

$$E_5 = -\frac{E_R Z^2}{n^2} = -\frac{217.76 \text{ eV}}{25} = -8.71 \text{ eV}. \quad (3.27)$$

Atomic energy levels for a Be^{+++} ion from $n = 1$ to $n = 5$ are plotted in Fig. 3.2. Also plotted are electronic transitions (1) from $n = 4$ to $n = 3$ resulting in photon 1 with energy of 10.6 eV and (2) from $n = 5$ to $n = 1$ resulting in photon 2 with energy of 209.05 eV.

(e) Energy released in the form of a photon following the $n = 5$ to $n = 1$ electronic transition is

$$E_\nu = E_5 - E_1 = (-8.71 \text{ eV}) - (-217.76 \text{ eV}) = 209.05 \text{ eV}, \quad (3.28)$$

(see Fig. 3.2) corresponding to the following wavelength λ

$$\lambda = \frac{hc}{E_\nu} = \frac{2\pi\hbar c}{E_\nu} = \frac{2\pi \times (1973 \text{ eV} \cdot \text{\AA})}{209.05 \text{ eV}} = 59.3 \text{ \AA}. \quad (3.29)$$

3.1.Q4

(86)

Accounting for the finite size of the nucleus, derive from basic principles the following equations for the Bohr theory of one-electron atoms:

- Angular momentum L_n of electron while in orbit with principal quantum number n .
- Kinetic energy E_K of the electron–nucleus system.
- Force F_e on electron while in orbit n .
- Using results from (a), (b), and (c) determine expressions for radius r_n of Bohr orbit n , velocity v_n of electron while in orbit n , and total energy E_n of electron while in orbit n .

SOLUTION:

Bohr initially derived his theory of one-electron atoms assuming that nuclear mass M is infinite and that the electron revolves about a point at the center of the nucleus. Experimental studies of hydrogen spectrum have shown a minute discrepancy of the order of one part in 2000 between measured data and theoretical calculations and the discrepancy was attributed to the finite size of the nucleus making both the electron as well as the nucleus to revolve about their common center-of-mass, as shown schematically in Fig. 3.3. In deriving the kinematics of the Bohr atom we thus consider the electron–nucleus system and derive equations of motion for the whole system rather than just for the orbital electron.

The following relationships will be useful in our calculations

$$r = r_e + r_M, \quad v = v_e + v_M, \quad m_e r_e = M r_M \quad \text{and} \quad \omega = \frac{v_e}{r_e} = \frac{v_M}{r_M}, \quad (3.30)$$

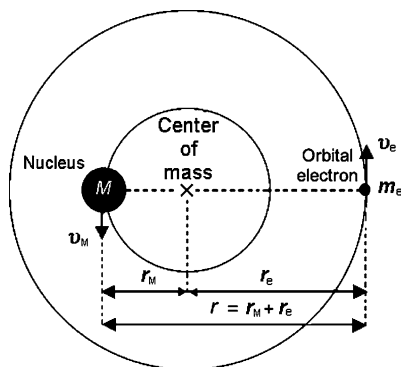


Fig. 3.3 Schematic diagram of the Rutherford–Bohr atomic model with one orbital electron of mass m_e and a finite nucleus of mass M . Both the orbital electron and the nucleus revolve about their common center-of-mass

where

m_e and M are the mass of electron and nucleus, respectively.
 r_e and r_M are the radius of electron and nucleus orbit, respectively.
 v_e and v_M are the velocity of electron and nucleus, respectively, while in orbit.
 ω is the angular frequency of the electron and nucleus revolving about their common center-of-mass (see Fig. 3.3).

We now express r_e and r_M as follows

$$r_e = r - r_M = r - \frac{m_e}{M}r_e \quad \text{or} \quad r_e = \frac{r}{1 + \frac{m_e}{M}} \quad (3.31)$$

and

$$r_M = r - r_e = r - \frac{M}{m_e}r_M \quad \text{or} \quad r_M = \frac{r}{1 + \frac{M}{m_e}}. \quad (3.32)$$

In a similar fashion we express v_e and v_M as

$$v_e = v - v_M = v - \frac{r_M}{r_e}v_e = v - \frac{m_e}{M}v_e \quad \text{or} \quad v_e = \frac{v}{1 + \frac{m_e}{M}} \quad (3.33)$$

and

$$v_M = v - v_e = v - \frac{r_e}{r_M}v_M = v - \frac{M}{m_e}v_M \quad \text{or} \quad v_M = \frac{v}{1 + \frac{M}{m_e}}. \quad (3.34)$$

(a) **Angular momentum** L for our electron-nucleus system is in general given as

$$L = I\omega = \sum_i m_i r_i^2 \omega = m_e r_e^2 \omega + M r_M^2 \omega, \quad (3.35)$$

where I is the rotational inertia of the electron–nucleus system given as $I = \sum_i m_i r_i^2$.

Using expressions for r_e and r_M given in (3.31) and (3.32), respectively, we now express (3.35) as

$$\begin{aligned} L &= \frac{m_e r^2 \omega}{(1 + \frac{m_e}{M})^2} + \frac{M r^2 \omega}{(1 + \frac{M}{m_e})^2} = r^2 \omega \left[\frac{m_e M^2}{(m_e + M)} + \frac{m_e^2 M}{(m_e + M)} \right] \\ &= \frac{m_e M}{m_e + M} r^2 \omega = \mu_M r^2 \omega, \end{aligned} \quad (3.36)$$

where μ_M is defined as the reduced mass of the electron–nucleus system

$$\mu_M = \frac{m_e M}{m_e + M}. \quad (3.37)$$

Using the result of (3.36) we now express the angular momentum L as a function of v and r as

$$L = \mu_M r^2 \omega = \mu_M r^2 \frac{v_e}{r_e} = \mu_M r^2 \frac{v}{(1 + \frac{M}{m_e})} \frac{(1 + \frac{M}{m_e})}{r} = \mu_M v r. \quad (3.38)$$

(b) **Kinetic energy** E_K of the electron–nucleus system is given as

$$E_K = \frac{1}{2} \sum_i m_i v_i^2 = \frac{1}{2} m_e v_e^2 + \frac{1}{2} M v_M^2. \quad (3.39)$$

Using expressions for v_e and v_M given in (3.33) and (3.34), respectively, we now express (3.39) as follows

$$\begin{aligned} E_K &= \frac{1}{2} \frac{m_e v^2}{(1 + \frac{m_e}{M})^2} + \frac{1}{2} \frac{M v^2}{(1 + \frac{M}{m_e})^2} = \frac{v^2}{2} \left[\frac{m_e M^2}{(m_e + M)} + \frac{m_e^2 M}{(m_e + M)} \right] \\ &= \frac{1}{2} \frac{m_e M v^2}{m_e + M} = \frac{1}{2} \mu_M v^2. \end{aligned} \quad (3.40)$$

(c) **Force** F_e exerted on the orbital electron is in general given as

$$F_e = \frac{Z e^2}{4\pi \epsilon_0 r^2} = \frac{m_e v_e^2}{r_e} = m_e \omega^2 r_e. \quad (3.41)$$

After inserting (3.31) and (3.33) into (3.41) we get the following expression for force F_e

$$F_e = m_e \frac{v^2}{(1 + \frac{m_e}{M})^2} \frac{(1 + \frac{m_e}{M})}{r} = \frac{m_e M}{m_e + M} \frac{v^2}{r} = \frac{\mu_M v^2}{r}. \quad (3.42)$$

(d) In (a), (b), and (c) we stated all equations that are required in the derivation of Rutherford–Bohr atom kinematics, accounting for the finite mass of the nucleus.

Combining (3.38) with the third Bohr postulate on quantization of angular momentum ($L = n\hbar$), we get the following expression for the angular momentum L

$$L_n = n\hbar = \mu_M v_n r_n, \quad (3.43)$$

and combining (3.41) with (3.43) we get the following result for the radius of orbit n

$$r_n = \frac{4\pi\epsilon_0 (\hbar c)^2 n^2}{e^2 \mu_M c^2 Z} = a_0 \frac{m_e n^2}{\mu_M Z} = a_0 \left(1 + \frac{m_e}{M}\right) \frac{n^2}{Z}, \quad (3.44)$$

where a_0 is defined as the Bohr radius constant ($a_0 = 0.5292 \text{ \AA}$).

Combining (3.43) with (3.44) results in the following expression for v_n/c

$$\frac{v_n}{c} = \frac{e^2 Z}{4\pi\epsilon_0 \hbar c n} = \alpha \frac{Z}{n}, \quad (3.45)$$

where α is the fine structure constant ($\alpha = 1/137$).

The total energy level of the electron in orbit n is calculated by adding the kinetic energy E_K and potential energy E_P to get

$$\begin{aligned} E_n = E_K + E_P &= \frac{1}{2} \mu_M v_n^2 - \frac{Ze^2}{4\pi\epsilon_0 r_n} = -\frac{1}{2} \left(\frac{e^2}{4\pi\epsilon_0} \right)^2 \frac{(\mu_M c^2)}{(\hbar c)^2} \left(\frac{Z}{n} \right)^2 \\ &= -E_R \frac{\mu_M}{m_e} \left(\frac{Z}{n} \right)^2 = -E_R \frac{1}{1 + \frac{m_e}{M}} \left(\frac{Z}{n} \right)^2, \end{aligned} \quad (3.46)$$

where E_R is the Rydberg energy constant ($E_R = 13.61 \text{ eV}$).

Equations for r_n (3.44), normalized velocity v_n/c (3.45), and electron energy level E_n (3.46) were determined by accounting for the finite nuclear mass, but are similar to those obtained for infinite nuclear mass (T3.3), (T3.5), and (T3.7) except for a correction factor $(1 + m_e/M) = m_e/\mu_M$ for the radius, no correction factor for velocity, and a correction factor $(1 + m_e/M)^{-1} = \mu_M/m_e$ for energy level.

3.1.Q5

(87)

For hydrogen atom:

- (a) Compare expressions for orbital radii r_n , electron orbital velocities v_n , and atomic energy levels E_n calculated assuming an infinite mass of the nucleus ($M \rightarrow \infty$) to those calculated for a finite nuclear mass M .
- (b) For the three parameters r_n , v_n and E_n determine the correction factor f to be applied to expressions for infinite nuclear mass ($M \rightarrow \infty$) to obtain expressions valid for finite nuclear mass.

- (c) Plot general correction factors of (b) for r_n , v_n , and E_n in the range $0 \leq m/M \leq 1$, where m is the mass of the orbiting particle and M is the mass of the heavier particle.
- (d) Determine and plot on graph (c) correction factors f_r , f_v , and f_E for (1) muonic hydrogen and (2) positronium. Muonic hydrogen atom consists of a proton p ($m_p c^2 = 1836 m_e c^2$) and negative muon μ^- ($m_{\mu^-} c^2 = 207 m_e c^2$) and positronium consists of a positron and electron.

SOLUTION:

Table 3.1 Summary of Bohr atom expressions for orbital radius r_n , electron orbital velocity v_n , and atomic energy level E_n for infinite nuclear mass in column (2), finite nuclear mass in column (3), appropriate constants in column (4), and correction factor in column (5). μ_M is the reduced mass of the electron–nucleus system

(1)	(2)	(3)	(4)	(5)
	Infinite nuclear mass M	Finite nuclear mass M	Bohr theory constants	Correction factor
Radius r_n	$a_0 \frac{n^2}{Z}$	$a_0 \frac{m_e}{\mu_M} \frac{n^2}{Z}$	$a_0 = \frac{4\pi\epsilon_0 \hbar^2}{e^2 m_e} = 0.5292 \text{ \AA}$	$f_r = \frac{m_e}{\mu_M} = 1 + \frac{m_e}{M}$
Velocity v_n	$ac \frac{Z}{n}$	$ac \frac{Z}{n}$	$a = \frac{e^2}{4\pi\epsilon_0 \hbar c} = \frac{1}{137}$	$f_v = 1$
Energy level E_n	$-E_R \frac{Z^2}{n^2}$	$-E_R \frac{\mu_M}{m_e} \frac{Z^2}{n^2}$	$E_R = \left(\frac{e^2}{4\pi\epsilon_0}\right)^2 \frac{m_e}{\hbar^2} = 13.61 \text{ eV}$	$f_E = \frac{\mu_M}{m_e} = \left(1 + \frac{m_e}{M}\right)^{-1}$

(a) Expressions for orbital radii r_n , electron orbital velocities v_n , and atomic energy levels E_n are derived in (T3.3), (T3.5), and (T3.7), respectively, assuming an infinite nuclear mass and in Prob. 86 accounting for the finite mass of the nucleus. The results are summarized in Table 3.1, columns (1) through (4).

(b) Correction factors to be applied to expressions for infinite nuclear mass ($M \rightarrow \infty$ column 2 in Table 3.1) to obtain expressions valid for finite nuclear mass (column 3) for the three parameters r_n , v_n , and E_n are as follows:

Correction factor f_r for orbital radius r_n of one-electron Bohr atom is given as

$$f_r = \frac{m_e}{\mu_M} = 1 + \frac{m_e}{M} = 1 + \frac{0.511}{938.3} = 1.0005. \tag{3.47}$$

Correction factor f_v for the velocity v_n of orbital electron is equal to 1, i.e., there is no correction for velocity when going from infinite to finite mass considerations.

Correction factor f_E for energy levels E_n of one-electron Bohr atom is

$$f_E = \frac{\mu_M}{m_e} = \left(1 + \frac{m_e}{M}\right)^{-1} = \left(1 + \frac{0.511}{938.3}\right)^{-1} \approx 1 - \frac{0.511}{938.3} = 0.9995. \quad (3.48)$$

Answers to this section are summarized in Table 3.1, column (5).

(c) The Bohr theory for hydrogen atom that initially assumed an infinite nuclear mass worked well because the nucleus (proton or deuteron or triton, etc.) exceeds the electron mass by at least a factor of $1836 = m_p c^2 / (m_e c^2)$. For other types of one-electron structures, such as the positronium Ps, muonium Mu, and muonic hydrogen H_μ where the two masses are close to one another, one must account for both masses and use the appropriate value for the orbiting particle mass as well as for the reduced mass μ_M of the system, as given in column (3) of Table 3.1. The correction factor, presented in column (5) of Table 3.1 can be generalized to all hydrogen-type structures in which one particle with a given charge and mass m revolves around another particle of opposite charge and mass M .

The general correction factor for mass m orbiting around larger mass M thus follows the following rules:

- (1) For radius r_n correction factor f_r can be generalized to read $f_r = \frac{m}{\mu_M} = 1 + \frac{m}{M}$.
- (2) For velocity v_n correction factor f_v remains equal to 1 irrespective of the ratio m/M .
- (3) For energy levels E_n corrections factor f_E is $f_E = \frac{\mu_M}{m} = \left(1 + \frac{m}{M}\right)^{-1}$.

Correction factors f_r , f_v , and f_E are plotted in Fig. 3.4 in the mass ratio m/M range between 0 and 1.

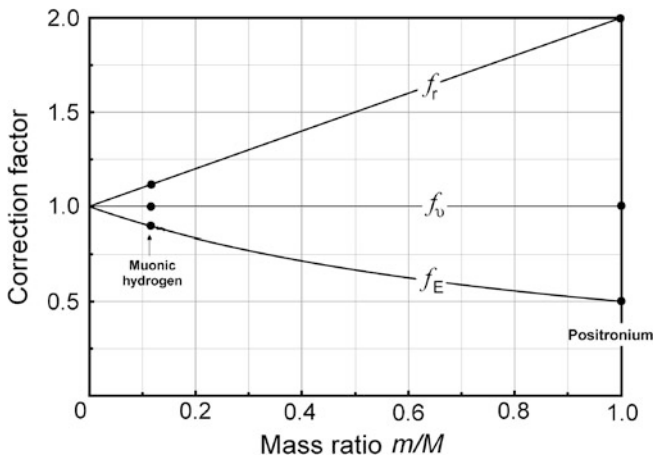


Fig. 3.4 Small mass m and large mass M revolve about a common center-of-mass. General correction factors f_r , f_v , and f_E to be applied to expressions for radius r , velocity v , and energy E valid for infinite large mass ($M \rightarrow \infty$) to obtain expressions valid for finite large mass M

- (d) Finite mass correction factors for (1) muonic hydrogen and (2) positronium.
- (1) Muonic hydrogen consists of negative muon ($m_{\mu^-}c^2 = 207m_e c^2$) and proton revolving about their common center-of-mass in a Bohr atom type configuration ($m_{\mu^-}/m_p = 0.113$).

$$f_r = 1 + \frac{m_{\mu^-}}{m_p} = 1 + \frac{207}{1836} = 1.113, \quad f_v = 1, \quad (3.49)$$

$$f_E = \left(1 + \frac{m_{\mu^-}}{m_p}\right)^{-1} = \left(1 + \frac{207}{1836}\right)^{-1} = 0.90.$$

- (2) Positronium consists of positron and electron revolving about their common center-of-mass in a Bohr atom type configuration ($m_{e^-}/m_{e^+} = 1$).

$$f_r = 1 + \frac{m_{e^-}}{m_{e^+}} = 1 + 1 = 2, \quad f_v = 1, \quad (3.50)$$

$$f_E = \left(1 + \frac{m_{e^-}}{m_{e^+}}\right)^{-1} = (1 + 1)^{-1} = 0.5.$$

Results of (3.49) and (3.50) are plotted in Fig. 3.4.

3.1.Q6

(88)

Reduced mass μ_M represents an effective mass of a two-body system, consisting of two masses: m and M . Defined as

$$\mu_M = \frac{mM}{m+M} \quad \text{or} \quad \frac{1}{\mu_M} = \frac{1}{m} + \frac{1}{M}, \quad (3.51)$$

reduced mass μ_M of a two-body system has units of mass and is used to simplify a two-body problem into an equivalent one-body problem with effective mass equal to the reduced mass. The reduced mass has many applications in physics and is used in Bohr theory of one-electron atoms to account for the finite mass of the nucleus.

Calculate the reduced mass μ_M for the following Bohr-like atomic structures: protium (hydrogen-1), deuterium, tritium, positronium, muonium, antihydrogen, and muonic hydrogen. For each of the seven structures also state its atomic constituents and their mass.

SOLUTION:

Answers to this problem are summarized in Table 3.2.

Table 3.2 Constituents and their reduced mass for the following Bohr-like atomic structures: protium, deuterium, tritium, positronium, muonium, antihydrogen, and muonic hydrogen

Bohr-like structure	Constituents M and m	Mass of constituents	Ratio $\frac{m}{M}$	Reduced mass μ_M
Protium H-1	M : proton p m : electron e^-	$M = 1836m_e$ $m = m_e$	5.45×10^{-4}	$0.9995m_e$
Antihydrogen \bar{H}	M : antiproton \bar{p} m : positron e^+	$M = 1836m_e$ $m = m_e$	5.45×10^{-4}	$0.9995m_e$
Deuterium H-2	M : p + 2 neutrons m : electron e^-	$M = 3670.5m_e$ $m = m_e$	2.72×10^{-4}	$0.9997m_e$
Tritium H-3	M : p + 3 neutrons m : electron e^-	$M = 5497m_e$ $m = m_e$	1.82×10^{-4}	$0.9998m_e$
Positronium Ps	M : positron e^+ m : electron e^-	$m = m_e$ $m = m_e$	1.0	$0.5m_e$
Muonium Mu	M : muon μ^+ m : electron e^-	$M = 207m_e$ $m = m_e$	4.83×10^{-3}	$0.995m_e$
Muonic hydrogen	M : proton p m : muon μ^-	$M = 1836m_e = 8.87m_\mu$ $m = 207m_e = m_\mu$	0.113	$186m_e = 0.90m_\mu$

3.1.Q7**(89)**

Deuterium (H-2) atom also known as heavy hydrogen is one of the two stable isotopes of hydrogen with a natural abundance of 0.016 %. The more common isotope of hydrogen is protium (H-1) with natural abundance of ~ 99.98 %. The nucleus of deuterium is called deuteron and contains one proton and one neutron; the nucleus of protium consists of one proton only. American physicist Harold Urey discovered deuterium in 1934. Heavy water is water consisting of highly enriched deuterium with respect to protium.

For deuterium atom ($Z = 1$) in the first excited state ($n = 2$) determine:

- Distance r between electron and deuteron (nucleus of deuterium atom).
- Radius r_e of the electron orbit.
- Radius r_d of the deuteron orbit.
- Speed v_e of electron in orbit.
- Speed v_d of deuteron in orbit.
- Energy $h\nu$ of the emitted photon upon the atom reverting to ground state.
- Recoil momentum p and recoil kinetic energy E_K upon the atom reverting to ground state.

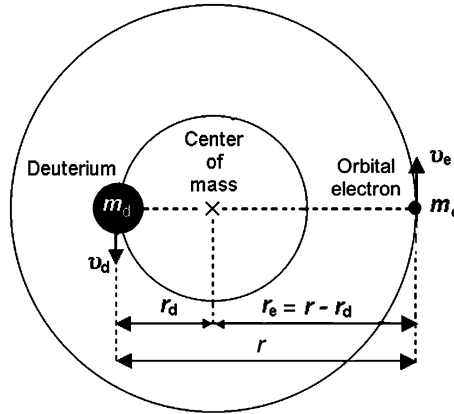


Fig. 3.5 Schematic diagram of deuterium atom consisting of deuteron nucleus with one proton and one neutron

SOLUTION:

To solve this problem we must account for the effect of the finite mass of the nucleus (deuteron: $m_d = 1875.6128 \text{ MeV}/c^2$) on the kinematics of the Rutherford–Bohr atom. When the finite mass of the nucleus is taken into consideration, both the orbital electron as well as nucleus revolve about their common center-of-mass, as shown in Fig. 3.5 where r_e stands for the radius of the electron orbit, r_d for the radius of the deuteron orbit, and $r = r_e + r_d$ the distance between the electron and deuteron.

General expressions for radius r_n , velocity v_n/c , and energy levels E_n of one-electron structures were derived in Prob. 86 accounting for the finite nuclear mass M . The results were as follows

$$r_n = a_0 \left(1 + \frac{m_e}{M}\right) \frac{n^2}{Z}, \quad \frac{v_n}{c} = \alpha \frac{Z}{n}, \quad \text{and} \quad E_n = -E_R \frac{1}{1 + \frac{m_e}{M}} \left(\frac{Z}{n}\right)^2. \quad (3.52)$$

(a) Distance r between electron and deuteron for $n = 2$ orbit is calculated from (3.44) as

$$r_{n=2} = a_0 \left(1 + \frac{m_e}{m_d}\right) \times \frac{4}{1} = 4a_0 \left(1 + \frac{0.511}{1875.6}\right) = 4.0011a_0 = 2.1174 \text{ \AA}. \quad (3.53)$$

(b) Radius r_e of the $n = 2$ electron orbit is calculated from (3.31) as

$$r_e = \frac{r}{1 + \frac{m_e}{m_d}} = 4a_0 = 2.1168 \text{ \AA}. \quad (3.54)$$

(c) Radius r_d of the $n = 2$ deuteron orbit is calculated from (3.32) as

$$r_d = \frac{r}{1 + \frac{m_d}{m_e}} = \frac{4.0011}{1 + \frac{1875.6128}{0.511}} = 1.09 \times 10^{-3} a_0 = 6 \times 10^{-4} \text{ \AA}. \quad (3.55)$$

(d) Total speed v of electron and deuteron in orbit is determined from (3.45) as

$$v = \alpha \frac{Z}{n} c = \frac{\alpha c}{2} = \frac{c}{2 \times 137} = 3.65 \times 10^{-3} c = 1.0949 \times 10^6 \text{ m/s.} \quad (3.56)$$

Electron speed v_e is calculated from (3.33) as

$$v_e = \frac{v}{1 + \frac{m_e}{m_d}} = \frac{3.65 \times 10^{-3} c}{1 + \frac{0.511}{1875.6}} = 3.649 \times 10^{-3} c = 1.0947 \times 10^6 \text{ m/s.} \quad (3.57)$$

Deuteron speed v_d is calculated from (3.34) as

$$v_d = \frac{v}{1 + \frac{m_d}{m_e}} = \frac{3.65 \times 10^{-3} c}{1 + \frac{1875.6}{0.511}} = 9.94 \times 10^{-7} c \approx 300 \text{ m/s.} \quad (3.58)$$

(e) To determine energy $h\nu$ of the photon emitted through $n = 2$ to $n = 1$ transition we must first determine energy levels for the ground state $n = 1$ and first excited state $n = 2$ of the deuterium atom from (3.46)

$$E_{n=1} = -E_R \frac{1}{1 + \frac{m_e}{m_d}} \left(\frac{Z}{n} \right)^2 = -(13.61 \text{ eV}) \times \frac{1}{1 + \frac{0.511}{1875.6}} \left(\frac{1}{1} \right)^2 = -13.61 \text{ eV} \quad (3.59)$$

and

$$E_{n=2} = -E_R \frac{1}{1 + \frac{m_e}{m_d}} \left(\frac{Z}{n} \right)^2 = -(13.61 \text{ eV}) \times \frac{1}{1 + \frac{0.511}{1875.6}} \left(\frac{1}{2} \right)^2 = -3.40 \text{ eV.} \quad (3.60)$$

Energy difference ΔE between the two energy levels is emitted in the form of a ultraviolet photon with energy $h\nu = \Delta E = 10.21 \text{ eV}$.

(g) Photon with energy $h\nu = 10.21 \text{ eV}$ has momentum $p_\nu = h\nu/c = 10.21 \text{ eV}/c$. As a result of momentum conservation recoil momentum of the deuteron atom is $p_A = 10.21 \text{ eV}/c$.

The recoil kinetic energy E_K of the atom is calculated from the recoil momentum p_A using the standard expression relating momentum with kinetic energy (T1.64). This equation can be turned into a quadratic expression for kinetic energy

$$E_K^2 + 2m_d c^2 E_K - p_A^2 c^2 = 0 \quad (3.61)$$

and has the following physically relevant solution for recoil kinetic energy E_K

$$\begin{aligned} E_K &= -m_d c^2 + \sqrt{(m_d c^2)^2 + p_A^2 c^2} \approx \frac{p_A^2 c^2}{2m_d c^2} \\ &= \frac{(10.21 \text{ eV})^2}{2 \times (1875.6 \times 106 \text{ eV})} = 3 \times 10^{-8} \text{ eV.} \end{aligned} \quad (3.62)$$

3.1.Q8

(90)

Calculate the difference in wavelength $\Delta\lambda$ and quantum energy ΔE of the lowest energy Balmer lines emitted by protium (hydrogen-1) and deuterium (hydrogen-2).

SOLUTION:

Facts to note:

- (1) Both protium and deuterium are one-electron structures of hydrogen but they differ in nuclear mass. Protium nucleus consists of one proton ($m_p c^2 = 938.2720$ MeV); deuterium of one proton and one neutron ($m_d c^2 = 1875.0128$ MeV).
- (2) The lowest energy Balmer line originates in an electronic transition from shell $n_i = 3$ to shell $n_f = 2$.
- (3) The difference in wavelengths and quantum energies results from the different nuclear rest energies of protium and deuterium.

Energy levels E_n of one-electron atom corrected for finite nuclear mass M according to (3.46) are expressed as follows (T3.17)

$$E_n = -E_R \frac{1}{1 + \frac{m_e}{M}} \frac{Z^2}{n^2}, \quad (3.63)$$

where

E_R is the Rydberg energy ($E_R = 13.605692$ eV).

Z is the atomic number of the one-electron atom (for hydrogen $Z = 1$).

m_e is the electron rest mass ($m_e = 0.510999$ MeV/ c^2).

Photon energy E_ν , emitted following an electronic transition from initial energy level n_i to final energy level n_f , is

$$E_\nu = h\nu = \frac{2\pi\hbar c}{\lambda} = E_R \frac{Z^2}{1 + \frac{m_e}{M}} \left[\frac{1}{n_f^2} - \frac{1}{n_i^2} \right] \quad (3.64)$$

resulting in the following quantum energies $E_\nu(\text{p})$ and $E_\nu(\text{d})$ of lowest Balmer lines for protium (p) and deuterium (d), respectively

$$E_\nu(\text{p}) = E_R \frac{Z^2}{1 + \frac{m_e}{m_p}} \left[\frac{1}{n_f^2} - \frac{1}{n_i^2} \right] = \frac{13.605692 \text{ eV}}{1 + \frac{0.510999}{938.2720}} \left[\frac{1}{4} - \frac{1}{9} \right] = 1.888651 \text{ eV} \quad (3.65)$$

and

$$E_\nu(\text{d}) = E_R \frac{Z^2}{1 + \frac{m_e}{m_d}} \left[\frac{1}{n_f^2} - \frac{1}{n_i^2} \right] = \frac{13.605692 \text{ eV}}{1 + \frac{0.510999}{1875.0128}} \left[\frac{1}{4} - \frac{1}{9} \right] = 1.889680 \text{ eV}. \quad (3.66)$$

Quantum energies $E_\nu(\text{p})$ and $E_\nu(\text{d})$ correspond to the following wavelengths λ_p and λ_d , respectively

$$\lambda_\text{p} = \frac{2\pi\hbar c}{E_\nu(\text{p})} = \frac{2\pi \times (1973.27 \text{ eV} \cdot \text{\AA})}{1.888651 \text{ eV}} = 6564.70 \text{ \AA} \quad (3.67)$$

and

$$\lambda_\text{d} = \frac{2\pi\hbar c}{E_\nu(\text{d})} = \frac{2\pi \times (1973.27 \text{ eV} \cdot \text{\AA})}{1.889680 \text{ eV}} = 6561.12 \text{ \AA}. \quad (3.68)$$

Quantum energy difference ΔE_ν and wavelength difference $\Delta\lambda$ between lowest Balmer line photons emitted by excited protium atoms and excited deuterium atoms are thus as follows

$$\Delta E_\nu = E_\nu(\text{d}) - E_\nu(\text{p}) = 1.889680 \text{ eV} - 1.888651 \text{ eV} = 1.03 \times 10^{-3} \text{ eV} \quad (3.69)$$

and

$$\Delta\lambda = |\lambda_\text{d} - \lambda_\text{p}| = |6561.12 \text{ \AA} - 6564.70 \text{ \AA}| = 3.58 \text{ \AA}. \quad (3.70)$$

3.1.Q9

(91)

The lowest energy Balmer photon is emitted from excited hydrogen atom.

- Plot the atomic energy level diagram for hydrogen for $n = 1$ through $n = 5$ and identify the Balmer line with the longest wavelength λ .
- Determine the energy E_ν and wavelength λ of the emitted Balmer photon.
- Determine the momentum p_ν of the emitted photon.
- Determine the recoil speed v_recoil of the hydrogen atom.
- Determine the recoil kinetic energy E_recoil of the hydrogen atom.

SOLUTION:

(a) Atomic energy level diagram for hydrogen atom is shown in Fig. 3.6. Also shown on the diagram is the electronic transition that produces the Balmer line ($n_f = 2$) with the longest wavelength, i.e., smallest energy ($n_i = 3$).

The energy levels of the hydrogen atom ($Z = 1$) are shown in Fig. 3.6 and calculated from the basic Bohr theory (T3.7) as follows

$$E_n = -E_\text{R} \frac{1}{n^2}, \quad (3.71)$$

resulting in $E_1 = -13.61 \text{ eV}$, $E_2 = -3.40 \text{ eV}$, $E_3 = -1.51 \text{ eV}$, $E_4 = -0.85 \text{ eV}$, and $E_5 = -0.54 \text{ eV}$.

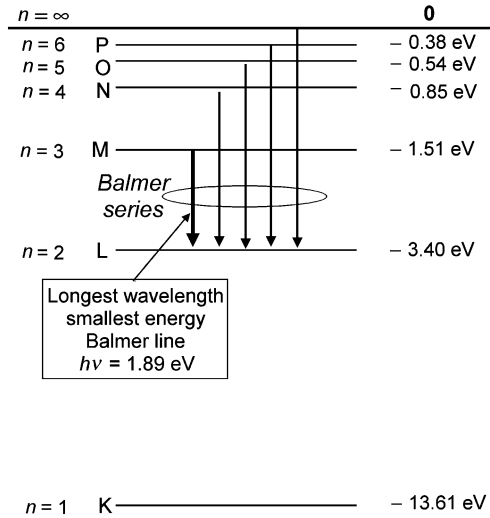


Fig. 3.6 Atomic energy level diagram for hydrogen atom. Also shown are lines from the Balmer spectral series with the longest wavelength/smallest energy line shown in *bold*

(b) As indicated in Fig. 3.6, the longest-wavelength Balmer line originates from a transition from $n_i = 3$ to $n_f = 2$ and is characterized by an energy difference of $\Delta E = E_3 - E_2 = -1.51 \text{ eV} - (-3.40 \text{ eV}) = 1.89 \text{ eV}$. Thus, the energy of the emitted photon $E_\nu = 1.89 \text{ eV}$ corresponding to a wavelength λ given as

$$\lambda = \frac{hc}{E_\nu} = \frac{2\pi\hbar c}{E_\nu} = \frac{2\pi \times (1973 \text{ eV} \cdot \text{\AA})}{1.89 \text{ eV}} = 6555 \text{ \AA}. \quad (3.72)$$

(c) Momentum p_ν of the emitted Balmer line photon is calculated from the general relativistic expression for total energy E of any particle (including a photon) with rest energy E_0

$$E = \sqrt{E_0^2 + p^2 c^2} \quad \text{or} \quad p = \frac{1}{c} \sqrt{E^2 - E_0^2}. \quad (3.73)$$

For a photon the rest energy $E_0 = 0$ and from (3.73) we get

$$p_\nu = \frac{E_\nu}{c} = \frac{h\nu}{c} = \frac{h}{\lambda} = \frac{2\pi\hbar}{\lambda} = \frac{2\pi\hbar c}{\lambda c} = \frac{2\pi \times (1973 \text{ eV} \cdot \text{\AA})}{(6555 \text{ \AA}) \times c} = 1.89 \text{ eV}/c. \quad (3.74)$$

(d) Recoil velocity v_{recoil} of the proton is calculated from the recoil momentum p_{recoil} of the proton which is equal to the momentum of the emitted Balmer photon. Thus, we have

$$p_{\text{recoil}} = m_p v_{\text{recoil}} = p_\nu = 1.89 \text{ eV}/c \quad (3.75)$$

and

$$v_{\text{recoil}} = \frac{p_\nu}{m_p} = \frac{1.89 \text{ eV}/c}{938.3 \times 10^6 \text{ eV}/c^2} = 2.01 \times 10^{-9} c = 0.603 \text{ m/s}. \quad (3.76)$$

(e) Recoil kinetic energy E_{recoil} of the hydrogen atom as a result of emission of longest-wavelength Balmer line is calculated with the classical expression for kinetic energy

$$\begin{aligned} E_{\text{recoil}} &= \frac{m_H v_{\text{recoil}}^2}{2} = \frac{m_H c^2}{2} \left(\frac{v_{\text{recoil}}}{c} \right)^2 = \frac{938.8 \times 10^6 \text{ eV}}{2} \times (2.01 \times 10^{-9})^2 \\ &= 1.9 \times 10^{-9} \text{ eV}. \end{aligned} \quad (3.77)$$

3.1.Q10

(92)

For doubly ionized lithium-7 atom (Li^{++} , $Z = 3$, $A = 7$, $m_{\text{Li-7}} = 6533.38 \text{ MeV}/c^2$):

- Calculate and plot the atomic energy level diagram for the 5 lowest energy levels. Use the correction for the finite nuclear mass in the calculation.
- Calculate the wave numbers k and corresponding wavelengths λ and quantum energies E_ν for the three lowest k values as well as for the series limit of the $n_f = 2$ spectral series and indicate the corresponding transitions in the energy level diagram plotted in (a).

SOLUTION:

(a) Energy levels $E_n(\text{Li}^{++})$ of doubly ionized lithium-7 atom incorporating the finite nuclear mass correction are calculated from the following expression (T3.17)

$$E_n = -E_R \frac{1}{1 + \frac{m_e}{M(\text{Li-7})}} \left(\frac{Z}{n} \right)^2 = -(13.61 \text{ eV}) \frac{1}{1 + \frac{0.511}{6533.83}} \left(\frac{3}{n} \right)^2 = -\frac{122.5 \text{ eV}}{n^2}. \quad (3.78)$$

The ionization potential of Li^{++} is thus 122.5 eV and the first 5 levels of the energy level diagram, shown in Fig. 3.7, are as follows

$$\begin{aligned} E_1 &= -122.5 \text{ eV}; & E_2 &= -30.6 \text{ eV}; & E_3 &= -13.6 \text{ eV}; \\ E_4 &= -7.7 \text{ eV}; & E_5 &= -4.9 \text{ eV}. \end{aligned} \quad (3.79)$$

(b) The wave number k for transitions from initial level $n_i > 2$ to final level $n_f = 2$ incorporating the correction for the finite nuclear mass is given as follows (Table T3.7)

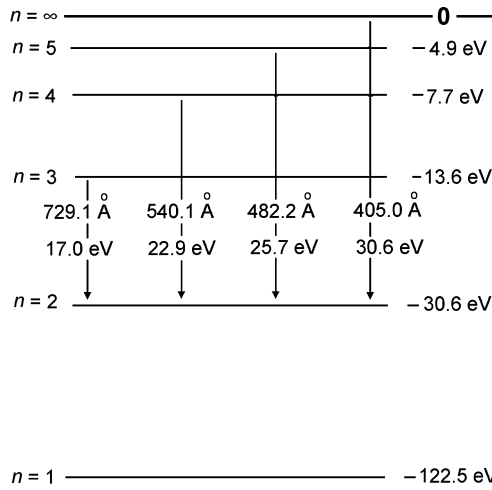


Fig. 3.7 Atomic energy level diagram of doubly ionized lithium atom Li^{++} . The three lowest energy electronic transitions as well as the limiting transition to $n_f = 2$ are also shown

$$\begin{aligned}
 k = \frac{1}{\lambda} &= R_\infty \frac{Z^2}{1 + \frac{m_e}{M_{\text{Li-7}}}} \left[\frac{1}{2^2} - \frac{1}{n_i^2} \right] = \frac{(109737 \text{ cm}^{-1}) \times 3^2}{1 + \frac{0.511}{6533.83}} \left[0.25 - \frac{1}{n_i^2} \right] \\
 &= (109728 \text{ cm}^{-1}) \times 9 \times \left[0.25 - \frac{1}{n_i^2} \right] = (987552 \text{ cm}^{-1}) \times \left[0.25 - \frac{1}{n_i^2} \right], \quad (3.80)
 \end{aligned}$$

where $R_\infty = 109737 \text{ cm}^{-1}$ is the Rydberg constant for infinite nuclear mass and $R_\infty/(1 + m_e/M_{\text{Li-7}}) = 109728 \text{ cm}^{-1}$ is the Rydberg constant for Li-7 incorporating the finite nuclear mass correction (see Table T3.2).

The first three lines of the $n_f = 2$ spectral series of Li-7 are given as follows

$$k(n_i = 3) = (987552 \text{ cm}^{-1}) \times (0.25 - 1/9) = 137160 \text{ cm}^{-1}, \quad (3.81)$$

$$k(n_i = 4) = (987552 \text{ cm}^{-1}) \times (0.25 - 1/16) = 185166 \text{ cm}^{-1}, \quad (3.82)$$

$$k(n_i = 5) = (987552 \text{ cm}^{-1}) \times (0.25 - 1/25) = 207387 \text{ cm}^{-1}, \quad (3.83)$$

$$\begin{aligned}
 k(n_i = \infty) &= (987552 \text{ cm}^{-1}) \times (0.25 - 1/\infty) = 246888 \text{ cm}^{-1} \\
 &\text{(limit of } n_f = 2 \text{ series),} \quad (3.84)
 \end{aligned}$$

corresponding to the following wavelengths λ

$$\lambda(n_i = 3) = 1/k(n_i = 3) = 1/(137160 \text{ cm}^{-1}) = 729.1 \text{ \AA}, \quad (3.85)$$

$$\lambda(n_i = 4) = 1/k(n_i = 4) = 1/(185166 \text{ cm}^{-1}) = 540.1 \text{ \AA}, \quad (3.86)$$

$$\lambda(n_i = 5) = 1/k(n_i = 5) = 1/(207387 \text{ cm}^{-1}) = 482.2 \text{ \AA}, \quad (3.87)$$

$$\begin{aligned}
 \lambda(n_i = \infty) &= 1/k(n_i = \infty) = 1/(246888 \text{ cm}^{-1}) = 405.0 \text{ \AA} \\
 &\text{(limit of } n_f = 2 \text{ series)} \quad (3.88)
 \end{aligned}$$

and the following quantum energies E_v

$$E_v(n_f = 2, n_i = 3) = 30.6 \text{ eV} - 13.6 \text{ eV} = 17.0 \text{ eV}, \quad (3.89)$$

$$E_v(n_f = 2, n_i = 4) = 30.6 \text{ eV} - 7.7 \text{ eV} = 22.9 \text{ eV}, \quad (3.90)$$

$$E_v(n_f = 2, n_i = 5) = 30.6 \text{ eV} - 4.9 \text{ eV} = 25.7 \text{ eV}, \quad (3.91)$$

$$E_v(n_f = 2, n_i = \infty) = 30.6 \text{ eV} - 0 \text{ eV} = 30.6 \text{ eV} \quad (\text{limit of } n_f = 2 \text{ series}) \quad (3.92)$$

3.1.Q11

(93)

In addition to one-electron atoms and ions, several more exotic, short-lived, and unusual “atomic” structures are known whose kinematics can be described using the same concepts as those applied to the standard Bohr atom. However, to achieve meaningful theoretical results, the use of appropriate reduced mass μ_M rather than electron mass m_e is mandatory, because μ_M for these structures can be significantly different from m_e in contrast to the situation with the standard electron-proton Bohr atom.

Positronium consists of a positron and electron revolving about their common center-of-mass that lies, because of their equal masses, halfway between them.

- (a) If such a system were a normal atom, how would its emission spectrum compare to that of hydrogen atom? Compare the lowest energy emission line from the Lyman series in hydrogen to the corresponding transition in positronium.
- (b) Estimate the time of collapse of the Bohr orbit for positronium.

SOLUTION:

- (a) The emission spectrum of hydrogen atom, as described by the wave number

$$k_H = R_H \left(\frac{1}{n_f^2} - \frac{1}{n_i^2} \right) = \frac{R_\infty}{1 + \frac{m_e}{m_p}} \left(\frac{1}{n_f^2} - \frac{1}{n_i^2} \right), \quad (3.93)$$

where R_H is the Rydberg constant for hydrogen given as (T3.19)

$$R_H = \frac{\mu_H}{m_e} R_\infty = \frac{1}{1 + \frac{m_e}{m_p}} R_\infty = 0.9995 R_\infty = 109677 \text{ cm}^{-1} \quad (3.94)$$

with

μ_H reduced mass of hydrogen ($\mu_H = m_e m_p / (m_e + m_p)$).

R_∞ Rydberg constant assuming an infinite nuclear mass ($R_\infty = 109737 \text{ cm}^{-1}$).

In a similar manner the emission spectrum of positronium would be expressed as

$$k_{\text{pos}} = R_{\text{pos}} \left(\frac{1}{n_f^2} - \frac{1}{n_i^2} \right) = \frac{R_{\infty}}{1 + \frac{m_e}{m_e}} \left(\frac{1}{n_f^2} - \frac{1}{n_i^2} \right) = \frac{R_{\infty}}{2} \left(\frac{1}{n_f^2} - \frac{1}{n_i^2} \right), \quad (3.95)$$

where R_{pos} is the Rydberg constant of positronium given as

$$R_{\text{pos}} = \frac{\mu_{\text{pos}}}{m_e} R_{\infty} = \frac{1}{1 + \frac{m_e}{m_e}} R_{\infty} = \frac{1}{2} R_{\infty} = 54868.5 \text{ cm}^{-1} \quad (3.96)$$

with μ_{pos} the positronium reduced mass $\mu_{\text{pos}} = m_e^2 / (2m_e) = 0.5m_e$.

As a consequence of the reduced mass, the frequencies, energy levels, and wave numbers associated with the spectral lines of positronium are about half of those corresponding to hydrogen atom. The actual ratio is given as $1/(1 + m_e/m_p) = 1/1.005 = 0.9995$ versus 0.5.

The lowest energy line from the Lyman spectral series of hydrogen originates from the $n_i = 2$ to $n_f = 1$ electronic transition. Its energy is given as

$$h\nu = E_2 - E_1 = -0.9995 E_R \left(\frac{1}{4} - 1 \right) \approx 10.2 \text{ eV} \quad (3.97)$$

and the corresponding line in positronium has the following energy

$$h\nu = -0.5 E_R \left(\frac{1}{4} - 1 \right) = \frac{3}{4} \times 0.5 E_R = 5.1 \text{ eV}. \quad (3.98)$$

(b) Problem 83 deals with the time of collapse t_{col} of the Bohr orbit for the ground state of hydrogen atom and produced the following result

$$t_{\text{col}}(\text{H}) = -\frac{3}{bE_1^3} = 1.4 \times 10^{-10} \text{ s}, \quad (3.99)$$

with E_1 the ground state energy of the hydrogen atom ($E_1 = -13.6 \text{ eV}$) and b_{H} the time of collapse constant given for hydrogen as

$$b_{\text{H}} = \frac{128\pi\epsilon_0 c}{3(m_e c^2)^2 e^2} = 8.51 \times 10^6 (\text{eV})^3 \cdot \text{s}^{-1}. \quad (3.100)$$

The time of collapse $t_{\text{col}}(\text{pos})$ of positronium will be of the same form as that of hydrogen in (3.99) except that we replace m_e in (3.100) with $\mu_{\text{pos}} = 0.5m_e$ and E_1 in (3.99) with $0.5E_1$ (ground state of positronium). We then get

$$\begin{aligned} t_{\text{col}}(\text{pos}) &= -\frac{3}{b_{\text{pos}} E_{\text{pos}}^3} = -\frac{3}{0.5^2 b_{\text{H}} 0.5^3 E_1^3} = -\frac{1}{0.5^5} t_{\text{col}}(\text{H}) \\ &= \frac{1.4 \times 10^{-10} \text{ s}}{3.125 \times 10^{-2}} = 4.5 \text{ ns} \end{aligned} \quad (3.101)$$

in fair agreement with measured lifetime of positronium of the order of 10^{-10} s .

3.1.Q12

(94)

Muonic atom is an atom in which an electron is replaced by a negative muon μ^- with a rest mass $m_\mu = 207m_e$ orbiting close to or within the nucleus. Hydrogen forms the simplest muonic atom consisting of a proton p and a negative muon μ^- .

For muonic hydrogen atom:

- Determine radius of the first and second Bohr orbit.
- Calculate and plot atomic energy level diagram for $n = 1$ to $n = 5$.
- Determine energy and wavelength of the most energetic photon that can be emitted by muonic hydrogen.
- Determine the energy of the photon with the longest wavelength λ in the Lyman series of muonic hydrogen.

SOLUTION:

(a) In order to determine the radii and energy levels of muonic hydrogen we first calculate its reduced mass μ_μ

$$\mu_\mu = \frac{m_\mu m_p}{m_\mu + m_p} = \frac{207m_e 1836m_e}{207m_e + 1836m_e} = 186m_e. \quad (3.102)$$

General equations for radii r_n and energy levels E_n of Bohr atom accounting for the finite nuclear mass are given as follows [see (T3.16) and (T3.17), respectively]

$$r_n = \frac{4\pi\epsilon_0 (\hbar c)^2 n^2}{e^2 \mu_\mu c^2 Z} = a_0 \frac{m_e n^2}{\mu_\mu Z} = \frac{a_0 n^2}{186 Z} \quad (3.103)$$

and

$$E_n = -\frac{1}{2} \left(\frac{e}{4\pi\epsilon_0} \right)^2 \frac{\mu_\mu c^2 Z^2}{(\hbar c)^2 n^2} = -E_R \frac{\mu_\mu Z^2}{m_e n^2}, \quad (3.104)$$

where a_0 is the Bohr radius constant (T3.4) equal to $a_0 = 0.5292 \text{ \AA}$ and E_R is the Rydberg energy ($E_R = 13.61 \text{ eV}$).

Radii of the first ($n = 1$) and second ($n = 2$) Bohr orbit of muonic hydrogen atom are as follows

$$r_1 = \frac{a_0 n^2}{186 Z} = \frac{0.5292 \text{ \AA}}{186} = 2.85 \times 10^{-3} \text{ \AA} = 285 \text{ fm} \quad (3.105)$$

and

$$r_2 = \frac{a_0 n^2}{186 Z} = \frac{(0.5292 \text{ \AA})}{186} \times \frac{2^2}{1} = 11.4 \times 10^{-3} \text{ \AA} = 1140 \text{ fm}. \quad (3.106)$$

(b) Energy levels E_n for $n = 1$ to $n = 5$ are calculated for muonic hydrogen from (3.104) as

$$E_n = -\frac{1}{2} \left(\frac{e}{4\pi\epsilon_0} \right)^2 \frac{\mu_\mu c^2 Z^2}{(\hbar c)^2 n^2} = -E_R \frac{\mu_\mu}{m_e} \frac{1}{n^2} = -\frac{(13.6 \text{ eV}) \times 186}{n^2} = \frac{2530 \text{ eV}}{n^2}. \quad (3.107)$$

Thus, as shown in Fig. 3.8, atomic energy levels of muonic hydrogen are:

$$\begin{aligned} E_1 &= -2530 \text{ eV}, \\ E_2 &= -2530 \text{ eV}/4 = -632.5 \text{ eV}, \\ E_3 &= -2530 \text{ eV}/9 = -281.1 \text{ eV}, \\ E_4 &= -2530 \text{ eV}/16 = -158.1 \text{ eV}, \\ E_5 &= -2530 \text{ eV}/25 = -101.2 \text{ eV}. \end{aligned}$$

(c) The most energetic photon that can be emitted from muonic hydrogen is produced by a muon moving from ∞ (where it was at rest) to the $n = 1$ energy level of muonic hydrogen (ground state of muonic hydrogen: $E_1 = -2530 \text{ eV}$). Energy $h\nu$ released as photon (Photon 1 in Fig. 3.8) in this muonic transition of 2530 eV corresponds to a photon wavelength λ of

$$\lambda = \frac{hc}{h\nu} = \frac{2\pi\hbar c}{h\nu} = \frac{12390 \text{ eV} \cdot \text{\AA}}{2530 \text{ eV}} = 4.9 \text{ \AA}. \quad (3.108)$$

(d) All lines of Lyman series end on level 1 and the highest wavelength (i.e., lowest energy in Lyman series belongs to photon generated in $n = 2$ to $n = 1$ transition, corresponding to energy of 1897.5 eV and shown as photon 2 in Fig. 3.8.

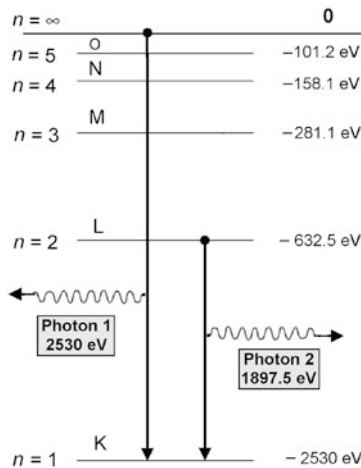


Fig. 3.8 Atomic energy level diagram for muonic hydrogen

3.1.Q13

(95)

Muonium, muonic hydrogen, and antihydrogen are exotic hydrogen-like structures whose spectral emissions can be predicted with the simple Bohr theory of one-electron atoms, similar to the approach taken in studies of protium (hydrogen-1) and deuterium spectra.

For four hydrogen-like atoms: protium, antihydrogen, muonium, and muonic hydrogen:

- List the constituents and their rest mass
- Calculate their reduced mass.
- Determine the lowest Lyman-type photon emission energy.

SOLUTION:

- Constituents as well as their mass for the four hydrogen-like atomic structures are given in rows (2) and (3) of Table 3.3.
- Reduced mass μ_M for the constituents of the four hydrogen-like structures is calculated using (3.51) and is given in row (4) of Table 3.3.
- Lowest Lyman-type photon emission energy for the four hydrogen-like structures is calculated as the difference between energy levels $(E_n)_i - (E_n)_f$ (see row (5) in Table 3.3) for $n_i = 2$ and $n_f = 1$ and is given in Table 3.3.

Table 3.3 Characteristics of four hydrogen-like atomic structures: H-1, $\bar{\text{H}}$, Mu, and H_μ

(1) Structure	Protium H-1	Antihydrogen $\bar{\text{H}}$	Muonium Mu	Muonic hydrogen H_μ
(2) Constituents	M : proton p m : electron e^-	M : antiproton \bar{p} m : positron e^+	M : muon μ^+ m : electron e^-	M : proton p m : muon μ^-
(3) Mass	$m_p = 1836m_e$	$m_p = 1836m_e$	$m_{\mu^+} = 207m_e$	$m_p = 1836m_e$ $m_{\mu^-} = 207m_e$
(4) Reduced mass μ_M	$0.9995m_e$	$0.9995m_e$	$0.995m_e$	$186m_e = 0.90m_{\mu^-}$
(5) Energy levels E_n	$-0.9995 \frac{E_R}{n^2}$	$-0.9995 \frac{E_R}{n^2}$	$-0.995 \frac{E_R}{n^2}$	$-186 \frac{E_R}{n^2}$
(6) Ground state E_1 (eV)	-13.61	-13.61	-13.54	-2531.5
(7) First excited state E_2 (eV)	-3.40	-3.40	-3.39	-632.9
(8) Lowest Lyman-type emission line	10.21 eV	10.21 eV	10.15 eV	1900 eV

3.1.Q14

(96)

An α particle colliding with an electron may capture the electron and form a singly ionized helium ion He^+ . The recombination energy is typically emitted in the form of a photon with energy $h\nu$ satisfying conservation of energy. The He^+ ion eventually meets another free electron and recombines with it to form a neutral helium atom.

- (a) An electron moving with velocity $v = 1.5 \times 10^7$ m/s recombines with an α particle to form a singly ionized helium atom in ground state. Determine the wavelength λ of the monoenergetic photon that is emitted in the recombination reaction.
- (b) An electron with kinetic energy $E_K = 1.6$ eV recombines with an α particle. A singly ionized helium atom is formed and a photon with wavelength $\lambda = 2478$ Å is emitted during the recombination process. Determine the excited energy level E_n into which the electron was captured and describe what happens to the singly ionized helium ion after the recombination process.
- (c) Plot a schematic diagram of the processes described in (a) and (b).

SOLUTION:

(a) We first determine the kinetic energy of the electron before recombination using (T1.58)

$$E_K = m_e c^2 \left[\frac{1}{\sqrt{1 - \frac{v^2}{c^2}}} - 1 \right] = (0.511 \times 10^6 \text{ eV}) \times \left[\frac{1}{\sqrt{1 - \frac{(1.5 \times 10^7)^2}{(3 \times 10^8)^2}}} - 1 \right] = 640 \text{ eV}. \quad (3.109)$$

The ground state ($n = 1$) of the singly ionized helium ion (He^+ ; $Z = 2$) is calculated from Bohr theory (T3.7) for single electron structures to get

$$E_n = E_1 = -E_R \left(\frac{Z}{n} \right)^2 = -(13.6 \text{ eV}) \times \left(\frac{2}{1} \right)^2 = -54.4 \text{ eV}, \quad (3.110)$$

where E_R is the Rydberg energy (13.6 eV).

Total energy E_v available for emission of photon in the electron– α particle recombination process is the kinetic energy of the incident electron ($E_K = 640$ eV) PLUS the binding energy E_B of the electron in the He^+ ground state ($E_B = |E_1| = 54.4$ eV), i.e.,

$$E_v = E_K + E_B = E_K + |E_1| = 640 \text{ eV} + 54.4 \text{ eV} = 694.4 \text{ eV} \quad (3.111)$$

corresponding to a photon with wavelength λ of

$$\lambda = \frac{hc}{E_\nu} = \frac{2\pi\hbar c}{E_\nu} = \frac{2\pi \times (1973 \text{ eV} \cdot \text{\AA})}{694.4 \text{ eV}} = 17.8 \text{ \AA}. \quad (3.112)$$

(b) We first calculate the energy E_ν of the emitted photon with $\lambda = 2478 \text{ \AA}$

$$E_\nu = h\nu = \frac{hc}{\lambda} = \frac{2\pi\hbar c}{\lambda} = \frac{2\pi \times (1973 \text{ eV} \cdot \text{\AA})}{2478 \text{ \AA}} = 5 \text{ eV}. \quad (3.113)$$

This photon energy consists of two components: (1) kinetic energy $E_K = 1.6 \text{ eV}$ of the electron and (2) binding energy $E_B(n)$ of the He^+ shell into which the electron is captured during the recombination process. Thus,

$$E_B = E_\nu - E_K = 5 \text{ eV} - 1.6 \text{ eV} = 3.4 \text{ eV} \quad (3.114)$$

and the binding energy $E_B(n)$ component of the photon energy is 3.4 eV .

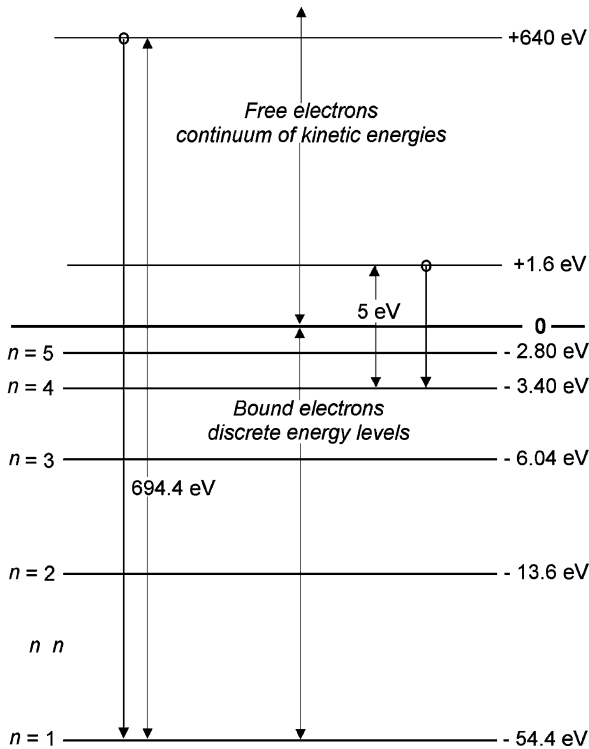


Fig. 3.9 Schematic diagram of processes described in (a) and (b)

Energy levels for the first 5 shells of the singly ionized helium ion H^+ are calculated from (3.109) and are as follows:

$$\begin{aligned} E_1 &= -54.4 \text{ eV}; & E_2 &= -13.6 \text{ eV}; & E_3 &= -6.04 \text{ eV}; \\ E_4 &= -3.40 \text{ eV}; & E_5 &= -2.18 \text{ eV}, \end{aligned} \quad (3.115)$$

indicating that, in the recombination process with the α particle, the electron was captured into the $n = 4$ shell and the two formed an excited singly ionized helium ion He^+ .

The excited He^+ ion will attain its ground state through one or two or three electronic transitions starting from the initial $n = 4$ excited state. Each transition is followed by emission of photon with energy equal to the difference in energy between the initial and final shell.

(c) Schematic diagram of processes described in (a) and (b) is given in Fig. 3.9.

3.1.Q15

(97)

An incident photon of energy $h\nu$ ionizes a hydrogen atom in ground state through photoelectric effect. The liberated electron, referred to as a photoelectron, subsequently combines with an α particle and forms a singly ionized helium atom (He^+) in second excited state, emitting a photon of wavelength $\lambda' = 858 \text{ \AA}$. Determine the incident photon energy $h\nu$.

SOLUTION:

The seven steps taken in solving this problem are listed below and shown with a schematic diagram in Fig. 3.10.

(1) Incident photon with energy $h\nu$ undergoes a photoelectric effect on a hydrogen atom in the ground state. In photoelectric effect the photon disappears and the electron is ejected from the atom as photoelectron with kinetic energy E_K equal to photon energy $h\nu$ MINUS the shell binding energy of the emitted photoelectron $E_B(n)$.

(2) Thus, the photoelectron is emitted from the ground state of hydrogen with kinetic energy E_K given as

$$E_K = h\nu - E_B(\text{H}; n = 1) = h\nu - 13.6 \text{ eV}. \quad (3.116)$$

Note: the energy level of the ground state of hydrogen is $E(\text{H}; n = 1) = E_1 = -13.6 \text{ eV}$; however, the binding energy of the electron in the ground state of hydrogen is $E_B(\text{H}; n = 1) = +13.6 \text{ eV}$.

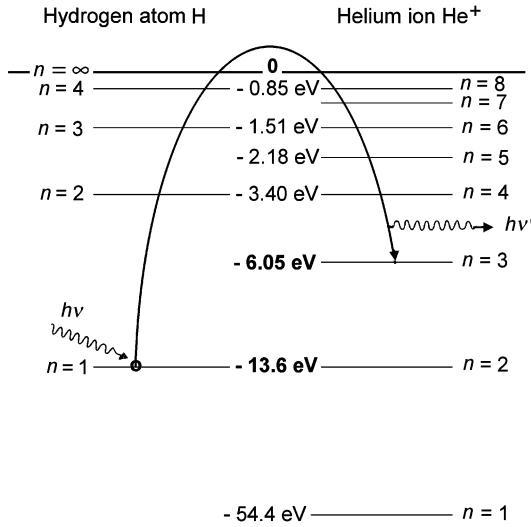


Fig. 3.10 Atomic energy level diagram for hydrogen atom and singly ionized helium ion with a schematic diagram of processes in which a photon $h\nu$ undergoes a photoelectric effect with a hydrogen atom in ground state producing a photoelectron which subsequently combines with an α particle to form a singly ionized helium ion in second excited state and emits a photon with energy $h\nu'$. The summary of results is as follows: $h\nu' = 14.4$ eV and $h\nu = 22$ eV. Kinetic energy E_K of the photoelectron that subsequently recombines with helium ion He^{++} is 22 eV $- 13.6$ eV = 8.4 eV

(3) The liberated photoelectron with kinetic energy E_K subsequently combines with an α particle to form a singly ionized helium atom (He^+) in the second excited state ($n = 3$).

(4) The (e, α) recombination process triggers emission of a photon with wavelength $\lambda = 858 \text{ \AA}$ corresponding to photon energy $h\nu'$ given as

$$h\nu' = \frac{2\pi\hbar c}{\lambda'} = \frac{2\pi \times (1973 \text{ eV} \cdot \text{\AA})}{858 \text{ \AA}} = 14.4 \text{ eV}. \tag{3.117}$$

(5) Energy of the emitted photon $h\nu'$ is equal to kinetic energy of the photoelectron E_K PLUS the binding energy $E_B(\text{He}^+; n = 3)$ of an electron in the second excited state of He^+ given as

$$E_B(\text{He}^+; n = 3) = E_R \left(\frac{Z}{n} \right)^2 = (13.6 \text{ eV}) \times \left(\frac{2^2}{3^2} \right) = 6.05 \text{ eV}. \tag{3.118}$$

(6) Thus, the emitted photon energy $h\nu'$ can be expressed as follows

$$h\nu' = E_K + E_B(\text{He}^+; n = 3) = h\nu - E_B(\text{H}; n = 1) + E_B(\text{He}^+; n = 3). \tag{3.119}$$

(7) The unknown incident photon energy $h\nu$ can finally from (3.119) be calculated as follows

$$\begin{aligned} h\nu &= h\nu' + E_{\text{B}}(\text{H}, n = 1) - E_{\text{B}}(\text{He}^+, n = 3) \\ &= 14.4 \text{ eV} + 13.61 \text{ eV} - 6.05 \text{ eV} = 22 \text{ eV}. \end{aligned} \quad (3.120)$$

3.2 Multi-electron Atoms

3.2.Q1

(98)

The periodic properties of elements can be predicted from the layout of the periodic table of elements and understood from an analysis of the electron configuration of atoms.

List and define at least 5 periodic characteristics of elements and briefly discuss their manifestation in the periodic table of elements.

SOLUTION:

The most notable periodic properties of elements are:

- (a) Ionization potential of atom.
- (b) Electron affinity.
- (c) Electronegativity and electropositivity.
- (d) Atomic radius.
- (e) Atomic volume.
- (f) Density of elements in condensed state.
- (g) Melting and boiling point.

(a) **Ionization potential (IP)** of an atom is defined as the energy required for removing the least bound orbital electron called valence electron from the outer shell of the atom. The Hartree approximation predicts an IP of 13.6 eV for all atoms; however, measurements show that there is a significant variation in IP as a function of atomic number Z . As Z increases from hydrogen ($Z = 1$), IP exhibits a periodic variation with Z and ranges from a maximum of 24.6 eV for helium ($Z = 4$) to a low of 3.8 eV for francium ($Z = 87$), with noble gases (He, Ne, Ar, Kr, Xe, Rn) exhibiting the highest value for a given period and alkali elements (Li, Na, K, Rb, Cs, Fr) the lowest value per period.

(b) **Electron affinity** reflects the energy that is released when a neutral atom acquires a free electron from its surroundings and transforms into a negative ion (anion). Electron affinity varies periodically with Z ; for example, group II A (alkali earth) elements have low electron affinity as a result of filled $l = 0$ subshells. On the other hand, group VII A elements (halogens) have a high electron affinity because

the addition of an extra outer shell electron rounds off the electron complement of the outer shell and group VIII elements (noble gases) have essentially zero electron affinity because their outer shell already contains a full complement of electrons. Elements of all other group have low electron affinity.

(c) Electronegativity reflects a molecule's ability to attract an electron and form a covalent bond. Thus electronegativity is a property of molecules while electron affinity is a property of individual atoms. In the periodic table of elements, electronegativity increases with Z along a given period and decreases with Z along a row. Hence fluorine is the most electronegative element and cesium is the least electronegative, since it has a low IP and a great ability to shed its outer shell electron. One can also state that cesium is a highly electropositive element (a donor of electron). The electronegative property of oxygen is very important for air filled ionization chambers used in radiation dosimetry.

(d) Atomic radius of a chemical element is a measure of the size of its atoms, usually assumed spherical and taken as the mean distance from the center of the atomic nucleus to the outermost electrons of the atom. Since the atomic boundary is not clearly outlined, several different definitions of atomic radius are in use, such as the Bohr radius, Hartree radius, Thomas-Fermi radius, root-mean-square radius, ionic radius, Van der Waals radius, and covalent radius. These radii refer to isolated atoms in the ground state, to atoms in ionized and excited states, or to atoms bound in ionic, covalent or Van der Waals bonds and can be determined either through measurement or theoretical calculations.

Atomic radii vary in a predictable fashion across the periodic table of elements, generally, with increasing atomic number Z :

- (i) decreasing along each period (row).
- (ii) increasing along each group (column).
- (iii) increasing sharply between the noble gas at the end of each period and the alkali element at the beginning of a new period.

(e) Atomic volume \mathcal{V}'_a is defined as the volume occupied by one mole (Avogadro number) of an element in condensed state. \mathcal{V}'_a is thus a macroscopic quantity that can be determined by dividing a mole of an element with the physical density of the element.

In each group of the periodic table \mathcal{V}'_a generally increases with Z because of an increasing number of electron shells. Each period of the periodic table starts with an alkali element, finishes with a noble gas, and has two maxima in \mathcal{V}'_a (the higher maximum for the alkali element in the lower maximum for the noble gas) and a minimum at the center of the period.

(f) Density of elements in condensed state varies with atomic number Z throughout the periodic table of elements. For a given period the density at the beginning increases with Z to reach a maximum at the center of the period and then decreases gradually toward the end of the period.

(g) **Melting and boiling points** exhibit some periodicity with increasing Z in conjunction with the behavior of the atomic volume: elements with low atomic volume generally have high melting point and elements with high atomic volume have low melting points. Thus in a given period, with increasing Z the melting point first increases, reaches a maximum at the center of the period (e.g., carbon and tungsten) and then decreases toward a minimum for a noble gas. The boiling points of elements show similar trends to those exhibited by melting points, however, the periodicity is less pronounced.

3.2.Q2**(99)**

When lead ($Z = 82$) is bombarded with energetic electrons, in addition to bremsstrahlung photons, characteristic photons are emitted. Wave numbers k (in cm^{-1}) of a few most energetic x-ray lines emitted are as follows:

$$k(\text{K abs. edge}) = 7.10 \times 10^8; k(\text{K-L}) = 5.92 \times 10^8; k(\text{K-M}) = 6.85 \times 10^8; \\ k(\text{K-N}) = 7.06 \times 10^8; k(\text{L-M}) = 0.94 \times 10^8; \text{ and } k(\text{L-N}) = 1.15 \times 10^8,$$

where “K abs. edge” designates the highest-energy characteristic photon emitted by lead and K, L, M, and N are shells with principal quantum numbers n equal to 1, 2, 3, and 4, respectively.

NOTE: In the k data above, the fine structure splitting of atomic energy levels is ignored and only the principal quantum number n is accounted for. Often in modern physics the wave number k is defined as $k = 2\pi/\lambda$; however, in this problem we use the traditional definition $k = 1/\lambda$.

- Based on information given above, construct the atomic energy level diagram for the K, L, M, and N shells of lead.
- Comment on the differences between the energy level diagram for lead and that for a one-electron atom such as hydrogen.

SOLUTION:

Before embarking on the energy level diagram, we must first determine the photon energy $h\nu$ corresponding to the wave numbers above, using the Planck law in the following form

$$E_\nu = h\nu = h \frac{c}{\lambda} = \frac{2\pi \hbar c}{\lambda} = 2\pi \hbar c k = 2\pi \times (197.3 \text{ MeV} \cdot \text{fm}) \times k \\ = (1239 \times 10^{-10} \text{ keV} \cdot \text{cm}) \times k. \quad (3.121)$$

- Atomic energy level diagram for lead.

Photon energies calculated from (3.121) for the various wave numbers of electronic transitions are provided in Table 3.4. These data now allow us to determine the

Table 3.4 Photon energies corresponding to various electronic transitions to K shell in lead

Transition	K-∞ K abs. edge	K-L	K-M	K-N	L-M	L-N
Wave number k (cm^{-1})	7.10×10^8	5.92×10^8	6.85×10^8	7.06×10^8	0.94×10^8	1.15×10^8
Photon energy $h\nu$ (keV)	88.0	73.3	84.9	87.5	11.6	14.2

energy levels for the four innermost shells of the energy level diagram of lead. The K absorption edge photon energy of +88 keV for lead gives us direct information on the K shell energy level [$E(\text{K}) = -88$ keV] as well as on the binding energy of the K shell electron $E_{\text{B}}(\text{K}) = +88$ keV.

Using the K shell energy level of $E(\text{K}) = -88$ keV determined from the K absorption edge energy, we can now calculate the L, M, and N shell energy levels with the help of photon energies listed in Table 3.4 as follows

$$E(\text{L}) = E(\text{K}) + h\nu_{\text{K-L}} = -88 \text{ keV} + 73.3 \text{ keV} = -14.7 \text{ keV}, \quad (3.122)$$

$$E(\text{M}) = E(\text{K}) + h\nu_{\text{K-M}} = -88 \text{ keV} + 84.9 \text{ keV} = -3.1 \text{ keV} \quad (3.123)$$

or

$$E(\text{M}) = E(\text{L}) + h\nu_{\text{L-M}} = -14.7 \text{ keV} + 11.6 \text{ keV} = -3.1 \text{ keV}, \quad (3.124)$$

$$E(\text{N}) = E(\text{K}) + h\nu_{\text{K-N}} = -88 \text{ keV} + 87.5 \text{ keV} = -0.5 \text{ keV} \quad (3.125)$$

or

$$E(\text{N}) = E(\text{L}) + h\nu_{\text{L-N}} = -14.7 \text{ keV} + 14.2 \text{ keV} = -0.5 \text{ keV}. \quad (3.126)$$

The energy level diagram for the four innermost shells (K, L, M, and N) of lead is plotted in Fig. 3.11. Also plotted are the transitions listed in Table 3.4. The arrows designating transitions point in the direction of electron transition, however, the transitions are labeled according to the IUPAC notation that follows the transition of the vacancy rather than the transition of an electron. Thus the transition designated with K-L designates a transition of an electron from the L to K shell while the electron vacancy makes a transition from the K to L shell.

(b) Table 3.4 provides energy differences between various atomic energy levels of lead, however, it does not provide the actual energy levels. For one-electron structures where energy levels are proportional to $1/n^2$ one can easily determine the actual energy levels from the knowledge of the transition energy and values of n for the two levels. On the other hand, in multi-electron atoms such as lead the situation is much more complicated because of nuclear charge screening by the complement of orbital electrons. Hartree proposed a simple, yet elegant, approximation to determine the atomic energy levels based on an effective charge that accounts for both the nuclear charge as well as its electron screening.

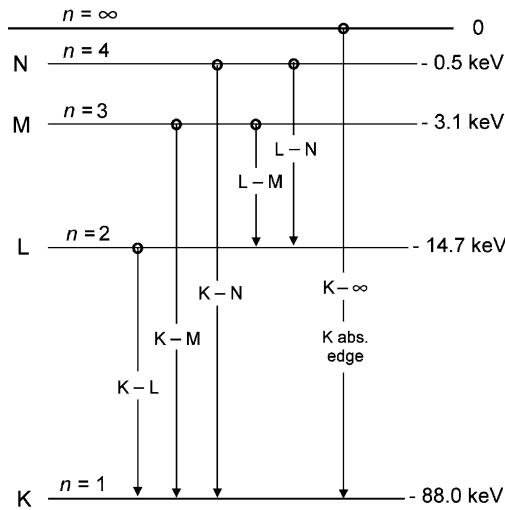


Fig. 3.11 The four innermost shells (K, L, M, and N) of lead atom and several examples of x-ray transitions

In Hartree approximation the atomic energy levels E_n of multi-electron atoms are expressed like in one-electron Bohr atom except that the atomic number Z of the Bohr atom is replaced by an effective atomic number $Z_{\text{eff}} = (Z - s_n)$, with s_n referred to as the screening constant for a given atomic shell n . The Hartree approximation works quite well for K shell ($n = 1$) energy levels of multi-electron atoms assuming a screening constant $s_K = s_{n=1} = 2$; for other shells the agreement is much poorer and the screening constants do not only depend on principal quantum number n but also on atomic number Z .

We now estimate the K shell energy level for lead using the Hartree approximation as

$$\begin{aligned}
 E(\text{K}) &= E_{n=1} = -E_{\text{R}} Z_{\text{eff}}^2 = -E_{\text{R}} (Z - s_{\text{K}}) \\
 &= -E_{\text{R}} (Z - 2)^2 = -(13.61 \text{ eV}) \times 80^2 = -87 \text{ keV}
 \end{aligned}
 \tag{3.127}$$

and note that the calculated value agrees reasonably well with the value of -88 keV obtained from the absorption edge photon and widely quoted in the literature as the energy level of the K shell in lead. Figure 3.12 shows a plot of K shell binding energy $E_{\text{B}}(\text{K})$ against atomic number Z for elements from $Z = 1$ to $Z = 100$. Solid curve represents measured data; dashed curve represents data calculated with Hartree approximation of (3.127) for $Z > 20$.

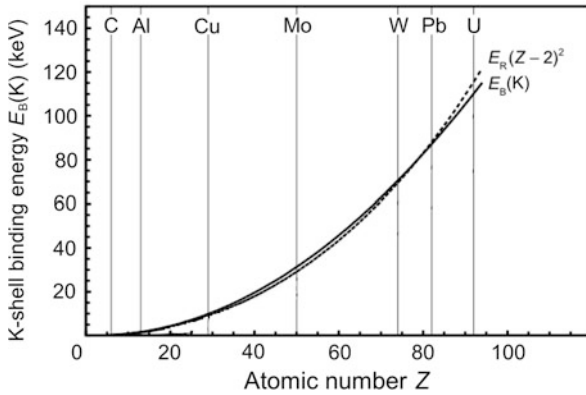


Fig. 3.12 K shell binding energy $E_B(K)$ against atomic number Z for elements from $Z = 1$ to $Z = 100$. *Solid curve* represents measured data; *dashed curve* represents data calculated with Hartree approximation of (3.126) for $Z > 20$

3.3 Experimental Confirmation of the Bohr Atomic Model

3.3.Q1

(100)

Hydrogen is the simplest atom in nature and its emission and absorption spectra are well understood. The spectrum of hydrogen is particularly important in astronomy because most of the Universe consists of hydrogen. Emission as well as absorption spectra of hydrogen are characterized with many series of lines each series ending (emission spectrum) or beginning (absorption spectrum) at the same atomic state.

On an atomic energy level diagram plot schematically the six known series of the emission spectrum of hydrogen and prepare a table that for each series lists the following parameters: final electron orbit n_f ; final energy E_f ; lowest photon energy; energy limit; and spectral range.

SOLUTION:

Correct prediction of line spectra emitted or absorbed by monoatomic gases, especially hydrogen, serves as an important confirmation of the Rutherford-Bohr atomic model. The following features of emission and absorption spectra of mono-atomic gases are notable:

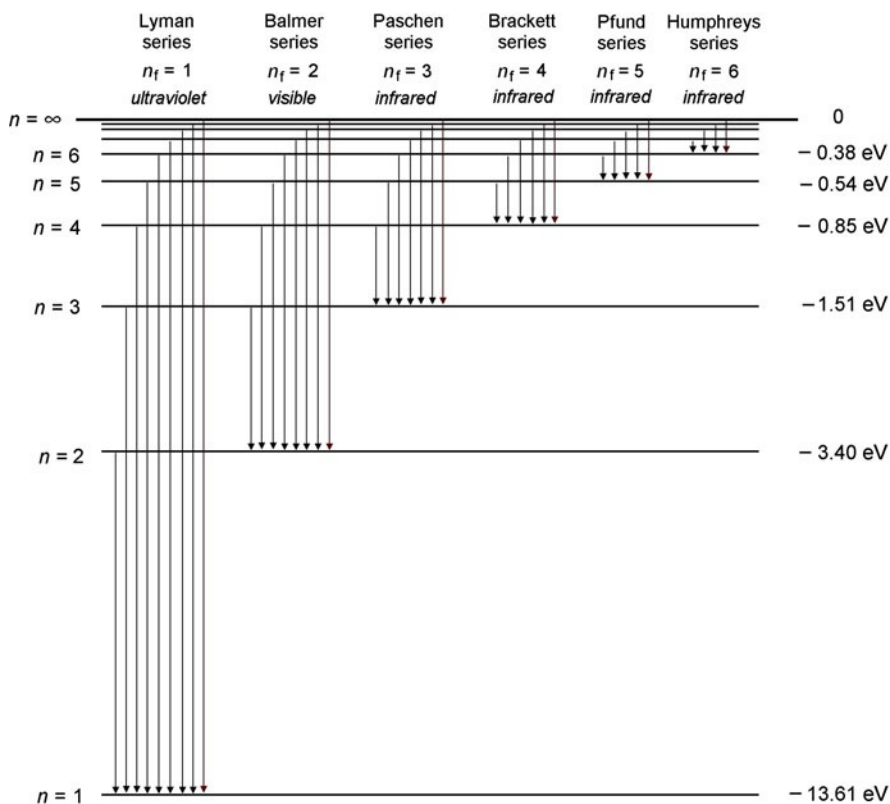


Fig. 3.13 Six known emission series spectra of hydrogen

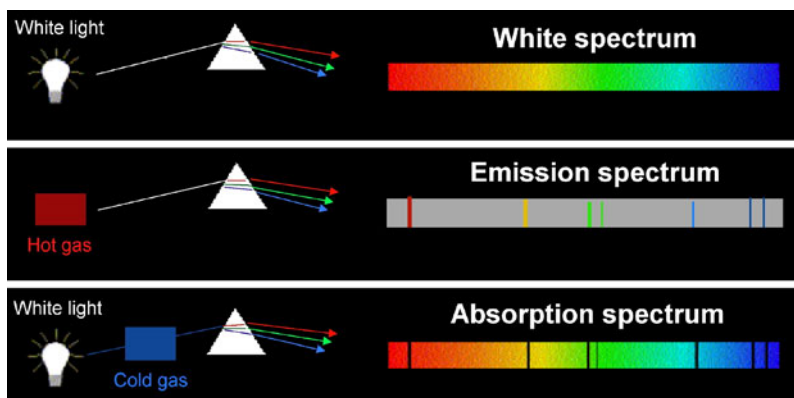
(1) The emission spectrum is measured by first collimating the emitted radiation by a slit and then passing the collimated slit-beam through an optical prism or diffraction grating. The prism or grating breaks the beam into its wavelength spectrum that is recorded on a photographic plate.

(2) In the measurement of absorption spectrum a continuous spectrum is made to pass through the gas under investigation. The photographic plate shows a set of unexposed lines that result from the absorption by the gas of distinct wavelengths of the continuous spectrum.

The six known emission series of hydrogen are: Lyman, Balmer, Paschen, Brackett, Pfund, and Humphreys. An atomic energy level diagram and its six emission series spectra are shown in Fig. 3.13 and the pertinent parameters of the six series are listed in Table 3.5. Figure 3.14 depicts the basic differences between a white spectrum, emission spectrum, and absorption spectrum.

Table 3.5 Basic parameters of the six spectral series of hydrogen

Name of series	Final orbit n_f	Final energy level E_f (eV)	Min. photon energy (eV)	Limit of series (eV)	Spectral range
Lyman	1	-13.61	10.21	13.61	ultraviolet
Balmer	2	-3.40	1.89	3.40	visible
Paschen	3	-1.51	0.66	1.51	infrared
Brackett	4	-0.85	0.31	0.85	infrared
Pfund	5	-0.54	0.16	0.54	infrared
Humphreys	6	-0.38	0.10	0.38	infrared

**Fig. 3.14** Basic differences between white spectrum, emission spectrum, and absorption spectrum

3.3.Q2

(101)

During 1913 Moseley carried out an important experiment the results of which lent irrefutable support for the nascent Rutherford-Bohr atomic model. Moseley studied the K_α and L_α characteristic x rays (K–L and K–M, respectively, in modern IUPAC notation) emitted by many then known elements between aluminum and gold in the Periodic Table of Elements and showed empirically that the frequency ν of an element's K_α and L_α radiation is proportional to the square of the element's atomic number Z , i.e.,

$$\nu = a(Z - s)^2 \quad \text{or} \quad \sqrt{\nu} = \sqrt{a}(Z - s), \quad (3.128)$$

where \sqrt{a} is the slope of the linear $\sqrt{\nu}$ versus Z plot and s is a screening constant. This relationship is now called the Moseley law and can be derived from first principles of physics in conjunction with Bohr atomic theory combined with Hartree theory of multi-electron atoms.

Table 3.6 Energy of K_α x-ray line for various elements with atomic number $13 \leq Z \leq 55$

(1)	Element	Unit	Al	Cr	Fe	Cu	Mo	Ag	Cs
(2)	Z		13	24	26	29	42	47	55
(3)	$h\nu_{K-L}$	(eV)	1485.5	5409.3	6397.5	8037.8	17426.9	22076.6	30800.0
(4)	$\sqrt{h\nu_{K-L}}$	($\sqrt{\text{eV}}$)	38.54	73.55	79.98	89.65	132.01	148.58	175.50

Table 3.6 gives atomic number z and photon energy $h\nu_{K-L}$ of the K_α , i.e., (K–L), characteristic line for various elements between aluminum ($Z = 13$) and cesium ($Z = 55$). K_α energy in row (3) of the table is the mean of energies of K_{α_1} (K–L₃) and K_{α_2} (K–L₂) characteristic x-ray lines for a given element in the table and available from the NIST.

- (a) Plot the data given in row (4) of Table 3.6 against atomic number Z given in row (2) for x-ray targets given in row (1) and establish that $\sqrt{\nu}$ is indeed proportional to Z .
- (b) From the Bohr theory of one-electron atom combined with the Hartree approximation for multi-electron atoms derive and plot the Moseley equation

$$\sqrt{h\nu_{K-L}} = k(Z - s_K), \quad (3.129)$$

where k is the slope of the equation equal to $k = 0.5\sqrt{3E_R}$ with E_R the Rydberg energy and $s_K = 1$ is the screening constant for the K shell containing one electron and one vacancy.

- (c) From the linear plot in (a) determine:
- (1) Slope k and screening constant s_K of (3.129).
 - (2) Rydberg energy E_R .
 - (3) Product $\hbar c$ of reduced Planck constant \hbar multiplied by the speed of light in vacuum c .

SOLUTION:

(a) In Fig. 3.15(A) we plot the square root of the K_α x-ray line energy $\sqrt{h\nu_{K-L}}$ against atomic number Z for the seven elements listed in Table 3.XY. A cursory examination of the data points shows that they fall on or close to a straight line, confirming the validity of Moseley law.

(b) Equation (3.128) is derived by considering the Bohr theory of one-electron structures in conjunction with the Hartree approximation proposed for use with multi-electron atoms. Hartree theory for multi-electron atoms provides the following general expression for atomic energy levels E_n (T3.36)

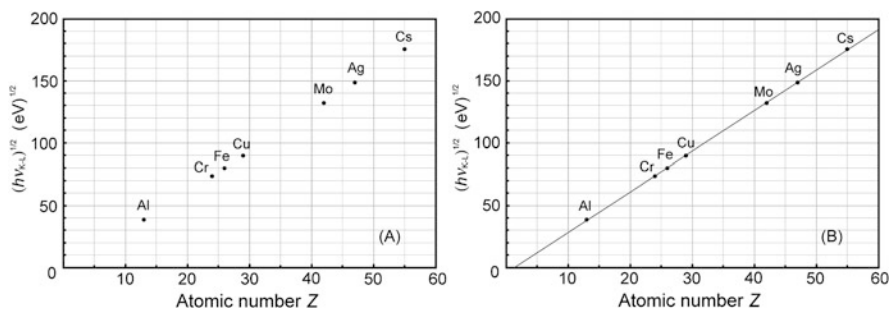


Fig. 3.15 Square root of K_{α} x-ray line energy against atomic number for 7 elements in Periodic Table of Elements between aluminum and cesium. (A) Plot of data summarized in Table 3.7 and obtained from the NIST. (B) Results of least square fit to the data set

$$E_n = -E_R \frac{Z_{\text{eff}}^2}{n^2}, \quad (3.130)$$

where

E_R is the Rydberg energy ($E_R = 13.61$ eV).

Z_{eff} is the effective atomic number that may be expressed as $Z - s$ with s defined as a screening constant.

n is the principal quantum number.

Photon energy $h\nu$ emitted following an electronic transition from initial level n_i to final level n_f is expressed as

$$h\nu = E_R Z_{\text{eff}}^2 \left(\frac{1}{n_f^2} - \frac{1}{n_i^2} \right). \quad (3.131)$$

Thus, energy $h\nu$ of a photon originating from a K–L (K_{α} in Siegbahn's notation) vacancy transition is given as

$$h\nu_{K-L} = E_R Z_{\text{eff}}^2 \left(\frac{1}{n_f^2} - \frac{1}{n_i^2} \right) = E_R (Z - s_K)^2 \left(1 - \frac{1}{4} \right) = \frac{3}{4} E_R (Z - s_K)^2 \quad (3.132)$$

$$\text{or } \sqrt{h\nu_{K-L}} = \frac{1}{2} \sqrt{3E_R} (Z - s_K) = k(Z - s_K),$$

where s_K is the K shell screening constant for one vacancy in the K shell. Hartree approximation predicts a value of $s_K = 2$ for the K shell screening constant of a neutral atom. For the K_{α} transition, however, the K shell screening constant is assumed to be $s_K = 1$ to account for the vacancy in the K shell that the electron feels when making the L shell to K shell transition.

(c) To determine the constants k and s_K we apply the method of least squares fit to data points of Fig. 3.15(A) and assume that we are dealing with a linear function of the following form: $y = kx + b$. Transformation of (3.122) into the form $y = kx + b$ results in

$$(1) \quad y = \sqrt{h\nu_{K-L}}; \quad (2) \quad x = Z; \quad \text{and} \quad (3) \quad b = ks_K. \quad (3.133)$$

The general solutions in the least squares theory for slope k and y intercept b are, respectively,

$$k = \frac{n \sum_{i=1}^n x_i y_i - \sum_{i=1}^n x_i \sum_{i=1}^n y_i}{n \sum_{i=1}^n x_i^2 - (\sum_{i=1}^n x_i)^2} \quad (3.134)$$

and

$$b = \frac{\sum_{i=1}^n x_i^2 \sum_{i=1}^n y_i - \sum_{i=1}^n x_i \sum_{i=1}^n x_i y_i}{n \sum_{i=1}^n x_i^2 - (\sum_{i=1}^n x_i)^2}, \quad (3.135)$$

where i is an index and n is the number of data points in a particular set of data. The following table shows the individual components of our data set: x_i , y_i ; x_i^2 , and $x_i y_i$ as well as their sums: $\sum_{i=1}^n x_i$, $\sum_{i=1}^n y_i$, $\sum_{i=1}^n x_i^2$, and $\sum_{i=1}^n x_i y_i$ for use in (3.134) and (3.135).

Table 3.7 Parameters x_i , y_i ; x_i^2 , and $x_i y_i$ used in least squares fit method to determine the slope k and y intercept for the linear relationship between $\sqrt{h\nu_{K-L}}$ and Z

i	x_i	y_i ($\sqrt{\text{eV}}$)	x_i^2	$x_i y_i$ ($\sqrt{\text{eV}}$)
1	13	38.56	169	501.217
2	24	73.55	576	1765.15
3	26	79.98	676	2079.59
4	29	89.65	841	2599.96
5	42	132.01	1764	5544.46
6	47	148.58	2209	6983.40
7	55	175.50	3025	9652.46
SUM	236	737.83 ($\sqrt{\text{eV}}$)	9260	29126.2 ($\sqrt{\text{eV}}$)

(1) From Table 3.7 in conjunction with (3.134) and (3.135) we get the following results for the slope k and the y axis intercept b of (3.132)

$$k = \frac{7 \times (29126.2 \sqrt{\text{eV}}) - 236 \times (737.83 \sqrt{\text{eV}})}{7 \times 9260 - (236)^2} = 3.26 \sqrt{\text{eV}} \quad (3.136)$$

and

$$b = \frac{9260 \times (737.83 \sqrt{\text{eV}}) - 236 \times (29126.2 \sqrt{\text{eV}})}{7 \times 9260 - (236)^2} = -4.54 \sqrt{\text{eV}}. \quad (3.137)$$

Thus, the slope of the linear equation $\sqrt{h\nu_{K-L}} = k(Z - s_K)$ is $k = 3.26 \sqrt{\text{eV}}$ and the screening constant is $s_K = b/k = 4.54/3.26 = 1.39$, in reasonable agreement with the generally accepted value for the screening constant of $s_K = 1$ in L to K electronic transitions producing the K_α characteristic x-ray lines. In Fig. 3.15(B)

we show the results of the least squares fit to the data set provided in Table 3.7 and parameters calculated in (3.136) and (3.137).

(2) Equation (3.132) suggests that the slope k of the linear $\sqrt{\nu}$ versus Z relationship is equal to $k = 0.5 \times \sqrt{3E_R}$ which means that in principle we should be able to determine the Rydberg energy E_R from this relationship. Rydberg energy is thus given as

$$E_R = \frac{k^2}{0.75} = \frac{3.26^2}{0.75} \text{ eV} = 14.2 \text{ eV} \quad (3.138)$$

in reasonably good agreement with the NIST value of $E_R = 13.61 \text{ eV}$.

(3) Bohr theory of one-electron atoms predicts the following expression for the Rydberg energy (T3.8)

$$E_R = \frac{1}{2} \left(\frac{e^2}{4\pi\epsilon_0} \right)^2 \frac{m_e c^2}{(\hbar c)^2}, \quad (3.139)$$

resulting in the following expression for $\hbar c$

$$\begin{aligned} \hbar c &= \frac{e^2}{4\pi\epsilon_0} \sqrt{\frac{m_e c^2}{2E_R}} = \frac{(1.6 \times 10^{-19} \text{ A} \cdot \text{s}) \times (\text{eV} \cdot \text{m})}{4\pi \times 8.85 \times 10^{-12} \text{ A} \cdot \text{s}} \sqrt{\frac{0.511 \times 10^6 \text{ eV}}{2 \times (14.2 \text{ eV})}} \\ &= 1.93 \times 10^{-7} \text{ eV} \cdot \text{m} = 1.93 \times 10^{-7} \times (10^{-6} \text{ MeV}) \times (10^{15} \text{ fm}) \\ &= 193 \text{ MeV} \cdot \text{fm} \end{aligned} \quad (3.140)$$

in reasonably good agreement with the NIST value stated as $\hbar c = 197.3 \text{ MeV} \cdot \text{fm}$.

3.3.Q3

(102)

Direct confirmation that the internal energy states of an atom are quantized came from an experiment carried out by James Franck and Gustav Hertz in 1914. The Franck-Hertz experiment provided experimental support for the Rutherford-Bohr model of the atom and for the quantization of atomic energy levels.

- Draw a schematic diagram of the Franck-Hertz experimental apparatus and explain its main characteristics.
- Figure 3.16(A) shows collector plate current I_{col} against accelerating voltage U for the Franck-Hertz experiment on mercury vapor and Fig. 3.16(B) shows a simple energy level diagram for outer shell electrons of mercury. Based on Fig. 3.16 explain the origin of the three

peaks in the I_{col} vs. U plot and provide answers to the following three questions:

- (1) Describe the ground state of mercury atom.
 - (2) Describe the first excited state of mercury atom.
 - (3) What is the ionization potential of mercury atom?
- (c) Assume that the Franck–Hertz apparatus is filled with low-pressure hydrogen gas rather than with mercury vapor. Sketch the I_{col} vs. U diagram for the first two peaks, explain their origin, and calculate the emitted spectral lines corresponding to the first two peaks in the I_{col} vs. U plot.

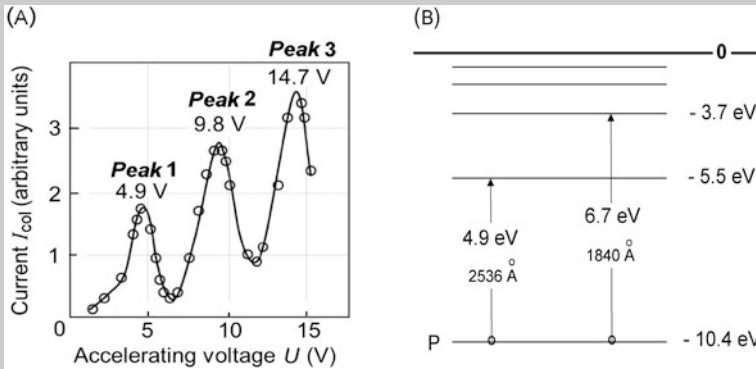


Fig. 3.16 (A) Typical collector plate current against accelerating voltage in mercury-filled Franck–Hertz apparatus. (B) Atomic energy level diagram for mercury. Only the outer P shell level of mercury in ground state is shown

SOLUTION:

(a) The Franck–Hertz apparatus is shown schematically in Fig. 3.17. An evacuated vessel containing three electrodes (cathode, anode, and collector plate) is filled with low-pressure mercury vapor. Electrons are emitted thermionically from the heated cathode and accelerated toward the perforated anode by positive potential U applied between the cathode and the anode. Some of the accelerated electrons pass through the perforated anode and land on the collector plate, provided their kinetic energy upon passing through the anode is sufficiently high to overcome a small retarding potential U_{ret} that is applied between the anode and the collector plate.

The experiment involves measuring the electron current I_{col} reaching the collector plate as a function of the accelerating voltage U . With an increasing potential U the current I_{col} at the plate increases with U until, at a potential of 4.9 V, it abruptly drops, indicating that some type of interaction between electrons and mercury atoms suddenly appears when the electrons attain kinetic energy of 4.9 eV. The interaction is interpreted as follows: an accelerated electron excites an outer shell mercury or-

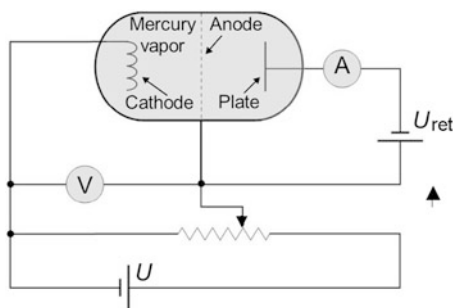


Fig. 3.17 Schematic diagram of the Franck-Hertz apparatus used in determination of excited states of gaseous atoms. V designates voltmeter, A designates ammeter

bitual electron from its ground state to its first excited state (4.9 eV) and in doing so loses 4.9 eV of its kinetic energy as well as its ability to overcome the retarding potential U_{ret} between the anode and the collector plate.

(b) The three peaks shown in the I_{col} vs. U plot of Fig. 3.16(A) have the following origins:

Peak 1: Accelerated electron exceeds kinetic energy E_K of 4.9 eV and excites an outer shell mercury electron from its ground state (energy level: -10.4 eV) to the first excited state with an energy level of -5.5 eV. Thus, the ionization potential of mercury is 10.4 eV; the first excitation potential is 4.9 eV.

Peak 2: Accelerated electron has sufficient kinetic energy ($E_K > 9.8$ eV) to produce excitation of two mercury atoms from the ground state to the first excited state.

Peak 3: Accelerated electron has sufficient kinetic energy ($E_K > 14.7$ eV) to produce excitation of three mercury atoms from the ground state to the first excited state.

Answers to the three specific questions in **(b)** are partially based on Fig. 3.16(B):

(1) Ground state of mercury (Hg) atom: atomic number Z of mercury is 80 and the electronic configuration of mercury is: K shell—2 electrons; L shell—8 electrons; M shell—18 electrons; N shell—32 electrons; O shell—18 electrons, and P (outer) shell—2 electrons.

In its ground state the mercury atom has both of its outer shell electrons in the P shell and the remaining 78 electrons are all in lower shells.

(2) The first excited state of Hg atom is when one of the two outer shell electrons is lifted from the P shell into the empty Q shell above the P shell. As shown in Fig. 3.16(B) the energy of the P shell is -10.4 eV while the energy of the Q shell is -5.5 eV. This means that the first excitation potential of Hg atom is $[-5.5 \text{ eV} - (-10.4 \text{ eV})] = 4.9 \text{ eV}$.

(3) As evident from Fig. 3.16(B), the minimum energy required for ionization of mercury atom, i.e., ionization potential of mercury atom, is 10.4 eV.

(c) Replacing mercury with hydrogen in the standard Franck-Hertz experiment is bound to result in a different structure of the I_{col} vs. U plot. To speculate on the two lowest voltage peaks in the I_{col} vs. U plot we present the simple energy level diagram of hydrogen in Fig. 3.18 with the ground state at -13.61 eV, first excited state at -3.40 eV, and second excited state at -1.51 eV. Thus, to move an electron from ground state of hydrogen to its first excited state requires energy of 10.21 eV and to its second excited state energy of 12.07 eV.

We would thus expect the first two peaks in a Franck-Hertz-type experiment with low-pressure hydrogen to occur at 10.21 V and 12.07 V. As far as emission of spectral lines as a consequence of the two peaks, we expect emission of a photon of energy $h\nu = 10.21$ eV corresponding to wavelength ($\lambda = 1213.6 \text{ \AA}$) correlated with the 10.21 V peak and emission of either one photon of energy $h\nu = 12.1$ eV ($\lambda = 1024 \text{ \AA}$) or two photons, one of energy $h\nu = 1.89$ eV ($\lambda = 6555.6 \text{ \AA}$) and the other of energy $h\nu = 10.21$ eV ($\lambda = 1213.6 \text{ \AA}$) correlated with the 12.07 V peak.

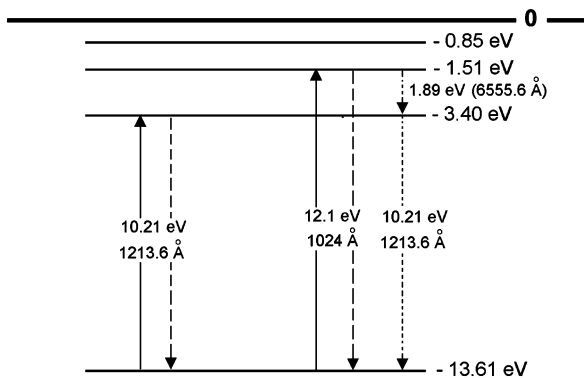


Fig. 3.18 Energy level diagram for hydrogen atom

3.4 Schrödinger Equation for Hydrogen Atom

3.4.Q1

(103)

Atomic radius can be estimated from atomic charge distributions measured with x-ray scattering experiments. When the so-measured results are compared with radii calculated with the hydrogen ground state wave function, one concludes that $\sqrt{\langle r^2 \rangle}$, the calculated square root of the expectation value

$\overline{r^2}$ (root-mean-square atomic radius), gives a better measure of the hydrogen atom size than does the Bohr radius.

- (a) Calculate $\sqrt{\overline{r^2}}$ for the hydrogen atom in the ground state.
 (b) Compare the result of (a) with the Bohr radius a_0 .

SOLUTION:

(a) The expectation value of $\overline{r^2}$ for the hydrogen atom in ground state is calculated from

$$\overline{r^2} = \iiint r^2 \psi^* \psi \, d\mathcal{V} = \iiint r^2 |R|^2 \, d\mathcal{V} = 4\pi \int r^4 |R|^2 \, dr, \quad (3.141)$$

where $R(r)$ is the spherically symmetric wave function given as (T3.71)

$$R(r) = \frac{1}{\sqrt{\pi a_0^3}} e^{-\frac{r}{a_0}} \quad (3.142)$$

and the volume element in spherical coordinates is given as $d\mathcal{V} = 4\pi r^2 \, dr$. Inserting (3.142) into (3.141) gives

$$\overline{r^2} = \frac{4}{a_0^3} \int_0^\infty r^4 e^{-\frac{2r}{a_0}} \, dr = \frac{4}{a_0^3} \left[\frac{4!}{(2/a_0)^5} \right] = \frac{4}{a_0^3} \times \frac{4 \times 3 \times 2 \times a_0^5}{32} = 3a_0^2. \quad (3.143)$$

(b) According to (3.143) the radius of hydrogen atom defined as $\sqrt{\overline{r^2}}$ amounts to

$$\sqrt{\overline{r^2}} = \sqrt{3a_0^2} = a_0 \sqrt{3} = (0.5292 \text{ \AA}) \sqrt{3} \approx 0.91 \text{ \AA}, \quad (3.144)$$

which is almost twice as large as the Bohr radius given as

$$a_0 = \frac{4\pi \varepsilon_0 (\hbar c)^2}{e^2 m_e c^2} = 0.5292 \text{ \AA} \quad (3.145)$$

in (T3.4).

Chapter 4 consists of **13 problems** that in 4 sections cover production of the two types of x rays: characteristic radiation and bremsstrahlung radiation in addition to two types of radiation remotely related to x rays: synchrotron radiation (also called magnetic bremsstrahlung) and Čerenkov radiation. Characteristic x rays and low energy bremsstrahlung produced in x-ray tubes are used extensively in diagnostic imaging while high energy x rays produced in linear accelerators provide the basis of modern radiotherapy.

Characteristic x rays are produced by electronic transitions in atoms triggered by vacancies in inner electronic shells of the absorber atom. Inner shell atomic vacancies are produced through one of 8 possible processes and migrate toward the outer atomic shell (valence shell) of the absorber atom through one or more steps. The energy released in an electronic transition from one electronic orbit to another is either emitted in the form of a characteristic photon or transferred to an orbital electron of the absorber atom by triggering release of this electron as an Auger electron. Bremsstrahlung x rays, on the other hand, are produced by an inelastic Coulomb interaction between light charged particle and the nucleus of the absorber atom. The spectrum of characteristic x-ray photons is discrete and characteristic of the absorber material; the spectrum of bremsstrahlung is continuous and contains photons with energy from 0 to the kinetic energy of the light charged particle that produced the photon.

The first few problems in this chapter (Sect. 4.1) address issues related to characteristic radiation, such as the Siegbahn and IUPAC notation for designation of electronic levels in an atom as well as rules governing production of characteristic x-ray line spectra. Problems in Sect. 4.2 deal with theoretical aspects of the production of bremsstrahlung radiation and the chapter concludes with several questions covering practical and theoretical aspects of and synchrotron radiation (Sect. 4.3) and Čerenkov radiation (Sect. 4.4).

4.1 X-Ray Line Spectra

4.1.Q1

(104)

An atom with an electronic vacancy in its inner shell is in a highly excited state and returns to its ground state through one or several electronic transitions. In each of these transitions an electron from a higher atomic shell fills the shell vacancy and the energy difference in binding energy between the initial and final shell or sub-shell is emitted from the atom in one of two ways: either (1) in the form of characteristic (fluorescence) radiation or (2) radiation-less in the form of Auger electrons, Coster–Kronig electrons, or super Coster–Kronig electrons.

-
- (a) Define an atomic shell vacancy, list the two types of shell vacancy, and briefly describe the ultimate fate of a shell vacancy.
 - (b) List at least 8 processes resulting in production of a primary atomic shell vacancy and briefly describe each process.
 - (c) Define the fluorescence yield ω and sketch a plot of ω against atomic number Z of the absorber for the K, L, and M electronic shells.

SOLUTION:

(a) A shell vacancy is defined as an electron missing from the normal complement of electrons in a given atomic shell. Two types of vacancy are known: (1) primary and (2) secondary.

(1) **Primary shell vacancy** occurs when an atomic electron is displaced from the atomic cloud through one of 8 known processes that fall into 5 categories: incident photon–atom interactions; nuclear effects; incident charged particle–atom Coulomb interactions, Auger effect, and positron annihilation. Primary vacancy can occur in any one of the electronic shells of an atom, making a positive ion (anion) out of the neutral atom.

(2) **Secondary shell vacancy** occurs when an electron makes a transition from a higher-level electronic shell to a lower-level electronic shell in an atom, meaning that the vacancy moves in the opposite direction. The transition energy is emitted in the form of characteristic (fluorescence) radiation or is transferred to an electron in a higher-level shell that is ejected as Auger electron leaving behind a primary vacancy.

Note: When a primary vacancy is created, the shell electron leaves the electronic cloud and the atom loses an electron through creation of a vacancy and thus undergoes the process of ionization. When a secondary vacancy occurs, an existing vacancy merely moves from a lower-level shell to a higher-level shell of the same

atom and no new vacancy is produced in the atom; however, the transition energy is emitted as a characteristic photon or is transferred to an Auger electron. All primary vacancies produced in an atom migrate to the outer shell of the positive ion either directly or through creation of intermediate secondary vacancies. Free electrons from the ion's environment will fill the ion's outer shell vacancies and the ion will revert to its original neutral state.

(b) Eight processes that result in production of a primary shell vacancy are as follows:

(1) **Photoelectric effect.** A photon-atom interaction whereby the photon is completely absorbed by the atom and its energy is given to an orbital shell electron. The orbital electron is ejected from the atom as a photoelectron leaving behind a shell vacancy.

(2) **Compton scattering.** A photon-orbital electron interaction whereby the photon is scattered with a lower energy by a loosely bound orbital electron and energy difference between the incident and scattered photon is absorbed by an orbital electron. The orbital electron is consequently ejected from the atom as a Compton (recoil) electron leaving behind a shell vacancy.

(3) **Triplet production.** A photon-orbital electron interaction whereby the photon interacts with the Coulomb field of an orbital electron of the absorber atom. The photon disappears and an electron-positron pair is created (materialization). To conserve momentum, the orbital electron absorbs part of the incident photon energy and is consequently ejected from the atom leaving behind a shell vacancy.

(4) **Charged particle Coulomb interaction** with atom. A charged particle as it traverses absorbing medium interacts through Coulomb force with orbital electrons and nuclei of atoms in the absorber. The orbital electrons absorb part of the charged particle energy and are either ejected from the atom or excited to higher energy levels leaving behind shell vacancies in the absorber atoms.

(5) **Internal conversion.** A nuclear decay process whereby the energy of an excited nucleus is given to an orbital electron. As a result the orbital electron is ejected from the absorber atom leaving behind a shell vacancy.

(6) **Electron capture.** A nuclear decay process whereby an excited nucleus captures an orbital electron from one of the inner shells of the atom. The captured electron leaves behind a shell vacancy and in the nucleus a proton is converted into a neutron.

(7) **Positron annihilation.** A positron traversing absorbing medium annihilates with an orbital electron in a process that creates several (most often two) annihilation quanta and an electronic vacancy in the absorber atom. Most frequently, the annihilation occurs after the positron lost all of its kinetic energy through Coulomb interactions with absorber atoms; however, more rarely annihilation can also occur

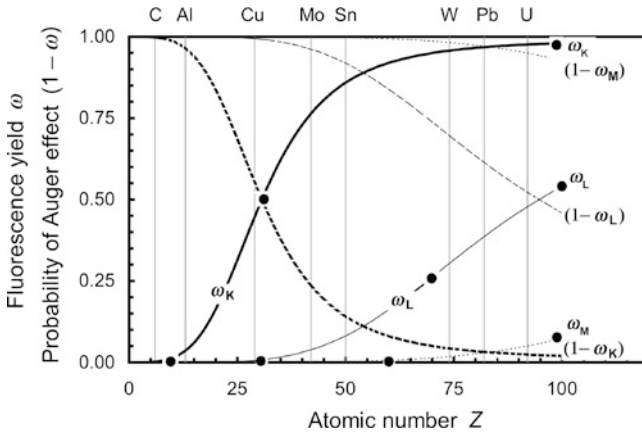


Fig. 4.1 Fluorescence yields ω_K , ω_L , and ω_M against atomic number Z . Also shown are probabilities for Auger effect $1 - \omega_K$, $1 - \omega_L$, and $1 - \omega_M$. Data are from Hubbell

when the positron still carries kinetic energy and the annihilation process is then called annihilation-in-flight.

(8) **Auger effect.** A process by which an atom with a vacancy in one of its orbital shells, except for the outer shell, relaxes. As an orbital electron makes a transition from a higher-level shell to fill the vacancy, the transition energy is emitted either in the form of characteristic (fluorescence) photon or is transferred to a higher-level shell electron that is emitted as an Auger electron leaving behind a primary shell vacancy.

The first three processes: photoelectric effect, Coulomb scattering, and triplet production (electronic pair production) fall into the category of photon interaction with absorber atom. The fourth process includes charged particle Coulomb interaction with orbital electrons of absorber atoms, while Internal conversion and electron capture fall into the category of nuclear effects.

(c) **Fluorescence yield** of a given shell (K, L, or M) is defined as the number of fluorescence (characteristic) photons emitted per vacancy in the shell. It can also be regarded as the probability, after creation of an electronic shell vacancy, of fluorescence photon emission as opposed to Auger electron emission.

Fluorescence yields ω_K , ω_L , and ω_M for K, L, and M electronic shell vacancies, respectively, are plotted in Fig. 4.1 against atomic number Z for all elements with $1 \leq Z \leq 100$. The anchor points for ω versus Z plot are clearly indicated in Fig. 4.1. The anchor points are:

For ω_K : $[Z \leq 10, \omega_K = 0]$; $[Z = 30, \omega_K = 0.50]$; $[Z \geq 90, \omega_K \approx 0.96]$
 For ω_L : $[Z \leq 30, \omega_L = 0]$; $[Z = 70, \omega_L = 0.25]$; $[Z = 100, \omega_L \approx 0.5]$
 For ω_M : $[Z < 70, \omega_M = 0]$; $[Z = 100, \omega_M \approx 0.05]$

The following features of fluorescence yield ω are noteworthy:

- (1) A plot of the fluorescence yield ω_K against absorber atomic number Z results in a sigmoid shaped curve with ω_K ranging from $\omega_K = 0$ for low atomic number ($Z < 10$) elements through $\omega_K = 0.5$ at $Z = 30$ to $\omega_K = 0.96$ at very high Z .
- (2) For the L-shell vacancy the fluorescence yield ω_L is zero at $Z < 30$ and then rises with Z to reach a value $\omega_L = 0.5$ at $Z = 100$.
- (3) Fluorescence yield ω_M is zero for all elements with $Z < 60$, and for $Z > 60$ it rises slowly with increasing Z to attain a value $\omega_M \approx 0.05$ for very high Z absorbers, indicating that fluorescence emission from the M shell and higher level electronic shells is essentially negligible for all absorbers, even those with very high atomic number Z .
- (4) For a given electronic shell a plot of $1 - \omega$ against atomic number Z shows the probability for Auger effect following creation of a vacancy in an electronic shell with the exception of the outer shell of the absorber atom.
- (5) For a given absorber, the higher is the shell level (i.e., the lower is the shell binding energy), the lower is the fluorescence yield ω and, consequently, the higher is the probability for Auger effect ($1 - \omega$).

4.1.Q2**(105)**

Atomic energy level diagram for tungsten ($Z = 74$) in ground state is shown in Fig. 4.1. Energy levels are identified using the spectroscopic notation (e.g., $1s_{1/2}$, $2s_{1/2}$, ... etc.) as well as the IUPAC x-ray notation (e.g., K, L_1 , L_2 , ... etc.).

- (a) For each energy level of tungsten provide in Fig. 4.2 the quantum numbers n , l , j , and m_j of electrons occupying the energy level.
- (b) For each energy level of tungsten provide in Fig. 4.2 the number of electrons residing in the level.
- (c) Complete Table 4.1 that deals with information pertinent to the shell and subshell structure of tungsten.
- (d) Based on information in Fig. 4.2 and Table 4.1 summarize the electronic configuration of the tungsten atom in the ground state according to the convention used in atomic physics.
- (e) Transition L_1-O_3 (referring to transition of vacancy rather than the actual transition of an electron) is indicated on the energy level diagram of Fig. 4.2. Is this an allowed or forbidden transition?
- (f) Assume that there is an electronic vacancy in the L_2 subshell. Following the standard selection rules for dipolar transitions and using the IUPAC notation, show on Fig. 4.2 and list separately all allowed electronic transitions to the L_2 subshell.

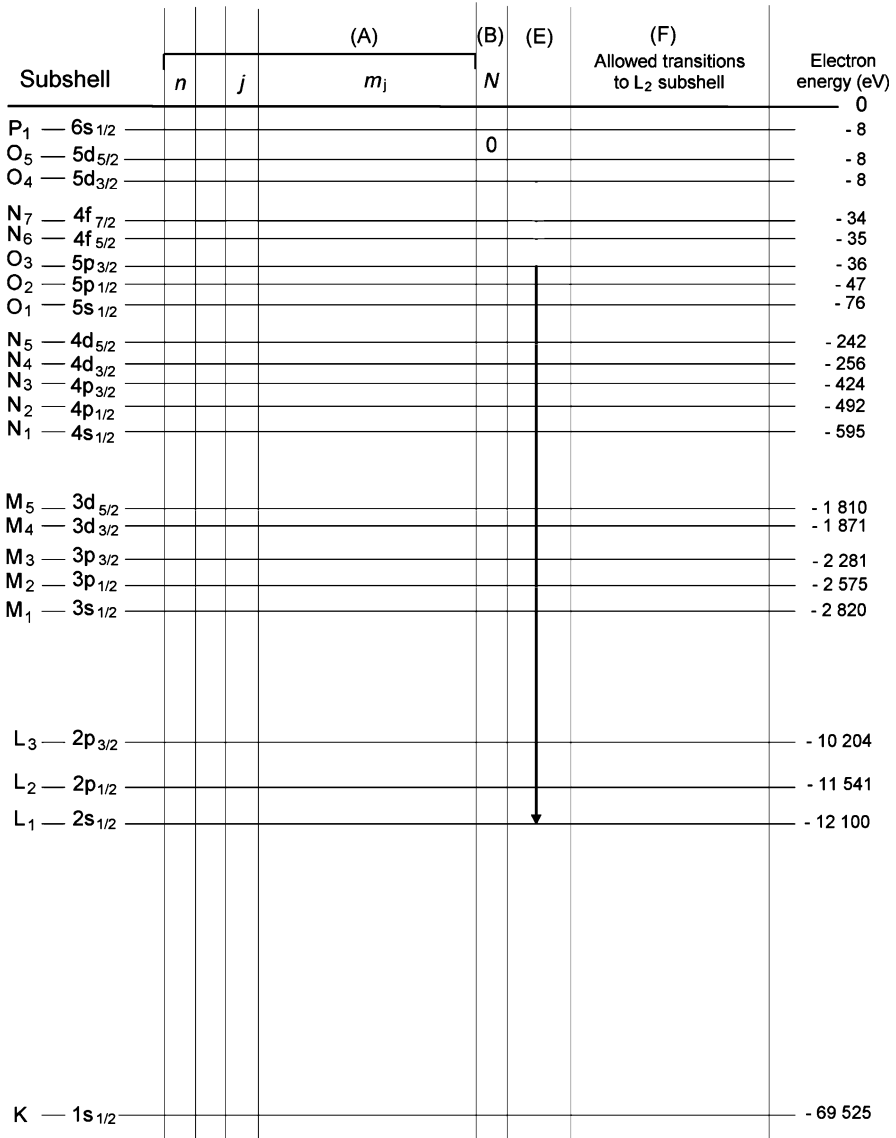


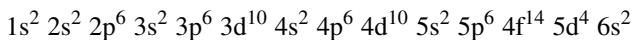
Fig. 4.2 Atomic energy level diagram of tungsten ($Z = 74$) including energy levels of the K shell and all subshells. *First column* shows the designation of subshells in the IUPAC notation and the *last column* shows the energy levels of the subshells in electron volts (eV)

Table 4.1 Main characteristics of the shell and subshell structure of tungsten

Principal quantum number n	Electronic shell	Shell population	Electronic subshell	Orbital quantum number	Subshell population
	K		1s		
	L		2s		
		–	2p		
	M		3s		
		–	3p		
		–	3d		
	N		4s		
		–	4p		
		–	4d		
		–	4f		
	O		5s		
		–	5p		
		–	5d		
	P		6s		

SOLUTION:

- (a) Quantum numbers n , ℓ , j , and m_j for each energy level of tungsten are provided in Fig. 4.3.
- (b) Number of electrons residing in each energy level is provided in Fig. 4.3 [column (B)].
- (c) Information pertinent to shell and subshell structure of tungsten is provided in Table 4.2.
- (d) Electronic configuration of tungsten in atomic ground state is given as:



- (e) The transition L_1-O_3 involves the vacancy transition from subshell L_1 to subshell O_3 , corresponding to the actual electron transition in the opposite direction from O_3 to L_1 . The question on whether this is an allowed or forbidden transition will be answered by checking the applicable selection rules $\Delta\ell = \pm 1$ and $\Delta j = 0, \pm 1$. Since in this transition $\Delta\ell = +1$ and $\Delta j = +1$, we conclude that this is an allowed transition.
- (f) All allowed transitions to the L_2 subshell are shown in Fig. 4.3 [column (F)] and listed separately in Table 4.3 that also shows $\Delta\ell$ and Δj for each allowed transition.

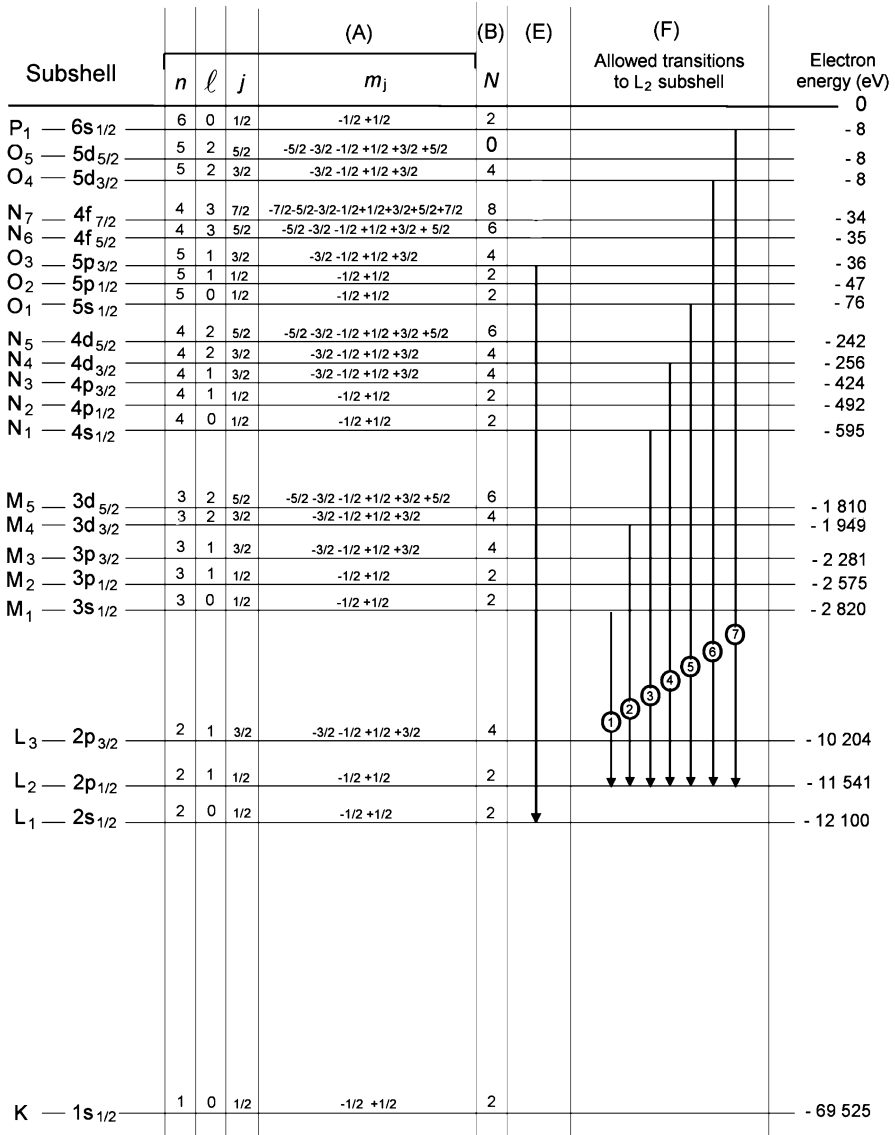


Fig. 4.3 Atomic energy level diagram of tungsten including shell and subshell structure following the IUPAC convention (*first column*); quantum numbers for individual subshells in column (A); number of electrons *N* in each subshell in column (B); transition L₁–O₃ (vacancy) in column (E); all allowed transitions (vacancy) from L₂ subshell in column (F); and energy level in electron volts for each subshell (*right hand column*)

Table 4.2 Main characteristics of shell and subshell structure of tungsten

Principal quantum number n	Electronic shell	Shell population	Electronic subshell	Orbital quantum number	Subshell population
1	K	2	1s	1	2
2	L	8	2s	1	2
			2p	2	6
3	M	18	3s	1	2
			3p	2	6
			3d	3	10
4	N	32	4s	1	2
			4p	2	6
			4d	3	10
			4f	4	14
5	O	12	5s	1	2
			5p	2	6
			5d	3	4
6	P	2	6s	1	2

Table 4.3 Allowed transitions to fill a vacancy in the L_2 subshell of tungsten atom

N	Transition	$\Delta\ell$	Δj
1	L_2-M_1	-1	0
2	L_2-M_4	+1	1
3	L_2-N_1	-1	0
4	L_2-N_4	+1	1
5	L_2-O_1	-1	0
6	L_2-O_4	+1	1
7	L_2-O_1	-1	0

4.1.Q3**(106)**

Atomic energy level diagram for tungsten is shown in Fig. 4.4. Assume that an electron from the M_2 subshell fills an electronic vacancy that was created in the K shell. As shown schematically on the graph, there are two possible options (A and B) available to the excited atom for release of energy made available during the M_2-K electronic transition.

- (a) List and briefly define at least six processes by which the K shell vacancy in the tungsten atom might have been produced.

- (b) Briefly describe options A and B for the release of the transition energy $E(M_2-K)$.
- (c) Discuss the branching ratio between options A and B.
- (d) Explain the fate of the M_2 vacancy that was produced in the initial M_2-K electronic transition.

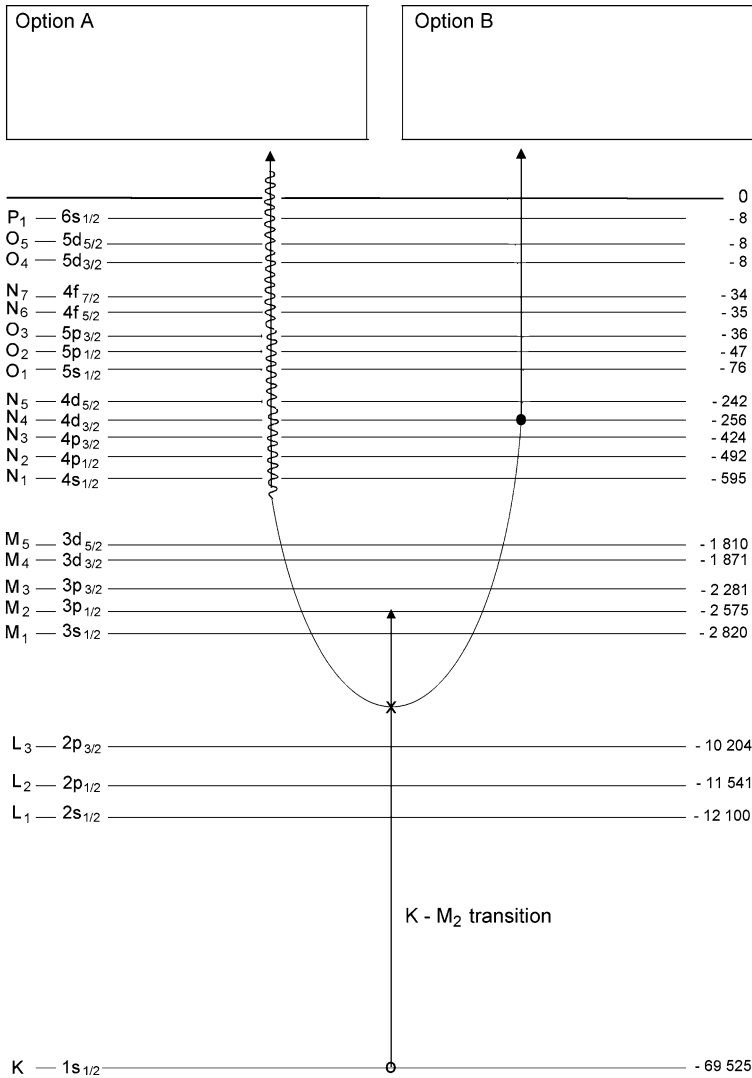


Fig. 4.4 Atomic energy level diagram of tungsten with a vacancy in the K shell that is filled by an electron from the M_2 subshell (transition $K-M_2$ describes the transition of the vacancy)

SOLUTION:

(a) The electronic vacancy in the K shell of tungsten could have been produced through an assortment of different effects that can be placed into three major categories of interactions (see Prob. 104) with the K shell orbital electron: *Coulomb inelastic collision* of light charged particle (electron or positron) or heavy charged particle (proton, deuteron, alpha, etc.); photon interactions (*photoelectric effect*, *Compton effect*, and *electronic pair production*) and nuclear effects (*internal conversion* or *K capture*).

(b) As shown schematically in Fig. 4.5, there are two options (A and B) available for dissipation of the K–M₂ transition energy $\Delta E = E(M_2) - E(K) = 66.95$ keV.

(1) In *option A* the transition energy is emitted in the form of a characteristic (fluorescence) photon that (i) is referred to as a K–M₂ photon because it originated from a vacancy transition from the K shell to the M₂ subshell and (ii) is referred to as characteristic photon because its energy of 66.95 keV is characteristic of the tungsten atom.

(2) In *option B* the transition energy $\Delta E = E(M_2) - E(K) = 66.95$ keV is transferred to an orbital electron from L shell or higher and the electron, referred to as an Auger electron, is ejected from the tungsten atom. In our example given in Fig. 4.5 the transition energy is transferred to a N₄ subshell orbital electron that is ejected from the nucleus as an e_{KM₂N₄} Auger electron with kinetic energy $E_K = \Delta E - E_B(N_4) = E(M_2) - E(K) - E_B(N_4) = 66.69$ keV through a process called the Auger effect.

(c) The branching between the two options (emission of a characteristic photon or ejection of an Auger electron) is governed by the fluorescence yield ω for the given atom and for the given atomic shell of the atom. The fluorescence yield for a given shell is defined as the number of fluorescence photons emitted per vacancy in the given shell. Alternatively, fluorescence yield can also be regarded as the probability, after the creation of a shell vacancy, of fluorescence emission as opposed to emission of Auger electron.

The fluorescence yield ω is plotted with solid curves for K, L, and M shell electron vacancies in Fig. 4.6 against atomic number for all elements. Also plotted (with dashed lines) is the probability for Auger effect ($1 - \omega$) against atomic number for all elements. As shown in Fig. 4.6, the fluorescence yield for the K shell vacancy in tungsten is $\omega_K = 0.95$, while the probability for Auger effect following a K shell vacancy in tungsten is $1 - \omega_K = 0.05$.

<p>Option A Emission of characteristic photon K-M₂ <i>Energy of emitted photon $h\nu(K-M_2)$</i></p> $h\nu(K-M_2) = E(M_2) - E(K)$ $= -2.575 \text{ keV} + 69.525 \text{ keV}$ $= 66.95 \text{ keV}$	<p>Option B Emission of Auger electron <i>Energy of ejected Auger electron $E_K(e_{KM_2N_4})$</i></p> $E_K(e_{KM_2N_4}) = E(M_2) - E(K) - E(N_4)$ $= -2.575 \text{ keV} + 69.525 \text{ keV} - 0.256 \text{ keV}$ $= 66.69 \text{ keV}$
---	---

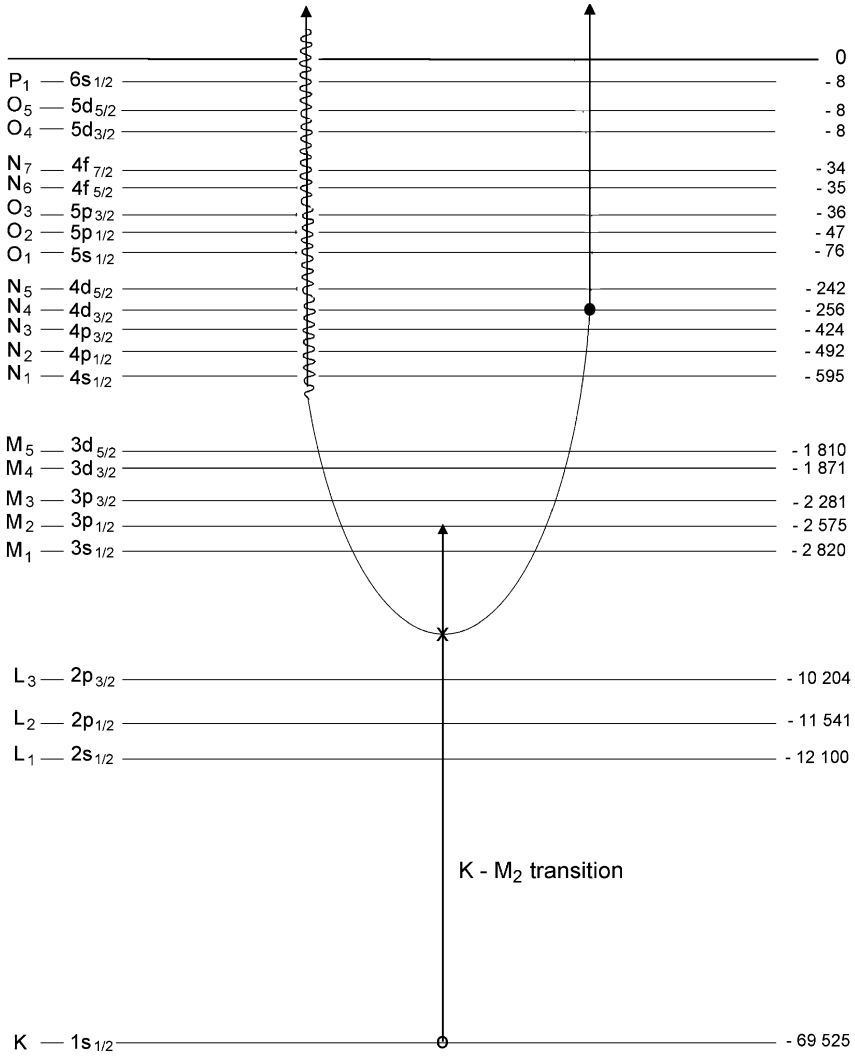


Fig. 4.5 Atomic energy level diagram of tungsten with an electronic vacancy in the K shell that is filled by an electron from the M₂ subshell. The two options: A as emission of characteristic (also called fluorescence) photon and B as emission of an Auger electron are described

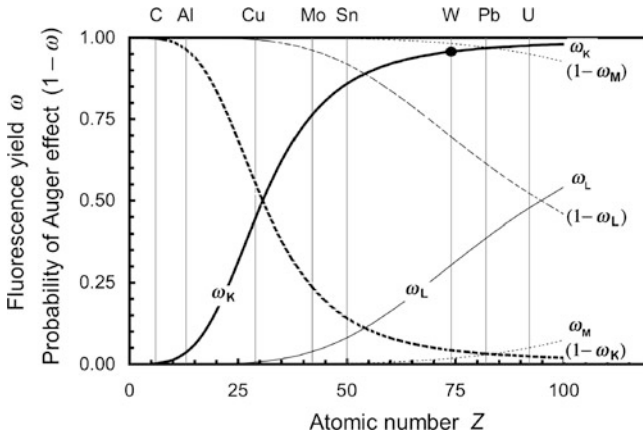


Fig. 4.6 Fluorescence yield (*solid curves*) and probability of Auger effect against atomic number for elements between $Z = 1$ to $Z = 100$

4.1.Q4

(107)

Figure 4.7 shows the atomic energy level diagram of tungsten atom consisting of the K shell and all subshells in addition to showing the electron population of each subshell.

- (a) Assume that there is a vacancy in the K shell and show three different possible paths of migration of the vacancy to the outer subshell P_1 . Each of the three paths should consist of at least 5 allowed transitions (steps). Identify each step in the IUPAC notation.
- (b) Assume that there is a vacancy in the N_2 subshell. The vacancy will be filled by an electron from a higher-level subshell and the transition will be accompanied either by emission of a characteristic photon or an Auger electron, Coster-Kronig electron or super Coster-Kronig electron. Show three possible electronic transitions to the N_2 subshell: one that could result in a standard Auger electron, one that could engender a Coster-Kronig electron, and one that could result in a super Coster-Kronig electron. For each of these electrons provide appropriate label in IUPAC notation and their kinetic energy.

SOLUTION:

Figure 4.8 deals with migration of two electronic vacancies (one in the K shell and the other in the N_2 subshell) toward the outer subshell (P_1) in a tungsten atom.

Figure 4.8(A) shows three examples of possible paths for the K shell vacancy migration toward the P_1 subshell (also referred to as the outer shell or valence shell of

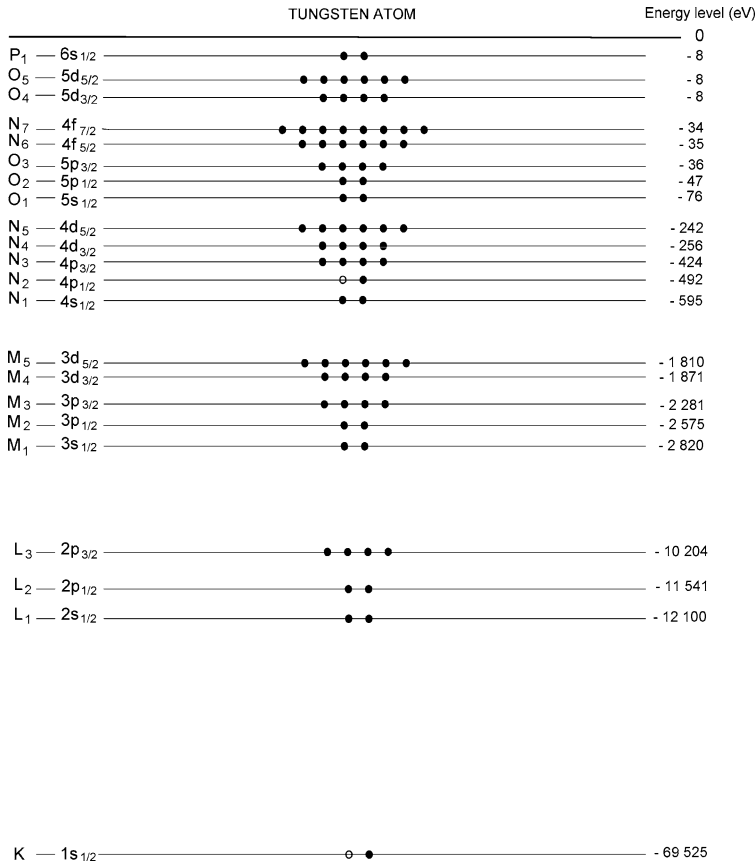


Fig. 4.7 Energy level diagram for tungsten atom ($Z = 74$). Electron vacancies in the K shell and the N₂ subshell are shown with *hollow circles*, the electrons in the K shell and all subshells are shown with *solid circle*

tungsten atom), each path progressing through 6 electronic transitions (steps). Each step is identified in the IUPAC notation and fulfills the dipolar selection rules on the angular momentum quantum number ($\Delta\ell = \pm 1$) as well as on the total angular momentum quantum number ($\Delta j = 0, \pm 1$). The K–L₂ and K–L₃ transitions were labeled K_{α_1} and K_{α_2} , respectively, in the classical Siegbahn notation.

Figure 4.8(B) shows the start of three possible pathways of the vacancy migration from the N₂ subshell toward the P₁ subshell. Each of these steps is followed by energy transfer to an orbital electron through three different types of Auger effect: standard Auger effect, Coster-Kronig effect, and super Coster-Kronig effect. The distinction among the three different effects is as follows:

- (i) In the standard Auger effect the primary transition occurs between two shells and the transition energy is transferred to an orbital electron from the initial shell or an even higher-level shell. The ejected electron is called an Auger electron.

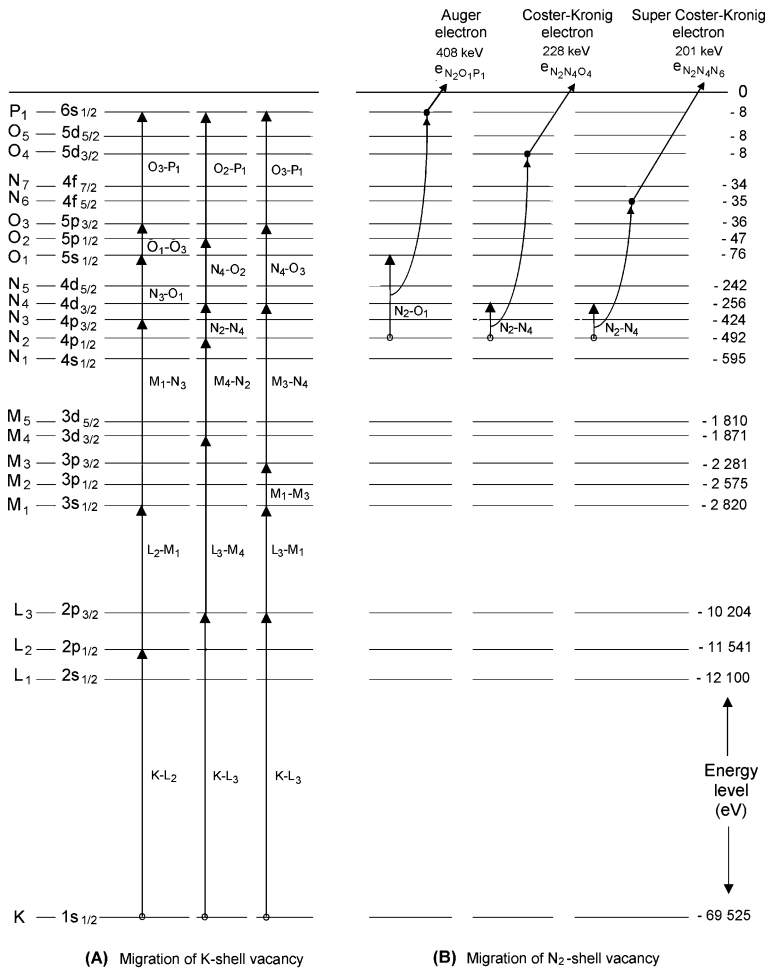


Fig. 4.8 Energy level diagram of tungsten atom. (A) shows three of many possible pathways that a vacancy in the K shell of tungsten can take in its migration to the outer subshell P₁. Each pathway contains 6 steps and each step is identified in the IUPAC notation. (B) deals with a vacancy in the N₂ subshell and shows three possible transitions, one resulting in ejection of an Auger electron through standard Auger effect, one resulting in ejection of a Coster-Kronig electron through Coster-Kronig effect, and one resulting in super Coster-Kronig electron through super Coster-Kronig effect

- (ii) In Coster-Kronig effect the transition energy originates from two subshells of a given shell and is transferred to an electron in another (higher-level) shell. The emitted electron is called a Coster-Kronig electron.
- (iii) In super Coster-Kronig effect the transition energy that, like in (ii), originates from two subshells of a given shell is transferred to a subshell electron within the shell in which the primary transition occurred. The emitted electron is called super Coster-Kronig electron.

4.1.Q5

(108)

Figure 4.9 displays an atomic energy level diagram of tungsten. An incident photon of energy $h\nu = 150 \text{ keV}$ interacts with a K-shell electron. In the interaction the photon disappears, the K-shell electron is ejected as a photoelectron and the vacancy, created in the K shell, migrates through many steps toward the P_1 subshell. Each step in the vacancy migration to the P_1 subshell and the subsequent return of the atom to ground state and to neutral state by attracting an electron from environment into the P_1 state is identified on the diagram with a box containing three labels: (A) Identification of the particle (photon or electron) produced or released or of energy transfer process; (B) Identification of the transition in the IUPAC notation; and (C) Specification of particle energy or transition energy in electron volts (eV).

- (a) Provide answers for each step in the vacancy migration.
- (b) Provide a summary for energy released in the form of photons and electrons.

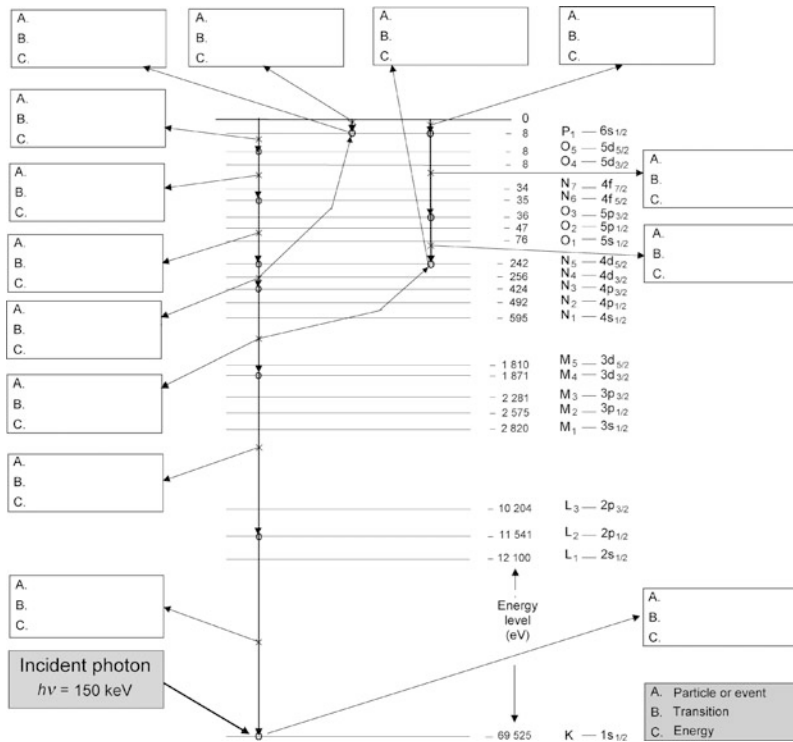


Fig. 4.9 Atomic energy level diagram of tungsten and an example of K-shell vacancy migration toward the outer shell and eventual neutralization of the atom

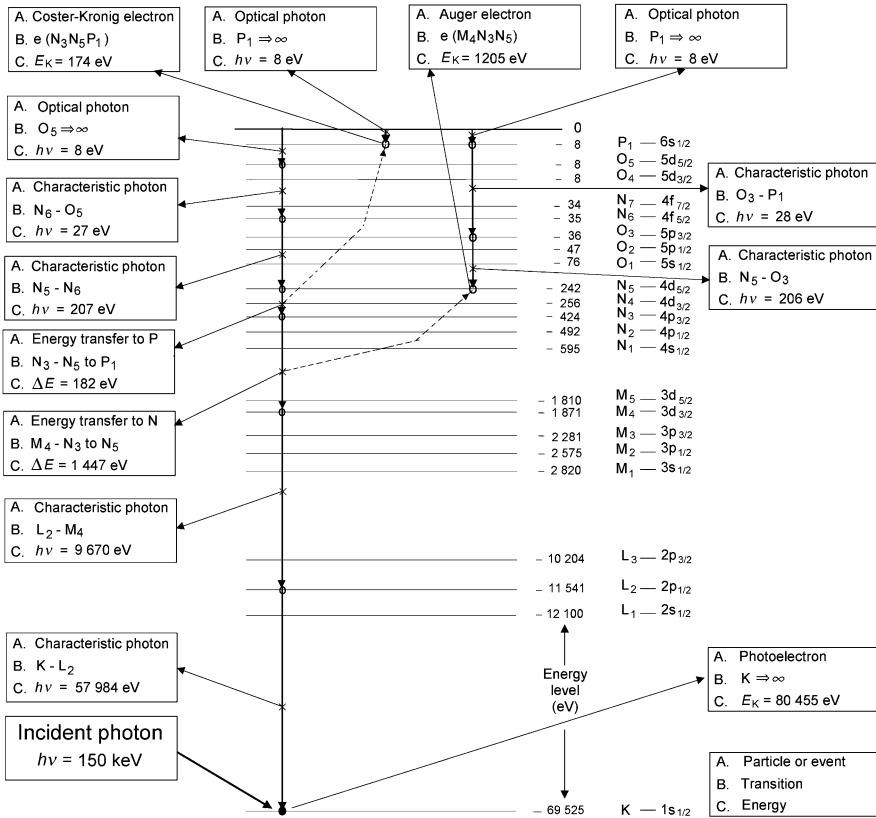


Fig. 4.10 Example of K-shell vacancy migration toward the outer shell of tungsten atom. The 6 transitions producing characteristic radiation and two transitions producing Auger electrons are clearly identified and their IUPAC notation as well as energy are also given. The tungsten atom was assumed to have been neutral before the incident photon interaction and the 3 optical photon transitions in the diagram represent the process of the tungsten ion acquiring 3 free electrons to become neutral again

SOLUTION:

(a) Each step in the vacancy migration to the outer shell of tungsten involves either production of a characteristic (fluorescence) photon or an Auger electron. Figure 4.10 provides answers (A), (B), and (C) for each individual step.

(b) Summary for the example of vacancy migration from K shell to P₁ subshell is given in Table 4.4. The migration in this example consists of 4 transitions producing a characteristic photon and 2 transitions producing an Auger electron. The 8 eV optical transitions result from neutralization of tungsten ion through attracting stationary electrons from the environment.

Table 4.4 Summary of an example of K-shell vacancy migration to P1 subshell in tungsten

	Transition		Energy (eV)
1	K-L ₂	Characteristic photon	57 984
2	L ₂ -M ₄	Characteristic photon	9 670
3	M ₄ -N ₃	Energy transfer to N5	1 447
4	N ₃ -N ₅	Energy transfer to P1	182
5	N ₅ -N ₆	Characteristic photon	207
6	N ₆ -O ₅	Characteristic photon	27
7	O ₅ -∞	Optical photon	8
		Total energy	69 525

Total energy released: 69 525 eV equals the binding energy of the K-shell electron.

Of the 69 525 eV energy that was released, 67 896 eV was released in the form of characteristic (fluorescence) photons and 1629 eV was transferred to other shells for release of Auger electrons.

Of the 1629 eV that was transferred to other shells, 1379 eV was released as kinetic energy of Auger electrons and 250 eV was released in the form of photons.

Summary of energy emission:

Photons: $67\,896\text{ eV} + 250\text{ eV} = 68\,146\text{ eV}$

Kinetic energy of Auger electrons: 1379 eV

Total energy: $68\,146\text{ eV} + 1379\text{ eV} = 69\,525\text{ eV}$

4.2 Emission of Radiation by Accelerated Charged Particle (Bremsstrahlung Production)

4.2.Q1

(109)

The intrinsic electromagnetic field of a charged particle moving with velocity v is affected by the magnitude of v and undergoes a Lorentz contraction in the direction of motion and expands in directions perpendicular to the direction of motion.

The electric field $\mathcal{E}_v(r, \theta, v)$ is given as

$$\mathcal{E}_v(r, \theta, v) = \mathcal{E}_0 C_v = \frac{q}{4\pi\epsilon_0 r^2} C_v, \quad (4.1)$$

where

\mathcal{E}_0 is the isotropic electric field produced by charged particle q for $v = 0$ and is expressed through the Coulomb law $\mathcal{E} = q/(4\pi\epsilon_0 r^2)$.

r is the distance from the charged particle q to the point of interest.

C_v is the electric field correction factor given as

$$C_v = \frac{1 - \beta^2}{(1 - \beta^2 \sin^2 \theta)^{3/2}}. \quad (4.2)$$

Define the field difference $[\mathcal{E}_v(r, \theta, v) - \mathcal{E}_0]$ as the Lorentz field $\mathcal{E}_L(r, \theta, v)$ and:

- (a) Determine and plot the relationship between $\mathcal{E}_L(r, \theta, v)$ and β as well as between $\mathcal{E}_L(r, \theta, v)$ and kinetic energy E_K/E_0 for $\theta = 0$ π (direction of field contraction).
- (b) Determine and plot the relationship between $\mathcal{E}_L(r, \theta, v)$ and β as well as between $\mathcal{E}_L(r, \theta, v)$ and kinetic energy E_K/E_0 for $\theta = \frac{1}{2}\pi$ (direction of field expansion).

SOLUTION:

(a) In the forward direction for $\theta = 0$ the electric field $\mathcal{E}_v(r, \theta = 0, v)$ of (4.1) simplifies to read

$$\mathcal{E}_v(r, \theta = 0, v) = \mathcal{E}_0 C_v|_{\theta=0} = \frac{\mathcal{E}_0(1 - \beta^2)}{(1 - \beta^2 \sin^2 \theta)^{3/2}} \Big|_{\theta=0} = \mathcal{E}_0(1 - \beta^2), \quad (4.3)$$

and the same result is obtained for the backward direction $\theta = \pi$

$$\mathcal{E}_v(r, \theta = \pi, v) = \mathcal{E}_0 C_v|_{\theta=\pi} = \frac{\mathcal{E}_0(1 - \beta^2)}{(1 - \beta^2 \sin^2 \theta)^{3/2}} \Big|_{\theta=\pi} = \mathcal{E}_0(1 - \beta^2). \quad (4.4)$$

Electric fields (4.3) and (4.4) result in the following expressions for the Lorentz electric field $\mathcal{E}_L(r, \theta, v)$ contraction as function of charged particle velocity $v/c = \beta$ and kinetic energy E_K , respectively

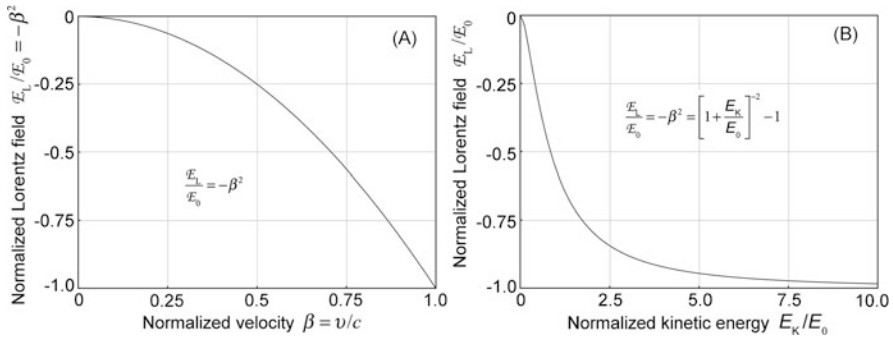


Fig. 4.11 Normalized Lorentz electric field $\mathcal{E}_L/\mathcal{E}_0$ against charged particle normalized velocity β [see (4.5)] in (A) and against charged particle normalized kinetic energy E_K/E_0 [see (4.6)] in (B) for $\theta = 0$ and $\theta = \pi$

$$\mathcal{E}_L(r, \theta = 0, v) = \mathcal{E}_L(r, \theta = \pi, v) = \mathcal{E}_v(r, \theta = 0, v) - \mathcal{E}_0 = -\mathcal{E}_0\beta^2 \quad (4.5)$$

and

$$\mathcal{E}_L(r, \theta = 0, v) = \mathcal{E}_L(r, \theta = \pi, v) = -\mathcal{E}_0\beta^2 = -\mathcal{E}_0 \left[1 - \frac{1}{\left(1 + \frac{E_K}{E_0}\right)^2} \right], \quad (4.6)$$

after we insert into (4.5) the well known relationship between β and E_K

$$E_K = E - E_0 = E_0 \left(\frac{1}{\sqrt{1 - \beta^2}} - 1 \right) \quad \text{or} \quad \beta^2 = 1 - \frac{1}{\left(1 + \frac{E_K}{E_0}\right)^2}. \quad (4.7)$$

Note: \mathcal{E}_0 is the isotropic electric field at $v = 0$, while E_0 is the rest energy of the charged particle.

Figure 4.11 shows a plot of $\mathcal{E}_L/\mathcal{E}_0$ for $\theta = 0$ and $\theta = \pi$ against β in part (A) and against E_K/E_0 in part (B).

(b) In directions perpendicular to the direction of motion of the charged particle the electric field $\mathcal{E}_v(r, \theta, v)$ of (4.1) simplifies to read

$$\mathcal{E}_v \left(r, \theta = \frac{1}{2}\pi, v \right) = \mathcal{E}_0 C_v \left(v, \theta = \frac{1}{2}\pi \right) = \frac{\mathcal{E}_0(1 - \beta^2)}{(1 - \beta^2 \sin^2 \theta)^{3/2}} \Big|_{\theta = \frac{1}{2}\pi} = \mathcal{E}_0 \frac{1}{\sqrt{1 - \beta^2}}, \quad (4.8)$$

resulting in the following expressions for the Lorentz field expansion as a function of velocity $v/c = \beta$ and kinetic energy E_K of the charged particle

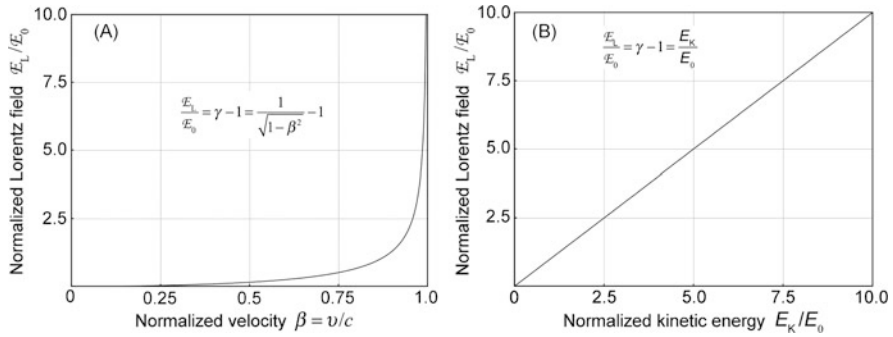


Fig. 4.12 Normalized Lorentz electric field \mathcal{E}_L/E_0 against charged particle normalized velocity β [see (4.9)] in (A) and against charged particle normalized kinetic energy E_K/E_0 [see (4.10)] in (B) for $\theta = \frac{1}{2}\pi$

$$\mathcal{E}_L\left(r, \theta = \frac{1}{2}\pi, v\right) = \mathcal{E}_v\left(r, \theta = \frac{1}{2}\pi, v\right) - \mathcal{E}_0 = \mathcal{E}_0\left[\frac{1}{\sqrt{1-\beta^2}} - 1\right] = \mathcal{E}_0(\gamma - 1) \tag{4.9}$$

and

$$\mathcal{E}_L\left(r, \theta = \frac{1}{2}\pi, v\right) = \mathcal{E}_v\left(r, \theta = \frac{1}{2}\pi, v\right) - \mathcal{E}_0 = \mathcal{E}_0(\gamma - 1) = \mathcal{E}_0\frac{E_K}{E_0} \tag{4.10}$$

after we insert into (4.9) the relationship between the Lorentz factor $\gamma = (1 - \beta^2)^{-1/2}$ and kinetic energy $E_K = E_0(\gamma - 1)$ with E_0 the rest energy of the charged particle. Figure 4.12 shows a plot of \mathcal{E}_L/E_0 for $\theta = \frac{1}{2}\pi$ against β in part (A) and against E_K/E_0 in part (B).

4.2.Q2 (110)

The intensity of bremsstrahlung radiation, defined as energy flow per unit area per unit time, is known as the Poynting vector \mathbf{S} and its magnitude $S = |\mathbf{S}|$ is given classically as (T4.17)

$$S = |\mathbf{S}| = \varepsilon_0 c \mathcal{E}^2 = \frac{q^2 a^2}{16\pi^2 \varepsilon_0 c^3 r^2} \sin^2 \theta \tag{4.11}$$

and relativistically as (T4.25)

$$S = |\mathbf{S}| = \varepsilon_0 c \mathcal{E}^2 = \frac{q^2 a^2}{16\pi^2 \varepsilon_0 c^3 r^2} \frac{\sin^2 \theta}{(1 - \beta \cos \theta)^5}, \tag{4.12}$$

where

- \mathcal{E} is the far field component of the electric field associated with a particle of charge q accelerated with acceleration \mathbf{a} .
- c is the speed of light in vacuum.
- β is charged particle velocity v normalized to c .
- r is the radius vector connecting charge q with point of interest P .
- θ is the angle between \mathbf{v} and \mathbf{r} .
- ϵ_0 is the electric constant.

Integrating $S(r, \theta)$ over area A , calculate the power P emitted by the accelerated charged particle in the form of bremsstrahlung radiation

- (a) Use the classical Poynting vector to derive the classical Larmor expression.
- (b) Use the relativistic Poynting vector to derive the relativistic Larmor expression.
- (c) Briefly describe the significance of the Larmor relationship.
- (d) Compare the classical result with the relativistic result. Does the relativistic result transform into the classical result for small velocity v ?

SOLUTION:

Power P (energy per unit time) emitted by the accelerated charged particle as bremsstrahlung radiation is calculated by integrating the intensity (Poynting vector) $S(r, \theta)$ over area A

$$P = \frac{dE}{dt} = \int S(r, \theta) dA \quad (4.13)$$

and recognizing that $dA = r^2 \sin \theta d\theta d\phi$ and the Poynting vector is defined as [see (T4.16)]

$$S = |\mathbf{S}| = \left| \frac{\mathcal{E} \times \mathbf{B}}{\mu_0} \right| = \frac{\mathcal{E}B}{\mu_0}. \quad (4.14)$$

(a) **Classical Larmor expression** is calculated inserting (4.11) into (4.13) as

$$\begin{aligned} P &= \frac{dE}{dt} = \int S(r, \theta) dA = \int_0^\pi S(r, \theta) r^2 \sin \theta d\theta \int_0^{2\pi} d\phi \\ &= -\frac{q^2 a^2}{8\pi \epsilon_0 c^3} \int_0^\pi (1 - \cos^2 \theta) d(\cos \theta) = \frac{q^2 a^2}{6\pi \epsilon_0 c^3}. \end{aligned} \quad (4.15)$$

(b) Relativistic Larmor expression is calculated inserting (4.12) into (4.13) to obtain

$$\begin{aligned} P &= \frac{dE}{dt} = \int S(r, \theta) dA = \int_0^\pi S(r, \theta) r^2 \sin \theta d\theta \int_0^{2\pi} d\phi \\ &= -\frac{q^2 a^2}{8\pi \epsilon_0 c^3} \int_0^\pi \frac{(1 - \cos^2 \theta) d(\cos \theta)}{(1 - \beta \cos \theta)^5} = \frac{q^2 a^2}{8\pi \epsilon_0 c^3} J(\theta), \end{aligned} \quad (4.16)$$

where the integral $J(\theta)$ is calculated by first making the substitution $\cos \theta = x$ and $d(\cos \theta) = dx$ to get

$$J = \int_{-1}^{+1} \frac{1 - x^2}{(1 - \beta x)^5} dx. \quad (4.17)$$

Next, we integrate (4.17) by parts, introducing new variables $u = 1 - x^2$ and $dv = (1 - \beta x)^{-5} dx$ with $du = -2x dx$ and $v = (4\beta)^{-1}(1 - \beta x)^{-4}$, to get

$$J = \int_{-1}^{+1} u dv = [uv]_{x=-1}^{x=+1} - \int_{-1}^{+1} v du = \frac{1}{2\beta} \int_{-1}^{+1} \frac{x dx}{(1 - \beta x)^4}. \quad (4.18)$$

Following another simplifying change in variables: $\zeta = 1 - \beta x$ or $x = (1 - \zeta)/\beta$ and $dx = -d\zeta/\beta$, one obtains the following simple integral

$$\begin{aligned} J &= \frac{1}{2\beta^3} \int_{1-\beta}^{1+\beta} \frac{1-\zeta}{\zeta^4} d\zeta = \frac{1}{2\beta^3} \left[-\frac{1}{3\zeta^3} + \frac{1}{2\zeta^2} \right]_{1-\beta}^{1+\beta} \\ &= \frac{1}{2\beta^3} \left[-\frac{1}{3(1+\beta)^3} + \frac{1}{2(1+\beta)^2} + \frac{1}{3(1-\beta)^3} - \frac{1}{2(1-\beta)^2} \right] \\ &= \frac{4}{3(1-\beta^2)^3} = \frac{4\gamma^6}{3}. \end{aligned} \quad (4.19)$$

Equation (4.19), when inserted into (4.16), gives the following result for the relativistic Larmor relationship

$$P = \frac{dE}{dt} = \int S(r, \theta) dA = \frac{q^2 a^2}{8\pi \epsilon_0 c^3} J(\theta) = \frac{q^2 a^2}{6\pi \epsilon_0 c^3} \gamma^6. \quad (4.20)$$

(c) Equations (4.15) and (4.20) are the classical and relativistic Larmor relationships, respectively, both predicting that the power P emitted in the form of bremsstrahlung radiation by an accelerated charged particle is proportional to $q^2 a^2$

- (1) q^2 , square of accelerated particle's charge.
- (2) a^2 , square of particle's acceleration.

The Larmor relationship represents one of the basic laws of nature and is of great importance to radiation physics. It is generally expressed as follows: “Any time a charged particle is accelerated or decelerated it emits part of its kinetic energy in the form of bremsstrahlung photons.” Since it is proportional to a^2 , as shown in (4.15) and (4.20), the power of bremsstrahlung production is inversely proportional to m^2 , the square of the particle's mass. Thus, proton by virtue of its relatively large mass m_p in comparison with the electron mass m_e ($m_p/m_e = 1836 \approx 2000$) produces much less bremsstrahlung radiation than does an electron, specifically about $(m_p/m_e)^2 \approx 4 \times 10^6$ times less. The radiation stopping power for electrons in comparison to that for protons is over six orders of magnitude larger at the same velocity and in the same absorbing material.

As a result of the inverse m^2 dependence, a heavy charged particle such as proton traversing a medium loses energy only through ionization (collision) losses and its radiation losses are negligible. Light charged particles undergo collision as well as radiation loss in traversing an absorbing medium and the total stopping power for light charged particles is the sum of collision stopping power and radiation stopping power.

(d) The classical and relativistic Larmor expressions differ only by the factor γ^6 in the relativistic expression. At low velocities v the normalized velocity $\beta \rightarrow 0$ and the Lorentz factor $\gamma \rightarrow 1$, resulting in identical Larmor expressions given in (4.15).

4.2.Q3

(111)

Intensity of bremsstrahlung radiation emitted by particle of charge q accelerated with acceleration \mathbf{a} is given by the Poynting vector \mathbf{S} as

$$S(r, \theta) = |\mathbf{S}| = \frac{q^2 a^2}{16\pi^2 \epsilon_0 c^3 r^2} \frac{\sin^2 \theta}{(1 - \beta \cos \theta)^5} = C_1 \frac{\sin^2 \theta}{(1 - \beta \cos \theta)^5}. \quad (4.21)$$

$S(r, \theta)$ is characterized by a characteristic angle θ_{\max} at which the intensity exhibits a maximum value for given q , a , r and β . The characteristic angle θ_{\max} is derived by setting $dS/d\theta|_{\theta=\theta_{\max}} = 0$ and is given by the following expression (T4.29)

$$\theta_{\max} = \arccos \left\{ \frac{1}{3\beta} (\sqrt{1 + 15\beta^2} - 1) \right\}. \quad (4.22)$$

The power P emitted in the form of bremsstrahlung is given as

$$P = \frac{q^2 a^2}{6\pi \epsilon_0 c^3} \gamma^6 = C_2 \gamma^6. \quad (4.23)$$

Calculate: **(a)** bremsstrahlung intensity $S(r, \theta = \theta_{\max})$ and **(b)** power P of emitted bremsstrahlung for given q , a , and r for charged particles with kinetic energy E_K of 1 keV, 100 keV, 1 MeV, and 100 MeV. Normalize your results to values calculated for $E_K = 1$ keV.

SOLUTION:

(a) Bremsstrahlung intensity S and **(b)** power P of emitted bremsstrahlung for various kinetic energies of charged particle were calculated with (4.21) and (4.23), respectively, and the results are provided in Table 4.5.

- (1) $\beta = \frac{v}{c} = \sqrt{1 - 1/(1 + E_K/E_0)^2}$ with E_0 rest energy of the charged particle.
A plot of β against kinetic energy E_K is shown in Fig. 4.13.
- (2) For θ_{\max} see (4.22) and (T4.29). A plot of θ_{\max} against E_K is shown in Fig. 4.14.
- (3) For $S(r, \theta)$ see (4.21) and (T4.25).
- (4) Lorentz factor $\gamma = (1 - \beta^2)^{-1/2}$.
- (6) For derivation of relativistic Larmor relationship consult Prob. 110(b).

Table 4.5 Bremsstrahlung intensity $S(r, \theta = \theta_{\max})$ and power P of emitted bremsstrahlung for various kinetic energies E_K of charged particle

		E_K			
		1 keV	100 keV	1 MeV	100 MeV
(1)	β	0.063	0.548	0.941	0.9999
(2)	θ_{\max} (deg)	81.2	35.0	10.0	0.4
(3)	$S(r, \theta_{\max})/C_1$	1.00	6.32	1.41×10^4	1.6×10^{15}
(4)	γ	1.002	1.20	2.96	70.71
(5)	γ^6	1.012	2.99	673	1.25×10^{11}
(6)	P/C_2	1.00	2.95	665	1.235×10^{11}

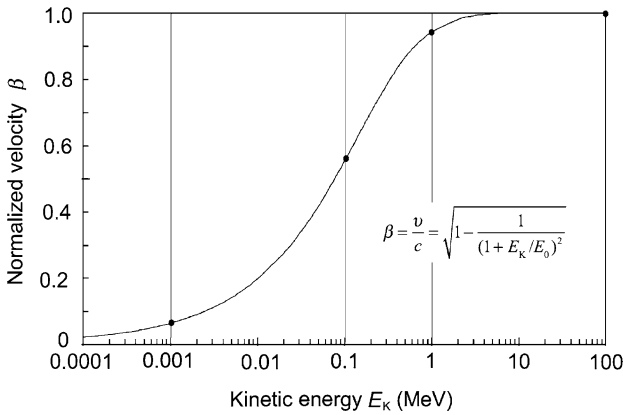


Fig. 4.13 Velocity v normalized to speed of light in vacuum c against kinetic energy E_K of the charged particle

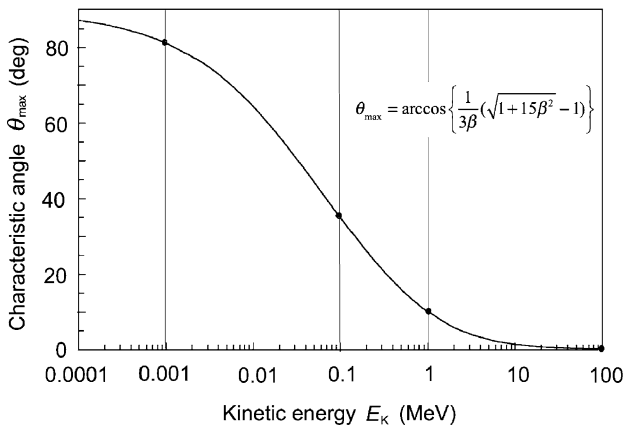


Fig. 4.14 Characteristic angle θ_{\max} against kinetic energy E_K of the charged particle

4.2.Q4

(112)

Maximum bremsstrahlung intensity produced by an accelerated light charged particle (CP) is emitted in a direction defined by the bremsstrahlung characteristic angle θ_{\max} expressed as follows (T4.29)

$$\theta_{\max} = \arccos \left\{ \frac{1}{3\beta} \left[\sqrt{1 + 15\beta^2} - 1 \right] \right\}, \quad (4.24)$$

where β is the normalized CP velocity related to CP kinetic energy E_K as follows (T2.6)

$$\beta = \left[1 - \left(1 + \frac{E_K}{E_0} \right)^{-2} \right]^{-\frac{1}{2}}, \quad (4.25)$$

with E_0 the rest energy of the light CP ($E_0 = m_e c^2 = 0.511$ MeV).

- (a) Show that the expression (4.24) in conjunction with (4.25) in the highly relativistic region where $\beta \rightarrow 1$ and $\gamma \rightarrow \infty$ can be simplified to read

$$\theta_{\max} \approx \frac{1}{2(1 + \frac{E_K}{E_0})}. \quad (4.26)$$

- (b) Show that the expression (4.24) in conjunction with (4.25) in the classical region where $\beta \rightarrow 0$ and $\gamma \rightarrow 1$ can be simplified to read

$$\theta_{\max} \approx \frac{1}{2} \left(\pi - 5 \sqrt{\frac{2E_K}{E_0}} \right). \quad (4.27)$$

- (c) Plot θ_{\max} of (4.24) against kinetic energy E_K in the E_K range 10^{-4} MeV $\leq E_K \leq 10^4$ MeV and show how the approximations derived in (a) and (b) fit the general θ_{\max} function.

SOLUTION:

- (a) **Extreme relativistic region.** Equation (4.24) that gives the general relationship between θ_{\max} and β can be also expressed as follows

$$\cos \theta_{\max} = \frac{1}{3\beta} \left[\sqrt{1 + 15\beta^2} - 1 \right]. \quad (4.28)$$

Since in the extreme relativistic region $\beta \rightarrow 1$, $\gamma \rightarrow \infty$, and $\theta_{\max} \rightarrow 0$, we can simplify (4.28) using the following steps:

- (1) Function $\cos \theta_{\max}$ is expanded into the following series

$$\cos \theta_{\max} = 1 - \frac{\theta_{\max}^2}{2!} + \frac{\theta_{\max}^4}{4!} - \frac{\theta_{\max}^6}{6!} + \dots + (-1)^n \frac{\theta_{\max}^{2n}}{(2n)!}. \quad (4.29)$$

- (2) The Lorentz factor $\gamma = 1/\sqrt{1 - \beta^2}$ is modified to give β as a function of γ

$$\beta^2 = 1 - \frac{1}{\gamma^2} \quad \text{and} \quad \frac{1}{\beta} = \frac{1}{\sqrt{1 - \frac{1}{\gamma^2}}} \approx 1 + \frac{1}{2\gamma^2} \quad \text{for } \gamma \rightarrow \infty. \quad (4.30)$$

- (3) The term $\frac{1}{3\beta}[\sqrt{1+15\beta^2}-1]$ is now written in terms of γ and Taylor expansion is used on the square root term $\sqrt{1-15/(16\gamma^2)} \approx 1-15/(32\gamma^2)$ for $\gamma \rightarrow \infty$

$$\begin{aligned} \frac{1}{3\beta}[\sqrt{1+15\beta^2}-1] &= \frac{1}{3}\left(1+\frac{1}{2\gamma^2}\right)\left[\sqrt{1+15\left(1-\frac{1}{\gamma^2}\right)}-1\right] \\ &\approx \frac{1}{3}\left(1+\frac{1}{2\gamma^2}\right)\left[4\left(1-\frac{15}{32\gamma^2}\right)-1\right] \\ &= \left(1+\frac{1}{2\gamma^2}\right)\left(1-\frac{5}{8\gamma^2}\right) \approx 1-\frac{1}{8\gamma^2}. \end{aligned} \quad (4.31)$$

- (4) We now take the first two terms of the $\cos \theta_{\max}$ series of (4.29) and neglect all higher order terms since $\theta_{\max} \rightarrow 0$ and merge them with (4.31) to get a simple expression for θ_{\max} as a function of γ and β

$$\cos \theta_{\max} = 1 - \frac{\theta_{\max}^2}{2} = 1 - \frac{1}{8\gamma^2} \quad \text{or} \quad \theta_{\max} \approx \frac{1}{2\gamma} = \frac{\sqrt{1-\beta^2}}{2}. \quad (4.32)$$

From (4.25) we note that

$$1 - \beta^2 = \frac{1}{\left(1 + \frac{E_K}{E_0}\right)^2} \quad \text{and} \quad \sqrt{1 - \beta^2} = \frac{1}{\left(1 + \frac{E_K}{E_0}\right)} \quad (4.33)$$

and, after inserting (4.33) into (4.32), we get the following simple expression for the bremsstrahlung characteristic angle θ_{\max} as a function of kinetic energy E_K of the bremsstrahlung-producing light charged particle in the extreme relativistic region

$$\theta_{\max} \approx \frac{1}{2\gamma} = \frac{\sqrt{1-\beta^2}}{2} = \frac{1}{2\left(1 + \frac{E_K}{E_0}\right)}. \quad (4.34)$$

- (b) Classical region.** We again start with (4.24), consider the classical region where $\beta \rightarrow 0$, $\gamma \rightarrow 1$, and $\theta_{\max} \rightarrow \frac{1}{2}\pi$, and get the following modified expression

$$\begin{aligned} \theta_{\max} &= \arccos \left\{ \frac{1}{3\beta}[\sqrt{1+15\beta^2}-1] \right\} \\ &\approx \arccos \left\{ \frac{1}{3\beta} \left[1 + \frac{15}{2}\beta^2 + \dots - 1 \right] \right\} = \arccos \left\{ \frac{5\beta}{2} \right\}, \end{aligned} \quad (4.35)$$

where we used the Taylor expansion of the square root term for small β . In classical mechanics we have the following simple expression for E_K as a function of β

$$E_K = \frac{m_e v^2}{2} = \frac{1}{2} m_e c^2 \beta^2 = \frac{1}{2} E_0 \beta^2 \quad \text{or} \quad \beta = \sqrt{\frac{2E_K}{E_0}}. \quad (4.36)$$

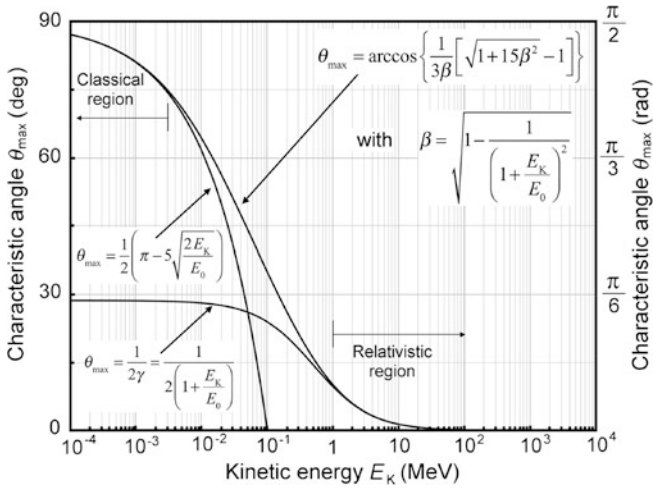


Fig. 4.15 Bremsstrahlung characteristic angle θ_{\max} against kinetic energy E_K of the electron producing bremsstrahlung. Three equations are shown: (1) general expression (4.24) in conjunction with (4.25), (2) approximation (4.26) holding in the extreme relativistic region, and (3) approximation (4.27) holding in the classical region

We now get the following expression for θ_{\max} as a function of kinetic energy E_K

$$\theta_{\max} \approx \arccos\sqrt{\frac{12.5E_K}{E_0}} \tag{4.37}$$

which, for $E_K \ll E_0$, allows the following series expansion of the $\arccos\sqrt{12.5E_K/E_0}$ function

$$\theta_{\max} \approx \arccos\sqrt{\frac{12.5E_K}{E_0}} \approx \frac{1}{2}\left(\pi - 5\sqrt{\frac{2E_K}{E_0}}\right), \tag{4.38}$$

obtained with the use of only the first two terms of the series expansion. The series expansion of the function $\arccos x$, converging for $|x| < 1$, is in general expressed as follows

$$\arccos x \approx \frac{\pi}{2} - \left[x + \frac{x^3}{2 \times 3} + \frac{1 \times 3x^5}{2 \times 4 \times 5} + \dots + \frac{1 \times 3 \times 5 \dots (2n-1)x^{2n+1}}{2 \times 4 \times 6 \times \dots (2n) \times (2n+1)}\right]. \tag{4.39}$$

(c) The three equations for θ_{\max} : the general equation (4.24) in conjunction with (4.25) and the two approximations, (4.26) for the extreme relativistic region where $\beta \rightarrow 1$, $\gamma \rightarrow \infty$, and $\theta_{\max} \rightarrow 0$, and (4.27) for the classical region where $\beta \rightarrow 0$, $\gamma \rightarrow 1$, and $\theta_{\max} \rightarrow \frac{1}{2}\pi$, are plotted in Fig. 4.15.

It is obvious that the two approximations represent excellent simplifications of (4.24) in their respective areas of applicability: (4.26) in the extreme relativistic region (for $E_K > 2$ MeV) and (4.27) in the classical region (for $E_K < 1$ keV).

4.2.Q5

(113)

In bremsstrahlung production the characteristic angle θ_{\max} is defined as the angle θ at which the maximum intensity of the emitted bremsstrahlung occurs. In (T4.29) θ_{\max} is expressed as follows

$$\theta_{\max} = \arccos \left\{ \frac{1}{3\beta} [\sqrt{1 + 15\beta^2} - 1] \right\}, \quad (4.40)$$

where β is the normalized velocity of the light charged particle producing bremsstrahlung.

- (a) Determine the characteristic angle θ_{\max} at which the electron kinetic energy E_K equals the electron rest energy $E_0 = m_e c^2 = 0.511$ MeV.
- (b) Derive an expression for electron kinetic energy E_K as a function of the characteristic bremsstrahlung angle θ_{\max} .
- (c) Use the expression for $E_K(\theta_{\max})$ derived in (b) to determine electron kinetic energy E_K at which maximum bremsstrahlung intensity is emitted with a characteristic angle θ_{\max} of 1° .
- (d) Show results of (a) and (c) on a plot of θ_{\max} against E_K for 0.0001 MeV $\leq E_K \leq 100$ MeV.

SOLUTION:

(a) To determine the bremsstrahlung characteristic angle θ_{\max} we will use (4.40) but must first determine the normalized electron velocity β for kinetic energy $E_K = E_0$ using the standard relativistic expression (T2.7) for $\beta(E_K)$

$$\beta = \sqrt{1 - \frac{1}{(1 + \frac{E_K}{E_0})}} = \sqrt{1 - \frac{1}{4}} = 0.866. \quad (4.41)$$

Next we insert β calculated in (4.41) into (4.40) and get

$$\begin{aligned} \theta_{\max} &= \arccos \left\{ \frac{1}{3\beta} [\sqrt{1 + 15\beta^2} - 1] \right\} \\ &= \arccos \left\{ \frac{1}{3 \times 0.866} \times [\sqrt{1 + 15 \times 0.866^2} - 1] \right\} \\ &= \arccos 0.9622 = 0.276 \text{ rad} = 15.8^\circ. \end{aligned} \quad (4.42)$$

Thus, the characteristic angle θ_{\max} for bremsstrahlung produced by a light charged particle whose kinetic energy E_K equals its rest energy E_0 is 15.8° (0.276 rad).

(b) To derive an expression for $E_K(\theta_{\max})$ we first solve (4.40) for β and then insert the derived expression for $\beta(\theta_{\max})$ into the standard relativistic expression for $E_K(\beta)$ expressed as follows

$$E_K = (\gamma - 1)E_0 = \left(\frac{1}{\sqrt{1 - \beta^2}} - 1 \right) m_e c^2. \quad (4.43)$$

To derive $\beta(\theta_{\max})$ we express (4.40) in the following form

$$\cos \theta_{\max} = \left\{ \frac{1}{3\beta} [\sqrt{1 + 15\beta^2} - 1] \right\} \quad (4.44)$$

and solve for β to get

$$9\beta^2 \cos^2 \theta_{\max} + 6\beta \cos \theta_{\max} + 1 = 1 + 15\beta^2 \quad \text{or} \quad 9\beta \cos^2 \theta_{\max} + 6 \cos \theta_{\max} = 15\beta. \quad (4.45)$$

The normalized velocity $\beta(\theta_{\max})$ is thus from (4.45) given as

$$\beta = \frac{6 \cos \theta_{\max}}{15 - 9 \cos^2 \theta_{\max}}. \quad (4.46)$$

(c) Inserting β of (4.46) into (4.43) results in the following general expression for $E_K(\theta_{\max})$ and the following kinetic energy E_K after insertion of $\theta_{\max} = 1^\circ$

$$\begin{aligned} E_K &= E_0 \left[\frac{1}{\sqrt{1 - \left(\frac{6 \cos \theta_{\max}}{15 - 9 \cos^2 \theta_{\max}} \right)^2}} - 1 \right] \\ &= (0.511 \text{ MeV}) \times \left[\frac{1}{\sqrt{1 - \left(\frac{6 \cos(1^\circ)}{15 - 9 \cos^2(1^\circ)} \right)^2}} - 1 \right] \\ &= 14.13 \text{ MeV}. \end{aligned} \quad (4.47)$$

The expression for $E_K(\theta_{\max})$ of (4.47) is somewhat cumbersome; however, it is possible to simplify it by using a simple approximation for θ_{\max} valid for relativistic kinetic energy E_K and given as follows (T4.36)

$$\theta_{\max} = \arccos \left\{ \frac{1}{3\beta} [\sqrt{1 + 15\beta^2} - 1] \right\} \approx \frac{1}{2\gamma} = \frac{1}{2} \sqrt{1 - \beta^2}. \quad (4.48)$$

We now express $1 - \beta^2$ in terms of θ_{\max} using (4.48) and then in terms of E_K/E_0 using (4.41) to get

$$1 - \beta^2 = 4\theta_{\max}^2 = \frac{1}{\left(1 + \frac{E_K}{E_0}\right)^2}. \quad (4.49)$$

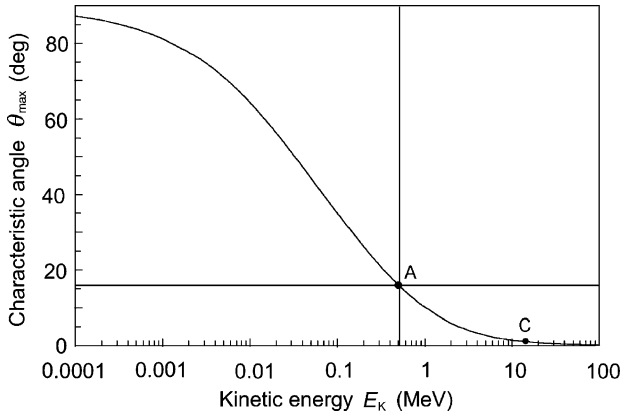


Fig. 4.16 Characteristic angle θ_{\max} against kinetic energy E_K of the light charged particle producing bremsstrahlung. Point A represents the result of calculation in (a), point C the result of calculation in (c)

In (4.49) we have a very simple relationship linking θ_{\max} with E_K and solving (4.49) for θ_{\max} results in a very simple expression (4.50) for E_K as a function of θ_{\max} . Inserting $\theta_{\max} = 1^\circ$ into (4.50) gives the same answer for E_K as did (4.47) above

$$E_K = E_0 \left[\frac{1}{2\theta_{\max}} - 1 \right] = (0.511 \text{ MeV}) \times \left[\frac{180}{2\pi} - 1 \right] = 14.13 \text{ MeV}. \quad (4.50)$$

Kinetic energy E_K of a light charged particle that produces bremsstrahlung with $\theta_{\max} = 1^\circ$ is 14.13 MeV.

(d) Results of (a) and (c) are shown as data points A and C, respectively, in Fig. 4.16 which represents a plot of bremsstrahlung characteristic angle θ_{\max} against kinetic energy E_K of the light charged particle producing bremsstrahlung radiation.

4.3 Synchrotron Radiation

4.3.Q1

(114)

Radiation emitted by a charged particle in circular motion in a cyclic accelerator or a storage ring is called *synchrotron radiation*. Since the effect occurs under the influence of a magnetic field that keeps the particle in a circular orbit, it is sometimes called *magnetic bremsstrahlung*.

- (a) Using Larmor relationship determine the general expression for power P radiated by a relativistic particle of charge q and velocity $v(t)$ moving in a circular orbit.

- (b) Using the result of (a) determine the general expression for energy loss ΔE per revolution for electrons and protons in a cyclic accelerator.
- (c) For electrons accelerated to 25 MeV in a betatron determine the energy loss per revolution if the central orbit radius $R = 0.5$ m.
- (d) For protons accelerated to 250 MeV in a synchrotron determine the energy loss per revolution if the radius R of the orbit is 3 m.

SOLUTION:

(a) The general Larmor relationship gives power P of radiation emitted by particle of charge q subjected to acceleration a

$$P = \frac{dE}{dt} = \frac{q^2 a^2}{6\pi \epsilon_0 c^3} \quad (4.51)$$

and the relativistic acceleration a for a particle in circular motion is given as

$$a = \frac{1}{m_0} \frac{dp}{dt'} = \frac{1}{m_0} \frac{d(\gamma m_0 v)}{dt} \frac{dt}{dt'} = \gamma^2 \frac{dv}{dt} = \gamma^2 \frac{v^2}{R}, \quad (4.52)$$

where p is the relativistic particle momentum, t' is the time in the reference frame of the particle, γ is the Lorentz factor [$\gamma = dt/dt' = 1/\sqrt{1-\beta^2}$], R is the radius of the circular orbit, and $dv/dt = v^2/R$ is the classical particle acceleration for circular motion.

The emitted power P of (4.51) is thus given as

$$P = \frac{q^2 a^2}{6\pi \epsilon_0 c^3} = \frac{c}{6\pi \epsilon_0} \frac{q^2 \gamma^4 \beta^4}{R^2} = \frac{c}{6\pi \epsilon_0} \frac{\beta^4}{(1-\beta^2)^2} \frac{q^2}{R^2} = \frac{c}{6\pi \epsilon_0} \frac{q^2 \beta^4}{R^2} \left[\frac{E}{E_0} \right]^4, \quad (4.53)$$

where we have used the standard expression for total energy E of a particle $E = \gamma E_0$, with E_0 the rest energy of the particle.

(b) Energy loss ΔE per revolution is calculated by multiplying power P of (4.53) with the time τ for one revolution, given as $\tau = 2\pi R/v$, to get

$$\Delta E = P\tau = \frac{c}{6\pi \epsilon_0} \frac{q^2 \beta^4}{R^2} \left[\frac{E}{E_0} \right]^4 \frac{2\pi R}{v} = \frac{q^2 \beta^3}{3\epsilon_0 R^2} \left[\frac{E}{E_0} \right]^4, \quad (4.54)$$

indicating that energy loss per revolution is inversely proportional to the radius R of the orbit and proportional to the fourth power of E/E_0 . For a given particle total energy E the energy loss ΔE is inversely proportional to the rest mass E_0 of the particle, therefore synchrotron radiation is much more important for electrons than for protons and it places a practical limitation on the maximum energy achievable in a betatron.

Energy loss per revolution for relativistic electrons ($\beta \approx 1$) is from (4.54) calculated as

$$\begin{aligned}\Delta E_{\text{electron}} &= \frac{q^2 \beta^3}{3\epsilon_0 R} \left[\frac{E}{E_0} \right]^4 \\ &= \frac{e \times 1.6 \times 10^{-19} \text{ A} \cdot \text{s}}{3 \times 8.85 \times 10^{-12} [\text{A} \cdot \text{s}/(\text{V} \cdot \text{m})] \times R \times (0.511 \text{ MeV})^4} \\ &= \left\{ 8.84 \times 10^{-8} \frac{\text{eV} \cdot \text{m}}{(\text{MeV})^4} \right\} \frac{E^4}{R},\end{aligned}\quad (4.55)$$

while energy loss per revolution for relativistic protons is from (4.54) calculated as

$$\begin{aligned}\Delta E_{\text{proton}} &= \frac{q^2 \beta^3}{3\epsilon_0 R} \left[\frac{E}{E_0} \right]^4 = \frac{e \times 1.6 \times 10^{-19} \text{ A} \cdot \text{s}}{3 \times 8.85 \times 10^{-12} [\text{A} \cdot \text{s}/(\text{V} \cdot \text{m})] \times R \times (938.3 \text{ MeV})^4} \\ &= \left\{ 7.78 \times 10^{-21} \frac{\text{eV} \cdot \text{m}}{(\text{MeV})^4} \right\} \frac{E^4}{R}.\end{aligned}\quad (4.56)$$

(c) Energy loss ΔE per revolution for 25 MeV electrons in a betatron with $R = 0.5$ m is according to (4.55) calculated as follows

$$\begin{aligned}\Delta E_{\text{electron}} &= \left\{ 8.84 \times 10^{-8} \frac{\text{eV} \cdot \text{m}}{(\text{MeV})^4} \right\} \frac{E^4}{R} \\ &= 8.84 \times 10^{-8} \frac{\text{eV} \cdot \text{m}}{(\text{MeV})^4} \frac{(25 + 0.511)^4 (\text{MeV})^4}{0.5 \text{ m}} = 0.075 \text{ eV}.\end{aligned}\quad (4.57)$$

(d) Energy loss ΔE per revolution for 250 MeV protons in a synchrotron with $R = 3$ m is according to (4.56) calculated as

$$\begin{aligned}\Delta E_{\text{proton}} &= \left\{ 7.78 \times 10^{-21} \frac{\text{eV} \cdot \text{m}}{(\text{MeV})^4} \right\} \frac{E^4}{R} \\ &= 7.78 \times 10^{-21} \frac{\text{eV} \cdot \text{m}}{(\text{MeV})^4} \frac{(250 + 938.3)^4 (\text{MeV})^4}{3 \text{ m}} = 5.2 \times 10^{-9} \text{ eV}.\end{aligned}\quad (4.58)$$

4.4 Čerenkov Radiation

4.4.Q1

(115)

Energetic charged particles moving through an optically transparent dielectric absorber with uniform velocity v_i that exceeds the phase velocity of light c_n in the particular absorber give rise to emission of photons called Čerenkov

radiation. The photons are emitted along the surface of a forward directed cone centered on the charged particle direction of motion and the cone is specified with the following relationship

$$\cos \theta_{\text{Cer}} = \frac{c_n}{v_i} + C_R = \frac{c}{n v_i} + C_R = \frac{1}{n \beta_i} + C_R \approx \frac{1}{n \beta_i}, \quad (4.59)$$

where n is the index of refraction for the transparent absorber, β_i is the velocity of the incident particle normalized to the speed of light in vacuum c , and C_R is a small correction accounting for the recoil of the charged particle as a result of the emission of a Čerenkov photon.

- (a) Use relativistic expressions for conservation of total energy and momentum to derive (4.59) corrected for the recoil of the charged particle as a result of the emission of the Čerenkov photon.
- (b) Show that the recoil correction C_R is exceedingly small and therefore can be neglected.

SOLUTION:

Figure 4.17 depicts the process of production of a Čerenkov photon. A relativistic particle moves with velocity v_i and momentum \mathbf{p}_i along the abscissa (x) axis. At the origin of the coordinate system a Čerenkov photon of energy $h\nu = hc/(\nu\lambda)$ and momentum \mathbf{p}_ν is produced and emitted at an angle θ_{Cer} , called Čerenkov angle, while the particle is deflected through an angle ϕ and continues with momentum \mathbf{p}_f and velocity v_f that is smaller than v_i .

- (a) The derivation of the Čerenkov angle equation is carried out similarly to the derivation of the Compton wavelength shift equation (T7.44) with the use of relativistic relationships for conservation of total energy E and momentum p .

The following well-known expressions will be used in the derivation:

$$p_i = \gamma_i m_0 v_i; \quad p_f = \gamma_f m_0 v_f; \quad p_\nu = \frac{h}{\lambda}; \quad \gamma_i = \frac{1}{\sqrt{1 - \beta_i^2}} = \left[1 - \frac{v_i^2}{c^2} \right]^{-\frac{1}{2}};$$

$$\gamma_f = \frac{1}{\sqrt{1 - \beta_f^2}} = \left[1 - \frac{v_f^2}{c^2} \right]^{-\frac{1}{2}}; \quad E_i = \gamma_i m_0 c^2 = \sqrt{E_0^2 + p_i^2 c^2};$$

$$E_f = \gamma_f m_0 c^2 = \sqrt{E_0^2 + p_f^2 c^2}; \quad E_\nu = h\nu = \frac{hc}{n\lambda};$$

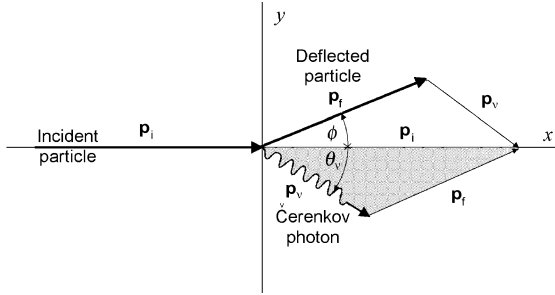


Fig. 4.17 Production of a Čerenkov photon. A relativistic particle moves in an absorber with velocity v_i and momentum p_i along the abscissa (x) axis. The particle velocity v_i exceeds the speed of light in the absorber and, as a result, Čerenkov radiation is produced and emitted in a direction defined by the Čerenkov angle θ_v . The particle is deflected under recoil angle ϕ and continues with momentum p_f and velocity v_f that is smaller than v_i

where m_0 is the rest mass of the particle while E_i , E_f , and E_v are, respectively, total incident energy of the charged particle, total final energy of the charged particle, and energy of the Čerenkov photon.

Conservation of energy in Čerenkov effect is expressed as follows:

$$E_i = E_f + E_v \quad \text{or} \quad \gamma_i m_0 c^2 = \gamma_f m_0 c^2 + \frac{hc}{n\lambda} \quad \text{or} \quad (4.60)$$

$$\sqrt{E_0^2 + p_i^2 c^2} = \sqrt{E_0^2 + p_f^2 c^2} + \frac{hc}{n\lambda}.$$

Conservation of momentum along the abscissa (x) axis:

$$p_i = p_f \cos \phi + p_v \cos \theta_v. \quad (4.61)$$

Conservation of momentum along the ordinate (y) axis:

$$0 = p_f \sin \phi - p_v \sin \theta_v. \quad (4.62)$$

Using the law of cosines in conjunction with Fig. 4.17 we express p_f^2 as follows

$$p_f^2 = p_i^2 + p_v^2 - 2p_i p_v \cos \theta_v, \quad (4.63)$$

and then derive another expression for p_f^2 , first rearranging the conservation of energy equation (4.60) as follows

$$\sqrt{E_0^2 + p_f^2 c^2} = \sqrt{E_0^2 + p_i^2 c^2} - \frac{hc}{n\lambda} \quad (4.64)$$

and then squaring (4.64) to get

$$p_f^2 c^2 = p_i^2 c^2 + \frac{h^2 c^2}{n^2 \lambda^2} - \frac{2hc}{n\lambda} \sqrt{E_0^2 + p_i^2 c^2} \equiv p_i^2 c^2 + \frac{h^2 c^2}{n^2 \lambda^2} - \frac{2hc}{n\lambda} E_i. \quad (4.65)$$

Table 4.6 Parameters of Čerenkov interaction between energetic electron or proton and water

	Rest energy m_0c^2 (MeV)	λ_C (Å) (1)	β_{thr} in water (2)	γ_{thr} at β_{thr} (3)	$\frac{1}{n\beta_{\text{thr}}}$	Recoil term (4)
Electron	$m_e c^2 = 0.511$	2.43×10^{-3}	0.752	1.52	1	1.14×10^{-6}
Proton	$m_p c^2 = 938.3$	1.32×10^{-5}	0.752	1.52	1	6.32×10^{-10}

(1) $\lambda_C = \frac{h}{m_0c}$; (2) $\beta_{\text{thr}} = \frac{1}{n}$; (3) $\gamma_{\text{thr}} = \frac{1}{\sqrt{1-\beta_{\text{thr}}^2}}$; (4) $\frac{\lambda_C}{2\beta_{\text{thr}}\gamma_{\text{thr}}\lambda} \left[1 - \frac{1}{n^2}\right]$

After multiplying (4.64) with c^2 , we equate the result with (4.65) and obtain the following expression for $\cos\theta_{\text{Cer}}$

$$\begin{aligned}
 \cos\theta_v &= \frac{2hc}{n\lambda} \frac{E_i}{2p_i p_v c^2} + \frac{p_v^2 c^2}{2p_i p_v c^2} - \frac{h^2 c^2}{n^2 \lambda^2} \frac{1}{2p_i p_v c^2} \\
 &= \frac{2hc}{n\lambda} \frac{(\gamma_i m_0 c^2)\lambda}{2(\gamma_i m_0 v_i)hc^2} + \frac{h^2 c^2 \lambda}{2\lambda^2 (\gamma_i m_0 v_i)hc^2} - \frac{h^2 c^2}{n^2 \lambda^2} \frac{\lambda}{2(\gamma_i m_0 v_i)hc^2} \\
 &= \frac{c}{n v_i} + \frac{h}{2\lambda(\gamma_i m_0 v_i)} \left[1 - \frac{1}{n^2}\right] = \frac{1}{n\beta_i} + \frac{1}{2} \frac{\lambda_{\text{dB}}}{\lambda} \left[1 - \frac{1}{n^2}\right] \\
 &= \frac{1}{n\beta_i} + \frac{1}{2\beta_i \gamma_i} \frac{\lambda_C}{\lambda} \left[1 - \frac{1}{n^2}\right] \approx \frac{1}{n\beta_i}, \tag{4.66}
 \end{aligned}$$

where λ_{dB} is the de Broglie wavelength of the charged particle (T2.1) given as

$$\lambda_{\text{dB}} = \frac{h}{p_i} = \frac{2\pi \hbar c}{E_K \sqrt{1 + \frac{2E_0}{E_K}}} = \frac{h}{\gamma_i m_0 v_i} = \frac{\lambda_C}{\beta_i \gamma_i}, \tag{4.67}$$

with λ_C the Compton wavelength of the charged particle (T7.44) defined as

$$\lambda_C = \frac{h}{m_0 c}. \tag{4.68}$$

The final term of (4.66) represents the charged particle recoil term in Čerenkov interaction.

(b) Čerenkov angle θ_{Cer} of (4.66) consists of two terms, both terms dependent on the velocity β_i of the incident particle and the index of refraction n of the transparent absorber. The second term, several orders of magnitude smaller than the first term $1/(n\beta_i)$, originates from the particle recoil and is usually neglected.

To assess the magnitude of the recoil term $\lambda_C(1 - 1/n^2)/(2\beta_i \gamma_i \lambda)$ we evaluate the term for passage of electrons and protons through water at threshold velocity $\beta_{\text{thr}} = 1/n = 1/1.33 = 0.752$ assuming a typical Čerenkov radiation wavelength λ of 4000 Å. The results, displayed in Table 4.6, show that the recoil term for electrons is 6 orders of magnitude smaller than the $1/(n\beta_i)$ term, while for protons the recoil

term is even smaller (1836 times smaller than that for electrons since $m_p/m_e = 1836$). It is thus reasonable in discussions of Čerenkov angle θ_{Cer} to neglect the recoil term and use a much simpler equation expressed as $\cos \theta_{\text{Cer}} = 1/(n\beta_i)$.

4.4.Q2

(116)

Čerenkov radiation is emitted in a forward directed cone centered on the charged particle direction of motion. The half-cone angle θ_{Cer} , referred to as the Čerenkov angle, depends on the index of refraction n of the transparent absorber and on the velocity β_i of the incident charged particle, and is defined by the following expression

$$\theta_{\text{Cer}} = \cos^{-1} \frac{1}{n\beta_i} = \cos^{-1} \left\{ n \sqrt{1 - \frac{1}{[1 + \frac{(E_K)_i}{E_0}]^2}} \right\}^{-1}, \quad (4.69)$$

where $(E_K)_i$ and β_i are the kinetic energy and velocity normalized to speed of light c in vacuum, respectively.

The normalized velocity β_i that can produce Čerenkov radiation in a transparent dielectric absorber ranges from a minimum β_i referred to as threshold normalized velocity β_{thr} up to $\beta_i = 1$, corresponding to a range in θ_{Cer} from a minimum Čerenkov angle $(\theta_{\text{Cer}})_{\text{min}}$ up to a maximum Čerenkov angle $(\theta_{\text{Cer}})_{\text{max}}$.

For four transparent dielectric absorbers: water ($n = 1.33$); Lucite ($n = 1.50$); sapphire ($n = 1.76$); and diamond ($n = 2.15$) traversed by electrons:

- (a) Determine the threshold velocity $(\beta_i)_{\text{thr}}$ and threshold kinetic energy $(E_K)_{\text{thr}}/E_0$.
- (b) Determine the minimum Čerenkov angle $(\theta_{\text{Cer}})_{\text{min}}$, maximum Čerenkov angle $(\theta_{\text{Cer}})_{\text{max}}$, and the dynamic range of θ_{Cer} in terms of normalized velocity β_i as well as normalized kinetic energy $(E_K)_i$ of the incident electron.
- (c) Plot θ_{Cer} against β_i for $0 \leq \beta_i \leq 1$.
- (d) Plot θ_{Cer} against $(E_K)_i/E_0$ for $0 \leq (E_K)_i/E_0 \leq 10$.

SOLUTION:

(a) A charged particle moving with uniform velocity in vacuum does not emit radiation either in the form of bremsstrahlung radiation or in the form of Čerenkov radiation. However, a charged particle moving with uniform velocity in a transparent dielectric absorber does not emit bremsstrahlung radiation but may emit Čerenkov radiation if the velocity of the charged particle exceeds the speed of light c in the transparent absorber.

Note: to emit bremsstrahlung radiation a charged particle must be accelerated or decelerated either in vacuum or in an absorber. Thus, for bremsstrahlung production the necessary condition is the acceleration of charged particle; for emission of Čerenkov radiation the necessary condition is transparent absorber and particle velocity exceeding speed of light in absorber.

(1) Threshold velocity $(\beta_i)_{\text{thr}}$ is defined as the minimum normalized velocity of a charged particle that produces Čerenkov radiation in a given dielectric absorber and this velocity is equal to the phase velocity of light c_n in the given absorber expressed as $c_n = c/n$ where c is the speed of light in vacuum ($c = 3 \times 10^8$ m/s) and n is the index of refraction of the dielectric absorber. Threshold velocity $(v_i)_{\text{thr}}$ is thus given as

$$(v_i)_{\text{thr}} = \frac{c}{n} \quad \text{or} \quad (\beta_i)_{\text{thr}} = \frac{(v_i)_{\text{thr}}}{c} = \frac{1}{n}. \quad (4.70)$$

Equation (4.70) was used to determine the normalized threshold velocity $(\beta_i)_{\text{thr}}$ for electrons propagating in four dielectric materials: water, Lucite, sapphire, and diamond. Results of the calculation are listed in column (3) of Table 4.7.

(2) Threshold kinetic energy $(E_K)_{\text{thr}}$ is defined as the minimum charged particle kinetic energy that produces Čerenkov radiation in a given transparent dielectric absorber. It is related to threshold velocity $(\beta_i)_{\text{thr}}$ through the standard relativistic E_K versus β relationship as (T2.7)

$$(E_K)_{\text{thr}} = E_0 \left[\frac{1}{\sqrt{1 - (\beta_i)_{\text{thr}}^2}} - 1 \right] = E_0 \left[\frac{1}{\sqrt{1 - \frac{1}{n^2}}} - 1 \right] \quad \text{or} \quad (4.71)$$

$$(\beta_i)_{\text{thr}} = \sqrt{1 - \frac{1}{\left[1 + \frac{(E_K)_{\text{thr}}}{E_0}\right]^2}}.$$

For the four transparent dielectrics of Table 4.7 (water, Lucite, sapphire, and diamond) (4.71) was used to determine the threshold kinetic energy $(E_K)_{\text{thr}}$ based on normalized threshold velocity $(\beta_i)_{\text{thr}}$ listed in column (3) and the results of the $(E_K)_{\text{thr}}$ calculation are listed in columns (4) and (5) of Table 4.7.

(b) In (4.66) we saw that Čerenkov radiation is emitted in a forward directed cone centered on the charged particle direction of motion. The cone is specified with the following Čerenkov angle θ_{Cer} given, based on consideration of energy and momentum conservation, as

$$\theta_{\text{Cer}} = \frac{1}{\beta_i n}. \quad (4.72)$$

For a given transparent dielectric the minimum Čerenkov angle $(\theta_{\text{Cer}})_{\text{min}}$ is related to the normalized threshold velocity $(\beta_i)_{\text{thr}}$ of (4.70) as follows

$$(\theta_{\text{Cer}})_{\text{min}} = \cos^{-1} \left\{ \frac{1}{(\beta_i)_{\text{thr}} n} \right\} = \cos^{-1} 1 = 0. \quad (4.73)$$

Table 4.7 Basic parameters of Čerenkov radiation produced by energetic electrons in various transparent dielectric materials

(1)	(2)	(3)	(4)	(5)	(6)	(7)
Dielectric absorber	n	$(\beta_i)_{\text{thr}} = \frac{1}{n}$	$(E_K)_{\text{thr}}/E_0$	$(E_K)_{\text{thr}}$ (MeV)	$(\theta_{\text{Cer}})_{\text{min}}$	$(\theta_{\text{Cer}})_{\text{max}}$
Water	1.33	0.752	0.517	0.264	0	41.2°
Lucite	1.50	0.667	0.342	0.175	0	48.2°
Sapphire	1.76	0.568	0.215	0.110	0	55.4°
Diamond	2.15	0.465	0.130	0.066	0	62.3°

The maximum Čerenkov angle $(\theta_{\text{Cer}})_{\text{max}}$ is determined from the following limit for $\beta_i \rightarrow 1$

$$(\theta_{\text{Cer}})_{\text{max}} = \lim_{\beta_i \rightarrow 1} \theta_{\text{Cer}} = \lim_{\beta_i \rightarrow 1} \cos^{-1} \left\{ \frac{1}{\beta_i n} \right\} = \cos^{-1} \frac{1}{n} \quad (4.74)$$

or

$$\begin{aligned} (\theta_{\text{Cer}})_{\text{max}} &= \lim_{(E_K)_i \rightarrow \infty} \theta_{\text{Cer}} \\ &= \lim_{(E_K)_i \rightarrow \infty} \cos^{-1} \left\{ \frac{1}{n} \left[1 - \left(1 + \frac{(E_K)_i}{E_0} \right)^{-2} \right]^{-\frac{1}{2}} \right\} \\ &= \cos^{-1} \frac{1}{n}. \end{aligned} \quad (4.75)$$

Equation (4.73) shows that $(\theta_{\text{Cer}})_{\text{min}} = 0$ for all transparent dielectric materials while, as shown by (4.75), $(\theta_{\text{Cer}})_{\text{max}}$ depends on the refractive index n of the material. Results of the calculation of $(\theta_{\text{Cer}})_{\text{max}}$ for four dielectric materials are listed in column (6) of Table 4.7.

The following conclusions can now be made with regard to Čerenkov angle θ_{Cer} :

- (1) For Čerenkov radiation to occur the charged particle velocity v_i must exceed the threshold velocity $(v_i)_{\text{thr}} = (\beta_i)_{\text{thr}}c = c/n$, where n is the index of refraction of the absorbing medium and c is the speed of light in vacuum.
- (2) The dynamic range of Čerenkov angles θ_{Cer} from $(\theta_{\text{Cer}})_{\text{min}} = 0$ to $(\theta_{\text{Cer}})_{\text{max}} = \cos^{-1} 1/n$ corresponds to:
 - (i) Range in β_i from $(\beta_i)_{\text{thr}} = 1/n$ to $\beta_i \rightarrow 1$ or
 - (ii) Range in $(E_K)_i$ from $(E_K)_{\text{thr}} = E_0[1/\sqrt{1 - (1/n)^2} - 1]$ to $(E_K)_i \rightarrow \infty$.
- (c) Plot of Čerenkov angle θ_{Cer} against normalized velocity β_i of (4.72) for electrons in various transparent dielectric absorbers (water, Lucite, sapphire, and diamond) in the range $0 \leq \beta_i \leq 1$ is shown in Fig. 4.18. For a given dielectric material the diagram provides $(\beta_i)_{\text{thr}} = 1/n$ at $\theta_{\text{Cer}} = 0$ and provides $(\theta_{\text{Cer}})_{\text{max}} = \cos^{-1}(1/n)$ at $\beta_i \rightarrow 1$.

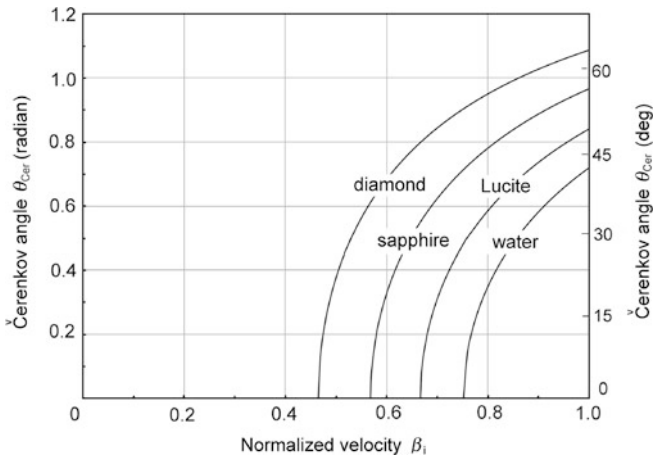


Fig. 4.18 Čerenkov angle θ_{Cer} against normalized velocity β_i of the incident electron

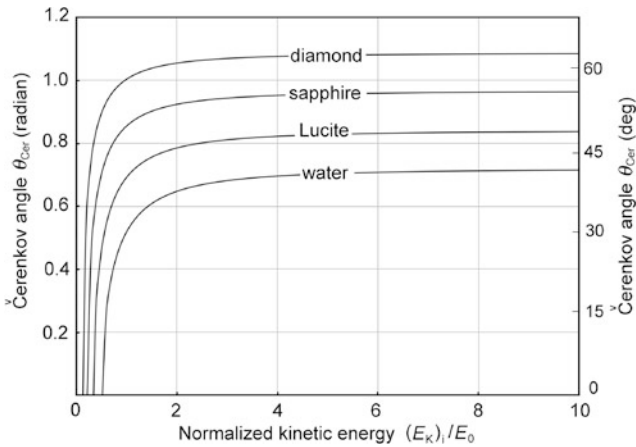


Fig. 4.19 Čerenkov angle θ_{Cer} against normalized kinetic energy $(E_K)_i/E_0$ of the incident electron

(d) Plot of Čerenkov angle θ_{Cer} against normalized kinetic energy $(E_K)_{\text{thr}}/E_0$ for electrons in various transparent dielectric absorbers in the range $0 \leq (E_K)_{\text{thr}}/E_0 \leq 10$ is shown in Fig. 4.19. For a given dielectric material the diagram provides $(E_K)_{\text{thr}}/E_0 = \{[1 - (1/n)^2]^{-1/2} - 1\}$ at $\theta_{\text{Cer}} = 0$ and provides $(\theta_{\text{Cer}})_{\text{max}} = \cos^{-1}(1/n)$ at $(E_K)_i \rightarrow \infty$.

Chapter 5 consists of **10 problems** covering two-particle collisions in 3 sections. Two particle collisions are well known in nuclear physics and radiation dosimetry. Typically, these collisions are characterized by an energetic projectile striking a stationary target and resulting in the most general case in an intermediate compound that subsequently decays into two reaction products.

Three categories of charged particles are considered as projectile: (1) light charged particles such as electron and positron, (2) heavy charged particle, such as proton and alpha particle, and (3) neutral particle, such as neutron. The possible targets are: (1) atoms as a whole, (2) atomic nuclei, and (3) atomic orbital electrons. The collisions are classified into three categories: (1) nuclear reactions, (2) elastic collisions, and (3) inelastic collisions.

The many types of interacting particles as well as the various possible categories of interactions result in a wide range of two-particle collisions of interest in nuclear physics and medical physics.

Problems in Sect. 5.1 deal with general aspects of two-particle collisions in classical physics, while Sect. 5.2 introduces nuclear reactions and addresses issues related to reaction Q value and threshold energy. Section 5.2 also deals with the relationship between reaction Q value and threshold energy and addresses the relationship between the two as well as the various methods to determine Q value, such as the atomic rest energy method, the nuclear rest energy method, and the binding energy method.

Section 5.3 concentrates on elastic two-particle collisions and energy transfer from the projectile to the target in this type of collision covering the general energy transfer as well as maximum energy transfer using classical and relativistic physics.

5.1 Collisions of Two Particles: General Aspects

5.1.Q1

(117)

An electron e of rest energy $m_e c^2 = 0.511$ MeV collides head-on with a stationary hydrogen atom H of rest energy $m_H c^2 \approx m_p c^2 + m_e c^2 = 938.272$ MeV + 0.511 MeV = 938.783 MeV.

- (a) Determine the fraction of the incident electron kinetic energy $(E_K^e)_i$ transferred as kinetic energy $(E_K^H)_f$ to the hydrogen atom, assuming that the collision is elastic.
- (b) Determine the minimum initial velocity v_i^e and minimum kinetic energy $(E_K^e)_i$ of the incident electron assuming that the collision is inelastic which means that the hydrogen atom, in addition to kinetic energy $(E_K^H)_f$ also acquires a characteristic energy E^* from the incident electron.

SOLUTION:

(a) For elastic one-dimensional collision, in conjunction with classical mechanics and the following notation:

v_i and v_f are the initial and final velocities, respectively, of the electron
 $u_i = 0$ and u_f are the initial and final velocities, respectively, of the hydrogen atom,

we consider conservation of momentum p and kinetic energy E_K as follows

$$p_i^e = p_f^e + p_f^H \quad \text{or} \quad m_e v_i = m_e v_f + m_H u_f \quad (5.1)$$

and

$$(E_K^e)_i = (E_K^e)_f + (E_K^H)_f \quad \text{or} \quad \frac{1}{2} m_e v_i^2 = \frac{1}{2} m_e v_f^2 + \frac{1}{2} m_H u_f^2. \quad (5.2)$$

We solve (5.1) for v_f and insert the result $v_f = v_i - (m_H/m_e)u_f$ into (5.2) to get

$$v_i = \frac{1}{2} \left(\frac{m_H}{m_e} + 1 \right) u_f \quad \text{or} \quad \frac{u_f}{v_i} = \frac{2m_e}{m_e + m_H}. \quad (5.3)$$

The fractional energy transfer $\Delta E_{\max}/(E_K^e)_i$ from the incident electron with kinetic energy $(E_K^e)_i$ to hydrogen atom $(E_K^H)_f$ is now given as follows

$$\begin{aligned} \frac{\Delta E_{\max}}{(E_K^e)_i} &= \frac{(E_K^H)_f}{(E_K^e)_i} = \frac{(E_K^e)_i - (E_K^e)_f}{(E_K^e)_i} = \frac{\frac{1}{2} m_H u_f^2}{\frac{1}{2} m_e v_i^2} = \frac{4m_e m_H}{(m_e + m_H)^2} \approx \frac{4m_e}{m_H} \\ &= 0.0022 = 0.22 \%. \end{aligned} \quad (5.4)$$

(b) In inelastic collision conservation of momentum remains the same as in elastic collision; however, the conservation of energy accounts also for the characteristic energy E^* that is transferred from the electron to hydrogen atom in addition to kinetic energy.

Conservation of momentum thus reads

$$m_e v_i = m_e v_f + m_H v_f \quad (5.5)$$

and conservation of energy

$$\frac{1}{2} m_e v_i^2 = \frac{1}{2} m_e v_f^2 + \frac{1}{2} m_H v_f^2 + E^*. \quad (5.6)$$

Again, we solve (5.5) for v_f and insert the result $v_f = v_i - (m_H/m_e)u_f$ into (5.6) to get the following quadratic equation for u_f as a function of v_i and E^*

$$\frac{m_H}{m_e} \left(\frac{m_H}{m_e} + 1 \right) u_f^2 - 2 \frac{m_H}{m_e} v_i u_f + 2 \frac{E^*}{m_e} = 0. \quad (5.7)$$

The two general solutions of (5.7) are

$$u_f = \frac{2 \frac{m_H}{m_e} v_i \pm \sqrt{\left(2 \frac{m_H}{m_e} v_i\right)^2 - 4 \frac{m_H}{m_e} \left(\frac{m_H}{m_e} + 1\right) \frac{2E^*}{m_e}}}{2 \frac{m_H}{m_e} \left(\frac{m_H}{m_e} + 1\right)}. \quad (5.8)$$

A physically meaningful solution to (5.7) requires that the radical in u_f be real and we thus get the following inequality

$$\left(2 \frac{m_H}{m_e} v_i\right)^2 \geq 4 \frac{m_H}{m_e} \left(\frac{m_H}{m_e} + 1\right) \frac{2E^*}{m_e}, \quad (5.9)$$

that gives the following result for the minimum required velocity $(v_i)_{\min}$ and minimum required kinetic energy $[(E_K^c)_i]_{\min}$ of the incident electron

$$(v_i)_{\min} = \sqrt{2E^* \frac{m_H + m_e}{m_e m_H}} \approx \sqrt{\frac{2E^*}{m_e}} \quad (5.10)$$

and

$$[(E_K^c)_i]_{\min} = \frac{m_e v_{\min}^2}{2} = E^* \left(1 + \frac{m_e}{m_H}\right). \quad (5.11)$$

The result for the minimum kinetic energy of (5.11) indicates that the incident electron must possess a kinetic energy that exceeds slightly the characteristic energy E^* .

5.1.Q2

(118)

Two billiard balls of unknown masses m_1 and m_2 collide, with the projectile m_1 moving with velocity v before collision and the target m_2 stationary before collision. After collision m_1 has a speed of $\frac{1}{2}v$ and moves at 90° to its original direction.

- Determine the direction of motion of billiard ball m_2 after the collision.
- Determine the ratio m_1/m_2 between the masses of the two billiard balls.
- Determine the velocity of billiard ball m_2 as a function of the incident velocity v of billiard ball m_1 .
- Determine the energy transfer fraction from ball m_1 to ball m_2 in the collision.

SOLUTION:

A schematic diagram of the collision is presented in Fig. 5.1, with m_1 and m_2 the two billiard balls; the origin of the Cartesian coordinate system at the center of the stationary ball m_2 before collision; $v_1 = v$ the velocity of ball m_1 before collision; $u_1 = \frac{1}{2}v$ the velocity of ball m_1 after collision; $v_2 = 0$ the velocity of ball m_2 before collision; u_2 the velocity of ball m_2 after collision; $\theta = \frac{1}{2}\pi$ the scattering angle of the projectile; and ϕ the recoil angle of the target.

Parameters of the collision process are evaluated using conservation of momentum p and kinetic energy E_K as follows:

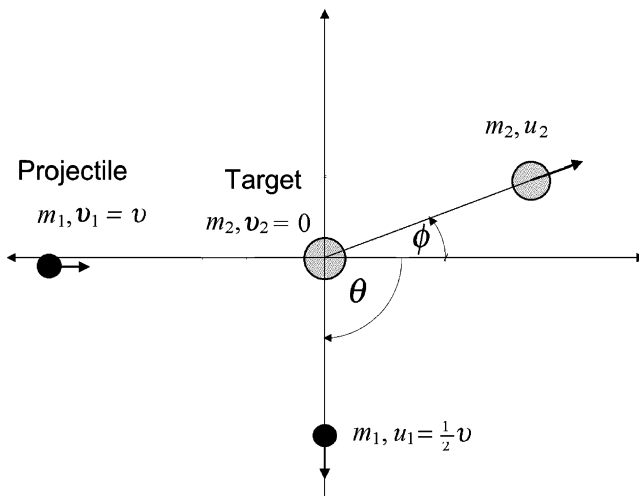


Fig. 5.1 Schematic diagram of the collision between billiard ball m_1 with billiard ball m_2 . The projectile m_1 is scattered with scattering angle $\theta = \frac{1}{2}\pi$, the target m_2 recoils with angle ϕ

Conservation of momentum (x component):

$$m_1 v_1 = m_1 u_1 \cos \theta + m_2 u_2 \cos \phi. \quad (5.12)$$

Conservation of momentum (y component):

$$0 = -m_1 u_1 \sin \theta + m_2 u_2 \sin \phi = -m_1 u_1 + m_2 u_2 \sin \phi. \quad (5.13)$$

Conservation of kinetic energy

$$\frac{1}{2} m_1 v_1^2 = \frac{1}{2} m_1 u_1^2 + \frac{1}{2} m_2 u_2^2. \quad (5.14)$$

(a) Recoil angle ϕ will be determined from (5.12) and (5.13) for conservation of momentum as follows (*note*: scattering angle $\theta = \frac{1}{2}\pi$). From (5.12) and (5.13) we get, respectively,

$$m_1 v_1 = m_2 u_2 \cos \phi \quad \text{or} \quad m_1 v = m_2 u_2 \cos \phi \quad (5.15)$$

and

$$m_1 u_1 = m_2 u_2 \sin \phi \quad \text{or} \quad m_1 \left(\frac{1}{2} v \right) = m_2 u_2 \sin \phi, \quad (5.16)$$

and from (5.15) and (5.16) it follows that $\tan \phi = \frac{1}{2}$ or $\phi = \arctan 0.5 = 26.57^\circ$.

(b) The ratio m_1/m_2 is calculated from the conservation of energy (5.14) in conjunction with (5.15) as follows

$$\frac{1}{2} m_1 v^2 = \frac{1}{2} m_1 \left(\frac{1}{2} v \right)^2 + \frac{1}{2} m_2 u_2^2 \quad \text{or} \quad \frac{m_1}{m_2} = \frac{4}{3} \left(\frac{u_2}{v} \right)^2 = \frac{4}{3} \left(\frac{m_1}{m_2} \right)^2 \cos^{-2} \phi, \quad (5.17)$$

where we used (5.15) to obtain $u_2/v = m_1/(m_2 \cos \phi)$ and insert it into (5.17) to get ratio m_1/m_2

$$\frac{m_1}{m_2} = \frac{3}{4} \cos^2 \phi = 0.60. \quad (5.18)$$

(c) Velocity u_2 as a function of incident velocity v is easily determined from (5.15) and (5.18)

$$u_2 = \frac{m_1}{m_2} \frac{v}{\cos \phi} = \frac{0.6v}{\cos(26.57^\circ)} = 0.67v. \quad (5.19)$$

(d) Energy transfer fraction $\Delta E_K/(E_K)_i$ where $(E_K)_i$ is the initial kinetic energy of ball m_1 is given as

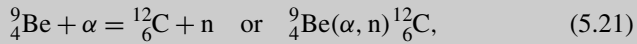
$$\Delta E_K = \frac{m_2 u_2^2}{2} = \frac{m_1 v^2}{2} - \frac{m_1 (\frac{1}{2} v)^2}{2} = \frac{3}{4} (E_K)_i \quad \text{or} \quad \frac{\Delta E_K}{(E_K)_i} = \frac{3}{4}. \quad (5.20)$$

5.2 Nuclear Reactions

5.2.Q1

(119)

In 1932 Chadwick discovered the neutron by bombarding beryllium ${}^9_4\text{Be}$ with α particles to produce neutron from the following nuclear reaction



where reactants ${}^9_4\text{Be}$ and α particle are the target and projectile, respectively, and ${}^{12}_6\text{C}$ and n are reaction products carbon-12 and neutron, respectively. In general, reaction energy is referred to as Q value; positive ($Q > 0$) in exothermic reaction and negative ($Q < 0$) in endothermic reaction.

- State three methods that can be used in calculation of Q value of a nuclear reaction.
- Determine Q value of the Chadwick nuclear reaction used in discovery of the neutron.
- Is the Chadwick reaction exothermic or endothermic? If it is exothermic, can the reaction occur spontaneously or at very low kinetic energy of α particle?

SOLUTION:

Figure 5.2 shows a schematic diagram of a binary nuclear reaction characterized as a two-particle collision of a projectile with rest mass M_1 , velocity v_1 , momentum p_1 , and kinetic energy $(E_K)_1$ striking a stationary target with mass M_2 and velocity $v_2 = 0$. An intermediate compound nucleus is produced temporarily and it decays into two reaction products, one of mass M_3 ejected with velocity v_3 at an angle ϕ to the incident projectile direction, and the other of mass M_4 ejected with velocity v_4 at an angle θ to the incident projectile direction of motion.

- (a) In any nuclear reaction the sum of total energies before the reaction $\sum_{i,\text{before}} E_i$ must equal the sum of total energies after the reaction $\sum_{i,\text{after}} E_i$, or

$$\sum_{i,\text{before}} E_i = \sum_{i,\text{after}} E_i \equiv \sum_i [(E_K)_i + M_i c^2] = \sum_i [(E_K)_i + M_i c^2]. \quad (5.22)$$

Any change in the sum of kinetic energies before and after the reaction is compensated by an equivalent change in the sum of rest energies before and after the reaction or an equivalent change in the sum of binding energies before and after the reaction. The so-called Q value of a nuclear reaction is used to quantify the change in kinetic energy.

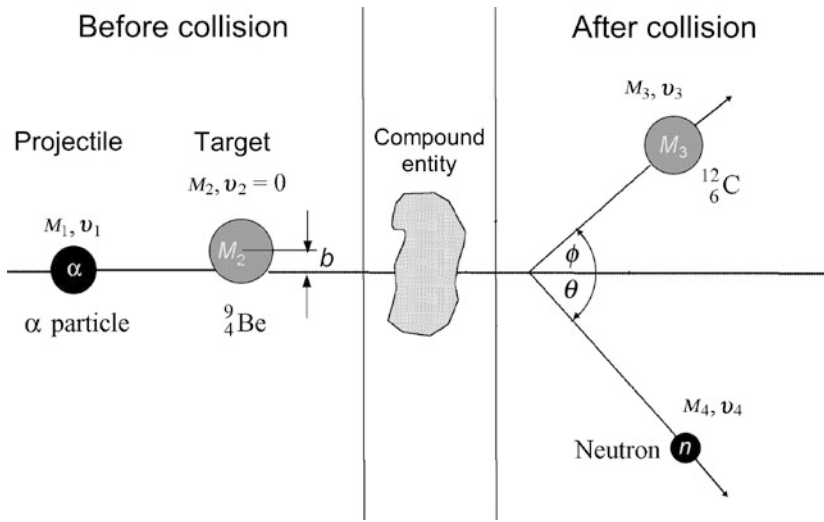


Fig. 5.2 Schematic diagram of a two-particle collision evolving into a nuclear reaction

Three methods for calculation of Q value of binary nuclear reactions are:

(1) *Kinetic energy method*: Subtract the kinetic energy of the reactants (projectile and target) before the reaction $\sum_{i,\text{before}} (E_K)_i$ from the sum of kinetic energies of the reaction products after the reaction $\sum_{i,\text{after}} (E_K)_i$, or

$$Q = \sum_{i,\text{after}} (E_K)_i - \sum_{i,\text{before}} (E_K)_i = [(E_K)_3 + (E_K)_4] - [(E_K)_1 + (E_K)_2]. \quad (5.23)$$

(2) *Rest energy method*: Subtract the sum of nuclear rest energies of the reaction products after the reaction $\sum_{i,\text{after}} M_i c^2$ from the sum of rest energies of reactants (projectile and target) before the reaction $\sum_{i,\text{before}} M_i c^2$, or

$$Q = \sum_{i,\text{before}} M_i c^2 - \sum_{i,\text{after}} M_i c^2 = (M_1 c^2 + M_2 c^2) - (M_3 c^2 + M_4 c^2). \quad (5.24)$$

Note that in (5.24) M stands for nuclear mass. If atomic masses \mathcal{M} rather than nuclear masses are used in calculations of Q values for nuclear reactions, in many instances the electron masses cancel out, so that there is no difference in the Q value result. However, in situations where electron masses do not cancel out, special care must be taken when using atomic masses to account for all electrons involved in the interaction.

(3) *Binding energy method*: Subtract the sum of total binding energies of reactants (projectile and target) before the reaction $\sum_{i,\text{before}} (E_B)_i$ from the sum of total

binding energies of reaction products after the reaction $\sum_{i,\text{after}}(E_B)_i$, or

$$Q = \sum_{i,\text{after}} (E_B)_i - \sum_{i,\text{before}} (E_B)_i = [(E_B)_3 + (E_B)_4] - [(E_B)_1 + (E_B)_2]. \quad (5.25)$$

(b) Q value of the Chadwick nuclear reaction ${}^9_4\text{Be}(\alpha, n){}^{12}_6\text{C}$ is calculated with the nuclear rest energy method as well as with the binding energy method, both described in (a). The results are summarized as follows:

Table 5.1 Summary of characteristics of the Chadwick 1932 neutron-discovery reaction

1				Nuclear rest energy (MeV)	Binding energy (MeV)
2	Projectile	m_1	α	3 727.3791	28.29569
3	Target	m_2	${}^9_4\text{Be}$	8 392.7499	58.16497
4	$\sum_{i,\text{before}}$			12 120.1290	86.46066
5	Reaction product	m_3	${}^{12}_6\text{C}$	11 174.8625	92.16175
6	Reaction product	m_4	n	939.5653	0
7	$\sum_{i,\text{after}}$			12 114.4278	92.16175

Q value calculated with the rest energy method is

$$Q = \sum_{i,\text{before}} M_i c^2 - \sum_{i,\text{after}} M_i c^2 = [m_\alpha c^2 + M({}^9_4\text{Be})c^2] - [M({}^{12}_6\text{C})c^2 + m_n c^2]$$

$$= 12120.1290 \text{ MeV} - 12 114.4278 \text{ MeV} = 5.701 \text{ MeV} \quad (5.26)$$

and with the binding energy method the result is the same, as expected

$$Q = \sum_{i,\text{after}} (E_B)_i - \sum_{i,\text{before}} (E_B)_i = [E_B({}^{12}_6\text{C}) + E_B(\text{n})] - [E_B(\alpha) + E_B({}^9_4\text{Be})]$$

$$= [92.16175 + 0] \text{ MeV} - [28.29569 + 58.16497] \text{ MeV} = 5.701 \text{ MeV}. \quad (5.27)$$

(c) The Chadwick nuclear reaction is exothermic with Q value of 5.7 MeV and thus, in principle, should occur spontaneously and release 5.7 MeV of energy irrespective of the kinetic energy of the incident α particle. However, the reaction cannot occur spontaneously or with low energy α particles because of the nuclear potential barrier that an α particle must overcome when it strikes a positively-charged target nucleus.

5.2.Q2

(120)

In Prob. 119 the Chadwick nuclear reaction ${}^9_4\text{Be}(\alpha, n){}^{12}_6\text{C}$ was shown to be exothermic with Q value of +5.7 MeV. This suggests that the inverse Chad-

wick reaction ${}^{12}_6\text{C}(n, \alpha){}^9_4\text{Be}$ is endothermic with Q value of -5.7 MeV and thus can occur only when the incident neutron possesses kinetic energy that is equal to or exceeds a threshold kinetic energy $(E_{\text{K}}^{\text{n}})_{\text{thr}}$.

- Derive the general expression for threshold kinetic energy $(E_{\text{K}})_{\text{thr}}$ of an endothermic nuclear reaction.
- Determine the relationship between threshold kinetic energy $(E_{\text{K}})_{\text{thr}}$ and Q value.
- Determine neutron threshold kinetic energy $(E_{\text{K}}^{\text{n}})_{\text{thr}}$ for the inverse Chadwick reaction.

SOLUTION:

(a) Threshold kinetic energy $(E_{\text{K}})_{\text{thr}}$ of an endothermic nuclear reaction is determined through the use of the so-called invariant $E^2 - p^2c^2 = \text{inv}$ applied to reactants (projectile and target) before the collision (in laboratory coordinate system) and to reaction products after the collision (in center-of-mass coordinate system), with

E total energy of the system either before or after collision.

p total momentum of the system either before or after collision.

c speed of light in vacuum.

Total energy and momentum before collision (in laboratory coordinate system):

$$E_{\text{before}} = E_{\text{thr}} + m_{20}c^2 = (E_{\text{K}})_{\text{thr}} + m_{10}c^2 + m_{20}c^2 = \sqrt{p_1^2c^2 + m_{10}c^2} + m_{20}c^2, \quad (5.28)$$

where E_{thr} is the total threshold energy of the projectile, $(E_{\text{K}})_{\text{thr}}$ is the kinetic energy of the projectile, and $p_1 = p_{\text{before}}$ is the momentum of the projectile, all given for before the collision and related through the standard relativistic expressions $E_{\text{thr}} = (E_{\text{K}})_{\text{thr}} + m_{10}c^2 = \sqrt{p_1^2c^2 + m_{10}c^2}$.

Total energy and momentum after collision (in center-of-mass coordinate system)

$$E_{\text{after}} = m_{30}c^2 + m_{40}c^2 \quad \text{and} \quad p_{\text{after}} = 0. \quad (5.29)$$

The invariant can now be expressed as follows:

$$\begin{aligned} E^2 - p^2c^2 &= E_{\text{before}}^2 - p_{\text{before}}^2c^2 \equiv (\sqrt{p_1^2c^2 + m_{10}c^2} + m_{20}c^2)^2 - p_1^2c^2 \\ &= E_{\text{after}}^2 - p_{\text{after}}^2c^2 \equiv (m_{30}c^2 + m_{40}c^2)^2 - 0, \end{aligned} \quad (5.30)$$

resulting in total threshold energy E_{thr} expressed as follows

$$E_{\text{thr}} = \frac{(m_{30}c^2 + m_{40}c^2)^2 - (m_{10}^2c^4 + m_{20}^2c^4)}{2m_{20}c^2} = (E_{\text{K}})_{\text{thr}} + m_{10}c^2 \quad (5.31)$$

and threshold kinetic energy $(E_K)_{\text{thr}}$

$$(E_K)_{\text{thr}} = \frac{(m_{30}c^2 + m_{40}c^2)^2 - (m_{10}c^2 + m_{20}c^2)^2}{2m_{20}c^2}. \quad (5.32)$$

(b) Q value for a nuclear reaction is defined as

$$Q = (m_{10}c^2 + m_{20}c^2) - (m_{30}c^2 + m_{40}c^2) \quad (5.33)$$

and can be expressed as follows

$$\begin{aligned} (m_{30}c^2 + m_{40}c^2)^2 &= [(m_{10}c^2 + m_{20}c^2) - Q]^2 \\ &= (m_{10}c^2 + m_{20}c^2)^2 - 2Q(m_{10}c^2 + m_{20}c^2) + Q^2. \end{aligned} \quad (5.34)$$

Inserting (5.34) into (5.32) results in the following expression for $(E_K)_{\text{thr}}$ in terms of Q

$$(E_K)_{\text{thr}} = -Q \left[\frac{m_{10}c^2 + m_{20}c^2}{m_{20}c^2} + \frac{Q}{2m_{20}c^2} \right] \approx -Q \left[1 + \frac{m_{10}}{m_{20}} \right], \quad (5.35)$$

where we can generally ignore the term $Q/(2m_{20}c^2)$, since $Q \ll 2m_{20}c^2$. In (5.35) the threshold kinetic energy of the projectile exceeds $|Q|$ by a relatively small amount to account for the conservation of energy and momentum in the nuclear reaction.

(c) Q value for the inverse Chadwick nuclear reaction ${}^{12}_6\text{C}(n, \alpha){}^9_4\text{Be}$ is determined either with the rest energy method or with the binding energy method

Rest energy method:

$$\begin{aligned} Q &= [m_n c^2 + M({}^{12}_6\text{C})c^2] - [m_\alpha c^2 + M({}^9_4\text{Be})c^2] \\ &= [939.5653 + 11174.8625] \text{ MeV} - [3727.3791 + 8392.7499] \text{ MeV} \\ &= -5.701 \text{ MeV}. \end{aligned} \quad (5.36)$$

Binding energy method:

$$\begin{aligned} Q &= [E_B({}^4_2\text{He}) + E_B({}^9_4\text{Be})] - [E_B(n) + E_B({}^{12}_6\text{C})] \\ &= [28.29569 + 58.16497] \text{ MeV} - [0 + 92.16175] = -5.70 \text{ MeV}. \end{aligned} \quad (5.37)$$

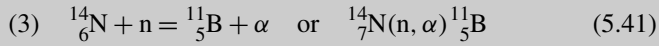
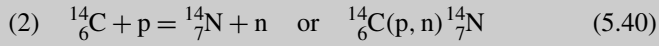
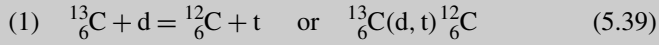
As shown in (5.35), the threshold kinetic energy of the neutron in the inverse Chadwick reaction is calculated as follows

$$\begin{aligned} (E_K^n)_{\text{thr}} &= -Q \left(1 + \frac{m_n}{M({}^{12}_6\text{C})} \right) = -(-5.70 \text{ MeV}) \times \left(1 + \frac{939.5653}{11174.8625} \right) \\ &= 6.18 \text{ MeV}. \end{aligned} \quad (5.38)$$

5.2.Q3

(121)

Consider the following three nuclear reactions:



For each reaction determine:

- (a) Q value.
- (b) Reaction type (exothermic or endothermic).
- (c) Threshold kinetic energy $(E_K)_{\text{thr}}$ of the projectile.
- (d) Coulomb barrier energy E_{Coul} .
- (e) Effective threshold energy $(E_K)_{\text{min}}$, i.e., minimum kinetic energy of the projectile required for the nuclear reaction to occur.

Summarize results of (a), (b), (c), (d), and (e) in Table 5.2A.

Table 5.2A Summary of results for the three nuclear reactions of Prob. 121

Nuclear reaction	Reaction Q value (MeV)	Reaction type	Threshold energy $(E_K)_{\text{thr}}$ (MeV)	Coulomb barrier E_{Coul} (MeV)	Effective threshold $(E_K)_{\text{min}}$ (MeV)
(1) ${}^{13}_6\text{C}(\text{d}, \text{t}){}^{12}_6\text{C}$					
(2) ${}^{14}_6\text{C}(\text{p}, \text{n}){}^{14}_7\text{N}$					
(3) ${}^{14}_7\text{N}(\text{n}, \alpha){}^{11}_5\text{B}$					

SOLUTION:

(a) Q value of a nuclear reaction $m_1(m_2, m_3)m_4$ is calculated either with the rest energy method

$$Q = (m_1c^2 + m_2c^2) - (m_3c^2 + m_4c^2) \quad (5.42)$$

or with the binding energy method

$$Q = [E_B(m_3) + E_B(m_4)] - [E_B(m_1) + E_B(m_2)]. \quad (5.43)$$

For a given nuclear reaction both methods give identical results when appropriate data given in Appendix A are used, as shown below for the three nuclear reactions.

Q value for nuclear reaction (1):

$$\begin{aligned} Q[{}^{13}_6\text{C}(\text{d}, \text{t}) {}^{12}_6\text{C}] &= [m_{\text{d}}c^2 + m({}^{13}_6\text{C})] - [m_{\text{t}}c^2 + m({}^{12}_6\text{C})] \\ &= [1875.6128 + 12109.4816] \text{ MeV} \\ &\quad - [2808.9209 + 11174.8625] \text{ MeV} \\ &= 1.311 \text{ MeV}, \end{aligned} \tag{5.44}$$

$$\begin{aligned} Q[{}^{13}_6\text{C}(\text{d}, \text{t}) {}^{12}_6\text{C}] &= [E_{\text{B}}(\text{t}) + E_{\text{B}}({}^{12}_6\text{C})] - [E_{\text{B}}(\text{d}) + E_{\text{B}}({}^{13}_6\text{C})] \\ &= [8.48182 + 92.16175] \text{ MeV} \\ &\quad - [2.22458 + 97.10812] \text{ MeV} \\ &= 1.311 \text{ MeV}. \end{aligned} \tag{5.45}$$

Q value for nuclear reaction (2):

$$\begin{aligned} Q[{}^{14}_6\text{C}(\text{p}, \text{n}) {}^{14}_7\text{N}] &= [m_{\text{p}}c^2 + m({}^{14}_6\text{C})c^2] - [m_{\text{n}}c^2 + m({}^{14}_7\text{N})] \\ &= [938.2720 + 13040.8703] \text{ MeV} \\ &\quad - [939.5654 + 13040.2028] \text{ MeV} \\ &= -0.6259 \text{ MeV}, \end{aligned} \tag{5.46}$$

$$\begin{aligned} Q[{}^{14}_6\text{C}(\text{p}, \text{n}) {}^{14}_7\text{N}] &= [E_{\text{B}}(\text{n}) + E_{\text{B}}({}^{14}_7\text{N})] - [E_{\text{B}}(\text{p}) + E_{\text{B}}({}^{14}_6\text{C})] \\ &= [0 + 104.65871] \text{ MeV} \\ &\quad - [0 + 105.28455] \text{ MeV} = -0.6258 \text{ MeV}. \end{aligned} \tag{5.47}$$

Q value for nuclear reaction (3):

$$\begin{aligned} Q[{}^{14}_7\text{N}(\text{n}, \alpha) {}^{11}_5\text{B}] &= [m_{\text{n}}c^2 + m({}^{14}_7\text{N})c^2] - [m_{\alpha}c^2 + m({}^{11}_5\text{B})] \\ &= [939.5655 + 13040.2028] \text{ MeV} \\ &\quad - [3727.3791 + 10252.5469] \text{ MeV} \\ &= -0.1577 \text{ MeV}, \end{aligned} \tag{5.48}$$

$$\begin{aligned} Q[{}^{14}_7\text{N}(\text{n}, \alpha) {}^{11}_5\text{B}] &= [E_{\text{B}}(\alpha) + E_{\text{B}}({}^{11}_5\text{B})] - [E_{\text{B}}(\text{n}) + E_{\text{B}}({}^{14}_7\text{N})] \\ &= [28.29569 + 76.20524] \text{ MeV} - [0 + 104.65871] \text{ MeV} \\ &= -0.1578 \text{ MeV}. \end{aligned} \tag{5.49}$$

(b) As established in **(a)**, nuclear reaction (1) has a positive Q value, while for reactions (2) and (3) Q values are negative. This implies that in reaction (1) mass is converted into kinetic energy shared by the reaction products and, because of the

energy release, the reaction is called exothermic. Conversely, for reactions (2) and (3) energy is converted into mass, and the reaction is called endothermic because it can only happen when the energy of the projectile matches or exceeds a well defined threshold energy.

(c) Threshold total energy of the projectile E_{thr} and the threshold kinetic energy $(E_K)_{\text{thr}}$ of the projectile are given as follows [see T(5.12) through T(5.15)]

$$E_{\text{thr}} = \frac{(m_{30}c^2 + m_{40}c^2)^2 - (m_{10}^2c^4 + m_{20}^2c^4)}{2m_{20}c^2} = (E_K)_{\text{thr}} + m_{10}c^2 \quad (5.50)$$

and

$$(E_K)_{\text{thr}} = \frac{(m_{30}c^2 + m_{40}c^2)^2 - (m_{10}c^2 + m_{20}c^2)^2}{2m_{20}c^2} \approx -Q \left(1 + \frac{m_{10}}{m_{20}} \right). \quad (5.51)$$

Threshold kinetic energy $(E_K)_{\text{thr}}$ for nuclear reaction (1):

$$(E_K)_{\text{thr}} = 0 \quad \text{since} \quad Q > 0. \quad (5.52)$$

Threshold kinetic energy $(E_K)_{\text{thr}}$ for nuclear reaction (2):

$$(E_K)_{\text{thr}} \approx -(-0.6259 \text{ MeV}) \times \left(1 + \frac{938.2720}{13040.8703} \right) = 0.671 \text{ MeV}. \quad (5.53)$$

Threshold kinetic energy $(E_K)_{\text{thr}}$ for nuclear reaction (3):

$$(E_K)_{\text{thr}} \approx -(-0.1577 \text{ MeV}) \times \left(1 + \frac{939.5655}{13040.2028} \right) = 0.170 \text{ MeV}. \quad (5.54)$$

(d) The Coulomb barrier is important in nuclear reactions where the projectile is a charged particle such as p, d, t, α , and heavy ion. Even in reactions with positive Q value resulting in $(E_K)_{\text{thr}} = 0$, for a positively charged projectile to penetrate the nucleus it must possess sufficient kinetic energy to overcome the Coulomb repulsion between the positively charged nucleus and the positively charged projectile. Thus in this situation, the Coulomb barrier E_{Coul} represents the effective threshold energy of the projectile unless, of course, $(E_K)_{\text{thr}} > E_{\text{Coul}}$ in which case $(E_K)_{\text{thr}}$ plays a role of the effective threshold kinetic energy.

The Coulomb barrier energy E_{Coul} is estimated from the Coulomb force F_{Coul} as follows

$$\begin{aligned} E_{\text{Coul}} &\approx \int_{\infty}^{R_{\text{sep}}} F_{\text{Coul}} \, dr = \frac{(Z_1 e)(Z_2 e)}{4\pi \epsilon_0} \int_{\infty}^{R_{\text{sep}}} \frac{dr}{r^2} = \frac{e^2}{4\pi \epsilon_0} \frac{Z_1 Z_2}{R_{\text{sep}}} \\ &\approx \frac{e^2}{4\pi \epsilon_0} \frac{Z_1 Z_2}{R_0 (\sqrt[3]{A_1} + \sqrt[3]{A_2})} = C \frac{Z_1 Z_2}{(\sqrt[3]{A_1} + \sqrt[3]{A_2})} \\ &\approx (1.15 \text{ MeV}) \times \frac{Z_1 Z_2}{(\sqrt[3]{A_1} + \sqrt[3]{A_2})}, \end{aligned} \quad (5.55)$$

Table 5.2B Summary of results for nuclear reactions (5.39), (5.40), and (5.41) of Prob. 121

Nuclear reaction	Reaction Q value (MeV)	Reaction type	Threshold energy $(E_K)_{\text{thr}}$ (MeV)	Coulomb barrier E_{Coul} (MeV)	Effective threshold kinetic energy $(E_K)_{\text{min}}$ (MeV)
(1) ${}^{13}_6\text{C}(d, t){}^{12}_6\text{C}$	+1.311	exothermic	0	2.0	$E_{\text{Coul}} = 2$ MeV
(2) ${}^{14}_6\text{C}(p, n){}^{14}_7\text{N}$	-0.6259	endothermic	0.671	2.11	$E_{\text{Coul}} = 2.11$ MeV
(3) ${}^{14}_7\text{N}(n, \alpha){}^{11}_5\text{B}$	-0.1577	endothermic	0.170	0	$(E_K)_{\text{thr}} = 0.17$ MeV

where

R_{sep} is the distance between the centers of the projectile and the target nucleus when the two are just touching (note: nuclear radius R is generally estimated as $R \approx R_0 \sqrt[3]{A}$ with the nuclear radius constant $R_0 = 1.25$ fm).

C is the Coulomb barrier constant [$e^2/(4\pi\epsilon_0 R_0) = 1.15$ MeV].

A is the atomic mass number of the target nucleus.

Z is the atomic number of the target nucleus.

For reaction (1) the Coulomb barrier energy E_{Coul} is

$$E_{\text{Coul}} \approx (1.15 \text{ MeV}) \times \frac{1 \times 6}{(\sqrt[3]{2} + \sqrt[3]{13})} = 2.0 \text{ MeV}. \quad (5.56)$$

For reaction (2) the Coulomb barrier energy E_{Coul} is

$$E_{\text{Coul}} \approx (1.15 \text{ MeV}) \times \frac{1 \times 6}{(\sqrt[3]{1} + \sqrt[3]{14})} = 2.11 \text{ MeV}. \quad (5.57)$$

For reaction (3) the Coulomb barrier energy E_{Coul} is $E_{\text{Coul}} = 0$ because the projectile (neutron) is not charged.

(e) Effective threshold energy $(E_K)_{\text{min}}$ is the minimum kinetic energy that the projectile must possess in order to trigger the nuclear reaction. For positively charged projectiles this energy is affected by the Coulomb barrier energy E_{Coul} and by Q value of the nuclear reaction; for neutral projectiles the Coulomb barrier does not play any role in determining the effective threshold energy.

For reaction (1) the effective threshold energy of the projectile $(E_K)_{\text{min}} = E_{\text{Coul}} = 2.0$ MeV.

For reaction (2) the effective threshold energy of the projectile $(E_K)_{\text{min}} = E_{\text{Coul}} = 2.11$ MeV.

For reaction (3) the effective threshold energy of the projectile $(E_K)_{\text{min}} = (E_K)_{\text{thr}} = 0.17$ MeV.

Summary of results for nuclear reactions (5.39), (5.40), and (5.41) is given in Table 5.2B.

5.3 Two-Particle Elastic Scattering: Energy Transfer

5.3.Q1

(122)

Center-of-Momentum or Center-of-Mass (CM) frame is an inertial frame where the momentum of the center of mass of a system is zero. In dealing with head-on (direct) elastic collision of two particles with masses m_1 and m_2 , the velocities of the two particles after the collision are reversed in the CM frame.

$$\mathbf{u}_{\text{CM},1} = -\mathbf{v}_{\text{CM},1} \quad \text{and} \quad \mathbf{u}_{\text{CM},2} = -\mathbf{v}_{\text{CM},2}, \quad (5.58)$$

where $\mathbf{v}_{\text{CM},1}$ and $\mathbf{u}_{\text{CM},1}$ are velocities of m_1 before and after the collision, respectively, and $\mathbf{v}_{\text{CM},2}$ and $\mathbf{u}_{\text{CM},2}$ are velocities of m_2 before and after the collision, respectively.

- (a) Using classical mechanics where the velocities of the two particles are much less than the speed of light, show that in a head-on elastic collision of two particles with masses m_1 and m_2 the velocities of the two particles after the collision are given by (5.58).
- (b) Calculate the classical maximum energy transfer ΔE_{max} and maximum momentum transfer Δp_{max} in a head-on elastic collision between two particles when the projectile particle of mass m_1 and velocity \mathbf{v} strikes a stationary target particle of m_2 .

SOLUTION:

(a) In the CM frame the total momentum of the two particles is zero. We apply conservation of momentum for before (indicated by label i) and after (indicated by label f) the collision to get

$$(\mathbf{p}_{\text{CM},1})_i + (\mathbf{p}_{\text{CM},2})_i = (\mathbf{p}_{\text{CM},1})_f + (\mathbf{p}_{\text{CM},2})_f = 0, \quad (5.59)$$

where $(\mathbf{p}_{\text{CM},1})_i = m_1 \mathbf{v}_{\text{CM},1}$ and $(\mathbf{p}_{\text{CM},2})_i = m_1 \mathbf{v}_{\text{CM},2}$ are, respectively, momenta of m_1 and m_2 before the collision, and $(\mathbf{p}_{\text{CM},2})_i = m_1 \mathbf{v}_{\text{CM},2}$ and $(\mathbf{p}_{\text{CM},2})_f = m_2 \mathbf{u}_{\text{CM},2}$ are, respectively, momenta of m_1 and m_2 after the collision. From (5.59) we get

$$(\mathbf{p}_{\text{CM},1})_i = -(\mathbf{p}_{\text{CM},2})_i \quad \text{and} \quad (\mathbf{p}_{\text{CM},1})_f = -(\mathbf{p}_{\text{CM},2})_f. \quad (5.60)$$

Since the collision between the two particles is elastic, total kinetic energy before collision is equal to total kinetic energy after the collision. Applying conservation of energy we get

$$\frac{(\mathbf{p}_{\text{CM},1})_i^2}{2m_1} + \frac{(\mathbf{p}_{\text{CM},2})_i^2}{2m_2} = \frac{(\mathbf{p}_{\text{CM},1})_f^2}{2m_1} + \frac{(\mathbf{p}_{\text{CM},2})_f^2}{2m_2}. \quad (5.61)$$

In (5.61) we used the classical relationship $E_K = p^2/2m$ where E_K is the particle kinetic energy, p is its momentum, and m is its mass. Inserting (5.60) into (5.61) we get the following expressions

$$\frac{(p_{CM,1})_i^2}{2(m_1 + m_2)} = \frac{(p_{CM,1})_f^2}{2(m_1 + m_2)} \quad \text{and} \quad \frac{(p_{CM,2})_i^2}{2(m_1 + m_2)} = \frac{(p_{CM,2})_f^2}{2(m_1 + m_2)}. \quad (5.62)$$

Two solutions are obtained from (5.62). Either

$$(\mathbf{p}_{CM,1})_f = (\mathbf{p}_{CM,1})_i \quad \text{and} \quad (\mathbf{p}_{CM,2})_f = (\mathbf{p}_{CM,2})_i \quad (5.63)$$

or

$$(\mathbf{p}_{CM,1})_f = -(\mathbf{p}_{CM,1})_i \quad \text{and} \quad (\mathbf{p}_{CM,2})_f = -(\mathbf{p}_{CM,2})_i. \quad (5.64)$$

The solution (5.63) states that the momenta of m_1 and m_2 did not change after the collision (i.e., no collision took place), and from (5.64) we conclude that the momenta of the two particles after the collision are opposite to their momenta before the collision. Hence, as stated in (5.58)

$$\mathbf{u}_{CM,1} = -\mathbf{v}_{CM,1} \quad \text{and} \quad \mathbf{u}_{CM,2} = -\mathbf{v}_{CM,2}. \quad (5.65)$$

(b) A head-on elastic collision between two particles, results in a maximum possible momentum transfer Δp_{\max} and maximum possible energy transfer ΔE_{\max} from the projectile m_1 to the target m_2 . Therefore,

$$\Delta p_{\max} = m_1 \mathbf{v} - m_1 \mathbf{u}_1 = m_2 \mathbf{u}_2, \quad (5.66)$$

and

$$\Delta E_{\max} = \frac{m_1 v^2}{2} - \frac{m_1 u_1^2}{2} = \frac{m_2 u_2^2}{2}, \quad (5.67)$$

where u_1 and u_2 are the velocities of the projectile m_1 and the target m_2 after collision, respectively.

A simple way to obtain u_2 is by using (5.58). In this approach, we use Galilean transformation to calculate the velocity of the target $\mathbf{v}_{CM,2}$ before the collision in the CM frame, apply (5.58) to get the velocity of the target $\mathbf{u}_{CM,2}$ after the collision in the CM frame, and then use Galilean transformation to calculate back the velocity of the target u_2 in the LAB frame after the collision. To apply this method, the velocity \mathbf{V}_{CM} of the CM frame with respect to the LAB frame needs to be determined.

The velocity of the CM frame \mathbf{V}_{CM} is the velocity of an inertial frame where the total momentum is equal to zero.

$$(\mathbf{p}_{CM,1})_i + (\mathbf{p}_{CM,2})_i = m_1 \mathbf{v}_{CM,1} + m_2 \mathbf{v}_{CM,2} = 0. \quad (5.68)$$

Let velocities of m_1 and m_2 in the LAB frame be, respectively, \mathbf{v}_1 and \mathbf{v}_2 . Using Galilean transformation the velocities of m_1 and m_2 in the CM frame are, respectively,

$$\mathbf{v}_{CM,1} = \mathbf{v}_1 - \mathbf{V}_{CM} \quad \text{and} \quad \mathbf{v}_{CM,2} = \mathbf{v}_2 - \mathbf{V}_{CM}. \quad (5.69)$$

Inserting (5.69) into (5.68) and solving for \mathbf{V}_{CM} we get

$$\mathbf{V}_{\text{CM}} = \frac{m_1 \mathbf{v}_1 + m_2 \mathbf{v}_2}{m_1 + m_2}. \quad (5.70)$$

For projectile with velocity $\mathbf{v}_1 = \mathbf{v}$ and a stationary target with $\mathbf{v}_2 = 0$, the velocity of the CM frame \mathbf{V}_{CM} is from (5.70) given by

$$\mathbf{V}_{\text{CM}} = \frac{m_1}{m_1 + m_2} \mathbf{v} \quad (5.71)$$

and the velocity of the target $\mathbf{v}_{\text{CM},2}$ before the collision in the CM frame is

$$\mathbf{v}_{\text{CM},2} = \mathbf{v}_2 - \mathbf{V}_{\text{CM}} = -\mathbf{V}_{\text{CM}}. \quad (5.72)$$

Using (5.58), the velocity of the target $\mathbf{u}_{\text{CM},2}$ after the collision in the CM frame is

$$\mathbf{u}_{\text{CM},2} = -\mathbf{v}_{\text{CM},2} = \mathbf{V}_{\text{CM}}. \quad (5.73)$$

The velocity \mathbf{u}_2 of the target after the collision in the LAB frame is obtained by applying an inverse Galilean transformation, thus,

$$\mathbf{u}_2 = \mathbf{u}_{\text{CM},2} + \mathbf{V}_{\text{CM}} = 2\mathbf{V}_{\text{CM}} = \frac{2m_1}{m_1 + m_2} \mathbf{v} = \frac{2}{m_1 + m_2} \mathbf{p}_i, \quad (5.74)$$

where $\mathbf{p}_i = m_1 \mathbf{v}$ is the initial momentum of the projectile m_1 .

Inserting (5.74) into (5.66) we get

$$\Delta p_{\text{max}} = m_2 \mathbf{u}_2 = \frac{2m_2}{m_1 + m_2} \mathbf{p}_i, \quad (5.75)$$

and inserting (5.74) into (5.67) we get

$$\Delta E_{\text{max}} = \frac{m_2 u_2^2}{2} = \frac{4m_2}{2(m_1 + m_2)^2} p_i^2 = \frac{4m_1 m_2}{(m_1 + m_2)^2} (E_K)_i, \quad (5.76)$$

where $(E_K)_i = p_i^2/2m_1$ is the initial kinetic energy of the projectile.

5.3.Q2

(123)

Relativistic analysis of the kinematics of a head-on (direct) elastic collision of two particles with rest masses m_{10} and m_{20} in the center-of-mass (CM) frame shows that the velocities of the two particles after the collision are opposite to their velocities before the collision.

$$u_{\text{CM},1} = -u_{\text{CM},1} \quad \text{and} \quad u_{\text{CM},2} = -u_{\text{CM},2}, \quad (5.77)$$

where $v_{CM,1}$ and $u_{CM,1}$ are velocities of m_{10} before and after the collision, respectively, and $v_{CM,2}$ and $u_{CM,2}$ are velocities of m_{20} before and after the collision, respectively.

- (a) Using relativistic mechanics show that the initial and final velocities in a head-on elastic collision of two particles with rest masses m_{10} and m_{20} are related by (5.77).
- (b) Calculate the relativistic maximum energy transfer ΔE_{\max} and relativistic maximum momentum transfer Δp_{\max} in a head-on elastic collision between two particles when the projectile particle of mass m_{10} and velocity v strikes a stationary target particle m_{20} .

SOLUTION:

(a) In the CM frame the total momentum of the two particles is zero. We apply conservation of momentum for before and after the collision to get

$$(p_{CM,1})_i + (p_{CM,2})_i = (p_{CM,1})_f + (p_{CM,2})_f = 0, \quad (5.78)$$

with $(p_{CM,1})_i$ and $(p_{CM,2})_i$ momenta of m_{10} and m_{20} , respectively, before collision and $(p_{CM,1})_f$ and $(p_{CM,2})_f$ momenta of m_{10} and m_{20} , respectively, after collision. From (5.78) we get

$$(p_{CM,1})_i = -(p_{CM,2})_i \quad \text{and} \quad (p_{CM,1})_f = -(p_{CM,2})_f. \quad (5.79)$$

Since the collision between the two particles is elastic, the total energy before collision is equal to the total energy after collision. Applying conservation of total energy we get

$$\begin{aligned} & \sqrt{E_{10}^2 + (p_{CM,1}c)_i^2} + \sqrt{E_{20}^2 + (p_{CM,2}c)_i^2} \\ &= \sqrt{E_{10}^2 + (p_{CM,1}c)_f^2} + \sqrt{E_{20}^2 + (p_{CM,2}c)_f^2}, \end{aligned} \quad (5.80)$$

where $E_{10} = m_{10}c^2$ and $E_{20} = m_{20}c^2$ are rest energies of m_{10} and m_{20} , respectively. In (5.80) we used the relativistic relationship $E = \sqrt{E_0^2 + (pc)^2}$ where E is the particle total energy, p is its momentum, $E_0 = m_0c^2$ is its rest energy, and c is the speed of light in vacuum.

Inserting (5.79) into (5.80) yields

$$\begin{aligned} & \sqrt{E_{10}^2 + (p_{CM,1}c)_i^2} + \sqrt{E_{20}^2 + (p_{CM,1}c)_i^2} \\ &= \sqrt{E_{10}^2 + (p_{CM,1}c)_f^2} + \sqrt{E_{20}^2 + (p_{CM,1}c)_f^2}, \end{aligned} \quad (5.81)$$

and

$$\begin{aligned} & \sqrt{E_{10}^2 + (p_{CM,2c})_i^2} + \sqrt{E_{20}^2 + (p_{CM,2c})_i^2} \\ &= \sqrt{E_{10}^2 + (p_{CM,2c})_f^2} + \sqrt{E_{20}^2 + (p_{CM,2c})_f^2}. \end{aligned} \quad (5.82)$$

Two possible solutions are obtained from (5.81) and (5.82). Either

$$(p_{CM,1})_f = (p_{CM,1})_i \quad \text{and} \quad (p_{CM,2})_f = (p_{CM,2})_i \quad (5.83)$$

or

$$(p_{CM,1})_f = -(p_{CM,1})_i \quad \text{and} \quad (p_{CM,2})_f = -(p_{CM,2})_i. \quad (5.84)$$

The solution (5.83) states that the momenta of m_{10} and m_{20} did not change after the collision (i.e., no collision took place) and from (5.84) we conclude that the momenta of the two particles after the collision are opposite in direction to their respective momenta before collision. Hence, as shown in (5.77),

$$u_{CM,1} = -v_{CM,1} \quad \text{and} \quad u_{CM,2} = -v_{CM,2}. \quad (5.85)$$

It should be noted that the respective total energies of the projectile $(E_{CM,1})_f$ and the target $(E_{CM,2})_f$ in the CM frame after the collision are equal to their respective energies before the collision, i.e.,

$$(E_{CM,1})_f = (E_{CM,1})_i \quad \text{and} \quad (E_{CM,2})_f = (E_{CM,2})_i. \quad (5.86)$$

(b) A head-on elastic collision between a projectile particle m_{10} with a stationary target m_{20} , results in a maximum possible momentum transfer Δp_{\max} and a maximum possible energy transfer ΔE_{\max} from the projectile m_{10} to the target m_{20} . Therefore,

$$\Delta p_{\max} = (p_1)_i - (p_1)_f = (p_2)_f, \quad (5.87)$$

and

$$\Delta E_{\max} = (E_2)_f - E_{20}, \quad (5.88)$$

where $(p_1)_i$ and $(p_1)_f$ are, respectively, momenta of the projectile m_{10} before and after the collision, $(p_2)_f$ is the momentum of the target m_{20} after the collision, $(E_2)_f$ is total energy of the target after the collision, and $E_{20} = m_{20}c^2$ is the rest energy of the target.

A simple way to obtain Δp_{\max} is by using (5.84). In this approach, we use the Lorentz transformation for energy and momentum to calculate the momentum $(p_{CM,2})_i$ and the total energy $(E_{CM,2})_i$ of the target before the collision in the CM frame, apply (5.84) to get the momentum of the target $(p_{CM,2})_f$ after the collision in the CM frame, and then use the inverse Lorentz transformation of energy and momentum to calculate back the momentum of the target $(p_2)_f$ in the LAB frame after the collision.

The Lorentz transformation of total energy E and momentum p in reference frame S to another reference frame S' moving with a relative speed of βc is

$$E' = \gamma(E - \beta pc) \quad \text{and} \quad p'c = \gamma(pc - \beta E), \quad (5.89)$$

where E' and p' are the total energy and momentum in S' , respectively, and $\gamma = (1 - \beta^2)^{-1/2}$. The inverse transformation of total energy E' and momentum p' back into reference frame S is given by

$$E = \gamma(E' + \beta p'c) \quad \text{and} \quad pc = \gamma(p'c + \beta E'). \quad (5.90)$$

The relativistic relative velocity β_{CM} of the CM frame with respect to the LAB frame for the two colliding particle system is determined as follows. Since the total initial momenta of the two particles is zero in the CM reference frame, we use (5.89) with $p'c = 0$ to get

$$0 = \gamma_{\text{CM}}(p_{\text{LAB}}c - \beta_{\text{CM}}E_{\text{LAB}}), \quad (5.91)$$

where p_{LAB} and E_{LAB} are, respectively, the total momentum and energy of the two particles in the LAB frame and $\gamma_{\text{CM}} = (1 - \beta_{\text{CM}}^2)^{-1/2}$. Since $\gamma_{\text{CM}} \geq 1$, the solution to (5.91) is

$$\beta_{\text{CM}} = \frac{p_{\text{LAB}}c}{E_{\text{LAB}}}. \quad (5.92)$$

For a system consisting of a projectile particle of rest mass m_{10} with momentum $(p_1)_i$ and a stationary target particle of rest mass m_{20} in the LAB reference frame, the initial momentum $(p_{\text{CM},2})_i$ and initial energy $(E_{\text{CM},2})_i$ of the target in the CM frame are, respectively,

$$(E_{\text{CM},2})_i = \gamma_{\text{CM}}[E_2 - \beta_{\text{CM}}(p_2)_i c] = \gamma_{\text{CM}}E_{20}, \quad (5.93)$$

and

$$(p_{\text{CM},2})_i = \gamma_{\text{CM}}[(p_2)_i c - \beta_{\text{CM}}E_2] = -\gamma_{\text{CM}}\beta_{\text{CM}}E_2 = -\gamma_{\text{CM}}\beta_{\text{CM}}E_{20}, \quad (5.94)$$

where $(p_2)_i = 0$ is the initial momentum of the target in the LAB frame and $E_2 = E_{20} = m_{20}c^2$ is the initial energy of the target in the LAB frame.

Inserting (5.94) into (5.84) and (5.93) into (5.86), we get

$$(p_{\text{CM},2})_f = -(p_{\text{CM},2})_i = \gamma_{\text{CM}}\beta_{\text{CM}}E_{20}, \quad (5.95)$$

and

$$(E_{\text{CM},2})_f = (E_{\text{CM},2})_i = \gamma_{\text{CM}}E_{20}. \quad (5.96)$$

Applying the inverse Lorentz transformation to obtain $(p_2)_f c$, we get

$$(p_2)_f c = \gamma_{\text{CM}}[(p_{\text{CM},2})_f + \beta_{\text{CM}}(E_{\text{CM},2})_f] = 2\gamma_{\text{CM}}^2\beta_{\text{CM}}E_{20}. \quad (5.97)$$

Using $\gamma_{\text{CM}} = (1 - \beta_{\text{CM}}^2)^{-1/2}$ and $\beta_{\text{CM}} = p_{\text{LAB}}c/E_{\text{LAB}}$, (5.97) becomes

$$(p_2)_f = \frac{2E_{\text{LAB}}p_{\text{LAB}}E_{20}}{E_{\text{LAB}}^2 - (p_{\text{LAB}}c)^2} = \Delta p_{\text{max}}. \quad (5.98)$$

Inserting $E_{\text{LAB}} = (\gamma m_{10} + m_{20})c^2$, $p_{\text{LAB}} = (p_1)_i = \frac{1}{c}\sqrt{(\gamma m_{10}c^2)^2 - (m_{10}c^2)^2}$, and $E_{20} = m_{20}c^2$ into (5.98) the relativistic maximum momentum transfer Δp_{max} is expressed as

$$\Delta p_{\text{max}} = \frac{2(\gamma m_{10} + m_{20})m_{20}}{m_{10}^2 + m_{20}^2 + 2\gamma m_{10}m_{20}}(p_1)_i. \quad (5.99)$$

To obtain the maximum energy transfer ΔE_{max} we apply the inverse Lorentz transformation given in (5.89) to get

$$(E_2)_f = \gamma_{\text{CM}}[(E_{\text{CM},2})_f + \beta_{\text{CM}}(p_{\text{CM},2})_f c] = (1 + \beta_{\text{CM}}^2)\gamma_{\text{CM}}^2 E_{20} = (2\gamma_{\text{CM}}^2 - 1)E_{20}. \quad (5.100)$$

Inserting (5.100) into (5.88) we get

$$\Delta E_{\text{max}} = (E_2)_f - E_{20} = 2(\gamma_{\text{CM}}^2 - 1)E_{20} = \frac{2(p_{\text{LAB}}c)^2 E_{20}}{E_{\text{LAB}}^2 - (p_{\text{LAB}}c)^2}. \quad (5.101)$$

Using $(p_{\text{LAB}}c)^2 = (p_1c)_i^2 = (\gamma + 1)E_{10}(E_{\text{K}})_i = (\gamma m_{10}c^2)^2 - (m_{10}c^2)^2$, where $(E_{\text{K}})_i$ is the initial kinetic energy for projectile m_{10} , the relativistic maximum energy transfer ΔE_{max} is expressed as

$$\Delta E_{\text{max}} = \frac{2(\gamma + 1)m_{10}m_{20}}{m_{10}^2 + m_{20}^2 + 2\gamma m_{10}m_{20}}(E_{\text{K}})_i. \quad (5.102)$$

5.3.Q3

(124)

An alpha particle of initial kinetic energy $(E_{\text{K}}^\alpha)_i = 5 \text{ MeV}$ collides with a stationary oxygen-17 (O-17) nucleus. The α particle is scattered at a scattering angle θ of 53.9° and the oxygen nucleus recoils at a recoil angle ϕ of 59.4° . The rest energy of the α particle $m_\alpha c^2$ is 3727.4 MeV, the rest energy of the oxygen-17 nucleus $m_{\text{O}}c^2$ is 15830.5 MeV. Use the following convention in your calculations:

v_α and $(E_{\text{K}}^\alpha)_i$ are velocity and kinetic energy, respectively, of the α particle before collision,

v_α and $(E_{\text{K}}^\alpha)_f$ are velocity and kinetic energy, respectively, of the α particle after collision,

v_{O} and $(E_{\text{K}}^{\text{O}})_f$ are velocity and kinetic energy, respectively, of the oxygen nucleus after collision.

- (a) Prepare a graph showing schematic representation of the scattering process.
- (b) Determine the ratio u_α/u_O of final velocities u_α and u_O for the α particle and the oxygen nucleus, respectively, after collision.
- (c) Determine the ratio v_α/u_α of velocities v_α and u_α of the α particle before and after collision, respectively.
- (d) Determine the energy transfer ΔE_K and the energy transfer fraction $\Delta E_K/(E_K^\alpha)_i$ from the α particle to the oxygen nucleus in the collision.
- (e) State conditions for maximum energy transfer ΔE_{\max} and the maximum energy transfer fraction $[\Delta E/(E_K^\alpha)_i]_{\max}$ that would occur under these conditions.

SOLUTION:

The required quantities for this question are calculated using conservation of momentum p and kinetic energy E_K as well as a graph showing a schematic diagram of the collision in Fig. 5.3.

Conservation of momentum (x component):

$$m_\alpha v_\alpha = m_\alpha u_\alpha \cos \theta + m_O u_O \cos \phi. \quad (5.103)$$

Conservation of momentum (y component):

$$0 = -m_\alpha u_\alpha \sin \theta + m_O u_O \sin \phi. \quad (5.104)$$

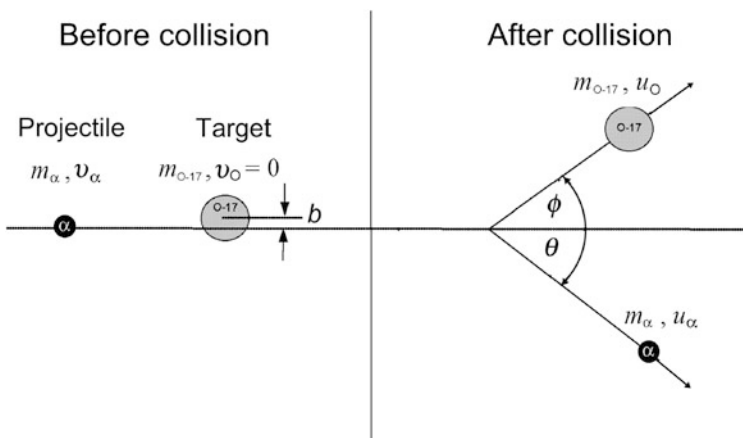


Fig. 5.3 Schematic representation of the scattering process

Conservation of kinetic energy:

$$(E_K^\alpha)_i = (E_K^\alpha)_f + (E_K^O)_f \quad \text{or} \quad \frac{1}{2}m_\alpha v_\alpha^2 = \frac{1}{2}m_\alpha u_\alpha^2 + \frac{1}{2}m_O u_O^2. \quad (5.105)$$

The mass ratio m_α/m_O and its inverse m_O/m_α appear in several equations used here, so we state them now

$$\frac{m_\alpha}{m_O} = \frac{3727.4}{15830.5} = 0.236 \quad \text{and} \quad \frac{m_O}{m_\alpha} = 4.24. \quad (5.106)$$

(a) A schematic representation of the scattering process is shown in Fig. 5.3.

(b) The velocity ratio u_α/u_O is determined from (5.104) as follows

$$\frac{u_\alpha}{u_O} = \frac{m_O \sin \phi}{m_\alpha \sin \theta} = 4.24 \times \frac{\sin(59.4^\circ)}{\sin(53.9^\circ)} = 4.52. \quad (5.107)$$

(c) The velocity ratio v_α/u_α is determined from (5.103) in conjunction with (5.107)

$$\begin{aligned} \frac{v_\alpha}{u_\alpha} &= \cos \theta + \frac{m_O u_O}{m_\alpha u_\alpha} \cos \phi = \cos(53.9^\circ) + \frac{4.24}{4.52} \cos(59.4^\circ) \\ &= 0.589 + 0.478 = 1.067. \end{aligned} \quad (5.108)$$

(d) Energy transfer ΔE is equal to kinetic energy of the oxygen nucleus after the collision and is calculated from the well-known equation (T5.25) derived from the conservation of energy and momentum considerations laid out in (5.103) through (5.105)

$$\begin{aligned} \Delta E &= (E_K^O)_f = \frac{4m_\alpha m_O}{(m_\alpha + m_O)^2} (E_K^\alpha)_i \cos^2 \phi \\ &= \frac{4 \times 3727.4 \times 15830.5}{(3727.4 + 15830.5)^2} \times (5 \text{ MeV}) \times \cos^2(59.4^\circ) = 0.8 \text{ MeV}. \end{aligned} \quad (5.109)$$

Energy transfer fraction $\Delta E/(E_K^\alpha)_i$ is now simply given as

$$\begin{aligned} \frac{\Delta E}{(E_K^\alpha)_i} &= \frac{4m_\alpha m_O}{(m_\alpha + m_O)^2} \cos^2 \phi = \frac{4 \times 3727.4 \times 15830.5}{(3727.4 + 15830.5)^2} \times \cos^2(59.4^\circ) \\ &= 0.617 \times 0.259 = 0.16, \end{aligned} \quad (5.110)$$

indicating that in our specific collision process (at recoil angle $\phi = 59.4^\circ$) 16 % of the incident α particle energy (0.8 MeV) is transferred to the oxygen nucleus and 84 % (4.2 MeV) is kept by the α particle.

(e) Maximum energy transfer fraction $[\Delta E/(E_K^\alpha)_i]_{\max}$ would occur in a head-on collision for recoil angle $\phi = 0$ and would amount to 61.7 %, as shown below

$$\left[\frac{\Delta E}{(E_K^\alpha)_i} \right]_{\max} = \frac{4m_\alpha m_O}{(m_\alpha + m_O)^2} \times \cos^2 0 = \frac{4 \times 3727.4 \times 15830.5}{(3727.4 + 15830.5)^2} = 0.617. \quad (5.111)$$

5.3.Q4

(125)

As derived in Prob. 123, the general expression for maximum energy transfer ΔE_{\max} from a projectile with rest energy $m_{10}c^2$ and incident kinetic energy $(E_K)_i$ to a target at rest ($v = 0$) with rest energy $m_{20}c^2$ in a head-on (direct hit) elastic collision is given as (T5.47)

$$\Delta E_{\max} = \frac{2(\gamma + 1)m_{10}m_{20}}{m_{10}^2 + m_{20}^2 + 2\gamma m_{10}m_{20}} (E_K)_i. \quad (5.112)$$

Several simplifying expressions are available for expressing $(\Delta E_K)_{\max}$ depending on the relative values of projectile rest mass m_{10} and target rest mass m_{20} as well as for $\gamma \rightarrow 1$ and $\gamma \rightarrow \infty$. Provide a summary of expressions for ΔE_{\max} under the following conditions:

- (a) Lorentz factor $\gamma \rightarrow 1$ (classical limit).
- (b) Lorentz factor $\gamma \rightarrow \infty$.
- (c) $m_{10} \ll m_{20}$.
- (d) $m_{10} = m_{20}$ (projectile m_{10} and target m_{20} are distinguishable).
- (e) $m_{10} = m_{20}$ (projectile m_{10} and target m_{20} are indistinguishable).
- (f) $m_{10} \gg m_{20}$.

SOLUTION:

(a) In the classical limit as $E_K \rightarrow 0$ (or $\gamma \rightarrow 1$), the classical limit of (5.112) reads as follows

$$\Delta E_{\max}^{\text{clas}} = \lim_{\substack{(E_K)_i \rightarrow \frac{m_{10}v_1^2}{2} \\ \gamma \rightarrow 1}} \Delta E_{\max} = \frac{4m_{10}m_{20}}{(m_{10} + m_{20})^2} (E_K)_i, \quad (5.113)$$

so that the maximum energy transfer fraction $\eta(E_K) = \Delta E_{\max}/(E_K)_i$ is independent of $(E_K)_i$ and depends solely on the rest masses m_{10} and m_{20} of the projectile P and target T, respectively. Equation (5.113) is well known in classical physics for determination of maximum energy transfer in classical collisions.

(b) In the limit as kinetic energy $(E_K)_i$ becomes very large $[(E_K)_i \rightarrow \infty]$, the Lorentz factor γ also approaches infinity and ΔE_{\max} approaches $(E_K)_i$

$$\lim_{\substack{(E_K)_i \rightarrow \infty \\ \gamma \rightarrow \infty}} \Delta E_{\max} = \lim_{\substack{(E_K)_i \rightarrow \infty \\ \gamma \rightarrow \infty}} \frac{2(\gamma + 1)m_{10}m_{20}}{m_{10}^2 + m_{20}^2 + 2\gamma m_{10}m_{20}} (E_K)_i = (E_K)_i. \quad (5.114)$$

(c) For projectile rest mass m_{10} much smaller than the target rest mass m_{20} , i.e., $m_{10} \ll m_{20}$, the following approximation applies

$$\begin{aligned} \Delta E_{\max} &= \frac{2(\gamma + 1)m_{10}m_{20}}{m_{10}^2 + m_{20}^2 + 2\gamma m_{10}m_{20}} (E_K)_i \approx \frac{2(\gamma + 1)}{\frac{m_{20}}{m_{10}} + 2\gamma} (E_K)_i \\ &= \frac{2m_{10}c^2}{\frac{m_{20}}{m_{10}} + 2\gamma} \times \frac{\beta^2}{1 - \beta^2}. \end{aligned} \quad (5.115)$$

In the classical limit $\gamma \rightarrow 1$ and $(E_K)_i \rightarrow \frac{1}{2}m_{10}v_1^2$, so that (5.115) transforms into

$$\Delta E_{\max}^{\text{class}} \approx \frac{4m_{10}}{m_{20}} (E_K)_i. \quad (5.116)$$

(d) When the projectile m_{10} and the target m_{20} are *distinguishable* and have equal mass, i.e., $m_{10} = m_{20}$, the maximum energy transfer $(\Delta E_K)_{\max}$ is equal to $(E_K)_i$ in general and the same holds in the classical limit.

(e) When the projectile m_{10} and the target m_{20} are *indistinguishable* and have equal mass, i.e., $m_{10} = m_{20}$, an assumption is made that the particle that leaves the collision site with the larger energy is the incident particle. This means that the maximum possible energy transfer $(\Delta E_K)_{\max}$ is equal to $\frac{1}{2}(E_K)_i$. Thus, $(\Delta E_K)_{\max} = \frac{1}{2}(E_K)_i$ both in general and in the classical limit.

(f) For projectile mass m_{10} much larger than the target mass m_{20} , i.e., $m_{10} \gg m_{20}$, the following approximation applies

$$\begin{aligned} (\Delta E_K)_{\max} &= \frac{2(\gamma + 1)m_{10}m_{20}}{m_{10}^2 + m_{20}^2 + 2\gamma m_{10}m_{20}} (E_K)_i \approx \frac{2(\gamma + 1)}{\frac{m_{10}}{m_{20}} + 2\gamma} (E_K)_i \\ &= \frac{2m_{10}c^2}{\frac{m_{10}}{m_{20}} + 2\gamma} \times \frac{\beta^2}{1 - \beta^2}. \end{aligned} \quad (5.117)$$

In the classical limit $\gamma \rightarrow 1$ and $(E_K)_i \rightarrow \frac{1}{2}m_{10}v_1^2$ so that (5.117) transforms into

$$(\Delta E_K)_{\max}^{\text{clas}} \approx 2m_{20}v_1^2. \quad (5.118)$$

Note: In (5.115) and (5.117) we used the following identity

$$(\gamma + 1)(E_K)_i = (\gamma + 1)(\gamma - 1)E_0 = (\gamma^2 - 1)E_0 = \frac{\beta^2}{1 - \beta^2}E_0. \quad (5.119)$$

Relativistic and classical maximum energy transfers from projectile P to target T in elastic head-on collision are summarized in Tables 5.3 and 5.4, respectively.

Table 5.3 Maximum energy transfer $(\Delta E_K)_{\max}$ from projectile P with incident kinetic energy $(E_K) = (\gamma - 1)m_{10}c^2$ and rest mass m_{10} to stationary target T with rest mass m_{20} in an elastic head-on collision. *Note:* $(\Delta E_K)_{\max}$ depends on mass of projectile P (m_{10}) and target T (m_{20}) as well as on the incident kinetic energy $(E_K)_i$ of the projectile

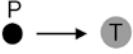

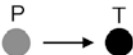
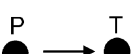

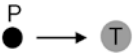

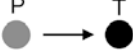
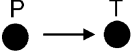

Projectile m_{10} Target m_{20}	Relative magnitude	Projectile & target	$(\Delta E_K)_{\max}$	Example
	$m_{10} \neq m_{20}$	Do not differ appreciably	$\frac{2(\gamma+1)m_{10}m_{20}(E_K)_i}{m_{10}^2+m_{20}^2+2\gamma m_{10}m_{20}}$	P: α particle T: carbon nucleus
	$m_{10} \ll m_{20}$	P much smaller than T	$\frac{2m_{10}c^2}{m_{20}+2\gamma} \times \frac{\beta^2}{1-\beta^2}$	P: electron T: nucleus
	$m_{10} = m_{20}$	P and T have equal mass and are distinguishable	$(E_K)_i = (\gamma - 1)m_{10}c^2$	P: positron T: orbital electron
	$m_{10} = m_{20}$	P and T have equal mass and are indistinguishable	$\frac{1}{2}(E_K)_i = \frac{1}{2}(\gamma - 1)m_{10}c^2$	P: electron T: orbital electron
	$m_{10} \gg m_{20}$	P much larger than T	$2m_{20}c^2 \frac{\beta^2}{1-\beta^2}$	P: heavy CP T: orbital electron

Table 5.4 Classical limit of the maximum energy transfer $(\Delta E_K)_{\max}$ from projectile P with incident velocity v_1 , kinetic energy $(E_K)_i = \frac{1}{2}m_{10}v_1^2$ and mass m_{10} to stationary target T with mass m_{20} in an elastic head-on collision. *Note:* $(\Delta E_K)_{\max}$ depends on mass of projectile P (m_{10}) and mass of target T (m_{20}) but does not depend on the incident kinetic energy $(E_K)_i$ of the projectile

Projectile m_{10} Target m_{20}	Relative magnitude	Comment on projectile & target	$(\Delta E_K)_{\max}$	Typical example
	$m_{10} \neq m_{20}$	Do not differ appreciably	$\frac{4m_{10}m_{20}}{(m_{10}+m_{20})^2} (E_K)_i$	P: Billiard ball (300 g) T: Billiard ball (500 g)
	$m_{10} \ll m_{20}$	P much smaller than T	$\sim 4 \frac{m_{10}}{m_{20}} (E_K)_i$ $= 2 \frac{m_{10}^2 v_1^2}{m_{20}}$	P: Styrofoam billiard ball T: Regular billiard ball
	$m_{10} = m_{20}$	P and T have equal mass and are distinguishable	$(E_K)_i = \frac{1}{2}m_{10}v_1^2$	P: Red billiard ball T: Red billiard ball
	$m_{10} = m_{20}$	P and T have equal mass and are indistinguishable	$\frac{1}{2}(E_K)_i = \frac{1}{4}m_{10}v_1^2$	P: Red billiard ball T: Black billiard ball
	$m_{10} \gg m_{20}$	P much larger than T	$\sim 4 \frac{m_{20}}{m_{10}} (E_K)_i$ $= 2m_{20}v_1^2$	P: Regular billiard ball T: Styrofoam billiard ball

5.3.Q5

(126)

The maximum energy transfer fraction $[\eta(E_K)]_{\max} = \Delta E_{\max}/(E_K)_i$ from a projectile with rest energy $m_{10}c^2$ and incident kinetic energy $(E_K)_i$ to a target at rest ($v = 0$) with rest energy $m_{20}c^2$ in a head-on (direct hit) elastic collision is given as (T5.47)

$$[\eta(E_K)]_{\max} = \frac{\Delta E_{\max}}{(E_K)_i} = \frac{2(\gamma + 1)m_{10}m_{20}}{m_{10}^2 + m_{20}^2 + 2\gamma m_{10}m_{20}}. \tag{5.120}$$

Determine the maximum energy transfer fraction $[\eta(E_K)]_{\max}$ and its classical limit $\eta_{\max}^{\text{class}}$ for a head-on elastic collision of an α particle ($m_{\alpha}c^2 = 3727.4 \text{ MeV}$) with:

- (a) Oxygen-16 nucleus ($m_{\text{O-16}}c^2 = 14895.1 \text{ MeV}$) and α particle kinetic energy $(E_K)_i$ of 5.5 MeV, 500 MeV, 2 GeV, and 20 GeV. Summarize your answers in row (3) of Table 5.5A and enter them on the O-16 curve of the graph $[\eta(E_K)]_{\max}$ vs $(E_K)_i$ of Fig. 5.4.
- (b) Lead-206 nucleus ($m_{\text{Pb-206}}c^2 = 191820 \text{ MeV}$) and α particle kinetic energy $(E_K)_i$ of 5.5 MeV, 500 MeV, 2 GeV, and 20 GeV. Summarize your answers in row (4) of Table 5.5A and enter them on the Pb-216 curve of the graph $[\eta(E_K)]_{\max}$ vs $(E_K)_i$ of Fig. 5.4.
- (c) Orbital electron of the target and α particle kinetic energy $(E_K)_i$ of 5.5 MeV, 500 MeV, 2 GeV, and 20 GeV. Summarize your answers in row (5) of Table 5.5A.
- (d) Determine the initial kinetic energy $(E_K)_i$ of α particle that would produce in an elastic head-on collision with lead-206 nucleus a maximum energy transfer fraction $[\eta(E_K)]_{\max}$ twice as large as that calculated for a 100 MeV α particle.

Table 5.5A Summary of results for Prob. 126 (a), (b), and (c)

(1)	$(E_K)_i$	Classical limit	5.5 MeV	500 MeV	2 GeV	20 GeV
(2)	$\gamma = \frac{1}{\sqrt{1-\beta^2}}$					
(3)	α vs O-16 $[\eta(E_K)]_{\max}$					
(4)	α vs Pb-206 $[\eta(E_K)]_{\max}$					
(5)	α vs electron $[\eta(E_K)]_{\max}$					

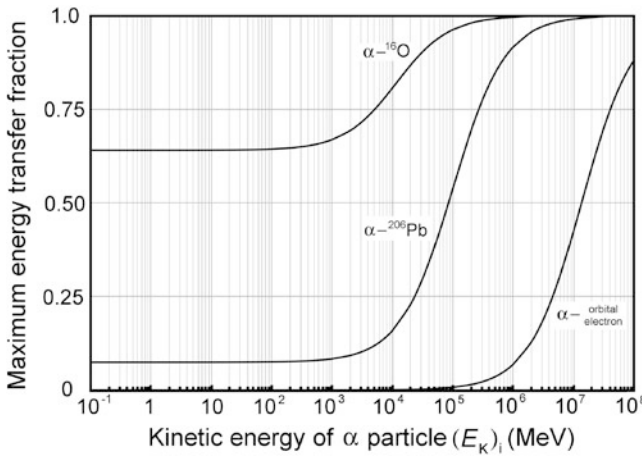


Fig. 5.4 Maximum energy transfer fraction $[\eta(E_K)]_{\max}$ against incident kinetic energy $(E_K)_i$ given in (5.120) for α particles interacting with oxygen-16 (O-16), lead-206 (Pb-206), and “free” orbital electron

SOLUTION:

Since the maximum energy transfer fraction $[\eta(E_K)]_{\max}$ is a function of the Lorentz factor γ of the projectile, we first calculate γ from kinetic energy E_K of the α particle using the basic definition of relativistic kinetic energy E_K (T1.58)

$$(E_K)_i = (\gamma - 1)m_\alpha c^2 \quad \text{or} \quad \gamma = 1 + \frac{(E_K)_i}{m_\alpha c^2} \tag{5.121}$$

and summarize the answers in row (2) of Table 5.5B.

(a) Elastic collision between projectile (α particle) and target [oxygen-16 (O-16) nucleus] for α -particle kinetic energies $(E_K)_i$ of 5.5 MeV, 500 MeV, 2 GeV, and 20 GeV.

The maximum energy transfer fraction $[\eta(E_K)]_{\max}$ is calculated from (T5.47)

$$[\eta(E_K)]_{\max} = \frac{(\Delta E_K)_{\max}}{(E_K)_i} = \frac{2(\gamma + 1)m_\alpha c^2 m_{O-16} c^2}{(m_\alpha c^2)^2 + (m_{O-16} c^2)^2 + 2\gamma m_\alpha c^2 m_{O-16} c^2} \tag{5.122}$$

and the results for the four α particle kinetic energies are displayed in row (3) of Table 5.5B and entered on the O-16 curve of Fig. 5.5.

The classical limit η_{clas} of $[\eta(E_K)]_{\max}$ is calculated from the classical expression (T5.48)

$$\eta_{\max}^{\text{class}} = \lim_{\gamma \rightarrow 1} \eta(E_K) = \frac{4m_\alpha c^2 m_{O-16} c^2}{(m_\alpha c^2 + m_{O-16} c^2)^2} = \frac{4 \times 3727.3 \times 14895.1}{(3727.3 + 14895.1)^2} = 0.64. \tag{5.123}$$

Table 5.5B Summary of results for Prob. 126 (a), (b), and (c)

(1) $(E_K)_i$	Classical limit	5.5 MeV	500 MeV	2 GeV	20 GeV
(2) $\gamma = \frac{1}{\sqrt{1-\beta^2}}$	1.0	1.0015	1.134	1.537	6.366
(3) α vs O-16 $[\eta(E_K)]_{\max}$	0.640	0.6405	0.655	0.693	0.868
(4) α vs Pb-206 $[\eta(E_K)]_{\max}$	0.075	0.075	0.079	0.093	0.229
(5) α vs electron $[\eta(E_K)]_{\max}$	5.482×10^{-4}	5.487×10^{-4}	5.490×10^{-4}	6.953×10^{-4}	20.2×10^{-4}

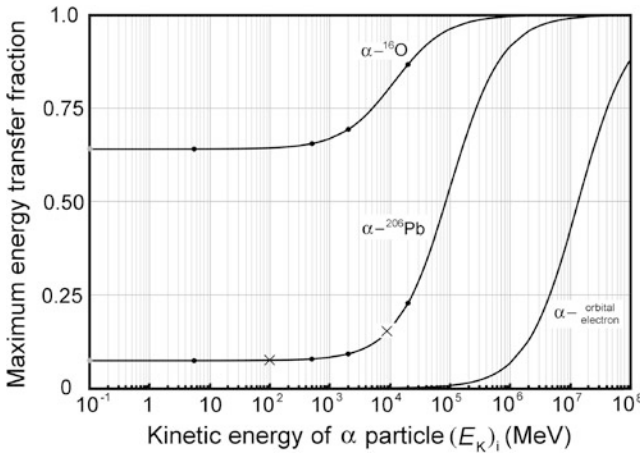


Fig. 5.5 Maximum energy transfer fraction $[\eta(E_K)]_{\max}$ against incident kinetic energy $(E_K)_i$ for α particles interacting with oxygen-16 (O-16), lead-206 (Pb-206), and “free” orbital electron. The black data points represent results of calculations of $[\eta(E_K)]_{\max}$ for α -¹⁶O collision of (a) and α -²⁰⁶Pb collision of (b) for α particle energies $(E_K)_i$ of 5.5 MeV, 500 MeV, 2 GeV, and 20 GeV. The two data points in grey represent the classical approximation of $[\eta(E_K)]_{\max}$ calculated in (c) with (5.127). The two data points designated by \times represent results of calculations in (d)

(b) Elastic collision between projectile (α particle) and target [lead-206 (Pb-206) nucleus] for α -particle kinetic energies $(E_K)_i$ of 5.5 MeV, 500 MeV, 2 GeV, and 20 GeV.

The maximum energy transfer fraction $[\eta(E_K)]_{\max}$ is calculated from

$$[\eta(E_K)]_{\max} = \frac{(\Delta E_K)_{\max}}{(E_K)_i} = \frac{2(\gamma + 1)m_\alpha c^2 m_{\text{Pb-206}} c^2}{(m_\alpha c^2)^2 + (m_{\text{Pb-206}} c^2)^2 + 2\gamma m_\alpha c^2 m_{\text{Pb-206}} c^2} \tag{5.124}$$

and the results for the four α particle kinetic energies are displayed in row (4) of Table 5.5B and superimposed on the Pb-206 curve of Fig. 5.5.

The classical limit η_{clas} of $[\eta(E_K)]_{\text{max}}$ is calculated as follows

$$\eta_{\text{max}}^{\text{class}} = \lim_{\gamma \rightarrow 1} \eta(E_K) = \frac{4m_\alpha c^2 m_{\text{Pb-206}} c^2}{(m_\alpha c^2 + m_{\text{Pb-206}} c^2)^2} = \frac{4 \times 3727.3 \times 191820}{(3727.3 + 191820)^2} = 0.075. \quad (5.125)$$

(c) Elastic collision between projectile (α particle) and target (orbital electron) for α -particle kinetic energies $(E_K)_i$ of 5.5 MeV, 500 MeV, 2 GeV, and 20 GeV. Maximum energy transfer fraction $\eta(E_K)$ is calculated from

$$[\eta(E_K)]_{\text{max}} = \frac{(\Delta E_K)_{\text{max}}}{(E_K)_i} = \frac{2(\gamma + 1)m_\alpha c^2 m_e c^2}{(m_\alpha c^2)^2 + (m_e c^2)^2 + 2\gamma m_\alpha c^2 m_e c^2} \quad (5.126)$$

and the results for the various α particle kinetic energies are displayed in row (5) of Table 5.5B. Classical limit η_{clas} of $\eta(E_K)$ is calculated as follows

$$\eta_{\text{max}}^{\text{class}} = \lim_{\gamma \rightarrow 1} \eta(E_K) = \frac{4m_\alpha c^2 m_e c^2}{(m_\alpha c^2 + m_e c^2)^2} = \frac{4 \times 3727.3 \times 0.511}{(3727.3 + 0.511)^2} = 5.482 \times 10^{-4}. \quad (5.127)$$

(d) To determine the unknown kinetic energy $(E_K)_i$ of the α particle we first determine the maximum energy transfer fraction $[\eta(E_K)]_{\text{max}}$ for a 100 MeV α particle colliding elastically with Pb-206 nucleus and then find $(E_K)_i$ for $[\eta(E_K)]_{\text{max}}$ at twice the 100 MeV value.

The maximum energy transfer fraction $[\eta(E_K)]_{\text{max}}$ is calculated from (5.120) with appropriate γ calculated using (5.121) to get

$$\gamma = 1 + \frac{E_K}{m_\alpha c^2} = 1 + \frac{100}{3727.3} = 1.027. \quad (5.128)$$

Insertion of (5.128) into (5.120) gives the following result for $[\eta(E_K)]_{\text{max}}$

$$\begin{aligned} [\eta(E_K)]_{\text{max}} &= \frac{(\Delta E_K)_{\text{max}}}{(E_K)_i} = \frac{2(\gamma + 1)m_\alpha c^2 m_{\text{Pb-206}} c^2}{(m_\alpha c^2)^2 + (m_{\text{Pb-206}} c^2)^2 + 2\gamma m_\alpha c^2 m_{\text{Pb-206}} c^2} \\ &= \frac{2 \times 2.027 \times 3727.4 \times 191820}{3727.4^2 + 191820^2 + 2 \times 1.027 \times 3727.4 \times 191820} = 0.076. \end{aligned} \quad (5.129)$$

Next we determine kinetic energy $(E_K)_i$ of an α particle with $[\eta(E_K)]_{\text{max}} = 0.152$ that is equal to twice the value at 100 MeV calculated as 0.07 in (5.129). Kinetic energy $(E_K)_i$ of the α particle is determined in a two-step process: first we solve (5.128) for γ and then we calculate $(E_K)_i$ from γ . Equation (5.128) is modified as follows

$$\eta(E_K) = \frac{(\Delta E_K)_{\text{max}}}{(E_K)_i} = \frac{2(\gamma + 1)m_\alpha c^2 m_{\text{Pb-206}} c^2}{(m_\alpha c^2)^2 + (m_{\text{Pb-206}} c^2)^2 + 2\gamma m_\alpha c^2 m_{\text{Pb-206}} c^2} = \frac{a(\gamma + 1)}{b + a\gamma}, \quad (5.130)$$

where a and b are constants given as follows

$$a = 2m_\alpha c^2 m_{\text{Pb-206}} c^2 \quad \text{and} \quad b = (m_\alpha c^2)^2 + (m_{\text{Pb-206}} c^2)^2. \quad (5.131)$$

We now solve (5.130) for γ and insert γ into (5.121) to get

$$(E_K)_i = (\gamma - 1)m_\alpha c^2 = \left(\frac{\eta \frac{b}{a} - 1}{1 - \eta} - 1 \right) m_\alpha c^2, \quad (5.132)$$

where

$$\begin{aligned} \frac{b}{a} &= \frac{(m_\alpha c^2)^2 + (m_{\text{Pb-206}} c^2)^2}{2m_\alpha c^2 m_{\text{Pb-206}} c^2} = \frac{1}{2} \left(\frac{m_\alpha c^2}{m_{\text{Pb-206}} c^2} + \frac{m_{\text{Pb-206}} c^2}{m_\alpha c^2} \right) \\ &= \frac{1}{2} \times \left(\frac{3727.3}{191820} + \frac{191820}{3727.3} \right) = 25.74. \end{aligned} \quad (5.133)$$

Initial kinetic energy $(E_K)_i$ of the α particle is thus calculated from (5.132) as

$$(E_K)_i = \left(\frac{0.152 \times 25.74 - 1}{1 - 0.152} - 1 \right) \times (3727.3 \text{ MeV}) = 9074 \text{ MeV} \approx 9.1 \text{ GeV}. \quad (5.134)$$

Chapter 6 consists of **22 problems** covering 11 sections devoted to general aspects of charged particle interactions with matter. A charged particle is surrounded by its Coulomb electric field that interacts with orbital electrons and the nucleus of all atoms it encounters as it penetrates into an absorber. Charged particle interactions with orbital electrons of the absorber result in collision loss; interactions with nuclei of the absorber result in radiation loss.

The energy transfer from the charged particle to matter in each individual atomic interaction is generally small, so that the particle undergoes a large number of interactions before its kinetic energy is fully spent. The parameter that is used to describe the gradual loss of energy of the charged particle, as it penetrates into an absorber, is referred to as stopping power. Two categories of stopping power are known: (1) collision stopping power that results from charged particle interaction with orbital electrons of the absorber atoms and (2) radiation stopping power that results from charged particle interaction with the nuclei of the absorber.

Chapter 6 starts with problems dealing with general aspects of energy transfer from charged particle to absorber and with general aspects of stopping power of absorbers (Sects. 6.1 and 6.2). Section 6.3 covers radiation stopping power and is followed by several problems on collision stopping power of absorbing media for heavy charged particles in Sect. 6.4 and for light charged particles in Sect. 6.5. Section 6.6 deals with total stopping power and the chapter concludes with problems related to various aspects of stopping power, such as radiation yield (Sect. 6.7), range of charged particle in absorber (Sect. 6.8), mean and restricted stopping power (Sects. 6.9 and 6.10) and practical aspects of bremsstrahlung targets (Sect. 6.11).

6.1 General Aspects of Energy Transfer from Charged Particle to Medium

6.1.Q1

(127)

A charged particle (CP) is surrounded by its Coulomb electric field that interacts with orbital electrons and the nucleus of all atoms it encounters, as it penetrates into an absorbing medium. In penetrating an absorber charged particles may experience a variety of interactions with atoms of the medium. Energy transfer from the charged particle to absorbing medium in each individual atomic interaction is generally but not necessarily small, so that the energetic particle typically undergoes a large number of interactions before its incident kinetic energy is fully spent.

- (a) Classify charged particles used in medicine for treatment of disease according to their mass.
- (b) Classify charged particle interactions with absorber atoms and provide a brief description of each interaction.
- (c) Prepare a block diagram for interactions between a charged particle and absorber atom listed in (b).
- (d) Of the CP interactions listed in (b) only a few contribute to CP energy loss. List and rank the energy loss processes in CP interactions with absorber atoms.

SOLUTION:

(a) Charged particles (CPs) of interest in medicine for treatment of disease are usually placed into three categories according to their rest mass:

- (1) Light charged particles (CPs), such as electrons and positrons with rest mass of $m_e = 0.511 \text{ MeV}/c^2$.
- (2) Intermediate charged particles (CPs), such as negative pions π^- with $m_{\pi^-} = 140m_e$.
- (3) Heavy charged particles (CPs), such as protons ($m_p = 1836m_e$), deuterons, α particles, carbon ions, etc.

In 1970s negative pions were touted as an exciting charged particle option for use in radiotherapy, however, during the past two decades the study of negative pions has largely been abandoned in favor of heavy charged particles such as protons because of simpler means of production and less expensive equipment maintenance.

(b) As energetic charged particles penetrate into an absorbing medium, they interact either with orbital electrons of absorber atoms or with the nucleus of absorbing atoms. These interactions are typically classified as follows:

- (1) Coulomb interaction between *CP and orbital electrons* of absorber atom resulting in:
- (i) Elastic scattering (no energy loss but change in direction of motion).
 - (ii) Inelastic collision referred to as soft or distant collision with impact parameter b much larger than radius of absorbing atom a , i.e., $b \gg a$, resulting in some energy loss (soft collision loss) through excitation or ionization of absorber atom.
 - (iii) Inelastic collision referred to as hard or direct collision with impact parameter b of the order of the radius of absorbing atom a , i.e., $b \approx a$, resulting in some energy loss (hard collision loss) through excitation or ionization of absorber atom.
 - (iv) In-flight annihilation (applicable to positrons only) of CP with orbital electron of absorber resulting in production of annihilation photons (radiation loss).
- (2) Coulomb interaction between *CP and nucleus* of absorber atom resulting in:
- (i) Elastic scattering (essentially no energy loss but change in direction of motion).
 - (ii) Inelastic scattering referred to as radiation loss with the impact parameter b much smaller than the radius of the absorber atom a , i.e., $b \ll a$, resulting in energy loss through production of bremsstrahlung (applicable to light CPs only).
 - (iii) Penetration of the nucleus of absorbing atom resulting in nuclear reaction (applicable to heavy and intermediate CPs and much less so to light CP).
 - (iv) Inelastic scattering resulting in Coulomb nuclear excitation and subsequent emission of gamma rays.
- (c) A block diagram of interactions between charged particle and atom is shown in Fig. 6.1.
- (d) The four entries in CP vs orbital electron interaction and the four entries in CP vs nucleus interaction cover the most important interaction processes of CP interaction with absorber atoms. However, the cross sections for individual interactions vary significantly from one interaction to another and from one particle to another.

(1) **CP interactions with orbital electrons of absorber atoms:**

Elastic collisions are possible but essentially negligible except at very low CP energies where the process is referred to as the Ramsauer effect.

Inelastic collisions represent the prevalent interaction between the CP and orbital electrons of the absorber and are split into two classes: hard and soft collisions, both classes causing excitation and ionization of absorber atoms. The energy transfer to orbital electrons is significantly higher in hard collisions in comparison to soft collisions; however, the number of soft collisions exceeds the number of hard collisions

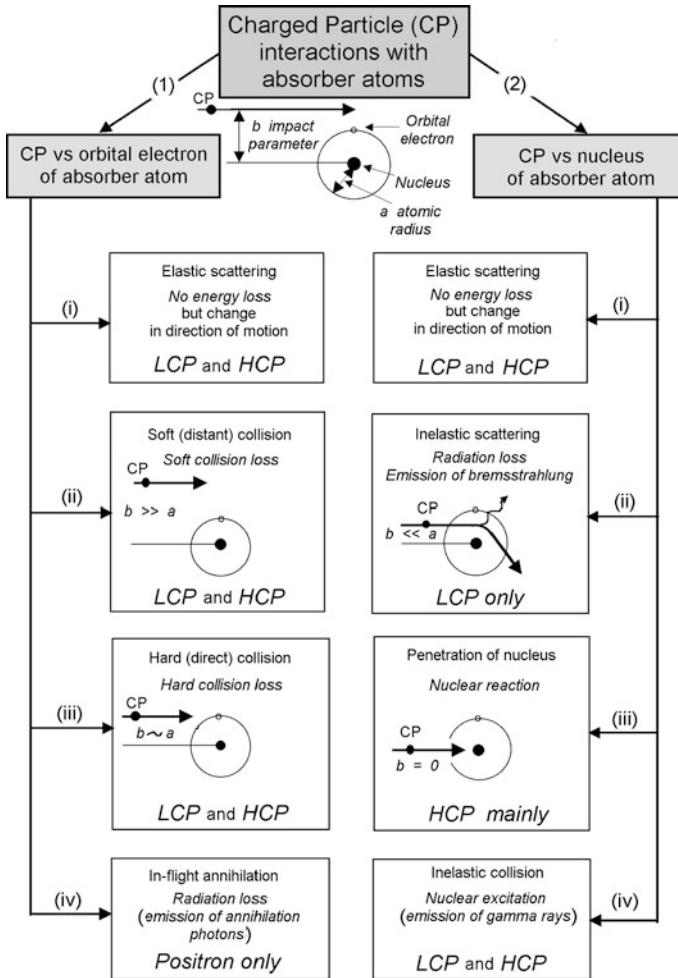


Fig. 6.1 Classification of charged particle (CP) interactions with absorber atoms. Intermediate CPs are ignored because they are no longer considered an option for radiotherapy. LCP and HCP stand for “light charged particles” and “heavy charged particles”, respectively

to such an extent that total energy transfer from the CP to orbital electrons of the absorber is roughly equal for the two classes of collision.

In-flight annihilation only applies to light CP and of these, only to positrons. It produces radiation loss that is added to the bremsstrahlung loss but contributes only a small amount to the total radiation loss and is often ignored in comparison with hard and soft collision loss.

(2) CP interactions with nuclei of absorber atoms:

Elastic Coulomb scattering of CPs on nuclei of absorber atoms are not pronounced for heavy CPs but are very pronounced for light CPs because of their rel-

atively small mass in comparison to that of nuclei. For heavy CPs there is some energy transfer from the CP to the nucleus as the recoil energy of the nucleus but this recoil energy is miniscule in comparison to energy losses inelastic collisions between the heavy CP and orbital electrons of the absorber atoms

Inelastic Coulomb scattering of CPs on nuclei is much less probable than elastic Coulomb scattering. It can be ignored for heavy CPs but it is of significance for light CPs because it serves as source as source of bremsstrahlung photons that play a very important role in modern physics in particular as well as science, industry, and medicine in general.

Penetration of the nucleus by a heavy or light CP that engenders a nuclear reaction is very important in its own right in nuclear physics but play only a minor role in energy transfer from CP to absorber atom. Thus, in energy transfer considerations this process is usually neglected.

Coulomb nuclear excitation by a heavy or light CP is of interest in nuclear physics but is of negligible importance in energy transfer considerations and is therefore ignored.

In summary, the most important processes of energy transfer from CP to atoms of absorber are the inelastic hard and soft collisions between the CP and orbital electrons of absorber engendering collision (ionization) loss and inelastic collisions between the CP and nucleus of absorber atoms engendering radiation (bremsstrahlung) loss.

6.2 General Aspects of Stopping Power

6.2.Q1

(128)

Stopping power plays an important role in study of charged particle interactions with absorbing media.

- (a) Define stopping power and explain the purpose it serves.
- (b) List and briefly describe the various known types of stopping power.
- (c) Mass stopping power S depends on physical properties of the absorber and the type of CP, yet, for a given heavy CP, it is constant within a factor of 2 for all absorbers. Explain.

SOLUTION:

(a) In traversing an absorbing medium a charged particle (CP) interacts with the atoms of the absorber and gradually loses its kinetic energy in a large number of small steps. The mean rate of energy loss per unit path length of the CP of kinetic energy E_K traversing an absorbing medium of atomic number Z is defined as

the stopping power of the absorbing medium. Stopping power depends on physical properties of the absorbing medium as well on properties of the CP traversing the absorbing medium. Stopping power is considered a property of the absorbing medium in which a CP propagates.

Stopping power has an important role in many facets of basic science and technology, and is used heavily in clinical radiation dosimetry based on ionization chambers.

(b) Various types of stopping power are known depending on: (1) the expression of path length of the CP propagating in the absorbing medium and (2) the mode of CP interaction with the atoms of the absorbing medium.

(1) With regard to penetration path length two types of stopping power are known: The rate of energy loss (typically expressed in MeV) per unit penetration path length (typically expressed in cm) is called the “*linear stopping power*” s . Linear stopping power is proportional to the number of absorber atoms N_a per volume \mathcal{V} and its typical units are MeV/cm and less commonly keV/ μm . Since $N_a/\mathcal{V} = \rho N_a/m = \rho N_A/A$, one concludes that the linear stopping power s is proportional to absorber density ρ and inversely proportional to its atomic mass number A . N_A is the Avogadro constant.

To minimize the effect of absorber density ρ on stopping power the penetration path length is often measured in g/cm^2 and the energy loss per unit path length is then called the “*mass stopping power*” S with typical unit $\text{MeV} \cdot \text{cm}^2/\text{g}$. The mass stopping power S is thus proportional to the number of absorber atoms N_a per absorber mass m that is proportional to N_A/A . In mass stopping power S the effect of absorber density is removed and the mass stopping power of all absorber materials is, within a factor of 2, constant for all absorbers.

Linear and mass stopping powers are thus defined as

$$s = -\frac{dE_K}{dx} \quad \text{and} \quad S = \frac{s}{\rho} = -\frac{dE_K}{\rho dx}, \quad \text{respectively,} \quad (6.1)$$

where dE_K is the energy lost by the CP in absorbing medium at penetration thickness dx .

(2) With regard to mode of interaction between the CP and atoms of absorbing medium the stopping power is divided into two major groups: inelastic collision interaction between CP and orbital electrons of the absorber result in collision (also referred to as electronic or ionization) stopping power; inelastic collision interaction between the CP and nucleus of absorber result in radiation stopping power. Inelastic collisions between CP and orbital electrons are further subdivided into soft collisions and hard collisions that result in hard collision stopping power and soft collision stopping power, as shown schematically in Fig. 6.2.

Total stopping power S_{tot} is defined as the sum of radiation stopping power S_{rad} and collision stopping power S_{col} consisting of a soft and a hard term. We thus have

$$S_{\text{tot}} = S_{\text{rad}} + S_{\text{col}} = S_{\text{rad}} + S_{\text{col}}^{\text{soft}} + S_{\text{col}}^{\text{hard}}. \quad (6.2)$$

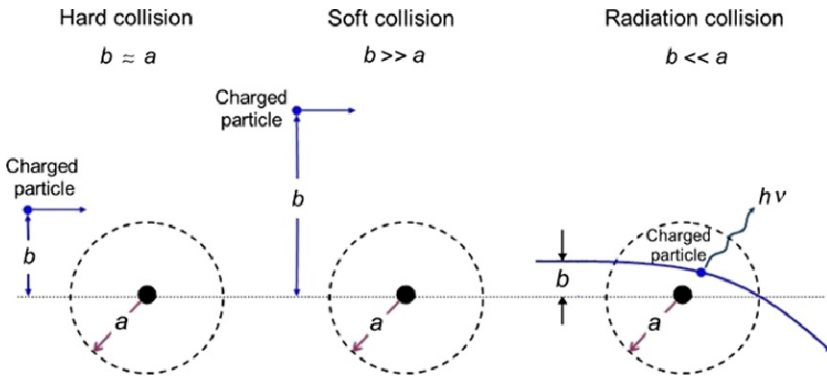


Fig. 6.2 Three different types of collision (hard, sof, and radiation collision) of a charged particle with a atom depending on the relative size of the impact parameter b and atomic radius a

Table 6.1 Collision stopping powers in $\text{MeV} \cdot \text{cm}^2/\text{g}$ of various materials for protons of various kinetic energies in the range from 0.1 MeV to 1 GeV. Date are from the NIST

Element	Atomic number	0.1 MeV	1 MeV	10 MeV	100 MeV	1000 MeV
Hydrogen	1	3487	676.4	101.9	15.2	4.50
Carbon	6	719	226.3	40.5	6.49	1.94
Aluminum	13	447.7	172.0	33.7	5.68	1.75
Copper	29	209.3	118.2	27.1	4.85	1.52
Silver	47	195.5	96.1	23.1	4.34	1.39
Tungsten	74	116.3	63.5	18.2	3.70	1.22
Lead	82	121.4	63.0	17.8	3.55	1.19
Uranium	92	141	58.8	16.9	3.41	1.14
Water		816	260.8	45.6	7.29	2.21
Air		730	222.9	40.1	6.44	1.96

(c) For heavy CPs the mass radiation stopping power S_{rad} is much smaller than the mass collision stopping power S_{col} , so that the total mass stopping power S_{tot} is roughly equal to S_{col} . Since S_{col} originates with inelastic collisions between the CP and orbital electrons of the absorber atoms, a conclusion can be made that S_{col} is proportional to the electron density N_e given as the number of electrons per mass of the absorber or $N_e/m = ZN_A/A$. Since Z/A is roughly constant in nature, slowly varying from 0.5 for low Z elements down to ~ 0.38 for high Z elements, we conclude that $Z/A \approx 0.5$ (with one notable exception of hydrogen for which $Z/A = 1$) and, therefore, S_{col} should not vary appreciably with atomic number of absorbers for a given CP of a given kinetic energy E_K . However, theoretical derivations of S_{col} reveal other Z -dependent terms that cause a decrease in S_{col} with increasing atomic number Z of the absorber.

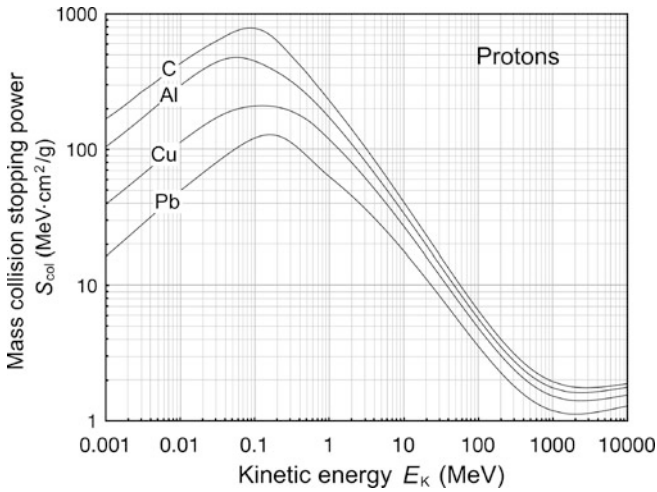


Fig. 6.3 Mass collision stopping power, i.e., total mass stopping power of various absorbing materials for protons against proton kinetic energy in the range from 1 keV to 10^4 MeV

This conclusion is substantiated in Table 6.1 and Fig. 6.3 that give S_{col} against E_K for protons in the range from 1 keV to 10^4 MeV for various absorber materials ranging from hydrogen ($Z = 1$) to uranium ($Z = 92$) in addition to water and air. Data are from the NIST www.physics.nist.gov/PhysRefData/Star/Text/PSTAR.html

6.3 Radiation Stopping Power

6.3.Q1

(129)

According to Bethe and Heitler the mass radiation stopping power S_{rad} of an absorbing material traversed by light charged particles (electrons or positrons) of kinetic energy E_K can be estimated with the following expression

$$S_{\text{rad}} = \alpha r_e^2 Z N_e (E_K + m_e c^2) B_{\text{rad}}, \quad (6.3)$$

where

α is the fine structure constant [$\alpha = e^2/(4\pi\epsilon_0\hbar c) = 1/137$].

r_e is the classical electron radius [$r_e = e^2/(4\pi\epsilon_0 m_e c^2) = 2.818$ fm].

N_e is the number of electrons per unit mass (electron density), i.e., $N_e = ZN_A/A$ with Z and A , respectively, the atomic number and atomic mass of the absorber.

$m_e c^2$ electron and positron rest energy ($m_e c^2 = 0.511$ MeV).

B_{rad} is a slowly varying function of the atomic number Z of the absorber and total energy $E_i = E_K + m_e c^2$ of the light charged particle (CP) with the following recommended mean values: $\bar{B}_{\text{rad}} \approx 16/3 \approx 5.3$ in the non-relativistic kinetic energy range where $E_K \ll m_e c^2$; $\bar{B}_{\text{rad}} \approx 6$ for $E_K \approx 1$ MeV; $\bar{B}_{\text{rad}} \approx 12$ for $E_K \approx 10$ MeV; and $\bar{B}_{\text{rad}} \approx 15$ for $E_K \approx 100$ MeV.

- (a) Based on mass radiation stopping power S_{rad} data available from the NIST and provided for electrons traversing four absorbers (carbon, copper, tin, and lead) in Table 6.2, determine numerical values for the function $B_{\text{rad}}(Z, E_i)$ for the four absorbers at kinetic energies of $E_K = 0.01$ MeV, 0.1 MeV, 1 MeV, 10 MeV, and 100 MeV.
- (b) Describe the dependence of function B_{rad} on kinetic energy E_K of the incident electron and atomic number Z of the absorber.
- (c) Based on your calculations, determine average (mean) values of B_{rad} and compare them to the values recommended in the literature and stated above.

Table 6.2 Mass radiation stopping power $S_{\text{rad}}^{\text{NIST}}$ from the NIST of four absorbers (carbon, copper, tin, and lead) for five kinetic energies E_K of the electron (0.01 MeV, 0.1 MeV, 1 MeV, 10 MeV, and 100 MeV). E_i stands for the total energy of the incident electron

1	E_K (MeV)	0.01	0.1	1	10	100	
2	E_i (MeV)	0.521	0.611	1.511	10.511	100.511	
3	Absorber	$\bar{S}_{\text{rad}}^{\text{NIST}}$	$B_{\text{rad}}^{\text{calc}}$	$\bar{S}_{\text{rad}}^{\text{NIST}}$	$B_{\text{rad}}^{\text{calc}}$	$\bar{S}_{\text{rad}}^{\text{NIST}}$	$B_{\text{rad}}^{\text{calc}}$
4	Carbon C	0.003	0.003	0.011	0.151	2.05	
5	Copper Cu	0.012	0.017	0.046	0.565	7.08	
6	Tin Sn	0.017	0.028	0.077	0.849	10.40	
7	Lead Pb	0.021	0.045	0.129	1.206	14.36	

SOLUTION:

(a) As given in (6.3), the mass radiation stopping power S_{rad} contains a fundamental constant $\sigma_0 = \alpha r_e^2 = 5.8 \times 10^{-28} \text{ cm}^2$ and is proportional to $ZN_e = Z^2 N_A/A$, total energy $E_i = E_K + m_e c^2$ of the incident light CP (electron or positron), and function B_{rad} . Since Table 6.2 provides S_{rad} from the NIST evaluated with a combination of theoretical bremsstrahlung cross sections described by Berger and Seltzer, it is easy to determine the function B_{rad} from (6.3) as follows

$$B_{\text{rad}} = \frac{S_{\text{rad}}}{\alpha r_e^2 Z N_e E_i} \tag{6.4}$$

Before embarking on the calculation of B_{rad} , we compile appropriate data for the four absorbers, such as Z , A , N_e and $\alpha r_e^2 Z N_e$ and present them in Table 6.3.

Table 6.3 Basic atomic properties of the four absorbers: carbon, copper, tin, and lead

1	Absorber	Atomic number Z	Atomic mass A	Electron density $N_e = ZN_A/A$	$\alpha r_e^2 Z N_e$ (cm ² /g)
2	Carbon C	6	12.01	3.008×10^{23}	1.046×10^{-3}
3	Copper Cu	29	63.5	2.749×10^{23}	4.623×10^{-3}
4	Tin Sn	50	118.7	2.537×10^{23}	7.352×10^{-3}
5	Lead Pb	82	207.2	2.383×10^{23}	11.33×10^{-3}

Table 6.4 Calculated values of B_{rad} for the four absorbers (carbon, copper, tin, and lead) at five kinetic energies E_K of the electron. Mass radiation stopping powers S_{rad} are from the NIST

1	E_K (MeV)	0.01	0.1	1	10	100					
2	E_i (MeV)	0.521	0.611	1.511	10.511	100.511					
3	Absorber	$\bar{S}_{\text{rad}}^{\text{NIST}}$	$B_{\text{rad}}^{\text{calc}}$	$\bar{S}_{\text{rad}}^{\text{NIST}}$	$B_{\text{rad}}^{\text{calc}}$	$\bar{S}_{\text{rad}}^{\text{NIST}}$	$B_{\text{rad}}^{\text{calc}}$	$\bar{S}_{\text{rad}}^{\text{NIST}}$	$B_{\text{rad}}^{\text{calc}}$	$\bar{S}_{\text{rad}}^{\text{NIST}}$	$B_{\text{rad}}^{\text{calc}}$
4	Carbon C	0.003	5.9	0.003	5.3	0.011	6.6	0.151	13.7	2.05	19.5
5	Copper Cu	0.012	5.1	0.017	6.1	0.046	6.6	0.565	11.6	7.08	15.2
6	Tin Sn	0.017	4.4	0.028	6.3	0.077	6.9	0.849	11.0	10.40	14.1
7	Lead Pb	0.021	3.5	0.045	6.4	0.129	7.5	1.206	10.1	14.36	12.6

We again note that N_e in the first approximation equals to $\frac{1}{2}N_A$; however, a closer look shows that $N_e \approx 0.5$ for low Z elements and then it slowly drops to reach $N_e \approx 0.4$ for high Z elements. One can still state that S_{rad} is approximately proportional to Z of the absorber; however, to make this statement with more confidence we need to examine the Z -dependence of B_{rad} for a given kinetic energy of the incident electron or positron.

We now calculate B_{rad} for each of the four absorbers at the five kinetic energies E_K using (6.4) and data that are summarized in Table 6.3. The calculated B_{rad} are displayed in Table 6.4.

(b) The dependence of the radiation stopping power B_{rad} on kinetic energy E_K of the light CP and atomic number Z of the absorber is determined from Fig. 6.4. The figure shows that for a given absorber Z at low kinetic energies E_K where $E_K \ll m_e c^2$ the parameter B_{rad} amounts to about 5.5. With increasing E_K the parameter remains almost constant and at $E_K \approx m_e c^2$ begins to rise slowly to reach a value of 6 at $E_K \approx 1$ MeV and then continues to rise slowly until it reaches saturation at around $E_K \approx 1000$ MeV. For a given E_K , on the other hand, B_{rad} is essentially constant (~ 5.5) at $E_K < 1$ MeV but at higher $E_K > 1$ MeV it is inversely proportional to Z with the spread in B_{rad} increasing with increasing kinetic energy E_K and amounting to $\sim 7 \pm 0.5$ at $E_K = 1$ MeV; $\sim 12 \pm 2$ at $E_K = 10$ MeV; $\sim 16 \pm 3.5$ at $E_K = 100$ MeV; and $\sim 17.5 \pm 4$ at $E_K = 1000$ MeV.

(c) Mean values of B_{rad} determined from the spread in B_{rad} displayed in Fig. 6.4 agrees well with the \bar{B}_{rad} recommended in the literature and indicated with the symbol \otimes in Fig. 6.4.

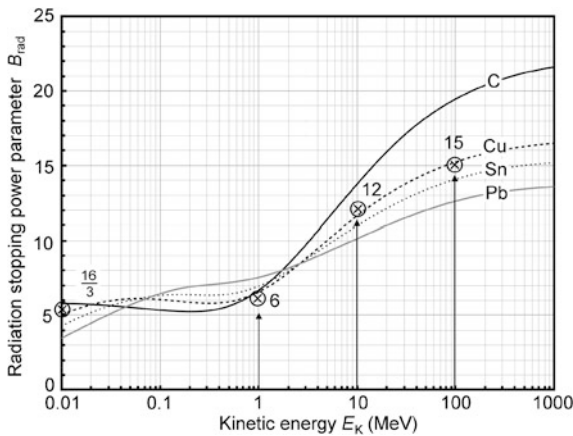


Fig. 6.4 Radiation stopping power parameter B_{rad} against kinetic energy E_K for four absorber materials: carbon, copper, tin, and lead. Symbols \otimes indicate values of B_{rad} at various kinetic energies E_K as recommended in the literature

6.4 Collision (Electronic) Stopping Power for Heavy Charged Particles

6.4.Q1

(130)

Energy transfer from energetic heavy charged particles (CP) to a medium (absorber) they traverse occurs mainly through Coulomb interactions of the CP with orbital electrons of absorber atoms (collision or electronic loss); inelastic Coulomb interactions between heavy CP and nuclei of the absorber atoms (radiation loss) are negligible and thus ignored.

- Plot a schematic diagram for a typical Coulomb interaction between a heavy CP and orbital electron of absorber that results in momentum transfer Δp and energy transfer ΔE from the CP to orbital electron. Clearly identify all parameters that influence the interaction.
- For a heavy CP of charge ze and kinetic energy E_K traversing an absorber of electron density N_e derive expressions for momentum transfer Δp and energy transfer ΔE from the heavy CP to orbital electron of absorber. Express the impact parameter b as a function of Δp and ΔE .
- Both Δp and ΔE depend on the impact parameter b and both have a range between a minimum and maximum value, corresponding to a maximum and minimum value of b , respectively. For the seven elements listed in Table 6.5 determine the maximum and minimum values of Δp , ΔE , and b for proton of incident kinetic energy $E_K = 10$ MeV.

- (d) Can an interaction between a heavy CP and absorber orbital electron occur when the impact parameter b is outside the range $b_{\min} \leq b \leq b_{\max}$? If so, what is the type of interaction? Do any interactions occur between the incident heavy CP and the nuclei of absorber atoms?

Table 6.5 Mean ionization/excitation potential I (eV) for various elements of interest to medical physics

1	Element	H	Al	Cu	Ag	Au	W	Pb
2	Atomic number Z	1	12	29	47	79	74	82
3	Ionization/excitation potential I (eV)	19	166	322	470	790	727	823

SOLUTION:

(a) Coulomb interaction between a heavy CP (charge ze and mass M) and an orbital electron (charge e and mass m_e) of an absorber atom is shown schematically in Fig. 6.5. Base on assumption that the heavy CP is positively charged, the orbital electron is located in the inner focus of the hyperbolic trajectory that, in principle, the heavy CP follows. *Note:* if the two particle charges were of equal sign, then the stationary particle would reside in the outer focus of the hyperbola as is the case in Rutherford scattering. The important parameters of the Coulomb interaction are: impact parameter b , scattering angle θ , and angle ϕ between the radius vector \mathbf{r} and the bisector of the hyperbolic trajectory of the CP.

(b) The momentum transfer (impulse) Δp from the CP to orbital electron is directed along a line that bisects the angle $\pi - \theta$, where θ is the scattering angle for the Coulomb interaction

$$\begin{aligned} \Delta p &= \int_{-\infty}^{\infty} F_{\Delta p} dt = \int_{-\infty}^{\infty} F_{\text{coul}} \cos \phi dt = \frac{ze^2}{4\pi\epsilon_0} \int_{-\frac{\pi-\theta}{2}}^{\frac{\pi-\theta}{2}} \frac{\cos \phi}{r^2} \left(\frac{dt}{d\phi} \right) d\phi \\ &= zr_e m_e c^2 \int_{-\frac{\pi-\theta}{2}}^{\frac{\pi-\theta}{2}} \frac{\cos \phi}{r^2} \left(\frac{dt}{d\phi} \right) d\phi, \end{aligned} \quad (6.5)$$

where

r is the distance between the heavy CP and the orbital electron.

ϕ is the angle between the radius vector r and the bisector of the hyperbola.

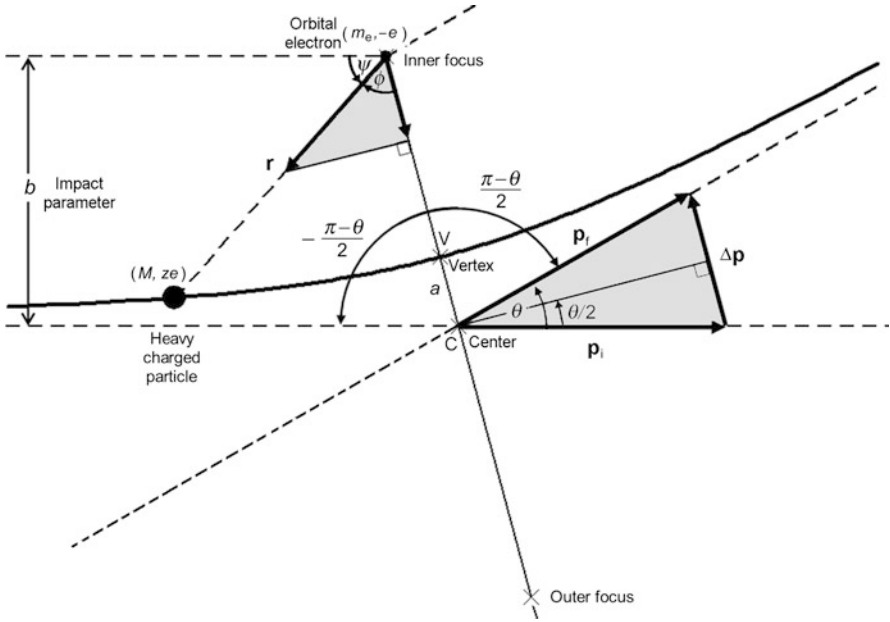


Fig. 6.5 Schematic diagram of a Coulomb collision between a positively charged heavy particle with mass M and an orbital electron with mass m_e . Since $M \gg m_e$, the scattering angle $\theta \approx 0$

The Coulomb force between the two charges (ze and e) is given as

$$F_{\text{coul}} = \frac{ze^2}{4\pi\epsilon_0 r^2} = \frac{zr_e m_e c^2}{r^2}, \tag{6.6}$$

with r_e the standard classical electron radius constant [$r_e = e^2/(4\pi\epsilon_0 m_e c^2) = 2.818 \text{ fm}$] and $m_e c^2$ rest energy of the electron [$m_e c^2 = 0.511 \text{ MeV}$]. The angular momentum L for the Coulomb collision process is defined as follows (see Fig. T2.4)

$$L = |\mathbf{r} \times M\mathbf{v}| = rMv \sin \psi = Mvb = M\omega r^2, \tag{6.7}$$

with

- ω angular frequency equal to $d\phi/dt$.
- v velocity of the heavy CP before the interaction.
- b impact parameter.

Using the conservation of angular momentum expressed in (6.7), we can now write (6.5) in a simpler form

$$\Delta p = \frac{zr_e m_e c^2}{vb} \int_{-\frac{\pi-\theta}{2}}^{\frac{\pi-\theta}{2}} \cos \phi \, d\phi = \frac{zr_e m_e c^2}{vb} [\sin \phi]_{-(\pi-\theta)/2}^{(\pi-\theta)/2} = \frac{2zr_e m_e c^2}{vb} \cos \frac{\theta}{2}. \tag{6.8}$$

In the case of heavy CP of charge ze and mass M interacting with a “stationary” electron of charge e and mass m_e , the scattering angle θ is essentially equal to zero because $M \gg m_e$. Thus, the momentum transfer Δp from (6.8) and energy transfer ΔE , respectively, are given as

$$\Delta p(b) = \frac{2zr_e m_e c^2}{vb} \quad (6.9)$$

and

$$\Delta E(b) = \frac{(\Delta p)^2}{2m_e} = \frac{2z^2 r_e^2 m_e c^2}{(v/c)^2 b^2}. \quad (6.10)$$

The impact parameter b as a function of Δp and ΔE can thus be expressed from (6.9) and (6.10) as follows

$$b = \frac{2zr_e m_e c^2}{v\Delta p} = \frac{zr_e}{(v/c)} \sqrt{\frac{2m_e c^2}{\Delta E}}. \quad (6.11)$$

(c) Intuitively, we might assume that the impact parameter b ranges from 0 to ∞ and that the energy transfer ΔE ranges from 0 to E_K , the kinetic energy of the incident heavy CP. However, a closer look at the underlying physics reveals that ΔE actually ranges from a minimum $\Delta E_{\min} > 0$ to a maximum $\Delta E_{\max} < E_K$ both clearly defined and corresponding to maximum and minimum values of b , respectively. Minimum energy transfer ΔE_{\min} is limited to the mean ionization/excitation potential I of the given absorber and ΔE_{\max} is limited by the maximum energy that can be transferred from particle M_0 to particle m_0 in a direct-hit collision, classically given as $\Delta E_{\max} = 2m_e v^2$ [see (T5.30)]. Using (6.9), (6.10), and (6.11) we can now express the minima and maxima in Δp , ΔE , and b as follows

$$\Delta p_{\min} = \frac{2zr_e m_e c^2}{vb_{\max}} = \sqrt{2m_e I} \quad \text{or} \quad b_{\max} = \frac{2zr_e m_e c^2}{v\Delta p_{\min}} = \frac{zr_e}{(v/c)} \sqrt{\frac{2m_e c^2}{I}}, \quad (6.12)$$

$$\Delta p_{\max} = \frac{2zr_e m_e c^2}{vb_{\min}} = 2m_e v \quad \text{or} \quad b_{\min} = \frac{2zr_e m_e c^2}{v\Delta p_{\max}} = \frac{zr_e}{(v/c)^2}, \quad (6.13)$$

$$\Delta E_{\min} = \frac{2z^2 r_e^2 m_e c^2}{(v/c)^2 b_{\max}^2} = I \quad \text{or} \quad b_{\max} = \frac{zr_e}{(v/c)} \sqrt{\frac{2m_e c^2}{\Delta E_{\min}}} = \frac{zr_e}{(v/c)} \sqrt{\frac{2m_e c^2}{I}}, \quad (6.14)$$

$$\Delta E_{\max} = \frac{2z^2 r_e^2 m_e c^2}{(v/c)^2 b_{\min}^2} = 2m_e v^2 \quad \text{or} \quad b_{\min} = \frac{zr_e}{(v/c)} \sqrt{\frac{2m_e c^2}{\Delta E_{\max}}} = \frac{zr_e}{(v/c)^2}. \quad (6.15)$$

Using the expressions above, we will determine the minima and maxima as follows: $\Delta p_{\min} = [\sqrt{m_e c^2 I}]/c$; $\Delta p_{\max} = 2m_e c^2 (v/c)/c$; $\Delta E_{\min} = I$; $\Delta E_{\max} =$

Table 6.6 Mean ionization/excitation potential I , minimum and maximum momentum transfer (Δp_{\min} and Δp_{\max}), minimum and maximum energy transfer (ΔE_{\min} and ΔE_{\max}), and minimum and maximum impact parameter (b_{\min} and b_{\max}) for 10 MeV proton traversing various absorbers of interest to medical physics

1	Element	H	Al	Cu	Ag	W	Au	Pb
2	Z	1	12	29	47	74	79	82
3	I (eV)	19	166	322	470	727	790	823
4	Δp_{\min} (keV/c)	3.12	9.21	12.83	15.50	19.27	20.09	20.51
5	Δp_{\max} (keV/c)	$\leftarrow 151.2 \rightarrow$						
6	ΔE_{\min} (eV)	19	166	322	470	727	790	823
7	ΔE_{\max} (eV)	$\leftarrow 21.5 \times 10^3 \rightarrow$						
8	b_{\min} (fm)	$\leftarrow 268 \rightarrow$						
9	b_{\max} (fm)	8832	2988	2145	1176	1428	1370	1342

$2m_e c^2 (\nu/c)^2$; $b_{\min} = z r_e (\nu/c)^{-2}$; and $b_{\max} = [z r_e (\nu/c)] \sqrt{2m_e c^2 / I}$. From these expressions it is evident that, on the one hand, the minima in Δp and ΔE are independent of the CP and depend only on the mean ionization/excitation potential I of the absorber; while, on the other hand, the maxima in Δp and ΔE are independent of the absorber but depend on the velocity ν of the CP. Results of these calculations are given in Table 6.6.

(c) To work on our problem involving a 10 MeV proton and various absorbers we will first determine the proton velocity $\beta = \nu/c$ at $E_K = 10$ MeV. Velocity is determined using the relativistic expression for kinetic energy $E_K = (\gamma - 1)m_p c^2$ to get

$$\beta^2 = 1 - \frac{1}{\left(1 + \frac{E_K}{m_p c^2}\right)^2} = 1 - \frac{1}{\left(1 + \frac{10}{938.3}\right)^2} = 0.021 \quad \text{or} \quad \beta = 0.148. \quad (6.16)$$

(d) The range of impact parameters b is from $b = 0$ to $b = \infty$; however, we must recognize that energy transfer ΔE from the CP to orbital electrons of the absorber atoms can occur only for impact parameters b in a much narrower window that extends from b_{\min} to b_{\max} , as shown for 10 MeV proton in various absorber materials in Table 6.6. The table also shows that ΔE_{\max} which is inversely proportional to b_{\min} is independent of absorber and depends only on the velocity ν of the CP, while ΔE_{\min} which is inversely proportional to b_{\max} depends on the absorber through the mean ionization/excitation potential I .

The answer to the question on whether or not a Coulomb interaction between a heavy CP and orbital electron is possible for impact parameters b outside the window $b_{\min} \leq b \leq b_{\max}$ is that it certainly can occur; however, in this situation

the interaction will be elastic and no energy transfer to absorber will occur. We also note that interactions between the CP and nuclei of the absorber certainly do occur, however, again, these interactions are elastic interactions that do not result in bremsstrahlung production.

6.4.Q2

(131)

The Bethe equation for collision stopping power S_{col} of an absorbing medium for a heavy charged particle (CP) such as proton, deuteron and α particle and heavier ions such as carbon ion and neon ion is in the most general form that includes the Fano corrections written as

$$\begin{aligned} S_{\text{col}} &= 4\pi N_e \left(\frac{e^2}{4\pi\epsilon_0} \right)^2 \frac{z^2}{m_e c^2 \beta^2} \left\{ \ln \frac{2m_e c^2}{I} + \ln \frac{\beta^2}{1-\beta^2} - \beta^2 - \frac{C}{Z} - \delta \right\} \\ &= C_1 \frac{N_e z^2}{\beta^2} \bar{B}_{\text{col}}. \end{aligned} \quad (6.17)$$

- Identify parameters, define constants, and provide numerical values of constants for the collision stopping power equation (6.17).
- Briefly discuss the shell correction C/Z to the collision stopping power equation (6.17).
- Briefly discuss the density correction δ to the collision stopping power equation (6.17).
- Discuss the dependence of S_{col} of (6.17) on the stopping medium (absorber).
- Discuss the dependence of S_{col} of (6.17) on heavy CP: mass $m_0 c^2$, velocity $\beta = v/c$, and charge ze .

SOLUTION:

(a) Parameters of the general **Bethe equation** incorporating the Fano corrections are as follows:

- N_e electron density ($N_e = ZN_A/A$) expressed in number of electrons per gram of absorber medium with Z the atomic number and A the atomic mass of the absorber. In the first approximation, $Z/A \approx 0.5$ for all elements with the notable exception of hydrogen for which $Z/A \approx 1$. A closer look at Z/A shows that for $Z \geq 2$ it slowly decreases from 0.5 for low Z elements to 0.38 for high Z elements. For example, Z/A for helium-4 is 0.5, for cobalt-60 it is 0.45, and for uranium-235 it is 0.39.
- ze charge of the heavy charged particle CP (for proton $z = 1$; for α particle $z = 2$).
- $m_e c^2$ rest energy of the electron ($m_e c^2 = 0.511$ MeV).

- β velocity of the heavy CP normalized to speed of light $c = 3 \times 10^8$ m/s in vacuum.
- I mean ionization/excitation potential of the absorber.
- C shell correction constant.
- δ density correction.
- C_1 is a collision stopping power constant independent of absorbing medium as well as of the physical characteristics of the CP. It is defined with the following expression

$$C_1 = 4\pi \left(\frac{e^2}{4\pi\epsilon_0} \right)^2 \frac{1}{m_e c^2} = 4\pi \left[\left(\frac{e^2}{4\pi\epsilon_0} \right) \frac{1}{(m_e c^2)} \right]^2 m_e c^2 = 4\pi r_e^2 m_e c^2$$

$$= 4\pi \times (2.818 \times 10^{-13} \text{ cm})^2 \times (0.511 \text{ MeV}) = 5.099 \times 10^{-25} \text{ MeV} \cdot \text{cm}^2, \quad (6.18)$$

where r_e is the classical radius of electron defined as

$$r_e = \left(\frac{e^2}{4\pi\epsilon_0} \right) \frac{1}{(m_e c^2)} = 2.818 \text{ fm}.$$

- \bar{B}_{col} is the so-called **atomic stopping number** that depends directly on velocity β of the charged particle and indirectly on the atomic number Z of the absorber through the mean ionization/excitation potential I . It is given as

$$\bar{B}_{\text{col}} = \left\{ \ln \frac{2m_e c^2}{I} + \ln \frac{\beta^2}{1 - \beta^2} - \beta^2 - \frac{C}{Z} - \delta \right\}. \quad (6.19)$$

(b) Shell correction. Bethe's derivation of S_{col} for heavy CPs traversing an absorber assumes that the velocity v of the CP is much larger than the velocity v_{orb} of orbital electrons of the absorber atoms. At high kinetic energy E_K of the CP this assumption ($v \gg v_{\text{orb}}$) is correct; however, at low E_K where $v \leq v_{\text{orb}}$ it does not hold, since orbital electrons do not participate in energy transfer from the CP when $v \leq v_{\text{orb}}$. This effect causes an overestimate in the mean ionization/excitation potential I at low E_K and, consequently, results in an underestimate in S_{col} calculated from an uncorrected Bethe equation.

Since K shell electrons are the fastest of all orbital electrons in an absorber atom, they are the first to be affected by low CP velocity with decreasing CP velocity, as the CP penetrates deeper into the absorber. Often thus, the shell correction is addressed as the K shell correction and all possible higher shell corrections are ignored.

The shell correction term C/Z that Fano introduced to correct for the overestimate in I is a function of the absorbing medium as well as of the incident particle velocity v ; however, for the same absorbing medium and the same particle velocity, it is the same for all particles including electrons and positrons.

(c) Density effect correction. Fano introduced a second correction term δ to the Bethe collision stopping power equation to account for the polarization or density

effect in condensed absorbing media. The effect influences the soft (distant) collision interactions by polarizing the condensed absorbing medium thereby decreasing the collision stopping power of the condensed medium in comparison with the same absorbing medium in the gaseous state. For heavy CPs the density correction is important at relativistic energies and negligible at intermediate and low energies; however, for electrons and positrons it plays a role in stopping power formulas at all energies.

(d) Dependence of S_{col} on the absorbing medium. S_{col} depends on atomic number Z of the absorber in two ways: (1) directly through the electron density $N_e = ZN_A/A$ of the absorber and (2) indirectly through the mean ionization/excitation potential I of the absorber.

S_{col} is directly proportional to Z/A and this implies that S_{col} decreases with increasing Z as a result of the slight Z/A dependence on Z . Note: for hydrogen $Z/A = 1$, but for all other elements, it is close to 0.5 ranging from 0.5 for low Z elements and, with increasing Z , slowly decreasing to ~ 0.4 for high Z elements.

The indirect dependence of S_{col} on absorber Z is brought about through the $-\ln I$ term in the stopping number \bar{B}_{col} , since I depends on Z , ranging from 19 eV for hydrogen ($Z = 1$) to ~ 900 eV for uranium ($Z = 92$). Thus, both the direct and indirect dependence of S_{col} on atomic number Z of the absorber causes S_{col} to diminish with increasing Z , however, the decrease in S_{col} is only slight despite the two orders of magnitude range in atomic number Z of the absorber.

(e) Dependence of S_{col} on physical characteristic of the charged particle.

(1) As shown in (6.17), S_{col} depends on CP velocity v and charge ze but does not depend either directly or indirectly on the rest mass m_0c^2 of the CP. A given absorbing material will have the same S_{col} for all heavy CPs of a given kinetic energy E_K and charge ze .

(2) Discussion of S_{col} dependence on velocity v must address three ranges in CP velocity: classical velocity v at low kinetic energy, intermediate velocity at intermediate kinetic energy, and relativistic velocity at high energy. Each one of these three velocity ranges is characterized with its own effect on S_{col} . As evident from (6.17), S_{col} depends on CP velocity $\beta = v/c$ through the $1/\beta^2$ term as well as through the $\{\ln[\beta^2/(1 - \beta^2)] - \beta^2\}$ term contained in the atomic stopping number \bar{B}_{col} .

At low kinetic energies E_K the Fano shell correction must be incorporated in the Bethe equation to account for the low velocity v of the CP and for non-participation of inner shell electrons in the stopping power process. In the intermediate energy region S_{col} is governed by the $1/\beta^2$ term that is proportional to $1/E_K$ and decreases rapidly with increasing E_K . In the high-energy relativistic region, where $\beta \approx 1$, collision stopping power S_{col} rises slowly with E_K as a result of the slow rise in the $\{\ln[\beta^2/(1 - \beta^2)] - \beta^2\}$ term which slowly increases with E_K .

(3) As far as the charge dependence of S_{col} is concerned, we see from (6.17) that S_{col} is linearly proportional to z^2 where ze stands for the charge of the CP. For example, $z = 1$ for proton and deuteron; $z = 2$ for α particle but $z = 1$ for singly ionized helium atom; and $z = 1$ for singly ionized carbon atom, $z = 2$ for doubly ionized carbon atom, and $z = 6$ for carbon nucleus. This implies, for example, that S_{col} of an absorber will differ by a factor of 4 in the case of proton and α particle of the same velocity β , i.e., $S_{\text{col}}(\alpha) = 4S_{\text{col}}(\text{p})$ for the same β .

6.4.Q3

(132)

Several empirical expressions have been proposed for calculation of the mean atomic ionization/excitation potential I that is used in calculations of collision stopping power equations. A few of these approximations are as follows:

$$(1) \quad I \approx 19 \text{ eV for hydrogen} \quad (6.20)$$

$$(2) \quad I(\text{in eV}) \approx 11.5Z; \quad \text{or} \quad I(\text{in eV}) \approx 11Z; \quad \text{or} \quad I(\text{in eV}) \approx 10.5Z \quad (6.21)$$

$$(3) \quad I(\text{in eV}) \approx 9.1Z(1 + 1.9Z^{-2/3}) \quad (6.22)$$

$$(4) \quad I(2 \leq Z \leq 13) \approx 11.2 + 11.7Z \quad \text{and} \quad I(Z > 13) \approx 52.8 + 8.71Z \quad (6.23)$$

$$(5) \quad I(Z < 13) = 7 + 12Z \quad \text{and} \quad I(Z > 13) = 9.76Z + 58.8Z^{-0.19} \quad (6.24)$$

Mean ionization/excitation potential I for chemical compounds such as water and for gas mixtures such as air are calculated with the Bragg additivity rule using the following expression

$$\ln I = \frac{\sum_i N_i Z_i \ln I_i}{\sum_i N_i Z_i}, \quad (6.25)$$

where

i designates an individual component of the chemical compound or of the gas mixture

Z_i is the atomic number of the individual component i

N_i is the number of atoms i in the chemical component or the percentage by weight of the component i in the gas mixture.

Using (6.24) in conjunction with (6.25) calculate:

- (a) Mean ionization/excitation potential I of water (H_2O).
- (b) Mean ionization/excitation potential I of Lucite ($\text{C}_5\text{H}_8\text{O}_2$)_n.

Table 6.7 Mean ionization/excitation potential of hydrogen, carbon, and oxygen

Element	Hydrogen	Carbon	Oxygen
Atomic number Z	1	6	8
Mean ionization/excitation potential I (eV)	19 eV from (6.24)	81.5 eV from (6.23)	104.6 eV from (6.23)

SOLUTION:

Before using (6.25) we must determine the mean atomic ionization/excitation potential for the following elements: hydrogen and oxygen as constituents of water (H_2O) and hydrogen, carbon, and oxygen as constituents of Lucite ($\text{C}_5\text{H}_8\text{O}_2$) $_n$. The appropriate data are presented in Table 6.7.

(a) Mean ionization/excitation potential of water is calculated from (6.25) as follows: We first calculate the two components of (6.25) and get

$$\sum_i N_i Z_i \ln I_i = 2 \times 1 \times \ln 19 + 1 \times 8 \times \ln 104.6 = 43.1 \quad (6.26)$$

and

$$\sum_i N_i Z_i = 2 \times 1 + 1 \times 8 = 10 \quad (6.27)$$

and then use (6.25) to get

$$\ln I = \frac{\sum_i N_i Z_i \ln I_i}{\sum_i N_i Z_i} = \frac{43.1}{10} = 4.31 \quad \text{or} \quad I = 74.4 \text{ eV}, \quad (6.28)$$

in good agreement with the value of 75 eV that is in common use for the mean ionization/excitation potential of water.

(b) Mean ionization/excitation potential I of Lucite ($\text{C}_5\text{H}_8\text{O}_2$) $_n$ is also calculated from (6.25) by first calculating the numerator and denominator of (6.25), respectively

$$\sum_i N_i Z_i \ln I_i = 5 \times 6 \times \ln 81.5 + 8 \times 1 \times \ln 19 + 2 \times 8 \times \ln 104.6 = 230 \quad (6.29)$$

and

$$\sum_i N_i Z_i = 5 \times 6 + 8 \times 1 + 2 \times 8 = 54 \quad (6.30)$$

and then using (6.25) to get

$$\ln I = \frac{\sum_i N_i Z_i \ln I_i}{\sum_i N_i Z_i} = \frac{230}{54} = 4.26 \quad (6.31)$$

resulting in

$$I = e^{4.26} = 71 \text{ eV} \quad (6.32)$$

in reasonable agreement with the value of 74 eV that is commonly used for the ionization/excitation potential of Lucite.

6.4.Q4

(133)

In general, the total stopping power for a given charged particle (CP) is the sum of collision stopping power and radiation stopping power. However, for heavy charged particles the total stopping power is equal to the collision stopping power, since the radiation stopping power for heavy charged particles is negligible in comparison with the collision stopping power.

- (a) Calculate the mass stopping power of water for a proton of kinetic energy $E_K = 100 \text{ MeV}$. Ignore the shell and density corrections. The atomic ionization/excitation potential of water I is 75 eV (see Prob. 132).
- (b) For 1 MeV and 10 MeV protons in water repeat the calculation carried out in (a).
- (c) Calculate the kinetic energy of the deuteron ($m_d c^2 = 1875.6 \text{ MeV}$) for which the stopping power of water is the same as that for the proton in (a).
- (d) Calculate the stopping power of water for α particle ($m_\alpha c^2 = 3727.3 \text{ MeV}$) having the same velocity as the proton in (a).
- (e) Compare the results obtained in (a) and (b) for protons and in (d) for α particles with data available from the NIST for stopping powers of water for protons and α particles www.nist.gov/pml/data/star/index.cfm.

SOLUTION:

(a) To calculate the mass stopping power of water for a 100 MeV proton we use the Bethe mass collision stopping power equation (T6.42) that reads

$$S_{\text{col}} = 4\pi N_e \left(\frac{e^2}{4\pi\epsilon_0} \right)^2 \frac{z^2}{m_e c^2 \beta^2} \left\{ \ln \frac{2m_e c^2}{I} + \ln \frac{\beta^2}{1 - \beta^2} - \beta^2 \right\} = C_1 \frac{N_e z^2}{\beta^2} B_{\text{col}}, \quad (6.33)$$

where

- N_e is the electron density ($N_e = ZN_A/A$) in number of electrons per gram of absorber medium with Z the atomic number and A the atomic mass of water.
 z is the number of electronic charges on the heavy CP (for proton $z = 1$; for α particle $z = 2$).
 β is velocity of the CP normalized to speed of light c in vacuum.

I is the mean ionization/excitation potential of water ($I = 75$ eV).

B_{col} is the so-called atomic stopping number that depends directly on velocity β of the CP and indirectly on the atomic number Z of the absorber (water in our case) through the mean ionization/excitation potential I and is given as

$$B_{\text{col}} = \left\{ \ln \frac{2m_e c^2}{I} + \ln \frac{\beta^2}{1 - \beta^2} - \beta^2 \right\}. \quad (6.34)$$

C_1 is a collision stopping power constant independent of absorbing medium as well as of the characteristics of the charged particle. It is expressed as [see (6.18) in Prob. 131]

$$\begin{aligned} C_1 &= \left(\frac{e^2}{4\pi\epsilon_0} \right)^2 \frac{4\pi}{m_e c^2} = 4\pi r_e^2 m_e c^2 = 4\pi (2.818 \times 10^{-13} \text{ cm})^2 \times (0.511 \text{ MeV}) \\ &= 5.099 \times 10^{-25} \text{ MeV} \cdot \text{cm}^2. \end{aligned} \quad (6.35)$$

Before we use (6.33) to calculate the stopping power of water, we must determine the electron density N_e of water and the velocity β of the 100 MeV proton.

(1) **Calculation of electron density** N_e is carried out as follows: 1 mole of water (H_2O) equals to 18.0153 g of water [see (T1.22)] and, by definition, contains 6.022×10^{23} molecules of water, each molecule containing 2 hydrogen atoms and one oxygen atom. Thus, 1 g of water contains $\frac{1}{18.0153} \times 6.022 \times 10^{23}$ molecules of water and, since each molecule of water contains 10 electrons, we conclude that the electron density of water N_e is

$$\begin{aligned} N_e &= \frac{1}{18.0153} \times \left(6.022 \times 10^{23} \frac{\text{molecule}}{\text{g}} \right) \times \left(10 \frac{\text{electron}}{\text{molecule}} \right) \\ &= 3.343 \times 10^{23} \text{ electron/g}. \end{aligned} \quad (6.36)$$

(2) **Calculation of 100-MeV-proton velocity** β is carried out using the standard expression (T2.7) relating relativistic particle velocity $\beta = v/c$ with kinetic energy E_K of the particle. The expression is easy to derive from the basic definition of relativistic kinetic energy E_K given as follows

$$E_K = (\gamma - 1)m_0 c^2 = \left(\frac{1}{\sqrt{1 - v^2/c^2}} - 1 \right) m_0 c^2, \quad (6.37)$$

from which we get the following expression for β

$$\beta^2 = \frac{v^2}{c^2} = 1 - \frac{1}{\left(1 + \frac{E_K}{m_p c^2}\right)^2} = 1 - \frac{1}{\left(1 + \frac{100}{938.3}\right)^2} = 0.183, \quad (6.38)$$

indicating that the velocity v of a 100 MeV proton is $0.428c$.

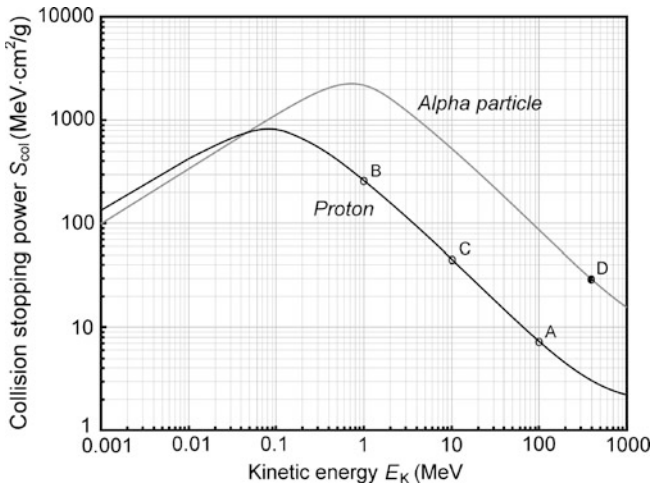


Fig. 6.6 Collision stopping power of water for proton and α particle in the kinetic energy range from 1 keV to 1 GeV. The continuous curves are data from the NIST, the four data points are results of our calculations of stopping power with the Bethe stopping power equation (6.33) that ignores the shell correction and the density correction

(3) **Calculation of the atomic stopping number B_{col}** proceeds as follows

$$\begin{aligned}
 B_{col} &= \left\{ \ln \frac{2m_e c^2}{I} + \ln \frac{\beta^2}{1 - \beta^2} - \beta^2 \right\} \\
 &= \ln \frac{2 \times 0.511 \times 10^6 \text{ eV}}{75 \text{ eV}} + \ln \frac{0.183}{1 - 0.183} - 0.183 \\
 &= 9.52 + (-1.50) - 0.183 = 7.84.
 \end{aligned}
 \tag{6.39}$$

(4) We now use (6.33) to get the final answer for **stopping power of water** and 100 MeV protons

$$\begin{aligned}
 S_{col} &= C_1 \frac{N_e z^2}{\beta^2} B_{col} = (5.099 \times 10^{-25} \text{ MeV} \cdot \text{cm}^2) \times \frac{3.343 \times 10^{23} \text{ g}^{-1}}{0.183} \times 7.84 \\
 &= 7.30 \text{ MeV} \cdot \text{cm}^2/\text{g} \quad (\text{see point A in Fig. 6.6}).
 \end{aligned}
 \tag{6.40}$$

(b) We now repeat, for 1 MeV and 10 MeV protons in water, the calculation carried out in (a), for each energy first calculating β^2 using (6.38) and B_{col} using (6.34) and then using (6.33) to get the final results for the mass stopping power.

For **1 MeV protons** we get the following results for β^2 , B_{col} , and S_{col}

$$\beta^2 = \frac{v^2}{c^2} = 1 - \frac{1}{\left(1 + \frac{E_k}{m_p c^2}\right)^2} = 1 - \frac{1}{\left(1 + \frac{1}{938.3}\right)^2} = 2.128 \times 10^{-3},
 \tag{6.41}$$

$$B_{\text{col}} = \ln \frac{2m_e c^2}{I} + \ln \frac{\beta^2}{1 - \beta^2} - \beta^2 = 9.520 - 6.150 - 2.128 \times 10^{-3} = 3.367 \quad (6.42)$$

and

$$\begin{aligned} S_{\text{col}} &= C_1 \frac{N_e z^2}{\beta^2} B_{\text{col}} = (5.099 \times 10^{-25} \text{ MeV} \cdot \text{cm}^2) \times \frac{3.343 \times 10^{23} \text{ g}^{-1}}{2.128 \times 10^{-3}} \times 3.367 \\ &= 269.7 \text{ MeV} \cdot \text{cm}^2/\text{g} \quad (\text{see point B in Fig. 6.6}). \end{aligned} \quad (6.43)$$

For **10 MeV protons** the results are as follows

$$\beta^2 = \frac{v^2}{c^2} = 1 - \frac{1}{\left(1 + \frac{E_K}{m_p c^2}\right)^2} = 1 - \frac{1}{\left(1 + \frac{10}{938.3}\right)^2} = 0.021, \quad (6.44)$$

$$\begin{aligned} B_{\text{col}}(10 \text{ MeV}) &= \ln \frac{2m_e c^2}{I} + \ln \frac{\beta^2}{1 - \beta^2} - \beta^2 \\ &= 9.520 - 3.842 - 0.021 = 5.657 \end{aligned} \quad (6.45)$$

and

$$\begin{aligned} S_{\text{col}} &= C_1 \frac{N_e z^2}{\beta^2} B_{\text{col}} = (5.099 \times 10^{-25} \text{ MeV} \cdot \text{cm}^2) \times \frac{3.343 \times 10^{23} \text{ g}^{-1}}{0.021} \times 5.657 \\ &= 45.9 \text{ MeV} \cdot \text{cm}^2/\text{g} \quad (\text{see point C in Fig. 6.6}). \end{aligned} \quad (6.46)$$

(c) To determine the kinetic energy E_K of a deuteron for which the stopping power of water is the same as that for a 100 MeV proton, we take a closer look at the functional dependence of (6.33) on physical properties of the charged particle and note that S_{col} has five components: C_1 , N_e , z , β , and B_{col} . Of these, C_1 , N_e , and B_{col} are independent of the charged particle, so that, for the mass stopping power of water to be the same for proton and deuteron, the two charged particles should have the same z (they do, since for both particles $z = 1$) and the same β . As shown in (6.38), $\beta^2 = 0.183$ for a 100 MeV proton, therefore we use (6.37) and determine the deuteron kinetic energy E_K that corresponds to $\beta^2 = 0.183$ as follows

$$\begin{aligned} E_K &= (\gamma - 1)m_0 c^2 = \left(\frac{1}{\sqrt{1 - \beta^2}} - 1\right)m_0 c^2 \\ &= \left(\frac{1}{\sqrt{1 - 0.183}} - 1\right) \times (1875.6 \text{ MeV}) \\ &= 199.5 \text{ MeV} \approx 2 \left(\frac{1}{\sqrt{1 - \beta^2}} - 1\right)m_p c^2 = 200 \text{ MeV}. \end{aligned} \quad (6.47)$$

Thus, for the same stopping power in water, the kinetic energy E_K of the charged particle is proportional to the rest energy of the charged particle.

Since the rest energy of the deuteron $m_d c^2$ is roughly twice the rest energy $m_p c^2$ of the proton, its kinetic energy E_K for the same velocity β is twice as high. Thus, the mass stopping power of water is the same ($7.30 \text{ MeV} \cdot \text{cm}^2/\text{g}$) for a 100 MeV proton and a 200 MeV deuteron because both charged particles have the same velocity β as well as the same atomic number $z = 1$.

(d) To calculate the stopping power of water for α particle having the same velocity as the proton, we again evaluate the functional dependence of (6.33) and note that, in addition to charged particle velocity β , the mass stopping power also depends on the square of the atomic number z . Since $z = 2$ for α particle compared to $z = 1$ for proton, we conclude that the mass stopping power of water is 4 times as large ($4 \times 7.30 \text{ MeV} \cdot \text{cm}^2/\text{g} = 29.2 \text{ MeV} \cdot \text{cm}^2/\text{g}$) for α particle as that for proton at the same velocity β of the two particles (see point D in Fig. 6.6).

From the discussion in **(c)** we also note that, at same velocity β , kinetic energy $E_K(\alpha)$ of an α particle is approximately 4-times as large as that of a proton

$$\begin{aligned} E_K(\alpha) &= (\gamma - 1)m_\alpha c^2 = \left(\frac{1}{\sqrt{1 - \beta^2}} \right) m_\alpha c^2 \\ &= \left(\frac{1}{\sqrt{1 - 0.183}} \right) \times (3727.3 \text{ MeV}) = 396.4 \text{ MeV}. \end{aligned} \quad (6.48)$$

(e) For 1 MeV, 10 MeV, and 100 MeV protons we calculated with Bethe equation (6.33) the following stopping powers of water: $269.7 \text{ MeV} \cdot \text{cm}^2/\text{g}$, $45.9 \text{ MeV} \cdot \text{cm}^2/\text{g}$, and $7.30 \text{ MeV} \cdot \text{cm}^2/\text{g}$, respectively, while the NIST, accounting for all known corrections, gives the following respective results: $260.8 \text{ MeV} \cdot \text{cm}^2/\text{g}$, $45.7 \text{ MeV} \cdot \text{cm}^2/\text{g}$, and $7.29 \text{ MeV} \cdot \text{cm}^2/\text{g}$. For an α particle with kinetic energy $E_K(\alpha) = 400 \text{ MeV}$ the NIST provides a stopping power of water of $29.2 \text{ MeV} \cdot \text{cm}^2/\text{g}$, while our rudimentary calculation yields $29.2 \text{ MeV} \cdot \text{cm}^2/\text{g}$. Thus, the agreement with the basic Bethe equation (6.33) and the one incorporating all currently known corrections is quite good.

Stopping power of water for proton and α particle available from the NIST is shown in Fig. 6.6 in the energy range from 1 keV to 1000 MeV and our calculated results are superimposed on the graph with data points. The good agreement between our calculation and the NIST data is evident.

6.4.Q5

(134)

Bethe equation for mass collision stopping power S_{col} of a stopping medium (absorber) for heavy charged particles (CP) is given as

$$S_{\text{col}} = 4\pi N_e \left(\frac{e^2}{4\pi\epsilon_0} \right)^2 \frac{z^2}{m_e c^2 \beta^2} \left\{ \ln \frac{2m_e c^2}{I} + \ln \frac{\beta^2}{1 - \beta^2} - \beta^2 \right\} = C_1 \frac{N_e z^2}{\beta^2} B_{\text{col}}, \quad (6.49)$$

with parameters defined in Prob. 131 and the Fano shell and density corrections neglected.

- (a) Determine the mass collision stopping power S_{col} of water for a proton with incident kinetic energy $E_K = 51$ MeV. Mean ionization/excitation potential I of water is 75 eV; electron density $N_e = ZN_A/A$ was determined in Prob. 133 as $N_e = 3.343 \times 10^{23}$ el/g.
- (b) Determine the incident kinetic energy E_K of a deuteron for which water has the same mass collision stopping power S_{col} as for the proton in (a).
- (c) Determine the incident kinetic energy E_K and mass collision stopping power S_{col} of water for the following particles: α particle, carbon-6 ion, and neon-10 ion having the same incident velocity $\beta = v/c$ as the proton in (a) and deuteron in (b).

SOLUTION:

(a) To use (6.49) for calculation of S_{col} of water we will need the following parameters: (1) constant C_1 , (2) velocity $\beta = v/c$ of proton with $E_K = 51$ MeV, and (3) collision stopping number of water for 51 MeV proton.

(1) From (6.18) in Prob. 131 we get the following expression for constant C_1

$$C_1 = 4\pi \left(\frac{e^2}{4\pi\epsilon_0} \right)^2 \frac{1}{m_e c^2} = 4\pi r_e^2 m_e c^2 = 4\pi \times (2.818 \times 10^{-13} \text{ cm})^2 \times (0.511 \text{ MeV}) \\ = 5.099 \times 10^{-25} \text{ MeV} \cdot \text{cm}^2. \quad (6.50)$$

(2) Velocity of the 51-MeV-proton is determined from the standard expression for relativistic kinetic energy E_K as follows

$$E_K = (\gamma - 1)E_0 = \left(\frac{1}{\sqrt{1 - \beta^2}} - 1 \right) m_p c^2, \quad (6.51)$$

from where it follows that

$$\beta^2 = 1 - \frac{1}{\left(1 + \frac{E_K}{m_p c^2}\right)^2} = 1 - \frac{1}{\left(1 + \frac{51}{938.3}\right)^2} = 0.10 \quad \text{and} \quad \beta = 0.01. \quad (6.52)$$

(3) Atomic stopping number B_{col} of proton in water is determined as follows

$$B_{\text{col}} = \left\{ \ln \frac{2m_e c^2}{I} + \ln \frac{\beta^2}{1 - \beta^2} - \beta^2 \right\} \\ = \ln \frac{2 \times 0.511 \times 10^6 \text{ eV}}{75 \text{ eV}} + \ln \frac{0.1}{0.9} - 0.1 = 9.52 - 2.197 - 0.10 = 7.22. \quad (6.53)$$

Now that we have all the required parameters we can determine S_{col} as follows

$$\begin{aligned} S_{\text{col}} &= C_1 \frac{N_e z^2}{\beta^2} B_{\text{col}} = (5.099 \times 10^{-25} \text{ MeV} \cdot \text{cm}^2) \times \frac{3.343 \times 10^{23}}{0.1 \text{ g}} \times 7.22 \\ &= 12.31 \frac{\text{MeV} \cdot \text{cm}^2}{\text{g}} \end{aligned} \quad (6.54)$$

and get a result that is in excellent agreement with the NIST mass collision stopping power S_{col} of $12.25 \text{ MeV} \cdot \text{cm}^2/\text{g}$ obtained for a 51 MeV proton.

(b) For a heavy CP to engender in absorber the same mass collision stopping power S_{col} as does a proton, it must have the same velocity β as well as the same charge number $z = 1$. Since for both proton and deuteron $z = 1$, for a deuteron to engender S_{col} of $12.31 \text{ MeV} \cdot \text{cm}^2/\text{g}$ in water, it must have the same velocity β of 0.01 as does a 51 MeV proton. Since the deuteron is heavier than the proton, its kinetic energy $E_K(\text{d})$ must be higher than that of the proton $E_K(\text{p})$. The ratio $E_K(\text{d})/E_K(\text{p})$ is determined from (6.51) as follows

$$E_K(\text{p}) = m_p c^2 \left(\frac{1}{\sqrt{1 - \beta^2}} - 1 \right) \quad \text{and} \quad E_K(\text{d}) = m_d c^2 \left(\frac{1}{\sqrt{1 - \beta^2}} - 1 \right), \quad (6.55)$$

from where it follows that the ratio $E_K(\text{d})/E_K(\text{p})$ is given as follows

$$\frac{E_K(\text{d})}{E_K(\text{p})} = \frac{m_d c^2}{m_p c^2} = \frac{1875.6}{938.3} \approx 2. \quad (6.56)$$

Thus, for a deuteron to engender the same stopping power in water as does a proton, it must have the same velocity as the proton, and this implies that it has a kinetic energy that is twice the kinetic energy of the proton. Mass collision stopping power S_{col} of water is therefore $12.31 \text{ MeV} \cdot \text{cm}^2/\text{g}$ for 51 MeV proton as well as for 102 MeV deuteron.

(c) We now calculate: (1) kinetic energy $E_K(m_0)$ of particle with rest mass m_0 and (2) mass collision stopping power S_{col} of water for various CPs (deuteron, α particle, carbon-6 ion, and neon-10 ion), all of velocity $\beta = 0.01$, as determined for 51 MeV proton in (a).

(1) Kinetic energy $E_K(m_0)$ of heavy CPs that all have the same velocity β is linearly proportional to CP's rest energy $E_0 = m_0 c^2$. Based on (6.56) we reach a general conclusion that kinetic energy of a given heavy CP of rest mass m_0 can be expressed in terms of kinetic energy of proton of rest mass m_p as

$$E_K(m_0) = \frac{m_0 c^2}{m_p c^2} E_K(m_p), \quad (6.57)$$

Table 6.8 Various parameters in calculation of kinetic energy E_K and mass stopping power of water for various heavy CPs (proton, deuteron, α particle, carbon-6 ion, and neon-10 ion)

1	Particle	Proton	Deuteron	α particle	Carbon-6	Neon-10
2	$E_0 = m_0 c^2$	938.3	1875.6	3727.3	11174.9	18617.7
3	$m_0 c^2 / m_p c^2$	1.0	2	3.97	11.91	19.84
4	$E_K(m_0)$	51	102	202.5	11175	18616
5	E_K/A (MeV/u)	51	~ 51	~ 51	~ 51	~ 51
6	z	1	1	2	6	10
7	$S_{\text{col}}(m_0, z)$ (MeV \cdot cm ² /g)	12.31	12.31	49.2	443.2	1231

provided that both CPs have the same velocity β . Kinetic energy $E_K(m_0)$ for proton, deuteron, α particle, carbon-6 ion, and neon-10 ion, all traveling with velocity $\beta = 0.01$, determined from (6.57) is listed in row (4) of Table 6.8, while kinetic energy of the various CPs stated in MeV/u is listed in row (5) of the table. It is evident that CPs with same MeV/u have the same velocity β and engender the same stopping number B_{col} in a given stopping material.

- (2) Mass collision stopping power $S_{\text{col}}(m_0, z)$ for the various CPs of rest mass m_0 , all with the same velocity $\beta = 0.01$, will now be expressed in terms of $S_{\text{col}}(m_p, z)$ of water for a proton. From (6.49) it is evident that, for a constant velocity β , $S_{\text{col}}(m_0, z)$ is linearly proportional with z^2 , where z is the number of charges that the CP carries, i.e.,

$$S_{\text{col}}(m_0, z) = z^2 S_{\text{col}}(m_p, z). \quad (6.58)$$

Results for $S_{\text{col}}(m_0, z)$ of water for proton, deuteron, α particle, carbon-6 ion, and neon-10 ion are summarized in row (7) of Table 6.8. Note that our S_{col} of water for α particles of $E_K = 202.5$ MeV is in excellent agreement with the NIST value of $S_{\text{col}} = 49.03$ MeV \cdot cm²/g for the same conditions.

6.4.Q6

(135)

Specific ionization j is defined as the number of primary and secondary ion pairs produced per unit length of the path traced by a charged particle (CP) traversing an absorber. It is usually expressed in ion pairs per millimeter (ip/mm) and increases with the charge of the CP. The specific ionization produced in the absorber by a CP at a given kinetic energy E_K is proportional to

the linear stopping power s of the absorber and the proportionality constant (at least for gases) is \overline{W} , the mean energy required to produce an ion pair in the absorber at particle energy E_K . For gases \overline{W} is essentially independent of particle energy and only slightly depends on the CP type. For example, \overline{W} of air is $\overline{W}_{\text{air}} = 33.97$ eV/ip for electrons and x rays, 35 eV/ip for protons, and 36 eV/ip for α particles.

- (a) Determine the specific ionization j resulting from the passage of a 10 MeV proton through standard air ($T = 0^\circ\text{C}$ and $p = 101.3$ kPa). Density of standard air $\rho_{\text{air}} = 1.293 \times 10^{-3}$ g/cm³; the mean ionization/excitation potential of air is $I_{\text{air}} = 86$ eV. Ignore the Fano shell and density corrections in the calculation of collision stopping powers.
- (b) Based on Fig. 6.7 that shows the mass collision stopping power S_{col} of standard air against proton kinetic energy E_K in the kinetic energy range from 10^{-3} MeV to 10^4 MeV, determine the maximum possible specific ionization j in standard air for protons. Stopping power data are from the NIST at http://physics.nist.gov/cgi-bin/Star/ap_table.pl.
- (c) Based on data from the NIST, given in Table 6.9A, prepare a plot of specific ionization j against residual range R_{residual} for a 10 MeV proton in standard air. In order to get a clear picture of the Bragg peak plot j only for the last 5 mm of the proton path in air.

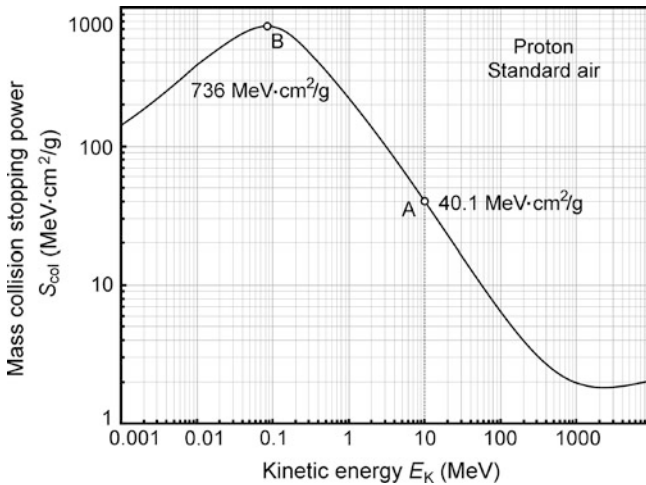


Fig. 6.7 Mass collision stopping power S_{col} of standard air against kinetic energy E_K of proton. Point A highlights S_{col} of standard air for a 10 MeV proton calculated in (a); point B highlights the maximum that occurs at 0.084 MeV and is used in calculation of the maximum specific ionization

Table 6.9A Mass collision stopping power S_{col} and CSDA range R_{CSDA} for protons in air in the kinetic energy E_K range from 0 to 10 MeV. The table is to be used to determine a plot of specific ionization against residual range for 10 MeV protons in standard air where E_K is kinetic energy of the proton propagating in standard air, S_{col} is mass collision stopping power of standard air, s_{col} is linear collision stopping power of standard air, j is specific ionization produced in standard air by protons of energy E_K , R_{CSDA} is the continuous slowing down approximation (CSDA) range in g/cm² for protons of energy E_K in standard air, r_{CSDA} is the CSDA range in mm of air for protons of energy E_K

1	E_K (MeV)	$S_{\text{col}}^{\text{a}}$ (MeV · cm ² /g)	s_{col} (MeV/cm)	j (i.p./mm)	$R_{\text{CSDA}}^{\text{a}}$ (g/cm ²)	R_{residual} (mm)
2	0.001	141.4			9.857×10^{-6}	
3	0.005	277.6			2.891×10^{-5}	
4	0.01	385.0			4.400×10^{-5}	
5	0.05	689.7			1.152×10^{-4}	
6	0.07	729.3			1.433×10^{-4}	
7	0.08	735.5			1.569×10^{-4}	
8	0.09	735.2			1.705×10^{-4}	
9	0.2	592.8			3.349×10^{-4}	
10	0.5	350.1			1.021×10^{-3}	
11	1	222.9			2.867×10^{-3}	
12	2	137.1			8.792×10^{-3}	
13	5	69.1			4.173×10^{-2}	
14	10	40.1			1.408×10^{-1}	

^aData are from the NIST at http://physics.nist.gov/cgi-bin/Star/ap_table.pl

SOLUTION:

(a) Mean specific ionization j of air for 10 MeV proton is determined using the following steps:

- (1) Use the Bethe equation (6.17) for heavy CP to determine mass collision stopping power S of air for 10 MeV proton as follows

$$S_{\text{col}} = C_1 \frac{N_e z^2}{\beta^2} B_{\text{col}}, \quad (6.59)$$

with parameters defined in Prob. 131.

- (2) Determine the electron density N_e of air for use in (6.59).
- (3) Determine β^2 for 10 MeV proton for use in (6.59).
- (4) Calculate the atomic stopping number B_{col} defined in (6.19) for use in (6.59).

- (5) Multiply S_{col} of (6.59) by density of standard air ($\rho_{\text{air}} = 1.293 \times 10^{-3} \text{ g/cm}^3$) to get the linear collision stopping power s_{col} .
- (6) Multiply s_{col} by $\overline{W}_{\text{air}}$, the mean energy required to produce an ion pair in air by a proton, to get the mean specific ionization j of air for a 10 MeV proton.

(1) Before we embark on calculation of the mass collision stopping power S_{col} we must determine the parameters of (6.59).

(2) **Electron density** N_e of air is calculated using the following composition of air per weight and molecular mass (see Table T8.2): nitrogen N: 75.8 %, $M_{\text{N}} = 14.0067$; oxygen O: 22.6 %, $M_{\text{O}} = 15.9994$; argon Ar: 0.93 %, $M_{\text{Ar}} = 39.948$; and carbon dioxide CO_2 : 0.03 %, $M_{\text{CO}_2} = 44$.

In one gram of air we thus have the following four constituents of importance: (0.758 g) of N + (0.226 g) of O + (0.0093 g) of Ar + (0.0003 g) of CO_2 and each one of the four components contributes the following number of electrons:

Nitrogen:

$$\begin{aligned} x_{\text{N}} &= \frac{(6.022 \times 10^{23} \text{ at/mol}) \times (0.758 \text{ g})}{14.0067 \text{ g/mol}} \times (7 \text{ el/at}) \\ &= 2.28125 \times 10^{23} \text{ el} \end{aligned} \quad (6.60)$$

Oxygen:

$$\begin{aligned} x_{\text{O}} &= \frac{(6.022 \times 10^{23} \text{ at/mol}) \times (0.226 \text{ g})}{15.9994 \text{ g/mol}} \times (8 \text{ el/at}) \\ &= 6.80512 \times 10^{22} \text{ el} \end{aligned} \quad (6.61)$$

Argon:

$$\begin{aligned} x_{\text{N}} &= \frac{(6.022 \times 10^{23} \text{ at/mol}) \times (0.0093 \text{ g})}{39.948 \text{ g/mol}} \times (18 \text{ el/at}) \\ &= 2.524 \times 10^{21} \text{ el} \end{aligned} \quad (6.62)$$

Carbon dioxide:

$$\begin{aligned} x_{\text{N}} &= \frac{(6.022 \times 10^{23} \text{ at/mol}) \times (0.0003 \text{ g})}{44 \text{ g/mol}} \times (28 \text{ el/at}) \\ &= 1.150 \times 10^{20} \text{ el} \end{aligned} \quad (6.63)$$

Electron density N_e of air is given by the sum of the components listed in (6.60) through (6.63) to yield $N_e = 2.99 \times 10^{23}$ electron/g.

(3) **Velocity** β of a 10 MeV proton is determined using the standard relationship (see T2.7)

$$\beta^2 = \frac{v^2}{c^2} = 1 - \frac{1}{\left(1 + \frac{E_{\text{K}}}{m_{\text{p}}c^2}\right)^2} = 1 - \frac{1}{\left(1 + \frac{10}{938.3}\right)^2} = 0.021. \quad (6.64)$$

(4) **Atomic stopping number** B_{col} is calculated as follows

$$\begin{aligned} B_{\text{col}} &= \left\{ \ln \frac{2m_e c^2}{I} + \ln \frac{\beta^2}{1 - \beta^2} - \beta^2 \right\} = \left\{ \ln \frac{1.022 \times 10^6}{86} + \ln \frac{0.021}{1 - 0.021} - 0.021 \right\} \\ &= \{9.3829 + (-3.842) - 0.021\} = 5.52. \end{aligned} \quad (6.65)$$

Finally, the mass collision stopping power S_{col} of air for a 10 MeV proton is

$$\begin{aligned} S_{\text{col}} &= C_1 \frac{N_e z^2}{\beta^2} B_{\text{col}} = (5.099 \times 10^{-25} \text{ MeV} \cdot \text{cm}^2) \times \frac{2.99 \times 10^{23} \text{ g}^{-1}}{0.021} \times 5.52 \\ &= 40.1 \text{ MeV} \cdot \text{cm}^2/\text{g} \quad (\text{shown as point A in Fig. 6.7}), \end{aligned} \quad (6.66)$$

in excellent agreement with the value of $40.1 \text{ MeV} \cdot \text{cm}^2/\text{g}$ that the NIST provides for dry air near sea level and 10 MeV proton at http://physics.nist.gov/cgi-bin/Star/ap_table.pl.

(5) **Linear collision stopping power** s_{col} is calculated by multiplying the mass collision stopping power S_{col} by density ρ

$$s_{\text{col}} = \rho S_{\text{col}} = (1.293 \times 10^{-3} \text{ g/cm}^3) \times (40.1 \text{ MeV} \cdot \text{cm}^2/\text{g}) = 0.0518 \text{ MeV/cm}. \quad (6.67)$$

Since $\overline{W}_{\text{air}}$ is 35 eV for protons in air, we get the following result for the mean specific ionization j of air for 10 MeV proton

$$j = \frac{s_{\text{col}}}{\overline{W}_{\text{air}}} = \frac{0.0518 \times 10^6 \text{ eV/cm}}{35 \text{ eV/ip}} = 1480 \text{ ip/cm} = 148 \text{ ip/mm}. \quad (6.68)$$

(b) As is evident from Fig. 6.7 (see point B), the maximum possible specific ionization j_{max} in air is produced when S_{col} against proton kinetic energy E_K is at its maximum and, for proton in standard air, this maximum occurs at $E_K = 0.084 \text{ MeV}$ and amounts to $S_{\text{col}}^{\text{max}} = 736 \text{ MeV} \cdot \text{cm}^2/\text{g}$.

Based on the discussion in (a), we now calculate j_{max} as follows

$$\begin{aligned} j_{\text{max}} &= \frac{s_{\text{col}}^{\text{max}}}{\overline{W}_{\text{air}}} = \frac{\rho_{\text{air}} S_{\text{col}}^{\text{max}}}{\overline{W}_{\text{air}}} \\ &= \frac{(1.293 \times 10^{-3} \text{ g/cm}^3) \times (736 \times 10^6 \text{ eV} \cdot \text{cm}^2/\text{g})}{35 \text{ eV/ip}} \\ &= 27190 \text{ ip/cm} = 2719 \text{ ip/mm}, \end{aligned} \quad (6.69)$$

in excellent agreement with the value of $j_{\text{max}} = 2750 \text{ ip/mm}$ stated by Evans (p. 656).

(c) To plot the specific ionization j against the residual range R_{residual} we first complete Table 6.9A which provides the NIST data on S_{col} and R_{CSDA} for protons (0.001 MeV to 10 MeV) in air.

Results of our calculation of j and R_{residual} are displayed in Table 6.9B. In Fig. 6.8 we plot the specific ionization j of Table 6.9B against residual range R_{residual} for the last 5 mm of the 10 MeV proton in air where the proton energy is already significantly diminished, rapidly approaches 0 and the ionization reaches its maximum value at the Bragg peak. *Note* that j_{max} occurs around the residual range of 1.2 mm where the proton energy falls to $E_K = 0.084$ MeV.

Table 6.9B Various physical parameters of 10 MeV proton traversing standard air

1	E_K (MeV)	S_{col} (NIST) (MeV · cm ² /g)	s_{col} (6.67) (MeV/cm)	j (6.68) (i.p./mm)	R_{CSDA} (NIST) (g/cm ²)	R_{residual} (mm)
2	0.001	141.4	0.148	442.2	9.857×10^{-6}	0.08
3	0.005	277.6	0.332	989.3	2.891×10^{-5}	0.22
4	0.01	385.0	0.469	1,399.0	4.400×10^{-5}	0.34
5	0.05	689.7	0.852	2,540.6	1.152×10^{-4}	0.90
6	0.07	729.3	0.902	2,688.7	1.433×10^{-4}	1.1
7	0.08	735.5	0.910	2,712.0	1.569×10^{-4}	1.2
8	0.09	735.2	0.909	2,711.6	1.705×10^{-4}	1.3
9	0.2	592.8	0.734	2,187.8	3.349×10^{-4}	2.6
10	0.5	350.1	0.433	1,292.3	1.021×10^{-3}	7.9
11	1	222.9	0.276	822.7	2.867×10^{-3}	22.2
12	2	137.1	0.170	506.1	8.792×10^{-3}	68
13	5	69.1	0.086	255.1	4.173×10^{-2}	323
14	10	40.1	0.050	147.9	1.408×10^{-1}	1089

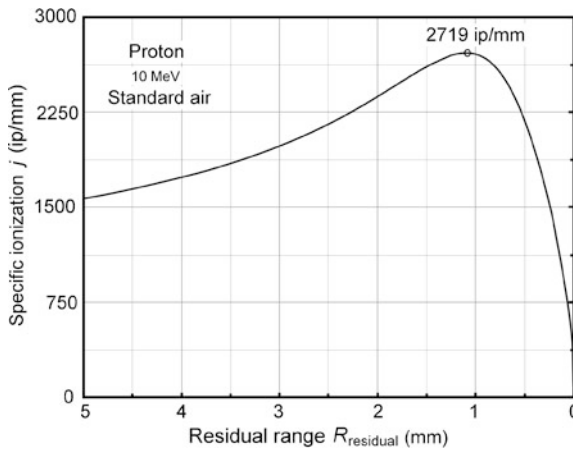


Fig. 6.8 Specific ionization produced in air by a 10 MeV proton traversing standard air at the last 5 mm of its track. The Bragg peak with maximum specific ionization $j_{\text{max}} = 2719$ ip/mm is clearly visible

6.4.Q7

(136)

The Bethe equation for the mass collision stopping power S_{col} of an absorber traversed by a heavy charged particle (CP) generally expressed as [see (6.17) in Prob. 131]

$$S_{\text{col}} = 4\pi \left(\frac{e^2}{4\pi\epsilon_0} \right)^2 \frac{z^2 N_e}{m_e c^2 \beta^2} \left\{ \ln \frac{2m_e c^2}{I} + \ln \frac{\beta^2}{1 - \beta^2} - \beta^2 \right\} \quad (6.70)$$

is often written in more condensed form as

$$S_{\text{col}} = C_1 \frac{z^2 N_e}{\beta^2} \{ f(\beta) - \ln I \}. \quad (6.71)$$

- (a) Show how (6.71) is obtained from (6.70).
- (b) Determine and plot $f(\beta)$ against kinetic energy E_K of the heavy CP for the following kinetic energies E_K in MeV: 0.01, 0.1, 1, 10, 100, and 1000.
- (c) Calculate the mass collision stopping power S_{col} of water for a 50 MeV proton using (6.71). Compare your result with data available from the NIST (<http://physics.nist.gov/PhysRefData/Star/Text/PSTAR.html>).
- (d) Use (6.71) to calculate the mass collision stopping power S_{col} of copper absorber traversed by α particles with kinetic energy E_K of 250 MeV. The mean ionization/excitation potential I of copper is 322 eV. Compare your result with data from the NIST (<http://physics.nist.gov/PhysRefData/Star/Text/ASTAR.html>).

SOLUTION:

(a) To evaluate the link between (6.71) and (6.70) we compare the two equations directly and first determine the collision stopping power constant C_1 [see (6.18) in Prob. 131]

$$\begin{aligned} C_1 &= 4\pi \left(\frac{e^2}{4\pi\epsilon_0} \right)^2 \frac{1}{m_e c^2} \equiv 4\pi r_e^2 m_e c^2 \\ &= 4\pi \times (2.818 \times 10^{-13} \text{ cm}^2) \times (0.511 \text{ MeV}) = 5.099 \times 10^{-25} \text{ MeV} \cdot \text{cm}^2 \end{aligned} \quad (6.72)$$

and then determine the functional form of the velocity function $f(\beta)$ by rewriting (6.70) in a more convenient form as

$$S_{\text{col}} = C_1 \frac{z^2 N_e}{\beta^2} \left\{ \ln \frac{2m_e c^2 \beta^2}{1 - \beta^2} - \beta^2 - \ln I \right\} \quad (6.73)$$

Table 6.10 Normalized velocity β and velocity function $f(\beta)$ for various proton kinetic energies E_K in the range from 0.01 MeV to 1000 MeV

E_K (MeV)	0.01	0.1	1	10	100	1000
β^2	2.1×10^{-5}	2.13×10^{-4}	0.00213	0.021	0.183	0.766
β	4.58×10^{-3}	0.0146	0.0462	0.145	0.428	0.875
$f(\beta)$	2.179	5.384	7.685	9.972	12.16	14.26

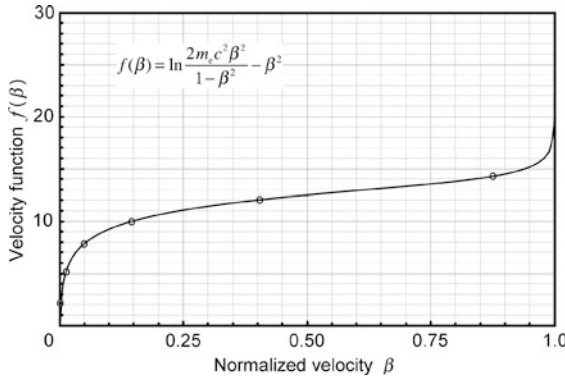


Fig. 6.9 Velocity function $f(\beta)$ against normalized heavy charged particle velocity β

which allows us to define $f(\beta)$ as follows

$$f(\beta) = \ln \frac{2m_e c^2 \beta^2}{1 - \beta^2} - \beta^2 = \ln \frac{1.022 \times 10^6 \beta^2}{1 - \beta^2} - \beta^2 \tag{6.74}$$

and also express the mass collision stopping power S_{col} , as shown in (6.71), where

- C_1 is the collision stopping power constant given in (6.72).
- $f(\beta)$ is the velocity function given in (6.74).
- $\ln I$ is the natural logarithm of the mean ionization/excitation potential of the absorber expressed in eV.

(b) The velocity function $f(\beta)$ against kinetic energy E_K of the heavy CP is determined by first calculating β for a given E_K and then inserting the calculated β into (6.74) to calculate $f(\beta)$. The results of the $f(\beta)$ calculation for E_K in MeV = 0.01, 0.1, 1, 10, 100, and 1000 for protons are listed in Table 6.10 and plotted in Fig. 6.9 against normalized velocity β and in Fig. 6.10 against kinetic energy E_K .

(c) As evident from (6.71), to determine the mass collision stopping power S_{col} of water for a proton with kinetic energy $E_K = 50$ MeV we need to know the electron density N_e of water, mean ionization/excitation potential I of water, and the velocity β of a 50 MeV proton. N_e of water has been determined in Prob. 133 as $N_e(\text{water}) = 3.343 \times 10^{23}$ electron/g. I of water has been determined in Prob. 132 as $I(\text{water}) = 74.4$ eV.

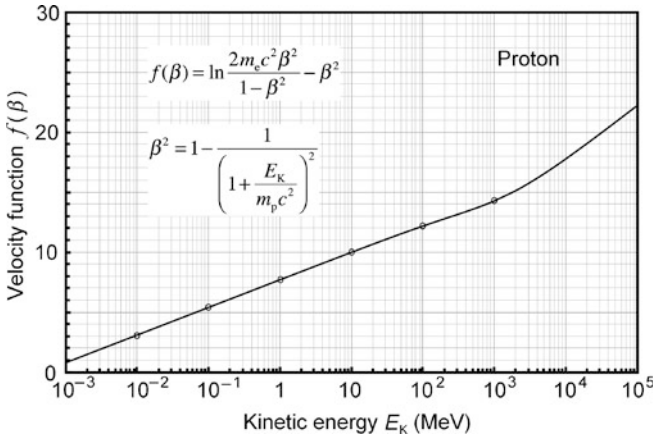


Fig. 6.10 Velocity function $f(\beta)$ against kinetic energy E_K for protons in the kinetic energy range from 10^{-3} MeV to 10^5 MeV

Normalized velocity β of a 50 MeV proton is calculated from the standard expression that follows from the basic definition for relativistic kinetic energy $E_K = [1/(1 - \beta^2)^{1/2} - 1]m_0c^2$, i.e.,

$$\beta^2 = 1 - \frac{1}{\left(1 + \frac{E_K}{m_p c^2}\right)^2} = 1 - \frac{1}{\left(1 + \frac{50}{938.3}\right)^2} = 0.099 \quad \text{or} \quad \beta = 0.314. \quad (6.75)$$

Velocity function $f(\beta)$ given in (6.74) yields the following value for a 50 MeV proton

$$f(\beta) = \ln \frac{1.022 \times 10^6 \beta^2}{1 - \beta^2} - \beta^2 = \ln \frac{1.022 \times 10^6 \times 0.099}{0.901} - 0.099 = 11.53. \quad (6.76)$$

The mass collision stopping power S_{col} of water is thus given as

$$\begin{aligned} S_{\text{col}} &= C_1 \frac{z^2 N_e}{\beta^2} \{f(\beta) - \ln I\} \\ &= (5.1 \times 10^{-25} \text{ MeV} \cdot \text{cm}^2) \times \frac{3.343 \times 10^{23} \text{ g}^{-1}}{0.099} \times 7.218 = 12.43 \text{ MeV} \cdot \text{cm}^2/\text{g} \end{aligned} \quad (6.77)$$

in excellent agreement with the value of $12.45 \text{ MeV} \cdot \text{cm}^2/\text{g}$ provided by the NIST for the collision stopping power of water for 50 MeV proton.

(d) To calculate S_{col} of copper absorber traversed by a 250 MeV α particle using (6.71) we first determine β^2 for the α particle and then calculate the velocity function $f(\beta)$ for the calculated β^2 . We then insert $f(\beta)$ into (6.71) to determine S_{col} .

Calculation of α particle velocity β from relativistic kinetic energy E_K

$$\beta^2 = 1 - \frac{1}{\left(1 + \frac{E_K}{m_p c^2}\right)^2} = 1 - \frac{1}{\left(1 + \frac{250}{3727.3}\right)^2} = 0.122 \quad \text{or} \quad \beta = 0.349. \quad (6.78)$$

Calculation of velocity function $f(\beta)$ using (6.74)

$$f(\beta) = \ln \frac{1.022 \times 10^6 \beta^2}{1 - \beta^2} - \beta^2 = \ln \frac{1.022 \times 10^6 \times 0.122}{1 - 0.122} - 0.122 = 11.74. \quad (6.79)$$

Calculation of mass collision stopping power S_{col} of copper for 250 MeV α particle

$$\begin{aligned} S_{\text{col}} &= C_1 \frac{z^2 N_e}{\beta^2} \{f(\beta) - \ln I\} = (5.099 \times 10^{-25} \text{ MeV} \cdot \text{cm}^2) \\ &\times \frac{4 \times 2.7485 \times 10^{23} \text{ g}^{-1}}{0.122} \times 5.965 = 27.41 \text{ MeV} \cdot \text{cm}^2/\text{g} \end{aligned} \quad (6.80)$$

in good agreement with the NIST value of 27.24 MeV \cdot cm²/g for mass collision stopping power of copper traversed by 250 MeV α particle.

6.5 Collision Stopping Power for Light Charged Particles

6.5.Q1

(137)

Mass collision stopping power S_{col} of a stopping medium (absorber) for light charged particles (CP) of kinetic energy E_K is given as follows

$$S_{\text{col}} = C_e \frac{N_e}{\beta^2} \left\{ \ln \frac{E_K^2}{I^2} + \ln \left(1 + \frac{\tau}{2} \right) + F^\pm(\tau) - \delta \right\}, \quad (6.81)$$

where

C_e is the stopping power constant for light CP (electron and positron).

$$\begin{aligned} C_e &= 2\pi r_e^2 m_e c^2 = 2\pi (2.818 \times 10^{-13} \text{ cm}^2) \times (0.511 \text{ MeV}) \\ &= 2.55 \times 10^{-25} \text{ MeV} \cdot \text{cm}^2. \end{aligned}$$

N_e is the electron density of the absorber: $N_e = ZN_A/A$.

r_e is the classical electron radius constant: $r_e = e^2/(4\pi\epsilon_0 m_e c^2) = 2.818$ fm.

τ is the electron kinetic energy E_K normalized to electron rest mass $m_e c^2 = 0.511$ MeV, i.e., $\tau = E_K/(m_e c^2)$.

$F^\pm(\tau)$ is the stopping power function of electron (F^-) and positron (F^+) given as follows

$$F^-(\tau) = \frac{1}{(\tau+1)^2} \left[1 + \frac{\tau^2}{8} - (2\tau+1)\ln 2 \right] \quad (6.82)$$

and

$$F^+(\tau) = 2\ln 2 - \frac{\tau(\tau+2)}{12(\tau+1)^2} \left[23 + \frac{14}{\tau+2} + \frac{10}{(\tau+2)^2} + \frac{4}{(\tau+2)^3} \right]. \quad (6.83)$$

- (a) Use (6.81) to calculate the mass collision stopping power S_{col} of lead absorber ($Z = 82$; $A = 207.2$ g/mol; $I = 823$ eV) for electrons with kinetic energies E_K of 100 keV, 1 MeV, and 10 MeV.
- (b) Compare S_{col} of lead calculated in (a) for electron kinetic energies E_K of 100 keV, 1 MeV, and 10 MeV with data obtained from the NIST or from *Appendix E* of Attix.
- (c) Plot the density effect parameter δ of lead against electron kinetic energy E_K in the range from $E_K = 10$ keV to $E_K = 100$ MeV. You can obtain the density effect parameter δ on-line from the NIST or from *Appendix E* of Attix.

SOLUTION:

(a) The problem will be solved in six steps, with the first five steps used to prepare suitable data for use in the last step that involves calculation of S_{col} with (6.81). The six steps are as follows:

- (1) Determine electron density N_e of the lead absorber

$$N_e = \frac{ZN_A}{A} = \frac{82 \times (6.022 \times 10^{23} \text{ mol}^{-1})}{207.2 \text{ g/mol}} = 2.388 \times 10^{23} \text{ electron/g.} \quad (6.84)$$

- (2) Determine the normalized kinetic energy τ for 100 keV, 1 MeV, and 10 MeV electrons using the following relationship

$$\tau = \frac{E_K}{m_e c^2}. \quad (6.85)$$

The calculated values of τ for electrons with kinetic energy E_K of 100 keV, 1 MeV, and 10 MeV are summarized in row 2 of Table 6.11.

Table 6.11 Summary of parameters used in calculation of mass collision stopping power S_{col} of lead for electrons with kinetic energy E_K of 100 keV, 1 MeV, and 10 MeV

1	Electron kinetic energy E_K	100 keV	1 MeV	10 MeV
2	Normalized kinetic energy τ	0.1957	1.957	19.57
3	Normalized electron velocity β	0.548	0.941	0.9988
4	β^2	0.30	0.886	0.9976
5	$1 - \beta^2$	0.70	0.114	0.0024
6	Stopping power function $F^-(\tau)$	0.028	-0.220	0.0497
7	Density effect parameter δ	0.0074	0.181	1.52
8	Calculated S_{col} (MeV \cdot cm ² /g)	1.969	0.994	1.198

- (3) Determine normalized electron velocity β for 100 keV, 1 MeV, and 10 MeV electrons using the following expressions

$$\beta^2 = 1 - \frac{1}{\left(1 + \frac{E_K}{m_e c^2}\right)^2} = 1 - \frac{1}{(1 + \tau)^2} \quad \text{and} \quad (6.86)$$

$$1 - \beta^2 = \frac{1}{\left(1 + \frac{E_K}{m_e c^2}\right)^2} = \frac{1}{(1 + \tau)^2}.$$

The calculated values of β , β^2 , and $1 - \beta^2$ are summarized in rows 3, 4, and 5 of Table 6.11, respectively.

- (4) Determine stopping power function for electron $F^-(\tau)$ using (6.82) for 100 keV, 1 MeV, and 10 MeV electron. The calculated values of $F^-(\tau)$ are summarized in row 6 of Table 6.11.
- (5) From the NIST (<http://physics.nist.gov/PhysRefData/Star/Text/ESTAR.html>) obtain the density effect parameter δ of lead absorber for 100 keV, 1 MeV, and 10 MeV electrons. The respective values of δ are listed in row 7 of Table 6.11.
- (6) Finally, employ (6.81) in conjunction with Table 6.11 that summarizes the supporting data required for use with (6.81) to determine S_{col} of lead for three electron kinetic energies E_K of 100 keV, 1 MeV, and 10 MeV.

Electron in lead: $E_K = 100 \text{ keV}$; $\tau = 0.1957$; $\beta = 0.548$

$$\begin{aligned} S_{\text{col}} &= C_e \frac{N_e}{\beta^2} \left\{ \ln \frac{E_K^2}{I^2} + \ln \left(1 + \frac{\tau}{2}\right) + F^\pm(\tau) - \delta \right\} \\ &= (2.55 \times 10^{-25} \text{ MeV} \cdot \text{cm}^2) \times \frac{2.383 \times 10^{23} \text{ g}^{-1}}{0.30} \\ &\quad \times \left\{ \ln \left(\frac{10^5}{823}\right)^2 + \ln \left(1 + \frac{0.1957}{2}\right) + F^-(0.1957) - 0.74 \times 10^{-3} \right\} \\ &= (0.2026 \text{ MeV} \cdot \text{cm}^2/\text{g}) \times \{9.60 + 0.093 + 0.028 - 0.0074\} \\ &= (0.2026 \text{ MeV} \cdot \text{cm}^2/\text{g}) \times 9.714 = 1.969 \text{ MeV} \cdot \text{cm}^2/\text{g}. \end{aligned} \quad (6.87)$$

Table 6.12 Comparison of mass collision stopping powers S_{col} of lead for electrons of kinetic energy of 100 keV, 1 MeV, and 10 MeV. Data calculated with (6.81) are displayed in row 2; data obtained from the NIST are shown in row 3; and data obtained from Appendix E of Attix are shown in row 4

1	Kinetic energy E_K of electron	100 keV	1 MeV	10 MeV
2	S_{col} [calculated with (6.81) in $\text{MeV} \cdot \text{cm}^2/\text{g}$]	1.969	0.994	1.198
3	S_{col} [from the NIST in $\text{MeV} \cdot \text{cm}^2/\text{g}$]	1.964	0.994	1.201
4	S_{col} [from Appendix E of Attix in $\text{MeV} \cdot \text{cm}^2/\text{g}$]	1.964	0.994	1.201

Electron in lead: $E_K = 1 \text{ MeV}$; $\tau = 1.957$; $\beta = 0.941$

$$\begin{aligned}
 S_{\text{col}} &= C_e \frac{N_e}{\beta^2} \left\{ \ln \frac{E_K^2}{I^2} + \ln \left(1 + \frac{\tau}{2} \right) + F^\pm(\tau) - \delta \right\} \\
 &= (2.55 \times 10^{-25} \text{ MeV} \cdot \text{cm}^2) \times \frac{2.383 \times 10^{23} \text{ g}^{-1}}{0.886} \\
 &\quad \times \left\{ \ln \left(\frac{10^6}{823} \right)^2 + \ln \left(1 + \frac{1.957}{2} \right) + F^-(1.957) - 0.181 \right\} \\
 &= (0.0686 \text{ MeV} \cdot \text{cm}^2/\text{g}) \times \{14.21 + 0.682 - 0.220 - 0.181\} \\
 &= (0.0686 \text{ MeV} \cdot \text{cm}^2/\text{g}) \times 14.49 = 0.994 \text{ MeV} \cdot \text{cm}^2/\text{g}. \quad (6.88)
 \end{aligned}$$

Electron in lead: $E_K = 10 \text{ MeV}$; $\tau = 19.57$; $\beta = 0.9988$

$$\begin{aligned}
 S_{\text{col}} &= C_e \frac{N_e}{\beta^2} \left\{ \ln \frac{E_K^2}{I^2} + \ln \left(1 + \frac{\tau}{2} \right) + F^\pm(\tau) - \delta \right\} \\
 &= (2.55 \times 10^{-25} \text{ MeV} \cdot \text{cm}^2) \times \frac{2.383 \times 10^{23} \text{ g}^{-1}}{0.9976} \\
 &\quad \times \left\{ \ln \left(\frac{10^7}{823} \right)^2 + \ln \left(1 + \frac{19.57}{2} \right) + F^-(19.57) - 1.52 \right\} \\
 &= (0.06091 \text{ MeV} \cdot \text{cm}^2/\text{g}) \times \{18.810 + 2.378 + 0.00497 - 1.52\} \\
 &= (0.06091 \text{ MeV} \cdot \text{cm}^2/\text{g}) \times 19.673 = 1.198 \text{ MeV} \cdot \text{cm}^2/\text{g}. \quad (6.89)
 \end{aligned}$$

(b) Table 6.12 displays mass collision stopping power S_{col} of lead for electrons with kinetic energies of 100 keV, 1 MeV, and 10 MeV: row 2 displays values calculated in (a) and row 3 values obtained from the NIST. The agreement between the calculated values of (a) and tabulated values from the NIST is excellent suggesting that (6.81) may be used in conjunction with (6.82) for estimation of mass collision stopping powers for electrons.

Figure 6.11 shows the mass collision stopping power S_{col} of water, aluminum, and lead for electrons against electron kinetic energy E_K with heavy solid lines and, for comparison, mass radiation stopping powers for same absorbers are shown with light solid lines. Similarly to stopping power behavior for heavy CPs, the data

for electrons show that higher atomic number absorbers have lower S_{col} than lower atomic number absorbers at same electron kinetic energies as a result of the Z/A term in electron density as well as the $(-\ln I)$ term, where I is the mean ionization/excitation potential of the absorbing medium.

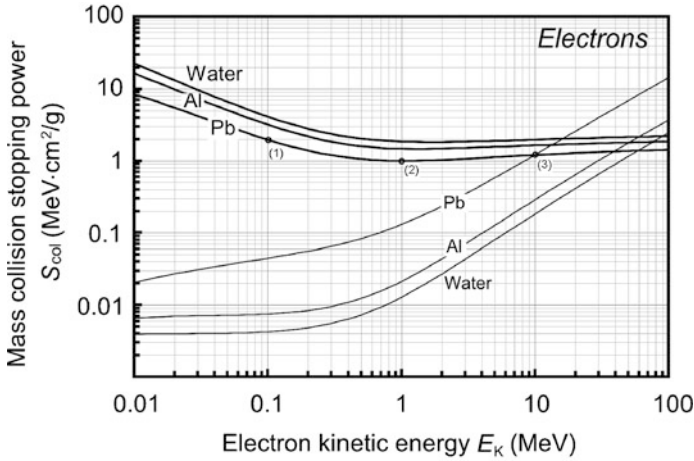


Fig. 6.11 Mass collision stopping power S_{col} of water, aluminum, and lead for electrons of kinetic energy in the range from 0.01 MeV to 100 MeV. The collision stopping power data are shown with *heavy solid lines*; for comparison the *light solid lines* show the mass radiation stopping power of same stopping media for electrons. Data were obtained from the NIST. Points (1), (2), and (3) display the data calculated with (6.81) in (a) for 100 keV, 1 MeV, and 10 MeV electrons in lead

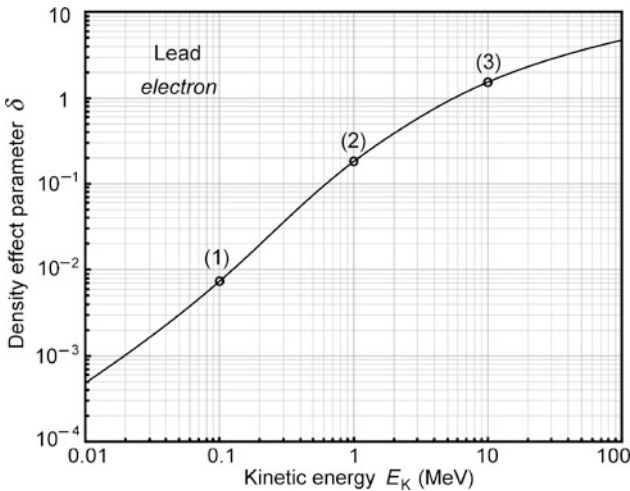


Fig. 6.12 Density effect parameter δ of lead against electron kinetic energy E_k . Points (1), (2), and (3) show data that were used in calculation of mass collision stopping power S_{col} of lead for electron energies of 100 keV, 1 MeV, and 10 MeV, respectively

(c) The density effect parameter δ is a function of the composition and density of the absorber as well as of the velocity v of the light CP traversing the absorber. Figure 6.12 shows δ plotted against electron or positron kinetic energy E_K of lead obtained from the NIST and also provided in *Appendix E* of Attix. Data used in (a) for the calculation of the mass collision stopping power S_{col} of lead for 100 keV, 1 MeV, and 10 MeV electrons are shown as points (1), (2), and (3), respectively. The dependence of S_{col} on stopping medium results from two factors in the collision stopping power expression given in (6.81). The two factors are the electron density $N_e = ZN_A/A$ and the mean ionization/excitation potential I , both lowering S_{col} with an increasing atomic number Z of the stopping medium.

6.5.Q2

(138)

Expressions for the mass collision stopping power S_{col} of a given absorber for electron and positron traversing the absorber are of the same form except for the difference in the stopping power functions F^- for electron and F^+ for positron. The two functions are given as follows

$$F^-(\tau) = \frac{1}{(\tau + 1)^2} \left[1 + \frac{\tau^2}{8} - (2\tau + 1) \ln 2 \right] \quad (6.90)$$

and

$$F^+(\tau) = 2 \ln 2 - \frac{\tau(\tau + 2)^2}{12(\tau + 1)^2} \left[23 + \frac{14}{\tau + 2} + \frac{10}{(\tau + 2)^2} + \frac{4}{(\tau + 2)^3} \right], \quad (6.91)$$

where τ is the kinetic energy of the electron and positron E_K normalized to the electron/positron rest energy $m_e c^2$, i.e., $\tau = E_K/(m_e c^2)$.

- (a) Figure 6.13 plots $F^-(\tau)$ and $F^+(\tau)$ against kinetic energy E_K . Calculate $F^-(\tau)$ and $F^+(\tau)$ for $E_K = 0.337$ MeV using (6.90) and (6.91), respectively, and verify that your results fit on the F^\pm graph of Fig. 6.13.
- (b) Determine analytically the following features of the two stopping power functions F^- and F^+ : (1) $\lim_{\tau \rightarrow 0} F^-$; (2) $\lim_{\tau \rightarrow 0} F^+$; (3) $\lim_{\tau \rightarrow \infty} F^-$; (4) $\lim_{\tau \rightarrow \infty} F^+$; (5) τ_0^- for $F^-(\tau_0^-) = 0$; and (6) τ_*^- for absolute minimum in F^- .
- (c) Use Fig. 6.13 to determine the following features of the stopping power function F^- and F^+ : (1) τ_0^+ for $F^+(\tau_0^+) = 0$; (2) τ' for $F^+(\tau') = F^-(\tau')$; and (3) τ_*^+ for absolute minimum in F^+ .
- (d) Comment on the behavior of the two stopping power functions F^- and F^+ with respect to the kinetic energy E_K of the electron and positron, respectively.

SOLUTION:

(a) We first determine $\tau = E_K/(m_e c^2) = 0.337/0.511 = 0.66$ for the light CP of kinetic energy $E_K = 0.337$ MeV and then insert τ into (6.90) and (6.91) to get

$$\begin{aligned} F^-(\tau) &= \frac{1}{(\tau+1)^2} \left[1 + \frac{\tau^2}{8} - (2\tau+1) \ln 2 \right] \\ &= \frac{1}{1.66^2} \left[1 + \frac{0.66^2}{8} - 2.32 \ln 2 \right] = -0.20, \end{aligned} \quad (6.92)$$

$$F^+(\tau) = 2 \ln 2 - \frac{0.66 \times 2.66}{12 \times 1.66^2} \left[23 + \frac{14}{2.66} + \frac{10}{2.66^2} + \frac{4}{2.66^3} \right] = -0.20. \quad (6.93)$$

As shown in Fig. 6.13, the two functions F^- and F^+ are identical and equal to -0.2 at 0.337 MeV.

(b) The stopping power functions for electron and positron are from (6.90) and (6.91) given as

$$\begin{aligned} F^-(\tau) &= \frac{1 + \frac{\tau^2}{8} - (2\tau+1) \ln 2}{(\tau+1)^2}, \\ F^+(\tau) &= 2 \ln 2 - \frac{\tau(\tau+2)}{12(\tau+1)^2} \left[23 + \frac{14}{\tau+2} + \frac{10}{(\tau+2)^2} + \frac{4}{(\tau+2)^3} \right]. \end{aligned}$$

(1)

$$\lim_{\tau \rightarrow 0} F^- = \lim_{\tau \rightarrow 0} \left\{ \frac{1}{(\tau+1)^2} \left[1 + \frac{\tau^2}{8} - (2\tau+1) \ln 2 \right] \right\} = 1 - \ln 2 = 0.3069. \quad (6.94)$$

(2)

$$\begin{aligned} \lim_{\tau \rightarrow 0} F^+(\tau) &= \left\{ 2 \ln 2 - \frac{\tau(\tau+2)}{12(\tau+1)^2} \left[23 + \frac{14}{\tau+2} + \frac{10}{(\tau+2)^2} + \frac{4}{(\tau+2)^3} \right] \right\} \\ &= 2 \ln 2 \approx 1.386. \end{aligned} \quad (6.95)$$

(3)

$$\lim_{\tau \rightarrow \infty} F^- = \lim_{\tau \rightarrow \infty} \left\{ \frac{\frac{1}{\tau^2} + \frac{1}{8} - \frac{2 \ln 2}{\tau} + \frac{\ln 2}{\tau^2}}{1 + \frac{2}{\tau} + \frac{1}{\tau^2}} \right\} = \frac{1}{8} = 0.125. \quad (6.96)$$

(4)

$$\begin{aligned} \lim_{\tau \rightarrow \infty} F^+ &= \lim_{\tau \rightarrow \infty} \left\{ 2 \ln 2 - \frac{1 + \frac{2}{\tau}}{12 + \frac{24}{\tau} + \frac{12}{\tau^2}} \left[23 + \frac{14}{\tau+2} + \frac{10}{(\tau+2)^2} + \frac{4}{(\tau+2)^3} \right] \right\} \\ &= 2 \ln 2 - \frac{23}{12} = -0.5304. \end{aligned} \quad (6.97)$$

(5)

$$F^-(\tau_0^-) \frac{1 + \frac{(\tau_0^-)^2}{8} - (2\tau_0^- + 1) \ln 2}{(\tau_0^- + 1)^2} = 0 \quad \text{or} \quad (6.98)$$

$$(\tau_0^-)^2 - (16 \ln 2)\tau - 8(\ln 2 - 1) = 0,$$

$$\tau_0^- = \frac{16 \ln 2 \pm \sqrt{(16 \ln 2)^2 + 32(\ln 2 - 1)}}{2} \quad \text{or} \quad (6.99)$$

$$(\tau_0^-)_1 = 0.225 \rightarrow E_K[(\tau_0^-)_1] = 0.115 \text{ MeV},$$

$$(\tau_0^-)_2 = 10.87 \rightarrow E_K[(\tau_0^-)_2] = 5.55 \text{ MeV}.$$

(6) To find the absolute minimum in F^- we set $dF^-/d\tau|_{\tau=\tau_*^-} = 0$ and get

$$\left. \frac{dF^-}{d\tau} \right|_{\tau=\tau_*^-} = -\frac{2}{(1+\tau)^3} \left[1 + \frac{\tau^2}{8} - (2\tau+1) \ln 2 \right] + \frac{1}{(1+\tau)^2} \left[\frac{2\tau}{8} - 2 \ln 2 \right] = 0 \quad (6.100)$$

resulting in

$$-2 + \tau \left(2 \ln 2 + \frac{1}{4} \right) = 0 \quad \text{and} \quad \tau_*^- = 1.222 \quad \text{or} \quad E_K^* = \tau_*^- m_e c^2 = 0.625 \text{ MeV}. \quad (6.101)$$

Results of calculations (1) through (6) are displayed in Fig. 6.13 as data points (1) through (6) on the F^- and F^+ stopping power curves.

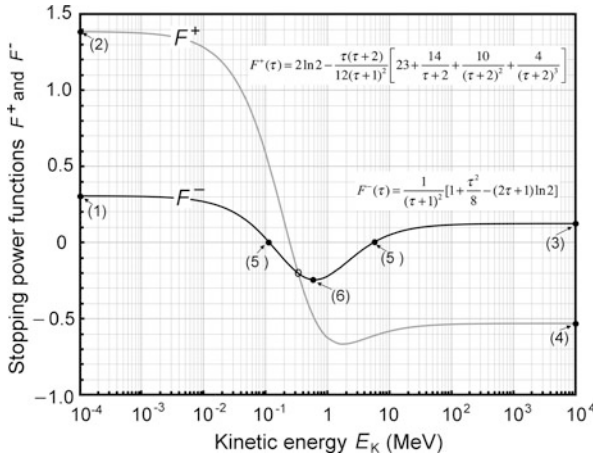


Fig. 6.13 Stopping power functions F^- and F^+ against kinetic energy E_K of the electron and positron, respectively. Data points (1) through (6) on F^+ and F^- curves represent data calculated in (b) in (6.94), (6.95), (6.96), (6.97), (6.98), and (6.100), respectively. The open circle point defines the point of intersection of the F^+ and F^- curves at kinetic energy $E_K = 0.337$ MeV, as calculated in (a)

(c) We now determine τ_0^+ , τ' , and τ_*^+ by reading the values directly from Fig. 6.13 and get: $\tau_0^+ = 0.482$ with $E_K(\tau_0^+) = \tau_0^+ m_e c^2 = 0.247$ MeV; $\tau' = -0.66$ with $E_K(\tau') = \tau' m_e c^2 = 0.337$, and $\tau_*^+ = 3.52$ with $E_K(\tau_*^+) = \tau_*^+ m_e c^2 = 1.8$ MeV.

(d) Mass collision stopping powers of a given material differ for electron and positron because of the differences in the two stopping power functions F^- and F^+ , respectively, plotted in Fig. 6.13. At low kinetic energies E_K , function $F^-(\tau)$ exceeds function $F^+(\tau)$ by a factor of $1.386/0.3069 \approx 4.5$, as determined in (b). Both F^- and F^+ then decrease with increasing E_K , become negative crossing the abscissa axis at ~ 0.115 MeV and ~ 0.24 MeV, respectively, and become equal (-0.2) at ~ 0.3 MeV. Both functions then go through their respective absolute minima at around $E_K \approx 1$ MeV and then attain saturation at very high E_K ; F^+ saturates at ~ -0.53 and F^- at ~ 0.125 , as also determined in (b).

6.6 Total Mass Stopping Power

6.6.Q1

(139)

For a given atomic number Z of the stopping medium, kinetic energy E_K of the light CP (electron or positron) at which both components of S_{tot} are identical is referred to as the critical kinetic energy E_K^{crit} . Radiation physics literature suggests that E_K^{crit} for a given stopping material Z can be estimated from the following empirical expression

$$E_K^{\text{crit}} = \frac{\text{const}}{Z} = \frac{800 \text{ MeV}}{Z}. \quad (6.102)$$

- (a) Fig. 6.14 plots S_{rad} and S_{col} for seven stopping materials: helium, carbon, aluminum, copper, silver, lead, and uranium against the kinetic energy E_K of the light CP. Data are from the NIST and the plot is for E_K in the vicinity of E_K^{crit} for the seven stopping materials. Curves in Fig. 6.14 are not labeled. Identify S_{rad} and S_{col} curves for the 7 stopping materials.
- (b) From appropriately labeled Fig. 6.14 determine the critical kinetic energy E_K^{crit} of the 7 stopping materials, plot E_K^{crit} against Z and compare with a plot of (6.102). Discuss how (6.102) is satisfied for the 7 elements and draw general conclusions on the validity of (6.102) for stopping materials in general.

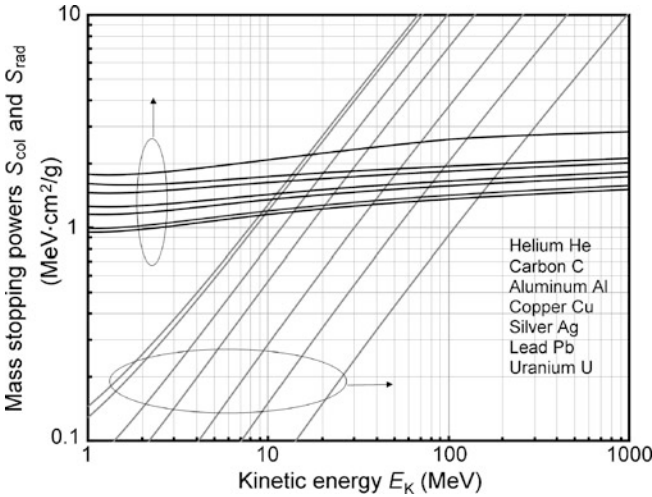


Fig. 6.14 Mass radiation stopping power S_{rad} and mass collision stopping powers S_{col} for seven stopping media around the region where the two stopping powers for a given stopping medium are equal

SOLUTION:

(a) We identify the stopping power curves of Fig. 6.14 through accounting for the following two facts related to stopping powers of light CPs:

(1) For all stopping materials irrespective of atomic number Z the collision component S_{col} of S_{tot} predominates at kinetic energies $E_K < 10$ MeV, while the radiation component S_{rad} of S_{tot} predominates at $E_K > 100$ MeV. In the intermediate region, where E_K is between 10 MeV and 100 MeV, the region of predominance depends on the atomic number Z of the stopping medium. Based on this we conclude that the heavy curves in Fig. 6.14 represent S_{col} of the 7 stopping media and the light curves represent S_{rad} of the 7 stopping media (see Fig. 6.15).

(2) At a given kinetic energy E_K of the light CP, S_{col} is inversely proportional to Z of the stopping medium as a result of two properties of the stopping medium: electron density $N_e = ZN_A/A$ and mean ionization/excitation potential I , as evident from (6.17). Both N_e and $\ln I$ decrease S_{col} with increasing Z . On the other hand, as shown in (6.3), S_{rad} is proportional to ZN_e which suggests a linear proportion of S_{rad} with Z , since Z/A in N_e is essentially constant for all stopping media.

In Fig. 6.14 we thus arrange the S_{col} curves in the order of increasing Z from top (He) to bottom (U) and the S_{rad} curves in reverse order with U on the top and He on the bottom, as shown in Fig. 6.15.

(b) We are now ready to determine critical kinetic energy E_K^{crit} for the seven materials using data from Fig. 6.15. E_K^{crit} is defined as the intercept between S_{col} and

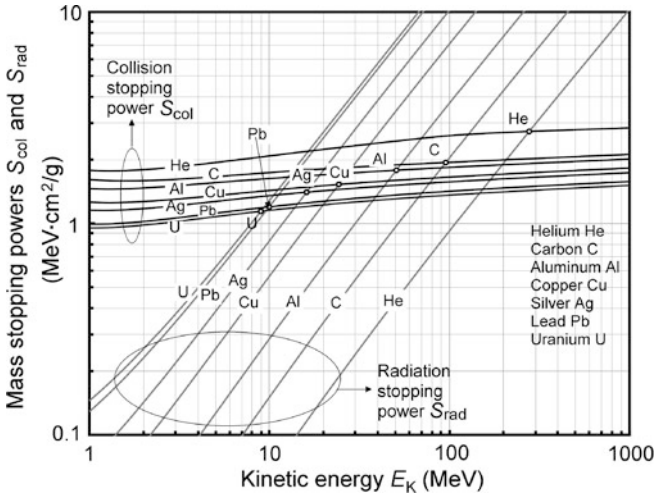


Fig. 6.15 Mass radiation and mass collision stopping powers, S_{rad} and S_{col} , respectively, for seven stopping media: helium, carbon, aluminum, copper, silver, lead, and uranium around the region where the two stopping powers for a given stopping medium are equal. Critical kinetic energy E_K^{crit} for the seven stopping media is identified with open circle data points

Table 6.13 Critical kinetic energy of various stopping media. Measured data are obtained from the NIST, calculated data are determined from (6.102)

(1) Stopping medium	Helium He	Carbon C	Alumin Al	Copper Cu	Silver Ag	Lead Pb	Uran U
(2) Atomic number Z	2	6	13	29	47	82	92
(3) E_K^{crit} (MeV) measured data	277	96	51	24.3	16	10	9
(5) $E_K^{crit} \times Z$ (MeV) measured data	554	576	663	705	752	820	823
(6) E_K^{crit} (MeV) calculated from (6.102)	400	133	61.5	27.6	17.0	9.8	8.7
(7) $E_K^{crit} \times Z$ (MeV) calculated from (6.102)	800	800	800	800	800	800	800
(8) $S_{col} = S_{rad}$ (MeV · cm ² /g)	2.73	1.95	1.79	1.53	1.41	1.20	1.14

S_{rad} curves for the given stopping material and we can now read E_K^{crit} directly from the graph. The results for the 7 stopping media are listed in Table 6.13 in row (3). Also listed in the table is atomic number Z of the stopping medium in row (2) as well as in row (6) the critical energy E_K^{crit} determined from (6.102).

The measured and calculated E_K^{crit} data are plotted in Fig. 6.16 against atomic number Z of the various stopping materials with data points and solid curve, respectively. The agreement between the two sets appears to be reasonable, suggesting that (6.102) is a good and simple empirical approximation for determination of E_K^{crit} .

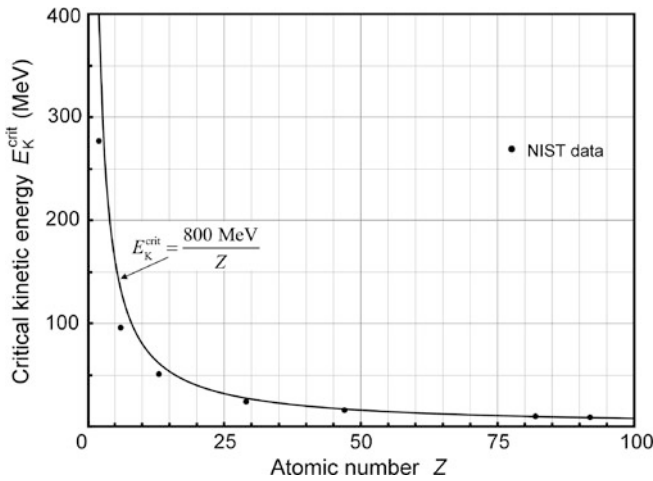


Fig. 6.16 Critical kinetic energy E_K^{crit} against atomic number Z for seven stopping materials ranging in Z from 6 to 92. The *solid curve* represents data calculated from (6.102), the *data points* represent data based on mass collision and mass radiation stopping power data obtained from the NIST

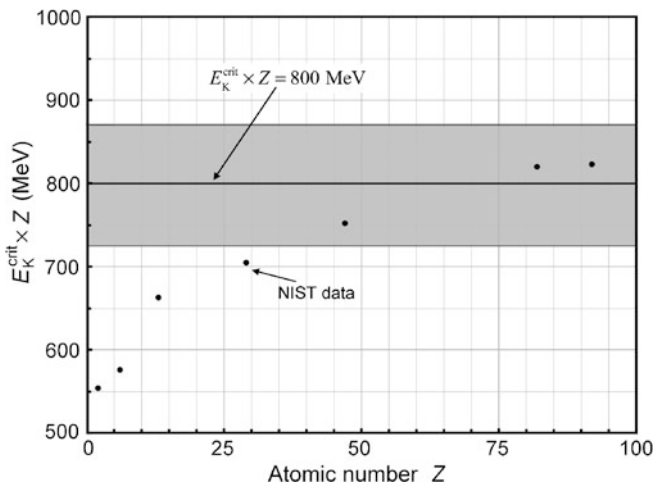


Fig. 6.17 Product of critical kinetic energy E_K^{crit} and atomic number Z against atomic number Z for seven stopping materials ranging in Z from 6 to 92. The *solid curve* represents data calculated from (6.102), the *data points* represent data based on mass collision and mass radiation stopping power data obtained from the NIST. The *grey area* represents $\pm 10\%$ deviation from (6.102)

However, a comparison between rows (3) and (5) of Table 6.13 suggests otherwise, especially for stopping media of low Z . We therefore re-plot the data in the form of $E_K^{\text{crit}} \times Z$ and get a better picture on the discrepancy between (6.102) and the NIST data, as shown in Fig. 6.17. The grey area in the figure shows a region of $\pm 10\%$

agreement with (6.102) and we note that for $Z < 30$ data calculated with (6.102) exceed the NIST data by more than 10 % and the discrepancy margin increases as Z decreases.

Figure 6.17 shows that (6.102) must be used with caution, especially at low atomic number Z where it overestimates the critical kinetic energy E_K^{crit} by ~ 50 %. At large Z (6.102) provides a more reliable means for estimation of the critical kinetic energy E_K^{crit} achieving an accuracy of about ± 5 %.

6.6.Q2

(140)

The ratio between the two components $S_{\text{col}}/S_{\text{rad}}$ of light charged particle (CP) stopping power at a given kinetic energy E_K of the light CP depends on E_K as well as on the atomic number Z of the stopping material and can be approximated with the following empirical expression

$$\frac{S_{\text{col}}}{S_{\text{rad}}} = \frac{E_K^{\text{crit}}}{E_K}, \quad (6.103)$$

where E_K^{crit} , the so-called critical kinetic energy, is the kinetic energy of the light CP at which the two components of S_{tot} are identical, i.e., $S_{\text{col}}(E_K^{\text{crit}}) = S_{\text{rad}}(E_K^{\text{crit}}) = \frac{1}{2}S_{\text{tot}}(E_K^{\text{crit}})$.

- (a) Figure 6.18 shows an unlabeled graph of S_{col} in one group and S_{rad} in another group. Each group of curves covers seven stopping materials: helium, carbon, aluminum, copper, silver, lead, and uranium against E_K of the light CP. Identify the two groups of curves and for each curve provide the stopping material.
- (b) Verify the validity of (6.103) for the following three stopping materials: carbon, copper, and lead. Obtain the stopping power and E_K^{crit} data for the three stopping materials from appropriately labeled Fig. 6.18.
- (c) For the three stopping materials of (b) plot your results and compare the NIST data on $S_{\text{col}}/S_{\text{rad}}$ with the ratio E_K^{crit} in the E_K range from 0.01 MeV to 1000 MeV. Make general comments on the validity of (6.103).

SOLUTION:

(a) Before we can identify the stopping power curves in Fig. 6.18 we should consider the following points:

- (1) Both S_{col} as given in (6.70) and S_{rad} as given in (6.3) depend upon atomic number Z of the stopping material as well as on kinetic energy E_K of the light CP.

- (2) Dependence of S_{col} on Z is manifested directly through electron density N_e that is proportional to Z/A and indirectly on ionization/excitation potential I through the $(- \ln I)$ term. Both Z/A and $(- \ln I)$ diminish S_{col} with increasing Z .
- (3) Dependence of S_{rad} on Z is manifested directly through the ZN_e factor that indicates direct proportionality of S_{rad} with Z , since N_e through Z/A exhibits only a slight dependence on Z . Note that in the first approximation $Z/A \approx 0.5$ for all elements, however, in reality Z/A ranges from 0.5 at low Z down to ~ 0.4 at high Z with only one notable exception of hydrogen for which $Z/A = 1$.
- (4) Dependence of S_{col} on E_K is divided into 3 regions: at relatively low kinetic energy, S_{col} is inversely proportional to E_K (i.e., goes as $1/E_K$), reaches a broad minimum at a few MeV as the light CP approaches speed of light c , and then slowly rises at relativistic energies above 10 MeV.
- (5) Dependence of S_{rad} on E_K is manifested directly through the $(E_K + m_e c^2)$ term and indirectly through the B_{rad} term that is constant for $E_K < m_e c^2$ and exhibits a slow rise with E_K increasing above 1 MeV.

(b) We now use Fig. 6.19 that is based on data from the NIST to determine S_{col} and S_{rad} for carbon, copper, and lead at the following kinetic energies in MeV: 0.01, 0.1, 1, 10, 100, and 1000. We also determine E_K^{crit} following the same procedure that was followed in Prob. 141. Our results are listed in Table 6.14 in which we also give the ratios $S_{\text{col}}/S_{\text{rad}}$ and E_K^{crit}/E_K . Since the table represents 3 stopping materials, one each for low Z , intermediate Z , and high Z , we can draw some general conclusions about the general validity of (6.103), as proscribed in (c).

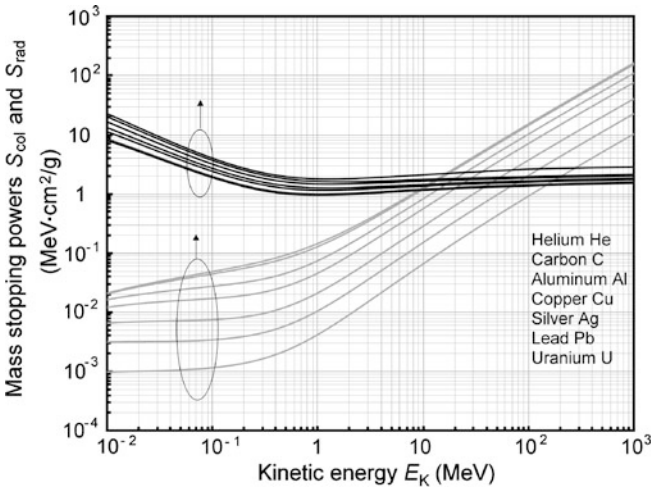


Fig. 6.18 Mass collision stopping power S_{col} and mass radiation stopping power S_{rad} for 7 stopping materials in the atomic number Z (range from 2 to 92) against kinetic energy E_K of the light CP

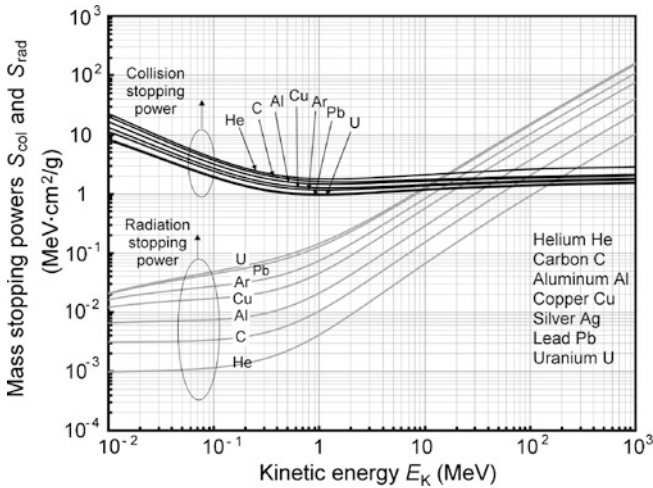


Fig. 6.19 Mass collision stopping power S_{col} and mass radiation stopping power S_{rad} for 7 stopping materials in the atomic number Z (range from 2 to 92) against kinetic energy E_K of the light CP. Data are from the NIST

Table 6.14 Ratios S_{col}/S_{rad} and E_K^{crit}/E_K of (6.103) of carbon, copper, and lead at various kinetic energies E_K of electron. Data are from the NIST

E_K (MeV)	Carbon $Z = 6$ $E_K^{crit} = 96 \text{ MeV}$				Copper $Z = 29$ $E_K^{crit} = 24.3 \text{ MeV}$				Lead $Z = 82$ $E_K^{crit} = 10 \text{ MeV}$			
	S_{rad}	S_{col}	$\frac{S_{col}}{S_{rad}}$	$\frac{E_K^{crit}}{E_K}$	S_{rad}	S_{col}	$\frac{S_{col}}{S_{rad}}$	$\frac{E_K^{crit}}{E_K}$	S_{rad}	S_{col}	$\frac{S_{col}}{S_{rad}}$	$\frac{E_K^{crit}}{E_K}$
0.01	0.003	20	6667	9600	0.012	13.2	1100	2430	0.02	8.5	425	1000
0.1	0.0035	3.7	1057	960	0.017	2.7	159	243	0.05	2	44.4	100
1	0.01	1.6	160	96	0.046	1.3	28.3	24.3	0.13	1	7.7	10
10	0.15	1.8	12	9.6	0.57	1.4	2.5	2.43	1.2	1.2	1	1
100	2	2	1	0.96	7	1.7	0.24	0.243	14	1.4	0.1	0.1
1000	22	2.1	0.1	0.1	76.5	1.85	0.024	0.024	155	1	0.01	0.01

(c) To visualize better the results of (6.103) presented in Table 6.14 we plot and compare the two ratios S_{col}/S_{rad} (shown as data points) and E_K^{crit}/E_K (shown with solid line) in Fig. 6.20. It is evident that the two ratios agree well for electron kinetic energy E_K above 1 MeV; however, for $E_K < 1$ MeV the agreement breaks down and $S_{col}/S_{rad} < E_K^{crit}/E_K$, the lower the kinetic energy the worse is the agreement, so that at kinetic energy $E_K = 0.001$ MeV ratio E_K^{crit}/E_K exceeds ratio S_{col}/S_{rad} by at least 50 %. We thus conclude that (6.103) is a reasonable approximation for estimation of the ratio S_{col}/S_{rad} at electron kinetic energy exceeding 1 MeV, however, for $E_K < 1$ MeV (6.103) is not reliable, especially for kinetic energy that is much smaller than 1 MeV.

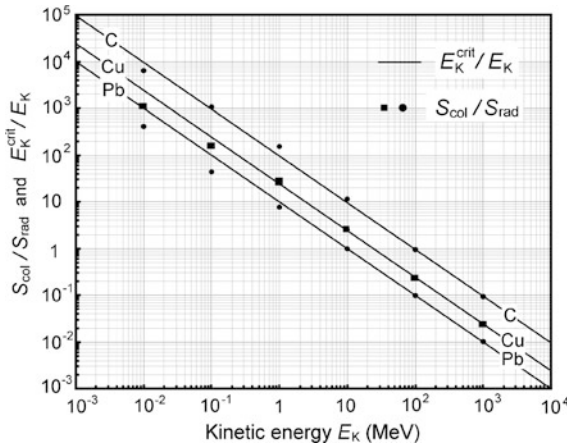


Fig. 6.20 Comparison of ratios $S_{\text{col}}/S_{\text{rad}}$ and $E_{\text{K}}^{\text{crit}}/E_{\text{K}}$ for carbon, copper and lead at various electron kinetic energies

6.7 Radiation Yield

6.7.Q1

(141)

The following data are provided in Table 6.15: mass radiation stopping power S_{rad} , mass collision stopping power S_{col} , total mass stopping power S_{tot} , ratio $S_{\text{rad}}/S_{\text{tot}}$, and ratio $S_{\text{col}}/S_{\text{tot}}$. Based on these data determine the following quantities for electrons with initial kinetic energy $(E_{\text{K}})_0$ of 4 MeV striking a lead absorber:

- Radiation yield $Y[(E_{\text{K}})_0]$.
- Energy E_{K} radiated in the form of bremsstrahlung photons (radiation loss) per incident electron.
- Energy E_{col} lost by the incident electron through ionization of lead atoms (collision loss) per incident electron.
- Based on data used in calculation of radiation yield $Y[(E_{\text{K}})_0]$ for $(E_{\text{K}})_0 = 4$ MeV in (a) plot $Y[(E_{\text{K}})_0]$ for electrons in lead with initial kinetic energies $(E_{\text{K}})_0$ between 0 and 4 MeV with kinetic energy E_{K} interval of 0.5 MeV.

SOLUTION:

(a) Radiation yield $Y[(E_{\text{K}})_0]$ of an electron with initial kinetic energy $(E_{\text{K}})_0$ striking an absorber is defined as that fraction of the initial kinetic energy $(E_{\text{K}})_0$ that is emitted as bremsstrahlung radiation with energy E_{rad} through the slowing down process of the electron in the absorber.

Table 6.15 Stopping power data of lead obtained from the NIST in electron kinetic energy range from 10^{-3} MeV to 10 MeV

(1)	(2)	(3)	(4)	(5)	(6)	(7)	(8)
n	E_K (MeV)	S_{rad} (MeV · cm ² /g)	S_{col} (MeV · cm ² /g)	S_{tot} (MeV · cm ² /g)	S_{rad}/S_{tot}	S_{col}/S_{tot}	$1/S_{tot}$ (MeV · cm ² /g) ⁻¹
1	0	0			0	1.0	
2	0.5	0.082	1.053	1.135	0.0725	0.9275	0.8811
3	1	0.129	0.994	1.123	0.1149	0.8851	0.8905
4	1.5	0.179	1.004	1.183	0.1513	0.8487	0.8453
5	2	0.232	1.024	1.256	0.1846	0.8153	0.7962
6	2.5	0.287	1.044	1.331	0.2156	0.7844	0.7513
7	3	0.343	1.063	1.406	0.2440	0.7560	0.7112
8	3.5	0.400	1.080	1.480	0.2703	0.7297	0.6757
9	4	0.458	1.095	1.553	0.2949	0.7057	0.6439
10	4.5	0.517	1.108	1.625	0.3181	0.6818	0.6154
11	5	0.577	1.120	1.697	0.3400	0.6600	0.5893
12	5.5	0.638	1.132	1.770	0.3605	0.6395	0.5650
13	6	0.699	1.142	1.841	0.3797	0.6203	0.5432
14	6.5	0.761	1.151	1.912	0.3980	0.6020	0.5230
15	7	0.823	1.160	1.983	0.4150	0.5850	0.5043
16	7.5	0.886	1.168	2.054	0.4314	0.5686	0.4869
17	8	0.950	1.175	2.125	0.4470	0.5529	0.4706
18	8.5	1.013	1.182	2.195	0.4615	0.5385	0.4556
19	9	1.077	1.189	2.266	0.4753	0.5247	0.4413
20	9.5	1.142	1.195	2.337	0.4887	0.5113	0.4279
21	10	1.206	1.201	2.407	0.5010	0.4990	0.4155
22	10.5	1.272	1.206	2.478	0.5133	0.4867	0.4036
23	11	1.337	1.212	2.549	0.5245	0.4755	0.3923
24	11.5	1.403	1.217	2.619	0.5357	0.4647	0.3818
25	12	1.469	1.221	2.690	0.5461	0.4539	0.3717
26	12.5	1.535	1.226	2.761	0.5560	0.4440	0.3622
27	13	1.602	1.230	2.832	0.5657	0.4343	0.3531
28	13.5	1.668	1.234	2.903	0.5746	0.4251	0.3445
29	14	1.735	1.238	2.974	0.5834	0.4163	0.3362
30	14.5	1.802	1.242	3.045	0.5918	0.4079	0.3284
31	15	1.870	1.246	3.116	0.6001	0.4000	0.3209

For a heavy charged particle the radiation yield $Y[(E_K)_0]$ is zero; however, for light CPs, such as electron and positron, $Y[(E_K)_0] \neq 0$ and can be determined from stopping power data as follows

$$Y[(E_K)_0] = \frac{\int_0^{(E_K)_0} \frac{S_{\text{rad}}(E_K)}{S_{\text{tot}}(E_K)} dE_K}{\int_0^{(E_K)_0} dE_K} = \frac{1}{(E_K)_0} \int_0^{(E_K)_0} \frac{S_{\text{rad}}(E_K)}{S_{\text{tot}}(E_K)} dE_K. \quad (6.104)$$

Since the ratio $S_{\text{rad}}(E_K)/S_{\text{tot}}(E_K)$ is generally not available in an analytical form, the integration in (6.104) is replaced with a numerical summation of $S_{\text{rad}}E_K/S_{\text{tot}}(E_K)$ using a suitable E_K interval ΔE_K

$$Y[(E_K)_0] = \frac{1}{(E_K)_0} \int_0^{(E_K)_0} \frac{S_{\text{rad}}(E_K)}{S_{\text{tot}}(E_K)} dE_K = \frac{1}{(E_K)_0} \sum_{i=1}^n \overline{\left(\frac{S_{\text{rad}}(E_K)}{S_{\text{tot}}(E_K)} \right)}_i \Delta E_K, \quad (6.105)$$

where $\overline{(S_{\text{rad}}(E_K)/S_{\text{tot}}(E_K))_i}$ stands for the average value of $(S_{\text{rad}}(E_K)/S_{\text{tot}}(E_K))_i$ for the interval i and $(S_{\text{rad}}(E_K)/S_{\text{tot}}(E_K))_i \Delta E_K$ represents the area of interval i in the summation procedure.

To calculate $Y[(E_K)_0]$ numerically we use the $S_{\text{rad}}/S_{\text{tot}}$ data provided in column (6) of Table 6.15, and for practical reasons we choose a relatively wide kinetic energy interval ΔE_K of 0.5 MeV for the summation. When a computer is used for this purpose, a much narrower interval would be chosen; however, for our proof of principle a manual calculation with an interval $\Delta E_K = 0.5$ MeV is adequate. Thus, for initial kinetic energy $(E_K)_0 = 4$ MeV we will have 8 energy intervals at 0.5 MeV each and, for convenience, we choose $E_K = 0$ for start of the first interval.

Results of our numerical integration in determination of $Y[(E_K)_0]$ for $(E_K)_0 = 4$ MeV are summarized in Table 6.16 and the intervals for the numerical integration are also displayed in Fig. 6.21. Based on data displayed in column (6) of Table 6.16 we now determine $Y[(E_K)_0]$ for $(E_K)_0 = 4$ MeV as follows

$$Y[(E_K)_0] = \frac{1}{(E_K)_0} \sum_{i=1}^{n=8} \overline{\left(\frac{S_{\text{rad}}(E_K)}{S_{\text{tot}}(E_K)} \right)}_i \Delta E_K = \frac{1}{4 \text{ MeV}} \times 0.7002 \text{ MeV} = 0.175, \quad (6.106)$$

indicating that 17.5 % of the 4 MeV incident electron kinetic energy is transformed into bremsstrahlung photons. It is noteworthy that our result for $Y[4 \text{ MeV}] = 0.175$ is in excellent agreement with the value of 0.176 stated by the NIST and undoubtedly obtained with a much finer interval length than our 0.5 MeV.

(b) Total energy E_{rad} radiated from a 4 MeV electron striking a lead absorber is given as

$$E_{\text{rad}} = (E_K)_0 \times Y[(E_K)_0] = (4 \text{ MeV}) \times 0.175 = 0.7002 \text{ MeV}, \quad (6.107)$$

indicating that out of the incident electron kinetic energy of 4 MeV, 0.7 MeV is emitted in the form of bremsstrahlung photons.

Table 6.16 Parameters in numerical integration used to determine the radiation yield $Y[(E_K)_0]$ and E_{rad} , the energy emitted in the form of bremsstrahlung photons for an electron of incident kinetic energy $(E_K)_0 = 4 \text{ MeV}$ traversing a lead absorber

(1)	(2)	(3)	(4)	(5)	(6)	(7)
n	E_K (MeV)	$\frac{S_{\text{rad}}(E_K)_i}{S_{\text{tot}}(E_K)_i}$	$\frac{S_{\text{rad}}(E_K)_i}{S_{\text{tot}}(E_K)_i}$	$(\frac{S_{\text{rad}}}{S_{\text{tot}}})_i \Delta E_K$ (MeV)	$\sum_{i=1}^n (\frac{S_{\text{rad}}}{S_{\text{tot}}})_i \Delta E_K$ (MeV)	$\frac{\sum_{i=1}^n (\frac{S_{\text{rad}}}{S_{\text{tot}}})_i \Delta E_K}{(E_K)_n}$
	0	0.00				
1			0.036	0.0180	0.0180	0.036
	0.5	0.072				
2			0.0937	0.0469	0.0649	0.065
	1	0.1149				
3			0.1331	0.0666	0.1315	0.088
	1.5	0.1573				
4			0.1680	0.0840	0.2155	0.108
	2	0.1846				
5			0.2001	0.1000	0.3155	0.126
	2.5	0.2156				
6			0.2298	0.1149	0.4304	0.143
	3	0.2440				
7			0.2572	0.1285	0.5589	0.160
	3.5	0.2730				
8			0.2826	0.1413	0.7002	0.175
	4	0.2949				

(c) To deal with E_{col} , the energy lost through ionization of lead atoms, of course, we could reason that if 0.7 MeV out of 4 MeV is transformed into bremsstrahlung energy then the difference $(4 - 0.7) \text{ MeV} = 3.3 \text{ MeV}$ is lost to ionization for a 4 MeV incident electron completely stopped in lead. This is our initial answer, but we will confirm it now by applying numerical integration using the $S_{\text{col}}/S_{\text{tot}}$ ratio given in column (7) of Table 6.15.

Figure 6.22 shows a plot of the ratio $S_{\text{col}}/S_{\text{tot}}$ from Table 6.15 against kinetic energy E_K of the electron and it also shows the integration intervals that we used in the numerical integration of $S_{\text{col}}/S_{\text{tot}}$, assuming an incident kinetic energy $(E_K)_0$ of the electron of 4 MeV. Table 6.17 displays the results of our numerical integration of $S_{\text{col}}/S_{\text{tot}}$ similar to Table 6.16 that was used in (a) to deal with the numerical integration of $S_{\text{col}}/S_{\text{tot}}$. Based on column (6) of Table 6.17 we determine E_{col} for

$(E_K)_0 = 4 \text{ MeV}$ as follows

$$E_{\text{col}} = \int_0^{(E_K)_0} \frac{S_{\text{col}}(E_K)}{S_{\text{tot}}(E_K)} dE_K = \sum_{i=1}^{n=8} \left(\frac{S_{\text{col}}(E_K)}{S_{\text{tot}}(E_K)} \right)_i \Delta E_K = 3.3 \text{ MeV}, \quad (6.108)$$

in excellent agreement with the estimation above that stated $E_{\text{col}} = (E_K)_0 - E_{\text{rad}}$.

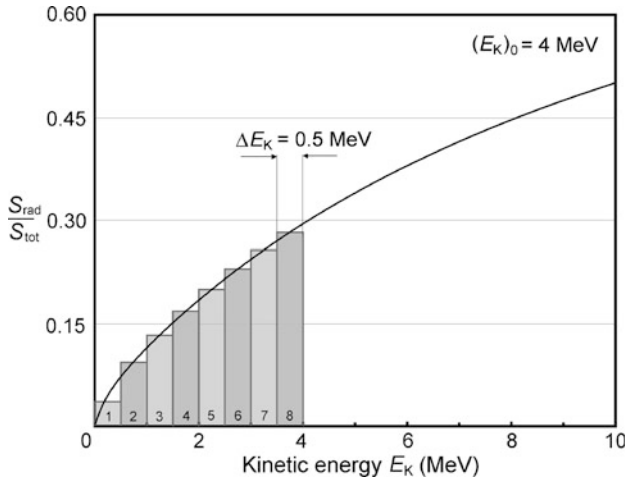


Fig. 6.21 Ratio $S_{\text{rad}}/S_{\text{tot}}$ of lead against kinetic energy of electrons. Also shown are energy intervals ΔE_K used in numerical integration of the $S_{\text{rad}}/S_{\text{tot}}$ ratio

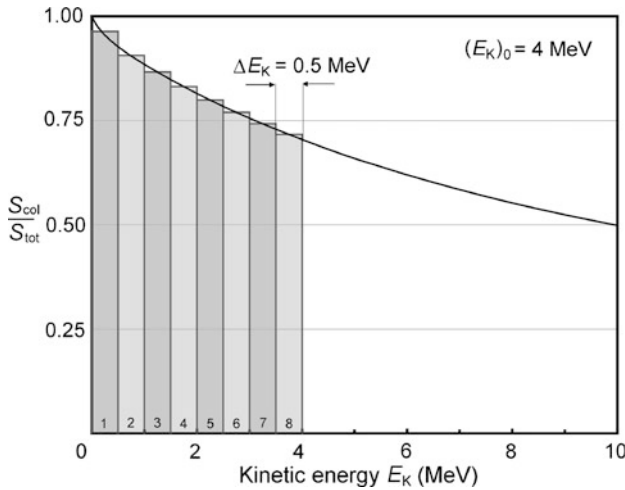


Fig. 6.22 Ratio $S_{\text{col}}/S_{\text{tot}}$ of lead against kinetic energy of electrons. Also shown are energy intervals ΔE_K used in numerical integration of the $S_{\text{col}}/S_{\text{tot}}$ ratio

Table 6.17 Parameters in numerical integration used to determine E_{col} , energy that the electron with incident kinetic energy $(E_K)_0 = 4$ MeV loses through ionization of lead atoms

(1)	(2)	(3)	(4)	(5)	(6)
n	E_K (MeV)	$\frac{S_{col}(E_K)_i}{S_{tot}(E_K)_i}$	$\frac{S_{col}(E_K)_i}{S_{tot}(E_K)_i}$	$(\frac{S_{col}}{S_{tot}})_i \Delta E_K$ (MeV)	$\sum_{i=1}^n (\frac{S_{col}}{S_{tot}})_i \Delta E_K$ (MeV)
	0.001	0.9996			
1			0.9639	0.4819	0.4819
	0.5	0.9275			
2			0.9064	0.4532	0.9351
	1	0.8851			
3			0.8669	0.4334	1.3685
	1.5	0.8487			
4			0.8320	0.4160	1.7845
	2	0.8153			
5			0.7998	0.4000	2.1845
	2.5	0.7844			
6			0.7702	0.3851	2.5696
	3	0.7560			
7			0.7429	0.3714	2.9410
	3.5	0.7297			
8			0.7174	0.3587	3.2997
	4	0.7057			

(d) With (6.106) we determined the radiation yield $Y[(E_K)_0]$ for initial kinetic energy $(E_K)_0$ of 4 MeV. We now use the same relationship (6.106) to plot the radiation yield $Y[(E_K)_0]$ against initial kinetic energy $(E_K)_0$ in the range $0 \leq Y[(E_K)_0] \leq 4$ MeV and present the appropriate data in column (7) of Table 6.16 as well as in Fig. 6.23. The solid line in the figure represents the NIST data, the data points are determined with (6.106) for a given $(E_K)_0$. Our calculated points agree well with the NIST data that show that $Y[(E_K)_0]$ increases with initial kinetic energy $(E_K)_0$ and asymptotically approaches 100 % at initial kinetic energies above 1000 MeV.

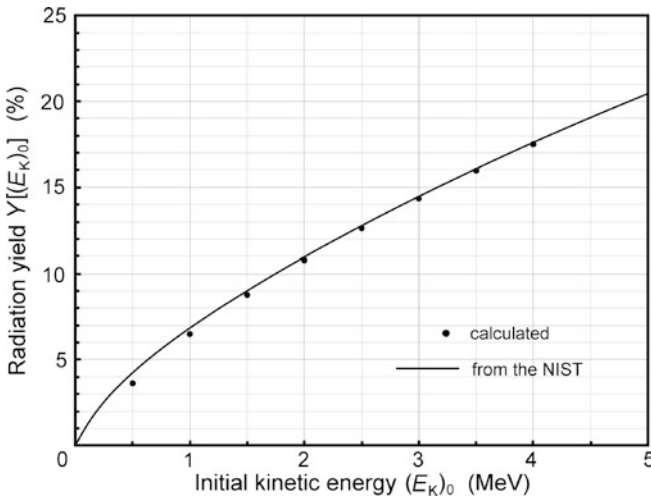


Fig. 6.23 Radiation yield $Y[(E_K)_0]$ against initial kinetic energy $(E_K)_0$ of lead for electrons in the initial kinetic energy range from 0 to 4 MeV. Solid curve represents data from the NIST, data points are our calculated values

6.8 Range of Charged Particles

6.8.Q1

(142)

Most of collision and radiation losses as a charged particle penetrates into an absorber transfer in individual interactions only a minute fraction of the CP kinetic energy E_K to orbital electrons of the absorber. It is therefore convenient, as proposed by Berger and Seltzer, in 1983 to think of the CP moving through an absorber as if it is losing its kinetic energy gradually and continuously in a process called continuous slowing down approximation (CSDA). The CSDA range R_{CSDA} is then defined as

$$R_{\text{CSDA}} = \int_0^{(E_K)_0} \frac{dE_K}{S_{\text{tot}}(E_K)} \quad (6.109)$$

and can be determined through integrating the reciprocal of total mass stopping power ($1/S_{\text{tot}}$) over kinetic energy E_K from 0 to initial kinetic energy $(E_K)_0$. For heavy CPs, R_{CSDA} is a very good approximation to the mean range \bar{R} of the CP in the absorbing medium, because of the essentially rectilinear path of the CP in the absorbing medium.

- (a) Use data available from the NIST to calculate the CSDA range R_{CSDA} in water for protons with incident kinetic energy $(E_K)_0$ of 100 MeV.
- (b) Using data calculated in (a) plot R_{CSDA} for protons in water against incident kinetic energy $(E_K)_0$ in the range from $0 \leq (E_K)_0 \leq 100$ MeV.

SOLUTION:

(a) In principle, to determine the CSDA range in water of protons with incident kinetic energy $(E_K)_0 = 100$ MeV we would use (6.109). However, since the reciprocal of the total mass stopping power S_{tot} is not available in an analytical form, we will resort to a numerical integration of $1/S_{\text{tot}}$ data and use a reasonably small energy interval ΔE_K of 5 MeV in the integration. The steps in the numerical integration were discussed in Prob. 141, so here we present only a summary of the six steps involved:

- (1) Decide on kinetic energy interval ΔE_K for the numerical integration. We will use 5 MeV for ΔE_K and thus need data for E_K in MeV of 0, 5, 10, 15, ..., 95, 100.
- (2) Obtain S_{col} in $\text{MeV} \cdot \text{cm}^2/\text{g}$ (<http://physics.nist.gov/PhysRefData/Star/Text/PSTAR.html>) from the NIST for protons in water for kinetic energies given in step (1). S_{tot} for heavy CP in general includes two terms: the predominant collision term S_{col} and a minor nuclear term S_{nuc} arising from elastic collisions between CP and the nucleus of the absorber. In our calculation we ignore the S_{nuc} term and assume that $S_{\text{tot}} \approx S_{\text{col}}$. *Note:* for heavy CP radiation stopping power S_{rad} is zero in contrast to the situation with light CPs (electrons and positrons) for which $S_{\text{tot}} = S_{\text{col}} + S_{\text{rad}}$.
- (3) Calculate $1/S_{\text{col}}$, the reciprocal of S_{col} , for E_K given in step (1). Figure 6.24 plots $1/S_{\text{col}}$ against E_K for protons in water and also shows the energy intervals ΔE_K used in the numerical integration.
- (4) Calculate $\overline{1/S_{\text{col}}}$, the average of $1/S_{\text{col}}$, for each energy interval ΔE_K . For example, for the last energy interval ΔE_K shown in Fig. 6.24 we calculate $\overline{1/S_{\text{col}}}$ as follows

$$\begin{aligned}
 \overline{1/S_{\text{col}}}(100 \text{ MeV}) &= 1/S_{\text{col}}(100 \text{ MeV}) - 1/S_{\text{col}}(95 \text{ MeV}) \\
 &= 0.5 \times [0.1372 (\text{MeV} \cdot \text{cm}^2/\text{g})^{-1} \\
 &\quad - 0.1320 (\text{MeV} \cdot \text{cm}^2/\text{g})^{-1}] \\
 &= 0.1346 (\text{MeV} \cdot \text{cm}^2/\text{g})^{-1}. \tag{6.110}
 \end{aligned}$$

- (5) Calculate the area for each energy interval, i.e., $(\overline{1/S_{\text{col}}})_i \times \Delta E_K$.

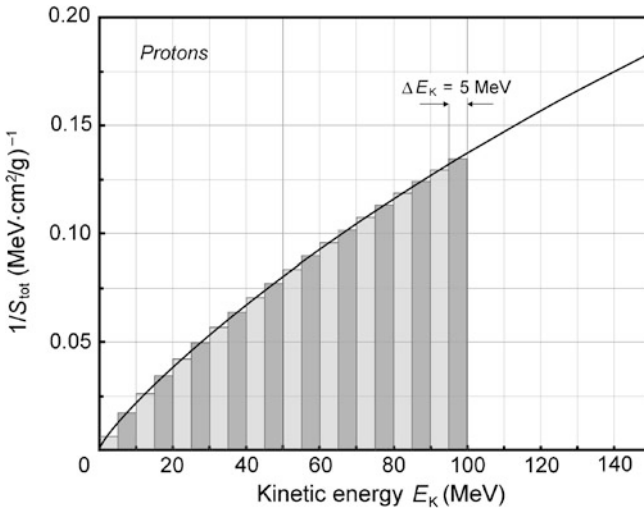


Fig. 6.24 Reciprocal of mass collision stopping power ($1/S_{\text{col}}$) of water against incident kinetic energy $(E_K)_0$ of protons. Also shown are kinetic energy intervals ΔE_K used in numerical integration of $1/S_{\text{col}}$ in calculation of CSDA range

(6) Sum up the areas $\overline{(1/S_{\text{col}})}_i \times \Delta E_K$ from area 1 to area n at $(E_K)_0$ to get

$$\sum_{i=1}^n \overline{(1/S_{\text{col}})}_i \times \Delta E_K = R_{\text{CSDA}}[(E_K)_0]. \quad (6.111)$$

Table 6.18 summarizes the six steps in the calculation of the CSDA range R_{CSDA} for 100 MeV protons in water and results in $R_{\text{CSDA}} = 7.71 \text{ g/cm}^2 = 7.71 \text{ cm}$. This result, despite a relatively large energy interval of $\Delta E_K = 5 \text{ MeV}$ agrees well with the tabulated value of $R_{\text{CSDA}} = 7.718 \text{ g/cm}^2$ obtained from the NIST.

(b) Data required for plotting of R_{CSDA} for protons in water in the kinetic energy interval $0 \leq (E_K)_0 \leq 100 \text{ MeV}$ are actually available from row (6) of Table 6.18 where they were used to determine through numerical integration R_{CSDA} for 100 MeV protons. These data obviously contain range information for all proton energies up to $(E_K)_0 = 100 \text{ MeV}$ and all we need to do is extract it from the table. For example, for $(E_K)_0 = 75 \text{ MeV}$ we get directly from column (15) and row (6) a CSDA range R_{CSDA} of 4.61 cm; for $(E_K)_0 = 20 \text{ MeV}$ we get directly from column (4) and row (6) a CSDA range of 0.42 cm, etc.

In Fig. 6.25 we plot the CSDA range R_{CSDA} in water of protons with kinetic energy between 0 and 125 MeV. The data points represent calculated values listed in row (6) of Table 6.18 and the solid curve represents R_{CSDA} obtained from the NIST. The agreement between our data calculated with numerical integration using a relatively large energy interval of 5 MeV and data obtained from the NIST is excellent.

Table 6.18 Summary of data for calculation of CSDA range in water for protons of kinetic energy of 100 MeV. (*) indicates data obtained from the NIST

n	1	2	3	4	5	6	7	8	9	10
1 E_K (MeV)	5	10	15	20	25	30	35	40	45	50
2 S_{tot} (*)	79.11	45.67	32.92	26.07	21.75	18.76	16.56	14.88	13.54	12.45
3 $1/S_{tot}$	0.0126	0.0219	0.0304	0.0384	0.0460	0.0533	0.0604	0.0672	0.0739	0.0803
4 $\overline{1/S_{tot}}$	0.0063	0.0173	0.0261	0.0344	0.0422	0.0500	0.0568	0.0638	0.0705	0.0771
5 $(1/S_{tot})\Delta E_K$	0.0316	0.0863	0.1307	0.1718	0.2108	0.2482	0.2842	0.3190	0.3527	0.3854
6 $\sum(1/S_{tot})\Delta E_K$	0.0316	0.1179	0.2486	0.4205	0.6313	0.8795	1.1637	1.4827	1.8353	2.2208
n	11	12	13	14	15	16	17	18	19	20
1 E_K (MeV)	55	60	65	70	75	80	85	90	95	100
2 S_{tot} (*)	11.54	10.78	10.13	9.559	9.063	8.625	8.236	7.888	7.573	7.289
3 $1/S_{tot}$	0.0867	0.0928	0.0987	0.1046	0.1103	0.1159	0.1214	0.1268	0.1320	0.1372
4 $\overline{1/S_{tot}}$	0.0835	0.0897	0.0957	0.1017	0.1075	0.1131	0.1187	0.1241	0.1294	0.1346
5 $(1/S_{tot})\Delta E_K$	0.4174	0.4486	0.4787	0.5083	0.5374	0.5657	0.5934	0.6205	0.6471	0.6731
6 $\sum(1/S_{tot})\Delta E_K$	2.6382	3.0868	3.5655	4.0738	4.6112	5.1769	5.7703	6.3908	7.0378	7.7109
n	21	22	23	24	25	26	27	28	29	30
1 E_K (MeV)	105	110	115	120	125	130	135	140	145	150
2 S_{tot} (*)	7.030	6.794	6.577	6.377	6.192	6.021	5.861	5.713	5.575	5.445
3 $1/S_{tot}$	0.1422	0.1472	0.1520	0.1568	0.1615	0.1661	0.1706	0.1750	0.1794	0.1837
4 $\overline{1/S_{tot}}$										
5 $(1/S_{tot})\Delta E_K$										
6 $\sum(1/S_{tot})\Delta E_K$										

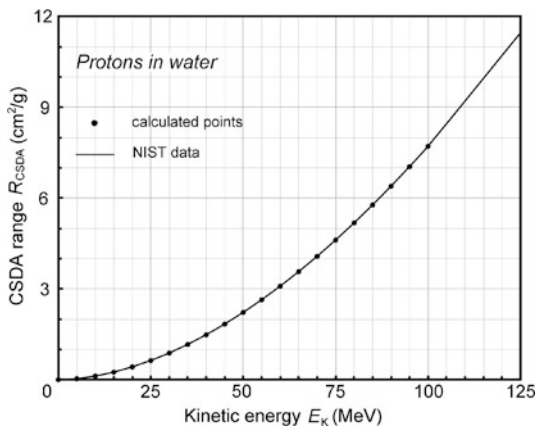


Fig. 6.25 CSDA range R_{CSDA} against incident kinetic energy $(E_K)_0$ for protons in water. Data points represent our calculated results; the solid curve represents data obtained from the NIST

6.8.Q2

(143)

According to the derivation of (T6.74), the CSDA range $R_{\text{CSDA}}^{M_0}[(E_K^{M_0})]$ of an arbitrary heavy charged particle (CP) of rest energy M_0c^2 , charge ze , and incident kinetic energy $(E_K^{M_0})_0$ in a given absorber can be written in terms of the CSDA range of a proton $R_{\text{CSDA}}^p[(E_K^p)]$ of rest energy $m_p c^2 = 938.3 \text{ MeV}$ and equivalent incident kinetic energy $(E_K^p)_0$ in the same absorber as

$$R_{\text{CSDA}}^{M_0}[(E_K^{M_0})_0] = C(M_0, z) R_{\text{CSDA}}^p[(E_K^p)_0], \quad (6.112)$$

where $C(M_0, z)$ is a correction factor dependent on rest mass M_0 and number z of electron charges e of the heavy CP given in (6.113) and $(E_K^p)_0$ is the equivalent incident kinetic energy of the proton related to the incident kinetic energy $(E_K^{M_0})_0$ of the heavy CP through the relationship given in (6.114)

$$C(M_0, z) = \frac{1}{z^2} \frac{M_0}{m_p} \quad (6.113)$$

and

$$(E_K^p)_0 = \frac{m_p}{M_0} (E_K^{M_0})_0. \quad (6.114)$$

-
- (a) Derive (6.112) from the basic definition of R_{CSDA} and S_{col} for non-relativistic heavy CPs.
- (b) Determine the mass/charge correction factor $C(M_0, z)$ for the following heavy CPs: deuteron d, triton t, α particle ${}^4_2\text{He}^{2+}$, carbon ion ${}^{12}_6\text{C}^{6+}$, and neon ion ${}^{20}_{10}\text{Ne}^{10+}$.
- (c) Determine the equivalent proton incident kinetic energy $(E_K^p)_0$ for the following heavy CPs: deuteron d, triton t, α particle ${}^4_2\text{He}^{2+}$, carbon ion ${}^{12}_6\text{C}^{6+}$, and neon ion ${}^{20}_{10}\text{Ne}^{10+}$, all of incident kinetic energy $(E_K^{M_0})_0$ of 500 MeV.
- (d) Based on Fig. 6.26 that gives the CSDA range R_{CSDA}^p of protons in water against incident kinetic energy $(E_K^p)_0$, determine the CSDA range $R_{\text{CSDA}}^{M_0}$ in water for the following heavy CPs: deuteron d, triton t, α particle ${}^4_2\text{He}^{2+}$, carbon ion ${}^{12}_6\text{C}^{6+}$, and neon ion ${}^{20}_{10}\text{Ne}^{10+}$, all of incident kinetic energy $(E_K^{M_0})_0$ of 500 MeV.

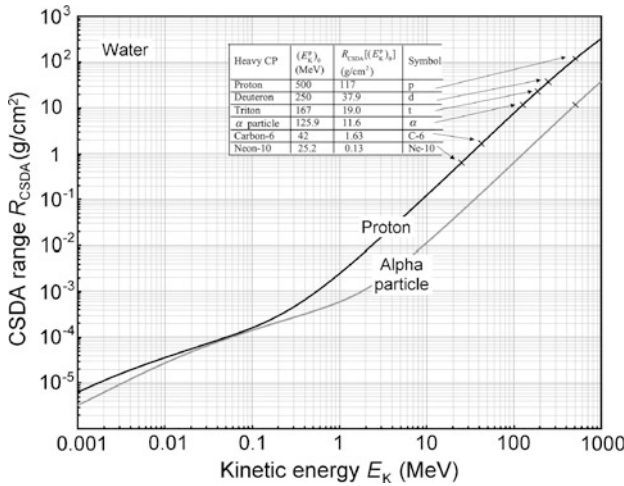


Fig. 6.26 Continuous slowing down approximation range R_{CSDA} in water for proton (solid dark curve) and α particle (grey curve) against incident kinetic energy $(E_K)_0$ based on data from the NIST. Incident kinetic energies $(E_K^M)_0$ of proton for deuteron, triton, α particle, carbon-6 ion, and neon-10 ion, all with incident kinetic energy $(E_K^{M_0})$ of 500 MeV, are indicated with tick marks on the proton curve

SOLUTION:

(a) The CSDA range $R_{CSDA}[(E_K^{M_0})]$ of a heavy CP with rest mass M_0 and charge ze traversing a stopping medium (absorber) is defined as

$$R_{CSDA}[(E_K^{M_0})] = \int_0^{(E_K^{M_0})} \frac{dE_K}{S_{col}(E_K)}, \tag{6.115}$$

where $(E_K^{M_0})$ is the incident kinetic energy of the CP and $S_{col}(E_K^{M_0})$ is the mass collision stopping power of the absorber for heavy particle of rest mass M_0 . For a non-relativistic heavy CP, $S_{col}(E_K^{M_0})$ is given by the Bethe stopping power equation as

$$\begin{aligned} S_{col}[(E_K^{M_0})] &= \frac{C_A z^2}{v^2} \ln \frac{2m_e v^2}{I} = \frac{C_A z^2}{2} \frac{2M_0}{M_0 v^2} \ln \left[\frac{4m_e}{I} \frac{M_0 v^2}{2M_0} \right] \\ &= \frac{C_A z^2}{2} \frac{M_0}{E_K^{M_0}} \ln \left[\frac{4m_e}{I} \frac{E_K^{M_0}}{M_0} \right], \end{aligned} \tag{6.116}$$

where

- C_A is a constant for a given absorber.
- v is the velocity of the heavy CP.
- m_e is the rest mass of the electron ($m_e = 0.511 \text{ MeV}/c^2$).

I is the ionization/excitation potential of the stopping medium (absorber).
 $E_K^{M_0}$ is the kinetic energy of the heavy CP, i.e., $E_K^{M_0} = \frac{1}{2}M_0v^2$ for non-relativistic heavy CP.

Combining (6.116) with (6.115) we get the following expression for $R_{\text{CSDA}}[(E_K^{M_0})]$

$$R_{\text{CSDA}}[(E_K^{M_0})_0] = \frac{2M_0}{C_A z^2} \int_0^{(E_K^{M_0})} \frac{\frac{E_K^{M_0}}{M_0} d\frac{E_K^{M_0}}{M_0}}{\ln\left[\frac{4m_e}{I} \frac{E_K^{M_0}}{M_0}\right]}, \quad (6.117)$$

which we now expand to make a link between the range $R_{\text{CSDA}}[(E_K^{M_0})]$ of the heavy CP of rest mass M_0 and charge ze and range $R_{\text{CSDA}}[(E_K^p)]$ of a proton of rest mass $m_p = 938.3$ MeV and charge e

$$\begin{aligned} R_{\text{CSDA}}[(E_K^{M_0})_0] &= \frac{M_0}{z^2 m_p} \left\{ \frac{2m_p}{C_A} \int_0^{E_K^{M_0}} \frac{\left(\frac{E_K^{M_0}}{m_p} \frac{m_p}{M_0}\right) d\left(\frac{E_K^{M_0}}{m_p} \frac{m_p}{M_0}\right)}{\ln\left[\left(\frac{4m_e}{I}\right)\left(\frac{E_K^{M_0}}{m_p} \frac{m_p}{M_0}\right)\right]} \right\} \\ &= \frac{M_0}{z^2 m_p} \left\{ \frac{2m_p}{C_A} \int_0^{E_K^p} \frac{\left(\frac{E_K^p}{m_p}\right) d\left(\frac{E_K^p}{m_p}\right)}{\ln\left[\left(\frac{4m_e}{I}\right)\left(\frac{E_K^p}{m_p}\right)\right]} \right\} \\ &= \frac{M_0}{z^2 m_p} R_{\text{CSDA}}^p[(E_K^p)_0] = C(M_0, z) R_{\text{CSDA}}[(E_K^p)_0], \quad (6.118) \end{aligned}$$

where $C(M_0, z)$ is a correction factor for mass M_0 and charge ze of the heavy CP given in (6.119) and $(E_K^p)_0$ is the equivalent incident kinetic energy of a proton that satisfies (6.112) and is related to $(E_K^{M_0})_0$, as shown in (6.120)

$$C(M_0, z) = \frac{M_0}{z m_p} \quad (6.119)$$

and

$$(E_K^p)_0 = \frac{m_p}{M_0} (E_K^{M_0})_0. \quad (6.120)$$

(b) The mass/charge correction factor $C(M_0, z)$ for the five heavy charged particles is determined using (6.113) and listed in column (7) of Table 6.19 which also lists the basic relevant physical properties of the five heavy charged particles in addition to proton.

(c) The equivalent proton incident kinetic energy $(E_K^p)_0$ for use in (6.112) in determination of the CSDA range of CPs heavier than the proton is calculated with (6.114) for five CPs (deuteron, triton, α particle, carbon-6 ion, and neon-10 ion), all with incident kinetic energy of 500 MeV and given in column (4) of Table 6.20.

Table 6.19 Physical properties relevant to calculation of CSDA range in water for a selection of six heavy charged particles: proton, deuteron, triton, α particle, carbon-6 ion, and neon-10 ion

(1)	(2)	(3)	(4)	(5)	(6)	(7)	(8)
(2)	Heavy CP		z	A	M_0c^2	$C(M_0, z)$	m_p/M_0
(3)	Proton	$^1_1\text{H} = \text{p}$	1	1	938.3	1.000	1.000
(4)	Deuteron	$^2_1\text{H} = \text{d}$	1	2	1875.6	1.999	0.500
(5)	Triton	$^3_1\text{H} = \text{t}$	1	3	2808.6	2.993	0.334
(6)	α particle	$^4_2\text{He} = \alpha$	2	4	3727.3	0.993	0.252
(7)	Carbon-6	$^{12}_6\text{C}^{6+}$	6	12	11174.9	0.331	0.084
(8)	Neon-10	$^{20}_{10}\text{Ne}^{10+}$	10	20	18617.7	0.198	0.050

Table 6.20 Various parameters of relevance to determination of the CSDA range in water for various heavy charged particles, all of incident kinetic energy of 500 MeV

(1)	(2)	(3)	(4)	(5)	(6)	(7)	(8)
(2)	Heavy CP		$(E_K^p)_0$	R_{CSDA}^p	$(E_K^{M_0})_0$	$(E_K^{M_0})_0/A$	$R_{\text{CSDA}}^{M_0}$
(3)	Proton	$^1_1\text{H} = \text{p}$	500	117	500	500	117
(4)	Deuteron	$^2_1\text{H} = \text{d}$	250	37.9	500	250	75.8
(5)	Triton	$^3_1\text{H} = \text{t}$	167	19	500	167	57.0
(6)	α particle	$^4_2\text{He} = \alpha$	125.9	11.6	500	125	11.5
(7)	Carbon-6	$^{12}_6\text{C}^{6+}$	42	1.63	500	41.7	0.54
(8)	Neon-10	$^{20}_{10}\text{Ne}^{10+}$	25.2	0.65	500	25	0.13

(d) The CSDA range of heavy CPs: proton, deuteron, triton, α particle, carbon ion, and neon ion, all with incident kinetic energy $(E_K^{M_0})_0$ of 500 MeV is determined with (6.112) and results are displayed in Table 6.20 and in Fig. 6.26. We note that 500 MeV proton, deuterons, and tritons have a range that exceeds the penetration in water required for radiotherapy, while carbon ions and neon ions at 500 MeV [i.e., at 42 MeV/u ($\sim 500 : 12$) and 25 MeV/u ($\sim 500 : 20$), respectively] exhibit CSDA ranges that are too low for use in practical radiotherapy.

6.9 Mean Stopping Power

6.9.Q1

(144)

In radiation dosimetry the main interest is in the energy absorbed per unit mass of the absorbing medium governed by collision losses of charged particles. It is often convenient to characterize a given radiation beam with elec-

trons of only one energy $(E_K)_0$ rather than with an electron spectrum $d\phi/dE_K$ that is present in practice. As shown by Johns and Cunningham [17], one can define mean mass collision stopping power $\bar{S}_{\text{col}}[(E_K)_0]$ with the following expression

$$\bar{S}_{\text{col}}[(E_K)_0] = (E_K)_0 \frac{1 - Y[(E_K)_0]}{R_{\text{CSDA}}[(E_K)_0]}. \quad (6.121)$$

- (a) Derive (6.121) from the definition of $\bar{S}_{\text{col}}[(E_K)_0]$ based on electron spectrum and given as

$$\bar{S}_{\text{col}}[(E_K)_0] = \frac{\int_0^{(E_K)_0} \frac{d\phi}{dE_K} S_{\text{col}}(E_K) dE_K}{\int_0^{(E_K)_0} \frac{d\phi}{dE_K} dE_K}. \quad (6.122)$$

- (b) Using data from the NIST {<http://physics.nist.gov/PhysRefData/Star/Text/ESTAR.html>} in conjunction with (6.121) determine $\bar{S}_{\text{col}}[(E_K)_0]$ of water for the following incident electron kinetic energies $(E_K)_0$ in MeV: 0.01, 0.05, 0.1, 0.5, 1, 5, 10, 50, 100, 500, and 1000.
- (c) Figure 6.27 is a plot of the mass collision stopping power $S_{\text{col}}[(E_K)_0]$ of water against incident kinetic energy $(E_K)_0$ of the electron. On the same graph plot the data you calculated for the mean mass collision stopping power $\bar{S}_{\text{col}}[(E_K)_0]$ for several $(E_K)_0$ in the range from 10^{-3} MeV to 10^3 MeV. Compare $S_{\text{col}}[(E_K)_0]$ curve with $\bar{S}_{\text{col}}[(E_K)_0]$ curve and explain the cause of the difference between the two curves.

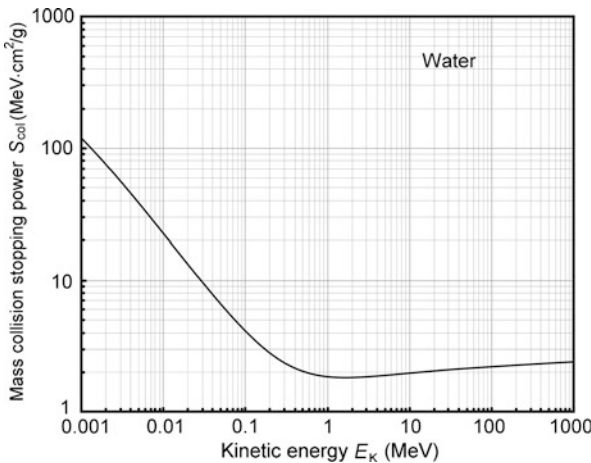


Fig. 6.27 Mass collision stopping power S_{col} of water for electrons against kinetic energy E_K of electrons in the electron kinetic energy range from 1 keV to 1000 MeV

SOLUTION:

(a) The electron spectrum $d\phi/dE_K$, ignoring all possible hard collisions, is expressed in terms of total mass stopping power $S_{\text{tot}}(E_K)$ as

$$\frac{d\phi(E_K)}{dE_K} = \frac{N}{S_{\text{tot}}(E_K)}, \quad (6.123)$$

where N is the number of mono-energetic electrons of kinetic energy $(E_K)_0$ set in motion per unit mass in the absorbing medium. These electrons will through their own slowing down process produce a spectrum of electrons in the medium ranging in energy from $(E_K)_0$ down to zero.

The mean value of $S_{\text{col}}(E_K)$ is calculated using the standard procedure for averaging physical quantities, as stated in (6.122). The integral in the denominator of (6.122) after insertion of (6.123) is given as follows

$$\int_0^{(E_K)_0} \frac{d\phi(E_K)}{dE_K} dE_K = N \int_0^{(E_K)_0} \frac{dE_K}{S_{\text{tot}}(E_K)} = N \times R_{\text{CSDA}}[(E_K)_0], \quad (6.124)$$

where we use the definition of the CSDA range given as [see (T6.69)]

$$R_{\text{CSDA}}[(E_K)_0] = \int_0^{(E_K)_0} \frac{dE_K}{S_{\text{col}}(E_K)}. \quad (6.125)$$

The integral in the numerator of (6.122), again after insertion of (6.123), is determined as follows

$$\begin{aligned} \int_0^{(E_K)_0} \frac{d\phi}{dE_K} S_{\text{col}}(E_K) dE_K &= N \int_0^{(E_K)_0} \frac{S_{\text{col}}(E_K)}{S_{\text{tot}}(E_K)} dE_K \\ &= N \int_0^{(E_K)_0} \frac{S_{\text{tot}}(E_K) - S_{\text{rad}}(E_K)}{S_{\text{tot}}(E_K)} dE_K \\ &= N \times (E_K)_0 - N \times (E_K)_0 Y[(E_K)_0] \\ &= N \times (E_K)_0 [1 - Y[(E_K)_0]], \end{aligned} \quad (6.126)$$

where we used:

- (1) Definition of total mass collision stopping power S_{tot} as a sum of two components [see (T6.63)], i.e.,

$$S_{\text{tot}} = S_{\text{col}} + S_{\text{rad}}. \quad (6.127)$$

- (2) Definition of radiation yield [see (T6.67)]

$$Y[(E_K)_0] = \frac{1}{(E_K)_0} \int_0^{(E_K)_0} \frac{S_{\text{rad}}(E_K)}{S_{\text{tot}}(E_K)} dE_K. \quad (6.128)$$

Table 6.21 Parameters of importance for calculation of the mean mass collision stopping power $\bar{S}_{\text{col}}[(E_K)_0]$ with (6.121). Data for $S_{\text{col}}[(E_K)_0]$, $Y[(E_K)_0]$, and $R_{\text{CSDA}}[(E_K)_0]$ were obtained from the NIST, data for column (5) were calculated with (6.121)

(1)	(2)	(3)	(4)	(5)
$(E_K)_0$ (MeV)	$S_{\text{col}}[(E_K)_0]$ (MeV · cm ² /g)	$Y[(E_K)_0]$	$R_{\text{CSDA}}[(E_K)_0]$ (g/cm ²)	$\bar{S}_{\text{col}}[(E_K)_0]$ (MeV · cm ² /g)
0.01	22.6	9.41×10^{-5}	2.52×10^{-4}	39.7
0.05	6.60	3.44×10^{-4}	4.32×10^{-3}	11.6
0.1	4.12	5.84×10^{-4}	1.43×10^{-2}	6.99
0.5	2.03	1.98×10^{-3}	1.77×10^{-1}	2.82
1	1.85	3.58×10^{-3}	4.37×10^{-1}	2.28
5	1.89	1.91×10^{-2}	2.55	1.92
10	1.97	4.07×10^{-2}	4.98	1.93
50	2.14	1.92×10^{-1}	19.8	2.04
100	2.20	3.19×10^{-1}	32.6	2.09
500	2.34	6.61×10^{-1}	77.0	2.20
1000	2.40	7.76×10^{-1}	100.2	2.24

Combining (6.122) with (6.124) and (6.126) we now get the expression presented in (6.121) for the mean mass collision stopping power of an absorber

$$\begin{aligned} \bar{S}_{\text{col}}[(E_K)_0] &= \frac{\int_0^{(E_K)_0} \frac{d\phi}{dE_K} S_{\text{col}}(E_K) dE_K}{\int_0^{(E_K)_0} \frac{d\phi}{dE_K} dE_K} = \frac{N \times (E_K)_0 [1 - Y[(E_K)_0]]}{N \times R_{\text{CSDA}}[(E_K)_0]} \\ &= (E_K)_0 \frac{[1 - Y[(E_K)_0]]}{R_{\text{CSDA}}[(E_K)_0]}. \end{aligned} \quad (6.129)$$

(b) To solve this part we open the NIST website, collect the required data on $S_{\text{col}}[(E_K)_0]$, $Y[(E_K)_0]$, and $R_{\text{CSDA}}[(E_K)_0]$ for electrons with incident kinetic energy $(E_K)_0$ in water, as prescribed for (b), and display these data in columns (1) through (4) of Table 6.21. Finally, we calculate the mean mass collision stopping power $\bar{S}_{\text{col}}[(E_K)_0]$ using (6.121) and display the results in column (5) of Table 6.21.

(c) Columns (2) and (5) of Table 6.21 as well as Fig. 6.28 show that for a given incident electron kinetic energy $(E_K)_0$ the mass collision stopping power $S_{\text{col}}[(E_K)_0]$ and the mean mass collision stopping power $\bar{S}_{\text{col}}[(E_K)_0]$ differ from one another. On the one hand, at $(E_K)_0 < 3$ MeV, $\bar{S}_{\text{col}}[(E_K)_0]$ exceeds $S_{\text{col}}[(E_K)_0]$; the lower is $(E_K)_0$, the larger is the difference. On the other hand, at $(E_K)_0 > 3$ MeV the situation is reversed and $\bar{S}_{\text{col}}[(E_K)_0] < S_{\text{col}}[(E_K)_0]$, however, the difference is not as pronounced as it is at low kinetic energies $(E_K)_0$.

The difference between $S_{\text{col}}[(E_K)_0]$ and $\bar{S}_{\text{col}}[(E_K)_0]$ is caused by the difference in definition of the two quantities: $S_{\text{col}}[(E_K)_0]$ gives the energy loss by the CP at the instant when its kinetic energy is $(E_K)_0$, while $\bar{S}_{\text{col}}[(E_K)_0]$ gives the mean mass

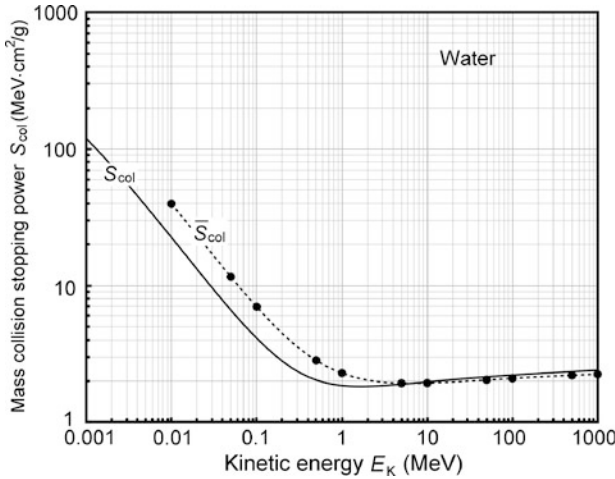


Fig. 6.28 Mass collision stopping power S_{col} of water against kinetic energy E_K of electrons (solid curve) from the NIST and mean mass collision stopping power \bar{S}_{col} of water against kinetic energy of electrons (data points and dashed curve) calculated using (6.121)

collision stopping power for all kinetic energies from $(E_K)_0$ down to zero. We note the following features:

- (1) For $(E_K)_0 < 3$ MeV, $S_{col}[(E_K)_0]$ increases with decreasing kinetic energy causing an increase in $\bar{S}_{col}[(E_K)_0]$.
- (2) For $(E_K)_0$ exceeding 3 MeV the situation is reversed; as $(E_K)_0$ decreases, $S_{col}[(E_K)_0]$ also decreases and this results in $\bar{S}_{col}[(E_K)_0] < S_{col}[(E_K)_0]$.
- (3) The two stopping powers, $S_{col}[(E_K)_0]$ and $\bar{S}_{col}[(E_K)_0]$, are identical at $(E_K)_0 \approx 5$ MeV, as shown in Fig. 6.28, indicating that the low- and high-energy effects involved in averaging the stopping power cancel one another.

6.10 Restricted Collision Stopping Power

6.10.Q1

(145)

Many expressions, at first glance unrelated to one another, have been used in the literature to describe the unrestricted mass collision stopping power S_{col} of absorbers for electrons. For example, the ICRU Report 37 uses the following form for S_{col}

$$S_{col} = C_e \frac{N_e}{\beta^2} \left\{ \ln \frac{E_K^2}{I^2} + \ln \left(1 + \frac{\tau}{2} \right) + (1 - \beta^2) \left[1 + \frac{\tau^2}{8} - (2\tau + 1) \ln 2 \right] - \delta \right\}, \tag{6.130}$$

while the book by Johns and Cunningham has

$$S_{\text{col}} = C_e \frac{N_e}{\beta^2} \left\{ \ln \frac{E_K^2 (E_K + 2E_0)}{2E_0 I^2} + \frac{E_K^2}{8(E_K + E_0)^2} - \frac{(2E_K + E_0)E_0 \ln 2}{(E_K + E_0)^2} + 1 - \beta^2 - \delta \right\}, \quad (6.131)$$

where C_e is a constant given as $C_e = 2\pi r_e^2 E_0 = 2.55 \times 10^{-25} \text{ MeV} \cdot \text{cm}^2$; N_e is the number of electrons per unit mass of absorber ($N_e = Z N_A / A$); E_K is kinetic energy of the electron; E_0 is rest energy of the electron; τ is kinetic energy E_K of the electron normalized to electron rest energy E_0 , i.e., $\tau = E_K / E_0$; δ is the so-called density effect parameter that accounts for density effect in condensed media; and I is the mean ionization/excitation potential of the absorber.

Bichsel recommends the following expression that can be used for both the unrestricted as well as the restricted mass collision stopping power

$$S_{\text{col}} = C_e \frac{N_e}{\beta^2} \left\{ \ln \frac{2(\tau + 2)E_0^2}{I^2} + F^-(\tau, \zeta) - \delta \right\}, \quad (6.132)$$

where F^- is in general defined as

$$F^- = -1 - \beta^2 + \ln[(\tau - \zeta)\zeta] + \frac{\tau}{\tau - \zeta} + \frac{1}{(\tau + 1)^2} \left[\frac{\zeta^2}{2} + (2\tau + 1) \ln \left(1 - \frac{\zeta}{\tau} \right) \right], \quad (6.133)$$

with ζ a special parameter defined as $\zeta = \tau / (2E_0)$ for unrestricted stopping power and as $\zeta = \Delta / E_0$ for restricted collision stopping power where Δ is equal to kinetic energy of the delta ray whose kinetic energy is just large enough to allow it to escape from the region of interest.

- (a) Show that (6.130) and (6.131) are equivalent.
- (b) Show that (6.132) incorporating (6.133) with $\zeta = \tau / (2E_0)$ is equivalent to (6.131).
- (c) Take (6.132) in conjunction with (6.133), insert $\zeta = \Delta / E_0$, and derive the expression for restricted mass collision stopping power given in the book by Johns and Cunningham as

$$L_{\Delta} = C_e \frac{N_e}{\beta^2} \left\{ \ln \frac{2(E_K + 2E_0)(E_K - \Delta)\Delta}{E_0 I^2} + \frac{E_K}{E_K - \Delta} + \frac{1}{(E_K + E_0)^2} \left[\frac{\Delta^2}{2} + E_0(2E_K + E_0) \ln \frac{E_K - \Delta}{E_K} \right] - 1 - \beta^2 - \delta \right\}. \quad (6.134)$$

SOLUTION:

(a) To prove equivalency of (6.130) with (6.131) we compare the terms inside the curly brackets of the two equations and transform (6.130) into (6.131) using the definition of the parameter $\tau = E_K/E_0$. Starting with (6.130) we get

$$\left\{ \ln \frac{E_K^2}{I^2} + \ln \left(1 + \frac{\tau}{2} \right) + (1 - \beta^2) \left[1 + \frac{\tau^2}{8} - (2\tau + 1) \ln 2 \right] - \delta \right\} \\ = \{ A + B + (C \times D) - \delta \}, \quad (6.135)$$

where

$$A = \ln \frac{E_K^2}{I^2}, \quad (6.136)$$

$$B = \ln \left(1 + \frac{\tau}{2} \right) = \ln \frac{E_K + 2E_0}{2E_0}, \quad (6.137)$$

$$A + B = \ln \frac{E_K^2}{I^2} + \ln \frac{(E_K + 2E_0)}{2E_0} = \ln \frac{E_K^2 (E_K + 2E_0)}{2E_0 I^2}, \quad (6.138)$$

$$C = 1 - \beta^2 = \frac{E_0^2}{(E_K + E_0)^2} = \frac{1}{(\tau + 1)^2}, \quad (6.139)$$

$$D = 1 + \frac{\tau^2}{8} - (2\tau + 1) \ln 2 = 1 + \frac{E_K}{8E_0} - \frac{2E_K + E_0}{E_0} \ln 2, \quad (6.140)$$

$$C \times D = 1 - \beta^2 + \frac{E_K^2}{8(E_K + E_0)^2} - \frac{(2E_K + E_0)E_0}{(E_K + E_0)^2} \ln 2. \quad (6.141)$$

Inserting parameters A , B , C , and D into (6.135) we now get the following expression for (6.135)

$$\{ A + B + (C \times D) - \delta \} \\ = \left\{ \ln \frac{E_K^2 (E_K + 2E_0)}{2E_0 I^2} + \frac{E_K^2}{8(E_K + E_0)^2} - \frac{(2E_K + E_0)E_0 \ln 2}{(E_K + E_0)^2} + 1 - \beta^2 - \delta \right\}. \quad (6.142)$$

Equation (6.142) is identical to (6.131), substantiating the contention that (6.130) and (6.131) are equivalent to one another. *Note:* Parameter C of (6.139) is determined from the basic definition of kinetic energy of the incident electron $E_K/E_0 = (1 - \beta^2)^{-1/2} - 1$.

(b) To prove the equivalency of (6.132) with (6.130) and (6.131) when parameter ζ of (6.132) is equal to the maximum possible energy transfer ΔE_{\max} from the incident electron of kinetic energy E_K to a delta ray electron normalized to electron rest energy E_0 .

According to convention on indistinguishable colliding particles, ΔE_{\max} equals to 50 % of the kinetic energy E_K of the incident electron. We thus use $\zeta = E_K/(2E_0)$ and modify (6.132) as follows

$$\left\{ \ln \frac{2(\tau + 2)E_0^2}{I^2} + F^- \left(\tau = \frac{E_K}{E_0}, \zeta = \frac{E_K}{2E_0} \right) - \delta \right\} = \{G + F^- - \delta\}, \quad (6.143)$$

with

$$G = \ln \frac{2(\tau + 2)E_0^2}{I^2} = \ln \frac{(E_K + 2E_0)E_0}{I^2}, \quad (6.144)$$

and

$$F^- = -1 - \beta^2 + H + J + K \times L, \quad (6.145)$$

where

$$H = \ln[(\tau - \zeta)\zeta] = \ln \left[\left(\frac{E_K}{E_0} - \frac{E_K}{2E_0} \right) \frac{E_K}{2E_0} \right] = \ln \frac{E_K^2}{4E_0^2}, \quad (6.146)$$

$$J = \frac{\tau}{\tau - \zeta} = \frac{E_K E_0}{E_0(E_K - \frac{1}{2}E_K)} = 2, \quad (6.147)$$

$$K = \frac{1}{(\tau + 1)^2} = \frac{E_0^2}{(E_K + E_0)^2} \quad [\text{see (6.139)}], \quad (6.148)$$

$$L = \frac{\zeta^2}{2} + (2\tau + 1) \ln \left(1 - \frac{\zeta}{\tau} \right) = \frac{E_K^2}{8E_0^2} - \frac{2E_K + E_0}{E_0} \ln 2, \quad (6.149)$$

$$\begin{aligned} K \times L &= \frac{E_0^2}{(E_K + E_0)^2} \times \left(\frac{E_K^2}{8E_0^2} - \frac{2E_K + E_0}{E_0} \ln 2 \right) \\ &= \frac{E_K^2}{8(E_K + E_0)^2} - \frac{(2E_K + E_0) \ln 2}{(E_K + E_0)^2}. \end{aligned} \quad (6.150)$$

Function F^- of (6.145) can now be expressed as follows

$$\begin{aligned} F^- &= -1 - \beta^2 + H + J + K \times L \\ &= -1 - \beta^2 + \ln \frac{E_K^2}{4E_0^2} + \frac{E_K^2}{8(E_K + E_0)^2} - \frac{(2E_K + E_0) \ln 2}{(E_K + E_0)^2}, \end{aligned} \quad (6.151)$$

leading to the following expression for (6.143)

$$\begin{aligned} & \left\{ \ln \frac{2(\tau+2)E_0^2}{I^2} + F^-\left(\tau = \frac{E_K}{E_0}, \zeta = \frac{E_K}{2E_0}\right) - \delta \right\} \\ &= \{G + F^- - \delta\} \\ &= \left\{ \ln \frac{(E_K + 2E_0)E_0}{I^2} + \frac{E_K^2}{8(E_K + E_0)^2} - \frac{(2E_K + E_0) \ln 2}{(E_K + E_0)^2} + 1 - \beta^2 - \delta \right\}. \end{aligned} \quad (6.152)$$

Equation (6.152) is identical to terms in curly bracket of (6.131) allowing us to conclude that (6.132) with $\zeta = E_K/(2E_0)$ is equivalent to (6.130) which, as shown in (a), in turn is equivalent to (6.131) for description of the mass unrestricted collision stopping power of various absorbers for electrons.

(c) In this section we use (6.132) in conjunction with (6.133) and insert into (6.133) for parameter ζ the δ ray threshold Δ normalized to electron rest energy E_0 , i.e., $\zeta = \Delta/E_0$, to derive (6.134) for restricted stopping power L_Δ . First, we write the terms in curly bracket of (6.132) as follows

$$\left\{ \ln \frac{2(\tau+2)E_0^2}{I^2} + F^-(\tau, \zeta) - \delta \right\} = \left\{ A + F^-\left(\tau = \frac{E_K}{E_0}, \zeta = \frac{\Delta}{E_0}\right) - \delta \right\} \quad (6.153)$$

where

$$A = \ln \frac{2(\tau+2)E_0^2}{I^2} = \ln \frac{2(E_K + 2E_0)E_0}{I^2} \quad (6.154)$$

and

$$\begin{aligned} & F^-\left(\tau = \frac{E_K}{E_0}, \zeta = \frac{\Delta}{E_0}\right) \\ &= -1 - \beta^2 + \ln \left[\left(\frac{E_K}{E_0} - \frac{\Delta}{E_0} \right) \frac{\Delta}{E_0} \right] + \frac{E_K}{E_K - \Delta} \\ &+ \frac{E_0^2}{(E_K - E_0)^2} \left[\frac{\Delta^2}{2E_0^2} + \left(\frac{2E_K}{E_0} + 1 \right) \ln \left(1 - \frac{\Delta}{E_K} \right) \right] - \delta \\ &= -1 - \beta^2 + \ln \frac{(E_K - \Delta)\Delta}{E_0^2} + \frac{E_K}{E_K - \Delta} \\ &+ \frac{1}{(E_K - E_0)^2} \left[\frac{\Delta^2}{2} + (2E_K + E_0)E_0 \ln \frac{E_K - \Delta}{E_K} \right] - \delta. \end{aligned} \quad (6.155)$$

Next, after inserting (6.154) and (6.155) into (6.153) we get the following expression for the restricted stopping power L_Δ , in agreement with the expression (6.134)

provided by Johns and Cunningham

$$L_{\Delta} = C_e \frac{N_e}{\beta^2} \left\{ \ln \frac{2(E_K + 2E_0)(E_K - \Delta)\Delta}{E_0 I^2} + \frac{E_K}{E_K - \Delta} + \frac{1}{(E_K + E_0)^2} \left[\frac{\Delta^2}{2} + E_0(2E_K + E_0) \ln \frac{E_K - \Delta}{E_K} \right] - 1 - \beta^2 - \delta \right\}. \quad (6.156)$$

6.10.Q2

(146)

Johns and Cunningham provide expressions for unrestricted and restricted mass collision stopping powers S_{col} and L_{Δ} , respectively, in the following format for electrons

$$S_{\text{col}} = C_e \frac{N_e}{\beta^2} \left\{ \ln \frac{E_K^2(E_K + 2E_0)}{2E_0 I^2} + \frac{E_K^2}{8(E_K + E_0)^2} - \frac{(2E_K + E_0)E_0 \ln 2}{(E_K + E_0)^2} + 1 - \beta^2 - \delta \right\} \quad (6.157)$$

and

$$L_{\Delta} = C_e \frac{N_e}{\beta^2} \left\{ \ln \frac{2(E_K + 2E_0)(E_K - \Delta)\Delta}{E_0 I^2} + \frac{E_K}{E_K - \Delta} + \frac{1}{(E_K + E_0)^2} \left[\frac{\Delta^2}{2} + E_0(2E_K + E_0) \ln \frac{E_K - \Delta}{E_K} \right] - 1 - \beta^2 - \delta \right\}, \quad (6.158)$$

where Δ is the delta ray electron threshold energy which is equal to kinetic energy of the delta ray electron whose kinetic energy is just large enough to allow it to escape from the region of interest. The other parameters of (6.157) and (6.158) are defined in Prob. 145.

- (a) Use expressions (6.157) and (6.158) to calculate S_{col} and L_{Δ} , respectively, of water for electrons with the following kinetic energy E_K in MeV: 0.01, 0.1, 1, 10, and 100 and the following delta ray threshold energies Δ in keV: 1, 10, and 100. The density effect parameter δ , as provided by the NIST [http://physics.nist.gov/cgi-bin/Star/e_table.pl] is as follows:

$E_K = 0.01$ MeV: $\delta = 0$; 0.1 MeV: 0 ; 1 MeV: 0.243 ; 10 MeV: 2.992 ; 100 MeV: 7.077 ; electron density: $N_e = 3.343 \times 10^{23}$ electron/g (Prob. 133); mean ionization/excitation potential: 75 eV (see Prob. 132).

- (b) Insert your results onto Fig. 6.29 that plots unrestricted mass collision stopping power S_{col} of water as well as restricted stopping power L_{Δ} (for Δ of 1 keV, 10 keV, and 100 keV) of water against electron kinetic energy E_K in the kinetic energy range from 1 keV to 100 MeV.
- (c) Calculate and plot the ratio L_{Δ}/S_{col} for the five kinetic energies E_K and three delta ray threshold energies Δ of (a) and (b). Comment on the meaning of the ratio L_{Δ}/S_{col} .
- (d) Show that (6.158) for restricted stopping power L_{Δ} transforms into (6.157) for unrestricted stopping power S_{col} when $\Delta = \Delta(E_K)_{max} = \frac{1}{2}E_K$ is used in (6.158).

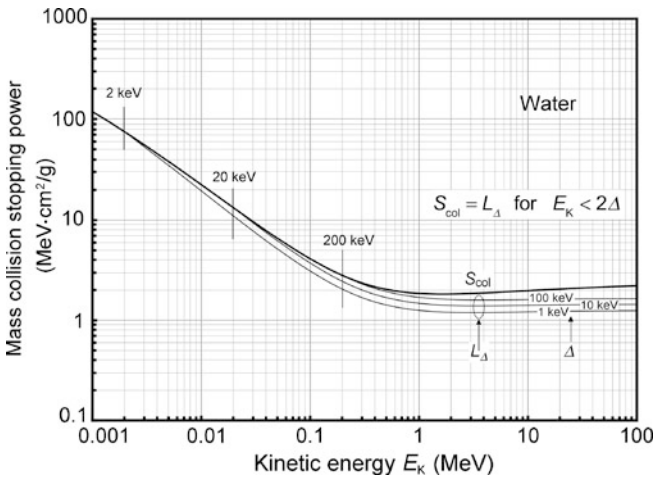


Fig. 6.29 Unrestricted mass collision stopping power S_{col} of water plotted with *heavy solid curve* as well as restricted stopping power L_{Δ} (for Δ of 1 keV, 10 keV, and 100 keV) of water plotted with *light solid curves* against electron kinetic energy E_K in the kinetic energy range from 1 keV to 100 MeV

SOLUTION:

(a) Expressions (6.157) for unrestricted mass collision stopping power S_{col} and (6.158) for restricted mass collision stopping power L_{Δ} were used to calculate S_{col} and L_{Δ} of water for the following kinetic energies E_K in MeV: 0.01, 0.1, 1, 10, and 100 and three delta ray threshold energies Δ of 1 keV, 10 keV, and 100 keV. Results are tabulated in Table 6.22 that also lists appropriate β^2 as well as the density effect parameter δ from the NIST.

Table 6.22 Unrestricted mass collision stopping power S_{col} (heavy solid curve) calculated from (6.157) as well as restricted stopping power L_{Δ} (light solid curves) calculated from (6.158) for delta ray threshold energies Δ of 1 keV, 10 keV, and 100 keV of water for electrons in kinetic energy range from 1 keV to 100 MeV

1	Kinetic energy E (MeV)	$\beta^2 = \frac{v^2}{c^2}$	δ from NIST	S_{col} (MeV/cm)	$L_{\Delta=1 \text{ keV}}$ (MeV/cm)	$L_{\Delta=10 \text{ keV}}$ (MeV/cm)	$L_{\Delta=100 \text{ keV}}$ (MeV/cm)
2	0.01	0.03802	0	22.600	19.630	–	–
3	0.10	0.30055	0	4.122	3.111	3.741	–
4	1.00	0.85563	0.243	1.852	1.256	1.477	1.695
5	10.00	0.99764	2.992	1.971	1.212	1.409	1.606
6	100.00	0.99997	7.077	2.206	1.248	1.442	1.639

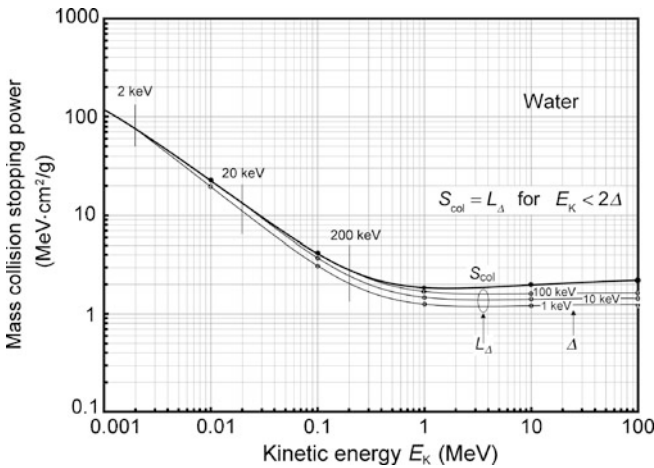


Fig. 6.30 Unrestricted mass collision stopping power S_{col} (heavy solid curve) as well as restricted stopping power L_{Δ} (light solid curves) for delta ray threshold energies Δ of 1 keV, 10 keV, and 100 keV of water for electrons in the kinetic energy range from 1 keV to 100 MeV obtained from the NIST. Superimposed onto the curves are S_{col} calculated from (6.157) and L_{Δ} calculated from (6.158)

(b) Figure 6.30 shows the unrestricted mass collision stopping power S_{col} (heavy solid curve) as well as restricted stopping power L_{Δ} (light solid curves) for delta ray threshold energies Δ of 1 keV, 10 keV, and 100 keV of water for electrons in the kinetic energy range from 1 keV to 100 MeV obtained from the NIST. Superimposed onto the curves are S_{col} calculated from (6.157) and L_{Δ} calculated from (6.158). Agreement between calculated data and data from the NIST is excellent.

(c) Ratio $L_{\Delta}/S_{\text{col}}$ of water for data of Table 6.22 is shown in Table 6.23 and plotted in Fig. 6.31. The following notable properties of $L_{\Delta}/S_{\text{col}}$ are apparent:

Table 6.23 Ratio $L_{\Delta}/S_{\text{col}}$ of water for data of Table 6.22 where L_{Δ} is the restricted mass collision stopping power and S_{col} is the unrestricted mass collision stopping power

1	Kinetic energy E (MeV)	S_{col}	$L_{\Delta=1 \text{ keV}}$	$\frac{L_{\Delta=1 \text{ keV}}}{S_{\text{col}}}$	$L_{\Delta=10 \text{ keV}}$	$\frac{L_{\Delta=10 \text{ keV}}}{S_{\text{col}}}$	$L_{\Delta=100 \text{ keV}}$	$\frac{L_{\Delta=100 \text{ keV}}}{S_{\text{col}}}$
2	0.01	22.600	19.630	0.869	–	–	–	–
3	0.10	4.122	3.111	0.755	3.741	0.908	–	–
4	1.00	1.852	1.256	0.678	1.477	0.800	1.695	0.915
5	10.00	1.971	1.212	0.615	1.409	0.715	1.606	0.815
6	100.00	2.206	1.248	0.566	1.442	0.654	1.639	0.743

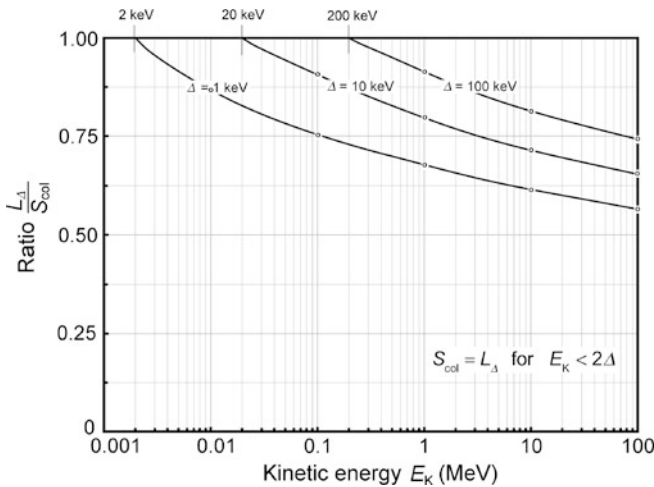


Fig. 6.31 Ratio $L_{\Delta}/S_{\text{col}}$ of water for data of Table 6.22 where L_{Δ} is the restricted mass collision stopping power and S_{col} is the unrestricted mass collision stopping power

- (1) For $E_K \leq 2\Delta$, where E_K is kinetic energy of the electron and Δ is threshold delta ray energy, $L_{\Delta} = S_{\text{col}}$ and thus $L_{\Delta}/S_{\text{col}} = 1$. Conclusion: No energy escapes the volume of interest.
- (2) As E_K increases beyond 2Δ , L_{Δ} becomes increasingly smaller in comparison to S_{col} indicating that an increasingly larger portion of incident kinetic energy escapes the volume of interest.
- (3) Ratio $L_{\Delta}/S_{\text{col}}$ can be considered the proportion of electron kinetic energy E_K that is absorbed locally. The proportion of E_K that escapes the volume of interest is $1 - L_{\Delta}/S_{\text{col}}$.

(d) To show that (6.158) for restricted stopping power L_{Δ} transforms into (6.157) for unrestricted stopping power S_{col} when delta ray threshold Δ attains its maximum possible value of $\Delta = \Delta(E_K)_{\text{max}} = \frac{1}{2}E_K$ we insert $\Delta = \frac{1}{2}E_K$ into (6.158) and get

$$\begin{aligned}
L_{\Delta=\frac{1}{2}E_K} &= C_e \frac{N_e}{\beta^2} \left\{ \ln \frac{2(E_K + 2E_0)(E_K - \frac{1}{2}E_K)\frac{1}{2}E_K}{E_0 I^2} + \frac{E_K}{E_K - \frac{1}{2}E_K} \right. \\
&\quad \left. + \frac{1}{(E_K + E_0)^2} \left[\frac{(\frac{1}{2}E_K)^2}{2} + E_0(2E_K + E_0) \ln \frac{E_K - \frac{1}{2}E_K}{E_K} \right] \right. \\
&\quad \left. - 1 - \beta^2 - \delta \right\} \\
&= C_e \frac{N_e}{\beta^2} \left\{ \ln \frac{E_K^2(E_K + 2E_0)}{2E_0 I^2} + \frac{E_K^2}{8(E_K + E_0)^2} - \frac{(2E_K + E_0)E_0 \ln 2}{(E_K + E_0)^2} \right. \\
&\quad \left. + 1 - \beta^2 - \delta \right\} = S_{\text{col}}. \tag{6.159}
\end{aligned}$$

6.11 Bremsstrahlung Targets

6.11.Q1

(147)

Diagnostic radiology and external beam radiotherapy rely heavily on x rays produced by energetic electrons striking metallic targets in x-ray tubes of x-ray machines or in disk-loaded waveguides of linear accelerators (linacs). X-ray targets come in many forms and are classified according to various attributes, such as: (1) Thickness, (2) Atomic number, (3) Photon spectrum and effective energy they produce, and (4) Physical integrity.

- (a) Categorize the interactions that an energetic electron experiences as it penetrates into an x-ray target.
- (b) Discuss categories of x-ray targets with respect to their thickness.
- (c) Discuss categories of x-ray targets with respect to their atomic number Z .

SOLUTION:

(a) X-ray targets serve as source of x rays and a common feature of all x-ray targets is that they are bombarded with energetic electrons that penetrate the target. The source of the energetic electrons most commonly is a heated filament ejecting electrons that are subsequently accelerated in an electrostatic field (provided in an x-ray tube) or electromagnetic field (provided in a linac wave guide) to attain kinetic energy of the order of 50 keV to 50 MeV for medical use and even higher kinetic energy for research purposes.

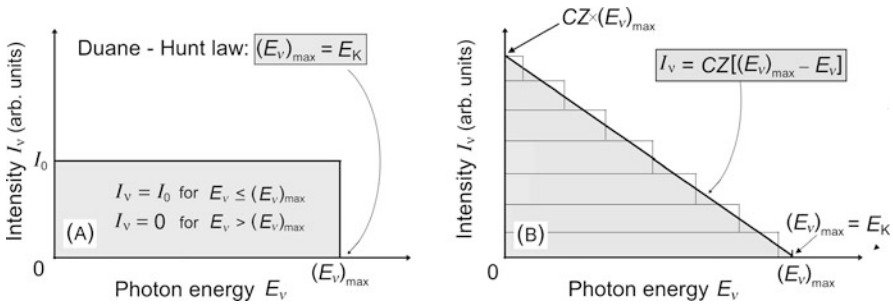


Fig. 6.32 Typical x-ray intensity spectra: **(A)** for thin target and **(B)** for thick target. Applied x-ray tube potential is U , maximum photon energy $(E_v)_{\max}$ is equal to eU which, according to Duane-Hunt law, is equal to kinetic energy E_K of incident electrons

Energetic electrons strike and penetrate the x-ray target and in traversing it interact through Coulomb interactions with constituents of target atoms, either orbital electrons or nuclei. The Coulomb interactions are either elastic collisions resulting in no energy loss but change in direction of motion or inelastic collisions involving some energy loss as well as change in direction of motion. There are four types of interaction available to incident electron striking an x-ray target and interacting with target atoms:

- (1) Elastic collision with orbital electron (no energy loss but change in direction of motion).
- (2) Elastic collision with nucleus (no energy loss but change in direction of motion).
- (3) Inelastic collision with orbital electron resulting in atomic excitation or ionization associated with energy loss and change in direction of motion (collision or ionization loss).
- (4) Inelastic collision with nucleus resulting in radiation energy loss, change in direction of motion, and production of bremsstrahlung x rays.

(b) Based on their thickness in comparison to the mean range \bar{R} of incident monoenergetic electrons in the target material, targets are classified into two main groups: thin targets and thick targets. Thickness of thin targets is much smaller than \bar{R} while thickness of thick targets is of the order of \bar{R} .

By definition, a *thin target* is so thin that incident electrons traverse it without any significant loss of kinetic energy, without significant elastic collisions, and with relatively small radiation loss. In a thin target essentially all radiation interactions are interactions between electrons of incident kinetic energy and the nuclei.

The bremsstrahlung radiation produced in a thin target by electrons of kinetic energy E_K has a constant intensity $I_v = I_0$ for $E_v = (E_v)_{\max}$ and zero intensity $I_v = 0$ for $E_v > (E_v)_{\max}$, as shown schematically in Fig. 6.32(A). The maximum photon energy $(E_v)_{\max}$ is equal to eU where U is the applied potential.

According to Duane-Hunt law, eU is equal to kinetic energy E_K of incident electrons striking the x-ray target. Since the x-ray intensity I_ν is proportional to the product $(\Delta N/\Delta E_\nu) \times E_\nu$, it follows that, in comparison with the number of photons of energy $(E_\nu)_{\max}$, the x-ray spectrum contains twice as many photons of energy $0.5(E_\nu)_{\max}$, 4 times as many photons of energy $0.25(E_\nu)_{\max}$, 10 times as many photons of energy $0.10(E_\nu)_{\max}$, etc.

A *thick target* is defined such that all electrons striking it are absorbed in the target and no electrons can traverse the thick target. In practice, the thickness of a thick target is about 110 % of \bar{R} to ensure that none of the incident electrons can exit the target. On the other hand, the thick target should be no thicker than necessary, so as to minimize the absorption of x rays in the target material.

The spectral distribution of thick target bremsstrahlung can be represented as a superposition of contributions from a large number of thin targets, each thin target traversed by a lower energy mono-energetic electron beam having a lower $(E_\nu)_{\max}$ than the previous thin target. In traversing each thin target, the electron loses a small portion of its kinetic energy and enters the next thin target with a lower energy until it attains zero kinetic energy in the last thin target, as shown schematically in Fig. 6.32(B) which depicts a thick target spectrum as a superposition of many thin target spectra of the type shown in Fig. 6.32(A). The beam intensity I_ν for a thick target as a function of photon energy E_ν may be described with the following empirical linear relationship

$$I_\nu \approx CZ[(E_\nu)_{\max} - E_\nu], \quad (6.160)$$

where C is a constant, Z is the atomic number of the thick target material, $(E_\nu)_{\max}$ is the maximum energy of the spectrum, and I_ν is the x-ray beam intensity at photon energy $E_\nu = h\nu$ with a maximum value $CZ(E_\nu)_{\max}$ at $E_\nu = 0$ and a value of 0 for $E_\nu \geq (E_\nu)_{\max}$.

(c) Atomic number Z and kinetic energy E_K of the incident electron beam affect the quality as well as yield of x rays produced by an x-ray target. With regard to atomic number, x-ray targets are classified as low Z targets, intermediate Z targets, and high Z targets. In general, the total intensity I of x rays produced by a thick target is estimated by integrating I_ν of (6.160) over the energy range from $E_\nu = 0$ to $E_\nu = (E_\nu)_{\max}$ to get

$$I = CZ \int_0^{(E_\nu)_{\max}} [(E_\nu)_{\max} - E_\nu] dE_\nu = \frac{1}{2} CZ \times (E_\nu)_{\max}^2 = \frac{1}{2} CZ (eU)^2 = \frac{1}{2} CZ E_K^2 \quad (6.161)$$

showing that the total photon intensity I emitted from the x-ray target is proportional to the target atomic number Z and the square of the accelerating potential U or kinetic energy E_K .

The statement of (6.161) that x-ray intensity I is proportional to ZE_K^2 reflects the total bremsstrahlung energy emitted per electron absorbed in the thick x-ray target or per electron incident onto the thick target, since the definition of a thick target stipulates that all electrons striking the target will be absorbed in the target.

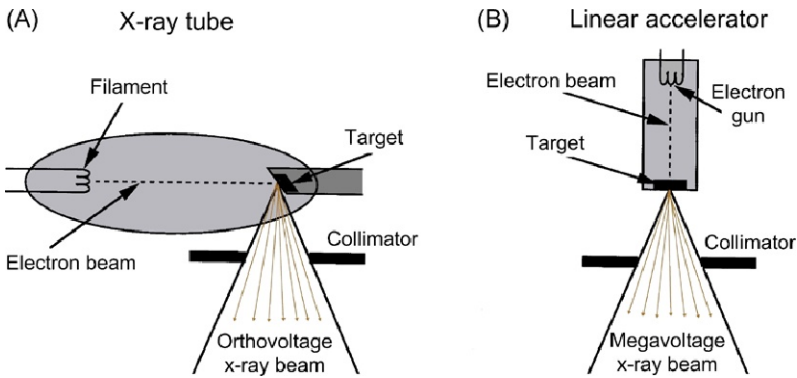


Fig. 6.33 Schematic comparison of x-ray production (A) in the diagnostic radiology orthovoltage range with an x-ray machine (maximum x-ray intensity orthogonally to the electron beam) and (B) in the radiotherapy megavoltage range with a linear accelerator (x rays emitted mainly in the direction of the electron beam)

X-ray yield thus depends on the atomic number Z of the target, as stated in (6.161), but this implies intensity integrated over all photon energies from 0 to maximum as well as over the full 4π solid angle. It is well known that intensity of x rays emanating from an x-ray target is not isotropic and the intensity distribution depends strongly on kinetic energy of the incident electrons. The intensity maximum in diagnostic radiology energy range is at 90° to the direction of the incident electron, while with increasing kinetic energy the intensity distribution is progressively more forward peaked. This is why with diagnostic x-ray tubes the patient imaging is carried out at 90° to the incident electron beam direction and in radiotherapy treatment the patient is positioned at 0° to the incident electron beam direction. This is shown schematically in Fig. 6.33.

6.11.Q2

(148)

X-ray targets play an important role in x-ray production and their performance is influenced by many physical and practical parameters, such as atomic number, composition and design of the target as well as kinetic energy and electron beam current of electrons striking the x-ray target.

- Briefly discuss the important features of x-ray generation in an x-ray target.
- The term “beam quality” is used to indicate the ability of an x-ray beam to penetrate a water phantom. List at least six x-ray beam quality “specifiers” or indices.

- (c) Betatrons used clinically in 1950s and 1960s typically operated in the 25 MV x-ray mode. When 25 MV linacs were introduced into clinical service in the early 1970s, percentage depth doses they produced in water were significantly shallower (less penetrating) than those produced by 25 MV betatrons. How was this surprising finding explained and rectified?

SOLUTION:

- (a) Brief characteristics of x-ray production in an x-ray target:

(1) In an x-ray tube or in a linac accelerating wave guide, energetic electrons strike a metallic target and a small fraction of their kinetic energy is emitted from the target in the form of x rays, while most of the kinetic energy carried by incident electrons is converted into heat.

(2) Efficiency for x-ray production, also called x-ray yield, depends on three parameters: target atomic number Z , kinetic energy E_K of the incident electrons striking the target, and electron beam current J . X-ray yield increases with increasing Z for constant J and E_K ; it increases with increasing J for constant Z and E_K ; and it increases with E_K for constant Z and J .

(3) Two types of x rays are produced in an x-ray target: characteristic x rays and bremsstrahlung photons, and both types are produced through energy loss that incident electrons experience in penetrating the target and interacting with atoms of the target.

Characteristic x rays are generated as a consequence of Coulomb collisions between incident electrons and orbital electrons of target atoms, producing excitation and ionization of target atoms, and creating vacancies in atomic shells of target atoms. As orbital electrons from higher orbits fill these vacancies, transition energy is emitted in the form of discrete photons or Auger electrons with energy that is characteristic of the target material, hence the name characteristic radiation. Energy loss by electrons through this type of interaction is referred to as collision loss or ionization loss and contributes to collision stopping power of the target material.

Bremsstrahlung photons are generated in x-ray targets through Coulomb interactions between incident electrons and nuclei of target atoms. Photon spectra produced in this type of interaction are continuous, ranging in energy from zero to a maximum energy $h\nu_{\max}$ equal to kinetic energy E_K of incident electrons (Duane-Hunt law). Energy loss by electrons through this type of interaction is called radiation loss and contributes to radiation stopping power of the target.

(4) Bremsstrahlung spectrum is continuous while characteristic photons contribute discrete spectral lines that are superimposed onto the continuous bremsstrahlung spectrum. The relative proportion of the number of characteristic photons

to bremsstrahlung photons in an x-ray beam spectrum varies with atomic number Z of the target and kinetic energy E_K of the incident electrons. For example, x-ray beams produced in a tungsten target by 100 keV electrons contain about 20 % of characteristic photons and 80 % of bremsstrahlung photons. In the megavoltage range the contribution of characteristic photons to the total spectrum is negligible in comparison to bremsstrahlung photons.

(5) In the diagnostic energy range (30 kVp to 150 kVp) most photons are produced at close to 90° from the direction of incident electrons striking the target. In the megavoltage radiotherapy energy range (4 MV to 50 MV), on the other hand, most photons are produced in the direction of the incident electron beam striking the target.

(6) Since most of the kinetic energy of the incident electron beam upon striking an x-ray target is transformed into heat, x-ray targets must have the following properties: high melting point, good thermal conductivity, and high x-ray yield, while x-ray producing equipment must have efficient means for cooling the x-ray target. Target cooling is less of a problem in megavoltage x-ray production than in the diagnostic energy range because the efficiency of x-ray production is at least an order of magnitude higher in the megavoltage range ($\sim 10\%$) in comparison to the diagnostic range ($< 1\%$).

Requirements for cooling of x-ray tubes used in imaging are more stringent than requirements for cooling of x-ray tubes used in radiotherapy for two reasons: to achieve short exposure times the instantaneous tube currents used in imaging are one to two orders of magnitude higher than in radiotherapy tubes. Moreover, focal spots in imaging tubes are much smaller than those in therapy tubes resulting in more sophisticated methods for cooling of imaging tubes (e.g., rotating anode) compared to therapy tubes which employ stationary targets.

(b) Beam quality specification or beam quality indices. Many beam quality indices have been developed and are in use, but none of them is simple, universal, and easy to use. Best-known indices are as follows:

(1) Measurement of **complete x-ray spectrum** produced in an x-ray target and emitted by x-ray producing equipment for diagnostic or therapeutic use gives the most rigorous description of beam quality. However, a complete x-ray spectrum is difficult to measure directly under clinical conditions because of the high photon fluence rate that causes significant photon pile up in the detector. Indirect techniques have been developed for this purpose, but are cumbersome. Examples are measurement with diffraction spectrometer using Bragg reflection on a single crystal and registering the intensity of x rays as a function of wavelength or measurement with high resolution detector using 90° Compton scattering from a known sample and reconstructing the actual spectrum from the scatter spectrum using the Klein-Nishina function.

(2) Measurement of **half-value layer (HVL)** is practical for beam quality description in the diagnostic x-ray energy region (superficial and orthovoltage x rays) because of strong dependence of the attenuation coefficient on photon energy. In the superficial energy region HVL is usually quoted in millimeters of aluminum, in the orthovoltage region in millimeters of copper. In the megavoltage region, however, HVL is not used for beam quality specification because in this region the attenuation coefficient is only a slowly varying function of photon energy.

To minimize effects of radiation scattered in the attenuator the HVL should be measured under “good geometry” conditions that imply a narrow radiation beam and a reasonable distance between the attenuator and the detector to minimize the number of scattered photons reaching the detector. Moreover, the ionization chamber used in HVL measurement should possess an air equivalent wall and a flat photon energy response throughout the beam energy spectrum.

(3) **Nominal accelerating potential (NAP)** was used in early radiation dosimetry protocols as a matter of convenience and is related to the kinetic energy of incident electrons striking the target. It is defined in terms of the ionization ratio measured with a $10 \times 10 \text{ cm}^2$ field in water phantom on central beam axis with an ionization chamber at 100 cm from the target and at depths in water of 20 cm and 10 cm. The measured dose ratio at the two depths in water was linked with a nominal accelerating potential which was then used for selection of dosimetric parameters.

(4) **Ratio of “tissue-phantom ratios” (TPR_{20,10})** at depths of $z = 20 \text{ cm}$ and $z = 10 \text{ cm}$ in water phantom for a $10 \times 10 \text{ cm}^2$ field at 100 cm from the target. TPR at depth z itself is defined as the ratio of doses D_Q and $D_{Q_{\text{ref}}}$ where D_Q is the dose at depth z and $D_{Q_{\text{ref}}}$ is the dose at a reference depth, typically chosen as 5 cm or 10 cm. TPR_{20,10} is used for megavoltage beam quality specification in many national and international dosimetry protocols. It is similar to the NAP concept, however, through the TPR ratio it accounts for the actual penetration of a given clinical beam in water.

(5) Megavoltage beam quality specification can also be quoted with **percentage depth dose (PDD)** for a $10 \times 10 \text{ cm}^2$ field at a depth of $z = 10 \text{ cm}$ in water phantom that is positioned at a distance of 100 cm from the target. Percentage depth dose at depth of 10 cm is defined as the ratio of doses D_Q and D_P multiplied by 100, where D_Q is dose at depth of 10 cm in water and D_P is the dose at depth of dose maximum in water for the given megavoltage beam. Effects of electron contamination of the thick target x-ray beam can be minimized with a lead scattering foil placed into the photon beam.

(c) During 1950s and 1960s betatrons provided the only viable and practical option for delivery of megavoltage external beam radiotherapy in the energy range above 10 MV. However, betatrons suffered some serious drawbacks in comparison with cobalt-60 teletherapy machines that were used for megavoltage radiotherapy during that time, such as low output ($\sim 0.5 \text{ Gy/min}$), relatively small field size ($< 20 \times 20 \text{ cm}^2$), non-isocentric mounting, and noisy operation, so that high-energy

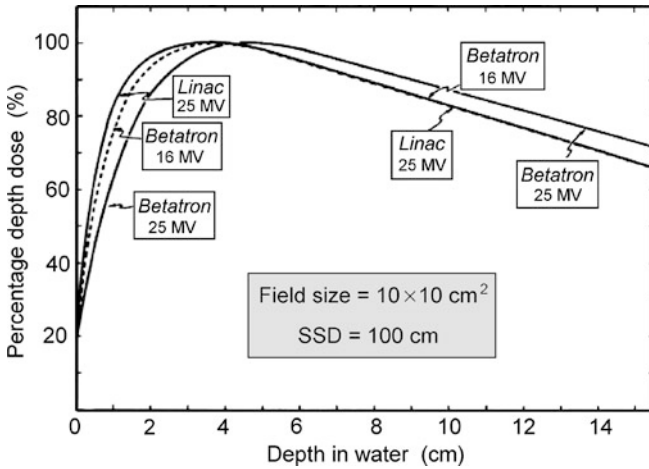


Fig. 6.34 Depth dose data measured with $10 \times 10 \text{ cm}^2$ field at target–water phantom distance of 100 cm for Varian Clinac-35 operated at 25 MV (solid curve), Allis-Chalmers betatron operated at 25 MV (solid curve) and Allis-Chalmers betatron operated at 16 MV (dashed curve)

linear accelerators (linacs) that solved these drawbacks were a welcome new development in radiotherapy in the early 1970s. The basic assumption in the development of high energy linacs was that, when run at 25 MV, they will provide the same beam quality as did the 25 MV betatrons but will ameliorate the weak points of betatrons and be, in comparison with betatrons, much more efficient and practical to use (output up to 10 Gy/min, field size up to $40 \times 40 \text{ cm}^2$ at 100 cm from the x-ray target, isocentric mounting, and quieter operation).

However, when percentage depth dose characteristics (beam penetration into water and tissue) were measured, it turned out that the beam produced with the 25 MV linac (Varian CI-35) was much less penetrating than that produced with a 25 MV betatron (Allis-Chalmers), as shown in Fig. 6.34 which also shows that the new 25 MV linac produced a beam that had depth dose characteristics of a betatron operated at 16 MV. This significant discrepancy was subsequently investigated and traced to differences in design and atomic number of x-ray target and flattening filter; two mundane, yet important, beam-forming and beam-shaping components, respectively, of the two megavoltage x-ray machines.

As for the flattening filter, betatron employed a filter made of aluminum, while the linac used a tungsten flattening filter to conserve space. However, in comparison to aluminum, tungsten softens the photon beam more than does a low Z filter and shifts the spectrum toward lower effective energy. Thus, to achieve the highest effective x-ray beam energy, a linac flattening filter should be made of low Z material. Since in this question, we are addressing x-ray targets, we now concentrate on x-ray targets of high-energy linacs.

In Fig. 6.35 we show schematically the way bremsstrahlung was produced in the two machines. Betatron used a thin tungsten target, while the linac used a thick tungsten target. Therefore, in the betatron the electrons have only one interaction

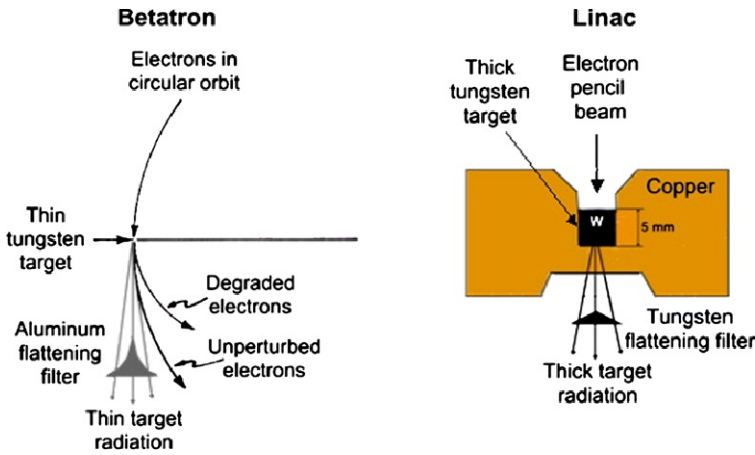


Fig. 6.35 Comparison of x-ray production with a thin target in a betatron to x-ray production with a thick target in a linear accelerator (linac)

with the thin target or no interaction at all, as they traverse the thin target. If the electrons have an inelastic collision with a target nucleus, they lose some of their energy, produce a bremsstrahlung photon, spiral in, as indicated in the figure, and hit the wall of the donut. If they do not experience a collision, they exit the thin target with kinetic energy intact, go around the circular orbit once more, and strike the target again. This means that in a 25 MV betatron each bremsstrahlung photon is produced by a 25 MeV electron incident on the thin target. On the other hand, in a 25 MV linac thick target bremsstrahlung is produced by electrons, undergoing multiple collisions, as they slow down from incident energy of 25 MeV to zero energy. This results in a photon spectrum that contains a larger proportion of lower energy photons than are present in betatron-produced bremsstrahlung beam and this, in turn, produces a less penetrating photon beam characterized as thick target spectrum.

For same incident electron kinetic energy, thin x-ray targets clearly produce more penetrating photon beams than do thick x-ray targets; however, thin targets can only be used in a betatron because of the presence of a strong magnetic field that sweeps into the donut wall the lower energy electrons that traverse the target after having had a bremsstrahlung interaction. To introduce this approach to a linac would be much more difficult as well as less practical than the traditional use of thick targets, therefore linacs use a thick target to ensure that no electrons can traverse the target and reach the flattening filter or the patient.

Thick target is the correct practical choice of target for linacs; however, the early choice of tungsten as the target material in high-energy linacs turned out less than optimal as far as beam quality was concerned. The choice was based on conventional wisdom that x-ray yield of thick targets depends linearly on the atomic number Z of the target, therefore, a high Z target was to maximize beam output for a given electron beam current passing through the target. However, a closer look at this

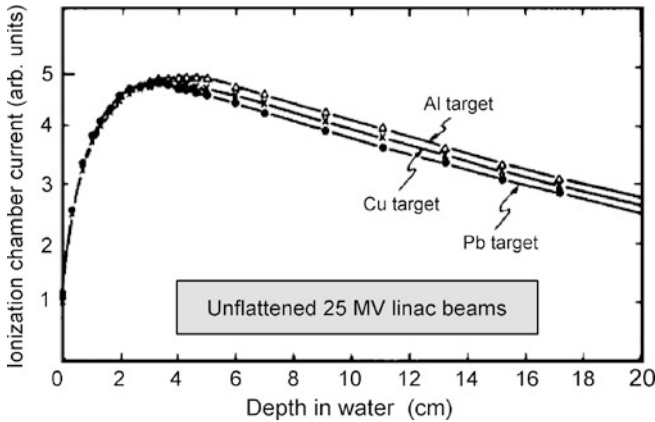


Fig. 6.36 Relative ionization chamber current against depth in water-equivalent phantom for an unflattened 25 MV linac beam with field size of $10 \times 10 \text{ cm}^2$ and target–phantom distance of 100 cm for three target materials: aluminum, copper, and lead. All depth dose curves were measured in the forward beam direction and normalized to the same beam current passing through the target

Z dependence shows that it accounts for x-ray output integrated over a full solid angle in 4π geometry, yet in radiotherapy one is only interested in a small solid angle in the forward direction which coincides with the direction of the electron beam striking the target. Furthermore, one actually strives to minimize the x-ray production in directions other than the forward direction in order to minimize the leakage radiation emanating from the linac.

In Fig. 6.36 we show central axis depth dose distributions measured in forward beam direction in a water-equivalent phantom against depth in phantom with various target materials: aluminum (low Z), copper (intermediate Z), and lead (high Z). The ordinate plots ionization chamber current against depth in phantom for a given charge delivered to the target.

Curves for the three target materials in Fig. 6.36 reveal several interesting features:

- (1) X-ray yield in the forward direction does **not** depend linearly on target atomic number Z .
- (2) Since aluminum target produces the highest x-ray yield in the forward direction, we can state that low Z targets are the most efficient in x-ray production in the forward direction; however, the difference between high Z and low Z targets is small, so that one can conclude that x-ray yield in the forward direction is essentially the same for all thick x-ray targets and thus is independent of atomic number Z of the target.
- (3) There is another important characteristic of target material evident from Fig. 6.36. In the forward direction low Z target does not only produce the highest x-ray yield by a small margin, more importantly, it also produces the most energetic beam that can also be described as the most penetrating beam or the beam with the highest effective energy.

The question now arises on how to reconcile the linear Z dependence of the integrated x-ray yield with the independence of x-ray yield in the forward direction upon Z of the target. Both statements have been proven experimentally, so we can explain the seeming contradiction as follows: x-ray yield in directions other than the forward direction depends on Z , so that a high Z target produces significantly more leakage radiation than a low Z target and this results in the linear dependence of the integrated x-ray yield upon Z .

Low Z targets thus have at least two advantages over high Z targets: in the forward direction they produce more penetrating beam and in all other directions around the target they produce less leakage radiation. Based on Fig. 6.36 one concludes that low Z target should be used in high-energy linac in order to:

- (1) Maximize the x-ray beam penetrating power for a given kinetic energy of electrons striking the x-ray thick target.
- (2) Minimize the leakage radiation emanating from the linac.

It is thus obvious that linac targets should be made of low Z materials. In comparison with x-ray tubes, requirements for very high melting point of the target material in linacs is more relaxed because of the higher x-ray yield and associated lower heat deposition in the target in the megavoltage energy range. Therefore, many materials that would not be suitable for x-ray tube targets can in principle be considered for target use in linacs.

However, materials used for linac targets must possess a high mass density to minimize the thickness of the thick linac target and it turns out that it is very difficult to identify a low Z material with a high density comparable to lead and tungsten. For example, the thickness of the thick target required for a 25 MV linac is as follows: 1 cm of lead, or 0.6 cm of tungsten, or 1.4 cm of copper, or 5 cm of aluminum. Aluminum is an excellent candidate from the point of view of atomic number; however, it is very impractical when the target thickness of 5 cm is considered. On the other hand, copper is a good candidate on both counts, atomic number ($Z = 29$) and density ($\rho \approx 9 \text{ g/cm}^3$), and is now the most common material used for x-ray targets in modern high-energy linacs.

In summary, both the x-ray target and flattening filter of high-energy linacs should be made of materials with as low as possible atomic number Z to maximize the beam effective energy and as high as possible mass density to minimize the space occupied by the two components.

Chapter 7 consists of **34 problems** spread over 7 sections dealing with various interactions that photons of energy exceeding the ionization potential of atoms can have with absorbing media. These photons belong to the category of indirectly ionizing radiation and they deposit energy in the absorbing medium through a two-step process: (1) in the first step energy is transferred from the photon to one, two or three energetic light charged particles and (2) in the second step the light charged particles deposit all or part of the transferred energy into the absorbing medium through collision loss with orbital electrons of the absorber atoms. The energy difference between energy transferred to charged particles and energy absorbed in the absorbing medium goes into bremsstrahlung (for electrons and positrons) and in-flight annihilation (for positrons only).

Section 7.1 contains several problems that address the general aspects of photon attenuation in absorbers dealing with: (1) various attenuation and absorption coefficients, (2) various characteristic absorber thicknesses, such as half-value layer, mean free path, and tenth-value layer as well as (3) issues related to narrow beam geometry versus broad beam geometry in photon attenuation measurements.

Sections 7.2 through 7.7 concentrate on individual photon interaction effects, dealing with all important aspects of relevance to individual effects starting with basic features and finishing with microscopic and macroscopic scale attenuation coefficients, energy transfer coefficients, and energy absorption coefficients. Section 7.2 addresses Thomson scattering and is followed by a set of 13 problems dealing with Compton (incoherent) scattering in Sect. 7.3 and Sect. 7.4 that concentrates on Rayleigh (coherent) scattering. Next section (Sect. 7.5) addresses various aspects of the photoelectric effect with six problems, Sect. 7.6 deals with both components of pair production (nuclear and electronic), and Sect. 7.7 concentrates on various aspects of photonuclear reactions.

7.1 General Aspects of Photon Interactions with Absorbers

7.1.Q1

(149)

Attenuation of a mono-energetic photon beam of intensity I and energy $h\nu$ in absorber of thickness x is described by an exponential function as follows

$$I(x) = I(0)e^{-\mu(Z,h\nu)x}, \quad (7.1)$$

where $I(0)$ is the intensity of the un-attenuated ($x = 0$) photon beam and $\mu(Z, h\nu)$ is the linear attenuation coefficient dependent on atomic number Z of absorber and energy $h\nu$ of the photon beam. In addition to μ , several other attenuation coefficients are also in use, most notably the mass attenuation coefficient μ_m and the atomic attenuation coefficient (cross section) ${}_a\mu$.

- Draw a typical attenuation curve for a mono-energetic photon beam $h\nu$ with incident intensity $I(0)$ against absorber thickness x , as given in (7.1). On the I vs x curve define the following characteristic thicknesses: half-value layer $x_{1/2}$, mean free path \bar{x} , and tenth-value layer $x_{1/10}$ and state the relationships among them.
- Complete the diagram for linear attenuation coefficient μ , mass attenuation coefficient μ_m and atomic attenuation coefficient ${}_a\mu$ provided in Fig. 7.1 by identifying the factors used in transferring from one attenuation coefficient to another.

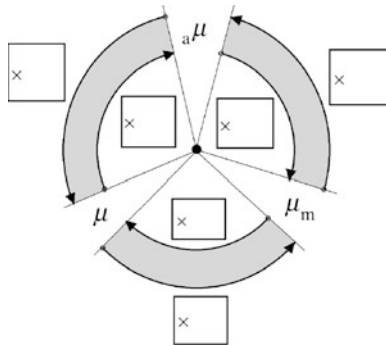


Fig. 7.1 Three important attenuation coefficients: linear μ , mass μ_m , and atomic ${}_a\mu$ as well as factors used in relationships among the three attenuation coefficients

SOLUTION:

- Figure 7.2 is a typical plot of intensity $I(x)$ against absorber thickness x for a mono-energetic photon beam measured under narrow beam geometry conditions.

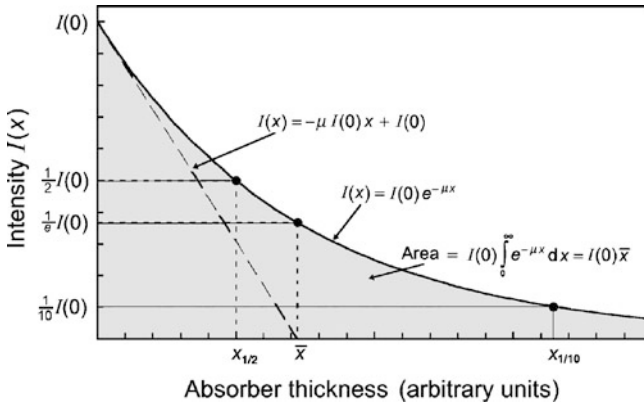


Fig. 7.2 Intensity $I(x)$ against absorber thickness x for a typical mono-energetic photon beam measured under narrow beam geometry conditions. Half-value layer (HVL) $x_{1/2}$, mean free path (MFP) \bar{x} , and tenth-value layer (TVL) $x_{1/10}$ are identified on the abscissa (x) axis

The functional relationship of $I(x)$ vs x is a perfect exponential function expressed in (7.1). The figure also highlights: (1) half-value layer $x_{1/2}$, (2) mean free path \bar{x} , and (3) tenth-value layer $x_{1/10}$. These parameters of exponential attenuation are defined as follows:

- (1) Half-value layer (HVL) $x_{1/2}$ is the thickness of absorber that attenuates the photon beam from intensity $I(0)$ to $\frac{1}{2}I(0)$, i.e., to 50 % of its original intensity $I(0)$.
- (2) Mean free path (MFP) \bar{x} is the thickness of absorber that attenuates the photon beam from intensity $I(0)$ to $e^{-1}I(0) = 0.368I(0)$, i.e., to 36.8 % of its original intensity $I(0)$.
- (3) Tenth-value layer (TVL) $x_{1/10}$ is the thickness of absorber that attenuates the photon beam from intensity $I(0)$ to $\frac{1}{10}I(0)$, i.e., to 10 % of its original intensity $I(0)$.

Relationships among the characteristic thicknesses: half-value layer (HVL) $x_{1/2}$, mean free path (MFP) \bar{x} , and tenth-value layer (TVL) $x_{1/10}$ are as follows

$$\mu = \frac{\ln 2}{x_{1/2}} = \frac{1}{\bar{x}} = \frac{\ln 10}{x_{1/10}} \quad \text{or} \quad x_{1/2} = (\ln 2)\bar{x} = \frac{\ln 2}{\ln 10}x_{1/10} \equiv 0.301x_{1/10}. \quad (7.2)$$

(b) The three most important attenuation coefficients are: atomic ${}_a\mu$, mass μ_m , and linear μ . The basic relationship between the linear attenuation coefficient μ and atomic attenuation coefficient (also known as atomic cross section) ${}_a\mu$ is expressed as

$$\mu = n \square {}_a\mu = \frac{N_a}{V} {}_a\mu = \rho \frac{N_a}{m} {}_a\mu = \rho \frac{N_A}{A} {}_a\mu, \quad (7.3)$$

where

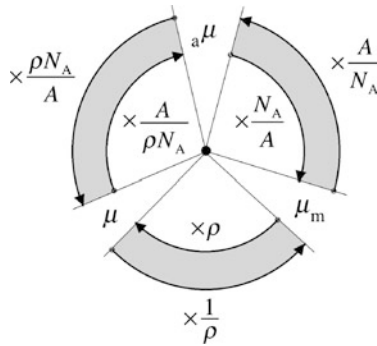


Fig. 7.3 General relationships among three most common attenuation coefficients: atomic $a\mu$, mass μ_m , and linear μ

- n is the number of absorber atoms N_a per absorber volume \mathcal{V} , i.e., $n = N_a/\mathcal{V}$.
- ρ is the mass density of the absorber, typically in g/cm^3 .
- m is the absorber mass, typically in g.
- N_A is the Avogadro number, typically number of atoms N_a per mole of the absorber ($N_A = 6.022 \times 10^{23} \text{ mol}^{-1}$).
- A is the molar mass (mass per mole) of the absorber expressed in g/mol.

The common relationships among the three attenuation coefficients: atomic $a\mu$, mass μ_m , and linear μ are displayed in Fig. 7.3.

7.1.Q2

(150)

Photon beam attenuation in a given absorber is governed by linear attenuation coefficient μ that in turn depends on energy $h\nu$ of the photon beam and atomic number Z of the absorber. In addition to linear attenuation coefficient μ , several other attenuation coefficients are also in common use, most importantly the mass attenuation coefficient μ_m and atomic attenuation coefficient (cross section) $a\mu$.

- (a) An attenuation experiment carried out on an unknown photon beam, using narrow beam geometry and various thicknesses x of lead (mass density $\rho = 11.36 \text{ g/cm}^3$, atomic mass $A = 207.2 \text{ g/mol}$) resulted in the following exposure rate \dot{X} data measured with a cylindrical ionization chamber of appropriate wall thickness. Plot the measured exposure rate \dot{X} against lead thickness x and, based on the graph, determine the linear attenuation coefficient μ for the unknown beam in lead.

x (mm Pb)	0	2	4	6	8	10	12	15	20	25	30	40	50
\dot{X} (R/min)	123.6	108.3	94.9	83.2	72.9	63.9	56.0	45.9	33.0	23.7	17.1	8.8	4.6

- (b) From the linear attenuation coefficient μ determined in (a) calculate the mass attenuation coefficient μ_m , atomic attenuation coefficient ${}_a\mu$ and mean free path \bar{x} for the unknown photon beam.
- (c) Based on the graph plotted in (a) describe the spectral distribution and the quality of the unknown photon beam. Use NIST data to determine the energy of the unknown photon beam based on the mass attenuation coefficient determined in (c).

SOLUTION:

(a) Figure 7.4(A) shows a plot of the measured attenuation data on a linear graph paper and the resulting attenuation curve appears exponential suggesting that our photon beam is mono-energetic. Data are re-plotted in Fig. 7.4(B) on semi-log graph paper, resulting in a straight line, confirming true exponential behavior of the measured data. Applying the least-squares fit to measured data we determine the best straight line through the measured points and we now have three options for the determination of the linear attenuation coefficient μ using: (1) slope of the straight line through the measured points, (2) half-value layer, and (3) tenth-value layer (TVL).

(1) **Slope of the straight line** is determined from the triangle drawn in Fig. 7.4(B) defined by two arbitrary points $P_1(x_1, y_1)$ and $P_2(x_2, y_2)$ on the straight line with $x_1 = 12$ mm, $y_1 = 56.0$ R/min and $x_2 = 30$ mm, $y_2 = 17.1$ R/min

$$\tan \phi = \frac{\ln y_1 - \ln y_2}{-(x_1 - x_2)} = \frac{\ln \frac{y_1}{y_2}}{x_2 - x_1} = \frac{\ln \frac{56.0}{17.1}}{(30 - 12) \text{ mm}} = 0.0659 \text{ mm}^{-1} = 0.659 \text{ cm}^{-1}. \quad (7.4)$$

We thus have the following result for the linear attenuation coefficient: $\mu = 0.659 \text{ cm}^{-1}$.

(2) **Half-value layer** $x_{1/2}$ of an absorber in a given photon beam $h\nu$ is defined as the thickness of the absorber that attenuates the photon beam from its original un-attenuated value of $I(0)$ to half of its original value or $\frac{1}{2}I(0)$. Assuming exponential attenuation of the photon beam, μ and $x_{1/2}$ are related directly as: $\mu = (\ln 2)/x_{1/2}$. With $I(0) = 123.6$ R/min we determine the characteristic thickness $x_{1/2}$ (for which $I(x_{1/2}) = \frac{1}{2}I(0) = 61.8$ R/min) as $x_{1/2} = 1.05$ cm of lead and this results in a linear attenuation coefficient μ of $\mu = 0.066 \text{ mm}^{-1}$ or 0.66 cm^{-1} .

(3) **Tenth-value layer** $x_{1/10}$ of an absorber in a given photon beam $h\nu$ is defined as the thickness of the absorber that attenuates the photon beam from its original un-attenuated value of $I(0)$ to one tenth of its original value or $\frac{1}{10}I(0)$. Assuming exponential attenuation of the photon beam μ and $x_{1/10}$ are related directly as: $\mu = (\ln 10)x_{1/10}$. With $I(0) = 123.6$ R/min we determine the characteristic

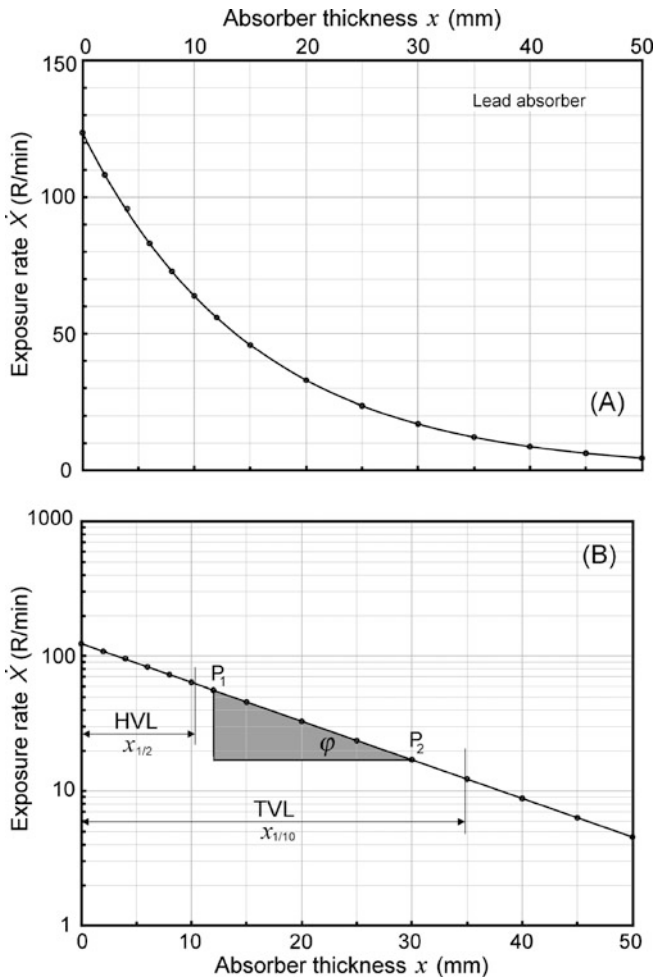


Fig. 7.4 Exposure rate \dot{X} against absorber thickness x for a narrow beam attenuation experiment using a photon beam and lead absorbers. In (A) data are plotted on a linear graph paper, in (B) they are plotted on a semi-log graph paper

thickness $x_{1/10}$ (for which $I(x_{1/10}) = \frac{1}{10}I(0) = 12.36$ R/min) as $x_{1/10} = 3.49$ of lead and this results in a linear attenuation coefficient μ of $\mu = 0.066$ mm⁻¹ or 0.66 cm⁻¹.

All three methods for determination of the linear attenuation coefficient μ result in the same value of $\mu = 0.66$ cm⁻¹.

(b) From the linear attenuation coefficient $\mu = 0.66$ cm⁻¹ determined in (a) we calculate the atomic and mass attenuation coefficients, ${}_a\mu$ and μ_m , respectively,

using the relationships provided in Fig. 7.3

$$\begin{aligned} {}_a\mu &= \mu \frac{A}{\rho N_A} = (0.66 \text{ cm}^{-1}) \times \frac{(207.2 \text{ g/mol})}{(11.36 \text{ g/cm}^3) \times (6.022 \times 10^{23} \text{ atom/mol})} \\ &= 20 \times 10^{-24} \frac{\text{cm}^2}{\text{atom}} = 20 \frac{\text{b}}{\text{atom}} \end{aligned} \quad (7.5)$$

and

$$\mu_m = \frac{\mu}{\rho} = \frac{0.66 \text{ cm}^{-1}}{11.36 \text{ cm}^2/\text{g}} = 0.058 \frac{\text{cm}^2}{\text{g}} \quad (7.6)$$

or

$$\mu_m = {}_a\mu \frac{N_A}{A} = \left(20 \times 10^{-24} \frac{\text{cm}^2}{\text{atom}} \right) \times \frac{6.022 \times 10^{23} \text{ atom/mol}}{207.2 \text{ g/mol}} = 0.058 \frac{\text{cm}^2}{\text{g}}. \quad (7.7)$$

From (7.2) we get the following expression for the mean free path \bar{x} of a photon beam

$$\bar{x} = \frac{1}{\mu} = \frac{x_{1/2}}{\ln 2} = \frac{1}{0.66 \text{ cm}^{-1}} = 1.52 \text{ cm}. \quad (7.8)$$

(c) A plot of measured data in Fig. 7.4(B) results in a straight line indicating perfect exponential attenuation behavior through several cycles in exposure rate. Since this type of behavior can only be achieved with mono-energetic photon beam, we conclude that the experiment was carried out using a mono-energetic gamma source rather than with an x-ray machine or linear accelerator that produce heterogeneous photon beams.

The half-value layer $x_{1/2}$ of our beam was established to be 1.05 cm of lead indicating a relatively high-energy gamma ray beam in the megavoltage range. Examination of the NIST data shows that a cobalt-60 gamma ray beam which produces an essentially mono-energetic beam with two photon energies close to each other (1.17 MeV and 1.33 MeV for a mean energy of 1.25 MeV) has an atomic attenuation coefficient ${}_a\mu$ in lead of ${}_a\mu = 20.2 \text{ b/atom}$ in good agreement with our estimated value of ${}_a\mu = 20 \text{ b/atom}$. We therefore conclude that the data for this problem were obtained using a cobalt-60 gamma ray machine.

7.1.Q3

(151)

Photons with energy in the ionizing radiation region have several options for interacting with matter. The specific interactions are referred to as effects and many of these effects carry the name of their discoverer.

- (a) List the 7 most important photon interactions with absorbing medium in medical physics.
- (b) For the seven photon interactions with absorbing medium listed in (a) prepare a table with the following entries: (1) Symbol used for attenuation coefficient, (2) Type of target, (3) Photon fate after interaction, and (4) Charged particles released or produced in the interaction.
- (c) Probability for photon interaction with absorber is described with the attenuation coefficient (often referred to as cross section). Complete Table 7.1A that addresses the basic properties of commonly used attenuation coefficients.
- (d) Photon attenuation in absorber can be described with various characteristic thicknesses of absorber. Complete Table 7.2A that deals with properties of various characteristic absorber thicknesses.

Table 7.1A Common attenuation coefficients used in describing photon interactions with absorber atoms

1	Coefficient	Symbol	Relationship to μ	SI unit	Common unit	Unit of absorber thickness
2	Linear attenuation coefficient	μ	–			
3	Mass attenuation coefficient					
4	Atomic attenuation coefficient					
5	Linear energy transfer coefficient					–
6	Mass energy transfer coefficient					–
7	Linear energy absorption coefficient					–
8	Mass energy absorption coefficient					–

Table 7.2A Characteristic absorber thicknesses and their relationship with the linear attenuation coefficient μ

1	Characteristic absorber thickness	Symbol	Relationship to attenuation coefficient μ	$\frac{I(x)}{I(0)}$	$100\frac{I(x)}{I(0)}$
2	Half-value layer (HVL)				
3	Mean free path (MFP)				
4	Tenth-value layer (TVL)				
5	Three mean free paths				
6	Five mean free paths				
7	Seven mean free paths				
8	Nine mean free paths				

SOLUTION:

(a) The 7 most important photon interactions with absorbing medium are: (1) Thomson scattering, (2) Compton effect, (3) Rayleigh scattering, (4) Photoelectric effect, (5) Nuclear pair production, (6) Electronic pair production, and (7) Photonuclear reaction (photodisintegration).

(b) Photons of energy in the ionizing radiation category have many options for interacting with matter. Seven of these are of importance to medical physics and radiation dosimetry; many others are more specialized and negligible in comparison with the important seven, but are nevertheless of academic interest in nuclear physics. The basic characteristics of the 7 most important photon interactions with absorbing medium are listed in Table 7.3.

(1) *Symbols used for designation of attenuation and absorption coefficients:* Of the seven important photon interactions with atoms of the absorber, two are designated with separate Greek letters: photoelectric effect with τ (tau) and pair production with κ (kappa) where κ_{NPP} stands for nuclear pair production and κ_{TP} for electronic (triplet) production. Four effects are designated with Greek letter sigma (σ) that is in nuclear physics used to designate general interaction cross sections. In radiation physics σ is used with a subscript to designate four specific types of photon interaction: σ_{Th} for Thomson scattering, σ_{C} for Compton effect, σ_{R} for Rayleigh scattering, and σ_{PN} for photodisintegration (photonuclear effect).

(2) **Type of target.** A closer look at photon interaction with absorber atom reveals that the interaction can be either with an orbital electron or nucleus.

- (i) Interaction with an orbital electron can be interaction with an essentially “free electron” (Thomson scattering and Compton effect) or interaction with a tightly bound electron (photoelectric effect) or interaction with the electric field of the electron (triplet production).

Table 7.3 Basic characteristics of the 7 most important photon interactions

0	Photon interaction with absorber	Symbol for attenuation coefficient	Type of target	Photon fate	Charged particles released
1	Thomson scattering	σ_{Th}	“Free” electron	Photon is scattered	None
2	Compton effect	σ_C	“Free” electron	Photon is scattered	Recoil (Compton) electron
3	Rayleigh scattering	σ_R	Whole atom	Photon is scattered	None
4	Photoelectric effect	τ	Whole atom	Photon disappears	Photoelectron
5	Nuclear pair production	κ_{NPP}	Nucleus	Photon disappears	Electron/positron pair
6	Electronic pair production	κ_{TP}	“Free” electron	Photon disappears	Electron/positron pair and orbital electron
7	Photonuclear reaction	σ_{PN}	Nucleus	Photon disappears	Various heavy charged particles

(ii) Interaction with the nucleus can be interaction with electric field of the nucleus (nuclear pair production) or actual direct interaction with the nucleus (photodisintegration).

(3) As far as the **fate of the photon** after interaction is concerned there are two possibilities: (i) photon disappearance and (ii) photon scattering.

(i) In photon disappearance the photon is completely absorbed (photoelectric effect, nuclear pair production, triplet production, and photodisintegration).

(ii) In photon scattering photon is scattered with no energy loss (Rayleigh scattering) or with concurrent loss of the energy (Compton effect).

(4) **Charged particles released or produced** in photon interaction with absorber atom.

(i) In Thomson and Rayleigh scattering there is no release or production of charged particles. In photoelectric effect, Compton effect, and triplet production orbital electrons are released from the absorber atom.

(ii) In pair production and triplet production an electron / positron pair is produced in the electric field of the nucleus and electric field of the orbital electron, respectively.

(iii) In photodisintegration heavy charged particles and neutrons may be released from the nucleus.

(c) Basic properties of the various attenuation coefficients used for describing attenuation of photons in absorbing media are given in Table 7.1B.

Table 7.1B Basic properties of attenuation coefficients used for describing attenuation of photons in absorbing media

1	Coefficient	Symbol	Relationship to μ	SI unit	Common unit	Unit of absorber thickness
2	Linear attenuation coefficient	μ	–	m^{-1}	cm^{-1}	cm
3	Mass attenuation coefficient	μ_m	$\mu_m = \frac{\mu}{\rho}$	$\frac{m^2}{kg}$	$\frac{cm^2}{g}$	$\frac{g}{cm^2}$
4	Atomic attenuation coefficient	$a\mu$	$a\mu = \frac{\mu}{n\Delta}$	$\frac{m^2}{atom}$	$\frac{cm^2}{atom}$	$\frac{atom}{cm^2}$
5	Linear energy transfer coefficient	μ_{tr}	$\mu_{tr} = \mu \bar{f}_{tr}$	m^{-1}	cm^{-1}	–
6	Mass energy transfer coefficient	$\frac{\mu_{tr}}{\rho}$	$\frac{\mu_{tr}}{\rho} = \frac{\mu}{\rho} \bar{f}_{tr}$	$\frac{m^2}{kg}$	$\frac{cm^2}{g}$	–
7	Linear energy absorption coefficient	μ_{ab}	$\mu_{ab} = \mu \bar{f}_{ab}$	m^{-1}	cm^{-1}	–
8	Mass energy absorption coefficient	$\frac{\mu_{ab}}{\rho}$	$\frac{\mu_{ab}}{\rho} = \frac{\mu}{\rho} \bar{f}_{ab}$	$\frac{m^2}{kg}$	$\frac{cm^2}{g}$	–

(d) Basic properties of the various characteristic absorber thicknesses used for describing attenuation of photon beams in absorbing media are given in Table 7.2B.

Table 7.2B Basic properties of various characteristic absorber thicknesses used for describing attenuation of photon beams in absorbing media

1	Characteristic absorber thickness	Symbol	Relationship to attenuation coefficient μ	$\frac{I(x)}{I(0)}$	$100 \frac{I(x)}{I(0)}$
2	Half-value layer (HVL)	$x_{1/2}$	$\frac{\ln 2}{\mu} = \frac{0.693}{\mu}$	0.500	50 %
3	Mean free path (MFP)	\bar{x}	$\frac{1}{\mu}$	$0.368 = \frac{1}{e}$	36.8 %
4	Tenth-value layer (TVL)	$x_{1/10}$	$\frac{\ln 10}{\mu} = \frac{2.303}{\mu}$	0.100	10 %
5	Three mean free paths	$3\bar{x}$	$\frac{3}{\mu}$	0.050	5 %
6	Five mean free paths	$5\bar{x}$	$\frac{5}{\mu}$	~0.007	0.7 %
7	Seven mean free paths	$7\bar{x}$	$\frac{7}{\mu}$	~0.001	~0.1%
8	Nine mean free paths	$9\bar{x}$	$\frac{9}{\mu}$	~0.0001	~0.01%

7.1.Q4

(152)

Attenuation properties of absorbing materials are important in radiation physics, since they provide useful data on interaction of radiation beams with

absorbers. These materials can be of biological origin, such as patients in diagnosis and treatment of disease with ionizing radiation, or condensed matter objects, such as those used in shielding of radiation sources.

Measurement of attenuation properties of photon beams in absorber are relatively simple, however, care must be exercised when results of measurements are interpreted. Attenuation can be measured in the so-called narrow beam (“good”) geometry or in broad beam geometry. The former is used in measurement of attenuation coefficients for a given beam energy and given absorber, the latter in determination of shielding requirements of radiation emitting installations.

- (a) Describe the salient features of narrow beam geometry and broad beam geometry and draw a schematic diagram for the two geometries.
- (b) The table below shows a comparison between two attenuation experiments on a radiation source using lead as absorber; experiment (1) was carried out under narrow beam geometry conditions, experiment (2) under broad beam conditions. Plot the data for both experiments on a semi-log plot, identify the source type (mono-energetic or heterogeneous beams), and indicate which beam was measured under narrow beam geometry conditions.
- (c) Determine the linear, atomic, and mass attenuation coefficients: μ , $a\mu$, and μ_m respectively, in lead for the narrow beam.
- (d) Determine the buildup factor B for two absorber thicknesses: 10 cm and 20 cm. Also determine the effective linear attenuation coefficient μ_{eff} for the broad beam.

Absorber thickness (cm)	0	0.5	1.0	1.5	2	5	10	15	20
Transmitted fraction (1)	1.000	0.719	0.517	0.372	0.267	0.037	1.36×10^{-3}	5.02×10^{-5}	1.85×10^{-4}
Transmitted fraction (2)	1.000	0.751	0.564	0.423	0.318	0.057	3.24×10^{-3}	18.5×10^{-5}	10.5×10^{-4}

SOLUTION:

(a) Narrow beam geometry technique in attenuation measurements of photon beams implies a narrowly collimated source of mono-energetic photons and a relatively small radiation detector. As shown in Fig. 7.5(A), a slab of absorber material of thickness x is placed between the source and detector. The absorber decreases the detector signal (intensity which is proportional to the number of photons striking the detector) from $I(0)$ measured without the absorber in place to signal $I(x)$ measured with absorber thickness x in the beam.

In contrast to the narrow beam geometry that is used in determination of the various attenuation coefficients for photon beam attenuation, one can also deal with

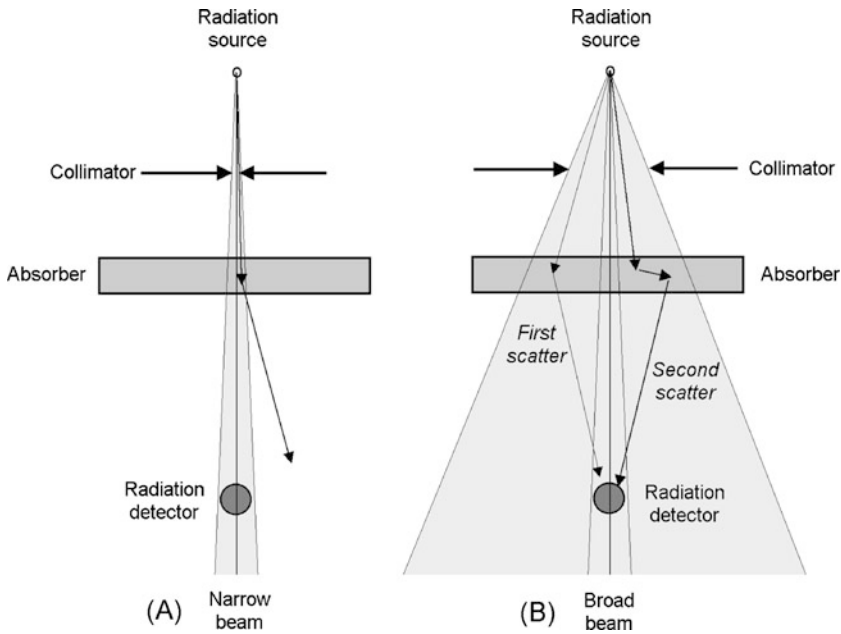


Fig. 7.5 Beam geometry for measurement of photon beam attenuation in absorbing materials. (A) Narrow beam geometry and (B) Broad beam geometry

the so-called broad beam geometry in which the detector reading is not only diminished by attenuation of the primary beam in the absorber, but is also increased by the radiation scattered from the absorber into the detector, as shown schematically in Fig. 7.5(B).

(b) The attenuation data for the two experiments are plotted in Fig. 7.6 on semi-log graph paper. Two straight lines arise, one for each experiment. Since the data fall on straight lines, we conclude that the radiation source used in experiments was a mono-energetic source.

The answer to the question on which of the two straight lines represents the narrow beam data is relatively simple, since we are dealing with a mono-energetic source and neither beam hardening nor beam softening effects are expected to happen in the lead absorber. The lower straight line that appears to give a less penetrating beam in Fig. 7.6 is attributed to narrow beam geometry and the higher straight line is attributed to broad beam geometry.

(c) The linear attenuation coefficient μ is calculated from the slope of the narrow beam attenuation line in Fig. 7.6

$$\mu = \frac{\ln \frac{y_0}{y_1}}{x_1 - x_0} = \frac{\ln \frac{1}{0.037}}{5 \text{ cm}} = 0.66 \text{ cm}^{-1}, \quad (7.9)$$

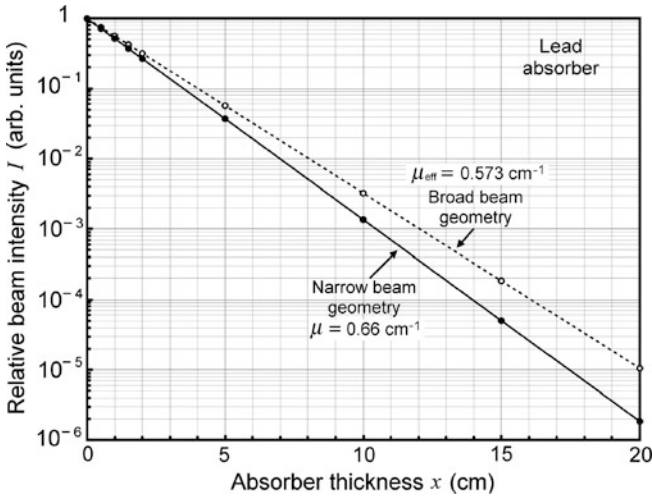


Fig. 7.6 Attenuation data plotted on semi-log graph paper against absorber thickness x . Two sets of data were taken, one set under narrow beam geometry conditions and the other under broad beam geometry conditions

while the atomic attenuation coefficient ${}_a\mu$ and the mass attenuation coefficient μ_m are calculated using μ and appropriate proportionality relationships

$$\begin{aligned} {}_a\mu &= \frac{A}{\rho N_A} \mu = \frac{207.2 \text{ g} \cdot \text{mol}^{-1}}{(11.36 \text{ g} \cdot \text{cm}^{-3}) \times (6.022 \times 10^{23} \text{ atom} \cdot \text{mol}^{-1})} \times (0.66 \text{ cm}^{-1}) \\ &= 20 \times 10^{-24} \frac{\text{cm}^2}{\text{atom}} = 2 \frac{\text{b}}{\text{atom}} \end{aligned} \quad (7.10)$$

and

$$\mu_m = \frac{\mu}{\rho} = \frac{0.66 \text{ cm}^{-1}}{11.36 \text{ g} \cdot \text{cm}^{-3}} = 0.058 \frac{\text{cm}^2}{\text{g}}. \quad (7.11)$$

(d) Figure 7.6 shows two sets of attenuation data, one set taken under narrow beam (good) geometry conditions and the other under broad beam (poor) geometry conditions. As shown in the figure, poor geometry may overestimate the measured half-value layer (HVL) of a photon beam and underestimate the attenuation coefficient of the beam by a significant amount.

The broad beam geometry in comparison with narrow beam geometry can be evaluated with two methods: (1) with the buildup factor B and (2) with an effective attenuation coefficient μ_{eff} :

(1) **Buildup factor** $B(x)$ in photon attenuation measurement is defined for a given absorber thickness x as the ratio between the signal $I_B(x)$ measured under broad

beam conditions to the signal $I_N(x)$ measured under narrow beam conditions

$$B(x) = \frac{I_B(x)}{I_N(x)} = \frac{I_B(x)}{I_N(0)e^{-\mu x}}. \quad (7.12)$$

For the two beams of Fig. 7.6 at a lead thickness $x = 10$ cm, the relative signal $I_B(10 \text{ cm})$ is 3.24×10^{-3} , while the relative signal $I_N(10 \text{ cm})$ is 1.36×10^{-3} resulting in a buildup factor of $B(10 \text{ cm}) = 2.38$. For the two beams of Fig. 7.6 at a lead thickness $x = 20$ cm, the relative signal $I_B(20 \text{ cm})$ is 10.5×10^{-6} , while the relative signal $I_N(20 \text{ cm})$ is 1.85×10^{-6} , resulting in a buildup factor of $B(20 \text{ cm}) = 5.68$.

Thus, the larger is the absorber thickness x , the larger is the buildup factor B . This conclusion has obvious implications in radiation physics: If attenuation measurements are carried out for the determination of attenuation coefficients, then it is imperative to use narrow beam geometry to ensure measurement accuracy. On the other hand, if measurements are being made for radiation safety purposes, the broad beam attenuation conditions should be used to ensure that all scattering effects in the absorber (shielding wall) are accounted for.

The buildup factor $B(x)$ encompasses the scattering events in the absorber; however, it must be measured for each specific absorber thickness x and is affected by photon beam energy as well as the geometry, absorber atomic number and thickness, and the quantity measured which can be photon fluence, photon energy fluence, beam intensity, beam exposure, kerma, or dose. For narrow beam geometry $B = 1$, for broad beam geometry $B > 1$ and under certain conditions it can amount to a factor of 10 or more. Since in broad beam attenuation photons interacting with the absorber may be scattered into the detector thereby contributing to the measured signal, the apparent attenuation is lower than that obtained under narrow beam conditions and results in an overestimation of the half-value layer of the beam and underestimation of the narrow beam attenuation coefficient of the beam.

(2) An alternative concept to the buildup factor $B(x)$ is the concept of **mean effective attenuation coefficient** $\bar{\mu}_{\text{eff}}$ expressed from (7.12) as follows

$$I_B(x) = I_N(x)B = I_N(0)Be^{-\mu x} = I_N(0)e^{-\bar{\mu}_{\text{eff}}x}. \quad (7.13)$$

Equation (7.13) yields the following result for $\bar{\mu}_{\text{eff}}$

$$\bar{\mu}_{\text{eff}} = \mu - \frac{\ln B(x)}{x}. \quad (7.14)$$

We now determine the mean effective attenuation coefficient $\bar{\mu}_{\text{eff}}$ for the broad beam of Fig. 7.6 as follows (first for $x = 10$ cm and then for $x = 20$ cm)

$$\bar{\mu}_{\text{eff}} = \mu - \frac{\ln B(x)}{x} = (0.660 \text{ cm}^{-1}) - \frac{\ln 2.38}{10 \text{ cm}} = 0.573 \text{ cm}^{-1} \quad (7.15)$$

and

$$\bar{\mu}_{\text{eff}} = \mu - \frac{\ln B(x)}{x} = (0.660 \text{ cm}^{-1}) - \frac{\ln 5.68}{20 \text{ cm}} = 0.573 \text{ cm}^{-1}. \quad (7.16)$$

We can also determine the mean effective attenuation coefficient $\bar{\mu}_{\text{eff}}$ directly from the broad beam data of Fig. 7.6 as follows

$$\bar{\mu}_{\text{eff}} = \frac{\ln \frac{y_0}{y_1}}{x_1 - x_0} = \frac{\ln \frac{1}{0.057}}{5 \text{ cm}} = 0.573 \text{ cm.} \quad (7.17)$$

Thus, all three methods of determining the $\bar{\mu}_{\text{eff}}$ yield the same result.

7.2 Thomson Scattering

7.2.Q1

(153)

Early information on atomic structure and composition gathered in the beginning of 20-th century has been deduced from x-ray scattering experiments on low atomic elements for which orbital electrons could be considered essentially free. Thomson developed the classical theory of x-ray scattering on free electrons and this type of scattering is now referred to as Thomson scattering; no longer of much practical value because it was superseded by other scattering effects but still important for historical reasons and for providing the limiting values of low energy Compton scattering.

- (a) Derive the differential electronic cross section for Thomson scattering $d_e\sigma_{\text{Th}}/d\Omega$ for polarized as well as for unpolarized radiation.
- (b) Plot the differential electronic cross section for Thomson scattering $d_e\sigma_{\text{Th}}/d\Omega$ for un-polarized radiation on a Cartesian coordinate system and polar coordinate system.

SOLUTION:

(a) The differential scattering cross section $d\sigma/d\Omega$ is in general defined as energy radiated per unit time per unit solid angle which is equal to $dP/d\Omega$ (where P stands for power) divided by incident energy per unit area per unit time (defined as Poynting vector S_{in}). The ratio $(dP/d\Omega)$ is emitted in the direction Θ and is equal to $r^2 S_{\text{out}}$ where S_{out} is the Poynting vector for the emitted scattered EM waves.

The electric fields \mathcal{E}_{in} for the harmonic incident radiation and \mathcal{E}_{out} for the scattered radiation are given, respectively, as

$$\mathcal{E}_{\text{in}} = \mathcal{E}_0 \sin \omega t \quad \text{and} \quad \mathcal{E}_{\text{out}} = \frac{e}{4\pi\epsilon_0} \frac{\ddot{x} \sin \Theta}{c^2 r}, \quad (7.18)$$

where

\mathcal{E}_0 is the amplitude of the incident harmonic oscillation.

- Θ is the angle between the direction of emission \mathbf{r} and the polarization vector of the incident wave \mathcal{E}_{in} or the direction of electron acceleration.
 \ddot{x} is the acceleration of the electron.

The equation of motion for the accelerated electron vibrating about its equilibrium position is given as follows

$$m_e \ddot{x} = e\mathcal{E} = e\mathcal{E}_0 \sin \omega t \quad \text{or} \quad \ddot{x} = \frac{e\mathcal{E}_0}{m_e} \sin \omega t. \quad (7.19)$$

Inserting \ddot{x} from (7.19) into (7.18) results in the following expression for electric field \mathcal{E}_{out}

$$\mathcal{E}_{\text{out}} = \frac{e^2 \mathcal{E}_0}{4\pi \epsilon_0 m_e c^2} \frac{\sin \omega t \sin \Theta}{r} = \frac{r_e}{r} \mathcal{E}_0 \sin \omega t \sin \Theta, \quad (7.20)$$

where r_e is a constant referred to as the classical electron radius and equal to $r_e = e^2 / (4\pi \epsilon_0 m_e c^2)$ or 2.818 fm.

Using (7.18) and (7.20) we now determine the Poynting vectors S_{in} and S_{out} as follows

$$S_{\text{in}} = \epsilon_0 c \mathcal{E}_{\text{in}}^2 = \epsilon_0 c \mathcal{E}_0^2 \sin^2 \omega t \quad (7.21)$$

and

$$S_{\text{out}} = \epsilon_0 c \mathcal{E}_{\text{out}}^2 = \epsilon_0 c r_e^2 \mathcal{E}_0^2 \frac{\sin^2 \omega t \sin^2 \Theta}{r^2}. \quad (7.22)$$

Based on the discussion above we now express the differential cross section for Thomson classical scattering as follows

$$\left. \frac{d_e \sigma_{\text{Th}}}{d\Omega} \right|_{\text{pol}} = \frac{dP/d\Omega}{S_{\text{in}}} = r^2 \frac{S_{\text{out}}}{S_{\text{in}}} = r_e^2 \sin^2 \Theta, \quad (7.23)$$

with the understanding that (7.23) represents the differential electronic cross section for Thomson scattering of polarized incident radiation on free electrons. For unpolarized beam, on the other hand, the cross section is calculated by averaging over all possible orientations of the polarizing vector governed by polarization angle ψ ranging from 0 to 2π .

$$\left. \frac{d_e \sigma_{\text{Th}}}{d\Omega} \right|_{\text{unpol}} = r^2 \frac{\overline{S_{\text{out}}}}{\overline{S_{\text{in}}}} = r_e^2 \overline{\sin^2 \Theta}. \quad (7.24)$$

The mean value of $\sin^2 \Theta$, i.e., $\overline{\sin^2 \Theta}$ for unpolarized radiation is determined with the help of Fig. 7.7 from which the following relationships are evident

$$\cos \Theta = \frac{a}{r}, \quad \sin \theta = \frac{b}{r}, \quad \text{and} \quad \cos \psi = \frac{a}{b}, \quad (7.25)$$

where angles Θ , scattering angle θ , and polarization angle ψ as well as parameters a and b are clearly defined in Fig. 7.7. Combining expressions of (7.25) we find the

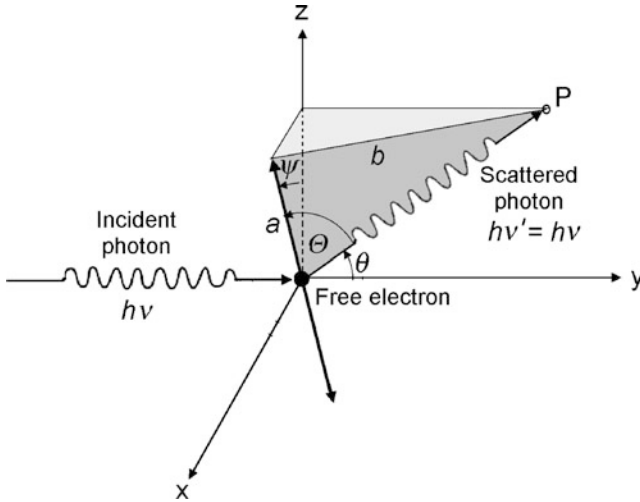


Fig. 7.7 Schematic diagram of Thomson scattering on free electron. The incident photon with energy $h\nu$ is scattered and emitted with a scattering angle θ . Note that angles θ and Θ are not coplanar (i.e., they are not in the same plane)

following expression for $\cos \Theta$ in terms of $\sin \theta$ and $\cos \psi$

$$\cos \Theta = \frac{a}{r} = \frac{b \cos \psi}{r} = \frac{r \sin \theta \cos \psi}{r} = \sin \theta \cos \psi. \quad (7.26)$$

The mean value of $\sin^2 \Theta$ is now determined by integration over the polarizing angle ψ from 0 to 2π and using the relationship $\sin^2 \Theta = 1 - \cos^2 \Theta$ to get

$$\begin{aligned} \overline{\sin^2 \Theta} &= \frac{\int_0^{2\pi} \sin^2 \Theta d\psi}{\int_0^{2\pi} d\psi} = \frac{1}{2\pi} \int_0^{2\pi} (1 - \cos^2 \Theta) d\psi = 1 - \frac{\sin^2 \theta}{2\pi} \int_0^{2\pi} \cos^2 \psi d\psi \\ &= 1 - \frac{\sin^2 \theta}{4\pi} [\sin \psi \cos \psi + \psi]_0^{2\pi} = 1 - \frac{1}{2} \sin^2 \theta = \frac{1}{2} (1 + \cos^2 \theta). \end{aligned} \quad (7.27)$$

Combining (7.27) with (7.24) we now write the electronic cross section for Thomson scattering of unpolarized radiation on free electron as follows

$$\frac{d_e \sigma_{\text{Th}}}{d\Omega} \Big|_{\text{unpol}} = r_e^2 \overline{\sin^2 \Theta} = \frac{r_e^2}{2} (1 + \cos^2 \theta) \quad \text{in cm}^2/\text{electron/sterad} \quad (7.28)$$

and plot (7.28) against scattering angle θ in Fig. 7.8(A) in Cartesian coordinate system and in Fig. 7.8(B) in polar coordinate system. At $\theta = 0$ and $\theta = \pi$ the Thomson differential electronic cross section in area per electron per steradian equals to $r_e^2 = (2.818 \text{ fm})^2 = 7.94 \times 10^{-26} \text{ cm}^2 = 79.4 \text{ mb}$ while at $\theta = \frac{1}{2}\pi$ it amounts to half of this value, indicating that in Thomson effect forward scattering and back scattering are twice as strong as is scattering at $\theta = \frac{1}{2}\pi$.

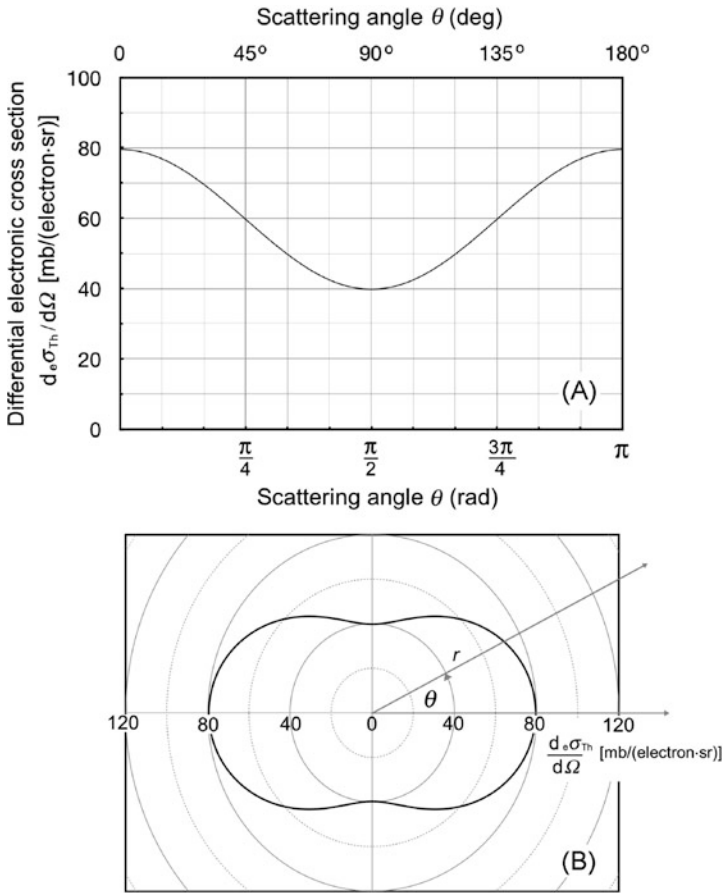


Fig. 7.8 Differential electronic cross section $d_e \sigma_{Th} / d\Omega$ per unit solid angle against the scattering angle θ for Thomson scattering of unpolarized radiation on free electron. (A) Plotted in Cartesian coordinate system; (B) Plotted in polar coordinate system

7.2.Q2

(154)

The differential electronic cross section per unit solid angle $d_e \sigma_{Th} / d\Omega$ for Thomson scattering of unpolarized radiation on free electron is expressed as (T7.39), as derived in Prob. 153

$$\left. \frac{d_e \sigma_{Th}}{d\Omega} \right|_{\text{unpol}} = \frac{r_e^2}{2} (1 + \cos^2 \theta), \tag{7.29}$$

where r_e is the so-called classical electron radius ($r_e = e^2 / (4\pi \epsilon_0 m_e c^2) = 2.818 \text{ fm}$ and θ is the scattering angle.

- (a) Starting from (7.29), derive the differential electronic cross section $d_e\sigma_{\text{Th}}/d\theta$ per unit scattering angle θ for Thomson scattering on free electrons.
- (b) Plot $d_e\sigma_{\text{Th}}/d\theta$ against scattering angle θ from $\theta = 0$ to $\theta = \pi$ and calculate the minima and maxima appearing on the plot.
- (c) Calculate the total electronic cross section ${}_e\sigma_{\text{Th}}$ for Thomson scattering starting with: (1) $d_e\sigma_{\text{Th}}/d\Omega$ of (7.29) and (2) $d_e\sigma_{\text{Th}}/d\theta$ derived in (b).
- (d) Define the Thomson total atomic cross section ${}_a\sigma_{\text{Th}}$ and discuss its limitations.

SOLUTION:

(a) The differential electronic cross section $d_e\sigma_{\text{Th}}/d\theta$ per unit scattering angle gives the fraction of the photon incident energy that is scattered into a cone contained between θ and $\theta + d\theta$. The function is expressed as follows

$$\frac{d_e\sigma_{\text{Th}}}{d\theta} = \frac{d_e\sigma_{\text{Th}}}{d\Omega} \frac{d\Omega}{d\theta} = \frac{r_e^2}{2} (1 + \cos\theta) 2\pi \sin\theta = \pi r_e^2 (1 + \cos\theta) \sin\theta. \quad (7.30)$$

Function $d_e\sigma_{\text{Th}}/d\theta$ plotted against scattering angle θ has two obvious minima, one at $\theta = 0$ and the other at $\theta = \pi$ where $\sin\theta = 0$. The other local extremes are determined by taking the derivative of (7.30) with respect to θ and setting the result equal to zero, i.e., $d^2_e\sigma_{\text{Th}}/d\theta^2 = 0$.

The derivative of (7.30) is as follows

$$\frac{d^2_e\sigma_{\text{Th}}}{d\theta^2} = \pi r_e^2 [(1 + \cos\theta) \cos\theta - 2 \cos\theta \sin^2\theta] = \pi r_e^2 \cos\theta (3 \cos^2\theta - 1) = 0. \quad (7.31)$$

Equation (7.31) can be satisfied under three conditions:

(1)

$$\cos\theta = 0 \quad \text{or} \quad \theta = \frac{1}{2}\pi, \quad (7.32)$$

(2)

$$\cos\theta = \frac{1}{\sqrt{3}} \quad \text{or} \quad \theta = \arccos 0.577 = 54.7^\circ, \quad (7.33)$$

(3)

$$\cos\theta = -1/\sqrt{3} \quad \text{or} \quad \theta = \arccos(-0.577) = 125.3^\circ. \quad (7.34)$$

The differential cross section is plotted against θ in Fig. 7.9 for $0 \leq \theta \leq \pi$ and exhibits three minima (at $\theta = 0$, $\frac{1}{2}\pi$, and π) and two maxima, one at $\theta = 54.7^\circ$ and the other at $\theta = 125.3^\circ$. The non-zero minimum in $d_e\sigma_{\text{Th}}/d\theta$ at $\theta = \frac{1}{2}\pi$ results in

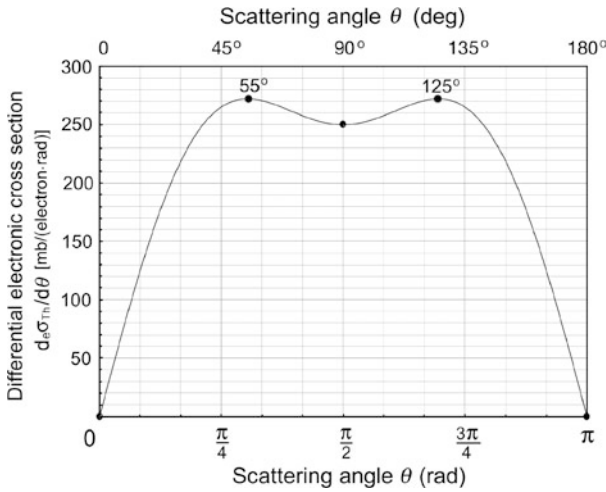


Fig. 7.9 Differential electronic cross section $d_e\sigma_{\text{Th}}/d\theta$ per unit angle θ for Thomson scattering plotted against the scattering angle θ

$d_e\sigma_{\text{Th}}/d\theta = \pi r_e^2 = 249.4$ mb/electron/rad and the maxima at $\theta = 54.7^\circ$ and $\theta = 125.3^\circ$ give $d_e\sigma_{\text{Th}}/d\theta = 271.6$ mb/electron/rad.

(c) The total electronic cross section ${}_e\sigma_{\text{Th}}$ for Thomson scattering can be calculated by: (1) integrating (7.29) over the full solid angle Ω or (2) integrating (7.30) over scattering angle θ from 0 to π .

- (1) We start with the differential electronic cross section $d_e\sigma_{\text{Th}}/d\Omega$ of (7.29) and integrate over solid angle as follows

$$\begin{aligned} {}_e\sigma_{\text{Th}} &= \int \frac{d_e\sigma_{\text{Th}}}{d\Omega} d\Omega = \frac{r_e^2}{2} \int_0^{2\pi} \left[\int_0^\pi (1 + \cos^2 \theta) \sin \theta d\theta \right] d\phi \\ &= \pi r_e^2 \left[\int_0^\pi d(\cos \theta) + \int_0^\pi \cos^2 \theta d(\cos \theta) \right] = \frac{8\pi}{3} r_e^2 = 0.665 \text{ b.} \end{aligned} \quad (7.35)$$

- (2) We start with the differential cross section $d_e\sigma_{\text{Th}}/d\theta$ of (7.30) and integrate over scattering angle θ as follows

$$\begin{aligned} {}_e\sigma_{\text{Th}} &= \int_0^\pi \frac{d_e\sigma_{\text{Th}}}{d\theta} d\theta = \pi r_e^2 \int_0^\pi \sin \theta (1 + \cos^2 \theta) d\theta \\ &= \pi r_e^2 \left[\int_0^\pi d(\cos \theta) + \int_0^\pi \cos^2 \theta d(\cos \theta) \right] = \frac{8\pi}{3} r_e^2 = 0.665 \text{ b.} \end{aligned} \quad (7.36)$$

The total area under the $d_e\sigma_{\text{Th}}/d\theta$ curve of Fig. 7.9 is equal to the total electronic scattering cross section ${}_e\sigma_{\text{Th}}$. Thus, ${}_e\sigma_{\text{Th}}$ can also be determined directly by measuring the area under the $d_e\sigma_{\text{Th}}/d\theta$ curve in Fig. 7.9 with an appropriately calibrated planimeter.

The total cross section ${}_e\sigma_{\text{Th}}$ determined in (7.35) and (7.36) is referred to as the Thomson classical scattering coefficient for a free electron (${}_e\sigma_{\text{Th}} = 0.665 \text{ b}$) and has the same value for all incident photon energies $h\nu$. Moreover, in Thomson scattering no energy is transferred from the incident photon to the free electron, so that the scattered photon has the same energy as the incident photon, i.e., $h\nu' = h\nu$.

(d) The atomic cross section for Thomson scattering ${}_a\sigma_{\text{Th}}$ is in terms of the electronic cross section ${}_e\sigma_{\text{Th}}$ given as

$${}_a\sigma_{\text{Th}} = {}_e\sigma_{\text{Th}} Z = \frac{8\pi}{3} r_e^2 Z, \quad (7.37)$$

showing a linear dependence upon atomic number Z , as elucidated experimentally for low atomic number elements by Charles G. Barkla, a U.K. physicist who received the Nobel Prize in Physics for his discovery of characteristic x rays.

For photon energies $h\nu$ exceeding the electron binding energy but small in comparison with the electron rest energy $m_e c^2 = 0.511 \text{ MeV}$, i.e., $E_B \ll h\nu \ll m_e c^2$, the atomic cross section ${}_a\sigma_{\text{Th}}$ measured at small θ approaches Thomson's value of (7.36). At larger θ and larger photon energies $h\nu$ where $h\nu$ approaches or exceeds 0.511 MeV , however, the Thomson classical theory breaks down and the intensity of coherently scattered radiation on free electrons diminishes in favor of incoherently Compton scattered radiation in which part of the incident photon energy is transferred to the recoiling electron and the photon is scattered with energy that is lower than the incident photon energy.

7.3 Incoherent Scattering (Compton Effect)

7.3.Q1

(155)

The basic Compton equation can be derived from principles of energy and momentum conservation [see (T7.47), (T7.53), and (T7.54)] and is expressed as follows

$$\Delta\lambda = \lambda_C(1 - \cos\theta), \quad (7.38)$$

where $\Delta\lambda$ is the change in photon wavelength, λ_C is the so-called Compton wavelength of the electron given as $\lambda_C = h/(m_e c)$, and θ is the scattering angle.

- (a) Use the Compton equation (7.38) to express the scattered photon energy $h\nu'$ in terms of the incident photon energy $h\nu$ and scattering angle θ .
- (b) Use the Compton equation (7.38) to express the recoil electron kinetic energy E_K in terms of the incident photon energy $h\nu$ and scattering angle θ .

- (c) Show that the fractional energy loss $\Delta(h\nu)/(h\nu)$ of a Compton-scattered photon can be expressed as

$$\frac{\Delta h\lambda}{h\lambda} = \frac{h\nu - h\nu'}{h\nu} = \frac{\Delta\lambda}{1 + \Delta\lambda}. \quad (7.39)$$

- (d) The term “Compton scattering” usually refers to inelastic scattering of a photon on loosely bound electrons of an absorber. However, other, more exotic, Compton phenomena are also known, such as for example, nuclear Compton effect and inverse Compton effect. Briefly describe these two phenomena.
- (e) Compare the maximum wavelength shift $\Delta\lambda_{\max}^e$ in standard photon-free electron Compton scattering to the maximum wavelength shift $\Delta\lambda_{\max}^p$ in Compton scattering of a photon from a proton.

SOLUTION:

- (a) We write the basic Compton equation as follows

$$\Delta\lambda = \lambda' - \lambda = \frac{c}{\nu'} - \frac{c}{\nu} = \frac{h}{m_e c} (1 - \cos\theta). \quad (7.40)$$

We now multiply (7.40) with ν/c to get

$$\frac{\nu}{\nu'} - 1 = \frac{h\nu}{m_e c^2} (1 - \cos\theta) \quad \text{and} \quad h\nu'(h\nu, \theta) = h\nu \frac{1}{1 + \varepsilon(1 - \cos\theta)}, \quad (7.41)$$

where $\varepsilon = \frac{h\nu}{m_e c^2}$ is the photon energy $h\nu$ normalized to the rest energy $m_e c^2$ of the electron.

- (b) From conservation of energy in a Compton process we have: $h\nu = h\nu' + E_K$ and we use this expression in conjunction with (7.41) to get E_K in terms of $h\nu$ and θ

$$E_K(h\nu, \theta) = h\nu - h\nu' = h\nu - h\nu \frac{1}{1 + \varepsilon(1 - \cos\theta)} = h\nu \frac{\varepsilon(1 - \cos\theta)}{1 + \varepsilon(1 - \cos\theta)}. \quad (7.42)$$

- (c) The fractional energy loss $\Delta(h\nu)/(h\nu)$ of the Compton-scattered photon is determined linking (7.39) with an expression for $\Delta\lambda/\lambda_C = 1 - \cos\theta$ obtained from (7.38) to get

$$\begin{aligned} \frac{\Delta h\nu}{h\nu} &= \frac{h\nu - h\nu'}{h\nu} = \frac{E_K}{h\nu} = \frac{\varepsilon(1 - \cos\theta)}{1 + \varepsilon(1 - \cos\theta)} = \frac{\varepsilon \frac{\Delta\lambda}{\lambda_C}}{1 + \varepsilon \frac{\Delta\lambda}{\lambda_C}} = \frac{\frac{\nu}{c} \Delta\lambda}{1 + \frac{\nu}{c} \Delta\lambda} \\ &= \frac{\Delta\lambda}{1 + \frac{\Delta\lambda}{\lambda}} = \frac{\Delta\lambda}{1 + \Delta\lambda}. \end{aligned} \quad (7.43)$$

(d) *Nuclear Compton effect* is a process in which an incident photon of energy $h\nu$ interacts with a nucleus, transfers some energy to nuclear recoil, and is emitted with diminished energy $h\nu'$ at scattering angle θ . This effect may occur but it is much less probable than the standard Compton effect in which a photon is scattered off a “free and stationary” orbital electron (see Prob. 182).

Inverse Compton effect is a process in which a low energy photon interacts with a highly relativistic electron and gains and the electron loses energy in contrast to the standard Compton effect where through the photon–“free and stationary electron” interaction the photon loses energy and the recoil electron gains energy (see Problems 161 and 162).

(e) Maximum wavelength shift $\Delta\lambda_{\max}$ occurs for a scattering angle $\theta = \pi$ and this type of scattering is referred to as backscattering. Scattering of photons on “free electrons” is the most common scattering of photon on an absorber; however, photon scattering on heavier charged particles is also possible, such as for example scattering of photons on protons.

For standard scattering of photon on a free electron with a scattering angle $\theta = \pi$ the Compton equation (7.38) gives

$$\begin{aligned}\Delta\lambda_{\max}^e &= \Delta\lambda^e|_{\theta=\pi} = 2\lambda_C^e = \frac{4\pi\hbar c}{m_e c^2} = \frac{4\pi \times (197.3 \text{ MeV} \cdot \text{fm})}{0.511 \text{ MeV}} \\ &= 4860 \text{ fm} = 0.0486 \text{ \AA},\end{aligned}\quad (7.44)$$

where λ_C^e is termed the Compton wavelength of electron: $\lambda_C^e = h/(m_e c) = 2430 \text{ fm} = 0.0243 \text{ \AA}$, numerically equal to the wavelength of a photon with energy $h\nu = m_e c^2 = 0.511 \text{ MeV}$.

For scattering of photon on a proton with a scattering angle $\theta = \pi$ the Compton equation (7.38) gives

$$\begin{aligned}\Delta\lambda_{\max}^p &= \Delta\lambda^p|_{\theta=\pi} = 2\lambda_C^p = \frac{4\pi\hbar c}{m_p c^2} = \frac{4\pi \times (197.3 \text{ MeV} \cdot \text{fm})}{938.3 \text{ MeV}} \\ &= 2.64 \text{ fm} = 2.64 \times 10^{-5} \text{ \AA},\end{aligned}\quad (7.45)$$

where λ_C^p is termed the Compton wavelength of proton: $\lambda_C^p = h/(m_p c) = 1.32 \text{ fm} = 1.32 \times 10^{-5} \text{ \AA}$, numerically equal to the wavelength of a photon with energy $h\nu = m_p c^2 = 938.3 \text{ MeV}$.

7.3.Q2

(156)

A photon may undergo several successive Compton scattering interactions (multiple Compton scattering).

- (a) Find a general expression for photon energy $h\nu_i$ after incident photon of energy $h\nu$ undergoes N Compton scattering events, each event through a scattering angle θ_i .

(b) Use the general expression for N successive Compton scattering events derived in (a) and calculate the photon energy $h\nu_N$ under the following conditions:

- (1) Single Compton scattering through $\theta_1 = 180^\circ$.
- (2) Two successive Compton scatterings, each one through 90° .
- (3) Three successive Compton scatterings, each one through 60° .
- (4) Four successive Compton scatterings, each one through 45° .
- (5) Ten successive Compton scatterings, each one through 18° .

SOLUTION:

(a) To derive a general expression for N scattering events we first expand the well known expression for single Compton scattering of photon with energy $h\nu$ through a scattering angle θ_1 to result in scattered photon $h\nu_1$ [(T7.71) and (7.41)]

$$h\nu_1 = h\nu \frac{1}{1 + \frac{h\nu}{E_0}(1 - \cos\theta_1)} \quad (7.46)$$

into expressions for two and three successive Compton scattering events, and then generalize the results to multiple (N) scattering events. In (7.46) E_0 is the electron rest energy (0.511 MeV).

From (7.46) we get the following expression for $h\nu_2$ following two successive Compton scattering events, first through scattering angle θ_1 and second through scattering angle θ_2

$$\begin{aligned} h\nu_2 &= h\nu_1 \frac{1}{1 + \frac{h\nu_1}{E_0}(1 - \cos\theta_2)} = h\nu \frac{1}{1 + \frac{h\nu}{E_0}(1 - \cos\theta_1)} \times \frac{1}{1 + \frac{h\nu}{E_0} \frac{(1 - \cos\theta_2)}{[1 + \frac{h\nu}{E_0}(1 - \cos\theta_1)]}} \\ &= h\nu \frac{1}{1 + \frac{h\nu}{E_0}(2 - \cos\theta_1 - \cos\theta_2)}. \end{aligned} \quad (7.47)$$

In a similar fashion we derive the final energy $h\nu_3$ for three successive Compton scattering events through scattering angles θ_1 , θ_2 and θ_3 and get

$$\begin{aligned} h\nu_3 &= h\nu_2 \frac{1}{1 + \frac{h\nu_2}{E_0}(1 - \cos\theta_3)} \\ &= h\nu \frac{1}{1 + \frac{h\nu}{E_0}(2 - \cos\theta_1 - \cos\theta_2)} \times \frac{1}{1 + \frac{h\nu}{E_0} \frac{(1 - \cos\theta_3)}{[1 + \frac{h\nu}{E_0}(2 - \cos\theta_1 - \cos\theta_2)]}} \\ &= h\nu \frac{1}{1 + \frac{h\nu}{E_0}(3 - \cos\theta_1 - \cos\theta_2 - \cos\theta_3)}. \end{aligned} \quad (7.48)$$

A closer look at expressions (7.46), (7.47), and (7.48) reveals the following recursive relationship for final photon energy $h\nu_N$ attained after N successive Coulomb scattering events through angles $\theta_1, \theta_2, \theta_3, \dots, \theta_N$

$$h\nu_N = h\nu \frac{1}{1 + \frac{h\nu}{E_0}(N - \sum_{i=1}^N \cos \theta_i)}. \quad (7.49)$$

(b) We now use the recursive relationship (7.49) to calculate the final photon energy $h\nu_N$ in N successive Compton scattering events, each event i characterized by scattering angle θ_i

(1)

$$N = 1; \theta_1 = 180^\circ; h\nu_1 = h\nu \frac{1}{1 + 2\frac{h\nu}{E_0}}, \quad (7.50)$$

(2)

$$N = 2; \theta_1 = \theta_2 = 90^\circ; h\nu_2 = h\nu \frac{1}{1 + 2\frac{h\nu}{E_0}}, \quad (7.51)$$

(3)

$$N = 3; \theta_1 = \theta_2 = \theta_3 = 60^\circ; h\nu_3 = h\nu \frac{1}{1 + 1.5\frac{h\nu}{E_0}}, \quad (7.52)$$

(4)

$$N = 4; \theta_1 = \theta_2 = \theta_3 = \theta_4 = 45^\circ; h\nu_4 = h\nu \frac{1}{1 + 1.172\frac{h\nu}{E_0}}, \quad (7.53)$$

(5)

$$N = 10; \theta_1 = \theta_2 = \theta_3 = \dots = \theta_{10} = 45^\circ; h\nu_{10} = h\nu \frac{1}{1 + 0.489\frac{h\nu}{E_0}}. \quad (7.54)$$

7.3.Q3

(157)

In Compton effect a photon interacts with a free electron and the electron is released as recoil (Compton) electron with kinetic energy E_K . The photon is scattered with energy $h\nu'$ that is smaller than the incident photon energy $h\nu$ and depends on the scattering angle θ . Consider a Compton interaction in which the recoil electron gains kinetic energy of 2 MeV and determine:

- (a) General expression for photon energy $h\nu$ as a function of the kinetic energy E_K of the recoil electron.
- (b) Minimum energy $h\nu_{\min}$ of the incident photon required for this Compton interaction (in which recoil electron kinetic energy $E_K = 2 \text{ MeV}$) to occur.
- (c) Scattering angle θ for this Compton interaction.
- (d) Recoil angle ϕ of the recoil electron for this Compton interaction.

SOLUTION:

(a) The general expression for photon energy $h\nu$ as a function of the kinetic energy E_K will be obtained from the expression for kinetic energy E_K as a function of the incident photon energy $h\nu$ and scattering angle θ that was derived in (7.42) of Prob. 155 and is given as follows

$$E_K = h\nu \frac{\varepsilon(1 - \cos\theta)}{1 + \varepsilon(1 - \cos\theta)} = E_\nu \frac{\frac{E_\nu}{E_0}(1 - \cos\theta)}{1 + \frac{E_\nu}{E_0}(1 - \cos\theta)} = \frac{E_\nu^2(1 - \cos\theta)}{E_0 + E_\nu(1 - \cos\theta)}, \quad (7.55)$$

where we use the following shorthand notation: $E_\nu = h\nu$ and $E_0 = m_e c^2$. Solving (7.55) for E_ν , we now get the following quadratic expression for E_ν

$$E_\nu^2(1 - \cos\theta) - E_K(1 - \cos\theta)E_\nu - E_K E_0 = 0 \quad (7.56)$$

with the following solution

$$E_\nu = \frac{E_K(1 - \cos\theta) \pm \sqrt{E_K^2(1 - \cos\theta)^2 + 4E_K E_0(1 - \cos\theta)}}{2(1 - \cos\theta)}. \quad (7.57)$$

Since the photon energy $E_\nu = h\nu$ can only be positive, (7.56) has only the following physically relevant solution

$$E_\nu = h\nu = \frac{1}{2} E_K \left[1 + \sqrt{1 + \frac{4E_0}{E_K(1 - \cos\theta)}} \right]. \quad (7.58)$$

(b) Equation (7.58) gives a general relationship between the incident photon energy $E_\nu = h\nu$ and recoil electron energy E_K in Compton effect. It is evident from (7.58) that for a given E_K the minimum energy $h\nu_{\min}$ will occur for maximum value of the function $(1 - \cos\theta)$ that ranges from $1 - \cos\theta = 0$ for $\theta = 0$ (forward scattering) through $1 - \cos\theta = 1$ for $\theta = \frac{1}{2}\pi$ (side scattering) to $1 - \cos\theta = 2$ for $\theta = \pi$ (backscattering).

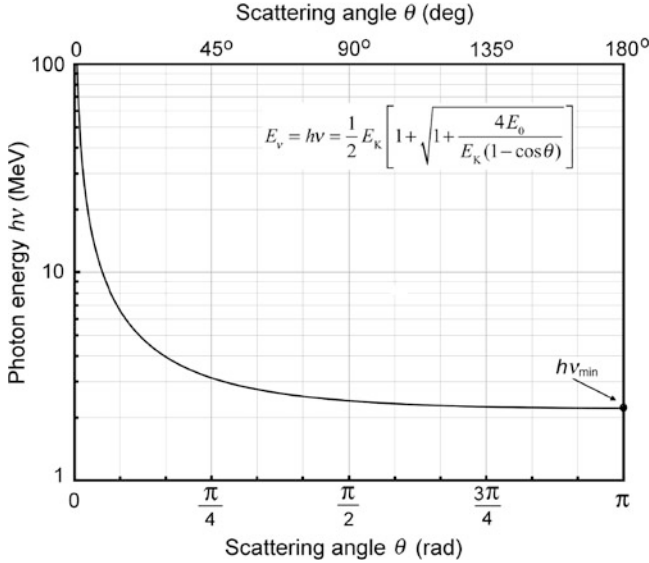


Fig. 7.10 Photon energy $h\nu$ against scattering angle θ relationship expressed in (7.58) for kinetic energy of recoil electron $E_K = 2$ MeV. The minimum photon energy $h\nu_{\min}$ required to produce recoil electron with $E_K = 2$ MeV is 2.23 MeV and it occurs at maximum scattering angle $\theta_{\max} = \pi$

Thus, for $E_K = 2$ MeV, the minimum required photon energy $h\nu_{\min}$ for Compton effect to occur is calculated from (7.58) by setting $\theta = \pi$ (backscattering) to get

$$\begin{aligned} h\nu_{\min} &= \frac{1}{2} E_K \left[1 + \sqrt{1 + \frac{4E_0}{E_K(1 - \cos \pi)}} \right] \\ &= \frac{2 \text{ MeV}}{2} \left[1 + \sqrt{1 + \frac{4 \times (0.511 \text{ MeV})}{(2 \text{ MeV}) \times 2}} \right] = 2.23 \text{ MeV}. \end{aligned} \quad (7.59)$$

To show that $h\nu = 2.23$ MeV is truly the minimum photon energy for Compton effect to occur and produce a recoil electron with $E_K = 2$ MeV, we plot in Fig. 7.10 the photon energy $E_\nu = h\nu$ against scattering angle θ for $E_K = 2$ MeV, as given in (7.58).

(c) As discussed in (b) and shown in Fig. 7.10, the minimum photon energy $h\nu_{\min}$ occurs at $\theta = \pi$ (backscattering). For electron recoil energy $E_K = 2$ MeV the minimum photon energy $h\nu_{\min} = 2.23$ MeV and it occurs at the maximum scattering angle $\theta_{\max} = \pi$.

(d) In Compton effect the scattering angle θ and the recoil angle ϕ are related through the following relationship (T7.68)

$$\tan \phi = \frac{1}{1 + \varepsilon} \cot \frac{\theta}{2}, \quad (7.60)$$

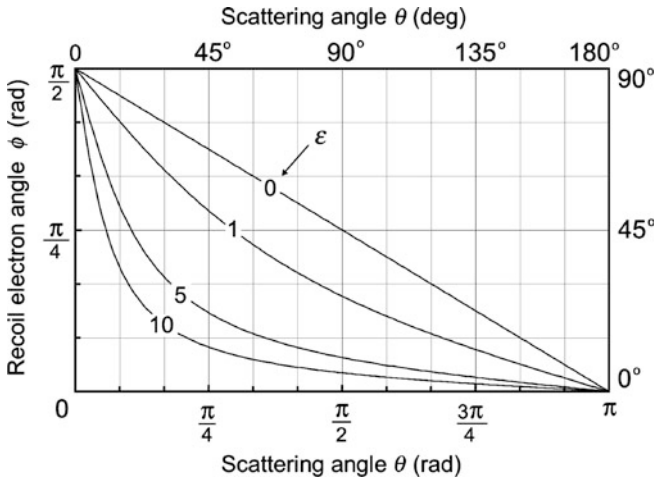


Fig. 7.11 Electron recoil angle ϕ against photon scattering angle θ for various values of parameter $\varepsilon = h\nu/(m_e c^2)$

plotted in Fig. 7.11 in the form of recoil angle ϕ against scattering angle θ for various values of the parameter ε , given as photon energy $E_\nu = h\nu$ normalized to the rest energy of the electron $E_0 = m_e c^2 = 0.511$ MeV. The figure shows that for scattering angle $\theta = \pi$ the recoil angle $\phi = 0$ irrespective of the value of ε . We thus conclude that for the Compton effect addressed in this problem the incident photon with energy $h\nu$ is backscattered with scattering angle $\theta = \pi$ and the recoil electron moves in the direction of the incident photon (recoil angle $\phi = 0$) with kinetic energy $E_K = 2$ MeV.

7.3.Q4

(158)

The differential Klein-Nishina electronic cross section per unit solid angle for Compton effect is given as follows

$$\frac{d_e \sigma_C^{KN}}{d\Omega} = \frac{r_e^2}{2} \left(\frac{\nu'}{\nu}\right)^2 \left\{ \frac{\nu'}{\nu} + \frac{\nu}{\nu'} - \sin^2 \theta \right\} \tag{7.61}$$

and can also be expressed as the product of the differential electronic cross section per unit solid angle for Thompson scattering $d_e \sigma_{Th}/d\Omega$ and the Klein-Nishina form factor F_{KN}

$$\frac{d_e \sigma_C^{KN}}{d\Omega} = \frac{d_e \sigma_{Th}}{d\Omega} F_{KN}, \tag{7.62}$$

where

$$\frac{d_e \sigma_{Th}}{d\Omega} = \frac{r_e^2}{2} (1 + \cos^2 \theta). \tag{7.63}$$

- (a) Deduce the Klein-Nishina form factor F_{KN} from (7.61) and (7.62).
 (b) Use the Klein-Nishina form factor derived in (a) and calculate its value for a grid of points defined by $\varepsilon = 0, 0.1, 0.5, 1, 5,$ and 10 and $\theta = 0, 45^\circ, 90^\circ, 135^\circ,$ and 180° . Present the calculated data in a tabular form.
 (c) Plot the data from (b) on a Cartesian plot of form factor $F_{\text{KN}}(\varepsilon, \theta)$ against scattering angle θ and sketch the shape of the form factor for the values of ε given in (b). State at least 5 notable features of the form factor $F_{\text{KN}}(\varepsilon, \theta)$.

SOLUTION:

(a) For Compton scattering, the energy of the scattered photon $h\nu'$ is given in terms of the incident photon energy $h\nu$ and scattering angle θ as follows

$$h\nu' = h\nu \frac{1}{1 + \varepsilon(1 - \cos\theta)} \quad \text{or} \quad \frac{h\nu'}{h\nu} = \frac{1}{1 + \varepsilon(1 - \cos\theta)} \quad \text{or} \quad (7.64)$$

$$\frac{h\nu}{h\nu'} = 1 + \varepsilon(1 - \cos\theta),$$

where ε is defined as $\varepsilon = h\nu/(m_e c^2)$, the photon incident energy $h\nu$ normalized to the rest energy of the electron $m_e c^2 = 0.511$ MeV.

The Klein-Nishina electronic cross section per unit solid angle $d_e\sigma_C^{\text{KN}}/d\Omega$ of (7.61) in conjunction with (7.64) is now expressed as follows

$$\begin{aligned} \frac{d_e\sigma_C^{\text{KN}}}{d\Omega} &= \frac{r_e^2}{2} \left(\frac{\nu'}{\nu} \right)^2 \left\{ \frac{\nu'}{\nu} + \frac{\nu}{\nu'} - \sin^2\theta \right\} \\ &= \frac{r_e^2}{2} \left[\frac{1}{1 + \varepsilon(1 - \cos\theta)} \right]^2 \left\{ \frac{1}{1 + \varepsilon(1 - \cos\theta)} \right. \\ &\quad \left. + [1 + \varepsilon(1 - \cos\theta)] - \sin^2\theta \right\}. \end{aligned} \quad (7.65)$$

Rearranging terms in (7.65) and using the trigonometric identity $1 - \sin^2\theta = \cos^2\theta$ we get the following expression for $d_e\sigma_C^{\text{KN}}/d\Omega$

$$\begin{aligned} \frac{d_e\sigma_C^{\text{KN}}}{d\Omega} &= \frac{r_e^2}{2} \left[\frac{1}{1 + \varepsilon(1 - \cos\theta)} \right]^2 \left\{ \cos^2\theta + \frac{1 + [1 + \varepsilon(1 - \cos\theta)]\varepsilon(1 - \cos\theta)}{1 + \varepsilon(1 - \cos\theta)} \right\} \\ &= \frac{r_e^2}{2} \left[\frac{1}{1 + \varepsilon(1 - \cos\theta)} \right]^2 \left\{ \cos^2\theta + \frac{1 + \varepsilon(1 - \cos\theta) + [\varepsilon(1 - \cos\theta)]^2}{1 + \varepsilon(1 - \cos\theta)} \right\} \end{aligned}$$

$$\begin{aligned}
&= \frac{r_e^2}{2} \left[\frac{1}{1 + \varepsilon(1 - \cos \theta)} \right]^2 \left\{ 1 + \cos^2 \theta + \frac{\varepsilon^2(1 - \cos \theta)^2}{1 + \varepsilon(1 - \cos \theta)} \right\} \\
&= \left\{ \frac{r_e^2}{2} (1 + \cos^2 \theta) \right\} \left\{ \left[\frac{1}{1 + \varepsilon(1 - \cos \theta)} \right]^2 \right. \\
&\quad \left. \times \left[1 + \frac{\varepsilon^2(1 - \cos \theta)^2}{[1 + \varepsilon(1 - \cos \theta)](1 + \cos^2 \theta)} \right] \right\}. \tag{7.66}
\end{aligned}$$

Recognizing the first term in the fourth row of (7.66) as the Thomson differential scattering cross section $d_e\sigma_{\text{Th}}/d\Omega$, Klein and Nishina named the second term, which depends on incident photon energy $h\nu$ through ε and also depends on the scattering angle θ , the scattering form factor. In their honor, this form factor is now referred to as the Klein-Nishina form factor $F_{\text{KN}}(h\nu, \theta)$.

The Klein-Nishina electronic cross section per unit solid angle $d_e\sigma_{\text{C}}^{\text{KN}}/d\Omega$ can thus be expressed in terms of the Thomson differential scattering cross section $d_e\sigma_{\text{Th}}/d\Omega$ multiplied by the Klein-Nishina form factor as

$$\frac{d_e\sigma_{\text{C}}^{\text{KN}}}{d\Omega} = \frac{d_e\sigma_{\text{Th}}}{d\Omega} F_{\text{KN}}(h\nu, \theta), \tag{7.67}$$

where the Klein-Nishina form factor is expressed as follows

$$F_{\text{KN}}(h\nu, \theta) = \left[\frac{1}{1 + \varepsilon(1 - \cos \theta)} \right]^2 \left[1 + \frac{\varepsilon^2(1 - \cos \theta)^2}{[1 + \varepsilon(1 - \cos \theta)](1 + \cos^2 \theta)} \right]. \tag{7.68}$$

(b) Table 7.4 presents values of the Klein-Nishina form factor $F_{\text{KN}}[\varepsilon = h\nu(m_e c^2)^{-1}, \theta]$ given in (7.68) and calculated for various values of ε and θ prescribed for (b).

Table 7.4 Klein-Nishina form factor $F_{\text{KN}}(\varepsilon, \theta) = F_{\text{KN}}[h\nu/(m_e c^2), \theta]$ given in (7.68) for various values of ε and θ prescribed in (b)

ε	θ				
	0°	45°	90°	135°	180°
0	1.0	1.0	1.0	1.0	1.0
0.1	1.0	0.944	0.834	0.742	0.706
0.5	1.0	0.770	0.519	0.367	0.313
1	1.0	0.625	0.375	0.234	0.185
5	1.0	0.260	0.144	0.067	0.046
10	1.0	0.159	0.083	0.036	0.024

(c) The Klein-Nishina form factor $F_{\text{KN}}(\varepsilon, \theta)$ is a complicated function of the energy parameter ε and scattering angle θ . Five notable features of $F_{\text{KN}}(\varepsilon, \theta)$ are:

- (1) $F_{\text{KN}}(\varepsilon, \theta) \leq 1$ for all θ and ε . Thus, the differential electronic Klein-Nishina cross section $d_e\sigma_{\text{C}}^{\text{KN}}/d\Omega$ for Compton scattering is smaller than or equal to the differential Thomson electronic cross section $d_e\sigma_{\text{Th}}/d\Omega$, i.e.,

$$\frac{d_e\sigma_{\text{C}}^{\text{KN}}}{d\Omega} \leq \frac{d_e\sigma_{\text{Th}}}{d\Omega} \quad \text{for all } \theta \text{ and } \varepsilon. \quad (7.69)$$

- (2) $F_{\text{KN}}(\varepsilon, \theta) = 1$ for $\theta = 0$ at any ε . Thus, the differential electronic Klein-Nishina cross section $d_e\sigma_{\text{C}}^{\text{KN}}/d\Omega$ for Compton scattering is equal to the differential Thomson electronic cross section $d_e\sigma_{\text{Th}}/d\Omega$, i.e.,

$$\frac{d_e\sigma_{\text{C}}^{\text{KN}}}{d\Omega} = \frac{d_e\sigma_{\text{Th}}}{d\Omega} \quad \text{for } \theta = 0 \text{ at any } \varepsilon. \quad (7.70)$$

- (3) $F_{\text{KN}}(\varepsilon, \theta) = 1$ for $\varepsilon = 0$ at any θ . Thus, the differential electronic Klein-Nishina cross section $d_e\sigma_{\text{C}}^{\text{KN}}/d\Omega$ for Compton scattering is equal to the differential Thomson electronic cross section $d_e\sigma_{\text{Th}}/d\Omega$, i.e.,

$$\frac{d_e\sigma_{\text{C}}^{\text{KN}}}{d\Omega} = \frac{d_e\sigma_{\text{Th}}}{d\Omega} \quad \text{for } \varepsilon = 0 \text{ at any } \theta. \quad (7.71)$$

- (4) For a given ε , $F_{\text{KN}}(\varepsilon, \theta)$ decreases with increasing θ from $F_{\text{KN}}(\varepsilon, \theta) = 1$ at $\theta = 0$.
- (5) For a given θ , $F_{\text{KN}}(\varepsilon, \theta)$ decreases with increasing ε from $F_{\text{KN}}(\varepsilon, \theta) = 1$ at $\varepsilon = 0$.

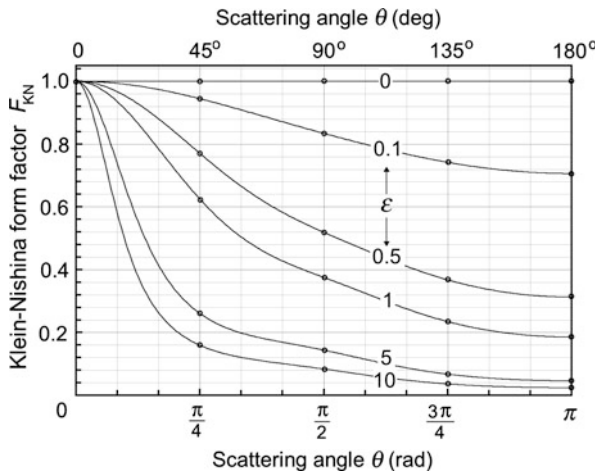


Fig. 7.12 Klein-Nishina $F_{\text{KN}}(\varepsilon, \theta)$ form factor (7.68) calculated for various values of $\varepsilon = hv/(m_e c^2)$ and scattering angle θ listed in Table 7.4. Data points are connected by hand

7.3.Q5

(159)

The Klein-Nishina differential electronic cross section per unit solid angle $d_e\sigma_C^{\text{KN}}/d\Omega$ for Compton effect is in its most simple form expressed as

$$\frac{d_e\sigma_C^{\text{KN}}}{d\Omega} = \frac{r_e^2}{2} \left(\frac{v'}{v} \right)^2 \left[\frac{v'}{v} + \frac{v}{v'} - \sin^2\theta \right], \quad (7.72)$$

where r_e is the classical electron radius (2.82 fm), $h\nu$ the incident photon energy, $h\nu'$ the scattered photon energy, and θ the scattering angle.

The Klein-Nishina total electronic cross section for Compton scattering ${}_e\sigma_C^{\text{KN}}$ can be calculated through integration of (7.72) over the solid angle Ω resulting in the following expression

$$\begin{aligned} \sigma_C^{\text{KN}} &= \int \left(\frac{d_e\sigma_C^{\text{KN}}}{d\Omega} \right) d\Omega = 2\pi r_e^2 \left[\frac{(1+\varepsilon)}{(1+2\varepsilon)^2} + \frac{\ln(1+2\varepsilon)}{2\varepsilon} \right. \\ &\quad \left. + \frac{2}{\varepsilon^2} - \left(\frac{1+\varepsilon}{\varepsilon^2} \right) \frac{\ln(1+2\varepsilon)}{\varepsilon} \right] \end{aligned} \quad (7.73)$$

with ε an energy parameter defined as $\varepsilon = h\nu/(m_e c^2)$ and standing for the incident photon energy $h\nu$ normalized to the electron rest energy $m_e c^2 = 0.511$ MeV.

- Derive the Klein-Nishina total electronic cross section for Compton scattering ${}_e\sigma_C^{\text{KN}}$ given in (7.73) from the differential electronic cross section $d_e\sigma_C^{\text{KN}}/d\Omega$ given in (7.72).
- Show that as $h\nu \rightarrow 0$, the Klein-Nishina total electronic cross section ${}_e\sigma_C^{\text{KN}}$ approaches the Thomson total electronic cross section ${}_e\sigma_{\text{Th}}$, i.e.,

$$\lim_{\varepsilon \rightarrow 0} {}_e\sigma_C^{\text{KN}} = {}_e\sigma_{\text{Th}} = \frac{8}{3} \pi r_e^2 = 0.665 \text{ b}. \quad (7.74)$$

- Use the expression for ${}_e\sigma_C^{\text{KN}}$ derived as (7.73) in (a) and calculate the anchor points for the graph ${}_e\sigma_C^{\text{KN}}$ against incident photon energy $h\nu$ for the following incident photon energies in MeV: 0.001, 0.1, 1, 10, and 100.
- Plot the calculated anchor points for ${}_e\sigma_C^{\text{KN}}$ vs $h\nu$ graph and sketch the ${}_e\sigma_C^{\text{KN}}$ curve in the photon energy range $0.001 \text{ MeV} \leq h\nu \leq 100 \text{ MeV}$.

SOLUTION:

(a) As shown in (7.73), ${}_e\sigma_C^{\text{KN}}$ is derived by integrating $d_e\sigma_C^{\text{KN}}/d\Omega$ over the solid angle Ω where $d\Omega = \sin\theta d\theta d\phi$. The angular θ dependence is implicit in (7.72),

so we first modify (7.72) to obtain explicit θ dependence by inserting into (7.72) the $h\nu'$ vs $h\nu$ relationships that read

$$h\nu' = h\nu \frac{1}{1 + \varepsilon(1 - \cos\theta)} \quad \text{or} \quad \frac{h\nu'}{h\nu} = \frac{1}{1 + \varepsilon(1 - \cos\theta)} \quad \text{or} \quad (7.75)$$

$$\frac{h\nu}{h\nu'} = 1 + \varepsilon(1 - \cos\theta).$$

Equation (7.72) in conjunction with (7.75) gives

$$\begin{aligned} \frac{d_e\sigma_C^{\text{KN}}}{d\Omega} &= \frac{r_e^2}{2} \left[\frac{1}{1 + \varepsilon(1 - \cos\theta)} \right]^2 \left\{ \frac{1}{1 + \varepsilon(1 - \cos\theta)} + [1 + \varepsilon(1 - \cos\theta)] - \sin^2\theta \right\} \\ &= \frac{r_e^2}{2} \left\{ \frac{1}{[1 + \varepsilon(1 - \cos\theta)]^3} + \frac{1}{1 + \varepsilon(1 - \cos\theta)} - \frac{\sin^2\theta}{[1 + \varepsilon(1 - \cos\theta)]^2} \right\} \end{aligned} \quad (7.76)$$

and the total electronic Klein-Nishina cross section for Compton effect ${}_e\sigma_C^{\text{KN}}$ is now expressed as

$$\begin{aligned} \sigma_C^{\text{KN}} &= \int \left(\frac{d_e\sigma_C^{\text{KN}}}{d\Omega} \right) d\Omega = \int_0^{2\pi} \left\{ \int_0^\pi \left(\frac{d_e\sigma_C^{\text{KN}}}{d\Omega} \right) \sin\theta d\theta \right\} d\phi \\ &= \pi r_e^2 \int_0^\pi \left\{ \frac{1}{[1 + \varepsilon(1 - \cos\theta)]^3} + \frac{1}{1 + \varepsilon(1 - \cos\theta)} \right. \\ &\quad \left. - \frac{\sin^2\theta}{[1 + \varepsilon(1 - \cos\theta)]^2} \right\} \sin\theta d\theta, \end{aligned} \quad (7.77)$$

and calculated through the following six steps:

- (1) Define a dimensionless variable x

$$x = 1 + \varepsilon(1 - \cos\theta). \quad (7.78)$$

- (2) Solve (7.78) for $\cos\theta$ and determine the differential of $\cos\theta$

$$\cos\theta = 1 - \frac{x-1}{\varepsilon} = \frac{1+\varepsilon}{\varepsilon} - \frac{x}{\varepsilon} \quad \text{and} \quad \sin\theta d\theta = \frac{dx}{\varepsilon}. \quad (7.79)$$

- (3) Use the trigonometric identity $\sin^2\theta + \cos^2\theta = 1$ to determine $-\sin^2\theta$ as follows

$$\begin{aligned} -\sin^2\theta &= \cos^2\theta - 1 = \left(\frac{1+\varepsilon}{\varepsilon} - \frac{x}{\varepsilon} \right)^2 - 1 \\ &= \frac{(1+\varepsilon)^2}{\varepsilon^2} - \frac{2(1+\varepsilon)x}{\varepsilon^2} + \frac{x^2}{\varepsilon} - 1 \\ &= \frac{1+2\varepsilon}{\varepsilon^2} - \frac{2(1+\varepsilon)x}{\varepsilon^2} + \frac{x^2}{\varepsilon^2}. \end{aligned} \quad (7.80)$$

(4) Write (7.77) as a sum of the following three integrals

$$\frac{e\sigma_C^{\text{KN}}}{\pi r_e^2} = \int_0^\pi \left\{ \frac{1}{[1 + \varepsilon(1 - \cos\theta)]^3} + \frac{1}{1 + \varepsilon(1 - \cos\theta)} - \frac{\sin^2\theta}{[1 + \varepsilon(1 - \cos\theta)]^2} \right\} \sin\theta \, d\theta = \mathcal{J}_1 + \mathcal{J}_2 + \mathcal{J}_3. \quad (7.81)$$

(5) Solve the three integrals of (7.81) separately

$$\begin{aligned} \mathcal{J}_1 &= \int_0^\pi \frac{\sin\theta \, d\theta}{[1 + \varepsilon(1 - \cos\theta)]^3} = \int_1^{1+2\varepsilon} \frac{dx}{\varepsilon x^3} = -\frac{1}{2\varepsilon} \left[\frac{1}{x^2} \right]_1^{1+2\varepsilon} \\ &= -\frac{1}{2\varepsilon} \left[\frac{1}{(1+2\varepsilon)^2} - 1 \right] = \frac{2(1+\varepsilon)}{(1+2\varepsilon)^2}, \end{aligned} \quad (7.82)$$

$$\mathcal{J}_2 = \int_0^\pi \frac{\sin\theta \, d\theta}{1 + \varepsilon(1 - \cos\theta)} = \int_1^{1+2\varepsilon} \frac{dx}{\varepsilon x} = \frac{1}{\varepsilon} [\ln x]_1^{1+2\varepsilon} = \frac{\ln(1+2\varepsilon)}{\varepsilon}, \quad (7.83)$$

$$\begin{aligned} \mathcal{J}_3 &= \int_0^\pi \frac{-\sin^2\theta}{[1 + \varepsilon(1 - \cos\theta)]^2} \sin\theta \, d\theta \\ &= \frac{1}{\varepsilon} \left[\int_1^{1+2\varepsilon} \left(\frac{1+2\varepsilon}{\varepsilon^2} \right) \frac{dx}{x^2} - 2 \int_1^{1+2\varepsilon} \left(\frac{1+\varepsilon}{\varepsilon^2} \right) \frac{dx}{x} + \int_1^{1+2\varepsilon} \frac{dx}{\varepsilon^2} \right] \\ &= \frac{1}{\varepsilon} \left[-\left(\frac{1+2\varepsilon}{\varepsilon^2} \right) \frac{1}{x} - 2 \left(\frac{1+\varepsilon}{\varepsilon^2} \right) \ln x + \frac{x}{\varepsilon^2} \right]_1^{1+2\varepsilon} \\ &= \frac{1}{\varepsilon} \left[-\frac{1}{\varepsilon^2} + \left(\frac{1+2\varepsilon}{\varepsilon^2} \right) - 2 \left(\frac{1+\varepsilon}{\varepsilon^2} \right) \ln(1+2\varepsilon) + 0 + \frac{1+2\varepsilon}{\varepsilon^2} - \frac{1}{\varepsilon^2} \right]. \end{aligned} \quad (7.84)$$

(6) The Klein-Nishina total electronic cross section for Compton scattering $e\sigma_C^{\text{KN}}$ is now given as the sum of the three integrals $\mathcal{J}_1 + \mathcal{J}_2 + \mathcal{J}_3$ given in (7.82), (7.83) and (7.84), respectively

$$\begin{aligned} e\sigma_C^{\text{KN}} &= \int \left(\frac{d_e\sigma_C^{\text{KN}}}{d\Omega} \right) d\Omega = \int_0^{2\pi} \left\{ \int_0^\pi \left(\frac{d_e\sigma_C^{\text{KN}}}{d\Omega} \right) \sin\theta \, d\theta \right\} d\phi \\ &= \{\mathcal{J}_1\} + \{\mathcal{J}_2\} + \{\mathcal{J}_3\} \\ &= \pi r_e^2 \left\{ \frac{2(1+\varepsilon)}{(1+2\varepsilon)^2} \right\} + \left\{ \frac{\ln(1+2\varepsilon)}{\varepsilon} \right\} + \left\{ \left(\frac{1+2\varepsilon}{\varepsilon^3} \right) - \frac{2}{\varepsilon^3} - 2 \left(\frac{1+\varepsilon}{\varepsilon^3} \right) \ln(1+2\varepsilon) + \frac{1+2\varepsilon}{\varepsilon^3} \right\} \end{aligned}$$

$$\begin{aligned}
&= 2\pi r_e^2 \left[\frac{1 + \varepsilon}{(1 + 2\varepsilon)^2} + \frac{\ln(1 + 2\varepsilon)}{2\varepsilon} + \frac{2}{\varepsilon^2} - \frac{(1 + \varepsilon) \ln(1 + 2\varepsilon)}{\varepsilon^3} \right] \\
&= 2\pi r_e^2 \mathcal{J}, \tag{7.85}
\end{aligned}$$

where \mathcal{J} is a function of ε only and is proportional to ${}_e\sigma_C^{\text{KN}}$ with the proportionality constant equal to $2\pi r_e^2 = 0.4990$ b. The third line in (7.85) represents one of the many possible forms in which the total Klein-Nishina electronic cross section may be presented. Another form, used in Hubbell's work and seemingly more complicated in comparison to the one derived in (7.85), is given in (T7.104). Both forms, of course, will provide identical results for a given photon energy $h\nu$ or energy parameter ε .

(b) The low energy limit of ${}_e\sigma_C^{\text{KN}}$ where parameter ε approaches zero is of importance, since the Compton effect, like Thomson scattering, is an interaction of incident photon $h\nu$ with free electron and one could thus expect that for $\varepsilon \rightarrow 0$ the cross section $\varepsilon \rightarrow 0$ approaches the Thomson cross section ${}_e\sigma_{\text{Th}} = \frac{8}{3}\pi r_e^2 = 0.665$ b. At first glance, however, ${}_e\sigma_C^{\text{KN}}$ of (7.85) appears to have a singularity for $\varepsilon = 0$, so we now take a closer look at (7.85) for $\varepsilon \rightarrow 0$.

First, we address the question of the form of (7.85) for ε very small, i.e., for $\varepsilon \ll 1$, and expand the two logarithmic terms in (7.85) into a series using the following known expansion

$$\ln(1 + x) \approx x - \frac{x^2}{2} + \frac{x^3}{3} - \frac{x^4}{4} + \dots + (-1)^{n+1} \frac{x^n}{n} \quad \text{for } -1 < x < +1. \tag{7.86}$$

The four terms of function \mathcal{J} , namely \mathcal{J}_1 , \mathcal{J}_2 , \mathcal{J}_3 , and \mathcal{J}_4 of (7.85) are now for $\varepsilon \ll 1$ expressed as follows

(1)

$$\mathcal{J}_1 = \frac{1 + \varepsilon}{(1 + 2\varepsilon)^2} \approx (1 + \varepsilon)(1 - 4\varepsilon) = 1 - 3\varepsilon - 4\varepsilon^2 \tag{7.87}$$

(2)

$$\begin{aligned}
\mathcal{J}_2 &= \frac{\ln(1 + 2\varepsilon)}{2\varepsilon} \approx \left\{ \frac{1}{2\varepsilon} \left[2\varepsilon - \frac{(2\varepsilon)^2}{2} + \frac{(2\varepsilon)^3}{3} - \dots \right] \right\} \\
&= \left\{ 1 - \varepsilon + \frac{4\varepsilon^2}{3} - \dots \right\} \tag{7.88}
\end{aligned}$$

(3)

$$\mathcal{J}_3 = \frac{2}{\varepsilon^2} \tag{7.89}$$

(4)

$$\begin{aligned}
\mathcal{J}_4 &= \left\{ -\frac{(1+\varepsilon)\ln(1+2\varepsilon)}{\varepsilon^3} \right\} \approx \left\{ -\frac{1+\varepsilon}{\varepsilon^3} \left[2\varepsilon - \frac{(2\varepsilon)^2}{2} + \frac{(2\varepsilon)^3}{3} - \dots \right] \right\} \\
&= \left\{ -(1+\varepsilon) \left[\frac{2}{\varepsilon^2} - \frac{2}{\varepsilon} + \frac{8}{3} - \dots \right] \right\} \\
&= \left\{ -\frac{2}{\varepsilon^2} + \frac{2}{\varepsilon} - \frac{8}{3} - \dots - \frac{2}{\varepsilon} + 2 - \frac{8\varepsilon}{3} \dots \right\} \\
&= \left\{ -\frac{2}{\varepsilon^2} - \frac{8}{3} + 2 - \frac{8\varepsilon}{3} \dots \right\} = \left\{ -\frac{2}{\varepsilon^2} - \frac{2}{3} \dots \right\} \tag{7.90}
\end{aligned}$$

The sum of the four terms: $\mathcal{J} = \{\mathcal{J}_1 + \mathcal{J}_2 + \mathcal{J}_3 + \mathcal{J}_4\}$ for $\varepsilon \ll 1$ can now be expressed as follows

$$\begin{aligned}
\{\mathcal{J}_1 + \mathcal{J}_2 + \mathcal{J}_3 + \mathcal{J}_4\} &= \left\{ [1 - 3\varepsilon - 4\varepsilon^2] + \left[1 - \varepsilon + \frac{4\varepsilon^2}{3} - \dots \right] \right. \\
&\quad \left. + \left[\frac{2}{\varepsilon^2} \right] + \left[-\frac{2}{\varepsilon^2} - \frac{2}{3} \dots \right] \right\} \\
&= \frac{4}{3} - 4\varepsilon - \frac{8}{3}\varepsilon^2 + \dots \tag{7.91}
\end{aligned}$$

The small ε approximation to ${}_e\sigma_C^{\text{KN}}$ expressed in (7.91) is obviously much simpler than (7.85), obviously does not suffer a singularity at $\varepsilon \rightarrow 0$, and lends itself to an easy evaluation of the ${}_e\sigma_C^{\text{KN}}$ limit for $\varepsilon \rightarrow 0$, as shown below

$$\begin{aligned}
\lim_{\varepsilon \rightarrow 0} ({}_e\sigma_C^{\text{KN}}) &= \lim_{\varepsilon \rightarrow 0} \{2\pi r_e^2 [\mathcal{J}_1 + \mathcal{J}_2 + \mathcal{J}_3 + \mathcal{J}_4]\} = \lim_{\varepsilon \rightarrow 0} \{2\pi r_e^2 [\mathcal{J}]\} \\
&= 2\pi r_e^2 \lim_{\varepsilon \rightarrow 0} \left\{ \frac{4}{3} - 4\varepsilon - \frac{8}{3}\varepsilon^2 + \dots \right\} = \frac{8\pi}{3} r_e^2 = {}_e\sigma_{\text{Th}} = 0.665 \text{ b.} \tag{7.92}
\end{aligned}$$

(c) We now use (7.73) to calculate ${}_e\sigma_C^{\text{KN}}$ for incident photon energies $h\nu$ in MeV of 0.001, 0.1, 1, 10, and 100. Results of our calculation are displayed in Table 7.5, where for each $h\nu$ we show the value of the four functions \mathcal{T}_1 , \mathcal{T}_2 , \mathcal{T}_3 , and \mathcal{T}_4 , Klein-Nishina total electronic cross section ${}_e\sigma_C^{\text{KN}}$, and anchor points for the ${}_e\sigma_C^{\text{KN}}$ vs $h\nu$ graph. A comparison between our calculated ${}_e\sigma_C^{\text{KN}}$ with ${}_e\sigma_C^{\text{KN}}$ available in the literature shows excellent agreement and attests to the veracity of (7.73) in calculation of ${}_e\sigma_C^{\text{KN}}$.

(d) Figure 7.13 plots ${}_e\sigma_C^{\text{KN}}$ against incident photon energy $h\nu$ and clearly exhibits the approach to the Thomson limit ${}_e\sigma_{\text{Th}} = 0.665 \text{ b}$ at low $h\nu$ as well as the fall off of ${}_e\sigma_C^{\text{KN}}$ with increasing $h\nu$ at high $h\nu$.

Table 7.5 Klein-Nishina total electronic cross section $e\sigma_C^{KN}$ for Compton scattering for various incident photon energies $h\nu$ calculated with (7.85). For very low incident photon energy $h\nu$, as shown in (7.92), the Compton total cross section $e\sigma_C^{KN}$ approaches the Thomson total cross section $e\sigma_{Th} = \frac{8}{3}\pi r_e = 0.665$ b

$h\nu$ (MeV)	0.001	0.1	1	10	100
$\epsilon = \frac{h\nu}{m_e c^2} = \frac{h\nu}{0.511 \text{ MeV}}$	1.95694×10^{-3}	0.1957	1.957	19.57	195.7
$J_1 = \frac{1+\epsilon}{(1+2\epsilon)^2}$	0.99416	0.6176	0.1225	0.0128	1.278
$J_2 = \frac{\ln(1+2\epsilon)}{2\epsilon}$	0.99805	0.8439	0.4066	0.0943	0.0153
$J_3 = \frac{2}{\epsilon^2}$	522242	52.2213	0.5222	0.0052	5.222×10^{-5}
$J_4 = \frac{(1+\epsilon)\ln(1+2\epsilon)}{\epsilon^3}$	-522242.7	-52.6953	-0.6281	-0.0101	-1.567×10^{-4}
$J = \sum_i J_i$	1.33221	0.9875	1.6794	0.1022	0.0166
$e\sigma_C^{KN} = 2\pi r_e^2 J$ (7.85)	0.66480	0.4928	0.2112	0.0510	0.0083
Anchor point	0.665	0.50	0.21	0.051	0.008

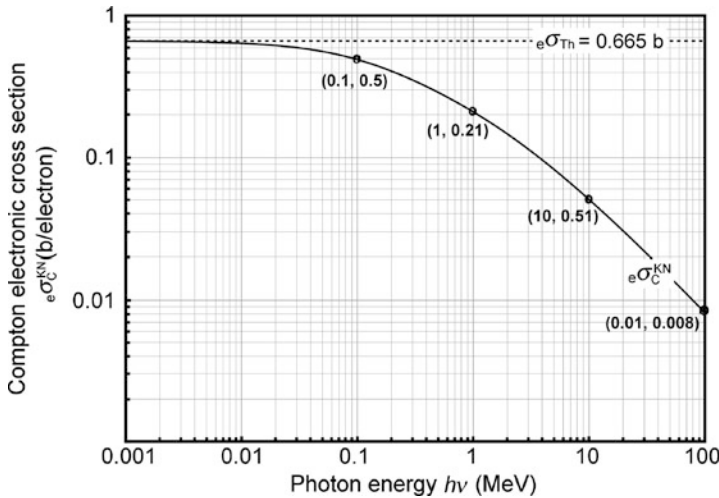


Fig. 7.13 Klein-Nishina total electronic cross section (attenuation coefficient) for Compton effect $e\sigma_C^{KN}$ on free electron against incident photon energy $h\nu$ determined from Klein-Nishina equation given in (7.85). At very low photon energies ($h\nu \rightarrow 0$) $e\sigma_C^{KN} \rightarrow e\sigma_{Th} = 0.665$ b. Data points on the graph represent the anchor points for the $e\sigma_C^{KN}$ vs $h\nu$ diagram

7.3.Q6

(160)

The Klein-Nishina differential electronic cross section $d_e\sigma_C^{KN}/dE_K$, expressing the initial energy spectrum of Compton recoil electrons averaged over all scattering angles θ , is calculated from the basic Klein-Nishina equation for $d_e\sigma_C^{KN}/d\Omega$.

- (a) Starting from the basic Klein-Nishina equation for the differential electronic cross section per unit solid angle for Compton effect $d_e\sigma_C^{\text{KN}}/d\Omega$ given as

$$\frac{d_e\sigma_C^{\text{KN}}}{d\Omega} = \frac{r_e^2}{2} \left(\frac{v'}{v} \right)^2 \left[\frac{v'}{v} + \frac{v}{v'} - \sin^2\theta \right], \quad (7.93)$$

show that $d_e\sigma_C^{\text{KN}}/dE_K$ can be expressed as

$$\frac{d_e\sigma_C^{\text{KN}}}{dE_K} = \frac{\pi r_e^2}{\varepsilon h\nu} \left[2 + \frac{E_K^2}{\varepsilon^2(h\nu - E_K)^2} - \frac{2E_K}{\varepsilon(h\nu - E_K)} + \frac{E_K^2}{\varepsilon^2(h\nu - E_K)^2} \right], \quad (7.94)$$

where r_e is the classical radius of the electron: $r_e = e^2/(4\pi\varepsilon_0 m_e c^2) = 2.818$ fm; $h\nu$ is the energy of the incident photon; $h\nu'$ is the energy of the scattered photon; θ is the scattering angle; and ε is an energy parameter defined as $\varepsilon = h\nu/(m_e c^2)$ with $m_e c^2 = 0.511$ MeV the rest energy of the electron.

- (b) For incident photon energy $h\nu$ of 1 MeV use (7.94) and determine the differential electronic cross section $d_e\sigma_C^{\text{KN}}/dE_K$ for Compton recoil electron kinetic energies from minimum possible kinetic energy $(E_K)_{\text{min}}$ to the maximum possible kinetic energy $(E_K)_{\text{max}}$ of recoil electrons in steps of 0.1 MeV.
- (c) Display the data calculated in (b) on a Cartesian plot to get a distribution of recoil electrons produced in Compton scattering of 1 MeV photons on free electrons. Comment on notable features of the plotted curve.

SOLUTION:

- (a) Before embarking on calculation of $d_e\sigma_C^{\text{KN}}/dE_K$, we recall that:

- (1) Energy of the scattered photon $h\nu'$ is given in terms of incident photon energy $h\nu$ and scattering angle θ as (T7.71)

$$h\nu'(h\nu, \theta) = h\nu \frac{1}{1 + \varepsilon(1 - \cos\theta)}, \quad (7.95)$$

- (2) Kinetic energy E_K of the Compton recoil electron is given as (T7.79)

$$E_K(h\nu, \theta) = h\nu \frac{\varepsilon(1 - \cos\theta)}{1 + \varepsilon(1 - \cos\theta)}, \quad (7.96)$$

- (3) From conservation of energy in Compton effect, $h\nu$, $h\nu'$, and E_K are related through the following

$$h\nu = h\nu' + E_K \quad \text{or} \quad h\nu' = h\nu - E_K. \quad (7.97)$$

From (7.95) we get the following expression for $\cos\theta$

$$\cos\theta = 1 - \frac{E_K}{\varepsilon(h\nu - E_K)}, \quad (7.98)$$

which, upon the use of trigonometric identity $\sin^2\theta = 1 - \cos^2\theta$, yields the following expression for $\sin^2\theta$

$$\sin^2\theta = \frac{2E_K}{\varepsilon(h\nu - E_K)} - \frac{E_K^2}{\varepsilon^2(h\nu - E_K)^2}. \quad (7.99)$$

We now turn to the calculation of electronic cross section $d_e\sigma_C^{\text{KN}}/dE_K$ using the chain rule for computing derivative of a composition of two or more functions. This allows us to express $d_e\sigma_C^{\text{KN}}/dE_K$ as a product of three simpler derivatives that may be determined individually as follows

$$\frac{d_e\sigma_C^{\text{KN}}}{dE_K} = \frac{d_e\sigma_C^{\text{KN}}}{d\Omega} \frac{d\Omega}{d\theta} \frac{d\theta}{dE_K}, \quad (7.100)$$

where

- (1) $d_e\sigma_C^{\text{KN}}/d\Omega$ is the standard Klein-Nishina equation given in (7.93) which, after incorporating (7.95), (7.98), and (7.99), reads as follows in terms of $h\nu$ and E_K

$$\begin{aligned} \frac{d_e\sigma_C^{\text{KN}}}{d\Omega} &= \frac{r_e^2}{2} \left(\frac{\nu'}{\nu} \right)^2 \left[\frac{\nu'}{\nu} + \frac{\nu}{\nu'} - \sin^2\theta \right] \\ &= \frac{r_e^2}{2} \left(\frac{h\nu - E_K}{h\nu} \right)^2 \left[\frac{h\nu - E_K}{h\nu} + \frac{h\nu}{h\nu - E_K} - \frac{2E_K}{\varepsilon(h\nu - E_K)} \right. \\ &\quad \left. + \frac{E_K^2}{\varepsilon^2(h\nu - E_K)^2} \right], \end{aligned} \quad (7.101)$$

- (2) $d\Omega/d\theta$ is determined from the standard definition of $d\Omega$

$$d\Omega = 2\pi \sin\theta d\theta \quad \text{or} \quad \frac{d\Omega}{d\theta} = 2\pi \sin\theta, \quad (7.102)$$

- (3) $d\theta/dE_K$ is determined from the standard expression for kinetic energy E_K of the Compton recoil electron given in (7.96). Using (7.96) we first determine $dE_K/d\theta$ as follows

$$\begin{aligned} \frac{dE_K}{d\theta} &= h\nu \frac{\varepsilon \sin\theta [1 + \varepsilon(1 - \cos\theta) - \varepsilon^2 \sin\theta(1 - \cos\theta)]}{[1 + \varepsilon(1 - \cos\theta)]^2} \\ &= \frac{\varepsilon(h\nu - E_K)^2}{h\nu} \sin\theta \end{aligned} \quad (7.103)$$

and then take the reciprocal of $dE_K/d\theta$ to get $d\theta/dE_K$ in terms $h\nu$, E_K , and θ

$$\frac{d\theta}{dE_K} = \frac{h\nu}{\varepsilon(h\nu - E_K)^2 \sin\theta}. \quad (7.104)$$

Insertion of (7.101), (7.102), and (7.103) into (7.100) results in the following expression for the differential electronic cross section $d_e\sigma_C^{KN}/dE_K$

$$\begin{aligned} \frac{d_e\sigma_C^{KN}}{dE_K} &= \left\{ \frac{d_e\sigma_C^{KN}}{d\Omega} \right\} \left\{ \frac{d\Omega}{d\theta} \right\} \left\{ \frac{d\theta}{dE_K} \right\} \\ &= \left\{ \frac{r_e^2}{2} \left(\frac{h\nu - E_K}{h\nu} \right)^2 \left[\frac{h\nu - E_K}{h\nu} + \frac{h\nu}{h\nu - E_K} \right. \right. \\ &\quad \left. \left. - \frac{2E_K}{\varepsilon(h\nu - E_K)} + \frac{E_K^2}{\varepsilon^2(h\nu - E_K)^2} \right] \right\} \\ &\quad \times \{2\pi \sin\theta\} \times \left\{ \frac{h\nu}{\varepsilon(h\nu - E_K)^2 \sin\theta} \right\} \\ &= \frac{\pi r_e^2}{\varepsilon h\nu} \left[\frac{h\nu - E_K}{h\nu} + \frac{h\nu}{h\nu - E_K} - \frac{2E_K}{\varepsilon(h\nu - E_K)} + \frac{E_K^2}{\varepsilon^2(h\nu - E_K)^2} \right] \\ &= \frac{\pi r_e^2}{\varepsilon h\nu} \left[2 + \frac{E_K^2}{h\nu(h\nu - E_K)} - \frac{2E_K}{\varepsilon(h\nu - E_K)} + \frac{E_K^2}{\varepsilon^2(h\nu - E_K)^2} \right]. \quad (7.105) \end{aligned}$$

(b) To calculate $d_e\sigma_C^{KN}/dE_K$ for 1 MeV photons undergoing Compton scattering we will use four well-defined steps:

- (1) First we use (7.96) to determine the minimum and maximum possible kinetic energies of the Compton recoil electrons, $(E_K)_{\min}$ and $(E_K)_{\max}$, respectively, for $h\nu = 1$ MeV photons. For these photons the energy parameter ε is given as $\varepsilon = h\nu/(m_e c^2) = 1/0.511 = 1.957$. From (7.96) we note that the minimum kinetic energy $(E_K)_{\min} = 0$ occurring at $\theta = 0$ and the maximum kinetic energy $(E_K)_{\max} = 2h\nu\varepsilon/(1 + 2\varepsilon) = 0.796$ MeV occurring at $\theta = \pi$. Thus, we will use (7.105) to calculate $d_e\sigma_C^{KN}/dE_K$ from 0 to $(E_K)_{\max} = 0.796$ MeV in steps of 0.1 MeV.
- (2) Next, we determine for incident photon energy $h\nu = 1$ MeV the value of the term in front of the square bracket of (7.105)

$$\begin{aligned} \frac{\pi r_e^2}{\varepsilon h\nu} &= \frac{\pi \times (2.181 \times 10^{-13} \text{ cm})^2}{1.957 \times (1 \text{ MeV} \cdot \text{electron})} \\ &= 1.275 \times 10^{-25} \frac{\text{cm}^2}{\text{MeV} \cdot \text{electron}} = 0.1275 \frac{\text{b}}{\text{MeV} \cdot \text{electron}}. \quad (7.106) \end{aligned}$$

Table 7.6 The four components of (7.105) for calculation of $d_e\sigma_C^{KN}/dE_K$ for various kinetic energies of recoil electron between $(E_K)_{\min} = 0$ and $(E_K)_{\max} = 0.796$ MeV for Compton interaction of 1 MeV photons with free electrons

E_K (MeV)	First term of (7.105)	$\frac{E_K^2}{h\nu(h\nu-E_K)}$	$-\frac{2E_K}{\varepsilon(h\nu-E_K)}$	$\frac{E_K^2}{\varepsilon^2(h\nu-E_K)^2}$	\sum of 4 terms	$\frac{d_e\sigma_C^{KN}}{dE_K}$ [b/(MeV · el)]
1	0	0	0	0	2.000	0.255
2	0.1	0.011	-0.114	0.003	1.900	0.242
3	0.2	0.05	-0.255	0.016	1.811	0.231
4	0.3	0.129	-0.438	0.048	1.739	0.222
5	0.4	0.267	-0.681	0.116	1.702	0.217
6	0.5	0.500	-1.022	0.261	1.739	0.222
7	0.6	0.900	-1.533	0.588	1.955	0.249
8	0.7	1.633	-2.385	1.422	2.670	0.340
9	0.796	3.106	-3.988	3.975	5.094	0.649

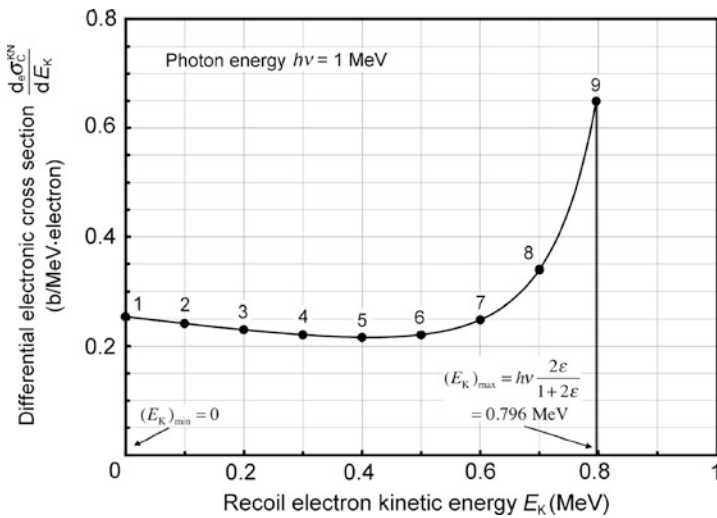


Fig. 7.14 Differential electronic cross section $d_e\sigma_C^{KN}/dE_K$ against kinetic energy E_K of recoil electron for 1 MeV photons undergoing Compton interactions with free electrons. Data points from (1) to (9) on the graph correspond to rows in Table 7.6

(3) For $E_K = (E_K)_{\min} = 0$ we note that

$$\begin{aligned} \frac{d_e\sigma_C^{KN}}{dE_K} &= \frac{2\pi r_e^2}{\varepsilon h\nu} = 2 \times 0.1275 \frac{b}{\text{MeV} \cdot \text{electron}} \\ &= 0.255 \frac{b}{\text{MeV} \cdot \text{electron}}. \end{aligned} \tag{7.107}$$

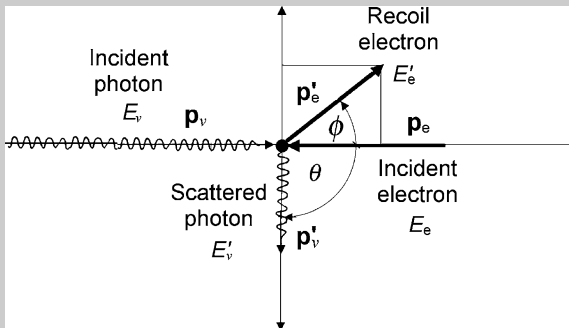
(4) Equation (7.105) will now be used to calculate $d_e\sigma_C^{KN}/dE_K$ in steps of 0.1 MeV from 0.1 MeV to the last point at 0.796 MeV. Detailed results of the calculation for the four terms of (7.105) and 9 recoil electron kinetic energies E_K between $(E_K)_{\min} = 0$ and $(E_K)_{\max} = 0.796$ MeV are displayed in Table 7.6.

(c) Differential electronic cross sections $d_e\sigma_C^{KN}/dE_K$ calculated with (7.105) and tabulated in Table 7.6 for 1 MeV photons interacting with free electrons in Compton effect are plotted in Fig. 7.14 against recoil electron kinetic energy E_K between $(E_K)_{\min} = 0$ and $(E_K)_{\max} = 0.796$ MeV.

7.3.Q7

(161)

A photon of energy $E_\nu = h\nu$ collides head-on with a free electron that is moving exactly in the opposite direction to that of the photon with speed $\beta = v/c$ and total energy $E_e = \gamma E_0$ where E_0 is the rest energy of the electron ($E_0 = m_e c^2 = 0.511$ MeV). The photon is scattered sideways with a scattering angle $\theta = 90^\circ$, as shown schematically below



(a) Show that energy $E'_\nu = h\nu'$ of the scattered photon can be expressed in terms of incident photon energy E_ν and incident electron velocity β as

$$E'_\nu = E_\nu \frac{1 + \beta}{1 + \frac{E_\nu}{E_e}} = E_\nu \frac{1 + \beta}{1 + \frac{\epsilon}{\gamma}} = E_\nu \frac{1 + \beta}{1 + \epsilon \sqrt{1 - \beta^2}}. \tag{7.108}$$

(b) Define the ratio of scattered photon energy over the incident photon energy E'_ν/E_ν as the scattered photon energy fraction f'_ν and determine $(f'_\nu)_{\min}$ and $(f'_\nu)_{\max}$ for the range of β from 0 to 1.

(c) Determine the kinetic energy E'_K of the Compton recoil electron.

SOLUTION:

(a) Energy of the scattered photon E'_ν will be determined through an evaluation of the conservation of total energy and momentum in the Compton process:

Conservation of total energy E in the Compton process is expressed as

$$E_\nu + E_e = E'_\nu + E'_e. \quad (7.109)$$

Conservation of momentum p in the direction normal to that of the incident photon E'_ν (y axis)

$$0 = p'_e \sin \phi - p'_\nu \quad \text{or} \quad 0 = p'_e \sin \phi - \frac{E'_\nu}{c}, \quad (7.110)$$

where p'_ν is the momentum of the scattered photon after the Compton interaction.

Conservation of momentum p in the direction of the incident photon E'_ν (x axis)

$$p_\nu - p_e = p'_e \cos \phi \quad \text{or} \quad \frac{E_\nu}{c} - p_e = p'_e \cos \phi, \quad (7.111)$$

where p_e and p_ν are momenta of the incident electron and incident photon, respectively, before Compton interaction and p'_e is the momentum of the recoil electron after Compton interaction.

We now write (7.110) and (7.111) in the following form

$$(p'_e)^2 \sin^2 \phi = \frac{(E'_\nu)^2}{c^2} \quad \text{and} \quad (p'_e)^2 \cos^2 \phi = \frac{(E_\nu)^2}{c^2} - 2p_e \frac{E_\nu}{c} + (p_e)^2. \quad (7.112)$$

Addition of the two equations of (7.112) and multiplication of the result with c^2 gives the following expression for $(p'_e)^2 c^2$

$$(p'_e)^2 c^2 = (E_\nu)^2 + (E'_\nu)^2 - 2p_e c E_\nu + (p_e)^2 c^2. \quad (7.113)$$

From conservation of total energy (7.109) and recalling that $(E'_e)^2 = (p'_e)^2 c^2 + E_0^2$ we now obtain another equation for $(p'_e)^2 c^2$ that reads as follows

$$(p'_e)^2 c^2 = (E_\nu)^2 + (E'_\nu)^2 - 2E_\nu E'_\nu + (E_e)^2 + 2E_\nu E_e - 2E'_\nu E_e - E_0^2. \quad (7.114)$$

We now have two equations [(7.113) and (7.114)] for $(p'_e)^2 c^2$ that, when merged, lead to the following expression

$$-2p_e c E_\nu + (p_e)^2 c^2 = -2E_\nu E'_\nu + (E_e)^2 + 2E_\nu E_e - 2E'_\nu E_e - E_0^2 \quad (7.115)$$

that can be simplified to the following, recalling that $(p_e)^2 c^2 + E_0^2 = (E_e)^2$ and dividing by $2E_\nu$

$$-p_e c + E'_\nu - E_e + \frac{E'_\nu}{E_\nu} E_e = 0. \quad (7.116)$$

Using the simple relationship $p_e c = \beta E_e$ linking particle momentum p_e with its total energy E_e (T1.65), we now express (7.116) as follows

$$-\beta E_e + E'_v - E_e + \frac{E'_v}{E_v} E_e = 0 \quad \text{or} \quad E'_v \left(\frac{E_e}{E_v} + 1 \right) = E_e (1 + \beta), \quad (7.117)$$

resulting in the following solution for energy of the scattered photon E'_v

$$E'_v = E_e \frac{1 + \beta}{1 + \frac{E_e}{E_v}} = E_v \frac{1 + \beta}{1 + \frac{E_v}{E_e}} = E_v \frac{1 + \beta}{1 + \frac{E_v}{\gamma E_0}} = E_v \frac{1 + \beta}{1 + \frac{\varepsilon}{\gamma}} = E_v \frac{1 + \beta}{1 + \sqrt{\varepsilon^2 - \beta^2}}, \quad (7.118)$$

where ε is defined as the ratio E_v/E_0 just like in standard Compton effect.

(b) Scattered photon energy fraction f'_v is defined by the ratio of the scattered photon energy E'_v over the incident photon energy E_v , i.e., $f'_v = E'_v/E_v$ which from (7.118) gives

$$f'_v = \frac{E'_v}{E_v} = \frac{1 + \beta}{1 + \varepsilon \sqrt{1 - \beta^2}}. \quad (7.119)$$

Equation (7.119) provides an interesting result, at first glance surprising, because it shows that the energy fraction f'_v can be smaller as well as larger than 1, in contrast to the standard Compton effect for which one assumes that the electron is free and stationary and this assumption results in $f'_v < 1$ as a rule.

Thus, in the case of Compton effect occurring on a free electron moving with velocity $\beta = v/c$, the scattered photon energy E'_v may exceed the incident photon energy E_v and this suggesting that the incident photon energy is augmented by an energy transfer from the energetic electron. This effect is not only of theoretical interest in physics; in astrophysics this type of Compton process actually occurs and is referred to as the *inverse Compton scattering*.

Let us now look at several interesting special situations related to scattered photon energy fraction f'_v : (1) $\lim_{\beta \rightarrow 0} f'_v$, (2) $\lim_{\beta \rightarrow 1} f'_v$, and (3) β at which $f'_v = 1$.

- (1) One would expect that $\lim_{\beta \rightarrow 0} f'_v$ gives a result that coincides with that obtained for the standard Compton effect in which electron velocity β is zero. That this indeed happens is shown as follows

$$(f'_v)_{\min} = \lim_{\beta \rightarrow 0} \frac{1 + \beta}{1 + \varepsilon \sqrt{1 - \beta^2}} = \frac{1}{1 + \varepsilon}, \quad (7.120)$$

in perfect agreement with the result for the standard Compton effect and side scattering with a scattering angle $\theta = 90^\circ$.

- (2) The other extreme in f'_v is attained for $\lim_{\beta \rightarrow 1} f'_v$

$$(f'_v)_{\max} = \lim_{\beta \rightarrow 1} \frac{1 + \beta}{1 + \varepsilon \sqrt{1 - \beta^2}} = 2, \quad (7.121)$$

indicating that photon scattered at 90° cannot exceed the incident photon energy E_ν by more than 100 % even when Compton effect occurs on an ultra-relativistic electron.

- (3) To calculate β at which $f'_\nu = 1$ (implying that the scattered photon energy E'_ν is equal to incident photon energy E_ν) we set (7.119) equal to 1 and solve for β

$$f'_\nu = \frac{E'_\nu}{E_\nu} = \frac{1 + \beta}{1 + \varepsilon\sqrt{1 - \beta^2}} = 1, \quad (7.122)$$

resulting in

$$\beta = \frac{\varepsilon}{\sqrt{1 + \varepsilon^2}}. \quad (7.123)$$

From (7.120) and (7.121) we conclude that the dynamic range of the scattered photon energy fraction f'_ν is from $(f'_\nu)_{\min} = (1 + \varepsilon)^{-1}$ in effect for side scattering ($\theta = 90^\circ$) in standard Compton scattering to $(f'_\nu)_{\max} = 2$ in Compton effect in which a photon interacts with an ultra-relativistic electron and is scattered at $\theta = \frac{1}{2}\pi$. Figure 7.15 shows a plot of f'_ν against normalized incident electron velocity β in the range from $\beta = 0$ to $\beta = 1$ for various values of ε , incident photon energy normalized to electron rest mass.

(c) Total energy E'_e of the recoil electron is calculated from the conservation of total energy relationship (7.109) in conjunction with (7.118) which gives the energy of the scattered photon E'_ν in terms of the incident photon energy E_ν and velocity β of the incident electron. We insert (7.118) into (7.109) and get the following expression for total energy of the recoil electron E'_e

$$\begin{aligned} E'_e &= E_\nu - E'_\nu + E_e = E_\nu \left[1 - \frac{1 + \beta}{1 + \varepsilon\sqrt{1 - \beta^2}} \right] + E_e \\ &= E_\nu \left[1 - \frac{1 + \beta}{1 + \varepsilon\sqrt{1 - \beta^2}} \right] + \frac{E_0}{\sqrt{1 - \beta^2}} = E_\nu \left[\frac{\varepsilon\sqrt{1 - \beta^2} - \beta}{1 + \varepsilon\sqrt{1 - \beta^2}} \right] + \frac{E_0}{\sqrt{1 - \beta^2}}, \end{aligned} \quad (7.124)$$

where we used the standard relativistic relationship between total energy E_e and rest energy E_0 $E_e = \gamma E_0 = E_0/\sqrt{1 - \beta^2}$ of a particle [see (T1.58)].

Recalling the relativistic relationship between E'_K and E'_e given as $E'_K = E'_e - E_0$, we now express the kinetic energy E'_K of the recoil electron, using (7.124), as follows

$$E'_K = E'_e - E_0 = E_\nu \left[\frac{\varepsilon\sqrt{1 - \beta^2} - \beta}{1 + \varepsilon\sqrt{1 - \beta^2}} \right] + E_0 \left[\frac{1}{\sqrt{1 - \beta^2}} - 1 \right]. \quad (7.125)$$

We now look at two interesting limits of E'_K , one for $\beta \rightarrow 0$ and the other for $\beta \rightarrow 1$:

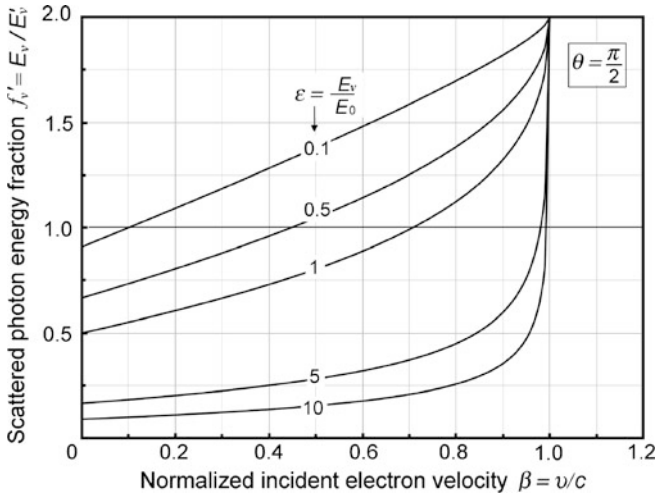


Fig. 7.15 Scattered photon energy fraction f'_v against normalized incident electron velocity β for various values of normalized incident photon energy ϵ

- (1) The limit of E'_K for $\beta \rightarrow 0$ should coincide with the result for the standard Compton effect on a stationary electron and photon scattering at $\theta = 90^\circ$ given as $E'_K = \epsilon/(1 + \epsilon)$ in (T7.79)

$$\lim_{\beta \rightarrow 0} E'_K = \lim_{\beta \rightarrow 0} E_v \left[\frac{\epsilon \sqrt{1 - \beta^2} - 1}{1 + \epsilon \sqrt{1 - \beta^2}} \right] + E_0 \left[\frac{1}{\sqrt{1 - \beta^2}} - 1 \right] = \frac{\epsilon}{1 + \epsilon}, \quad (7.126)$$

in full agreement with the standard Compton scattering on stationary electron and photon scattered with a scattering angle of $\theta = 90^\circ$ (side scattering).

- (2) The limit of E'_K for $\beta \rightarrow 1$ represents Compton effect on an ultra-relativistic electron and reads as follows

$$\lim_{\beta \rightarrow 1} E'_K = \lim_{\beta \rightarrow 1} E_v \left[\frac{\epsilon \sqrt{1 - \beta^2} - 1}{1 + \epsilon \sqrt{1 - \beta^2}} \right] + E_0 \left[\frac{1}{\sqrt{1 - \beta^2}} - 1 \right] = -E_v + \infty. \quad (7.127)$$

At first glance, (7.127) appears surprising, however, since β cannot reach 1 for a particle, the result simply means that $\lim_{\beta \rightarrow 1} E'_K = -E_v + E_K$, where E_K is the kinetic energy of the ultra-relativistic electron for which $\beta \rightarrow 1$. This result agrees well with (7.121) which states that the scattered photon cannot acquire from the incident electron energy larger than E_v which combined with the incident photon energy E_v at most doubles the energy of the scattered photon to $2E_v$, irrespective of the magnitude of the incident electron energy E_K .

As a test of the validity of our determination of the scattered photon energy E'_v (7.118) and the recoil electron total energy E'_e (7.124) we insert (7.118) and (7.124)

into the conservation of total energy expressed in (7.109) and get

$$\begin{aligned}
 E_\nu + E_e &= E'_\nu + E'_e = \left[E_\nu \frac{1 + \beta}{1 + \varepsilon\sqrt{1 - \beta^2}} \right] + \left[E_\nu \frac{\varepsilon\sqrt{1 - \beta^2} - \beta}{1 + \varepsilon\sqrt{1 - \beta^2}} + \frac{E_0}{\sqrt{1 - \beta^2}} \right] \\
 &= E_\nu + E_e,
 \end{aligned} \tag{7.128}$$

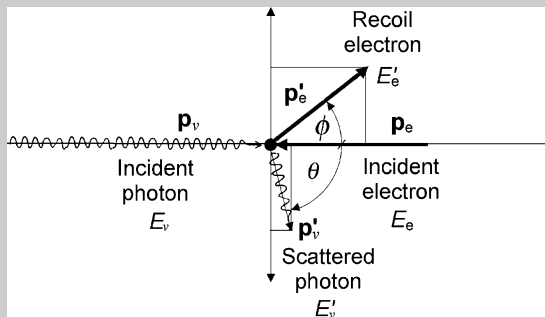
clearly confirming the validity of our results.

7.3.Q8

(162)

Problem 161 deals with Compton scattering of a photon with energy E_ν on a free, yet moving electron. The incident photon E_ν and the incident electron with total energy of E_e are collinear and moving in opposite directions; the scattered photon is scattered with energy E'_ν and scattering angle $\theta = \frac{1}{2}\pi$ and the Compton electron recoils with recoil angle ϕ .

Analyze the same scattering process as the one described in Prob. 161 but allow, as shown in the sketch below, the scattering angle θ to attain any value between 0 (forward scattering) and π (back-scattering).



Under these conditions, representing a more general case of the inverse Compton effect discussed in Prob. 161, determine the general relationships for:

- Scattered photon energy E'_ν and scattered photon energy fraction f'_ν as a function of incident photon energy E_ν , scattering angle θ , and normalized velocity β of the incident electron. The scattered photon energy fraction f'_ν is defined as the ratio E'_ν/E_ν .
- Kinetic energy E'_K of the recoil electron as a function of incident photon energy E_ν , scattering angle θ , and normalized velocity β of the incident electron.

SOLUTION:

(a) Like in Prob. 161, our approach to solving this general problem will be to apply the principle of conservation of total energy E and momentum p from before to after the scattering event.

(1) Conservation of total energy E is expressed as follows

$$E_\nu + E_e = E'_\nu + E'_e \quad \text{or} \quad (E'_e)^2 = (E_\nu + E_e)^2 - 2(E_\nu + E_e)E'_\nu + (E'_\nu)^2, \quad (7.129)$$

where

E_ν and E'_ν are energies of the incident and scattered photon, respectively.
 E_e and E'_e are total energies of the incident and recoil electron, respectively, given as follows

$$E_e^2 = p_e^2 c^2 + E_0^2 \quad \text{and} \quad (E'_e)^2 = (p'_e)^2 c^2 + E_0^2 \quad (7.130)$$

with p_e and p'_e the momenta of incident and recoil electron and E_0 the rest energy of the electron ($E_0 = m_e c^2 = 0.511 \text{ MeV}$).

(2) Conservation of momentum (abscissa x axis)

$$E_\nu - p_e c = E'_\nu \cos \theta + p'_e c \cos \phi \quad \text{or} \quad (E_\nu - p_e c - E'_\nu \cos \theta)^2 = (p'_e)^2 c^2 \cos^2 \phi. \quad (7.131)$$

(3) Conservation of momentum (ordinate y axis)

$$E'_\nu \sin \phi = p'_e c \sin \theta \quad \text{or} \quad (E'_\nu)^2 \sin^2 \phi = (p'_e)^2 c^2 \sin^2 \phi. \quad (7.132)$$

Adding (7.131) and (7.132) results in the following expression for electron recoil momentum p'_e

$$\begin{aligned} (p'_e)^2 c^2 &= (E_\nu - p_e c)^2 - 2(E_\nu - p_e c)E'_\nu \cos \theta + (E'_\nu)^2 \\ &= [(E_\nu)^2 - 2E_\nu p_e c + (p_e)^2 c^2] - 2(E_\nu - p_e c)E'_\nu \cos \theta + (E'_\nu)^2. \end{aligned} \quad (7.133)$$

We now introduce (7.131) into (7.133) for $(p_e)^2 c^2$ and for $(p'_e)^2 c^2$ and get

$$(E'_e)^2 - E_0^2 = (E_\nu)^2 - 2E_\nu p_e c + (E_e)^2 - E_0^2 - 2(E_\nu - p_e c)E'_\nu \cos \theta + (E'_\nu)^2. \quad (7.134)$$

Cancelling E_0^2 in (7.134) and introducing (7.129) for $(E'_e)^2$ we now obtain the following equation

$$\begin{aligned} (E'_e)^2 &\equiv (E_\nu + E_e)^2 - 2(E_\nu + E_e)E'_\nu + (E'_\nu)^2 \\ &= (E_\nu + E_e)^2 - 2E_\nu E_e - 2E_\nu p_e c - 2(E_\nu - p_e c)E'_\nu \cos \theta + (E'_\nu)^2. \end{aligned} \quad (7.135)$$

After cancelling $(E_\nu + E_e)^2$ and $(E'_\nu)^2$ in (7.135) we are left with the following components

$$[(E_\nu + E_e) - (E_\nu - p_e c) \cos \theta] E'_\nu = E_\nu E_e + E_\nu p_e c, \quad (7.136)$$

that can be rearranged to yield the following expression for the scattered photon energy fraction f'_ν defined as the ratio of the scattered photon energy E'_ν over the incident photon energy E_ν

$$f'_\nu = \frac{E'_\nu}{E_\nu} = \frac{E_e + p_e c}{E_\nu(1 - \cos \theta) + E_e + p_e c \cos \theta} \equiv \frac{1 + \frac{p_e c}{E_e}}{\frac{E_e}{E_e}(1 - \cos \theta) + 1 + \frac{p_e c}{E_e} \cos \theta}. \quad (7.137)$$

Finally, after introducing

$$\frac{p_e c}{E_e} = \frac{\gamma E_0 \beta}{\gamma E_0} = \beta \quad \text{and} \quad \frac{E_\nu}{E_e} = \frac{E_\nu}{\gamma E_0} = \frac{\varepsilon}{\gamma} = \varepsilon \sqrt{1 - \beta^2}, \quad (7.138)$$

we express the scattered photon energy fraction f'_ν as follows

$$f'_\nu = \frac{E'_\nu}{E_\nu} = \frac{1 + \beta}{1 + \beta \cos \theta + \varepsilon \sqrt{1 - \beta^2}(1 - \cos \theta)}. \quad (7.139)$$

A closer look at the expression (7.139) for the scattered photon energy fraction f'_ν shows that, similar to the calculation in Prob. 161 in which the scattering angle θ is $\frac{1}{2}\pi$, the scattered photon fraction can exceed 1 in contrast to the standard Compton effect where $f'_\nu \leq 1$. We now take a look at the range of f'_ν by evaluating several special situations related to the scattered photon energy fraction f'_ν : (1) $(f'_\nu)_{\min} = \lim_{\beta \rightarrow 0} f'_\nu$, (2) $(f'_\nu)_{\max} = \lim_{\beta \rightarrow 1} f'_\nu$, and (3) β at which $f'_\nu = 1$.

- (1) One would expect that $\lim_{\beta \rightarrow 0} f'_\nu$ gives a result that coincides with that obtained for the standard Compton effect in which electron velocity β is zero. That this indeed happens is shown as follows

$$\begin{aligned} (f'_\nu)_{\min} &= \lim_{\beta \rightarrow 0} f'_\nu = \lim_{\beta \rightarrow 0} \frac{1 + \beta}{1 + \beta \cos \theta + \varepsilon \sqrt{1 - \beta^2}(1 - \cos \theta)} \\ &= \frac{1}{1 + \varepsilon(1 - \cos \theta)}, \end{aligned} \quad (7.140)$$

in perfect agreement with the result for standard Compton effect where $\beta = 0$ and θ is any scattering angle between 0 and π .

- (2) The other extreme in f'_ν is attained for $\lim_{\beta \rightarrow 1} f'_\nu$ as follows

$$(f'_\nu)_{\max} = \lim_{\beta \rightarrow 1} f'_\nu = \lim_{\beta \rightarrow 1} \frac{1 + \beta}{1 + \beta \cos \theta + \varepsilon \sqrt{1 - \beta^2}(1 - \cos \theta)} = \frac{1}{1 + \cos \theta}, \quad (7.141)$$

ranging from $f'_\nu = 1$ for $\theta = 0$ through $f'_\nu = 2$ for $\theta = \frac{1}{2}\pi$ to $f'_\nu \rightarrow \infty$ for $\theta = \pi$.

- (3) To calculate β at which $f'_\nu = 1$ (implying that the scattered photon energy E'_ν is equal to incident photon energy E_ν) we set (7.139) equal to 1 and solve for β

$$f'_\nu = \frac{E'_\nu}{E_\nu} = \frac{1 + \beta}{1 + \beta \cos \theta + \varepsilon \sqrt{1 - \beta^2}(1 - \cos \theta)} = 1, \quad (7.142)$$

resulting in

$$\beta = \frac{\varepsilon}{\sqrt{1 + \varepsilon^2}}. \quad (7.143)$$

- (b) To determine kinetic energy E'_K of the recoil electron we first determine the total energy E'_e of the recoil electron and then calculate E'_K from E'_e using the standard relativistic relationship $E'_K = E'_e - E_0$ where E_0 is the rest energy of the electron. E'_e is calculated from the conservation of energy relationship of (7.129) in conjunction with (7.139) which gives the energy E'_ν of the scattered photon. Combining (7.139) with (7.129) we get the following expression for total recoil electron energy E'_e

$$\begin{aligned} E'_e &= E_\nu - E'_\nu + E_e = E_\nu \left[1 - \frac{1 + \beta}{1 + \beta \cos \theta + \varepsilon \sqrt{1 - \beta^2}(1 - \cos \theta)} \right] + E_e \\ &= E_\nu \frac{(\varepsilon \sqrt{1 - \beta^2} - \beta)(1 - \cos \theta)}{1 + \beta \cos \theta + \varepsilon \sqrt{1 - \beta^2}(1 - \cos \theta)} + E_e. \end{aligned} \quad (7.144)$$

Kinetic energy E'_K of the recoil electron is then given as

$$E'_K = E'_e - E_0 = E_\nu \frac{(\varepsilon \sqrt{1 - \beta^2})(1 - \cos \theta)}{1 + \beta \cos \theta + \varepsilon \sqrt{1 - \beta^2}(1 - \cos \theta)} + E_K, \quad (7.145)$$

where E_K is kinetic energy of the incident electron.

The validity of (7.145) can be verified by adding the two energies E'_ν of (7.139) and E'_e of (7.144) after the Coulomb interaction and comparing the result with the sum of the two energies ($E_\nu + E_e$) before the Coulomb interaction.

We now look at two interesting limits concerning E'_K , one for $\beta \rightarrow 0$ and the other for $\beta \rightarrow \infty$.

- (1) The limit of E'_K for $\beta \rightarrow 0$ should coincide with the result for the standard Compton effect on a stationary electron ($\beta = 0$) and photon scattering at scattering angle θ given as $E'_K = \varepsilon(1 - \cos \theta)/[1 + \varepsilon(1 - \cos \theta)]$ in (T7.79)

$$\begin{aligned} \lim_{\beta \rightarrow 0} E'_K &= \lim_{\beta \rightarrow 0} E_\nu \frac{(\varepsilon \sqrt{1 - \beta^2})(1 - \cos \theta)}{1 + \beta \cos \theta + \varepsilon \sqrt{1 - \beta^2}(1 - \cos \theta)} + E_K \\ &= E_\nu \frac{\varepsilon(1 - \cos \theta)}{1 + \varepsilon(1 - \cos \theta)} \end{aligned} \quad (7.146)$$

in full agreement with the standard Compton scattering on stationary electron ($\beta = 0$).

- (2) The limit of E'_K for $\beta \rightarrow 1$ represents Compton effect on an ultra-relativistic electron with kinetic energy E_K and reads as follows

$$\lim_{\beta \rightarrow 1} E'_K = \lim_{\beta \rightarrow 1} E_\nu \frac{(\varepsilon \sqrt{1 - \beta^2})(1 - \cos \theta)}{1 + \beta \cos \theta + \varepsilon \sqrt{1 - \beta^2}(1 - \cos \theta)} + E_K = E_K. \quad (7.147)$$

7.3.Q9**(163)**

A photon of energy $h\nu = 10.22$ MeV undergoes Compton scattering in a lead absorber ($Z = 82$, $A = 207.2$ g/mol, $\rho = 11.36$ g/cm³). Determine:

- Energy E_K^C transferred from incident photon to charged particles for the following scattering angles θ : 0° , 45° , 90° and 180° .
- Energy $h\nu'$ of the scattered photon for the following scattering angles θ : 0° , 30° , 60° , 90° , and 180° .
- Mean energy transfer fraction \bar{f}_C and mean energy \bar{E}_K^C transferred to charged particles in Compton effect.
- Klein-Nishina total electronic cross section ${}_e\sigma_C^{KN}$ and mass energy transfer coefficient $(\sigma_C^{KN})_{tr}/\rho$ for Compton effect of 10.22 MeV photons in lead.
- Maximum angle θ_{max} through which the photon can be scattered and still be able to undergo a triplet production interaction in the field of a K-shell electron in lead absorber.

SOLUTION:

- (a) Energy E_K^C transferred from incident photon $h\nu$ to recoil electron is given by (T7.79)

$$E_K^C(\theta) = h\nu \frac{\varepsilon(1 - \cos \theta)}{1 + \varepsilon(1 - \cos \theta)} = h\nu \frac{\frac{h\nu}{m_e c^2}(1 - \cos \theta)}{1 + \frac{h\nu}{m_e c^2}(1 - \cos \theta)}, \quad (7.148)$$

where $\varepsilon = \frac{h\nu}{m_e c^2} = \frac{10.22}{0.511} = 20$.

Inserting scattering angles θ of 0° , 45° , 90° , and 180° into (7.148) we get the following results for recoil electron energy E_K^C : 0, 8.73 MeV, 9.73 MeV, and 9.97 MeV, corresponding to the following scattered photon energies $h\nu'(\theta) = h\nu - E_K^C(\theta)$ of 10 MeV, 1.49 MeV, 0.49 MeV, and 0.25 MeV.

- (b) Energy $h\nu'$ of the scattered photon is calculated from (T7.71)

$$h\nu'(\theta) = h\nu \frac{1}{1 + \varepsilon(1 - \cos \theta)}, \quad (7.149)$$

where again $\varepsilon = h\nu/(m_e c^2) = 10.22/0.511 = 20$.

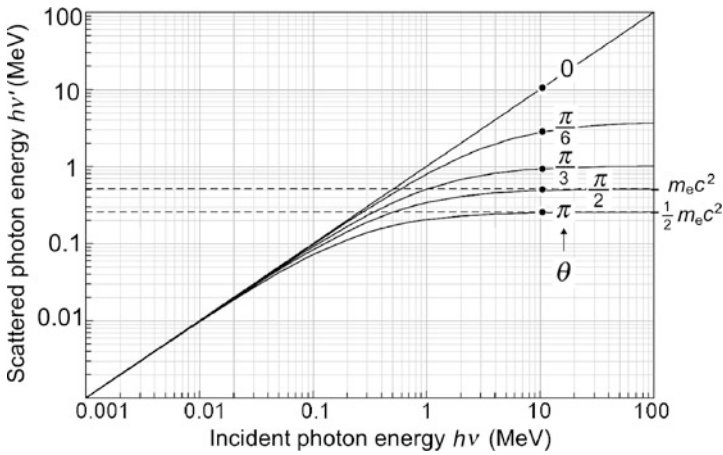


Fig. 7.16 Scattered photon energy $h\nu'$ against incident photon energy $h\nu$ for various scattering angles θ in the range from 0 to 180°

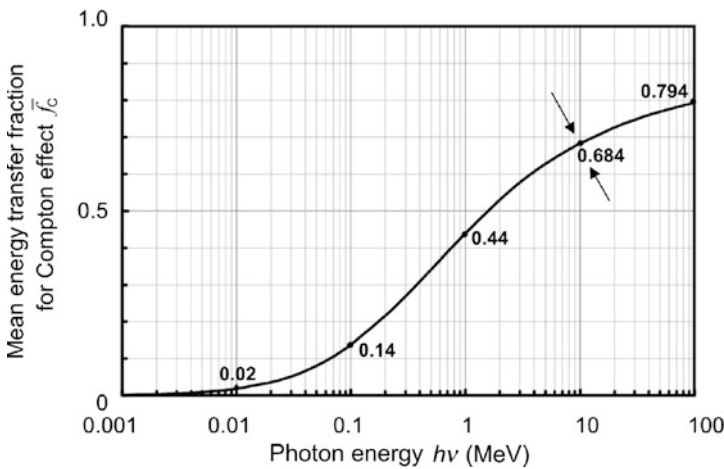


Fig. 7.17 The Compton graph showing the mean energy transfer fraction \bar{f}_C against incident photon energy $h\nu$ for Compton scattering

Inserting scattering angles θ of 0, 30°, 60°, 90°, and 180° into (7.149) we get the following results for scattered photon energy $h\nu'$: 10 MeV, 2.78 MeV, 0.93 MeV, 0.49 MeV, and 0.25 MeV, corresponding to the following recoil electron energies $E_K^C(\theta) = h\nu - h\nu'(\theta)$ of 0, 7.44 MeV, 9.29 MeV, 9.73 MeV, and 9.97 MeV. A graph depicting the general relationship between $h\nu'$ and $h\nu$ for various scattering angles θ is given in Fig. 7.16. Energies $h\nu'$ calculated for 10.22 MeV photons at various scattering angles in this section are shown in Fig. 7.16 as data points at $h\nu = 10.22$ MeV.

(c) Mean energy transfer fraction \bar{f}_C and mean energy \bar{E}_K^C transferred from a 10.22 MeV incident photon to charged particles in Compton effect are obtained directly from the Compton graph for which the point $\bar{f}_C = 0.68$ at $h\nu = 10$ MeV is one of the anchor points. As shown in Fig. 7.17, we get the following results for $\bar{f}_C(h\nu = 10.22 \text{ MeV})$ and $\bar{E}_K^C(h\nu = 10.22 \text{ MeV})$

$$\bar{f}_C(h\nu = 10.22 \text{ MeV}) \approx 0.69 \quad \text{and} \quad \bar{E}_K^C(h\nu = 10.22 \text{ MeV}) \approx 6.9 \text{ MeV}. \quad (7.150)$$

(d) Klein-Nishina total electronic Compton cross section $e\sigma_C^{\text{KN}}$ and mass energy transfer coefficient $(\sigma_C^{\text{KN}})_{\text{tr}}/\rho$ are obtained from the Klein-Nishina cross section graph for which the point $e\sigma_C^{\text{KN}}(10 \text{ MeV}) = 0.051 \text{ b/electron}$ is one of the anchor points. Thus we get

$$e\sigma_C^{\text{KN}}(10.22 \text{ MeV}) \approx 0.050 \times 10^{-24} \text{ cm}^2/\text{electron} = 0.050 \text{ b/electron} \quad (7.151)$$

and

$$\begin{aligned} (\sigma_C^{\text{KN}})_{\text{tr}}/\rho|_{10.22 \text{ MeV}} &= \frac{ZN_A}{A} e\sigma_C^{\text{KN}} \frac{\bar{E}_K^C}{h\nu} = \frac{ZN_A}{A} e\sigma_C^{\text{KN}} \bar{f}_C \\ &\approx \frac{(82 \text{ el/atom}) \times (6.022 \times 10^{23} \text{ atom} \cdot \text{mol}^{-1})}{207.2 \text{ g} \cdot \text{mol}^{-1}} (0.050 \text{ b/el}) \\ &\quad \times 0.69 = 8.22 \times 10^{-3} \frac{\text{cm}^2}{\text{g}}. \end{aligned} \quad (7.152)$$

From (7.151) we note that the Klein-Nishina electronic Compton energy transfer coefficient $(e\sigma_C^{\text{KN}})_{\text{tr}}$ is equal to $\bar{f}_C \cdot e\sigma_C^{\text{KN}} = 0.69 \times 0.05 \text{ b/electron} = 0.035 \text{ b/electron}$. The two electronic coefficients $e\sigma_C^{\text{KN}}$ and $(e\sigma_C^{\text{KN}})_{\text{tr}}$ for photon energy $h\nu = 10.22 \text{ MeV}$ are plotted as data points on $e\sigma_C^{\text{KN}}$ and $(e\sigma_C^{\text{KN}})_{\text{tr}}$ curves of Fig. 7.18.

(e) We will determine the maximum scattering angle θ_{max} recognizing the following two conditions:

- (1) The range of scattered photon energies in Compton effect is from $h\nu' = h\nu$ for $\theta = 0$ (forward scattering) to $h\nu' = h\nu/(1 + 2\varepsilon)$ for $\theta = 180^\circ$ with $\varepsilon = h\nu/(m_e c^2 = 10.22/0.511 = 20)$.
- (2) Threshold energy $h\nu_{\text{thr}}$ for triplet production (electronic pair production) is $4m_e c^2$ or 2.044 MeV. Therefore, we must determine the scattering angle θ at which the scattered photon energy $h\nu'$ is equal to 2.044 MeV and this will then be the maximum scattering angle θ_{max} at which triplet production is still possible. Scattering angles exceeding θ_{max} will produce scattered photons whose energy is below the threshold for triplet production of 2.044 MeV.

We now determine θ_{max} using (7.149) with appropriate values for $h\nu$ (10.22 MeV) and $h\nu'$ (2.044 MeV) and get the following relationship incorporating $h\nu'$, $h\nu$, and θ

$$h\nu'(\theta_{\text{max}}) = h\nu \frac{1}{1 + \varepsilon(1 - \cos \theta_{\text{max}})} \quad (7.153)$$

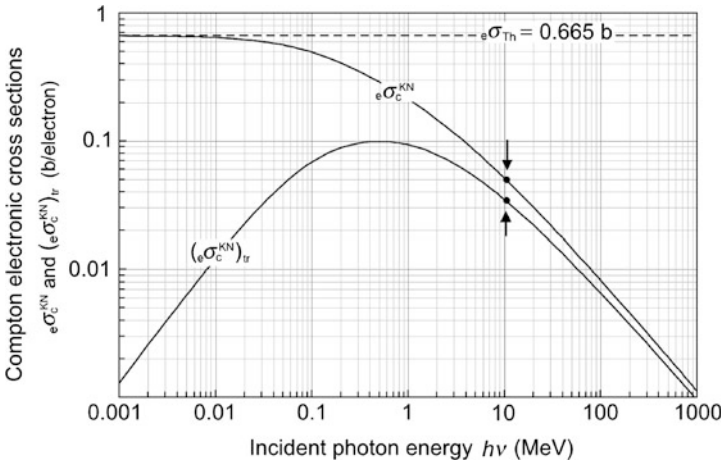


Fig. 7.18 Compton electronic cross section $e\sigma_C^{KN}$ and Compton electronic energy transfer cross section $(e\sigma_C^{KN})_{tr}$ for a free electron against incident photon energy $h\nu$. The two data points at incident photon energy $h\nu = 10.22$ MeV represent results of our calculations of $e\sigma_C^{KN}$ and $(e\sigma_C^{KN})_{tr}$ in (d)

or

$$\frac{h\nu'(\theta_{\max})}{h\nu} \equiv a = \frac{2.044}{10.22} = 0.2 = \frac{1}{1 + \varepsilon(1 - \cos\theta_{\max})}. \tag{7.154}$$

Solving (7.154) for $\cos\theta_{\max}$ results in the following θ_{\max}

$$\cos\theta_{\max} = \frac{a(1 + \varepsilon) - 1}{a\varepsilon} = \frac{0.2 \times (1 + 20) - 1}{0.2 \times 20} = 0.8 \quad \text{or} \tag{7.155}$$

$$\theta_{\max} = \arccos 0.8 = 36.9^\circ.$$

7.3.Q10

(164)

Scattering plays an important role in atomic and nuclear physics and much of the current knowledge on atomic and nuclear structure has been acquired from scattering experiments combined with scattering theories based on atomic and nuclear form factors, respectively. Form factors represent a Fourier transformation of a spatial density distribution (most commonly charge distribution) from geometric to the so-called K space and depend on the type of scattering (elastic or inelastic) as well as on the type of incident radiation beam (x ray, electron, or neutron).

Cross sections for Rayleigh (coherent) scattering are expressed as product of Thomson electronic cross section multiplied by the square of the atomic

form factor $F(x, Z)$, while differential atomic cross sections for Compton (incoherent) scattering are expressed as product of Klein-Nishina differential electronic cross section with the incoherent scattering function $S(x, Z)$ which is related to the atomic form factor $F(x, Z)$. Theoretical derivation of $F(x, Z)$ is very complex for all elements except hydrogen for which the ground state wave function is well known and simple.

- (a) Derive the atomic form factor $F(x, Z)$ of hydrogen $F(x, Z = 1) = F(x, H)$.
- (b) On a log-log graph paper plot the atomic form factor of hydrogen $F(x, H)$ derived in (a) against the momentum transfer variable x .

SOLUTION:

(a) Atomic form factor $F(\mathbf{K}, Z)$ for an atom of atomic number Z represents a Fourier transform of the atomic charge distribution and is defined by the following integral

$$F(\mathbf{K}, Z) = \iiint \rho(\mathbf{r}) e^{i\mathbf{K}\mathbf{r}} d\mathcal{V}, \quad (7.156)$$

where

$\rho(\mathbf{r})$ is the total electron density at \mathbf{r} .

\mathbf{K} is the momentum transfer vector with magnitude $|\mathbf{K}| = K$ defined as [(T1.106) and (T2.122)]

$$|\mathbf{K}| = K = \frac{|\Delta\mathbf{p}|}{\hbar} = \frac{\Delta p}{\hbar} = \frac{2h}{\hbar\lambda} \sin \frac{\theta}{2} = \frac{4\pi}{\lambda} \sin \frac{\theta}{2} = 4\pi x, \quad (7.157)$$

with $\Delta\mathbf{p}$ the momentum transferred from the incident photon to the scatterer (T1.119), λ the wavelength of the incident photon, and x the momentum transfer variable defined as [$x = \sin(\frac{1}{2}\theta)/\lambda$] where θ is the scattering angle and λ is the wavelength, h is the Planck constant, and \hbar is the reduced Planck constant [$\hbar = h/(2\pi)$].

For a spherically symmetric charge distribution (central potential) $F(\mathbf{K}, Z)$ may be simplified as follows

$$\begin{aligned} F(\mathbf{K}, Z) &= F(K, Z) = \iiint \rho(\mathbf{r}) e^{i\mathbf{K}\mathbf{r}} d\mathcal{V} \\ &= \int_0^{2\pi} \int_0^\pi \int_0^\infty \rho(r) e^{iKr \cos\theta} r^2 dr \sin\theta d\theta d\phi \\ &= 2\pi \int_0^\infty r^2 \rho(r) \left\{ \int_{-1}^{+1} e^{iKr \cos\theta} d(\cos\theta) \right\} dr \end{aligned}$$

$$\begin{aligned}
 &= 4\pi \int_0^\infty r^2 \rho(r) \frac{e^{iKr} - e^{-iKr}}{2iKr} dr \\
 &= \frac{4\pi}{K} \int_0^\infty r \rho(r) \sin(Kr) dr.
 \end{aligned} \tag{7.158}$$

For atomic hydrogen the Schrödinger equation yields the following ground state wave function (T3.71)

$$\psi_{100} = \frac{1}{\sqrt{\pi a_0^3}} e^{-\frac{r}{a_0}}, \tag{7.159}$$

where a_0 is the Bohr radius constant equal to $a_0 = \hbar c / (am_e c^2) = 0.5292 \text{ \AA}$. Electron density $\rho(r)$ for electron in ground state of hydrogen is given as

$$\rho(r) = |\psi_{100}|^2 = \frac{1}{\pi a_0^3} e^{-\frac{2r}{a_0}}, \tag{7.160}$$

and inserting (7.160) into (7.158) yields the following expression for the atomic form factor $F(K, Z = 1) = F(K, H)$ of hydrogen in ground state

$$F(K, H) = \frac{4}{K a_0^3} \int_0^\infty r e^{-\frac{2r}{a_0}} \sin(Kr) dr = \frac{4}{K a_0^3} j. \tag{7.161}$$

Integral j is of the following form $j = \int_0^\infty z e^{-\beta z} \sin(bz) dz$ and can be solved through several tedious steps of integration by parts or through finding the solution in an extensive table of integrals where one can find the following entry

$$\int_0^\infty z^n e^{-\beta z} \sin(bz) dz = (-1)^n \frac{\partial^n}{\partial \beta^n} \left(\frac{b}{b^2 + \beta^2} \right). \tag{7.162}$$

For $n = 1$, (7.162) gives the following solution for integral j

$$j = \int_0^\infty z e^{\beta z} \sin(bz) dz = \frac{2\beta b}{(b^2 + \beta^2)^2} = \frac{4K}{a_0(K^2 + \frac{4}{a_0^2})^2} = \frac{4K a_0^3}{(4 + K^2 a_0^2)^2}, \tag{7.163}$$

where the fourth and fifth terms of (7.163) were obtained by inserting into (7.163) the following parameters: $z = r$, $b = K$, and $\beta = 2/a_0$.

The atomic form factor $F(K, H)$ for hydrogen in the ground state is now given as follows

$$F(K, H) = \frac{4}{K a_0^3} j = \frac{16}{(4 + K^2 a_0^2)^2} = \frac{1}{(1 + \frac{K^2 a_0^2}{4})^2}. \tag{7.164}$$

Since from (7.157) we note that $K = 4\pi x$, we can express $F(K, H)$ in the format used by Hubbell and the NIST as follows

$$F(K, H) = F(x, H) = \frac{1}{(1 + 4\pi^2 a_0^2 x^2)^2} = \frac{1}{(1 + C_f x^2)^2}, \tag{7.165}$$

where C_f is a form factor constant equal to $C_f = 4\pi^2 a_0^2 = 4\pi^2 (0.5292 \text{ \AA})^2 = 11.056 \text{ \AA}^2$.

Four special regions are of interest for the atomic form factor of (7.165):

- (1) Limit for $x \rightarrow 0$:

$$\lim_{x \rightarrow 0} F(x, H) = \lim_{x \rightarrow 0} \frac{1}{(1 + C_f x^2)^2} = 1. \tag{7.166}$$

- (2) Region of small x where $C_f x \ll 1$:

$$F(x, H) \approx 1 - 2C_1 x^2. \tag{7.167}$$

- (3) Region of intermediate x :

$$F(x, H) \text{ is given by (7.165)}. \tag{7.168}$$

- (2) Region of large x where $C_f x^2 \gg 1$ we get:

$$F(x, H) \approx (C_f x^2)^{-2}. \tag{7.169}$$

- (3) Limit for $x \rightarrow \infty$:

$$\lim_{x \rightarrow \infty} F(x, H) = \lim_{x \rightarrow \infty} \frac{1}{(1 + 4\pi^2 a_0^2 x^2)^2} = 0. \tag{7.170}$$

(b) A log-log plot of the atomic form factor $F(x, H)$ of hydrogen against the momentum transfer variable x determined from (7.165) is shown in Fig. 7.19 over 4 cycles in x and 8 cycles in $F(x, H)$. Limiting values for $x \rightarrow 0$ and $x \rightarrow \infty$ as well as regions of small x , intermediate x and large x are clearly identified.

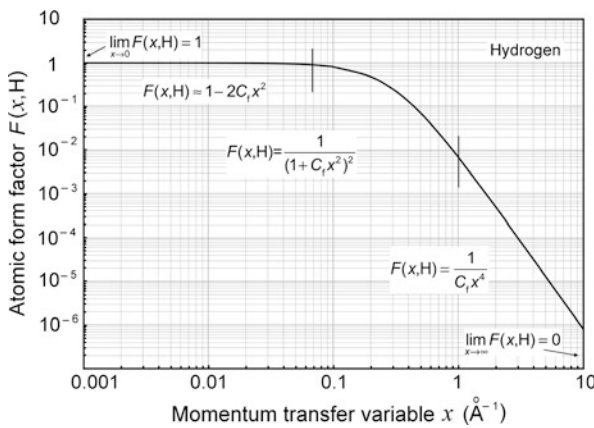


Fig. 7.19 Atomic form factor $F(x, H)$ against momentum transfer variable x for hydrogen as determined from (7.165)

7.3.Q11

(165)

Compton scattering theory assumes a photon interaction with a free and stationary electron, but this assumption becomes problematic when photon energy is comparable to the binding energy of the atomic electron to the nucleus. Various methods have been developed to account for these binding effects and most notable of them is Hubbell's method based on the incoherent scattering function $S(x, Z)$, with x the momentum transfer variable defined as $x = (\sin \frac{1}{2}\theta)/\lambda$, λ the wavelength of the incident photon, θ the scattering angle, and Z the atomic number of the absorber. Hubbell has shown that the incoherent scattering function $S(x, Z)$ of hydrogen is linked to the atomic form factor $F(x, Z)$ of hydrogen through the following relationship

$$S(x, Z = 1) = S(x, \text{H}) = 1 - [F(x, \text{H})]^2 = 1 - \frac{1}{[1 + 4\pi a_0^2 x^2]^4}, \quad (7.171)$$

with the form factor $F(x, \text{H})$ calculated from first principles and the wave function of the hydrogen atom ground state, as shown in Prob. 164.

-
- (a) For hydrogen determine the atomic form factor $F(x, \text{H})$ and the incoherent scattering function $S(x, \text{H})$ using (7.171) for the following values of x in \AA^{-1} : 0.001, 0.01, 0.1, 1, 10, and 100. Plot $F(x, \text{H})$ and $S(x, \text{H})$ against the momentum transfer variable x .
- (b) For hydrogen derive an equation for the incoherent scattering function $S(x, \text{H})$ as a function of scattering angle θ and incident photon energy E_ν . For $E_\nu = h\nu = 1$ keV calculate $S(\theta, \text{H})$ for the following scattering angles θ : 30° , 60° , 90° , 135° , and 180° . Using calculated data sketch $S(\theta, \text{H})$ against θ for the full range of θ from 0° to 180° .

SOLUTION:

(a) Atomic form factor $F(x, \text{H})$ of hydrogen was derived in Prob. 164 from first principles using the ground state wave function of hydrogen. Expressed as a function of the momentum transfer variable x , the atomic form factor of hydrogen is in (7.171) implicitly given as

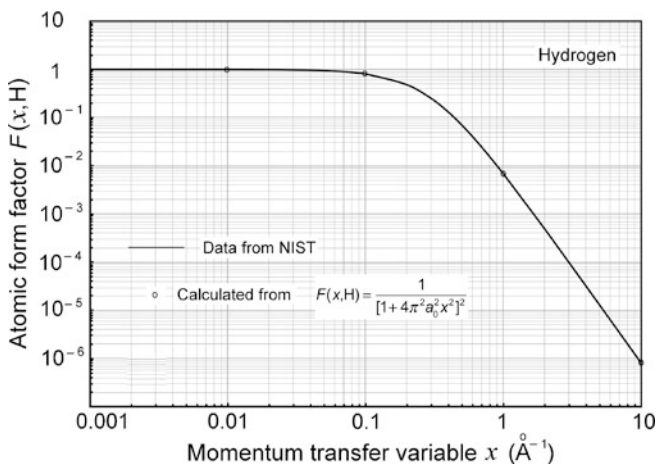
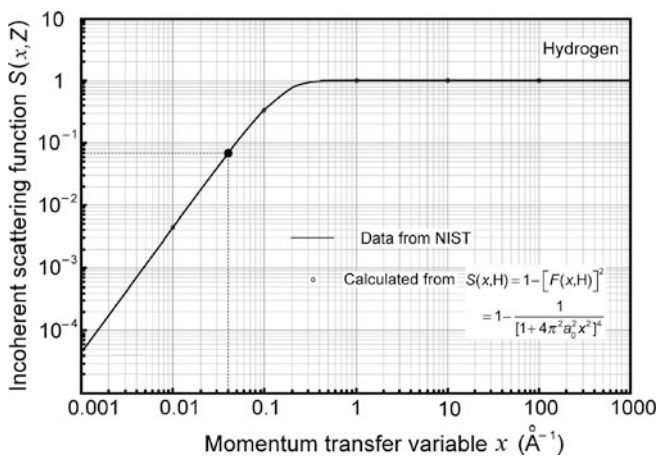
$$F(x, Z = 1) = F(x, \text{H}) = \frac{1}{(1 + 4\pi^2 a_0^2 x^2)^2}, \quad (7.172)$$

while $S(x, \text{H})$ is given as

$$S(x, \text{H}) = 1 - \frac{1}{(1 + 4\pi^2 a_0^2 x^2)^4}. \quad (7.173)$$

Table 7.7 Atomic form factor $F(x, H)$ and incoherent scattering function $S(x, H)$, both of hydrogen, against momentum transfer variable x

x (\AA^{-1})	$F(x, H)$	$S(x, H)$
0.001	1.000	4.42×10^{-5}
0.01	0.998	4.41×10^{-3}
0.1	0.811	0.343
1	6.88×10^{-3}	1.000
10	8.17×10^{-7}	1.000

**Fig. 7.20** Atomic form factor $F(x, H)$ of hydrogen against momentum transfer variable x . *Solid curves* represent data from the NIST, data points (\bullet) represent values calculated from (7.172)**Fig. 7.21** Incoherent scattering function $S(x, H)$ of hydrogen against momentum transfer variable x . *Solid curves* represent data from the NIST, data points (\bullet) represent values calculated from (7.173)

In Table 7.7 we show results of our calculation of $F(x, H)$ and $S(x, H)$ for various values of the momentum transfer variable x using (7.172) and (7.173), respectively. Our calculated data are in excellent agreement with $F(x, H)$ and $S(x, H)$ tables available from the NIST, as shown in Figs. 7.20 and 7.21, which show the NIST data with solid line curves and our calculation results with data points.

In contrast to analytic expressions available for calculation of $F(x, H)$ and $S(x, H)$ for hydrogen, no such expressions are available for multi-electron elements, and Hubbell determined $F(x, H)$ and $S(x, H)$ for all other elements ranging in Z from 2 to 100 using various assumptions, theories, and approximations. Hubbell's data are available from the NIST approaching the following limiting values for $x \rightarrow 0$ and $x \rightarrow \infty$

$$\begin{aligned} \lim_{x \rightarrow 0} F(x, Z) &= Z; & \lim_{x \rightarrow \infty} F(x, Z) &\rightarrow 0 \quad \text{and} \\ \lim_{x \rightarrow 0} S(x, Z) &= 0; & \lim_{x \rightarrow \infty} S(x, Z) &= Z. \end{aligned} \quad (7.174)$$

(b) To plot the incoherent scattering function $S(x, H)$ against scattering angle θ for a given incident photon energy $E_\nu = h\nu$ we first express the momentum transfer variable x as a function of E_ν as well as θ and then we introduce the expression for $x(E_\nu, \theta)$ into (7.173) to get $S(\theta, H)$ for a given E_ν . Momentum transfer variable x is related to E_ν and θ as follows

$$x = \frac{1}{\lambda} \sin \frac{\theta}{2} = \frac{\nu}{c} \sin \frac{\theta}{2} = \frac{h\nu}{2\pi\hbar c} \sin \frac{\theta}{2} = \frac{E_\nu}{(1239.7 \text{ MeV} \cdot \text{fm})} \sin \frac{\theta}{2}. \quad (7.175)$$

Inserting (7.175) into (7.173) results in the following expression for $S(E_\nu, \theta, H)$

$$S(x, H) = 1 - \frac{1}{[1 + 4\pi^2 a_0^2 (\frac{E_\nu \sin(\theta/2)}{1239.7 \text{ MeV} \cdot \text{fm}})^2]^4} = 1 - \frac{1}{[1 + \frac{71939.3}{(\text{MeV})^2} E_\nu^2 \sin^2 \frac{\theta}{2}]^4}. \quad (7.176)$$

In (7.176) photon energy E_ν is a parameter and inserting its given value provides information on the incoherent scattering function against scattering angle θ . Inserting $E_\nu = 1 \text{ keV}$ into (7.176) gives the following $S(\theta, H)$ as a function of θ for incident photon energy of 1 keV

$$\begin{aligned} S(\theta, H) &= 1 - \frac{1}{[1 + 71939.3 \frac{1}{(\text{MeV})^2} \times (0.001 \text{ MeV})^2 \times \sin^2 \frac{\theta}{2}]^4} \\ &= 1 - \frac{1}{[1 + 7.19393 \times 10^{-2} \times \sin^2(\theta/2)]^4}. \end{aligned} \quad (7.177)$$

Table 7.8 Incoherent scattering function $S(\theta, Z)$ of hydrogen calculated from (7.177) for various scattering angles θ and photon energy $E_\nu = 1$ keV

θ	0°	30°	60°	90°	135°	180°
$S(\theta, H)$	0	0.0190	0.0688	0.1318	0.2121	0.2426

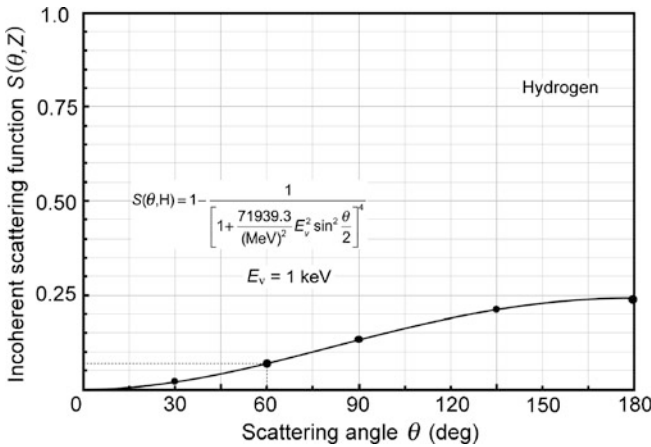


Fig. 7.22 Sketch of the incoherent scattering function $S(\theta, Z)$ against scattering angle θ for photon energy $E_\nu = 1$ keV. Data points shown with solid circles are calculated from (7.177)

We used (7.177) to calculate $S(\theta, H)$ for $h\nu = 1$ keV with various scattering angles θ and obtained results listed in Table 7.8. Next we plot the data of Table 7.8 and obtain a sketch of the incoherent scattering function $S(\theta, H)$ for photon energy $E_\nu = h\nu = 1$ keV plotted against scattering angle θ in Fig. 7.22. From (7.177) it is evident that, for a given incident photon energy E_ν , the incoherent scattering function $S(\theta, H)$ reaches its maximum value at $\theta = \pi$ and this can also be concluded from Fig. 7.22 and Table 7.8.

7.3.Q12

(166)

Compton electronic cross sections are calculated with Klein-Nishina (KN) equations valid for free electrons while the KN atomic cross sections are calculated from Compton electronic cross sections by a simple multiplication with atomic number Z of the absorber. However, at low incident photon energies the calculated KN atomic cross sections significantly exceed measured data and this discrepancy has been attributed to binding effects of electrons to the nuclei of absorber atoms.

Various methods have been developed to account for electronic binding effects and most notable of them is Hubbell's method based on the incoherent scattering function $S(x, Z)$ that expresses the Compton differential atomic cross section $d_a\sigma_C/d\Omega$ as (T7.116)

$$\frac{d_a\sigma_C}{d\Omega} = \frac{d_e\sigma_C^{\text{KN}}}{d\Omega} \times S(x, Z) = \frac{d_e\sigma_{\text{Th}}}{d\Omega} \times F_{\text{KN}} \times S(x, Z), \quad (7.178)$$

where $d_e\sigma_C^{\text{KN}}/d\Omega$ is the differential Klein-Nishina electronic cross section for Compton scattering (T7.90), $d_e\sigma_{\text{Th}}/d\Omega$ is the Thomson differential cross section for free electron, F_{KN} is the Klein-Nishina form factor, and the momentum transfer variable x is defined as $x = \sin(\theta/2)\lambda$, with λ the wavelength of the incident photon.

For hydrogen the incoherent scattering function $S(x, \text{H})$ is related to the atomic form factor $F(x, \text{H})$ through the following relationship where a_0 is the Bohr radius (0.5292 Å), as described in Prob. 164

$$S(x, \text{H}) = 1 - [F(x, \text{H})]^2 = 1 - \frac{1}{[1 + 4\pi^2 a_0^2 x^2]^4}. \quad (7.179)$$

-
- (a) Using (7.178) calculate the Compton differential atomic cross sections $d_a\sigma_C/d\Omega$ and $d_a\sigma_C/d\theta$ for photon energy $E_\nu = 1$ keV and scattering angle $\theta = 60^\circ$. Sketch the two basic components of $d_a\sigma_C/d\Omega$: (1) Thomson differential electronic cross section $d_e\sigma_{\text{Th}}/d\Omega$ and (2) Klein-Nishina form factor F_{KN} in the θ range from 0 to π and show how your calculated values for $E_\nu = 1$ keV and $\theta = 60^\circ$ fit on the graph.
- (b) Verify your results for $d_a\sigma_C/d\Omega$ and $d_a\sigma_C/d\theta$ calculated in (a) by plotting them onto $d_a\sigma_C/d\Omega$ and $d_a\sigma_C/d\theta$ graphs available for photon energy $E_\nu = 1$ keV.

SOLUTION:

Binding energy corrections to Klein-Nishina equations are treated in the impulse approximation taking into account all orbital electrons of the absorber atom. This involves applying a multiplicative correction function $S(x, Z)$ (referred to as the incoherent scattering function) to the Klein-Nishina differential atomic cross sections, as expressed in (7.178). For the one-electron atom (hydrogen) Hubbell showed that the incoherent scattering function $S(x, Z)$ is linked to the atomic form factor $F(x, Z)$ of hydrogen through (7.179).

(a) To calculate the Compton differential atomic cross section $d_a\sigma_C/d\Omega$ of hydrogen at incident photon energy $E_\nu = h\nu = 1$ keV and scattering angle $\theta = 60^\circ$ we start with (7.178)

$$\frac{d_a\sigma_C}{d\Omega} = \frac{d_e\sigma_C^{\text{KN}}}{d\Omega} \times S(x, H) = \frac{d_e\sigma_{\text{Th}}}{d\Omega} \times F_{\text{KN}}(\theta, E_\nu) \times S(\theta, E_\nu, H) \quad (7.180)$$

and introduce expressions for its three component factors:

- (1) Thomson differential electronic cross section $d_e\sigma_{\text{Th}}/d\Omega$ (T7.39).
- (2) Klein-Nishina form factor $F_{\text{KN}}(\theta, E_\nu)$ (see T7.90).
- (3) Incoherent scattering function $S(\theta, E_\nu, H)$.

To understand better the contribution of the individual factors to $d_a\sigma_C/d\Omega$ we will evaluate these factors separately and subsequently multiply them as required by (7.178) to get $d_a\sigma_C/d\Omega$ for $E_\nu = 1$ keV and $\theta = 60^\circ$.

- (1) Thomson differential electronic cross sections $d_e\sigma_{\text{Th}}/d\Omega$ and $d_e\sigma/d\theta$ for Thomson scattering on free electron are expressed as follows [(T7.39) and (T7.40)]

$$\frac{d_e\sigma_{\text{Th}}}{d\Omega} = \frac{r_e^2}{2} (1 + \cos^2 \theta) \quad \text{and} \quad \frac{d_e\sigma_{\text{Th}}}{d\theta} = \pi r_e^2 (1 + \cos^2 \theta) \sin \theta, \quad (7.181)$$

giving for our specific case of $E_\nu = 1$ keV and $\theta = 60^\circ$ the following results

$$\begin{aligned} \frac{d_e\sigma_{\text{Th}}}{d\Omega} &= \frac{r_e^2}{2} (1 + \cos^2 \theta) = \frac{(2.812 \times 10^{-13} \text{ cm})^2}{2 \text{ el} \cdot \text{sr}} \times (1 + \cos^2 60^\circ) \\ &= \frac{7.94 \times 10.26 \text{ cm}^2}{2 \text{ el} \cdot \text{sr}} \times (1.25) = 4.96 \times 10^{-26} \frac{\text{cm}^2}{\text{el} \cdot \text{sr}} = 49.6 \frac{\text{mb}}{\text{el} \cdot \text{sr}} \end{aligned} \quad (7.182)$$

and

$$\begin{aligned} \frac{d_e\sigma_{\text{Th}}}{d\theta} &= \frac{d_e\sigma_{\text{Th}}}{d\Omega} \frac{d\Omega}{d\theta} = \frac{r_e^2}{2} (1 + \cos^2 \theta) 2\pi \sin \theta \\ &= \pi \times (2.818 \times 10^{-13} \text{ cm})^2 \times (1 + \cos^2 60^\circ) \\ &\quad \times (\sin 60^\circ) / [(\text{el} \cdot \text{sr}) \times (\text{sr}/\text{rad})] \\ &= \pi \times [7.941 \times 10^{-26} \text{ cm}^2 / (\text{el} \cdot \text{rad})] \times 1.25 \times 0.886 \\ &= 2.700 \times 10^{-25} \text{ cm}^2 / (\text{el} \cdot \text{rad}) = 270 \text{ mb} / (\text{el} \cdot \text{rad}). \end{aligned} \quad (7.183)$$

Figure 7.23 depicts $d_e\sigma_{\text{Th}}/d\Omega$ for the full range of θ from 0 to π and also shows the position of $d_e\sigma_{\text{Th}}/d\Omega = 49.6 \text{ mb}/(\text{el} \cdot \text{sr})$ calculated in (7.182) for $\theta = 60^\circ$.

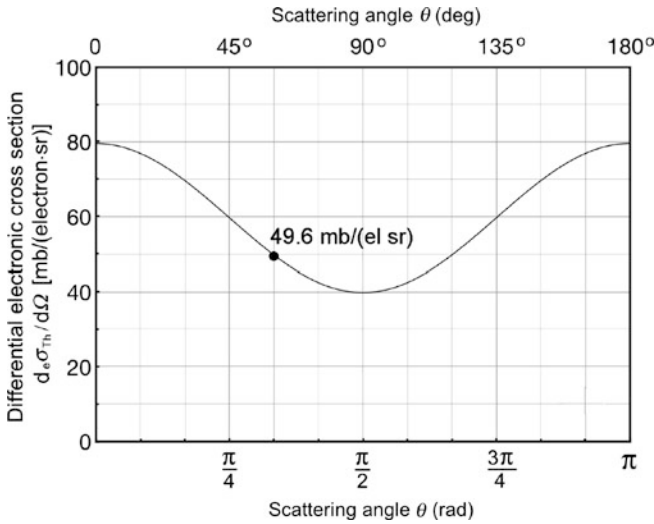


Fig. 7.23 Thomson differential electronic cross section $d_e\sigma_{Th}/d\Omega$ per unit solid angle against the scattering angle θ on the range from 0 to $\theta = \pi$ for Thomson scattering on free electron, as given in (7.181). $d_e\sigma_{Th}/d\Omega = 49.6 \text{ mb}/(\text{el} \cdot \text{sr})$, calculated in (7.182) for $\theta = 60^\circ$, is also shown on the cross section curve

(2) Klein-Nishina form factor $F_{KN}(\theta, E_\nu)$ is in general given as follows (T.7.90)

$$F_{KN} = \frac{1}{[1 + \varepsilon(1 - \cos\theta)]^2} \left\{ 1 + \frac{\varepsilon^2(1 - \cos\theta)^2}{[1 + \varepsilon(1 - \cos\theta)](1 + \cos^2\theta)} \right\} \quad (7.184)$$

and, after inserting values for our case of $E_\nu = 1 \text{ keV}$ and $\theta = 60^\circ$, we get

$$\begin{aligned} F_{KN} &= \frac{1}{[1 + 1.957 \times 10^{-3} \times (1 - \cos 60^\circ)]^2} \\ &\quad \times \left\{ 1 + \frac{(1.957 \times 10^{-3})^2 \times (1 - \cos 60^\circ)^2}{[1 + 1.957 \times 10^{-3} \times (1 - \cos 60^\circ)](1 + \cos^2 60^\circ)} \right\} \\ &= \frac{1}{[1 + 1.957 \times 10^{-3} \times 0.5]^2} \times \left\{ \frac{1 + 3.830 \times 10^{-6} \times 0.25}{[1 + 1.957 \times 10^{-3} \times 0.5] \times 1.25} \right\} \approx 0.998. \end{aligned} \quad (7.185)$$

Figure 7.24 depicts the Klein-Nishina form factor F_{KN} against the scattering angle θ for various values of the energy parameter $\varepsilon = E_\nu/(m_e c^2)$ and also shows on the graph the location of the $F_{KN} = 0.998$ point for $E_\nu = 1 \text{ keV}$ ($\varepsilon = 1/511 = 1.957 \times 10^{-3}$) and $\theta = 60^\circ$.

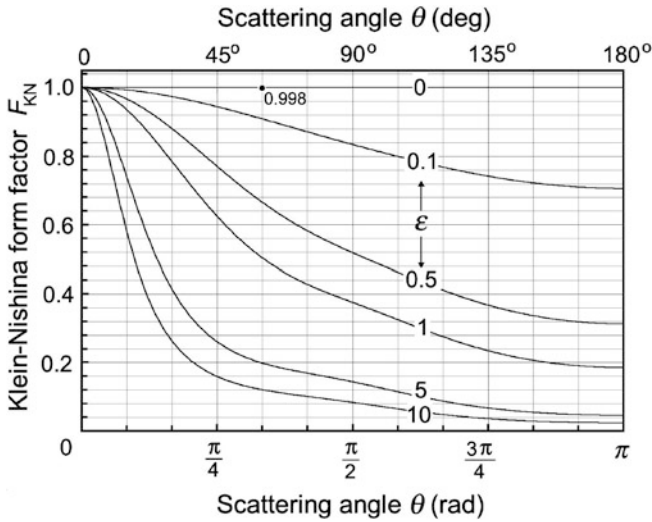


Fig. 7.24 Klein-Nishina form factor F_{KN} against scattering angle θ as per (7.184) in the range from $\theta = 0$ to $\theta = \pi$. K_{KN} determined in (7.185) for scattering angle $\theta = 60^\circ$ is indicated on the graph

- (2A) As implicitly suggested in (7.178), the Klein-Nishina differential cross section $d_e\sigma_C^{KN}/d\Omega$ is given by the following product

$$\frac{d_e\sigma_C^{KN}}{d\Omega} = \frac{d_e\sigma_{Th}}{d\Omega} \times F_{KN} = \left(49.6 \frac{\text{mb}}{\text{el} \cdot \text{sr}} \right) \times 0.998 = 49.5 \frac{\text{mb}}{\text{el} \cdot \text{sr}}. \tag{7.186}$$

- (2B) The Klein-Nishina differential cross section $d_e\sigma_C^{KN}/d\theta$ for free electron, $E_\nu = 1 \text{ keV}$, and $\theta = 60^\circ$ is now expressed as follows

$$\begin{aligned} \frac{d_e\sigma_C^{KN}}{d\theta} &= \frac{d_e\sigma_{Th}}{d\theta} \times F_{KN} = [270 \text{ mb}/(\text{el} \cdot \text{rad})] \times 0.998 \\ &= 269.5 \text{ mb}/(\text{el} \cdot \text{rad}), \end{aligned} \tag{7.187}$$

where we used $d_e\sigma_{Th}/d\theta = 270 \text{ mb}/(\text{el} \cdot \text{rad})$ of (7.183) and $F_{KN} = 0.998$ of (7.185).

- (3) To express the incoherent scattering function $S(x, H)$ as a function of scattering angle θ for a given incident photon energy $E_\nu = h\nu$ we first express the momentum transfer variable x as a function of E_ν as well as θ , and then we introduce the expression for $x(E_\nu, \theta)$ into (7.179) to get $S(\theta, H)$ for a given E_ν . The momentum transfer variable x is related to E_ν and θ as follows

$$x = \frac{1}{\lambda} \sin \frac{\theta}{2} = \frac{\nu}{c} \sin \frac{\theta}{2} = \frac{h\nu}{2\pi\hbar c} \sin \frac{\theta}{2} = \frac{E_\nu}{(1239.7 \text{ MeV} \cdot \text{fm})} \sin \frac{\theta}{2}. \tag{7.188}$$

Inserting (7.183) into (7.179) results in the following expression for $S(E_\nu, \theta, H)$

$$S(x, H) = 1 - \frac{1}{[1 + 4\pi^2 a_0^2 (\frac{E_\nu \sin(\theta/2)}{1239.7 \text{ MeV}\cdot\text{fm}})^2]^4} = 1 - \frac{1}{[1 + \frac{71939.3}{(\text{MeV})^2} E_\nu^2 \sin^2 \frac{\theta}{2}]^4}. \quad (7.189)$$

The incoherent scattering function $S(x, H)$ for incident photon energy $E_\nu = 1$ keV and scattering angle $\theta = 60^\circ$ is calculated from (7.189) as follows:

$$\begin{aligned} S(60^\circ, H) &= 1 - \frac{1}{[1 + 7.19393 \times 10^{-2} \times \sin^2(30^\circ)]^4} \\ &= 1 - \frac{1}{(1 + 7.19393 \times 10^{-2} \times 0.25)^4} \\ &= 1 - \frac{1}{(1.01798)^4} = 1 - \frac{1}{1.0739} = 0.0688. \end{aligned} \quad (7.190)$$

Combining the results of (7.182), (7.185), and (7.190) we now get the Compton atomic differential cross sections $d_a\sigma_C/d\Omega$ and $d_a\sigma_C/d\theta$ for photon energy $E_\nu = 1$ keV and scattering angle $\theta = 60^\circ$ as follows

$$\begin{aligned} \frac{d_a\sigma_C}{d\Omega} &= \frac{d_a\sigma_{\text{Th}}}{d\Omega} \times F_{\text{KN}} \times S(x, H) \\ &= \left(49.6 \frac{\text{mb}}{\text{el} \cdot \text{sr}}\right) \times 0.998 \times 0.0688 \frac{\text{el}}{\text{atom}} = 3.41 \frac{\text{mb}}{\text{atom} \cdot \text{sr}} \end{aligned} \quad (7.191)$$

and

$$\frac{d_a\sigma_C}{d\theta} = \frac{d_a\sigma_C}{d\Omega} 2\pi \sin \theta = 3.41 \frac{\text{mb}}{\text{el} \cdot \text{sr}} \times 2\pi \times \sin 60^\circ \left(\frac{\text{sr}}{\text{rad}}\right) = 18.6 \text{ mb}/(\text{el} \cdot \text{rad}). \quad (7.192)$$

(d) Figure 7.25 depicts two differential cross sections plotted per unit solid angle Ω against scattering angle θ for incident photon energy $E_\nu = h\nu = 1$ keV. The upper curve represents the Klein-Nishina differential electronic cross section $d_e\sigma_C^{\text{KN}}/d\Omega$ for free electron and the lower curve is for the Compton differential atomic cross section $d_a\sigma_C/d\Omega$ of hydrogen. The two data points show results of our calculations for scattering angle $\theta = 60^\circ$: $d_e\sigma_C^{\text{KN}}/d\Omega = 49.5 \text{ mb}/(\text{el} \cdot \text{sr})$ given in (7.186) and $d_a\sigma_C/d\Omega = 3.41 \text{ mb}/(\text{atom} \cdot \text{sr})$ given in (7.191).

Figure 7.26 depicts two differential cross sections plotted per unit scattering angle θ against scattering angle θ for incident photon energy $E_\nu = 1$ keV. The upper curve represents the differential Klein-Nishina electronic cross section $d_e\sigma_C^{\text{KN}}/d\theta$ for free electron and the lower curve is for the differential Compton atomic cross section $d_a\sigma_C/d\theta$ for hydrogen. The two data points show our results for scattering angle $\theta = 60^\circ$: $d_e\sigma_C^{\text{KN}}/d\theta = 269.5 \text{ mb}/(\text{el} \cdot \text{rad})$ calculated in (7.187) and $d_a\sigma_C/d\theta = 18.6 \text{ mb}/(\text{atom} \cdot \text{rad})$ calculated in (7.192).

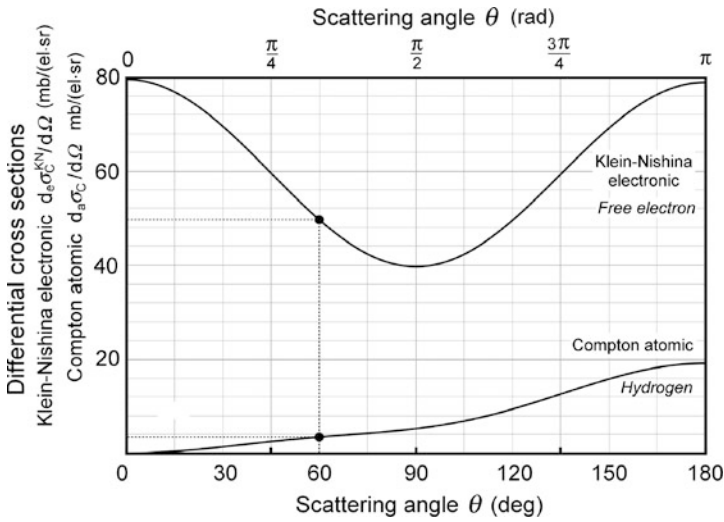


Fig. 7.25 Differential cross section per unit solid angle plotted against scattering angle θ for incident photon energy $E_\nu = h\nu = 1$ keV. The *upper curve* represents Klein-Nishina differential electronic cross section $d_e\sigma_C^{KN}/d\Omega$ of free electron; the *lower curve* represents differential atomic cross section $d_a\sigma_C/d\Omega$ of hydrogen. The two data points are results of our calculations presented in (7.186) and (7.191), respectively

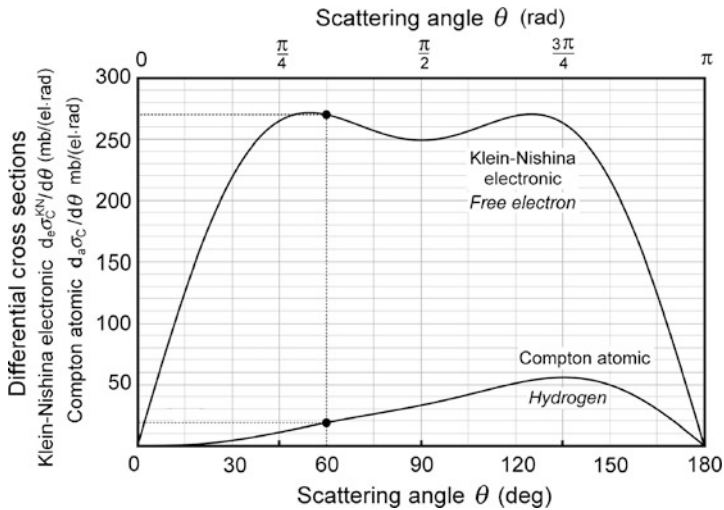


Fig. 7.26 Differential cross section per unit solid angle plotted against scattering angle θ for incident photon energy $E_\nu = h\nu = 1$ keV. The *upper curve* represents Klein-Nishina differential electronic cross section $d_e\sigma_C^{KN}/d\theta$ of free electron; the *lower curve* represents differential atomic cross section $d_a\sigma_C/d\theta$ of hydrogen. The two data points are results of our calculations presented in (7.187) and (7.192), respectively

7.4 Incoherent (Rayleigh) Scattering

7.4.Q1

(167)

Much of the early information on composition and structure of atoms was derived from experiments based on scattering of photons on atoms and two broad categories of photon scattering on atoms were developed: coherent and incoherent. In coherent scattering the energy of the scattered photon $h\nu'$ is equal to the incident photon energy $h\nu$; consequently, coherent scattering can also be called elastic scattering. In incoherent scattering $h\nu$ exceeds $h\nu'$; consequently, incoherent scattering can also be referred to as inelastic scattering.

Both, the coherent and incoherent scattering, are characterized by scattering angle θ and momentum transfer $|\Delta\mathbf{p}| = \Delta p$ from the incident photon with momentum $|\mathbf{p}| = p$ to the scattering center S. Momentum transfer is thus the vector difference between momentum \mathbf{p} of the incident photon and momentum \mathbf{p}' of the scattered photon, i.e., $\Delta\mathbf{p} = \mathbf{p} - \mathbf{p}'$.

- (a) Show that momentum transfer Δp in coherent photon scattering can be expressed as

$$\Delta p = |\Delta\mathbf{p}| = 2\frac{h\nu}{c} \sin\frac{\theta}{2} = 2hx. \quad (7.193)$$

- (b) Show that momentum transfer Δp in incoherent photon scattering can be expressed as

$$\begin{aligned} \Delta p = |\Delta\mathbf{p}| &= \left[2\frac{h\nu}{c} \sin\frac{\theta}{2} \right] \frac{\sqrt{1 + (\varepsilon^2 + \varepsilon) \sin^2\frac{\theta}{2}}}{1 + 2\varepsilon \sin^2\frac{\theta}{2}} \\ &= 2hx \frac{\sqrt{1 + (\varepsilon^2 + \varepsilon) \sin^2\frac{\theta}{2}}}{1 + 2\varepsilon \sin^2\frac{\theta}{2}}. \end{aligned} \quad (7.194)$$

In (7.193) and (7.194)

$h\nu$ is the incident photon energy with h the Planck constant and ν photon frequency.

c is the speed of light in vacuum ($c \approx 3 \times 10^8$) m/s.

θ is the scattering angle.

ε is incident photon energy normalized to rest energy of electron ($m_e c^2 = 0.511$ MeV).

x is momentum transfer variable defined as

$$x = \frac{1}{\lambda} \sin \frac{\theta}{2}, \quad (7.195)$$

where λ is the wavelength of the incident photon ($\lambda = c/\nu$).

- (c) A photon with energy $h\nu = 20$ keV undergoes Rayleigh scattering on a carbon atom. Scattering angle θ is 20° . Calculate the momentum transfer variable x , momentum transfer Δp , and recoil energy $(E_K)_T$ transferred from the photon to the carbon atom.

SOLUTION:

Photon scattering on a scattering center S is depicted in Fig. 7.27 for both the coherent scattering in (A) and (B) and for incoherent scattering in (C). Initial photon momentum (momentum of the incident photon) is \mathbf{p} (vector quantity with magnitude $|\Delta\mathbf{p}| = p$), final photon momentum (momentum of the scattered photon) is \mathbf{p}' (vector quantity with magnitude $|\Delta\mathbf{p}'| = p'$). The angle between \mathbf{p} and \mathbf{p}' is the scattering angle θ ranging from $\theta = 0$ (forward scattering) through $\theta = 90^\circ$ (side scattering) to $\theta = 180^\circ$ (backscattering). Photon momentum p_ν is related to photon energy $E_\nu \equiv h\nu$ through the following well-known expression (T1.76)

$$p_\nu = \frac{E_\nu}{c} = \frac{h\nu}{c} = \frac{h}{\lambda}. \quad (7.196)$$

(a) In coherent scattering where $p = p'$ the momentum vectors form an isosceles triangle (i.e., triangle in which two sides are equal in length). The scattering center S is located at the triangle vertex formed by the two equal-length sides of the triangle ($|\mathbf{p}| = |\mathbf{p}'|$). The triangle altitude through this vertex is perpendicular to the base of the triangle ($|\Delta\mathbf{p}|$) and coincides with the scattering angle bisector cutting the momentum triangle into two equal rectangular triangles, as shown in Fig. 7.27(A). The two angles opposite to the scattering angle θ are equal to one another.

For the shaded right-angled triangle of Fig. 7.27(A) we can now state the following simple trigonometric relationship connecting $\frac{1}{2}\theta$ and $\frac{1}{2}\Delta p$

$$\sin \frac{\theta}{2} = \frac{\Delta p}{2p} \quad \text{or} \quad \Delta p = 2p \sin \frac{\theta}{2} = 2 \frac{h\nu}{c} \sin \frac{\theta}{2} = 2 \frac{h}{\lambda} \sin \frac{\theta}{2} = 2hx, \quad (7.197)$$

showing that the momentum transfer Δp is proportional to the momentum transfer variable x defined in (7.195) which depends upon photon energy $h\nu$ and scattering angle θ .

Momentum transfer expression (7.197) can also be derived directly from the shaded momentum triangle depicted in Fig. 7.27(B) using the law of cosines on the shaded triangle defined by the three vector momenta: \mathbf{p} , \mathbf{p}' , and $\Delta\mathbf{p}$ as follows

$$(\Delta p)^2 = p^2 + (p')^2 - 2pp' \cos \theta. \quad (7.198)$$

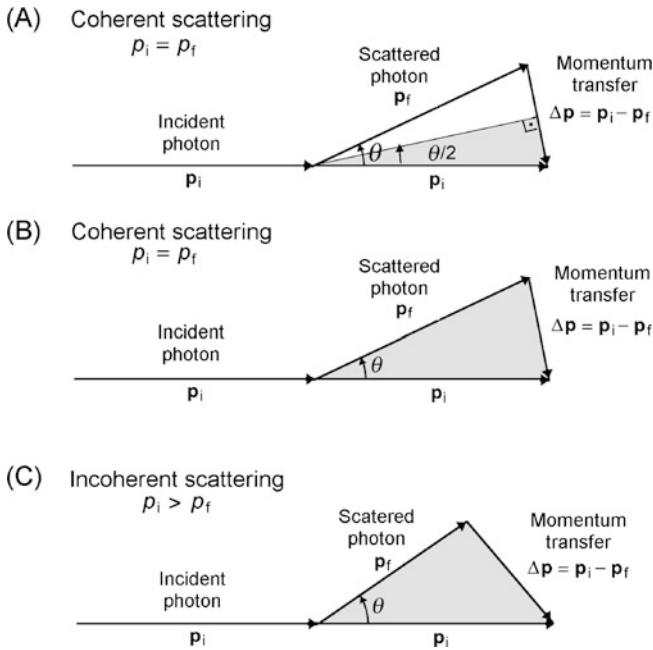


Fig. 7.27 Momentum diagram for photon scattering on scattering center S. (A) and (B) represents coherent scattering, (C) represents incoherent scattering

Since in coherent scattering $p = p'$, we simplify (7.198) to read

$$\Delta p = \sqrt{2p^2(1 - \cos\theta)} = \sqrt{4p^2 \sin^2 \frac{\theta}{2}} = 2p \sin \frac{\theta}{2} = 2 \frac{h\nu}{c} \sin \frac{\theta}{2} = 2 \frac{h}{\lambda} \sin \frac{\theta}{2} = 2hx, \tag{7.199}$$

in perfect agreement with (7.197).

(b) In incoherent scattering the photon not only changes direction of motion, it also loses some of its energy, resulting in $p > p'$. All sides of the momentum triangle in this situation are unequal (scalene triangle) and the three angles are also unequal. To derive the momentum transfer Δp for incoherent scattering we now apply the law of cosines on the shaded triangle of Fig. 7.27(C) and get an expression identical to (7.198) linking magnitudes of the three momenta \mathbf{p} , \mathbf{p}' and $\Delta \mathbf{p}$. However, since $p \neq p'$, the derivation of Δp is significantly more complicated for incoherent scattering than it was for coherent scattering in (a).

Introducing (7.196) into (7.198) we start the derivation of Δp for incoherent scattering with the following expression

$$c^2(\Delta p)^2 = (h\nu)^2 + (h\nu')^2 - 2(h\nu)(h\nu') \cos\theta. \tag{7.200}$$

Recalling the relationship between incident photon energy $h\nu$ and scattered photon energy $h\nu'$ that applies for incoherent (Compton) scattering (T7.71)

$$h\nu' = h\nu \frac{1}{1 + \varepsilon(1 - \cos\theta)} = h\nu \frac{1}{1 + 2\varepsilon \sin^2 \frac{\theta}{2}} \quad (7.201)$$

and inserting (7.201) into (7.200) we now get

$$\begin{aligned} c^2(\Delta p)^2 &= 2(h\nu)^2 \left\{ \frac{1 + 2\varepsilon \sin^2 \frac{\theta}{2} + 2\varepsilon^2 \sin^4 \frac{\theta}{2} - \cos\theta - 2\varepsilon \cos\theta \sin^2 \frac{\theta}{2}}{[1 + 2\varepsilon \sin^2 \frac{\theta}{2}]^2} \right\} \\ &= 2(h\nu)^2 \left\{ \frac{2\varepsilon \sin^2 \frac{\theta}{2} + 2\varepsilon^2 \sin^4 \frac{\theta}{2} + 2 \sin^2 \frac{\theta}{2} - 2\varepsilon \sin^2 \frac{\theta}{2} + 4\varepsilon \sin^4 \frac{\theta}{2}}{[1 + 2\varepsilon \sin^2 \frac{\theta}{2}]^2} \right\} \\ &= 4(h\nu)^2 \left\{ \frac{(\varepsilon^2 + 2\varepsilon) \sin^4 \frac{\theta}{2} + \sin^2 \frac{\theta}{2}}{[1 + 2\varepsilon \sin^2 \frac{\theta}{2}]^2} \right\} \\ &= 4(h\nu)^2 \left(\sin^2 \frac{\theta}{2} \right) \frac{[1 + (\varepsilon^2 + 2\varepsilon) \sin^2 \frac{\theta}{2}]}{[1 + 2\varepsilon \sin^2 \frac{\theta}{2}]^2}. \end{aligned} \quad (7.202)$$

Momentum transfer Δp in incoherent scattering is from (7.202) expressed as

$$\Delta p = 2 \left(\frac{h\nu}{c} \sin \frac{\theta}{2} \right) \frac{\sqrt{1 + (\varepsilon^2 + 2\varepsilon) \sin^2 \frac{\theta}{2}}}{1 + 2\varepsilon \sin^2 \frac{\theta}{2}} = 2h\nu \frac{\sqrt{1 + (\varepsilon^2 + 2\varepsilon) \sin^2 \frac{\theta}{2}}}{1 + 2\varepsilon \sin^2 \frac{\theta}{2}}, \quad (7.203)$$

where x again is the momentum transfer variable and ε is the incident photon energy $h\nu$ normalized to the electron rest energy $m_e c^2 = 0.511$ MeV.

(c) Momentum transfer variable x is calculated from (7.195) and (7.197) as follows

$$x = \frac{1}{\lambda} \sin \frac{\theta}{2} = \frac{h\nu}{2\pi \hbar c} \sin \frac{\theta}{2} = \frac{(20 \text{ keV})}{2\pi \times (1.973 \text{ keV} \cdot \text{\AA})} \sin \frac{10^\circ}{2} = 0.141 \text{ \AA}^{-1}. \quad (7.204)$$

Momentum transfer Δp to carbon atom for $x = 0.141 \text{ \AA}^{-1}$ is from (7.199)

$$\Delta p = 2hx = \frac{4\pi \hbar c x}{c} = \frac{4\pi (1.973 \text{ keV} \cdot \text{\AA}) \times (0.141 \text{ \AA}^{-1})}{c} = 3.49 \text{ keV}. \quad (7.205)$$

Energy transfer $(E_K)_{\text{tr}}$ to carbon atom for $\Delta p = 3.49 \times 10^3 \text{ eV}/c$ is calculated as

$$(E_K)_{\text{tr}} = \frac{(\Delta p)^2}{2M_C} = \frac{c^2(\Delta p)^2}{2M_C c^2} = \frac{(3.49 \times 10^3 \text{ eV})^2}{2 \times (11.175 \times 10^9 \text{ eV})} = 5.45 \times 10^{-4} \text{ eV}. \quad (7.206)$$

Energy transfer to carbon atom in a typical Rayleigh scattering event is exceedingly small and negligible, allowing us to label coherent scattering as elastic scattering.

7.4.Q2

(168)

Rayleigh differential atomic cross section $d_a\sigma_R/d\Omega$ per unit solid angle is given as (T7.127)

$$\frac{d_a\sigma_R}{d\Omega} = \frac{d_e\sigma_{Th}}{d\Omega} [F(x, Z)]^2 = \frac{r_e^2}{2} (1 + \cos^2\theta) [F(x, Z)]^2, \quad (7.207)$$

where $d_e\sigma_{Th}/d\Omega$ is the Thomson differential electronic cross section, r_e is the so-called classical radius of the electron, and $F(x, Z)$ is the atomic form factor which is a function of atomic number Z and momentum transfer variable x defined as $x = \sin(\theta/2)/\lambda$.

- (a) Derive and sketch an expression for the momentum transfer function $\chi = x/E_\nu$ as a function of the scattering angle θ .
- (b) Calculate the momentum transfer variable x for scattering angle $\theta = 60^\circ$ and incident photon energy of $E_\nu = h\nu = 1$ keV.
- (c) Using result of (b) and atomic form factor table from the NIST, determine atomic form factor $F(x, Z)$ of carbon for photon energy $E_\nu = 1$ keV and scattering angle $\theta = 60^\circ$.
- (d) Using (7.207) and the results from part (c) calculate the Rayleigh differential atomic cross sections $d_a\sigma_R/d\Omega$ and $d_a\sigma_R/d\theta$ of carbon for photon energy $h\nu = 1$ keV and scattering angle of $\theta = 60^\circ$.
- (e) Using same method as in (d) determine $d_a\sigma_R/d\Omega$ and $d_a\sigma_R/d\theta$ for photons of energy $E_\nu = 1$ keV scattered at $\theta = 0$ (forward scattering) and $\theta = \pi$ (backscattering).
- (f) Verify your results calculated in (d) and (e) by entering them onto $d_a\sigma_R/d\Omega$ and $d_a\sigma_R/d\theta$ graphs given in Figs. 7.30 and 7.31, respectively, for Rayleigh scattering of $E_\nu = 1$ keV photons in a carbon absorber.

SOLUTION:

(a) The momentum transfer variable x is a function of the scattering angle θ as well as the wavelength λ of the incident photon and is defined as (T7.120)

$$x = \frac{\sin(\theta/2)}{\lambda} = \frac{\nu \sin(\theta/2)}{c} = \frac{h\nu \sin(\theta/2)}{2\pi\hbar c} = \frac{E_\nu \sin(\theta/2)}{1239.7 \text{ MeV} \cdot \text{fm}}, \quad (7.208)$$

where $E_\nu = h\nu$ is incident photon energy, h is Planck constant, and c is the speed of light. In (7.208) we used the standard relationship between photon wavelength λ and energy E_ν

$$E_\nu = h\nu = \frac{hc}{\lambda} = \frac{2\pi\hbar c}{\lambda} = \frac{2\pi \times (197.3 \text{ MeV} \cdot \text{fm})}{\lambda} = \frac{1239.7 \text{ MeV} \cdot \text{fm}}{\lambda}. \quad (7.209)$$

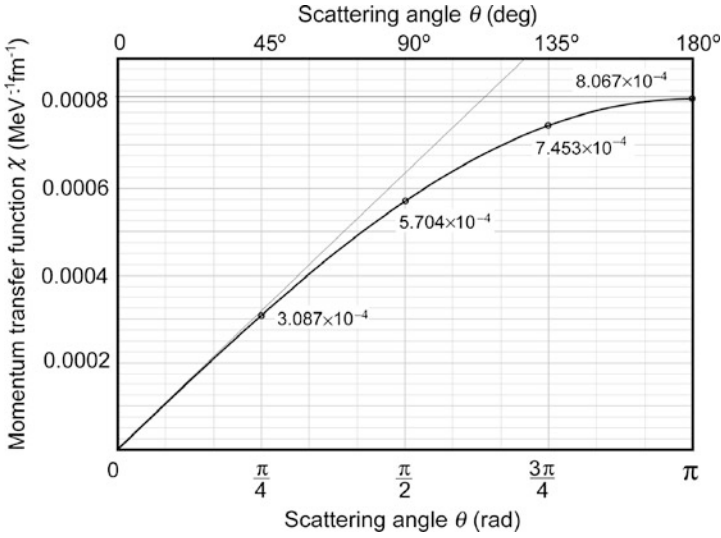


Fig. 7.28 Momentum transfer function χ against scattering angle θ from $\theta = 0$ to $\theta = \pi$

We now write (7.208) in the form x/E_ν to remove the dependence on photon energy E_ν and get the energy-independent momentum transfer function χ

$$\chi = \frac{x}{E_\nu} = \frac{\sin(\theta/2)}{1239.7 \text{ MeV} \cdot \text{fm}} = (8.067 \times 10^{-4} \text{ MeV}^{-1} \cdot \text{fm}^{-1}) \sin \frac{\theta}{2} = C \sin \frac{\theta}{2}, \quad (7.210)$$

where C is a constant equal to $(2\pi \hbar c)^{-1} = 8.067 \times 10^{-4} \text{ MeV}^{-1} \cdot \text{fm}^{-1}$.

Function χ depends on scattering angle θ only and is depicted in Fig. 7.28 in the full scattering angle θ range from 0 to π . It is a simple trigonometric function exhibiting the following two notable properties:

- (1) For small scattering angles θ , it increases linearly with θ as $\chi = \frac{1}{2}C\theta$.
- (2) At large angles where ($\theta \rightarrow \pi$), it saturates at a constant $\bar{C} = 8.067 \times 10^{-4} \text{ MeV}^{-1} \cdot \text{fm}^{-1}$.

From (7.210) we note that the momentum transfer variable x is a linear function of the photon energy $E_\nu = h\nu$ with the slope of the linear function given by the value of the momentum transfer function χ at a given scattering angle θ .

(b) To calculate the momentum transfer variable x for scattering angle $\theta = 60^\circ$ and incident photon energy $E_\nu = 1 \text{ keV}$, we first determine the momentum transfer function χ at $\theta = 60^\circ$ from (7.210) or Fig. 7.28 and obtain $\chi = 0.0004 \text{ MeV}^{-1} \cdot \text{fm}^{-1}$.

Table 7.9 Atomic form factor $F(x, Z)$ of carbon against momentum transfer variable x

x (\AA^{-1})	$F(x, 6)$	x (\AA^{-1})	$F(x, 6)$	x (\AA^{-1})	$F(x, 6)$
0	6.0000	0.2	3.5775	3.5	8.0432×10^{-2}
0.005	5.9974	0.25	2.9614	4	5.2230×10^{-2}
0.01	5.9898	0.3	2.5015	5	2.4330×10^{-2}
0.015	5.9771	0.4	1.9512	6	1.2650×10^{-2}
0.02	5.9594	0.5	1.6856	7	7.1471×10^{-2}
0.025	5.9369	0.6	1.5353	8	4.3194×10^{-3}
0.03	5.9093	0.7	1.4245	10	1.8363×10^{-3}
0.04	5.8406	0.8	1.3206	15	3.7767×10^{-4}
0.05	5.7544	0.9	1.2165	20	1.2157×10^{-4}
0.07	5.5369	1	1.1121	50	3.2386×10^{-6}
0.09	5.2702	1.25	0.86482	80	5.0734×10^{-7}
0.1	5.1225	1.5	0.65662	100	2.1123×10^{-7}
0.125	4.7407	2	0.37202	1000	3.5964×10^{-11}
0.15	4.3310	2.5	0.21455	1.0×10^6	1.6609×10^{-20}
0.175	3.9371	3	0.12832	1.0×10^9	1.6810×10^{-29}

Next, we determine the momentum transfer variable x from (7.210) as

$$\begin{aligned}
 x \left(1 \text{ keV}, \frac{1}{3} \pi \right) &= \chi \left(\frac{1}{3} \pi \right) E_\nu = (0.0004 \text{ MeV}^{-1} \cdot \text{fm}^{-1}) \times (0.001 \text{ MeV}) \\
 &= 4 \times 10^{-7} \text{ fm}^{-1} = 0.04 \text{ \AA}^{-1}.
 \end{aligned} \tag{7.211}$$

(c) Atomic form factors $F(x, Z)$ for elements from $Z = 1$ to $Z = 92$ as a function of the momentum transfer variable x , tabulated by Hubbell, are available from the NIST and cover a range of values of x from 0 all the way to 10^9 \AA^{-1} . In Table 7.9 we present Hubbell's NIST data for the atomic form factor of carbon and for the entry of $x = 0.04 \text{ \AA}^{-1}$ obtain a form factor of $F(x = 0.04 \text{ \AA}^{-1}, Z = 6) = 5.8406$ (shown in bold face in the table). Of course, if the exact x is not found in the form factor table, one can resort to a linear interpolation of appropriate entries found in the table.

(d) Rayleigh atomic differential cross section $d_a \sigma_R / d\Omega$ is given by (7.207) and contains two components: Thomson differential electronic cross section $d_e \sigma_{\text{Th}} / d\Omega$ multiplied by the square of the atomic form factor $F(x, Z)$. To determine $d_a \sigma_R / d\Omega$ of carbon at $\theta = 60^\circ$ and $E_\nu = 1 \text{ keV}$ we must first calculate $d_e \sigma_{\text{Th}} / d\Omega$ and determine $F(x, Z)$ for the two parameters θ and E_ν , and then use (7.207). The form factor $F(x, Z)$ was determined from the NIST tables in (c).

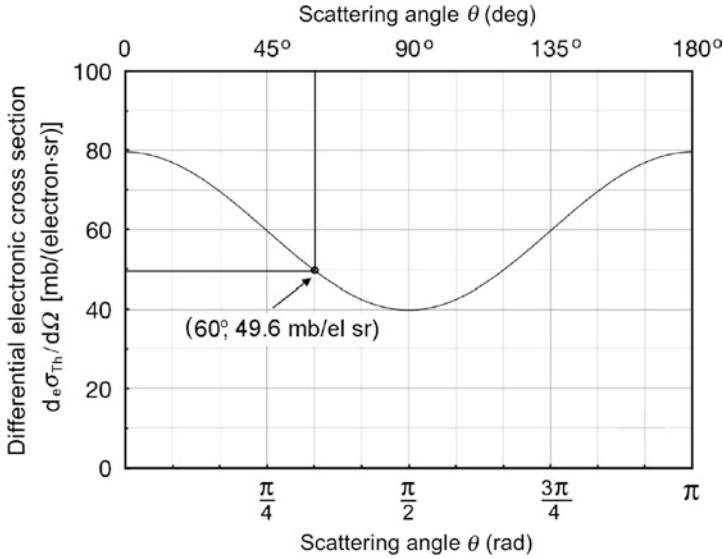


Fig. 7.29 Differential electronic cross section $d_e\sigma_{\text{Th}}/d\Omega$ per unit solid angle against the scattering angle θ for Thomson scattering on free electron. $d_e\sigma_{\text{Th}}/d\Omega$ calculated in (7.212) for scattering angle $\theta = 60^\circ$ is shown as measured point on the cross section curve

The Thomson cross section $d_e\sigma_{\text{Th}}/d\Omega$ for $\theta = 60^\circ$ is calculated as follows

$$\begin{aligned} \frac{d_e\sigma_{\text{Th}}}{d\Omega} &= \frac{r_e^2}{2} (1 + \cos^2 \theta) = \frac{(2.818 \times 10^{-13} \text{ cm})^2}{2 \text{ el} \cdot \text{sr}} \times (1 + \cos^2 60^\circ) \\ &= \frac{7.94 \times 10^{-26} \text{ cm}^2}{2 \text{ el} \cdot \text{sr}} \times (1.25) = 4.96 \times 10^{-26} \frac{\text{cm}^2}{\text{el} \cdot \text{sr}} = 49.6 \frac{\text{mb}}{\text{el} \cdot \text{sr}} \quad (7.212) \end{aligned}$$

and shown in Fig. 7.29 in the full scattering angle range from $\theta = 0$ to $\theta = \pi$.

Equation (7.207) now yields the following result for the Rayleigh differential atomic cross section $d_a\sigma_{\text{R}}/d\Omega$ for photon of energy $E_\nu = h\nu = 1 \text{ keV}$, scattered at $\theta = 60^\circ$

$$\frac{d_a\sigma_{\text{R}}}{d\Omega} = \frac{d_e\sigma_{\text{Th}}}{d\Omega} [F(x, Z)]^2 = \left(49.6 \times 10^{-3} \frac{\text{b}}{\text{at} \cdot \text{sr}} \right) \times (5.8406)^2 = 1.692 \frac{\text{b}}{\text{at} \cdot \text{sr}} \quad (7.213)$$

Atomic Rayleigh differential cross section $d_a\sigma_{\text{R}}/d\Omega$ at $E_\nu = h\nu = 1 \text{ keV}$ and $\theta = 60^\circ$ is calculated as follows

$$\begin{aligned} \frac{d_a\sigma_{\text{R}}}{d\theta} &= \frac{d_a\sigma_{\text{R}}}{d\Omega} \frac{d\Omega}{d\theta} = \frac{d_a\sigma_{\text{R}}}{d\Omega} 2\pi \sin \theta \\ &= \left(1.692 \frac{\text{b}}{\text{atom} \cdot \text{sr}} \right) \times 2\pi \sin(60^\circ) \frac{\text{sr}}{\text{rad}} = 9.207 \frac{\text{b}}{\text{atom} \cdot \text{rad}} \quad (7.214) \end{aligned}$$

(e) We now use the same method as in (d) and calculate $d_a\sigma_R/d\Omega$ and $d_a\sigma_R/d\theta$ for photons of energy $E_\nu = 1$ keV scattered at $\theta = 0$ and $\theta = \pi$.

(1) Let us first look at $\theta = \pi$. The momentum transfer function χ is determined as follows

$$\begin{aligned}\chi &= C \sin \frac{\theta}{2} = (8.067 \times 10^{-4} \text{ MeV}^{-1} \cdot \text{fm}^{-1}) \times \sin \frac{\pi}{2} \\ &= 8.067 \times 10^{-4} \text{ MeV}^{-1} \cdot \text{fm}^{-1}.\end{aligned}\quad (7.215)$$

The momentum transfer variable x at $E_\nu = 1$ keV and $\theta = \pi$ is given as

$$x = E_\nu \chi = (10^{-3} \text{ MeV}) \times (8.067 \times 10^{-4} \text{ MeV}^{-1} \cdot \text{fm}^{-1}) = 0.08067 \text{ \AA}^{-1}.\quad (7.216)$$

A linear interpolation of entries for $x = 0.07 \text{ \AA}^{-1}$ and $x = 0.09 \text{ \AA}^{-1}$ in Table 7.9 yields the following atomic form factor $F(x = 0.08067 \text{ \AA}^{-1}, Z = 6) = 5.3946$ for carbon at $h\nu = 1$ keV and $\theta = \pi$. Insertion of this form factor into (7.207) gives the following result for $d_a\sigma_R/d\Omega$

$$\begin{aligned}\frac{d_a\sigma_R}{d\Omega} &= \frac{d_e\sigma_{\text{Th}}}{d\Omega} [F(x, Z)]^2 = \left(79.4 \times 10^{-3} \frac{\text{b}}{\text{atom} \cdot \text{sr}} \right) \times (5.3946)^2 \\ &= 2.311 \frac{\text{b}}{\text{atom} \cdot \text{sr}}.\end{aligned}\quad (7.217)$$

Similarly, for $d_a\sigma_R/d\theta$ we get from (7.214)

$$\frac{d_a\sigma_R}{d\theta} = \frac{d_a\sigma_R}{d\Omega} \frac{d\Omega}{d\theta} = \frac{d_a\sigma_R}{d\Omega} 2\pi \sin \theta = \left(2.311 \frac{\text{b}}{\text{atom} \cdot \text{sr}} \right) \times 2\pi \sin \pi = 0.\quad (7.218)$$

(2) At $\theta = 0$ the momentum transfer function χ as well as the momentum transfer variable are both equal to zero and $d_a\sigma_R/d\Omega = 2.858 \text{ b}/(\text{atom} \cdot \text{sr})$, exactly $36r_c^2 \text{ b}/(\text{atom} \cdot \text{sr})$ or $Z^2 d_e\sigma_{\text{Th}}(\theta = 0)/d\Omega$. This follows from $F(x = 0, Z) = Z$ valid at all photon energies E_ν and atomic numbers Z . Just like for $\theta = 180^\circ$ in (7.218), at $\theta = 0$ the differential cross section $d_a\sigma_R/d\theta = 0$.

(f) Figures 7.30 and 7.31 depict $d_a\sigma_R/d\Omega$ and $d_a\sigma_R/d\theta$, respectively, against scattering angle θ for $h\nu = 1$ keV in the full range of θ from $\theta = 0$ to $\theta = \pi$. Cross sections calculated for $\theta = 60^\circ$ in (d) as well as for $\theta = 0$ and $\theta = \pi$ in (e) are clearly shown as data points on the graphs and agree well with the curves plotted in the two figures. Differential atomic Rayleigh cross sections $d_a\sigma_R/d\Omega$ and $d_a\sigma_R/d\theta$ of carbon calculated for scattering angles θ of 0° , 60° , and 180° in (d) and (e) are summarized in Table 7.10.

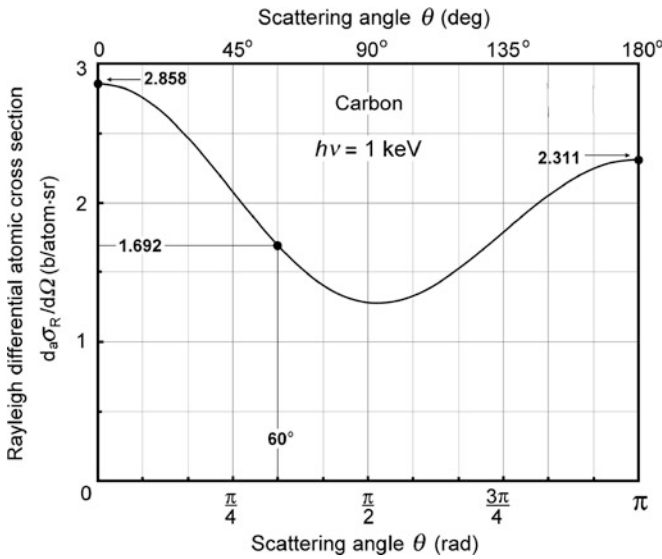


Fig. 7.30 Rayleigh differential atomic cross section of carbon $d_a\sigma_R/d\Omega$ per unit solid angle against the scattering angle θ for Rayleigh scattering of photon with energy $h\nu = 1 \text{ keV}$. Data points correspond to results from calculations in (d) for $\theta = 60^\circ$ and in (e) for $\theta = 0$ as well as $\theta = \pi$

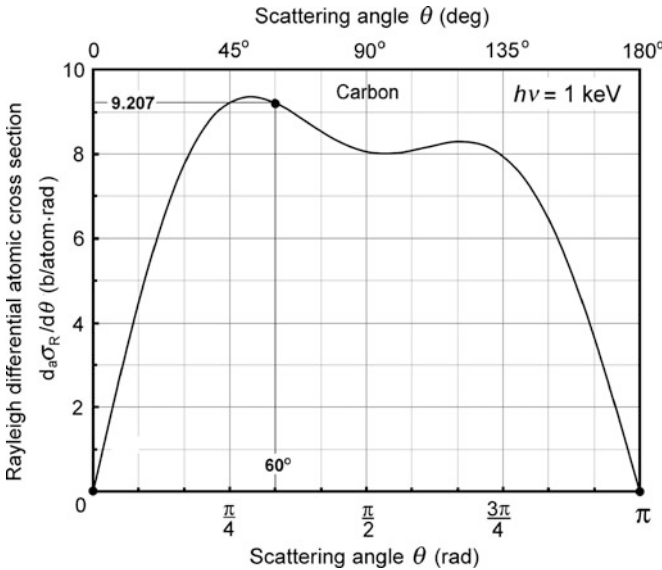


Fig. 7.31 Rayleigh differential atomic cross section of carbon $d_a\sigma_R/d\Omega$ per unit scattering angle against the scattering angle θ for Rayleigh scattering of photon with energy $h\nu = 1 \text{ keV}$. Data points correspond to results from calculations in (d) for $\theta = 60^\circ$ and in (e) for $\theta = 0$ as well as $\theta = \pi$

Table 7.10 Summary of differential atomic Rayleigh cross sections of carbon calculated in (d) and (e) for photons of energy of 1 keV

Scattering angle θ degrees	Differential cross section $d_a\sigma_R/d\Omega$ b/(atom sr)	Differential cross section $d_a\sigma_R/d\theta$ b/(atom rad)
0	2.858	0
60	1.692	9.207
180	2.311	0

7.5 Photoelectric Effect

7.5.Q1

(169)

Photoelectric (PE) effect is the term used to describe an interaction between a photon of energy $h\nu$ and a tightly bound orbital electron of an absorber atom. In the interaction the photon is absorbed completely and an orbital electron is ejected as photoelectron with kinetic energy E_K^{pe} .

- Draw a schematic diagram of the photoelectric effect occurring in the K shell of a multi-electron absorber atom.
- Prove that the photoelectric effect cannot happen on a free electron.
- Explain the meaning of terms: “loosely bound” electron and “tightly bound” electron.
- It is generally assumed that the kinetic energy E_K^c of the photoelectron released from the atom undergoing a PE process is given as $E_K^c = h\nu - E_B$, where E_B is the binding energy of the electron to the atom undergoing the PE process. However, since the PE process occurs in a photon interaction with a tightly bound electron, the atom M involved in the PE process must recoil with a certain non-zero, albeit small, recoil kinetic energy E_K^{M+} . Do not neglect the recoil kinetic energy of the atom and calculate the kinetic energy E_K^c of the photoelectron and the kinetic energy E_K^{M+} of the recoil ion. Determine the ratio E_K^{M+}/E_K^c to justify neglecting E_K^{M+} in comparison with E_K^c .

SOLUTION:

(a) A schematic diagram of the PE effect is depicted in Fig. 7.32. A photon with energy $h\nu$, exceeding the K-shell electron binding energy $E_B(K)$, interacts with a K-shell electron of a multi-electron atom. The photon is absorbed and the K-shell electron is ejected from the atom as a photoelectron with kinetic energy $E_K \approx h\nu - E_B(K)$. The vacancy in the K shell is subsequently filled with a higher orbit electron and the energy of the electronic transition is emitted in the form of a characteristic (fluorescence) photon or as an Auger electron.

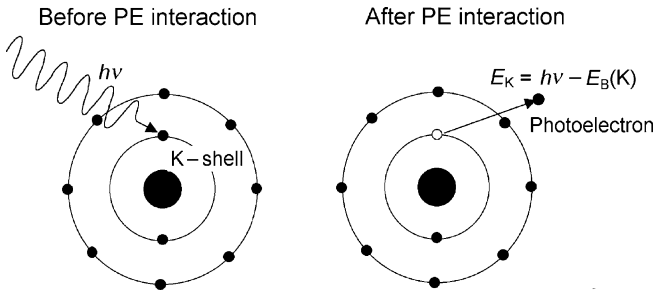


Fig. 7.32 Schematic diagram of the photoelectric effect

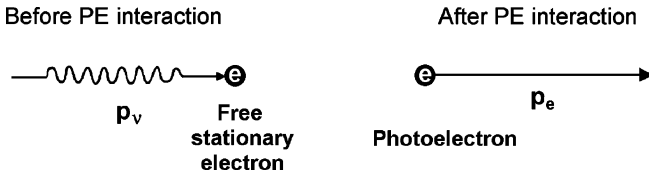


Fig. 7.33 Schematic diagram of a “gedanken experiment” (thought experiment) in which a photon undergoes a PE interaction with a free and stationary electron

(b) *Photon-free electron PE interaction is not possible* because it would violate the principle of total energy and momentum conservation. To prove this statement let us create a “gedanken experiment” (thought experiment) in which photon-free electron PE interaction is possible (Fig. 7.33) and evaluate how it satisfies the conservation of total energy and momentum.

(1) **Total energy E** before and after PE interaction:

Before PE interaction (photon + free electron at rest)

$$E_{\text{before}} = h\nu + m_e c^2 \tag{7.219}$$

After PE interaction (photoelectron)

$$E_{\text{after}} = E_K^e + m_e c^2 \tag{7.220}$$

Total energy conservation:

$$E_{\text{before}} = E_{\text{after}} \quad \text{or} \quad h\nu + m_e c^2 = E_K^e + m_e c^2 \quad \text{or} \quad h\nu = E_K^e, \tag{7.221}$$

where $h\nu$ his energy of the photon, $m_e c^2$ is the rest energy of the electron, and E_K^e is kinetic energy of the photoelectron.

(2) **Momentum p** before and after PE interaction:

Before PE interaction (photon + free electron at rest)

$$p_{\text{before}} = p_\nu = \frac{h\nu}{c} \tag{7.222}$$

After PE interaction (photoelectron)

$$p_{\text{after}} = p_e = \frac{E_K^e}{c} \sqrt{1 + \frac{2m_e c^2}{E_K^e}} \quad (7.223)$$

Momentum conservation:

$$p_{\text{before}} = p_{\text{after}} \quad \text{or} \quad \frac{h\nu}{c} = \frac{E_K^e}{c} \sqrt{1 + \frac{2m_e c^2}{E_K^e}} \quad \text{or} \quad h\nu > E_K^e, \quad (7.224)$$

where p_ν is the momentum of the photon and p_e is the momentum of the photoelectron.

Equations (7.221) and (7.224) clearly contradict one another, since from conservation of energy stated in (7.221) we establish that $h\nu = E_K^e$ and from conservation of momentum stated in (7.224) we establish that $h\nu > E_K^e$. Based on this we conclude that in a photon–free electron interaction the photon and free electron alone cannot simultaneously conserve the total energy and momentum and this makes a photon–free electron PE interaction impossible.

The extra energy and momentum carried by the photon that is not transferred to the photoelectron is actually transferred to a third entity, the parent atom of the photoelectron. However, this extra energy and momentum can be transferred to the parent atom only when the electron is bound to the parent atom, the tighter is the binding, the more probable is the PE event, under the condition, of course, that the photon energy $h\nu$ must exceed the binding energy E_B of the electron to the nucleus.

(c) In the context of photon interactions with absorber atoms the two terms “loosely bound” electron and “tightly bound” electron are often explained casually by stating that a tightly bound electron is an inner shell atomic electron, while a loosely bound electron is an outer shell atomic electron. Since this is not true in general (for example, a K-shell electron in lead appears loosely bound to a 10 MeV photon), it is better to explain the two terms by comparing the energy of the interacting photon $h\nu$ with the binding energy E_B of a given atomic electron. We then get the following definitions:

- (1) **Loosely bound electron** is an electron whose binding energy E_B is small in comparison with photon energy $h\nu$, i.e., $E_B \ll h\nu$. An interaction between a photon and a loosely bound electron is considered to be an interaction between a photon and a “free” (i.e., unbound electron).
- (2) **Tightly bound electron** is an electron whose binding energy E_B is comparable to, larger than, or slightly smaller than the photon energy $h\nu$. For photon interaction to occur with a tightly bound electron, binding energy E_B of the electron must be of the order of, but smaller than the photon energy $h\nu$, i.e., $E_B \lesssim h\nu$. Interaction between photon and a tightly bound electron is considered an interaction between a photon and the atom as a whole.

(d) Energy E_{tr} available in a PE process for transfer to photoelectron and residual ion M^+ is given as $E_{\text{tr}} = h\nu - E_{\text{B}}$, where $h\nu$ is the incident photon energy and E_{B} is the binding energy of the electron ejected as photoelectron. Energy E_{tr} is shared as kinetic energy between photoelectron E_{K}^{e} and residual ion $E_{\text{K}}^{M^+}$ in inverse proportion to their mass. Thus, we can state

$$E_{\text{tr}} = E_{\text{K}}^{\text{e}} + E_{\text{K}}^{M^+} = \frac{M^+}{M^+ + m_{\text{e}}} E_{\text{tr}} + \frac{m_{\text{e}}}{M^+ + m_{\text{e}}} E_{\text{tr}} = \frac{M^+}{M} (h\nu - E_{\text{B}}) + \frac{m_{\text{e}}}{M} (h\nu - E_{\text{B}}), \quad (7.225)$$

recognizing that $M = M^+ + m_{\text{e}}$, with M the mass of the parent atom, M^+ the mass of the residual ion, and m_{e} the photoelectron mass. From (7.225) we now express E_{K}^{e} and $E_{\text{K}}^{M^+}$ as

$$E_{\text{K}}^{\text{e}} = \frac{M^+}{M} E_{\text{tr}} = \frac{M^+}{M} (h\nu - E_{\text{B}}) \quad \text{and} \quad E_{\text{K}}^{M^+} = \frac{m_{\text{e}}}{M} E_{\text{tr}} = \frac{m_{\text{e}}}{M} (h\nu - E_{\text{B}}). \quad (7.226)$$

The ratio $E_{\text{K}}^{\text{e}}/E_{\text{K}}^{M^+}$ shows that the recoil energy of the residual ion is exceedingly small and can be neglected. Thus, it is reasonable to state that $E_{\text{K}}^{\text{e}} \approx E_{\text{tr}} = h\nu - E_{\text{B}}$.

7.5.Q2

(170)

A 100 keV photon has a photoelectric (PE) interaction with a K-shell electron in lead atom. The K-shell binding energy $E_{\text{B}}(\text{K})$ of lead is 88 keV; atomic weight of lead is 207.2 u and atomic rest energy $\mathcal{M}(\text{Pb})c^2$ is $207.2 \times 931.494 \text{ MeV} = 193005.5568 \text{ MeV}$.

- Determine kinetic energy E_{K}^{e} of the ejected photoelectron as well as the recoil kinetic energy $E_{\text{K}}^{\text{Pb}^+}$ of the residual lead ion.
- Determine the magnitude of the momenta \mathbf{p}_{ν} , \mathbf{p}_{e} , and \mathbf{p}_{Pb^+} of the incident photon, ejected photoelectron, and recoil residual lead ion, respectively.
- Draw a diagram with momentum vectors for the PE interaction of a 100 keV photon with a K-shell electron in lead atom. Do not neglect the recoil of the residual lead ion.

SOLUTION:

(a) In PE interaction between a photon and an atomic electron the photon is completely absorbed, the electron is ejected as a photoelectron with a well-defined kinetic energy, and the residual ion recoils with a small kinetic energy. When a 100 keV photon undergoes a PE interaction with a K-shell electron of lead, photon disappears and its energy $h\nu$ of 100 keV is distributed as follows:

- A component of photon energy in the amount of 88 keV equal to the binding energy $E_{\text{B}}(\text{K})$ of the K-shell electron in lead is used up to release the K-shell electron as a photoelectron.

- (2) Energy difference $(E_K)_{\text{tr}}$ between photon energy $h\nu$ and electron binding energy $E_B(\text{K})$ is transferred to the photoelectron and residual lead ion as kinetic energy E_K^{e} and $E_K^{\text{Pb}^+}$, respectively,

$$(E_K)_{\text{tr}} = h\nu - E_B(\text{K}) = E_K^{\text{e}} + E_K^{\text{Pb}^+}. \quad (7.227)$$

- (3) The transferred energy $(E_K)_{\text{tr}}$ is shared between the photoelectron and residual ion in the inverse proportion to their mass. Using (7.227) and recalling that $\mathcal{M}(\text{Pb}) = \mathcal{M}(\text{Pb}^+) + m_e$, where \mathcal{M} designates atomic mass, i.e., nuclear mass M plus mass of orbital electrons, we expand $(E_K)_{\text{tr}}$ as

$$\begin{aligned} (E_K)_{\text{tr}} = E_K^{\text{e}} + E_K^{\text{Pb}^+} &= \frac{\mathcal{M}(\text{Pb}^+)}{\mathcal{M}(\text{Pb}^+) + m_e} (E_K)_{\text{tr}} + \frac{m_e}{\mathcal{M}(\text{Pb}^+) + m_e} (E_K)_{\text{tr}} \\ &= \frac{\mathcal{M}(\text{Pb}^+)}{\mathcal{M}(\text{Pb})} (E_K)_{\text{tr}} + \frac{m_e}{\mathcal{M}(\text{Pb})} (E_K)_{\text{tr}} \\ &= \frac{\mathcal{M}(\text{Pb}^+)}{\mathcal{M}(\text{Pb})} [h\nu - E_B(\text{K})] + \frac{m_e}{\mathcal{M}(\text{Pb})} [h\nu - E_B(\text{K})], \end{aligned} \quad (7.228)$$

resulting in the following expressions for E_K^{e} and $E_K^{\text{Pb}^+}$

$$E_K^{\text{e}} = \frac{\mathcal{M}(\text{Pb}^+)}{\mathcal{M}(\text{Pb})} [h\nu - E_B(\text{K})] \quad \text{and} \quad E_K^{\text{Pb}^+} = \frac{m_e}{\mathcal{M}(\text{Pb})} [h\nu - E_B(\text{K})]. \quad (7.229)$$

Inserting appropriate values into (7.229) we get the following results for kinetic energy E_K^{e} of the photoelectron and recoil kinetic energy $E_K^{\text{Pb}^+}$ of the residual lead ion

$$\begin{aligned} E_K^{\text{e}} &= \frac{\mathcal{M}^{\text{Pb}^+}}{\mathcal{M}^{\text{Pb}}} [h\nu - E_B(\text{K})] = \left(1 - \frac{m_e}{\mathcal{M}^{\text{Pb}}}\right) [h\nu - E_B(\text{K})] \\ &= \left(1 - \frac{0.511}{193005.5568}\right) \times [100 \text{ keV} - 88 \text{ keV}] \\ &= (1 - 2.6476 \times 10^{-6}) \times (12 \text{ keV}) = 11.999968 \text{ keV}, \end{aligned} \quad (7.230)$$

$$\begin{aligned} E_K^{\text{Pb}^+} &= \frac{m_e}{\mathcal{M}^{\text{Pb}}} [h\nu - E_B(\text{K})] = \left(\frac{0.511}{193005.5568}\right) \times [100 \text{ keV} - 88 \text{ keV}] \\ &= 2.6476 \times 10^{-6} \times (12 \text{ keV}) = 3.177 \times 10^{-5} \text{ keV} = 3.177 \times 10^{-2} \text{ eV}. \end{aligned} \quad (7.231)$$

In summary, in 100 keV photon interaction with a K-shell electron in lead, 88 keV is used up to release the electron from the atom and the remaining 12 keV is shared as kinetic energy between the photoelectron and residual lead ion. Equations (7.230) and (7.231) show that the photoelectron, by virtue of its much smaller mass

compared to the residual ionic mass, picks up the larger portion by far of the 12 keV available and the residual ion acquires an exceedingly small portion of the 12 keV as recoil kinetic energy. This recoil energy is so small that it is usually neglected in studies of the PE effect. An assumption is thus made that the photoelectron acquires the full amount of the available energy, i.e., $E_K^e \approx h\nu - E_B$, however, for rigorous work we must recognize that the recoil energy of the residual ion is finite, albeit small, preventing the PE effect occurring on free electrons.

(b) Magnitude of momenta involved in a 100 keV photon PE interaction with K-shell electron in lead is determined using the standard expressions for calculation of photon momentum p_ν (T1.76) and particle momentum (T1.64)

(1) Magnitude of the incident photon momentum p_ν

$$|\mathbf{p}_\nu| = p_\nu = \frac{E_\nu}{c} = \frac{h\nu}{c} = \frac{100 \text{ keV}}{c} = 100 \text{ keV}/c. \quad (7.232)$$

(2) Magnitude of the ejected photoelectron momentum p_e

$$\begin{aligned} |\mathbf{p}_e| = p_e &= \frac{E_K^e}{c} \sqrt{1 + \frac{2m_e c^2}{E_K^e}} \\ &= \frac{(11.999968 \text{ keV})}{c} \sqrt{1 + \frac{2 \times 0.511}{11.999968 \times 10^{-3}}} = 111.39 \text{ keV}/c. \end{aligned} \quad (7.233)$$

(3) Magnitude of the recoil momentum p_{Pb^+} of the residual lead ion

$$\begin{aligned} |\mathbf{p}_{\text{Pb}^+}| = p_{\text{Pb}^+} &= \frac{E_K^{\text{Pb}^+}}{c} \sqrt{1 + \frac{2\mathcal{M}(\text{Pb}^+)c^2}{E_K^{\text{Pb}^+}}} \\ &= \frac{(3.177 \times 10^{-5} \text{ keV})}{c} \sqrt{1 + \frac{2 \times 193005.0458}{3.2 \times 10^{-8}}} = 110.75 \text{ keV}/c. \end{aligned} \quad (7.234)$$

(c) Like in general PE effect, three vector momenta play a role in the PE interaction of a 100 keV photon with a K-shell electron in lead atom: (1) momentum of the incident photon \mathbf{p}_ν , (2) momentum of the ejected photoelectron \mathbf{p}_e , and (3) recoil momentum of the residual lead ion \mathbf{p}_{Pb^+} . The three vector momenta form a triangle and we know the sides of the triangle, since they are defined by the magnitudes of the vectors that were determined in **(b)**. The triangle is depicted in Fig. 7.34 and in principle can be drawn simply on the basis of its three sides. On the other hand, we can use the trigonometric cosine law and calculate the angles ϕ and φ to facilitate the drawing of the momentum triangle for the PE effect.

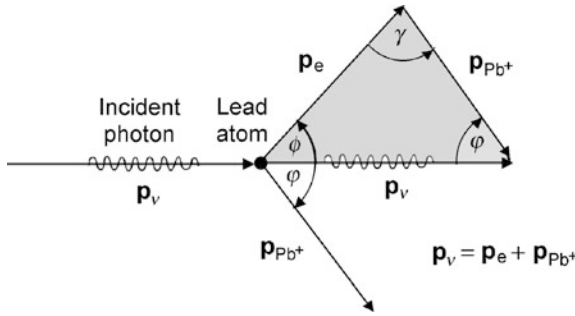


Fig. 7.34 Vector diagram for a PE interaction of a 100 keV photon with K-shell electron in lead atom

With help of Fig. 7.34 and the law of cosines we calculate angles ϕ and φ as follows

$$p_{\text{Pb}^+}^2 = p_v^2 + p_e^2 - 2p_v p_e \cos \phi \quad \text{or}$$

$$\phi = \arccos \frac{p_v^2 + p_e^2 - p_{\text{Pb}^+}^2}{2p_v p_e} = \arccos \frac{100^2 + 111.39^2 - 110.75^2}{2 \times 100 \times 111.39} \quad (7.235)$$

$$= \arccos 0.455 = 62.9^\circ$$

and

$$p_e^2 = p_v^2 + p_{\text{Pb}^+}^2 - 2p_v p_{\text{Pb}^+} \cos \varphi \quad \text{or}$$

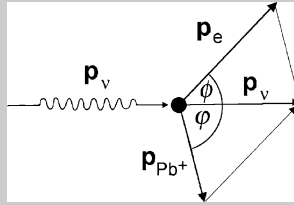
$$\varphi = \arccos \frac{p_v^2 + p_{\text{Pb}^+}^2 - p_e^2}{2p_v p_{\text{Pb}^+}} = \arccos \frac{100^2 + 110.75^2 - 111.39^2}{2 \times 100 \times 110.75} \quad (7.236)$$

$$= \arccos 0.440 = 63.9^\circ.$$

7.5.Q3

(171)

The most important parameters in photoelectric (PE) interaction of energetic photons with absorber atoms are: (1) Incident photon energy $h\nu$; (2) Atomic number Z of the absorber atom; (3) Binding energy E_B of the ejected electron; (4) Kinetic energy $(E_K)_{\text{tr}}$ transferred from incident photon to photoelectron E_K^e and residual ion $E_K^{M^+}$; (5) Momenta of incident photon \mathbf{p}_v , ejected photoelectron \mathbf{p}_e , and residual ion \mathbf{p}_{M^+} ; and (6) Emission angle ϕ of the photoelectron and recoil angle φ of the residual ion.



For photons of energy $h\nu = 0.1 \text{ MeV}$, 1 MeV , 10 MeV , 100 MeV , and 1000 MeV undergoing a PE interaction with a K-shell electron in lead determine:

- Kinetic energy $(E_K)_{\text{tr}}$ transferred from incident photon to photoelectron E_K^e and residual lead ion $E_K^{\text{Pb}^+}$.
- Momentum of the incident photon \mathbf{p}_ν ; ejected photoelectron \mathbf{p}_e , and residual ion \mathbf{p}_{Pb^+} .
- Ejection angle ϕ of the photoelectron and recoil angle φ of the residual lead ion Pb^+ .
- Plot momentum vector diagrams for PE interaction of photons with energy of 0.1 MeV , 1 MeV , 10 MeV , and 100 MeV . Adjust scale of each graph to normalize the incident photon momentum to $1 \text{ MeV}/c$.
- Conservation of energy and momentum seem to suggest a uniquely defined ejection angle ϕ of the photoelectron for a given photon energy $h\nu$ yet experiments showed a broad distribution of ejection angles (see Evans). Explain the reason for the discrepancy.

K-shell binding energy $E_B(\text{K})$ of lead is 88 keV ; atomic weight of lead is 207.2 u ; atomic rest energy of lead $\mathcal{M}(\text{Pb})c^2$ is 193005.5568 MeV ; and atomic rest energy of residual lead ion is $\mathcal{M}(\text{Pb}^+)c^2 = \mathcal{M}(\text{Pb})c^2 - m_e c^2 = 193005.0458 \text{ MeV}$. For definition of parameters see sketch above.

SOLUTION:

- Energy $(E_K)_{\text{tr}}$ transferred from incident photon to the photoelectron as E_K^e and to the recoil residual ion as $E_K^{\text{Pb}^+}$ is equal to the difference between photon energy $h\nu$ and binding energy $E_B(\text{K})$ of K-shell electron in lead

$$(E_K)_{\text{tr}} = E_K^e + E_K^{\text{Pb}^+} = h\nu - E_B(\text{K}) = h\nu - 0.088 \text{ MeV}. \quad (7.237)$$

Energy $(E_K)_{\text{tr}}$ transferred from photon to lead atom given in (7.237) is shared between the photoelectron and residual lead ion in inverse proportion to their mass.

Thus, E_K^e and $E_K^{\text{Pb}^+}$ are given as

$$E_K^e = \frac{\mathcal{M}(\text{Pb}^+)}{\mathcal{M}(\text{Pb}^+) + m_e} (E_K)_{\text{tr}} = \frac{\mathcal{M}(\text{Pb}^+)}{\mathcal{M}(\text{Pb})} (E_K)_{\text{tr}} \quad (7.238)$$

and

$$E_K^{\text{Pb}^+} = \frac{m_e}{\mathcal{M}(\text{Pb}^+) + m_e} (E_K)_{\text{tr}} = \frac{m_e}{\mathcal{M}(\text{Pb})} (E_K)_{\text{tr}}. \quad (7.239)$$

Results of our calculation of $(E_K)_{\text{tr}}$, E_K^e , and $E_K^{\text{Pb}^+}$ based on (7.237), (7.238), and (7.239), respectively, for the five photon energies are given in rows (2), (3), and (4) of Table 7.11.

(b) Magnitude of momenta of the incident photon \mathbf{p}_ν ; ejected photoelectron \mathbf{p}_e , and residual ion $\mathbf{p}_{\mathcal{M}^+}$ involved in PE interaction of incident photon of energy $h\nu$ with a K-shell electron in lead is determined using the standard expressions for calculation of photon momentum $p_\nu = |\mathbf{p}_\nu|$ (T1.76) and particle momentum $p = |\mathbf{p}|$ (T1.64), respectively, as

$$p_\nu = |\mathbf{p}_\nu| = \frac{E_\nu}{c} = \frac{h\nu}{c}, \quad (7.240)$$

$$p_e = |\mathbf{p}_e| = \frac{E_K^e}{c} \sqrt{1 + \frac{2m_e c^2}{E_K^e}} \quad \text{and} \quad p_{\text{Pb}^+} = |\mathbf{p}_{\text{Pb}^+}| = \frac{E_K^{\text{Pb}^+}}{c} \sqrt{1 + \frac{2\mathcal{M}(\text{Pb}^+)c^2}{E_K^{\text{Pb}^+}}}. \quad (7.241)$$

Results of our calculation of p_ν with (7.240) and p_e as well as p_{Pb^+} with (7.241) for the five photon energies are listed in rows (5), (6), and (7) of Table 7.11.

(c) Ejection angle ϕ of the photoelectron and recoil angle φ of the residual lead ion are calculated using the rule of cosine on the triangle formed by the three vector momenta \mathbf{p}_ν , \mathbf{p}_e , and $\mathbf{p}_{\mathcal{M}^+}$. The two expressions for ϕ and φ are given as follows

$$\phi = \arccos \frac{p_\nu^2 + p_e^2 - p_{\text{Pb}^+}^2}{2p_\nu p_e} \quad (7.242)$$

and

$$\varphi = \arccos \frac{p_\nu^2 + p_{\text{Pb}^+}^2 - p_e^2}{2p_\nu p_{\text{Pb}^+}}. \quad (7.243)$$

Results of our calculation of ejection angle ϕ with (7.242) and recoil angle φ with (7.243) for the five photon energies are listed in rows (8) and (9), respectively, of Table 7.11.

(d) Figure 7.35 shows four graphs of vector momenta \mathbf{p}_ν , \mathbf{p}_e , and $\mathbf{p}_{\mathcal{M}^+}$ for PE interaction of energetic photons with K-shell electron in lead. Part (A) is for photon

Table 7.11 Various parameters important for photoelectric (PE) interaction of photon of energy $h\nu$ with a K-shell electron in lead absorber

(1) $E_\nu = h\nu$ (MeV)	0.1	1.0	10	100	1000
(2) $(E_K)_{tr}$ (MeV)	0.012	0.912	9.912	99.912	999.912
(3) E_K^c (MeV)	0.0119997	0.9119976	9.9119738	99.9117354	999.909352
(4) $E_K^{Pb^+}$ (MeV)	3.178×10^{-8}	2.415×10^{-6}	2.625×10^{-5}	2.646×10^{-4}	2.648×10^{-3}
(5) p_ν (MeV/c)	0.1	1	10	100	1000
(6) p_e (MeV/c)	0.111391	1.328081	10.410440	100.421435	1000.42022
(7) p_{Pb^+} (MeV/c)	0.110751	0.965508	3.183017	10.105717	31.969748
(8) ϕ	62.9°	46.4°	17.8°	15.8°	1.8°
(9) φ	63.9°	85.0°	88.2°	89.5°	90.2°

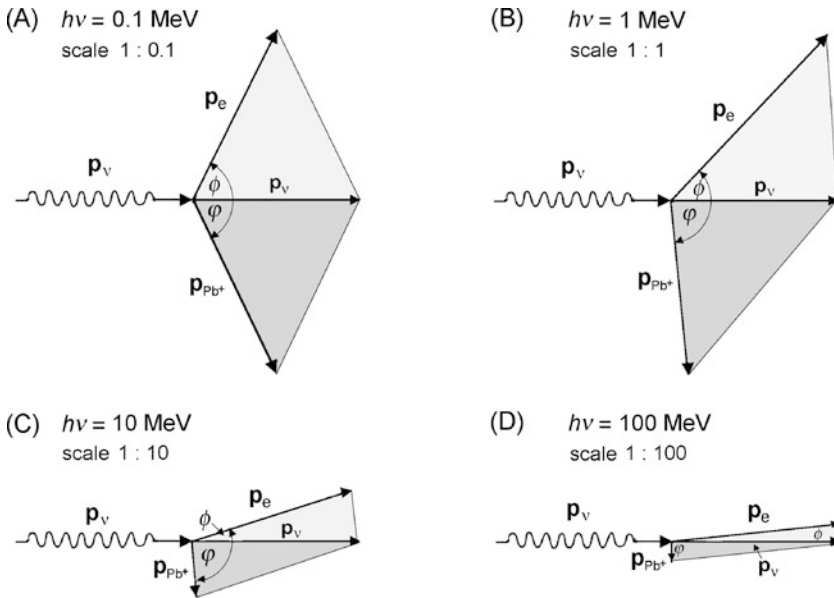


Fig. 7.35 Vector diagrams for PE interaction between photon of energy $h\nu$ with K-shell electron in lead absorber. Three momentum vectors are shown for each photoelectric (PE) interaction: momentum \mathbf{p}_ν of incident photon, momentum \mathbf{p}_e of the ejected photoelectron, and recoil momentum \mathbf{p}_{Pb^+} of the residual lead ion. (A) is for $h\nu = 0.1$ MeV and scale of 1:0.1; (B) for 1 MeV and scale 1:1; (C) for 10 MeV and scale of 1:10; and (D) for 100 MeV and scale 1:100

energy $h\nu = 0.1$ MeV and scale of 1:0.1; (B) for 1 MeV and scale 1:1; (C) for 10 MeV and scale 1:10; and (D) for 100 MeV and scale 1:100. Magnitudes of vectors are plotted with decreasing scales such that the magnitude of \mathbf{p}_ν appears the same in all four graphs.

From the four graphs of Fig. 7.35 and Table 7.11 we note several interesting features of the three momenta in PE interaction between an energetic photon and K-shell electron in lead:

- (1) At incident photon energy $h\nu$ exceeding, but of the order of, $E_B(\text{K})$, magnitudes of \mathbf{p}_e and \mathbf{p}_{Pb^+} are similar to the magnitude of \mathbf{p}_ν .
- (2) With increasing incident photon energy $h\nu$ the magnitude of \mathbf{p}_e remains similar to the magnitude of \mathbf{p}_ν , while the magnitude of \mathbf{p}_{Pb^+} decreases significantly.
- (3) At $h\nu = 0.1$ MeV the photoelectron ejection angle ϕ and residual lead ion recoil angle φ are about 60° . As photon energy $h\nu$ increases, ϕ decreases and photoelectron is ejected more and more in the direction of the incident photon (forward direction).
- (4) As photon energy $h\nu$ increases from 0.1 MeV, recoil angle φ increases from 60° and rapidly approaches 90° indicating that at high photon energies the residual lead ion recoils in a direction perpendicular to the incident photon.
- (5) Irrespective of photon energy $h\nu$, as long as $h\nu > E_B(\text{K})$, kinetic energy E_K^e of the photo-electron equals photon energy $h\nu$ less the binding energy $E_B(\text{K})$ of the K-shell electron.
- (6) Irrespective of photon energy $h\nu$, as long as $h\nu > E_B(\text{K})$, kinetic energy $E_K^{\text{Pb}^+}$ of the recoil residual lead ion is exceedingly small, the ratio $E_K^{\text{Pb}^+}/E_K^e$ amounting to only $\sim 3 \times 10^{-6}$ and justifying the standard approximation in PE effect: $(E_K)_{\text{tr}} = h\nu - E_B(\text{K}) \approx E_K^e$ and $E_K^{\text{Pb}^+} \approx 0$.

(e) As shown in (a) and (b), conservation of total energy and momentum applied to PE effect suggest a discrete energy distribution of photoelectrons (E_K^e) as well as uniquely defined ejection angles ϕ of the photoelectron. While discrete E_K^e are born out by experiment, uniquely defined ϕ are not, since photoelectrons tend to be emitted within a wide range of angles ϕ . For a given photon energy $h\nu$ the directional distribution of photoelectrons exhibits a bell-type curve that peaks around 60° at relatively low $h\nu$ and then tends more and more toward forward direction as photon energy $h\nu$ increases. Evans describes this behavior by defining a bipartition angle as a function of photon energy $h\nu$. The bipartition angle for a specific quantity is defined as the half-angle of the cone into which one half of the quantity is scattered. We note that the ejection angle ϕ , calculated in (c), roughly follows the bipartition angle introduced for the PE effect by Evans.

Evans explains the problem in ejection angle ϕ by stipulating that the photon indeed transfers its full momentum $p_\nu = h\nu/c$ to the photoelectron and residual ion but it also adds a small and varying transverse momentum that arises from the electric field of the EM wave interacting with charged photoelectron and residual ion. The extra momentum fluctuates depending on the polarity of the electric field of the EM wave causing a spread in ϕ around the angle calculated in (c) from conservation of energy and momentum principles.

7.5.Q4

(172)

The probability P_j of the photoelectric effect, if it occurs, to occur within the j subshell of an absorber atom is determined with the help of the photoelectric effect mass attenuation coefficient τ/ρ plotted against the photon energy $h\nu$ encompassing K, L, and M absorption edges. In general, P_j is expressed as

$$P_j = \left(1 - \sum_{n=0}^{j-1} P_n \right) \xi_j, \quad (7.244)$$

where $P_0 = 0$; $\sum P_j = 1$; and ξ_j is an absorption edge parameter defined for subshell j as

$$\xi_j = \frac{(\tau/\rho)_j^H - (\tau/\rho)_j^L}{(\tau/\rho)_j^H}, \quad (7.245)$$

with H and L designating the high and low values, respectively, of the mass attenuation coefficient τ/ρ at the given absorption edge j .

- (a) Plot the photoelectric mass attenuation coefficient τ/ρ for tungsten ($Z = 74$) for photon energies in the interval from 10 keV to 100 keV. On the plot show the K, L_1 , L_2 , and L_3 absorption edges and determine the high and low mass attenuation coefficient values $(\tau/\rho)_j^H$ and $(\tau/\rho)_j^L$, respectively, for use in (7.245).
- (b) Calculate the absorption edge parameter ξ_j for the K shell as well as the L_1 , L_2 , and L_3 subshells.
- (c) For a photon with energy $h\nu \geq E_B(\text{K})$, where $E_B(\text{K})$ is the K-shell binding energy, determine the probabilities of the photoelectric (PE) effect P_K and P_L to occur in the K shell and in the L shell, respectively.
- (d) Repeat the calculation of (c) for a photon with energy $E_B(L_1) \leq h\nu < E_B(\text{K})$ where $E_B(L_1)$ is the binding energy of the L_1 subshell.

SOLUTION:

(a) A plot of the photoelectric mass attenuation coefficient τ/ρ for tungsten in the energy range between 10 keV and 100 keV is shown in Fig. 7.36. Data were obtained from the XCOM database that was compiled by Burger et al. and is available online from the NIST at the following URL: <http://www.nist.gov/pml/data/xcom/index.cfm>. The database contains photon cross section data for the photoelectric effect, Compton and Rayleigh scattering, and pair production photon interactions.

As illustrated in Fig. 7.36, the mass attenuation coefficient for the PE effect as a function of the incident photon energy $h\nu$ exhibits a characteristic saw-tooth structure in which the sharp discontinuities, referred to as the absorption edge, arise

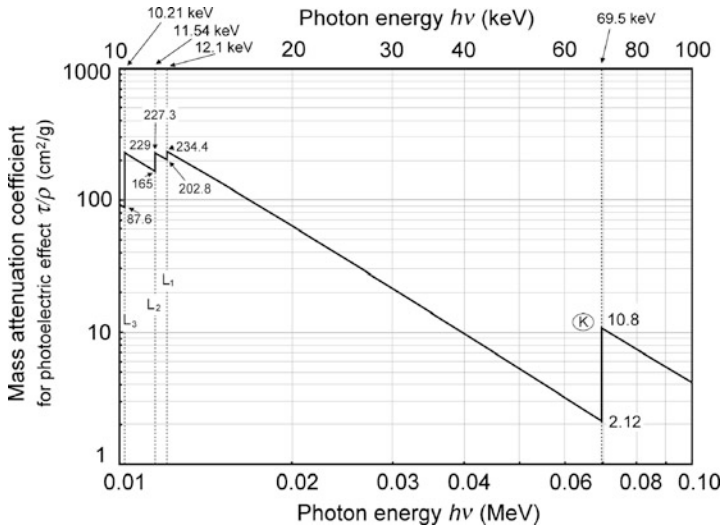


Fig. 7.36 Photoelectric mass attenuation coefficient τ/ρ against incident photon energy $h\nu$ for tungsten in the energy range from 10 keV to 100 keV covering the K and L absorption edges. High and low τ/ρ values at the K absorption edge as well as the three L sub-edges are shown to aid in the derivation of the absorption edge parameters ξ_j

whenever the photon energy coincides with the binding energy of a particular electron shell.

Four tungsten discontinuities in PE attenuation coefficient τ/ρ occur at photon energies $h\nu = E_B(K) = 69.5$ keV, $h\nu = E_B(L_1) = 12.1$ keV, $h\nu = E_B(L_2) = 11.54$ keV, and $h\nu = E_B(L_3) = 10.21$ keV. Similar discontinuities in attenuation coefficient, of course, also occur in higher-level subshells such as those residing in the M, N, and O shells.

(b) Absorption edge parameter ξ_j for subshell j is given in (7.245). For the K shell, we get

$$\xi_K = \frac{(\tau/\rho)_K^H - (\tau/\rho)_K^L}{(\tau/\rho)_K^H} = \frac{10.80 \text{ cm}^2/\text{g} - 2.118 \text{ cm}^2/\text{g}}{10.80 \text{ cm}^2/\text{g}} = 0.804. \quad (7.246)$$

Similarly, the absorption edge parameters ξ_{L_1} , ξ_{L_2} , ξ_{L_3} are:

$$\xi_{L_1} = \frac{(\tau/\rho)_{L_1}^H - (\tau/\rho)_{L_1}^L}{(\tau/\rho)_{L_1}^H} = \frac{234.4 \text{ cm}^2/\text{g} - 102.8 \text{ cm}^2/\text{g}}{234.4 \text{ cm}^2/\text{g}} = 0.135, \quad (7.247)$$

$$\xi_{L_2} = \frac{(\tau/\rho)_{L_2}^H - (\tau/\rho)_{L_2}^L}{(\tau/\rho)_{L_2}^H} = \frac{227.3 \text{ cm}^2/\text{g} - 165.0 \text{ cm}^2/\text{g}}{227.3 \text{ cm}^2/\text{g}} = 0.274, \quad (7.248)$$

Table 7.12 High and low values of PE mass attenuation coefficient at absorption edges, $(\tau/\rho)_j^H$ and $(\tau/\rho)_j^L$, respectively, as well as the absorption edge parameter ξ_j for the K, L₁, L₂, and L₃ subshells of tungsten

Subshell	$E_B(j)$ (keV)	$(\tau/\rho)_j^H$ (cm ² /g)	$(\tau/\rho)_j^L$ (cm ² /g)	ξ_j
K	69.5	10.8	2.118	0.804
L ₁	12.1	234.4	202.8	0.135
L ₂	11.54	227.3	165.0	0.274
L ₃	10.21	229.0	87.59	0.618

and

$$\xi_{L_3} = \frac{(\tau/\rho)_{L_3}^H - (\tau/\rho)_{L_3}^L}{(\tau/\rho)_{L_3}^H} = \frac{229.0 \text{ cm}^2/\text{g} - 87.59 \text{ cm}^2/\text{g}}{229.0 \text{ cm}^2/\text{g}} = 0.618, \quad (7.249)$$

respectively. Table 7.12 summarizes the calculated results of (7.246) through (7.249).

(c) For photons with energies $h\nu \geq E_B(\text{K})$ to undergo a PE effect with tungsten atom the photon can in principle be absorbed by any one of the 74 orbital electrons and the electron undergoing the PE interaction is then ejected from the atom. The probability P_j of an electron that undergoes PE effect to be ejected from a specific subshell j can be determined using the recursive relationship given in (7.244). *Note:* P_j is the probability of PE effect, **if it occurs**, to occur in subshell j . It is important not to misconstrue P_j as the probability for the PE effect to happen, as this probability is governed by the attenuation coefficient τ .

For K-shell electrons (7.244) gives the following probability P_K

$$P_K = \left(1 - \sum_{n=0}^0 P_0 \right) \xi_K = \xi_K = 0.804, \quad (7.250)$$

showing that, for an incident photon with $h\nu \geq E_B(\text{K})$ interacting with a tungsten atom, there is an 80.4 % probability that its energy is absorbed by one of the two K-shell electrons. Consequently, the probability of the photon interacting with one of the other 72 electrons is only 19.6 %. This heavy emphasis on K-shell electrons results from the weighting of PE interactions in favor of tightly bound electrons; that is, the tighter is the electron binding to the nucleus, the larger is the electron's probability of PE interaction.

To determine the probability P_L for the L shell we must first calculate the probabilities P_{L_1} , P_{L_2} , and P_{L_3} for the L₁, L₂, and L₃ subshells, respectively, as follows

$$P_{L_1} = \left(1 - \sum_{n=0}^1 P_j \right) \xi_{L_1} = (1 - P_K) \xi_{L_1} = (1 - 0.804) \times 0.135 = 0.026, \quad (7.251)$$

$$\begin{aligned}
 P_{L_2} &= \left(1 - \sum_{n=0}^2 P_j\right) \xi_{L_2} = (1 - P_K - P_{L_1}) \xi_{L_2} \\
 &= (1 - 0.804 - 0.026) \times 0.274 = 0.047
 \end{aligned} \tag{7.252}$$

and

$$\begin{aligned}
 P_{L_3} &= \left(1 - \sum_{n=0}^3 P_j\right) \xi_{L_3} = (1 - P_K - P_{L_1} - P_{L_2}) \xi_{L_3} \\
 &= (1 - 0.804 - 0.026 - 0.047) \times 0.618 = 0.076.
 \end{aligned} \tag{7.253}$$

From (7.251), (7.252), and (7.253) we get the probability for the L-shell P_L as the sum of P_{L_1} , P_{L_2} , and P_{L_3}

$$P_L = P_{L_1} + P_{L_2} + P_{L_3} = 0.026 + 0.047 + 0.076 = 0.149. \tag{7.254}$$

Therefore, when a photon with energy $h\nu \geq E_B(K) = 69.5$ keV undergoes a PE interaction with a tungsten atom, the probability of the photoelectron being ejected from the K shell is 80.4 %, as calculated in (7.250), from the L-shell it is 14.9 %, as determined in (7.254), and from higher shells it amounts to the remaining 4.7 %.

(d) Calculation of probabilities for K-shell P_K and the L-shell P_L for an incident photon with energy $E_B(L_1) \leq h\nu < E_B(K)$ follows the same steps as in **(c)** with one exception; in this energy range between $E_B(L_1)$ and $E_B(K)$, since the incident photon energy is less than the binding energy $E_B(K)$ the two K-shell electrons cannot participate in PE interactions, so that P_K is equal to 0. P_{L_1} , P_{L_2} , and P_{L_3} are then from (7.244) and ξ_j of Table 7.12 calculated as follows

$$P_{L_1} = \left(1 - \sum_{n=0}^1 P_j\right) \xi_{L_1} = (1 - P_K) \xi_{L_1} = (1 - 0) \times 0.135 = 0.135, \tag{7.255}$$

$$\begin{aligned}
 P_{L_2} &= \left(1 - \sum_{n=0}^2 P_j\right) \xi_{L_2} = (1 - P_K - P_{L_1}) \xi_{L_2} = (1 - 0 - 0.135) \times 0.274 = 0.237, \\
 &\tag{7.256}
 \end{aligned}$$

and

$$\begin{aligned}
 P_{L_3} &= \left(1 - \sum_{n=0}^3 P_j\right) \xi_{L_3} = (1 - P_K - P_{L_1} - P_{L_2}) \xi_{L_3} \\
 &= (1 - 0 - 0.135 - 0.237) \times 0.618 = 0.388
 \end{aligned} \tag{7.257}$$

respectively, and the probability P_L for the L-shell now is given as the following sum, similar to that of (7.254)

$$P_L = P_{L_1} + P_{L_2} + P_{L_3} = 0.135 + 0.237 + 0.388 = 0.760. \tag{7.258}$$

For photon with energy between the binding energy of the L_1 subshell and K shell, i.e., for $E_B(L_1) \leq h\nu < E_B(K)$, when it undergoes a PE interaction with a tungsten atom, the probability for interaction in the K shell is zero, the probability for interaction in the L shell, according to (7.258), is 76 % and the probability for interaction in higher-level shells is 24 %. The conclusion that we can reach based on (7.250) and (7.258) is that when PE interaction occurs, by far the highest probability is for it to occur with a shell or subshell whose binding energy is below $h\nu$ by the least amount.

7.5.Q5

(173)

Cross sections (attenuation coefficients) for the photoelectric (PE) interaction of photons with absorbers are readily available from the literature; however, the most authoritative and up to date source is available at the NIST (<http://physics.nist.gov/PhysRefData/Xcom/html/xcom1.html>). Based on Fig. 7.37 that plots the NIST photoelectric (PE) atomic cross section ${}_a\tau$ for 5 absorbers ranging in atomic number Z from $Z = 1$ (hydrogen) to $Z = 82$ (lead) against photon energy $h\nu$ ranging from 10^{-3} MeV to 10^4 MeV make the following estimates for absorbers in general:

- Dependence of ${}_a\tau$ on energy $h\nu$ of the incident photon.
- Dependence of ${}_a\tau$ on atomic number Z of the absorber.
- Dependence of the photoelectric mass attenuation coefficient τ/ρ on atomic number Z of the absorber.

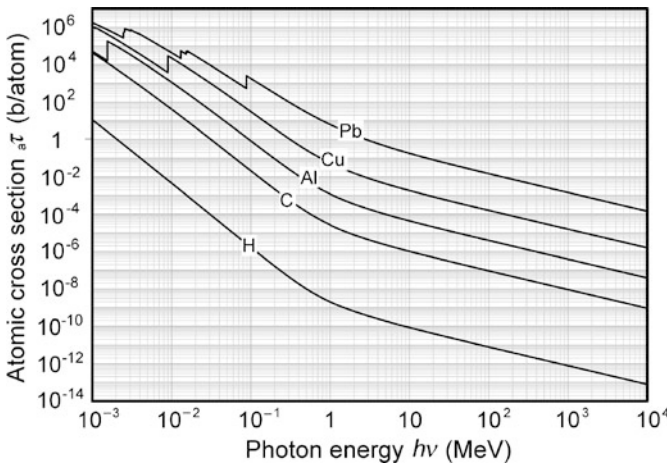


Fig. 7.37 Photoelectric atomic cross section (attenuation coefficient) ${}_a\tau$ against photon energy $h\nu$ for various absorbers ranging from hydrogen ($Z = 1$) to lead ($Z = 82$). Data are from the NIST

SOLUTION:

A cursory inspection of Fig. 7.37, which plots the photoelectric cross section ${}_a\tau$ against photon energy $h\nu$ (in the range $1 \text{ keV} \leq h\nu \leq 10^4 \text{ MeV}$) for various absorbers (in the atomic number Z range $1 \leq Z \leq 82$), exhibits several general features of ${}_a\tau$:

- (1) For a given atomic number Z , ${}_a\tau$ is a smooth, continuous function except for sharp discontinuities called absorption edge that occur when $h\nu$ is in the vicinity of electron binding energy E_B of atomic shells.
- (2) For a given Z , as energy $h\nu$ increases above the energy of an absorption edge, ${}_a\tau$ decreases with increasing $h\nu$.
- (3) Energy of a given absorption edge increases with Z of absorber.
- (4) For a given photon energy $h\nu$, ${}_a\tau$ increases with increasing Z of absorber.

(a) An investigation of the ${}_a\tau$ dependence upon photon energy $h\nu$ (Fig. 7.37) for a given absorber Z reveals that, at $h\nu$ above the K-shell absorption edge, ${}_a\tau$ on a ${}_a\tau$ versus $h\nu$ log-log plot exhibits three distinct regions: two linear regions (1 and 3) connected by transition region 2. Since linearity on a log-log plot suggests a power function, we conclude that ${}_a\tau$ can be described by two power functions of the form ${}_a\tau \propto (h\nu)^k$, each with its own exponent k . In region 1 where $h\nu < \sim 0.5 \text{ MeV}$, $k \approx -3$ predominates; in region 3, where $h\nu > \sim 10 \text{ MeV}$, $k = -1$ predominates, and in region 2, where $0.5 \text{ MeV} < h\nu < 10 \text{ MeV}$, ${}_a\tau$ is affected by both exponents k , as shown in Fig. 7.38. Exponents are negative because ${}_a\tau$ decreases with increasing photon energy $h\nu$. The intercept between extrapolated linear line of region 1 with that of region 3 occurs at approximately 1.5 MeV for all absorbers.

Theoretical derivation of the photoelectric cross section ${}_a\tau$ is, in contrast to the derivation of Compton cross sections, very complex. Heitler derived ${}_a\tau$ above the K absorption edge using non-relativistic Born approximation and obtained the following expression

$${}_a\tau = 32^{1/2} {}_e\sigma_{\text{Th}} \alpha^4 Z^5 \varepsilon^{7/2} = 32^{1/2} {}_e\sigma_{\text{Th}} \alpha^4 Z^5 (h\nu/m_e c^2)^{7/2}, \quad (7.259)$$

where ${}_e\sigma_{\text{Th}}$ is Thomson electronic cross section and α is fine structure constant.

(b) To investigate the dependence of photoelectric atomic cross section ${}_a\tau$ on absorber atomic number Z we re-plot in Fig. 7.39 the data of Fig. 7.38 and depict on a log-log scale ${}_a\tau$ against Z for the following incident photon energies $E_\nu = h\nu$ in MeV: 0.001, 0.01, 0.1, 1, 10, and 100. For a given E_ν the data points appear to be following a straight line on the log-log plot indicating a power function relationship of the form ${}_a\tau \propto Z^n$, where n is the exponent of the power function. At first glance the exponent n appears to be between 3 and 5, since each straight line rises at a rate of 3 cycles to 5 cycles in ${}_a\tau$ per each cycle increase in Z .

A closer look at the ${}_a\tau$ versus Z graph reveals two notable features of the straight line behavior, i.e., ${}_a\tau$ versus Z^n behavior:

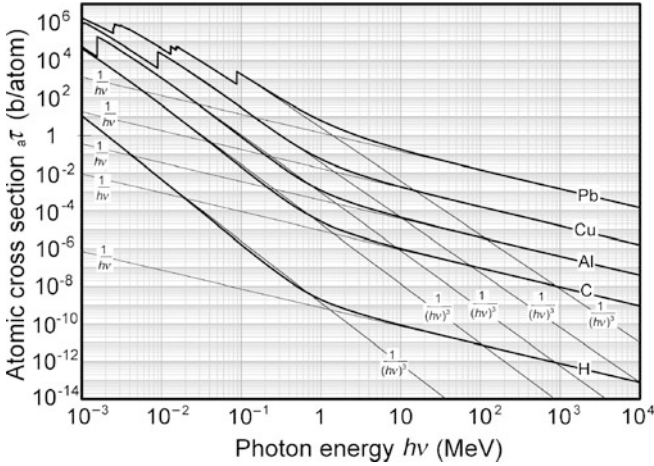


Fig. 7.38 Atomic cross section $a\tau$ against incident photon energy $h\nu$ for 5 absorbers: hydrogen, carbon, aluminum, copper, and lead. At photon energy $h\nu$ below 1 MeV the $a\tau$ dependence on photon energy $h\nu$ goes approximately as $a\tau \propto 1/(h\nu)^3$ and at photon energy above 10 MeV the $a\tau$ dependence on photon energy goes as $a\tau \propto 1/(h\nu)$, as shown in the figure

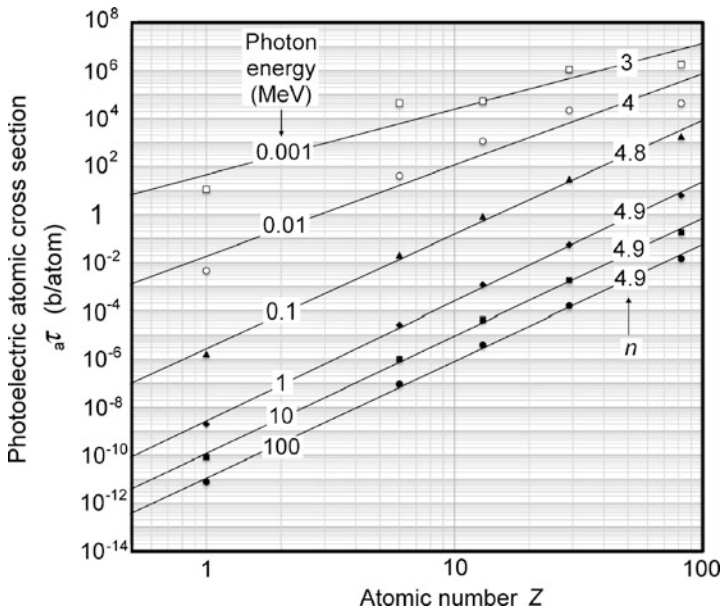


Fig. 7.39 Photoelectric atomic cross section $a\tau$ against atomic number Z of the absorber

- (1) Data points for higher photon energy ($E_\nu > 0.1$ MeV) fit a straight line much better than those for lower photon energy ($E_\nu < 0.1$ MeV). The reason for this is attributed to absorption edges causing significant discontinuities in $a\tau$ at

photon energy in the vicinity of absorption edges. Since the highest absorption edge energy of any element is below 150 keV, the adverse effect of absorption edges on ${}_a\tau$ versus Z dependence is not present at E_ν above 150 keV.

- (2) Exponent n ranges from $n \approx 3$ at low photon energy up to $n \approx 5$ at high photon energy. In the literature n is usually stated as $n = 4$ at low photon energy rising to $n = 4.6$ at high photon energy. Our range in exponent n , based on Fig. 7.39, is somewhat broader but we must recognize that we made no attempts at averaging out the discontinuities in ${}_a\tau$ at absorption edges.

On the basis of data plotted in Fig. 7.39 we arrive at the general conclusion that photoelectric atomic cross section ${}_a\tau$ is roughly proportional to atomic number Z to the fourth power, i.e., ${}_a\tau \propto Z^4$.

(c) Photoelectric mass attenuation coefficient τ/ρ dependence on atomic number Z is derived from the dependence of photoelectric atomic cross section ${}_a\tau$ on Z that was determined in (b) as ${}_a\tau \propto Z^4$. The basic relationship between photoelectric linear attenuation coefficient τ and ${}_a\tau$ goes as: $\tau = n^\square {}_a\tau$, where n^\square is the number of atoms N_a per volume \mathcal{V} of the absorber. We thus have the following relationship between τ/ρ and ${}_a\tau$

$$\frac{\tau}{\rho} = \frac{n^\square {}_a\tau}{\rho} = \frac{N_a}{\rho \mathcal{V}} ({}_a\tau) = \frac{N_a}{m} ({}_a\tau) = \frac{N_A}{A} ({}_a\tau) \approx \frac{N_A}{2Z} ({}_a\tau) \propto \frac{Z^4}{Z} = Z^3, \quad (7.260)$$

where we used $N_a/m = N_A/A$ and $A \approx 2Z$. *Note:* For all elements $Z/A \approx 0.5$, with one notable exception of hydrogen for which $Z/A = 1$. Actually, Z/A slowly decreases from 0.5 for low Z elements to ~ 0.4 for high Z elements. For example, Z/A for helium-4 is 0.5, for cobalt-60 it is 0.45, and for uranium-235 it is 0.39. From (7.260) we see that $\tau/\rho \propto Z^3$, since ${}_a\tau \propto Z^4$.

7.6 Pair Production

7.6.Q1

(174)

Pair production is the term used to describe production of an electron-positron pair (materialization) out of energy (photon) in either the electric field of the nucleus of an absorber atom (called nuclear pair production) or in the electric field of an orbital electron of an absorber atom (called triplet production or electronic pair production). The threshold for nuclear pair production is slightly larger than the sum of the rest masses of the electron and positron.

- (a) Draw schematic diagrams for the nuclear pair production process and for the electronic pair production process.
- (b) Calculate the energy transferred from photons to charged particles (CPs) when an x-ray beam containing $N(0) = 10^5$ photons passes through a lead sheet of thickness $x = 1.5$ cm. Assume that all photon interactions are of the pair production type and that the pair production process in lead for 10 MeV photons has a cross section (atomic attenuation coefficient) ${}_a\kappa(\text{Pb}, 10 \text{ MeV}) = 12.4 \times 10^{-24} \text{ cm}^2/\text{atom}$.
- (c) A 10 MeV photon interacts with an absorber in a pair production process. Calculate the kinetic energy E_K of the positron produced in the interaction, if the electron emerges from the interaction with kinetic energy $E_K = 2 \text{ MeV}$.
- (d) A positron with kinetic energy $E_K = 2 \text{ MeV}$ is annihilated by a stationary electron. Calculate the total energy that is radiated in the form of photons.

SOLUTION:

(a) The two pair production processes (nuclear and electronic) are shown schematically in Fig. 7.40. In both processes the photon disappears and an electron-positron pair (matter) is produced out of photon energy. This is referred to as “materialization” and requires an expenditure of energy equivalent of two electronic rest energies ($2m_e c^2 = 1.022 \text{ MeV}$). The rest of the photon energy ($h\nu - 2m_e c^2$) is transferred to charged particles released in the absorber.

(b) To calculate the energy that is transferred from the photon beam to the 1.5 cm thick lead absorber we first determine the number of interactions \mathcal{N} that the photon beam will have in the absorber and then multiply this number by the mean energy transfer in pair production $\bar{E}_{\text{tr}}^{\text{PP}}$ from photon to charged particles.

To calculate the number of pair production interactions in the slab we will need the linear attenuation coefficient for pair production κ that is related to the atomic attenuation coefficient (cross section) ${}_a\kappa$ as follows

$$\begin{aligned} \kappa &= n \square {}_a\kappa = \rho \frac{N_A}{A} {}_a\kappa \\ &= (11.34 \text{ g/cm}^2) \times \frac{6.022 \times 10^{23} \text{ atom/mol}}{207.2 \text{ g/mol}} \times (12.4 \times 10^{-24} \text{ cm}^2/\text{atom}) \\ &= 0.409 \text{ cm}^{-1}. \end{aligned} \tag{7.261}$$

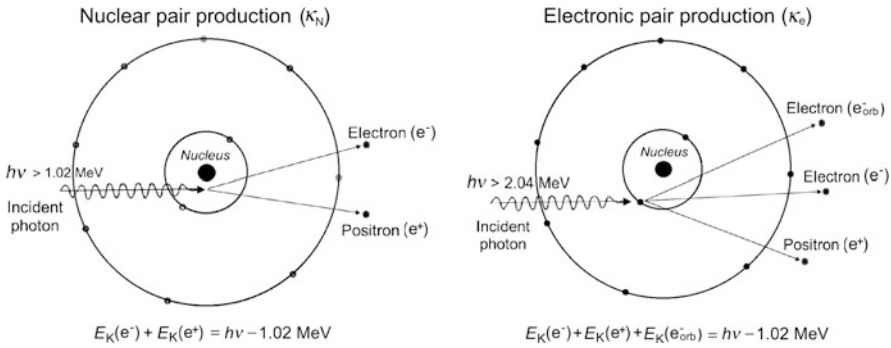


Fig. 7.40 Schematic diagrams of nuclear pair production and triplet production

Number of photons $N(x)$ transmitted through the lead slab of thickness $x = 1.5 \text{ cm}$ is given as

$$\begin{aligned}
 N(x) &= N(0)e^{-\kappa x} = 10^5 \times e^{-(0.409 \text{ cm}^{-1}) \times (1.5 \text{ cm})} = 10^5 \times e^{-0.6135} \\
 &= 0.541 \times 10^5 \text{ photons.}
 \end{aligned}
 \tag{7.262}$$

The number of photons $\mathcal{N}(x)$ interacting in the slab will be

$$\mathcal{N}(x) = N(0) - N(x) = N(0)[1 - e^{-\kappa x}] = 0.459 \times 10^5 \text{ photons.}
 \tag{7.263}$$

In general, in each pair production interaction the energy E_{tr}^{PP} transferred from the photon to CPs is the photon energy $h\nu$ less the rest masses of the two CPs (electron: $m_e c^2 = 0.511 \text{ MeV}$ and positron: $m_{e^+} c^2 = 0.511 \text{ MeV}$) produced out of energy, i.e., $E_{tr}^{PP} = h\nu - 2m_e c^2$. For photons of energy $h\nu = 10 \text{ MeV}$, the energy transferred to CPs is $10 \text{ MeV} - 1.022 \text{ MeV} = 8.978 \text{ MeV}$.

Since there are 0.459×10^5 pair production events in the 1.5 cm thick lead slab and in each event energy of 8.978 MeV is transferred to kinetic energy of CPs, the total kinetic energy of CPs is

$$\begin{aligned}
 E_K(\text{CPs}) &= 0.459 \times 10^5 \times 8.978 \text{ MeV} \\
 &= 4.11 \times 10^5 = (4.11 \times 10^{11} \text{ eV}) \times (1.6 \times 10^{-19} \text{ J/eV}) \\
 &= 6.58 \times 10^{-8} \text{ J.}
 \end{aligned}
 \tag{7.264}$$

(c) The energy E_{tr}^{PP} transferred from a 10 MeV photon to CPs in a pair production event is given as $E_{tr}^{PP} = h\nu - 2m_e c^2 = 10 \text{ MeV} - 1.022 \text{ MeV} = 8.978 \text{ MeV}$. This energy is shared between the electron and the positron that are produced in a pair production process. Thus, if the electron carries away a kinetic energy E_K of 2 MeV from the total available energy of 8.978 MeV, then the positron will get the remaining part of E_{tr}^{PP} which is $8.98 \text{ MeV} - 2 \text{ MeV} = 6.978 \text{ MeV}$. Thus, the kinetic energy of the positron in this pair production event is 6.978 MeV.

(d) The process of positron annihilation by a stationary electron before the positron expended all of its kinetic energy is referred to as in-flight annihilation. In general, the total energy radiated from the annihilation-in-flight event is equal to the kinetic energy E_K of the positron plus the sum of rest energies of the electron and positron, i.e., $2m_e c^2 = 1.022 \text{ MeV}$.

In our example, thus, the total energy radiated from the annihilation in flight event is $2 \text{ MeV} + 1.022 \text{ MeV} = 3.022 \text{ MeV}$.

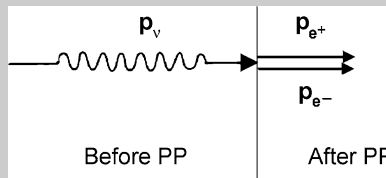
7.6.Q2

(175)

In pair production (PP) an electron-positron pair is produced (materialization) out of energy (photon) either in (1) electric field of a nucleus of an absorber atom (nuclear PP) or in (2) electric field of an orbital electron of an absorber atom (electronic PP also called triplet production).

(a) Show that materialization (production of matter out of energy) in pair production cannot occur in free space. Make the following simplifying assumptions:

- (1) Electron and positron are produced with identical kinetic energies and
- (2) All momenta involved in the materialization process are collinear, as shown schematically in the following diagram



(b) Show that materialization in pair production cannot occur in free space in general, as shown schematically in the following diagram with $E_K^{e^+} \neq E_K^{e^-}$ and momenta are not collinear

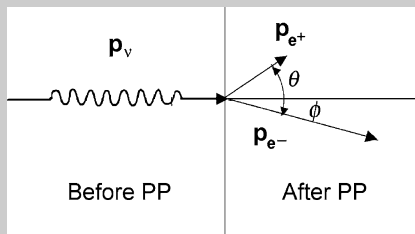


Table 7.13 Parameters of pair production before and after pair production interaction in free space under special conditions of $E_K^- = E_K^+$ and all momenta collinear

BEFORE PP interaction in free space	AFTER PP interaction in free space
Total energy	
$E_\nu = h\nu$	$E_{\text{pair}} = E_K^- + E_K^+ + 2E_0 = 2\gamma E_0 = 2\gamma m_e c^2$
Charge	
$q = 0$ (photon)	$q = 0$ (electron e^- and positron e^+)
Momentum	
$p_\nu = \frac{E_\nu}{c} = \frac{h\nu}{c}$	$p_{\text{pair}} = 2\gamma m_e v = E_{\text{pair}} \frac{v}{c^2}$

SOLUTION:

When the incident photon energy $E_\nu = h\nu$ exceeds $2m_e c^2 = 1.022$ MeV, where $m_e c^2$ is the rest energy of the electron as well as of its anti-particle, the positron, the production of an electron-positron pair in conjunction with a complete absorption of the incident photon by absorber atom becomes energetically possible.

For pair production (PP) effect to occur, three quantities must be conserved: (1) total energy, (2) charge, and (3) momentum. Thus, to study the possibility of pair production occurring in free space we must evaluate conservation of the three quantities assuming that photon transformation into an electron-positron pair occurs in free space.

(a) First we evaluate the simpler special case in which kinetic energies of the electron and positron, E_K^- and E_K^+ , respectively, are identical upon production, and both particles move colinearly in the direction of the incident photon. The parameters before and after PP interaction are presented in Table 7.13.

In (7.269) we assumed that total energy is conserved [see (7.266)] and obtained a result $p_\nu = p_{\text{pair}} c/v$. Since the particle velocity v is always smaller than speed of light c in vacuum, this result indicates a violation of the momentum conservation principle and leads to a conclusion that both the total energy and momentum could not be conserved simultaneously if pair production occurred in free space. Photon momentum p_ν before the PP interaction is always larger than p_{pair} , the combined momentum of the electron and positron after the PP interaction. Thus, the incident photon possesses momentum excess that cannot be absorbed by the electron-positron pair but must be absorbed by a collision partner, be it an atomic nucleus of the absorber atom (nuclear PP) or orbital electron of the absorber atom (electronic PP).

(1) Conservation of total energy:

$$E_{\text{before}} = E_{\text{after}} \quad (7.265)$$

$$E_\nu = h\nu \equiv E_{\text{pair}} = E_K^- + E_K^+ + 2E_0 = 2\gamma E_0 = 2\gamma m_e c^2 \quad (7.266)$$

Table 7.14 Parameters of pair production before and after general pair production interaction in free space

BEFORE PP interaction in free space	AFTER PP interaction in free space
Total energy	
$E_\nu = h\nu$	$E_{\text{pair}} = E_K^{e^-} + E_K^{e^+} + 2E_0 = E_K^{e^-} + E_K^{e^+} + 2m_e c^2$
Charge	
$q = 0$ (photon)	$q = 0$ (electron e^- and positron e^+)
Momentum along abscissa (x) axis	
$(p_\nu)_x = \frac{E_\nu}{c} = \frac{h\nu}{c}$	$(p_{\text{pair}})_x = p_{e^+} \cos \theta + p_{e^-} \cos \phi$
Momentum along ordinate (y) axis	
$(p_\nu)_y = 0$	$(p_{\text{pair}})_y = p_{e^+} \sin \theta - p_{e^-} \sin \phi$

(2) Conservation of charge:

$$q_{\text{before}} = q_{\text{after}} \quad (7.267)$$

Charge before pair production interaction is zero (photon) and charge after PP interaction is also zero (negative e^- plus positive e^+).

(3) Conservation of momentum:

$$p_{\text{before}} = p_{\text{after}} \quad (7.268)$$

$$p_\nu = \frac{E_\nu}{c} = \frac{h\nu}{c} \equiv \frac{E_{\text{pair}}}{c} = \frac{2\gamma m_e c^2}{c} = \frac{(2\gamma m_e \nu)c}{\nu} = p_{\text{pair}} \frac{c}{\nu} \quad (7.269)$$

(b) In this section we look at a general case of PP occurring in free space, with electron and positron acquiring different kinetic energies (i.e., $E_K^{e^-} \neq E_K^{e^+}$) and different emission angles ϕ and θ , respectively. Like in **(a)**, we lay out the conservation of total energy, charge and momentum equations, however, for the momentum conservation we now get two equations, one for the abscissa (x) axis and the other for the ordinate (y) axis.

The Cartesian coordinate system is oriented such that the incident photon is directed in the positive direction of the abscissa axis, and the pair production event occurs at the origin $(0, 0)$ of the coordinate system. Table 7.14 lists the parameters of general pair production in free space and the conservation of total energy, charge, and momentum are expressed as follows:

(1) Conservation of total energy:

$$E_{\text{before}} = E_{\text{after}} \quad (7.270)$$

$$E_\nu = h\nu \equiv E_{\text{pair}} = E_K^{e^-} + E_K^{e^+} + 2E_0 = E_K^{e^-} + E_K^{e^+} + 2m_e c^2 \quad (7.271)$$

(2) Conservation of charge:

$$q_{\text{before}} = q_{\text{after}} \quad (7.272)$$

Charge before is 0 (photon) and charge after is also zero (negative e^- plus positive e^+).

(3) Conservation of momentum along the abscissa axis:

$$(p_{\text{before}})_x = (p_{\text{after}})_x \quad (7.273)$$

$$(p_\nu)_x = \frac{E_\nu}{c} = \frac{h\nu}{c} \equiv p_{e^+} \cos \theta + p_{e^-} \cos \phi \quad (7.274)$$

(4) Conservation of momentum along the ordinate axis:

$$(p_{\text{before}})_y = (p_{\text{after}})_y \quad (7.275)$$

$$(p_\nu)_y = 0 = p_{e^+} \sin \theta - p_{e^-} \sin \phi \quad (7.276)$$

Equations (7.271), (7.274), and (7.276) are similar to those that were used in derivation of the wavelength shift $\Delta\lambda$ in Compton effect, so we will investigate them using the same approach. We express (7.274) and (7.276), respectively, as follows

$$(E_\nu - p_{e^+} c \cos \theta)^2 \equiv E_\nu^2 - 2E_\nu p_{e^+} c \cos \theta + p_{e^+}^2 c^2 \cos^2 \theta = (p_{e^+} c \cos \theta)^2 \quad (7.277)$$

and

$$(p_{e^+} c \sin \theta)^2 = (p_{e^-} c \sin \phi)^2. \quad (7.278)$$

Addition of (7.277) and (7.278) results in

$$E_\nu^2 - 2E_\nu p_{e^+} c \cos \theta + p_{e^+}^2 c^2 = p_{e^-}^2 c^2. \quad (7.279)$$

Recalling the standard relativistic relationship between momentum p , rest energy E_0 , and kinetic energy E_K of a particle expressed as $p^2 c^2 = (E_K + E_0)^2 - E_0^2 = E_K^2 + 2E_K E_0$, we now express (7.279) as follows

$$E_\nu^2 - 2E_\nu p_{e^+} c \cos \theta + (E_K^{e^+} + E_0)^2 = (E_K^{e^-} + E_0)^2. \quad (7.280)$$

From conservation of total energy (7.271) we note that

$$E_K^{e^-} + E_0 = E_\nu - E_K^{e^+} - E_0 \quad (7.281)$$

and introduce (7.281) into (7.280) to get, after convenient cancellation of several terms, a simple expression

$$p_{e^+} c \cos \theta \equiv \left[\sqrt{(E_K^{e^+})^2 + 2E_K^{e^+} E_0} \right] \cos \theta = E_K^{e^+} + E_0. \quad (7.282)$$

Squaring (7.282) and rearranging the terms we finally get the following expression for $\cos^2 \theta$

$$\cos^2 \theta = \frac{(E_K^{e^+} + E_0)^2}{(E_K^{e^+})^2 + 2E_K^{e^+} E_0} = 1 + \frac{E_0^2}{(E_K^{e^+})^2 + 2E_K^{e^+} E_0} \geq 1. \quad (7.283)$$

In similar fashion we can derive from (7.274) and (7.275) an expression for $\cos^2 \phi$ that reads

$$\cos^2 \phi = \frac{(E_K^{e^-} + E_0)^2}{(E_K^{e^-})^2 + 2E_K^{e^-} E_0} = 1 + \frac{E_0^2}{(E_K^{e^-})^2 + 2E_K^{e^-} E_0} \geq 1. \quad (7.284)$$

Since $E_0 \neq 0$, we conclude that (7.283) and (7.284) are always larger than 1 and, since cosine of any angle will always be smaller or equal to 1, we also conclude that (7.283) and (7.284) do not describe a viable physical process. This means that conservation of total energy and momentum cannot be fulfilled simultaneously in general pair production occurring in free space.

7.6.Q3

(176)

Nuclear reactions are characterized by the following simple equation: $a + A = B + b + Q$, where a is the projectile, A is the stationary target, b and B are reaction products, and Q is reaction energy usually referred to as the reaction Q value. When a nuclear reaction releases energy ($Q > 0$), it is called exothermic or exoergic; when it absorbs energy to get started ($Q < 0$), it is called endothermic or endoergic. A special case of nuclear reaction is elastic collision in which $Q = 0$ and no energy is produced nor consumed.

In principle, an exothermic reaction can occur spontaneously; an endothermic reaction, on the other hand, cannot get started unless the projectile has kinetic energy equal to or exceeding a threshold energy, whose value in the center-of-mass system is equal to the absolute Q value. At threshold energy, the reaction can just take place but the reaction products have zero kinetic energy.

Using the invariant $E^2 - p^2 c^2 = \text{inv}$, where E is the total energy of the particles and p is the momentum before interaction in the laboratory system and after interaction in the center-of-mass system, calculate:

- (a) Threshold energy $E_{\text{thr}}^{\text{NPP}}$ for nuclear pair production.
- (b) Threshold energy $E_{\text{thr}}^{\text{EPP}}$ for electronic pair production (triplet production).
- (c) Threshold total energy E_{thr} and threshold kinetic energy $(E_K)_{\text{thr}}$ for a general nuclear reaction expressed as: $a + A = B + b$.

SOLUTION:

In physics the invariant is defined as a quantity that does not change when it undergoes a transformation from one reference frame to another, such as, for example, when going from laboratory frame before a nuclear interaction to center-of-mass frame or to center-of-momentum (COM) frame after interaction. COM frame is defined as an inertial frame in which the center of mass is at rest and thus has no velocity.

(a) Threshold energy $(E_\nu)_{\text{thr}}^{\text{NPP}}$ for nuclear pair production

- (1) *Before interaction* (photon with energy E_ν + atomic nucleus with rest energy $m_A c^2$)

Total energy:

$$E_{\text{before}} = (E_\nu)_{\text{thr}}^{\text{NPP}} + m_A c^2 \quad (7.285)$$

Momentum:

$$p_{\text{before}} = \frac{(E_\nu)_{\text{thr}}^{\text{NPP}}}{c} \quad (7.286)$$

Invariant before:

$$\begin{aligned} E_{\text{before}}^2 - p_{\text{before}}^2 c^2 &= \{(E_\nu)_{\text{thr}}^{\text{NPP}} + m_A c^2\}^2 - \left[\frac{(E_\nu)_{\text{thr}}^{\text{NPP}}}{c} \right]^2 c^2 \\ &= \{[(E_\nu)_{\text{thr}}^{\text{NPP}}]^2 + 2(E_\nu)_{\text{thr}}^{\text{NPP}} m_A c^2 + [m_A c^2]^2\} \\ &\quad - [(E_\nu)_{\text{thr}}^{\text{NPP}}]^2. \end{aligned} \quad (7.287)$$

- (2) *After interaction* (nucleus with rest energy $m_A c^2$ + electron/positron pair with combined rest energy $2m_e c^2$)

Total energy:

$$E_{\text{after}} = m_A c^2 + 2m_e c^2 \quad (7.288)$$

Momentum:

$$p_{\text{after}} = 0 \quad (7.289)$$

Invariant after:

$$\begin{aligned} E_{\text{after}}^2 - p_{\text{after}}^2 c^2 &= \{m_A c^2 + 2m_e c^2\}^2 - 0 \\ &= \{(m_A c^2)^2 + 4(m_A c^2)(m_e c^2) + 4(m_e c^2)^2\} - 0 \end{aligned} \quad (7.290)$$

We now equate the two invariants (7.287) and (7.290) and solve for the threshold energy $(E_\nu)_{\text{thr}}^{\text{NPP}}$

$$(E_\nu)_{\text{thr}}^{\text{NPP}} = \frac{4m_e c^2 (m_A c^2 + m_e c^2)}{2m_A c^2} = 2m_e c^2 \left(1 + \frac{m_e c^2}{m_A c^2} \right). \quad (7.291)$$

(b) Threshold energy $(E_\nu)_{\text{thr}}^{\text{EPP}}$ for **electronic pair production**

(1) *Before interaction* (photon with energy E_ν + atomic orbital electron with rest energy $m_e c^2$)

Total energy:

$$E_{\text{before}} = (E_\nu)_{\text{thr}}^{\text{EPP}} + m_e c^2 \quad (7.292)$$

Momentum:

$$p_{\text{before}} = \frac{(E_\nu)_{\text{thr}}^{\text{EPP}}}{c} \quad (7.293)$$

Invariant before:

$$\begin{aligned} E_{\text{before}}^2 - p_{\text{before}}^2 c^2 &= [(E_\nu)_{\text{thr}}^{\text{EPP}} + m_e c^2]^2 - \left[\frac{(E_\nu)_{\text{thr}}^{\text{EPP}}}{c} \right]^2 c^2 \\ &= \{ [(E_\nu)_{\text{thr}}^{\text{EPP}}]^2 + 2(E_\nu)_{\text{thr}}^{\text{EPP}} m_e c^2 + [m_e c^2]^2 \} \\ &\quad - [(E_\nu)_{\text{thr}}^{\text{EPP}}]^2. \end{aligned} \quad (7.294)$$

(2) *After interaction* (atomic orbital electron with rest mass $m_e c^2$ + electron/positron pair with combined rest mass $2m_e c^2$)

Total energy:

$$E_{\text{after}} = 3m_e c^2 \quad (7.295)$$

Momentum:

$$p_{\text{after}} = 0$$

Invariant after:

$$E_{\text{after}}^2 - p_{\text{after}}^2 c^2 = [3m_e c^2]^2 - 0 = 9(m_e c^2)^2. \quad (7.296)$$

We now equate the two invariants of (7.294) and (7.296) and solve for the threshold energy $(E_\nu)_{\text{thr}}^{\text{EPP}}$

$$(E_\nu)_{\text{thr}}^{\text{EPP}} = \frac{8(m_e c^2)^2}{2m_A c^2} = 4m_e c^2. \quad (7.297)$$

(c) Threshold total energy $E_{\text{thr}}^{\text{a}}$ and threshold kinetic energy $(E_K)_{\text{thr}}$ for a **general nuclear reaction expressed as: $a + A = B + b$.**

(1) *Before nuclear reaction* in laboratory system

(projectile a with total energy $E_{\text{thr}}^{\text{a}} = (E_K^{\text{a}})_{\text{thr}} + m_a c^2$ + stationary target with rest energy $m_A c^2$)

Total energy:

$$E_{\text{before}} = \sqrt{(m_a c^2)^2 + p_a^2 c^2} + m_A c^2 \quad (7.298)$$

Momentum:

$$p_{\text{before}} = \frac{(E_{\nu})_{\text{thr}}^{\text{EPP}}}{c} \quad (7.299)$$

Invariant before:

$$\begin{aligned} E_{\text{before}}^2 - p_{\text{before}}^2 c^2 &= \left\{ \sqrt{(m_a c^2)^2 + p_a^2 c^2} + m_A c^2 \right\}^2 - p_a^2 c^2 \\ &= (m_a c^2)^2 + p_a^2 c^2 + 2E_{\text{thr}}^a m_A c^2 + (m_A c^2)^2 - p_a^2 c^2. \end{aligned} \quad (7.300)$$

- (2) *After interaction* in center of mass system
(reaction products B and b with rest energies $m_B c^2$ and $m_b c^2$, respectively)
Total energy:

$$E_{\text{after}} = m_B c^2 + m_b c^2 \quad (7.301)$$

Momentum:

$$p_{\text{after}} = 0 \quad (7.302)$$

Invariant after:

$$E_{\text{after}}^2 - p_{\text{after}}^2 c^2 = [m_B c^2 + m_b c^2]^2 - 0. \quad (7.303)$$

We now equate the two invariants of (7.300) and (7.303) and solve for threshold total energy E_{thr}^a and obtain the following result

$$E_{\text{thr}}^a = \frac{[m_B c^2 + m_b c^2]^2 - [(m_a c^2)^2 + (m_A c^2)^2]}{2m_A c^2}. \quad (7.304)$$

Threshold kinetic energy $(E_K^a)_{\text{thr}}$ of projectile a is the difference between the projectile's threshold total energy E_{thr}^a given in (7.304) and its rest energy $m_a c^2$

$$\begin{aligned} (E_K^a)_{\text{thr}} &= E_{\text{thr}}^a - m_a c^2 = \frac{[m_B c^2 + m_b c^2]^2 - [(m_a c^2)^2 + (m_A c^2)^2]}{2m_A c^2} - m_a c^2 \\ &= \frac{[m_B c^2 + m_b c^2]^2 - [m_A c^2 + m_a c^2]^2}{2m_A c^2}. \end{aligned} \quad (7.305)$$

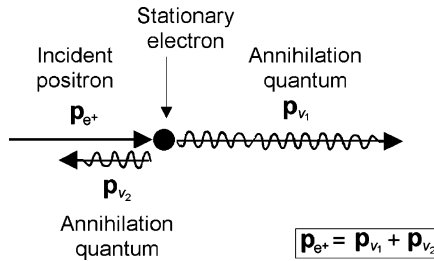


Fig. 7.41 Annihilation-in-flight on stationary electron for positron with kinetic energy E_K

7.6.Q4

(177)

A pair production event is followed by a two-quantum annihilation of the positron when the kinetic energy of the positron is E_K (in-flight annihilation). Energies of the two photons produced are $h\nu_1$ and $h\nu_2$. Assume that the positron and the two photons are co-linear and:

- (a) Draw a schematic diagram of the annihilation event.
- (b) Determine the general relationship for energies $h\nu_1$ and $h\nu_2$ of the two quanta emitted.
- (c) Show that in the extreme relativistic case, where $E_K \gg m_e c^2$, one of the two quanta has energy $h\nu_1 = E_K + \frac{3}{2}m_e c^2$, while the other quantum has energy $h\nu_1 = \frac{1}{2}m_e c^2$.
- (d) Determine the magnitudes of momenta for the incident positron and the two quanta for $E_K \gg m_e c^2$ and ensure that the schematic diagram of (a) reflects the relative magnitude of the momenta.

SOLUTION:

(a) A simple schematic diagram for positron-electron annihilation event is shown in Fig. 7.41.

(b) Derivation of the general expressions for $h\nu_1$ and $h\nu_2$ is based on principles of conservation of energy and momentum.

Conservation of energy:

$$E_{e^+} + m_e c^2 \equiv (E_K + m_e c^2) + m_e c^2 = h\nu_1 + h\nu_2 \quad \text{or} \quad E_K + 2m_e c^2 = h\nu_1 + h\nu_2, \quad (7.306)$$

where E_{e^+} is the total energy of the incident positron, $m_e c^2$ is the electron rest mass (0.511 MeV), and $m_e c^2$ is the positron rest mass (0.511 MeV).

Conservation of momentum p :

$$p_{e^+} \equiv \frac{E_K}{c} \sqrt{1 + \frac{2m_e c^2}{E_K}} = -p_{v_1} + p_{v_2} \equiv -\frac{h\nu_1}{c} + \frac{h\nu_2}{c} \quad \text{or} \quad (7.307)$$

$$E_K \sqrt{1 + \frac{2m_e c^2}{E_K}} = -h\nu_1 + h\nu_2,$$

where p stands for momentum, for a particle such as positron, related to E_K through the standard relationship $E^2 \equiv (E_K + m_0 c^2)^2 = p^2 c^2 + m_0 c^2$, as discussed in (T1.62).

Equations (7.306) and (7.307) provide two equations for two unknowns and adding them results in the following expression for $h\nu_2$

$$E_K \left[1 + \sqrt{1 + \frac{2m_e c^2}{E_K}} \right] + 2m_e c^2 = 2h\nu_2 \quad \text{or} \quad (7.308)$$

$$h\nu_2 = \frac{1}{2} E_K \left[1 + \sqrt{1 + \frac{2m_e c^2}{E_K}} \right] + m_e c^2.$$

Direct insertion of (7.308) into (7.306) results in the following expression for $h\nu_1$

$$h\nu_1 = \frac{1}{2} E_K \left[1 - \sqrt{1 + \frac{2m_e c^2}{E_K}} \right]. \quad (7.309)$$

(c) We now evaluate $h\nu_1$ and $h\nu_2$ for $E_K \gg m_e c^2$ and get the following expressions

$$h\nu_1 = \frac{1}{2} E_K \left[1 - \sqrt{1 + \frac{2m_e c^2}{E_K}} \right] \approx \frac{1}{2} E_K - \frac{1}{2} E_K \left(1 + \frac{m_e c^2}{E_K} \right) = \frac{1}{2} m_e c^2 \quad (7.310)$$

and

$$h\nu_2 = \frac{1}{2} E_K \left[1 + \sqrt{1 + \frac{2m_e c^2}{E_K}} \right] + m_e c^2$$

$$\approx \frac{1}{2} E_K + \frac{1}{2} E_K \left(1 + \frac{m_e c^2}{E_K} \right) + m_e c^2 = E_K + \frac{3}{2} m_e c^2. \quad (7.311)$$

(d) Magnitudes of momenta \mathbf{p}_{e^+} , \mathbf{p}_{v_1} , and \mathbf{p}_{v_2} are as follows:

(1) Magnitude of momentum \mathbf{p}_{e^+} , as shown in (7.307)

$$|\mathbf{p}_{e^+}| = p_{e^+} = \frac{E_K}{c} \sqrt{1 + \frac{2m_e c^2}{E_K}} \approx \frac{E_K}{c} \left(1 + \frac{m_e c^2}{E_K} \right) = \frac{1}{c} (E_K + m_e c^2). \quad (7.312)$$

(2) Magnitude of momentum \mathbf{p}_{v_1} using (7.310)

$$|\mathbf{p}_{v_1}| = p_{v_1} = \frac{h\nu_1}{c} = \frac{1}{2c} E_K \left[1 - \sqrt{1 + \frac{2m_e c^2}{E_K}} \right] \approx \frac{1}{c} \left(\frac{1}{2} m_e c^2 \right). \quad (7.313)$$

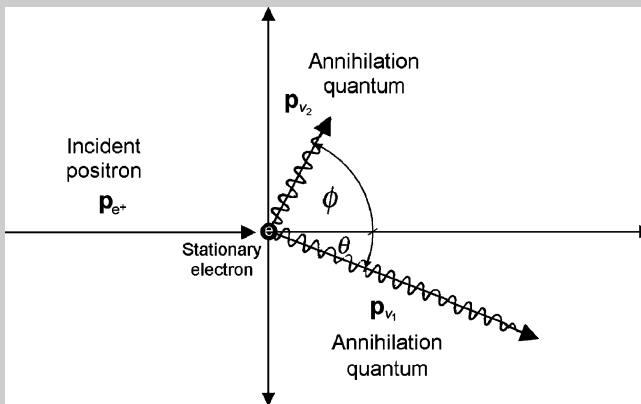
(3) Magnitude of momentum \mathbf{p}_{v_2} using (7.311)

$$|\mathbf{p}_{v_1}| = p_{v_1} = \frac{h\nu_1}{c} = \frac{1}{2c} E_K \left[1 + \sqrt{1 + \frac{2m_e c^2}{E_K}} \right] \approx \frac{1}{c} \left(E_K + \frac{3}{2} m_e c^2 \right). \quad (7.314)$$

7.6.Q5

(178)

A positron with kinetic energy $E_K = 2E_0 = 2m_e c^2$ undergoes an in-flight annihilation event with a stationary electron resulting in emission of two photons (annihilation quanta) $h\nu_1$ and $h\nu_2$, as shown in the diagram below.



Assume that $h\nu_1 = 2h\nu_2$ and determine:

- Energies $h\nu_1$ and $h\nu_2$ of the two annihilation quanta.
- Emission angles θ and ϕ of the two annihilation quanta.

SOLUTION:

(a) Since we know the energy relationship between the two quanta ($h\nu_1 = 2h\nu_2$), we can determine the actual energies of the two quanta directly from the principle of conservation of energy in the annihilation process. The conservation of total energy is expressed as follows

$$E_{e^+} + m_e c^2 \equiv (E_K + m_e c^2) + m_e c^2 = E_K + 2E_0 = h\nu_1 + h\nu_2, \quad (7.315)$$

where E_{e^+} is the total energy of the incident positron, $m_{e^+}c^2$ rest energy of the positron, given as $E_0 = 0.511$ MeV, and $m_{e^-}c^2$ rest energy of the electron, also given as $E_0 = 0.511$ MeV.

Inserting $E_K = 2E_0$ and $h\nu_1 = 2h\nu_2$ into (7.315) gives the following results for $h\nu_1$ and $h\nu_2$

$$h\nu_1 = \frac{8}{3}E_0 = \frac{8}{3}m_e c^2 \quad \text{and} \quad h\nu_2 = \frac{4}{3}E_0 = \frac{4}{3}m_e c^2. \quad (7.316)$$

(b) To determine the emission angles θ and ϕ we set up two conservation of momentum equations, one for the abscissa axis and the other for the ordinate axis on a Cartesian coordinate system oriented such that the incident positron travels in the positive direction along the abscissa axis. The two conservation of momentum equations read as follows:

(1) *Conservation of momentum along abscissa axis*

$$p_{e^+} = \frac{1}{c}\sqrt{E_K^2 + 2E_0E_K} = \frac{h\nu_1}{c}\cos\theta + \frac{h\nu_2}{c}\cos\phi. \quad (7.317)$$

After multiplying (7.317) with c and inserting $E_K = 2E_0$, $h\nu_1 = \frac{8}{3}E_0$, and $h\nu_2 = \frac{4}{3}E_0$ into (7.319) we get the following expression relating θ and ϕ

$$3\sqrt{2} = 4\cos\theta + 2\cos\phi \quad \text{or} \quad \cos\theta = \frac{3}{4}\sqrt{2} - \frac{1}{2}\cos\phi. \quad (7.318)$$

(2) *Conservation of momentum along ordinate axis*

$$\frac{h\nu_1}{c}\sin\theta = \frac{h\nu_2}{c}\sin\phi. \quad (7.319)$$

After multiplying (7.319) with c and inserting $E_K = 2E_0$, $h\nu_1 = \frac{8}{3}E_0$, and $h\nu_2 = \frac{4}{3}E_0$ into (7.319) we get the following expression relating θ and ϕ

$$\sin\theta = \frac{1}{2}\sin\phi. \quad (7.320)$$

Equations (7.318) and (7.320) serve as two equations for two unknowns (θ and ϕ). Squaring the two equations opens an elegant approach to finding the actual values of θ and ϕ

$$\cos^2\theta = \left(\frac{3\sqrt{2}}{4} - \frac{1}{2}\cos\phi\right)^2 = \frac{9}{2} - \frac{3\sqrt{2}}{4}\cos\phi + \frac{1}{4}\cos^2\phi \quad (7.321)$$

and

$$\sin^2\theta = \frac{1}{4}\sin^2\phi. \quad (7.322)$$

Adding (7.321) and (7.322) gives the following equation for $\cos \phi$

$$(\sin^2 \theta + \cos^2 \theta) = \frac{9}{2} - \frac{3\sqrt{2}}{4} \cos \phi + \frac{1}{4} (\sin^2 \phi + \cos^2 \phi). \quad (7.323)$$

Recalling that $\sin^2 x + \cos^2 x = 1$ and solving (7.323) for $\cos \phi$ gives the following result

$$\cos \phi = 0.3536 \quad \text{and} \quad \phi = \arccos 0.3536 = 69.3^\circ. \quad (7.324)$$

Inserting (7.324) into (7.320) gives the following result for $\sin \theta$

$$\sin \theta = \frac{1}{2} \sin \phi = \frac{1}{2} \sqrt{1 - \cos^2 \phi} = 0.4677 \quad \text{and} \quad \theta = \arcsin 0.4677 = 27.9^\circ. \quad (7.325)$$

A more general approach for finding θ and ϕ is possible through the use of the cosine rule for the determination of the two emission angles. A closer look at the schematic diagram of the annihilation process shown in Fig. 7.42 reveals that momenta \mathbf{p}_{ν_1} , \mathbf{p}_{ν_2} , and \mathbf{p}_{e^+} form two triangles for which angles θ and ϕ can be determined through the use of the cosine rule as follows

(1) Cosine rule applied to triangle 1 in Fig. 7.42 results in the following expression for $\cos \theta$

$$p_{\nu_2}^2 = p_{\nu_1}^2 + p_{e^+}^2 - 2p_{\nu_1} p_{e^+} \cos \theta. \quad (7.326)$$

Solving (7.326) for $\cos \theta$ gives the following explicit expression for $\cos \theta$

$$\cos \theta = \frac{p_{\nu_1}^2 + p_{e^+}^2 - p_{\nu_2}^2}{2p_{\nu_1} p_{e^+}} = \frac{(\frac{8}{3})^2 + (2\sqrt{2})^2 - (\frac{4}{3})^2}{2 \times \frac{8}{3} \times 2\sqrt{2}} = 0.884, \quad (7.327)$$

resulting in $\theta = \arccos 0.884 = 27.9^\circ$.

(2) Cosine rule applied to triangle 2 in Fig. 7.42 results in the following expression for $\cos \phi$

$$p_{\nu_2}^2 = p_{\nu_1}^2 + p_{e^+}^2 - 2p_{\nu_1} p_{e^+} \cos \phi. \quad (7.328)$$

Solving (7.328) for $\cos \phi$ gives the following explicit expression for $\cos \phi$

$$\cos \phi = \frac{p_{\nu_1}^2 + p_{e^+}^2 - p_{\nu_2}^2}{2p_{\nu_1} p_{e^+}} = \frac{(\frac{4}{3})^2 + (2\sqrt{2})^2 - (\frac{8}{3})^2}{2 \times \frac{4}{3} \times 2\sqrt{2}} = 0.354, \quad (7.329)$$

resulting in $\phi = \arccos 0.354 = 69.3^\circ$.

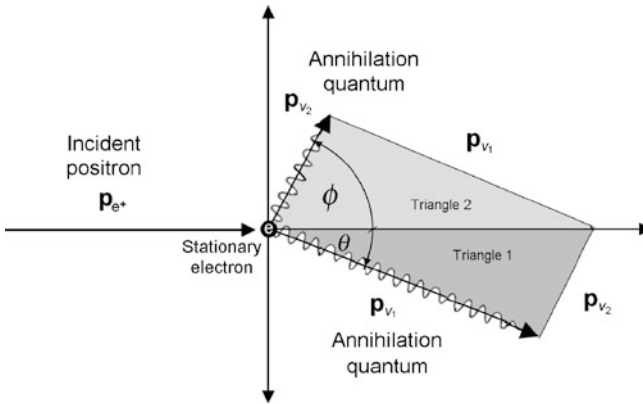


Fig. 7.42 Schematic diagram of the positron in-flight annihilation process

7.7 Photonuclear Reactions

7.7.Q1

(179)

Photonuclear (PN) reaction (also called nuclear photoelectric effect or photo-disintegration) is a term used to describe direct interaction between an energetic photon (x ray or gamma ray) and a nucleus of the absorber atom. The nucleus absorbs the photon and often ejects a neutron [in a (γ, n) process] or a proton [in a (γ, p) process]. Less common are ejection of a deuteron [in a (γ, d) process], ejection of multiple nucleons [in (γ, nn) and (γ, np) processes], and induction of nuclear fission in the so-called photo-fission process. For a particle to be ejected from the nucleus the photon energy must exceed the particle binding energy E_B to the nucleus. PN reactions are endothermic and the minimum photon energy that can induce a given PN reaction is called the threshold energy $h\nu_{thr}^{PN}$ for the PN reaction. Three methods have been developed for the calculation of the PN threshold energy: (1) Rest energy method, (2) Binding energy method, and (3) Relativistic invariant method.

Derive expressions for threshold energy E_{thr}^{PN} in a photonuclear reaction based upon:

- (a) Rest energies of the target, projectile, and reaction products.
- (b) Binding energies of the target, projectile, and reaction products.
- (c) Relativistic invariant: $E^2 - p^2c^2 = inv$ for before and after the PN reaction.
- (d) Use the three methods to calculate threshold energy $E_{thr}^{PN} = h\nu_{thr}^{PN}$ of the ${}^{208}_{82}\text{Pb}(\gamma, n){}^{207}_{82}\text{Pb}$ photonuclear reaction.

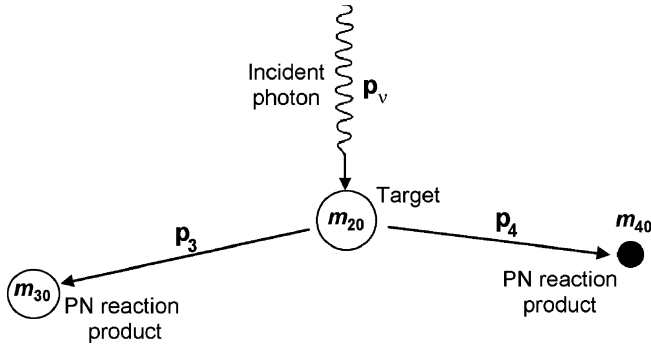


Fig. 7.43 Schematic diagram of a photoneuclear reaction with photon as projectile and nucleus m_{20} as target. Reaction products consist of heavier nucleus m_{30} and nucleon or light nucleus m_{40}

SOLUTION:

The schematic diagram of a PN reaction is similar to that of a general endothermic nuclear reaction (see Fig. T5.1) except that the projectile, which in general nuclear reaction is a particle with rest mass m_{10} and rest energy $m_{10}c^2$, in a PN reaction is an energetic photon with energy $h\nu$, rest energy $m_{10}c^2 = 0$, and momentum $|\mathbf{p}_v| = p_v = h\nu/c$, as shown in Fig. 7.43.

Threshold kinetic energy $(E_K)_{\text{thr}}$ of an endothermic nuclear reaction can be determined:

- (1) either indirectly by first determining the Q value of the nuclear reaction and then calculating the threshold energy from the known Q value
- (2) or directly by using the relativistic invariant method.

Q value of a nuclear reaction is determined either with the *rest energy method* or with the *binding energy method*. Once Q value is known, threshold energy $(E_K)_{\text{thr}}$ of a nuclear reaction is calculated from the general expression linking $(E_K)_{\text{thr}}$ with the Q value (T5.15) of a nuclear reaction given as

$$(E_K)_{\text{thr}} = -Q \left(1 + \frac{m_{10}}{m_{20}} \right), \quad (7.330)$$

where m_{10} is the rest mass of the reaction projectile and m_{20} is the rest mass of the reaction target. *Note:* In the case of PN reaction, the projectile is a photon with rest mass $m_{10} = 0$, resulting in the following simple expression for PN reaction threshold energy

$$E_{\text{thr}}^{\text{PN}} = h\nu_{\text{thr}}^{\text{PN}} = -Q. \quad (7.331)$$

(a) Rest energy method: Q value of a PN reaction is determined (T5.7) by subtracting the sum of rest energies of reaction products after the PN reaction

$(m_{30}c^2 + m_{40}c^2)$ from the rest energy of the target $m_{20}c^2$ to get

$$Q = \sum_{i,\text{before}} m_i c^2 - \sum_{i,\text{after}} m_i c^2 = m_{20}c^2 - (m_{30}c^2 + m_{40}c^2). \quad (7.332)$$

Since $E_{\text{thr}}^{\text{PN}} = h\nu_{\text{thr}}^{\text{PN}} = -Q$ from (7.331), we get from (7.332) the following expression for the threshold energy $E_{\text{thr}}^{\text{PN}}$

$$E_{\text{thr}}^{\text{PN}} = h\nu_{\text{thr}}^{\text{PN}} = -Q = (m_{30}c^2 + m_{40}c^2) - m_{20}c^2. \quad (7.333)$$

(b) Binding energy method: alternatively to the rest energy method, the Q value of a PN reaction can be calculated by subtracting the binding energy $E_{\text{B}}(m_{20})$ of the target from the sum of binding energies of reaction products m_{30} and m_{40}

$$Q = \sum_{i,\text{after}} E_{\text{B}}(m_i) - \sum_{i,\text{before}} E_{\text{B}}(m_i) = E_{\text{B}}(m_{30}) + E_{\text{B}}(m_{40}) - E_{\text{B}}(m_{20}). \quad (7.334)$$

Since $E_{\text{thr}}^{\text{PN}} = h\nu_{\text{thr}}^{\text{PN}} = -Q$ from (7.331), we get from (7.334) the following expression for threshold energy $E_{\text{thr}}^{\text{PN}}$

$$E_{\text{thr}}^{\text{PN}} = h\nu_{\text{thr}}^{\text{PN}} = -Q = E_{\text{B}}(m_{20}) - [E_{\text{B}}(m_{30}) + E_{\text{B}}(m_{40})]. \quad (7.335)$$

(c) Relativistic invariant method: The relativistic invariant is expressed as

$$E^2 - p^2c^2 = \text{inv}, \quad (7.336)$$

where E stands for the total energy of a system, p stands for the momentum of a system, and c is the speed of light in vacuum.

Using the relativistic invariant method, the threshold energy E_{thr} for an endothermic nuclear reaction is in general calculated by equating the invariant for the projectile-target ensemble before the nuclear reaction with the invariant for the ensemble of reaction products after the nuclear reaction and solving for E_{thr} . The invariant for the projectile-target ensemble is determined in the laboratory coordinate system for projectile total energy E equal to threshold energy E_{thr} that in turn is given as $E_{\text{thr}} = (E_{\text{K}})_{\text{thr}} + m_{10}c^2$ with $(E_{\text{K}})_{\text{thr}}$ threshold kinetic energy of the projectile and $m_{10}c^2$ its rest energy. The invariant for the ensemble of reaction products after the reaction is determined in the center-of-mass coordinate system resulting in total energy given as the sum of rest energies of reaction products and total momentum p equal to zero.

Thus, for a general endothermic nuclear reaction the invariant before the reaction $\mathcal{J}_{\text{before}}$ is expressed as

$$\mathcal{J}_{\text{before}} = [\sqrt{p_1^2c^2 + (m_{10}c^2)^2} + m_{20}c^2]^2 - p_1^2c^2 \quad (7.337)$$

and the invariant $\mathcal{J}_{\text{after}}$ after the reaction

$$\mathcal{J}_{\text{after}} = (m_{30}c^2 + m_{40}c^2) - 0. \quad (7.338)$$

From $\mathcal{J}_{\text{before}} = \mathcal{J}_{\text{after}}$ and recalling that $\sqrt{p_1^2 c^2 + (m_{10} c^2)^2} = E_{\text{thr}} = (E_{\text{K}})_{\text{thr}} + m_{10} c^2$, we obtain the following results for threshold energies E_{thr} and $(E_{\text{K}})_{\text{thr}}$ of and endothermic nuclear reaction

$$E_{\text{thr}} = \frac{[m_{30} c^2 + m_{40} c^2]^2 - [(m_{10} c^2)^2 + (m_{20} c^2)^2]}{2m_{20} c^2} = (E_{\text{K}})_{\text{thr}} + m_{10} c^2 \quad (7.339)$$

and

$$(E_{\text{K}})_{\text{thr}} = \frac{[m_{30} c^2 + m_{40} c^2]^2 - [m_{10} c^2 + m_{20} c^2]^2}{2m_{20} c^2}. \quad (7.340)$$

For the special case of photonuclear reaction where the projectile is an energetic photon ($m_{10} c^2 = 0$), the threshold energy $E_{\text{thr}}^{\text{PN}}$ is given by inserting $m_{10} c^2 = 0$ into (7.339) or (7.340) to get

$$E_{\text{thr}}^{\text{PN}} = h\nu_{\text{thr}}^{\text{PN}} = \frac{[m_{30} c^2 + m_{40} c^2]^2 - [m_{20} c^2]^2}{2m_{20} c^2}. \quad (7.341)$$

In summary, there are three methods for calculation of threshold energy $E_{\text{thr}}^{\text{PN}} = h\nu_{\text{thr}}^{\text{PN}}$ of a photonuclear reaction and they provide the following expressions for $E_{\text{thr}}^{\text{PN}} = h\nu_{\text{thr}}^{\text{PN}}$:

(1) *Rest energy method*

$$E_{\text{thr}}^{\text{PN}} = h\nu_{\text{thr}}^{\text{PN}} = (m_{30} c^2 + m_{40} c^2) - m_{20} c^2 \quad (7.342)$$

(2) *Binding energy method*

$$E_{\text{thr}}^{\text{PN}} = h\nu_{\text{thr}}^{\text{PN}} = E_{\text{B}}(m_{20}) - [E_{\text{B}}(m_{30}) + E_{\text{B}}(m_{40})] \quad (7.343)$$

(3) *Relativistic invariant method*

$$E_{\text{thr}}^{\text{PN}} = h\nu_{\text{thr}}^{\text{PN}} = \frac{[m_{30} c^2 + m_{40} c^2]^2 - [m_{20} c^2]^2}{2m_{20} c^2} \quad (7.344)$$

For a given PN reaction one obtains the same end result for threshold energy $E_{\text{thr}}^{\text{PN}} = h\nu_{\text{thr}}^{\text{PN}}$ irrespective of which method one uses, provided, of course, that appropriate data are inserted into the three Eqs. (7.342), (7.343), and (7.344).

(d) Threshold for the photonuclear reaction ${}^{208}_{82}\text{Pb}(\gamma, n){}^{207}_{82}\text{Pb}$ is calculated as follows using appropriate data for (7.342), (7.343), and (7.344) from Appendix A:

(1) *Rest energy method:*

$$\begin{aligned} E_{\text{thr}}^{\text{PN}} &= h\nu_{\text{thr}}^{\text{PN}} = (m_{30} c^2 + m_{40} c^2) - m_{20} c^2 = [M({}^{207}_{82}\text{Pb})c^2 + m_n c^2] \\ &\quad - [M({}^{208}_{82}\text{Pb})c^2 + 0] \\ &= [192754.8983 \text{ MeV} + 939.5654 \text{ MeV}] - [193687.0956 \text{ MeV} + 0] \\ &= 7.37 \text{ MeV} \end{aligned} \quad (7.345)$$

(2) *Binding energy method:*

$$\begin{aligned}
 E_{\text{thr}}^{\text{PN}} &= h\nu_{\text{thr}}^{\text{PN}} = E_{\text{B}}(m_{20}) - [E_{\text{B}}(m_{30}) + E_{\text{B}}(m_{40})] = [E_{\text{B}}(^{208}_{82}\text{Pb})] \\
 &\quad - [E_{\text{B}}(^{207}_{82}\text{Pb}) + 0] \\
 &= 1636.4457 \text{ MeV} - 1629.0779 \text{ MeV} = 7.37 \text{ MeV}
 \end{aligned} \tag{7.346}$$

(3) *Relativistic invariant method:*

$$\begin{aligned}
 E_{\text{thr}}^{\text{PN}} &= h\nu_{\text{thr}}^{\text{PN}} = \frac{[m_{30}c^2 + m_{40}c^2]^2 - [m_{20}c^2]^2}{2m_{20}c^2} \\
 &= \frac{[M(^{207}_{82}\text{Pb})c^2 + m_{\text{n}}c^2]^2 - [M(^{208}_{82}\text{Pb})c^2]^2}{2M(^{208}_{82}\text{Pb})c^2} \\
 &= \frac{[192754.8983 \text{ MeV} + 939.5654 \text{ MeV}]^2 - [193687.0956 \text{ MeV}]^2}{2 \times (193687.0956 \text{ MeV})} \\
 &= 7.37 \text{ MeV}
 \end{aligned} \tag{7.347}$$

As shown in (7.345), (7.346), and (7.347), the three methods (rest energy, binding energy, and relativistic invariant) for calculation of threshold energy of photonuclear reaction give identical results.

7.7.Q2

(180)

Nuclear reaction $^{206}_{82}\text{Pb}(\gamma, \text{n})^{205}_{82}\text{Pb}$ is an example of a typical photonuclear (PN) reaction in which a high-energy photon with energy $h\nu$ exceeding the PN reaction threshold energy $E_{\text{thr}}^{\text{PN}} = h\nu_{\text{thr}}^{\text{PN}}$ induces a PN reaction that causes photonuclear decay of the target nucleus $^{206}_{82}\text{Pb}$ into $^{205}_{82}\text{Pb}$ and emission of a fast neutron with kinetic energy $(E_{\text{K}})_{\text{n}}$.

(a) Calculate the threshold energy $E_{\text{thr}}^{\text{PN}} = h\nu_{\text{thr}}^{\text{PN}}$ for the PN reaction $^{206}_{82}\text{Pb}(\gamma, \text{n})^{205}_{82}\text{Pb}$ using three methods that have been developed for determination of PN reaction threshold:

- (1) Rest energy method.
- (2) Binding energy method.
- (3) Relativistic invariant method.

Relevant data on rest energies and binding energies are provided in Appendix A.

(b) Determine the kinetic energy of the neutron $(E_{\text{K}})_{\text{n}}$ and the recoil nucleus $(E_{\text{K}})_{\text{Pb-205}}$ in a PN reaction of a 10 MeV photon with a Pb-206 nucleus.

- (c) Calculate the magnitude of the momentum of the incident photon $p_\nu = |\mathbf{p}_\nu|$, emitted fast neutron $p_n = |\mathbf{p}_n|$, and recoil Pb-205 nucleus $p_{\text{Pb-205}} = |\mathbf{p}_{\text{Pb-205}}|$ for PN reaction of a 10 MeV photon with a Pb-206 nucleus.
- (d) Draw a vector diagram of momentum \mathbf{p}_ν before the PN reaction and momenta $\mathbf{p}_{\text{Pb-205}}$ as well as \mathbf{p}_n after the PN reaction.

SOLUTION:

(a) Threshold energy of a photonuclear reaction is defined as the minimum photon energy that can trigger a particular photonuclear reaction. As derived in Prob. 179, there are three methods for calculation of threshold energy $E_{\text{thr}}^{\text{PN}} = h\nu_{\text{thr}}^{\text{PN}}$ of a photonuclear reaction: (1) Rest energy method, (2) Binding energy method, and (3) Relativistic invariant method.

We now determine $E_{\text{thr}}^{\text{PN}} = h\nu_{\text{thr}}^{\text{PN}}$ of the ${}^{206}_{82}\text{Pb}(\gamma, n){}^{205}_{82}\text{Pb}$ PN reaction using the three methods.

(1) *Rest energy method:*

$$\begin{aligned} E_{\text{thr}}^{\text{PN}} &= h\nu_{\text{thr}}^{\text{PN}} = (m_{30}c^2 + m_{40}c^2) - m_{20}c^2 = [M({}^{205}_{82}\text{Pb})c^2 + m_n c^2] \\ &\quad - [M({}^{206}_{82}\text{Pb})c^2 + 0] \\ &= [190890.604 \text{ MeV} + 939.565 \text{ MeV}] - [191822.082 \text{ MeV} + 0] \\ &= 8.087 \text{ MeV} \end{aligned} \quad (7.348)$$

(2) *Binding energy method:*

$$\begin{aligned} E_{\text{thr}}^{\text{PN}} &= h\nu_{\text{thr}}^{\text{PN}} = E_B(m_{20}) - [E_B(m_{30}) + E_B(m_{40})] = [E_B({}^{206}_{82}\text{Pb}) + 0] \\ &\quad - [E_B({}^{205}_{82}\text{Pb}) + 0] \\ &= 1622.326 \text{ MeV} - 1614.239 \text{ MeV} = 8.087 \text{ MeV} \end{aligned} \quad (7.349)$$

(3) *Relativistic invariant method:*

$$\begin{aligned} E_{\text{thr}}^{\text{PN}} &= h\nu_{\text{thr}}^{\text{PN}} = \frac{[m_{30}c^2 + m_{40}c^2]^2 - [m_{20}c^2]^2}{2m_{20}c^2} \\ &= \frac{[M({}^{205}_{82}\text{Pb})c^2 + m_n c^2]^2 - [M({}^{206}_{82}\text{Pb})c^2]^2}{2M({}^{206}_{82}\text{Pb})c^2} \\ &= \frac{[190890.604 \text{ MeV} + 939.565 \text{ MeV}]^2 - [191822.082 \text{ MeV}]^2}{2 \times (191822.082 \text{ MeV})} \\ &= 8.087 \text{ MeV} \end{aligned} \quad (7.350)$$

As evident from (7.348), (7.349), and (7.350), the three methods for calculation of threshold energy $E_{\text{thr}}^{\text{PN}} = h\nu_{\text{thr}}^{\text{PN}}$ of PN reaction ${}^{206}_{82}\text{Pb}(\gamma, n){}^{205}_{82}\text{Pb}$ yield identical results of 8.087 MeV.

(b) Since the threshold photon energy for the ${}^{206}_{82}\text{Pb}(\gamma, n){}^{205}_{82}\text{Pb}$ PN reaction is 8.087 MeV, the reaction products (Pb-205 nucleus and a neutron) resulting from the PN reaction induced by a 10 MeV photon in a Pb-206 nucleus will share the energy difference between the photon energy $h\nu = 10$ MeV and the threshold energy $E_{\text{thr}}^{\text{PN}} = h\nu_{\text{thr}}^{\text{PN}} = 8.087$ MeV. The threshold energy of 8.087 MeV is used up to enable the PN reaction and the excess energy above the threshold energy is shared as kinetic energy $(E_{\text{K}})_{\text{tr}}$ between the liberated neutron and the Pb-205 nucleus, i.e.,

$$\begin{aligned} (E_{\text{K}})_{\text{tr}} &= h\nu - h\nu_{\text{thr}}^{\text{PN}} = 10 \text{ MeV} - 8.087 \text{ MeV} = 1.913 \text{ MeV} \\ &= (E_{\text{K}})_{\text{n}} + (E_{\text{K}})_{\text{Pb-205}} \\ &= \frac{m({}^{205}_{82}\text{Pb})c^2}{m({}^{205}_{82}\text{Pb})c^2 + m_{\text{n}}c^2} (E_{\text{K}})_{\text{tr}} + \frac{m_{\text{n}}c^2}{m({}^{205}_{82}\text{Pb})c^2 + m_{\text{n}}c^2} (E_{\text{K}})_{\text{tr}}, \end{aligned} \quad (7.351)$$

each receiving a fraction of the transferred energy in inverse proportion to their rest masses. From (7.351) we determine kinetic energies $(E_{\text{K}})_{\text{n}}$ and $(E_{\text{K}})_{\text{Pb-205}}$ as follows

$$(E_{\text{K}})_{\text{n}} = \frac{m({}^{205}_{82}\text{Pb})c^2}{m({}^{205}_{82}\text{Pb})c^2 + m_{\text{n}}c^2} (E_{\text{K}})_{\text{tr}} = \frac{190890.604}{191830.204} \times (1.913 \text{ MeV}) = 1.9036 \text{ MeV} \quad (7.352)$$

and

$$\begin{aligned} (E_{\text{K}})_{\text{Pb-205}} &= \frac{m_{\text{n}}c^2}{m({}^{205}_{82}\text{Pb})c^2 + m_{\text{n}}c^2} (E_{\text{K}})_{\text{tr}} \\ &= \frac{939.565}{191830.204} \times (1.913 \text{ MeV}) = 0.0094 \text{ MeV}, \end{aligned} \quad (7.353)$$

indicating that most of the energy available for transfer to reaction products (1.913 MeV) goes to the lighter reaction product (neutron).

(c) The magnitude of the photon momentum \mathbf{p}_{ν} before PN reaction is given as follows

$$|\mathbf{p}_{\nu}| = p_{\nu} = \frac{h\nu}{c} = \frac{10 \text{ MeV}}{c} = 10 \text{ MeV}/c. \quad (7.354)$$

As shown in (7.352), after the PN reaction, the neutron kinetic energy $(E_{\text{K}})_{\text{n}}$ is 1.9036 MeV and kinetic energy $(E_{\text{K}})_{\text{Pb-205}}$ of the recoil nucleus Pb-205 is 0.0094 MeV. These two kinetic energies correspond to the following magnitudes

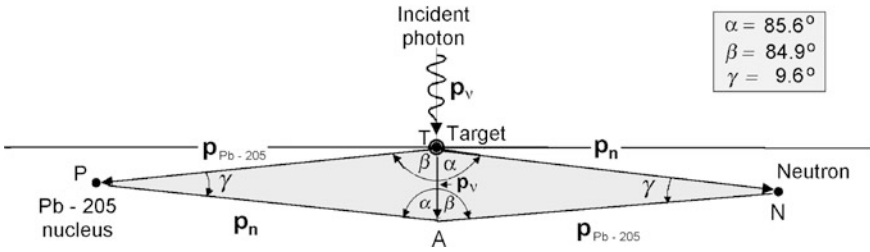


Fig. 7.44 Schematic diagram of the photonuclear reaction triggered by a 10 MeV photon interacting with a Pb-206 nucleus. Incident photon momentum $|\mathbf{p}_v| = p_v = 10 \text{ MeV}/c$ before the reaction; momenta of the emitted neutron and recoil nucleus Pb-205 after the reaction are $|\mathbf{p}_n| = p_n = 59.84 \text{ MeV}/c$ and $|\mathbf{p}_{\text{Pb-205}}| = p_{\text{Pb-205}} = 59.91 \text{ MeV}/c$, respectively

of momenta \mathbf{p}_n and $\mathbf{p}_{\text{Pb-205}}$, respectively

$$\begin{aligned}
 |\mathbf{p}_n| = p_n &= \frac{(E_K)_n}{c} \sqrt{1 + \frac{2m_n c^2}{(E_K)_n}} \\
 &= \frac{1.9036 \text{ MeV}}{c} \times \sqrt{1 + \frac{2 \times 939.565}{1.9036}} = 59.84 \text{ MeV}/c \quad (7.355)
 \end{aligned}$$

and

$$\begin{aligned}
 |\mathbf{p}_{\text{Pb-205}}| = p_{\text{Pb-205}} &= \frac{(E_K)_{\text{Pb-205}}}{c} \sqrt{1 + \frac{2m(^{205}\text{Pb})c^2}{(E_K)_{\text{Pb-205}}}} \\
 &= \frac{0.0094 \text{ MeV}}{c} \times \sqrt{1 + \frac{2 \times 190890.604}{0.0094}} = 59.91 \text{ MeV}/c. \quad (7.356)
 \end{aligned}$$

(d) Magnitudes of momenta of the incident photon \mathbf{p}_v , emitted neutron \mathbf{p}_n , and recoil nucleus $\mathbf{p}_{\text{Pb-205}}$ were determined in **(c)**; however, to plot the momenta as vectors we must, in addition to vector magnitudes, also determine their direction relative to the direction of the incident photon. For convenience we choose the incident photon directed vertically down, and, based on the principle of momentum conservation, we conclude that the resultant momentum of the neutron and Pb-205 recoil nucleus must have the same magnitude as that of the incident photon and must also be directed vertically down. This can be achieved if \mathbf{p}_n and $\mathbf{p}_{\text{Pb-205}}$ are directed almost perpendicularly to \mathbf{p}_v and moving in almost opposite directions to one another, as shown in Fig. 7.44.

As evident from Fig. 7.44, vectors \mathbf{p}_v , \mathbf{p}_n , and $\mathbf{p}_{\text{Pb-205}}$ form two triangles: TNA and TPA and are characterized by angles α , β , and γ . To determine the exact directions of \mathbf{p}_n and $\mathbf{p}_{\text{Pb-205}}$ relative to that of \mathbf{p}_v we now apply the trigonometric law of cosines to calculate angles α , β , and γ .

(1) Angle α :

$$p_{\text{Pb-205}}^2 = p_v^2 + p_n^2 - 2p_v p_n \cos \alpha \quad (7.357)$$

or

$$\alpha = \arccos \frac{p_v^2 + p_n^2 - p_{\text{Pb-205}}^2}{2p_v p_n} = \arccos \frac{10^2 + 59.84^2 - 59.91^2}{2 \times 10 \times 59.84} = 85.6^\circ. \quad (7.358)$$

(2) Angle β :

$$p_n^2 = p_v^2 + p_{\text{Pb-205}}^2 - 2p_v p_{\text{Pb-205}} \cos \beta \quad (7.359)$$

or

$$\beta = \arccos \frac{p_v^2 + p_{\text{Pb-205}}^2 - p_n^2}{2p_v p_{\text{Pb-205}}} = \arccos \frac{10^2 + 59.91^2 - 59.84^2}{2 \times 10 \times 59.91} = 84.9^\circ. \quad (7.360)$$

(3) Angle γ :

$$p_v^2 = p_{\text{Pb-205}}^2 + p_n^2 - 2p_{\text{Pb-205}} p_n \cos \gamma \quad (7.361)$$

or

$$\gamma = \arccos \frac{p_{\text{Pb-205}}^2 + p_n^2 - p_v^2}{2p_{\text{Pb-205}} p_n} = \arccos \frac{59.91^2 + 59.84^2 - 10^2}{2 \times 59.91 \times 59.84} = 9.6^\circ. \quad (7.362)$$

The sum of angles α , β , and γ is 180° satisfying the rule that the sum of internal angles in a triangle must be 180° .

Summary:

- (1) Threshold $E_{\text{thr}}^{\text{PN}}$ for the PN reaction ${}^{206}_{82}\text{Pb}(\gamma, n){}^{205}_{82}\text{Pb}$ is 8.087 MeV.
- (2) In a 10 MeV direct photon interaction with a ${}^{206}_{82}\text{Pb}$ nucleus, threshold energy of 8.087 MeV is used to trigger the PN reaction and the energy difference between the incident photon energy $h\nu = 10$ MeV and the threshold energy $E_{\text{thr}}^{\text{PN}} = 8.087$ MeV in the amount of 1.913 MeV is transferred as kinetic energy to reaction products (neutron and Pb-205 nucleus).
- (3) Neutron and Pb-205 nucleus share energy of 1.913 MeV in inverse proportion to their masses. Neutron receives 1.9036 MeV (99.5 %) and Pb-205 nucleus 0.0094 MeV (0.5 %), corresponding to a momentum of 59.84 MeV/c for neutron and 59.91 MeV/c for the Pb-205 nucleus.

7.7.Q3

(181)

Photonuclear (PN) reactions are characterized by reaction threshold defined as the minimum photon energy $E_{\text{thr}}^{\text{PN}} = h\nu_{\text{thr}}^{\text{PN}}$ that can trigger a PN reaction. Three methods have been developed for determination of threshold energy $E_{\text{thr}}^{\text{PN}} = h\nu_{\text{thr}}^{\text{PN}}$ based either on rest energy of the target and reaction products, binding energy of the target and reaction products, or on the relativistic invari-

ant for before and after the photonuclear interaction. Equations for the three methods were derived in Prob. 180 and are summarized as follows:

(1) Rest energy method:

$$E_{\text{thr}}^{\text{PN}} = h\nu_{\text{thr}}^{\text{PN}} = (m_{30}c^2 + m_{40}c^2) - m_{20}c^2, \quad (7.363)$$

(2) Binding energy method:

$$E_{\text{thr}}^{\text{PN}} = h\nu_{\text{thr}}^{\text{PN}} = E_{\text{B}}(m_{20}) - [E_{\text{B}}(m_{30}) + E_{\text{B}}(m_{40})], \quad (7.364)$$

(3) Relativistic invariant method:

$$E_{\text{thr}}^{\text{PN}} = h\nu_{\text{thr}}^{\text{PN}} = \frac{[m_{30}c^2 + m_{40}c^2]^2 - [m_{20}c^2]^2}{2m_{20}c^2}, \quad (7.365)$$

where m_{20} is the rest mass of the target nucleus and m_{30} and m_{40} are rest masses of reaction products.

Calculate threshold energies $E_{\text{thr}}^{\text{PN}} = h\nu_{\text{thr}}^{\text{PN}}$ for the following PN reactions:

- (a) $d(\gamma, n)p$ (b) $t(\gamma, n)d$ (c) ${}^3_2\text{He}(\gamma, d)p$
 (d) ${}^3_2\text{He}(\gamma, 2p)n$ (e) ${}^7_3\text{Li}(\gamma, p){}_2^6\text{He}$ (f) ${}^9_4\text{Be}(\gamma, n){}_4^8\text{Be}$
 (g) ${}^{16}_8\text{O}(\gamma, \alpha){}_6^{12}\text{C}$

For each PN reaction use all three methods of threshold calculation and show that they yield identical results.

SOLUTION:

(a) Threshold for PN reaction $d(\gamma, n)p = {}^2_1\text{H}(\gamma, n)p$: (induced deuteron breakup)

(1)

$$\begin{aligned} E_{\text{thr}}^{\text{PN}} &= h\nu_{\text{thr}}^{\text{PN}} = (m_{30}c^2 + m_{40}c^2) - m_{20}c^2 = [M(d)c^2 + 0] - [m_n c^2 + m_p c^2] \\ &= [1875.6128 \text{ MeV} + 0] - [939.5654 \text{ MeV} + 938.2720 \text{ MeV}] \\ &= 2.225 \text{ MeV} \end{aligned} \quad (7.366)$$

(2)

$$\begin{aligned} E_{\text{thr}}^{\text{PN}} &= h\nu_{\text{thr}}^{\text{PN}} = E_{\text{B}}(m_{20}) - [E_{\text{B}}(m_{30}) + E_{\text{B}}(m_{40})] \\ &= E_{\text{B}}(d) - [E_{\text{B}}(n) + E_{\text{B}}(p)] \\ &= E_{\text{B}}(d) - [0 + 0] = 2.225 \text{ MeV} \end{aligned} \quad (7.367)$$

(3)

$$\begin{aligned}
 E_{\text{thr}}^{\text{PN}} = h\nu_{\text{thr}}^{\text{PN}} &= \frac{[m_{30}c^2 + m_{40}c^2]^2 - [m_{20}c^2]^2}{2m_{20}c^2} = \frac{[m_{\text{n}}c^2 + m_{\text{p}}c^2]^2 - [m_{\text{d}}c^2]^2}{2m_{\text{d}}c^2} \\
 &= \frac{[939.5654 \text{ MeV} + 938.2720 \text{ MeV}]^2 - [1875.6128 \text{ MeV}]^2}{2 \times (1875.6128 \text{ MeV})} \\
 &= 2.226 \text{ MeV} \tag{7.368}
 \end{aligned}$$

(b) Threshold for PN reaction $t(\gamma, n)d = {}^3_1\text{H}(\gamma, n){}_1^2\text{H}$: (induced triton breakup)

(1)

$$\begin{aligned}
 E_{\text{thr}}^{\text{PN}} = h\nu_{\text{thr}}^{\text{PN}} &= (m_{30}c^2 + m_{40}c^2) - m_{20}c^2 = [m_{\text{d}}c^2 + m_{\text{n}}c^2] - m_{\text{t}}c^2 \\
 &= [1875.6128 \text{ MeV} + 939.5654 \text{ MeV}] - [2808.9269 \text{ MeV}] \\
 &= 6.26 \text{ MeV} \tag{7.369}
 \end{aligned}$$

(2)

$$\begin{aligned}
 E_{\text{thr}}^{\text{PN}} = h\nu_{\text{thr}}^{\text{PN}} &= E_{\text{B}}(m_{20}) - [E_{\text{B}}(m_{30}) + E_{\text{B}}(m_{40})] \\
 &= E_{\text{B}}(\text{t}) - [E_{\text{B}}(\text{d}) + E_{\text{B}}(\text{p})] \\
 &= 8.48182 \text{ MeV} - [2.22458 \text{ MeV} + 0] = 6.26 \text{ MeV} \tag{7.370}
 \end{aligned}$$

(3)

$$\begin{aligned}
 E_{\text{thr}}^{\text{PN}} = h\nu_{\text{thr}}^{\text{PN}} &= \frac{[m_{30}c^2 + m_{40}c^2]^2 - [m_{20}c^2]^2}{2m_{20}c^2} = \frac{[m_{\text{d}}c^2 + m_{\text{n}}c^2]^2 - [m_{\text{t}}c^2]^2}{2m_{\text{t}}c^2} \\
 &= \frac{[1875.6128 \text{ MeV} + 939.5654 \text{ MeV}]^2 - [2808.9269 \text{ MeV}]^2}{2 \times [2808.9269 \text{ MeV}]} \\
 &= 6.26 \text{ MeV} \tag{7.371}
 \end{aligned}$$

(c) Threshold for PN reaction ${}^3_2\text{He}(\gamma, d)p$: (two body breakup channel)

(1)

$$\begin{aligned}
 E_{\text{thr}}^{\text{PN}} = h\nu_{\text{thr}}^{\text{PN}} &= (m_{30}c^2 + m_{40}c^2) - m_{20}c^2 = [M(\text{d})c^2 + m_{\text{p}}c^2] - [M({}^3_2\text{He})] \\
 &= [1875.6128 \text{ MeV} + 938.2720 \text{ MeV}] - [2808.3913 \text{ MeV}] = 5.49 \text{ MeV} \\
 &\tag{7.372}
 \end{aligned}$$

(2)

$$\begin{aligned}
 E_{\text{thr}}^{\text{PN}} = h\nu_{\text{thr}}^{\text{PN}} &= E_{\text{B}}(m_{20}) - [E_{\text{B}}(m_{30}) + E_{\text{B}}(m_{40})] \\
 &= E_{\text{B}}({}^3_2\text{He}) - [E_{\text{B}}(\text{d}) + E_{\text{B}}(\text{p})] \\
 &= 7.7181 \text{ MeV} - 2.2246 \text{ MeV} = 5.49 \text{ MeV} \tag{7.373}
 \end{aligned}$$

(3)

$$\begin{aligned}
 E_{\text{thr}}^{\text{PN}} &= h\nu_{\text{thr}}^{\text{PN}} = \frac{[m_{30}c^2 + m_{40}c^2]^2 - [m_{20}c^2]^2}{2m_{20}c^2} \\
 &= \frac{[M(\text{d})c^2 + m_{\text{p}}c^2]^2 - [M({}_2^3\text{He})c^2]^2}{2M({}_2^3\text{He})c^2} \\
 &= \frac{[1875.6128 \text{ MeV} + 938.2720 \text{ MeV}]^2 - [2808.3913 \text{ MeV}]^2}{2 \times (2808.3913 \text{ MeV})} \\
 &= 5.50 \text{ MeV} \tag{7.374}
 \end{aligned}$$

(d) Threshold for PN reaction ${}_2^3\text{He}(\gamma, 2\text{p})\text{n}$: (three body break up channel)

(1)

$$\begin{aligned}
 E_{\text{thr}}^{\text{PN}} &= h\nu_{\text{thr}}^{\text{PN}} = (m_{30}c^2 + m_{40}c^2) - m_{20}c^2 = [2m_{\text{p}}c^2 + m_{\text{n}}c^2] - [M({}_2^3\text{He})c^2] \\
 &= [2 \times (938.2720 \text{ MeV}) + (939.5654 \text{ MeV})] - [2808.3913 \text{ MeV}] \\
 &= 7.72 \text{ MeV} \tag{7.375}
 \end{aligned}$$

(2)

$$\begin{aligned}
 E_{\text{thr}}^{\text{PN}} &= h\nu_{\text{thr}}^{\text{PN}} = E_{\text{B}}(m_{20}) - [E_{\text{B}}(m_{30}) + E_{\text{B}}(m_{40})] = E_{\text{B}}({}_2^3\text{He}) - [0 + 0] \\
 &= 7.72 \text{ MeV} \tag{7.376}
 \end{aligned}$$

(3)

$$\begin{aligned}
 E_{\text{thr}}^{\text{PN}} &= h\nu_{\text{thr}}^{\text{PN}} = \frac{[m_{30}c^2 + m_{40}c^2]^2 - [m_{20}c^2]^2}{2m_{20}c^2} \\
 &= \frac{[2m_{\text{p}}c^2 + m_{\text{n}}c^2] - [M({}_2^3\text{He})c^2]}{2M({}_2^3\text{He})c^2} \\
 &= \frac{[2 \times (938.2720 \text{ MeV}) + (939.5654 \text{ MeV})]^2 - [2808.3913 \text{ MeV}]^2}{2 \times (2808.3913 \text{ MeV})} \\
 &= 7.73 \text{ MeV} \tag{7.377}
 \end{aligned}$$

(e) Threshold for PN reaction ${}_3^7\text{Li}(\gamma, \text{p}){}_2^6\text{He}$: (induced proton emission)

(1)

$$\begin{aligned}
 E_{\text{thr}}^{\text{PN}} &= h\nu_{\text{thr}}^{\text{PN}} = (m_{30}c^2 + m_{40}c^2) - m_{20}c^2 \\
 &= [M({}_2^6\text{He})c^2 + m_{\text{p}}c^2] - [M({}_3^7\text{Li})c^2] \\
 &= [5605.5372 \text{ MeV} + 938.2720 \text{ MeV}] - [6533.8330 \text{ MeV}] = 9.98 \text{ MeV} \tag{7.378}
 \end{aligned}$$

(2)

$$\begin{aligned}
 E_{\text{thr}}^{\text{PN}} &= h\nu_{\text{thr}}^{\text{PN}} = E_{\text{B}}(m_{20}) - [E_{\text{B}}(m_{30}) + E_{\text{B}}(m_{40})] \\
 &= E_{\text{B}}({}_3^7\text{Li}) - [E_{\text{B}}({}_2^6\text{He}) + 0] \\
 &= 39.2446 \text{ MeV} - 29.2682 \text{ MeV} = 9.98 \text{ MeV}
 \end{aligned} \tag{7.379}$$

(3)

$$\begin{aligned}
 E_{\text{thr}}^{\text{PN}} &= h\nu_{\text{thr}}^{\text{PN}} = \frac{[m_{30}c^2 + m_{40}c^2]^2 - [m_{20}c^2]^2}{2m_{20}c^2} \\
 &= \frac{[M({}_2^6\text{He})c^2 + m_{\text{p}}c^2]^2 - [M({}_3^7\text{Li})c^2]^2}{2M({}_3^7\text{Li})c^2} \\
 &= \frac{[5605.5372 \text{ MeV} + 938.2720 \text{ MeV}]^2 - [6533.8330 \text{ MeV}]^2}{2 \times (6533.8330 \text{ MeV})} \\
 &= 9.98 \text{ MeV}
 \end{aligned} \tag{7.380}$$

(f) Threshold for PN reaction ${}_4^9\text{Be}(\gamma, \text{n}){}_4^8\text{Be}$: (induced neutron emission)

(1)

$$\begin{aligned}
 E_{\text{thr}}^{\text{PN}} &= h\nu_{\text{thr}}^{\text{PN}} = (m_{30}c^2 + m_{40}c^2) - m_{20}c^2 \\
 &= [M({}_4^8\text{Be})c^2 + m_{\text{n}}c^2] - [M({}_4^9\text{Be})c^2] \\
 &= [7454.8500 \text{ MeV} + 939.5654 \text{ MeV}] - [8392.7499 \text{ MeV}] = 1.67 \text{ MeV}
 \end{aligned} \tag{7.381}$$

(2)

$$\begin{aligned}
 E_{\text{thr}}^{\text{PN}} &= h\nu_{\text{thr}}^{\text{PN}} = E_{\text{B}}(m_{20}) - [E_{\text{B}}(m_{30}) + E_{\text{B}}(m_{40})] \\
 &= E_{\text{B}}({}_4^9\text{Be}) - [E_{\text{B}}({}_4^8\text{Be}) + 0] \\
 &= 58.1650 \text{ MeV} - 56.4996 \text{ MeV} = 1.67 \text{ MeV}
 \end{aligned} \tag{7.382}$$

(3)

$$\begin{aligned}
 E_{\text{thr}}^{\text{PN}} &= h\nu_{\text{thr}}^{\text{PN}} = \frac{[m_{30}c^2 + m_{40}c^2]^2 - [m_{20}c^2]^2}{2m_{20}c^2} \\
 &= \frac{[M({}_4^8\text{Be})c^2 + m_{\text{n}}c^2]^2 - [M({}_4^9\text{Be})c^2]^2}{2M({}_4^9\text{Be})c^2} \\
 &= \frac{[7454.8500 \text{ MeV} + 939.5654 \text{ MeV}]^2 - [8392.7499 \text{ MeV}]^2}{2 \times (8392.7499 \text{ MeV})} \\
 &= 1.67 \text{ MeV}
 \end{aligned} \tag{7.383}$$

(g) Threshold for PN reaction ${}^{16}_8\text{O}(\gamma, \alpha){}^{12}_6\text{C}$: (induced α particle emission)

(1)

$$\begin{aligned}
 E_{\text{thr}}^{\text{PN}} &= h\nu_{\text{thr}}^{\text{PN}} = (m_{30}c^2 + m_{40}c^2) - m_{20}c^2 \\
 &= [M({}^{12}_6\text{C})c^2 + m_{\alpha}c^2] - [M({}^{16}_8\text{O})c^2] \\
 &= [11174.8625 \text{ MeV} + 3727.3791 \text{ MeV}] - [14895.0796 \text{ MeV}] \\
 &= 7.16 \text{ MeV}
 \end{aligned} \tag{7.384}$$

(2)

$$\begin{aligned}
 E_{\text{thr}}^{\text{PN}} &= h\nu_{\text{thr}}^{\text{PN}} = E_{\text{B}}(m_{20}) - [E_{\text{B}}(m_{30}) + E_{\text{B}}(m_{40})] \\
 &= E_{\text{B}}({}^{16}_8\text{O}) - [E_{\text{B}}({}^{12}_6\text{C}) - E_{\text{B}}(\alpha)] \\
 &= 127.6193 \text{ MeV} - [92.1618 \text{ MeV} + 28.2957 \text{ MeV}] = 7.16 \text{ MeV}
 \end{aligned} \tag{7.385}$$

(3)

$$\begin{aligned}
 E_{\text{thr}}^{\text{PN}} &= h\nu_{\text{thr}}^{\text{PN}} = \frac{[m_{30}c^2 + m_{40}c^2]^2 - [m_{20}c^2]^2}{2m_{20}c^2} \\
 &= \frac{[M({}^{12}_6\text{C})c^2 + m_{\alpha}c^2] - [M({}^{16}_8\text{O})c^2]}{2M({}^{16}_8\text{O})c^2} \\
 &= \frac{[11174.8625 \text{ MeV} + 3727.3791 \text{ MeV}]^2 - [14895.0796 \text{ MeV}]^2}{2 \times (14895.0796 \text{ MeV})} \\
 &= 7.16 \text{ MeV}
 \end{aligned} \tag{7.386}$$

7.7.Q4

(182)

Photonuclear reaction (also referred to as photodisintegration) occurs in a direct interaction between an energetic photon and an absorber nucleus. It causes nuclear disintegration with emission of a neutron or charged particle such as proton, deuteron, α particle, fission fragments, etc. If the photon disappears, the reaction may be called nuclear photoelectric effect; if inelastic scattering occurs between the photon and the nucleus, the effect may be referred to as nuclear Compton effect.

A (γ, p) photonuclear reaction produces a proton with kinetic energy $E'_{\text{K}} = 6 \text{ MeV}$.

(a) Describe in general terms the prominent features of this (γ, p) photonuclear reaction.

- (b) Calculate the minimum photon energy $(E_\nu)_{\min}$ required for the (γ, p) reaction to occur.
- (c) Calculate the energy of the scattered photon E'_ν for $(E_\nu)_{\min}$ determined in (b).
- (d) Determine the momentum of the incident photon with energy determined in (b), scattered photon with energy determined in (c), and recoil proton with kinetic energy $E'_K = 6 \text{ MeV}$.
- (e) Draw a schematic diagram of this photonuclear reaction using relative scale according to momenta determined in (d). Verify that principles of energy and momentum conservation are upheld.

SOLUTION:

(a) Since no mention is made of the parent nucleus, we assume that the (γ, p) photon-nucleus interaction is a nuclear Compton effect in which the photon is scattered by a “free and stationary” proton. We also assume that, similarly to the standard electronic Compton interaction, at a given incident photon energy E_ν , the recoil proton will acquire the maximum possible energy from the incident photon at a photon scattering angle θ of 180° . Conversely, we can also assume that a given recoil proton kinetic energy E'_K will be attained with a minimum required incident photon kinetic energy $(E_\nu)_{\min}$ when the scattering angle θ is 180° .

(b) From the standard electronic Compton effect we know that the energy transfer from incident photon to recoil particle is in general given as

$$E'_K = E_\nu \frac{\varepsilon(1 - \cos\theta)}{1 + \varepsilon(1 - \cos\theta)} \quad \text{and for } \theta = \pi \text{ it is given as } E'_K = E_\nu \frac{2\varepsilon}{1 + 2\varepsilon}, \quad (7.387)$$

where ε is the incident photon energy E_ν normalized to the rest energy m_0c^2 of the recoil particle, i.e., $\varepsilon = E_\nu/(m_0c^2)$. The recoil particle in standard Compton effect is the electron ($m_e c^2 = 0.511 \text{ MeV}$); in nuclear Compton (γ, p) scattering it is the proton ($m_p c^2 = 938.3 \text{ MeV}$).

Since the minimum incident photon energy $(E_\nu)_{\min}$ for the given recoil proton energy $E'_K = 6 \text{ MeV}$ will be attained at $\theta = \pi$, as described in (7.387), we get the following expression relating E'_K with $(E_\nu)_{\min}$

$$E'_K = (E_\nu)_{\min} \frac{2\varepsilon}{1 + 2\varepsilon} = \frac{2(E_\nu)_{\min}^2}{m_p c^2 + 2(E_\nu)_{\min}}. \quad (7.388)$$

Equation (7.388) can be rearranged into a quadratic equation for $(E_\nu)_{\min}$ given as

$$2(E_\nu)_{\min}^2 - 2E'_K(E_\nu)_{\min} - E'_K m_p c^2 = 0, \quad (7.389)$$

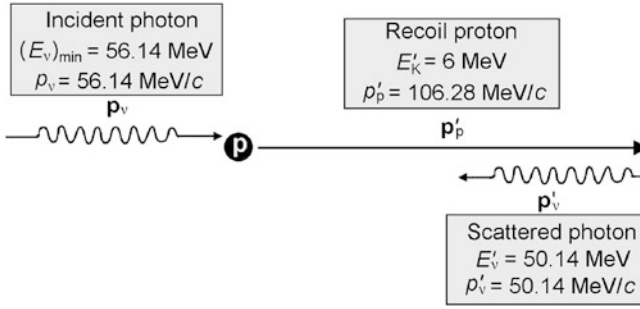


Fig. 7.45 Schematic diagram of the (γ, p) Compton photonuclear reaction

with the following physically relevant solution

$$\begin{aligned} (E_\nu)_{\min} &= \frac{E'_K + \sqrt{(E'_K)^2 + 2E'_K m_p c^2}}{2} \\ &= \frac{6 \text{ MeV} + \sqrt{36 (\text{MeV})^2 + 2 \times 6 \times 938.3 (\text{MeV})^2}}{2} = 56.14 \text{ MeV}. \end{aligned} \quad (7.390)$$

(c) The scattered photon energy E'_ν is determined from the conservation of energy as follows

$$E'_\nu = (E_\nu)_{\min} - E'_K = 56.14 \text{ MeV} - 6 \text{ MeV} = 50.14 \text{ MeV}. \quad (7.391)$$

(d) Momenta of the incident photon of energy $(E_\nu)_{\min} = 56.14 \text{ MeV}$ and the scattered photon of energy $E'_\nu = 50.14 \text{ MeV}$ are as follows

$$p_\nu = |\mathbf{p}_\nu| = \frac{(E_\nu)_{\min}}{c} = 56.14 \text{ MeV}/c \quad \text{and} \quad p'_\nu = |\mathbf{p}'_\nu| = \frac{E'_\nu}{c} = 50.14 \text{ MeV}/c. \quad (7.392)$$

Momentum of the recoil proton of kinetic energy $E'_K = 6 \text{ MeV}$ is determined from the standard expression relating relativistic momentum p with kinetic energy E_K of a particle as (T1.64)

$$p_p = |\mathbf{p}_p| = \frac{E'_K}{c} \sqrt{1 + \frac{2m_p c^2}{E'_K}} = \frac{6 \text{ MeV}}{c} \sqrt{1 + \frac{2 \times 938.3}{6}} = 106.28 \text{ MeV}/c. \quad (7.393)$$

(e) A schematic diagram of the photon–“free” proton (γ, p) photonuclear reaction with a scattering angle $\theta = 180^\circ$ is shown in Fig. 7.45. The recoil proton kinetic energy E'_K is 6 MeV with proton recoil momentum p'_p of 106.28 MeV/c; incident photon energy is $E_\nu = 56.14 \text{ MeV}$ with incident photon momentum p_ν of 56.14 MeV/c; and scattered photon energy is $E'_\nu = 50.14 \text{ MeV}$ with scattered photon momentum p'_ν of 50.14 MeV/c. From the data presented in Fig. 7.45 we note that the principles of energy and momentum conservation in nuclear Compton effect are upheld.

Chapter 8 contains **15 questions** spread over 7 sections that cover energy transfer to light charged particles and energy absorption in absorbing medium in photon interaction with matter. Energy transfer exceeds or is equal to energy absorption, and the difference between the two is attributed to energy radiated from the charged particles in the form of photons, either bremsstrahlung or, under certain conditions, annihilation photons. Many types of photon interaction with absorbing medium are known. Some of these are only of theoretical interest and help in understanding of the general photon interaction phenomena, others are of great importance in medical physics, since they play a fundamental role in imaging, radiotherapy as well as radiation dosimetry.

Section 8.1 addresses the macroscopic attenuation coefficients that in general represent a sum of attenuation coefficients for all individual interactions that an ionizing photon may have with atoms of the absorber. The interactions of interest in the context of attenuation coefficients are the photoelectric effect, Rayleigh scattering, Compton effect, and pair production, consisting of the nuclear and electronic component.

Section 8.2 deals with issues related to energy transfer from photons to charged particles, while Sect. 8.3 concentrates on energy absorption in the absorber and also deals with the mean radiation fraction (with its two main components: the bremsstrahlung fraction and in-flight annihilation fraction) as well as the mean energy absorption fraction. Section 8.4 consists of problems dealing with attenuation coefficients of compounds and mixtures; Sect. 8.5 addresses various effects that follow photon interactions with the absorber.

The chapter concludes with problems highlighting a summary of photon interactions with absorber atoms (Sect. 8.6) and Sect. 8.7 contains two problems presenting a simple Monte Carlo simulation history of highenergy photons interacting with a water phantom.

8.1 Macroscopic Attenuation Coefficient

8.1.Q1

(183)

The mass attenuation coefficients for photoelectric effect τ/ρ , Rayleigh scattering σ_R/ρ , Compton scattering σ_C/ρ , nuclear pair production κ_{NPP}/ρ and electronic pair production (triplet production) κ_{TP}/ρ for photons with energy $h\nu = 5 \text{ MeV}$ in tungsten are:

$$\begin{aligned}\tau/\rho &= 9.04 \times 10^{-4} \text{ cm}^2/\text{g}; \\ \sigma_R/\rho &= 1.01 \times 10^{-4} \text{ cm}^2/\text{g}; \\ \sigma_C/\rho &= 2.01 \times 10^{-2} \text{ cm}^2/\text{g}; \\ \kappa_{\text{NPP}}/\rho &= 1.98 \times 10^{-2} \text{ cm}^2/\text{g}; \\ \kappa_{\text{TP}}/\rho &= 7.91 \times 10^{-5} \text{ cm}^2/\text{g}.\end{aligned}$$

Physical density ρ and atomic mass A of tungsten are 19.3 g/cm^3 and 183.84 g/mol , respectively.

For photons of energy $h\nu = 5 \text{ MeV}$ interacting with a tungsten absorber calculate:

- (a) Mass attenuation coefficient μ/ρ .
- (b) Linear attenuation coefficient μ .
- (c) Atomic attenuation coefficients ${}_a\tau$, ${}_a\sigma_R$, ${}_a\sigma_C$, ${}_a\kappa_{\text{NPP}}$, and ${}_a\kappa_{\text{TP}}$ for photoelectric effect, Rayleigh scattering, nuclear pair production and triplet production, respectively.
- (d) Atomic attenuation coefficient ${}_a\mu$.
- (e) Electronic attenuation coefficients ${}_e\sigma_C$ and ${}_e\kappa_{\text{TP}}$ for Compton effect and triplet production, respectively.

SOLUTION:

As shown in (T8.1) through (T8.4), for an absorber of density ρ , atomic number Z , and atomic mass A , the expressions for the linear attenuation coefficient μ , mass attenuation coefficient μ_m , and atomic attenuation coefficient (cross section) ${}_a\mu$ are given as a sum of contributions μ_i from the four individual effects.

- (1) Linear attenuation coefficient μ

$$\mu = \sum_i \mu_i = \tau + \sigma_R + \sigma_C + \kappa, \quad (8.1)$$

- (2) Mass attenuation coefficient μ_m

$$\mu_m = \frac{\mu}{\rho} = \sum_i \left(\frac{\mu}{\rho} \right)_i = \frac{1}{\rho} (\tau + \sigma_R + \sigma_C + \kappa) = \frac{\tau}{\rho} + \frac{\sigma_R}{\rho} + \frac{\sigma_C}{\rho} + \frac{\kappa}{\rho}, \quad (8.2)$$

(3) Atomic attenuation coefficient (cross section) ${}_a\mu$

$${}_a\mu = \frac{1}{\rho} \frac{A}{N_A} \mu = \frac{1}{\rho} \frac{A}{N_A} \sum_i \mu_i = \frac{1}{\rho} \frac{A}{N_A} (\tau + \sigma_R + \sigma_C + \kappa) = {}_a\tau + {}_a\sigma_R + {}_a\sigma_C + {}_a\kappa, \quad (8.3)$$

where τ , σ_R , σ_C , and κ are the linear attenuation coefficients for the photoelectric effect, Rayleigh scattering, Compton effect, and pair production, respectively. The linear pair production attenuation coefficient κ is usually expressed as the sum of the linear nuclear pair production attenuation coefficient κ_{NPP} and the linear electronic pair production (triplet production) attenuation coefficient κ_{TP} .

(a) As given in (8.2), the mass attenuation coefficient μ/ρ for 5 MeV photons in tungsten absorber is calculated as a sum of four individual components

$$\begin{aligned} \frac{\mu}{\rho} &= \sum_i \left(\frac{\mu}{\rho} \right)_i = \frac{\tau}{\rho} + \frac{\sigma_R}{\rho} + \frac{\sigma_C}{\rho} + \left(\frac{\kappa_{\text{TP}}}{\rho} + \frac{\kappa_{\text{NPP}}}{\rho} \right) = \frac{\tau}{\rho} + \frac{\sigma_R}{\rho} + \frac{\sigma_C}{\rho} + \frac{\kappa}{\rho} \\ &= [9.04 \times 10^{-4} + 1.01 \times 10^{-4} + 2.01 \times 10^{-2} + (1.98 \times 10^{-2} + 7.91 \times 10^{-5})] \frac{\text{cm}^2}{\text{g}} \\ &= 4.10 \times 10^{-2} \frac{\text{cm}^2}{\text{g}}. \end{aligned} \quad (8.4)$$

(b) Linear attenuation coefficient μ is calculated from the mass attenuation coefficient μ/ρ as follows

$$\mu = \mu_m \rho = \left(\frac{\mu}{\rho} \right) \times \rho = 4.10 \times 10^{-2} \frac{\text{cm}^2}{\text{g}} \times 19.3 \frac{\text{g}}{\text{cm}^3} = 0.792 \text{ cm}^{-1}. \quad (8.5)$$

(c) Atomic attenuation coefficients ${}_a\mu_i$ are calculated from the two basic nuclear physics expressions relating linear and mass attenuation coefficients with the atomic coefficient

$$\mu_i = n \square {}_a\mu_i \quad \text{or} \quad \frac{\mu_i}{\rho} = \frac{n \square}{\rho} {}_a\mu_i = \frac{N_A}{A} {}_a\mu_i, \quad (8.6)$$

where

$n \square$ is the number of atoms N_a per volume V , i.e., $n \square = N_a/V = \rho N_a/m = \rho N_A/A$.

m is the mass of the absorber.

N_A is the Avogadro number ($6.022 \times 10^{23} \text{ mol}^{-1}$).

ρ is the mass density of the absorber.

Atomic attenuation coefficients for the four types of photon interaction of 5 MeV photons with tungsten atoms are thus given as follows:

(1) *Photoelectric effect*

$$\begin{aligned}
 {}_a\tau &= \frac{A}{N_A} \left(\frac{\tau}{\rho} \right) = \frac{183.84 \text{ g/mol}}{6.022 \times 10^{23} \text{ atom/mol}} \times (9.04 \times 10^{-4} \text{ cm}^2/\text{g}) \\
 &= 2.76 \times 10^{-25} \frac{\text{cm}^2}{\text{atom}} = 0.276 \frac{\text{b}}{\text{atom}}, \quad (8.7)
 \end{aligned}$$

(2) *Rayleigh scattering*

$$\begin{aligned}
 {}_a\sigma_R &= \frac{A}{N_A} \left(\frac{\sigma_R}{\rho} \right) = \frac{183.84 \text{ g/mol}}{6.022 \times 10^{23} \text{ atom/mol}} \times (1.01 \times 10^{-4} \text{ cm}^2/\text{g}) \\
 &= 3.09 \times 10^{-26} \frac{\text{cm}^2}{\text{atom}} = 3.09 \times 10^{-2} \frac{\text{b}}{\text{atom}}, \quad (8.8)
 \end{aligned}$$

(3) *Compton effect*

$$\begin{aligned}
 {}_a\sigma_C &= \frac{A}{N_A} \left(\frac{\sigma_C}{\rho} \right) = \frac{183.84 \text{ g/mol}}{6.022 \times 10^{23} \text{ atom/mol}} \times (2.01 \times 10^{-2} \text{ cm}^2/\text{g}) \\
 &= 6.14 \times 10^{-24} \frac{\text{cm}^2}{\text{atom}} = 6.14 \frac{\text{b}}{\text{atom}}, \quad (8.9)
 \end{aligned}$$

(4) *Pair production*

Atomic attenuation coefficient ${}_a\kappa$ for pair production has two components: nuclear ${}_a\kappa_{\text{NPP}}$ and electronic (triplet) ${}_a\kappa_{\text{TP}}$

$$\begin{aligned}
 {}_a\kappa_{\text{NPP}} &= \frac{A}{N_A} \left(\frac{\kappa_{\text{NPP}}}{\rho} \right) = \frac{183.84 \text{ g/mol}}{6.022 \times 10^{23} \text{ atom/mol}} \times (1.98 \times 10^{-2} \text{ cm}^2/\text{g}) \\
 &= 6.05 \times 10^{-24} \frac{\text{cm}^2}{\text{atom}} = 6.05 \frac{\text{b}}{\text{atom}} \quad (8.10)
 \end{aligned}$$

and

$$\begin{aligned}
 {}_a\kappa_{\text{TP}} &= \frac{A}{N_A} \left(\frac{\kappa_{\text{TP}}}{\rho} \right) = \frac{183.84 \text{ g/mol}}{6.022 \times 10^{23} \text{ atom/mol}} \times (7.91 \times 10^{-6} \text{ cm}^2/\text{g}) \\
 &= 2.42 \times 10^{-27} \frac{\text{cm}^2}{\text{atom}} = 2.42 \times 10^{-3} \frac{\text{b}}{\text{atom}}. \quad (8.11)
 \end{aligned}$$

Note: Since ${}_a\kappa_{\text{NPP}} \gg {}_a\kappa_{\text{TP}}$, one can assume that ${}_a\kappa \approx {}_a\kappa_{\text{NPP}} = 6.05 \text{ b/atom}$.

(d) As given in (8.3), the atomic attenuation coefficient ${}_a\mu$ for 5 MeV photons interacting with tungsten is given by the sum of the four individual components

given in (8.7) through (8.10). We thus have the following result for ${}_a\mu$

$$\begin{aligned} {}_a\mu &= \sum_i {}_a\mu_i = {}_a\tau + {}_a\sigma_R + {}_a\sigma_C + {}_a\kappa \\ &= (0.276 + 3.09 \times 10^{-2} + 6.14 + 6.05) \frac{\text{b}}{\text{atom}} = 12.5 \frac{\text{b}}{\text{atom}}. \end{aligned} \quad (8.12)$$

Using (8.6) in conjunction with (8.12) we can verify the consistency of results for the mass and linear attenuation coefficients obtained in (8.4) and (8.5), respectively, as

$$\begin{aligned} \mu &= n \square {}_a\mu = \rho \frac{N_A}{A} {}_a\mu \\ &= (19.3 \text{ g/cm}^3) \times \frac{(6.022 \times 10^{23} \text{ atom/mol})}{(183.84 \text{ g/mol})} \times (12.5 \times 10^{-24} \text{ cm}^2/\text{atom}) \\ &= 0.792 \text{ cm}^{-1} \end{aligned} \quad (8.13)$$

and

$$\begin{aligned} \mu_m &= \frac{\mu}{\rho} = \frac{0.792 \text{ cm}^{-1}}{19.3 \text{ g/cm}^3} = 4.10 \times 10^{-2} \text{ cm}^2/\text{g} \equiv \frac{n \square}{} {}_a\mu = \frac{N_A}{A} {}_a\mu \\ &= \frac{(6.022 \times 10^{23} \text{ atom/mol})}{(183.84 \text{ g/mol})} \times (12.5 \times 10^{-24} \text{ cm}^2/\text{atom}) \\ &= 4.10 \times 10^{-2} \text{ cm}^2/\text{g}. \end{aligned} \quad (8.14)$$

(e) *Electronic Compton attenuation coefficient* ${}_e\sigma_C$ is calculated from the atomic Compton attenuation coefficient ${}_a\sigma_C$ as follows

$$\begin{aligned} {}_e\sigma_C &= \frac{{}_a\sigma_C}{Z} = \frac{6.14 \times 10^{-24} \text{ cm}^2/\text{atom}}{74 \text{ electron/atom}} = 8.30 \times 10^{-26} \text{ cm}^2/\text{electron} \\ &= 0.083 \text{ b/electron}. \end{aligned} \quad (8.15)$$

Electronic triplet production attenuation coefficient ${}_e\kappa_{TP}$ is calculated from the atomic triplet production attenuation coefficient ${}_a\kappa_{TP}$ as follows

$${}_e\kappa_{TP} = \frac{{}_a\kappa_{TP}}{Z} = \frac{2.42 \times 10^{-3} \text{ b/atom}}{74 \text{ electron/atom}} = 3.27 \times 10^{-5} \text{ b/electron}. \quad (8.16)$$

8.2 Energy Transfer from Photons to Charged Particles in Absorber

8.2.Q1

(184)

The five most important photon interactions with matter are the photoelectric effect, Rayleigh scattering, Compton effect, nuclear pair production, and triplet production. Of these, Rayleigh scattering is elastic and does not transfer any energy to charged particles, so it is ignored in the context of energy transfer. Three of the remaining four effects (photoelectric, Compton, and triplet production) produce vacancies in absorber atoms, and these vacancies engender either characteristic (fluorescence) photons or Auger electrons or both.

- State and sketch the mean energy transfer fractions for the photoelectric effect \bar{f}_{PE} , Rayleigh scattering \bar{f}_{R} , Compton effect \bar{f}_{C} , and pair production \bar{f}_{PP} as a function of incident photon energy $h\nu$.
- Determine the mean energy transfer fractions \bar{f}_{PE} , \bar{f}_{R} , \bar{f}_{C} , and \bar{f}_{PP} for 5 MeV photons interacting with a tungsten absorber.

SOLUTION:

(a) The total mean energy transfer fraction $\bar{f}_{\text{tr}}(h\nu, Z)$ is defined as the fraction of photon energy $h\nu$ that is transferred to kinetic energy of charged particles produced or released in the absorber during various possible photon interactions with absorber atoms. It is generally expressed as the sum of four components, each component representing a specific effect that contributes to photon attenuation in the absorber (photoelectric effect, Rayleigh scattering, Compton effect, and pair production).

The mean energy transfer fractions for individual photon interactions are expressed as follows

$$\bar{f}_{\text{PE}} = \frac{\bar{E}_{\text{tr}}^{\text{PE}}}{h\nu} = \frac{h\nu - \bar{X}_{\text{PE}}}{h\nu} = \frac{h\nu - \sum_j P_j \omega_j h\nu_j}{h\nu} = 1 - \frac{\sum_j P_j \omega_j h\nu_j}{h\nu}, \quad (8.17)$$

$$\bar{f}_{\text{R}} = 0, \quad (8.18)$$

$$\bar{f}_{\text{C}} = \frac{\bar{E}_{\text{tr}}^{\text{C}}}{h\nu} = \frac{h\nu - h\nu' - \bar{X}_{\text{C}}}{h\nu} = 1 - \frac{h\nu' + \bar{X}_{\text{C}}}{h\nu} \approx 1 - \frac{h\nu'}{h\nu}, \quad (8.19)$$

$$\bar{f}_{\text{NPP}} = \frac{\bar{E}_{\text{tr}}^{\text{NPP}}}{h\nu} = \frac{h\nu - 2m_{\text{e}}c^2}{h\nu} = 1 - \frac{2m_{\text{e}}c^2}{h\nu} = 1 - \frac{2m_{\text{e}}c^2}{h\nu}, \quad (8.20)$$

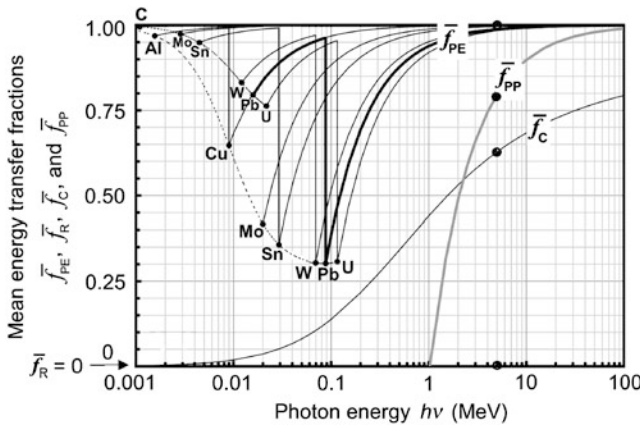


Fig. 8.1 Mean energy transfer fractions \bar{f}_i plotted against photon energy $h\nu$ for the four main photon interactions with absorber atoms: \bar{f}_{PE} for photoelectric effect, \bar{f}_R for Rayleigh scattering, \bar{f}_C for Compton effect, and \bar{f}_{PP} for pair production. The data points show the mean energy transfer fractions for the four interactions at photon energy of 5 MeV interacting with tungsten absorber

$$\begin{aligned} \bar{f}_{TP} &= \frac{\bar{E}_{tr}^{TP}}{h\nu} = \frac{h\nu - 2m_e c^2 - \bar{X}_{TP}}{h\nu} = 1 - \frac{2m_e c^2 + \bar{X}_{TP}}{h\nu} \\ &\approx 1 - \frac{2m_e c^2}{h\nu}, \end{aligned} \tag{8.21}$$

where \bar{X}_{PE} , \bar{X}_C , and \bar{X}_{TP} are the mean fluorescence emission energies for the photoelectric effect, Compton effect, and triplet production, and $h\nu'$ is the mean energy of the scattered photon. In the photoelectric effect it is customary to add the kinetic energy of the Auger electrons to that of the photoelectron; in Compton effect and the triplet production the kinetic energy of possible Auger electrons is neglected.

The mean energy transfer fractions \bar{f}_{PE} , \bar{f}_R , \bar{f}_C , and \bar{f}_{PP} are very important in radiation dosimetry in particular and medical physics in general. It is therefore imperative that a medical physics student be able to sketch and explain the four mean energy transfer fractions in the photon energy $h\nu$ range from 1 keV to 1000 MeV. Figure 8.1 shows the mean energy transfer fractions \bar{f}_{PE} , \bar{f}_R , \bar{f}_C , and \bar{f}_{PP} for the photoelectric effect, Rayleigh scattering, Compton effect and pair production. The graph seems quite busy but a closer look actually shows that the fractions for individual effects are relatively easy to understand and to reproduce once a few facts are recognized. The following points are useful to note:

- (1) Of the four fractions, \bar{f}_{PE} for photoelectric effect seems the most cumbersome since it depends not only on energy $h\nu$ of the photon but also on the atomic number Z of the absorber, as a result of the Z -dependence of (i) P_j , the probability for photoelectric effect, if it occurs, to occur in j shell or sub-shell; (ii) ω_j , the fluorescence yield; and (iii) $h\bar{\nu}_j$, the mean fluorescence photon energy.

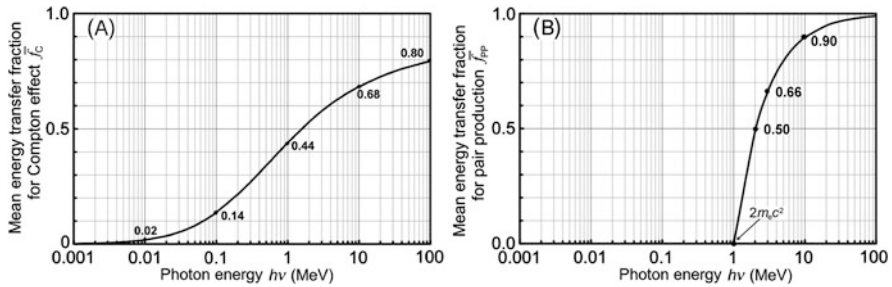


Fig. 8.2 Mean energy transfer fractions (A) \bar{f}_C for Compton effect and (B) \bar{f}_{PP} for pair production. Anchor points listed in Table 8.1 that help with sketching the two curves are highlighted

Table 8.1 Anchor points for mean energy transfer fractions \bar{f}_C and \bar{f}_{PP}

$h\nu$ (MeV)	0.001	0.01	0.1	1.0	5	10	100	1000
\bar{f}_C	0	0.02	0.14	0.44	–	0.68	0.80	0.85
\bar{f}_{PP}	–	–	–	~ 0	0.5	0.9	~ 1	~ 1

- (2) For a given absorber Z , \bar{f}_{PE} ranges from its lowest value at the K absorption edge [$h\nu = E_B(K)$] to $\bar{f}_{PE} = 1$ both at low photon energies where $h\nu < E_B(M)$ and at high photon energies where $h\nu > 10$ MeV.
- (3) Energy dependence of \bar{f}_R for Rayleigh scattering is trivial since $\bar{f}_R = 0$ irrespective of photon $h\nu$ and Z of the absorber.
- (4) \bar{f}_C and \bar{f}_{PP} for Compton effect and pair production, respectively, depend on photon energy $h\nu$ but are independent of the atomic number Z of the absorber. For all absorbers, the range of \bar{f}_C is from $\bar{f}_C < 0.02$ for $h\nu < 10$ keV to $\bar{f}_C > 0.85$ for $h\nu > 1000$ MeV. For all absorbers, the range of \bar{f}_{PP} is from $\bar{f}_{PP} = 0$ for $h\nu \leq 1.02$ MeV through $\bar{f}_{PP} = 0.5$ at $h\nu = 2$ MeV to $\bar{f}_{PP} \approx 1$ for $h\nu > 10$ MeV.
- (5) Not depending on Z of the absorber, \bar{f}_C , and \bar{f}_{PP} are given for all absorbers by only one curve each, and the two curves can be easily reproduced by knowing a few anchor points for each curve, as shown in Fig. 8.2, (A) and (B), respectively, and listed in Table 8.1.

(b) Mean energy transfer fractions \bar{f}_{PE} , \bar{f}_R , \bar{f}_C , and \bar{f}_{PP} for 5 MeV photon can be read directly from Fig. 8.1 and are marked on the figure as data points for $h\nu = 5$ MeV. The individual mean energy transfer fractions for 5 MeV photon interacting with a tungsten absorber are as follows

$$\bar{f}_{PE} \approx 1.0, \quad \bar{f}_R = 0, \quad \bar{f}_C = 0.62, \quad \text{and} \quad \bar{f}_{PP} = 0.795. \quad (8.22)$$

8.2.Q2

(185)

Using the mass attenuation coefficient data for aluminum and tungsten available from the NIST XCOM database: physics.nist.gov/PhysRefData/Xcom/html/xcom1.html

- Calculate the relative weights w_i of the photoelectric effect w_{PE} , Rayleigh scattering w_R , Compton scattering w_C , and pair production (nuclear and electronic combined) w_{PP} , for aluminum and tungsten for photon energies $h\nu$ of 0.001 MeV, 0.1 MeV, 1 MeV, 10 MeV, and 100 MeV.
- Enter and verify the data calculated in (a) on the two graphs presented in Fig. 8.3 that plots in (A) for aluminum and (B) for tungsten the relative weights w_i for the photoelectric effect, Rayleigh scattering, Compton effect, and pair production against photon energy $h\nu$ in the range from 0.001 MeV to 100 MeV.
- Discuss the general behavior of the relative weights w_i against photon energy of the four main types of photon interaction with absorber atoms.

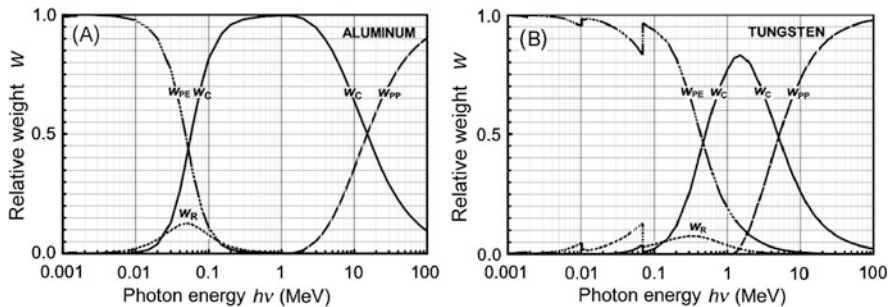


Fig. 8.3 Relative weights w_i plotted for aluminum in (A) and tungsten in (B) against photon energy $h\nu$ for the four main photon interactions with absorber atoms: photoelectric effect w_{PE} , Rayleigh scattering w_R , Compton effect w_C , and pair production w_{PP} . Data calculated using the NIST XCOM database

SOLUTION:

Out of the large number of possible photon interactions with absorber atoms known in nuclear physics, in medical physics we usually account for the four most prominent interactions: photoelectric effect (PE), Rayleigh scattering (R), Compton effect (C), and pair production (PP). Relative weight w_i for each of these interactions i is

given by the following ratios

$$w_i = \frac{\mu_i/\rho}{\mu/\rho} \quad (8.23)$$

with

$$\begin{aligned} w_{\text{PE}} &= \frac{\tau/\rho}{\mu/\rho}; & w_{\text{R}} &= \frac{\sigma_{\text{R}}/\rho}{\mu/\rho}; \\ w_{\text{C}} &= \frac{\sigma_{\text{C}}/\rho}{\mu/\rho}; & \text{and } \frac{\kappa_{\text{PP}}/\rho}{\mu/\rho} &= \frac{\kappa_{\text{NPP}}/\rho + \kappa_{\text{TP}}/\rho}{\mu}, \end{aligned} \quad (8.24)$$

where μ_i/ρ is the mass attenuation coefficient for interaction i and μ/ρ is the total mass attenuation coefficient equal to the sum of mass attenuation coefficients for each of the four individual interactions i , as indicated below

$$\frac{\mu}{\rho} = \sum_i \frac{\mu_i}{\rho} = \frac{\tau}{\rho} + \frac{\sigma_{\text{R}}}{\rho} + \frac{\sigma_{\text{C}}}{\rho} + \frac{\kappa}{\rho}. \quad (8.25)$$

From (8.24) and (8.25) we note that the sum of the weights w_i for the individual photon interaction effects must by definition equal to 1, i.e.,

$$\sum_i w_i = w_{\text{PE}} + w_{\text{R}} + w_{\text{C}} + w_{\text{PP}} = \frac{\tau/\rho}{\mu/\rho} + \frac{\sigma_{\text{R}}/\rho}{\mu/\rho} + \frac{\sigma_{\text{C}}/\rho}{\mu/\rho} + \frac{\kappa_{\text{PP}}/\rho}{\mu/\rho} = 1. \quad (8.26)$$

(a) Based on data available from the NIST we now calculate the relative weights w_i of the photoelectric effect w_{PE} , Rayleigh scattering w_{R} , Compton scattering w_{C} , and pair production (nuclear and electronic combined) w_{PP} for aluminum and tungsten for selected photon energies $h\nu$ of 0.001 MeV, 0.1 MeV, 1 MeV, 10 MeV, and 100 MeV. NIST data for aluminum are presented in Table 8.1 and for tungsten in Table 8.2.

(b) The relative weights for the photoelectric effect w_{PE} , Rayleigh scattering w_{R} , Compton effect w_{C} , and pair production w_{PP} for various photons in the energy range between 1 keV and 100 MeV interacting with aluminum and tungsten absorber were calculated with (8.24) in (a) and are listed in Tables 8.2 and 8.3, respectively. We entered the calculated w_i on the graphs of Fig. 8.4 to verify our calculated data. The agreement between the graphs based on NIST data and our calculated w_i is excellent allowing us to make the following conclusions on the photon energy dependence of w_i :

- (1) On semi-log photon energy diagram w_{PE} and w_{PP} exhibit a sigmoid shape, w_{PE} decreasing from 1 with photon energy increasing from 1 keV and w_{PP} increasing from 0 with photon energy increasing from 1 MeV.
- (2) For the photoelectric effect w_{PE} is approximately equal to 1 at relatively low photon energies $h\nu$ of the order of the K-shell binding energy $E_{\text{B}}(\text{K})$. With increasing photon energy, w_{PE} decreases and asymptotically approaches 0. It attains a 50 % point at ~ 40 keV for low Z absorbers such as aluminum and at

Table 8.2 Relative weights w_i for photoelectric effect w_{PE} , Rayleigh scattering w_R , Compton effect w_C , and pair production w_{PP} in **aluminum** absorber for various photon energies $h\nu$ in the range from 0.001 MeV to 100 MeV

(1) $h\nu$ (MeV)	0.001	0.01	0.1	1.0	10.0	100.0
(2) τ/ρ (cm ² /g)	1.18×10^3	25.6	1.84×10^{-2}	2.64×10^{-5}	9.66×10^{-7}	8.64×10^{-8}
(3) σ_R/ρ (cm ² /g)	2.26	0.551	1.32×10^{-2}	1.44×10^{-4}	1.44×10^{-6}	1.44×10^{-8}
(4) σ_C/ρ (cm ² /g)	1.43×10^{-2}	0.106	0.139	6.13×10^{-2}	1.48×10^{-2}	2.40×10^{-3}
(5) κ_{NPP}/ρ (cm ² /g)	0	0	0	0	8.00×10^{-3}	2.12×10^{-2}
(6) κ_{TP}/ρ (cm ² /g)	0	0	0	0	3.39×10^{-4}	1.56×10^{-3}
(7) μ/ρ (cm ² /g)	1.182×10^3	26.3	0.171	6.15×10^{-2}	2.31×10^{-2}	2.52×10^{-2}
(8) w_{PE}	0.998	0.975	0.108	4.30×10^{-4}	4.17×10^{-5}	3.34×10^{-6}
(9) w_R	1.91×10^{-3}	2.10×10^{-2}	7.74×10^{-2}	2.34×10^{-3}	6.22×10^{-5}	5.72×10^{-7}
(10) w_C	1.21×10^{-5}	4.04×10^{-3}	0.815	0.997	0.640	9.54×10^{-2}
(11) w_{PP}	0	0	0	0	0.360	0.905
(12) $\sum_i w_i$	~ 1.00	~ 1.00	~ 1.00	~ 1.00	~ 1.00	~ 1.00

Table 8.3 Relative weights w_i for photoelectric effect w_{PE} , Rayleigh scattering w_R , Compton effect w_C , and pair production w_{PP} in **tungsten** absorber for various photon energies $h\nu$ in the range from 0.001 MeV to 100 MeV

(1) $h\nu$ (MeV)	0.001	0.01	0.1	1.0	10.0	100.0
(2) τ/ρ (cm ² /g)	3.67×10^3	92.4	4.15	1.28×10^{-2}	3.75×10^{-4}	3.08×10^{-5}
(3) σ_R/ρ (cm ² /g)	11.4	4.45	0.182	2.48×10^{-3}	2.53×10^{-5}	2.53×10^{-7}
(4) σ_C/ρ (cm ² /g)	4.43×10^{-3}	4.79×10^{-2}	0.102	5.09×10^{-2}	1.24×10^{-2}	2.01×10^{-3}
(5) κ_{NPP}/ρ (cm ² /g)	0	0	0	0	3.44×10^{-2}	8.09×10^{-2}
(6) κ_{TP}/ρ (cm ² /g)	0	0	0	0	2.79×10^{-4}	1.19×10^{-3}
(7) μ/ρ (cm ² /g)	3.68×10^3	26.3	4.43	6.62×10^{-2}	4.75×10^{-2}	8.79×10^{-2}
(8) w_{PE}	0.997	0.954	0.936	0.193	7.90×10^{-3}	3.50×10^{-4}
(9) w_R	3.10×10^{-3}	4.50×10^{-2}	4.10×10^{-2}	3.75×10^{-2}	5.33×10^{-4}	2.88×10^{-6}
(10) w_C	1.18×10^{-6}	4.94×10^{-4}	2.30×10^{-2}	0.769	0.261	2.29×10^{-2}
(11) w_{PP}	0	0	0	0	0.730	0.977
(12) $\sum_i w_i$	~ 1.00	~ 1.00	~ 1.00	~ 1.00	~ 1.00	~ 1.00

~ 500 keV for high Z absorbers such as tungsten. For low Z absorbers $w_{PE} \approx 0$ for photon energies exceeding 100 keV; for high Z absorbers $w_{PE} = 0$ at photon energies exceeding 10 MeV.

- (3) For Rayleigh scattering w_R follows a bell shaped distribution and reaches a peak value of about 0.1 or less indicating that the relative weight of Rayleigh scattering does not amount to more than about 10 % of the total attenuation.

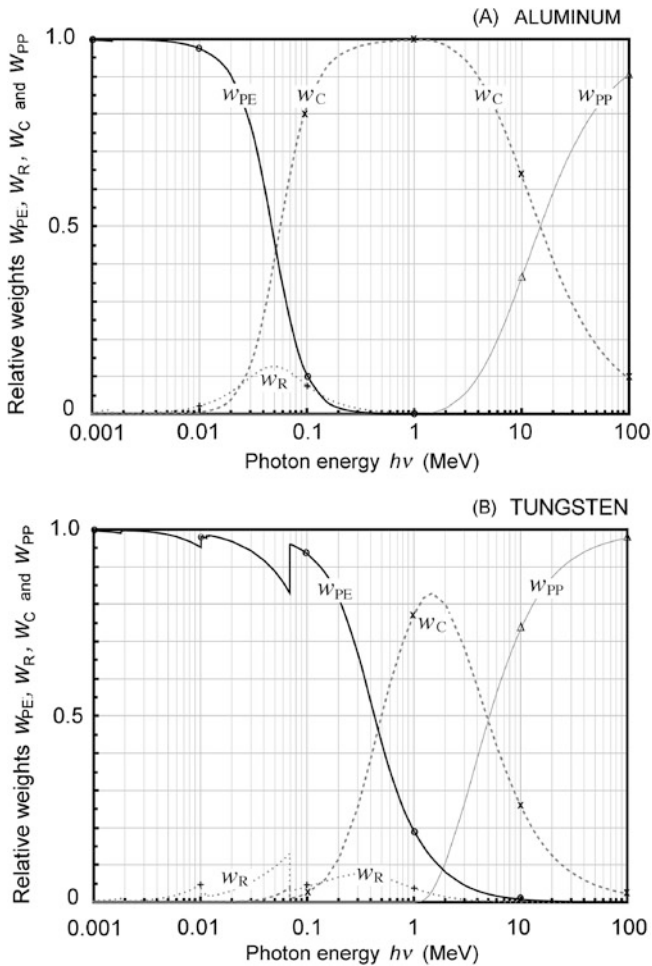


Fig. 8.4 Relative weights w_i for photoelectric effect w_{PE} , Rayleigh scattering w_R , Compton effect w_C , and pair production w_{PP} in aluminum in (A) and tungsten in (B) for various photon energies $h\nu$ in the range from 0.001 MeV to 100 MeV. Our calculated data are shown as data points on the graphs

- (4) For Compton scattering w_C also follows a bell shaped distribution and for all absorbers it peaks at ~ 1.5 MeV. For low Z absorbers the distribution is broad and peaks at $w_C = 1$; for high Z absorbers the distribution is narrow and peaks at $w_C \approx 0.7$.
- (5) For pair production w_{PP} exhibits a sigmoid curve shape starting at the pair production threshold photon energy of 1.022 MeV. With increasing photon energy the distribution rises rapidly from $w_{PP} = 0$ to reach a saturation value of $w_{PP} = 1$ at high photon energies. The point of 50% saturation ($w_{PP} = 0.5$) occurs at photon energy of ~ 20 MeV for low Z absorbers and at only ~ 5 MeV for high Z absorbers.

8.2.Q3

(186)

Total mean energy transfer fraction $\bar{f}_{\text{tr}}(h\nu, Z)$ is defined as the mean fraction of photon energy $h\nu$ that is transferred to kinetic energy of charged particles produced or released in the absorber during the various possible photon interactions with absorber atoms.

- (a) Determine $\bar{f}_{\text{tr}}(h\nu = 4 \text{ MeV}, Z = 82)$ for 4 MeV photons interacting with a lead absorber.
- (b) Determine \bar{E}_{tr} , mean energy transferred from 4 MeV photon to charged particles released or produced in lead absorber.

The following NIST data for 4 MeV photons in lead may prove useful in the calculations: ${}_a\tau = 0.593 \text{ b/atom}$, ${}_a\sigma_{\text{R}} = 0.066 \text{ b/atom}$, ${}_a\sigma_{\text{C}} = 7.879 \text{ b/atom}$, ${}_a\kappa = 5.904 \text{ b/atom}$.

SOLUTION:

(a) The total mean energy transfer fraction \bar{f}_{tr} for the four most common photon interactions (photoelectric, Rayleigh, Compton, and pair production) is expressed as follows (T8.6)

$$\begin{aligned}\bar{f}_{\text{tr}} &= \frac{\bar{E}_{\text{tr}}}{h\nu} = \sum_i \frac{\mu_i/\rho}{\mu/\rho} \bar{f}_i = \left\{ \frac{\tau/\rho}{\mu/\rho} \bar{f}_{\text{PE}} + \frac{\sigma_{\text{R}}/\rho}{\mu/\rho} \bar{f}_{\text{R}} + \frac{\sigma_{\text{C}}/\rho}{\mu/\rho} \bar{f}_{\text{C}} + \frac{\kappa/\rho}{\mu/\rho} \bar{f}_{\text{PP}} \right\} \\ &= \sum_i w_i \frac{a\mu_i}{a\mu} = \sum_i w_i \bar{f}_i = \{w_{\text{PE}}\bar{f}_{\text{PE}} + w_{\text{R}}\bar{f}_{\text{R}} + w_{\text{C}}\bar{f}_{\text{C}} + w_{\text{PP}}\bar{f}_{\text{PP}}\} \\ &= \sum_i \frac{\mu_i}{\mu} \frac{\bar{E}_{\text{tr}}^i}{h\nu} = \frac{1}{h\nu} \{w_{\text{PE}}\bar{E}_{\text{tr}}^{\text{PE}} + w_{\text{R}}\bar{E}_{\text{tr}}^{\text{R}} + w_{\text{C}}\bar{E}_{\text{tr}}^{\text{C}} + w_{\text{PP}}\bar{E}_{\text{tr}}^{\text{PP}}\},\end{aligned}\quad (8.27)$$

where

\bar{f}_i is the mean energy transfer fraction for photon interaction i : \bar{f}_{PE} , \bar{f}_{R} , \bar{f}_{C} , and \bar{f}_{PP} .

w_i is the relative weight of photon interaction i : w_{PE} , w_{R} , w_{C} , and w_{PP} .

\bar{E}_{tr}^i is the mean energy transferred from photon to charged particles for interaction i .

\bar{E}_{tr} is the mean energy transferred from photon to charged particles averaged over all possible photon interactions at a given photon energy $h\nu$ and absorber atomic number Z .

As shown in (8.27), to determine the total mean energy transfer fraction \bar{f}_{tr} for 4 MeV photons interacting with lead absorber we need:

- (1) Mean energy transfer fractions \bar{f}_i for each of the four major photon interactions with lead.
- (2) Relative weights w_i for the four major photon interactions with lead absorber.

(1) To determine the mean energy transfer fractions \bar{f}_i we use the definitions for energy transfer fractions applicable to the individual effects as follows:

- (i) Mean energy transfer fraction \bar{f}_{PE} in photoelectric effect is given by (T7.161)

$$\begin{aligned}\bar{f}_{PE} &= 1 - \frac{P_K \omega_K \eta_K E_B(K)}{h\nu} = 1 - \frac{0.788 \times 0.968 \times 0.915 \times 0.088}{4} \\ &= 1 - 0.015 = 0.985,\end{aligned}\quad (8.28)$$

where

P_K is the probability for the photoelectric effect, if it occurs, to occur in the K shell of an absorber atom. Probability P_K ranges from $P_K \approx 1$ for low atomic number Z absorbers to $P_K \approx 0.75$ for high Z absorbers.

ω_K is the fluorescence yield for the K shell strongly dependent on absorber atomic number Z .

η_K is the fluorescence efficiency defined for emission of K-shell fluorescence photon as the mean fraction of the K-shell binding energy carried by the fluorescence photon. Fluorescence efficiency η_K decreases slowly from $\eta_K \approx 0.97$ for low Z absorbers, reaches a broad minimum of $\eta_K \approx 0.9$ at $Z \approx 50$ and then rises slowly to reach $\eta_K = 0.95$ for high Z absorbers.

$E_B(K)$ is binding energy of the K-shell electron.

In open literature we find the following data for use in (8.28) for 4 MeV photons in lead $P_K = 0.788$, $\omega_K = 0.968$, $\eta_K = 0.915$, and $E_B(K) = 88$ keV.

Mean energy transfer \bar{E}_{tr}^{PE} in photoelectric effect

$$\bar{E}_{tr}^{PE} = \bar{f}_{PE} h\nu = 0.985 \times (4 \text{ MeV}) = 3.94 \text{ MeV}.\quad (8.29)$$

- (ii) Mean energy transfer fraction \bar{f}_R in Rayleigh scattering is equal to 0 for all photon energies and for all absorber atomic numbers

$$\bar{f}_R = 0\quad (8.30)$$

Mean energy transfer \bar{E}_{tr}^R in Rayleigh scattering

$$\bar{E}_{tr}^R = 0\quad (8.31)$$

- (iii) Mean energy transfer fraction \bar{f}_C in Compton effect is determined from the Compton graph (Fig. T7.18)

$$\bar{f}_C = 0.61\quad (8.32)$$

Mean energy transfer $\bar{E}_{\text{tr}}^{\text{C}}$ in Compton effect is given as

$$\bar{E}_{\text{tr}}^{\text{C}} = \bar{f}_{\text{C}} h\nu = 0.61 \times (4 \text{ MeV}) = 2.44 \text{ MeV} \quad (8.33)$$

(iv) Mean energy transfer fraction \bar{f}_{PP} in pair production is given by

$$\bar{f}_{\text{PP}} = 1 - \frac{2m_e c^2}{h\nu} = 1 - \frac{2 \times 0.511}{4} = 0.745 \quad (8.34)$$

Mean energy transfer $\bar{E}_{\text{tr}}^{\text{PP}}$ in pair production is

$$\bar{E}_{\text{tr}}^{\text{PP}} = \bar{f}_{\text{PP}} h\nu = 0.745 \times (4 \text{ MeV}) = 2.978 \text{ MeV} \quad (8.35)$$

(2) To determine the relative weights w_i for the four interaction effects of 4 MeV photons with lead we will use the definition $w_i = {}_a\mu_i / {}_a\mu$. Therefore, we first calculate the atomic attenuation coefficient ${}_a\mu$ for 4 MeV photons in lead and get

$$\begin{aligned} {}_a\mu &= {}_a\tau + {}_a\sigma_{\text{R}} + {}_a\sigma_{\text{C}} + {}_a\kappa \\ &= (0.593 + 0.066 + 7.879 + 5.904) \text{ b/atom} \\ &= 14.442 \text{ b/atom} = 14.442 \times 10^{-24} \text{ cm}^2/\text{atom}. \end{aligned} \quad (8.36)$$

The relative weights w_i of photoelectric effect w_{PE} , Rayleigh scattering w_{R} , Compton effect w_{C} , and pair production w_{PP} are calculated as follows

$$w_{\text{PE}} = \frac{{}_a\tau}{{}_a\mu} = \frac{0.593}{14.442} = 0.041, \quad (8.37)$$

$$w_{\text{R}} = \frac{{}_a\sigma_{\text{R}}}{{}_a\mu} = \frac{0.066}{14.442} = 4.6 \times 10^{-3}, \quad (8.38)$$

$$w_{\text{C}} = \frac{{}_a\sigma_{\text{C}}}{{}_a\mu} = \frac{7.879}{14.442} = 0.546, \quad (8.39)$$

$$w_{\text{PP}} = \frac{{}_a\kappa}{{}_a\mu} = \frac{5.904}{14.442} = 0.409. \quad (8.40)$$

Addition of the four w_i of (8.37) through (8.40) results in 1.0006 instead of 1.00... and the small discrepancy is attributed to rounding off of attenuation coefficients to three significant figures.

(3) Total mean energy transfer fraction \bar{f}_{tr} for 4 MeV photons in lead absorber is

$$\begin{aligned} \bar{f}_{\text{tr}} &= \{w_{\text{PE}} \bar{f}_{\text{PE}} + w_{\text{R}} \bar{f}_{\text{R}} + w_{\text{C}} \bar{f}_{\text{C}} + w_{\text{PP}} \bar{f}_{\text{PP}}\} \\ &= \{0.041 \times 0.985 + 0 + 0.546 \times 0.610 + 0.409 \times 0.745\} = 0.678. \end{aligned} \quad (8.41)$$

Table 8.4 Summary of data and results for 4 MeV photons interacting with lead absorber

	Photoelectric effect	Rayleigh scattering	Compton effect	Pair production	Summation
Cross section (cm ² /atom)	$a\tau = 0.593$	$a\sigma_R = 0.066$	$a\sigma_C = 7.879$	$a\kappa = 5.904$	$a\mu = 14.442$
w_i	$w_{PE} = 0.041$	$w_R = 0.0046$	$w_C = 0.546$	$w_{PP} = 0.409$	$\sum_i w_i \approx 1.000$
\bar{f}_i	$\bar{f}_{PE} = 0.985$	$\bar{f}_R = 0$	$\bar{f}_C = 0.610$	$\bar{f}_{PP} = 0.745$	–
$w_i \bar{f}_i$	$w_{PE} \bar{f}_{PE} = 0.040$	$w_R \bar{f}_R = 0$	$w_C \bar{f}_C = 0.333$	$w_{PP} \bar{f}_{PP} = 0.305$	$\bar{f}_{tr} = 0.678$
\bar{E}_{tr}^i	$\bar{E}_{tr}^{PE} = 3.94 \text{ MeV}$	$\bar{E}_{tr}^R = 0$	$\bar{E}_{tr}^C = 2.44 \text{ MeV}$	$\bar{E}_{tr}^{PP} = 2.978 \text{ MeV}$	–

w_i is relative weight for individual effect i

\bar{f}_i is the mean energy transfer fraction for individual effect i

$w_i \bar{f}_i$ is the mean weighted energy transfer fraction for individual effect i

\bar{E}_{tr}^i is mean energy transfer for individual effect i

(b) Mean energy \bar{E}_{tr} transferred from a 4 MeV photon to charged particles released or produced in lead absorber can be determined in two ways, both giving the same result:

- (1) Directly using the total mean energy transfer fraction \bar{f}_{tr} as

$$\bar{E}_{tr} = \bar{f}_{tr} h\nu = 0.678 \times (4 \text{ MeV}) = 2.71 \text{ MeV}. \quad (8.42)$$

- (2) Indirectly using mean energy transfers \bar{E}_{tr}^i in individual effects weighted by appropriate relative weights w_i as follows

$$\begin{aligned} \bar{E}_{tr} &= \sum_i w_i \bar{E}_{tr}^i = w_{PE} \bar{E}_{tr}^{PE} + w_R \bar{E}_{tr}^R + w_C \bar{E}_{tr}^C + w_{PP} \bar{E}_{tr}^{PP} \\ &= 0.041 \times (3.94 \text{ MeV}) + 0 + 0.546 \times (2.44 \text{ MeV}) + 0.409 \times (2.978 \text{ MeV}) \\ &= (0.161 + 0 + 1.332 + 1.218) \text{ MeV} = 2.71 \text{ MeV}. \end{aligned} \quad (8.43)$$

Data and results for 4 MeV photons interacting with lead absorber are summarized in Table 8.4. The calculated mean energy transfer fractions \bar{f}_i (i.e., \bar{f}_{PE} , \bar{f}_R , \bar{f}_C , and \bar{f}_{PP}) are entered as data points on a graph in Fig. 8.5 showing \bar{f}_i against photon energy $h\nu$ in the energy range from 1 keV to 100 MeV. The calculated relative weights w_i (i.e., w_{PE} , w_R , w_C , and w_{PP}) are entered as data points on a graph in Fig. 8.6 showing w_i against photon energy $h\nu$ in the energy range from 1 keV to 100 MeV.

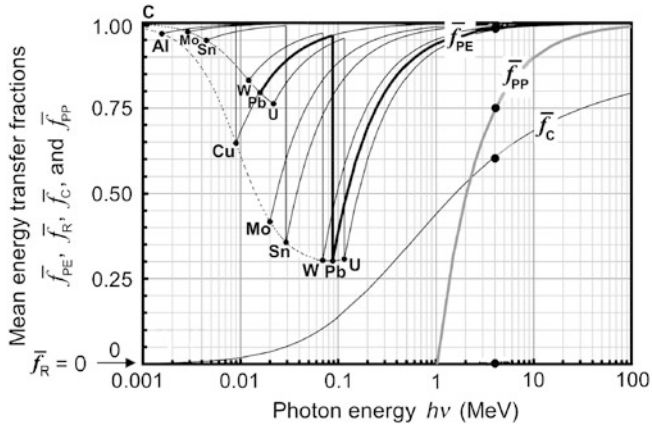


Fig. 8.5 Mean energy transfer fractions \bar{f}_i plotted against photon energy $h\nu$ for the four main photon interactions with absorber atoms: f_{PE} for photoelectric effect, f_R for Rayleigh scattering, f_C for Compton effect, and f_{PP} for pair production. The data points show the mean energy transfer fractions for the four interactions at photon energy of 4 MeV interacting with lead absorber

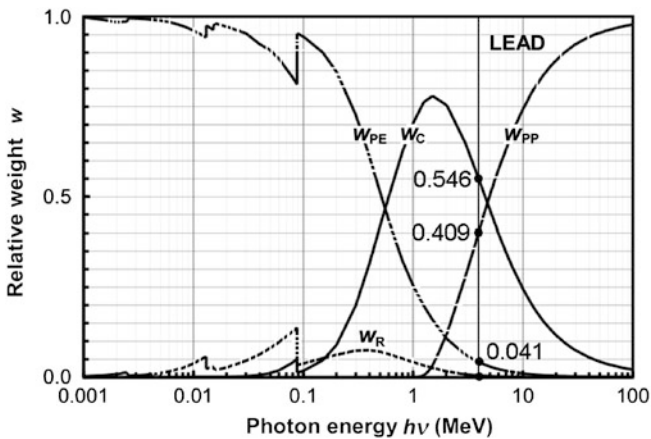


Fig. 8.6 Relative weights w_i for the main photon interactions with lead absorber: photoelectric effect w_{PE} , Rayleigh scattering w_R , Compton effect w_C , and pair production w_{PP} . Data were calculated using the NIST XCOM database. The data points highlight results of our calculation of w_i for 4 MeV photons interacting with a lead absorber

8.3 Energy Transfer and Energy Absorption

8.3.Q1

(187)

At photon energy $h\nu$ of 4 MeV in lead absorber ($Z = 82$, $A = 207.2$ g/mol, $\rho = 11.36$ g/cm³) the atomic attenuation coefficients for photoelectric effect, Rayleigh scattering, Compton scattering, nuclear pair production, and triplet production according to the NIST are as follows: ${}_a\tau = 0.5928 \times 10^{-24}$ cm²/atom, ${}_a\sigma_R = 0.0660 \times 10^{-24}$ cm²/atom, ${}_a\sigma_C = 7.879 \times 10^{-24}$ cm²/atom, ${}_a\kappa^{\text{NPP}} = 5.891 \times 10^{-24}$ cm²/atom, and ${}_a\kappa^{\text{TP}} = 0.013 \times 10^{-24}$ cm²/atom. Mean radiation fraction $\bar{g} = 0.13$

For 4 MeV photons interacting with lead absorber determine:

- Atomic attenuation coefficient ${}_a\mu$.
- Mass attenuation coefficient μ/ρ .
- Linear attenuation coefficient μ .
- Mass energy transfer coefficient μ_{tr}/ρ .
- Mass energy absorption coefficient μ_{ab}/ρ .
- Total mean energy absorption fraction \bar{f}_{ab} .
- Mean energy \bar{E}_{ab} absorbed in lead absorber.

SOLUTION:

(a) Atomic attenuation coefficient ${}_a\mu$ is given as the sum of the individual atomic attenuation coefficients for photons in lead at $h\nu = 4$ MeV

$$\begin{aligned} {}_a\mu &= {}_a\tau + {}_a\sigma_R + {}_a\sigma_C + ({}_a\kappa^{\text{NPP}} + {}_a\kappa^{\text{TP}}) = {}_a\tau + {}_a\sigma_R + {}_a\sigma_C + {}_a\kappa \\ &= [0.5928 + 0.0660 + 7.879 + (5.891 + 0.013)] \times 10^{-24} \text{ cm}^2/\text{atom} \\ &= 14.442 \times 10^{-24} \text{ cm}^2/\text{atom} = 14.442 \text{ b/atom.} \end{aligned} \quad (8.44)$$

(b) Mass attenuation coefficient μ/ρ is calculated from the atomic attenuation coefficient ${}_a\mu$ as follows

$$\begin{aligned} \frac{\mu}{\rho} &= \frac{N_A}{A} {}_a\mu = \frac{(6.022 \times 10^{23} \text{ atom/mol}^{-1}) \times (14.442 \times 10^{-24} \text{ cm}^2/\text{atom})}{207.2 \text{ g/mol}} \\ &= 0.0420 \text{ cm}^2/\text{g.} \end{aligned} \quad (8.45)$$

(c) Linear attenuation coefficient μ is calculated from the mass attenuation coefficient μ/ρ as

$$\mu = \mu_m \rho = \left(0.0420 \frac{\text{cm}^2}{\text{g}}\right) \times \left(11.36 \frac{\text{g}}{\text{cm}^3}\right) = 0.4771 \text{ cm}^{-1}. \quad (8.46)$$

(d) Mass energy transfer coefficient μ_{tr}/ρ is calculated from its basic definition given as

$$\frac{\mu_{\text{tr}}}{\rho} = \frac{\mu}{\rho} \frac{\bar{E}_{\text{tr}}}{h\nu}, \quad (8.47)$$

where \bar{E}_{tr} is the mean energy transferred from 4 MeV photon to charged particles released or created through photon interactions in lead absorber, calculated for $h\nu = 4$ MeV photons in Prob. 186(b) as $\bar{E}_{\text{tr}} = 2.71$ MeV. We thus have

$$\frac{\mu_{\text{tr}}}{\rho} = \frac{\mu}{\rho} \frac{\bar{E}_{\text{tr}}}{h\nu} = \left(0.0420 \frac{\text{cm}^2}{\text{g}}\right) \times \left(\frac{2.71}{4}\right) = 0.0285 \frac{\text{cm}^2}{\text{g}}. \quad (8.48)$$

(e) Mass energy absorption coefficient μ_{ab}/ρ is calculated from the mass energy transfer coefficient μ_{tr}/ρ as follows

$$\frac{\mu_{\text{ab}}}{\rho} = \frac{\mu_{\text{tr}}}{\rho} (1 - \bar{g}) = \left(0.0285 \frac{\text{cm}^2}{\text{g}}\right) \times (1 - 0.13) = 0.0248 \frac{\text{cm}^2}{\text{g}}. \quad (8.49)$$

(f) Total mean energy absorption fraction \bar{f}_{ab} is calculated from its basic definition

$$\bar{f}_{\text{ab}} = \bar{f}_{\text{tr}}(1 - \bar{g}) = \frac{\bar{E}_{\text{tr}}}{h\nu} (1 - \bar{g}) = \frac{2.71}{4} \times (1 - 0.13) = 0.678 \times 0.87 = 0.59. \quad (8.50)$$

(g) Mean energy \bar{E}_{ab} absorbed in lead absorber is calculated using the mean energy absorption fraction \bar{f}_{ab} calculated in (f)

$$\bar{E}_{\text{ab}} = \bar{f}_{\text{ab}} h\nu = 0.59 \times (4 \text{ MeV}) = 2.36 \text{ MeV} \quad (8.51)$$

or using mean energy \bar{E}_{tr} transferred to charged particles determined in Prob. 186(b)

$$\bar{E}_{\text{ab}} = \bar{E}_{\text{tr}}(1 - \bar{g}) = (2.71 \text{ MeV}) \times (1 - 0.13) = 2.36 \text{ MeV}, \quad (8.52)$$

where \bar{g} is the mean radiation fraction accounting for radiation energy loss of charged particles released or created by photons in the absorber through bremsstrahlung, annihilation in flight and production of fluorescence radiation.

8.3.Q2

(188)

Mono-energetic 10 MeV photons interact with manganese absorber ($A = 54.94$ g/mol, $Z = 25$, and $\rho = 7.43$ g/cm³). Atomic attenuation coefficients

for photoelectric effect ${}_a\tau$ and Rayleigh scattering ${}_a\sigma_R$ for 10 MeV photons in manganese are 9.3×10^{-4} b/atom and 3.7×10^{-4} b/atom, respectively. Assume that the mean radiation fraction \bar{g} is ~ 0.11 .

Based on information provided above, determine (clearly stating all assumptions and approximations you make in each individual step in your calculations):

- (a) Mass attenuation coefficient μ/ρ .
- (b) Mean energy transfer fraction for photoelectric effect \bar{f}_{PE} .
- (c) Mean energy transfer fraction for Rayleigh scattering \bar{f}_R .
- (d) Mean energy transfer fraction for Compton scattering \bar{f}_C .
- (e) Mean energy transfer fraction for pair production \bar{f}_{PP} .
- (f) Total mean energy transfer fraction \bar{f}_{tr} .
- (g) Mean energy \bar{E}_{tr} transferred from 10 MeV-photon to charged particles in photon interaction.
- (h) Mean kinetic energy of each charged particle produced in an interaction of a 10 MeV photon with manganese atom.
- (i) Mass energy transfer coefficient μ_{tr}/ρ .
- (j) Mass energy absorption coefficient μ_{ab}/ρ .
- (k) Mean energy absorbed in manganese in a 10 MeV photon interaction with manganese atom.

SOLUTION:

(a) **Mass attenuation coefficient** μ/ρ is given as a sum of four attenuation coefficients: photoelectric PE (τ/ρ), Rayleigh R (σ_R/ρ), Compton C (σ_C/ρ), and pair production PP (κ/ρ) as follows

$$\mu_m = \frac{\mu}{\rho} = \frac{\tau}{\rho} + \frac{\sigma_R}{\rho} + \frac{\sigma_C}{\rho} + \frac{\kappa}{\rho} = \frac{N_A}{A} ({}_a\tau + {}_a\sigma_R + {}_a\sigma_C + {}_a\kappa). \quad (8.53)$$

Two of the required atomic attenuation coefficients (${}_a\tau$ and ${}_a\sigma_R$) were given above, the other two (${}_a\sigma_C$ and ${}_a\kappa$) we estimate from commonly known radiation physics facts that can be extracted from Fig. 8.7(A) showing Compton electronic coefficient ${}_a\sigma_C$ against incident photon energy $h\nu$ and from Fig. 8.7(B) showing regions of relative predominance of specific photon interactions. Anchor points for the two graphs are marked with x and allow us to sketch the two graphs with reasonable accuracy and use them to estimate the value of physical quantities of relevance in our calculations.

Figure 8.7(A) plots Klein-Nishina coefficients of free electrons representing Compton electronic cross section ${}_e\sigma_C$ against photon energy $h\nu$. The anchor point at $h\nu = 10$ MeV amounts to ${}_e\sigma_C(10 \text{ MeV}) = 0.05$ b/atom $= 0.05 \times 10^{-24}$ cm²/atom and is now used for calculation of the Compton atomic cross section, i.e., Compton

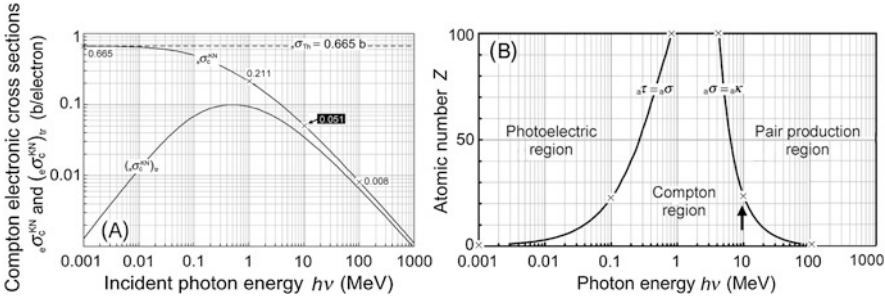


Fig. 8.7 Two graphs of importance in radiation physics. **(A)** Compton Klein-Nishina coefficients for free electrons (Compton atomic attenuation coefficients) against incident photon energy $h\nu$ with the following anchor points: (Thomson low energy limit, 0.665 b/atom); (1 MeV, 0.21 b/atom); (10 MeV, 0.051 b/atom); and (100 MeV, 0.008 b/atom). **(B)** Regions of predominance of the three most important processes of photon interaction with absorber atom. Anchor points of the graph are: ($h\nu = 0.001$ MeV, $Z = 0$); (0.1 MeV, 25); (1 MeV, 100); (4 MeV, 100); (10 MeV, 25); and (100 MeV, 0). *Arrows* mark points of interest in our calculation

atomic attenuation coefficient ${}_a\sigma_C$ of manganese at photon energy $h\nu = 10$ MeV

$$\begin{aligned} {}_a\sigma_C(10 \text{ MeV, Mn}) &= Z \times {}_e\sigma_C(10 \text{ MeV}) = (25 \text{ el/atom}) \times 0.051 \times 10^{-24} \text{ cm}^2/\text{el} \\ &= 1.275 \times 10^{-24} \text{ cm}^2/\text{atom}. \end{aligned} \tag{8.54}$$

From Fig. 8.7(B) we note that manganese falls on one of the anchor points ($Z = 25$, $\nu = 10$ MeV). This suggests that at 10 MeV in manganese the attenuation coefficients for Compton effect and pair production are identical and furthermore that attenuation coefficients for photoelectric effect and Rayleigh scattering in comparison with Compton and pair production attenuation coefficients may be neglected in the first approximation. Since, as shown in Fig. 8.7(B), the Compton and pair production atomic coefficients are approximately equal for 10 MeV photons interacting with manganese, the atomic attenuation coefficient ${}_a\mu$ is determined as

$$\begin{aligned} {}_a\mu(10 \text{ MeV, Mn}) &= {}_a\tau + {}_a\sigma_R + {}_a\sigma_C + {}_a\kappa \\ &= (9.3 \times 10^{-4} + 3.7 \times 10^{-4} + 1.275 + 1.275) \text{ b/atom} \\ &\approx 2{}_a\sigma_C(10 \text{ MeV, Mn}) = 2.55 \text{ b/atom} = 2.55 \times 10^{-24} \text{ cm}^2/\text{atom} \end{aligned} \tag{8.55}$$

and the mass attenuation coefficient μ/ρ is then from (8.53) given as

$$\frac{\mu}{\rho} = \frac{N_A}{A} {}_a\mu \approx \frac{(6.022 \times 10^{23} \text{ atom/mol}) \times (2.55 \times 10^{-24} \text{ cm}^2/\text{atom})}{54.94 \text{ g/mol}} = 0.0280 \frac{\text{cm}^2}{\text{g}}. \tag{8.56}$$

(b) Mean energy transfer fraction for photoelectric effect \bar{f}_{PE} at $h\nu = 10$ MeV is very close to unity; however, since the photoelectric effect attenuation coefficient τ/ρ is 3 orders of magnitude smaller than coefficients for Compton effect σ_C/ρ and

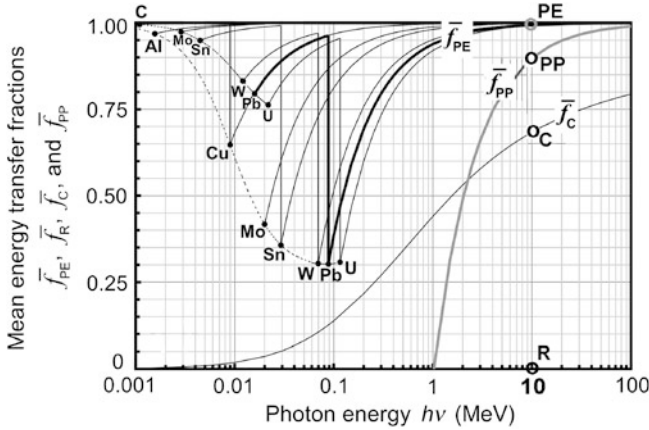


Fig. 8.8 Mean energy transfer fractions \bar{f}_i for photoelectric effect \bar{f}_{PE} , Rayleigh scattering $\bar{f}_R = 0$, Compton effect \bar{f}_C , and pair production \bar{f}_{PP} for 8 absorbers with atomic numbers Z ranging from 13 for aluminum to 92 for uranium. Mean energy transfer fractions calculated in (b), (c), (d), and (e) for 10 MeV photons are indicated on the graph with circular data points

pair production κ/ρ , the photoelectric effect makes a negligible contribution to the mean energy transferred to charged particles.

(c) Mean energy transfer fraction for Rayleigh scattering \bar{f}_R is by definition equal to zero, because there is no energy transfer from photon to charged particles in Rayleigh scattering.

(d) Mean energy transfer fraction for Compton effect \bar{f}_C is provided from the Compton graph in which the point of $h\nu = 10$ MeV and $\bar{f}_C = 0.68$ serves as an anchor point. We thus know that in manganese ($Z = 25$) at $h\nu = 10$ MeV the Compton mean energy transfer fraction is 0.68 and the mean energy transferred to the recoil electron is $\bar{E}_{tr}^C = \bar{f}_C h\nu = 6.8$ MeV.

(e) Mean energy transfer fraction for pair production \bar{f}_{PP} at $h\nu = 10$ MeV is calculated as

$$\bar{f}_{PP} = 1 - \frac{2m_e c^2}{h\nu} = 1 - \frac{1.022}{10} = 0.898 \quad \text{or} \quad \bar{E}_{tr}^{PP} = \bar{f}_{PP} h\nu \approx 9 \text{ MeV.} \quad (8.57)$$

Mean energy transfer fractions \bar{f}_i for photoelectric effect \bar{f}_{PE} , Rayleigh scattering $\bar{f}_R = 0$, Compton effect \bar{f}_C , and pair production \bar{f}_{PP} determined in (b), (c), (d), and (e), respectively, are plotted with data points in Fig. 8.8. The figure also plots the four mean energy transfer fractions against photon energy for 8 absorbers ranging in Z from 13 for aluminum to 92 for uranium. *Note:* At all energies and for all absorbers $\bar{f}_R = 0$ because, in Rayleigh scattering, no energy gets transferred from the photon to charged particles. Of the remaining three energy transfer fractions, only \bar{f}_{PP} depends on atomic number Z , the other two (\bar{f}_C and \bar{f}_{PE}) are independent of Z .

(f) In general, the **total mean energy transfer fraction** \bar{f}_{tr} is a sum of four weighted mean energy transfer fractions: photoelectric $w_{\text{PE}}\bar{f}_{\text{PE}}$, Rayleigh $w_{\text{R}}\bar{f}_{\text{R}}$, Compton $w_{\text{C}}\bar{f}_{\text{C}}$, and pair production $w_{\text{PP}}\bar{f}_{\text{PP}}$ where w_i stands for the relative weight of interaction i

$$\begin{aligned}\bar{f}_{\text{tr}} &= \frac{\bar{E}_{\text{tr}}}{h\nu} = \sum_i w_i \bar{f}_i = w_{\text{PE}}\bar{f}_{\text{PE}} + w_{\text{R}}\bar{f}_{\text{R}} + w_{\text{C}}\bar{f}_{\text{C}} + w_{\text{PP}}\bar{f}_{\text{PP}} \\ &= \frac{a\tau}{a\mu}\bar{f}_{\text{PE}} + \frac{a\sigma_{\text{R}}}{a\mu}\bar{f}_{\text{R}} + \frac{a\sigma_{\text{C}}}{a\mu}\bar{f}_{\text{C}} + \frac{a\kappa}{a\mu}\bar{f}_{\text{PP}} \\ &= \frac{1}{a\mu}(a\tau\bar{f}_{\text{PE}} + a\sigma_{\text{R}}\bar{f}_{\text{R}} + a\sigma_{\text{C}}\bar{f}_{\text{C}} + a\kappa\bar{f}_{\text{PP}}),\end{aligned}\quad (8.58)$$

where w_i is the relative weight of given effect i for photon energy $h\nu$ and absorber atomic number Z defined as the ratio between the atomic attenuation coefficient $a\mu_i$ for the given effect i and the total atomic attenuation coefficient $a\mu$ which, as given in (8.53), is the sum of individual atomic attenuation coefficients, i.e., $a\mu = \sum a\mu_i$.

Thus, the total mean energy transfer fraction in the interaction of 10 MeV photons with manganese atoms would in general account for the four major effects that the photon can experience in interacting with manganese atom. However, for our specific case we know:

- (1) \bar{f}_{R} is always zero, so \bar{f}_{R} does not contribute to \bar{f}_{tr} .
- (2) $\bar{f}_{\text{PE}} \approx 1$; however, the probability for a photoelectric interaction is 3 orders of magnitude lower than that for Compton effect and pair production allowing us to ignore the \bar{f}_{PE} contribution to \bar{f}_{tr} through an assumption that $w_{\text{PE}} \approx 0$.
- (3) Since the probabilities for Compton effect and pair production in 10 MeV photon interaction with manganese atom are essentially identical, we assign a weight of 0.5 to each one of the two attenuation coefficients.

Thus, we have: $w_{\text{C}} \approx w_{\text{PP}} \approx 0.5$ and using (8.58) we now get the following result for \bar{f}_{tr}

$$\begin{aligned}\bar{f}_{\text{tr}} &= w_{\text{PE}}\bar{f}_{\text{PE}} + w_{\text{R}}\bar{f}_{\text{R}} + w_{\text{C}}\bar{f}_{\text{C}} + w_{\text{PP}}\bar{f}_{\text{PP}} \\ &= 0 + 0 + 0.5 \times 0.68 + 0.5 \times 0.898 = 0.789.\end{aligned}\quad (8.59)$$

(g) **Mean energy \bar{E}_{tr} transferred to charged particles** in interaction of a 10-MeV photon with manganese atom is determined from the simple expression

$$\begin{aligned}\bar{E}_{\text{tr}} &= \bar{f}_{\text{tr}}h\nu = (w_{\text{PE}}\bar{f}_{\text{PE}} + w_{\text{R}}\bar{f}_{\text{R}} + w_{\text{C}}\bar{f}_{\text{C}} + w_{\text{PP}}\bar{f}_{\text{PP}})h\nu \\ &= 0.789 \times (10 \text{ MeV}) = 7.9 \text{ MeV}.\end{aligned}\quad (8.60)$$

Note: since the cross sections for Compton effect and pair production are the same, a simple average between $\bar{E}_{\text{tr}}^{\text{C}}$ and $\bar{E}_{\text{tr}}^{\text{PP}}$ will give us the combined mean energy transfer in 10 MeV photon interaction with manganese absorber, i.e.,

$$\bar{E}_{\text{tr}} \approx \frac{\bar{E}_{\text{tr}}^{\text{C}} + \bar{E}_{\text{tr}}^{\text{PP}}}{2} = \frac{6.8 \text{ MeV} + 9 \text{ MeV}}{2} = 7.9 \text{ MeV}.\quad (8.61)$$

(h) To determine the **mean kinetic energy \bar{E}_{tr} transferred** from photon to individual charged particles in 10 MeV photon interaction with manganese atom we again assume that there is equal rate for Compton and pair production interactions and we again neglect photoelectric and Rayleigh scattering. Thus, for each Compton interaction that produces a 6.8 MeV recoil electron, we get an electron-positron pair with combined kinetic energy of 9 MeV or 4.5 MeV on average for each particle of the pair. The mean kinetic energy for all charged particles released (recoil electron) or produced (electron and positron of the pair) is thus given as the mean value of kinetic energies of the three particles

$$\bar{E}_K = \frac{6.8 \text{ MeV} + 4.5 \text{ MeV} + 4.5 \text{ MeV}}{3} = 5.3 \text{ MeV}. \quad (8.62)$$

(i) **Mass energy transfer coefficient μ_{tr}/ρ** is calculated using the basic definition of the mass energy transfer coefficient as follows (T7.19)

$$\frac{\mu_{tr}}{\rho} = \frac{\mu}{\rho} \frac{\bar{E}_{tr}}{h\nu} = \frac{\mu}{\rho} \bar{f}_{tr} = 0.0280 \times \frac{7.9}{10} \frac{\text{cm}^2}{\text{g}} = 0.0221 \frac{\text{cm}^2}{\text{g}}. \quad (8.63)$$

(j) **Mass energy absorption coefficient μ_{ab}/ρ** is calculated by multiplying μ_{tr}/ρ by $(1 - \bar{g})$ where \bar{g} is the mean radiation fraction for 10 MeV photon interaction with manganese atom

$$\begin{aligned} \frac{\mu_{ab}}{\rho} &= \frac{\mu_{tr}}{\rho} (1 - \bar{g}) = \frac{\mu}{\rho} \frac{\bar{E}_{ab}}{h\nu} = 0.0221 \times (1 - 0.11) \frac{\text{cm}^2}{\text{g}} \\ &= 0.0221 \times 0.89 \frac{\text{cm}^2}{\text{g}} = 0.0197 \frac{\text{cm}^2}{\text{g}}. \end{aligned} \quad (8.64)$$

(k) **Mean energy \bar{E}_{ab} absorbed** in manganese absorber in 10 MeV photon interaction with manganese atom is determined from the basic definition of the mass energy absorption coefficient μ_{ab}/ρ given as (T7.20)

$$\frac{\mu_{ab}}{\rho} = \frac{\mu}{\rho} \frac{\bar{E}_{ab}}{h\nu} \quad (8.65)$$

from where it follows that

$$\bar{E}_{ab} = h\nu \frac{\mu_{ab}/\rho}{\mu/\rho} = (10 \text{ MeV}) \times \frac{0.0193}{0.0274} = 7 \text{ MeV}. \quad (8.66)$$

Note: A comparison of our results with those provided by the NIST shows that our estimate for the atomic attenuation coefficient for 10 MeV photons in manganese is about 3 % too low (2.55 b/atom vs. NIST value of 2.62 b/atom). Considering the many approximations that we made in our simplified calculation, a discrepancy of less than 3 % seems acceptable.

8.3.Q3

(189)

A narrow x-ray beam containing $N = 10^{21}$ photons of energy $h\nu = 5$ MeV strikes perpendicularly a 14 mm thick slab of gold ($Z = 79$, $A = 197$ g/mol, $\rho = 19.3$ g/cm³).

- List at least 4 possible interactions of importance to medical physics that the 5 MeV photons can have in the gold slab.
- Figure 8.9 plots three atomic attenuation coefficients for gold. Identify and label the three curves with the appropriate interaction. Also label the abscissa (x) axis with appropriate values for the energy scale.
- Determine the mass attenuation coefficient μ/ρ for 5 MeV photons in gold.
- Determine the half value layer $x_{1/2}$ in gold for the narrow photon beam.
- Determine the total mean energy transfer fraction \bar{f}_{tr} .
- Determine the mean energy transferred to charged particles \bar{E}_{tr} for interaction of 5-MeV photon with gold atom.
- Determine the mass energy transfer coefficient μ_{tr}/ρ for 5 MeV photons interacting with gold atom.
- Given that the radiation fraction \bar{g} in gold for 5 MeV photons is 0.15, determine the mass energy absorption coefficient μ_{ab}/ρ for 5 MeV photons interacting with gold atom.
- Determine the mean energy absorbed in the gold slab for each 5 MeV photon interaction with gold atom.
- For each interaction listed in (a) determine the number of interactions occurring in the gold slab.

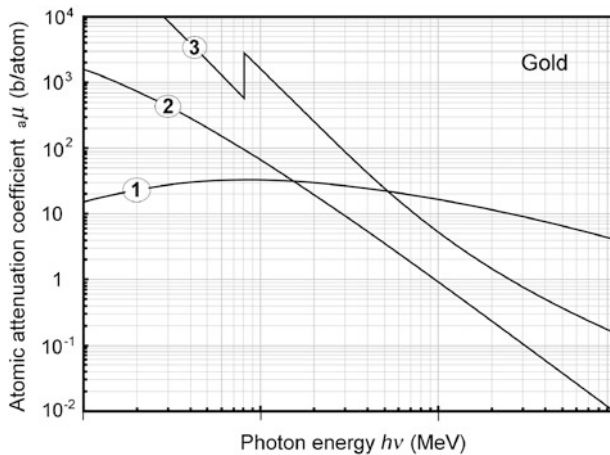


Fig. 8.9 Atomic attenuation coefficient $a\mu$ against photon energy $h\nu$ for three photon–gold atom interactions

SOLUTION:

(a) At energy of 5 MeV a photon can have all mainstream interactions with a gold atom. The list of 5 interactions thus reads as follows: (1) Photoelectric effect, (2) Rayleigh scattering, (3) Compton effect, (4) Nuclear pair production, and (5) Triplet production. The last two interactions are often jointly referred to as pair production.

(b) The three curves of Fig. 8.9 are plots of three types of atomic attenuation coefficients for interaction of photons with gold atoms: curve (1) is for Compton effect, curve (2) for Rayleigh scattering, and curve (3) for photoelectric effect. Curve for pair production is not shown but that does not mean that pair production cannot occur with a 5 MeV photon. Figure 8.10(A) shows completed Fig. 8.9 with photon energy scale on the abscissa axis and curves (1), (2), and (3) appropriately labeled.

(c) To get the mass and linear attenuation coefficients μ/ρ and μ , respectively, we first calculate the atomic attenuation coefficient ${}_a\mu$ based on information available from Fig. 8.9. We obtain the following atomic coefficients for $h\nu = 5$ MeV in gold absorber from Fig. 8.9: ${}_a\tau = 0.35$ b/atom, ${}_a\sigma_R = 0.04$ b/atom, and ${}_a\sigma_C = 7.0$ b/atom. Since the atomic coefficient for pair production ${}_a\kappa$ cannot be negligible, we consult the graph displaying regions of predominance for the main photon interactions and we notice that gold ($Z = 79$) at 5 MeV lands on the curve that displays $(h\nu, Z)$ values for which ${}_a\sigma_C = {}_a\kappa$.

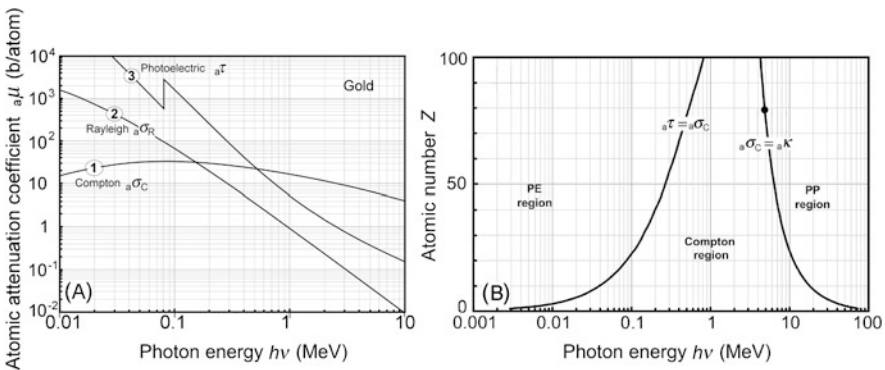


Fig. 8.10 (A) Atomic attenuation coefficients for photoelectric effect ${}_a\tau$, Rayleigh scattering ${}_a\sigma_R$, and Compton effect ${}_a\sigma_C$ against photon energy $h\nu$ in the energy range $0.01 \text{ MeV} \leq h\nu \leq 10 \text{ MeV}$. (B) Representation of the relative predominance of photoelectric effect, Compton effect, and pair production in a $(h\nu, Z)$ diagram where $h\nu$ is photon energy and Z the atomic number of absorber. The dot on the ${}_a\sigma_C = {}_a\kappa$ curve indicates the point for 5 MeV photon interacting with gold ($Z = 79$) at which ${}_a\sigma_C = {}_a\kappa$

We thus conclude that $a\kappa$ is equal to $a\sigma_C$ for 5 MeV photons in gold and we get: $a\kappa \approx a\sigma_C \approx 7$ b/atom. *Atomic attenuation coefficient* is then given as follows

$$a\mu = a\tau + a\sigma_R + a\sigma_C + a\kappa = (0.35 + 0.04 + 7.0 + 7.0) \text{ b/atom} = 14.4 \text{ b/atom} \quad (8.67)$$

mass attenuation coefficient μ/ρ

$$\frac{\mu}{\rho} = \frac{N_A}{A} a\mu = \frac{6.022 \times 10^{23} \text{ mol}^{-1}}{197 \text{ g} \cdot \text{mol}^{-1}} \times (14.4 \times 10^{-24} \text{ cm}^2) = 0.044 \frac{\text{cm}^2}{\text{g}}, \quad (8.68)$$

and *linear attenuation coefficient* μ

$$\mu = \frac{\mu}{\rho} \rho = \left(0.044 \frac{\text{cm}^2}{\text{g}}\right) \times \left(19.3 \frac{\text{g}}{\text{cm}^3}\right) = 0.85 \text{ cm}^{-1}. \quad (8.69)$$

(d) Half-value layer $x_{1/2}$ of a beam is that thickness of an absorber that decreases a narrow photon beam intensity to 50 % of its original value. Half-value layer of a 5 MeV beam in gold absorber is related to the linear attenuation coefficient μ as follows

$$x_{1/2} = \frac{\ln 2}{\mu} = \frac{0.693}{0.85 \text{ cm}^{-1}} = 0.81 \text{ cm}. \quad (8.70)$$

(e) Total mean energy transfer fraction \bar{f}_{tr} is defined as the sum of four weighted mean energy transfer fractions: photoelectric $w_{PE}\bar{f}_{PE}$, Rayleigh $w_R\bar{f}_R$, Compton $w_C\bar{f}_C$, and pair production $w_{PP}\bar{f}_{PP}$ where w_i stands for the relative weight of interaction i

$$\begin{aligned} \bar{f}_{tr} &= \frac{\bar{E}_{tr}}{h\nu} = \sum_i w_i \bar{f}_i = w_{PE}\bar{f}_{PE} + w_R\bar{f}_R + w_C\bar{f}_C + w_{PP}\bar{f}_{PP} \\ &= \frac{a\tau}{a\mu} \bar{f}_{PE} + \frac{a\sigma_R}{a\mu} \bar{f}_R + \frac{a\sigma_C}{a\mu} \bar{f}_C + \frac{a\kappa}{a\mu} \bar{f}_{PP} \\ &= \frac{1}{a\mu} (a\tau \bar{f}_{PE} + a\sigma_R \bar{f}_R + a\sigma_C \bar{f}_C + a\kappa \bar{f}_{PP}). \end{aligned} \quad (8.71)$$

We now estimate the mean energy transfer fractions \bar{f}_i and their weights w_i for the four main interactions that a 5 MeV photon can have with gold atom (photoelectric, Rayleigh, Compton, and pair production).

(1) *Photoelectric effect:*

$$\bar{f}_{PE} = 1 - \frac{P_K \omega_K \eta_K E(K)}{h\nu} = 1 - \frac{0.8 \times 0.96 \times 0.91 \times (0.0807 \text{ MeV})}{5 \text{ MeV}} = 0.989, \quad (8.72)$$

where

- P_K is the probability for the photoelectric effect, if it occurs, to occur in the K shell of gold atom. The range of P_K in nature is from $P_K \approx 1$ for low atomic number Z materials slowly dropping to $P_K \approx 0.8$ for high Z materials. We take $P_K = 0.8$ for gold atom.
- ω_K is the fluorescence yield, ranging in nature from $\omega_K = 0$ for $Z \leq 10$, through $\omega_K = 0.5$ for $Z = 30$, and saturating at $\omega_K = 0.98$ at very high Z . For gold we estimate $\omega_K = 0.96$.
- η_K is the fluorescence efficiency defined as the mean fraction of the K shell binding energy $E_B(K)$ carried by the fluorescence photon, ranging in nature from $\eta_K \approx 0.98$ at low Z , slowly dropping to reach a minimum at $\eta_K \approx 0.9$ at intermediate Z , and then slowly rising to reach $\eta_K \approx 0.93$ at high Z . For gold we estimate $\eta_K = 0.91$.
- $E_B(K)$ is the binding energy of K shell electrons that can be estimated with reasonable accuracy with the Hartree approximation: $E_B(K) \approx E_R(Z-2)^2 = (13.6 \text{ eV}) \times 77^2 = 80.7 \text{ keV}$.

Mean energy transferred to electrons in photoelectric effect \bar{E}_{tr}^{PE} is thus given as

$$\bar{E}_{tr}^{PE} = \bar{f}_{PE} h\nu = (5 \text{ MeV}) \times 0.989 = 4.95 \text{ MeV}. \quad (8.73)$$

Photoelectric weight w_{PE} is determined from the simple expression $w_{PE} = {}_a\tau / {}_a\mu = 0.35/14.4 = 0.024$.

(2) *Rayleigh scattering*: Since in Rayleigh scattering there is no energy transfer from the photon to charged particles, we conclude that the mean energy transfer fraction for Rayleigh scattering is zero ($\bar{f}_R = 0$).

Weight for Rayleigh scattering is determined as $w_R = {}_a\sigma_R / {}_a\mu = 0.04/14.4 = 2.8 \times 10^{-3}$.

(3) *Compton effect*: The mean energy transfer fraction for Compton effect \bar{f}_C is determined from the Compton graph from which we get $\bar{f}_C = 0.62$ and the Compton weight w_C is determined as $w_C = {}_a\sigma_C / {}_a\mu = 7/14.4 = 0.486$. The mean energy transfer \bar{E}_{tr}^C to recoil electron in Compton effect is $\bar{E}_{tr}^C = \bar{f}_C h\nu = 0.62 \times (5 \text{ MeV}) = 3.1 \text{ MeV}$.

(4) *Pair production* (including nuclear pair production and triplet production): The mean energy transfer fraction for pair production \bar{f}_{PP} is determined as

$$\bar{f}_{PP} = 1 - 2m_e c^2 / (h\nu) = 1 - 1.022/5 = 0.796, \quad (8.74)$$

resulting in the following mean energy transfer \bar{E}_{tr}^{PP} from photon to charged particles (electron and positron) in pair production of 5 MeV photon $\bar{E}_{tr}^{PP} = \bar{f}_{PP} h\nu = 0.796 \times (5 \text{ MeV}) = 3.98 \text{ MeV}$. Pair production weight w_{PP} is calculated from $w_{PP} = {}_a\kappa / {}_a\mu = 7/14.4 = 0.486$.

The total mean energy transfer fraction \bar{f}_{tr} is now calculated as

$$\begin{aligned}\bar{f}_{\text{tr}} &= \frac{\bar{E}_{\text{tr}}}{h\nu} = \sum_i w_i \bar{f}_i = w_{\text{PE}} \bar{f}_{\text{PE}} + w_{\text{R}} \bar{f}_{\text{R}} + w_{\text{C}} \bar{f}_{\text{C}} + w_{\text{PP}} \bar{f}_{\text{PP}} \\ &= 0.024 \times 0.989 + 0 + 0.486 \times 0.62 + 0.486 \times 0.796 = 0.712.\end{aligned}\quad (8.75)$$

(f) Mean energy transferred from photon to charged particles in 5 MeV photon interaction with gold atom is now easily determined from (8.75) as follows

$$\bar{E}_{\text{tr}} = \bar{f}_{\text{tr}} h\nu = 0.712 \times (5 \text{ MeV}) = 3.56 \text{ MeV}.\quad (8.76)$$

(g) Mass energy transfer coefficient μ_{tr}/ρ is determined from its basic definition

$$\frac{\mu_{\text{tr}}}{\rho} = \frac{\mu}{\rho} \frac{\bar{E}_{\text{tr}}}{h\nu} = \frac{\mu}{\rho} \bar{f}_{\text{tr}} = \left(0.044 \frac{\text{cm}^2}{\text{g}}\right) \times 0.712 = 0.0313 \frac{\text{cm}^2}{\text{g}}.\quad (8.77)$$

(h) Mass energy absorption coefficient μ_{ab}/ρ is determined from μ_{tr}/ρ and the mean radiation fraction \bar{g} as follows

$$\frac{\mu_{\text{ab}}}{\rho} = \frac{\mu_{\text{tr}}}{\rho} (1 - \bar{g}) = \left(0.0313 \frac{\text{cm}^2}{\text{g}}\right) \times (1 - 0.15) = 0.0266 \frac{\text{cm}^2}{\text{g}}.\quad (8.78)$$

(i) Mean energy absorbed in the gold slab for each 5 MeV photon interaction with gold atom

$$\bar{E}_{\text{ab}} = \bar{f}_{\text{ab}} h\nu = \bar{f}_{\text{tr}} (1 - \bar{g}) h\nu = 0.712 \times (1 - 0.15) \times (5 \text{ MeV}) = 3.03 \text{ MeV}.\quad (8.79)$$

(j) Number N of photons transmitted through the gold slab of $t = 1.4$ cm is

$$N = N_0 e^{-\mu t} = 10^{21} \times e^{-0.85 \times 1.4} = 0.304 \times 10^{21}.\quad (8.80)$$

Number of photons \mathcal{N} that undergo an interaction with gold atoms in traversing the gold slab

$$\mathcal{N} = N_0 - N = (1 - 0.304) \times 10^{21} = 0.696 \times 10^{21}.\quad (8.81)$$

Distribution of interactions is given by the individual weights w_i for interaction i

Number of photoelectric (PE) interactions

$$= w_{\text{PE}} \times \mathcal{N} = 0.024 \times 0.696 \times 10^{21} = 1.67 \times 10^{19}\quad (8.82)$$

Number of Rayleigh interactions

$$= w_{\text{R}} \times \mathcal{N} = 0.004 \times 0.696 \times 10^{21} = 1.95 \times 10^{18}\quad (8.83)$$

Number of Compton interactions

$$= w_{\text{C}} \times \mathcal{N} = 0.486 \times 0.696 \times 10^{21} = 3.38 \times 10^{20}\quad (8.84)$$

Number of pair production (PP) interactions

$$= w_{pp} \times \mathcal{N} = 0.486 \times 0.696 \times 10^{21} = 3.38 \times 10^{20} \quad (8.85)$$

8.3.Q4

(190)

Photons with energy $h\nu$ of 2 MeV interact with lead ($Z = 82$, $A = 207.2$ g/mol, $\rho = 11.34$ g/cm³) and light charged particles may be released or produced in the lead absorber through photoelectric effect, Rayleigh scattering, Compton effect, nuclear pair production, and triplet production. Determine and briefly explain

- (1) Maximum kinetic energy $(E_K)_{\max}$ that may be transferred from the incident photon with energy $h\nu$ to charged particles (CPs),
- (2) Mean kinetic energy \bar{E}_{tr} that is transferred from the incident photon $h\nu$ to CPs, and
- (3) Mean energy transfer fraction \bar{f}_i

for each of the five main photon interaction processes:

- (a) Photoelectric effect
- (b) Rayleigh scattering
- (c) Compton effect
- (d) Nuclear pair production
- (e) Triplet production
- (g) Summarize your results of (a), (b), (c), (d), and (e) by completing Table 8.5A.

Table 8.5A Maximum and mean energy transfer as well as mean energy transfer fraction for 2 MeV photon interacting with lead absorber through various photon interactions with lead atoms

Photon ($h\nu = 2$ MeV) interaction with lead absorber	$(E_K)_{\max}$	\bar{E}_{tr}	\bar{f}_i
(a) Photoelectric effect	$(E_K^{PE})_{\max} =$	$\bar{E}_{tr}^{PE} =$	$\bar{f}_{PE} =$
(b) Rayleigh scattering	$(E_{tr}^R)_{\max} =$	$\bar{E}_{tr}^R =$	$\bar{f}_R =$
(c) Compton effect	$(E_{tr}^C)_{\max} =$	$\bar{E}_{tr}^C =$	$\bar{f}_C =$
(d) Nuclear pair production	$(E_{tr}^{NPP})_{\max} =$	$(\bar{E}_{tr}^{NPP})_{\max} =$	$\bar{f}_{NPP} =$
(e) Triplet production	$(E_{tr}^{TP})_{\max} =$	$(\bar{E}_{tr}^{TP})_{\max} =$	$\bar{f}_{TP} =$

SOLUTION:

(a) In **photoelectric effect** the photon interacts with a tightly bound orbital electron of the absorber atom. If the photon energy ν exceeds the binding energy E_B

of the orbital electron, the electron is ejected from the atom as a photoelectron with kinetic energy $E_K = h\nu - E_B$.

Since in our case the photon energy $h\nu = 2$ MeV exceeds the binding energy of the K shell electron in lead [$E_B(\text{K}) = 0.088$ MeV], if photoelectric effect does occur, it will most likely occur with a K shell electron ($\sim 80\%$ probability), rather than with any of the higher shell electrons.

(1) Maximum kinetic energy $(E_{\text{tr}}^{\text{PE}})_{\text{max}}$ transferred from 2-MeV photon to CPs in photoelectric effect will be attained when the binding energy of the K shell vacancy is transferred in full to Auger electrons. The combined energy of the photoelectron [$E_K = 2$ MeV $-$ 0.088 MeV $=$ 1.912 MeV] and Auger electrons with total kinetic energy $E_K = 0.088$ MeV is then equal to $(E_{\text{tr}}^{\text{PE}})_{\text{max}}$ which in turn equals to $h\nu = 2$ MeV. Thus, in this situation, the total energy of the photon $h\nu$ is transferred to charged particles (electrons) in the form of the photoelectron that receives 1.912 MeV and several Auger electrons that receive a combined total kinetic energy of 0.088 MeV. Maximum energy transfer $(E_{\text{tr}}^{\text{PE}})_{\text{max}}$ thus equals to 2 MeV.

(2) Mean energy $\bar{E}_{\text{tr}}^{\text{PE}}$ transferred from 2 MeV photon to CPs in photoelectric effect will be between two extremes, $(E_K)_{\text{min}} = h\nu - E_B(\text{K})$ and $(E_K)_{\text{max}} = h\nu$, and is in radiation physics expressed as follows (T7.161)

$$\bar{E}_{\text{tr}}^{\text{PE}} = h\nu - P_K \omega_K \eta_K E_B(\text{K}), \quad (8.86)$$

where

- P_K is the probability for the photoelectric effect, if it occurs, to occur in the K shell of lead atom. The range of P_K in nature is from $P_K \approx 1$ for low atomic number Z materials slowly dropping to $P_K \approx 0.8$ for high Z materials. We take $P_K = 0.8$ for the lead atom.
- ω_K is the fluorescence yield, ranging in nature from $\omega_K = 0$ for $Z \leq 10$, through $\omega_K = 0.5$ for $Z = 30$, and saturating at $\omega_K = 0.98$ at very high Z . For lead we estimate $\omega_K = 0.97$.
- η_K is the fluorescence efficiency defined as the mean fraction of the K shell binding energy $E_B(\text{K})$ carried by the fluorescence photon, ranging in nature from $\eta_K \approx 0.98$ at low Z , slowly dropping to reach a minimum at $\eta_K \approx 0.90$ at intermediate Z , and then slowly rising to reach $\eta_K \approx 0.93$ at high Z . For lead we estimate $\eta_K = 0.93$.
- $E_B(\text{K})$ is the binding energy of K shell electrons that can be estimated with reasonable accuracy with the Hartree approximation. For lead: $E_B(\text{K}) \approx E_R(Z - 2)^2 = (13.6 \text{ eV}) \times 82^2 \approx 88 \text{ keV}$.

For photoelectric interaction between a 2 MeV photon and lead atom the mean energy transferred to charged particles (photoelectron and Auger electrons) is thus estimated with (8.86) as $\bar{E}_{\text{tr}}^{\text{PE}} = 2 \text{ MeV} - 0.8 \times 0.97 \times 0.93 \times 0.088 \text{ MeV} = 1.936 \text{ MeV}$.

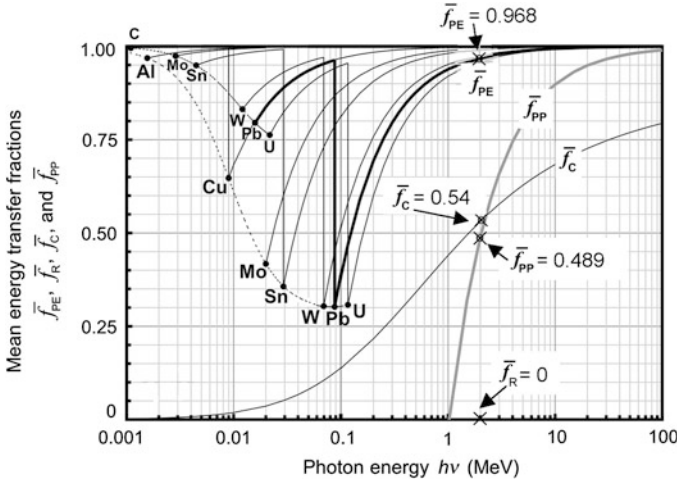


Fig. 8.11 Mean energy transfer fractions \bar{f}_{PE} , \bar{f}_R , \bar{f}_C , and \bar{f}_{PP} against photon energy $h\nu$. The location of points designating mean transfer fractions for $h\nu = 2$ MeV is also shown on the graph

(3) Mean energy transfer fraction \bar{f}_{PE} for photoelectric effect is given by the ratio $\bar{E}_{tr}^{PE} / h\nu$ resulting in

$$\bar{f}_{PE} = \frac{\bar{E}_{tr}^{PE}}{h\nu} = \frac{h\nu - P_K \omega_K \eta_K E_B(K)}{h\nu} = 1 - \frac{P_K \omega_K \eta_K E_B(K)}{h\nu} = \frac{1.936}{2} = 0.968, \tag{8.87}$$

as shown in Fig. 8.11.

(b) Rayleigh scattering is an interaction between incident photon and the whole complement of atomic orbital electrons. It is therefore characterized as photon scattering on tightly bound atomic electrons. In the interaction the atom is neither excited nor ionized; after the interaction the bound electrons revert to their original state, the atom as a whole absorbs the transferred momentum but its recoil energy, because of its large mass, is very small and the incident photon scattered with scattering angle θ has essentially the same energy as the original photon. Since in Rayleigh scattering no electrons are released or produced, there is no energy transfer to CPs and therefore $(E_{tr}^R)_{\max} = \bar{E}_{tr}^R = \bar{f}_R = 0$.

(c) Compton effect is the term used to describe a photon interaction with a loosely bound atomic orbital electron and, in theoretical studies, an assumption is usually made that the interacting electron is “free and stationary”.

(1) Maximum energy $(E_{tr}^C)_{\max}$ transferred from a 2 MeV photon to Compton recoil electron is determined from the following well-known Compton expression (T7.81)

$$(E_{tr}^C)_{\max} = h\nu \frac{2\varepsilon}{1 + 2\varepsilon} = (2 \text{ MeV}) \frac{2 \times 3.91}{1 + 2 \times 3.91} = 1.77 \text{ MeV}, \tag{8.88}$$

where ε is an energy parameter defined as the ratio between the incident photon energy $h\nu$ and the rest energy of the electron $m_e c^2 = 0.511$ MeV, i.e., $\varepsilon = h\nu/m_e c^2$.

(2) Mean energy $\bar{E}_{\text{tr}}^{\text{C}}$ transferred from a 2 MeV photon to Compton recoil electron is determined from the Compton graph that actually plots the mean energy transfer fraction \bar{f}_{C} against photon energy $h\nu$ and, as shown in Fig. 8.11, at $h\nu = 2$ MeV amounts to $\bar{f}_{\text{C}} = 0.54$. This means that $\bar{E}_{\text{tr}}^{\text{C}}$ which is by definition equal to $\bar{f}_{\text{C}} h\nu$ amounts to 0.54×2 MeV = 1.08 MeV.

(3) Compton mean energy transfer fraction \bar{f}_{C} , as discussed in (2) above, is $\bar{f}_{\text{C}} = 0.54$.

(d) Nuclear pair production is the term used to describe pair production (electron-positron materialization) in the field of the nucleus. The photon disappears and an electron-positron pair is produced with the two particles sharing the available total kinetic energy $E_{\text{tr}}^{\text{PP}} = h\nu - 2m_e c^2$, where $h\nu$ is the incident photon energy.

(1) Maximum energy $(E_{\text{tr}}^{\text{PP}})_{\text{max}}$ transferred from 2-MeV photon to CPs is given as the photon energy $h\nu$ less the rest energies of the electron and positron that were produced out of energy in the pair production interaction. $(E_{\text{tr}}^{\text{PP}})_{\text{max}}$ is thus given as $h\nu - 2m_e c^2$ and this kinetic energy is shared between the electron and the positron in such a way that the sum of E_{K} (electron) and E_{K} (positron) always amounts to $(E_{\text{tr}}^{\text{NPP}})_{\text{max}} = h\nu - 2m_e c^2$. For 2-MeV photon we get

$$(E_{\text{tr}}^{\text{NPP}})_{\text{max}} = h\nu - 2m_e c^2 = 2 \text{ MeV} - 1.022 \text{ MeV} = 0.978 \text{ MeV}. \quad (8.89)$$

(2) Mean energy $\bar{E}_{\text{tr}}^{\text{NPP}}$ transferred from 2-MeV photon to CPs is equal $(E_{\text{tr}}^{\text{NPP}})_{\text{max}} = 0.978$ MeV.

(3) The mean energy transfer fraction \bar{f}_{NPP} for nuclear pair production, is calculated from the ratio $(\bar{E}_{\text{tr}}^{\text{NPP}})_{\text{max}}/h\nu$ and amounts to $\bar{f}_{\text{NPP}} = 0.978/2 = 0.489$, as shown in Fig. 8.11.

(e) Electronic pair production, also called triplet production, is a photon interaction in which a pair production event occurs in the field of an orbital electron of the absorber. The photon disappears and three particles leave the interaction site: electron-positron pair as well as the interacting orbital electron. Here, the three particles share the available energy of $h\nu - 2m_e c^2$. Since the threshold energy $h\nu_{\text{thr}}$ for triplet production is $4m_e c^2 = 2.044$ MeV, a 2-MeV photon cannot undergo triplet production and there is no energy transfer to charged particles. Thus, $(E_{\text{tr}}^{\text{TP}}) = \bar{E}_{\text{tr}}^{\text{TP}} = \bar{f}_{\text{TP}} = 0$ for $h\nu = 2$ MeV.

(g) Table 8.5B presents a summary of results for calculation of maximum energy transfer $(E_{\text{K}})_{\text{max}}$, mean energy transfer \bar{E}_{tr} , and mean energy transfer fraction \bar{f}_i for 2 MeV photons interacting with lead absorber atoms through **(a)** photoelectric effect, **(b)** Rayleigh scattering, **(c)** Compton effect, **(d)** nuclear pair production, and **(e)** triplet production.

Table 8.5B Summary of results for calculation of maximum energy transfer $(E_K)_{\max}$, mean energy transfer \bar{E}_{tr} , and mean energy transfer fraction \bar{f}_i for 2 MeV photons interacting with lead absorber atoms through photoelectric effect, Rayleigh scattering, Compton effect, nuclear pair production, and triplet production

Photon ($h\nu = 2$ MeV) interaction with lead absorber	$(E_K)_{\max}$	\bar{E}_{tr}	\bar{f}_i
(a) Photoelectric effect	$(E_K^{\text{PE}})_{\max} = 2$ MeV	$\bar{E}_{\text{tr}}^{\text{PE}} = 1.936$ MeV	$\bar{f}_{\text{PE}} = 0.968$
(b) Rayleigh scattering	$(E_{\text{tr}}^{\text{R}})_{\max} = 0$	$\bar{E}_{\text{tr}}^{\text{R}} = 0$	$\bar{f}_{\text{R}} = 0$
(c) Compton effect	$(E_{\text{tr}}^{\text{C}})_{\max} = 1.77$ MeV	$\bar{E}_{\text{tr}}^{\text{C}} = 1.08$ MeV	$\bar{f}_{\text{C}} = 0.54$
(d) Nuclear pair production	$(E_{\text{tr}}^{\text{NPP}})_{\max} = 0.978$ MeV	$(\bar{E}_{\text{tr}}^{\text{NPP}})_{\max} = 0.978$ MeV	$\bar{f}_{\text{NPP}} = 0.489$
(e) Triplet production	$(E_{\text{tr}}^{\text{TP}})_{\max} = 0$	$(\bar{E}_{\text{tr}}^{\text{TP}})_{\max} = 0$	$\bar{f}_{\text{TP}} = 0$

8.4 Coefficients of Compounds and Mixtures

8.4.Q1

(191)

Discovered in 1907, Bakelite ($\text{C}_{45}\text{H}_{38}\text{O}_7$) is a synthetic resin based on a chemical combination of phenol and formaldehyde and belonging to the group of thermosetting polymers. In addition to being an excellent electric insulator, it is also resistant to chemical solvents and heat. Because of its excellent chemical and physical properties, it is also used as air equivalent material for various types of ionization chambers.

For photons with energy of 100 keV and 10 MeV interacting with Bakelite absorber determine:

- Proportion by weight of the constituent elements of Bakelite.
- Mass attenuation coefficient μ/ρ of Bakelite.
- Mass energy transfer coefficient μ_{tr}/ρ of Bakelite.
- Mass energy absorption coefficient μ_{ab}/ρ of Bakelite.
- Mean energy \bar{E}_{tr} transferred from photon to charged particles (electrons and positrons) in Bakelite absorber.
- Mean energy \bar{E}_{ab} absorbed in the Bakelite absorber.
- Mean energy \bar{E}_{rad} radiated from charged particles in the form of radiation loss consisting of bremsstrahlung photons and annihilation quanta from in-flight annihilation in Bakelite.

Atomic weight: Hydrogen H—1.00794; Carbon C—12.0107; Oxygen O—15.9994.

Table 8.6 Mass attenuation coefficients μ/ρ , mass energy transfer coefficient μ_{tr}/ρ , and mass energy absorption coefficient μ_{ab}/ρ for photons of energy $h\nu = 100 \text{ keV}$ and $h\nu = 10 \text{ MeV}$ interacting with carbon. (*)Data for mass attenuation coefficient are from the NIST. (***)Data for the mass energy transfer coefficient and mass energy absorption coefficient are from Johns, HE and Cunningham, JR

Element	HYDROGEN ($Z = 6$)		CARBON C ($Z = 1$)		OXYGEN O ($Z = 8$)	
	100 keV	10 MeV	100 keV	10 MeV	100 keV	10 MeV
$\mu/\rho \text{ (cm}^2/\text{g)}^{(*)}$	0.2944	0.0325	0.1514	0.0196	0.1551	0.0209
$\mu_{\text{tr}}/\rho \text{ (cm}^2/\text{g)}^{(**)}$	0.0406	0.0277	0.0213	0.0143	0.0234	0.0155
$\mu_{\text{ab}}/\rho \text{ (cm}^2/\text{g)}^{(***)}$	0.0406	0.0225	0.0213	0.0138	0.0234	0.0149

SOLUTION:

At a given photon energy $h\nu$ the attenuation coefficients μ , energy transfer coefficients μ_{tr} , and energy absorption coefficients μ_{ab} of a compound or mixture of elements are approximated by a summation of the weighted mean of the masses of constituent elements, as follows

$$\mu = \sum_j w_j \mu_j, \quad \mu_{\text{tr}} = \sum_j w_j (\mu_{\text{tr}})_j, \quad \mu_{\text{ab}} = \sum_j w_j (\mu_{\text{ab}})_j, \quad (8.90)$$

where w_j is the proportion by weight of the j -th constituent element.

(a) The proportion by mass of the constituent elements (C, H, and O) of Bakelite is determined as follows:

(1) Bakelite $\text{C}_{45}\text{H}_{38}\text{O}_7$ according to its chemical formula contains 45 atoms of carbon, 38 atoms of hydrogen, and 7 atoms of oxygen. The molecular weight \mathcal{M}_{Bak} of Bakelite thus is:

$$\mathcal{M}_{\text{Bak}} = 45 \times 12.0107 + 38 \times 1.0079 + 7 \times 15.9994 = 690.7775 \text{ g/mol.} \quad (8.91)$$

(2) Proportion by mass of hydrogen in Bakelite

$$w_{\text{H}} = \frac{38 \times 1.0079}{690.7775} = 0.0555 \quad (8.92)$$

(3) Proportion by mass of carbon in Bakelite

$$w_{\text{C}} = \frac{45 \times 12.0107}{690.7775} = 0.7824 \quad (8.93)$$

(4) Proportion by mass of oxygen in Bakelite

$$w_{\text{O}} = \frac{7 \times 15.9994}{690.7775} = 0.1621 \quad (8.94)$$

(b) *Mass attenuation coefficient* μ/ρ of Bakelite for photon energy $h\nu$ will be calculated with (8.90) and data from Table 8.6 for the three constituents of Bakelite as follows

$$\left(\frac{\mu}{\rho}\right)_{\text{Bak}}^{h\nu} = \sum_j w_j \left(\frac{\mu}{\rho}\right)_j^{h\nu} = w_C \left(\frac{\mu}{\rho}\right)_C^{h\nu} + w_H \left(\frac{\mu}{\rho}\right)_H^{h\nu} + w_O \left(\frac{\mu}{\rho}\right)_O^{h\nu}. \quad (8.95)$$

For photon energy $h\nu = 100$ keV in Bakelite using (8.95) we get

$$\begin{aligned} \left(\frac{\mu}{\rho}\right)_{\text{Bak}}^{100 \text{ keV}} &= \sum_j w_j \left(\frac{\mu}{\rho}\right)_j^{100 \text{ keV}} \\ &= w_C \left(\frac{\mu}{\rho}\right)_C^{100 \text{ keV}} + w_H \left(\frac{\mu}{\rho}\right)_H^{100 \text{ keV}} + w_O \left(\frac{\mu}{\rho}\right)_O^{100 \text{ keV}} \\ &= (0.7824 \times 0.1514 + 0.0555 \times 0.2944 + 0.1621 \times 0.1551) \text{ cm}^2/\text{g} \\ &= 0.1600 \text{ cm}^2/\text{g} \end{aligned} \quad (8.96)$$

and for photon energy $h\nu = 10$ MeV in Bakelite

$$\begin{aligned} \left(\frac{\mu}{\rho}\right)_{\text{Bak}}^{10 \text{ MeV}} &= \sum_j w_j \left(\frac{\mu}{\rho}\right)_j^{10 \text{ MeV}} \\ &= w_C \left(\frac{\mu}{\rho}\right)_C^{10 \text{ MeV}} + w_H \left(\frac{\mu}{\rho}\right)_H^{10 \text{ MeV}} + w_O \left(\frac{\mu}{\rho}\right)_O^{10 \text{ MeV}} \\ &= (0.7824 \times 0.0196 + 0.0555 \times 0.0325 + 0.1621 \times 0.0209) \text{ cm}^2/\text{g} \\ &= 0.0206 \text{ cm}^2/\text{g}. \end{aligned} \quad (8.97)$$

(c) *Mass energy transfer coefficient* μ_{tr}/ρ of Bakelite for photon energy $h\nu$ will be calculated with (8.90) and data from Table 8.6 for the three constituents of Bakelite as follows

$$\left(\frac{\mu_{\text{tr}}}{\rho}\right)_{\text{Bak}}^{h\nu} = \sum_j w_j \left(\frac{\mu_{\text{tr}}}{\rho}\right)_j^{h\nu} = w_C \left(\frac{\mu_{\text{tr}}}{\rho}\right)_C^{h\nu} + w_H \left(\frac{\mu_{\text{tr}}}{\rho}\right)_H^{h\nu} + w_O \left(\frac{\mu_{\text{tr}}}{\rho}\right)_O^{h\nu}. \quad (8.98)$$

For photon energy $h\nu = 100$ keV in Bakelite using (8.98) we get

$$\begin{aligned} \left(\frac{\mu_{\text{tr}}}{\rho}\right)_{\text{Bak}}^{100 \text{ keV}} &= \sum_j w_j \left(\frac{\mu_{\text{tr}}}{\rho}\right)_j^{100 \text{ keV}} \\ &= w_C \left(\frac{\mu_{\text{tr}}}{\rho}\right)_C^{100 \text{ keV}} + w_H \left(\frac{\mu_{\text{tr}}}{\rho}\right)_H^{100 \text{ keV}} + w_O \left(\frac{\mu_{\text{tr}}}{\rho}\right)_O^{100 \text{ keV}} \end{aligned}$$

$$\begin{aligned}
 &= (0.7824 \times 0.0213 + 0.0555 \times 0.0406 + 0.1621 \times 0.0234) \text{ cm}^2/\text{g} \\
 &= 0.0227 \text{ cm}^2/\text{g} \quad (8.99)
 \end{aligned}$$

and for photon energy $h\nu = 10 \text{ MeV}$ in Bakelite

$$\begin{aligned}
 \left(\frac{\mu_{\text{tr}}}{\rho}\right)_{\text{Bak}}^{10 \text{ MeV}} &= \sum_j w_j \left(\frac{\mu_{\text{tr}}}{\rho}\right)_j^{10 \text{ MeV}} \\
 &= w_{\text{C}} \left(\frac{\mu_{\text{tr}}}{\rho}\right)_{\text{C}}^{10 \text{ MeV}} + w_{\text{H}} \left(\frac{\mu_{\text{tr}}}{\rho}\right)_{\text{H}}^{10 \text{ MeV}} + w_{\text{O}} \left(\frac{\mu_{\text{tr}}}{\rho}\right)_{\text{O}}^{10 \text{ MeV}} \\
 &= (0.7824 \times 0.0143 + 0.0555 \times 0.0227 + 0.1621 \times 0.0155) \text{ cm}^2/\text{g} \\
 &= 0.0150 \text{ cm}^2/\text{g}. \quad (8.100)
 \end{aligned}$$

(d) *Mass energy absorption coefficient* μ_{ab}/ρ of Bakelite for photon energy $h\nu$ will be calculated with (8.90) and data from Table 8.6 for the three constituents of Bakelite as follows

$$\left(\frac{\mu_{\text{ab}}}{\rho}\right)_{\text{Bak}}^{h\nu} = \sum_j w_j \left(\frac{\mu_{\text{ab}}}{\rho}\right)_j^{h\nu} = w_{\text{C}} \left(\frac{\mu_{\text{ab}}}{\rho}\right)_{\text{C}}^{h\nu} + w_{\text{H}} \left(\frac{\mu_{\text{ab}}}{\rho}\right)_{\text{H}}^{h\nu} + w_{\text{O}} \left(\frac{\mu_{\text{ab}}}{\rho}\right)_{\text{O}}^{h\nu}. \quad (8.101)$$

For photon energy $h\nu = 100 \text{ keV}$ in Bakelite using (8.101) we get

$$\begin{aligned}
 \left(\frac{\mu_{\text{ab}}}{\rho}\right)_{\text{Bak}}^{100 \text{ keV}} &= \sum_j w_j \left(\frac{\mu_{\text{ab}}}{\rho}\right)_j^{100 \text{ keV}} \\
 &= w_{\text{C}} \left(\frac{\mu_{\text{ab}}}{\rho}\right)_{\text{C}}^{100 \text{ keV}} + w_{\text{H}} \left(\frac{\mu_{\text{ab}}}{\rho}\right)_{\text{H}}^{100 \text{ keV}} + w_{\text{O}} \left(\frac{\mu_{\text{ab}}}{\rho}\right)_{\text{O}}^{100 \text{ keV}} \\
 &= (0.7824 \times 0.0213 + 0.0555 \times 0.0406 + 0.1621 \times 0.0234) \text{ cm}^2/\text{g} \\
 &= 0.0227 \text{ cm}^2/\text{g} \quad (8.102)
 \end{aligned}$$

and for photon energy $h\nu = 10 \text{ MeV}$ in Bakelite

$$\begin{aligned}
 \left(\frac{\mu_{\text{ab}}}{\rho}\right)_{\text{Bak}}^{10 \text{ MeV}} &= \sum_j w_j \left(\frac{\mu_{\text{ab}}}{\rho}\right)_j^{10 \text{ MeV}} \\
 &= w_{\text{C}} \left(\frac{\mu_{\text{ab}}}{\rho}\right)_{\text{C}}^{10 \text{ MeV}} + w_{\text{H}} \left(\frac{\mu_{\text{ab}}}{\rho}\right)_{\text{H}}^{10 \text{ MeV}} + w_{\text{O}} \left(\frac{\mu_{\text{ab}}}{\rho}\right)_{\text{O}}^{10 \text{ MeV}} \\
 &= (0.7824 \times 0.0138 + 0.0555 \times 0.0225 + 0.1621 \times 0.0149) \text{ cm}^2/\text{g} \\
 &= 0.0145 \text{ cm}^2/\text{g}. \quad (8.103)
 \end{aligned}$$

(e) Mean energy \bar{E}_{tr} transferred from photon with energy $h\nu$ to charged particles (electron and positron) in Bakelite absorber is determined from the standard expression linking mass energy transfer coefficient μ_{tr}/ρ with mass attenuation coefficient μ/ρ , as shown in (T8.5)

$$\frac{\mu_{\text{tr}}}{\rho} = \bar{f}_{\text{tr}} \frac{\mu}{\rho} = \frac{\bar{E}_{\text{tr}} \mu}{h\nu \rho} \quad \text{or} \quad \bar{E}_{\text{tr}} = h\nu \frac{\mu_{\text{tr}}/\rho}{\mu/\rho}. \quad (8.104)$$

Mean energy transferred from photons of energy $h\nu = 100$ keV to charged particles in Bakelite from (8.104) is

$$\bar{E}_{\text{tr}} = h\nu \frac{\mu_{\text{tr}}/\rho}{\mu/\rho} = (100 \text{ keV}) \times \frac{0.0227}{0.1600} = 14.2 \text{ keV}, \quad (8.105)$$

while mean energy transferred from photons of energy $h\nu = 10$ MeV to charged particles is

$$\bar{E}_{\text{tr}} = h\nu \frac{\mu_{\text{tr}}/\rho}{\mu/\rho} = (10 \text{ MeV}) \times \frac{0.0150}{0.0206} = 7.28 \text{ MeV}. \quad (8.106)$$

(f) Mean energy \bar{E}_{ab} absorbed in the Bakelite absorber is determined from the standard expression linking mass energy absorption coefficient μ_{ab}/ρ with mass attenuation coefficient μ/ρ as follows

$$\frac{\mu_{\text{ab}}}{\rho} = \bar{f}_{\text{ab}} \frac{\mu}{\rho} = \frac{\bar{E}_{\text{ab}} \mu}{h\nu \rho} \quad \text{or} \quad \bar{E}_{\text{ab}} = h\nu \frac{\mu_{\text{ab}}/\rho}{\mu/\rho}. \quad (8.107)$$

Mean energy absorbed in Bakelite through a 100 keV photon interaction with Bakelite is

$$\bar{E}_{\text{ab}} = h\nu \frac{\mu_{\text{ab}}/\rho}{\mu/\rho} = (100 \text{ keV}) \times \frac{0.0227}{0.1600} = 14.2 \text{ keV} \quad (8.108)$$

and for a 10 MeV photon

$$\bar{E}_{\text{ab}} = h\nu \frac{\mu_{\text{ab}}/\rho}{\mu/\rho} = (10 \text{ MeV}) \times \frac{0.0145}{0.0206} = 7.04 \text{ MeV}. \quad (8.109)$$

(g) Mean energy \bar{E}_{rad} radiated from charged particles released or produced in Bakelite absorber is equal to energy difference between the energy transferred \bar{E}_{tr} to charged particles in Bakelite absorber and energy absorbed \bar{E}_{ab} in the Bakelite absorber, i.e., $\bar{E}_{\text{rad}} = \bar{E}_{\text{tr}} - \bar{E}_{\text{ab}}$.

For 100 keV incident photon we have

$$\bar{E}_{\text{rad}} = \bar{E}_{\text{tr}} - \bar{E}_{\text{ab}} = 14.2 \text{ keV} - 14.2 \text{ keV} = 0 \quad (8.110)$$

and for 10 MeV photon

$$\bar{E}_{\text{rad}} = \bar{E}_{\text{tr}} - \bar{E}_{\text{ab}} = 7.28 \text{ MeV} - 7.04 \text{ MeV} = 0.24 \text{ MeV}. \quad (8.111)$$

8.5 Effects Following Photon Interactions with Absorber

8.5.Q1

(192)

Six modes of photon interaction with absorber atoms are of importance to medical physics. Each of these interaction modes has its own peculiar characteristics, some of these are common to several of the six modes and others are specific to the given mode. For the six interaction modes of importance to medical physics describe the events that follow each one of these interactions.

- (a) Photoelectric effect
- (b) Rayleigh scattering
- (c) Compton scattering
- (d) Nuclear pair production
- (e) Electronic pair production
- (f) Photonuclear reaction

SOLUTION:

(a) *Photoelectric effect*, an interaction between the incident photon and a tightly bound orbital electron of the absorber atom, is considered an interaction between the photon and whole atom. The photon disappears and the orbital electron, called photoelectron, is ejected from the absorber atom leaving behind a shell vacancy in the absorber atom. The fate of the vacancy is discussed in (g), the fate of the photoelectron in (h).

(b) *Rayleigh scattering*, also called coherent scattering, refers to an interaction of the incident photon with a full complement of orbital electrons tightly bound to the nucleus of the absorber atom. This means that the photon interacts with the whole atom. The scattered photon is emitted with scattering angle θ and with energy identical to that of the incident photon. No vacancy is produced in the absorber atom and the incident photon loses no energy except for the negligible amount of energy used up as recoil energy of the absorber atom.

(c) *Compton effect*, also known as incoherent scattering and Compton scattering, is an interaction of the incident photon with a loosely bound, essentially “free electron”. The incident photon is scattered with scattering angle θ and some of its incident energy is transferred to the emitted electron, referred to as the Compton or recoil electron.

The scattered photon leaves the interaction site with a lower energy than that of the incident photon and in a direction different from that of the incident photon. The Compton electron leaves behind an electronic vacancy in the absorber atom and the fate of the vacancy as well as the fate of the Compton electron are discussed in (g) and (h), respectively.

(d) *Nuclear pair production* refers to a photon interaction in which a photon disappears under the influence of the nuclear electric field and an electron-positron pair is produced (materialization) out of the photon energy. No electronic vacancy is produced in this interaction, however, the electron and positron leaving the interaction site are moving through the absorbing medium and losing energy in collisions with absorber atoms discussed in (h). In addition, positron undergoes annihilation with an available free electron, as discussed in (i).

(e) *Electronic pair production*, also known as triplet production, is a photon interaction that occurs in the electric field of an orbital electron. The photon disappears and an electron-positron pair is produced. The incident photon energy is shared among three particles: orbital electron that enabled the interaction as well as the electron and positron produced in the interaction. As the three particles travel through the absorber, they lose their energy through collisions with atoms of the absorber, as discussed in (h). In addition the positron undergoes annihilation with an available free electron, as discussed in (i).

(f) *Photonuclear reaction*, also known as photodisintegration or nuclear photoelectric effect, is a direct interaction between the incident photon with nucleus of an absorber atom. The photon disappears and the nucleus ejects a neutron, proton, or even heavier particle that move through the absorbing medium and lose energy through Coulomb collisions or nuclear reactions. No vacancies are produced in the absorber atom and no energetic electrons are generated in the initial interaction. In medical physics, the photonuclear reaction is more of a curiosity than of real importance, so that most of the time it is ignored in comparison to the other modes of photon interaction with absorber atoms.

(g) *Electronic vacancies* are produced in absorber atoms by ejection of orbital electrons through the following photon interaction modes with absorber atoms: photoelectric effect (ejection of photoelectron), Compton effect (ejection of Compton recoil electron), and electronic pair production or triplet production (ejection of orbital electron). The three effects are significantly different from one another, however, they have vacancy formation in common and the fate of a vacancy does not at all depend on how it was created; all vacancies evolve along the same path and in the same manner.

If the *shell vacancy* occurs in a shell other than the outer (valence) shell of the absorber atom, an orbital electron from a higher level shell will fill the original vacancy (leaving behind a vacancy in its own shell) and the transition energy will be emitted either as a characteristic (fluorescence) photon or will be transferred

to a higher shell orbital electron. This electron will be ejected from the absorber atom as an Auger electron, leaving behind a new electronic vacancy in the absorber atom.

In electronic transition from higher to lower electronic shell, the vacancy makes a transition in the opposite direction and eventually migrates to the outer atomic shell of the absorber atom. Each emitted Auger electron, on the other hand, adds a new vacancy to the absorber atom that will also migrate to the outer atomic shell. Free electrons from the surroundings of the absorber atom will eventually fill the outer shell vacancies and this will return the absorber atom into its original neutral state that was in effect before the incident photon interaction occurred.

(h) Energetic charged particles (electrons and positrons) produced or released in several modes of incident photon interaction with absorber atom all travel through the absorber and lose kinetic energy in Coulomb interactions be it with orbital electrons or with nuclei of absorber atoms. These charged particles (CPs) can be photoelectron from photoelectric effect, Compton electron from Compton scattering, pair production electron and positron from nuclear pair production, or the orbital electron as well as the pair production electron and positron from triplet production.

Coulomb interactions between energetic CP and orbital electrons of absorber atom contribute to collision loss of the charged particle and cause ionization and excitation of absorber atoms that eventually result in absorbed dose through collision stopping power. Coulomb interactions between the energetic CPs (electrons and positrons) and nucleus of absorber atoms contribute to radiation loss of the CP and cause production of bremsstrahlung photons that generally escape the region of interest.

(i) Positrons produced in nuclear as well as electronic pair production move through absorber in a similar manner as electrons and lose their kinetic energy through Coulomb interactions with orbital electrons and nuclei of absorber atoms producing collision and radiation loss. However, upon losing their kinetic energy positrons undergo annihilation with a free electron from the environment and produce two 511 MeV photons (annihilation photons) leaving the annihilation site in opposite directions to satisfy conservation of energy and momentum principles.

In rare instances in a process referred to as in-flight annihilation, positron annihilation occurs before the positron expended all of its kinetic energy. One or more photons are produced in the annihilation process and photon energy must be such that conservation of energy and momentum principles are upheld.

Events following the six modes of photon interactions with absorber atoms that are of importance in medical physics are summarized in Fig. 8.12.

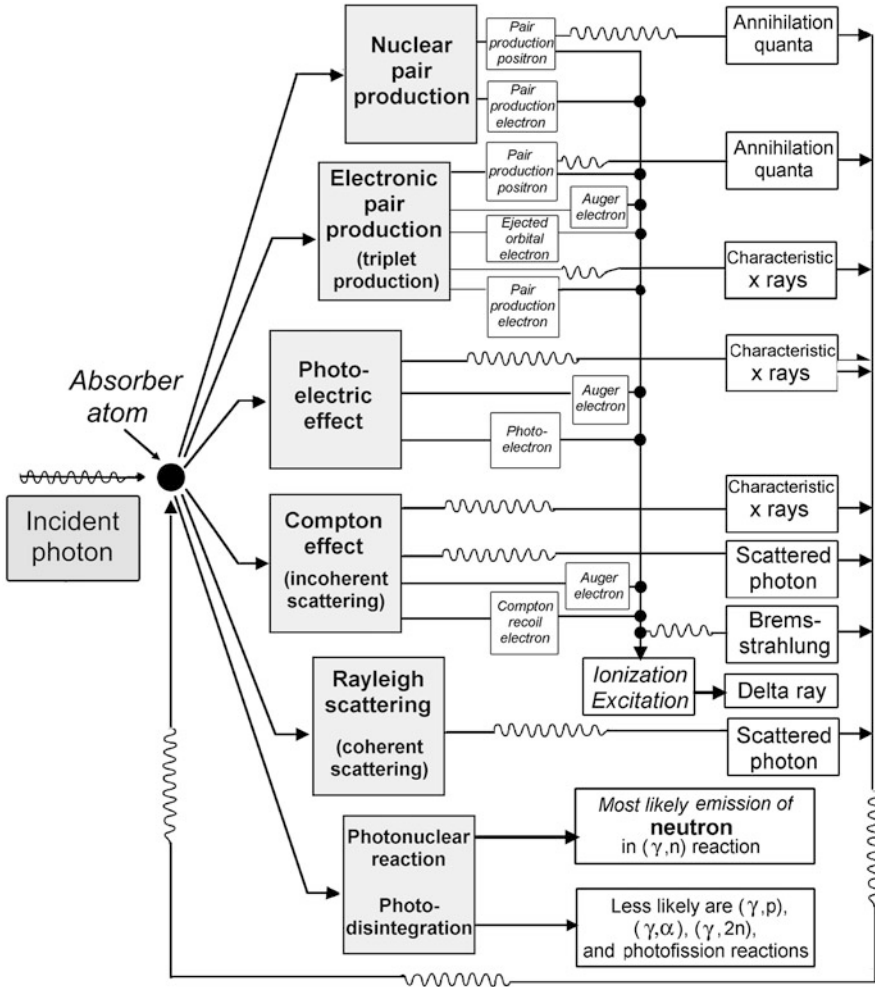


Fig. 8.12 Schematic diagram of the six modes available to incident photons for interaction with absorber atoms of importance to medical physics. Also shown are the particles released in or produced in the absorber during a given photon interaction as well as the effects that follow a given photon interaction, such as emission of characteristic radiation, Auger electrons, annihilation quanta, and bremsstrahlung photons. The figure also indicates that the secondary photons (Rayleigh- and Compton scattered photons, characteristic photons, annihilation quanta, and bremsstrahlung photons) can start their own photon interaction cycle in the absorber

8.6 Summary of Photon Interactions with Absorbers

8.6.Q1

(193)

Over a dozen different modes of photon interaction with absorber atoms have been identified in nuclear physics and six of these are of significance in medical physics, since they form the basis for use of radiation in imaging and therapy of disease. The six interactions or effects are:

- (A) Photoelectric effect
- (B) Rayleigh scattering
- (C) Compton effect
- (D) Nuclear pair production
- (E) Electronic pair production (also known as triplet production)
- (F) Photonuclear reactions (also known as photodisintegration)

For each photon interaction with absorber atoms:

- (a) State the entity with which the photon interacts (absorber atom, nucleus of absorber atom, or orbital electron of absorber atom).
- (b) List interactions that result in shell vacancy in absorber atom.
- (c) List interactions that release charged particles in the absorber and identify the charged particles.
- (d) List interactions that produce charged particles in the absorber and identify the charged particles.
- (e) Draw a schematic diagram.

SOLUTION:

Answers to (a), (b), (c), and (d) are given in Table 8.7, to (e) in Fig. 8.13.

Table 8.7 Various properties of photon interaction with absorber atoms such as the entity with which interaction occurs, production of shell vacancy, release or production of charged particles

Mode of photon interaction	Photoelectric	Rayleigh scattering	Compton	Nuclear pair prod.	Electronic pair prod.	Photonuclear
(a) Entity	Whole atom	Whole atom	Orbital electron	Electric field of nucleus	Electric field of orb. elect.	Nucleus
(b) Shell vacancy	Yes	No	Yes	No	Yes	No
(c) Charged particle release	Photoelectron	–	Compton electron	–	Orbital electron	–
(d) Charged particle production	–	–	–	Electron, Positron	Electron, Positron	Proton, etc.

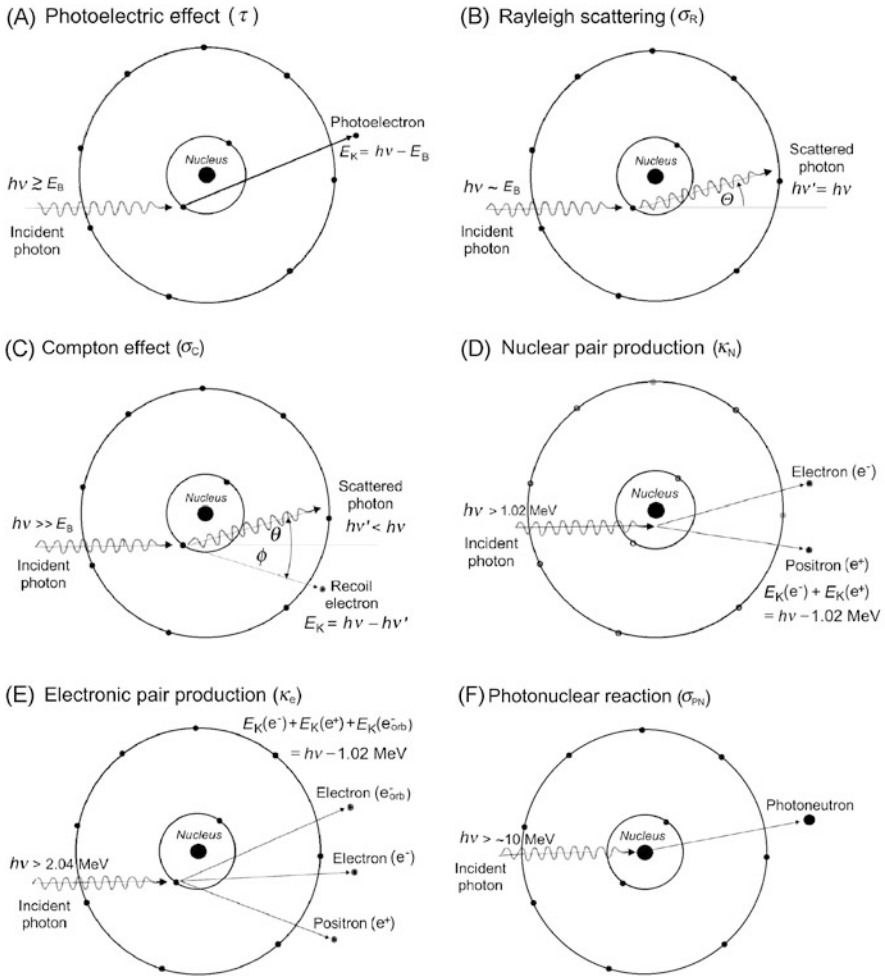


Fig. 8.13 Schematic diagrams of the six most important modes of photon interaction with atoms of absorber: (A) Photoelectric effect, (B) Rayleigh scattering, (C) Compton effect, (D) Nuclear pair production, (E) Electronic pair production, and (F) Photodisintegration. Modes (A), (B), (C), and (E) represent photon interactions with orbital electrons of absorber, modes (D) and (E) interactions with the nucleus of absorber. The nuclear and electronic pair production are usually handled together under the header “pair production”, and photoneutron are usually ignored, so that in medical physics often an assumption is made that there are only four important modes of photon interaction with absorber atoms: photoelectric effect, Rayleigh scattering, Compton scattering, and pair production

8.6.Q2

(194)

Mono-energetic photons of energy $h\nu = 60$ MeV interact with copper absorber ($Z = 29$, $A = 63.54$ g/mol, $\rho = 8.96$ g/cm³). Atomic attenuation coefficients (cross sections) of copper at $h\nu = 60$ keV are:

$${}_a\tau = 139.60 \times 10^{-24} \text{ cm}^2/\text{atom for photoelectric effect (PE)}$$

$${}_a\sigma_C = 13.93 \times 10^{-24} \text{ cm}^2/\text{atom for Compton effect (C)}$$

$${}_a\sigma_R = 11.29 \times 10^{-24} \text{ cm}^2/\text{atom for Rayleigh scattering (R)}$$

For interaction of 60 keV photons with copper absorber determine:

- (a) Mass attenuation coefficient μ/ρ .
- (b) Mean energy \bar{E}_{tr} transferred to electrons in copper absorber.
- (c) Mean energy transfer fraction \bar{f}_{tr} .
- (d) Mass energy transfer coefficient μ_{tr}/ρ .
- (e) Mass energy absorption coefficient μ_{ab}/ρ .

SOLUTION:

(a) *Mass attenuation coefficient* μ/ρ is the sum of mass attenuation coefficients for photoelectric effect τ/ρ , Compton effect σ_C/ρ , and Rayleigh scattering σ_R/ρ (T8.2)

$$\begin{aligned} \frac{\mu}{\rho} &= \frac{\tau}{\rho} + \frac{\sigma_C}{\rho} + \frac{\sigma_R}{\rho} + \frac{\kappa}{\rho} = \frac{N_A}{A} {}_a\mu = \frac{N_A}{A} ({}_a\tau + {}_a\sigma_C + {}_a\sigma_R + {}_a\kappa) \\ &= \frac{6.022 \times 10^{23} \text{ atom} \cdot \text{mol}^{-1}}{63.54 \text{ g} \cdot \text{mol}^{-1}} \times (139.60 + 13.93 + 11.29 + 0) \times 10^{-24} \frac{\text{cm}^2}{\text{atom}} \\ &= \frac{6.022 \times 10^{23} \text{ atom} \cdot \text{mol}^{-1}}{63.54 \text{ g} \cdot \text{mol}^{-1}} \times 164.82 \times 10^{-24} \frac{\text{cm}^2}{\text{atom}} = 1.562 \frac{\text{cm}^2}{\text{g}}. \end{aligned} \quad (8.112)$$

Note: Attenuation coefficient for pair production κ is equal to zero for photons of energy $h\nu = 60$ keV because this energy is below the threshold energy of 1.02 MeV for pair production.

(b) *Mean energy* \bar{E}_{tr} transferred to electrons from photon of energy 60 keV interacting with copper absorber is determined through considering mean energy transfer \bar{E}_{tr}^i from each individual effect that contributes to photon interaction and adding the weighted mean values to obtain the total combined mean value (T8.12)

$$\bar{E}_{\text{tr}} = \sum_i w_i \bar{E}_{\text{tr}}^i = w_{\text{PE}} \bar{E}_{\text{tr}}^{\text{PE}} + w_{\text{C}} \bar{E}_{\text{tr}}^{\text{C}} + w_{\text{R}} \bar{E}_{\text{tr}}^{\text{R}} + w_{\text{PP}} \bar{E}_{\text{tr}}^{\text{PP}}. \quad (8.113)$$

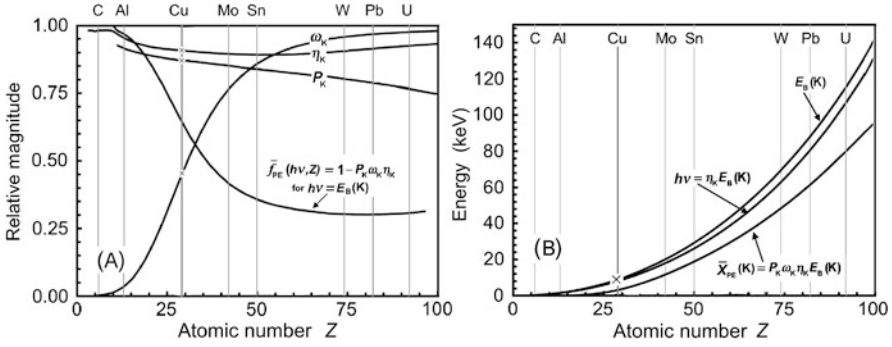


Fig. 8.14 Various atomic parameters for the K shell of the absorber relevant to photoelectric effect plotted against atomic number Z of the absorber: **(A)** Fluorescence yield ω_K , photoelectric probability P_K , and fluorescence efficiency η_K ; **(B)** K-shell binding energy $E_B(K)$, mean fluorescence photon energy $\eta_K E_B(K)$, and mean fluorescence emission energy $P_K \omega_K \eta_K E_B(K)$

Note: In our problem $\bar{E}_{tr}^R = 0$ (this is true in general, because there is no energy transfer to charged particles in Rayleigh scattering) and $\bar{E}_{tr}^{PP} = 0$ because 60 keV is below the threshold energy of 1.02 MeV for pair production.

- (1) Mean energy \bar{E}_{tr}^{PE} transferred to photoelectron and Auger electrons in photoelectric effect is calculated as (T7.161)

$$\bar{E}_{tr}^{PE} = h\nu - P_K \omega_K \eta_K E_B(K) = 60 \text{ keV} - 0.86 \times 0.45 \times 0.91 \times 9 \text{ keV} = 56.86 \text{ keV}, \tag{8.114}$$

with parameters $P_K = 0.86$ (photoelectric probability for K shell, if photoelectric effect happens), $\omega_K = 0.45$ (fluorescence yield for K shell), and $\eta_K = 0.91$ (fluorescence efficiency for K shell), plotted against atomic number Z of absorber in Fig. 8.14(A) and $E_B(K) = 9 \text{ keV}$ binding energy of K shell plotted against atomic number Z of absorber in Fig. 8.14(B) or estimated with Hartree approximation given as follows: $E_B(K) \approx (13.61 \text{ eV}) \times (Z - 2)^2$.

- (2) Mean energy \bar{E}_{tr}^C transferred to recoil electron in Compton effect is obtained from the ‘‘Compton Graph’’ which plots the mean energy transfer fraction \bar{f}_C for the Compton effect against incident photon energy $h\nu$. From the ‘‘Compton Graph’’ we find $\bar{f}_C = 0.10$ at $h\nu = 60 \text{ keV}$, as shown in Fig. 8.15. Since $\bar{f}_C = \bar{E}_{tr}^C / h\nu$, we get $\bar{E}_{tr}^C = 0.1 \times 60 \text{ keV} = 6 \text{ keV}$.

- (3) Mean energy \bar{E}_{tr}^R transferred to electrons in Rayleigh scattering is zero, since in Rayleigh scattering no energy is transferred to electrons, i.e., $\bar{E}_{tr}^R = 0$.

- (4) We now use (8.113) to determine the total mean energy transfer \bar{E}_{tr} to electrons in interaction of 60 keV photons with copper absorber

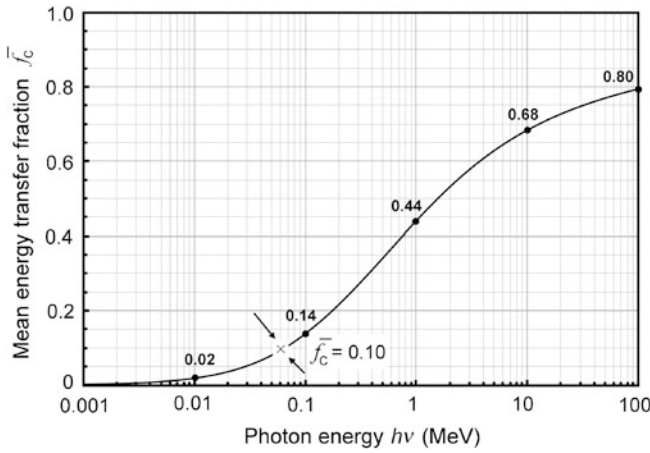


Fig. 8.15 The “Compton Graph” plotting the mean energy transfer fraction \bar{f}_C against photon energy $h\nu$ for Compton effect. Anchor points for the Compton curve are shown with *solid circles*, result of our calculation of the mean Compton energy transfer fraction \bar{f}_C at $h\nu = 60$ keV is shown by \times

$$\begin{aligned}\bar{E}_{\text{tr}} &= \sum_i w_i \bar{E}_{\text{tr}}^i = w_{\text{PE}} \bar{E}_{\text{tr}}^{\text{PE}} + w_{\text{C}} \bar{E}_{\text{tr}}^{\text{C}} + w_{\text{R}} \bar{E}_{\text{tr}}^{\text{R}} = \frac{a\tau}{a\mu} \bar{E}_{\text{tr}}^{\text{PE}} + \frac{a\sigma_{\text{C}}}{a\mu} \bar{E}_{\text{tr}}^{\text{C}} + \frac{a\sigma_{\text{R}}}{a\mu} \bar{E}_{\text{tr}}^{\text{R}} \\ &= \frac{139.60}{164.82} \times 56.86 \text{ keV} + \frac{13.93}{164.82} \times 6 \text{ keV} + \frac{11.29}{164.82} \times 0 = 48.7 \text{ keV}. \quad (8.115)\end{aligned}$$

(c) *Mean energy transfer fraction* \bar{f}_{tr} can be determined directly from (8.115) or through a weighted summation of transfer fractions for the individual effects that contribute to 60 keV photon interactions with copper absorber (T8.5)

$$\begin{aligned}\bar{f}_{\text{tr}} &= \frac{\bar{E}_{\text{tr}}}{h\nu} = \frac{48.7}{60} = 0.812 \equiv w_{\text{PE}} \bar{f}_{\text{PE}} + w_{\text{C}} \bar{f}_{\text{C}} + w_{\text{R}} \bar{f}_{\text{R}} \\ &= \frac{139.60}{164.82} \times \frac{56.86}{60} + \frac{13.93}{164.82} \times \frac{6}{60} = 0.812. \quad (8.116)\end{aligned}$$

(d) *Mass energy transfer coefficient* μ_{tr}/ρ is calculated from its basic definition as follows

$$\frac{\mu_{\text{tr}}}{\rho} = \bar{f}_{\text{tr}} \frac{\mu}{\rho} = 0.812 \times 1.562 \frac{\text{cm}^2}{\text{g}} = 1.268 \text{ cm}^2/\text{g}. \quad (8.117)$$

(e) *Mass energy absorption coefficient* μ_{ab}/ρ is in general given as (T8.14)

$$\frac{\mu_{\text{ab}}}{\rho} = \frac{\mu}{\rho} \frac{\bar{E}_{\text{ab}}}{h\nu} = \frac{\mu}{\rho} \frac{\bar{E}_{\text{tr}} - \bar{E}_{\text{rad}}}{h\nu} = \frac{\mu_{\text{tr}}}{\rho} (1 - \bar{g}) = \bar{f}_{\text{tr}} \frac{\mu}{\rho} (1 - \bar{g}), \quad (8.118)$$

where \bar{g} is the mean radiation fraction consisting of two main components: mean bremsstrahlung fraction \bar{g}_{B} and mean in-flight annihilation fraction \bar{g}_{A} . However,

here we are dealing with interaction of 60 keV photons with copper absorber and at this relatively low photon energy the mean radiation fraction \bar{g} is 0. This means that μ_{ab}/ρ is approximately equal to μ_{tr}/ρ , since essentially none of the energy transferred from photons to electrons in the copper absorber is re-emitted in the form of bremsstrahlung. We can thus conclude that all of the energy transferred to charged particles in the absorber is also absorbed in the absorber.

8.6.Q3**(195)**

Photons with energy $h\nu = 10$ MeV interact with carbon absorber. Mean energy \bar{E}_{tr} transferred from the photons to charged particles is 7.30 MeV; mean energy \bar{E}_{ab} absorbed by the carbon absorber is 7.06 MeV.

- (a) Based on these rudimentary data present a schematic diagram of the average interaction and fill-in as many missing links as you can.
- (b) Describe and evaluate the most probable events that lead to the mean values quoted above.

SOLUTION:

(a) The main steps in developing a picture of the 10-MeV-photon interaction with carbon absorber are as follows:

- (1) In the first approximation we assume that we are dealing with Compton effect (C) only and, based on their lower probabilities, we ignore the other possible photon interactions with carbon atoms, such as the photoelectric effect (PE) and pair production (PP). Thus, the incident photon energy $h\nu = 10$ MeV is shared between the recoil (Compton) electron kinetic energy $E'_K = 7.3$ MeV and the scattered (Compton) photon $h\nu' = h\nu - E'_K = 2.7$ MeV.
- (2) Before we can make a realistic diagram of the Compton interaction representing the 10 MeV photon interaction with carbon nuclei, we must know all parameters of the interaction: incident photon energy $E_\nu = h\nu$ and momentum p_ν , scattered photon energy $E'_\nu = h\nu'$ and momentum p'_ν , recoil electron kinetic energy E'_K and momentum p'_e , photon scattering angle θ , and electron recoil angle ϕ . We already have the three required energies: $E_\nu = 10$ MeV, $E'_\nu = 2.7$ MeV, and $E'_K = 7.3$ MeV.
- (3) The required photon momenta are determined as follows (T1.76)

$$p_\nu = \frac{E_\nu}{c} = 10 \text{ MeV}/c \quad \text{and} \quad p'_\nu = \frac{E'_\nu}{c} = 2.7 \text{ MeV}/c, \quad (8.119)$$

while the recoil electron momentum is determined using the standard p vs E'_K relationship (T1.64)

$$p'_e = \frac{E'_K}{c} \sqrt{1 + \frac{2E_0}{E'_K}} = \frac{7.3 \text{ MeV}}{c} \times \sqrt{1 + \frac{2 \times 0.511}{7.3}} = 7.8 \text{ MeV}/c. \quad (8.120)$$

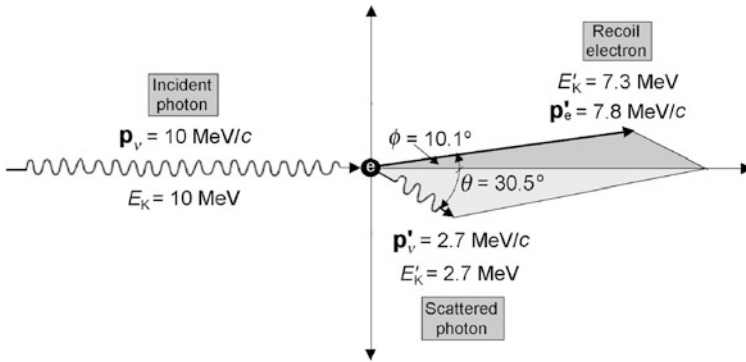


Fig. 8.16 Schematic diagram of the “first approximation (Compton effect)” to the 10 MeV photon interaction with carbon absorber

- (4) The photon scattering angle θ , corresponding to scattered photon energy $h\nu' = 2.7 \text{ MeV}$, is determined from the standard expression (T7.71) linking $h\nu'$, $h\nu$, and θ where ε is the incident photon energy normalized to electron rest energy $\varepsilon = h\nu/(m_e c^2) = 10/0.511 = 19.57$.

$$\frac{h\nu'}{h\nu} = \frac{1}{1 + \varepsilon(1 - \cos\theta)} \equiv a = \frac{2.7}{10} = 0.27. \quad (8.121)$$

Solving (8.121) for $\cos\theta$ gives

$$\cos\theta = \frac{a(\varepsilon + 1) - 1}{a\varepsilon} = \frac{0.27 \times (19.57 + 1) - 1}{0.27 \times 19.57} = 0.862 \quad (8.122)$$

and

$$\theta = \arccos 0.862 = 30.5^\circ. \quad (8.123)$$

- (5) The electron recoil angle ϕ , corresponding to electron recoil kinetic energy $E'_k = 7.3 \text{ MeV}$, is determined from the simple expression relating ϕ , θ , and ε as follows (T7.68)

$$\tan\phi = \frac{1}{1 + \varepsilon} \cot\frac{\theta}{2} = \frac{1}{1 + \varepsilon} \left(\tan\frac{\theta}{2} \right)^{-1} = \frac{1}{1 + 19.57} (\tan 15.25^\circ)^{-1} = 0.178 \quad (8.124)$$

or

$$\theta = \arctan 0.178 = 10.1^\circ. \quad (8.125)$$

- (6) We are now ready to plot the “first approximation” diagram of the 10 MeV photon interaction with carbon absorber. The plot is provided in Fig. 8.16 and shows a 10 MeV incident photon undergoing a Compton effect on a free and stationary electron. The electron recoils with kinetic energy $E'_k = 7.3 \text{ MeV}$ and the recoil angle ϕ is 10.1° . The photon is scattered with energy $h\nu' = 2.7 \text{ MeV}$ and the scattering angle θ is 30.5° .

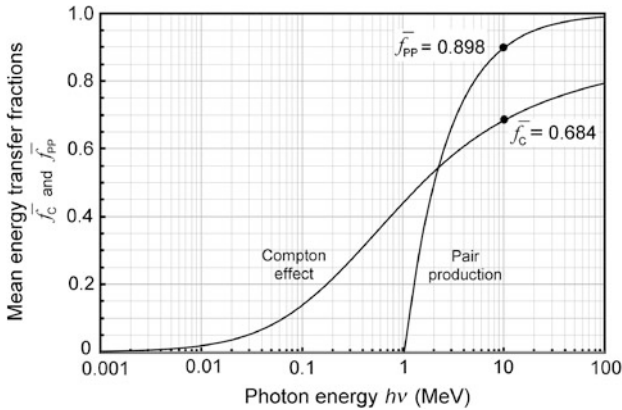


Fig. 8.17 Mean energy transfer fractions for Compton scattering and pair production \bar{f}_C and \bar{f}_{PP} , respectively, against incident photon energy $h\nu$. Mean transfer fraction for Compton effect is referred to as the “Compton Graph” because of its importance to radiation dosimetry. As highlighted in the graph, at $h\nu = 10$ MeV, $\bar{f}_C = 0.684$ and $\bar{f}_{PP} = 0.898$

(7) The released recoil electron with kinetic energy $E'_K = 7.3$ MeV travels through the carbon absorber and experiences Coulomb interactions with orbital electrons of carbon atoms resulting in collision loss and with nuclei of carbon atoms resulting in elastic scattering as well as some radiation loss. The collision loss is deposited locally in the absorber (7.06 MeV); radiation loss (bremsstrahlung) escapes from the absorber with energy of $(7.3 \text{ MeV} - 7.06 \text{ MeV} = 0.24 \text{ MeV})$.

(b) The basic picture of the 10 MeV photon interaction with carbon absorber is described in (a) and depicted schematically in Fig. 8.16; however, a closer look at possible interactions, in addition to Compton effect, reveals a much more elaborate and interesting picture.

- (1) For example, it is well known from the “Compton graph” (see Fig. 8.17) that the mean energy \bar{E}_{tr}^C transferred to Compton recoil electron from 10 MeV photons is 6.84 MeV. Since our problem states that the mean energy transferred from 10 MeV photons to charged particles (CPs) in carbon amounts to 7.3 MeV, it is obvious that there must be at least one more effect, in addition to Compton effect, that contributes to the energy transfer.
- (2) Recalling the diagram on the relative predominance of the three main photon interactions (PE, C, and PP) with matter and entering our point of ($h\nu = 10$ MeV, $Z = 6$) onto the graph, as shown in Fig. 8.18, reveals that the point clearly falls into the Compton domain of predominance, however, while we can ignore the PE probability, the point is relatively close to the 50-50 $\sigma_C = \kappa$ curve which defines equal weight for Compton effect and pair production (PP) suggesting that we should also consider the probability of PP, in addition to probability of C, to understand better the source of the 7.3 MeV mean energy transfer to charged particles.

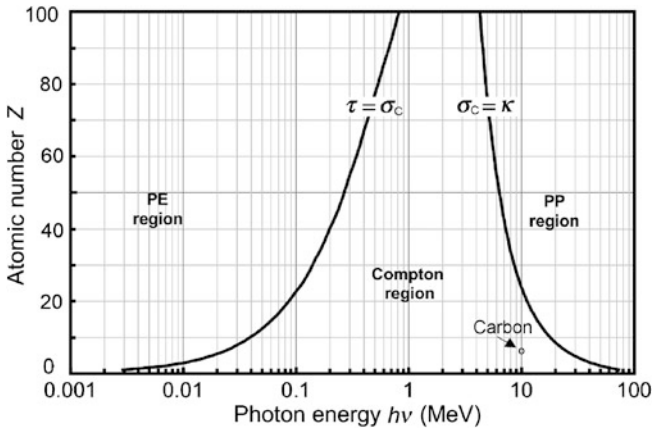


Fig. 8.18 Domains of relative predominance of the three main processes of photon interaction with absorber atom: photoelectric effect τ , Compton effect σ_C , and pair production κ in a $(h\nu, Z)$ graph where $h\nu$ is photon energy and Z is the absorber atomic number. The two curves in the graph connect points where photoelectric and Compton cross section are equal ($\tau = \sigma_C$) and points where Compton and pair production cross sections are equal ($\sigma_C = \kappa$)

- (3) In contrast to Compton effect where the mean energy transfer to CPs from 10 MeV photons is $\bar{E}_{tr}^C = 6.84$ MeV, in pair production the mean energy transfer \bar{E}_{tr}^{PP} is $h\nu - 2m_e c^2 = 8.98$ MeV, as also shown in Fig. 8.17.
- (4) The location of the point ($h\nu = 10$ MeV, $Z = 6$) in Fig. 8.18 suggests less than complete predominance of the Compton effect and a non-negligible contribution of pair production, so we now make a reasonable guess and assume the following weights of the two effects: $w_C \approx 0.80$ % and $w_{PP} \approx 20$ %. Using these weights we now estimate the following mean energy transferred from 10 MeV photons to CPs in carbon absorbers

$$\begin{aligned} \bar{E}_{tr} &= \sum_i w_i \bar{E}_{tr}^i = w_C \bar{E}_{tr}^C + w_{PP} \bar{E}_{tr}^{PP} \\ &= 0.80 \times 6.84 \text{ MeV} \times + 0.20 \times 8.98 \text{ MeV} = 7.27 \text{ MeV}, \quad (8.126) \end{aligned}$$

in good agreement with the value of 7.3 MeV quoted above, confirming the choice of weights we made with 80 % for Compton scattering and 20 % for pair production as reasonably good guess.

Mass attenuation coefficients σ_C/ρ and κ/ρ provided by the NIST are $1.539 \times 10^{-2} \text{ cm}^2/\text{g}$ and $0.421 \times 10^{-2} \text{ cm}^2/\text{g}$, respectively, resulting in weights w_C for Compton effect of 78.5 % and w_{PP} for pair production of 21.5 %. Our guess of 80 % Compton and 20 % pair production is thus in reasonably good agreement with the NIST. The NIST mass attenuation coefficients τ/ρ and σ_R/ρ are $5.059 \times 10^{-8} \text{ cm}^2/\text{g}$ and $3.853 \times 10^{-7} \text{ cm}^2/\text{g}$, respectively, substantiating our neglect of these two coefficients in comparison with Compton and pair production coefficients.

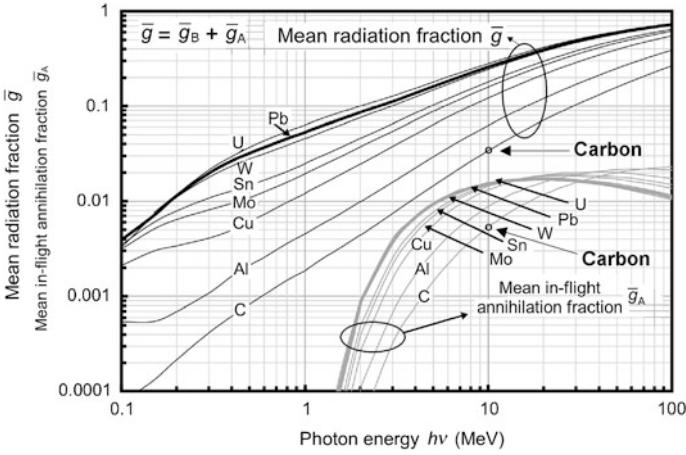


Fig. 8.19 Mean radiation fraction \bar{g} and mean in-flight annihilation fraction \bar{g}_A against photon energy $h\nu$ for eight selected absorbers including carbon. Data were calculated using the $g/EGSnrMP$ code obtained from the NRC, Ottawa. Mean radiation fractions \bar{g} and \bar{g}_A for 10 MeV photons are highlighted on the graphs

- (5) The next issue that we need to consider is the mean energy absorbed in carbon quoted above as \bar{E}_{ab} . In (a) we assumed the energy difference $\bar{E}_{tr} - \bar{E}_{ab}$ equal to 0.24 MeV is the mean energy \bar{E}_{rad} emitted by CPs in the form of bremsstrahlung. In the first approximation this is correct; however, the presence of pair production introduces positrons into the picture and positrons, as they travel through the absorber, may lose energy in the form of in-flight annihilation in addition to bremsstrahlung, so that the energy of 0.24 MeV should not be attributed only to bremsstrahlung, as was done in (a).
- (6) In Fig. 8.19 we show the mean radiation fraction \bar{g} (which is the sum of the mean bremsstrahlung fraction \bar{g}_B and the mean in-flight annihilation fraction \bar{g}_A) as well as the mean in-flight annihilation fraction \bar{g}_A against incident photon energy $h\nu$ for various absorbers including carbon. It is obvious that \bar{g}_A is a relatively small component of \bar{g} , making the mean bremsstrahlung fraction \bar{g}_B the predominant component of \bar{g} . From Fig. 8.19 we also note that \bar{g} at $h\nu = 10$ MeV is ~ 0.033 in good agreement with $\bar{E}_{rad} = 0.24$ MeV emitted in the form of radiation out of 7.3 MeV transferred to CPs since $\bar{g} = 0.24/7.3 = 0.033$. We also note that at $h\nu = 10$ MeV the in-flight annihilation fraction $\bar{g}_A \approx 0.0055$ and the bremsstrahlung fraction $\bar{g}_B \approx \bar{g} - \bar{g}_A = 0.033 - 0.0055 = 0.0275$, indicating that $\sim 17\%$ of $\bar{g} = 0.033$ is contributed by in-flight annihilation, while $\sim 83\%$ comes directly from the bremsstrahlung component. We thus conclude that the radiation loss of 0.24 MeV in the interaction of a 10 MeV photon with carbon 0.20 MeV escapes through bremsstrahlung and 0.04 through in-flight annihilation.

8.7 Sample Calculations

8.7.Q1

(196)

Diagram in Fig. 8.20 shows a simple Monte Carlo history of a 20 MeV photon in a water phantom that is divided into five volume elements (voxels), labeled A, B, C, D, and E. As a guide through various processes some photon energies $h\nu$ and charged particle kinetic energies E_K are given at interaction points (indicated by bullet points \bullet and identified by integer numbers 1 through 8) or at voxel boundaries (indicated by asterisks $*$).

- (a) Indicate and briefly describe interaction mechanisms occurring at interaction points labeled 1 through 8. For interactions [1] and [3], in addition to interaction energies, also determine angles θ and ϕ .
- (b) Determine energy E_{tr} transferred from photon to charged particles in voxels A, B, C, D, and E.
- (c) Determine net energy E_{tr}^{net} transferred from photon to charged particles in voxels A, B, C, D, and E.
- (d) Determine energy E_{ab} absorbed in voxels A, B, C, D, and E.

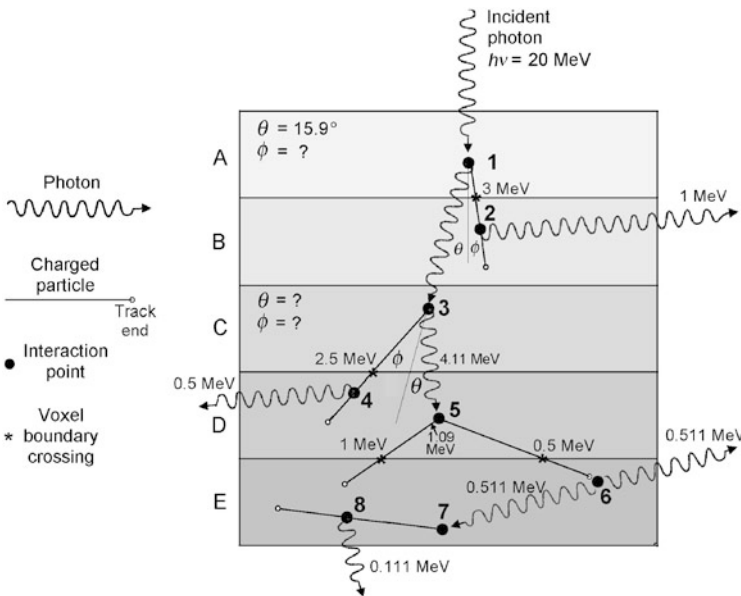


Fig. 8.20 A simple Monte Carlo history of a 20 MeV photon in a water phantom divided into five volume elements

SOLUTION:

(a) Analysis of a typical Monte Carlo history of a 20 MeV photon traversing a water phantom consisting of 5 volume elements (voxels).

Interaction [1]—Voxel A: Compton scattering

To make progress through the Monte Carlo history we need energy $h\nu'$ of the scattered photon, kinetic energy E_K of the Compton recoil electron, and recoil angle ϕ of the recoil electron.

- (1) Incident photon energy $h\nu$ is given as: $h\nu = 20$ MeV and $\varepsilon = \frac{h\nu}{m_e c^2} = \frac{20}{0.511} = 39.14$.
- (2) Scattering angle $\theta = 15.9^\circ$ (see diagram).
- (3) Scattered photon energy $h\nu'$ is calculated from the standard expression for $h\nu'$ as a function of incident photon energy $h\nu$ and scattering angle θ (T7.71)

$$h\nu' = \frac{h\nu}{1 + \varepsilon(1 - \cos\theta)} = \frac{20 \text{ MeV}}{1 + 39.14 \times (1 - \cos 15.9^\circ)} = 8 \text{ MeV}. \quad (8.127)$$

- (4) Recoil angle ϕ of the Compton recoil electron is calculated from (T7.67) as

$$\cot \phi = \frac{1}{\tan \phi} = (1 + \varepsilon) \tan \frac{\theta}{2} = (1 + 39.14) \times \tan 7.95^\circ = 5.61 = \frac{1}{0.1784} \quad (8.128)$$

and

$$\phi = \arctan 0.1784 = 10.11^\circ. \quad (8.129)$$

- (5) Kinetic energy E_K of the recoil electron is the energy transferred from the photon to charged particles (recoil electron in Compton scattering) and is determined from the principle of energy conservation as energy difference between incident $h\nu$ and scattered $h\nu'$ photon

$$E_K = h\nu - h\nu' = 20 \text{ MeV} - 8 \text{ MeV} = 12 \text{ MeV}. \quad (8.130)$$

The recoil electron in traversing voxel A loses 9 MeV through collision loss in voxel A and enters voxel B with kinetic energy $E_K = 3$ MeV.

Interaction [2]—Voxel B: Radiation loss (bremsstrahlung photon with $h\nu = 1$ MeV)

Recoil electron, produced in interaction [1], enters voxel B with kinetic energy $E_K = 3$ MeV and loses all of this energy in voxel B: 2 MeV in collision loss with orbital electrons in voxel B that contributes to absorbed energy E_{ab} in voxel B and 1 MeV in radiation loss (bremsstrahlung) that escapes voxel B and the water phantom.

Interaction [3]—Voxel C: Compton scattering

- (1) Incident photon energy $h\nu = 8 \text{ MeV}$ or $\varepsilon = h\nu/(m_e c^2) = 8/0.511 = 15.66$ (from interaction [1]).
- (2) Scattered photon energy $h\nu' = 4.11 \text{ MeV}$ (see diagram).
- (3) Scattering angle θ is calculated from (8.127) linking incident photon energy $h\nu$ and the scattered photon energy $h\nu'$ and scattering angle θ

$$h\nu' = \frac{h\nu}{1 + \varepsilon(1 - \cos\theta)} \quad \text{or} \quad \cos\theta = 1 - \frac{1}{\varepsilon} \left(\frac{h\nu}{h\nu'} - 1 \right) \quad (8.131)$$

resulting in the following expression for scattering angle θ as a function of $h\nu$ and $h\nu'$

$$\begin{aligned} \theta &= \arccos \left[1 - \frac{1}{\varepsilon} \left(\frac{h\nu}{h\nu'} - 1 \right) \right] = \arccos \left[1 - \frac{1}{15.66} \left(\frac{8}{4.11} - 1 \right) \right] \\ &= \arccos 0.94 = 20^\circ. \end{aligned} \quad (8.132)$$

- (4) Recoil electron angle ϕ is calculated from standard expression linking ϕ and θ (T7.67)

$$\cot\phi = \frac{1}{\tan\phi} = (1 + \varepsilon) \tan \frac{\theta}{2} = (1 + 15.66) \tan 10^\circ = 2.94 = \frac{1}{0.34} \quad (8.133)$$

resulting in

$$\phi = \arctan 0.34 = 18.79^\circ. \quad (8.134)$$

- (5) Recoil electron kinetic energy E_K , similar to (8.130), is given as

$$E_K = h\nu - h\nu' = 8 \text{ MeV} - 4.11 \text{ MeV} = 3.89 \text{ MeV}. \quad (8.135)$$

This is the energy transferred from photon to charged particles (electron) in voxel C. The recoil electron, produced in interaction [3], loses 1.39 MeV (3.89 MeV – 2.5 MeV) through collision loss in voxel C and enters voxel D with kinetic energy $E_K = 2.5 \text{ MeV}$, as indicated in the diagram. Energy 1.39 MeV is deposited (absorbed) in voxel C.

Interaction [4]—Voxel D: Radiation loss (bremsstrahlung photon with $h\nu = 0.5 \text{ MeV}$)

Recoil electron, produced in interaction [3], enters voxel D with kinetic energy $E_K = 2.5 \text{ MeV}$. It loses 0.5 MeV through radiation loss (bremsstrahlung) in interaction [4] in voxel D. This bremsstrahlung photon escapes from voxel D and the water phantom and the rest of recoil electron's kinetic energy (2 MeV) is lost through collision loss that is deposited (absorbed) in voxel D.

Interaction [5]—Voxel D: Nuclear pair production

- (1) Scattered photon of energy $h\nu = 4.11$ MeV, originating in interaction [3], undergoes nuclear pair production in voxel D. Photon disappears and an electron–positron pair with combined kinetic energy E_K of 3.09 MeV is created. Note: 1.02 MeV of the incident photon energy of 4.11 MeV is used up for creation of the electron–positron pair (materialization) and the rest (4.11 MeV $-$ 1.02 MeV $=$ 3.09 MeV) goes into combined kinetic energy of the electron and positron. Thus, the energy transferred from photon to charged particles (electron and positron) in interaction 5 is 3.09 MeV. As shown on the diagram, the electron of the electron–positron pair receives kinetic energy of $E_K = 1.09$ MeV, which means that the positron received the difference between 3.09 MeV and 1.09 MeV, i.e., $E_K = 2$ MeV.
- (2) Kinetic energy $E_K = 1.09$ MeV of the pair production electron is lost through collision loss, of this 0.09 MeV is lost in voxel D and 1 MeV in voxel E.
- (3) The positron also loses all of its kinetic energy (2 MeV) through collision loss: 1.5 MeV is lost and absorbed in voxel D and 0.5 MeV in voxel E.

Interaction [6]—Voxel E: Positron annihilation

Positron produced in interaction [5] receives kinetic energy 2 MeV, travels through voxels D and E, and loses all of its kinetic energy through collision loss. This energy of 2 MeV is thus absorbed in voxels D and E; 1.5 MeV in voxel D and 0.5 MeV in voxel E. When the positron reaches zero kinetic energy in voxel E, it annihilates with a “free and stationary” electron in interaction [6] and two annihilation quanta, each of energy 0.511 MeV are produced travelling in opposite directions to one another. One of the two annihilation quanta escapes voxel E as well as water phantom, the other annihilation quantum has interaction [7] in voxel E.

Interaction [7]—Voxel E: Photoelectric effect

The photoelectric effect between the annihilation quantum of energy 0.511 MeV and a low atomic number atom in the water phantom results in photon disappearance and emission of an orbital electron referred to as a photoelectron. The binding energy of the emitted orbital electron is negligible in comparison to the 0.511 MeV energy of the annihilation quantum, so that one can assume that the photoelectron kinetic energy is ~ 0.511 MeV and that the energy transferred from photon to charged particles (photoelectron in this case) is 0.511 MeV.

Interaction [8]—Voxel E: Radiation loss (bremsstrahlung photon with $h\nu = 0.111$ MeV)

Photoelectron, released in interaction [7] with kinetic energy of 0.511 MeV, travels through voxel E and loses its kinetic energy through collision loss as well as radiation loss through production of a bremsstrahlung photon of energy 0.111 MeV

in interaction [8]. The bremsstrahlung photon escapes voxel E as well as the water phantom. The collision loss of the photoelectron amounts to 0.4 MeV (0.511 MeV – 0.111 MeV) and is absorbed in voxel E.

(b) Energy transferred from photons to charged particles (electrons and positrons) E_{tr} in a given voxel of the water phantom

Voxel A—Interaction [1]: Kinetic energy of Compton electron $E_K = E_{tr} = 12$ MeV.

Voxel B—No energy transfer from photons to charged particles; $E_{tr} = 0$.

Voxel C—Interaction [3]: Kinetic energy of Compton electron $E_K = E_{tr} = 3.89$ MeV.

Voxel D—Interaction [5]: Kinetic energy of electron–positron pair $E_K = E_{tr} = 3.09$ MeV.

Voxel E—Interaction [7]: Kinetic energy of photoelectron $E_K = E_{tr} \approx 0.511$ MeV.

(c) Net energy transferred from photons to charged particles E_{tr}^{net} in a given voxel of the water phantom is defined as energy transferred E_{tr} to charged particles less energy subsequently lost by these charged particles in radiation collisions E_{rad} , such as production of bremsstrahlung (for electrons and positrons) or in-flight annihilation (for positrons). Thus, $E_{tr}^{net} = E_{tr} - E_{rad}$, irrespective of where the radiation loss occurs.

Voxel A—Interaction [1]: Compton electron is released with kinetic energy $E_K = 12$ MeV, however, it subsequently loses $E_{rad} = 1$ MeV of energy to bremsstrahlung production. Thus, net energy transfer is given as follows: $E_{tr}^{net} = E_{tr} - E_{rad} = 12$ MeV – 1 MeV = 11 MeV.

Voxel B—No net energy transfer from photons to charged particles, since $E_{tr} = 0$.

Voxel C—Interaction [3]: Compton electron is released with kinetic energy $E_K = 3.89$ MeV but it subsequently loses $E_{rad} = 0.5$ MeV of energy to bremsstrahlung production. Thus we have $E_{tr}^{net} = E_{tr} - E_{rad} = 3.89$ MeV – 0.5 MeV = 3.39 MeV.

Voxel D—Interaction [5]: Electron–pair is created and released with combined kinetic energy $E_K = E_{tr} = 3.09$ MeV. Since neither the electron nor the positron lose any of their kinetic energy through radiation loss, we have $E_{tr}^{net} = E_{tr} = 3.09$ MeV.

Voxel E—Interaction [7]: Photoelectron is released with kinetic energy $E_K = E_{tr} \approx 0.511$ MeV, but it subsequently loses $E_{rad} = 0.111$ MeV to bremsstrahlung production. Thus, we get $E_{tr}^{net} = E_{tr} - E_{rad} \approx 0.511$ MeV – 0.111 MeV = 0.4 MeV.

(d) Energy absorbed E_{ab} in a given voxel of the water phantom

Voxel A—Compton electron, released in interaction [1] with kinetic energy of 12 MeV, travels through voxels A and B. It crosses the boundary between voxels A and B with a kinetic energy of 3 MeV which means that it lost 9 MeV through collision loss in voxel A. This also indicates that $E_{ab} = 9$ MeV in voxel A.

Table 8.8 Summary of results for the simple Monte Carlo history depicted in Fig. 8.20

Voxel	A	B	C	D	E
E_{tr}	12 MeV	0	3.89 MeV	3.09 MeV	0.511 MeV
$E_{\text{tr}}^{\text{net}}$	11 MeV	0	3.39 MeV	3.09 MeV	0.4 MeV
E_{ab}	9 MeV	2 MeV	1.39 MeV	3.59 MeV	0.9 MeV

Voxel B—Compton electron, released in voxel A in interaction 1 arrives at the boundary between voxels A and B with kinetic energy of 3 MeV. Since its track ends in voxel B and it loses 1 MeV to bremsstrahlung, we conclude that $E_{\text{ab}} = 2$ MeV for voxel B.

Voxel C—Compton electron released with $E_{\text{K}} = 3.89$ MeV in interaction [3] in voxel C travels from voxel C to voxel D and crosses the boundary with a kinetic energy of 2.5 MeV. This means that it lost $(3.89 \text{ MeV} - 2.5 \text{ MeV}) = 1.39$ MeV through collision loss in voxel C and this energy was absorbed in voxel C as $E_{\text{ab}} = 1.39$ MeV.

Voxel D—Compton electron from interaction [3] enters voxel D with kinetic energy of 2.5 MeV. It loses this energy in voxel D mainly through collision loss of 2 MeV, absorbed in voxel D and contributing to E_{ab} in voxel D, and radiation loss of 0.5 MeV in interaction [4]. In voxel D we also have interaction [5] that releases an electron–positron pair with kinetic energy of 3.09 MeV. Both electron and positron travel across the boundary between voxels D and A, crossing the boundary with $E_{\text{K}} = 1$ MeV for the electron and $E_{\text{K}} = 0.5$ MeV for the positron. Since in interaction [5] the electron was released with $E_{\text{K}} = 1.09$ MeV and the positron with $E_{\text{K}} = 2$ MeV, we conclude that the electron lost 0.09 MeV through collision loss in voxel D, while the positron lost 1.5 MeV through collision loss in voxel D. We thus get $E_{\text{ab}} = 2 \text{ MeV} + 0.09 \text{ MeV} + 1.5 \text{ MeV} = 3.59 \text{ MeV}$, with 2 MeV contributed by the Compton electron produced in interaction [3] (that entered voxel D with energy 2.5 MeV and lost 0.5 MeV to bremsstrahlung), 0.09 MeV contributed by the pair production electron produced in interaction [5] (that was released with energy 1.09 MeV and left voxel D with energy 1 MeV), and 1.5 MeV contributed by the pair production positron produced in interaction [5] (that was released with energy 2 MeV and left voxel D with energy 0.5 MeV).

Voxel E—Positron from interaction [5] enters voxel E with $E_{\text{K}} = 0.5$ MeV and loses all of this energy through collision loss before interaction [6]. It thus contributes 0.5 MeV to E_{ab} in voxel E. Photoelectron is released with kinetic energy of 0.511 MeV in interaction [8]. It loses 0.111 MeV of kinetic energy through radiation (bremsstrahlung loss) and 0.4 MeV through collision loss that is absorbed in voxel E. We thus have $E_{\text{ab}} = 0.9$ MeV consisting of 0.5 MeV of absorbed energy from the positron of interaction [5] and 0.4 MeV from the photoelectron of interaction [7].

A summary of (b), (c), and (d) is provided in Table 8.8.

8.7.Q2

(197)

Diagram in Fig. 8.21 shows a simple Monte Carlo history of a 15 MeV photon in a water phantom that is divided into three volume elements (voxels), labeled A, B, and C. As a guide through various processes some photon energies $h\nu$ and charged particle kinetic energies E_K are given at interaction points (indicated by bullet points \bullet and identified by integer numbers 1 through 7) or at voxel boundaries (indicated by asterisks $*$).

- (a) Indicate and briefly describe interaction mechanisms occurring at interaction points labeled 1 through 7. For interactions [4] and [5], in addition to interaction energies, also determine angles θ and ϕ .
- (b) Determine energy E_{tr} transferred from photon to charged particles in voxels A, B, and C.
- (c) Determine net energy E_{tr}^{net} transferred from photon to charged particles in voxels A, B, and C.
- (d) Determine energy E_{ab} absorbed in voxels A, B, and C.

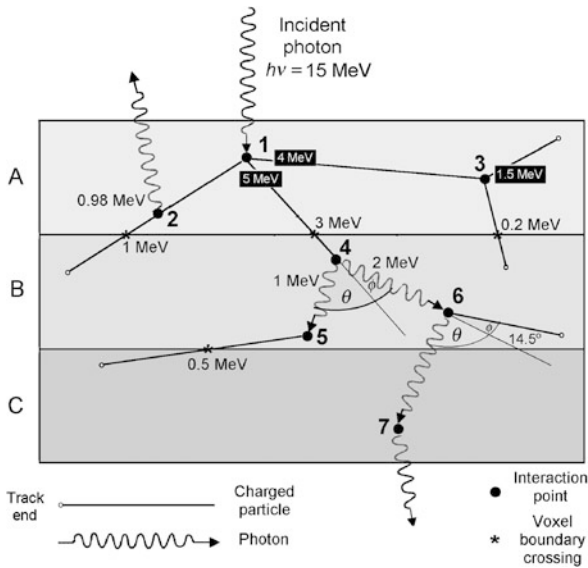


Fig. 8.21 Typical Monte Carlo history of a 15 MeV photon striking a water phantom divided into three voxels: A, B, and C

SOLUTION:

(a) Analysis of a typical Monte Carlo history of a 15 MeV photon traversing a water phantom consisting of 3 volume elements (voxels).

Interaction [1]—Voxel A: Triplet production also known as electronic pair production

At interaction point [1] the incident 15 MeV-photon interacts with the electric field of an orbital electron. The photon disappears and 1.02 MeV of its energy is used up in the creation of an electron–positron pair. The remaining photon energy of 13.98 MeV ($15 \text{ MeV} - 1.02 \text{ MeV}$) is transferred to three charged particles released in the triplet interaction: orbital electron that enabled the pair production process in its Coulomb field and the electron–positron pair (i.e., electron and positron) produced by the electronic pair production interaction.

As shown in the diagram, initial kinetic energies of two of the three charged particles of the triplet are 4 MeV and 5 MeV. This means that the third charged particle receives the remaining available energy of 4.98 MeV, making the kinetic energy that is transferred to charged particles equal to 13.98 MeV. Since, as evident from the diagram, the 4 MeV and the 4.98 MeV charged particles do not annihilate with an orbital electron in their path, we conclude that the charged particle of the triplet with initial kinetic energy of 5 MeV must be the positron.

Interaction [2]—Voxel A: Radiation loss (bremsstrahlung photon with $h\nu = 0.98 \text{ MeV}$)

Electron released in interaction [1] with kinetic energy of 4.98 MeV travels through voxel A and loses energy mainly through collision interactions with orbital electrons of the absorber. However, at interaction point [2] the electron experiences an inelastic collision with a nucleus of the absorber and loses 0.98 MeV of energy to a bremsstrahlung photon, which leaves voxel A as well as the water phantom. After the radiation loss at point [2] the electron continues losing energy through collision losses, crosses the boundary between voxels A and B with kinetic energy $E_K = 1 \text{ MeV}$ and then loses all of this energy in voxel B. Total collision loss of the 4.98 MeV electron is thus 4 MeV ($4.98 \text{ MeV} - 0.98 \text{ MeV}$); of this, collision loss is 3 MeV in voxel A and 1 MeV in voxel B. These collision losses contribute to the absorbed energy in a given voxel.

Interaction [3]—Voxel A: Hard electron-electron collision

The 4 MeV electron produced in interaction [1] travels through voxel A and loses the major part of its energy in voxel A through collision loss with orbital electrons and through a hard electron-electron collision at interaction point [3] where a δ electron with kinetic energy of 1.5 MeV is released. The δ electron travels through voxel A and loses all of its kinetic energy through collision losses in voxel A. The original electron continues its path through voxel A, crosses the boundary between voxels A and B with kinetic energy of 0.2 MeV and loses this energy through collision loss in voxel B.

Interaction [4]—Voxel B: In-flight annihilation of the positron

Positron receiving kinetic energy of 5 MeV at interaction point [1] travels through voxel A and loses energy through collision loss with orbital electrons and enters voxel B with kinetic energy of 3 MeV. Thus, it loses 2 MeV of its kinetic energy in voxel A.

After crossing the boundary between voxels A and B the positron travels through voxel B and undergoes collision losses until at interaction point [4] it experiences in-flight annihilation with an orbital electron of the absorber. As shown in the diagram, two photons are produced in the in-flight annihilation process: one with energy $h\nu_1 = 1$ MeV and the other with energy $h\nu_2 = 2$ MeV.

- (1) In order to determine angles θ and ϕ with respect to the positron trajectory we must calculate the kinetic energy of the positron at the interaction point [4]. We do this by invoking the conservation of total energy principle for the in-flight annihilation process recalling that: Total energy before annihilation = Total energy after annihilation, or

$$E_K^{e^+} + m_{e^+}c^2 + m_{e^-}c^2 = h\nu_1 + h\nu_2. \quad (8.136)$$

We thus have the following expression for kinetic energy of the positron before in-flight annihilation

$$\begin{aligned} E_K^{e^+} &= h\nu_1 + h\nu_2 - m_{e^+}c^2 - m_{e^-}c^2 \\ &= (1 + 2 - 0.511 - 0.511) \text{ MeV} + 1.98 \text{ MeV}. \end{aligned} \quad (8.137)$$

- (2) From the three equations for conservation of total energy and momentum one can derive the following implicit expressions for angles ϕ and θ ((T7.215) and (T7.216), respectively) containing the ratio of the two photon energies $h\nu_1$ and $h\nu_2$ as well as parameters E and A

$$\frac{h\nu_1}{h\nu_2} = \frac{E^2 + A^2 - 2EA \cos \phi}{E^2 - A^2} = \frac{E^2 - A^2}{E^2 + A^2 - 2EA \cos \theta}, \quad (8.138)$$

where parameters E and A are defined as follows

$$E = E_K^{e^+} + 2m_e c^2 \quad \text{and} \quad A = E_K^{e^+} \sqrt{1 + \frac{2m_e c^2}{E_K^{e^+}}}. \quad (8.139)$$

In (8.137) we determined the kinetic energy of the positron at the time of in-flight annihilation as $E_K^{e^+} = 1.98$ MeV and this results in $E = 3$ MeV and $A = 2.44$ MeV for the two parameters of (8.139).

- (3) Annihilation quantum emission angles θ and ϕ , respectively, are determined from (8.138) as follows

$$\begin{aligned}\theta &= \arccos \frac{E^2 + A^2 - (E^2 - A^2) \frac{h\nu_2}{h\nu_1}}{2EA} \\ &= \arccos \frac{[3^2 + 2.44^2 - (3^2 - 2.44^2) \times 2]}{2 \times 3 \times 2.44} \\ &= \arccos \frac{8.862}{14.64} = \arccos 0.605 = 52.75^\circ\end{aligned}\quad (8.140)$$

and

$$\begin{aligned}\phi &= \arccos \frac{E^2 + A^2 - (E^2 - A^2) \frac{h\nu_1}{h\nu_2}}{2EA} \\ &= \arccos \frac{[3^2 + 2.44^2 - (3^2 - 2.44^2) \times 0.5]}{2 \times 3 \times 2.44} \\ &= \arccos \frac{13.431}{14.64} = \arccos 0.917 = 23.45^\circ.\end{aligned}\quad (8.141)$$

Interaction [5]—Voxel B: Photoelectric effect

The 1 MeV annihilation quantum $h\nu_1$ produced at interaction point [4] propagates through voxel B and interacts at interaction point [5] with an orbital electron through photoelectric effect. The interaction results in photon $h\nu_1$ disappearance and the orbital electron is emitted as photoelectron with kinetic energy that is essentially equal to the photon energy of 1.0 MeV, since the binding energy of the orbital electron in water is negligible in comparison to the energy of the photon. The 1 MeV electron travels through voxel B, crosses the boundary between voxels B and C with kinetic energy of 0.5 MeV, and finally stops in voxel C. In its track, the 1 MeV photoelectron loses all of its energy through collision losses, half in voxel B and the remaining half in voxel C.

Interaction [6]—Voxel B: Compton scattering

The 2 MeV annihilation quantum $h\nu_2$ produced at interaction point [4] propagates through voxel B and interacts at interaction point [6] with an orbital electron through Compton scattering. To make progress through the Monte Carlo history we need energy $h\nu'$ of the scattered photon, kinetic energy E_K of the Compton recoil electron, and angle θ of the scattered photon $h\nu'$ with respect to the incident photon $h\nu$.

- (1) For interaction point [6] incident photon energy $h\nu$ is given as: $h\nu = 2.0$ MeV and parameter $\varepsilon = h\nu/(m_e c^2) = 2/0.511 = 3.914$.
- (2) Recoil electron angle $\phi = 14.5^\circ$ (see diagram).
- (3) Scattered photon angle θ is calculated from (T7.67) as

$$\tan \frac{\theta}{2} = \frac{1}{1 + \varepsilon} \cot \phi = \frac{1}{1 + 3.914} \cot 14.5^\circ = 0.787 \quad \text{or} \quad (8.142)$$

$$\theta = 2 \times \arctan 0.787 = 76.4^\circ.$$

- (4) Scattered photon energy $h\nu'$ is determined using the standard expression for $h\nu'$ as a function of incident photon energy $h\nu$ and scattering angle θ (T7.71)

$$h\nu' = \frac{h\nu}{1 + \varepsilon(1 - \cos \theta)} = \frac{2.0 \text{ MeV}}{1 + 3.914 \times (1 - \cos 76.4^\circ)} = 0.5 \text{ MeV}. \quad (8.143)$$

- (5) Kinetic energy E_K of the recoil electron is the energy transferred from the photon to charged particles (recoil electron in Compton scattering) and is determined from the principle of energy conservation as energy difference between incident $h\nu$ and scattered photon $h\nu'$

$$E_K = h\nu - h\nu' = 2.0 \text{ MeV} - 0.5 \text{ MeV} = 1.5 \text{ MeV}. \quad (8.144)$$

The recoil electron loses all of its energy of 1.5 MeV in voxel B through collision loss with orbital electrons of absorber atoms.

Interaction [7]—Voxel C: Rayleigh scattering

The scattered photon, produced in interaction [6] with energy $h\nu = 0.5$ MeV, enters voxel C and undergoes a Rayleigh scattering interaction with an atom at interaction point [7]. No energy is transferred to charged particles in Rayleigh scattering and the energy of the scattered photon $h\nu'$ is essentially equal to the energy of the incident photon $h\nu$. The Rayleigh-scattered photon with energy 0.5 MeV escapes voxel C and the water phantom.

(b) Energy transferred from photons to charged particles (electrons and positrons) E_{tr} in a given voxel of the water phantom:

Voxel A—Interaction [1]: Kinetic energy of the electron–positron pair and the orbital electron which enabled the triplet production process $E_{tr} = 15 \text{ MeV} - 1.02 \text{ MeV} = 13.98 \text{ MeV}$.

Voxel B—Interactions [5] and [6]: Kinetic energies of the photoelectron (1 MeV) and the Compton electron (1.5 MeV) result in $E_{tr} = 1 \text{ MeV} + 1.5 \text{ MeV} = 2.5 \text{ MeV}$.

Voxel C—No energy transferred from photons to electrons in voxel C, resulting in $E_{tr} = 0$.

(c) Net energy transferred from photons to charged particles E_{tr}^{net} in a given voxel of the water phantom is defined as energy transferred E_{tr} to charged particles

less energy subsequently lost by these charged particles in radiation collisions E_{rad} , such as production of bremsstrahlung (for electrons and positrons) or in-flight annihilation (for positrons). Thus, $E_{\text{tr}}^{\text{net}} = E_{\text{tr}} - E_{\text{rad}}$ irrespective of where the radiation loss occurs.

Voxel A—Interaction [1]: Three charged particles are released with a combined energy of $E_{\text{tr}} = 13.98$ MeV.

- (1) The 4.98 MeV electron loses $E_{\text{rad}} = 0.98$ MeV of energy to bremsstrahlung production at interaction point [2] resulting in net energy transfer of $(4.98 \text{ MeV} - 0.98 \text{ MeV}) = 4$ MeV.
- (2) The positron loses part of its initial kinetic energy of 5 MeV through in-flight annihilation process in voxel B at interaction point [4]. Since the in-flight annihilation occurs when the positron has kinetic energy of 1.98 MeV (see discussion in (a) for interaction point [4]), we conclude that the net energy transfer for the positron is 3.02 MeV $(5 \text{ MeV} - 1.98 \text{ MeV})$.
- (3) Total net energy transfer $E_{\text{tr}}^{\text{net}}$ in voxel A accounting for the three charged particles released in triplet production at interaction point [1] is $E_{\text{tr}}^{\text{net}} = E_{\text{tr}} - E_{\text{rad}}$ where $E_{\text{tr}} = 13.98$ MeV from (b) and E_{rad} is energy that the electron loses to bremsstrahlung at interaction point [2] plus kinetic energy of the positron (1.98 MeV) at interaction point [4] where the positron undergoes in-flight annihilation. Thus, $E_{\text{tr}}^{\text{net}} = 13.98 \text{ MeV} - (0.98 + 1.98) \text{ MeV} = 11.02$ MeV.

Voxel B—Energy transferred to the photoelectron in interaction [5] as well as energy transferred to the Compton electron in interaction [6] is lost in collision losses only, thus, $E_{\text{rad}} = 0$. Therefore, the net energy transferred $E_{\text{tr}}^{\text{net}}$ is equal to energy transferred E_{tr} , i.e., $E_{\text{tr}}^{\text{net}} = E_{\text{tr}} = 1 \text{ MeV} + 1.5 \text{ MeV} = 2.5$ MeV.

Voxel C—No net energy transfer from photons to charged particles, since there is no energy transfer from photons to charged particles in voxel C, i.e., $E_{\text{tr}}^{\text{net}} = E_{\text{tr}} = 0$.

(d) Energy absorbed E_{ab} in a given voxel of the water phantom

Voxel A—At interaction point [1] in voxel A three charged particles (2 electrons and a positron) are released with a combined kinetic energy of 13.98 MeV.

- (1) The 4 MeV triplet electron loses 3.8 MeV in voxel A through collision losses resulting in a 3.8 MeV energy deposition in voxel A. At interaction point [3] the electron has a hard collision with an orbital electron that is ejected as a δ ray that deposits all of its kinetic energy of 1.5 MeV in voxel A. The δ ray energy forms part of the 3.8 MeV energy deposited by the 4 MeV electron in voxel A.
- (2) The 5 MeV triplet positron travels through voxel A, loses kinetic energy through collision losses, and reaches the boundary between voxels A and B with kinetic energy 3 MeV. This means that it lost 2 MeV in voxel A and thus contributes 2 MeV to the absorbed energy in voxel A.

- (3) The 4.98 MeV triplet electron travels through voxel A and reaches the boundary between voxels A and B with a kinetic energy of 1 MeV. Of the 3.98 MeV energy that it lost in voxel A, 0.98 MeV is through radiation collision at interaction point [2] and 3 MeV is through collision losses. The contribution of this electron to total energy absorption in voxel A is thus 3 MeV.

Total contribution to absorbed energy in voxel A from charged particles is thus equal to

$$E_{ab} = 3.8 \text{ MeV} + 2 \text{ MeV} + 3 \text{ MeV} = 8.8 \text{ MeV}.$$

Voxel B—Several electrons and a positron contribute to energy deposition in voxel B.

- (1) The two electrons that are produced at interaction point [1] in voxel A enter voxel B with a combined energy of 1.2 MeV that is deposited completely in voxel B.
- (2) The positron produced at interaction point [1] enters voxel B with kinetic energy of 3.0 MeV of which 1.02 MeV is deposited in voxel B and the remaining 1.98 MeV is used up for production of two annihilation quanta ($h\nu_1 = 1 \text{ MeV}$ and $h\nu_2 = 2 \text{ MeV}$) in in-flight annihilation of the positron with $E_K = 1.98 \text{ MeV}$.
- (3) One of the annihilation quanta ($h\nu_1$) undergoes photoelectric effect at interaction point [5] in voxel B and the photoelectron is released with kinetic energy of $\sim 1 \text{ MeV}$. The photoelectron loses all of its kinetic energy through collision losses, 0.5 MeV in voxel B and 0.5 MeV in voxel C.
- (4) The $h\nu_2 = 2 \text{ MeV}$ annihilation quantum undergoes Compton effect at interaction point [6] in voxel B and releases a Compton electron of kinetic energy of 1.5 MeV. The Compton electron loses all of its kinetic energy in voxel B through collision losses.

The absorbed energy in voxel B is thus a sum of contributions from: (1) Electrons released in interaction [1] (1.2 MeV); (2) Positron produced in interaction [1] (1.02 MeV); (3) Photoelectron released in interaction [5] (0.5 MeV); and (4) Compton recoil electron released in interaction [6] (1.5 MeV). Thus, absorbed energy in voxel B is:

$$E_{ab} = 1.2 \text{ MeV} + 1.02 \text{ MeV} + 0.5 \text{ MeV} + 1.5 \text{ MeV} = 4.22 \text{ MeV}.$$

Voxel C—The photoelectron produced in interaction [5] enters voxel C with a kinetic energy of 0.5 MeV and loses all of this energy through collision losses in voxel C. Therefore, the absorbed energy in voxel C is $E_{ab} = 0.5 \text{ MeV}$.

A summary of (b), (c), and (d) is provided in Table 8.9 and Fig. 8.22.

Table 8.9 Summary of energy transferred E_{tr} , net energy transferred E_{tr}^{net} , and energy absorbed E_{ab} for 15 MeV photon striking a water phantom divided into voxels A, B, and C

Voxel	A	B	C
E_{tr}	13.98 MeV	2.5 MeV	0
E_{tr}^{net}	11.02 MeV	2.5 MeV	0
E_{ab}	8.8 MeV	4.22 MeV	0.5 MeV

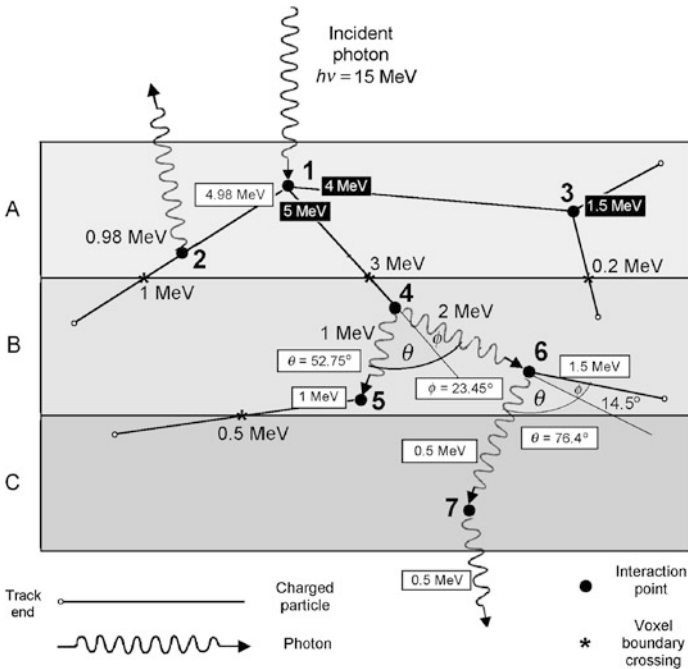


Fig. 8.22 Summary of calculations of Monte Carlo history for 15 MeV photon striking a water phantom consisting of three voxels: A, B, and C. The interaction points marked with ● are as follows: [1] Triplet production, [2] Radiation loss (bremsstrahlung), [3] Hard electron-electron collision, [4] In-flight annihilation, [5] Photoelectric effect, [6] Compton scattering, [7] Rayleigh scattering

Chapter 9 consists of **13 problems** covering 6 sections that deal with various aspects of neutron interactions with matter. Neutrons, by virtue of their neutrality, are considered indirectly ionizing radiation that exhibits a quasi exponential penetration into the absorber and deposits energy in an absorber through a two-step process: (1) energy transfer to heavy charged particles and (2) energy deposition in the absorber through Coulomb interactions of these charged particles with atoms of the absorber. As they penetrate into the absorber, neutrons may undergo elastic and inelastic scattering as well as trigger nuclear reactions, such as neutron capture, spallation, and fission.

Two distinct categories of neutron are of direct importance in medical physics: (1) thermal neutrons used in boron neutron capture therapy (BNCT) and (2) fast neutrons used in external beam radiotherapy. Indirectly, thermal neutrons also play an important role in production of radionuclide sources for use in external beam radiotherapy, in remote afterloading brachytherapy, and nuclear medicine imaging. A nuclear reactor and two types of thermal neutron interaction are used for production of radioactive sources: (1) neutron activation of suitable target material and (2) fission reaction induced by thermal neutron in fissile target material.

Section 9.1 presents long questions on general aspects of neutron interactions with absorber nuclei and Sect. 9.2 deals with various processes by which neutrons interact with nuclei of the absorber, such as elastic, inelastic, and non-elastic scattering as well as neutron capture, spallation, and fission.

Section 9.3 presents a problem on neutron kerma and Sect. 9.4 presents a problem on the neutron kerma factor. Section 9.5 introduces two problems on neutron dose deposition in tissue by thermal neutrons, intermediate neutrons, and fast neutrons. The last section (Sect. 9.6) provides problems on the use of neutrons in medicine either (1) for boron neutron capture therapy (BNCT), (2) production of fast neutron beams for radiotherapy, or (3) use of neutron emitters in brachytherapy.

9.1 General Aspects of Neutron Interactions with Absorbers

9.1.Q1

(198)

Neutrons, like photons, belong to the category of indirectly ionizing radiation. Used in science, industry, and medicine, they come in a wide spectrum of kinetic energy E_K^n , ranging from 10^{-8} eV for ultra-cold neutrons up to few GeV for relativistic cosmic neutrons. Neutrons transfer energy to absorbing medium through an intermediate step in which energy is transferred from the neutron to a charged particle which in turn transfers energy to the absorber medium through Coulomb interactions between the liberated charged particle and orbital electrons of the absorber. Thus, energy deposition in absorber by a neutron beam occurs through secondary charged particles, such as protons, α -particles, and recoiling nuclei. As they penetrate into absorbing medium, neutrons may undergo elastic, inelastic, or non-elastic scattering or they may trigger nuclear reactions, such as neutron capture, spallation, and fission.

Two distinct categories of neutrons are of direct importance in medical physics:

- (1) Thermal neutrons used in boron-neutron capture therapy (BNCT).
- (2) Fast neutrons used in external beam radiotherapy and brachytherapy.

Indirectly, thermal neutrons play an important role in production of radionuclide sources that are used in external beam radiotherapy, brachytherapy, and nuclear medicine imaging. In neutron dosimetry three regions of neutron kinetic energy are of importance: thermal, intermediate, and fast neutron region.

-
- (a) Discuss the basic properties of neutrons relevant to the use of neutrons in medicine for diagnosis (imaging) and therapy (radiotherapy) of disease.
 - (b) Calculate the velocity of neutrons with kinetic energy E_K of 10^{-7} eV (ultra-cold neutron), 10^{-4} eV (cold neutron), 0.025 eV (thermal neutron), 1 MeV (fast neutron), 14.1 MeV (fast neutron from d-t reaction), 100 MeV (cosmic neutron) and 1 GeV (cosmic neutron).

SOLUTION:

- (a) Basic properties of neutrons with emphasis on use in medicine.
 - (1) Neutron is a subatomic particle in the family of hadrons, composed of three quarks and exhibiting strong interaction with other hadrons.
 - (2) Ernest Rutherford in 1920 postulated the existence of the neutron and William Chadwick in 1932 discovered it at the University of Cambridge in the U.K.

- (3) The symbol for the neutron is n or n^0 . It possesses no electric charge and its rest mass m_n is slightly larger than that of the proton.
Rest mass of neutron: $m_n = 939.6 \text{ MeV}/c^2$; rest mass of proton: $m_p = 938.3 \text{ MeV}/c^2$.
- (4) Neutron is stable when it is bound in atomic nucleus; however, a free (extra-nuclear) neutron is unstable (radioactive) and decays through β^- decay into a proton, electron, and electronic antineutrino ($n^0 \rightarrow p^+ + e^- + \bar{\nu}_e$) with a mean lifetime $\tau \approx 14.9 \text{ min}$ or half-life $t_{1/2} = \tau \ln 2 \approx 10.3 \text{ min}$. In unstable nuclei that harbor an excess number of neutrons, neutron can also decay through β^- decay, however, the half life of this β^- decay is a characteristic of the decaying nucleus and different from that of the free neutron.
- (5) Free neutrons easily pass through atoms, because they have no electrical charge, thereby forming highly penetrating, indirectly ionizing, radiation beams that interact with matter only through direct collisions with nuclei of absorber atoms. Interactions of neutrons with orbital electrons of absorber atoms are generally not of any importance and are thus ignored.
- (6) Neutron detection is more complex than detection of directly ionizing charged particles and indirectly ionizing photons. Most common methods for detection of neutrons rely on neutron capture (neutron absorption) by the nucleus of an absorber atom or on elastic scattering of neutrons off nuclei of absorber.
- (7) The secondary charged particles released by fast neutrons in the absorbing medium produce a dose build-up similar to that that occurs in megavoltage photon beams. The depth of dose maximum z_{\max} of a clinical fast neutron beam depends on the energy and spectrum of the beam and for a source-surface distance of 100 cm and field size of $10 \times 10 \text{ cm}^2$ is of the order from 0.5 cm to 1.5 cm. Beyond z_{\max} there is a continuous quasi-exponential fall-off in the dose with increasing depth in water as a result of:
- (i) Attenuation of the neutron beam by absorbing medium (water).
 - (ii) Increase in distance from the source (inverse square law).

In contrast to megavoltage x-ray beams, the field size of neutron beams has a significant effect on depth dose characteristics because of the high probability for neutron scattering within the neutron beam.

- (8) Fast neutron beams are significantly more complex and more expensive to use in radiotherapy than are megavoltage x-ray beams, yet, from a physics point-of-view, they produce no better dose distributions than do megavoltage x-ray beams. However, from a radiobiological point-of-view, fast neutrons offer a distinct advantage over megavoltage x-ray beams because of the so-called oxygen enhancement ratio (OER) which amounts to 3 for x rays while it is much closer to 1 for fast neutron beams.

It turns out that the presence of oxygen in a cell acts as a radiosensitizer, making radiation more damaging for a given delivered dose. Since tumor cells are typically poorly oxygenated (tumor hypoxia) in comparison to normal cells, a given dose of x rays causes more damage to well oxygenated normal cells than to hypoxic tumor cells. Thus, in comparison to normal tissue, the oxygen effect decreases the sensitivity of tumor tissue to megavoltage x rays

Table 9.1 Results of calculation of neutron velocity v against kinetic energy E_K for neutrons ranging in kinetic energy from 10^{-7} eV to 1 GeV. Velocities in bold face are calculated with the relativistic equation (9.2) while velocities in standard font are calculated for comparison purposes with the classical equation (9.1)

(1)	Neutron	Kinetic energy E_K	$\frac{v}{c}$ (classical)	$\frac{v}{c}$ (relativistic)	$v(\frac{m}{s})$
(2)	Ultra-cold	10^{-7} eV	1.46×10^{-8}	–	4.4
(3)	Cold	10^{-4} eV	4.61×10^{-7}	–	138.4
(4)	Thermal	0.025 eV	7.29×10^{-6}	–	~ 2200
(5)	Fast	1 MeV	0.04614	0.04610	$\sim 1.38 \times 10^7$
(6)	Fast	14.1 MeV	0.1732	0.1713	$\sim 5.14 \times 10^7$
(7)	Cosmic	100 MeV	0.4614	0.4279	$\sim 1.28 \times 10^8$
(8)	Cosmic	1 GeV	–	0.8748	$\sim 2.62 \times 10^8$

and decreases the tumor control probability. It is generally believed that fast neutron irradiation overcomes this effect, because the OER of fast neutrons is much smaller than that of megavoltage x rays.

- (9) For use in radiotherapy, neutron beams are produced either with a cyclotron or a neutron generator. In a cyclotron protons or deuterons are accelerated to kinetic energies of 50 MeV to 80 MeV and strike a thick beryllium target to produce fast neutrons that are collimated into a clinical neutron beam. The neutron beam produced with a beryllium target has beam penetration and build-up characteristics similar to those of 4 MV to 10 MV megavoltage x-ray beams. In a neutron generator deuterons (d) are accelerated to 250 keV and strike a tritium (t) target to produce a 14.1 MeV neutron beam with depth dose characteristics similar to those obtained for a cobalt-60 teletherapy γ -ray beam.

- (b) Velocity of a neutron with a given kinetic energy E_K and rest energy $m_n c^2 = 939.6$ MeV is calculated from the classical expression for kinetic energy (T2.5)

$$E_K = \frac{m_n v^2}{2} = \frac{m_n c^2}{2} \left(\frac{v}{c} \right)^2 \quad \text{or} \quad \frac{v}{c} = \sqrt{\frac{2E_K}{m_n c^2}} \quad (9.1)$$

for relatively slow neutrons with velocity $v < 0.01c$ and from the relativistic expression for E_K (T2.7)

$$E_K = m_n c^2 \left(\frac{1}{\sqrt{1 - \frac{v^2}{c^2}}} - 1 \right) \quad \text{or} \quad \frac{v}{c} = \sqrt{1 - \frac{1}{\left(1 + \frac{E_K}{m_n c^2}\right)^2}} \quad (9.2)$$

for fast neutrons with velocity $v > 0.01c$.

Results of our neutron velocity calculations are displayed in Table 9.1 and plotted in Fig. 9.1 in the form of $\log v/c$ against $\log E_K$ which appears to follow a power

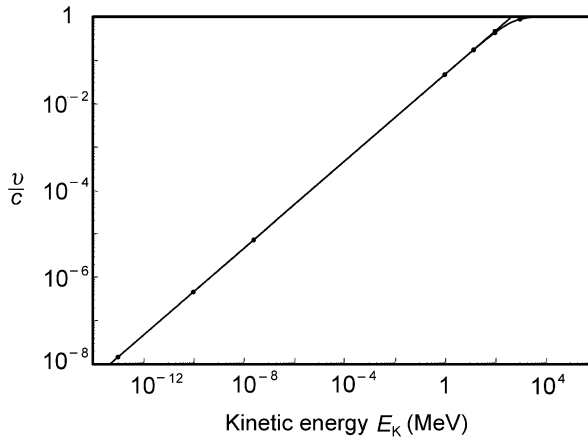


Fig. 9.1 Normalized velocity v/c against neutron kinetic energy E_K

function of exponent $1/2$ [classical expression (9.1)], except for saturation occurring at very high (relativistic) kinetic energies where (9.2) must be used and (9.1) is no longer applicable.

9.1.Q2

(199)

Neutrons are classified, similarly to x rays and γ rays, as indirectly ionizing radiation that deposits energy in absorbing medium through an intermediate step involving release of secondary charged particles in the attenuating medium. Whereas photons interact with atomic electrons and release electrons and positrons in the attenuating medium, neutrons interact with nuclei of the attenuator and release nuclear particles, such as protons, deuterons, α particles, and heavier nuclear recoils.

- Define neutron fluence ϕ and neutron fluence rate (neutron flux density) $\dot{\phi}$.
- Define total microscopic neutron cross section σ and total macroscopic cross section Σ .
- Describe attenuation of a collimated neutron beam in attenuating medium.
- Define the mean free path Λ of neutrons and reaction rate \dot{R} of neutrons.
- A lead attenuator (atomic number $Z = 82$, mass density $\rho = 11.3 \text{ g/cm}^3$, atomic weight $A = 207.2 \text{ g/mol}$) of thickness $z = 2 \text{ cm}$ attenuates a collimated neutron beam of kinetic energy $E_K^n = 10 \text{ MeV}$ from neutron fluence rate $\dot{\phi} = 2 \times 10^{12} \text{ cm}^{-2} \cdot \text{s}^{-1}$ to a fluence rate of $\dot{\phi} = 1.43 \times 10^{12} \text{ cm}^{-2} \cdot \text{s}^{-1}$. For this neutron beam interacting with lead attenuator calculate:

- (1) Total macroscopic cross section Σ .
- (2) Total microscopic cross section σ .
- (3) Mean free path Λ .
- (4) Neutron reaction rate \dot{R} at a depth of 1 cm in lead attenuator.

SOLUTION:

(a) Neutron fluence φ and neutron fluence rate $\dot{\varphi}$ are two basic physical quantities used for describing neutron beams and neutron fields. A neutron radiation field is established by neutron sources in conjunction with an attenuating medium that causes absorption as well as scattering of neutrons.

- (1) Neutron fluence φ , according to the ICRU, is defined as the quotient of ΔN by Δa or $\varphi = \Delta N / \Delta a$, with ΔN the number of particles that enter a sphere of cross sectional area Δa .
- (2) Neutron fluence rate or neutron flux density $\dot{\varphi}$, in addition to neutron kinetic energy E_K , is a convenient parameter used for describing the presence of free neutrons in an attenuating medium. Several closely related definitions of neutron fluence rate (neutron flux) are in use:
 - (i) According to the ICRU, neutron fluence rate $\dot{\varphi}$ is the quotient of $\Delta\varphi$ by Δt where $\Delta\varphi$ is the increment of neutron fluence in the time interval Δt ;
 - (ii) Fluence rate $\dot{\varphi}$ is also defined as the number of neutrons passing through a particular cross sectional area in any direction per unit time; and
 - (iii) Fluence rate $\dot{\varphi}$ is the product of neutron velocity v and neutron density (number of free neutrons per unit volume of the attenuator) n given as $\dot{\varphi} = nv$.

Typical unit of neutron fluence φ is cm^{-2} , expressing number of neutrons per cm^2 . Typical unit of neutron fluence rate or flux density $\dot{\varphi}$ is $\text{cm}^{-2} \cdot \text{s}^{-1}$, expressing number of neutrons per cm^2 per second.

(b) Neutrons being uncharged particles interact with nuclei of attenuating media through direct collisions rather than via Coulomb interactions. Many modes of interaction between incident neutron and nuclei of attenuating medium are available to a neutron propagating through an attenuating medium.

- (1) *Total microscopic cross sections.* The probability of a given type of interaction i is expressed in terms of a microscopic cross section σ_i for the given target nucleus. For a given target nucleus and a given neutron kinetic energy E_K^n a set of partial microscopic cross sections σ_i is usually available for the various possible interaction modes i . At a given E_K^n and target nucleus, the sum $\sum_i \sigma_i$ is referred to as the total microscopic cross section σ . Units of microscopic cross sections are cm^2/atom , m^2/atom , and barns per atom (b/atom).

- (2) *Total macroscopic cross section* Σ for a given attenuating medium is obtained by multiplying the total microscopic cross section σ (sum of all relevant partial microscopic cross sections) with the atomic density n^\square

$$\Sigma = n^\square \sigma \quad (\text{in units of cm}^{-1} \text{ or m}^{-1}), \quad (9.3)$$

with the atomic density n^\square defined as the number of atoms or nuclei N_a per volume \mathcal{V} of the attenuator

$$n^\square = \frac{N_a}{\mathcal{V}} = \rho \frac{N_a}{m} = \rho \frac{N_A}{A} \quad (\text{in units of cm}^{-3} \text{ or m}^{-3}), \quad (9.4)$$

where N_A is the Avogadro number ($6.022 \times 10^{23} \text{ mol}^{-1}$), ρ is mass density of the attenuator, and A is the atomic weight or atomic mass number in g/mol.

Like the microscopic cross section σ , the macroscopic cross section Σ depends on neutron kinetic energy E_K^n and physical properties of the attenuating medium. Relationship (9.4) is similar to the relationship in photon interactions with matter where the linear attenuation coefficient μ for a given photon interaction is a product of the atomic attenuation coefficient (also known as atomic cross section) ${}_a\mu$ and the atomic density n^\square or $\mu = n^\square {}_a\mu$.

- (c) Just as the linear attenuation coefficient μ is used for description of photon beam attenuation in attenuating medium, so is the macroscopic cross section Σ used for describing *attenuation of collimated neutron beams* in attenuating medium. The decrease in beam intensity dI is proportional to the neutron beam intensity I , microscopic cross section σ of the attenuator, atomic density n^\square of attenuator, and thickness dx of the attenuating medium

$$dI = -I\sigma n^\square dx = -I\Sigma dx \quad \text{or} \quad I = I_0 e^{-\Sigma x}, \quad (9.5)$$

where Σ is the macroscopic cross section of the attenuating medium for neutrons with kinetic energy E_K^n .

- (d) Macroscopic quantities: cross section Σ , mean free path Λ , and reaction rate \dot{R} of neutrons traversing an attenuating medium depend upon atomic density n^\square of the attenuating medium and kinetic energy E_K^n of the incident neutron.

- (1) Similarly to mean free path of photons, the *mean free path* Λ of neutrons is defined as that thickness Λ of attenuator that attenuates the neutron intensity I from original intensity I_0 to I_0/e or, expressed mathematically, we can say

$$I(\Lambda) = \frac{I_0}{e} = 0.368 I_0 = I_0 e^{-\Sigma \Lambda} \quad \text{or} \quad e^{-1} = e^{-\Sigma \Lambda} \quad \text{or} \quad \Lambda = \frac{1}{\Sigma}. \quad (9.6)$$

Mean free path Λ also is a measure of the mean distance that a neutron of given kinetic energy travels through a given attenuating medium before interacting with a nucleus. This definition is similar to the definition of mean free path \bar{x} of photons in attenuating medium, where $\bar{x} = 1/\mu$ with μ the linear attenuation coefficient.

- (2) *Reaction rate* \dot{R} between neutrons and nuclei of attenuator is defined as the product of the macroscopic cross section Σ and neutron fluence rate $\dot{\phi}$ or

$$\dot{R} = \Sigma \dot{\phi} = (n^{\square} \Sigma)(n\nu), \quad (9.7)$$

indicating that the reaction rate \dot{R} is linearly proportional to the atomic density n^{\square} , microscopic cross section σ , neutron density n , and velocity of neutrons ν . From (9.7) we note that the unit of reaction rate \dot{R} is $\text{cm}^{-3} \cdot \text{s}^{-1}$.

- (e) Attenuation of a collimated neutron beam in an attenuator is expressed as

$$I = I_0 e^{-\Sigma x}, \quad (9.8)$$

where I_0 and I are the incident fluence rate ($2 \times 10^{12} \text{ cm}^{-2} \cdot \text{s}^{-1}$) and transmitted fluence rate ($1.43 \times 10^{12} \text{ cm}^{-2} \cdot \text{s}^{-1}$), respectively, and Σ is the macroscopic cross section. Based on (9.8) and data provided on lead we now calculate:

- (1) Total macroscopic cross section Σ .
- (2) Total microscopic cross section σ .
- (3) Mean free path Λ .
- (4) Neutron reaction rate \dot{R} at a depth of 1 cm in lead attenuator.

- (1) Solving (9.8) for Σ we get the following result for the macroscopic cross section Σ

$$\Sigma = \frac{1}{x} \ln \frac{I_0}{I} = \frac{1}{(2 \text{ cm})} \ln \frac{2 \times 10^{22}}{1.43 \times 10^{22}} = 0.168 \text{ cm}^{-1}. \quad (9.9)$$

- (2) Next we calculate the microscopic cross section σ using (9.4) as follows

$$\begin{aligned} \sigma &= \frac{\Sigma}{n^{\square}} = \frac{A \Sigma}{\rho N_A} = \frac{(207.2 \text{ g} \cdot \text{mol}^{-1}) \times (0.168 \text{ cm}^{-1})}{(11.3 \text{ g/cm}^3) \times (6.022 \times 10^{23} \text{ mol}^{-1})} \\ &= 5.12 \times 10^{-24} \text{ cm}^{-2}/\text{atom} = 5.12 \text{ b/atom}. \end{aligned} \quad (9.10)$$

- (3) Mean free path Λ is calculated using (9.6) as follows

$$\Lambda = \frac{1}{\Sigma} = \frac{1}{0.168 \text{ cm}^{-1}} = 5.95 \text{ cm}. \quad (9.11)$$

This means that a 10 MeV neutron travels on average about 6 cm in lead before it experiences one of the possible nuclear interactions with a lead nucleus of the attenuator.

- (4) Reaction rate \dot{R} of a neutron beam is, according to (9.7), expressed as $\dot{R} = \Sigma \dot{\phi}$, where Σ is the total macroscopic cross section determined in (9.9)

as $\Sigma = 0.168 \text{ cm}^{-1}$ and $\dot{\phi}$ is the fluence rate at depth of $x = 1 \text{ cm}$ in lead determined from (9.5) as follows

$$\begin{aligned} I(x = 1 \text{ cm}) &= I_0 e^{-\Sigma x} = (2 \times 10^{12} \text{ cm}^{-2} \cdot \text{s}^{-1}) e^{-(0.168 \text{ cm}^{-1}) \times (1 \text{ cm})} \\ &= 1.69 \times 10^{12} \text{ cm}^{-2} \cdot \text{s}^{-1}. \end{aligned} \quad (9.12)$$

Reaction rate \dot{R} at a depth of $x = 1 \text{ cm}$ in lead is now calculated as

$$\dot{R} = \Sigma \dot{\phi} = (0.168 \text{ cm}^{-1}) \times (1.69 \times 10^{12} \text{ cm}^{-2} \cdot \text{s}^{-1}) = 2.84 \times 10^{12} \text{ cm}^{-3} \cdot \text{s}^{-1}. \quad (9.13)$$

9.2 Neutron Interactions with Nuclei of the Absorber

9.2.Q1

(200)

Neutrons by virtue of being neutral particles can approach a target nucleus without any interference from a Coulomb repulsive or attractive force, since they, unlike protons and electrons, are not affected by nuclear charge. Once in close proximity to the target nucleus, neutrons can interact with it through the short-range attractive nuclear forces and trigger various nuclear reactions.

- (a) List and briefly describe at least 5 principal processes by which neutrons interact with nuclei of an absorber.
- (b) Provide a list and a brief description of the best-known neutron sources of use in medicine and of importance in medical physics.

SOLUTION:

(a) Six **principal processes** by which neutrons interact with nuclei of the absorber are:

- (1) Elastic scattering.
- (2) Inelastic scattering.
- (3) Non-elastic scattering.
- (4) Neutron capture.
- (5) Spallation.
- (6) Fission.

A brief description of each of these neutron interactions is as follows:

(1) *Elastic scattering* of neutron on absorber nucleus is the most important process for slowing down neutrons. The neutron collides with a nucleus of mass M that recoils with an angle ϕ with respect to the neutron initial direction of motion and

the neutron is scattered by a scattering angle θ . Total energy and momentum are conserved in the elastic scattering interaction which means that kinetic energy lost by the neutron is equal to recoil energy of the target nucleus. The lighter is the target nucleus, the larger is the energy transfer from the neutron to the nucleus in an elastic scattering process; however, the target nucleus remains in the ground state.

(2) *Inelastic scattering* of neutron with absorber nucleus is similar to elastic scattering except that some of neutron's kinetic energy is transferred to the nucleus not only to manifest itself as nuclear recoil kinetic energy but also to raise the nucleus from the ground state to an excited state. The nucleus de-excites by emitting high-energy γ rays and the neutron is scattered and moves on with kinetic energy that is lower than its incident energy. For inelastic scattering to occur, kinetic energy of the incident neutron must exceed the excitation energy of the nucleus. In contrast to elastic scattering, inelastic scattering is a threshold process and, when it occurs, neutron loses more energy in inelastic than in an elastic collision with absorber nucleus in order to account for the energy of the emitted γ ray. Therefore, only fast neutrons undergo inelastic scattering.

(3) *Non-elastic scattering* is in certain respect similar to inelastic scattering except that the secondary particle that is emitted is not a neutron. On the other hand, non-elastic scattering can also be considered neutron capture, except that the term neutron capture usually applies to capture of thermal neutron while non-elastic scattering typically deals with fast neutrons. An example of non-elastic scattering is

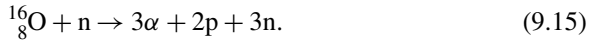


(4) *Neutron capture* is a term used to describe a nuclear reaction in which a thermal neutron collides with a target nucleus leading to neutron absorption in the target nucleus, formation of a new nuclide of different atomic mass number and/or atomic number from those of the target nucleus, and emission of a proton [(n, p) reaction: neutron capture with particle emission] or gamma ray [(n, γ) reaction: neutron capture with emission of γ radiation] in the process. Neutron capture, even after an immediate emission of a particle or γ ray, often results in an unstable radionuclide which decays with its own half-life that can range from a fraction of a second to many years depending on the nature of the neutron capture product. The majority of artificial radionuclides produced during the past decades have been discovered by means of thermal neutron capture in stable samples placed into nuclear fission reactors. When neutron capture is used for production of radionuclides or for analysis of trace elements in material samples, it is usually referred to as neutron activation instead of neutron capture.

(5) *Spallation* is defined as fragmentation of a target into many smaller components as a result of impact or stress. Consequently, nuclear spallation is defined as disintegration of a target nucleus into many small residual components such as α particles and nucleons (protons and neutrons) upon bombardment with a suitable

projectile such as light or heavy ion beams or neutrons. Nuclear spallation can also occur naturally in earth's atmosphere as a result of exposure of nuclides to energetic cosmic rays such as protons.

An example of spallation is as follows



Most of the energy released in the spallation process is carried away by the heavier fragments that deposit their energy in the absorber locally. On the other hand, neutrons and de-excitation γ rays produced in spallation carry their energy to a remote location. Spallation can be used for production of radionuclides and for generation of intense neutron beams in spallation neutron generators.

(6) *Fission* is a particular type of neutron interaction produced by bombardment of certain very high atomic number nuclei ($Z \geq 92$) by thermal or fast neutrons. The target nucleus fragments into two daughter nuclei of lighter mass and the fission process is accompanied with production of several fast neutrons. Nuclei that are capable of undergoing fission are called fissionable nuclei in general; nuclei that undergo fission with thermal neutrons are called fissile nuclei. Fission fragments combined with the nuclei that are subsequently formed through radioactive decay of fission fragments are called fission products.

(b) Neutron source is defined as a device that emits mono-energetic neutrons or a spectrum of neutrons. A wide variety of neutron sources are available ranging from small, encapsulated sources through particle accelerators and neutron generators to nuclear fission reactors.

(1) *Nuclear fission reactor* is the most abundant source of neutrons producing neutrons with an energy spectrum in the range from a few keV to over 10 MeV and average neutron energy of 2 MeV. Neutrons produced in research nuclear reactors are used for neutron scattering experiments, non-destructive testing, production of radionuclides for use in science, industry and medicine, and on a limited scale have been and still are also used in boron neutron capture therapy.

(2) *Particle accelerators* generate neutron beams by means of nuclear reactions with accelerated projectiles (protons or deuterons) striking a suitable target (typically of low atomic number) resulting in a product nucleus and a mono-energetic neutron beam. Best-known nuclear reactions for neutron production with neutron generators are exothermic reactions ${}^3_1\text{H}(d, n){}^4_2\text{He}$ with a Q value of 17.6 MeV and ${}^2_1\text{H}(d, n){}^3_2\text{He}$ with a Q value of 3.3 MeV. Cyclotron-produced fast neutrons rely on acceleration of protons to about 50 MeV and directing them onto a beryllium target in which fast neutrons are produced for use in radiotherapy. Most intense pulsed neutron beams for industrial research are produced by spallation neutron sources that are accelerator based.

(3) *Radioactive neutron sources* are produced by means of mixing an α emitter (such as radium-226 or americium-241) with a light metal (such as beryllium or boron) in powder form and encapsulating the mixture to make a neutron source generating neutrons through (α, n) reactions. The source intensity is governed by the half-life of the α emitter and the energy spectrum of emitted neutrons is continuous with maximum energy equal to the sum of the reaction Q value and kinetic energy of the α particle striking the nucleus.

(4) *Photoneutron sources* make use of photonuclear (γ, n) reactions and use mixtures of a mono-energetic γ emitter with beryllium metal. Photonuclear sources with mono-energetic γ emitters produce mono-energetic neutrons in contrast to (α, n) neutron sources that produce a spectrum of neutrons because of the random energy degradation of the α particles before they interact with the nucleus. The intensity of the photonuclear sources is governed by the half-life of the γ emitter component of the neutron source.

(5) *Spontaneous fission neutron sources* contain encapsulated high atomic number elements that undergo spontaneous fission and emit neutrons in the process. The best-known example of an intense spontaneous neutron fission source is californium-252 that was found useful in a wide range of specialized areas of science, industry, and medicine, such as the study of fission, neutron activation analysis, neutron radiography, well logging, nuclear reactor start up, and brachytherapy.

9.2.Q2

(201)

Elastic scattering of neutrons interacting with atomic nuclei of absorber is the most probable interaction of neutrons with absorbing medium for neutrons with kinetic energy $E_K \leq 2$ MeV. The other possible interactions are inelastic scattering, neutron capture, spallation, and fission. In the energy range below 10 MeV the elastic scattering of neutrons can be treated classically, as shown schematically in Fig. 9.2 for two-particle elastic collision between projectile m_1 (neutron) moving with velocity v_1 and a stationary target m_2 (nucleus of absorber), with θ the scattering angle of the projectile, ϕ the recoil angle of the target, and b the so-called impact parameter. After collision projectile m_1 continues with velocity u_1 and the target recoils with velocity u_2 .

- (a) Use the classical principles of energy and momentum conservation to derive an expression for energy transfer ΔE_K from the projectile m_1 to the stationary target m_2 in laboratory coordinate system.
- (b) Using the general expression for ΔE_K derived in (a), express ΔE_K for the specific example of neutron elastic scattering on a nucleus of the absorbing medium. Also state the energy transfer fraction f_{tr} , maximum energy transfer fraction $(f_{tr})_{max}$, and mean energy transfer fraction \bar{f}_{tr} for elastic scattering of neutrons on target nuclei of atomic mass A .

- (c) Using the expression derived in (b) for kinetic energy transfer ΔE_K from $\overline{neutron}$ to target nucleus in elastic scattering, determine mean energy $\overline{\Delta E_K}$ transferred from neutron to target nucleus in elastic scattering.
- (d) Determine an expression for mean energy $\overline{E_K^n}$ that a neutron carries from an elastic scattering event with target nucleus of atomic weight A . Calculate post-elastic scattering neutron kinetic energy as a fraction of incident neutron energy $(E_K^n)_0$ for the following target nuclei: hydrogen ($A = 1$), cadmium ($A = 112$), and uranium ($A = 238$).

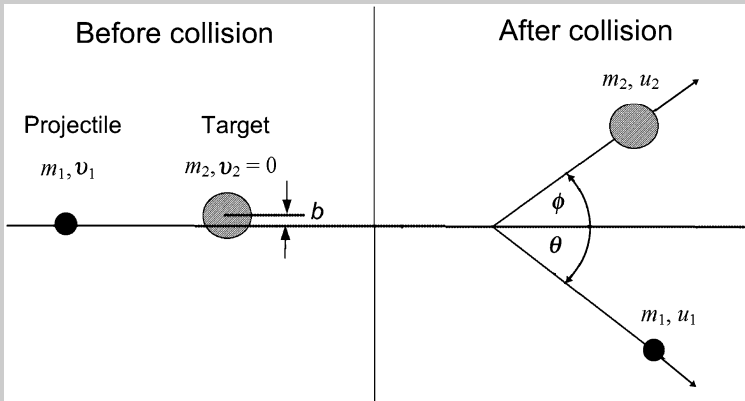


Fig. 9.2 Schematic diagram of an elastic collision between a projectile with mass m_1 and velocity v_1 striking a stationary target m_2 . Projectile is scattered with a scattering angle θ , target recoils with recoil angle ϕ , and the impact parameter is b . After the collision the velocity of the projectile is u_1 and the velocity of the recoiling target is u_2

SOLUTION:

(a) The kinetic energy transfer ΔE_K from projectile m_1 to the target m_2 is determined classically in laboratory coordinate system using the conservation of energy and momentum laws as follows (see Fig. 9.2):

(1) Conservation of kinetic energy:

$$(E_K)_0 + 0 = \frac{1}{2}m_1v_1 + 0 = \frac{1}{2}m_1u_1 + \frac{1}{2}m_2u_2, \tag{9.16}$$

where $(E_K)_0$ is the kinetic energy of the projectile (incident particle) m_1 .

(2) Conservation of momentum along abscissa (x) axis (note: the incident particle is moving along the abscissa axis in the positive direction):

$$m_1v_1 = m_1u_1 \cos \theta + m_2u_2 \cos \phi. \tag{9.17}$$

(3) *Conservation of momentum along ordinate (y) axis:*

$$0 = m_1 u_1 \sin \theta - m_2 u_2 \sin \phi. \quad (9.18)$$

Equations (9.17) and (9.18) can, respectively, be written as follows

$$(m_1 v_1 - m_2 u_2 \cos \phi)^2 = (m_1 u_1 \cos \theta)^2 \quad (9.19)$$

and

$$(m_1 u_1 \sin \theta)^2 \equiv m_1^2 u_1^2 - m_1^2 u_1^2 \cos^2 \theta = (m_2 u_2 \sin \phi)^2. \quad (9.20)$$

Inserting (9.19) into (9.20) gives the following expression

$$m_2^2 u_2^2 = m_1^2 u_1^2 - m_1^2 v_1^2 + 2m_1 v_1 m_2 u_2 \cos \phi, \quad (9.21)$$

which, after inserting (9.16) multiplied by $2m_1$, reads

$$m_2^2 u_2^2 = 2m_1 v_1 m_2 u_2 \cos \phi - m_1 m_2 u_2^2 \quad (9.22)$$

or

$$2m_1 v_1 \cos \phi = (m_1 + m_2) u_1. \quad (9.23)$$

Since $\Delta E_K = \frac{1}{2} m_2 u_2^2$ [i.e., energy transfer ΔE_K from the projectile (incident particle) m_1 with kinetic energy $(E_K)_0$ to the target of mass m_2 is equal to recoil energy of the target $\frac{1}{2} m_2 u_2^2$], we get the following general expression for energy transfer ΔE_K

$$\Delta E_K = \frac{4m_1 m_2}{(m_1 + m_2)^2} (E_K)_0 \cos^2 \phi, \quad (9.24)$$

showing that the energy ΔE_K transferred from the projectile to the recoiling target is governed by the recoil angle ϕ . With regard to recoil angle ϕ there are two special angles to consider:

- (1) In an elastic, head-on collision, the recoil angle ϕ of the target is zero and ΔE_K attains its maximum value $(\Delta E_K)_{\max}$ for given projectile mass m_1 , target mass m_2 , and kinetic energy $(E_K)_0$ of the projectile expressed as a consequence of $\cos 0^\circ = 1$ as

$$(\Delta E_K)_{\max} = \frac{4m_1 m_2}{(m_1 + m_2)^2} (E_K)_0 \cos^2 0^\circ = \frac{4m_1 m_2}{(m_1 + m_2)^2} (E_K)_0. \quad (9.25)$$

- (2) In grazing angle interaction between projectile and target, the recoil angle ϕ of the target is 90° , resulting in no energy transfer ($\Delta E_K = 0$), as a consequence of $\cos 90^\circ = 0$.
- (3) All other recoil angles are between 0° and 90° and the energy transfer from incident particle (neutron) to recoiling target (nucleus) is between $(\Delta E_K)_{\max}$ and 0.

(b) For the specific case of neutron scattering on an absorber nucleus we simplify the general classical expression (9.24) making the following changes:

- (1) Projectile m_1 is the incident neutron with mass m_n and incident kinetic energy $(E_K^n)_0$.
- (2) Target is the nucleus of the attenuating medium with mass consisting of A nucleons (atomic mass number), i.e., $m_2 \approx Am_n$ where we assume that proton mass m_p and neutron mass m_n are approximately equal ($m_p = 938.3 \text{ MeV}/c^2 \approx m_n = 939.6 \text{ MeV}/c^2$).

With A the atomic weight of the target nucleus we now get the following simple expression for (9.24)

$$\Delta E_K = \frac{4m_n[Zm_p + (A - Z)m_n]}{\{m_n + [Zm_p + (A - Z)m_n]\}^2} (E_K^n)_0 \cos^2 \phi \approx \frac{4A}{(1 + A)^2} (E_K^n)_0 \cos^2 \phi, \quad (9.26)$$

or we can state that the energy transfer fraction $f_{\text{tr}} = \Delta E_K / (E_K^n)_0$ that is, the fraction of kinetic energy of the incident neutron transferred to the stationary target, is

$$f_{\text{tr}} = \frac{\Delta E_K}{(E_K^n)_0} = \frac{4A}{(1 + A)^2} \cos^2 \phi. \quad (9.27)$$

Like in the general case described by (9.24), we again have two special angles: $\phi = 0$ and $\phi = 90^\circ$. For direct, head-on collision where the nucleus recoils with $\phi = 0$ the energy transfer ΔE_K and energy transfer fraction f_{tr} attain its maximum possible value, respectively, since $\cos 0^\circ = 1$ in (9.26) and (9.27)

$$(\Delta E_K)_{\text{max}} = \Delta E_K|_{\phi=0} = \frac{4A}{(1 + A)^2} (E_K)_0 \quad (9.28)$$

and

$$(f_{\text{tr}})_{\text{max}} = f_{\text{tr}}|_{\phi=0} = \frac{(\Delta E_K)_{\text{max}}}{(E_K^n)_0} = \frac{4A}{(1 + A)^2}. \quad (9.29)$$

Note that for a direct hit ($\phi = 0$), the maximum energy transfer fraction $(f_{\text{tr}})_{\text{max}}$ that is transferred from the incident neutron to recoil nucleus has the following properties:

- (1) Depends only on the atomic mass number A (atomic weight) of the target nucleus.
- (2) Is equal to 1 when the target nucleus is the hydrogen nucleus (proton) with ($A = 1$).
- (3) Decreases from $(f_{\text{tr}})_{\text{max}} = 1$ as the target mass increases from $A = 1$.

For grazing incidence where the nucleus recoils with $\phi = 90^\circ$ the energy transfer fraction f_{tr} attains its minimum value of $f_{\text{tr}} = 0$, as a result of $\cos 90^\circ = 0$ in (9.27)

$$(f_{\text{tr}})_{\text{min}} = \frac{\Delta E_K|_{\phi=90^\circ}}{(E_K^n)_0} = 0 \quad \text{or} \quad \Delta E_K|_{\phi=90^\circ} = 0. \quad (9.30)$$

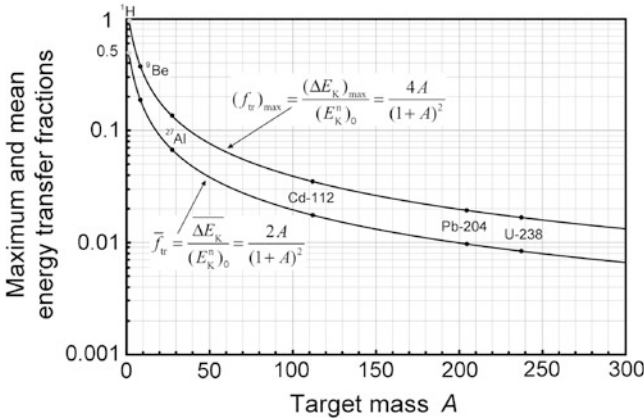


Fig. 9.3 Maximum and mean energy transfer fractions $(f_{tr})_{\max}$ and \bar{f}_{tr} for elastic collision of neutrons with moderator nuclei of atomic weight A

(c) Mean kinetic energy transfer $\overline{\Delta E_K}$ from neutron to target nucleus is calculated by averaging (9.26) over the recoil angle ϕ of the target nucleus as follows

$$\overline{\Delta E_K} = \frac{4A}{(1+A)^2} (E_K^n)_0 \overline{\cos^2 \phi}, \quad (9.31)$$

with $\overline{\cos^2 \phi}$ determined as

$$\overline{\cos^2 \phi} = \frac{\int_0^{\pi/2} \cos^2 \phi \, d\phi}{\int_0^{\pi/2} d\phi} = \frac{1}{\pi} \int_0^{\pi/2} \frac{1 + \cos(2\phi)}{2} d(2\phi) = \frac{1}{\pi} \left[\phi + \frac{\sin(2\phi)}{2} \right]_0^{\pi/2} = \frac{1}{2}. \quad (9.32)$$

Mean energy transfer $\overline{\Delta E_K}$ from neutron to target nucleus is thus given as follows

$$\overline{\Delta E_K} = \frac{4A}{(1+A)^2} (E_K^n)_0 \overline{\cos^2 \phi} = \frac{2A}{(1+A)^2} (E_K^n)_0 \quad (9.33)$$

and similarly for the mean energy transfer fraction \bar{f}_{tr}

$$\bar{f}_{tr} = \frac{\overline{\Delta E_K}}{(E_K^n)_0} = \frac{2A}{(1+A)^2}. \quad (9.34)$$

Equations (9.29) and (9.32) show that to moderate neutrons (that is to slow them down) with the fewest number of elastic collisions, target nuclei with as low as possible atomic weight A should be used as absorber medium. Thus, the most efficient nucleus for this purpose is hydrogen with $A = 1$ for which $(\Delta E_K)_{\max} = (E_K)_0$, $\overline{\Delta E_K} = \frac{1}{2}(E_K)_0$, and $\bar{f}_{tr} = \frac{1}{2}$ as seen by inserting $A = 1$ into (9.28), (9.29), and (9.32), respectively.

In Fig. 9.3 we plot, against atomic mass number A , the maximum energy transfer fraction $(f_{tr})_{\max}$ given in (9.29) and the mean energy transfer fraction \bar{f}_{tr} given

in (9.32) and show that the two energy transfer fractions decline rapidly roughly as $1/A$ with increasing A from their high values of 1 and 0.5, respectively, for hydrogen and amount to only 0.017 and 0.0085, respectively, for uranium-238, as also indicated in Fig. 9.3. Several other nuclides are also identified in the graph.

(d) Mean kinetic energy $\overline{E_K^n}$ of post-elastic collision neutron is calculated as mean energy transfer $\overline{\Delta E_K}$ from neutron to target nucleus subtracted from incident neutron energy $(E_K^n)_0$

$$\overline{E_K^n} = (E_K^n)_0 - \overline{\Delta E_K} = (E_K^n)_0 \left[1 - \frac{2A}{(1+A)^2} \right] = (E_K^n)_0 \frac{1+A^2}{(1+A)^2}. \quad (9.35)$$

Fractions of incident energy $(E_K^n)_0$ that a neutron retains after elastic collision with a given target nucleus are calculated from (9.35) as follows: $\overline{E_K^n}/(E_K^n)_0 = (1+A^2)/(1+A)^2$; $\overline{E_K^n}/(E_K^n)_0 = 0.5$ for H ($A = 1$); 0.858 for C ($A = 12$); 0.982 for Cd ($A = 112$); and 0.992 for U ($A = 238$).

9.2.Q3

(202)

Moderation (slowing down) of neutrons in nuclear reactors is very important for sustaining fission reaction. Neutrons generated in a typical fission reaction have kinetic energy $(E_K^n)_0$ of about 2 MeV, while thermal neutrons of kinetic energy $(E_K^n)_T \approx 0.025$ eV are required for efficient fission of uranium-235 (highest fission capture cross section) and for sustaining a fission chain reaction. A moderator is used for reduction of kinetic energy (thermalization) of neutrons generated in fission reactions and this is achieved through multiple, mainly elastic, scattering of neutrons whereby some of the neutron kinetic energy is transferred to the moderator in each scattering event. The mean energy $\overline{\Delta E_K}$ transferred from neutron to target nucleus of the moderator in each scattering interaction depends on incident neutron energy $(E_K^n)_0$ as well as on the atomic mass number A of the target nucleus and is given by

$$\overline{\Delta E_K} = (E_K^n)_0 \frac{2A}{(1+A)^2}. \quad (9.36)$$

- (a) Derive a recurrence equation to describe neutron kinetic energy $(E_K^n)_m$ after an incident neutron with initial kinetic energy $(E_K^n)_0$ undergoes a sequence of m elastic scattering collisions with nuclei of atomic mass number A .
- (b) Use the recurrence equation derived in (a) to determine the required number of elastic scattering interactions to moderate neutrons with $(E_K^n)_0 = 2$ MeV down to thermal energy $(E_K^n)_m = 0.025$ MeV in hydrogen, carbon, cadmium, lead, and uranium.

SOLUTION:

(a) The simplest manner in which one can derive a recurrence equation to recursively define a sequence of events is to write the first few terms of the sequence and from a comparison of the terms deduce the recurrence equation. Moderation (slowing down) of neutrons by elastic scattering is a good example of a sequence that can be described by a recurrence equation and we derive the general equation by laying out the first few terms of the neutron slowing down process through elastic scattering.

For each elastic scattering event the mean energy $\overline{\Delta E_K}$ transferred from the incident neutron of kinetic energy $(E_K^n)_{\text{inc}}$ to the moderator is derived in (9.35) and given in (9.36). Consequently, we can write the kinetic energy of the neutron after each elastic scattering event as the difference between $(E_K^n)_{\text{inc}}$ and $\overline{\Delta E_K}$ as follows

$$(E_K^n)_{\text{after}} = (E_K^n)_{\text{inc}} - \overline{\Delta E_K} = (E_K^n)_{\text{inc}} \left[1 - \frac{2A}{(1+A)^2} \right] = (E_K^n)_{\text{inc}} \left[\frac{1+A^2}{(1+A)^2} \right]. \quad (9.37)$$

The first few elastic scattering events in the slowing down of a neutron in a sequence of elastic scattering events are now expressed as follows:

- (1) We start with an incident neutron with kinetic energy $(E_K^n)_0$ striking the moderator of atomic weight A . As suggested in (9.37), the kinetic energy $(E_K^n)_1$ of the neutron after the first elastic scattering interaction is given as

$$(E_K^n)_1 = (E_K^n)_0 \left[\frac{1+A^2}{(1+A)^2} \right]. \quad (9.38)$$

- (2) Incident kinetic energy for the second scattering event is now $(E_K^n)_1$ so that, according to (9.37) in conjunction with (9.38), we write the neutron kinetic energy $(E_K^n)_2$ after the second scattering event as

$$(E_K^n)_2 = (E_K^n)_1 \left[\frac{1+A^2}{(1+A)^2} \right] = (E_K^n)_0 \left[\frac{1+A^2}{(1+A)^2} \right]^2. \quad (9.39)$$

- (3) The third scattering event starts with neutron of kinetic energy $(E_K^n)_2$ and the neutron kinetic energy $(E_K^n)_3$ after the third scattering event with the help of (9.37) and (9.39) is

$$(E_K^n)_3 = (E_K^n)_2 \left[\frac{1+A^2}{(1+A)^2} \right] = (E_K^n)_0 \left[\frac{1+A^2}{(1+A)^2} \right]^3. \quad (9.40)$$

- (4) The recurrence equation is now becoming obvious: after m elastic scattering interactions (with m an integer), neutron energy $(E_K^n)_m$ can be written as

follows

$$(E_K^n)_m = (E_K^n)_0 \left[\frac{1 + A^2}{(1 + A)^2} \right]^m \quad (9.41)$$

or

$$\frac{(E_K^n)_0}{(E_K^n)_m} = \left[\frac{(1 + A)^2}{1 + A^2} \right]^m = \left[1 + \frac{2A}{1 + A^2} \right]^m, \quad (9.42)$$

where $(E_K^n)_0$ is the kinetic energy of the incident neutron entering moderator A and starting the elastic scattering slowing down sequence.

(b) The process of slowing down energetic neutrons to thermal energy of 0.025 eV with elastic scattering in a moderator medium is referred to as thermalization of neutrons. The mean number m of elastic scattering interactions is easily determined by solving the recurrence equation (9.42) for m as follows

$$m = \frac{\ln \frac{(E_K^n)_0}{(E_K^n)_T}}{\ln \left[1 + \frac{2A}{1 + A^2} \right]}, \quad (9.43)$$

where

$(E_K^n)_T$ is the final kinetic energy of the neutron after thermalization through m scattering events.

$(E_K^n)_0$ is the initial kinetic energy of the neutron when it strikes the moderator.

A is the atomic mass number (atomic weight) of the moderator.

The number m of elastic scattering events for thermalization of $(E_K^n)_0 = 2$ MeV neutrons in hydrogen ($A = 1$), carbon ($A = 12$), cadmium ($A = 112$), lead ($A = 207$), and uranium ($A = 238$), respectively, is determined as follows

$$m_H = \frac{\ln[(2 \times 10^6)/0.025]}{\ln[1 + (2 \times 1)/(1 + 1^2)]} \approx 27, \quad (9.44)$$

$$m_C = \frac{\ln[(2 \times 10^6)/0.025]}{\ln[1 + (2 \times 12)/(1 + 12^2)]} \approx 119, \quad (9.45)$$

$$m_{Cd} = \frac{\ln[(2 \times 10^6)/0.025]}{\ln[1 + (2 \times 112)/(1 + 112^2)]} \approx 1029, \quad (9.46)$$

$$m_{Pb} = \frac{\ln[(2 \times 10^6)/0.025]}{\ln[1 + (2 \times 207)/(1 + 207^2)]} \approx 1893, \quad (9.47)$$

$$m_U = \frac{\ln[(2 \times 10^6)/0.025]}{\ln[1 + (2 \times 238)/(1 + 238^2)]} \approx 2175. \quad (9.48)$$

In Fig. 9.4 we plot the mean number of elastic collisions m given by (9.43) against atomic weight A for three kinetic energies $(E_K)_0$ of incident neutrons:

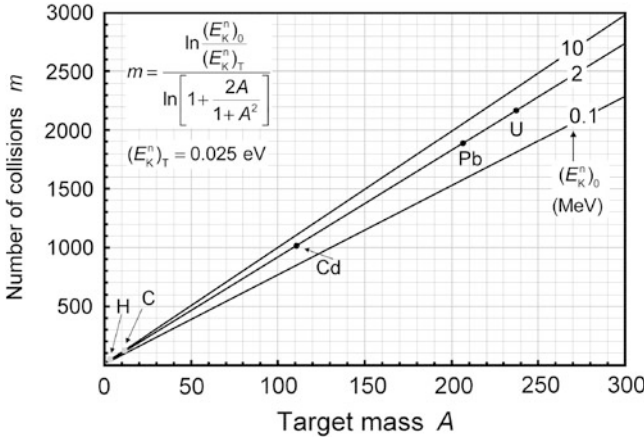


Fig. 9.4 Mean number of elastic collisions m against atomic weight A for three kinetic energies of incident neutrons: 0.1 MeV, 2 MeV, and 10 MeV

100 keV, 2 MeV, and 10 MeV. The data points on the $(E_K^n)_0 = 2$ MeV line are data that were calculated for various target materials in (9.44) through (9.48).

For a given incident neutron energy $(E_K^n)_0$ the plot of m against A is very close to a linear function even though (9.43) appears to be a complicated function. However, it turns out that $\ln[1 + 2A/(1 + A^2)]$ can easily be expanded into a series as follows

$$\ln(1 + x) \approx x - \frac{1}{2}x^2 + \frac{1}{3}x^3 - \frac{1}{4}x^4 + \dots \quad \text{for } -1 < x < 1. \quad (9.49)$$

By setting $x = 2A/(1 + A^2)$ and using only the first two terms of the series (9.49) we obtain the following simplification for $\ln[1 + 2A/(1 + A^2)]$ of (9.43)

$$\ln\left[1 + \frac{2A}{1 + A^2}\right] \approx \frac{2A}{1 + A^2} \left[1 - \frac{A}{1 + A^2}\right] \approx \frac{\frac{2A}{1 + A^2}}{1 + \frac{A}{1 + A^2}} = \frac{2A}{1 + A + A^2}. \quad (9.50)$$

Inserting (9.50) into (9.43) we get the following approximation for the mean number of elastic scattering events required to moderate a neutron from incident kinetic energy $(E_K^n)_0$ of a few MeV down to thermal energy $(E_K^n)_T$ which typically amounts to 0.025 eV

$$m = \frac{\ln\left(\frac{(E_K^n)_0}{(E_K^n)_T}\right)}{\ln\left[1 + \frac{2A}{1 + A^2}\right]} \approx \frac{1 + A + A^2}{2A} \ln\left(\frac{(E_K^n)_0}{(E_K^n)_T}\right). \quad (9.51)$$

9.3 Neutron Kerma

9.3.Q1

(203)

Neutron interactions with absorber are classified into two main groups (scattering and absorption) that in turn are split into several components. Each component is characterized by an interaction probability commonly referred to as cross section. Kerma and dose, of importance in radiation dosimetry, depend on neutron fluence and interaction cross section that in turn depends on neutron energy and type of interaction between the neutron and nuclei of attenuating medium.

- (a) Classify neutron interactions with attenuating medium. For each interaction define the microscopic cross section σ and briefly discuss its dependence on neutron velocity v and kinetic energy E_K .
- (b) Define kerma in general for photons and neutrons and describe how kerma is calculated for neutrons.

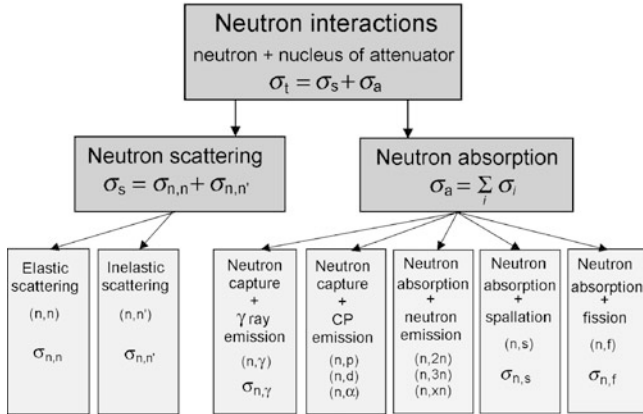
SOLUTION:

(a) Neutron interactions with nuclei of an attenuator are summarized in Table 9.2. The interactions fall into two main categories: neutron scattering and neutron absorption.

Neutron scattering is further subdivided into two categories: (1) elastic scattering and (2) inelastic scattering. In both types of scattering a portion of neutron's kinetic energy is transferred to the recoiling nucleus of the attenuator.

- (1) In *elastic scattering* the kinetic energy of the recoiling nucleus is equal to the kinetic energy that the neutron loses in the elastic scattering interaction, i.e., kinetic energy is conserved in the interaction.
- (2) In *inelastic scattering*, on the other hand, in addition to transferring energy to kinetic energy of the recoil nucleus, some of the energy that the neutron loses in the interaction is used to excite the recoil nucleus into an available nuclear exciting state. Consequently, kinetic energy is not conserved in the inelastic interaction even though the total energy is. Since energy to excite a given nucleus is discrete, inelastic scattering is an interaction process characterized by threshold energy.
- (3) An additional category of scattering termed *non-elastic scattering* is often added to the elastic and inelastic scattering categories. It refers to energetic neutron interaction with attenuator nucleus in which the energetic neutron is absorbed and a charged particle rather than a neutron is emitted. This type of interaction could also be categorized as neutron capture, however, the term "neutron capture" is usually reserved for absorption of thermal neutrons rather than energetic neutrons.

Table 9.2 Classification of neutron interactions with nucleus of attenuator



Neutron absorption is subdivided into five diverse categories that all have one common feature: penetration of the neutron into the attenuator nucleus, neutron disappearance from the neutron beam, emission of various particles, and transformation of the attenuator nucleus into a new, usually radioactive, nuclide. Often neutron absorption is referred to as neutron capture and the term implies absorption of a thermal neutron.

The five categories of neutron absorption are:

- (1) *Neutron activation* (n, γ) nuclear reaction also referred to as thermal neutron capture. This reaction is most commonly triggered with thermal neutrons in a nuclear reactor and produces a radioactive isotope of target nucleus.
- (2) *Neutron capture accompanied by release of nuclear charged particles*, such as protons in (n, p) reaction, deuterons in (n, d) reaction, and α particles in (n, α) reaction. This reaction plays an important role in the calculation and measurement of kerma and absorbed dose in radiotherapy and radiation dosimetry. Neutron capture accompanied by emission of a γ ray rather than charged particle is also very common.
- (3) *Neutron absorption that releases more than one neutron*. Emission of only one neutron is indistinguishable from a scattering event, so it falls under the scattering category. However, emission of more than one neutron multiplies the number of neutrons in the beam and affects the neutron fluence, so it is accounted for in this category.
- (4) *Spallation neutron reaction*. At very high neutron energy the penetration of the nucleus by a neutron can add a sufficient amount of energy to the nucleus to cause nuclear fragmentation into many small residual components.
- (5) *Fission*. Certain high atomic number Z target nuclei when bombarded with thermal or fast neutrons can split into two nuclei of smaller Z accompanied by release of several energetic neutrons that can be used for sustaining a fission chain reaction.

Nuclei of attenuator atoms are associated with cross sections that are proportional to the probability of specific interaction between incident neutron and nucleus of the attenuator and are measured in units of cm^2/atom , m^2/atom , or, most often in barns/atom (b/atom) where $1 \text{ b} = 10^{-24} \text{ cm}^2$. A specific microscopic cross section σ_i can be associated with each one of the various neutron interactions with the nuclei of the attenuating medium, as indicated in Table 9.2.

Total microscopic cross section σ or reaction probability is given as the sum of partial cross sections σ_i applicable for the individual interactions. Often, a particular calculation of a given physical problem requires the application of a specific microscopic cross section σ_i only. Since the individual cross sections σ_i depend on neutron kinetic energy E_K and, consequently, on neutron velocity v as well as on composition of the target nucleus, there are large variations in total microscopic cross section σ from one target nucleus to another. At low E_K the elastic cross section $\sigma_{n,n}$ is nearly constant with increasing kinetic energy E_K , whereas the inelastic cross section $\sigma_{n,n'}$ and all capture cross sections decrease with increasing E_K and are proportional to $1/v$, where v is the neutron velocity.

Values of partial cross sections σ_i are tabulated and usually given in units of cm^2/atom ; however, cross sections are usually combined first into one of the two major microscopic cross sections: scattering cross section σ_s (where $\sigma_s = \sigma_{n,n} + \sigma_{n,n'}$) and absorption cross section σ_a (where $\sigma_a = \sigma_{n,\gamma} + \sigma_{n,xn'} + \sigma_{n,cp} + \sigma_{n,s} + \sigma_{n,f}$) for a given target nucleus and are then added to form the total microscopic cross section $\sigma = \sigma_s + \sigma_a$ under the understanding that not all specific cross sections listed in Table 9.2 will be relevant for a given attenuating material at a given neutron energy.

(d) Kerma, an acronym for kinetic energy released in matter by indirectly ionizing radiation, is used in radiation dosimetry of photon and neutron beams. It is defined as energy that is transferred from neutral particles (photons or neutrons) to charged particles (CPs) per unit mass at a point-of-interest in the absorbing medium. In the case of photons the CPs released are electrons and positrons; in the case of neutrons they are protons and heavier ions.

Kerma is closely related to absorbed dose but the two quantities differ from each other because of radiation transport effects that manifest themselves through the finite range of the secondary charged particles released in the absorbing medium by indirectly ionizing radiation. Because of the very short range of heavy CPs released in absorbing medium by neutrons compared to the range of electrons and positrons released by photons, the charged particle equilibrium (CPE) is attained much faster in neutron beams than in photon beams.

(1) For mono-energetic photons of energy $h\nu$ traversing an attenuating medium of atomic number Z and mass density ρ , kerma K at point-of-interest P in the attenuator is related to the photon energy fluence ψ at point P through the mass energy transfer coefficient (μ_{tr}/ρ) for given photon energy $h\nu$ and attenuator atomic number Z . The mass energy transfer coefficient (μ_{tr}/ρ) is expressed as

$$\frac{\mu_{\text{tr}}}{\rho} = \frac{\mu}{\rho} \frac{\bar{E}_{\text{tr}}}{h\nu} = \frac{\mu}{\rho} \bar{f}_{\text{tr}}, \quad (9.52)$$

where

- ρ is the mass density of the attenuator.
- μ is the linear attenuation coefficient in units of cm^{-1} or m^{-1} for a given photon energy $h\nu$ and attenuator atomic number Z .
- μ_{tr} is the linear energy transfer coefficient in units of cm^{-1} or m^{-1} for a given photon energy $h\nu$ and attenuator atomic number Z .
- \bar{E}_{tr} is mean energy transferred from photons of energy $h\nu$ to charged particles (electrons and positrons) at point P in the attenuator of atomic number Z .
- \bar{f}_{tr} is the mean energy transfer fraction for photons of energy $h\nu$ and attenuating medium of atomic number Z .

Photon kerma K_γ at point P is thus expressed for *mono-energetic photons* as

$$K_\gamma = \psi \frac{\mu_{\text{tr}}}{\rho} = \phi h\nu \frac{\mu}{\rho} \frac{\bar{E}_{\text{tr}}}{h\nu} = \phi h\nu \frac{\mu}{\rho} \bar{f}_{\text{tr}} = \phi \frac{\mu}{\rho} \bar{E}_{\text{tr}}, \quad (9.53)$$

where

- ϕ is the photon fluence in cm^{-2} or m^{-2} expressing number of photons per area.
- ψ is the photon energy fluence in $\text{MeV} \cdot \text{cm}^{-2}$ or $\text{J} \cdot \text{m}^{-2}$.

For a *spectrum of photons* energy fluence $\psi'(h\nu)$ at point-of-interest P and mass energy transfer coefficient $(\mu_{\text{tr}}/\rho)_{h\nu,Z}$ as a function of photon energy $h\nu$ and attenuator atomic number Z , the kerma at point P is determined through the following integration

$$K = \int_{h\nu=0}^{h\nu_{\text{max}}} \psi'(h\nu) \left(\frac{\mu_{\text{tr}}}{\rho} \right)_{h\nu,Z} dh\nu, \quad (9.54)$$

where $\psi'(h\nu)$ is the differential distribution of photon energy fluence.

(2) The situation with neutron kerma is similar, yet not identical, to that of photons. For mono-energetic neutrons of kinetic energy E_{K}^{n} traversing an attenuating medium of mass density ρ and atomic number Z , the kerma at point P in the attenuating medium is related to neutron fluence ϕ through the neutron kerma factor $(F_{\text{n}})_{h\nu,Z}$ that is characteristic of both $h\nu$ and Z and expressed as follows

$$(F_{\text{n}})_{h\nu,Z} = \frac{\Sigma}{\rho} \frac{1}{\Delta E_{\text{K}}} = \frac{\Sigma}{\rho} \frac{\Delta E_{\text{K}}}{E_{\text{K}}^{\text{n}}} E_{\text{K}}^{\text{n}} = \frac{\Sigma_{\text{tr}}}{\rho} E_{\text{K}}^{\text{n}}, \quad (9.55)$$

where

- Σ is the total macroscopic cross section in units of cm^{-1} or m^{-1} for neutron interaction in attenuating medium Z for neutrons of kinetic energy E_{K}^{n} .

$\overline{\Delta E_K}$ is mean energy transferred from neutrons to charged particles (mainly protons) at point P in the attenuator.

Σ_{tr}/ρ is a parameter that plays a role of mass energy transfer coefficient and is for neutrons given by

$$\frac{\Sigma_{tr}}{\rho} = \frac{\Sigma}{\rho} \frac{\Delta E_K}{E_K^n}. \quad (9.56)$$

Kerma K_n for mono-energetic neutrons of kinetic energy E_K^n is thus expressed in terms of the neutron kerma factor F_n as follows

$$K_n = F_n \varphi = \frac{\Sigma}{\rho} \overline{\Delta E_K} = \frac{n^\square \sigma}{\rho} \overline{\Delta E_K}, \quad (9.57)$$

where we used the standard relationship between the macroscopic interaction cross section Σ and microscopic cross section σ

$$\Sigma = n^\square \sigma, \quad (9.58)$$

with n^\square the number of atoms (nuclei) per volume of the attenuating medium.

Kerma factors F_n are available from the literature in tabular format for various elements and compounds for a range of neutron kinetic energies E_K^n from thermal neutrons to fast neutrons (see, for example, the ICRU Report 26 or textbook by Attix).

For neutrons with an energy spectrum of neutron fluence $\varphi'(E_K^n)$ the following integral is used in calculation of neutron kerma

$$K_n = \int_{E_K^n=0}^{(E_K^n)_{\max}} \varphi'(E_K^n) (F_n)_{E_K^n, Z} dE_K^n, \quad (9.59)$$

where $(F_n)_{E_K^n, Z}$ represents neutron kerma factor as a function of E_K^n for a given attenuator medium Z.

9.4 Neutron Kerma Factor

9.4.Q1

(204)

Neutron kerma factor F_n plays an important role in neutron dosimetry similarly to the role that mass energy transfer coefficient μ_{tr}/ρ plays in photon dosimetry. However, F_n and μ_{tr}/ρ are defined differently to account for the differences in describing neutron fields in comparison to photon fields.

Photon fields are usually described by photon energy fluence ψ resulting in kerma expressed as $K = (\mu_{tr}/\rho)\psi$, while neutron fields are described by neutron fluence φ resulting in kerma expressed as $K = F_n\varphi$.

Total microscopic interaction cross section σ for neutrons with kinetic energy E_K^n of 10 MeV is 0.94 b in hydrogen and 1.25 b in oxygen. For $E_K^n = 10$ MeV neutrons determine:

- Total macroscopic interaction cross sections Σ of hydrogen and oxygen both at standard temperature and pressure (STP) of 0 °C and 101.3 kPa, respectively.
- Total macroscopic interaction cross section Σ of water.
- Neutron kerma factor F_n of hydrogen and oxygen at standard temperature and pressure.
- Neutron kerma factor F_n of water.
- Verify your results calculated in (c) and (d) on the graph of Fig. 9.5A that plots F_n against E_K^n for various attenuating media including hydrogen, oxygen, and water.

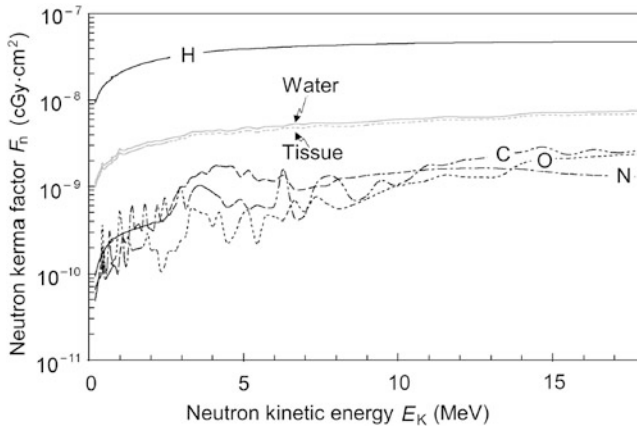


Fig. 9.5A Neutron kerma factor F_n against neutron kinetic energy E_K for various materials of interest in medical physics. Data were obtained from the NIST

SOLUTION:

- The total macroscopic interaction cross sections of hydrogen Σ_{H_2} and oxygen Σ_{O_2} are calculated from the following expression linking the macroscopic and microscopic cross sections

$$\Sigma = n \square \sigma, \quad (9.60)$$

where σ is the total microscopic cross section for the given neutron interaction and n^\square is the atomic (nuclear) density, i.e., number of atoms (nuclei) per volume \mathcal{V} of the attenuating medium expressed as $n^\square = N_a/\mathcal{V} = \rho N_a/m = \rho N_A/A$. Since hydrogen and oxygen are gases, we determine the appropriate nuclear densities n^\square at STP (0 °C and 101.3 kPa) invoking the ideal gas law which states that 1 mol of ideal gas at STP occupies a volume of 22.4 liters, i.e., $22.4 \times 10^3 \text{ cm}^3$.

- (1) Hydrogen gas in molecular form (H_2) has a molecular weight of $M = 2 \times 1.00794 \text{ g/mol}$ and since, according to ideal gas law, 1 mol of hydrogen gas at STP corresponds to a volume \mathcal{V} of $22.4 \times 10^2 \text{ cm}^3$, we obtain the following mass density of hydrogen gas

$$\rho_{\text{H}_2} = \frac{2 \times (1.00794 \text{ g/mol})}{22.4 \times 10^3 \text{ cm}^3/\text{mol}} = 9 \times 10^{-5} \text{ g/cm}^3. \quad (9.61)$$

- (2) Oxygen gas in molecular form (O_2) has a molecular weight of $M = 2 \times 15.9994 \text{ g/mol}$ and since, according to ideal gas law, 1 mol of oxygen gas at STP corresponds to a volume \mathcal{V} of $22.4 \times 10^2 \text{ cm}^3$, we obtain the following mass density of oxygen gas

$$\rho_{\text{O}_2} = \frac{2 \times (15.9994 \text{ g/mol})}{22.4 \times 10^3 \text{ cm}^3/\text{mol}} = 1.429 \times 10^{-3} \text{ g/cm}^3. \quad (9.62)$$

We now use (9.60) to determine macroscopic interaction cross sections Σ_{H_2} and Σ_{O_2} of hydrogen at STP and oxygen at STP, respectively, for neutrons with $E_K^n = 10 \text{ MeV}$.

- (1) Total macroscopic cross section of hydrogen Σ_{H_2} at STP for 10 MeV neutron

$$\begin{aligned} \Sigma_{\text{H}_2} &= n_{\text{H}_2}^\square \sigma_{\text{H}_2} = \rho_{\text{H}_2} \frac{N_A}{A_{\text{H}_2}} \sigma_{\text{H}_2} \\ &= \frac{(9 \times 10^{-5} \text{ g/cm}^3) \times (6.022 \times 10^{23} \text{ mol}^{-1}) \times (0.94 \times 10^{-24} \text{ cm}^2)}{2 \times 1.00794 \text{ g} \cdot \text{mol}^{-1}} \\ &= 2.53 \times 10^{-5} \text{ cm}^{-1}. \end{aligned} \quad (9.63)$$

- (2) Total macroscopic cross section of oxygen Σ_{O_2} at STP for 10 MeV neutron

$$\begin{aligned} \Sigma_{\text{O}_2} &= n_{\text{O}_2}^\square \sigma_{\text{O}_2} = \rho_{\text{O}_2} \frac{N_A}{A_{\text{O}_2}} \sigma_{\text{O}_2} \\ &= \frac{(1.429 \times 10^{-3} \text{ g/cm}^3) \times (6.022 \times 10^{23} \text{ mol}^{-1}) \times (1.25 \times 10^{-24} \text{ cm}^2)}{2 \times 15.9994 \text{ g} \cdot \text{mol}^{-1}} \\ &= 3.36 \times 10^{-5} \text{ cm}^{-1}. \end{aligned} \quad (9.64)$$

(b) Total macroscopic interaction cross section of water $\Sigma_{\text{H}_2\text{O}}$ for 10 MeV neutrons is calculated from the sum of contributions from hydrogen and oxygen nuclei constituting the water molecule

$$\Sigma_{\text{H}_2\text{O}} = \sum_i n_i^\square \sigma_i = n_{\text{H}}^\square \sigma_{\text{H}} + n_{\text{O}}^\square \sigma_{\text{O}}. \quad (9.65)$$

To find the atomic (nuclear) densities n_{H}^\square and n_{O}^\square , i.e., number of hydrogen and oxygen atoms (nuclei), respectively, per volume of water, we first determine the molecular density $n_{\text{H}_2\text{O}}^\square$ of water (i.e., number of water molecules per cm^3 of water) as follows

$$\begin{aligned} n_{\text{H}_2\text{O}}^\square &= \frac{N_{\text{mol}}}{\mathcal{V}} = \rho_{\text{H}_2\text{O}} \frac{N_{\text{mol}}}{m_{\text{H}_2\text{O}}} \\ &= \rho_{\text{H}_2\text{O}} \frac{N_{\text{A}}}{A_{\text{H}_2\text{O}}} = \frac{(1 \text{ g} \cdot \text{cm}^{-3}) \times (6.022 \times 10^{23} \text{ mol}^{-1})}{18.01528 \text{ g} \cdot \text{mol}^{-1}} \\ &= 3.343 \times 10^{22} \text{ cm}^{-3}. \end{aligned} \quad (9.66)$$

Since the molecular density of water is 3.343×10^{22} molecules per cm^3 and each water molecule contains 2 atoms of hydrogen and 1 atom of oxygen, we conclude that the atomic density of hydrogen in water n_{H}^\square is $2 \times 3.343 \times 10^{22} = 6.686 \times 10^{22}$ hydrogen atoms per cm^3 of water, while the atomic density of oxygen in water n_{O}^\square is 3.343×10^{22} oxygen atoms per cm^3 of water.

The macroscopic interaction cross section of water $\Sigma_{\text{H}_2\text{O}}$ for 10 MeV neutrons is now calculated as follows

$$\begin{aligned} \Sigma_{\text{H}_2\text{O}} &= n_{\text{H}}^\square \sigma_{\text{H}} + n_{\text{O}}^\square \sigma_{\text{O}} \\ &= (6.686 \times 10^{22} \text{ cm}^{-3}) \times (0.94 \times 10^{-24} \text{ cm}^2) \\ &\quad + (3.343 \times 10^{22} \text{ cm}^{-3}) \times (1.25 \times 10^{-24} \text{ cm}^2) \\ &= 0.0628 \text{ cm}^{-1} + 0.0418 \text{ cm}^{-1} = 0.1046 \text{ cm}^{-1}. \end{aligned} \quad (9.67)$$

(c) Neutron kerma factor F_{n} of hydrogen and oxygen for 10 MeV neutrons is calculated from the following expression

$$F_{\text{n}} = \frac{\Sigma}{\rho} \frac{\overline{\Delta E_{\text{K}}}}{\Delta E_{\text{K}}} = \frac{n^\square \sigma}{\rho} \frac{\overline{\Delta E_{\text{K}}}}{\Delta E_{\text{K}}} = \frac{N_{\text{a}}}{\rho \mathcal{V}} \sigma \frac{\overline{\Delta E_{\text{K}}}}{\Delta E_{\text{K}}} = \frac{N_{\text{A}}}{A} \sigma \frac{\overline{\Delta E_{\text{K}}}}{\Delta E_{\text{K}}} = \frac{N_{\text{A}}}{A} \sigma \frac{2A}{(1+A)^2} E_{\text{K}}^{\text{n}}, \quad (9.68)$$

where

Σ is the total macroscopic interaction cross section of attenuating medium for neutrons.

ρ is the density of attenuating medium (hydrogen or oxygen).

n^\square atomic (nuclear) density of attenuating medium: $n^\square = N_{\text{a}}/\mathcal{V}$ with N_{a} number of atoms and \mathcal{V} volume of attenuating medium.

- σ is the total microscopic interaction cross section of attenuating medium for neutrons.
- N_A is the Avogadro number: 6.022×10^{23} atoms (nuclei) per mol.
- A is the atomic mass number (atomic weight) of the attenuating medium.
- $\overline{\Delta E_K}$ is mean energy transferred from neutrons to charged particles at point-of-interest in attenuating medium calculated for neutrons of kinetic energy E_K^n from the following expression

$$\overline{\Delta E_K} = \frac{2A}{(1+A)^2} E_K^n. \quad (9.69)$$

- (1) Mean energy transfer $\overline{\Delta E_K}$ from neutron with kinetic energy $E_K^n = 10$ MeV interacting with hydrogen nucleus ($A = 1$) is from (9.69) given as

$$\overline{\Delta E_K} = \frac{2A}{(1+A)^2} E_K^n = \frac{2}{2^2} \times (10 \text{ MeV}) = 5 \text{ MeV}. \quad (9.70)$$

- (2) Mean energy transfer $\overline{\Delta E_K}$ from neutron with kinetic energy $E_K^n = 10$ MeV interacting with oxygen nucleus ($A = 16$) is from (9.69) given as

$$\overline{\Delta E_K} = \frac{2A}{(1+A)^2} E_K^n = \frac{2 \times 16}{(1+16)^2} \times (10 \text{ MeV}) = 1.11 \text{ MeV}. \quad (9.71)$$

We now determine the neutron kerma factors F_n of hydrogen and oxygen using (9.68) in conjunction with (9.70) and (9.71), respectively

- (1) Neutron kerma factor of hydrogen (F_n)_H for 10 MeV neutrons is given as

$$\begin{aligned} (F_n)_H &= \frac{N_A}{A_H} \sigma_H (\overline{\Delta E_K})_H = \frac{(6.022 \times 10^{23} \text{ mol}^{-1}) \times (0.94 \times 10^{-24} \text{ cm}^2) \times (5 \text{ MeV})}{(1.00794 \text{ g} \cdot \text{mol}^{-1})} \\ &\quad \times \frac{(1.602 \times 10^{-13} \text{ J/MeV}) \times (10^2 \text{ cGy/Gy})}{(10^{-3} \text{ kg/g})} \\ &= 4.49 \times 10^{-8} \text{ cGy} \cdot \text{cm}^2. \end{aligned} \quad (9.72)$$

- (2) Neutron kerma factor of oxygen (F_n)_O for 10 MeV neutrons is given as

$$\begin{aligned} (F_n)_O &= \frac{N_A}{A_O} \sigma_O (\overline{\Delta E_K})_O = \frac{(6.022 \times 10^{23} \text{ mol}^{-1}) \times (1.25 \times 10^{-24} \text{ cm}^2) \times (1.11 \text{ MeV})}{(15.9994 \text{ g} \cdot \text{mol}^{-1})} \\ &\quad \times \frac{(1.602 \times 10^{-13} \text{ J/MeV}) \times (10^2 \text{ cGy/Gy})}{(10^{-3} \text{ kg/g})} \\ &= 8.36 \times 10^{-10} \text{ cGy} \cdot \text{cm}^2. \end{aligned} \quad (9.73)$$

(d) Neutron kerma factor $(F_n)_{\text{H}_2\text{O}}$ of water for 10 MeV neutrons is determined by summing up contributions to kerma factor from hydrogen and oxygen. Thus, 1 mol of water contains N_A molecules of water and, since each water molecule contains two hydrogen atoms (nuclei) as well as one oxygen atom (nucleus), one can say that 1 mol of water contains $2N_A$ atoms (nuclei) of hydrogen as well as N_A atoms of oxygen. $(F_n)_{\text{H}_2\text{O}}$ is thus calculated as follows

$$\begin{aligned}
 (F_n)_{\text{H}_2\text{O}} &= \sum_i \frac{n_i}{\rho_{\text{H}_2\text{O}}} \overline{\sigma_i(\Delta E_K)_i} = \sum_i \frac{N_A}{A_{\text{H}_2\text{O}}} \overline{\sigma_i(\Delta E_K)_i} \\
 &= \frac{2N_A}{A_{\text{H}_2\text{O}}} \overline{\sigma_{\text{H}}(\Delta E_K)_{\text{H}}} + \frac{N_A}{A_{\text{H}_2\text{O}}} \overline{\sigma_{\text{O}}(\Delta E_K)_{\text{O}}} \\
 &= \frac{2 \times (6.022 \times 10^{23} \text{ mol}^{-1}) \times (0.94 \times 10^{-24} \text{ cm}^2) \times (5 \text{ MeV})}{18.0153 \text{ g} \cdot \text{mol}^{-1}} \\
 &\quad \times \frac{(1.6 \times 10^{-13} \text{ J/MeV}) \times (10^2 \text{ cGy/Gy})}{(10^{-3} \text{ kg/g})} \\
 &= \frac{(6.022 \times 10^{23} \text{ mol}^{-1}) \times (1.25 \times 10^{-24} \text{ cm}^2) \times (1.11 \text{ MeV})}{(18.0153 \text{ g} \cdot \text{mol}^{-1})} \\
 &\quad \times \frac{(1.6 \times 10^{-13} \text{ J/MeV}) \times (10^2 \text{ cGy/Gy})}{(10^{-3} \text{ kg/g})} \\
 &= 0.503 \times 10^{-8} \text{ cGy} \cdot \text{cm}^2 + 0.074 \times 10^{-8} \text{ cGy} \cdot \text{cm}^2 \\
 &= 5.77 \times 10^{-9} \text{ cGy} \cdot \text{cm}^2. \tag{9.74}
 \end{aligned}$$

Neutron kerma factor F_n is usually given in units of $\text{cGy} \cdot \text{cm}^2$ meaning cGy per $\text{neutron}/\text{cm}^2$. This follows from the definition of neutron kerma $K = F_n \varphi$, so that the kerma factor $F_n = K/\varphi$ is sometimes referred to as fluence-to-kerma factor.

In neutron beam dosimetry kerma and dose in tissue are obtained by multiplying kerma and dose measured with an instrument that is generally not perfectly tissue equivalent by the ratio of kerma factors of the two attenuating media. This approach is similar to photon beam dosimetry where kerma and dose in tissue are obtained by multiplying kerma and dose in non-tissue equivalent medium by the ratio of mass energy transfer coefficients and ratio of mass energy absorption coefficients, respectively, of the two attenuating media. *Note:* unlike in photon beams, in neutron beams there is no energy loss to bremsstrahlung by charged particles released in the attenuating medium.

(e) Figure 9.5B provides the neutron kerma factor F_n against neutron kinetic energy E_K^n for various materials of interest in medical physics including hydrogen, oxygen, and water; the three materials used in this question. Data points at $E_K^n = 10 \text{ MeV}$ show results of our calculations of kerma factor in (c) and (d) in good agreement with the graphs published by the ICRU, Report 26.

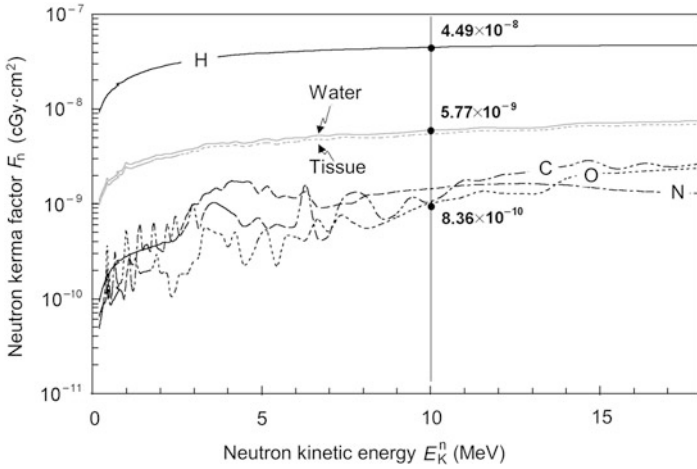


Fig. 9.5B Neutron kerma factor F_n against neutron kinetic energy E_K^n for various materials including hydrogen, oxygen, and water; materials used in this question. Data points at $E_K^n = 10$ MeV show results of our calculations in (c) and (d)

9.5 Neutron Dose Deposition in Tissue

9.5.Q1

(205)

Neutrons, by virtue of their neutrality, similarly to photons, deposit dose in tissue through a two-step process:

- Step 1: Energy transfer from neutron to heavy charged particles (CPs), such as protons and heavier nuclei in tissue (resulting in kerma).
- Step 2: Energy deposition in tissue by heavy CPs through Coulomb interactions of CPs with atoms of tissue (resulting in absorbed dose).

Soft tissue elemental composition is of importance in neutron dosimetry and is given by the ICRU in fraction by weight as follows: hydrogen H—0.102; carbon—0.123; nitrogen—0.035; oxygen—0.729; and many other elements combined to contribute 0.011.

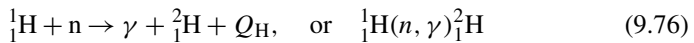
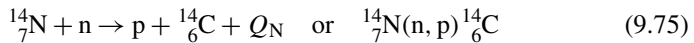
- (a) Three regions of neutron kinetic energy E_K^n are of importance in neutron dosimetry. Define the three regions, give examples of nuclear reactions for each of the three regions, and explain the mechanism for energy deposition in tissue for each nuclear reaction.

- (b) Based on the ICRU elemental tissue composition data calculate the number of hydrogen, carbon, nitrogen, and oxygen nuclei per unit mass of tissue.
- (c) Calculate the mean energy transfer fraction $f_{tr}^n = \overline{\Delta E_K} / E_K^n$ for neutrons interacting elastically with atoms of hydrogen, carbon, nitrogen, and oxygen.

SOLUTION:

(a) Depending on their kinetic energy E_K^n , neutrons are classified into many categories ranging from ultra-cold neutrons through thermal and intermediate neutrons to fast and relativistic neutrons. However, for dosimetric purposes, it is convenient to separate neutrons into only three categories: (1) thermal neutron region for $E_K^n < 1$ eV, (2) intermediate energy region for $1 \text{ eV} < E_K^n < 10 \text{ keV}$, and (3) fast neutron region for $E_K^n > 10 \text{ keV}$. A brief description of the three energy regions follows below and is summarized in Table 9.3.

(1) Dose deposition by neutrons of kinetic energy $E_K^n < 1$ eV (thermal neutron dosimetric region) in human tissue is governed by thermal neutron capture (absorption) reactions of neutron with $^{14}_7\text{N}$ and ^1_1H atoms in tissue producing the following two reactions:



where Q_N and Q_H are reaction Q values that are both positive, making the reactions exothermic.

(2) Intermediate kinetic energy neutrons $1 \text{ eV} < E_K^n < 10 \text{ keV}$ primarily interact with hydrogen nuclei of tissue through elastic scattering interaction and dose is deposited in tissue by the recoil energy picked up by hydrogen nuclei (proton) in the elastic scattering interaction. The mean energy transfer per one collision of neutron with hydrogen atom is 50 % of the kinetic energy of the neutron.

(3) Dose delivered to human tissue by interactions of fast neutrons ($E_K^n > 10 \text{ keV}$) with atoms of human tissue is mainly due to elastic collisions of neutrons with atoms of tissue, most importantly with hydrogen atoms, because of the high efficiency of mean energy transfer from neutron to hydrogen atom (proton) in elastic collisions. Also of some importance are fast neutron interactions with carbon and oxygen atoms of tissue via inelastic collision processes that release α particles in reactions of the type $(n, n'\alpha)$ and via non-elastic processes producing α particles and heavier ions. The α particles and heavier ions released in the fast neutron interactions are responsible for the dose deposition in tissue.

Table 9.3 Principal neutron interactions resulting in tissue kerma and types of energy deposition resulting in tissue dose

Energy region	Principal interactions	Mechanism of energy deposition in tissue
Thermal $E_K^n < 1 \text{ eV}$	Neutron capture	
	$^1_1\text{H}(n, \gamma)^2_1\text{H}$ $\sigma_{^1_1\text{H}} = 0.33 \text{ b/atom}$	$E_\gamma = 2.225 \text{ MeV}$
	$^{14}_7\text{N}(n, p)^{12}_6\text{C}$ $\sigma_{^{14}_7\text{N}} = 1.8 \text{ b/atom}$	$E_K^p = 0.58 \text{ MeV}$
	$^{14}_7\text{N}(n, \gamma)^{15}_7\text{N}$ $\sigma_{^{14}_7\text{N}} \approx 0.06 \text{ b/atom}$	$E_\gamma = 10.8 \text{ MeV}$
Intermediate $1 \text{ eV} < E_K^n < 10 \text{ keV}$	Elastic scattering	
	$^1_1\text{H}(n, n)^1_1\text{H}$ $\bar{E}_K^p \approx \frac{1}{2} E_K^n$	
Fast $E_K^n > 10 \text{ keV}$	Elastic scattering	
	$^1_1\text{H}(n, n)^1_1\text{H}$ $\bar{E}_K^p \approx \frac{1}{2} E_K^n$	
	Inelastic scattering	
	$^{12}_6\text{C}(n, n')3\alpha$ $(E_K^n)_{\text{thr}} \approx 9 \text{ MeV}$	E_K^α
Non-elastic scattering		
	$^{12}_6\text{C}(n, \alpha)^9_4\text{Be}$ $(E_K^n)_{\text{thr}} \approx 6 \text{ MeV}$	E_K^α and E_γ^{Be}
	$^{16}_8\text{O}(n, \alpha)^{13}_6\text{C}$ $(E_K^n)_{\text{thr}} \approx 4 \text{ MeV}$	E_K^α

Table 9.4 Physical characteristics of elemental constituents of human tissue

(1)	Tissue element	Hydrogen H	Carbon C	Nitrogen N	Oxygen O
(2)	Atomic number Z	1	6	7	8
(3)	Atomic weight A	1.008	12.01	14.01	16.00
(4)	Fraction by weight f_w	0.102	0.123	0.035	0.729
(5)	N_X/m_{tissue} (atom/g tissue)	6.09×10^{22}	0.62×10^{22}	0.15×10^{22}	2.74×10^{22}
(6)	$\bar{f}_{\text{tr}} = \overline{\Delta E_K}/E_K^n$	0.50	0.142	0.124	0.111

(b) The main constituent elements of human tissue are hydrogen H, carbon C, nitrogen N, and oxygen O and their fractions by weight f_X according to the ICRU are, respectively, 0.102, 0.123, 0.035, and 0.729. The number of atoms (nuclei) of a given element X per unit mass of tissue, N_X/m_{tissue} , is determined as follows:

- (1) Number of atoms X per mole A_X of element X is constant and referred to as the Avogadro number $N_A = 6.022 \times 10^{23} \text{ mol}^{-1}$.
- (2) Number of atoms X per gram of element X is given by N_A/A_X .
- (3) Number of atoms X per gram of tissue, N_X/m_{tissue} , is given as $N_X/m_{\text{tissue}} = f_X N_A/A_X$.

Results of the calculation of N_X/m_{tissue} for H, C, N, and O are listed in row (5) of Table 9.4 and show that per unit mass of tissue hydrogen H atoms (nuclei) are the most abundant with $6.09 \times 10^{22} \text{ atom/g}$, followed by oxygen O atoms with $2.74 \times 10^{22} \text{ atom/g}$. Carbon C and nitrogen N make a much lower contribution to N_X/m_{tissue} , the number of atoms (nuclei) per unit mass of tissue with $0.62 \times 10^{22} \text{ atom/g}$ and $0.15 \times 10^{22} \text{ atom/g}$, respectively.

N_X/m_{tissue} is of importance in determination of neutron kerma and absorbed dose, since both of these dosimetric quantities are linearly proportional to N_X/m_{tissue} .

(c) Mean energy transfer fraction \bar{f}_{tr} for elastic scattering of neutrons is calculated using the following expression

$$\bar{f}_{\text{tr}} = \frac{\overline{\Delta E_{\text{K}}}}{E_{\text{K}}^{\text{n}}} = \frac{2A}{(1+A)^2}, \quad (9.77)$$

where

$\overline{\Delta E_{\text{K}}}$ is the mean energy transferred from the incident neutron with kinetic energy E_{K}^{n} to the target (nucleus) of the attenuating medium.

A is the atomic weight of the target atom (nucleus) in the attenuating medium.

Equation (9.77) is derived from the standard classical equation for energy transfer ΔE_{K} from projectile with mass m_1 to the stationary target with mass m_2 in elastic collision (T5.25)

$$\Delta E_{\text{K}} = \frac{4m_1m_2}{(m_1+m_2)^2} (E_{\text{K}})_0 \cos^2 \phi, \quad (9.78)$$

where

$(E_{\text{K}})_0$ is the kinetic energy of the projectile (incident particle) m_1 .

ϕ is the recoil angle of the target measured with respect to the direction of incident neutron.

Equation (9.77) can be obtained from (9.78) with the following assumptions:

- (1) The incident particle (projectile) is the neutron: $m_1 = m_{\text{n}}$.
- (2) Kinetic energy of the projectile is the kinetic energy of the incident neutron: $(E_{\text{K}})_0 = E_{\text{K}}^{\text{n}}$.
- (3) Mean energy transfer $\overline{\Delta E_{\text{K}}}$ from projectile m_1 to stationary target m_2 is given as

$$\begin{aligned} \overline{\Delta E_{\text{K}}} &= \frac{4m_1m_2}{(m_1+m_2)^2} (E_{\text{K}})_0 \overline{\cos^2 \phi} = \frac{2m_1m_2}{(m_1+m_2)^2} (E_{\text{K}})_0, \quad \text{since} \\ \overline{\cos^2 \phi} &= \frac{1}{2}. \end{aligned} \quad (9.79)$$

- (4) The target is the nucleus of attenuator atom, i.e., $m_2 = Zm_{\text{p}} + (A-Z)m_{\text{n}} \approx Am_{\text{n}}$, where we assume that the proton mass m_{p} and the neutron mass m_{n} are approximately equal.
- (5) Equation (9.78) for the mean energy transfer fraction \bar{f}_{tr} from neutron to nucleus of attenuating medium can now be written in the simplified form of (9.77) as follows

$$\bar{f}_{\text{tr}} = \frac{\overline{\Delta E_{\text{K}}}}{(E_{\text{K}})_0} = \frac{2m_1m_2}{(m_1+m_2)^2} = \frac{\overline{\Delta E_{\text{K}}}}{E_{\text{K}}^{\text{n}}} \approx \frac{2A}{(1+A)^2}. \quad (9.80)$$

Mean energy transfer fractions \bar{f}_{tr} for hydrogen, carbon, nitrogen, and oxygen were calculated with (9.77) and results are displayed in row (6) of Table 9.4. Hydrogen is obviously the best nuclear target for energy transfer from neutron to target in elastic scattering, on the average receiving 50 % of neutron kinetic energy per elastic scattering collision. As shown in Table 9.4, \bar{f}_{tr} rapidly decreases with increasing number of nucleon A in the target, amounting to 0.142, 0.124, and 0.111 for carbon, nitrogen, and oxygen, respectively.

9.5.Q2

(206)

Neutrons with kinetic energy below 10 eV fall into the thermal neutron dosimetric energy region that is categorized by thermal neutron capture interactions with elemental hydrogen ${}^1_1\text{H}$ and elemental nitrogen ${}^{14}_7\text{N}$ in tissue. Nitrogen ${}^{14}_7\text{N}$ actually offers two neutron capture reactions, reaction (1) ${}^{14}_7\text{N}(n, p){}^{13}_6\text{C}$ with cross section of $\sigma({}^{14}_7\text{N}) \approx 1.18$ b/atom and reaction (2) ${}^{14}_7\text{N}(n, \gamma){}^{15}_6\text{N}$ with a much smaller cross section of $\sigma({}^{14}_7\text{N}) \approx 0.06$ b/atom. Hydrogen ${}^1_1\text{H}$ contributes to neutron capture through reaction (3) ${}^1_1\text{H}(n, \gamma){}^2_1\text{H}$ with a cross section of $\sigma({}^1_1\text{H}) = 0.33$ b/atom.

- (a) Nuclear reactions are characterized with a Q value that can be positive, zero, or negative. Define the Q value for a nuclear reaction and describe the two methods that are used for its determination in a typical nuclear reaction.
- (b) Calculate the Q values of the three neutron capture reactions that represent the most prominent interactions of thermal neutrons with tissue. In your calculations use the two methods described in (a) and show that both methods yield the same results for a given thermal neutron capture reaction. Appropriate rest energy and binding energy data are given in Appendix A.
- (c) For each of the three reactions determine the kinetic energies of the recoil nucleus and particles released [proton in reaction (1) and γ photons in reactions (2) and (3)].

SOLUTION:

(a) Two methods are used for determination of reaction Q value:

(1) Rest energy method in which we subtract the sum of nuclear rest energies of reaction products after the reaction $\sum_{i,\text{after}} M_i c^2$ from the sum of nuclear rest energies of reactants (projectile and target) before the reaction $\sum_{i,\text{before}} M_i c^2$, or

$$Q = \sum_{i,\text{before}} M_i c^2 - \sum_{i,\text{after}} M_i c^2. \quad (9.81)$$

(2) Binding energy method in which we subtract the sum of nuclear binding energies of reactants before the reaction $\sum_{i,\text{before}} E_B(i)$ from the sum of nuclear binding energies of reaction products after the reaction $\sum_{i,\text{after}} E_B(i)$, or

$$Q = \sum_{i,\text{after}} E_B(i) - \sum_{i,\text{before}} E_B(i). \quad (9.82)$$

(b) Two thermal neutron capture reactions are important in thermal neutron interactions with tissue: ${}^1_1\text{H}(n, \gamma){}^2_1\text{H}$ and ${}^{14}_7\text{N}(n, p){}^{14}_6\text{C}$. Another thermal neutron reaction ${}^{14}_7\text{N}(n, \gamma){}^{15}_7\text{N}$ is possible for thermal neutrons interacting with tissue but it has a much smaller probability than the ${}^{14}_7\text{N}(n, p){}^{14}_6\text{C}$ reaction.

(1) Thermal neutron capture reaction ${}^{14}_7\text{N}(n, p){}^{14}_6\text{C}$ can be written as



and its Q value is determined as follows:

Rest energy method

$$\begin{aligned} Q &= \sum_{i,\text{before}} M_i c^2 - \sum_{i,\text{after}} M_i c^2 = [M({}^{14}_7\text{N}) + m_n c^2] - [m_p c^2 + M({}^{14}_6\text{C})] \\ &= [13040.2028 \text{ MeV} + 939.5653 \text{ MeV}] - [938.2720 \text{ MeV} + 13040.8703 \text{ MeV}] \\ &= [13979.7681 \text{ MeV} - 13979.1423 \text{ MeV}] = 0.626 \text{ MeV}. \end{aligned} \quad (9.84)$$

Binding energy method

$$\begin{aligned} Q &= \sum_{i,\text{after}} E_B(i) - \sum_{i,\text{before}} E_B(i) = [0 + E_B({}^{14}_6\text{C})] - [E_B({}^{14}_7\text{N}) + 0] \\ &= 105.2846 \text{ MeV} - 104.6587 \text{ MeV} = 0.626 \text{ MeV}. \end{aligned} \quad (9.85)$$

(2) Thermal neutron capture reaction ${}^{14}_7\text{N}(n, \gamma){}^{15}_7\text{N}$ can be written as



and its Q value is determined as follows:

Rest energy method

$$\begin{aligned} Q &= \sum_{i,\text{before}} M_i c^2 - \sum_{i,\text{after}} M_i c^2 = [M({}^{14}_7\text{N}) + m_n c^2] - [0 + M({}^{15}_7\text{N})] \\ &= [13040.2028 \text{ MeV} + 939.5653 \text{ MeV}] - [13968.9350 \text{ MeV}] \\ &= [13979.7681 \text{ MeV} - 13968.9350 \text{ MeV}] = 10.83 \text{ MeV}. \end{aligned} \quad (9.87)$$

Binding energy method

$$\begin{aligned}
 Q &= \sum_{i,\text{after}} E_B(i) - \sum_{i,\text{before}} E_B(i) = [0 + E_B(^{15}_7\text{N})] - [E_B(^{14}_7\text{N}) + 0] \\
 &= 115.4914 \text{ MeV} + 104.6587 \text{ MeV} = 10.83 \text{ MeV}.
 \end{aligned} \tag{9.88}$$

(3) Thermal neutron capture reaction $^1_1\text{H}(n, \gamma)^2_1\text{H}$ can be written as



and its Q value is determined as follows

Rest energy method

$$\begin{aligned}
 Q &= \sum_{i,\text{before}} M_i c^2 - \sum_{i,\text{after}} M_i c^2 = [M(^1_1\text{H}) + m_n c^2] - [0 + M(^2_1\text{H})] \\
 &= [938.2720 \text{ MeV} + 939.5653 \text{ MeV}] - [0 + 1875.6128 \text{ MeV}] \\
 &= [1877.8373 \text{ MeV} - 1875.6128 \text{ MeV}] = 2.225 \text{ MeV}.
 \end{aligned} \tag{9.90}$$

Binding energy method

$$Q = \sum_{i,\text{after}} E_B(i) - \sum_{i,\text{before}} E_B(i) = E_B(^2_1\text{H}) - 0 = 2.225 \text{ MeV}. \tag{9.91}$$

Q values for the three thermal neutron capture reactions have been calculated with the rest energy method and the binding energy method and, for a given nuclear reaction, the two techniques provided identical results.

(c) For a typical nuclear reaction triggered by projectile with mass m_{10} and kinetic energy $(E_K)_0$ striking a stationary target m_{20} and resulting in two reaction products with masses m_{30} and m_{40} , the Q value is defined as

$$Q = (m_{10}c^2 + m_{20}c^2) - (m_{30}c^2 + m_{40}c^2). \tag{9.92}$$

Conservation of total energy in nuclear reaction, on the other hand, results in the following expression

$$[m_{10}c^2 + (E_K)_0] + [m_{20}c^2 + 0] = [m_{30}c^2 + (E_K)_3] + [m_{40}c^2 + (E_K)_4], \tag{9.93}$$

where $(E_K)_3$ and $(E_K)_4$ are kinetic energies of the reaction products m_{30} and m_{40} and the other quantities were defined above. Insertion of (9.92) into (9.93) results in the following simplification of (9.93)

$$(E_K)_0 + Q = (E_K)_3 + (E_K)_4. \tag{9.94}$$

Equation (9.94) can now be further simplified for thermal neutron capture reaction since the incident thermal neutron energy $(E_K)_0 = E_K^n = 0.025 \text{ eV} \approx 0$.

Thus, for thermal neutron capture reaction we can state that the sum of kinetic energies of the reaction products equals to Q value of the reaction

$$Q = (E_K)_3 + (E_K)_4 = \frac{|\mathbf{p}_{m_{30}}|^2}{2m_{30}} + \frac{|\mathbf{p}_{m_{40}}|^2}{2m_{40}} = \frac{p^2}{2} \left[\frac{1}{m_{30}} + \frac{1}{m_{40}} \right], \quad (9.95)$$

where $|\mathbf{p}_{m_{30}}|$ and $|\mathbf{p}_{m_{40}}|$ are momenta of reaction products m_{30} and m_{40} and we use the classical expression for kinetic energy of a particle. Total momentum before the capture reaction is zero, so that to fulfill the principle of momentum conservation the two momenta after the reaction must be equal in magnitude, i.e., $|\mathbf{p}_{m_{30}}| = |\mathbf{p}_{m_{40}}| = p$, and opposite in direction.

We now address the three neutron capture reactions of thermal neutrons with tissue atoms, two of the reactions produce a recoil atom and a γ ray and one reaction produces a recoil atom and a proton.

(1) Q value for reaction ${}^{14}_7\text{N}(n, p){}^{14}_6\text{C}$ was determined in (b) as $Q = 0.626$ MeV. This energy is shared as kinetic energy between two reaction products: proton and ${}^{14}_6\text{C}$ nucleus in the inverse proportion of their masses, since both reaction products carry away the same momentum but in opposite directions. Equation (9.95) for this reaction is expressed as follows

$$Q = E_K^p + E_K^{14\text{C}} = \frac{p^2}{2} \left[\frac{1}{m_p} + \frac{1}{M({}^{14}_7\text{C})} \right] = \frac{p^2}{2} \left[\frac{M({}^{14}_7\text{C}) + m_p}{m_p M({}^{14}_7\text{C})} \right]. \quad (9.96)$$

After rearranging (9.96) we get the following expression for p^2

$$p^2 = 2Q \frac{m_p M({}^{14}_7\text{C})}{M({}^{14}_7\text{C}) + m_p}, \quad (9.97)$$

so that we now express kinetic energy of the proton E_K^p as

$$\begin{aligned} E_K^p &= \frac{p^2}{2m_p} = Q \frac{M({}^{14}_7\text{C})}{M({}^{14}_7\text{C}) + m_p} = Q \frac{M({}^{14}_7\text{C})c^2}{M({}^{14}_7\text{C})c^2 + m_p c^2} \\ &= (0.626 \text{ MeV}) \times \frac{13040.8703}{13040.8703 + 938.2720} = 0.584 \text{ MeV} \end{aligned} \quad (9.98)$$

and kinetic energy of the ${}^{14}_6\text{C}$ nucleus as

$$\begin{aligned} E_K^{14\text{C}} &= \frac{p^2}{2M({}^{14}_7\text{C})} = Q \frac{m_p}{M({}^{14}_7\text{C}) + m_p} = Q \frac{m_p c^2}{M({}^{14}_7\text{C})c^2 + m_p c^2} \\ &= (0.626 \text{ MeV}) \times \frac{938.2720}{13040.8703 + 938.2720} = 0.042 \text{ MeV}. \end{aligned} \quad (9.99)$$

From (9.98) and (9.99) we note that in neutron capture reaction ${}^{14}_7\text{N}(n, p){}^{14}_6\text{C}$ the proton and the ${}^{14}_6\text{C}$ nucleus share the $Q = 0.626$ MeV available energy in the

inverse proportion of their rest masses, so that the proton carries away kinetic energy of $E_K^p = 0.584$ MeV and the $^{14}_6\text{C}$ nucleus carries away kinetic energy of $E_K^{^{14}_6\text{C}} = 0.042$ MeV.

Dose deposition in tissue from thermal neutron absorption is a two-step process. In the first step, energy is transferred from neutron to charged particles via thermal neutron capture contributing to tissue kerma. In the second step, energy is transferred from charged particles to tissue via Coulomb interactions with orbital electrons of tissue atoms, contributing to tissue dose.

In contrast to reaction (1) that in addition to recoil nucleus produces a proton, capture reactions (2) and (3) in addition to recoil nucleus produce a γ photon. The magnitude of the photon momentum p_ν is equal to the magnitude of the recoil nucleus momentum $p(m_{30})$ and the two momenta are opposite in direction to satisfy conservation of momentum in thermal neutron capture (*note*: total momentum before reaction is zero, since the neutron is of thermal energy and the target is stationary). The presence of γ photon after reaction requires a modification of (9.92) and (9.94) to read

$$Q = (m_{10}c^2 + m_{20}c^2) - (m_{30}c^2 + 0) \quad (9.100)$$

and

$$Q = (E_K)_3 + E_\nu = \frac{p_\nu^2}{2m_{30}} + p_\nu c. \quad (9.101)$$

Solving (9.101) for p_ν results in the following quadratic equation

$$p_\nu^2 + 2m_{30}p_\nu c - 2m_{30}Q = 0, \quad (9.102)$$

with the following physical solution for the magnitude of the photon and recoil nucleus momenta

$$p_\nu = \frac{-2m_{30}c + \sqrt{4m_{30}^2c^2 + 8m_{30}Q}}{2} = \frac{m_{30}c^2}{c} \left[\sqrt{1 + \frac{2Q}{m_{30}c^2}} - 1 \right]. \quad (9.103)$$

We now apply (9.103) to reactions (2) and (3) to determine p_ν .

(2) In neutron capture reaction $^{14}_7\text{N}(n, \gamma) ^{13}_7\text{N}$ we determined the Q value as $Q = 10.83$ MeV and m_{30} of (9.103) is $M(^{13}_7\text{N})$, resulting in the following p_ν

$$\begin{aligned} p_\nu &= \frac{M(^{14}_6\text{C})c^2}{c} \left[\sqrt{1 + \frac{2Q}{M(^{13}_7\text{N})c^2}} - 1 \right] \\ &= \frac{12111.1912 \text{ MeV}}{c} \left[\sqrt{1 + \frac{2 \times 10.83}{12111.1912}} - 1 \right] \\ &= \frac{12111.1912 \text{ MeV}}{c} \times (8.94 \times 10^{-4}) = 10.826 \text{ MeV}/c. \end{aligned} \quad (9.104)$$

The photon momentum p_ν and recoil momentum $p(^{13}_7\text{N}) = p_\nu = 10.826 \text{ MeV}/c$ give the following γ photon energy

$$E_\gamma = h\nu = p_\nu c = (10.826 \text{ MeV}/c) \times c = 10.826 \text{ MeV} \quad (9.105)$$

and kinetic energy of the recoil nucleus $E_K^{^{13}_7\text{N}}$

$$E_K^{^{13}_7\text{N}} = \frac{p_\nu^2 c^2}{2M(^{13}_7\text{N})c^2} = \frac{10.826^2}{2 \times 12111.1912} \text{ MeV} = 4.8 \times 10^{-3} \text{ MeV}. \quad (9.106)$$

(3) In neutron capture reaction $^1_0\text{n}(\gamma)^2_1\text{H}$ we determined the Q value as $Q = 2.225 \text{ MeV}$ and m_{30} of (9.103) is $M(^2_1\text{H})$, resulting in the following p_ν

$$\begin{aligned} p_\nu &= \frac{M(^2_1\text{H})c^2}{c} \left[\sqrt{1 + \frac{2Q}{M(^2_1\text{H})c^2}} - 1 \right] = \frac{1875.6128 \text{ MeV}}{c} \left[\sqrt{1 + \frac{2 \times 2.225}{1875.6128}} - 1 \right] \\ &= \frac{1875.6128 \text{ MeV}}{c} \times (1.19 \times 10^{-3}) = 2.224 \text{ MeV}/c. \end{aligned} \quad (9.107)$$

The photon momentum p_ν and recoil momentum $p(^2_1\text{H}) = p_\nu = 2.224 \text{ MeV}/c$ give the following γ photon energy

$$E_\gamma = h\nu = p_\nu c = (2.224 \text{ MeV}/c) \times c = 2.224 \text{ MeV} \quad (9.108)$$

and kinetic energy of the recoil nucleus E_K^{d} , where d stands for the deuteron produced in the neutron capture reaction

$$E_K^{^2_1\text{H}} = E_K^{\text{d}} = \frac{p_\nu^2 c^2}{2M(^2_1\text{H})c^2} = \frac{2.224^2}{2 \times 1875.6128} \text{ MeV} = 1.3 \times 10^{-3} \text{ MeV}. \quad (9.109)$$

From (9.105) and (9.106) as well as from (9.108) and (9.109) it is evident that the γ photon acquires most of the energy available from the Q value (of the order of 99.95 %) and the recoil nucleus, because of its large mass, receives only a small fraction of the available energy (0.05 %). In the first approximation, one can ignore the nuclear recoil energy and assume the full amount of the available Q value of the neutron thermal capture reaction is acquired by the photon when a photon is one of the reaction products.

9.6 Neutron Beams in Medicine

9.6.Q1

(207)

Boron neutron capture therapy (BNCT) is a binary radiotherapy modality used in treatment of brain lesions. First, the patient is injected with a tumor seeking drug containing a stable boron-10 nuclide that has a high cross section for thermal neutron capture ($\sigma = 3838 \text{ b}$) that is over three orders of magnitude larger than the thermal neutron cross section of other nuclides (H, C, N, and O) constituting human tissue. In the second step, the patient is exposed to thermal neutrons which trigger a biologically destructive nuclear reaction in boron-10 accumulated in the tumor, thereby significantly increasing, at least in principle, the therapeutic ratio and the tumor control probability (TCP).

Thermal neutron capture reaction in boron-10 proceeds as shown in Fig. 9.6 below

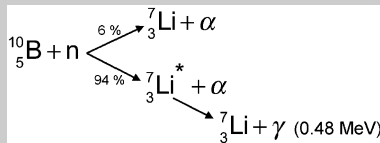


Fig. 9.6 Boron-10 thermal neutron capture reaction

- (a) Calculate Q value of the neutron capture reaction. Use both the rest energy method and the binding energy method. Appropriate nuclear data are provided in Appendix A.
- (b) Determine the kinetic energy E_K^n of the α particle and the $^7_3\text{Li}^{3+}$ ion for both branches of the neutron capture reaction.
- (c) Determine whether or not it is possible for the α particles produced in the thermal neutron capture reaction $^{10}_5\text{B}(n, \alpha)^7_3\text{Li}$ to produce $^{13}_7\text{N}$ in the following reaction: $^{10}_5\text{B}(\alpha, n)^{13}_7\text{N}$.

SOLUTION:

(a) As shown in Fig. 9.6, boron-10 exposed to thermal neutrons may undergo a neutron capture nuclear reaction that produces two reaction products (^7_3Li ion and α particle) with two possible branches: ($^7_3\text{Li}, \alpha$) and ($^7_3\text{Li}^*, \alpha$) with a branching ratio of 6 % vs. 94 %. The lithium-7 excited state de-excites to ground state with emission of a γ ray of energy $E_\gamma = 0.48 \text{ MeV}$.

Q value for both branches of the ($^{10}_5\text{B}, n$) neutron capture reaction is calculated as follows [(T5.7) and (T5.8)]

(1) **Rest energy method:**

$$\begin{aligned}
 Q &= \sum_{i,\text{before}} M_i c^2 - \sum_{i,\text{after}} M_i c^2 = [M({}^{10}_5\text{B})c^2 + m_n c^2] - [m_\alpha c^2 + M({}^7_3\text{Li})c^2] \\
 &= [9324.4362 \text{ MeV} + 939.5654 \text{ MeV}] - [3727.3791 \text{ MeV} + 6533.8329 \text{ MeV}] \\
 &= 10264.0016 \text{ MeV} - 10261.2120 \text{ MeV} = 2.79 \text{ MeV}. \tag{9.110}
 \end{aligned}$$

(2) **Binding energy method:**

$$\begin{aligned}
 Q &= \sum_{i,\text{after}} E_B(i) - \sum_{i,\text{before}} E_B(i) = [E_B({}^7_3\text{Li}) + E_B({}^4_2\text{He})] - [E_B({}^{10}_5\text{B}) + 0] \\
 &= [39.2446 \text{ MeV} + 28.2957 \text{ MeV}] - [64.7507 \text{ MeV} + 0] \\
 &= 2.79 \text{ MeV}. \tag{9.111}
 \end{aligned}$$

Q value for both branches of the (${}^{10}_5\text{B}, n$) neutron capture reaction is 2.79 MeV; however, in the first branch (${}^7_3\text{Li}, \alpha$) the two ions released share the full Q value in energy while in the second branch, which also produces a 0.48 MeV γ ray in the de-excitation process of ${}^7_3\text{Li}^*$, the two ions share the remaining energy $Q - E_\gamma = 2.79 \text{ MeV} - 0.48 \text{ MeV} = 2.31 \text{ MeV}$.

(b) Kinetic energy of reaction products in the neutron capture reaction is determined from the known Q value for the reaction calculated in (a).

(1) Kinetic energies of the α particle and the ${}^7_3\text{Li}^{3+}$ ion produced in the (${}^7_3\text{Li}, \alpha$) branch of the boron-10 neutron capture reaction are calculated as follows. The two reaction products share the Q value energy in the inverse proportion of their masses, since the momenta of the two reaction products (α particle and ${}^7_3\text{Li}$ ion) are equal in magnitude but opposite in direction to satisfy the conservation of momentum principle in thermal neutron capture reaction. *Note:* Total momentum before reaction is zero, so total momentum after capture reaction must also be zero.

Q value can be expressed as follows

$$Q = E_K^{\text{Li}} + E_K^\alpha = \frac{p_{\text{Li}}^2}{2M({}^7_3\text{Li})} + \frac{p_\alpha^2}{2m_\alpha} = \frac{p^2}{2} \left[\frac{1}{M({}^7_3\text{Li})} + \frac{1}{m_\alpha} \right] = \frac{p^2}{2} \frac{m_\alpha + M({}^7_3\text{Li})}{M({}^7_3\text{Li})m_\alpha}, \tag{9.112}$$

where E_K^{Li} and E_K^α are kinetic energy of the ${}^7_3\text{Li}$ ion and α particle, respectively, and p stands for $|\mathbf{p}_{\text{Li}}| = p_{\text{Li}}$ as well as for $|\mathbf{p}_\alpha| = p_\alpha$, since the magnitudes of the two momentum vectors are equal.

Solving (9.112) for p^2 allows us to express the kinetic energies E_K^{Li} and E_K^α , respectively, as follows

$$\begin{aligned} E_K^{\text{Li}} &= \frac{p^2}{2M({}^7_3\text{Li})} = Q \frac{m_\alpha c^2}{M({}^7_3\text{Li})c^2 + m_\alpha c^2} \\ &= (2.79 \text{ MeV}) \times \frac{3727.3791}{6533.8330 + 3727.3791} = (2.79 \text{ MeV}) \times 0.363 = 1.01 \text{ MeV} \end{aligned} \quad (9.113)$$

and

$$\begin{aligned} E_K^\alpha &= \frac{p^2}{2m_\alpha c^2} = Q \frac{M({}^7_3\text{Li})}{M({}^7_3\text{Li})c^2 + m_\alpha c^2} \\ &= (2.79 \text{ MeV}) \times \frac{6533.8330}{6533.8330 + 3727.3791} = (2.79 \text{ MeV}) \times 0.637 = 1.78 \text{ MeV}. \end{aligned} \quad (9.114)$$

(2) Kinetic energies of the α particle and the ${}^7_3\text{Li}^{3+}$ excited ion produced in the $({}^7_3\text{Li}^*, \alpha)$ branch of the boron-10 neutron capture reaction are calculated as follows. The excited nucleus ${}^7_3\text{Li}^*$ attains the ground state of ${}^7_3\text{Li}$ through emission of a γ ray of energy $E_\gamma = 0.48 \text{ MeV}$. Thus, the energy difference $Q - E_\gamma = 2.31 \text{ MeV}$ rather than the full energy of the Q value is available for sharing between the ${}^7_3\text{Li}$ ion and α particle and the energy is again shared in the inverse proportion of the masses of the two ions. For this branch of the boron-10 neutron capture reaction kinetic energies E_K^{Li} and E_K^α , respectively, are given as follows

$$\begin{aligned} E_K^{\text{Li}} &= \frac{p^2}{2M({}^7_3\text{Li})} = (Q - E_\gamma) \frac{m_\alpha c^2}{M({}^7_3\text{Li})c^2 + m_\alpha c^2} \\ &= (2.31 \text{ MeV}) \times \frac{3727.3791}{6533.8330 + 3727.3791} = (2.31 \text{ MeV}) \times 0.363 = 0.84 \text{ MeV} \end{aligned} \quad (9.115)$$

and

$$\begin{aligned} E_K^\alpha &= \frac{p^2}{2m_\alpha c^2} = (Q - E_\gamma) \frac{M({}^7_3\text{Li})}{M({}^7_3\text{Li})c^2 + m_\alpha c^2} \\ &= (2.31 \text{ MeV}) \times \frac{6533.8330}{6533.8330 + 3727.3791} = (2.31 \text{ MeV}) \times 0.637 = 1.47 \text{ MeV}. \end{aligned} \quad (9.116)$$

(c) Neutron capture reaction ${}^{10}_5\text{B}(n, \alpha){}^7_3\text{Li}$ proceeds in two branches, the 6 % branch producing 1.78 MeV α particles and the 94 % branch producing 1.47 MeV α particles [see (b)]. To establish whether or not reaction ${}^{10}_5\text{B}(\alpha, n){}^{13}_7\text{N}$ can run with these α particles we first evaluate the reaction Q value using the rest energy method

and the binding energy method as follows

$$\begin{aligned}
 Q &= \sum_{i,\text{before}} M_i c^2 - \sum_{i,\text{after}} M_i c^2 = [M({}^{10}_5\text{B})c^2 + m_n c^2] - [m_n c^2 + M({}^{13}_7\text{N})c^2] \\
 &= [9324.4362 \text{ MeV} + 3727.3791 \text{ MeV}] - [939.5654 \text{ MeV} + 1211.1910 \text{ MeV}] \\
 &= 13051.8153 \text{ MeV} - 13050.7564 \text{ MeV} = 1.059 \text{ MeV}, \tag{9.117}
 \end{aligned}$$

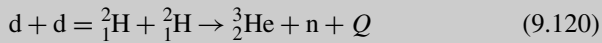
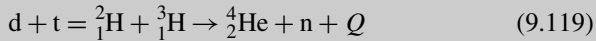
$$\begin{aligned}
 Q &= \sum_{i,\text{after}} E_B(i) - \sum_{i,\text{before}} E_B(i) = [0 + E_B({}^{13}_7\text{N})] - [E_B({}^{10}_5\text{B}) + E_B({}^4_2\text{He})] \\
 &= [0 + 94.1053 \text{ MeV}] - [64.7507 \text{ MeV} + 28.2957 \text{ MeV}] = 1.059 \text{ MeV}. \tag{9.118}
 \end{aligned}$$

Since Q value of the reaction ${}^{10}_5\text{B}(\alpha, n){}^{13}_7\text{N}$ is positive, the reaction is exothermic and can proceed without any threshold energy restrictions.

9.6.Q2

(208)

Primary sources of neutrons are: nuclear reactors, neutron emitting radionuclides, and accelerator-based neutron generators. The latter are small, relatively low voltage (of the order of 100 kV) accelerators based on deuterium-tritium (d-t) and deuterium-deuterium (d-d) fusion reactions:



Neutron generators based on the d-t fusion reaction are more common than those based on the d-d reaction because the neutron yield of the d-t reaction is up to 100 times larger than that of the d-d reaction.

- (a) Using both the rest energy method and the binding energy method, determine Q value of the two fusion reactions used in neutron generators. Appropriate data are available in Appendix A.
- (b) Determine kinetic energy of the neutron and the helium ions produced in the two fusion reactions.
- (c) Determine the velocity v/c of neutrons produced in the d-t and d-d fusion reactions of (9.119) and (9.120), respectively. Plot v/c against kinetic energy E_K^n of neutron and enter onto the graph your calculated values for the d-t and d-d fusion reactions.

SOLUTION:

- (a) Q values of the fusion reactions used for fast-neutron production in neutron generators.

(1) Q value of the d-t fusion reaction: Rest energy method.

$$\begin{aligned} Q &= \sum_{i,\text{before}} M_i c^2 - \sum_{i,\text{after}} M_i c^2 = [m_d c^2 + m_t c^2] - [M({}_2^4\text{He})c^2 + m_n c^2] \\ &= [1875.6128 \text{ MeV} + 2808.9209 \text{ MeV}] - [3727.3791 \text{ MeV} + 939.5654 \text{ MeV}] \\ &= 4684.5337 \text{ MeV} - 4666.9445 \text{ MeV} = 17.59 \text{ MeV}. \end{aligned} \quad (9.121)$$

Q value of the d-t fusion reaction: Binding energy method.

$$\begin{aligned} Q &= \sum_{i,\text{after}} E_B(i) - \sum_{i,\text{before}} E_B(i) = [E_B({}_2^4\text{He}) + 0] - [E_B(\text{d}) + E_B(\text{t})] \\ &= [28.2957 \text{ MeV} + 0] - [2.2246 \text{ MeV} + 8.4818 \text{ MeV}] \\ &= 28.2957 \text{ MeV} - 10.7064 \text{ MeV} = 17.59 \text{ MeV}. \end{aligned} \quad (9.122)$$

Both the rest energy method and the binding energy method give the same result for the Q value of the d-t fusion reaction: 17.59 MeV.

(2) Q value of the d-d fusion reaction: Rest energy method.

$$\begin{aligned} Q &= \sum_{i,\text{before}} M_i c^2 - \sum_{i,\text{after}} M_i c^2 = [m_d c^2 + m_d c^2] - [M({}_2^3\text{He})c^2 + m_n c^2] \\ &= [1875.6128 \text{ MeV} + 1875.6128 \text{ MeV}] - [2808.6128 \text{ MeV} + 939.5654 \text{ MeV}] \\ &= 3751.2256 \text{ MeV} - 3747.9567 \text{ MeV} = 3.27 \text{ MeV}. \end{aligned} \quad (9.123)$$

Q value of the d-d fusion reaction: Binding energy method

$$\begin{aligned} Q &= \sum_{i,\text{after}} E_B(i) - \sum_{i,\text{before}} E_B(i) = [E_B({}_2^3\text{He}) + 0] - [E_B(\text{d}) + E_B(\text{d})] \\ &= [7.7181 \text{ MeV} + 0] - [2.2246 \text{ MeV} + 2.2246 \text{ MeV}] \\ &= 7.7181 \text{ MeV} - 4.4492 \text{ MeV} = 3.27 \text{ MeV}. \end{aligned} \quad (9.124)$$

Both the rest energy method and the binding energy method give the same result for the Q value of the d-d fusion reaction: 3.27 MeV.

(b) *Kinetic energy of the two reaction products* of the d-t fusion reaction are calculated assuming that the kinetic energy of the deuteron projectile is negligible in comparison to kinetic energies E_K^α and E_K^n of the reaction products after the reaction. Under this assumption the reaction Q value of 17.59 MeV is shared as kinetic energy of the two reaction products in inverse proportions to the masses of reaction products. Since the total momentum before the reaction is ~ 0 , we conclude that the momenta of the two reaction products are equal in magnitude and opposite in direction, i.e.,

$$|\mathbf{p}_\alpha| = |\mathbf{p}_n| = p. \quad (9.125)$$

(1) Kinetic energy of the reaction products of the d-t fusion reaction is determined from the Q value calculated in (9.123) and (9.124). The expression for the Q value of the d-t fusion reaction is written as

$$Q = E_K^{\text{He-4}} + E_K^n = \frac{p_{\text{He-4}}^2}{2M({}_2^4\text{He})} + \frac{p_n^2}{2m_n} = \frac{p^2}{2} \left[\frac{1}{M({}_2^4\text{He})} + \frac{1}{m_n} \right] = \frac{p^2}{2} \frac{m_n + M({}_2^4\text{He})}{m_n M({}_2^4\text{He})}. \quad (9.126)$$

After solving (9.126) for p^2 and inserting p^2 into equations for E_K^α and E_K^n we get the following results for kinetic energy of the α particle and neutron, respectively

$$\begin{aligned} E_K^{\text{He-4}} &= \frac{p^2}{2M({}_2^4\text{He})} = Q \frac{(m_n c^2)}{M({}_2^4\text{He}) + m_n c^2} \\ &= (17.59 \text{ MeV}) \times \frac{939.5654}{3727.3791 + 939.5654} \\ &= (17.59 \text{ MeV}) \times 0.20 = 3.54 \text{ MeV} \end{aligned} \quad (9.127)$$

and

$$\begin{aligned} E_K^n &= \frac{p^2}{2m_n} = Q \frac{M({}_2^4\text{He})}{M({}_2^4\text{He}) + m_n c^2} \\ &= (17.59 \text{ MeV}) \times \frac{3727.3791}{3727.3791 + 939.5654} \\ &= (17.59 \text{ MeV}) \times 0.80 = 14.05 \text{ MeV}. \end{aligned} \quad (9.128)$$

(2) Kinetic energies of the two reaction products (${}^3_2\text{He}$ ion and neutron) of the d-d fusion reaction are calculated using the same assumptions that were used for the d-t reactions above. Kinetic energy of the $E_K^{\text{He-3}}$ ion and kinetic energy E_K^n of the neutron are calculated with (9.126), (9.127) and (9.128), respectively, all three equations modified to account for the rest mass of the ${}^3_2\text{He}$ ion. The expression for Q value of the d-d fusion reaction is written as

$$Q = E_K^{\text{He-3}} + E_K^n = \frac{p_{\text{He-3}}^2}{2M({}_2^3\text{He})} + \frac{p_n^2}{2m_n} = \frac{p^2}{2} \left[\frac{1}{M({}_2^3\text{He})} + \frac{1}{m_n} \right] = \frac{p^2}{2} \frac{m_n + M({}_2^3\text{He})}{m_n M({}_2^3\text{He})}. \quad (9.129)$$

After solving (9.129) for p^2 , kinetic energies of ${}^3_2\text{He}$ ion and neutron are calculated as follows

$$\begin{aligned} E_K^{\text{He-3}} &= \frac{p^2}{2M({}_2^3\text{He})} = Q \frac{(m_n c^2)}{M({}_2^3\text{He})c^2 + m_n c^2} \\ &= (3.27 \text{ MeV}) \times \frac{939.5654}{2808.3913 + 939.5654} \\ &= (3.27 \text{ MeV}) \times 0.251 = 0.82 \text{ MeV} \end{aligned} \quad (9.130)$$

and

$$\begin{aligned}
 E_K^n &= \frac{p^2}{2m_n} = Q \frac{M({}_2^3\text{He})}{M({}_2^3\text{He}) + m_n c^2} \\
 &= (3.27 \text{ MeV}) \times \frac{2808.3913}{2808.3913 + 939.5654} \\
 &= (3.27 \text{ MeV}) \times 0.749 = 2.45 \text{ MeV}. \tag{9.131}
 \end{aligned}$$

The d-t fusion reaction is the easiest fusion reaction to ignite and occurs when the deuteron and triton have essentially negligible kinetic energy in comparison to 17.59 MeV of energy that is released in the d-t fusion reaction. In both d-t as well as d-d fusion reaction neutrons are produced in a suitable target and emitted almost isotropically. Neutron and helium ion (α particle in d-t reaction and ${}_2^3\text{He}$ ion in d-d reaction) are emitted in directions opposite to each other in order to conserve the total momentum that before the interaction is essentially zero.

(c) Velocity of neutrons produced in d-t reaction with kinetic energy of 14.05 MeV and in d-d reaction with kinetic energy of 3.27 MeV is calculated from the standard relativistic expression for kinetic energy that is given as follows (T1.58). In (9.132) E_K^n is kinetic energy of the neutron, γ is the Lorentz factor (T1.43), and $m_n c^2$ is the rest energy of the neutron (939.6 MeV).

$$E_K^n = (\gamma - 1)m_n c^2 = \left(\frac{1}{\sqrt{1 - \frac{v^2}{c^2}}} - 1 \right) m_n c^2. \tag{9.132}$$

Solving (9.132) for v/c results in the following expression (T2.7)

$$\frac{v}{c} = \sqrt{1 - \frac{1}{\left(1 + \frac{E_K^n}{m_n c^2}\right)^2}}, \tag{9.133}$$

resulting in $v/c = 0.17$ for neutron kinetic energy of $E_K^n = 14.05$ MeV produced in the d-t fusion reaction and in $v/c = 0.072$ for neutron kinetic energy of $E_K^n = 2.45$ MeV produced in the d-d fusion reaction. A plot of (9.133) showing v/c against kinetic energy E_K^n of a neutron in the kinetic energy range from 1 keV to 100 MeV is presented in Fig. 9.7.

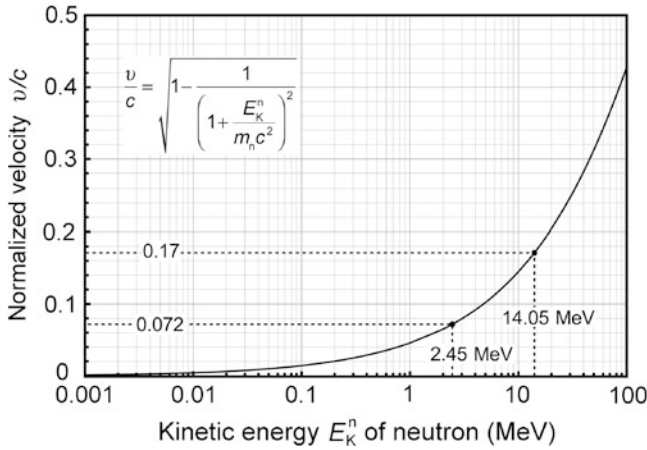


Fig. 9.7 Neutron velocity v normalized to speed of light c in vacuum against kinetic energy E_K^n of the neutron. The two data points on the graph represent neutron velocities calculated for the 2.45 MeV and 14.05 MeV neutrons produced in the d-d and d-t reaction, respectively

9.6.Q3

(209)

The most common and efficient means for production of clinical neutron beam in a cyclotron is to accelerate protons p or deuterons d in the energy range from 50 MeV to 70 MeV onto a thick beryllium-9 target. This results in neutron spectra that are characteristic of the particular nuclear reaction used, with the maximum neutron energy in the spectrum given as the sum of the incident charged particle kinetic energy and the reaction Q value for the particular nuclear reaction that produces the neutrons.

Neutron-generating nuclear reactions occurring in the beryllium-9 target are as follows



and



- Calculate Q values for reactions (9.134) and (9.135) and for the two nuclear reactions determine if the reactions are exothermic or endothermic. Appropriate nuclear data are given in Appendix A.
- For endothermic reactions of (a) calculate the threshold energy, i.e., the minimum kinetic energy that the incident charged particle must possess in order to trigger the nuclear reaction.

SOLUTION:

(a) Q values of reactions (9.134) and (9.135) are calculated either with the rest energy method or with the binding energy method.

(1) Q value for reaction ${}^9_4\text{Be} + \text{p} \rightarrow \text{n} + {}^9_3\text{B} + Q$ determined with the rest energy method:

$$\begin{aligned} Q &= \sum_{i,\text{before}} M_i c^2 - \sum_{i,\text{after}} M_i c^2 = [M({}^9_4\text{Be})c^2 + m_p c^2] - [m_n c^2 + M({}^9_3\text{B})c^2] \\ &= [8392.7499 \text{ MeV} + 938.2703 \text{ MeV}] - [939.5654 \text{ MeV} + 8393.3071 \text{ MeV}] \\ &= 9331.0202 \text{ MeV} - 9332.8725 \text{ MeV} = -1.85 \text{ MeV}. \end{aligned} \quad (9.136)$$

Q value for reaction ${}^9_4\text{Be} + \text{p} \rightarrow \text{n} + {}^9_3\text{B} + Q$ determined with the binding energy method:

$$\begin{aligned} Q &= \sum_{i,\text{after}} E_B(i) - \sum_{i,\text{before}} E_B(i) = [0 + E_B({}^9_3\text{B})] - [E_B({}^9_4\text{Be}) + 0] \\ &= [0 + 56.3145 \text{ MeV}] - [58.1650 \text{ MeV} + 0] = -1.85 \text{ MeV}. \end{aligned} \quad (9.137)$$

Q value for reaction ${}^9_4\text{Be} + \text{p} \rightarrow \text{n} + {}^9_3\text{B}$ is negative ($Q = -1.85 \text{ MeV}$) which means that the reaction is endothermic and the incident proton must possess a minimum kinetic energy, referred to as the threshold kinetic energy ($E_K^{\text{p}}{}_{\text{thr}}$), in order to be able to trigger the nuclear reaction. The threshold total energy and the threshold kinetic energy of the proton to be able to trigger neutron production in a beryllium thick target will be determined in (b).

(2) Q value for reaction ${}^9_4\text{Be} + \text{d} \rightarrow \text{n} + {}^{10}_5\text{B} + Q$ determined with the rest energy method:

$$\begin{aligned} Q &= \sum_{i,\text{before}} M_i c^2 - \sum_{i,\text{after}} M_i c^2 = [M({}^9_4\text{Be})c^2 + m_d c^2] - [m_n c^2 + M({}^{10}_5\text{B})c^2] \\ &= [8392.7499 \text{ MeV} + 1875.6128 \text{ MeV}] \\ &\quad - [939.5654 \text{ MeV} + 9324.4362 \text{ MeV}] \end{aligned} \quad (9.138)$$

$$= 10268.3627 \text{ MeV} - 10264.0016 \text{ MeV} = +4.36 \text{ MeV}. \quad (9.139)$$

Q value for reaction ${}^9_4\text{Be} + \text{d} \rightarrow \text{n} + {}^{10}_5\text{B} + Q$ determined with the binding energy method:

$$\begin{aligned} Q &= \sum_{i,\text{after}} E_B(i) - \sum_{i,\text{before}} E_B(i) = [0 + E_B({}^{10}_5\text{B})] - [E_B({}^9_4\text{Be}) + E_B(\text{d})] \\ &= [0 + 64.7507 \text{ MeV}] - [58.1650 \text{ MeV} + 2.2246 \text{ MeV}] \\ &= +4.36 \text{ MeV}. \end{aligned} \quad (9.140)$$

Q value for reaction ${}^9_4\text{Be} + \text{d} \rightarrow \text{n} + {}^{10}_5\text{B}$ is positive ($Q = +4.36$ MeV) which means that the reaction is exothermic and there is no minimum energy prescribed for the deuteron to trigger the nuclear reaction.

(b) Fast neutrons are produced in accelerators in which either protons or deuterons are first accelerated to relatively high kinetic energy and then bombard a thick beryllium target in which a spectrum of fast neutrons is produced. As shown in (a), Q value of the ${}^9_4\text{Be}(p, \text{n}){}^9_5\text{B}$ reaction is negative at -1.85 MeV, while Q value of the ${}^9_4\text{Be}(\text{d}, \text{n}){}^{10}_5\text{B}$ reaction is positive at $+4.36$ MeV.

A positive Q value suggests that the reaction is exothermic (also called exoergic), has no threshold, and results in release of energy. On the other hand, a negative Q value suggests that the reaction is endothermic (also called endoergic) and that for the reaction to take place the incident proton (projectile) energy must exceed a minimum energy that is referred to as the reaction threshold energy.

The threshold energy for a general endothermic collision of projectile m_{10} with stationary target m_{20} that results in two reaction products (m_{30} and m_{40}) is determined through the use of the so-called relativistic invariant

$$E^2 - p^2c^2 = \text{invariant}, \quad (9.141)$$

where E is the total energy before the collision and the total energy after the collision, p is the total momentum before and after the collision, and c is the speed of light in vacuum.

The invariant is valid for both the *laboratory coordinate system* and for the *center-of-mass coordinate system* and, for convenience, the conditions before the collision are written for the laboratory system while the conditions after the collision are written for the center-of-mass system. The conditions for before and after the collision are written as follows:

(1) Before collision:

$$\text{Total energy before collision: } E_{\text{thr}} + m_{20}c^2 = \sqrt{m_{10}^2c^4 + p_1^2c^2} + m_{20}c^2, \quad (9.142)$$

where E_{thr} is the total threshold energy of the projectile.

Total momentum before collision: p_1

(2) After collision:

$$\text{Total energy after collision: in the center-of-mass system: } m_{30}c^2 + m_{40}c^2 \quad (9.143)$$

Total momentum after collision: in the center-of-mass system: 0

The invariant of (9.141) for before and after the collision is now expressed as follows

$$E^2 - p^2c^2 = \left(\sqrt{m_{10}^2c^4 + p_1^2c^2} + m_{20}c^2 \right)^2 - p_1^2c^2 = (m_{30}c^2 + m_{40}c^2)^2 - 0. \quad (9.144)$$

Solving for $E_{\text{thr}} = \sqrt{m_{10}^2 c^4 + p_1^2 c^2}$ results in the following expression for the total threshold energy for the collision (nuclear reaction)

$$E_{\text{thr}} = \frac{(m_{30}c^2 + m_{40}c^2)^2 - (m_{10}^2c^4 + m_{20}^2c^4)}{2m_{20}c^2}. \quad (9.145)$$

Noting that $E_{\text{thr}} = (E_{\text{K}})_{\text{thr}} + m_{10}c^2$, where $(E_{\text{K}})_{\text{thr}}$ is the threshold kinetic energy of the projectile, we get the following expression for $(E_{\text{K}})_{\text{thr}}$

$$(E_{\text{K}})_{\text{thr}} = \frac{(m_{30}c^2 + m_{40}c^2)^2 - (m_{10}c^2 + m_{20}c^2)^2}{2m_{20}c^2}. \quad (9.146)$$

The threshold kinetic energy $(E_{\text{K}})_{\text{thr}}$ of the projectile given in (9.146) may now be written in terms of the nuclear reaction Q value as follows:

- (1) Recalling that Q value for the general endothermic nuclear reaction is written as (T5.5)

$$Q = m_{10}c^2 + m_{20}c^2 + m_{30}c^2 + m_{40}c^2, \quad (9.147)$$

we rearrange the terms of (9.147) to get the following expression

$$(m_{30}c^2 + m_{40}c^2)^2 = (m_{10}c^2 + m_{20}c^2)^2 + Q^2 - 2Q(m_{10}c^2 + m_{20}c^2). \quad (9.148)$$

- (2) Inserting the relationship of (9.147) into (9.146) we obtain

$$(E_{\text{K}})_{\text{thr}} = -Q \left[\frac{m_{10}c^2 + m_{20}c^2}{m_{20}c^2} - \frac{Q}{2m_{20}c^2} \right] \approx -Q \left(1 + \frac{m_{10}}{m_{20}} \right), \quad (9.149)$$

where, since $Q \ll m_{20}c^2$, we can ignore the $\frac{Q}{2m_{20}c^2}$ term in (9.149).

In (9.149) the threshold kinetic energy $(E_{\text{K}})_{\text{thr}}$ of projectile exceeds the $|Q|$ value by a relatively small amount to account for conservation of both energy and momentum in the collision.

Reaction ${}^9_4\text{Be}(p, n){}^9_5\text{B}$ in (a) is endothermic, so we now determine its threshold total energy E_{thr} and its threshold kinetic energy $(E_{\text{K}})_{\text{thr}}$ using (9.145) and (9.146), respectively.

- (1) Threshold total energy E_{thr} is calculated as follows

$$\begin{aligned} E_{\text{thr}} &= \frac{(m_{30}c^2 + m_{40}c^2)^2 - (m_{10}^2c^4 + m_{20}^2c^4)}{2m_{20}c^2} \\ &= \frac{[m_{\text{n}}c^2 + M({}^9_5\text{B})c^2]^2 - [m_{\text{p}}^2c^4 + (M({}^9_4\text{Be}))^2c^4]}{2M({}^9_4\text{Be})c^2} \\ &= \frac{[939.5654 \text{ MeV} + 8393.3071 \text{ MeV}]^2 - [(938.2720 \text{ MeV})^2 + (8392.7499 \text{ MeV})^2]}{2 \times (8392.7499 \text{ MeV})} \\ &= 940.33 \text{ MeV}. \end{aligned} \quad (9.150)$$

(2) Threshold kinetic energy $(E_K)_{\text{thr}}$ is calculated from the following expression

$$\begin{aligned}
 (E_K)_{\text{thr}} &\equiv E_{\text{thr}} - m_p c^2 = \frac{(m_{30}c^2 + m_{40}c^2)^2 - (m_{10}c^2 + m_{20}c^2)^2}{2m_{20}c^2} \\
 &= \frac{[m_n c^2 + M({}_3^9\text{B})c^2]^2 - [m_p c^2 + M({}_4^9\text{Be})c^2]^2}{2M({}_4^9\text{Be})c^2} \\
 &= \frac{[939.5654 \text{ MeV} + 8393.3071 \text{ MeV}]^2 - [938.2720 \text{ MeV} + 8392.7499 \text{ MeV}]^2}{2 \times (8392.7499 \text{ MeV})} \\
 &= 2.06 \text{ MeV}.
 \end{aligned} \tag{9.151}$$

Threshold kinetic energy $(E_K)_{\text{thr}}$ can also be determined using Q value of the endothermic reaction, as stated in (9.149)

$$\begin{aligned}
 (E_K)_{\text{thr}} &\approx -Q \left[1 + \frac{m_{10}}{m_{20}} \right] = -Q \left[1 + \frac{m_p}{M({}_4^9\text{Be})} \right] \\
 &= -(-1.85 \text{ MeV}) \times \left[1 + \frac{938.2720}{8392.7499} \right] \\
 &= (1.85 \text{ MeV}) \times 1.11 = 2.06 \text{ MeV}.
 \end{aligned} \tag{9.152}$$

Threshold kinetic energy $(E_K)_{\text{thr}}$ of the proton in the ${}_4^9\text{Be}(p, n){}_3^9\text{B}$ reaction exceeds the $|Q|$ value of the reaction by a relatively small amount of 11 % to account for conservation of both energy and momentum in the reaction.

9.6.Q4

(210)

Californium (Cf) is a synthetic radioactive transuranic element in the actinide series with an atomic number Z of 98 and 20 known radioisotopes. Of these only Cf-252, as an intense neutron emitter, is of commercial interest and was found useful in a wide range of specialized areas of science, industry, and medicine, such as the study of fission, neutron activation analysis, neutron radiography, well logging, nuclear reactor start up, and brachytherapy of cancer.

Californium-252 decays through two radioactive decay modes: (1) α decay with half life $(t_{1/2})_\alpha = 2.73$ years and branching fraction (ratio) of 0.969 and (2) spontaneous fission accompanied by emission of neutrons with half life of $(t_{1/2})_{\text{SF}} = 85.5$ years and branching fraction (ratio) of 0.031. Mean neutron fraction \bar{f}_n , i.e., the mean number of neutrons emitted per each spontaneous fission decay is $\bar{f}_n = 3.8$.

- (a) Determine the effective half-life $(t_{1/2})_{\text{eff}}$ of a $^{252}_{98}\text{Cf}$ neutron source.
- (b) Determine the monthly decay (in %) of a $^{252}_{98}\text{Cf}$ neutron source.
- (c) Determine specific activity a_{SF} for spontaneous fission of $^{252}_{98}\text{Cf}$.
- (d) Determine specific activity a_{α} for α decay of $^{252}_{98}\text{Cf}$.
- (e) Determine specific activity a_{eff} for decay of $^{252}_{98}\text{Cf}$.
- (f) Determine the neutron production rate of $^{252}_{98}\text{Cf}$ in number of neutrons per second.
- (g) Calculate Q value for α decay of $^{252}_{98}\text{Cf}$ into $^{248}_{96}\text{Cm}$ (curium) and determine the kinetic energy E_{K}^{α} of the emitted α particle.

SOLUTION:

(a) The effective half-life $(t_{1/2})_{\text{eff}}$ is calculated via the total decay constant λ of $^{252}_{98}\text{Cf}$ which follows the general rule of radioactivity stipulating that when more than one mode of decay is available to the radioactive nucleus (branching), the total decay constant λ is the sum of the partial decay constants λ_i applicable to each mode. We thus have

$$\lambda = \sum_i \lambda_i = \lambda_{\alpha} + \lambda_{\text{SF}} = \frac{\ln 2}{(t_{1/2})_{\alpha}} + \frac{\ln 2}{(t_{1/2})_{\text{SF}}} = (\ln 2) \left[\frac{1}{(t_{1/2})_{\alpha}} + \frac{1}{(t_{1/2})_{\text{SF}}} \right] = \frac{\ln 2}{(t_{1/2})_{\text{eff}}}. \quad (9.153)$$

The effective half-life $(t_{1/2})_{\text{eff}}$ of a $^{252}_{98}\text{Cf}$ source is calculated as follows

$$\frac{1}{(t_{1/2})_{\text{eff}}} = \frac{1}{(t_{1/2})_{\alpha}} + \frac{1}{(t_{1/2})_{\text{SF}}} = \frac{1}{2.73 \text{ y}} + \frac{1}{85.5 \text{ y}} = 0.378 \text{ y}^{-1}, \quad (9.154)$$

resulting in $(t_{1/2})_{\text{eff}} = 2.645 \text{ y}$.

(b) The monthly decay (in %) of a $^{252}_{98}\text{Cf}$ neutron source is calculated by assuming exponential source decay and an effective half-life $(t_{1/2})_{\text{eff}} = 2.645 \text{ y}$, as determined in (9.154). The monthly rate of source decay is expressed with the ratio I/I_0 , where I_0 is the source intensity at a given distance d from the source on day 0 (time: $t = 0$) and I is the source intensity at the same distance d from the source on day 30 (time: $t = 30$ days). I/I_0 is given as follows

$$\frac{I}{I_0} = e^{-\frac{\ln 2}{(t_{1/2})_{\text{eff}}} t} = e^{-\frac{(\ln 2) \times 30}{2.645 \times 365}} = e^{-0.0216} = 0.979 \quad (9.155)$$

indicating that in one month a $^{252}_{98}\text{Cf}$ neutron source will decay by 2.1 %.

(c) Specific activity a_{SF} of $^{252}_{98}\text{Cf}$ for spontaneous fission is calculated from activity \mathcal{A}_{SF} for spontaneous fission defined as $\mathcal{A}_{\text{SF}} = \lambda_{\text{SF}} N$ where N stands for the number

of radioactive atoms, N_A is the Avogadro number ($6.022 \times 10^{23} \text{ mol}^{-1}$), and A is the atomic mass number in g/mol

$$\begin{aligned} a_{\text{SF}} &= \frac{\mathcal{A}_{\text{SF}}}{m} = \frac{\lambda_{\text{SF}} N}{m} = \frac{\lambda_{\text{SF}} N_A}{A} = \frac{\ln 2}{(t_{1/2})_{\text{SF}}} \frac{N_A}{A} \\ &= \frac{(\ln 2) \times (6.022 \times 10^{23} \text{ mol}^{-1})}{(85.5 \text{ y}) \times (365 \text{ day/y}) \times (24 \text{ h/day}) \times (3600 \text{ s/h}) \times (252 \text{ g} \cdot \text{mol}^{-1})} \\ &= 6.143 \times 10^{11} \text{ s}^{-1} \cdot \text{g}^{-1} = 0.6143 \text{ TBq} \cdot \text{g}^{-1}. \end{aligned} \quad (9.156)$$

(d) Specific activity a_α of $^{252}_{98}\text{Cf}$ for α decay is calculated from activity \mathcal{A}_α for α decay defined as $\mathcal{A}_\alpha = \lambda_\alpha N$

$$\begin{aligned} a_\alpha &= \frac{\mathcal{A}_\alpha}{m} = \frac{\lambda_\alpha N}{m} = \frac{\lambda_\alpha N_A}{A} = \frac{\ln 2}{(t_{1/2})_\alpha} \frac{N_A}{A} \\ &= \frac{(\ln 2) \times (6.022 \times 10^{23} \text{ mol}^{-1})}{(2.73 \text{ y}) \times (365 \text{ day/y}) \times (24 \text{ h/day}) \times (3600 \text{ s/h}) \times (252 \text{ g} \cdot \text{mol}^{-1})} \\ &= 19.24 \times 10^{12} \text{ s}^{-1} \cdot \text{g}^{-1} = 19.24 \text{ TBq} \cdot \text{g}^{-1}. \end{aligned} \quad (9.157)$$

(e) Specific activity a_{eff} of $^{252}_{98}\text{Cf}$ is simply the sum of specific activities for α decay and for spontaneous fission

$$a_{\text{eff}} = a_\alpha + a_{\text{SF}} = 19.24 \text{ TBq/s} + 0.61 \text{ TBq/g} = 19.85 \text{ TBq/g}. \quad (9.158)$$

We can obtain the same result calculated directly from activity \mathcal{A} of $^{252}_{98}\text{Cf}$ defined as $\mathcal{A} = \lambda N$

$$\begin{aligned} a_{\text{eff}} &= \frac{\mathcal{A}}{m} = \frac{\lambda N}{m} = \frac{\lambda N_A}{A} = \frac{\ln 2}{(t_{1/2})_{\text{eff}}} \frac{N_A}{A} \\ &= \frac{(\ln 2) \times (6.022 \times 10^{23} \text{ mol}^{-1})}{(2.645 \text{ y}) \times (365 \text{ day/y}) \times (24 \text{ h/day}) \times (3600 \text{ s/h}) \times (252 \text{ g} \cdot \text{mol}^{-1})} \\ &= 19.85 \times 10^{12} \text{ s}^{-1} \cdot \text{g}^{-1} = 19.85 \text{ TBq} \cdot \text{g}^{-1} \\ &= \frac{19.85 \times 10^{12} \text{ Bq} \cdot \text{g}^{-1}}{3.7 \times 10^{10} \text{ Bq/Ci}} = 536.5 \text{ Ci/g}. \end{aligned} \quad (9.159)$$

(f) Neutron production rate in units of $\text{g}^{-1} \cdot \text{s}^{-1}$ is calculated by multiplying the specific activity a_{SF} of $^{252}_{98}\text{Cf}$ for spontaneous fission by the neutron factor \bar{f}_n (defined as the mean number of neutrons produced by each spontaneous fission decay) to get

$$\bar{f}_n a_{\text{SF}} = 3.8 \times (0.6143 \times 10^{12} \text{ s}^{-1} \cdot \text{g}^{-1}) = 2.33 \times 10^{12} \text{ s}^{-1} \cdot \text{g}^{-1}. \quad (9.160)$$

- (1) Industrial sources contain up to 50 mg of emitting of the order of $\sim 10^{11}$ neutrons per second $[(50 \times 10^{-3} \text{ g}) \times (2.33 \times 10^{12} \text{ s}^{-1} \cdot \text{g}^{-1}) \approx 10^{11} \text{ s}^{-1}]$.
- (2) High dose rate brachytherapy (HDR) source requires about 500 μg of $^{252}_{98}\text{Cf}$ per source emitting of the order of $\sim 10^9$ neutron/s $[(500 \times 10^{-6} \text{ g}) \times (2.33 \times 10^{12} \text{ s}^{-1} \cdot \text{g}^{-1}) \approx 10^9 \text{ s}^{-1}]$.

(g) Q value for α decay of $^{252}_{98}\text{Cf}$ into $^{248}_{96}\text{Cm}$ is calculated in a manner similar to the calculation of Q value for nuclear reactions using either (1) rest energy method or (2) binding energy method.

- (1) Rest energy method for α decay: $^{252}_{98}\text{Cf} \rightarrow ^{248}_{96}\text{Cm} + \alpha$

$$\begin{aligned} Q_{\alpha} &= \sum_{i,\text{before}} M_i c^2 - \sum_{i,\text{after}} M_i c^2 = [M(^{252}_{98}\text{Cf})] - [M(^{248}_{96}\text{Cm})c^2 + m_{\alpha}c^2] \\ &= [234762.4495 \text{ MeV}] - [231028.8556 \text{ MeV} + 3727.3791 \text{ MeV}] \\ &= [234762.4495 \text{ MeV}] - [234756.2347 \text{ MeV}] = 6.215 \text{ MeV}. \quad (9.161) \end{aligned}$$

- (2) Binding energy method for α decay: $^{252}_{98}\text{Cf} \rightarrow ^{248}_{96}\text{Cm} + \alpha$

$$\begin{aligned} Q_{\alpha} &= \sum_{i,\text{after}} E_B(i) - \sum_{i,\text{before}} E_B(i) = [E_B^{\text{Cm-248}} + E_B^{\text{Cm-248}}] - [E_B^{\text{Cf-252}}] \\ &= [1859.1902 \text{ MeV} + 28.2957 \text{ MeV}] - [1881.2748 \text{ MeV}] \\ &= [1887.4859 \text{ MeV}] - [1881.2748 \text{ MeV}] = 6.212 \text{ MeV}. \quad (9.162) \end{aligned}$$

- (3) Q value of the α decay is shared between the α particle and the recoil Cm-248 nucleus in inverse proportions to the rest energies, so that α particle receives about 98 % of the energy available in Q value.

Chapter 10 consists of **13 problems** spread over 8 sections dealing with the kinetics of radioactivity also known as radioactive decay, nuclear transformation, and nuclear disintegration. Radioactivity is a spontaneous process by which an unstable parent nucleus emits a particle or electromagnetic radiation and transforms into a more stable daughter nucleus that may or may not be stable. An unstable nucleus will decay further in a decay series until a stable nuclear configuration is reached.

The radioactive decay is governed by the formalism based on the definition of activity and the radioactive decay constant. Henri Becquerel discovered the process of natural radioactivity in 1896 and soon thereafter in 1898 Pierre Curie and Marie Skłodowska-Curie discovered radium and polonium and coined the term “radioactivity to describe emission of “emanations” from unstable natural elements. Frédéric Joliot and Irène Joliot-Curie discovered artificial radioactivity in 1934.

The first problem of this chapter (Sect. 10.1) deals with general aspects of radioactivity, such as activity, specific activity, decay constant, half-life, mean lifetime, and units of activity. Section 10.2 contains two problems addressing the simple kinetics of radioactive parent decaying into a stable daughter. Section 10.3 is dedicated to several long problems that deal with radioactive series decay from various angles to improve the understanding of the radioactive chain decay.

Section 10.4 introduces the concept of the general form of daughter activity, while Sect. 10.5 deals with the various equilibriums in parent-daughter activities, such as secular, transient, and ideal equilibrium. Next (Sect. 10.6) come two problems on general radioactive decay series with many chain links that are handled with Bateman equations, a problem in Sect. 10.7 on decay kinetics for a mixture of two or more independently decaying radionuclides, and the chapter concludes with a problem addressing the issue of branching decay and branching fraction (Sect. 10.8).

10.1 General Aspects of Radioactivity

10.1.Q1

(211)

During the past century radioactivity has revolutionized science, played an important role in industrial development, introduced several new branches of physics, and helped in establishing medical physics as a branch of physics of importance to both physics and medicine.

- (a) Define radioactivity and list a few other terms that are used to describe the process.
- (b) For the following phenomena name the scientist credited with the discovery and the year of discovery: (1) Natural radioactivity, (2) Radium and polonium, (3) Exponential laws of radioactivity, (4) Artificial radioactivity, and (5) Fission.
- (c) Name and define the characteristic parameter that is used to describe a given radioactive process. Discuss the dependence of this parameter on prevailing physical conditions in radioactive atom's environment.
- (d) In a radioactive substance that contains a large number N of identical radioactive atoms, what is the probability that a given atom will decay during a time interval Δt ? Are there any restrictions on the magnitude of Δt ?
- (e) Define activity \mathcal{A} of a radioactive substance and state its relationship with the number N of radioactive atoms present in the sample. State the unit of activity in the SI system of units and in the old (traditional) system of units. Also state the relationship between the two systems.
- (f) Both hertz (Hz) and becquerel (Bq) are units of a physical quantity and equal to $1/s$. What is the difference between the two units and which physical quantities do they represent?
- (g) Define specific activity a and show how it is determined for a given radionuclide. State the unit of specific activity in the SI system of units and in the old (traditional) system of units.

SOLUTION:

(a) Radioactivity is a process by which an unstable parent nucleus transforms spontaneously into one or several daughter nuclei that are more stable than the parent nucleus by having larger binding energies per nucleon than does the parent nucleus. The daughter nucleus may be stable or may also be unstable and decay further through a chain of radioactive decays until a stable nuclear configuration is reached. Radioactive decay is usually accompanied by emission of energetic particles, γ rays or both.

In addition to radioactivity, other terms used to describe spontaneous nuclear decay are radioactive decay, nuclear disintegration, nuclear transformation, and nuclear transmutation.

(b) Discoveries related to radioactivity:

- (1) Natural radioactivity: Henri Becquerel (1896).
- (2) Radium and polonium: Marie Curie-Skłodowska and Pierre Curie (1898).
- (3) Exponential laws of radioactivity: Ernest Rutherford and Frederick Soddy (1902).
- (4) Artificial radioactivity: Frédéric Joliot and Irène Joliot-Curie (1934).
- (5) Fission: Lise Meitner, Otto Frisch, Otto Hahn, and Friedrich W. Strassmann (1938).

(c) All radioactive decay processes are governed by the same general formalism that is based on the definition of the activity $\mathcal{A}(t)$ and on the total radioactive decay constant λ that is a characteristic parameter for each radioactive decay process with dimensions of reciprocal time usually in s^{-1} . The decay constant λ is independent of the age of the radioactive atom and is essentially independent of physical conditions such as temperature, pressure, and chemical state of the atom's environment.

(d) The total radioactive decay constant λ multiplied by a time interval Δt that is much smaller than $1/\lambda$ represents the probability that any particular atom of radioactive substance containing a large number $N(t)$ of identical radioactive atoms will decay in that time interval.

(e) Activity $\mathcal{A}(t)$ of a radioactive substance containing a large number $N(t)$ of identical radioactive atoms represents the total number of decays per unit time and is defined as a product between $N(t)$ and decay constant λ , i.e.,

$$\mathcal{A}(t) = \lambda N(t). \quad (10.1)$$

SI unit of activity is the becquerel (Bq) defined as $1 \text{ Bq} = 1 \text{ s}^{-1}$. The old unit of activity, the curie (Ci), was initially defined as the activity of 1 g of radium-226 and given as $1 \text{ Ci} = 3.7 \times 10^{10} \text{ s}^{-1}$. The activity of 1 g of radium-226 was subsequently measured to be $3.665 \times 10^{10} \text{ s}^{-1}$; however, the definition of the curie was kept at $3.7 \times 10^{10} \text{ s}^{-1}$. The current value of the activity of 1 g of radium-226 is thus 0.988 Ci or $3.665 \times 10^{10} \text{ Bq}$. The SI unit becquerel and the traditional unit curie are related as follows

$$1 \text{ Ci} = 3.7 \times 10^{10} \text{ Bq} = 0.037 \text{ TBq} \quad \text{and} \quad 1 \text{ Bq} = 2.703 \times 10^{-11} \text{ Ci}. \quad (10.2)$$

(f) Becquerel (Bq) and hertz (Hz) both correspond to 1 s^{-1} ; however, becquerel refers to physical quantity "activity" and hertz refers to periodic motion ("frequency").

(g) Specific activity a of a radioactive substance is defined as the activity \mathcal{A} per unit mass m

$$a = \frac{\mathcal{A}}{m} = \frac{\lambda N}{m} = \frac{\lambda N_A}{A} = \frac{(\ln 2)N_A}{t_{1/2}A}, \quad (10.3)$$

where N_A is the Avogadro number ($6.022 \times 10^{23} \text{ mol}^{-1}$), A is the atomic mass number, and $t_{1/2}$ is the half life of the radioactive substance. The units of specific activity are Bq/kg (SI unit) and Ci/g (traditional unit). The relationship between the two units is given as: $1 \text{ Ci/g} = 37 \text{ TBq/kg}$.

10.2 Decay of Radioactive Parent into a Stable Daughter

10.2.Q1 (212)

In its simplest form the radioactive decay is characterized by a radioactive parent nucleus P decaying with decay constant λ_P into a stable daughter nucleus D



The rate of depletion of the number of radioactive parent nuclei $N_P(t)$ is equal to the activity $\mathcal{A}_P(t)$ at time t , i.e.,

$$\frac{dN_P(t)}{dt} = -\mathcal{A}_P(t) = -\lambda_P N_P(t). \quad (10.5)$$

- (a) Solve the differential equation (10.5) to obtain the number of parent nuclei $N_P(t)$ at time t in terms of the number of parent nuclei $N_P(0)$ at time $t = 0$.
- (b) Using the results of (a) express the activity $\mathcal{A}_P(t)$ at time t in terms of the activity $\mathcal{A}_P(0)$ at time $t = 0$.
- (c) Half-life $(t_{1/2})_P$ of a radioactive substance P is defined as the time during which the number of radioactive nuclei of the substance decays to half of the initial value $N_P(0)$ present at time $t = 0$. Show that

$$(t_{1/2})_P = \frac{\ln 2}{\lambda_P}. \quad (10.6)$$

- (d) Obtain an expression for the average (mean) lifetime τ_P of a radioactive parent substance P and derive the relationship between mean lifetime τ_P and half-life $(t_{1/2})_P$.

SOLUTION:

(a) The fundamental differential equation (10.5) for describing radioactive decay can be rewritten in general integral form to get

$$\int_{N_P(0)}^{N_P(t)} \frac{dN_P(t)}{N_P(t)} = - \int_0^t \lambda_P dt. \quad (10.7)$$

Integration of both sides of (10.7) results in the following solution

$$\ln \frac{N_P(t)}{N_P(0)} = -\lambda_P t, \quad (10.8)$$

which can also be expressed as

$$N_P(t) = N_P(0)e^{-\lambda_P t}. \quad (10.9)$$

(b) The activity $\mathcal{A}_P(t)$ is proportional to the number of parent nuclei $N_P(t)$ and the proportionality constant is the decay constant λ_P , i.e.,

$$\mathcal{A}_P(t) = \lambda_P N_P(t). \quad (10.10)$$

Multiplying both sides of (10.9) by the decay constant λ_P and recalling (10.10) we get

$$\lambda_P N_P(t) = \lambda_P N_P(0)e^{-\lambda_P t} \quad \text{or} \quad \mathcal{A}_P(t) = \mathcal{A}_P(0)e^{-\lambda_P t}. \quad (10.11)$$

(c) The definition of half-life $(t_{1/2})_P$ of a radioactive substance in conjunction with (10.9) implies the following relationship

$$N_P[t = (t_{1/2})_P] = \frac{1}{2} N_P(0) = N_P(0)e^{-\lambda_P (t_{1/2})_P}, \quad (10.12)$$

while in conjunction with (10.11) it gives the following expression

$$\mathcal{A}_P[t = (t_{1/2})_P] = \frac{1}{2} \mathcal{A}_P(0) = \mathcal{A}_P(0)e^{-\lambda_P (t_{1/2})_P}. \quad (10.13)$$

Cancelling $N_P(0)$ in (10.12) or cancelling $\mathcal{A}_P(0)$ in (10.13) we first get

$$\frac{1}{2} = e^{-\lambda_P (t_{1/2})_P} \quad \text{or} \quad \ln \frac{1}{2} = -\lambda_P (t_{1/2})_P. \quad (10.14)$$

Solving (10.14) for $(t_{1/2})_P$ we obtain the following relationship linking half-life $(t_{1/2})_P$ of the parent nucleus with its decay constant λ_P

$$(t_{1/2})_P = \frac{\ln 2}{\lambda_P} \quad \text{or} \quad \lambda_P = \frac{\ln 2}{(t_{1/2})_P}. \quad (10.15)$$

(d) The actual lifetime of any radioactive parent nucleus P can vary from 0 to ∞ ; however, for a large number N_P of parent nuclei we can define the average (mean) lifetime or expectation value τ_P of radioactive parent substance P that equals the sum of lifetimes of all individual atoms divided by the initial number $N_P(0)$ of radioactive nuclei.

The average (mean) lifetime τ_P thus represents the average life expectancy of all nuclei in radioactive substance P at time $t = 0$; i.e.,

$$\mathcal{A}_P(0)\tau_P = \mathcal{A}_P(0) \int_0^\infty e^{-\lambda_P t} dt = \frac{\mathcal{A}_P(0)}{\lambda_P} = N_P(0). \quad (10.16)$$

Therefore, mean lifetime τ_P , half-life $(t_{1/2})_P$, and the decay constant λ_P are related through the following expression

$$\tau_P = \frac{1}{\lambda_P} = \frac{(t_{1/2})_P}{\ln 2}. \quad (10.17)$$

Inserting (10.17) into (10.9), the mean life τ_P can also be defined as the time required for the number of radioactive atoms $N_P(t)$ to fall from its initial value $N_P(0)$ at time $t = 0$ to a value of $e^{-1}N_P(0)$ corresponding to $0.368N_P(0)$ or to 36.8 % of $N_P(0)$ at time $t = \tau_P$. In similar fashion, inserting (10.17) into (10.11), the mean life τ_P can be defined as the time required for the activity of radioactive substance $\mathcal{A}_P(t)$ to fall from its initial value $\mathcal{A}_P(0)$ at time $t = 0$ to a value of $e^{-1}\mathcal{A}_P(0)$ corresponding to $0.368\mathcal{A}_P(0)$ or to 36.8 % of $\mathcal{A}_P(0)$ at time $t = \tau_P$.

The mean (average) survival time τ_P of a parent nucleus P can also be determined using the standard method for finding the average (mean) of a continuous variable as follows

$$\tau_P = \frac{\int_0^\infty t e^{-\lambda_P t} dt}{\int_0^\infty e^{-\lambda_P t} dt} = \frac{\frac{1}{\lambda_P^2}}{\frac{1}{\lambda_P}} = \frac{1}{\lambda_P}, \quad (10.18)$$

where the integral in the numerator of (10.18) is determined using the method of integration by parts.

10.2.Q2

(213)

Data in Table 10.1 represent measured activity \mathcal{A}_P in millicuries (mCi) as a function of time t for an unknown radionuclide P that decays into a stable daughter D. For the unknown radionuclide substance P:

- Plot the data of Table 10.1 in the format of activity \mathcal{A}_P against time t on Cartesian and semi-logarithmic graph paper and estimate the decay half-life $(t_{1/2})_P$ of radionuclide P.
- Using the least squares fit to measured data determine the decay constant λ_P .
- Determine the half-life $(t_{1/2})_P$.
- Determine the mean lifetime τ_P .

Table 10.1 Measured activity \mathcal{A}_P measured at various times t after the first measurement $\mathcal{A}_P(0)$ at time $t = 0$ for radioactive parent P decaying into stable daughter D

Time t (min)	0	1	2	3	4	5	6	8	10	12
Activity $\mathcal{A}_P(t)$ (mCi)	3.6	3.2	2.8	2.4	2.1	1.9	1.6	1.3	1.0	0.7

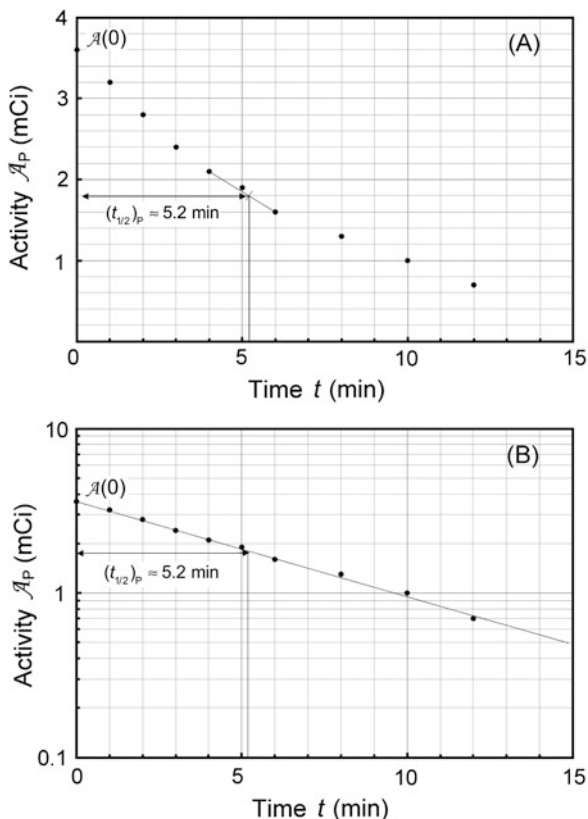


Fig. 10.1 Data of Table 10.1 for activity of parent P decaying into daughter D plotted in (A) on Cartesian scale and in (B) on semi-logarithmic scale. Rough estimate of half-life $(t_{1/2})_P = 5.2$ min is 5.2 minutes

SOLUTION:

(a) Measured data presented in Table 10.1 are depicted in Fig. 10.1 with activity \mathcal{A}_P plotted on the ordinate (y axis) and time t on the abscissa (x axis). Part (A) is plotted on Cartesian scale, part (B) on semi-logarithmic (log-lin) scale. Both graphs support the assumption that the relationship between activity \mathcal{A}_P and time t is exponential.

Activity $\mathcal{A}_P(t)$ at time t of parent nuclide P decaying into stable daughter D is described by the following exponential expression

$$\mathcal{A}_P(t) = \mathcal{A}_P(0)e^{-\lambda_P t}, \quad (10.19)$$

where $\mathcal{A}_P(0)$ is the parent activity at time $t = 0$ and λ_P is a decay parameter referred to as the decay constant related to half-life $(t_{1/2})_P$ and mean lifetime τ_P as follows

$$\lambda_P = \frac{\ln 2}{(t_{1/2})_P} = \frac{1}{\tau_P}. \quad (10.20)$$

Based on graphs in Fig. 10.1 we can estimate the half-life $(t_{1/2})_P$ of the unknown radioactive substance P by estimating the time required for the activity \mathcal{A}_P to decrease from $\mathcal{A}_P(0) = 3.6$ mCi to $0.5\mathcal{A}_P(0) = 1.8$ mCi. This direct approach results in an estimate of $(t_{1/2})_P \approx 5.2$ min.

(b) To improve on the rough estimate of $(t_{1/2})_P \approx 5.2$ min in **(a)** we now apply the method of linear curve fitting based on least-squares fit to measured data. To determine the decay constant λ_P from the data presented in Table 10.1 we first transform (10.19) into a linear function by applying the natural algorithm to both sides of (10.19) as follows

$$\ln \mathcal{A}_P(t) = \ln \mathcal{A}_P(0) - \lambda_P t. \quad (10.21)$$

Equation (10.21) is a linear equation of the standard form $y = b + ax$ with dependent variable y given as $\ln \mathcal{A}_P(t)$, ordinate (y) axis intercept b given as $\ln \mathcal{A}_P(0)$, dependent variable x given as t , and slope a given as $-\lambda_P$. We assume that values of the independent variable x_i are set accurately and values of the dependent variable y_i are measurements subject to some small uncertainty.

Next we apply the method of least squares fit using the following standard least squares fit expressions for the slope a of the linear function (10.21) and the y intercept b of the linear function

$$a = \frac{n \sum_{i=1}^n x_i y_i - \sum_{i=1}^n x_i \sum_{i=1}^n y_i}{n \sum_{i=1}^n x_i^2 - (\sum_{i=1}^n x_i)^2} \quad (10.22)$$

and

$$b = \frac{\sum_{i=1}^n x_i^2 \sum_{i=1}^n y_i - \sum_{i=1}^n x_i \sum_{i=1}^n x_i y_i}{n \sum_{i=1}^n x_i^2 - (\sum_{i=1}^n x_i)^2}, \quad (10.23)$$

where i is the running index and n is the number of data points in a particular set of data. In Table 10.2 we show the individual components (x_i , y_i , x_i^2 , and $x_i y_i$) of the data set used for the least squares fit method. In addition, row (12) of the table gives the calculated sums $\sum_{i=1}^n x_i$, $\sum_{i=1}^n y_i$, $\sum_{i=1}^n x_i^2$, and $\sum_{i=1}^n x_i y_i$ for use in (10.22) and (10.23) in determination of a and b .

Data in row (12) of Table 10.2 in conjunction with (10.22) and (10.23) give the following results for the slope a and y intercept b , respectively,

Table 10.2 Parameters x_i , y_i , x_i^2 , and $x_i y_i$ for the data set presented in Table 10.1 representing measured activity $\mathcal{A}_P(t)$ as a function of time t for a radioactive parent nucleus P decaying into a stable daughter D. Row (12) of the table provides the sum of the individual components for parameters x_i , y_i , x_i^2 , and $x_i y_i$

(1)	i	x_i	y_i	x_i^2	$x_i y_i$
(2)	1	0	1.281	0	0.000
(3)	2	1	1.163	1	1.163
(4)	3	2	1.030	4	2.059
(5)	4	3	0.875	9	2.626
(6)	5	4	0.742	16	2.968
(7)	6	5	0.642	25	3.209
(8)	7	6	0.470	36	2.820
(9)	8	8	0.262	64	2.099
(10)	9	10	0.000	100	0
(11)	10	12	-0.357	144	-4.280
(12)	SUM $\sum_{i=1}^n$	51	6.109	399	12.665

$$a = \frac{n \sum_{i=1}^n x_i y_i - \sum_{i=1}^n x_i \sum_{i=1}^n y_i}{n \sum_{i=1}^n x_i^2 - (\sum_{i=1}^n x_i)^2} = \frac{10 \times 12.665 - 51 \times 6.109}{10 \times 399 - (51)^2} = -0.133 \quad (10.24)$$

and

$$b = \frac{\sum_{i=1}^n x_i^2 \sum_{i=1}^n y_i - \sum_{i=1}^n x_i \sum_{i=1}^n x_i y_i}{n \sum_{i=1}^n x_i^2 - (\sum_{i=1}^n x_i)^2} = \frac{399 \times 6.109 - 51 \times 12.665}{10 \times 399 - (51)^2} = 1.290. \quad (10.25)$$

A plot of the data points (x_i, y_i) from Table 10.2 as well as the line $y = b + ax$ with slope $a = -0.133$ and y intercept $b = 1.29$ is shown in Fig. 10.2. From (10.24) and (10.25) we can now determine the decay constant λ_P and the initial activity $\mathcal{A}_P(0)$ as follows

$$\lambda_P = -a = 0.133 \text{ min}^{-1} \quad (10.26)$$

and

$$\mathcal{A}_P(0) = e^b = e^{1.29} = 3.63 \text{ mCi}. \quad (10.27)$$

(c) Half-life $(t_{1/2})_P$ of the radionuclide P is determined from the well-known relationship between $(t_{1/2})_P$ and λ_P given in (10.20) as

$$(t_{1/2})_P = \frac{\ln 2}{\lambda_P} = \frac{\ln 2}{0.133 \text{ min}^{-1}} = 5.21 \text{ min}. \quad (10.28)$$

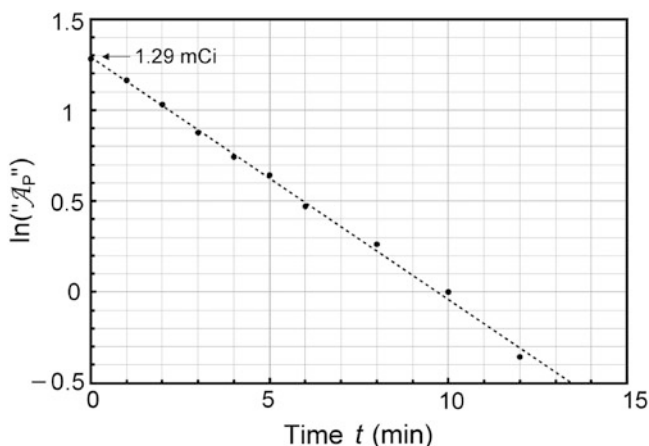


Fig. 10.2 Plot of the data points (x_i, y_i) from Table 10.2 as well as the line $y = b + ax$ with slope $a = -0.133$ and y intercept $b = 1.29$

Mean lifetime τ_P of the radionuclide P is also determined from (10.20)

$$\tau_P = \frac{1}{\lambda_P} = \frac{1}{0.133 \text{ min}^{-1}} = 7.52 \text{ min.} \quad (10.29)$$

10.3 Radioactive Series Decay

10.3.Q1

(214)

Radioactive decay through a series of radioactive transformations is much more common than the simple radioactive decay from a radioactive parent into stable daughter. The radioactive decay series forms a decay chain starting with the parent radionuclide and moves through several generations to eventually end with a stable nuclide.

Consider the simple chain $P \rightarrow D \rightarrow G$ where both the parent P and daughter D are radioactive and the granddaughter G is stable. The parent decays with a decay constant λ_P while the daughter decays with a decay constant λ_D . For this simple decay series:

- (a) State the differential equations governing the kinetics of the radioactive parent and radioactive daughter.

(b) Solve the differential equations in (a) with the following initial conditions:

- (1) Initial number of parent nuclei $N_P(t)$ at time $t = 0$ is $N_P(0)$.
- (2) Initial number of daughter nuclei $N_D(t = 0) = N_D(0) = 0$.

to get expressions for the number of parent nuclei N_P and for the number of daughter nuclei $N_D(t)$ as a function of time t .

- (c) Using the results of (b) obtain an expression for activity of the daughter $\mathcal{A}_D(t)$.
- (d) The expression for the daughter activity $\mathcal{A}_D(t)$ derived in (c) should predict $\mathcal{A}_D(t) = 0$ for $t = 0$ [recall the initial condition $N_D(0) = 0$] as well as for $t \rightarrow \infty$ (recall that at $t = \infty$ all daughter nuclei will have decayed). This means that $\mathcal{A}_D(t)$ must reach a maximum value $(\mathcal{A}_D)_{\max}$ at a characteristic time $(t_{\max})_D$ somewhere between the two extremes: $t = 0$ and $t = \infty$, i.e., $0 < (t_{\max})_D < \infty$. Derive an expression for the characteristic time $(t_{\max})_D$.
- (e) Show that for $\lambda_P \gtrsim \lambda_D$ (but not $\lambda_P = \lambda_D$) and for $\lambda_P \lesssim \lambda_D$ (but not $\lambda_P = \lambda_D$) the characteristic time $(t_{\max})_D$ can be approximated by $(t_{\max})_D \approx 1/\sqrt{\lambda_P \lambda_D}$. To verify this approximation calculate $(t_{\max})_D$ with this approximation and compare results with the expression derived in (d) for the following two radioactive series decays: (1) Series decay with $\lambda_P = 2.1 \text{ y}^{-1}$ and $\lambda_D = 2.0 \text{ y}^{-1}$ and (2) Series decay with $\lambda_P = 5.1 \text{ s}^{-1}$ and $\lambda_D = 5.5 \text{ s}^{-1}$.

SOLUTION:

(a) The differential equations governing the kinetics of the parent P and the daughter D nuclei in the simple $P \rightarrow D \rightarrow G$ decay chain describe the rate of change in the number of parent nuclei $N_P(t)$ and in the number of daughter nuclei $N_D(t)$.

- (1) For the parent, the rate of change $dN_P(t)/dt$ in the number of parent nuclei is given by the standard expression dealing with nuclear decay

$$\frac{dN_P(t)}{dt} = -\lambda_P N_P(t), \quad (10.30)$$

with the minus sign indicating a decrease in the number of parent nuclei $N_P(t)$ with increasing time t .

- (2) The rate of change $dN_D(t)/dt$ in the number of daughter nuclei D is equal to the supply of new daughter nuclei D through the decay of P given as $\lambda_P N_P(t)$ and the loss of daughter nuclei D from the decay of D to G given as $[-\lambda_D N_D(t)]$. The rate of change dN_D/dt is expressed as

$$\frac{dN_D(t)}{dt} = \lambda_P N_P(t) - \lambda_D N_D(t). \quad (10.31)$$

(b) Equation (10.30) shows that the parent P follows a straightforward radioactive decay process with the initial condition $N_P(t=0) = N_P(0)$ and the following solution

$$N_P(t) = N_P(0)e^{-\lambda_P t}. \quad (10.32)$$

The solution to (10.31) for the daughter, on the other hand, is more complicated and will be determined after inserting (10.32) into (10.31) to get the following expression for the rate of change in the number of daughter nuclei

$$\frac{dN_D(t)}{dt} = \lambda_P N_P(0)e^{-\lambda_P t} - \lambda_D N_D(t). \quad (10.33)$$

The general solution of the differential equation given by (10.33) is given as

$$N_D(t) = N_P(0)[pe^{-\lambda_P t} + de^{-\lambda_D t}], \quad (10.34)$$

where p and d are constants to be determined using the following four steps:

1. Differentiate (10.34) with respect to time t to obtain

$$\frac{dN_D(t)}{dt} = N_P(0)[-p\lambda_P e^{-\lambda_P t} - d\lambda_D e^{-\lambda_D t}]. \quad (10.35)$$

2. Insert (10.34) and (10.35) into (10.33) and rearrange the terms to get

$$e^{-\lambda_P t}[-p\lambda_P - \lambda_P + p\lambda_D] = 0. \quad (10.36)$$

3. The factor in square brackets of (10.36) must be equal to zero to satisfy the equation for all possible values of t , yielding the following expression for the constant p

$$p = \frac{\lambda_P}{\lambda_D - \lambda_P}. \quad (10.37)$$

4. The coefficient d depends on the initial condition for $N_D(t)$ at $t = 0$. With the standard initial condition $N_D(0) = 0$ we get the following simple equation from (10.34)

$$p + d = 0 \quad (10.38)$$

which upon insertion of (10.37) provides the following result for constant d

$$d = -p = -\frac{\lambda_P}{\lambda_D - \lambda_P} = \frac{\lambda_P}{\lambda_P - \lambda_D}. \quad (10.39)$$

After inserting (10.37) and (10.39) into (10.34) we get the following expression for the number of daughter nuclei $N_D(t)$ as a function of time t

$$N_D(t) = N_P(0) \frac{\lambda_P}{\lambda_D - \lambda_P} [e^{-\lambda_P t} - e^{-\lambda_D t}]. \quad (10.40)$$

(c) The simple $P \rightarrow D \rightarrow G$ radioactive series decay with radioactive parent P decaying through radioactive daughter D into stable grand-daughter G is characterized by equations describing the number of parent nuclei $N_P(t)$ and number of daughter nuclei $N_D(t)$ given by (10.32) and (10.40), respectively. Activities $\mathcal{A}_P(t)$ and $\mathcal{A}_D(t)$ of the parent and daughter, respectively, in a radioactive sample are also of interest and can be determined by recalling that, in general, the activity $\mathcal{A}(t)$ of a radionuclide is the product of its decay constant λ and the number $N(t)$ of radioactive nuclei present in the sample.

We thus get the following expressions for the activity of the parent $\mathcal{A}_P(t)$ from (10.32) and activity of the daughter $\mathcal{A}_D(t)$ from (10.40), respectively

$$\mathcal{A}_P(t) = \lambda_P N_P(t) = \lambda_P N_P(0) e^{-\lambda_P t} = \mathcal{A}_P(0) e^{-\lambda_P t} \quad (10.41)$$

and

$$\begin{aligned} \mathcal{A}_D(t) &= \lambda_D N_D(t) = \lambda_D N_P(0) \frac{\lambda_P}{\lambda_D - \lambda_P} [e^{-\lambda_P t} - e^{-\lambda_D t}] \\ &= \lambda_P N_P(0) \frac{\lambda_D}{\lambda_D - \lambda_P} [e^{-\lambda_P t} - e^{-\lambda_D t}] = \mathcal{A}_P(0) \frac{\lambda_D}{\lambda_D - \lambda_P} [e^{-\lambda_P t} - e^{-\lambda_D t}], \end{aligned} \quad (10.42)$$

where $\mathcal{A}_P(0)$ is the activity of the parent at time $t = 0$.

A test of the limiting value of $\mathcal{A}_D(t)$ given in (10.42) for $t = 0$ and $t \rightarrow \infty$ yields zero, as it should according to: (1) initial condition $N_D(0) = 0$ and (2) at $t = \infty$ all daughter nuclei will have decayed. From (10.42) we note: (1) $\lim_{t \rightarrow 0} \mathcal{A}_D(t) = 0$ and (2) $\lim_{t \rightarrow \infty} \mathcal{A}_D(t) = 0$.

(d) The characteristic time $(t_{\max})_D$ at which the daughter activity $\mathcal{A}_D(t)$ attains its maximum value $(\mathcal{A}_D)_{\max}$ is determined by setting $d\mathcal{A}_D/dt = 0$ at $t = (t_{\max})_D$ and solving for $(t_{\max})_D$ to get

$$\begin{aligned} \left. \frac{d\mathcal{A}_D(t)}{dt} \right|_{t=(t_{\max})_D} &= N_P(0) \frac{\lambda_D \lambda_P}{\lambda_D - \lambda_P} \frac{d}{dt} [e^{-\lambda_P t} - e^{-\lambda_D t}]_{t=(t_{\max})_D} \\ &= N_P(0) \frac{\lambda_D \lambda_P}{\lambda_D - \lambda_P} [-\lambda_P e^{-\lambda_P (t_{\max})_D} + \lambda_D e^{-\lambda_D (t_{\max})_D}] = 0. \end{aligned} \quad (10.43)$$

From (10.43) we first get

$$\lambda_P e^{-\lambda_P (t_{\max})_D} = \lambda_D e^{-\lambda_D (t_{\max})_D} \quad (10.44)$$

then

$$\frac{\lambda_P}{\lambda_D} = e^{(\lambda_P - \lambda_D) \times (t_{\max})_D} \quad (10.45)$$

and finally get the following general result for $(t_{\max})_D$

$$(t_{\max})_D = \frac{\ln \frac{\lambda_P}{\lambda_D}}{\lambda_P - \lambda_D}. \quad (10.46)$$

(e) For $\lambda_P \gtrsim \lambda_D$ and $0 < \varepsilon \ll 1$ we assume the following relationship between decay constants λ_P and λ_D of the parent and daughter, respectively

$$\lambda_P = \lambda_D(1 + \varepsilon) \quad \text{or} \quad \lambda_P(1 - \varepsilon) \approx \lambda_D. \quad (10.47)$$

Inserting (10.47) into (10.46) we get

$$(t_{\max})_D = \frac{\ln \frac{\lambda_P}{\lambda_D}}{\lambda_P - \lambda_D} \approx \frac{\ln(1 + \varepsilon)}{\varepsilon \lambda_D}. \quad (10.48)$$

The logarithm in (10.48) can be simplified with Taylor expansion into a series as follows

$$\ln(1 + \varepsilon) \approx \varepsilon - \frac{1}{2}\varepsilon^2 + \frac{1}{3}\varepsilon^3 - \frac{1}{4}\varepsilon^4 + \dots. \quad (10.49)$$

For very small ε we insert (10.47) and the first two terms of the Taylor series (10.49) into (10.48) and get the following expression for $(t_{\max})_D$

$$(t_{\max})_D \approx \frac{\ln(1 + \varepsilon)}{\varepsilon \lambda_D} \approx \frac{1 - \frac{1}{2}\varepsilon}{\lambda_D} \approx \frac{\sqrt{1 - \varepsilon}}{\lambda_D} \approx \frac{1}{\sqrt{\lambda_P \lambda_D}}. \quad (10.50)$$

Similarly, for $\lambda_P \lambda_D$ and $0 < \varepsilon \ll 1$ we assume the following relationship

$$\lambda_P = \lambda_D(1 - \varepsilon) \quad \text{or} \quad \lambda_P(1 + \varepsilon) = \lambda_D. \quad (10.51)$$

Inserting (10.51) into (10.48) we get

$$(t_{\max})_D = \frac{\ln \frac{\lambda_P}{\lambda_D}}{\lambda_P - \lambda_D} \approx \frac{\ln(1 - \varepsilon)}{-\varepsilon \lambda_D}. \quad (10.52)$$

The logarithm in (10.52) can be simplified with Taylor expansion into a series as follows

$$\ln(1 - \varepsilon) \approx -\left[\varepsilon + \frac{1}{2}\varepsilon^2 + \frac{1}{3}\varepsilon^3 + \frac{1}{4}\varepsilon^4 + \dots \right]. \quad (10.53)$$

For very small ε we insert (10.51) and the first two terms of the Taylor expansion (10.53) into (10.52) and get the following expression for $(t_{\max})_D$

$$(t_{\max})_D \approx \frac{\ln(1 - \varepsilon)}{\varepsilon \lambda_D} \approx \frac{1 + \frac{1}{2}\varepsilon}{\lambda_D} \approx \frac{\sqrt{1 + \varepsilon}}{\lambda_D} \approx \frac{1}{\sqrt{\lambda_P \lambda_D}}. \quad (10.54)$$

We now compare results of $(t_{\max})_D$ calculation with the general expression for $(t_{\max})_D$ given in (10.46) and with the approximation given in (10.51) and (10.54).

- (1) Series decay with $\lambda_P = 2.1 \text{ y}^{-1}$ and $\lambda_D = 2.0 \text{ y}^{-1}$ for which $\lambda_P \lambda_D$

$$(t_{\max})_D = \frac{\ln \frac{\lambda_P}{\lambda_D}}{\lambda_P - \lambda_D} = \frac{\ln \frac{2.1}{2.0}}{2.1 - 2.0} \text{ y}^{-1} = 0.4879 \text{ y}, \quad (10.55)$$

$$(t_{\max})_D \approx \frac{1}{\sqrt{\lambda_P \lambda_D}} = \frac{1}{\sqrt{2.1 \times 2.0}} \text{ y} = 0.48795 \text{ y}. \quad (10.56)$$

- (2) Series decay with $\lambda_P = 5.1 \text{ s}^{-1}$ and $\lambda_D = 5.5 \text{ s}^{-1}$

$$(t_{\max})_D = \frac{\ln \frac{\lambda_P}{\lambda_D}}{\lambda_P - \lambda_D} = \frac{\ln \frac{5.1}{5.5}}{5.1 - 5.5} \text{ y}^{-1} = 0.1888 \text{ y}, \quad (10.57)$$

$$(t_{\max})_D \approx \frac{1}{\sqrt{\lambda_P \lambda_D}} = \frac{1}{\sqrt{2.1 \times 2.0}} \text{ y} = 0.1888 \text{ y}. \quad (10.58)$$

10.3.Q2

(215)

The molybdenum-99 (Mo-99) \rightarrow technetium-99m (Tc-99m) \rightarrow technetium-99 (Tc-99) decay series plays an important role in nuclear medicine, since it serves as the source of Tc-99m, the most widely used radionuclide for nuclear imaging tests. The series parent radionuclide Mo-99 decays through β^- decay with a half-life $(t_{1/2})_{\text{Mo-99}} = 66.0$ hours into daughter radionuclide Tc-99m. Subsequently, the daughter Tc-99m decays through gamma emission with a half-life $(t_{1/2})_{\text{Tc-99m}} = 6.02$ hours to the granddaughter radionuclide Tc-99. The Tc-99 radionuclide has a much longer half-life $[(t_{1/2})_{\text{Tc-99}} = 2.1 \times 10^5 \text{ y}]$ in comparison with Mo-99 and Tc-99m and decays through β^- decay to ruthenium-99 (Ru-99).

Starting with a pure 10 mCi (0.37 GBq) Mo-99 source:

- State or derive equations for activities of the Mo-99 parent and Tc-99m daughter as a function of time.
- Calculate the characteristic time $(t_{\max})_{\text{Tc-99m}}$ at which the Tc-99m daughter radionuclide attains its maximum activity.
- Determine the maximum activity $\mathcal{A}_D[(t_{\max})_{\text{Tc-99m}}]$ of the Tc-99m radionuclide.
- Show that activities of the parent $\mathcal{A}_P[(t_{\max})_{\text{Tc-99m}}]$ and the daughter $\mathcal{A}_D[(t_{\max})_{\text{Tc-99m}}]$ are equal at the characteristic time $(t_{\max})_{\text{Tc-99m}}$.

- (e) Sketch the activities of the Mo-99 parent and Tc-99m daughter as a function of time and highlight the salient features of the two radioactive decay curves.

SOLUTION:

- (a) Activities of the parent $\mathcal{A}_P(t) = \mathcal{A}_{\text{Mo-99}}(t)$ and of the daughter $\mathcal{A}_D(t) = \mathcal{A}_{\text{Tc-99m}}(t)$ as a function of time t are, respectively, given by [see (T10.10) and (T10.35), respectively]

$$\mathcal{A}_P(t) = \mathcal{A}_P(0)e^{-\lambda_P t} \quad (10.59)$$

or

$$\mathcal{A}_{\text{Mo-99}}(t) = \mathcal{A}_{\text{Mo-99}}(0)e^{-\lambda_{\text{Mo-99}} t} \quad (10.60)$$

and

$$\mathcal{A}_D(t) = \mathcal{A}_P(0) \frac{\lambda_D}{\lambda_D - \lambda_P} [e^{-\lambda_P t} - e^{-\lambda_D t}] \quad (10.61)$$

or

$$\mathcal{A}_{\text{Tc-99m}}(t) = \mathcal{A}_{\text{Mo}}(0) \frac{\lambda_{\text{Tc-99m}}}{\lambda_{\text{Tc-99m}} - \lambda_{\text{Mo-99}}} [e^{-\lambda_{\text{Mo-99}} t} - e^{-\lambda_{\text{Tc-99m}} t}], \quad (10.62)$$

where

- $\mathcal{A}_P(0)$ is the activity of the parent P at time $t = 0$.
 λ_P is the decay constant for the parent P radionuclide.
 λ_D is the decay constant for the daughter D radionuclide.

Decay constants λ for molybdenum-99 and technetium-99m are obtained from their known half-lives $t_{1/2}$ using the standard relationship $\lambda = (\ln 2)/t_{1/2}$. Thus, for Mo-99 we have

$$\lambda_P = \lambda_{\text{Mo-99}} = \frac{\ln 2}{(t_{1/2})_{\text{Mo-99}}} = \frac{\ln 2}{66.0 \text{ h}} = 1.05 \times 10^{-2} \text{ h}^{-1} \quad (10.63)$$

and for Tc-99m

$$\lambda_D = \lambda_{\text{Tc-99m}} = \frac{\ln 2}{(t_{1/2})_{\text{Tc-99m}}} = \frac{\ln 2}{6.02 \text{ h}} = 0.115 \text{ h}^{-1}. \quad (10.64)$$

Inserting (10.63) and (10.64) into (10.59) and (10.61) and using the initial activity $\mathcal{A}_P(0) = 10 \text{ mCi}$ of the parent (Mo-99) radionuclide we get

$$\mathcal{A}_P(t) = \mathcal{A}_{\text{Mo-99}}(t) = (10 \text{ mCi}) \times e^{-(1.05 \times 10^{-2} \text{ h}^{-1}) \times t} \quad (10.65)$$

and

$$\begin{aligned}
 \mathcal{A}_D(t) &= \mathcal{A}_{\text{Tc-99m}}(t) \\
 &= (10 \text{ mCi}) \times \frac{0.115}{0.115 - 1.05 \times 10^{-2}} \left[e^{-(1.05 \times 10^{-2} \text{ h}^{-1}) \times t} - e^{-(0.115 \text{ h}^{-1}) \times t} \right] \\
 &= (11.0 \text{ mCi}) \times \left[e^{-(1.05 \times 10^{-2} \text{ h}^{-1}) \times t} - e^{-(0.115 \text{ h}^{-1}) \times t} \right]. \quad (10.66)
 \end{aligned}$$

(b) Activity of the parent $\mathcal{A}_P(t)$ falls exponentially with increasing time t ; however, activity of the daughter $\mathcal{A}_D(t)$ initially increases from zero to reach a maximum at a specific characteristic time $(t_{\max})_D$ and then decreases with increasing time t to return to zero at $t \rightarrow \infty$.

The characteristic time $(t_{\max})_D$ is determined by setting $d\mathcal{A}_D(t)/dt = 0$ at $t = (t_{\max})_D$. Differentiating (10.61) results in

$$\frac{d\mathcal{A}_D(t)}{dt} = \mathcal{A}_P(0) \frac{\lambda_D}{\lambda_D - \lambda_P} \left[\lambda_D e^{-\lambda_D t} - \lambda_P e^{-\lambda_P t} \right] \quad (10.67)$$

and setting $d\mathcal{A}_D(t)/dt = 0$ at $t = (t_{\max})_D$ we get

$$\lambda_D e^{-\lambda_D (t_{\max})_D} = \lambda_P e^{-\lambda_P (t_{\max})_D}. \quad (10.68)$$

Solving (10.68) for $(t_{\max})_D$ finally yields the following result for characteristic time $(t_{\max})_D$

$$(t_{\max})_D = \frac{\ln \frac{\lambda_P}{\lambda_D}}{\lambda_P - \lambda_D}. \quad (10.69)$$

For the $\text{Mo-99} \rightarrow \text{Tc-99m} \rightarrow \text{Tc-99}$ decay series the characteristic time $(t_{\max})_D$ at which $\mathcal{A}_{\text{Tc-99m}}(t)$ attains its maximum value is calculated as follows

$$(t_{\max})_D = (t_{\max})_{\text{Tc-99m}} = \frac{\ln \frac{1.05 \times 10^{-2}}{0.115}}{(1.05 \times 10^{-2} \text{ h}^{-1} - 0.115 \text{ h}^{-1})} = 22.88 \text{ h} \approx 23 \text{ h}. \quad (10.70)$$

(c) Maximum activity $\mathcal{A}_D[(t_{\max})_D]$ of the daughter Tc-99m at $(t_{\max})_D$ is obtained by inserting into (10.66) the characteristic time $t = (t_{\max})_D \approx 22.88 \text{ hr}$ that was calculated in (10.70) to get

$$\begin{aligned}
 \mathcal{A}_D[(t_{\max})_D] &= \mathcal{A}_{\text{Tc-99m}}[(t_{\max})_{\text{Tc-99m}}] \\
 &= (11.0 \text{ mCi}) \times \left[e^{-1.05 \times 10^{-2} \times 22.88} - e^{-0.115 \times 22.88} \right] \\
 &= 7.86 \text{ mCi}. \quad (10.71)
 \end{aligned}$$

(d) Daughter activity $\mathcal{A}_D(t)$ in (10.61) can be expressed as a function of parent activity $\mathcal{A}_P(t)$ as follows

$$\mathcal{A}_D(t) = \mathcal{A}_P(0) e^{-\lambda_P t} \frac{\lambda_D}{\lambda_D - \lambda_P} \left[1 - e^{-(\lambda_D - \lambda_P)t} \right] = \mathcal{A}_P(t) \frac{\lambda_D}{\lambda_D - \lambda_P} \left[1 - e^{-(\lambda_D - \lambda_P)t} \right], \quad (10.72)$$

and at characteristic time $(t_{\max})_{\text{D}}$ (10.72) becomes

$$\mathcal{A}_{\text{D}}[(t_{\max})_{\text{D}}] = \mathcal{A}_{\text{P}}[(t_{\max})_{\text{D}}] \frac{\lambda_{\text{D}}}{\lambda_{\text{D}} - \lambda_{\text{P}}} [1 - e^{-(\lambda_{\text{D}} - \lambda_{\text{P}})(t_{\max})_{\text{D}}}] \quad (10.73)$$

Inserting (10.69) for $(t_{\max})_{\text{D}}$ into (10.73) gives the following expression for $\mathcal{A}_{\text{D}}[t = (t_{\max})_{\text{D}}]$

$$\begin{aligned} \mathcal{A}_{\text{D}}[(t_{\max})_{\text{D}}] &= \mathcal{A}_{\text{P}}[(t_{\max})_{\text{D}}] \frac{\lambda_{\text{D}}}{\lambda_{\text{D}} - \lambda_{\text{P}}} \left[1 - e^{-(\lambda_{\text{D}} - \lambda_{\text{P}}) \frac{\ln \frac{\lambda_{\text{P}}}{\lambda_{\text{D}}}}{\lambda_{\text{P}} - \lambda_{\text{D}}}} \right] \\ &= \mathcal{A}_{\text{P}}[(t_{\max})_{\text{D}}] \frac{\lambda_{\text{D}}}{\lambda_{\text{D}} - \lambda_{\text{P}}} \left[1 - \frac{\lambda_{\text{P}}}{\lambda_{\text{D}}} \right] = \mathcal{A}_{\text{P}}[(t_{\max})_{\text{D}}], \end{aligned} \quad (10.74)$$

showing explicitly that at $t = (t_{\max})_{\text{D}}$ the parent and daughter activities are equal.

We now determine the maximum activity of the daughter Tc-99m in $\mathcal{A}_{\text{D}}[(t_{\max})_{\text{D}}]$ using (10.65) with $t = (t_{\max})_{\text{D}} \approx 22.88$ hr

$$\mathcal{A}_{\text{D}}[(t_{\max})_{\text{D}}] = \mathcal{A}_{\text{P}}[(t_{\max})_{\text{D}}] = (10 \text{ mCi}) \times e^{-1.05 \times 10^{-2} \times 22.88} = 7.86 \text{ mCi} \quad (10.75)$$

and obtain the same result as we did with (10.66) for the daughter activity $\mathcal{A}_{\text{D}}[(t_{\max})_{\text{D}}]$. Thus, at $t = (t_{\max})_{\text{D}}$ activities of the parent and the daughter are equal in general and, in our case with 10 mCi parent at $t = 0$, the activity of parent and daughter are 7.86 mCi and $(t_{\max})_{\text{D}} \approx 23$ h.

(e) The parent (Mo-99) and daughter (Tc-99m) activities $\mathcal{A}_{\text{P}}(t)$ and $\mathcal{A}_{\text{D}}(t)$, respectively, are shown in Fig. 10.3 plotted against time t using (10.65) and (10.66), respectively. A sketch of the two activity curves can be drawn based on a few important features or anchor points shown on the curves. The following features of $\text{P} \rightarrow \text{D} \rightarrow \text{G}$ radioactive decay series should be considered:

- (1) Parent activity $\mathcal{A}_{\text{P}}(t) = \mathcal{A}_{\text{Mo-99}}(t)$ follows exponential decay starting at $\mathcal{A}_{\text{Mo-99}}(0) = 10 \text{ mCi}$ (see Point 1 in Fig. 10.3).
- (2) Since $(t_{1/2})_{\text{Mo}} = 66 \text{ h}$, we know that $\mathcal{A}_{\text{Mo-99}}(66 \text{ h}) = 5 \text{ mCi}$ (see Point 4 in Fig. 10.3), $\mathcal{A}_{\text{Mo-99}}(132 \text{ h}) = 2.5 \text{ mCi}$, etc.
- (3) Daughter activity $\mathcal{A}_{\text{D}}(t) = \mathcal{A}_{\text{Tc-99m}}(t)$ is zero at $t = 0$ (initial condition: see Point 2 in Fig. 10.3). With increase in time, $\mathcal{A}_{\text{Tc-99m}}(t)$ first increases, reaches a peak of 7.86 mCi (see Point 3 in Fig. 10.3) as determined in (c), at a characteristic time $(t_{\max})_{\text{Tc-99m}} \approx 23 \text{ h}$ as determined in (b).

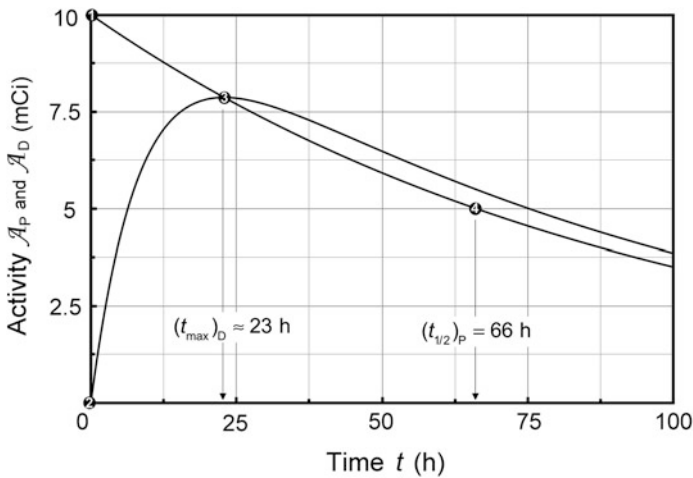


Fig. 10.3 Activity of parent (Mo-99) and daughter (Tc-99m), $\mathcal{A}_P(t)$ and $\mathcal{A}_D(t)$, respectively, against time t . Point (1): initial condition $\mathcal{A}_{\text{Mo-99}}(0) = 10$ mCi; point (2): initial condition $\mathcal{A}_{\text{Tc-99m}}(0) = 0$; point (3) characteristic time $(t_{\text{max}})_{\text{Tc-99m}} \approx 23$ h and $\mathcal{A}_{\text{Tc-99m}}[(t_{\text{max}})_{\text{Tc-99m}}] = 7.86$ mCi; and point (4) half-life of Mo-99 $(t_{1/2})_{\text{Mo-99}} = 66$ h

10.3.Q3

(216)

Figure 10.4 shows three activity $\mathcal{A}(t)$ curves plotted against time t for the radioactive series decay: Molybdenum-99 (Mo-99) \rightarrow Technetium-99m (Tc-99m) \rightarrow Technetium-99 (Tc-99) starting with a pure 10 mCi (0.37 GBq) Mo-99 source. Half-lives $(t_{1/2})_P = (t_{1/2})_{\text{Mo-99}} = 66$ h and $(t_{1/2})_D = (t_{1/2})_{\text{Tc-99m}} = 6.02$ h correspond to decay constants $\lambda_P = \lambda_{\text{Mo-99}} = 1.05 \times 10^{-2} \text{ h}^{-1}$ and $\lambda_D = \lambda_{\text{Tc-99m}} = 0.115 \text{ h}^{-1}$, respectively. The following three points should be noted:

- (1) Curve 1 is exponential and represents the parent P radionuclide Mo-99 decay into daughter D radionuclide Tc-99m starting with activity $\mathcal{A}_P(0) = 10$ mCi at time $t = 0$.
- (2) Curve 2 shows the activity $\mathcal{A}_D(t)$ of daughter radionuclide for initial condition $\mathcal{A}_D(0) = 0$.
- (3) Curve 3 represents the total activity $\mathcal{A}_{\text{tot}}(t)$ of the Mo-Tc sample as the sum of the parent and daughter activity as a function of time starting with $\mathcal{A}_{\text{tot}}(0) = 10$ mCi at time $t = 0$.

- (a) State or derive equations for the three activity curves shown in Fig. 10.4.
- (b) For curve 2 of Fig. 10.4 verify that $\lim_{t \rightarrow 0} \mathcal{A}_D(t) = 0$ and $\lim_{t \rightarrow \infty} \mathcal{A}_D(t) = 0$ and determine the characteristic time $(t_{\text{max}})_D$ at which activity $\mathcal{A}_D(t)$ reaches its maximum value.

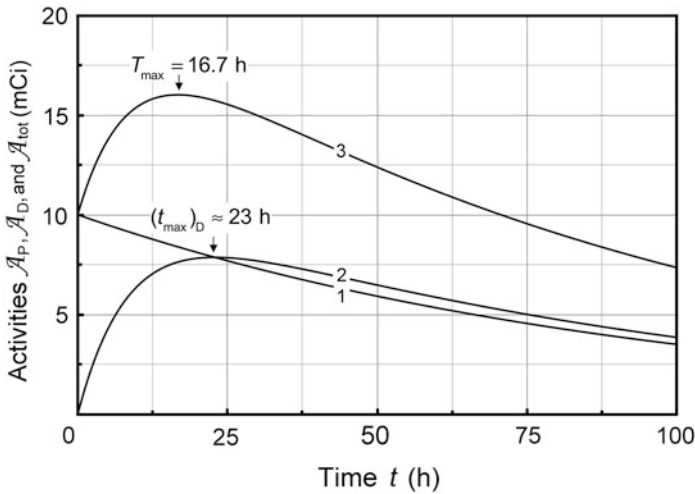


Fig. 10.4 Activities of parent Mo-99 (curve 1) and daughter Tc-99m (curve 2) against time t for molybdenum-99 \rightarrow technetium-99m \rightarrow technetium-99 radioactive decay series for a pure molybdenum source with initial activity of 10 mCi at time $t = 0$. Also shown is the total activity of the sample (curve 3) against time given as the sum of the parent and daughter activities

- (c) For curve 3 of Fig. 10.4 verify that $\lim_{t \rightarrow 0} \mathcal{A}_{\text{tot}}(t) = 10 \text{ mCi}$ and $\lim_{t \rightarrow \infty} \mathcal{A}_{\text{tot}}(t) = 0$.
- (d) Derive a general expression for calculation of the characteristic time T_{max} at which curve 3 of Fig. 10.4 representing the total activity $\mathcal{A}_{\text{tot}}(t)$ of the Mo-Tc sample attains its maximum value.
- (e) Calculate T_{max} for curve 3 of Fig. 10.4.
- (f) Calculate the maximum total activity $\mathcal{A}_{\text{tot}}(t)$ at $t = T_{\text{max}}$ for curve 3 of Fig. 10.4.

SOLUTION:

(a) Since the daughter product Tc-99m of the Mo-99 \rightarrow Tc-99m \rightarrow Tc-99 radioactive decay series is a metal, it remains in the molybdenum sample unless it is separated for medical purpose from the sample by means of a solvent (elution process). When left in the Mo-99 sample, the total activity $\mathcal{A}_{\text{tot}}(t)$ of the sample is the sum of the parent (Mo-99) activity $\mathcal{A}_{\text{P}}(t)$ and the daughter (Tc-99m) activity $\mathcal{A}_{\text{D}}(t)$. The daughter Tc-99m decays into granddaughter G (Tc-99) which is a radionuclide with a very long half-life of 211000 years, so that we assume that G in our decay series is stable.

Expressions for the three decay curves of Fig. 10.4 are as follows:

- (1) Curve 1 represents a simple exponential decay of the parent nucleus expressed as (T10.10)

$$\mathcal{A}_P(t) = \mathcal{A}_P(0)e^{-\lambda_P t}, \quad (10.76)$$

with the initial condition $\mathcal{A}_P(0) = 10$ mCi.

- (2) Curve 2 represents the activity $\mathcal{A}_D(t)$ of the daughter radionuclide and is expressed as follows (T10.35)

$$\mathcal{A}_D(t) = \mathcal{A}_P(0) \frac{\lambda_D}{\lambda_D - \lambda_P} [e^{-\lambda_P t} - e^{-\lambda_D t}], \quad (10.77)$$

with the initial condition $\mathcal{A}_D(0) = 0$.

- (3) Curve 3 represents the total activity $\mathcal{A}_{\text{tot}}(t)$ of the Mo-Tc sample and is given as a sum of $\mathcal{A}_P(t)$ of (10.76) and $\mathcal{A}_D(t)$ of (10.77) as follows

$$\begin{aligned} \mathcal{A}_{\text{tot}}(t) &= \mathcal{A}_P(t) + \mathcal{A}_D(t) = \mathcal{A}_P(0)e^{-\lambda_P t} + \mathcal{A}_P(0) \frac{\lambda_D}{\lambda_D - \lambda_P} [e^{-\lambda_P t} - e^{-\lambda_D t}] \\ &= \frac{\mathcal{A}_P(0)}{\lambda_D - \lambda_P} [(2\lambda_D - \lambda_P)e^{-\lambda_P t} - \lambda_D e^{-\lambda_D t}]. \end{aligned} \quad (10.78)$$

- (b) Daughter activity $\mathcal{A}_D(t)$ is given by (10.77) and the limits for (1) $t \rightarrow 0$ and (2) $t \rightarrow \infty$ are

- (1)

$$\lim_{t \rightarrow 0} \mathcal{A}_D(t) = \mathcal{A}_P(0) \frac{\lambda_D}{\lambda_D - \lambda_P} \lim_{t \rightarrow 0} [e^{-\lambda_P t} - e^{-\lambda_D t}] = \mathcal{A}_P(0) \frac{\lambda_D}{\lambda_D - \lambda_P} [1 - 1] = 0 \quad (10.79)$$

and

- (2)

$$\lim_{t \rightarrow \infty} \mathcal{A}_D(t) = \mathcal{A}_P(0) \frac{\lambda_D}{\lambda_D - \lambda_P} \lim_{t \rightarrow \infty} [e^{-\lambda_P t} - e^{-\lambda_D t}] = \mathcal{A}_P(0) \frac{\lambda_D}{\lambda_D - \lambda_P} [0 - 0] = 0 \quad (10.80)$$

- (3) Characteristic time $(t_{\text{max}})_D$ at which $\mathcal{A}_D(t)$ reaches its maximum is determined by setting $d\mathcal{A}_D(t)/dt = 0$ at $t = (t_{\text{max}})_D$ and solving for $(t_{\text{max}})_D$ to get the following result for Tc-99m (T10.37) using the following decay constants for Tc-99m: $\lambda_P = \lambda_{\text{Mo-99}} = 1.05 \times 10^{-2} \text{ h}^{-1}$ and $\lambda_D = \lambda_{\text{Tc-99m}} = 0.115 \text{ h}^{-1}$

$$\begin{aligned} (t_{\text{max}})_D &= \frac{\ln \frac{\lambda_P}{\lambda_D}}{\lambda_P - \lambda_D} = \frac{\ln \frac{1.05 \times 10^{-2}}{0.115}}{1.05 \times 10^{-2} \text{ h}^{-1} - 0.115 \text{ h}^{-1}} = \frac{-2.394}{-0.1045 \text{ h}^{-1}} \\ &= 22.9 \text{ h}. \end{aligned} \quad (10.81)$$

- (c) Total activity $\mathcal{A}_{\text{tot}}(t)$ is given by (10.78) and the limits for $t \rightarrow 0$ and $t \rightarrow \infty$ are as follows

$$\begin{aligned} \lim_{t \rightarrow 0} \mathcal{A}_{\text{tot}}(t) &= \frac{\mathcal{A}_P(0)}{\lambda_D - \lambda_P} \lim_{t \rightarrow 0} [(2\lambda_D - \lambda_P)e^{-\lambda_P t} - \lambda_D e^{-\lambda_D t}] = \frac{\mathcal{A}_P(0)}{\lambda_D - \lambda_P} (\lambda_D - \lambda_P) \\ &= \mathcal{A}_P(0) \end{aligned} \quad (10.82)$$

and

$$\lim_{t \rightarrow \infty} \mathcal{A}_{\text{tot}}(t) = \frac{\mathcal{A}_{\text{P}}(0)}{\lambda_{\text{D}} - \lambda_{\text{P}}} \lim_{t \rightarrow \infty} [(2\lambda_{\text{D}} - \lambda_{\text{P}})e^{-\lambda_{\text{P}}t} - \lambda_{\text{D}}e^{-\lambda_{\text{D}}t}] = \frac{\mathcal{A}_{\text{P}}(0)}{\lambda_{\text{D}} - \lambda_{\text{P}}} [0 - 0] = 0. \quad (10.83)$$

(d) As curve 3 of Fig. 10.4 shows, $\mathcal{A}_{\text{tot}}(t)$ is equal to $\mathcal{A}_{\text{P}}(0) = 10$ mCi at $t = 0$ where $\mathcal{A}_{\text{D}}(0) = 0$, and then rises with increasing time t until it reaches a peak at a characteristic time $t = T_{\text{max}}$. After the peak, total activity $\mathcal{A}_{\text{tot}}(t)$ decreases toward 0 with increasing t following the decrease of both $\mathcal{A}_{\text{P}}(t)$ and $\mathcal{A}_{\text{D}}(t)$ toward 0 at $t = \infty$. Characteristic time T_{max} should not be confused with $(t_{\text{max}})_{\text{D}}$, the characteristic time at which the daughter activity $\mathcal{A}_{\text{D}}(t)$ attains its maximum value, since the two characteristic times are not equal.

(e) T_{max} is determined by setting $d\mathcal{A}_{\text{tot}}/dt = 0$ at $t = T_{\text{max}}$ and solving for T_{max} as follows

$$\left. \frac{d\mathcal{A}_{\text{tot}}}{dt} \right|_{t=T_{\text{max}}} = \frac{\mathcal{A}_{\text{P}}(0)}{\lambda_{\text{D}} - \lambda_{\text{P}}} [-(2\lambda_{\text{D}} - \lambda_{\text{P}})\lambda_{\text{P}}e^{-\lambda_{\text{P}}T_{\text{max}}} + \lambda_{\text{D}}^2e^{-\lambda_{\text{D}}T_{\text{max}}}] = 0. \quad (10.84)$$

Equation (10.84) can be simplified to read

$$(2\lambda_{\text{D}} - \lambda_{\text{P}})\lambda_{\text{P}}e^{-\lambda_{\text{P}}T_{\text{max}}} = \lambda_{\text{D}}^2e^{-\lambda_{\text{D}}T_{\text{max}}}, \quad (10.85)$$

resulting in the following general expression for T_{max}

$$T_{\text{max}} = \frac{\ln \frac{(2\lambda_{\text{D}} - \lambda_{\text{P}})\lambda_{\text{P}}}{\lambda_{\text{D}}^2}}{\lambda_{\text{P}} - \lambda_{\text{D}}} \quad (10.86)$$

and the following solution for our problem with decay constants $\lambda_{\text{P}} = \lambda_{\text{Mo-99}} = 1.05 \times 10^{-2} \text{ h}^{-1}$ and $\lambda_{\text{D}} = \lambda_{\text{Tc-99m}} = 0.115 \text{ h}^{-1}$

$$T_{\text{max}} = \frac{\ln \frac{(2\lambda_{\text{D}} - \lambda_{\text{P}})\lambda_{\text{P}}}{\lambda_{\text{D}}^2}}{\lambda_{\text{P}} - \lambda_{\text{D}}} = \frac{\ln \frac{(2 \times 0.115 - 1.05 \times 10^{-2}) \times 1.05 \times 10^{-2}}{0.115 \times 0.115}}{(1.05 \times 10^{-2} - 0.115) \text{ h}^{-1}} = 16.72 \text{ h}. \quad (10.87)$$

(f) The maximum in total activity \mathcal{A}_{tot} occurs at $T_{\text{max}} = 16.72$ h, as determined in (e). At $t = T_{\text{max}}$ the total activity has the following magnitude

$$\begin{aligned} \mathcal{A}_{\text{tot}}(T_{\text{max}}) &= \frac{\mathcal{A}_{\text{P}}(0)}{\lambda_{\text{D}} - \lambda_{\text{P}}} [(2\lambda_{\text{D}} - \lambda_{\text{P}})e^{-\lambda_{\text{P}}T_{\text{max}}} - \lambda_{\text{D}}e^{-\lambda_{\text{D}}T_{\text{max}}}] \\ &= \frac{10 \text{ mCi}}{(0.115 - 1.05 \times 10^{-2})} [(2 \times 0.115 - 1.05 \times 10^{-2})e^{-1.05 \times 10^{-2} \times 16.72} \\ &\quad - 0.115e^{-0.115 \times 16.72}] \\ &= 16.02 \text{ mCi}. \end{aligned} \quad (10.88)$$

Equation (10.88) shows that the total activity $\mathcal{A}_{\text{tot}}(t)$ of a pure molybdenum-99 source increases with time from $t = 0$ until it reaches peak activity $\mathcal{A}_{\text{tot}}(T_{\text{max}})$ at a

characteristic time T_{\max} and then it decreases with time until it reaches zero activity at time $t \rightarrow \infty$. In contrast, the daughter activity \mathcal{A}_D reaches its maximum value at its own characteristic time $(t_{\max})_D$ that is larger than the characteristic time T_{\max} .

For initial activity of a pure molybdenum source of 10 mCi, the total sample activity reaches its maximum of 16.02 mCi at a characteristic time T_{\max} of 16.72 hours. The daughter activity, on the other hand, reaches its maximum at a characteristic time $(t_{\max})_D$ of 23 hours.

10.3.Q4

(217)

Consider the simplest radioactive decay series: $P \rightarrow D \rightarrow G$, where both the parent P and daughter D are radioactive and the granddaughter G is stable.

- State or derive expressions for $N_P(t)$, $N_D(t)$ where $N_P(t)$ is the number of parent nuclei, $N_D(t)$ the number of daughter nuclei, and $N_G(t)$ the number of grand-daughter nuclei, all as a function of time t , where $0 \leq t \leq \infty$. Use the following initial conditions: $N_P(t=0) = N_P(0) > 0$, $N_D(t=0) = 0$, and $N_G(t=0) = 0$.
- Validate the expression for $N_G(t)$ derived in (a) by showing that: (1) $\lim_{t \rightarrow 0} N_G(t) = 0$ and (2) $\lim_{t \rightarrow \infty} N_G(t) = N_P(0)$.
- Calculate the sum $N_P(t) + N_D(t) + N_G(t)$ using expressions for $N_P(t)$, $N_D(t)$, and $N_G(t)$ from (a). Do you get the result you expected?
- Figure 10.5 shows 3 curves representing $N_P(t)$, $N_D(t)$, and $N_G(t)$ normalized such that $N_P(t=0) = 1$ and plotted against time t for the decay series $\text{Mo-99} \rightarrow \text{Tc-99m} \rightarrow \text{Tc-99}$ with $\lambda_P = 1.05 \times 10^{-2} \text{ h}^{-1}$, $\lambda_D = 0.115 \text{ h}^{-1}$, and $\lambda_G \approx 0$. Identify the 3 curves.

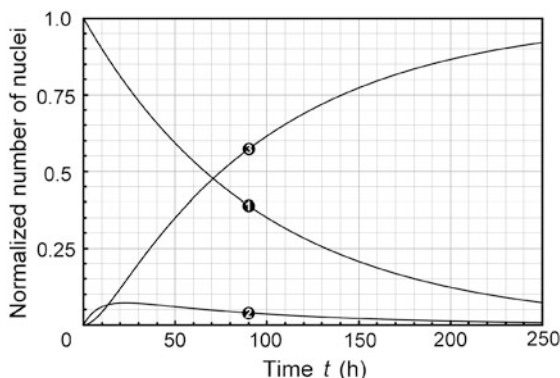


Fig. 10.5 Normalized number of nuclei N_P , N_D , and N_G against time t for the radioactive decay series $\text{Mo-99} \rightarrow \text{Tc-99m} \rightarrow \text{Tc-99}$

- (e) Of the 3 curves in Fig. 10.5, curve 1 decreases from 1 exponentially with time; curve 2 starts at zero, increases with time, exhibits a peak and then decreases with time; and curve 3 increases with time from zero and approaches 1 asymptotically. For curve 2, calculate the time t_{\max} at which the curve attains its peak value and determine the normalized peak value.

SOLUTION:

(a) Expressions for $N_P(t)$ and $N_D(t)$ are well known [see, for example, (T10.9) and (T10.34), respectively], so they will not be derived here. $N_P(t)$ exhibits a pure exponential behavior and $N_D(t)$ accounts for the supply of new daughter nuclei through the decay of P given as $\lambda_P N_P(t)$ and the loss of daughter nuclei D from the concurrent decay of D to G given as $-\lambda_D N_D(t)$, where λ_P and λ_D are the decay constants of parent P and daughter D, respectively.

For initial conditions $N_P(t=0) = N_P(0)$ and $N_D(t=0) = 0$ we have the following expressions for $N_P(t)$ and $N_D(t)$, respectively

$$\frac{dN_P(t)}{dt} = -\lambda_P N_P(t) \quad \text{or} \quad N_P(t) = N_P(0)e^{-\lambda_P t} \quad (10.89)$$

and

$$\frac{dN_D(t)}{dt} = \lambda_P N_P(t) - \lambda_D N_D(t) \quad \text{or} \quad N_D(t) = N_P(0) \frac{\lambda_P}{\lambda_D - \lambda_P} [e^{-\lambda_P t} - e^{-\lambda_D t}]. \quad (10.90)$$

Functional dependence of $N_G(t)$ is less known and can be derived by recognizing that the rate of change (growth) of G is governed by the decay of D, expressed as follows

$$\frac{dN_G(t)}{dt} = \lambda_D N_D(t). \quad (10.91)$$

Inserting (10.90) into (10.91) we get the following expression for $dN_G(t)/dt$

$$\frac{dN_G(t)}{dt} = N_P(0) \frac{\lambda_D \lambda_P}{\lambda_D - \lambda_P} [e^{-\lambda_P t} - e^{-\lambda_D t}]. \quad (10.92)$$

Upon integration of (10.92) from 0 to t we get the following expression for $N_G(t)$

$$N_G(t) = N_P(0) \frac{\lambda_D \lambda_P}{\lambda_D - \lambda_P} \left[-\frac{e^{-\lambda_P t}}{\lambda_P} + \frac{e^{-\lambda_D t}}{\lambda_D} \right] + C, \quad (10.93)$$

where C is an integration constant, for initial condition $N_G(t=0) = 0$ given as

$$N_G(t=0) = N_P(0) \frac{\lambda_D \lambda_P}{\lambda_D - \lambda_P} \left[-\frac{1}{\lambda_D} + \frac{1}{\lambda_P} \right] + C = N_P(0) \frac{\lambda_P - \lambda_D}{\lambda_D - \lambda_P} + C = 0 \quad (10.94)$$

or

$$C = N_P(0). \quad (10.95)$$

Based on (10.93) incorporating (10.95) the number of grand-daughter nuclei $N_G(t)$ as a function of time t is given as follows

$$\begin{aligned} N_G(t) &= N_P(0) \left\{ 1 - \frac{\lambda_D \lambda_P}{\lambda_D - \lambda_P} \left[\frac{e^{-\lambda_P t}}{\lambda_P} - \frac{e^{-\lambda_D t}}{\lambda_D} \right] \right\} \\ &= N_P(0) \left\{ 1 - \frac{\lambda_D e^{-\lambda_P t}}{\lambda_D - \lambda_P} + \frac{\lambda_P e^{-\lambda_D t}}{\lambda_D - \lambda_P} \right\}. \end{aligned} \quad (10.96)$$

In summary, the number of parent nuclei $N_P(t)$ is given by (10.89), the number of daughter nuclei $N_D(t)$ by (10.90), and the number of granddaughter nuclei $N_G(t)$ by (10.96).

(b) The limits of $N_G(t)$ for $t \rightarrow 0$ and $t \rightarrow \infty$ resulting from (10.96) are as follows

(1)

$$\begin{aligned} \lim_{t \rightarrow 0} N_G(t) &= N_P(0) \lim_{t \rightarrow 0} \left\{ 1 - \frac{\lambda_D e^{-\lambda_P t}}{\lambda_D - \lambda_P} + \frac{\lambda_P e^{-\lambda_D t}}{\lambda_D - \lambda_P} \right\} \\ &= N_P(0) \left\{ 1 - \frac{\lambda_D}{\lambda_D - \lambda_P} + \frac{\lambda_P}{\lambda_D - \lambda_P} \right\} = 0 \end{aligned} \quad (10.97)$$

(2)

$$\lim_{t \rightarrow \infty} N_G(t) = N_P(0) \lim_{t \rightarrow \infty} \left\{ 1 - \frac{\lambda_D e^{-\lambda_P t}}{\lambda_D - \lambda_P} + \frac{\lambda_P e^{-\lambda_D t}}{\lambda_D - \lambda_P} \right\} = N_P(0). \quad (10.98)$$

(c) Since the initial conditions for our radioactive sample stipulate that at $t = 0$ we are dealing with a pure parent radioactive source, i.e., $N_P(t = 0) = N_P(0)$, $N_D(t = 0) = 0$, and $N_G(t = 0) = 0$, we conclude that at any time $t > 0$ the sum of all nuclei $N_P(t)$, $N_D(t)$, and $N_G(t)$ must be equal to $N_P(0)$, the initial number of nuclei in the decay series. We now prove that this conclusion is correct by producing a sum consisting of $N_P(t)$ given in (10.89), $N_D(t)$ given in (10.90), and $N_G(t)$ given in (10.96) as follows

$$\begin{aligned} &N_P(t) + N_D(t) + N_G(t) \\ &= N_P(0)e^{-\lambda_P t} \\ &\quad + N_P(0) \frac{\lambda_P}{\lambda_D - \lambda_P} [e^{-\lambda_P t} - e^{-\lambda_D t}] + N_P(0) \left\{ 1 - \frac{\lambda_D e^{-\lambda_P t}}{\lambda_D - \lambda_P} + \frac{\lambda_P e^{-\lambda_D t}}{\lambda_D - \lambda_P} \right\} \\ &= N_P(0) \left(e^{-\lambda_P t} + \frac{\lambda_P e^{-\lambda_P t}}{\lambda_D - \lambda_P} - \frac{\lambda_P e^{-\lambda_D t}}{\lambda_D - \lambda_P} + 1 - \frac{\lambda_D e^{-\lambda_P t}}{\lambda_D - \lambda_P} + \frac{\lambda_P e^{-\lambda_D t}}{\lambda_D - \lambda_P} \right) \\ &= N_P(0). \end{aligned} \quad (10.99)$$

(d) The curves of Fig. 10.5 represent the number of nuclei of either the parent (Mo-99), daughter (Tc-99m), or grand-daughter (Tc-99) for the radioactive decay series starting with a pure source of molybdenum-99 radionuclide. The three curves are identified as follows:

- (1) Curve 1 depicts decay of the parent radionuclide Mo-99.
- (2) Curve 2 depicts growth and decay of the daughter radionuclide Tc-99m.
- (3) Curve 3 depicts growth of the granddaughter nuclide Tc-99 under the assumption that, because of its very long half-life, Tc-99 is essentially stable.

(e) The characteristic time $(t_{\max})_D$ in which the $N_D(t)$ curve reaches its maximum is determined by setting $dN_D/dt = 0$ at $t = (t_{\max})_D$. Differentiating (10.90) results in

$$\frac{dN_D(t)}{dt} = N_P(0) \frac{\lambda_P}{\lambda_D - \lambda_P} [-\lambda_P e^{-\lambda_P t} + \lambda_D e^{-\lambda_D t}] \quad (10.100)$$

and after setting $dN_D/dt = 0$ at $t = (t_{\max})_D$ we get

$$\lambda_P e^{-\lambda_P (t_{\max})_D} = \lambda_D e^{-\lambda_D (t_{\max})_D}. \quad (10.101)$$

Solving (10.101) for $(t_{\max})_D$ finally yields the following general result for characteristic time $(t_{\max})_D$ at which the daughter attains its maximum number of nuclei in the radioactive decay series

$$(t_{\max})_D = \frac{\ln \frac{\lambda_P}{\lambda_D}}{\lambda_P - \lambda_D} = \frac{\ln \frac{\lambda_D}{\lambda_P}}{\lambda_D - \lambda_P}. \quad (10.102)$$

For our specific case of Mo-99 \rightarrow Tc-99m \rightarrow Tc-99 radioactive decay series the characteristic time $(t_{\max})_D$ is calculated as follows

$$(t_{\max})_D = (t_{\max})_{\text{Tc-99m}} = \frac{\ln \frac{\lambda_P}{\lambda_D}}{\lambda_P - \lambda_D} = \frac{\ln \frac{1.05 \times 10^{-2}}{0.115}}{(1.05 \times 10^{-2} \text{ h}^{-1} - 0.115 \text{ h}^{-1})} = 22.88 \text{ h}. \quad (10.104)$$

This result matches the characteristic time $(t_{\max})_D$ in which the daughter in a radioactive decay series reaches its maximum activity [see Prob. 216(b)]

The normalized peak value of $N_D(t)/N_P(0)$ at $[t = (t_{\max})_D]$ is calculated by inserting $t = (t_{\max})_D$ into (10.96) to get the following result

$$\begin{aligned} \frac{N_D(t)}{N_P(0)} &= \frac{\lambda_P}{\lambda_D - \lambda_P} [e^{-\lambda_P (t_{\max})_D} - e^{-\lambda_D (t_{\max})_D}] \\ &= \frac{1.05 \times 10^{-2}}{(0.115 - 1.05 \times 10^{-2})} [e^{-1.05 \times 10^{-2} \times 22.88} - e^{-0.115 \times 22.88}] = 0.072. \end{aligned} \quad (10.105)$$

10.4 General Form of Daughter Activity

10.4.Q1

(218)

The parent P and daughter D activities $\mathcal{A}_P(t)$ and $\mathcal{A}_D(t)$, respectively, in a Parent \rightarrow Daughter \rightarrow Granddaughter decay series (chain) can be expressed in a general form covering all possible physical situations. This is achieved by:

- (1) Defining the ratio λ_P/λ_D as the decay factor m where λ_P and λ_D are the decay constants of parent and daughter, respectively.
- (2) Normalizing time t to the parent half-life $(t_{1/2})_P$ to get new variable $x = t/(t_{1/2})_P$.
- (3) Normalizing the parent activity $\mathcal{A}_P(t)$ to initial parent activity $\mathcal{A}_P(0)$ to get a new variable $y_P = \mathcal{A}_P(t)/\mathcal{A}_P(0) = \exp(-\lambda_P t)$.
- (4) Normalizing the daughter activity $\mathcal{A}_D(t)$ to initial parent activity $\mathcal{A}_P(0)$ to get a new variable $y_D = \mathcal{A}_D(t)/\mathcal{A}_P(0)$.

-
- (a) Transform the equation that describes the parent activity $\mathcal{A}_P(t)$ into a general form of y_P as a function of dimensionless variable x .
 - (b) Transform the equation that describes the daughter activity $\mathcal{A}_D(t)$ into a general form of y_D as a function of dimensionless variable x and decay factor m .
 - (c) Use the L'Hôpital rule to obtain the general form of the daughter activity y_D derived in (b) when the decay factor $m = 1$.
 - (d) Characteristic time t_{\max} is the time in which the daughter activity $\mathcal{A}_D(t)$ reaches its maximum value. Determine $(x_D)_{\max}$ as a function of decay factor m for all possible positive m including $m = 1$.
 - (e) Determine $(y_D)_{\max}$ as a function of m for all possible positive m including $m = 1$.
 - (f) Evaluate the relationship between $(y_D)_{\max}$ and $(x_D)_{\max}$ for all possible positive values of m including $m = 1$.
 - (g) Calculate and plot data points for the following two functions:
 - (1) General parent activity y_P for $0 \leq x \leq 10$ in steps of 1.
 - (2) General daughter activity y_D for $m = 1$ and $0 \leq x \leq 10$ in steps of 1.

Sketch the two curves through the data points and identify the region of $m > 1$ and the region of $m < 1$.

SOLUTION:

The general variables x , y_P , and y_D as well as the decay factor m are defined as follows

$$x = \frac{1}{(t_{1/2})_P}, \quad (10.106)$$

$$y_P = \frac{\mathcal{A}_P(t)}{\mathcal{A}_P(0)}, \quad (10.107)$$

$$y_D = \frac{\mathcal{A}_D(t)}{\mathcal{A}_P(0)}, \quad (10.108)$$

$$m = \frac{\lambda_P}{\lambda_D}. \quad (10.109)$$

(a) The standard form of parent activity $\mathcal{A}_P(t)$, expressed as follows (T10.10) irrespective of the status of the daughter (stable or radioactive)

$$\mathcal{A}_P(t) = \mathcal{A}_P(0)e^{-\lambda_P t} = \mathcal{A}_P(0)e^{-\frac{(\ln 2)t}{(t_{1/2})_P}}, \quad (10.110)$$

is, after incorporating (10.106) and (10.107), written as (T10.47)

$$y_P = \frac{\mathcal{A}_P(t)}{\mathcal{A}_P(0)} = e^{-\frac{(\ln 2)t}{(t_{1/2})_P}} = e^{-x \ln 2^{-x}} = 2^{-x} = \frac{1}{2^x}. \quad (10.111)$$

(b) The standard form of daughter activity $\mathcal{A}_D(t)$, expressed as follows (T10.35) irrespective of the stability status of the granddaughter (stable or radioactive)

$$\mathcal{A}_D(t) = \mathcal{A}_P(0) \frac{\lambda_D}{\lambda_D - \lambda_P} [e^{-\lambda_P t} - e^{-\lambda_D t}], \quad (10.112)$$

is, after incorporating (10.106), (10.108), and (10.110), written as (T10.45)

$$\begin{aligned} y_D &= \frac{\mathcal{A}_D(t)}{\mathcal{A}_P(0)} = \frac{1}{1-m} [e^{-x \ln 2} - e^{-\frac{x}{m} \ln 2}] = \frac{1}{1-m} [e^{\ln 2^{-x}} - e^{\ln 2^{-\frac{x}{m}}}] \\ &= \frac{1}{1-m} \left[\frac{1}{2^x} - \frac{1}{2^{x/m}} \right]. \end{aligned} \quad (10.113)$$

(c) Equation (10.113) for y_D as a function of x has physical meaning for all positive values of decay factor m except for $m = 1$ for which y_D is not defined. However, since for $m = 1$, (10.113) gives $y_D = 0/0$, we can apply the l'Hôpital rule and determine the function that governs y_D at $m = 1$ as follows

$$y_D|_{m=1} = \lim_{m \rightarrow 1} \frac{\frac{d}{dm} \left[\frac{1}{2^x} - \frac{1}{2^{x/m}} \right]}{\frac{d}{dm} (1-m)} = \lim_{m \rightarrow 1} \frac{-2^{-\frac{x}{m}} (\ln 2) \frac{x}{m^2}}{-1} = (\ln 2) \frac{x}{2^x}. \quad (10.114)$$

(d) The characteristic time $(t_{\max})_D$ which represents the time of maximum daughter activity and is written as (T10.37)

$$(t_{\max})_D = \frac{\ln \frac{\lambda_P}{\lambda_D}}{\lambda_P - \lambda_D} \quad (10.115)$$

can be expressed in general form incorporating (10.106) and (10.108) into (10.115) as follows

$$(x_D)_{\max} = \frac{(t_{\max})_D}{(t_{1/2})_P} = \frac{\lambda_P \ln \frac{\lambda_P}{\lambda_D}}{(\ln 2)(\lambda_P - \lambda_D)} = \frac{\ln \frac{\lambda_P}{\lambda_D}}{(\ln 2)(1 - \frac{\lambda_D}{\lambda_P})} = \frac{m \ln m}{(\ln 2)(m - 1)}. \quad (10.116)$$

Equation (10.116) has physical meaning for all positive m except for $m = 1$ for which it is not defined, since it gives $(x_D)_{\max} = 0/0$. Again we apply l'Hôpital rule to get a finite value for $(x_D)_{\max}|_{m=1}$ as follows

$$(x_D)_{\max}|_{m=1} = \lim_{m \rightarrow 1} \frac{\frac{d(m \ln m)}{dm}}{(\ln 2) \frac{d(m-1)}{dm}} = \lim_{m \rightarrow 1} \frac{(\ln m + 1)}{\ln 2} = \frac{1}{\ln 2} = 1.4427. \quad (10.117)$$

(e) The maximum daughter activity $(y_D)_{\max}$ can be determined by inserting $(x_D)_{\max}$ into y_D given by (10.113). However, since at the point of maximum daughter activity both the parent and the daughter have identical activities equal to $(y_D)_{\max}$, it is much easier to obtain $(y_D)_{\max}$ by inserting $(x_D)_{\max}$ into y_P given by (10.110)

$$(y_D)_{\max} = y_P[(x_D)_{\max}] = \frac{1}{2^{(x_D)_{\max}}} = 2^{\frac{m \ln m}{(\ln 2)(1-m)}} = e^{\frac{m}{1-m} \ln m}. \quad (10.118)$$

Equation (10.118) is valid for all positive m except for $m = 1$ in which case $(y_D)_{\max}$ can be determined by applying the l'Hôpital rule to (10.118) as follows

$$(y_D)_{\max}|_{m=1} = \lim_{m \rightarrow 1} \exp \frac{\frac{d(m \ln m)}{dm}}{\frac{d(1-m)}{dm}} = \lim_{m \rightarrow 1} \exp \frac{\ln m + 1}{-1} = e^{-1} = \frac{1}{e} = 0.368. \quad (10.119)$$

(f) It is easy to show that the relationship for positive m but $m \neq 1$ between $(y_D)_{\max}$ given by (10.118) and $(x_D)_{\max}$ given by (10.116) is a simple exponential expression

$$(y_D)_{\max} = e^{\frac{m}{1-m} \ln m} = e^{-\frac{m}{m-1} \ln m} = e^{-(\ln 2)(x_D)_{\max}} = 2^{-(x_D)_{\max}}, \quad (10.120)$$

while for $m = 1$, $(y_D)_{\max} = 1/e = 0.368$, as shown in (10.119), and $(x_D)_{\max} = 1/\ln 2 = 1.4427$, as shown in (10.117).

(g) Data points for $y_P(x)$ are calculated from (10.111) and for $y_D(x)$ from (10.113) and results for $0 \leq x \leq 10$ in steps of 1 are displayed in Table 10.3 and plotted in Fig. 10.6. The maximum value of y_D for $m = 1$ is $1/e = 0.368$ and occurs at $x = 1/\ln 2 = 1.4427$ which is also the intersection point of y_P and y_D curves.

Table 10.3 Data points for y_P and y_D at various values of x for $0 \leq x \leq 10$

x	0	1	2	3	4	5	6	7	8	9	10
y_P	1	0.5	0.25	0.125	0.063	0.031	0.016	0.008	0.004	0.002	0.001
y_D	0	0.347	0.347	0.259	0.173	0.108	0.065	0.038	0.022	0.012	0.007

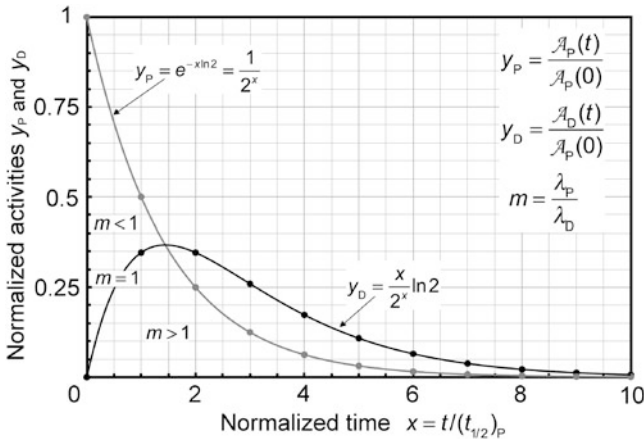


Fig. 10.6 Normalized activities y_P and y_D against normalized time x . The y_D curve is for decay factor $m = 1$ and has no physical meaning, however, it separates the y_D curves for $m > 1$ ($\lambda_P > \lambda_D$) from y_D curves for $m < 1$ ($\lambda_P < \lambda_D$) and is governed by the simple function given in (10.114)

10.5 Equilibria in Parent-Daughter Activities

10.5.Q1

(219)

In many parent $P \rightarrow$ daughter $D \rightarrow$ granddaughter G relationships after a certain time t the parent and daughter activities $\mathcal{A}_P(t)$ and $\mathcal{A}_D(t)$, respectively, reach a constant ratio that is independent of a further increase in time t . This condition is referred to as radioactive equilibrium and can be analysed by examining the behavior of the activity ratio $\mathcal{A}_D(t)/\mathcal{A}_P(t)$ which can be expressed as follows [see (T10.35)]

$$\zeta = \frac{\mathcal{A}_D(t)}{\mathcal{A}_P(t)} = \frac{\lambda_D}{\lambda_D - \lambda_P} [1 - e^{-(\lambda_D - \lambda_P)t}]. \quad (10.121)$$

- (a) Show that by introducing into (10.121) a parameter called the decay factor $m = \lambda_D/\lambda_P$ and new variables $x = t/(t_{1/2})_P$, $y_P = \mathcal{A}_P(t)/\mathcal{A}_P(0)$, and $y_D = \mathcal{A}_D(t)/\mathcal{A}_P(0)$ we get the following expression for activity ratio ζ

$$\zeta = \frac{\mathcal{A}_D(t)}{\mathcal{A}_P(t)} = \frac{y_D}{y_P} = \frac{1}{1-m} \left[1 - 2^{\frac{m-1}{m}x} \right]. \quad (10.122)$$

- (b) Expression (10.122) for $\zeta(x)$ is valid for all positive m except for $m = 1$ (or $\lambda_P = \lambda_D$) for which it is not defined since it results in $\zeta(x) = 0/0$. Despite this indeterminate result there is a functional relationship between $\zeta(x)$ and x for $m = 1$. Determine the function.
- (c) Figure 10.7 plots the activity ratio $\zeta(x)$ of (10.122) against time variable x for selected values of the decay factor m in the range from 0.1 to 10. Based on the figure, discuss the relationship between radioactive equilibrium and decay factor m .
- (d) Summarize in a table the four special regions for the decay factor m between $0 < m < \infty$.

SOLUTION:

- (a) The radioactive parent activity $\mathcal{A}_P(t)$ is given as (T10.10)

$$\mathcal{A}_P(t) = \mathcal{A}_P(0)e^{-\lambda_P t} = \lambda_P N_P(0)e^{-\lambda_P t} = \mathcal{A}_P(0)e^{-\frac{(\ln 2)}{(t_{1/2})_P} t}, \quad (10.123)$$

while the radioactive daughter activity $\mathcal{A}_D(t)$ is (T10.35)

$$\mathcal{A}_D(t) = \mathcal{A}_P(t) \frac{\lambda_D}{\lambda_D - \lambda_P} \left[1 - e^{-(\lambda_D - \lambda_P)t} \right], \quad (10.124)$$

where $\mathcal{A}_P(0)$ is the initial activity of the parent at time $t = 0$, λ_P is the decay constant of the parent radionuclide, and λ_D is the decay constant of the daughter radionuclide. The initial daughter activity $\mathcal{A}_D(0)$ is assumed to be zero at $t = 0$.

The activity ratio ζ is defined as the ratio between the daughter and parent activities at time t that from (10.124) can be expressed as follows after introducing the definitions for the new variable $x = t/(t_{1/2})_P$ and the decay factor $m = \lambda_P/\lambda_D$

$$\begin{aligned} \zeta &= \frac{\mathcal{A}_D(t)}{\mathcal{A}_P(t)} = \frac{\lambda_D}{\lambda_D - \lambda_P} \left[1 - e^{-(\lambda_D - \lambda_P)t} \right] = \frac{1}{1 - \frac{\lambda_P}{\lambda_D}} \left[1 - e^{-(\ln 2) \left(\frac{\lambda_D}{\lambda_P} - 1 \right) \frac{t}{(t_{1/2})_P}} \right] \\ &= \frac{1}{1-m} \left[1 - 2^{\frac{m-1}{m}x} \right]. \end{aligned} \quad (10.125)$$

- (b) Since $\zeta(x)$ of (10.122) and (10.125) for $m = 1$ or $\lambda_P = \lambda_D$ results in $\zeta(x) = 0/0$, we can determine the $\zeta(x)$ function for $m = 1$ by applying the l'Hôpital rule to

convert the indeterminate form into a determinate form which allows the evaluation of the $m \rightarrow 1$ limit as follows

$$\begin{aligned}\zeta(x)|_{m=1} &= \lim_{m \rightarrow 1} \frac{\frac{d}{dm} [1 - 2^{\frac{m-1}{1}x}]}{\frac{d(1-m)}{dm}} = \lim_{m \rightarrow 1} \frac{\{-2^{\frac{m-1}{m}x} (\ln 2) [\frac{x}{m} - \frac{m-1}{m^2}x]\}}{-1} \\ &= \lim_{m \rightarrow 1} \frac{-2^{\frac{m-1}{m}x} (\ln 2) \frac{x}{m^2}}{-1} = (\ln 2)x.\end{aligned}\quad (10.126)$$

Equation (10.126) shows that $\zeta(x)$ for $m = 1$ is a simple linear function of the type $y = b + ax$ for which the y intercept is $b = 0$ and the slope is $a = \ln 2 = 0.6931 \dots$, resulting in an angle of 34.7° between the abscissa and the straight line of the linear function.

(c) In Fig. 10.8 we show a plot of the linear expression given in (10.126) and derived in (b) for the activity ratio $\zeta(x)$ for $m = 1$ superimposed on $\zeta(x)$ curves plotted in Fig. 10.7 for various m between 0.1 and 10. The $m = 1$ linear equation actually separates two distinct regions of the activity ratio $\zeta(x)$: (1) Region where $m > 1$ and (2) Region where $0 < m < 1$.

(1) For the $m > 1$ region we write (10.125) as follows

$$\zeta(x) = \frac{1}{m-1} [e^{\frac{m-1}{m}x \ln 2} - 1]. \quad (10.127)$$

Since $m > 1$, $\zeta(x)$ in (10.127) rises exponentially with x , implying that the ratio $\mathcal{A}_D(t)/\mathcal{A}_P(t)$ also increases with time t and thus no equilibrium between $\mathcal{A}_P(t)$ and $\mathcal{A}_D(t)$ will ensue with an increasing time t . The exponential growth of $\zeta(x)$ for $m > 1$ with time t is clearly shown with dashed curves in Fig. 10.8 in the range of decay factor $1 < m < \infty$.

Thus, for $m > 1$, which means that $\lambda_P > \lambda_D$ or that half-life of the daughter exceeds that of the parent [$(t_{1/2})_D > (t_{1/2})_P$] or one can say that the daughter is longer-lived than the parent, the activity ratio $\zeta(x)$ increases exponentially with time t and no equilibrium can be reached between the parent activity $\mathcal{A}_P(t)$ and $\mathcal{A}_D(t)$ for any time t .

(2) For the $0 < m < 1$ region we rearrange the terms in (10.125) to get a clearer picture as follows

$$\zeta(x) = \frac{1}{1-m} [1 - e^{-(\ln 2)(\frac{1-m}{m})x}] = \frac{1}{1-m} [1 - 2^{-\frac{1-m}{m}x}] \quad (10.128)$$

and notice that the exponential term diminishes with increasing x and exponentially approaches zero as $x \rightarrow \infty$. This means that at large x the activity ratio $\zeta(x)$ saturates at a constant value that is independent of x and is equal to $1/(1-m)$. Under these conditions the parent activity $\mathcal{A}_P(t)$ and the daughter activity $\mathcal{A}_D(t)$ are said to be in transient equilibrium and are governed by the

following relationship

$$\zeta(x) = \frac{\mathcal{A}_D(t)}{\mathcal{A}_P(t)} = \frac{y_D}{y_P} = \frac{1}{1-m} = \frac{1}{1-\frac{\lambda_P}{\lambda_D}} = \frac{\lambda_D}{\lambda_D - \lambda_P} = \text{const} > 1 \quad (10.129)$$

provided, of course, that $\lambda_P < \lambda_D$, i.e., $(t_{1/2})_P > (t_{1/2})_D$.

Thus, for $0 < m < 1$, which means that $\lambda_P < \lambda_D$ or that the half-life of the daughter is shorter than the half-life of the parent [$(t_{1/2})_D < (t_{1/2})_P$] or one can say that the daughter is shorter-lived than the parent, the activity ratio $\zeta(x)$ at some large time saturates at a constant value given by (10.129) and larger than 1. The constancy of the ratio $\mathcal{A}_D(t)/\mathcal{A}_P(t)$ at large t implies a transient equilibrium between $\mathcal{A}_P(t)$ and $\mathcal{A}_D(t)$.

- (3) A special case of transient equilibrium occurs when the daughter is much shorter-lived than the parent [$(t_{1/2})_D \ll (t_{1/2})_P$] or we can say that $m \ll 1$ to get the following expression for (10.128)

$$\begin{aligned} \zeta(x) &= \frac{\mathcal{A}_D}{\mathcal{A}_P} = \frac{1}{1-m} \left[1 - e^{-(\ln 2)\left(\frac{1-m}{m}\right)x} \right] = \frac{1}{1-m} \left[1 - 2^{-\frac{1-m}{m}x} \right] \\ &\approx 1 - e^{-(\ln 2)\frac{x}{m}} = 1 - e^{-\lambda_D t}. \end{aligned} \quad (10.130)$$

Equation (10.130) becomes equal to unity for a relatively large time $x \gg (x_D)_{\max}$ where $(x_D)_{\max}$ is the normalized time of maximum daughter activity which indicates that $\mathcal{A}_D(t) \approx \mathcal{A}_P(t)$ or $\zeta \approx 1$, so that the parent and daughter decay together at the rate of the parent. This special case of transient equilibrium in which the daughter and parent activities are essentially identical is referred to as secular equilibrium.

(d) Important features of the four special regions characterized by the decay factor m between $m = 0$ and $m = \infty$ are summarized in Table 10.4. Region where $m \rightarrow 0$ results in secular equilibrium between the parent and daughter activities $\mathcal{A}_P(t)$ and $\mathcal{A}_D(t)$, respectively, and the region where $0 < m < 1$ results in transient equilibrium between the parent and daughter activities. Regions where $m = 1$ and $m > 1$ do not result in equilibrium between the parent and daughter activities. The relationship between $\mathcal{A}_P(t)$ and $\mathcal{A}_D(t)$ expressed by a linear function $\zeta(x) = (\ln 2)x$ for $m = 1$ separates the secular equilibrium region characterized by $m \rightarrow 0$ and the transient equilibrium region characterized by $0 < m < 1$ from the non-equilibrium region where $1 < m < \infty$.

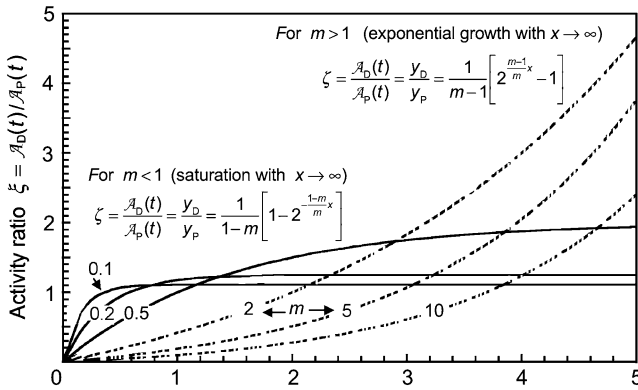


Fig. 10.7 Activity ratio $\zeta(x)$ against normalized time x for several decay factors m in the range from 0.1 through 1 to 10 calculated using (10.122)

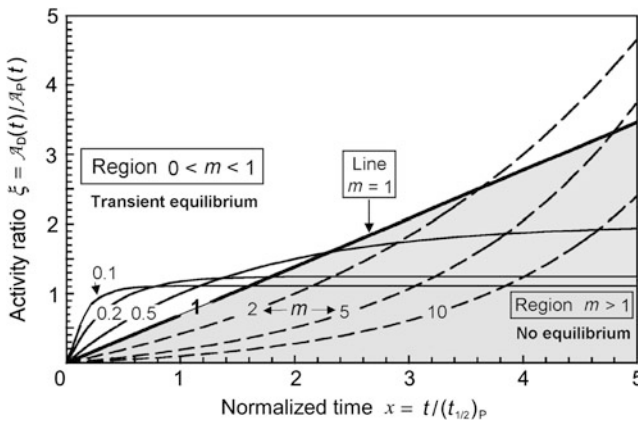


Fig. 10.8 Activity ratio $\zeta(x)$ against normalized time x for several decay factors m in the range from 0.1 through 1 to 10 calculated using (10.122) except for $\zeta(m = 1)$ which gives a linear function determined in (10.126). The linear function for $m = 1$ separates the region of transient equilibrium where $0 < m < 1$ from the region of no equilibrium where $m > 1$

Table 10.4 Four distinct regions of the decay factor m

Decay factor m	Relative value	Equilibrium	Relationship for $\xi = \frac{A_D(t)}{A_P(t)}$	
$m \approx 0$	$\lambda_D \gg \lambda_P$	Secular	$\xi = 1$	
$0 < m < 1$	$\lambda_D > \lambda_P$	Transient	$\xi = \frac{1}{1-m} = \frac{\lambda_D}{\lambda_D - \lambda_P}$	See (10.129)
$m = 1$	$\lambda_D = \lambda_P$	No	$\xi = \frac{t \ln 2}{(t_{1/2})_P} = x \ln 2$	See (10.126)
$m > 1$	$\lambda_D < \lambda_P$	No	$\xi = \frac{1}{m-1} \left\{ e^{\frac{m-1}{m} \frac{t \ln 2}{(t_{1/2})_P}} - 1 \right\}$	See (10.127)

10.6 Bateman Equations for Radioactive Decay Chain

10.6.Q1

(220)

Ernest Rutherford and Frederick Soddy introduced the exponential laws of radioactive decay in 1902 to explain results of their experiments on the thorium series of radionuclides. In 1910 Harry Bateman extended the series decay formalism from the simple radioactive decay series Parent \rightarrow Daughter \rightarrow Granddaughter to a general chain of decaying nuclei with an arbitrary number of radioactive chain links designated as follows: $N_1 \rightarrow N_2 \rightarrow N_3 \rightarrow \dots \rightarrow N_{i-1} \rightarrow N_i$, where N stands for number of nuclei in a given generation of nuclear progeny. The initial conditions stipulate that only the first generation parent nuclei are present in a sample at time $t = 0$, i.e., $N_1(t = 0) = N_1(0)$ and $N_2(0) = N_3(0) = \dots = N_{n-1}(0) = N_n(0) = 0$.

Bateman equations are usually given as a set of equations that give the number of atoms $N_n(t)$ of each nuclide of a radioactive decay chain produced after a given time t recognizing that at $t = 0$ (initial condition) only a given number of parent nuclei $N_1(0)$ were present. For generation n the set of Bateman equation and constants is usually presented in the following simple format

$$N_n(t) = C_1 e^{-\lambda_1 t} + C_2 e^{-\lambda_2 t} + C_3 e^{-\lambda_3 t} + \dots + C_n e^{-\lambda_n t}, \quad (10.131)$$

where C_1, C_2, \dots, C_n are constants given as follows

$$C_1 = N_1(0) \frac{\lambda_1 \lambda_2 \dots \lambda_{i-1}}{(\lambda_2 - \lambda_1)(\lambda_3 - \lambda_1) \dots (\lambda_i - \lambda_1)}, \quad (10.132)$$

$$C_2 = N_1(0) \frac{\lambda_1 \lambda_2 \dots \lambda_{n-1}}{(\lambda_1 - \lambda_2)(\lambda_3 - \lambda_2) \dots (\lambda_n - \lambda_2)}, \quad (10.133)$$

$$\vdots$$

$$C_n = N_1(0) \frac{\lambda_1 \lambda_2 \dots \lambda_{n-1}}{(\lambda_1 - \lambda_n)(\lambda_3 - \lambda_n) \dots (\lambda_{n-1} - \lambda_n)}. \quad (10.134)$$

-
- (a) Consolidate the Bateman equation and its constants into a single expression for generation n in radioactive decay series.
 - (b) Use the consolidated Bateman equation determined in (a) to express the number of nuclei for the first four generations of a radioactive decay chain.
 - (c) Based on results of (b) determine the activities of decay series progeny for the first four generations of a radioactive decay chain.

SOLUTION:

(a) The number $N_n(t)$ of nuclei of generation n can be expressed by a simple sum as follows

$$N_n(t) = \sum_{m=1}^n C_m e^{-\lambda_m t}, \quad (10.135)$$

while the constants C_1, C_2, \dots, C_n can be expressed by simple products as follows

$$C_m = N_1(0) \frac{\prod_{i=1}^{n-1} \lambda_i}{\prod_{\substack{i=1 \\ i \neq m}}^n (\lambda_i - \lambda_m)}. \quad (10.136)$$

Inserting (10.136) into (10.135) we obtain a single expression for $N_n(t)$

$$N_n(t) = \sum_{m=1}^n C_m e^{-\lambda_m t} = N_1(0) \sum_{m=1}^n \left[\frac{\prod_{i=1}^{n-1} \lambda_i}{\prod_{\substack{i=1 \\ i \neq m}}^n (\lambda_i - \lambda_m)} \right] e^{-\lambda_m t}. \quad (10.137)$$

(b) Equation (10.131) is used to determine the number of radioactive nuclei present for a given generation in nuclear decay series at a given time $t \geq 0$ with $t = 0$ defining the initial conditions $N_1(t = 0) = N_1(0)$ and $N_2(t = 0) = N_3(t = 0) = \dots = N_n(t = 0) = 0$.

(1) First generation ($n = 1$)—Number of parent nuclei $N_1(t)$ is expressed with the standard equation for description of exponential decay of radioactive nuclides

$$C_1 = N_1(0) \frac{\prod_{m=1}^{n-1} \lambda_i}{\prod_{\substack{i=1 \\ i \neq m}}^n (\lambda_i - \lambda_m)} = N_1(0), \quad (10.138)$$

$$N_1(t) = \sum_{m=1}^{n=1} C_m e^{-\lambda_m t} = C_1 e^{-\lambda_1 t} = N_1(0) e^{-\lambda_1 t}. \quad (10.139)$$

(2) Second generation ($n = 2$)—Number of daughter nuclei $N_2(t)$

$$C_1 = N_1(0) \frac{\prod_{i=1}^1 \lambda_i}{\prod_{\substack{i=1 \\ i \neq 1}}^1 (\lambda_i - \lambda_1)} = N_1(0) \frac{\lambda_1}{\lambda_2 - \lambda_1}, \quad (10.140)$$

$$C_2 = N_1(0) \frac{\prod_{i=1}^1 \lambda_i}{\prod_{\substack{i=1 \\ i \neq 2}}^1 (\lambda_i - \lambda_2)} = N_1(0) \frac{\lambda_1}{\lambda_1 - \lambda_2}, \quad (10.141)$$

$$N_2(t) = \sum_{m=1}^{n=2} C_m e^{-\lambda_m t} = C_1 e^{-\lambda_1 t} + C_2 e^{-\lambda_2 t} = N_1(0) \frac{\lambda_1}{\lambda_2 - \lambda_1} [e^{-\lambda_1 t} - e^{-\lambda_2 t}]. \quad (10.142)$$

(3) Third generation ($n = 3$)—Number of granddaughter nuclei $N_3(t)$

$$C_1 = N_1(0) \frac{\prod_{i=1}^2 \lambda_i}{\prod_{\substack{i=1 \\ i \neq 1}}^3 (\lambda_i - \lambda_1)} = N_1(0) \frac{\lambda_1 \lambda_2}{(\lambda_2 - \lambda_1)(\lambda_3 - \lambda_1)}, \quad (10.143)$$

$$C_2 = N_1(0) \frac{\prod_{i=1}^2 \lambda_i}{\prod_{\substack{i=1 \\ i \neq 2}}^3 (\lambda_i - \lambda_2)} = N_1(0) \frac{\lambda_1 \lambda_2}{(\lambda_1 - \lambda_2)(\lambda_3 - \lambda_2)}, \quad (10.144)$$

$$C_3 = N_1(0) \frac{\prod_{i=1}^2 \lambda_i}{\prod_{\substack{i=1 \\ i \neq 3}}^3 (\lambda_i - \lambda_3)} = N_1(0) \frac{\lambda_1 \lambda_2}{(\lambda_1 - \lambda_3)(\lambda_2 - \lambda_3)}, \quad (10.145)$$

$$\begin{aligned} N_3(t) &= \sum_{m=1}^{n=3} C_m e^{-\lambda_m t} = C_1 e^{-\lambda_1 t} + C_2 e^{-\lambda_2 t} + C_3 e^{-\lambda_3 t} \\ &= N_1(0) \lambda_1 \lambda_2 \left[\frac{e^{-\lambda_1 t}}{(\lambda_2 - \lambda_1)(\lambda_3 - \lambda_1)} + \frac{e^{-\lambda_2 t}}{(\lambda_1 - \lambda_2)(\lambda_3 - \lambda_2)} \right. \\ &\quad \left. + \frac{e^{-\lambda_3 t}}{(\lambda_1 - \lambda_3)(\lambda_2 - \lambda_3)} \right]. \end{aligned} \quad (10.146)$$

(4) Fourth generation ($n = 4$)—Number of great granddaughter nuclei $N_4(t)$

$$C_1 = N_1(0) \frac{\prod_{i=1}^3 \lambda_i}{\prod_{\substack{i=1 \\ i \neq 1}}^4 (\lambda_i - \lambda_1)} = N_1(0) \frac{\lambda_1 \lambda_2 \lambda_3}{(\lambda_2 - \lambda_1)(\lambda_3 - \lambda_1)(\lambda_4 - \lambda_1)}, \quad (10.147)$$

$$C_2 = N_1(0) \frac{\prod_{i=1}^3 \lambda_i}{\prod_{\substack{i=1 \\ i \neq 2}}^4 (\lambda_i - \lambda_2)} = N_1(0) \frac{\lambda_1 \lambda_2 \lambda_3}{(\lambda_1 - \lambda_2)(\lambda_3 - \lambda_2)(\lambda_4 - \lambda_2)}, \quad (10.148)$$

$$C_3 = N_1(0) \frac{\prod_{i=1}^3 \lambda_i}{\prod_{\substack{i=1 \\ i \neq 3}}^4 (\lambda_i - \lambda_3)} = N_1(0) \frac{\lambda_1 \lambda_2 \lambda_3}{(\lambda_1 - \lambda_3)(\lambda_2 - \lambda_3)(\lambda_4 - \lambda_3)}, \quad (10.149)$$

$$C_4 = N_1(0) \frac{\prod_{i=1}^3 \lambda_i}{\prod_{\substack{i=1 \\ i \neq 4}}^4 (\lambda_i - \lambda_4)} = N_1(0) \frac{\lambda_1 \lambda_2 \lambda_3}{(\lambda_1 - \lambda_4)(\lambda_2 - \lambda_4)(\lambda_3 - \lambda_4)}, \quad (10.150)$$

$$\begin{aligned} N_4(t) &= \sum_{m=1}^{n=3} C_m e^{-\lambda_m t} = C_1 e^{-\lambda_1 t} + C_2 e^{-\lambda_2 t} + C_3 e^{-\lambda_3 t} + C_4 e^{-\lambda_4 t} \\ &= N_1(0) \lambda_1 \lambda_2 \lambda_3 \left[\frac{e^{-\lambda_1 t}}{(\lambda_2 - \lambda_1)(\lambda_3 - \lambda_1)(\lambda_4 - \lambda_1)} \right. \end{aligned}$$

$$\begin{aligned}
& + \frac{e^{-\lambda_2 t}}{(\lambda_1 - \lambda_2)(\lambda_3 - \lambda_2)(\lambda_4 - \lambda_2)} + \frac{e^{-\lambda_3 t}}{(\lambda_1 - \lambda_3)(\lambda_2 - \lambda_3)(\lambda_4 - \lambda_3)} \\
& + \frac{e^{-\lambda_4 t}}{(\lambda_1 - \lambda_4)(\lambda_2 - \lambda_4)(\lambda_3 - \lambda_4)} \Big]. \quad (10.151)
\end{aligned}$$

(c) Activities $\mathcal{A}_n(t)$ of progeny in a radioactive decay series are calculated using results obtained from Bateman equation in (b).

(1) Parent activity $\mathcal{A}_1(t)$ at time t is given by the product of the parent decay constant λ_1 and the number of parent nuclei $N_1(t)$ present at time t in the sample, as given in (10.139)

$$\mathcal{A}_1(t) = \lambda_1 N_1(t) = \lambda_1 N_1(0) e^{-\lambda_1 t} = \mathcal{A}_1(0) e^{-\lambda_1 t}. \quad (10.152)$$

(2) Daughter activity $\mathcal{A}_2(t)$ at time t is given by the product of the daughter decay constant λ_2 and the number of parent nuclei $N_2(t)$ present at time t in the sample, as given in (10.142)

$$\mathcal{A}_2(t) = \lambda_2 N_2(t) = N_1(0) \frac{\lambda_1 \lambda_2}{\lambda_2 - \lambda_1} [e^{-\lambda_1 t} - e^{-\lambda_2 t}] = \mathcal{A}_1(0) \frac{\lambda_2}{\lambda_2 - \lambda_1} [e^{-\lambda_1 t} - e^{-\lambda_2 t}], \quad (10.153)$$

where $\mathcal{A}_1(0)$ is the initial activity of the parent nuclei.

(3) Granddaughter activity $\mathcal{A}_3(t)$ at time t is given by the product of the granddaughter decay constant λ_3 and the number of granddaughter nuclei $N_3(t)$ present at time t in the sample as given in (10.146)

$$\begin{aligned}
\mathcal{A}_3(t) &= \lambda_3 N_3(t) \\
&= N_1(0) \lambda_1 \lambda_2 \lambda_3 \left[\frac{e^{-\lambda_1 t}}{(\lambda_2 - \lambda_1)(\lambda_3 - \lambda_1)} + \frac{e^{-\lambda_2 t}}{(\lambda_1 - \lambda_2)(\lambda_3 - \lambda_2)} \right. \\
&\quad \left. + \frac{e^{-\lambda_3 t}}{(\lambda_1 - \lambda_3)(\lambda_2 - \lambda_3)} \right]. \quad (10.154)
\end{aligned}$$

(4) Great granddaughter activity $\mathcal{A}_4(t)$ at time t is given by the product of the decay constant λ_4 of the great grand daughter and the number of great granddaughter nuclei $N_4(t)$ present at time t in the sample, as given in (10.151)

$$\begin{aligned}
\mathcal{A}_4(t) &= \lambda_4 N_4(t) \\
&= N_1(0) \lambda_1 \lambda_2 \lambda_3 \lambda_4 \left[\frac{e^{-\lambda_1 t}}{(\lambda_2 - \lambda_1)(\lambda_3 - \lambda_1)(\lambda_4 - \lambda_1)} \right. \\
&\quad + \frac{e^{-\lambda_2 t}}{(\lambda_1 - \lambda_2)(\lambda_3 - \lambda_2)(\lambda_4 - \lambda_2)} + \frac{e^{-\lambda_3 t}}{(\lambda_1 - \lambda_3)(\lambda_2 - \lambda_3)(\lambda_4 - \lambda_3)} \\
&\quad \left. + \frac{e^{-\lambda_4 t}}{(\lambda_1 - \lambda_4)(\lambda_2 - \lambda_4)(\lambda_3 - \lambda_4)} \right]. \quad (10.155)
\end{aligned}$$

10.6.Q2

(221)

In Prob. 220 we determined general expressions for the number $N(t)$ as well as activity $\mathcal{A}(t)$ of the parent P, daughter D, granddaughter G, and great granddaughter GG nuclei present at time $t > 0$ for radioactive decay series. The initial conditions at time $t = 0$ were that the initial number of parent nuclei $N_1(t = 0)$ was $N_1(0)$ and no other descendants were present at $t = 0$.

In this problem we will assume a specific radioactive decay series, starting with initial parent activity $\mathcal{A}_1(0) = 2.5$ mCi and zero initial activity of all other descendants. The half-lives of first four generations of descendants are as follows: $(t_{1/2})_1 = 1.5$ d, $(t_{1/2})_2 = 0.2$ d, $(t_{1/2})_3 = 3.5$ d, and $(t_{1/2})_4 = 1.3$ d. For this radioactive decay series:

- Determine expressions for the number of parent $N_1(t)$, daughter $N_2(t)$, granddaughter $N_3(t)$, and great granddaughter $N_4(t)$ nuclei as a function of time t .
- Determine expressions for the activity of the parent $\mathcal{A}_1(t)$, daughter $\mathcal{A}_2(t)$, granddaughter $\mathcal{A}_3(t)$, and great granddaughter $\mathcal{A}_4(t)$ as a function of time t .
- Calculate $N_1(t)$, $N_2(t)$, $N_3(t)$, and $N_4(t)$ for time t of 2.5 d.
- Calculate $\mathcal{A}_1(t)$, $\mathcal{A}_2(t)$, $\mathcal{A}_3(t)$, and $\mathcal{A}_4(t)$ for time t of 2.5 d.
- Enter results calculated in (c) onto curves in Fig. 10.9(A) which show $N_1(t)$, $N_2(t)$, $N_3(t)$, and $N_4(t)$ against time t .
- Enter results calculated in (c) onto curves in Fig. 10.9(B) which show $\mathcal{A}_1(t)$, $\mathcal{A}_2(t)$, $\mathcal{A}_3(t)$, and $\mathcal{A}_4(t)$ against time t .
- Identify the curves in Figs. 10.9(A) and 10.9(B).

SOLUTION:

In Prob. 220 the Bateman equation and Bateman constants were consolidated into one general equation which was used to determine general expressions for the number of nuclei and activity for the first four generations of a radioactive decay series: P \rightarrow D \rightarrow G \rightarrow GG. The general Bateman equation is written as follows

$$N_n(t) = \sum_{m=1}^n C_m e^{-\lambda_m t} = N_1(0) \sum_{m=1}^n \left[\frac{\prod_{i=1}^{n-1} \lambda_i}{\prod_{\substack{i=1 \\ i \neq m}}^n (\lambda_i - \lambda_m)} \right] e^{-\lambda_m t}. \quad (10.156)$$

- The general expressions for the number of nuclei $N_1(t)$, $N_2(t)$, $N_3(t)$, and $N_4(t)$ were given as follows with $N_1(0)$ the initial number of parent nuclei and λ_i the decay constant of generation i .

$$N_1(t) = N_1(0) e^{-\lambda_1 t}, \quad (10.157)$$

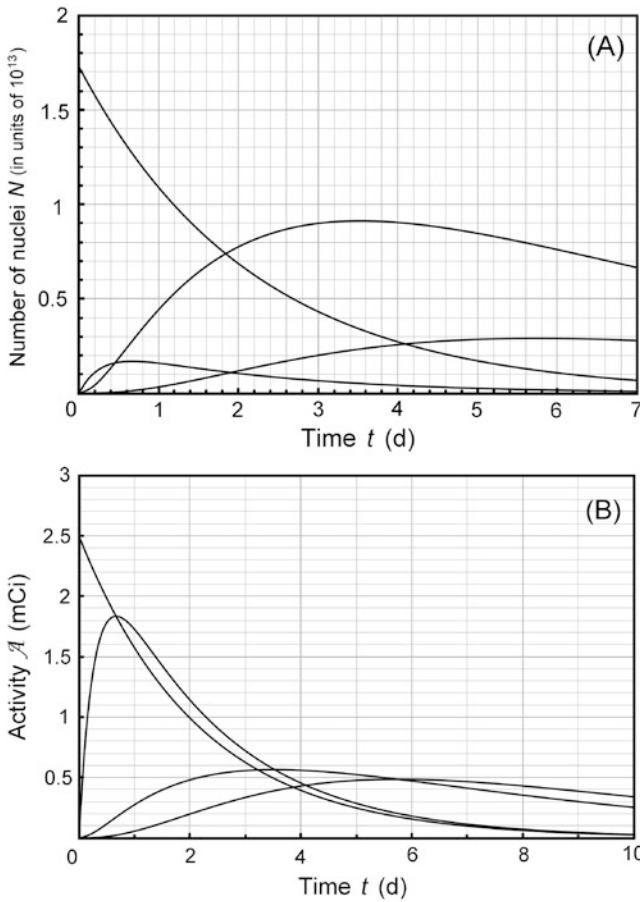


Fig. 10.9 Number of nuclei n in (A) and activity $\mathcal{A}(t)$ in (B) both against time t for parent, daughter, granddaughter, and great granddaughter of the specified radioactive decay series

$$N_2(t) = N_1(0) \frac{\lambda_1}{\lambda_2 - \lambda_1} [e^{-\lambda_1 t} - e^{-\lambda_2 t}], \tag{10.158}$$

$$N_3(t) = N_1(0) \lambda_1 \lambda_2 \left[\frac{e^{-\lambda_1 t}}{(\lambda_2 - \lambda_1)(\lambda_3 - \lambda_1)} + \frac{e^{-\lambda_2 t}}{(\lambda_1 - \lambda_2)(\lambda_3 - \lambda_2)} + \frac{e^{-\lambda_3 t}}{(\lambda_1 - \lambda_3)(\lambda_2 - \lambda_3)} \right], \tag{10.159}$$

$$N_4(t) = N_1(0) \lambda_1 \lambda_2 \lambda_3 \left[\frac{e^{-\lambda_1 t}}{(\lambda_2 - \lambda_1)(\lambda_3 - \lambda_1)(\lambda_4 - \lambda_1)} + \frac{e^{-\lambda_2 t}}{(\lambda_1 - \lambda_2)(\lambda_3 - \lambda_2)(\lambda_4 - \lambda_2)} + \frac{e^{-\lambda_3 t}}{(\lambda_1 - \lambda_3)(\lambda_2 - \lambda_3)(\lambda_4 - \lambda_3)} \right]$$

$$+ \frac{e^{-\lambda_4 t}}{(\lambda_1 - \lambda_4)(\lambda_2 - \lambda_4)(\lambda_3 - \lambda_4)} \Big]. \quad (10.160)$$

- (2) The general expressions for activities $\mathcal{A}_1(t)$, $\mathcal{A}_2(t)$, $\mathcal{A}_3(t)$, and $\mathcal{A}_4(t)$ were given as follows with $\mathcal{A}_1(0)$, the initial activity of the parent radionuclide

$$\mathcal{A}_1(t) = \lambda_1 N_1(t) = \mathcal{A}(0)e^{-\lambda_1 t}, \quad (10.161)$$

$$\mathcal{A}_2(t) = \lambda_2 N_2(t) = \mathcal{A}_1(0) \frac{\lambda_2}{\lambda_2 - \lambda_1} [e^{-\lambda_1 t} - e^{-\lambda_2 t}], \quad (10.162)$$

$$\mathcal{A}_3(t) = \lambda_3 N_3(t) = N_1(0) \lambda_1 \lambda_2 \lambda_3 \left[\frac{e^{-\lambda_1 t}}{(\lambda_2 - \lambda_1)(\lambda_3 - \lambda_1)} + \frac{e^{-\lambda_2 t}}{(\lambda_1 - \lambda_2)(\lambda_3 - \lambda_2)} + \frac{e^{-\lambda_3 t}}{(\lambda_1 - \lambda_3)(\lambda_2 - \lambda_3)} \right], \quad (10.163)$$

$$\begin{aligned} \mathcal{A}_4(t) &= \lambda_4 N_4(t) \\ &= N_1(0) \lambda_1 \lambda_2 \lambda_3 \lambda_4 \left[\frac{e^{-\lambda_1 t}}{(\lambda_2 - \lambda_1)(\lambda_3 - \lambda_1)(\lambda_4 - \lambda_1)} + \frac{e^{-\lambda_2 t}}{(\lambda_1 - \lambda_2)(\lambda_3 - \lambda_2)(\lambda_4 - \lambda_2)} + \frac{e^{-\lambda_3 t}}{(\lambda_1 - \lambda_3)(\lambda_2 - \lambda_3)(\lambda_4 - \lambda_3)} + \frac{e^{-\lambda_4 t}}{(\lambda_1 - \lambda_4)(\lambda_2 - \lambda_4)(\lambda_3 - \lambda_4)} \right]. \end{aligned} \quad (10.164)$$

- (3) Decay constant λ_i is related to half-life $(t_{1/2})_i$ through the standard expression

$$\lambda_i = \frac{\ln 2}{(t_{1/2})_i}. \quad (10.165)$$

- (4) Initial number of parent nuclei $N_1(0)$ is related to initial parent activity $\mathcal{A}_1(0)$ as follows

$$\begin{aligned} N_1(0) &= \frac{\mathcal{A}_1(0)}{\lambda_1} = \frac{\mathcal{A}_1(0)}{\ln 2} (t_{1/2})_1 \\ &= \frac{(2.5 \text{ mCi}) \times (1.5 \text{ d})}{\ln 2} \times (3.7 \times 10^7 \text{ s}^{-1} / \text{mCi}) \times (24 \text{ h/d}) \times (3600 \text{ s/h}) \\ &= 1.73 \times 10^{13}. \end{aligned} \quad (10.166)$$

- (5) Table 10.5 provides a summary of relevant specific data for the first four generations of the radioactive decay series analyzed in this problem.

(a) Expressions for the number of parent $N_1(t)$, daughter $N_2(t)$, granddaughter $N_3(t)$, and great granddaughter $N_4(t)$ nuclei as a function of time t is obtained by inserting (10.165) and appropriate decay constants into (10.157), (10.158), (10.159), and (10.160), respectively

Table 10.5 Summary of relevant specific data for the first four generations of the radioactive decay series of Prob. 221

Radionuclide	Parent	Daughter	Granddaughter	Great granddaughter
Generation n	$n = 1$	$n = 2$	$n = 3$	$n = 4$
Half-life $(t_{1/2})_n$	$(t_{1/2})_1 = 1.5$ d	$(t_{1/2})_2 = 0.2$ d	$(t_{1/2})_3 = 3.5$ d	$(t_{1/2})_4 = 1.3$ d
Decay constant λ (d^{-1})	0.462	3.466	0.198	0.533

(1)

$$N_1(t) = N_1(0)e^{-\lambda_1 t} = 1.73 \times 10^{13} \times e^{-(0.462 \text{ d}^{-1})t}, \quad (10.167)$$

(2)

$$\begin{aligned} N_2(t) &= N_1(0) \frac{\lambda_1}{\lambda_2 - \lambda_1} [e^{-\lambda_1 t} - e^{-\lambda_2 t}] \\ &= 2.66 \times 10^{-12} \times [e^{-(0.462 \text{ d}^{-1})t} - e^{-(3.466 \text{ d}^{-1})t}], \end{aligned} \quad (10.168)$$

(3)

$$\begin{aligned} N_3(t) &= N_1(0) \lambda_1 \lambda_2 \left[\frac{e^{-\lambda_1 t}}{(\lambda_2 - \lambda_1)(\lambda_3 - \lambda_1)} + \frac{e^{-\lambda_2 t}}{(\lambda_1 - \lambda_2)(\lambda_3 - \lambda_2)} \right. \\ &\quad \left. + \frac{e^{-\lambda_3 t}}{(\lambda_1 - \lambda_3)(\lambda_2 - \lambda_3)} \right] \\ &= -3.49 \times 10^{13} \times e^{-(0.462 \text{ d}^{-1}) \times t} + 2.82 \times 10^{-13} \times e^{-(3.466 \text{ d}^{-1}) \times t} \\ &\quad + 3.21 \times 10^{13} \times e^{-(0.198 \text{ d}^{-1}) \times t}, \end{aligned} \quad (10.169)$$

(4)

$$\begin{aligned} N_4(t) &= N_1(0) \lambda_1 \lambda_2 \lambda_3 \left[\frac{e^{-\lambda_1 t}}{(\lambda_2 - \lambda_1)(\lambda_3 - \lambda_1)(\lambda_4 - \lambda_1)} \right. \\ &\quad + \frac{e^{-\lambda_2 t}}{(\lambda_1 - \lambda_2)(\lambda_3 - \lambda_2)(\lambda_4 - \lambda_2)} + \frac{e^{-\lambda_3 t}}{(\lambda_1 - \lambda_3)(\lambda_2 - \lambda_3)(\lambda_4 - \lambda_3)} \\ &\quad \left. + \frac{e^{-\lambda_4 t}}{(\lambda_1 - \lambda_4)(\lambda_2 - \lambda_4)(\lambda_3 - \lambda_4)} \right] \\ &= -9.73 \times 10^{13} \times e^{-(0.462 \text{ d}^{-1}) \times t} - 1.91 \times 10^{11} \times e^{-(3.466 \text{ d}^{-1}) \times t} \\ &\quad + 1.90 \times 10^{13} \times e^{-(0.198 \text{ d}^{-1}) \times t} + 7.85 \times 10^{13} \\ &\quad \times e^{-(0.533 \text{ d}^{-1}) \times t}. \end{aligned} \quad (10.170)$$

(b) Expressions for the activity of the parent $\mathcal{A}_1(t)$, daughter $\mathcal{A}_2(t)$, granddaughter $\mathcal{A}_3(t)$, and great granddaughter $\mathcal{A}_4(t)$ as a function of time t is obtained by inserting $\mathcal{A}_1(0) = 2.5$ mCi and appropriate decay constants into (10.161), (10.162), (10.163), and (10.164), respectively

$$(1) \quad \mathcal{A}_1(t) = \lambda_1 N_1(t) = \mathcal{A}_1(0)e^{-\lambda_1 t} = [2.5 \times e^{-(0.462 \text{ d}^{-1}) \times t}] \text{ mCi}, \quad (10.171)$$

$$(2) \quad \begin{aligned} \mathcal{A}_2(t) &= \lambda_2 N_2(t) \mathcal{A}_1(0) \frac{\lambda_2}{\lambda_2 - \lambda_1} [e^{-\lambda_1 t} - e^{-\lambda_2 t}] \\ &= 2.88 \times [e^{-(0.462 \text{ d}^{-1}) \times t} - e^{-(3.466 \text{ d}^{-1}) \times t}] \text{ mCi}, \end{aligned} \quad (10.172)$$

$$(3) \quad \begin{aligned} \mathcal{A}_3(t) &= \lambda_3 N_3(t) = N_1(0) \lambda_1 \lambda_2 \lambda_3 \left[\frac{e^{-\lambda_1 t}}{(\lambda_2 - \lambda_1)(\lambda_3 - \lambda_1)} \right. \\ &\quad \left. + \frac{e^{-\lambda_2 t}}{(\lambda_1 - \lambda_2)(\lambda_3 - \lambda_2)} + \frac{e^{-\lambda_3 t}}{(\lambda_1 - \lambda_3)(\lambda_2 - \lambda_3)} \right] \\ &= [-2.16 \times e^{-(0.462 \text{ d}^{-1}) \times t} + 0.175 \times e^{-(3.466 \text{ d}^{-1}) \times t} \\ &\quad + 1.99 \times e^{-(0.198 \text{ d}^{-1}) \times t}] \text{ mCi}, \end{aligned} \quad (10.173)$$

$$(4) \quad \begin{aligned} \mathcal{A}_4(t) &= \lambda_4 N_4(t) = N_1(0) \lambda_1 \lambda_2 \lambda_3 \lambda_4 \left[\frac{e^{-\lambda_1 t}}{(\lambda_2 - \lambda_1)(\lambda_3 - \lambda_1)(\lambda_4 - \lambda_1)} \right. \\ &\quad \left. + \frac{e^{-\lambda_2 t}}{(\lambda_1 - \lambda_2)(\lambda_3 - \lambda_2)(\lambda_4 - \lambda_2)} + \frac{e^{-\lambda_3 t}}{(\lambda_1 - \lambda_3)(\lambda_2 - \lambda_3)(\lambda_4 - \lambda_3)} \right. \\ &\quad \left. + \frac{e^{-\lambda_4 t}}{(\lambda_1 - \lambda_4)(\lambda_2 - \lambda_4)(\lambda_3 - \lambda_4)} \right] \\ &= [-2.16 \times e^{-(0.462 \text{ d}^{-1}) \times t} + 0.175 \times e^{-(3.466 \text{ d}^{-1}) \times t} \\ &\quad + 1.99 \times e^{-(0.198 \text{ d}^{-1}) \times t} + 1.99 \times e^{-(0.198 \text{ d}^{-1}) \times t}] \text{ mCi}. \end{aligned} \quad (10.174)$$

(c) Numbers of nuclei $N_1(t)$, $N_2(t)$, $N_3(t)$, and $N_4(t)$ present at time $t = 2.5$ d are calculated inserting $t = 2.5$ d into (10.167), (10.168), (10.169), and (10.170), respectively.

$$(1) \quad N_1(t) = 1.73 \times 10^{13} \times e^{-0.462 \times 2.5} = 5.45 \times 10^{12}, \quad (10.175)$$

$$(2) \quad N_2(t) = 2.66 \times 10^{12} \times [e^{-0.462 \times 2.5} - e^{-3.466 \times 2.5}] = 0.838 \times 10^{12}, \quad (10.176)$$

$$(3) \quad \begin{aligned} N_3(t) &= -3.49 \times 10^{13} \times e^{-0.462 \times 2.5} + 2.82 \times 10^{13} \times e^{-3.466 \times 2.5} \\ &\quad + 3.21 \times 10^{13} \times e^{-0.198 \times 2.5} = 8.58 \times 10^{12} \end{aligned} \quad (10.177)$$

(4)

$$\begin{aligned}
 N_4(t) &= -9.73 \times 10^{13} \times e^{-0.462 \times 2.5} - 1.91 \times 10^{13} \times e^{-3.466 \times 2.5} \\
 &\quad + 1.9 \times 10^{13} \times e^{-0.198 \times 2.5} + 7.85 \times 10^{13} \times e^{-0.533 \times 2.5} \\
 &= 1.64 \times 10^{12}.
 \end{aligned} \tag{10.178}$$

(d) Activities $\mathcal{A}_1(t)$, $\mathcal{A}_2(t)$, $\mathcal{A}_3(t)$, and $\mathcal{A}_4(t)$ present at time $t = 2.5$ d are calculated by multiplication of the number of nuclei $N_1(t)$, $N_2(t)$, $N_3(t)$, and $N_4(t)$, respectively, with appropriate decay constant λ

(1)

$$\begin{aligned}
 \mathcal{A}_1(t) &= \lambda_1 N_1(t) = \frac{(0.462 \text{ d}^{-1}) \times 5.45 \times 10^{12}}{(24 \text{ h/d}) \times (3.6 \times 10^3 \text{ s/h}) \times (3.7 \times 10^7 \text{ mCi/s})} \\
 &= 0.788 \text{ mCi},
 \end{aligned} \tag{10.179}$$

(2)

$$\begin{aligned}
 \mathcal{A}_2(t) &= \lambda_2 N_2(t) = \frac{(3.466 \text{ d}^{-1}) \times 0.838 \times 10^{12}}{(24 \text{ h/d}) \times (3.6 \times 10^3 \text{ s/h}) \times (3.7 \times 10^7 \text{ mCi/s})} \\
 &= 0.909 \text{ mCi},
 \end{aligned} \tag{10.180}$$

(3)

$$\begin{aligned}
 \mathcal{A}_3(t) &= \lambda_3 N_3(t) = \frac{(0.198 \text{ d}^{-1}) \times 8.58 \times 10^{12}}{(24 \text{ h/d}) \times (3.6 \times 10^3 \text{ s/h}) \times (3.7 \times 10^7 \text{ mCi/s})} \\
 &= 0.531 \text{ mCi},
 \end{aligned} \tag{10.181}$$

(4)

$$\begin{aligned}
 \mathcal{A}_4(t) &= \lambda_4 N_4(t) = \frac{(0.533 \text{ d}^{-1}) \times 1.64 \times 10^{12}}{(24 \text{ h/d}) \times (3.6 \times 10^3 \text{ s/h}) \times (3.7 \times 10^7 \text{ mCi/s})} \\
 &= 0.273 \text{ mCi}.
 \end{aligned} \tag{10.182}$$

Results of **(c)** and **(d)** are summarized in Table 10.6.

(e) Data calculated in **(c)** for the numbers of nuclei $N_1(t)$, $N_2(t)$, $N_3(t)$, and $N_4(t)$ present at time $t = 2.5$ d are superimposed onto curves plotting number of nuclei $N(t)$ against time t , as shown in Fig. 10.10.

(f) Data calculated in **(d)** for activities $\mathcal{A}_1(t)$, $\mathcal{A}_2(t)$, $\mathcal{A}_3(t)$, and $\mathcal{A}_4(t)$ present at time $t = 2.5$ d are superimposed onto curves plotting activities $\mathcal{A}_1(t)$, $\mathcal{A}_2(t)$, $\mathcal{A}_3(t)$, and $\mathcal{A}_4(t)$ against time t , as shown in Fig. 10.11.

Table 10.6 Summary of results of (c) and (d)

	$P(i = 1)$	$D(i = 2)$	$G(i = 3)$	$GG(i = 4)$
$N_i(t = 0)$	1.73×10^{13}	0	0	0
$N_i(t = 2.5\text{d})$	0.545×10^{13}	0.084×10^{13}	0.858×10^{13}	0.164×10^{13}
$\mathcal{A}_i(t = 0)$	2.5 mCi	0	0	0
$\mathcal{A}_i(t = 2.5\text{d})$	0.788 mCi	0.909 mCi	0.531 mCi	0.273 mCi

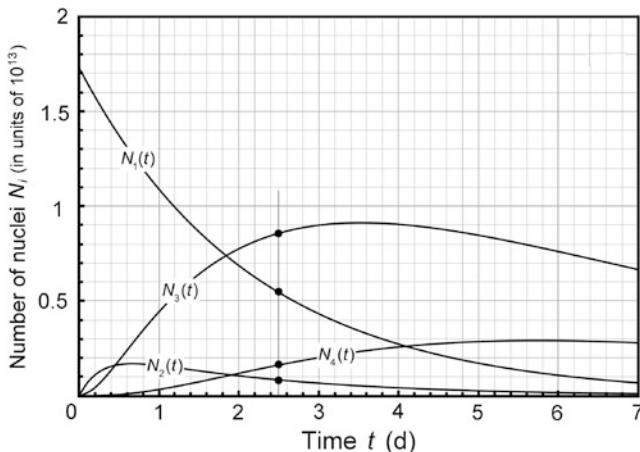


Fig. 10.10 Number $N_i(t)$ of nuclei against time t for parent $N_1(t)$ given in (10.167), daughter $N_2(t)$ given in (10.168), granddaughter $N_3(t)$ given in (10.169), and great granddaughter $N_4(t)$ given in (10.170) of the specified radioactive decay series. Numbers of nuclei calculated in (c) for $t = 2.5$ d are shown as data points superimposed onto the curves plotted for the numbers of nuclei

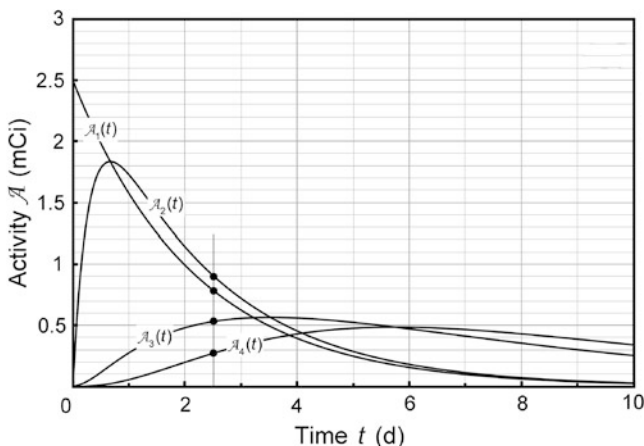


Fig. 10.11 Activity $\mathcal{A}_i(t)$ against time t for parent $\mathcal{A}_1(t)$ given in (10.171), daughter $\mathcal{A}_2(t)$ given in (10.172), granddaughter $\mathcal{A}_3(t)$ given in (10.173), and great granddaughter $\mathcal{A}_4(t)$ given in (10.174) of the specified radioactive decay series. Activities calculated in (d) for $t = 2.5$ d are shown with data points superimposed onto the activity curves

10.7 Mixture of Two or More Independently Decaying Radionuclides in a Sample

10.7.Q1

(222)

An unknown mixture of two or more independently decaying radionuclides, each with its own half-life and decay constant, will produce a composite decay curve that does not result in a straight line when plotted on a semi-logarithmic plot, unless, of course, all radionuclides have identical or very similar half-lives. In principle, the decay curves of the individual radionuclides can be resolved graphically, if their half-lives differ sufficiently and if at most three radioactive components are present.

A solution contains an unknown amount of gold-198 (Au-198) and iodine-131 (I-131) beta emitters. If the total activity $\mathcal{A}(t)$ of the solution at time $t = 0$ is $0.140 \mu\text{Ci}$ (5.18 kBq) and drops to half of its initial value in 3 days,

- Calculate the initial activities $\mathcal{A}_{\text{Au}}(0)$ and $\mathcal{A}_{\text{I}}(0)$ of Au-198 and I-131, respectively, in the solution. Half-lives of Au-198 and I-131 are 2.70 d and 8.05 d, respectively.
- Calculate the total activity $\mathcal{A}(t)$ of the solution at time $t = 15$ d.
- Calculate the time t as well as the total activity $\mathcal{A}(t)$ at which the activities of Au-198 and I-131 in the solution are equal.
- Plot on a semi-logarithmic graph the activities $\mathcal{A}_{\text{Au}}(t)$ and $\mathcal{A}_{\text{I}}(t)$ of Au-198 and I-131, respectively, and the total activity $\mathcal{A}(t)$ in the solution as a function of time. Show on the plot the activities at $t = 3$ d, $t = 15$ d, and at time t determined in (c).

SOLUTION:

(a) Activities $\mathcal{A}_{\text{Au}}(t)$ and $\mathcal{A}_{\text{I}}(t)$ of Au-198 and I-131 beta emitters, respectively, in a solution can be described with the standard exponential decay law governing radioactivity. We thus express activity $\mathcal{A}_{\text{Au}}(t)$ as a function of time t in the solution as

$$\mathcal{A}_{\text{Au}}(t) = \mathcal{A}_{\text{Au}}(0)e^{-\lambda_{\text{Au}}t} = \mathcal{A}_{\text{Au}}(0)e^{-\frac{\ln 2}{(t_{1/2})_{\text{Au}}}t} \quad (10.183)$$

and activity $\mathcal{A}_{\text{I}}(t)$ as a function of time t in the solution as

$$\mathcal{A}_{\text{I}}(t) = \mathcal{A}_{\text{I}}(0)e^{-\lambda_{\text{I}}t} = \mathcal{A}_{\text{I}}(0)e^{-\frac{\ln 2}{(t_{1/2})_{\text{I}}}t}, \quad (10.184)$$

where the decay constant λ is related to half-life $t_{1/2}$ through the relationship $\lambda = (\ln 2)/t_{1/2}$ and

$\mathcal{A}_{\text{Au}}(0)$ and $\mathcal{A}_{\text{I}}(0)$ are the initial activities at $t = 0$ of Au-198 and I-131, respectively.

λ_{Au} and λ_{I} are the decay constants of Au-198 and I-131, respectively.

$(t_{1/2})_{\text{Au}}$ and $(t_{1/2})_{\text{I}}$ are the half-lives of Au-198 and I-131, respectively.

Total activity $\mathcal{A}(t)$ of the radioactive solution as a function of time t is in general the sum of $\mathcal{A}_{\text{Au}}(t)$ given in (10.183) and $\mathcal{A}_{\text{I}}(t)$ given in (10.184), i.e.,

$$\mathcal{A}(t) = \mathcal{A}_{\text{Au}}(t) + \mathcal{A}_{\text{I}}(t) = \mathcal{A}_{\text{Au}}(0)e^{-\frac{\ln 2}{(t_{1/2})_{\text{Au}}}t} + \mathcal{A}_{\text{I}}(0)e^{-\frac{\ln 2}{(t_{1/2})_{\text{I}}}t}. \quad (10.185)$$

Data for our problem stipulate that the initial activity $\mathcal{A}(0)$ at $t = 0$ of our radioactive solution is 0.140 μCi , while its activity $\mathcal{A}(t)$ at $t = 3$ days is 0.070 μCi . Using (10.184) we now express $\mathcal{A}(0)$ at $t = 0$ and $\mathcal{A}(t)$ at $t = 3$ d, respectively, as follows

$$\mathcal{A}(0) = \mathcal{A}(t = 0) = \mathcal{A}_{\text{Au}}(0) + \mathcal{A}_{\text{I}}(0) = 0.140 \mu\text{Ci} \quad (10.186)$$

and

$$\begin{aligned} \mathcal{A}(t = 3 \text{ d}) &= \mathcal{A}_{\text{Au}}(t) + \mathcal{A}_{\text{I}}(t) = \mathcal{A}_{\text{Au}}(0)e^{-\frac{\ln 2}{(t_{1/2})_{\text{Au}}}t} + \mathcal{A}_{\text{I}}(0)e^{-\frac{\ln 2}{(t_{1/2})_{\text{I}}}t} \\ &= \mathcal{A}_{\text{Au}}(0)e^{-\frac{(\ln 2) \times (3 \text{ d})}{2.70 \text{ d}}} + \mathcal{A}_{\text{I}}(0)e^{-\frac{(\ln 2) \times (3 \text{ d})}{8.05 \text{ d}}} = 0.463\mathcal{A}_{\text{Au}}(0) + 0.772\mathcal{A}_{\text{I}}(0) \\ &= 0.070 \mu\text{Ci}. \end{aligned} \quad (10.187)$$

In (10.186) and (10.187) we have two equations for two unknowns: $\mathcal{A}_{\text{Au}}(0)$ and $\mathcal{A}_{\text{I}}(0)$. Solving (10.186) for $\mathcal{A}_{\text{Au}}(0)$ and inserting $\mathcal{A}_{\text{Au}}(0) = 0.140 \mu\text{Ci} - \mathcal{A}_{\text{I}}(0)$ into (10.187) we obtain the following results:

$$\mathcal{A}_{\text{Au}}(0) = 0.123 \mu\text{Ci} \quad \text{and} \quad \mathcal{A}_{\text{I}}(0) = 0.017 \mu\text{Ci}. \quad (10.188)$$

(b) To calculate the total activity of the solution at time $t = 15$ d we use (10.185) in conjunction with the initial activities $\mathcal{A}_{\text{Au}}(0)$ and $\mathcal{A}_{\text{I}}(0)$ at time $t = 0$ given in (10.188) and get

$$\begin{aligned} \mathcal{A}(t) &= \mathcal{A}_{\text{Au}}(t) + \mathcal{A}_{\text{I}}(t) = \mathcal{A}_{\text{Au}}(0)e^{-\frac{\ln 2}{(t_{1/2})_{\text{Au}}}t} + \mathcal{A}_{\text{I}}(0)e^{-\frac{\ln 2}{(t_{1/2})_{\text{I}}}t} \\ &= (0.123 \mu\text{Ci}) \times e^{-\frac{(\ln 2) \times (15 \text{ d})}{2.70 \text{ d}}} + (0.017 \mu\text{Ci}) \times e^{-\frac{(\ln 2) \times (15 \text{ d})}{8.05 \text{ d}}} \\ &= 2.62 \times 10^{-3} \mu\text{Ci} + 4.67 \times 10^{-3} \mu\text{Ci} = 7.29 \times 10^{-3} \mu\text{Ci}. \end{aligned} \quad (10.189)$$

(c) To determine the time $t = t_{\text{eq}}$ at which the activities $\mathcal{A}_{\text{Au}}(t)$ and $\mathcal{A}_{\text{I}}(t)$ are equal we write (10.183) and (10.184) in the following form

$$\mathcal{A}_{\text{Au}}(t_{\text{eq}}) = \mathcal{A}_{\text{Au}}(0)e^{-\frac{\ln 2}{(t_{1/2})_{\text{Au}}}t_{\text{eq}}} = \mathcal{A}_{\text{I}}(t_{\text{eq}}) = \mathcal{A}_{\text{I}}(0)e^{-\frac{\ln 2}{(t_{1/2})_{\text{I}}}t_{\text{eq}}}. \quad (10.190)$$

Solving (10.190) for t_{eq} we first get the general result

$$t_{\text{eq}} = \frac{(t_{1/2})_{\text{Au}}(t_{1/2})_{\text{I}} \ln \frac{\mathcal{A}_{\text{Au}}(0)}{\mathcal{A}_{\text{I}}(0)}}{[(t_{1/2})_{\text{B}} - (t_{1/2})_{\text{A}}] \ln 2} \tag{10.191}$$

and after inserting the initial activities $\mathcal{A}_{\text{Au}}(0)$ and $\mathcal{A}_{\text{I}}(0)$ from (10.188) we determine t_{eq} as

$$t_{\text{eq}} = \frac{(2.70 \text{ d}) \times (8.05 \text{ d}) \times \ln \frac{0.123}{0.017}}{(8.05 \text{ d} - 2.70 \text{ d}) \times \ln 2} = 11.6 \text{ d.} \tag{10.192}$$

Activity $\mathcal{A}(t)$ of the radioactive solution at $t = t_{\text{eq}} = 11.6 \text{ d}$ is calculated from (10.185)

$$\begin{aligned} \mathcal{A}(t = t_{\text{eq}}) &= \mathcal{A}_{\text{Au}}(t_{\text{eq}}) + \mathcal{A}_{\text{I}}(t_{\text{eq}}) = 2\mathcal{A}_{\text{Au}}(t_{\text{eq}}) = 2\mathcal{A}_{\text{I}}(t_{\text{eq}}) \\ &= \mathcal{A}_{\text{Au}}(0)e^{-\frac{\ln 2}{(t_{1/2})_{\text{Au}}}t_{\text{eq}}} + \mathcal{A}_{\text{I}}(0)e^{-\frac{\ln 2}{(t_{1/2})_{\text{I}}}t_{\text{eq}}} \\ &= (0.123 \text{ }\mu\text{Ci}) \times e^{-\frac{(\ln 2) \times (11.6 \text{ d})}{2.70 \text{ d}}} + (0.017 \text{ }\mu\text{Ci}) \times e^{-\frac{(\ln 2) \times (11.6 \text{ d})}{8.05 \text{ d}}} \\ &= 6.26 \times 10^{-3} \text{ }\mu\text{Ci} + 6.26 \times 10^{-3} \text{ }\mu\text{Ci} = 0.0125 \text{ }\mu\text{Ci.} \end{aligned} \tag{10.193}$$

(d) The radioactive solution investigated in this problem consists of two beta emitters: gold-198 and iodine-131 of unknown initial activities. Based on known solution's total initial activity $\mathcal{A}(0)$ and total activity at $t = 3 \text{ h}$, activities $\mathcal{A}_{\text{Au}}(t)$, $\mathcal{A}_{\text{I}}(t)$, and $\mathcal{A}(t)$ were determined and are plotted against time t in Fig. 10.12.

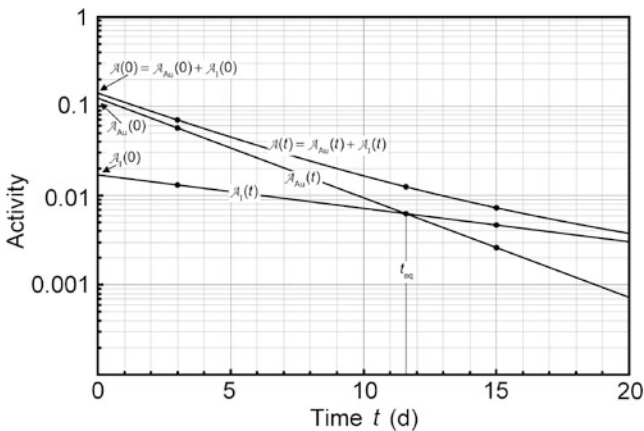


Fig. 10.12 Activities $\mathcal{A}_{\text{Au}}(t)$ of (10.183), $\mathcal{A}_{\text{I}}(t)$ of (10.184), and $\mathcal{A}(t)$ of (10.185) against time t

10.8 Branching Decay and Branching Fraction

10.8.Q1

(225)

In many instances decay of a radionuclide can proceed by more than one mode of decay and the radionuclide is said to undergo branching decay to two or more different daughter nuclides. In general, the total decay constant λ_P for the parent decay is the sum of the partial decay constants $(\lambda_P)_i$ for each possible branch or mode of decay

$$\lambda_P = \sum_i^N (\lambda_P)_i = (\ln 2) \sum_i^N \frac{1}{(t_{1/2})_P^i}, \quad (10.194)$$

where N is the number of decay branches or modes available and $(t_{1/2})_P^i$ is the half-life of the parent radionuclide for decay in mode i . The branching fraction f_i of mode i is defined as the ratio $f_i = (\lambda_P)_i / \lambda_P = (t_{1/2})_P / (t_{1/2})_P^i$.

Bismuth-212 (Bi-212) with a half-life $(t_{1/2})_{\text{Bi-212}} = 60.55 \text{ min} = 3633 \text{ s}$ decays into two radio-nuclides: (1) thalium-208 (Tl-208) through α alpha decay with a branching fraction $f_\alpha = 0.36$ and (2) polonium-212 (Po-212) through β^- beta decay with a branching fraction $f_{\beta^-} = 0.64$. Both daughters subsequently decay into stable lead-208 (Pb-208) nuclide: thallium-208 through β^- decay with a half-life $(t_{1/2})_{\text{Tl-208}} = 183.2 \text{ s}$ and polonium-212 through α decay with a half-life $(t_{1/2})_{\text{Po-212}} = 0.3 \mu\text{s}$.

- For bismuth-212 determine: (1) decay constant $\lambda_{\text{Bi-212}}$; (2) partial decay constant $(\lambda_\alpha)_{\text{Bi-212}}$ for α decay; (3) partial decay constant $(\lambda_{\beta^-})_{\text{Bi-212}}$ for β^- decay; (4) half-life $(t_{1/2})_{\text{Bi-212}}^\alpha$ for α decay; and (5) half-life $(t_{1/2})_{\text{Bi-212}}^{\beta^-}$ for β^- decay. Verify the self-consistency of results.
- Express the activities of (1) thalium-208 and (2) polonium-212 as a function of time t and initial parent activity $\mathcal{A}_{\text{Bi-212}}(0)$ for initial conditions: $N_{\text{Tl-208}}(0) = N_{\text{Po-212}}(0) = 0$.
- Prepare a table for the four nuclides involved in series decay of bismuth-212 into lead-208 and provide the following rows to serve as summary of the Bi-212 series decay: (1) Name of nuclide, (2) Symbol, (3) Designation, (4) Atomic number Z , (5) Atomic mass number A , (6) Type of decay, (7) Branching ratio, (8) Half-life $t_{1/2}$, and (9) Decay constant λ .
- Express the accumulation of the granddaughter nuclide (Pb-208) as a function of time for the initial conditions: $N_P(t=0) = N_{\text{Bi-212}}(0)$ and $N_G(0) = N_{\text{Pb-208}}(0) = 0$.

(e) Figure 10.13 shows five curves depicting the number of various nuclei against time t for series decay of Bi-212 through either Tl-208 or Po-212 into Pb-208 with initial conditions $N_{\text{Pb-212}}(t = 0) = N_{\text{Pb-212}}(0)$ and $N_{\text{Tl-208}}(0) = N_{\text{Po-212}}(0) = N_{\text{Pb-208}}(0) = 0$. All curves are normalized to $N_{\text{Bi-212}}(0) = 1$. Based on results in (a) through (d) identify the five curves.

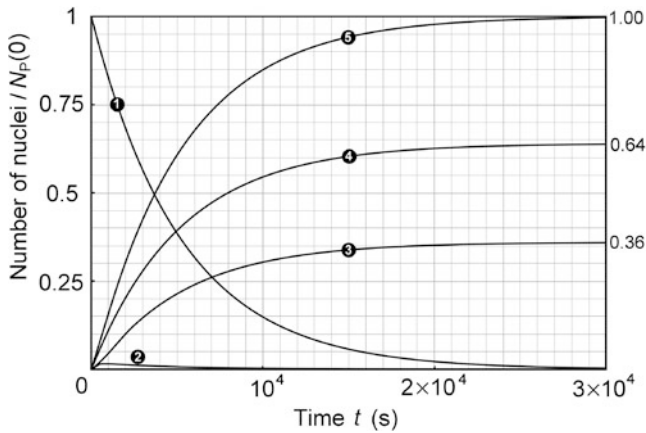


Fig. 10.13 Number of various nuclei against time t for the series decay of Bi-212 through either Tl-208 or Po-212 into Pb-208. All curves are normalized to $N_{\text{Bi-212}}(0) = 1$ with initial conditions $N_{\text{Pb-212}}(t = 0) = N_{\text{Pb-212}}(0)$ and $N_{\text{Tl-208}}(0) = N_{\text{Po-212}}(0) = N_{\text{Pb-208}}(0) = 0$

SOLUTION:

(a) Radioactive decay of bismuth-212 nucleus can proceed by two modes of decay: either α decay into thallium-208 or β^- decay into polonium-212. Therefore, in addition to total decay constant $\lambda_{\text{Bi-212}}$ and half-life $(t_{1/2})_{\text{Bi-212}}$, Bi-212 is also characterized by its partial decay constants $(\lambda_\alpha)_{\text{Bi-212}}$ and $(\lambda_{\beta^-})_{\text{Bi-212}}$ for α and β^- decay, respectively, as well as by half-lives $(t_{1/2})_{\text{Bi-212}}^\alpha$ and $(t_{1/2})_{\text{Bi-212}}^{\beta^-}$ for α and β^- decay, respectively.

- (1) Decay constant $\lambda_{\text{Bi-212}}$ for bismuth-212 is calculated from the standard relationship between decay constant λ and half-life $t_{1/2}$ as follows

$$\lambda_{\text{Bi-212}} = \frac{\ln 2}{(t_{1/2})_{\text{Bi-212}}} = \frac{\ln 2}{(60.55 \text{ min}) \times (60 \text{ s/min})} = 1.91 \times 10^{-4} \text{ s}^{-1}. \tag{10.195}$$

- (2) Partial decay constant $(\lambda_\alpha)_{\text{Bi-212}}$ for α decay of Bi-212 is calculated using the definition of branching fraction $f_i = (\lambda_P)_i / \lambda_P = (t_{1/2})_P / (t_{1/2})_P^i$

$$(\lambda_\alpha)_{\text{Bi-212}} = f_\alpha \lambda_{\text{Bi-212}} = 0.36 \times (1.91 \times 10^{-4} \text{ s}^{-1}) = 6.876 \times 10^{-5} \text{ s}^{-1}. \tag{10.196}$$

- (3) In same manner we calculate the partial decay constant $(\lambda_{\beta^-})_{\text{Bi-212}}$ for β^- decay of Bi-212

$$(\lambda_{\beta^-})_{\text{Bi-212}} = f_{\beta^-} \lambda_{\text{Bi-212}} = 0.64 \times (1.91 \times 10^{-4} \text{ s}^{-1}) = 12.224 \times 10^{-5} \text{ s}^{-1}. \quad (10.197)$$

- (4) Half-life $(t_{1/2})_{\text{Bi-212}}^{\alpha}$ for α decay of Bi-212 is calculated from the standard relationship (CC) linking decay constant λ and half-life $t_{1/2}$

$$(t_{1/2})_{\text{Bi-212}}^{\alpha} = \frac{\ln 2}{(\lambda_{\alpha})_{\text{Bi-212}}} = \frac{\ln 2}{6.876 \times 10^{-5} \text{ s}^{-1}} = 10081 \text{ s} = 168 \text{ min}. \quad (10.198)$$

- (5) Half-life $(t_{1/2})_{\text{Bi-212}}^{\beta^-}$ for β^- decay of Bi-212 is given as

$$(t_{1/2})_{\text{Bi-212}}^{\beta^-} = \frac{\ln 2}{(\lambda_{\beta^-})_{\text{Bi-212}}} = \frac{\ln 2}{12.224 \times 10^{-5} \text{ s}^{-1}} = 5670.4 \text{ s} = 94.51 \text{ min}. \quad (10.199)$$

A simple test can be carried out to verify the self-consistency of results in this section. According to (10.194) our calculations should satisfy the following equation

$$\begin{aligned} \lambda_{\text{Bi-212}} &= (\lambda_{\alpha})_{\text{Bi-212}} + (\lambda_{\beta^-})_{\text{Bi-212}} = 6.876 \times 10^{-5} \text{ s}^{-1} + 12.224 \times 10^{-5} \text{ s}^{-1} \\ &= 1.91 \times 10^{-4} \text{ s}^{-1}. \end{aligned} \quad (10.200)$$

- (6) Equation (10.200) can also be written so as to link the half-lives of individual branches of the parent with the half-life of the parent as follows

$$\frac{\ln 2}{(t_{1/2})_{\text{Bi-212}}} = \frac{\ln 2}{(t_{1/2})_{\text{Bi-212}}^{\alpha}} + \frac{\ln 2}{(t_{1/2})_{\text{Bi-212}}^{\beta^-}} \quad (10.201)$$

or

$$\begin{aligned} (t_{1/2})_{\text{Bi-212}} &= \frac{[(t_{1/2})_{\text{Bi-212}}^{\alpha}] \times [(t_{1/2})_{\text{Bi-212}}^{\beta^-}]}{[(t_{1/2})_{\text{Bi-212}}^{\alpha}] + [(t_{1/2})_{\text{Bi-212}}^{\beta^-}]} = \frac{10081 \times 5670.4}{10081 + 5670.4} \text{ s} \\ &= 3629.1 \text{ s} = 60.5 \text{ min} \end{aligned} \quad (10.202)$$

and

$$\begin{aligned} f_{\alpha} &= \frac{(t_{1/2})_{\text{Bi-212}}}{(t_{1/2})_{\text{Bi-212}}^{\alpha}} = \frac{3629.1}{10081} = 0.36 \quad \text{and} \\ f_{\beta^-} &= \frac{(t_{1/2})_{\text{Bi-212}}}{(t_{1/2})_{\text{Bi-212}}^{\beta^-}} = \frac{3629.1}{5670.4} = 0.64. \end{aligned} \quad (10.203)$$

(b) In multichannel decays of the parent P several daughters appear, each one characterized by its own growth and decay kinematics. The rate of change dN_D/dt in the number of given daughter D nuclei is equal to the supply of new daughter nuclei through the decay of P channeled into the branch i containing D and expressed as $(\lambda_P)_i N_P(0)e^{-(\lambda_P)_i t} = f_i \lambda_P N_P(0)e^{-f_i \lambda_P t}$ less the loss of daughter nuclei D from the decay of D into G given by $[-\lambda_D N_D(t)]$, where λ_D is the decay constant of the daughter D. The rate of change dN_D/dt is thus given by

$$\frac{dN_D(t)}{dt} = (\lambda_P)_i N_P(0)e^{-\lambda_P t} - \lambda_D N_D(t) = f_i \lambda_P N_P(0)e^{-\lambda_P t} - \lambda_D N_D(t). \quad (10.204)$$

Equation (10.204) has the following solution (T10.35) for the number of daughter nuclei N_D as a function of time t

$$N_D(t) = f_i N_P(0) \frac{\lambda_P}{\lambda_D - \lambda_P} [e^{-\lambda_P t} - e^{-\lambda_D t}] \quad (10.205)$$

and for the activity of daughter nuclide $\mathcal{A}_D(t)$ as a function of time t

$$\begin{aligned} \mathcal{A}_D(t) &= \lambda_D N_D(t) = \lambda_D f_i N_P(0) \frac{\lambda_P}{\lambda_D - \lambda_P} [e^{-\lambda_P t} - e^{-\lambda_D t}] \\ &= f_i \mathcal{A}_P(0) \frac{\lambda_D}{\lambda_D - \lambda_P} [e^{-\lambda_P t} - e^{-\lambda_D t}]. \end{aligned} \quad (10.206)$$

Before addressing the calculation of activity of Tl-208 and Po-212 [$\mathcal{A}_{\text{Tl-208}}(t)$ and $\mathcal{A}_{\text{Po-212}}(t)$, respectively], we determine decay constants of the two daughter products of Bi-212 (Tl-208 and Po-212) from their half-lives

$$\lambda_{\text{Tl-208}} \frac{\ln 2}{(t_{1/2})_{\text{Tl-208}}} = \frac{\ln 2}{183.2 \text{ s}} = 3.784 \times 10^{-3} \text{ s}^{-1}, \quad (10.207)$$

$$\lambda_{\text{Po-212}} \frac{\ln 2}{(t_{1/2})_{\text{Po-212}}} = \frac{\ln 2}{0.3 \times 10^{-6} \text{ s}} = 2.31 \times 10^6 \text{ s}^{-1}. \quad (10.208)$$

(1) From (10.205) we get the following expression for the activity of thallium (Th-208) daughter as a result of the decay of the bismuth-212 parent

$$\begin{aligned} \mathcal{A}_{\text{Tl-208}}(t) &= f_\alpha \mathcal{A}_{\text{Bi-212}}(0) \frac{\lambda_{\text{Tl-208}}}{\lambda_{\text{Tl-208}} - \lambda_{\text{Bi-212}}} [e^{-\lambda_{\text{Bi-212}} t} - e^{-\lambda_{\text{Tl-208}} t}] \\ &= 0.36 \mathcal{A}_{\text{Bi-212}}(0) \frac{3.784 \times 10^{-3}}{3.784 \times 10^{-3} - 1.91 \times 10^{-4}} \\ &\quad \times [e^{-(1.91 \times 10^{-4} \text{ s}^{-1}) t} - e^{-(3.784 \times 10^{-3} \text{ s}^{-1}) t}] \\ &= 0.379 \times [e^{-(1.91 \times 10^{-4} \text{ s}^{-1}) t} - e^{-(3.784 \times 10^{-3} \text{ s}^{-1}) t}] \mathcal{A}_{\text{Bi-212}}(0). \end{aligned} \quad (10.209)$$

Table 10.7 Properties of nuclides associated with series decay of bismuth-212

(1) Radionuclide	Thallium	Lead	Bismuth	Polonium
(2) Symbol	Tl	Pb	Bi	Po
(3) Designation	Daughter	Granddaughter	Parent	Daughter
(4) Z	81	82	83	84
(5) A	208	208	212	212
(6) Decay type	β^-	stable	α and β^-	α
(7) Branching f	$f_{\beta^-} = 1$	–	$f_{\alpha} = 0.36, f_{\beta^-} = 0.64$	$f_{\alpha} = 1$
(8) Half-life $t_{1/2}$	183.2 s	stable	60.55 min	0.3 μ s
(9) Decay constant λ	$3.784 \times 10^{-3} \text{ s}^{-1}$	stable	$1.91 \times 10^{-4} \text{ s}^{-1}$	$2.31 \times 10^6 \text{ s}^{-1}$

(2) In similar manner we get from (10.206) the following expression for the activity of polonium-212 (Po-212) daughter nuclide as a result of the decay of the bismuth-212 parent nuclide

$$\begin{aligned}
 \mathcal{A}_{\text{Po-212}}(t) &= f_{\beta^-} \mathcal{A}_{\text{Bi-212}}(0) \frac{\lambda_{\text{Po-212}}}{\lambda_{\text{Po-212}} - \lambda_{\text{Bi-212}}} [e^{-\lambda_{\text{Bi-212}}t} - e^{-\lambda_{\text{Po-212}}t}] \\
 &= 0.64 \mathcal{A}_{\text{Bi-212}}(0) \frac{2.31 \times 10^6}{2.31 \times 10^6 - 1.91 \times 10^{-4}} \\
 &\quad \times [e^{-(1.91 \times 10^{-4} \text{ s}^{-1})t} - e^{-(2.31 \times 10^6 \text{ s}^{-1})t}] \\
 &= 0.64 \times [e^{-(1.91 \times 10^{-4} \text{ s}^{-1})t} - e^{-(2.31 \times 10^6 \text{ s}^{-1})t}] \mathcal{A}_{\text{Bi-212}}(0).
 \end{aligned}
 \tag{10.210}$$

(c) Table 10.7 summarizes properties of nuclides involved in the 2-bransh decay of bismuth-212 into lead-208. Figure 10.14 shows a schematic diagram of the series decay of Bi-212 through either Tl-208 or Po-212 into Pb-208.

(d) In a radioactive decay series the growth of granddaughter G nuclide starting with the initial condition $N_G(t = 0) = 0$ is calculated from the expression for the rate of change dN_G/dt in the number of granddaughter nuclei. For a stable granddaughter nuclide the rate of accumulation of G is equal to the rate of decay of the daughter nuclide D, i.e.,

$$\frac{dN_G}{dt} = \lambda_D N_D(t) = f_i \frac{\lambda_D \lambda_P}{\lambda_D - \lambda_P} [e^{-\lambda_P t} - e^{-\lambda_D t}], \tag{10.211}$$

where $N_D(t)$ is the number of daughter nuclei at time t given in (10.205). Since in our example of bismuth-212 decay series, the lead-208 nuclide is accumulated through two channels, one represented by β^- decay of thallium-208 and the other by α decay of polonium-212, we calculate the contribution of each channel separately and then add the two contributions to obtain the total contribution from both channels.

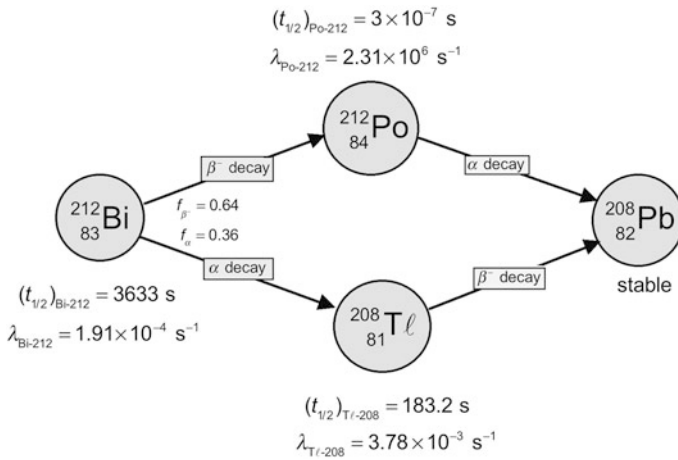


Fig. 10.14 Schematic diagram of the bismuth-212 decay series concluding with lead-208

Upon integration of (10.211) from 0 to t we get the following expression for $N_G(t)$

$$N_G(t) = f_i N_P(0) \frac{\lambda_D \lambda_P}{\lambda_D - \lambda_P} \left[-\frac{e^{-\lambda_P t}}{\lambda_P} + \frac{e^{-\lambda_D t}}{\lambda_D} \right] + C, \tag{10.212}$$

where C is an integration constant. For the initial condition $N_G(t = 0) = 0$ (10.211) is given as

$$N_G(t = 0) = f_i N_P(0) \frac{\lambda_D \lambda_P}{\lambda_D - \lambda_P} \left[-\frac{1}{\lambda_D} + \frac{1}{\lambda_P} \right] + C = f_i N_P(0) \frac{\lambda_P - \lambda_D}{\lambda_D - \lambda_P} + C = 0 \tag{10.213}$$

and results in the following simple expression for constant C

$$C = f_i N_P(0). \tag{10.214}$$

Inserting (10.214) into (10.212) we get the following expression for the number of granddaughter nuclei $N_G(t)$ accumulated from the decay of daughter D

$$\begin{aligned} N_G(t) &= f_i N_P(0) \left\{ 1 - \frac{\lambda_D \lambda_P}{\lambda_D - \lambda_P} \left[-\frac{e^{-\lambda_P t}}{\lambda_P} + \frac{e^{-\lambda_D t}}{\lambda_D} \right] \right\} \\ &= f_i N_P(0) \left\{ 1 - \frac{\lambda_D e^{-\lambda_P t}}{\lambda_D - \lambda_P} + \frac{\lambda_P e^{-\lambda_D t}}{\lambda_D - \lambda_P} \right\}. \end{aligned} \tag{10.215}$$

(1) Accumulation of Pb-208 nuclei as a result of Tl-208 decay is now given as

$$\begin{aligned} N_{Pb-208}^{Tl-208}(t) &= 0.36 N_P(0) \left\{ 1 - 1.053 \times e^{-(1.91 \times 10^{-4} \text{ s}^{-1})t} + 5.309 \times 10^{-2} \right. \\ &\quad \left. \times e^{-(3.78 \times 10^{-3} \text{ s}^{-1})t} \right\}. \end{aligned} \tag{10.216}$$

(2) Accumulation of Pb-208 nuclei as a result of Po-212 decay is now given as

$$N_{\text{Pb-208}}^{\text{Po-212}}(t) = 0.64N_{\text{P}}(0)\{1 - e^{-(1.91 \times 10^{-4} \text{ s}^{-1})t} + 8.230 \times 10^{-11} \times e^{-(2.31 \times 10^6 \text{ s}^{-1})t}\}. \quad (10.217)$$

The total accumulation of Pb-208 nuclei as a function of time t is given by the sum of (10.216) and (10.217) as follows

$$\begin{aligned} N_{\text{Pb-208}}(t) &= N_{\text{Pb-208}}^{\text{Tl-208}}(t) + N_{\text{Pb-208}}^{\text{Po-212}}(t) \\ &= 0.36N_{\text{P}}(0)\{1 - 1.053 \times e^{-(1.91 \times 10^{-4} \text{ s}^{-1})t} + 5.309 \times 10^{-2} \\ &\quad \times e^{-(3.78 \times 10^{-3} \text{ s}^{-1})t}\} \\ &\quad + 0.64N_{\text{P}}(0)\{1 - e^{-(1.91 \times 10^{-4} \text{ s}^{-1})t} + 8.230 \times 10^{-11} \\ &\quad \times e^{-(2.31 \times 10^6 \text{ s}^{-1})t}\} \\ &= N_{\text{P}}(0)[1 - 1.02e^{-(1.91 \times 10^{-4} \text{ s}^{-1})t} + 1.91e^{-(3.78 \times 10^{-3} \text{ s}^{-1})t} \\ &\quad + 5.27 \times 10^{-11} e^{-(2.3 \times 10^6 \text{ s}^{-1})t}]. \end{aligned} \quad (10.218)$$

(d) Five curves, all normalized to $N_{\text{Bi-212}}(0) = 1$ and all dealing with the series decay of parent nucleus Bi-212 through either the Tl-208 branch or the Po-212 branch to the granddaughter Pb-208 nucleus, are shown in Fig. 10.13.

- (1) Curve 1 plots the number of Bi-212 nuclei against time t , exhibiting the standard radioactive decay characteristics with a half-life $(t_{1/2})_{\text{Bi-212}}$ of 60.55 min = 3633 s and a decay constant $\lambda_{\text{Bi-212}}$ of $1.91 \times 10^{-4} \text{ s}^{-1}$.
- (2) Curve 2 shows the growth and decay of the daughter product $N_{\text{Tl-208}}(t)$ against time t . Half-life and decay constant of the $N_{\text{Tl-208}}$ radionuclide are, respectively, $(t_{1/2})_{\text{Tl-208}} = 183.2 \text{ s}$ and $\lambda_{\text{Tl-208}} = 3.78 \times 10^{-3} \text{ s}^{-1}$. Because of the relatively short half-life of thallium-208 compared to the half-life of the parent nucleus Bi-212, the number of Tl-208 nuclei transforms rapidly into the Pb-208 nucleus causing a relatively rapid accumulation of lead nuclei through the thallium branch.

We should note that the curve representing the growth and decay of the Po-212 nuclei is not discernible on the scale of Fig. 10.13 because of the extremely short half-life of the polonium-212 nucleus.

- (3) Curve 3 represents the accumulation of Pb-208 nuclei as a result of the decay of Bi-212 through the thallium decay branch. Since the Pb-208 nucleus is stable, the accumulation curve exhibits the standard exponential growth shape and saturates at 0.36 which is the branching fraction of the Bi-212 α decay through the Tl-208 branch.
- (4) Curve 4 also represents the accumulation of Pb-208 nuclei as a result of Bi-212 decay, in this case through the polonium decay branch. This curve too exhibits the standard exponential growth but saturates at 0.64 which is the branching fraction of the Bi-212 β^- decay through the Po-212 branch.

- (5) Curve 5 is for the total accumulation of Pb-208 through both branches of the Bi-212 decay and is given as the sum of the two exponential curves: curve 3 for the Tl-208 branch and curve 4 for the Po-212 branch. Since both curve 3 and curve 4 are exponential, curve 5 is also exponential and saturates at the sum of saturations of the two curves ($0.36 + 0.64 = 1$).

Chapter 11 consists of **22 problems** covering 13 sections that deal with most important modes of radioactive decay. Radioactive nuclides, either naturally occurring or artificially produced by nuclear reactions, are unstable and strive to reach more stable nuclear configurations through various processes of spontaneous radioactive decay that involve transformation to a more stable nuclide and emission of energetic particles. The early investigators of radioactivity explained the macroscopic kinetics of radioactive decay soon after Becquerel's discovery of natural radioactivity in 1896 through the work of Marie Skłodowska-Curie, Pierre Curie, Ernest Rutherford and Frederick Soddy. However, it took several decades before the various radioactive decay modes were fully understood on a microscopic scale.

Currently, the most important modes of radioactive decay are: alpha, beta minus, beta plus, electron capture, gamma and internal conversion. In addition to these standard modes, questions in this chapter also cover proton and neutron decay as well as spontaneous fission as interesting examples of spontaneous radioactive decay despite their limited relevance to medical physics.

Section 11.1 of this chapter contains one problem covering a general introduction to radioactive decay processes, Sect. 11.2 covers theoretical and practical aspects of alpha decay, Sect. 11.3 deals with general aspects of beta decay, while Sects. 11.4 and 11.5 cover beta minus and beta plus decay, respectively.

Electron capture decay is addressed in Sect. 11.6. Sections 11.7 and 11.8, respectively, cover gamma decay and its competing process, internal conversion. Section 11.9 addresses spontaneous fission and Sects. 11.10 and 11.11 deal with proton emission decay and neutron emission decay, respectively. Next comes Sect. 11.12 that contains several problems concentrating on the Chart of Nuclides (also called Segrè chart) and the chapter concludes with problems in Sect. 11.13 that deal with a summary of issues related to radioactive decay modes.

11.1 Introduction to Radioactive Decay Processes

11.1.Q1

(224)

Radioactive nuclides, either naturally occurring or produced artificially by nuclear reactions, are unstable and strive to reach more stable nuclear configurations through various processes of spontaneous radioactive decay that involve nuclear transformation to a more stable nuclide and emission of energetic particles.

- (a) A closer look at radioactive decay processes reveals that they are divided into six main categories. Provide a list of the six main categories of nuclear decay.
- (b) Two of the six nuclear decay categories are divided into subcategories. Identify these two categories and list their subcategories.
- (c) On a microscopic scale there are nine major modes of radioactive decay. List the nine modes of nuclear decay.
- (d) For each of the major nine modes of nuclear decay identify the particle that is released in the nuclear decay mode.
- (e) List the most important physical quantities that must be conserved in nuclear decay.
- (f) For radioactive nuclear decay define the disintegration or decay energy that is often also referred to as Q value of radioactive decay.
- (g) Explain the meaning of terms: “neutron-rich” and “proton rich”.

SOLUTION:

- (a) The six main categories of radioactive nuclear decay are:
 - (1) Alpha (α) decay
 - (2) Beta (β) decay
 - (3) Gamma (γ) decay
 - (4) Spontaneous fission (SF)
 - (5) Proton emission (PE) decay
 - (6) Neutron emission (NE) decay
- (b) The two categories of radioactive nuclear decay that are divided into subcategories are:
 - (1) Beta (β) decay that is subdivided into: beta minus (β^-) decay, beta plus (β^+) decay, and electron capture (EC) decay.
 - (2) Gamma (γ) decay that is subdivided into gamma emission (GE) decay and internal conversion (IC) decay.

Table 11.1 Modes of radioactive nuclear decay and particles released in nuclear decays

	Mode of radioactive nuclear decay	Particles released in radioactive nuclear decay
(1)	α	α particle (helium nucleus)
(2)	β^-	Electron e^- and electronic antineutrino $\bar{\nu}_e$
(3)	β^+	Positron e^+ and electronic neutrino ν_e
(4)	EC (electron capture)	Electronic neutrino ν_e
(5)	Gamma emission	γ ray photon
(6)	IC (internal conversion)	Atomic orbital electron e_{orb}
(7)	SF (spontaneous fission)	Neutron and fission product nuclei
(8)	Proton emission	Proton
(9)	Neutron emission	Neutron

(c) The nine major modes of radioactive nuclear decay are:

- (1) α decay
- (2) β^- decay
- (3) β^+ decay
- (4) Electron capture (EC)
- (5) γ emission decay
- (6) Internal conversion (IC)
- (7) Spontaneous fission (SF)
- (8) Proton emission decay
- (9) Neutron emission decay

(d) In each mode of radioactive nuclear decay the parent P nucleus transforms into a daughter D nucleus that differs from the parent nucleus in one or more of the following parameters: atomic number Z , neutron number N , and atomic mass number A . In addition, in each mode of nuclear decay one or more particles are released, as listed in Table 11.1.

(e) Most important physical quantities that must be conserved in radioactive nuclear decay are:

- (1) Total energy
- (2) Momentum
- (3) Total charge
- (4) Atomic number
- (5) Atomic mass number (number of nucleons)

(f) Total energy of particles released by the nuclear transformation process is equal to the net decrease in the rest energy of the neutral atom, from parent P to daughter D. The disintegration (decay) energy, often referred to as Q value for the radioactive decay, is defined as follows

$$Q = \{M(P) - [M(D) + m]\}c^2, \quad (11.1)$$

where $M(P)$, $M(D)$, and m are the nuclear rest masses (in unified atomic mass units u) of the parent, daughter, and emitted particles, respectively. The energy equivalent of u is 931.5 MeV.

Often atomic masses rather than nuclear masses are used in calculations of Q values for radioactive decay. In many decay modes the electron masses cancel out, so that it makes no difference if atomic or nuclear masses are used in (11.1). On the other hand, there are situations where electron masses do not cancel out (e.g., β^+ decay) and there special care must be taken to account for all electrons involved when atomic rest masses are used in (11.1).

For radioactive decay to be energetically possible the Q value must be greater than zero. This means that spontaneous radioactive decay processes release energy and are called exoergic or exothermic. For $Q > 0$, the energy equivalent of the Q value is shared as kinetic energy between the particles emitted in the decay process and the daughter product. Since the daughter has a much larger mass than the other emitted particles, the kinetic energy acquired by the daughter is usually negligibly small.

(g) In light (low atomic number) elements nuclear stability is achieved when the number of neutrons N and the number of protons Z is approximately equal ($N \approx Z$). As the atomic number increases, the N/Z ratio for stable nuclei increases from 1 at low Z elements to about 1.5 for heavy stable elements.

- (1) If a nucleus has a N/Z ratio that is too low for nuclear stability, it has an excess of protons and is called proton-rich. It decays through conversion of a proton into a neutron and emits a positron and a neutrino (β^+ decay). Alternatively, the nucleus may capture an orbital electron, transform a proton into a neutron and emit a neutrino (electron capture). A direct emission of a proton is also possible, but less likely, unless the nuclear imbalance is very high.
- (2) If a nucleus has a N/Z ratio too high for nuclear stability, it has an excess of neutrons and is called neutron-rich. It decays through conversion of a neutron into a proton and emits an electron and anti-neutrino. This process is referred to as β^- decay. If the N/Z ratio is extremely high, a direct emission of a neutron is possible.

11.2 Alpha Decay

11.2.Q1

(225)

Alpha (α) decay was the first mode of radioactive decay detected and investigated after Henri Becquerel discovered natural radioactivity in 1896. It played an important role in early modern physics experiments that lead to the

currently accepted Rutherford-Bohr atomic model and is characterized by a nuclear transformation in which an unstable parent nucleus P attains a more stable nuclear configuration in daughter D through ejection of an α particle.

- (a) Briefly discuss the history of α decay and explain its historical significance for physics in particular and science in general.
- (b) List three methods that are used to calculate decay energy $Q_\alpha(P)$ that is often also referred to as Q value of α decay
- (c) List and briefly describe the important features of α decay.
- (d) Q value of α decay is of similar magnitude but not equal to kinetic energy $(E_K)_\alpha$ of the α particle ejected in α decay. Explain the difference between the two energies.
- (e) $(E_K)_\alpha$ is often expressed as $(E_K)_\alpha \approx Q_\alpha(P)[1 - 4/A_P]$. Show and explain the derivation of this approximation.

SOLUTION:

(a) Alpha particles produced in natural α decay were used in one of the most important experiments in history of physics and science in general when Hans Geiger and Ernest Marsden carried out their momentous 1909 study of α particle scattering on a gold foil. Based on their experimental results that clearly contradicted the then-prevailing Thomson atomic model, Ernest Rutherford proposed a completely new atomic model with two main features:

- (1) Mass and positive charge of the atom are concentrated in the atomic nucleus the size of which is of the order of 10^{-15} m = 1 fm, i.e., 5 orders of magnitude smaller than the size of the atom.
- (2) Negatively charged electrons revolve about the nucleus in a cloud, the radius of which is of the order 10^{-10} = 1 Å.

Despite importance of α particles in early nuclear physics experiments, attempts to explain alpha decay theoretically were unsuccessful until 1928 when George Gamow unraveled its exact nature by introducing into physics the quantum-mechanical concept of tunneling of α particles through a potential barrier.

(b) Similarly to the calculation of the Q value of a nuclear reaction in which a projectile strikes a nuclear target to produce two reaction products, in nuclear α decay of parent P nucleus that results in daughter D nucleus and emission of an α particle, the α decay Q value or Q_α can be determined with three methods:

- (1) *Atomic rest energy method* in which one subtracts the sum of atomic rest energies of decay products after the α decay ($\sum_{i, \text{ after}} \mathcal{M}_i c^2$) from atomic rest

energy of the parent atom $\mathcal{M}(\text{P})c^2$

$$Q_\alpha = \mathcal{M}(\text{P})c^2 - \sum_{i, \text{ after}} \mathcal{M}_i c^2 = \{ \mathcal{M}(\text{P}) - [\mathcal{M}(\text{D}) + \mathcal{M}({}_2^4\text{He})] \} c^2. \quad (11.2)$$

- (2) *Nuclear rest energy method* in which one subtracts the sum of nuclear rest energies of decay products after the decay ($\sum_{i, \text{ after}} M_i c^2$) from the rest energy of the parent nucleus $M(\text{P})c^2$

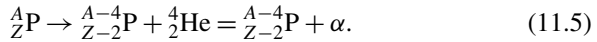
$$Q_\alpha = M(\text{P})c^2 - \sum_{i, \text{ after}} M_i c^2 = \{ M(\text{P}) - [M(\text{D}) + m_\alpha] \} c^2. \quad (11.3)$$

- (3) *Nuclear binding energy method* in which the binding energy $E_B(\text{P})$ of the parent nucleus before decay is subtracted from the sum of binding energies of decay products after the decay ($\sum_{i, \text{ after}} E_B(\text{P})$)

$$Q_\alpha = \sum_{i, \text{ after}} E_B(i) - E_B(\text{P}) = [E_B(\text{D}) + E_B({}_2^4\text{He})] - E_B(\text{P}). \quad (11.4)$$

(c) The prominent features of α decay are summarized as follows:

- (1) In α decay, the number of protons Z and the number of neutrons N is conserved by producing a ${}_2^4\text{He}$ nucleus (α particle) and lowering the parent's atomic mass number A_P by 4 and parent's atomic number Z_P by 2 to get a daughter with $A_D = A_P - 4$ and $Z_D = Z_P - 2$, i.e.,



- (2) The energetic α particle emitted in α decay slows down in moving through the absorber medium and eventually captures two electrons from its surroundings to become a neutral ${}_2^4\text{He}$ atom.
- (3) Typical kinetic energies of α particles released by naturally occurring radionuclides are between 4 MeV and 9 MeV, corresponding to a range in air of about 1 cm to 10 cm, respectively, and in tissue of about 10^{-3} cm and 10^{-2} cm, respectively.
- (4) α decay occurs commonly in nuclei with $Z > 82$ because in this range of atomic number Z decay energies Q_α determined in (b) are positive and of the order of ~ 4 MeV to ~ 9 MeV.
- (5) Total decay energy Q_α must be positive for α decay to occur and the $Q_\alpha > 0$ results mainly from the high total binding energy of the ${}_2^4\text{He}$ nucleus (29.3 MeV) that is significantly higher than for nuclei of ${}_2^3\text{He}$, ${}_1^3\text{He}$, and ${}_1^2\text{He}$ for which spontaneous ejection from parent nuclei energetically is not feasible.
- (6) Ejection of a heavy nucleus from the parent nucleus is energetically possible (large Q value); however, the effect of tunneling through the potential barrier is then also much more difficult for the heavy nucleus in comparison with tunneling for the α particle.

(7) Emission of heavy particles from parent nuclei with $Z > 92$ is possible and represents a mode of radioactive decay competing with α decay and referred to as *spontaneous fission*.

(d) In α decay the principles of energy and momentum conservation must be upheld and as a result α decay energy Q_α is shared between daughter atom and α particle. For a stationary parent nucleus the momentum before decay is zero, implying that the α particle and daughter atom together must have zero momentum after decay. This can be achieved only if the two decay products (α particle and daughter atom) acquire momenta opposite in direction and equal in magnitude

$$0 = \mathbf{p}_\alpha + \mathbf{p}_{\text{Po-218}} \quad (11.6)$$

or

$$|\mathbf{p}_\alpha| \equiv p_\alpha = \sqrt{\frac{(E_K)_\alpha}{2m_\alpha}} = |\mathbf{p}_{\text{Po-218}}| \equiv p_{\text{Po-218}} = \sqrt{\frac{(E_K)_{\text{Po-218}}}{2\mathcal{M}_{\text{Po-218}}}}, \quad (11.7)$$

where \mathbf{p}_α and \mathbf{p}_D are vector momenta of the α particle and daughter atom, respectively, and $|\mathbf{p}_\alpha| \equiv p_\alpha$ and $|\mathbf{p}_D| = p_D$ are magnitudes of the momentum vectors of the α particle and daughter atom, respectively.

Considering total energy conservation we recognize that kinetic energies of decay products in α decay are relatively small allowing us to use classical mechanics for expression of energy conservation to get the following expression for the decay energy $Q_\alpha(P)$

$$\begin{aligned} Q_\alpha(P) &= (E_K)_\alpha + (E_K)_D = \frac{p_\alpha^2}{2m_\alpha} + \frac{p_D^2}{2\mathcal{M}_D} = \frac{p_\alpha^2}{2} \left[\frac{1}{m_\alpha} + \frac{1}{\mathcal{M}_D} \right] \\ &= (E_K)_\alpha \left[1 + \frac{m_\alpha}{\mathcal{M}_D} \right] = (E_K)_D \left[1 + \frac{\mathcal{M}_D}{m_\alpha} \right]. \end{aligned} \quad (11.8)$$

From (11.8) we extract the following expressions for kinetic energies $(E_K)_\alpha$ and $(E_K)_D$ of α decay products

$$(E_K)_\alpha = Q_\alpha(P) \left[1 + \frac{m_\alpha}{\mathcal{M}_D} \right]^{-1} \quad \text{and} \quad (E_K)_D = Q_\alpha(P) \left[1 + \frac{\mathcal{M}_D}{m_\alpha} \right]^{-1}, \quad (11.9)$$

where $Q_\alpha(P)$ is the α decay energy (Q value) determined through one of the three methods introduced in (b). Noting that in α decay $m_\alpha \ll \mathcal{M}_D$, (11.9) suggests that the α particle and daughter D atom will share the decay energy $Q_\alpha(P)$ in the inverse proportion of their masses, resulting in a large portion of the available energy Q_α going to the α particle and only a small percentage of Q_α transferred to the daughter atom.

(e) Equations (11.9) for kinetic energies $(E_K)_\alpha$ and $(E_K)_D$ of the α particle and daughter atom, respectively, can be approximated as follows provided that $m_\alpha \ll \mathcal{M}_D$

$$\begin{aligned}
 (E_K)_\alpha &= \frac{Q_\alpha(P)}{1 + \frac{m_\alpha}{M_D}} \approx \frac{Q_\alpha(P)}{1 + \frac{m_\alpha}{M_P - m_\alpha}} = Q_\alpha(P) \frac{M_P - m_\alpha}{M_P} \\
 &\approx Q_\alpha(P) \frac{A_P - A_{\text{He}}}{A_P} = Q_\alpha(P) \frac{A_P - 4}{A_P}, \quad (11.10)
 \end{aligned}$$

where A_P is the atomic mass number of the parent nucleus and $A_{\text{He}} = 4$ is the atomic mass number of the helium nucleus.

Similarly, we get the following approximation for the recoil kinetic energy $(E_K)_D$ of the daughter atom D

$$(E_K)_D = \frac{Q_\alpha(P)}{1 + \frac{M_D}{m_\alpha}} = \frac{Q_\alpha(P)m_\alpha}{m_\alpha + M_D} \approx Q_\alpha(P) \frac{m_\alpha}{M_P} \approx \frac{4}{A_P}. \quad (11.11)$$

11.2.Q2

(226)

Radon is an inert noble gas that mixes with air and has 36 known isotopes, all radioactive. It occurs naturally as the decay product of uranium or thorium, and its most common isotope is radon-222 which is a daughter product of radium-226 decay. Radon daughters are solids that attach themselves to dust particles in air and pose a radiation risk to humans when inhaled causing bronchial and lung tissue damage possibly leading to lung cancer.

- (a) Determine decay energy Q_α for the α decay of radon-222 into polonium-218. Use and compare three methods for Q_α calculation: (1) Atomic rest energy method, (2) Nuclear rest energy method, and (3) Nuclear binding energy method. All required atomic and nuclear data are provided in Appendix A.
- (b) Determine kinetic energy $(E_K)_\alpha$ of the α particle emitted in the Rn-222 α decay.
- (c) Determine recoil kinetic energy $(E_K)_{\text{Po-218}}$ of polonium-218 daughter in Rn-222 α decay.
- (d) Find a decay scheme of radon-222 in the literature and verify whether or not your result of (b) agrees with the decay scheme you found in the literature.

SOLUTION:

(a) Decay energy or Q value of the radioactive nuclear α decay can be calculated with three methods and all three are expected to give the same result (see T11.1). The three methods are: (1) Atomic rest energy method (T11.3), (2) Nuclear rest energy method (T11.3), and (3) Nuclear binding energy method (T11.4).

(1) *Atomic rest energy method:*

$$\begin{aligned}
 Q_\alpha(^{222}_{86}\text{Rn}) &= \{ \mathcal{M}(^{222}_{86}\text{Rn}) - \mathcal{M}(^{218}_{84}\text{Po}) - \mathcal{M}(^4_2\text{He}) \} c^2 \\
 &= (222.017571u - 218.008973u - 4.002603u) \\
 &= (5.995 \times 10^{-3}u) \times (931.494028 \text{ MeV}/u) \\
 &= 5.58 \text{ MeV}.
 \end{aligned} \tag{11.12}$$

(2) *Nuclear rest energy method:*

$$\begin{aligned}
 Q_\alpha(^{222}_{86}\text{Rn}) &= \{ M(^{222}_{86}\text{Rn}) - M(^{218}_{84}\text{Po}) - m_\alpha \} c^2 \\
 &= (206764.1025 - 203031.1324 - 3727.3791) \text{ MeV} \\
 &= 5.59 \text{ MeV}.
 \end{aligned} \tag{11.13}$$

(3) *Nuclear binding energy method:*

$$\begin{aligned}
 Q_\alpha(^{222}_{86}\text{Rn}) &= E_B(^{218}_{84}\text{Po}) + E_B(^4_2\text{He}) - E_B(^{222}_{86}\text{Rn}) \\
 &= (1685.47305 + 28.29569 - 1708.17777) \text{ MeV} \\
 &= 5.59 \text{ MeV}.
 \end{aligned} \tag{11.14}$$

(b) We now use the principles of (1) total energy conservation and (2) momentum conservation to determine kinetic energy $(E_K)_\alpha$ of the α particle ejected in the α decay of radon-222 and recoil energy $(E_K)_{\text{Po-218}}$ of the polonium-218 daughter product. The two conservation principles are for α decay expressed as follows:

(1) For total energy conservation we recognize that kinetic energies in α decay are relatively small allowing us to use classical mechanics for expression of energy conservation

$$Q_\alpha(^{222}_{86}\text{Rn}) = (E_K)_\alpha + (E_K)_{\text{Po-218}} = \frac{p_\alpha^2}{2m_\alpha} + \frac{p_{\text{Po-218}}^2}{2\mathcal{M}_{\text{Po-218}}}. \tag{11.15}$$

(2) For momentum conservation we note that momentum before α decay is zero causing the two momenta \mathbf{p}_α and $\mathbf{p}_{\text{Po-218}}$ after the α decay to be opposite in direction and equal in magnitude

$$\mathbf{0} = \mathbf{p}_\alpha + \mathbf{p}_{\text{Po-218}} \tag{11.16}$$

or

$$|\mathbf{p}_\alpha| \equiv p_\alpha = \sqrt{\frac{(E_K)_\alpha}{2m_\alpha}} = |\mathbf{p}_{\text{Po-218}}| \equiv p_{\text{Po-218}} = \sqrt{\frac{(E_K)_{\text{Po-218}}}{2\mathcal{M}_{\text{Po-218}}}}, \tag{11.17}$$

where

p_α	is the magnitude of α particle momentum.
$p_{\text{Po-218}}$	is the magnitude of the polonium-218 atomic recoil momentum.
m_α	is the rest mass of the α particle.
$\mathcal{M}_{\text{Po-218}}$	is the rest mass of the polonium-218 atom (218.008973 u) \times (931.494028 MeV/u) = 203074.0564 MeV/ c^2 .

Using (11.15) we can now express the conservation of energy as

$$Q_\alpha(^{222}_{86}\text{Rn}) = (E_K)_\alpha + (E_K)_{\text{Po-218}} = \frac{p_\alpha^2}{2m_\alpha} + \frac{p_{\text{Po-218}}^2}{2\mathcal{M}_{\text{Po-218}}} = \frac{p_\alpha^2}{2} \left[\frac{1}{m_\alpha} + \frac{1}{\mathcal{M}_{\text{Po-218}}} \right] \quad (11.18)$$

from where it follows that

$$p_\alpha^2 = p_{\text{Po-218}}^2 = 2Q_\alpha(^{222}_{86}\text{Rn}) \left[\frac{1}{m_\alpha} + \frac{1}{\mathcal{M}_{\text{Po-218}}} \right]^{-1}. \quad (11.19)$$

Inserting (11.19) into (11.18) we now get the following expressions for $(E_K)_\alpha$ and $(E_K)_{\text{Po-218}}$

$$(E_K)_\alpha = \frac{p_\alpha^2}{2m_\alpha} = \frac{Q_\alpha(^{222}_{86}\text{Rn})}{m_\alpha} \left[\frac{1}{m_\alpha} + \frac{1}{\mathcal{M}_{\text{Po-218}}} \right]^{-1} = \frac{Q_\alpha(^{222}_{86}\text{Rn})}{\left[1 + \frac{m_\alpha}{\mathcal{M}_{\text{Po-218}}} \right]} \quad (11.20)$$

$$= \frac{5.59 \text{ MeV}}{\left[1 + \frac{3727.3791}{203074.0564} \right]} = \frac{5.59 \text{ MeV}}{1.0184} = 5.49 \text{ MeV} \quad (11.21)$$

and

$$(E_K)_{\text{Po-218}} = \frac{p_{\text{Po-218}}^2}{2\mathcal{M}_{\text{Po-218}}} = \frac{Q_\alpha(^{222}_{86}\text{Rn})}{\mathcal{M}_{\text{Po-218}}} \left[\frac{1}{m_\alpha} + \frac{1}{\mathcal{M}_{\text{Po-218}}} \right]^{-1} = \frac{Q_\alpha(^{222}_{86}\text{Rn})}{\left[1 + \frac{\mathcal{M}_{\text{Po-218}}}{m_\alpha} \right]} \\ = \frac{5.59 \text{ MeV}}{\left[1 + \frac{203074.0564}{3727.3791} \right]} = \frac{5.59 \text{ MeV}}{55.48} = 0.10 \text{ MeV}. \quad (11.22)$$

Same results can be obtained with the approximations presented in (T11.7) as

$$(E_K)_\alpha = Q_\alpha(^{222}_{86}\text{Rn}) \left[1 - \frac{4}{A_{\text{Rn-222}}} \right] = (5.59 \text{ MeV}) \times \left[1 - \frac{4}{222} \right] = 5.49 \text{ MeV} \quad (11.23)$$

and

$$(E_K)_{\text{Po-218}} \approx Q_\alpha(^{222}_{86}\text{Rn}) \frac{4}{A_{\text{Rn-222}}} = (5.59 \text{ MeV}) \times \frac{4}{222} = 0.10 \text{ MeV}. \quad (11.24)$$

(d) In Fig. 11.1 we show the energy level diagram we found in the literature for α decay of radon-222 into polonium-218. Our calculated kinetic energy $(E_K)_\alpha = 5.49 \text{ MeV}$ of the α particle that radon-222 emits in its decay into polonium-218 agrees well with the published data.

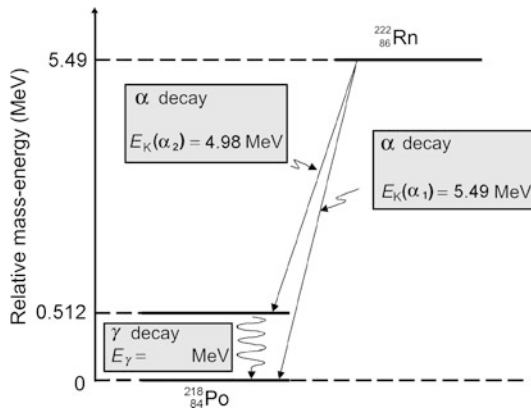


Fig. 11.1 Energy level diagram for α decay of radon-222 into polonium-218. The relative mass-energy levels for the ground states of the two radionuclides are calculated for the respective atomic masses of the two radionuclides given in Appendix A

11.3 Beta Decay

11.3.Q1

(227)

The term beta decay encompasses 3 modes of radioactive decay in which the atomic number Z between the parent and the daughter nuclide changes by one unit (± 1), while the atomic mass number A remains constant. Thus, the number of nucleons and the total charge are both conserved in the beta decay processes and one can say that the daughter D is an isobar of the parent P , since the two contain the same number of nucleons.

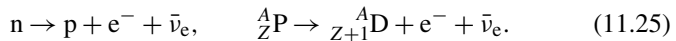
- List and briefly discuss the three radioactive decay processes that belong to the beta decay category.
- Often a β decay process of the parent is accompanied by emission of characteristic x rays or Auger electrons emitted by the daughter nucleus. Describe the mechanisms of these events.
- In α decay the emitted α particles are mono-energetic for a given α decay process. In β decay, however, β particles (electrons in β^- decay or positrons in β^+ decay) are emitted with a spectral distribution. Explain why this is so and sketch a typical β emission spectrum for electrons and positrons.
- In β^- and β^+ decay the daughter D recoils with kinetic energy $(E_K)_D$ ranging from 0 to a maximum value. Explain the conditions under which (1) $(E_K)_D = 0$ and (2) $(E_K)_D = \text{max}$.

- (e) Q value of β decay (also referred to as decay energy Q_β) can be expressed as the sum of kinetic energies of β decay products after β decay. Derive an expression for Q_β as a function of the maximum energy $(E_\beta)_{\max}$ of the beta particle after β decay.
- (f) From the result for Q_β in (e) express $(E_\beta)_{\max}$ as a function of Q_β and show that in the first approximation $(E_\beta)_{\max} \approx Q_\beta(1 - \eta_\beta)$, where η_β is a very small correction factor. Determine the correction factor η_β .

SOLUTION:

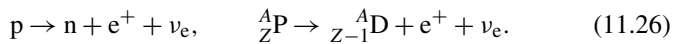
(a) Three processes fall into the category of β decay:

- (1) *Beta minus* (β^-) decay with the following characteristics: $Z \rightarrow Z + 1$; $A = \text{const.}$



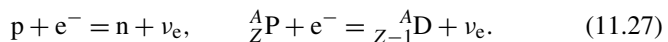
A neutron-rich radioactive nucleus transforms a neutron into proton and ejects an electron and an antineutrino. Free (extra-nuclear) neutrons actually decay into protons through the β^- decay process with a lifetime τ of 11.24 min. This decay is possible since the neutron rest mass exceeds that of the proton.

- (2) *Beta plus* (β^+) decay with the following characteristics: $Z \rightarrow Z - 1$; $A = \text{const.}$



A proton-rich radioactive nucleus transforms a proton into neutron and ejects a positron and a neutrino. Free (extra-nuclear) protons cannot decay into neutrons through a β^+ decay process because the rest mass of the proton is smaller than that of the neutron.

- (3) *Electron capture* with the following characteristics: $Z \rightarrow Z - 1$; $A = \text{const.}$



A proton-rich radioactive nucleus captures an inner shell orbital electron (usually K shell), transforms a proton into a neutron, and ejects a neutrino.

(b) In many cases, β decay of a parent nucleus does not lead directly to the ground state of the daughter nucleus; rather it leads to an *unstable* or even *metastable excited state* of the daughter. The excited state de-excites through emission of gamma rays or through emission of internal conversion electrons. Of course, the orbital shell vacancies produced by the electron capture or internal conversion process will be followed by emission of discrete characteristic photons or Auger electrons, as is the case with all atomic shell vacancies no matter how they are produced.

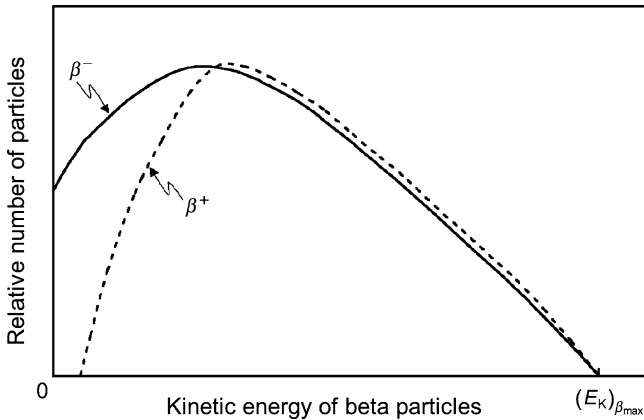


Fig. 11.2 Typical β particle energy spectra for β^- and β^+ decay normalized to the maximum energy of the β particles

Beta decay can only take place when the binding energy of the daughter nucleus $E_B(D)$ exceeds the binding energy of the parent nucleus $E_B(P)$.

(c) For a given β decay, similarly to the situation in α decay, the β -decay energy is uniquely defined by the difference in mass-energy between the parent and daughter nuclei. However, in contrast to the α decay where the energy of the emitted α particles is also uniquely defined, the β particles emitted in β decay are not monoenergetic, rather they exhibit a continuous spectral kinetic energy distribution with only the maximum kinetic energy $(E_e)_{\max}$ corresponding to the β decay energy.

This apparent contravention of the energy conservation law was puzzling physicists for many years until in 1930 *Wolfgang Pauli* postulated the existence of the neutrino to explain the continuous spectrum of electrons emitted in β decay. In 1934 *Enrico Fermi* expanded on Pauli's neutrino idea and developed a theory of β^- and β^+ decay. The theory includes the neutrino or the antineutrino as the third particle sharing the available decay energy and momentum with the β particle and the recoil nucleus. With the emission of a third particle, the neutrino or antineutrino, the momentum and energy can be conserved in β decay.

Typical shapes of β^- and β^+ spectra are shown in Fig. 11.2. In general, the spectra exhibit low values at small kinetic energies, reach a maximum at a certain kinetic energy, and then decrease with kinetic energy until they reach zero at a maximum energy $[(E_K)_\beta]_{\max}$ that corresponds to the β decay energy Q_β , if we neglect the small recoil energy acquired by the daughter nucleus.

The shapes of β^- and β^+ spectra differ at low kinetic energies owing to the charge of the β particles: electrons in β^- decay are attracted to the nucleus; positrons in β^+ decay are repelled by the nucleus. The charge effects cause an energy shift to lower energies for electrons and to higher energies for positrons, as is clearly shown in Fig. 11.2.

For use in internal dosimetry calculations of β sources the effective energy $[(E_K)_\beta]_{\text{eff}}$ of β decay spectra is usually estimated as

$$[(E_K)_\beta]_{\text{eff}} = \frac{1}{3} [(E_K)_\beta]_{\text{max}}. \quad (11.28)$$

(d) Because of the presence of the third decay product (the elusive neutrino or antineutrino) in β decay that shares the available decay energy Q_β , the recoil energy $(E_K)_D$ can take on values between zero and a maximum value.

(1) Recoil kinetic energy of the daughter decay product is zero, i.e., $(E_K)_D = 0$, when the electron and antineutrino in β^- decay or positron and neutrino in β^+ decay are emitted with the same momentum but in opposite directions.

(2) Maximum recoil kinetic energy $(E_K)_D = [(E_K)_D]_{\text{max}} = \text{max}$ of the daughter, on the other hand, occurs when either one of the two light decay particles (electron or antineutrino in β^- decay; positron or neutrino in β^+ decay) is emitted with the maximum available kinetic energy $[(E_K)_\beta]_{\text{max}}$.

(e) Q value of β decay or β -decay energy Q_β is expressed as the sum of kinetic energies of decay products after the β decay. For simplicity we use $[(E_K)_D]_{\text{max}}$ and $(E_K)_{\text{max}}$ in the sum to get

$$Q_\beta = [(E_K)_D]_{\text{max}} + [(E_K)_\beta]_{\text{max}} \quad (11.29)$$

and then express $[(E_K)_D]_{\text{max}}$ in terms of $[(E_K)_\beta]_{\text{max}}$.

Maximum recoil kinetic energy of the daughter $[(E_K)_D]_{\text{max}}$ is determined using the principles of energy and momentum conservation and accounting for the relativistic mass changes of the β particle (electron or positron) and using classical mechanics for recoil kinetic energy $[(E_K)_D]_{\text{max}}$ of the daughter.

Since the parent momentum before β decay is zero, the total momentum shared by the daughter D and the β particle e^\pm (under the special condition of neutrino or antineutrino energy equaling zero) must also equal to 0 after the β decay and this means that the two vector momenta \mathbf{p}_D and \mathbf{p}_{e^\pm} after β decay must be opposite in direction and equal in magnitude. The magnitudes of the two momenta are thus related as follows

$$M(D)v_D = p_D \equiv |\mathbf{p}_D| = |\mathbf{p}_{e^\pm}| \equiv p_{e^\pm} = \gamma_{e^\pm} m_e v_{e^\pm} = \frac{m_e v_{e^\pm}}{\sqrt{1 - \beta_{e^\pm}^2}} = \frac{m_e c \beta_{e^\pm}}{\sqrt{1 - \beta_{e^\pm}^2}}, \quad (11.30)$$

where

- m_e is the rest mass of the β particle (electron or positron): $m_e = 0.511 \text{ MeV}/c^2$.
- γ_{e^\pm} is the Lorentz factor of the beta particle: $\gamma_{e^\pm} = (1 - \beta_{e^\pm}^2)^{-1/2}$.
- β_{e^\pm} is the velocity v_{e^\pm} of the β particle normalized to speed of light c .

$\mathcal{M}(\text{D})$ is the atomic rest mass of the daughter β decay product.

β_{e^\pm} is the velocity of the daughter D after β decay.

Maximum recoil kinetic energy $[(E_K)_\text{D}]_\text{max}$ of the daughter is expressed as follows

$$[(E_K)_\text{D}]_\text{max} = \frac{p_\text{D}^2}{2\mathcal{M}(\text{D})c^2} = \frac{(m_e c^2)^2}{2\mathcal{M}(\text{D})c^2} \frac{\beta_{e^\pm}^2}{1 - \beta_{e^\pm}^2}. \quad (11.31)$$

From the standard expression for $[(E_K)_\beta]_\text{max} = (\gamma_{e^\pm} - 1)m_e c^2$ we determine the following expression for $\beta_{e^\pm}^2/(1 - \beta_{e^\pm}^2)$

$$\frac{\beta_{e^\pm}^2}{1 - \beta_{e^\pm}^2} = \frac{2[(E_K)_\beta]_\text{max}}{m_e c^2} + \left[\frac{[(E_K)_\beta]_\text{max}}{m_e c^2} \right]^2. \quad (11.32)$$

Inserting (11.32) into (11.31) we obtain the following result for the maximum recoil kinetic energy of the daughter D after β decay

$$[(E_K)_\text{D}]_\text{max} = \frac{m_e c^2}{\mathcal{M}(\text{D})c^2} [(E_K)_\beta]_\text{max} + \frac{1}{2\mathcal{M}(\text{D})c^2} [(E_K)_\beta]_\text{max}^2. \quad (11.33)$$

Beta decay energy Q_β is now given by the following expression

$$\begin{aligned} Q_\beta &= [(E_K)_\beta]_\text{max} + [(E_K)_\text{D}]_\text{max} \\ &= [(E_K)_\beta]_\text{max} + \left[\frac{m_e c^2}{\mathcal{M}(\text{D})c^2} [(E_K)_\beta]_\text{max} + \frac{1}{2\mathcal{M}(\text{D})c^2} [(E_K)_\beta]_\text{max}^2 \right] \\ &= [(E_K)_\beta]_\text{max} + [(E_K)_\beta]_\text{max} \left[\frac{m_e c^2 + \frac{1}{2} [(E_K)_\beta]_\text{max}}{\mathcal{M}(\text{D})c^2} \right], \end{aligned} \quad (11.34)$$

showing clearly that in beta minus decay as well as in beta plus decay by far the larger energy component is the component $[(E_K)_\beta]_\text{max}$ that is shared between the electron and antineutrino in beta minus decay and by the positron and neutrino in beta plus decay. Recoil energy $[(E_K)_\text{D}]_\text{max}$ given to the daughter, even at its maximum spelled out in (11.33), is extremely small and generally neglected in comparison with $[(E_K)_\beta]_\text{max}$.

Equation (11.34) can be written in the form of a quadratic equation for $[(E_K)_\beta]_\text{max}$ as a function of Q_β

$$\frac{1}{2\mathcal{M}(\text{D})c^2} [(E_K)_\beta]_\text{max}^2 + \left[1 + \frac{m_e c^2}{\mathcal{M}(\text{D})c^2} \right] [(E_K)_\beta]_\text{max} - Q_\beta = 0, \quad (11.35)$$

with the following physically-relevant solution [note: $[(E_K)_\beta]_\text{max} > 0$]

$$[(E_K)_\beta]_\text{max} = \mathcal{M}(\text{D})c^2 \left\{ - \left[1 + \frac{m_e c^2}{\mathcal{M}(\text{D})c^2} \right] + \sqrt{\left[1 + \frac{m_e c^2}{\mathcal{M}(\text{D})c^2} \right]^2 + \frac{2Q_\beta}{\mathcal{M}(\text{D})c^2}} \right\}. \quad (11.36)$$

(f) To evaluate (11.36) further we write it in the following form

$$[(E_K)_\beta]_{\max} = \mathcal{M}(\text{D})c^2 \left[1 + \frac{m_e c^2}{\mathcal{M}(\text{D})c^2} \right] \left\{ \sqrt{1 + \frac{2Q_\beta}{\mathcal{M}(\text{D})c^2} \left[1 + \frac{m_e c^2}{\mathcal{M}(\text{D})c^2} \right]^{-2}} - 1 \right\}. \quad (11.37)$$

The second term under the square root is obviously much smaller than 1 since it is governed by the ratio $2Q_\beta/[\mathcal{M}(\text{D})c^2]$, allowing us to expand the square root into a series and keeping only the first two terms to get

$$\begin{aligned} [(E_K)_\beta]_{\max} &\approx \mathcal{M}(\text{D})c^2 \left[1 + \frac{m_e c^2}{\mathcal{M}(\text{D})c^2} \right] \left\{ 1 + \frac{Q_\beta}{\mathcal{M}(\text{D})c^2} \left[1 + \frac{m_e c^2}{\mathcal{M}(\text{D})c^2} \right]^{-2} + \dots - 1 \right\} \\ &= \frac{Q_\beta}{1 + \frac{m_e c^2}{\mathcal{M}(\text{D})c^2}} \approx Q_\beta \left[1 - \frac{m_e c^2}{\mathcal{M}(\text{D})c^2} \right] = Q_\beta(1 - \eta), \end{aligned} \quad (11.38)$$

where η_β is a small correction factor for β decay given as $\eta_\beta = m_e c^2/(\mathcal{M}(\text{D})c^2)$ and this ratio multiplied by Q_β is actually the maximum recoil kinetic energy $[(E_K)_\text{D}]_{\max}$ of the daughter after the β decay

$$[(E_K)_\text{D}]_{\max} = Q_\beta - [(E_K)_\beta]_{\max} = Q_\beta - Q_\beta(1 - \eta_\beta) = \eta_\beta Q_\beta = \frac{m_e c^2}{\mathcal{M}(\text{D})c^2} Q_\beta. \quad (11.39)$$

11.4 Beta Minus Decay

11.4.Q1

(228)

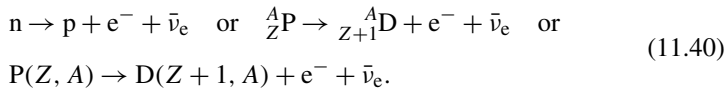
Several radionuclides decaying by beta minus (β^-) decay are used in medicine for external beam radiotherapy, brachytherapy, and nuclear imaging. Parent P radionuclide decays by β^- decay into excited daughter D that instantaneously or through metastable decay, decays into its ground state and emits the excitation energy in the form gamma rays.

- State expressions for β^- decay energy Q_{β^-} (Q value of β^- decay) based on: (1) nuclear rest energy of parent P and daughter D; (2) atomic rest energy of parent P and daughter D.
- Decay energy Q_{β^-} for β^- decay can be written as the sum of maximum recoil kinetic energy $[(E_K)_\text{D}]_{\max}$ of the daughter and maximum kinetic energy $[(E_K)_\beta]_{\max}$ of the β^- particle (electron) ejected from the nucleus in β^- decay. State the expressions for $[(E_K)_\text{D}]_{\max}$ and $[(E_K)_\beta]_{\max}$ in terms of Q_{β^-} .

- (c) Decay of a free (extra-nuclear) neutron into a proton p, electron e, and electronic anti-neutrino $\bar{\nu}_e$ is the simplest example of β^- decay. Calculate the Q value $Q_{\beta^-}(n)$ of a neutron undergoing β^- decay. Appropriate rest energies of neutron, proton, and electron are available in Appendix A.
- (d) For β^- decay of neutron determine the maximum kinetic energy $[(E_K)_\beta]_{\max}$ of the ejected electron and the maximum recoil kinetic energy $[(E_K)_D]_{\max}$ of the proton.

SOLUTION:

(a) Beta minus (β^-) decay is characterized by a spontaneous transformation of a neutron into a proton in a neutron-rich nucleus concurrently with ejection of an electron and antineutrino



Similarly to the case of nuclear reaction and the case of α decay, the decay energy $Q_{\beta^-}(\text{P})$ for beta minus decay can be determined either with (1) nuclear rest energy method or (2) atomic rest energy method.

- (1) In the nuclear rest energy method, one subtracts the sum of rest energies of decay products after the β^- decay (daughter D, electron e^- , and antineutrino $\bar{\nu}_e$) from the rest energy of the parent nucleus $M(\text{P})c^2$. Decay energy Q_{β^-} for the β^- decay process must be positive for β^- decay to occur and is given in terms of nuclear rest mass M as follows

$$Q_{\beta^-}(\text{P}) = M(\text{P})c^2 - \sum_{i, \text{ after}} M_i c^2 = \{M(Z, A) - [M(Z + 1, A) + m_e + 0]\}c^2, \quad (11.41)$$

where the term in square brackets represents the sum of nuclear rest masses of decay products: daughter $M(Z + 1, A)$, electron m_e , and 0 representing the rest mass of antineutrino. However, in terms of nuclear rest masses, the condition $Q_{\beta^-} > 0$ is a necessary but not sufficient condition for β^- decay to occur. As indicated in (11.41), β^- decay can occur to a neutron-rich unstable parent nucleus only when the mass $M(Z, A)$ of the parent P nucleus exceeds the mass $M(Z + 1, A)$ of the daughter D nucleus by more than one electron rest mass m_e , i.e., $M(Z, A) > M(Z + 1, A) + m_e$.

- (2) Adding and subtracting $Zm_e c^2$ to the right-hand side of (11.41) and neglecting the electron binding energies to the nucleus we obtain

$$Q_{\beta^-}(\text{P}) = \{[M(Z, A) + Zm_e] - [M(Z + 1, A) + m_e + 0 + Zm_e]\}c^2$$

$$= \{[\mathcal{M}(Z, A)] - [\mathcal{M}(Z + 1, A)]\}c^2, \quad (11.42)$$

where $\mathcal{M}(Z, A)$ and $\mathcal{M}(Z + 1, A)$ represent the *atomic rest masses* of the parent and daughter, respectively, noting that the following expressions link atomic and nuclear masses, \mathcal{M} and M , respectively

$$\mathcal{M}(Z, A) = M(Z, A) + Zm_e \quad (11.43)$$

and

$$\mathcal{M}(Z + 1, A) = M(Z + 1, A) + (Z + 1)m_e. \quad (11.44)$$

For the β^- decay to occur, as stated in (11.42), $Q_{\beta^-}(\text{P})$ must be positive, and we conclude from (11.42) that, in terms of atomic masses, the atomic mass of the parent $\mathcal{M}(Z, A)$ must exceed the atomic mass of the daughter $\mathcal{M}(Z + 1, A)$; i.e., $\mathcal{M}(Z, A) > \mathcal{M}(Z + 1, A)$, in contrast consideration of nuclear masses where, as stated in (11.41), the rest mass of parent nucleus $M(Z, A)$ must exceed the mass of the daughter nucleus $M(Z + 1, A)$ by more than one electron rest mass m_e for β^- decay to be feasible.

(b) Expressions for maximum kinetic energy $[(E_K)_\beta]_{\max}$ of the electron ejected in β^- decay were derived in Prob. 227 (11.37) and can be restated in relativistic format as follows

$$[(E_K)_\beta]_{\max} = \mathcal{M}(\text{D})c^2 \left[1 + \frac{m_e c^2}{\mathcal{M}(\text{D})} c^2 \right] \left\{ \sqrt{1 + \frac{2Q_\beta}{\mathcal{M}(\text{D})c^2} \left[1 + \frac{m_e c^2}{\mathcal{M}(\text{D})c^2} \right]^{-2}} - 1 \right\} \quad (11.45)$$

and, after recognizing that $m_e c^2 \ll \mathcal{M}(\text{D})c^2$, (11.45) is simplified greatly to read

$$[(E_K)_\beta]_{\max} \approx Q_\beta \left[1 - \frac{m_e c^2}{\mathcal{M}(\text{D})c^2} \right] = Q_\beta(1 - \eta) \quad (11.46)$$

and provides the following result for maximum recoil kinetic energy $[(E_K)_\text{D}]_{\max}$ of the daughter

$$[(E_K)_\text{D}]_{\max} = Q_\beta - [(E_K)_\beta]_{\max} = Q_\beta - Q_\beta(1 - \eta) = \eta Q_\beta = \frac{m_e c^2}{\mathcal{M}(\text{D})c^2} Q_\beta. \quad (11.47)$$

(c) Decay energy Q_{β^-} of neutron undergoing β^- decay is calculated using either the nuclear rest energy method of (11.41) or atomic rest energy method of (11.42). In the nuclear energy method the rest energy of the parent (neutron) must exceed the rest energy of the daughter (proton) by more than one electronic rest mass $m_e c^2 = 0.5110$ MeV.

As shown in Appendix A, $M(Z, A)c^2 = m_n c^2 = 939.5654$ MeV and $M(Z + 1, A)c^2 = m_p c^2 = 938.2720$ MeV, leading us to the conclusion that the parent nucleus (neutron) rest energy exceeds the daughter nucleus (proton) rest energy by 1.2934 MeV, an amount larger than the minimum of one electron rest mass required for β^- decay to be feasible.

(1) Using the nuclear rest energy method (11.41) we obtain the following result for Q_{β^-}

$$\begin{aligned} Q_{\beta^-}(\text{n}) &= \{M(Z, A) - [M(Z + 1, A) + m_e]\} = m_n c^2 - m_p c^2 - m_e c^2 \\ &= 939.5654 \text{ MeV} - 938.2720 \text{ MeV} - 0.5110 \text{ MeV} = 0.7824 \text{ MeV}. \end{aligned} \quad (11.48)$$

(2) Same result will be obtained using the atomic rest energy method (11.42) by assuming that the daughter product is the hydrogen atom

$$\begin{aligned} Q_{\beta^-}(\text{n}) &= \{\mathcal{M}(Z, A) - \mathcal{M}(Z + 1, A)\} = m_n c^2 - \mathcal{M}({}^1\text{H})c^2 \\ &= 939.5654 \text{ MeV} - (1.007825u) \times (931.494028 \text{ MeV}/u) \\ &= 939.5654 \text{ MeV} - 938.7830 \text{ MeV} = 0.7824 \text{ MeV}. \end{aligned} \quad (11.49)$$

(d) Maximum kinetic energy $[(E_K)_\beta]_{\max}$ of the beta particle and maximum recoil energy $[(E_K)_D]_{\max}$ of the daughter nucleus are calculated from (11.46) and (11.47), respectively, as follows

$$\begin{aligned} [(E_K)_\beta]_{\max} &= Q_{\beta^-}(\text{n}) \left[1 - \frac{m_e c^2}{m_p c^2} \right] = (0.7824 \text{ MeV}) \times \left[1 - \frac{0.5110}{938.272} \right] \\ &= 0.7820 \text{ MeV} \end{aligned} \quad (11.50)$$

and

$$\begin{aligned} [(E_K)_D]_{\max} &= Q_{\beta^-}(\text{n}) - [(E_K)_\beta]_{\max} = Q_{\beta^-}(\text{n}) \left[\frac{m_e c^2}{m_p c^2} \right] \\ &= (0.7824 \text{ MeV}) \times \left[\frac{0.5110}{938.272} \right] = 4 \times 10^{-4} \text{ MeV}. \end{aligned} \quad (11.51)$$

In neutron β^- decay the proton (daughter product) acquires only a minute fraction that amounts to at most $[(E_K)_D]_{\max} = 4 \times 10^{-4} \text{ MeV}$ of the total decay energy $Q_{\beta^-} = 0.7824 \text{ MeV}$. The rest of the decay energy (0.7820 MeV) is carried away by the ejected beta particle and antineutrino in random proportions; however, the sum of kinetic energies carried by the two particles (electron and neutrino) must be equal to the maximum kinetic energy available for the two particles $[(E_K)_\beta]_{\max} = 0.7820 \text{ MeV}$. *Note:* Kinetic energy of the two particles (0.7820 MeV) plus recoil kinetic energy of the daughter product (0.0004 MeV) is equal to the decay energy $Q_{\beta^-} = 0.7824 \text{ MeV}$.

11.4.Q2

(229)

Most notable β^- emitters of significance in medical physics are: cobalt-60 ($^{60}_{27}\text{Co}$), cesium-137 ($^{137}_{55}\text{Cs}$), and europium-152 ($^{152}_{63}\text{Eu}$) as radiation sources for external beam radiotherapy and iodine-131 ($^{131}_{53}\text{I}$) for thyroid nuclear imaging and thyroid ablation.

Calculate for the following radionuclides:

- (1) Cobalt-60.
 - (2) Iodine-131.
 - (3) Cesium-137.
 - (4) Europium-152.
- (a) Specific activity a .
 - (b) Binding energy per nucleon E_B/A .
 - (c) Decay energy Q_{β^-} . Use both the atomic and nuclear rest energy method in the calculation of Q_{β^-} . Appropriate nuclear and atomic data are provided in Appendix A.
 - (d) Summarize in a tabular format your results obtained in (a), (b), and (c).

SOLUTION:

- (a) Specific activity a of a radionuclide is defined as activity \mathcal{A} per unit mass m

$$a = \frac{\mathcal{A}}{m} = \frac{\lambda N}{m} = \frac{(\ln 2)N}{t_{1/2}m} = \frac{(\ln 2)N_A}{t_{1/2}A}, \quad (11.52)$$

where, for a given radionuclide, λ is the decay constant [$\lambda = (\ln 2)/t_{1/2}$] with $t_{1/2}$ the half-life, N_A is the Avogadro number ($6.022 \times 10^{23} \text{ mol}^{-1}$), and A is the atomic mass. From (11.52) we note that specific activity a is inversely proportional to both the half-life $t_{1/2}$ as well as atomic mass A .

- (1) Specific activity a of cobalt-60 ($t_{1/2} = 5.26 \text{ a}$):

$$\begin{aligned} a_{\text{Co-60}} &= \frac{(\ln 2) \times (6.022 \times 10^{23} \text{ mol}^{-1})}{(60 \text{ g} \cdot \text{mol}^{-1}) \times (5.26 \text{ a}) \times (365 \text{ d/a}) \times (24 \text{ h/d}) \times (3600 \text{ s/h})} \\ &= 4.194 \times 10^{13} \text{ s}^{-1}/\text{g} = 4.194 \times 10^{13} \text{ Bq/g} \\ &= 4.194 \times 10^4 \text{ GBq/g} = 1133 \text{ Ci/g}. \end{aligned} \quad (11.53)$$

- (2) Specific activity a of iodine-131 ($t_{1/2} = 8.02 \text{ d}$):

$$a_{\text{I-131}} = \frac{(\ln 2) \times (6.022 \times 10^{23} \text{ mol}^{-1})}{(131 \text{ g} \cdot \text{mol}^{-1}) \times (8.02 \text{ d}) \times (24 \text{ h/d}) \times (3600 \text{ s/h})}$$

$$\begin{aligned}
 &= 4.6 \times 10^{15} \text{ s}^{-1}/\text{g} \\
 &= 4.6 \times 10^6 \text{ Bq/g} = 4.6 \times 10^6 \text{ GBq/g} = 124280 \text{ Ci/g.} \quad (11.54)
 \end{aligned}$$

(3) Specific activity a of cesium-137 ($t_{1/2} = 30 \text{ a}$)

$$\begin{aligned}
 a_{\text{Cs-137}} &= \frac{(\ln 2) \times (6.022 \times 10^{23} \text{ mol}^{-1})}{(137 \text{ g} \cdot \text{mol}^{-1}) \times (30 \text{ a}) \times (365 \text{ d/a}) \times (24 \text{ h/d}) \times (3600 \text{ s/h})} \\
 &= 3.22 \times 10^{12} \text{ s}^{-1}/\text{g} = 3.22 \times 10^{12} \text{ Bq/g} \\
 &= 3.22 \times 10^3 \text{ GBq/g} = 87 \text{ Ci/g.} \quad (11.55)
 \end{aligned}$$

(4) Specific activity a of europium-152 ($t_{1/2} = 13.52 \text{ a}$):

$$\begin{aligned}
 a_{\text{Eu-152}} &= \frac{(\ln 2) \times (6.022 \times 10^{23} \text{ mol}^{-1})}{(152 \text{ g} \cdot \text{mol}^{-1}) \times (13.52 \text{ a}) \times (365 \text{ d/a}) \times (24 \text{ h/d}) \times (3600 \text{ s/h})} \\
 &= 6.44 \times 10^{12} \text{ s}^{-1}/\text{g} = 6.44 \times 10^{12} \text{ Bq/g} \\
 &= 6.44 \times 10^4 \text{ GBq/g} = 174.1 \text{ Ci/g.} \quad (11.56)
 \end{aligned}$$

(b) The sum of masses of individual components of a nucleus that contains Z protons and $A - Z$ neutrons is larger than the actual mass of the nucleus. This difference in mass is called the mass defect (deficit) Δm and its energy equivalent Δmc^2 is called the total binding energy E_B of the given nucleus (Z, A). The binding energy per nucleon E_B/A of a nucleus, i.e., the total binding energy of a nucleus E_B divided by the number of nucleons A , varies with the number of nucleons, is of the order of $\sim 8 \text{ MeV/nucleon}$, and is determined as follows

$$\frac{E_B}{A} = \frac{\Delta mc^2}{A} = \frac{Zm_p c^2 + (A - Z)m_n c^2 - Mc^2}{A}, \quad (11.57)$$

where $m_p c^2$ is the proton rest energy (938.272013 MeV), $m_n c^2$ is the neutron rest energy (939.565346 MeV), and Mc^2 is the rest energy of nucleus (Z, A).

(1) Binding energy per nucleon of cobalt-60 ($Z = 27, A = 60$):

$$\begin{aligned}
 \left. \frac{E_B}{A} \right|_{\text{Co-60}} &= \frac{27 \times 938.272013 \text{ MeV} + 33 \times 939.565346 \text{ MeV} - 55814.2014 \text{ MeV}}{60} \\
 &= \frac{524.7994 \text{ MeV}}{60} = 8.7467 \text{ MeV.} \quad (11.58)
 \end{aligned}$$

(2) Binding energy per nucleon of iodine-131 ($Z = 53, A = 131$):

$$\begin{aligned}
 \left. \frac{E_B}{A} \right|_{\text{I-131}} &= \frac{53 \times 938.272013 \text{ MeV} + 78 \times 939.565346 \text{ MeV} - 121911.1907 \text{ MeV}}{131} \\
 &= \frac{1103.32300 \text{ MeV}}{131} = 8.4223 \text{ MeV.} \quad (11.59)
 \end{aligned}$$

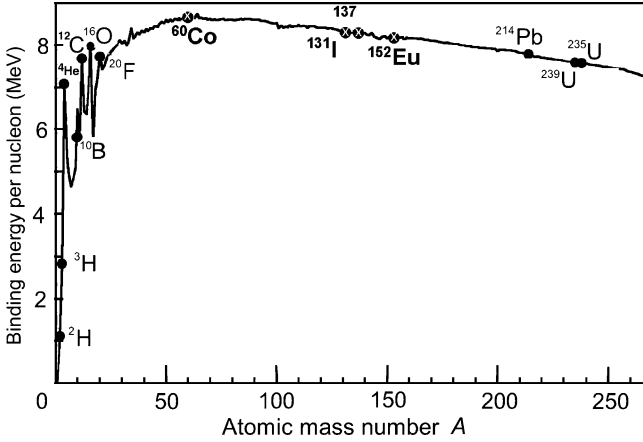


Fig. 11.3 Binding energy per nucleon E_B/A in MeV/nucleon against atomic mass number A

- (3) Binding energy per nucleon of cesium-137 ($Z = 55$, $A = 137$):

$$\begin{aligned} \left. \frac{E_B}{A} \right|_{\text{Cs-137}} &= \frac{55 \times 938.272013 \text{ MeV} + 82 \times 939.565346 \text{ MeV} - 127500.0283 \text{ MeV}}{137} \\ &= \frac{1149.2908 \text{ MeV}}{137} = 8.389 \text{ MeV}. \end{aligned} \quad (11.60)$$

- (4) Binding energy per nucleon of europium-152 ($Z = 63$, $A = 152$):

$$\begin{aligned} \left. \frac{E_B}{A} \right|_{\text{Eu-152}} &= \frac{63 \times 938.272013 \text{ MeV} + 89 \times 939.565346 \text{ MeV} - 141480.2400 \text{ MeV}}{152} \\ &= \frac{1252.21613 \text{ MeV}}{152} = 8.238 \text{ MeV}. \end{aligned} \quad (11.61)$$

Figure 11.3 plots binding energy per nucleon against atomic mass number A in the range of A from 1 to 250. Results calculated in (b) for Co-60, I-131, Cs-137, and Eu-152 are also shown. In general, the larger is the binding energy per nucleon E_B/A of an atom, the larger is the stability of its nucleus. Thus, the most stable nuclei in nature are the ones with $A \approx 60$ (iron, cobalt, and nickel).

(c) Beta minus Q value also known as β^- decay energy Q_{β^-} can be determined either with the atomic rest energy method or with the nuclear rest energy method, which, respectively, can be expressed as follows

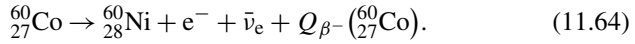
$$Q_{\beta^-}(\text{P}) = \{M(Z, A) - M(Z + 1, A)\}c^2 \quad (11.62)$$

and

$$Q_{\beta^-}(\text{P}) = \{M(Z, A) - M(Z + 1, A) - m_e\}c^2, \quad (11.63)$$

where P stands for parent nucleus with atomic number Z and atomic mass number A , M stands for nuclear rest mass, \mathcal{M} stands for atomic rest mass, and m_e is the rest mass of the electron.

- (1) Beta minus decay energy Q_{β^-} for cobalt-60 decay into nickel-60 ($t_{1/2} = 5.26$ a)



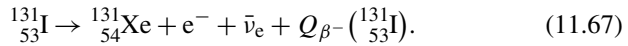
Atomic rest energy method

$$\begin{aligned} Q_{\beta^-}({}^{60}_{27}\text{Co}) &= \{\mathcal{M}(Z, A) - \mathcal{M}(Z + 1, A)\}c^2 = \{\mathcal{M}({}^{60}_{27}\text{Co}) - \mathcal{M}({}^{60}_{28}\text{Ni})\}c^2 \\ &= [59.933822u - 59.930791u]c^2 \\ &= 3.031 \times 10^{-3} \times (931.494028 \text{ MeV}) = 2.824 \text{ MeV}. \end{aligned} \quad (11.65)$$

Nuclear rest energy method

$$\begin{aligned} Q_{\beta^-}({}^{60}_{27}\text{Co}) &= \{M(Z, A) - M(Z + 1, A) - m_e\}c^2 \\ &= \{M({}^{60}_{27}\text{Co}) - M({}^{60}_{28}\text{Ni}) - m_e\}c^2 \\ &= 55814.2014 \text{ MeV} - 55810.8665 \text{ MeV} - 0.5110 \text{ MeV} \\ &= 2.824 \text{ MeV}. \end{aligned} \quad (11.66)$$

- (2) Beta minus decay energy Q_{β^-} for iodine-131 decay into xenon-131 ($t_{1/2} = 8.02$ d)



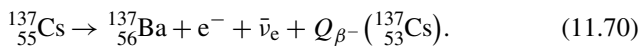
Atomic rest energy method

$$\begin{aligned} Q_{\beta^-}({}^{131}_{53}\text{I}) &= \{\mathcal{M}(Z, A) - \mathcal{M}(Z + 1, A)\}c^2 = \{\mathcal{M}({}^{131}_{53}\text{I}) - \mathcal{M}({}^{131}_{54}\text{Xe})\}c^2 \\ &= [130.906125u - 130.905082u]c^2 \\ &= 1.043 \times 10^{-3} \times (931.494028 \text{ MeV}) = 0.972 \text{ MeV}. \end{aligned} \quad (11.68)$$

Nuclear rest energy method

$$\begin{aligned} Q_{\beta^-}({}^{131}_{53}\text{I}) &= \{M(Z, A) - M(Z + 1, A) - m_e\}c^2 \\ &= \{M({}^{131}_{53}\text{I}) - M({}^{131}_{54}\text{Xe}) - m_e\}c^2 \\ &= 121911.1907 \text{ MeV} - 121909.7081 \text{ MeV} - 0.5110 \text{ MeV} \\ &= 0.972 \text{ MeV}. \end{aligned} \quad (11.69)$$

- (3) Beta minus decay energy Q_{β^-} for cesium-137 decay into barium-137 ($t_{1/2} = 30$ a)



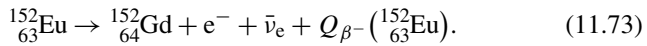
Atomic rest energy method

$$\begin{aligned} Q_{\beta^-}({}^{137}_{55}\text{Cs}) &= \{\mathcal{M}(Z, A) - \mathcal{M}(Z + 1, A)\}c^2 = \{\mathcal{M}({}^{137}_{55}\text{Cs}) - \mathcal{M}({}^{137}_{56}\text{Ba})\}c^2 \\ &= [136.907084u - 136.905821u]c^2 \\ &= 1.263 \times 10^{-3} \times (931.494028 \text{ MeV}) = 1.176 \text{ MeV}. \end{aligned} \quad (11.71)$$

Nuclear rest energy method

$$\begin{aligned} Q_{\beta^-}({}^{137}_{55}\text{Cs}) &= \{M(Z, A) - M(Z + 1, A) - m_e\}c^2 \\ &= \{M({}^{137}_{55}\text{Cs}) - M({}^{137}_{56}\text{Ba}) - m_e\}c^2 \\ &= 127500.0283 \text{ MeV} - 127498.3408 \text{ MeV} \\ &\quad - 0.5110 \text{ MeV} = 1.176 \text{ MeV}. \end{aligned} \quad (11.72)$$

- (4) Beta minus decay energy Q_{β^-} for europium-152 decay into gadolinium-152 ($t_{1/2} = 13.52 \text{ a}$)



Atomic rest energy method

$$\begin{aligned} Q_{\beta^-}({}^{152}_{63}\text{Eu}) &= \{\mathcal{M}(Z, A) - \mathcal{M}(Z + 1, A)\}c^2 = \{\mathcal{M}({}^{152}_{63}\text{Eu}) - \mathcal{M}({}^{152}_{64}\text{Gd})\}c^2 \\ &= [151.921745u - 151.919791u]c^2 \\ &= 1.954 \times 10^{-3} \times (931.494028 \text{ MeV}) = 1.820 \text{ MeV}. \end{aligned} \quad (11.74)$$

Nuclear rest energy method

$$\begin{aligned} Q_{\beta^-}({}^{152}_{63}\text{Eu}) &= \{M(Z, A) - M(Z + 1, A) - m_e\}c^2 \\ &= \{M({}^{152}_{63}\text{Eu}) - M({}^{152}_{64}\text{Gd}) - m_e\}c^2 \\ &= 141482.0052 \text{ MeV} - 141479.6741 \text{ MeV} - 0.5110 \text{ MeV} \\ &= 1.820 \text{ MeV}. \end{aligned} \quad (11.75)$$

Beta minus decay energy $Q_{\beta^-}(\text{P})$ was calculated for four radionuclides (Co-60, I-131, Cs-137, and Eu-152) that decay with β^- decay and are of importance in medical physics, three of them (Co-60, Cs-137, and Eu-152) as radiation sources for external beam radiotherapy and I-131 for thyroid imaging or ablation. Europium-152 has not been used clinically yet, however, studies have shown its potential usefulness as radiation source. In addition to β^- decay (27.9 %), Eu-152 also decays with electron capture (72.1 %) and β^+ decay (0.03 %). The other three radionuclides decay only through β^- decay (100 %).

Decay energies $Q_{\beta^-}(\text{P})$ for the four radionuclides were calculated with the atomic rest energy method and with the nuclear rest energy method. For a given radionuclide both methods gave identical results, as shown above.

Table 11.2 Various nuclear parameters for four radionuclides of importance to medical physics

(1)	Radionuclide	Specific activity a (Ci/g)	Binding energy per nucleon E_B/A (MeV)	Beta minus decay energy Q_{β^-} (MeV)
(2)	Cobalt-60	1133	8.75	2.824
(3)	Iodine-131	124280	8.42	0.972
(4)	Cesium-137	87	8.39	1.176
(5)	Europium-152	174	8.24	1.820

(d) Summary of results on specific activity a , binding energy per nucleon E_B/A , and β^- decay energy Q_{β^-} for radionuclides: cobalt-60, iodine-131, cesium-137, and europium-152 is presented in Table 11.2.

11.5 Beta Plus Decay

11.5.Q1

(230)

Beta plus (β^+) decay is characterized by the production of positrons that appear in a spectral distribution with maximum positron energy specific to the particular β^+ decay. As in the β^- decay, the daughter recoil kinetic energy in β^+ decay is essentially negligible. Radionuclides undergoing β^+ decay are often called positron emitters and are used in medicine for functional imaging with a special imaging technique called positron emission tomography (PET).

- (a) List at least 5 positron emitting radionuclides that can be attached to biological markers and used in PET imaging.
- (b) Briefly discuss the main characteristics of PET imaging:
 - (1) Information that it provides.
 - (2) Production of radionuclides for use in PET studies.
 - (3) Acquisition of PET scans.
- (c) State expressions for β^+ decay energy Q_{β^+} (Q value of β^+ decay) based on:
 - (1) Nuclear rest energy of parent P and daughter D.
 - (2) Atomic rest energy of parent P and daughter D.
- (d) Show a schematic representation of a typical radioactive beta plus β^+ decay transition from a parent nucleus P(Z, A) to ground state of a daughter nucleus D($Z - 1, A$) based on:

- (1) Atomic rest energies.
- (2) Nuclear rest energies.

Appropriate atomic and nuclear data are available from Appendix A. Show the correspondence between the two graphs.

SOLUTION:

The most frequently used positron emitters are: carbon-11 ($^{11}_6\text{C}$); nitrogen-13 ($^{13}_7\text{N}$); oxygen-15 ($^{15}_8\text{O}$); fluorine-18 ($^{18}_9\text{F}$); and rubidium-82 ($^{82}_{37}\text{Rb}$).

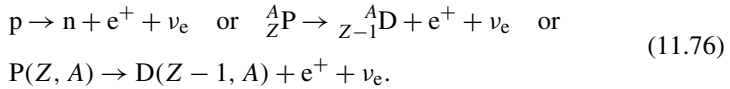
Of these, fluorine-18 is the most frequently used radionuclide in PET scanning. It is applied for labeling the deoxyglucose biological marker thereby forming the radiopharmaceutical fluorodeoxyglucose (FDG) for use in studies involving glucose metabolism in cancer diagnosis.

(b) Main characteristics of PET imaging are as follows:

- (1) PET is a nuclear medicine molecular imaging technique that provides information on metabolic function of organs or tissues by detecting how cells process certain compounds such as, for example, glucose. Cancer cells metabolize glucose at a much higher rate than normal tissues. By detecting increased radiolabelled glucose metabolism with a high degree of sensitivity, PET identifies cancerous cells, even at an early stage when other imaging modalities may miss them.
- (2) The radionuclides used in PET studies are most commonly produced by bombardment of an appropriate stable nuclide with protons from a cyclotron thereby producing positron-emitting radionuclides that are subsequently used for labeling biochemical substances and producing radioactive tracers. Another means of production of proton-rich radionuclides is by using a suitable generator, such as, for example, a rubidium-82 generator containing strontium-82 that decays by electron capture into positron emitting rubidium-82.
- (3) In a PET study one administers a positron-emitting radionuclide by injection or inhalation. The radionuclide circulates through the bloodstream to reach a particular organ. The positrons emitted by the radionuclide have a very short range in tissue (of the order of 1 mm) and undergo annihilation with an available atomic orbital electron typically at the end of their tracks. This process generally results in emission of two gamma photons called annihilation quanta, each with energy of 0.511 MeV, moving away from the point of production in nearly opposite directions.
- (4) Decay events are detected by coincidence detection of the annihilation quanta with a timing window of the order of few nanoseconds. Typical detectors are scintillators coupled with a photomultiplier tube (PMT) or photodiode and

arranged in a ring about the patient. The line connecting the two detectors triggered in coincidence is called the coincidence line and many such lines are formed during acquisition of a PET scan. Spatial activity distribution in the organ of interest within the field-of-view is reconstructed from the measured projections with the help of mathematical algorithms.

(c) Beta plus (β^+) decay is characterized by a spontaneous transformation of a proton into a neutron in a proton-rich nucleus concurrently with ejection of a positron and electronic neutrino



Similarly to the case of nuclear reaction, α decay, and β^- decay, the decay energy $Q_{\beta^+}(\text{P})$ for beta plus decay can be determined either with (1) nuclear rest energy method or (2) atomic rest energy method.

(1) In the *nuclear rest energy method*, one subtracts the sum of rest energies of decay products after the β^+ decay (daughter D, positron e^+ , and electronic neutrino ν_e) from the rest energy of the parent nucleus $M(\text{P})c^2$. Decay energy $Q_{\beta^+}(\text{P})$ for the β^+ decay process must be positive for β^+ decay to occur and is given in terms of nuclear rest mass M as follows

$$Q_{\beta^+}(\text{P}) = M(\text{P})c^2 - \sum_i M_i c^2 = \{M(Z, A) - [M(Z - 1, A) + m_e + 0]\}c^2, \quad (11.77)$$

where the term in square brackets represents the sum of nuclear rest masses of decay products: daughter $M(Z - 1, A)$, positron m_e , and 0 representing the rest mass of neutrino. However, in terms of nuclear rest masses, the condition $Q_{\beta^+} > 0$ is a necessary but not sufficient condition for β^+ decay to occur.

As indicated in (11.77), β^+ decay can occur to a proton-rich unstable parent nucleus only when the mass $M(Z, A)$ of the parent P nucleus exceeds the mass $M(Z - 1, A)$ of the daughter D nucleus by more than one positron rest mass m_e , i.e., $M(Z, A) > M(Z - 1, A) + m_e$.

(2) Adding and subtracting $Zm_e c^2$ to the right-hand side of (11.77) and neglecting the electron binding energies to the nucleus we obtain the following expression for $Q_{\beta^+}(\text{P})$ for the *atomic rest energy method*

$$\begin{aligned} Q_{\beta^+}(\text{P}) &= \{[M(Z, A) + Zm_e] - [M(Z - 1, A) + Zm_e + m_e]\}c^2 \\ &= \{[M(Z, A) + Zm_e] - [M(Z - 1, A) + (Z - 1)m_e + 2m_e]\}c^2 \\ &= \{\mathcal{M}(Z, A) - [\mathcal{M}(Z - 1, A) + 2m_e]\}c^2, \end{aligned} \quad (11.78)$$

where $M(Z, A)$ and $M(Z - 1, A)$ stand for nuclear rest masses of the parent and daughter, respectively, and $\mathcal{M}(Z, A)$ and $\mathcal{M}(Z - 1, A)$ stand for atomic

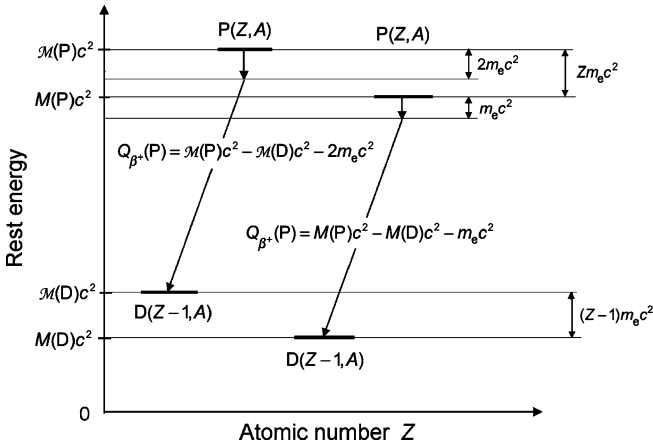


Fig. 11.4 Schematic diagram for β^+ decay; atomic rest energy *on the left* and nuclear rest energy *on the right*

rest masses of the parent and daughter, respectively, noting that the following expressions link atomic and nuclear masses, \mathcal{M} and M , respectively

$$\mathcal{M}(Z, A) = M(Z, A) + Zm_e \tag{11.79}$$

and

$$\mathcal{M}(Z - 1, A) = M(Z - 1, A) + (Z - 1)m_e. \tag{11.80}$$

From (11.78) a conclusion can be made that, for β^+ decay to occur, the atomic mass of the parent $\mathcal{M}(Z, A)$ must exceed the atomic mass of the daughter $\mathcal{M}(Z - 1, A)$ by more than two positron rest masses, or, in terms of rest energies

$$\mathcal{M}(Z, A)c^2 > \mathcal{M}(Z - 1, A)c^2 + 2m_e c^2. \tag{11.81}$$

(d) From (11.77) and (11.78) we note that $Q_{\beta^+}(P)$ can be expressed in terms of nuclear masses M or in terms of atomic masses \mathcal{M} of parent $P(Z, A)$ and daughter $D(Z - 1, A)$ as follows

$$\begin{aligned} Q_{\beta^+}(P) &= \{M(Z, A) - [M(Z - 1, A) + m_e]\}c^2 \\ &= \{\mathcal{M}(Z, A) - [\mathcal{M}(Z - 1, A) + 2m_e]\}c^2. \end{aligned} \tag{11.82}$$

A schematic diagram of β^+ decay is shown in Fig. 11.4 using atomic masses on the left and nuclear masses on the right for the parent $P(Z, A)$ and daughter $D(Z - 1, A)$. Of course, both methods must yield identical results for $Q_{\beta^+}(P)$, as evident from the two energy level diagrams in Fig. 11.4. The magnitude of $Q_{\beta^+}(P)$ resulting from the atomic rest energy method in the left diagram is identical to that resulting from the nuclear rest energy method shown in the right diagram.

11.5.Q2

(231)

The most frequently used positron emitters in clinical studies with PET scanners are: carbon-11 (C-11), nitrogen-13 (N-13), oxygen-15 (O-15), fluorine-18 (F-18), and rubidium-82 (Rb-82).

- (a) Determine the beta plus decay energy Q_{β^+} (also known as the Q value for β^+ decay) for the five most frequently used positron emitters: C-11, N-13, O-15, F-18, and Rb-82. In your calculation of Q_{β^+} (P) use both the atomic rest energy method as well as the nuclear rest energy method and convince yourself that both methods provide the identical results for a given radionuclide. Appropriate atomic and nuclear data are provided in Appendix A.
- (b) Determine the maximum energy $[(E_K)_\beta]_{\max}$ of the positron emitted in β^+ decay of positron emitters listed in (a).
- (c) Prepare a table in which you list for the 5 most frequently used positron emitters of (a) and (b) the following parameters: Row (1): positron emitter; row (2): atomic number Z ; row (3): atomic mass number A ; row (4): half-life $t_{1/2}$; row (5): daughter product; row (6): decay energy Q_{β^+} ; row (7): maximum positron energy $[(E_K)_\beta]_{\max}$ normalized to Q_{β^+} ; row (8): maximum recoil kinetic energy of the daughter $[(E_K)_D]_{\max}$ normalized to Q_{β^+} ; row (9): means of production (machine); and row (10): means of production (nuclear reaction).

If you do not know certain parameters, use available literature to find the answers.

SOLUTION:

(a) Q value for β^+ decay of positron emitters is determined either with the atomic rest energy method or with the nuclear rest energy method. The two methods were studied in detail in Prob. 232 and their relevant expressions can be summarized as follows:

- (1) For the atomic rest energy method with \mathcal{M} designating atomic mass

$$\begin{aligned} Q_{\beta^+}(\text{P}) &= \mathcal{M}(\text{P})c^2 - [\mathcal{M}(\text{D}) + 2m_e]c^2 \\ &= \mathcal{M}(Z, A)c^2 - [\mathcal{M}(Z - 1, A) + 2m_e]c^2. \end{aligned} \quad (11.83)$$

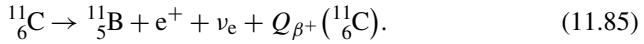
- (2) For the nuclear rest energy method with M designating nuclear mass

$$Q_{\beta^+}(\text{P}) = M(\text{P})c^2 - [M(\text{D}) + m_e]c^2 = M(Z, A)c^2 - [M(Z - 1, A) + m_e]c^2. \quad (11.84)$$

Of course, both methods are expected to give identical results when used to calculate $Q_{\beta^+}(P)$ for the same positron emitter. We will use both methods in the calculation of $Q_{\beta^+}(P)$.

(1) **Carbon-11** is a positron emitter produced in a cyclotron by bombardment of nitrogen-14 with a proton beam resulting in the following nuclear reaction: ${}^{14}_7\text{N}(p, \alpha){}^{11}_6\text{C}$.

The beta plus decay of C-11 proceeds as follows:



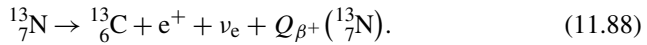
Decay energy $Q_{\beta^+}({}^{11}_6\text{C})$ is calculated with the atomic rest energy \mathcal{M} and nuclear rest energy M

$$\begin{aligned} Q_{\beta^+}({}^{11}_6\text{C}) &= [\mathcal{M}({}^{11}_6\text{C}) - \mathcal{M}({}^{11}_5\text{B}) - 2m_e]c^2 \\ &= [11.011434u - 11.009305u]c^2 - 2m_e c^2 \\ &= (2.129 \times 10^{-3}u) \times (931.494028 \text{ MeV}/u) - 1.022 \text{ MeV} \\ &= 0.960 \text{ MeV}, \end{aligned} \quad (11.86)$$

$$\begin{aligned} Q_{\beta^+}({}^{11}_6\text{C}) &= M({}^{11}_6\text{C})c^2 - M({}^{11}_5\text{B})c^2 - m_e c^2 \\ &= 10254.0190 \text{ MeV} - 10252.5469 \text{ MeV} - 0.511 \text{ MeV} \\ &= 0.960 \text{ MeV}. \end{aligned} \quad (11.87)$$

(2) **Nitrogen-13** is a positron emitter produced in a cyclotron by bombardment of oxygen-16 with a proton beam resulting in the following nuclear reaction: ${}^{16}_8\text{O}(p, \alpha){}^{13}_7\text{N}$.

The beta plus decay of N-13 proceeds as follows:



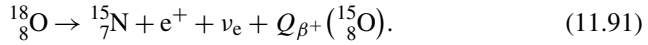
Decay energy $Q_{\beta^+}({}^{13}_7\text{N})$ is calculated with the atomic rest energy \mathcal{M} and nuclear rest energy M

$$\begin{aligned} Q_{\beta^+}({}^{13}_7\text{N}) &= [\mathcal{M}({}^{13}_7\text{N}) - \mathcal{M}({}^{13}_6\text{C}) - 2m_e]c^2 \\ &= [13.005739u - 13.003355u]c^2 - 2m_e c^2 \\ &= (2.384 \times 10^{-3}u) \times (931.494028 \text{ MeV}/u) - 1.022 \text{ MeV} \\ &= 1.198 \text{ MeV}, \end{aligned} \quad (11.89)$$

$$\begin{aligned} Q_{\beta^+}({}^{13}_7\text{N}) &= M({}^{13}_7\text{N})c^2 - M({}^{13}_6\text{C})c^2 - m_e c^2 \\ &= 12111.1910 \text{ MeV} - 12109.4816 \text{ MeV} - 0.511 \text{ MeV} \\ &= 1.198 \text{ MeV}. \end{aligned} \quad (11.90)$$

(3) **Oxygen-15** is a positron emitter produced in a cyclotron by bombardment of nitrogen-15 with a proton beam resulting in the following nuclear reactions $^{15}_7\text{N}(p, n)^{15}_8\text{O}$ or by bombardment of nitrogen-14 with a deuteron beam resulting in the following reaction: $^{15}_7\text{N}(d, n)^{15}_8\text{O}$.

The beta plus decay of O-15 proceeds as follows:



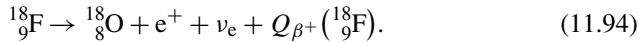
Decay energy $Q_{\beta^+}(^{15}_8\text{O})$ is calculated with the atomic rest energy \mathcal{M} and nuclear rest energy M

$$\begin{aligned} Q_{\beta^+}(^{15}_8\text{O}) &= [\mathcal{M}(^{15}_8\text{O}) - \mathcal{M}(^{15}_7\text{N}) - 2m_e]c^2 \\ &= [15.003066u - 15.000109]c^2 - 2m_e c^2 \\ &= (2.957 \times 10^{-3}u) \times (931.494028 \text{ MeV}/u) - 1.022 \text{ MeV} \\ &= 1.732 \text{ MeV}, \end{aligned} \quad (11.92)$$

$$\begin{aligned} Q_{\beta^+}(^{15}_8\text{O}) &= M(^{15}_8\text{O})c^2 - M(^{15}_7\text{N})c^2 - m_e c^2 \\ &= 13971.1784 \text{ MeV} - 13968.9350 \text{ MeV} - 0.511 \text{ MeV} \\ &= 1.732 \text{ MeV}. \end{aligned} \quad (11.93)$$

(4) **Fluorine-18** is a positron emitter produced in a cyclotron by bombardment of oxygen-18 with a proton beam resulting in the following nuclear reaction: $^{18}_8\text{O}(p, n)^{18}_9\text{F}$.

The beta plus decay of F-18 proceeds as follows:



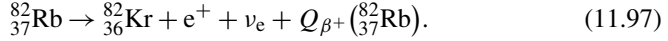
Decay energy $Q_{\beta^+}(^{18}_9\text{F})$ is calculated with the atomic rest energy \mathcal{M} and nuclear rest energy M

$$\begin{aligned} Q_{\beta^+}(^{18}_9\text{F}) &= [\mathcal{M}(^{18}_9\text{F}) - \mathcal{M}(^{18}_8\text{O}) - 2m_e]c^2 \\ &= [18.000938u - 17.999160]c^2 - 2m_e c^2 \\ &= (1.778 \times 10^{-3}u) \times (931.494028 \text{ MeV}/u) - 1.022 \text{ MeV} \\ &= 0.634 \text{ MeV}, \end{aligned} \quad (11.95)$$

$$\begin{aligned} Q_{\beta^+}(^{18}_9\text{F}) &= M(^{18}_9\text{F})c^2 - M(^{18}_8\text{O})c^2 - m_e c^2 \\ &= 16763.1673 \text{ MeV} - 16762.0221 \text{ MeV} - 0.511 \text{ MeV} \\ &= 0.634 \text{ MeV}. \end{aligned} \quad (11.96)$$

(5) **Rubidium-82** is a positron emitter produced in a rubidium-82 generator by electron capture decay of strontium-82 ($t_{1/2} = 25.4$ d) through the following decay reaction ${}_{38}^{82}\text{Sr} + e^- = {}_{37}^{82}\text{Rb} + \nu_e$.

The beta plus decay of Rb-82 proceeds as follows:



Decay energy $Q_{\beta^+}({}_{37}^{82}\text{Rb})$ is calculated with the atomic rest energy \mathcal{M} and nuclear rest energy M

$$\begin{aligned} Q_{\beta^+}({}_{37}^{82}\text{Rb}) &= [\mathcal{M}({}_{37}^{82}\text{Rb}) - \mathcal{M}({}_{36}^{82}\text{Kr}) - 2m_e]c^2 \\ &= [81.918209u - 81.913484]c^2 - 2m_e c^2 \\ &= (4.725 \times 10^{-3}u) \times (931.494028 \text{ MeV}/u) - 1.022 \text{ MeV} \\ &= 3.379 \text{ MeV}, \end{aligned} \quad (11.98)$$

$$\begin{aligned} Q_{\beta^+}({}_{37}^{82}\text{Rb}) &= M({}_{37}^{82}\text{Rb})c^2 - M({}_{36}^{82}\text{Kr})c^2 - m_e c^2 \\ &= 76287.4155 \text{ MeV} - 76283.5252 \text{ MeV} - 0.511 \text{ MeV} \\ &= 3.379 \text{ MeV}. \end{aligned} \quad (11.99)$$

(b) In the first approximation, maximum kinetic energy $[(E_K)_\beta]_{\max}$ of the positron emitted in β^+ decay can be considered equal to the decay energy Q_{β^+} , neglecting the exceedingly small recoil kinetic energy $[(E_K)_D]_{\max}$ of the daughter atom. If, however, recoil energy $[(E_K)_D]_{\max}$ is not neglected, then $[(E_K)_\beta]_{\max}$ is slightly smaller than Q_{β^+} and given as (T11.23)

$$[(E_K)_\beta]_{\max} = \mathcal{M}(D)c^2 \left[1 + \frac{m_e c^2}{\mathcal{M}(D)c^2} \right] \left\{ \sqrt{1 + \frac{2Q_{\beta^+}}{\mathcal{M}(D)c^2} \left[1 + \frac{m_e c^2}{\mathcal{M}(D)c^2} \right]^{-2}} - 1 \right\}. \quad (11.100)$$

Recognizing that $m_e c^2 \ll \mathcal{M}(D)c^2$, we simplify (11.100) to read

$$[(E_K)_\beta]_{\max} \approx Q_{\beta^+} \left[1 - \frac{m_e c^2}{\mathcal{M}(D)c^2} \right] \quad (11.101)$$

and we will use this approximation to determine maximum energy $[(E_K)_\beta]_{\max}$ of the beta particle for the five positron emitters used most frequently in clinical PET scanning.

(1) **Carbon-11** ${}_{6}^{11}\text{C} \rightarrow {}_{5}^{11}\text{B} + e^+ + \nu_e + Q_{\beta^+}({}_{6}^{11}\text{C})$, $Q_{\beta^+}({}_{6}^{11}\text{C}) = 0.960$ MeV

$$[(E_K)_\beta]_{\max} \approx Q_{\beta^+}({}_{6}^{11}\text{C}) \left[1 - \frac{m_e c^2}{\mathcal{M}({}_{6}^{11}\text{C})c^2} \right]$$

$$\begin{aligned}
 &= Q_{\beta^+}({}^{11}_6\text{C}) \left[1 - \frac{0.511}{11.009305 \times 931.494} \right] \\
 &= Q_{\beta^+}({}^{11}_6\text{C}) [1 - 4.98 \times 10^{-5}]. \quad (11.102)
 \end{aligned}$$

(2) **Nitrogen-13** ${}^{13}_7\text{N} \rightarrow {}^{13}_6\text{C} + e^+ + \nu_e + Q_{\beta^+}({}^{13}_7\text{N})$, $Q_{\beta^+}({}^{13}_7\text{N}) = 1.198 \text{ MeV}$

$$\begin{aligned}
 [(E_K)_\beta]_{\max} &\approx Q_{\beta^+}({}^{13}_7\text{N}) \left[1 - \frac{m_e c^2}{\mathcal{M}({}^{13}_6\text{C})c^2} \right] \\
 &= Q_{\beta^+}({}^{13}_7\text{N}) \times \left[1 - \frac{0.511}{13.003355 \times 931.494} \right] \\
 &= Q_{\beta^+}({}^{13}_7\text{N}) \times [1 - 4.22 \times 10^{-5}]. \quad (11.103)
 \end{aligned}$$

(3) **Oxygen-15** ${}^{15}_8\text{O} \rightarrow {}^{15}_7\text{N} + e^+ + \nu_e + Q_{\beta^+}({}^{15}_8\text{O})$, $Q_{\beta^+}({}^{15}_8\text{O}) = 1.732 \text{ MeV}$

$$\begin{aligned}
 [(E_K)_\beta]_{\max} &\approx Q_{\beta^+}({}^{15}_8\text{O}) \left[1 - \frac{m_e c^2}{\mathcal{M}({}^{15}_7\text{N})c^2} \right] \\
 &= Q_{\beta^+}({}^{15}_8\text{O}) \left[1 - \frac{0.511}{15.000109 \times 931.494} \right] \\
 &= Q_{\beta^+}({}^{15}_8\text{O}) [1 - 3.66 \times 10^{-5}]. \quad (11.104)
 \end{aligned}$$

(4) **Fluorine-18** ${}^{18}_9\text{F} \rightarrow {}^{18}_8\text{O} + e^+ + \nu_e + Q_{\beta^+}({}^{18}_9\text{F})$, $Q_{\beta^+}({}^{18}_9\text{F}) = 0.634 \text{ MeV}$

$$\begin{aligned}
 [(E_K)_\beta]_{\max} &\approx Q_{\beta^+}({}^{18}_9\text{F}) \left[1 - \frac{m_e c^2}{\mathcal{M}({}^{18}_8\text{O})c^2} \right] \\
 &= Q_{\beta^+}({}^{18}_9\text{F}) \left[1 - \frac{0.511}{17.999160 \times 931.494} \right] \\
 &= Q_{\beta^+}({}^{18}_9\text{F}) [1 - 3.05 \times 10^{-5}]. \quad (11.105)
 \end{aligned}$$

(5) **Rubidium-82** ${}^{82}_{37}\text{Rb} \rightarrow {}^{82}_{36}\text{Kr} + e^+ + \nu_e + Q_{\beta^+}({}^{82}_{37}\text{Rb})$, $Q_{\beta^+}({}^{82}_{37}\text{Rb}) = 3.379 \text{ MeV}$

$$\begin{aligned}
 [(E_K)_\beta]_{\max} &\approx Q_{\beta^+}({}^{82}_{37}\text{Rb}) \left[1 - \frac{m_e c^2}{\mathcal{M}({}^{82}_{36}\text{Kr})c^2} \right] \\
 &= Q_{\beta^+}({}^{82}_{37}\text{Rb}) \left[1 - \frac{0.511}{81.913484 \times 931.494} \right] \\
 &= Q_{\beta^+}({}^{82}_{37}\text{Rb}) [1 - 0.67 \times 10^{-5}]. \quad (11.106)
 \end{aligned}$$

(c) Table 11.3 presents various characteristics of the positron emitting radionuclides most frequently used in clinical PET scanning: carbon-11, nitrogen-13, oxygen-15, fluorine-18, and rubidium-82.

Table 11.3 Various characteristics of five positron emitters most frequently used for clinical PET scanning

1	Positron emitter	Carbon-11	Nitrogen-13	Oxygen-15	Fluorine-18	Rubidium-82
2	Atomic number Z	6	7	8	9	37
3	Atomic mass A	11	13	15	18	82
4	Half-life $t_{1/2}$	20.4 min	10 min	2.05 min	110 min	1.3 min
5	Daughter product	Boron-11	Carbon-13	Nitrogen-13	Oxygen-18	Krypton-82
6	Decay energy Q_{β^+}	0.960 MeV	1.198 MeV	1.732 MeV	0.634 MeV	3.379 MeV
7	$[(E_K)_{\beta}]_{\max}/Q_{\beta^+}$	$1-4.98 \times 10^{-5}$	$1-4.22 \times 10^{-5}$	$1-3.66 \times 10^{-5}$	$1-3.05 \times 10^{-5}$	$1-0.67 \times 10^{-5}$
8	$[(E_K)_{\beta}]_{\max}/Q_{\beta^+}$	4.98×10^{-5}	4.22×10^{-5}	3.66×10^{-5}	3.05×10^{-5}	0.67×10^{-5}
9	Production machine	Cyclotron	Cyclotron	Cyclotron	Cyclotron	Strontium generator
10	Nuclear reaction	${}^{14}_7\text{N}(p, \alpha){}^{11}_6\text{C}$	${}^{16}_8\text{O}(p, \alpha){}^{13}_7\text{N}$	${}^{15}_7\text{N}(d, n){}^{15}_8\text{O}$	Cyclotron ${}^{18}_8\text{O}(p, n){}^{18}_9\text{F}$	–

11.6 Electron Capture

11.6.Q1

(232)

Electron capture (EC) radioactive decay may occur in proton-rich, unstable parent nuclei, when an atomic electron ventures inside the nuclear volume, is captured by a proton, and triggers a proton to neutron transformation causing ejection of an energetic neutrino. EC decay is a competing process to β^+ decay; however, conditions on EC decay as far as relative atomic masses are concerned are less restrictive than those imposed on β^+ decay that results in positron emission and subsequent positron annihilation with emission of annihilation quanta.

- (a) Derive expressions for EC decay energy based on: (1) nuclear rest energies and (2) atomic rest energies of the parent P and daughter D.
- (b) Compare restrictions on EC decay with those imposed on β^+ decay.
- (c) Derive an expression for energy E_ν of the mono-energetic neutrino emitted in EC decay as a function of EC decay energy Q_{EC} and rest energy $\mathcal{M}(D)c^2$ of the daughter atom. Also derive an expression for the recoil kinetic energy $(E_K)_D$ of the daughter atom in EC decay.

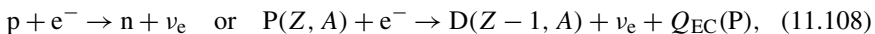
SOLUTION:

(a) Decay energy Q_{EC} or Q value for EC decay is determined from the standard expression for calculating Q value of a nuclear reaction written in its most general format as follows

$$Q_{EC} = \sum_{i, \text{before}} M_i c^2 - \sum_{i, \text{after}} M_i c^2, \quad (11.107)$$

where M stands for nuclear rest masses and the labels “before” and “after” refer to before EC decay and after EC decay, respectively. For EC decay to occur Q_{EC} must be positive.

Electron capture decay is described as follows



indicating that in EC decay parent P and daughter D must have identical atomic mass number A (parent and daughter are said to be isobars) but the atomic number Z decreases by 1 and the number of neutrons increases by 1.

(1) Equation (11.107) is for EC decay expressed in terms of nuclear rest masses M as follows

$$Q_{EC}(P) = [M(P)c^2 + m_e c^2] - [M(D)c^2 + m_{\nu_e} c^2]$$

$$= [M(Z, A)c^2 + m_e c^2] - [M(Z - 1, A) + 0], \quad (11.109)$$

where we make an assumption that the rest energy of neutrino is equal to zero ($m_{\nu_e} c^2 \approx 0$).

From (11.109) we note that for $Q_{EC} > 0$, i.e., for EC decay to occur, the parent nuclear rest energy $M(P)c^2 = M(Z, A)$ combined with the rest energy of an electron $m_e c^2$ must exceed the daughter nuclear rest energy $M(D)c^2 = M(Z - 1, A)$, i.e.,

$$M(P)c^2 + m_e c^2 > M(D)c^2. \quad (11.110)$$

(2) Equation (11.109) expresses EC decay energy in terms of nuclear rest energies as follows

$$Q_{EC}(P) = [M(Z, A)c^2 + m_e c^2] - [M(Z - 1, A)]. \quad (11.111)$$

Adding and subtracting $Zm_e c^2$ to the right hand side of (11.111) and rearranging the terms results in the following

$$\begin{aligned} Q_{EC}(P) &= [M(Z, A)c^2 + Zm_e c^2] - [M(Z - 1, A)c^2 + Zm_e c^2 - m_e c^2] \\ &= [\mathcal{M}(Z, A)c^2] - [\mathcal{M}(Z - 1, A)c^2], \end{aligned} \quad (11.112)$$

where we have used the following standard relationships between atomic rest energy \mathcal{M} and nuclear rest energy M and ignored the binding energy of orbital electrons to the nucleus, as is the standard practice

$$\mathcal{M}(Z, A)c^2 = M(Z, A)c^2 + Zm_e c^2 \quad (11.113)$$

and

$$\mathcal{M}(Z - 1, A)c^2 = M(Z - 1, A)c^2 + (Z - 1)m_e c^2. \quad (11.114)$$

From (11.112) it is evident that, in terms of atomic masses, EC decay can occur if the atomic rest energy of the parent $\mathcal{M}(Z, A)c^2$ exceeds the atomic rest energy of the daughter $\mathcal{M}(Z - 1, A)c^2$

$$\mathcal{M}(Z, A)c^2 > \mathcal{M}(Z - 1, A)c^2. \quad (11.115)$$

Thus, in electron capture decay, the atomic rest energy difference between the parent P and the daughter D is shared between the neutrino and recoil daughter.

(b) EC decay can occur on a proton-rich radionuclide when the parent atomic rest mass $\mathcal{M}(P)$ simply exceeds the daughter atomic rest mass $\mathcal{M}(D)$, i.e., $\mathcal{M}(P) > \mathcal{M}(D)$, in contrast to β^+ decay that is energetically possible only when the parent atomic rest mass $\mathcal{M}(P)$ exceeds that of the daughter $\mathcal{M}(D)$ by a minimum of two electronic masses, i.e., $\mathcal{M}(P) > \mathcal{M}(D) + 2m_e c^2$.

The following additional conditions apply to EC decay:

- (1) When the condition $Q_{EC} > 0$ is satisfied but Q_{β^+} is negative, the β^+ decay will not happen because it is energetically forbidden and EC decay will happen alone.
- (2) When $Q_{\beta^+} > 0$ then Q_{EC} is always positive and both decays (β^+ and EC) can happen. The branching ratios $\lambda_{EC}/\lambda_{\beta^+}$ vary considerably from one radionuclide to another, for example, from a low of 0.03 for fluorine-18 to several hundred for some other proton-rich radionuclides.
- (3) In contrast to β^- and β^+ decay in which three decay products share the decay energy and produce a continuous spectral distribution, in EC decay the two decay products (neutrino and recoil daughter) do not have a continuous spectral distribution; rather they are given discrete (mono-energetic) energies. Mono-energetic neutrinos produce a line spectrum with energy E_ν , while the daughter has a discrete recoil kinetic energy $(E_K)_D$ governed by the EC decay energy Q_{EC} .
- (4) Recall that the three decay products in β^- decay are: electron, antineutrino, and recoil daughter; in β^+ decay they are: positron, neutrino, and recoil daughter. In EC decay there are only two decay products: neutrino and recoil daughter.

(c) In EC decay kinetic energy $(E_K)_D$ of the recoil daughter atom and energy E_ν of the mono-energetic neutrino are determined using conservation of momentum and energy principles.

Conservation of momentum

- (1) Before EC decay the total momentum $\mathbf{p} = 0$ (assuming that the parent atom is stationary).
- (2) After EC decay the total momentum carried by recoil daughter atom \mathbf{p}_D and mono-energetic neutrino \mathbf{p}_ν must also be zero ($\mathbf{p}_D + \mathbf{p}_\nu = 0$), meaning that the two momenta \mathbf{p}_D and \mathbf{p}_ν are opposite in direction and identical in magnitude

$$|\mathbf{p}_D| \equiv p_D = \mathcal{M}(D)v_D = |\mathbf{p}_\nu| \equiv p_\nu = \frac{E_\nu}{c}, \quad \text{or} \quad v_D = \sqrt{\frac{E_\nu}{\mathcal{M}(D)c}}, \quad (11.116)$$

where

$\mathcal{M}(D)$ is the mass of the recoil daughter atom.

v_D is the velocity of the daughter recoil atom.

E_ν is the energy of the mono-energetic neutrino emitted in the EC decay.

Conservation of energy

- (1) Before EC the total energy is the EC decay energy Q_{EC} less the binding energy E_B of the orbital electron that is captured by the nucleus ($Q_{EC} - E_B$).

(2) After EC decay the total available energy ($Q_{\text{EC}} - E_{\text{B}}$) is shared between the two decay products (neutrino and recoil daughter atom)

$$Q_{\text{EC}} - E_{\text{B}} = E_{\nu} + (E_{\text{K}})_{\text{D}}. \quad (11.117)$$

Recoil energy $(E_{\text{K}})_{\text{D}}$ of the daughter atom can be classically expressed as

$$(E_{\text{K}})_{\text{D}} = \frac{p_{\text{D}}^2}{2\mathcal{M}(\text{D})} = \frac{\mathcal{M}(\text{D})v_{\text{D}}^2}{2} = \frac{E_{\nu}^2}{2\mathcal{M}(\text{D})c^2}. \quad (11.118)$$

Inserting (11.118) into (11.117) we now obtain the following quadratic equation for the energy E_{ν} of the mono-energetic neutrino emitted in the EC decay

$$\frac{1}{2\mathcal{M}(\text{D})}E_{\nu}^2 + E_{\nu} - (Q_{\text{EC}} - E_{\text{B}}) = 0, \quad (11.119)$$

with the following physically relevant solution

$$E_{\nu} = \left\{ \sqrt{1 + \frac{2(Q_{\text{EC}} - E_{\text{B}})}{\mathcal{M}(\text{D})c^2}} - 1 \right\} \mathcal{M}(\text{D})c^2. \quad (11.120)$$

Since $2(Q_{\text{EC}} - E_{\text{B}}) \ll \mathcal{M}(\text{D})c^2$, we can simplify (11.120) to read

$$\begin{aligned} E_{\nu} &= \left\{ \sqrt{1 + \frac{2(Q_{\text{EC}} - E_{\text{B}})}{\mathcal{M}(\text{D})c^2}} - 1 \right\} \mathcal{M}(\text{D})c^2 \\ &= \left\{ 1 + \frac{Q_{\text{EC}} - E_{\text{B}}}{\mathcal{M}(\text{D})c^2} + \dots - 1 \right\} \mathcal{M}(\text{D})c^2 = Q_{\text{EC}} - E_{\text{B}}. \end{aligned} \quad (11.121)$$

Incorporating (11.121) into (11.118) recoil kinetic energy of the daughter atom $(E_{\text{K}})_{\text{D}}$ is now expressed as follows

$$(E_{\text{K}})_{\text{D}} = \frac{E_{\nu}^2}{2\mathcal{M}(\text{D})c^2} = \frac{(Q_{\text{EC}} - E_{\text{B}})^2}{2\mathcal{M}(\text{D})c^2}. \quad (11.122)$$

Equations (11.121) and (11.122) express the energy E_{ν} of the mono-energetic neutrino and the recoil kinetic energy $(E_{\text{K}})_{\text{D}}$ of the daughter atom as a function of the EC decay energy Q_{EC} . However, since in many EC situations the binding energy of K or L shell orbital electrons is much smaller than the EC decay energy ($E_{\text{B}} \ll Q_{\text{EC}}$), we can, in the first approximation, assume that $E_{\nu} \approx Q_{\text{EC}}$ and $(E_{\text{K}})_{\text{D}} \approx 0$. This means that the energy of the mono-energetic neutrino is assumed to be equal to the EC decay energy.

11.6.Q2

(233)

Iridium-192 ($^{192}_{77}\text{Ir}$) serves as an important radiation source in remote after-loading brachytherapy. It decays with a half-life of 74 days into either stable platinum-192 ($^{192}_{78}\text{Pt}$) or stable osmium-192 ($^{192}_{76}\text{Os}$). The iridium source is produced in a nuclear reactor through a thermal neutron activation process on stable iridium-191.

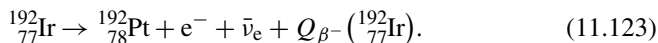
- (a) Establish which nuclear decay processes may be involved in the decay of iridium-192 into daughter products platinum-192 and osmium-192.
- (b) For iridium-192 calculate the decay energies for the decay processes established in (a). Relevant data for Ir-192, Os-192, and Pt-192 are available in Appendix A.
- (c) For each decay process of iridium-192 determined in (b) calculate energies of all decay products.

SOLUTION:

(a) There are 8 major radioactive decays that may possibly play a role in the decay of Ir-192 into Os-192 and Pt-192. The 8 decays are listed in Table 11.4 and, for each decay, the table lists ΔZ , the change in atomic number Z , and ΔA , the change in atomic mass number A . A cursory analysis of ΔZ and ΔA for the decay of Ir-192 into either Os-192 or Pt-192 shows that ΔA for both decays is 0, while for the decay Ir-192 \rightarrow Os-192 the change in Z is $\Delta Z = +1$ and for the decay Ir-192 \rightarrow Pt-192 it is $\Delta Z = -1$.

A comparison of these findings with data of Table 11.4 shows that 4 out of 8 decays satisfy the $\Delta Z = \pm 1$ condition and that 5 out of 8 decays satisfy the $\Delta A = 0$ condition. However, only 3 out of 8 decays (β^- , β^+ and EC) satisfy both conditions simultaneously and we conclude that, out of potential 8 decay processes, only β^- decay, β^+ decay, and electron capture may play a role in nuclear decay of Ir-192. Further analysis will be required to establish which of these three decays are actually implicated in the radioactive decay of iridium-192.

(1) The decay $^{192}_{77}\text{Ir} \rightarrow ^{192}_{78}\text{Pt}$ is characterized with $\Delta A = 0$ and $\Delta Z = -1$ suggesting a β^- decay process in which a neutron transforms into a proton and an electron and antineutrino are ejected from the nucleus



(2) The decay $^{192}_{77}\text{Ir} \rightarrow ^{192}_{76}\text{Os}$ is characterized with $\Delta A = 0$ and $\Delta Z = +1$ suggesting a β^+ decay process in which a proton transforms into a neutron and a positron and neutrino are ejected from the nucleus

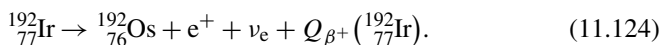


Table 11.4 Change in atomic number Z and atomic mass number A in 8 major radioactive nuclear decays

Decay	α	β^-	β^+	EC	γ	IC	PE	NE
ΔZ	+2	-1	+1	+1	0	0	+1	0
ΔA	+4	0	0	0	0	0	+1	+1

Legend:

EC = electron capture, IC = internal conversion, PE = proton emission, NE = neutron emission
 $\Delta Z = Z_b - Z_a$ and $\Delta A = A_b - A_a$ where “b” stands for before decay and “a” stands for after decay

(3) The decay ${}^{192}_{77}\text{Ir} \rightarrow {}^{192}_{76}\text{Os}$ characterized with $\Delta A = 0$ and $\Delta Z = +1$ could also be attributed to electron capture decay in which an orbital electron ventures into the nucleus, is captured, and causes a transformation of a proton into a neutron and ejection of a neutrino from the nucleus



(b) Next step is to evaluate decay energies for the three possible decay processes (β^- , β^+ , and EC) that were identified in (a) with help of Table 11.4. For a given decay to occur, decay energy Q_{decay} must be positive; however, if Q_{decay} is just barely positive, not much energy will be released in the decay process. Decay energy Q_{decay} is in the most general form written as

$$Q_{\text{decay}} = \sum_{i,\text{before}} M_i c^2 - \sum_{i,\text{after}} M_i c^2, \quad (11.126)$$

where M_i are nuclear masses and masses of other particles involved in decay. Based on (11.123) β^- , β^+ , and EC decay energies can now be expressed as follows using either the nuclear mass M method or the atomic mass \mathcal{M} method for the parent P and daughter D

$$Q_{\beta^-} = M(\text{P})c^2 - M(\text{D})c^2 - m_e c^2 = \mathcal{M}(\text{P})c^2 - \mathcal{M}(\text{D})c^2, \quad (11.127)$$

$$Q_{\beta^+} = M(\text{P})c^2 - M(\text{D})c^2 - m_e c^2 = \mathcal{M}(\text{P})c^2 - \mathcal{M}(\text{D})c^2 - 2m_e c^2, \quad (11.128)$$

$$Q_{\text{EC}} = M(\text{P})c^2 + m_e c^2 - M(\text{D})c^2 = \mathcal{M}(\text{P})c^2 - \mathcal{M}(\text{D})c^2, \quad (11.129)$$

where \mathcal{M} in (11.127), (11.128), and (11.129) stands for the atomic mass and $\mathcal{M}c^2$ for the atomic rest energy. Both approaches spelled out in (11.127) through (11.129), of course, provide the same results when appropriate nuclear or atomic data are used in the calculation.

(1) **Beta minus decay energy** Q_{β^-} is calculated with (11.127) as follows

$$Q_{\beta^-}({}^{192}_{77}\text{Ir}) = \mathcal{M}(\text{P})c^2 - \mathcal{M}(\text{D})c^2 = \mathcal{M}({}^{192}_{77}\text{Ir})c^2 - \mathcal{M}({}^{192}_{78}\text{Pt})c^2$$

$$\begin{aligned}
&= [191.962602u - 191.961035u]c^2 \\
&= (1.567 \times 10^{-3}u) \times (931.494028 \text{ MeV}/u) \\
&= 1.460 \text{ MeV}.
\end{aligned} \tag{11.130}$$

Decay energy for β^- decay of Ir-192 was calculated to be 1.460 MeV confirming β^- decay of Ir-192 into Pt-192 as one of the processes contributing to the Ir-192 decay. Note that same result can be obtained, if the nuclear rest energy method stated in (11.127) is used in the calculation.

$$\begin{aligned}
Q_{\beta^-}({}^{192}_{77}\text{Ir}) &= M(\text{P})c^2 - M(\text{D})c^2 - m_e c^2 \\
&= 178772.6733 \text{ MeV} - 178770.7027 \text{ MeV} - 0.511 \text{ MeV} \\
&= 1.460 \text{ MeV}.
\end{aligned} \tag{11.131}$$

(2) **Beta plus decay energy** Q_{β^+} is calculated with (11.128) as follows

$$\begin{aligned}
Q_{\beta^+}({}^{192}_{77}\text{Ir}) &= \mathcal{M}(\text{P})c^2 - \mathcal{M}(\text{D})c^2 = \mathcal{M}({}^{192}_{77}\text{Ir})c^2 - \mathcal{M}({}^{192}_{76}\text{Os})c^2 - 2m_e c^2 \\
&= [191.962602u - 191.961479u]c^2 - 2m_e c^2 \\
&= (1.123 \times 10^{-3}u) \times (931.494028 \text{ MeV}/u) - 1.022 \text{ MeV} \\
&= 0.024 \text{ MeV}.
\end{aligned} \tag{11.132}$$

Decay energy for β^+ decay of Ir-192 was calculated to be 0.024 MeV. Since the result is positive, β^+ decay is energetically possible but the energy available for sharing among the decay products is very small making the β^+ decay of Ir-192 improbable in comparison with its competing process, the electron capture. Note that same result can be obtained, if the nuclear rest energy method stated in (11.128) is used in the calculation

$$\begin{aligned}
Q_{\beta^+}({}^{192}_{77}\text{Ir}) &= M(\text{P})c^2 - M(\text{D})c^2 - m_e c^2 \\
&= 178772.6733 \text{ MeV} - 178772.1383 \text{ MeV} - 0.5110 \text{ MeV} \\
&= 0.024 \text{ MeV}.
\end{aligned} \tag{11.133}$$

(3) **Electron capture decay energy** Q_{EC} is calculated with (11.129) as follows

$$\begin{aligned}
Q_{\text{EC}}({}^{192}_{77}\text{Ir}) &= \mathcal{M}(\text{P})c^2 - \mathcal{M}(\text{D})c^2 = \mathcal{M}({}^{192}_{77}\text{Ir})c^2 - \mathcal{M}({}^{192}_{76}\text{Os})c^2 \\
&= [191.962602u - 191.961479u]c^2 \\
&= (1.123 \times 10^{-3}u) \times (931.494028 \text{ MeV}/u) \\
&= 1.046 \text{ MeV}.
\end{aligned} \tag{11.134}$$

Decay energy Q_{EC} for EC decay of Ir-192 was calculated to be 1.046 MeV, confirming the EC decay of Ir-192 into Os-192 as one of the decay processes contributing to

the decay of Ir-192. Note that same result can be obtained, if the nuclear rest energy method stated in (11.129) is used in the calculation

$$\begin{aligned} Q_{\text{EC}}(^{192}_{77}\text{Ir}) &= M(\text{P})c^2 + m_e c^2 - M(\text{D})c^2 \\ &= 178772.6733 \text{ MeV} + 0.5110 \text{ MeV} - 178772.1383 \text{ MeV} \\ &= 1.046 \text{ MeV}. \end{aligned} \quad (11.135)$$

(c) Energy of decay products in the Ir-192 radioactive decay is determined using conservation of momentum and total energy principles.

(1) **Beta minus decay of Ir-192:**

$$^{192}_{77}\text{Ir} \rightarrow ^{192}_{78}\text{Pt} + e^- + \bar{\nu}_e + Q_{\beta^-}(^{192}_{77}\text{Ir}). \quad (11.136)$$

The decay products in Ir-192 β^- decay are: electron e^- , antineutrino $\bar{\nu}_e$, and the daughter atom Pt-192. Energy of β^- decay products exhibits a spectral distribution and we will here evaluate only the maxima in the spectrum: $[(E_K)_{\beta^-}]_{\text{max}}$ and $[(E_K)_{\text{Pt-192}}]_{\text{max}}$ as representative values of energy transfer in β^- decay of Ir-192.

The β^- decay energy $Q_{\beta^-}(^{192}_{77}\text{Ir})$ is shared between the emitted electron as $[(E_K)_{\beta^-}]_{\text{max}}$ and recoil daughter atom as $[(E_K)_{\text{Pt-192}}]_{\text{max}}$ when the neutrino energy is zero. Hence,

$$Q_{\beta^-}(^{192}_{77}\text{Ir}) = [(E_K)_{\beta^-}]_{\text{max}} + [(E_K)_{\text{Pt-192}}]_{\text{max}} \quad (11.137)$$

and the two momenta $\mathbf{p}_{\beta^-} \equiv \mathbf{p}_{e^-}$ and $\mathbf{p}_D \equiv \mathbf{p}_{\text{Pt-192}}$ are opposite in direction and equal in magnitude. Thus, we can write the magnitude of vector $\mathbf{p}_{\text{Pt-192}}$ as follows

$$|\mathbf{p}_{\text{Pt-192}}| \equiv p_{\text{Pt-192}} = p_{e^-} = \frac{m_e c \beta_{e^-}}{\sqrt{1 - \beta_{e^-}^2}}, \quad (11.138)$$

where

m_e is the rest mass of the β particle (electron): $m_e = 0.511 \text{ MeV}/c^2$.

β_{e^-} is the velocity of the electron normalized to the speed of light c in vacuum.

Combining (11.138) with the classical expression for maximum kinetic energy $[(E_K)_{\text{Pt-192}}]_{\text{max}}$ of the daughter atom Pt-192 we get

$$[(E_K)_{\text{Pt-192}}]_{\text{max}} = \frac{p_{\text{Ir-192}}^2}{2M(^{192}_{78}\text{Pt})c^2} = \frac{p_{e^-}^2}{2M(^{192}_{78}\text{Pt})c^2} = \frac{(m_e c^2)^2}{2M(^{192}_{78}\text{Pt})c^2} \frac{\beta_{e^-}^2}{1 - \beta_{e^-}^2}. \quad (11.139)$$

From the standard expression for $[(E_K)_{\beta^-}]_{\text{max}} = [(1 - \beta_{e^-}^2)^{-1/2} - 1]m_e c^2$ we determine the following expression for $\beta_{e^-}^2/(1 - \beta_{e^-}^2)$

$$\frac{\beta_{e^-}^2}{1 - \beta_{e^-}^2} = \frac{2[(E_K)_{\beta^-}]_{\text{max}}}{m_e c^2} + \left[\frac{[(E_K)_{\beta^-}]_{\text{max}}}{m_e c^2} \right]^2. \quad (11.140)$$

Combining (11.140) with (11.139) we get the following expression for the maximum recoil kinetic energy $[(E_K)_{\text{Pt-192}}]_{\text{max}}$ of the daughter atom

$$\begin{aligned} [(E_K)_{\text{Pt-192}}]_{\text{max}} &= \frac{m_e c^2}{\mathcal{M}(\text{D})c^2} [(E_K)_\beta]_{\text{max}} + \frac{1}{2\mathcal{M}(\text{D})c^2} [(E_K)_\beta]_{\text{max}}^2 \\ &= Q_{\beta^-}({}^{192}\text{Ir}) - [(E_K)_{\beta^-}]_{\text{max}}. \end{aligned} \quad (11.141)$$

Equation (11.141) can be written in the form of a quadratic equation for $[(E_K)_{\beta^-}]_{\text{max}}$ as a function of the decay energy $Q_{\beta^-}({}^{192}\text{Ir})$

$$\frac{1}{2\mathcal{M}({}^{192}\text{Pt})c^2} [(E_K)_{\beta^-}]_{\text{max}}^2 + \left[1 + \frac{m_e c^2}{\mathcal{M}({}^{192}\text{Pt})c^2} \right] [(E_K)_{\beta^-}]_{\text{max}} - Q_{\beta^-}({}^{192}\text{Ir}) = 0 \quad (11.142)$$

with the following physically-relevant solution [note: $[(E_K)_\beta]_{\text{max}} > 0$]

$$\begin{aligned} [(E_K)_{\beta^-}]_{\text{max}} &= \mathcal{M}({}^{192}\text{Pt})c^2 \left\{ - \left[1 + \frac{m_e c^2}{\mathcal{M}({}^{192}\text{Pt})c^2} \right] \right. \\ &\quad \left. + \sqrt{\left[1 + \frac{m_e c^2}{\mathcal{M}({}^{192}\text{Pt})c^2} \right]^2 + \frac{2Q_{\beta^-}}{\mathcal{M}({}^{192}\text{Pt})c^2}} \right\}. \end{aligned} \quad (11.143)$$

The second term under the square root is obviously much smaller than 1 since it is governed by the ratio $2Q_{\beta^-}/[\mathcal{M}(\text{D})c^2]$, allowing us to expand the square root into a series and keeping only the first two terms of the series to get

$$\begin{aligned} [(E_K)_{\beta^-}]_{\text{max}} &\approx \mathcal{M}({}^{192}\text{Pt})c^2 \left[1 + \frac{m_e c^2}{\mathcal{M}({}^{192}\text{Pt})c^2} \right] \\ &\quad \times \left\{ 1 + \frac{Q_{\beta^-}({}^{192}\text{Ir})}{\mathcal{M}({}^{192}\text{Pt})c^2} \left[1 + \frac{m_e c^2}{\mathcal{M}({}^{192}\text{Pt})c^2} \right]^{-2} + \dots - 1 \right\} \\ &= \frac{Q_{\beta^-}({}^{192}\text{Ir})}{1 + \frac{m_e c^2}{\mathcal{M}({}^{192}\text{Pt})c^2}} \approx Q_{\beta^-}({}^{192}\text{Ir}) \left[1 - \frac{m_e c^2}{\mathcal{M}({}^{192}\text{Pt})c^2} \right] \\ &= (1 - \eta) Q_{\beta^-}({}^{192}\text{Ir}), \end{aligned} \quad (11.144)$$

where η is a small correction given as $\eta = m_e c^2/(\mathcal{M}({}^{192}\text{Pt})c^2)$ and this correction η multiplied by $Q_{\beta^-}({}^{192}\text{Ir})$ is actually the maximum recoil kinetic energy $[(E_K)_{\text{Pt-192}}]_{\text{max}}$ of the daughter expressed as

$$\begin{aligned} [(E_K)_{\text{Pt-192}}]_{\text{max}} &= Q_{\beta^-}({}^{192}\text{Ir}) - [(E_K)_{\beta^-}]_{\text{max}} = \eta Q_{\beta^-}({}^{192}\text{Ir}) \\ &= \frac{m_e c^2}{\mathcal{M}({}^{192}\text{Pt})c^2} Q_{\beta^-}({}^{192}\text{Ir}). \end{aligned} \quad (11.145)$$

We now use (11.144) to calculate $[(E_K)_{\beta^-}]_{\max}$ and (11.145) to calculate $[(E_K)_{\text{Pt-192}}]_{\max}$ for β^- decay of Ir-192 for which β^- decay energy was calculated in (11.130) to be 1.46 MeV. The maximum kinetic energy of the emitted beta particle (electron) is essentially equal to the decay energy $Q_{\beta^-}({}^{192}_{77}\text{Ir})$

$$\begin{aligned} [(E_K)_{\beta^-}]_{\max} &\approx Q_{\beta^-}({}^{192}_{77}\text{Ir}) \left[1 - \frac{m_e c^2}{\mathcal{M}({}^{192}_{78}\text{Pt})c^2} \right] \\ &= (1.46 \text{ MeV}) \left[1 - \frac{0.511}{191.961035 \times 931.494028} \right] \\ &= (1.46 \text{ MeV}) [1 - 2.86 \times 10^{-6}] \approx 1.46 \text{ MeV} \\ &= Q_{\beta^-}({}^{192}_{77}\text{Ir}). \end{aligned} \quad (11.146)$$

From (11.146) we note that the maximum energy of the electron emitted by the nucleus in β^- decay of Ir-192 is essentially equal to the β^- decay energy $Q_{\beta^-}({}^{192}_{77}\text{Ir}) = 1.46 \text{ MeV}$, so that essentially all energy available for sharing between the beta particle (electron) and the recoil atom is picked up by the electron as $[(E_K)_{\beta^-}]_{\max}$ and an exceedingly small amount $[(E_K)_{\text{Pt-192}}]_{\max}$, as stated in (11.145), is carried by the Pt-192 recoil atom, as shown below

$$\begin{aligned} [(E_K)_{\text{Pt-192}}]_{\max} &= \frac{m_e c^2}{\mathcal{M}({}^{192}_{78}\text{Pt})c^2} Q_{\beta^-}({}^{192}_{77}\text{Ir}) \\ &= \frac{0.511}{191.961035 \times 931.494028} \times (1.46 \text{ MeV}) \\ &= 4.17 \times 10^{-6} \text{ MeV} = 4.17 \text{ eV}. \end{aligned} \quad (11.147)$$

(2) **Decay energy for β^+ decay** of Ir-192 was in (11.132) given as 0.0241 MeV, making β^+ decay of Ir-192 allowed but of very low probability in comparison with electron capture decay.

(3) **Decay energy Q_{EC} for EC decay** of Ir-192 was in (11.134) calculated as 1.046 MeV. The decay products of Ir-192 electron capture decay into Os-192 are the neutrino and the Os-192 recoil atom and the two share the decay energy Q_{EC} corrected for the binding energy E_B of the captured electron. The energy conservation can thus be expressed as follows

$$Q_{\text{EC}} - E_B = E_\nu + (E_K)_{\text{Os-192}}. \quad (11.148)$$

As shown in Prob. 234, neutrino energy E_ν and daughter recoil kinetic energy $(E_K)_{\text{Os-192}}$ are given, respectively, as follows

$$E_\nu \approx Q_{\text{EC}} - E_B = 1.046 \text{ MeV} - 0.0765 \text{ MeV} = 0.97 \text{ MeV}, \quad (11.149)$$

and

$$\begin{aligned}(E_K)_{\text{Os-192}} &= \frac{(Q_{\text{EC}} - E_B)^2}{2\mathcal{M}({}^{192}_{76}\text{Os})c^2} = \frac{(1.046 \text{ MeV} - 0.0765 \text{ MeV})^2}{2 \times (191.961479u) \times (931.494028 \text{ MeV}/u)} \\ &= 2.6 \times 10^{-6} \text{ MeV} = 2.6 \text{ eV}\end{aligned}\quad (11.150)$$

again, like in the case of β^- decay, indicating that the kinetic energy of the recoil atom in comparison to neutrino energy in EC decay or beta particle energy in β^- decay is exceedingly small as a result of the large atomic rest mass compared to that of neutrino or electron.

In (11.149) and (11.150) we first assumed that the captured electron comes from the K shell of the Ir-192 atom and then we used the Hartree approximation (T3.38) to calculate the K shell binding energy to the Ir-192 nucleus

$$E_B(\text{K}) \approx E_R(Z_{\text{Ir}} - 2)^2 = (13.61 \text{ eV}) \times (77 - 2)^2 \approx 77 \text{ keV} = 0.0765 \text{ MeV}\quad (11.151)$$

in excellent agreement with the value of 76.1 keV provided for iridium by the NIST.

11.7 Gamma Decay

11.7.Q1

(234)

Alpha decay as well as the three beta decay modes may produce a daughter nucleus in an excited state without expending the full amount of the decay energy available. The daughter nucleus will reach its ground state (i.e., it will de-excite) through one of the following two processes:

- (1) Emit the excitation energy in the form of a γ photon (γ ray) in a radioactive decay process referred to as gamma (γ) emission decay.
- (2) Transfer the excitation energy to one of its associated atomic orbital electrons in a process called internal conversion (IC). The orbital electron is ejected from the atom and referred to as an internal conversion electron.

- (a) A few of the important gamma emitters in medical physics, for reason of historical significance, environmental hazard, or contemporary use in medicine, are: radium-226, radon-222, cobalt-60, cesium-137, molybdenum-99, and iridium-192.

Find in the literature and sketch the decay schemes for these radionuclides.

- (b) A closer look at the decay schemes plotted in (a) reveals that the gamma rays actually come from the daughter product, yet we identify them as if they originated in the parent radionuclide. Explain. Define the terms isomer and metastable state.
- (c) Determine decay energy Q_γ for γ emission decay of cobalt-60 into nickel-60.

SOLUTION:

(a) The six examples of radionuclides of importance to medical physics were chosen for the following reasons:

- (1) Radium-226 for its historical importance in early radiotherapy both as external or internal source of radiation. It is no longer used in medicine because it, as well as its daughter product radon-222, are dangerous as cancer inducing substances.
- (2) Radon-222, as environmentally hazardous gas, is a daughter product of radium-226 α decay. It was used as sealed encapsulated brachytherapy source in the past, but has been replaced by other safer and more practical radionuclides.
- (3) Cobalt-60 as the most practical sealed source for external beam radiotherapy. It has been used for this purpose since the early 1950s and still offers reasonably inexpensive means for radiotherapy in the developing world. In developed countries linear accelerators have largely replaced cobalt-60 teletherapy machines for use in radiotherapy.
- (4) Cesium-137 is still used as radiation source in blood irradiators but its use is declining because of security concerns.
- (5) Molybdenum-99 as the radioactive source of technetium-99m produced in technetium generators and used heavily in nuclear medicine imaging.
- (6) Iridium-192 as sealed source in modern high dose rate remote afterloading brachytherapy machines.

(b) In most radioactive α or β decays the daughter nucleus de-excitation occurs instantaneously (i.e., within 10^{-12} s), so that we refer to the emitted γ rays as if they were produced by the parent nucleus. For example, as shown in Fig. 11.5, for the cobalt-60 β^- decay into nickel-60, the γ rays following the β^- decay actually originate from nuclear de-excitations of nickel-60, yet, for convenience, we refer to these γ rays as the cobalt-60 γ rays. Similarly, we refer to γ photons following the β^- decay of cesium-137 into barium-137m as cesium-137 γ rays even though the γ photons actually originate from a transition in the barium-137 nucleus.

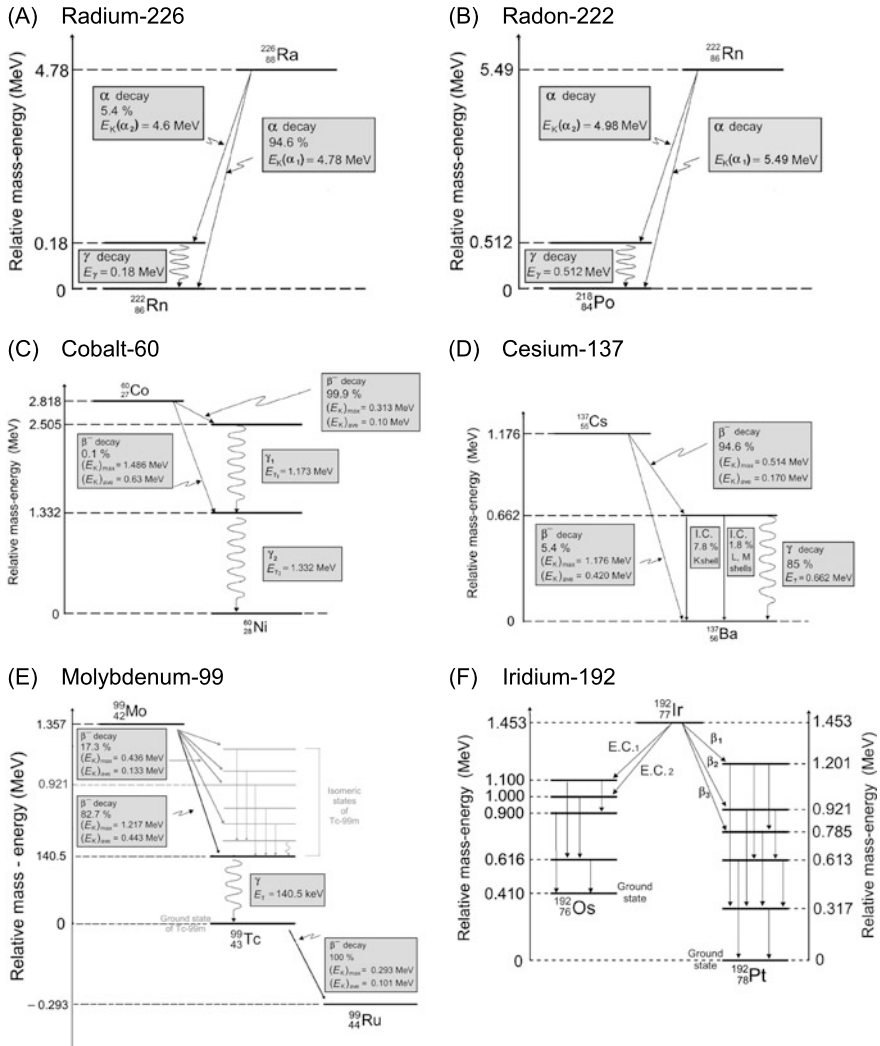


Fig. 11.5 Decay schemes for various radionuclides of importance to medical physics: (A) Radium-226; (B) Radon-222; (C) Cobalt-60; (D) Cesium-137; (E) Molybdenum-99; and (F) Iridium-192. All decays have a gamma emission decay component following α decay of radium-226 and radon-222, β^- decay of cobalt-60, cesium-137, molybdenum-99, and iridium-192, or electron capture decay of iridium-192

In certain α or β decays, the excited daughter nucleus does not immediately decay to its ground state; rather, it de-excites with a time delay:

- (1) The excited state of the daughter is then referred to as a *metastable state* and the process of de-excitation is called an *isomeric transition*. The metastable states are characterized by their own half-lives $t_{1/2}$ and mean (average) lives τ .

- (2) The nucleus in a metastable state is identified with a letter m next to the atomic mass number designation, as shown in Fig. 11.5 in (E) for technetium-99m or $^{99m}_{43}\text{Tc}$ with a half-life of 6.01 hours.
- (3) The term *isomer* is used for designation of nuclei that have the same atomic number Z and same atomic mass number A but differ in energy states.

In addition to α and β decay there are many other modes for producing nuclei in excited states that subsequently undergo γ decay. For example, excited states with energies up to 8 MeV may be produced with neutron capture (n, γ) reactions as well as with other nuclear reactions, such as (p, γ) and (α, γ), etc. Examples of γ rays following α and β decays are given in Fig. 11.5 in (A) and (B) for α decay and in (C), (D), (E) and (F) for β^- decay, and in (E) also for electron capture decay.

(c) In general, the decay energy Q_γ in single γ emission decay is the sum of the emitted γ -ray energy E_γ and the recoil kinetic energy $(E_K)_D$ of the daughter or

$$Q_\gamma(D) = E_\gamma + (E_K)_D. \quad (11.152)$$

Conservation of momentum and energy considerations allow us to evaluate further the decay energy Q_γ of (11.152). Momentum before γ decay is zero, so that after γ decay total momentum resulting from the γ -ray photon \mathbf{p}_γ and recoil atom \mathbf{p}_D must also equal to zero. Thus, the two vector momenta \mathbf{p}_γ and \mathbf{p}_D must be opposite in direction and equal in magnitude, i.e.,

$$\mathbf{p}_\gamma + \mathbf{p}_D = 0 \quad \text{or} \quad |\mathbf{p}_\gamma| \equiv p_\gamma = \frac{E_\gamma}{c} = |\mathbf{p}_D| \equiv p_D. \quad (11.153)$$

The partition of energy between the γ photon energy $E_\gamma = p_\gamma c$ and the recoil daughter kinetic energy $(E_K)_D$ can now be expressed as follows

$$(E_K)_D = \frac{p_D^2}{2\mathcal{M}(D)} = \frac{p_\gamma^2}{2\mathcal{M}(D)} = \frac{E_\gamma^2}{2\mathcal{M}(D)c^2}, \quad (11.154)$$

where $\mathcal{M}(D)c^2$ is the rest energy of the daughter atom.

The γ decay energy $Q_\gamma(D)$ after inserting (11.154) into (11.152) is now expressed as follows

$$Q_\gamma(D) = E_\gamma + (E_K)_D = E_\gamma \left[1 + \frac{E_\gamma}{2\mathcal{M}(D)c^2} \right]. \quad (11.155)$$

Equation (11.155) shows that the recoil kinetic energy of the daughter $(E_K)_D$ represents only a small fraction of the γ -ray energy E_γ and is therefore negligible in comparison to E_γ for most practical purposes and therefore one may conclude that $Q_\gamma(D) \approx E_\gamma$. However, if one wishes to calculate the recoil kinetic energy $(E_K)_D$ of the daughter one must use (11.154).

The label for “daughter” in gamma decay is used in parallel with the same label used in other nuclear decays that are clearly defined with parent decaying into

daughter. In gamma decay the parent and daughter represent the same nucleus, except that the parent nucleus is in an excited state and the daughter nucleus is in a lower excited state or the ground state.

For the cobalt-60 gamma rays, as shown in Fig. 11.5, the cobalt-60 nucleus decays through β^- decay into nickel-60 (Ni-60) in 2nd excited state. The Ni-60 nucleus immediately de-excites through two transitions, first from 2nd excited state to 1st excited state emitting a γ photon of energy $E_{\gamma_1} = 1.173$ MeV and then from 1st excited state to ground state emitting a γ photon of energy $E_{\gamma_2} = 1.332$ MeV.

Decay energy Q_γ is the sum of two decay energies, Q_{γ_1} for the first γ ray transition and Q_{γ_2} for the second γ ray transition both calculated with (11.155) and appropriate data. We get

$$\begin{aligned} Q_\gamma &= Q_{\gamma_1} + Q_{\gamma_2} = \left[E_{\gamma_1} + \frac{E_{\gamma_1}^2}{2\mathcal{M}({}^{60}_{28}\text{Ni})c^2} \right] + \left[E_{\gamma_2} + \frac{E_{\gamma_2}^2}{2\mathcal{M}({}^{60}_{28}\text{Ni})c^2} \right] \\ &= E_{\gamma_1} + E_{\gamma_2} + \frac{E_{\gamma_1}^2 + E_{\gamma_2}^2}{2\mathcal{M}({}^{60}_{28}\text{Ni})c^2} = 2.505 \text{ MeV} + 2.8 \times 10^{-5} \text{ MeV} \\ &\approx 2.505 \text{ MeV}. \end{aligned} \tag{11.156}$$

From (11.156) we note that recoil kinetic energy $(E_K)_{\text{Ni-60}}$ of the daughter atom Ni-60 is 28 eV.

11.8 Internal Conversion

11.8.Q1

(235)

In α or β decay the daughter nucleus is often left in an excited state and may attain the ground state through emission of one or several γ ray photons. However, γ emission decay is not the only option for de-excitation of the daughter nucleus. The de-excitation energy may also be transferred from the parent nucleus almost in full to an orbital electron of the same atom in a process referred to as internal conversion (IC). A small portion of the nuclear de-excitation energy Q_γ is required to overcome the binding energy E_B of the electron in its atomic shell. The remaining part of the decay energy Q_γ is shared as kinetic energy between the conversion electron $(E_K)_{\text{IC}}$ and the recoil daughter nucleus $(E_K)_{\text{D}}$

$$Q_{\text{IC}} = Q_\gamma - E_B = (E_K)_{\text{IC}} + (E_K)_{\text{D}}, \tag{11.157}$$

where Q_{IC} is the decay energy for internal conversion.

- (a) Derive relationships for IC decay energy Q_{IC} as well as kinetic energy of the internal conversion electron $(E_K)_{IC}$ and recoil daughter atom $(E_K)_D$.
- (b) The radioactive decay scheme of cesium-137, shown in Fig. 11.6, is an excellent example of β^- decay resulting not only in spectrum of beta particles (electrons) but also in γ rays (0.662 keV) through γ emission decay as well as IC electrons through IC decay. The β^- decay energy Q_{β^-} ($^{137}_{55}\text{Cs}$) is 1.176 MeV. Using expressions derived in (a) determine kinetic energy $(E_K)_{IC}$ of the IC electron ejected from the K shell of the barium-137 daughter atom as well as the recoil kinetic energy $(E_K)_{Ba-137}$ of the barium-137 daughter atom.
- (c) Define the internal conversion (IC) factor α_{IC} and from the decay scheme of cesium-137 displayed in Fig. 11.6 determine the total conversion factor α_{IC} for de-excitation of barium-137 into ground state in β^- decay of cesium-137 into barium-137.

SOLUTION:

(a) Equation (11.157) gives the IC decay energy Q_{IC} as the corresponding γ decay energy Q_γ less the binding energy E_B of the IC electron. Q_γ is the sum of photon energy E_γ and recoil kinetic energy $(E_K)_D$ of the daughter atom and, since $(E_K)_D$ is exceedingly small in comparison with E_γ , we can say that, in the first approximation, $Q_\gamma \approx E_\gamma$. Similarly, for IC we can say that $Q_{IC} = (E_K)_{IC} + (E_K)_D \approx (E_K)_{IC}$ since $(E_K)_{IC} \gg (E_K)_D$.

Now we turn to the calculation of kinetic energy $(E_K)_{IC}$ of the IC electron and kinetic energy $(E_K)_D$ of the recoil atom using conservation of momentum and total energy principles. Before the IC event the daughter atom is stationary and its momentum is zero. Therefore, after the IC event, the two vector momenta \mathbf{p}_{IC} of the IC electron and \mathbf{p}_D of the recoil daughter atom of mass $\mathcal{M}(D)$ and rest energy $\mathcal{M}(D)c^2$ must be opposite in direction and equal in magnitude. The magnitudes of the two momenta are thus related as follows

$$|\mathbf{p}_D| \equiv p_D = \sqrt{2(E_K)_D \mathcal{M}(D)} = |\mathbf{p}_{IC}| = p_{IC} = \frac{m_e c \beta_{IC}}{\sqrt{1 - \beta_{IC}^2}}, \quad (11.158)$$

where

m_e is the rest mass of the IC electron ($m_e = 0.511 \text{ MeV}/c^2$).

β_{IC} is the velocity of the IC electron normalized to speed of light in vacuum ($c \approx 3 \times 10^8 \text{ m/s}$).

$\mathcal{M}(D)$ is the rest mass of the daughter atom.

Recoil kinetic energy $(E_K)_D$ of the daughter atom can classically be expressed as

$$(E_K)_D = \frac{p_D^2}{2\mathcal{M}(D)} = \frac{p_{IC}^2}{2\mathcal{M}(D)} = \frac{(m_e c^2)^2}{2\mathcal{M}(D)c^2} \frac{\beta_{IC}^2}{(1 - \beta_{IC}^2)} = \frac{E_0^2}{2\mathcal{M}(D)c^2} \frac{\beta_{IC}^2}{(1 - \beta_{IC}^2)}, \quad (11.159)$$

after insertion of relativistic (11.158) into the classical expression for kinetic energy $(E_K)_D$. Note that E_0 is the rest energy of the IC electron.

We now express $\beta_{IC}^2/(1 - \beta_{IC}^2)$ in terms of the kinetic energy $(E_K)_{IC}$ of the IC electron. From the standard expression for relativistic kinetic energy $(E_K)_{IC}$ of the IC electron

$$(E_K)_{IC} = \left(\frac{1}{\sqrt{1 - \beta_{IC}^2}} - 1 \right) m_e c^2 = \left(\frac{1}{\sqrt{1 - \beta_{IC}^2}} - 1 \right) E_0, \quad (11.160)$$

we first get the following expression

$$\frac{1}{1 - \beta_{IC}^2} = \left[1 + \frac{(E_K)_{IC}}{E_0} \right]^2 = 1 + 2 \frac{(E_K)_{IC}}{E_0} + \frac{(E_K)_{IC}^2}{E_0^2}. \quad (11.161)$$

Equation (11.161) after slight rearrangement yields the following expression for $\beta_{IC}^2/(1 - \beta_{IC}^2)$

$$\frac{1}{1 - \beta_{IC}^2} - 1 = \frac{\beta_{IC}^2}{1 - \beta_{IC}^2} = 2 \frac{(E_K)_{IC}}{E_0} + \frac{(E_K)_{IC}^2}{E_0^2}. \quad (11.162)$$

After inserting (11.162) into (11.159) and rearranging the terms we get the following quadratic equation for $(E_K)_{IC}$ as a function of $(E_K)_D$

$$\frac{1}{2\mathcal{M}(D)c^2} (E_K)_{IC}^2 + \frac{E_0}{\mathcal{M}(D)c^2} (E_K)_{IC} - (E_K)_D = 0 \quad (11.163)$$

or as a function of Q_{IC} , after inserting $(E_K)_D = Q_{IC} - (E_K)_{IC}$ into (11.163)

$$\frac{1}{2\mathcal{M}(D)c^2} (E_K)_{IC}^2 + \left[1 + \frac{E_0}{\mathcal{M}(D)c^2} \right] (E_K)_{IC} - Q_{IC} = 0. \quad (11.164)$$

The quadratic equation (11.164) has the following physically relevant solution $(E_K)_{IC} > 0$

$$\begin{aligned} (E_K)_{IC} &= \mathcal{M}(D)c^2 \left\{ \sqrt{\left[1 + \frac{E_0}{\mathcal{M}(D)c^2} \right]^2 + \frac{2Q_{IC}}{\mathcal{M}(D)c^2}} - \left[1 + \frac{E_0}{\mathcal{M}(D)c^2} \right] \right\} \\ &= \mathcal{M}(D)c^2 \left[1 + \frac{E_0}{\mathcal{M}(D)c^2} \right] \left\{ \sqrt{1 + \frac{2Q_{IC}}{\mathcal{M}(D)c^2} \left[1 + \frac{E_0}{\mathcal{M}(D)c^2} \right]^{-2}} - 1 \right\}. \end{aligned} \quad (11.165)$$

Since the second term under the square root is much smaller than 1 as a result of $Q_{IC} \ll \mathcal{M}(\text{D})c^2$ and $E_0 \ll \mathcal{M}(\text{D})c^2$, we expand the square root term into a Taylor series and keep only the first two terms to get

$$\begin{aligned}(E_K)_{IC} &= \mathcal{M}(\text{D})c^2 \left[1 + \frac{E_0}{\mathcal{M}(\text{D})c^2} \right] \left\{ 1 + \frac{Q_{IC}}{\mathcal{M}(\text{D})c^2} \left[1 + \frac{E_0}{\mathcal{M}(\text{D})c^2} \right]^{-2} + \cdots - 1 \right\} \\ &= \frac{Q_{IC}}{\left[1 + \frac{E_0}{\mathcal{M}(\text{D})c^2} \right]} \approx Q_{IC} \left[1 - \frac{E_0}{\mathcal{M}(\text{D})c^2} \right] = Q_{IC}(1 - \eta) \\ &= (Q_\gamma - E_B)(1 - \eta),\end{aligned}\tag{11.166}$$

where η is a small correction factor to account for the kinetic energy of the recoil daughter atom.

We now estimate $(E_K)_D$ incorporating (11.166) into (11.157) to get

$$\begin{aligned}(E_K)_D &= Q_{IC} - (E_K)_{IC} = Q_{IC} - Q_{IC}(1 - \eta) = \eta Q_{IC} = \frac{E_0}{\mathcal{M}(\text{D})c^2} Q_{IC} \\ &= \frac{E_0}{\mathcal{M}(\text{D})c^2} (Q_\gamma - E_B).\end{aligned}\tag{11.167}$$

(b) We now use (11.166) to determine kinetic energy $(E_K)_{IC}$ of the IC electron and (11.167) to determine recoil kinetic energy $(E_K)_D$ of the daughter atom.

(1) We note that to use (11.166) we need the gamma decay energy Q_γ which we can approximate with photon energy $E_\gamma = 662$ keV. In addition to Q_γ , we also need the binding energy of the K shell electron in barium-137 atom and we estimate this binding energy with the Hartree approximation method (see (T3.38))

$$E_B(\text{K shell Ba}) \approx Z_{\text{eff}}^2 e_R = (56 - 2)^2 \times 13.61 \text{ eV} \approx 40 \text{ keV}.\tag{11.168}$$

Equation (11.166) now gives the following result for $(E_K)_{IC}$

$$\begin{aligned}(E_K)_{IC} &= (Q_\gamma - E_B)(1 - \eta) = (Q_\gamma - E_B) \left[1 - \frac{E_0}{\mathcal{M}(\text{D})c^2} \right] \\ &= (0.662 \text{ MeV} - 0.040 \text{ MeV}) \times \left[1 - \frac{0.511}{136.9 \times 931.5} \right] \\ &= (0.622 \text{ MeV}) \times (1 - 4.0 \times 10^{-6}) \approx 0.622 \text{ MeV}.\end{aligned}\tag{11.169}$$

(2) In (11.169) it is reasonable to neglect the ratio $E_0/[\mathcal{M}({}_{56}^{137}\text{Ba})c^2]$ because it is exceedingly small, however, in calculation of the daughter recoil kinetic energy we must use it, if we want to determine the extremely small recoil energy. Equation (11.167) thus gives

$$(E_K)_D = \frac{E_0}{\mathcal{M}(\text{D})c^2} (Q_\gamma - E_B)$$

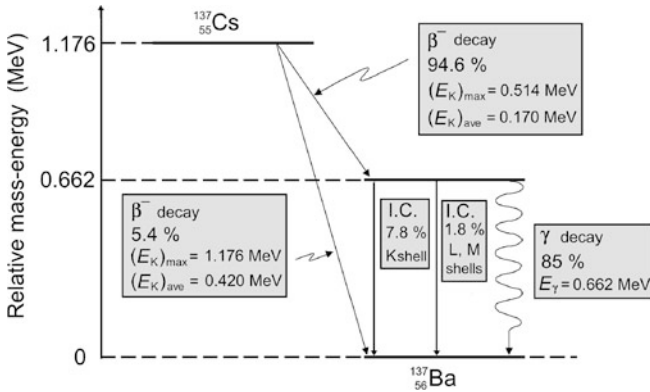


Fig. 11.6 Decay scheme for β^- decay of cesium-137 into barium-137. Relative mass-energy levels (decay energies or Q values) for the ground states of the two nuclides were calculated from either atomic rest energies or nuclear rest energies listed in Appendix A

$$\begin{aligned}
 &= \frac{0.511}{136.9 \times 931.5} \times (0.662 \text{ MeV} - 0.040 \text{ MeV}) \\
 &\approx 2.5 \text{ eV}.
 \end{aligned}
 \tag{11.170}$$

Note that the recoil kinetic energy $(E_K)_D$ is indeed very small in comparison with decay energies in nuclear physics but nonetheless of the order of magnitude of importance in atomic physics.

(c) In typical nuclear de-excitation process two competing nuclear processes are possible: γ -ray emission and internal conversion electron emission. In contrast to the fluorescence yield ω that is defined as the number of characteristic photons emitted per vacancy in a given atomic shell, the total internal conversion factor α_{IC} is defined as the ratio

$$\alpha_{IC} = \frac{\text{conversion probability}}{\gamma\text{-emission probability}} = \frac{N_{IC}}{N_\gamma},
 \tag{11.171}$$

where N_{IC} is the number of conversion electrons ejected from all atomic shells per unit time and N_γ is the number of γ photons emitted per unit time. In addition to the total internal conversion factor one can also define partial internal conversion factors according to the shell from which the electron was ejected.

The internal conversion factor α_{IC} in cesium-137 decay is determined based on the decay scheme and associated relevant data presented in Fig. 11.6.

- (1) Decay energy Q_{β^-} ($^{137}_{55}\text{Cs}$) is 1.176 MeV determined either with atomic rest energy data or with nuclear rest energy data for cesium-137 and barium-137 listed in Appendix A.
- (2) Of 100 β^- decays of $^{137}_{55}\text{Cs}$ radionuclide 94.6 decays land in the first excited state of the barium-137 ($^{137}_{56}\text{Ba}$) daughter nucleus which is 0.662 MeV above the

ground state of Ba-137. The maximum energy of the beta particle (electron) emitted in this transition is $1.176 \text{ MeV} - 0.662 \text{ MeV} = 0.514 \text{ MeV}$, ignoring the minute recoil of the barium-137 daughter nucleus.

(3) Of 100 β^- decays of $^{137}_{55}\text{Cs}$ radionuclide 5.4 decays proceed directly to the ground state of Ba-137 and the maximum energy of the emitted beta particle (electron) is 1.176 MeV, ignoring the minute recoil energy of the Ba-137 daughter atom.

(4) The 94.6 transitions from Cs-137 to first excited state of Ba-137 will result in 85 γ ray photons of energy $E_\gamma = 662 \text{ keV}$ and 9.6 IC electrons—7.8 of these will be ejected from the K shell of the Ba-137 atom and 1.8 will be ejected from the L shell of the Ba-137 atom.

(5) The internal conversion factor α_{IC} is defined as the ratio between IC probability and γ emission probability or as the ratio between the number N_{IC} of IC electrons ejected and the number N_γ of γ ray photons emitted. For Cs-137 the IC factor α_{IC} is thus given as

$$\alpha_{\text{IC}} = \frac{N_{\text{IC}}}{N_\gamma} = \frac{7.8 + 1.8}{85} = 0.113. \quad (11.172)$$

11.9 Spontaneous Fission

11.9.Q1

(236)

Spontaneous fission (SF) is a radioactive decay process by which a nucleus of atomic number $Z \geq 92$ splits spontaneously into two fission fragments and emits 2 to 4 neutrons as well as a significant amount of energy. SF usually competes with α decay and is, like α decay, explained theoretically as a quantum mechanical tunneling process.

Flerov and Petržak discovered SF in 1940 when they noticed that uranium-238, in addition to α decay, may undergo the process of spontaneous fission. The half-life $t_{1/2}$ of uranium-238 (U-238) is $4.47 \times 10^9 \text{ a}$. The rate of SF decay was measured to be about 24 SF decays per gram of U-238 per hour and the neutron factor f_n (neutron yield per SF decay) is about 2.1.

For uranium-238 ($^{238}_{92}\text{U}$) determine:

- (a) Decay constant λ .
- (b) Decay rate per gram per second.
- (c) Specific activity in Ci/g.
- (d) Half-life $(t_{1/2})_{\text{SF}}$ and decay constant λ_{SF} for SF decay.
- (e) How many times more probable is α decay compared to SF decay?
- (f) Production rate of neutrons (neutron yield) per gram per second.

SOLUTION:

(a) *Decay constant* λ of U-238 is determined from the standard relationship between half-life $t_{1/2}$ and decay constant λ

$$\begin{aligned}\lambda &= \frac{\ln 2}{t_{1/2}} = \frac{\ln 2}{(4.47 \times 10^9 \text{ a}) \times (365 \text{ d/a}) \times (24 \text{ h/d}) \times (3600 \text{ s/h})} \\ &= 4.92 \times 10^{-18} \text{ s}^{-1}.\end{aligned}\quad (11.173)$$

(b) *Decay rate* of U-238 per gram per second is by definition equal to the specific activity a defined as activity \mathcal{A} per unit mass m (in Bq/g where $1 \text{ Bq} = 1 \text{ s}^{-1}$) calculated as follows (T10.2)

$$\begin{aligned}a &= \frac{\mathcal{A}}{m} = \frac{\lambda N}{m} = \frac{\lambda N_A}{A} = \frac{(4.92 \times 10^{-18} \text{ s}^{-1}) \times (6.022 \times 10^{23} \text{ mol}^{-1})}{(238 \text{ g} \cdot \text{mol})} \\ &= 12449 \text{ Bq/g}.\end{aligned}\quad (11.174)$$

(c) *Specific activity* of U-238 a in Ci/g is determined from specific activity in Bq/g recalling the well known relationships $1 \text{ Ci} = 3.7 \times 10^{10} \text{ Bq}$ or $1 \text{ Bq} = 2.703 \times 10^{-11} \text{ Ci}$ to get

$$\begin{aligned}a &= 12449 \text{ Bq/g} = 12449 \times (2.703 \times 10^{-11} \text{ Ci/g}) = 3.36 \times 10^{-7} \text{ Ci/g} \\ &= 0.336 \text{ } \mu\text{Ci/g}.\end{aligned}\quad (11.175)$$

(d) *Half-life* $(t_{1/2})_{\text{SF}}$ for SF decay of U-238 will be determined from the measured SF decay rate of 24 SF decays per hour per gram of U-238. This decay rate is essentially the specific activity a_{SF} of U-238 for spontaneous decay given as

$$\begin{aligned}a_{\text{SF}} &= \lambda_{\text{SF}} \frac{N_A}{A} = \frac{(\ln 2)}{(t_{1/2})_{\text{SF}}} \frac{N_A}{A} = 24 \text{ h}^{-1} \cdot \text{g}^{-1} = 6.67 \times 10^{-3} \text{ s}^{-1} \cdot \text{g}^{-1} \\ &= 6.67 \times 10^{-3} \text{ Bq/g}\end{aligned}\quad (11.176)$$

from where it follows that the half-life $(t_{1/2})_{\text{SF}}$ for SF decay is given as

$$(t_{1/2})_{\text{SF}} = \frac{(\ln 2)}{a_{\text{SF}}} \frac{N_A}{A} = \frac{(\ln 2) \times (6.022 \times 10^{23} \text{ mol}^{-1})}{(24 \text{ h}^{-1} \cdot \text{g}^{-1}) \times (238 \text{ g} \cdot \text{mol}^{-1})} = 7.31 \times 10^{19} \text{ h}$$

$$= \frac{7.31 \times 10^{19} \text{ h}}{(24 \text{ h/d}) \times 365 \text{ d/a}} = 8.3 \times 10^{15} \text{ a.} \quad (11.177)$$

Decay constant λ_{SF} for SF decay of U-238 is given by the standard expression linking half-life $t_{1/2}$ and decay constant λ as (T10.3)

$$\begin{aligned} \lambda_{\text{SF}} &= \frac{\ln 2}{(t_{1/2})_{\text{SF}}} = \frac{\ln 2}{(8.3 \times 10^{15} \text{ a}) \times (365 \text{ d/a}) \times (24 \text{ h/d}) \times (3600 \text{ s/h})} \\ &= 2.65 \times 10^{-24} \text{ s}^{-1}. \end{aligned} \quad (11.178)$$

(e) Decay constant λ calculated in (a) is actually the *total decay constant* of U-238 equal to the sum of two partial decay constants: λ_{α} for α decay and λ_{SF} for SF decay. However, since, as shown by a comparison of (11.173) and (11.178), the SF decay constant $\lambda_{\text{SF}} = 2.65 \times 10^{-24} \text{ s}^{-1}$ is more than six orders of magnitude smaller than the total decay constant $\lambda = 4.92 \times 10^{-18} \text{ s}^{-1}$, we can assume that the α decay constant λ_{α} is approximately equal to the total decay constant λ , i.e., $\lambda_{\alpha} \approx \lambda$. This allows us to conclude that the probabilities for α decay and SF decay are proportional to decay constants for the two decay modes making α decay a factor of $[4.92 \times 10^{-18} / (2.65 \times 10^{-24})] = 1.85 \times 10^6$ more probable than SF decay, or simply spontaneous fission probability per decay is 5.4×10^{-7} .

(f) *Neutron yield* of U-238 per gram per second is given by the neutron factor $f_n = 2.1$ multiplied by the specific activity a_{SF} for SF decay calculated in (d)

$$f_n a_{\text{SF}} = 2.1 \times (6.67 \times 10^{-3} \text{ s}^{-1} \cdot \text{g}^{-1}) = 14 \times 10^{-3} \text{ s}^{-1} \cdot \text{g}^{-1} \approx 50 \text{ h}^{-1} \cdot \text{g}^{-1}. \quad (11.179)$$

Equation (11.179) shows that 1 gram of U-238 produces ~ 50 neutrons per hour through SF decay.

11.10 Proton Emission Decay

11.10.Q1

(237)

Proton-rich nuclides normally approach stability through β^+ decay or α decay. However, in the extreme case of very large proton excess a nucleus may also move toward stability through emission of one or even two protons. Proton emission (PE) decay is thus a competing process to β^+ and α decay and is, similarly to α decay and spontaneous fission (SF), an example of particle tunneling through the nuclear barrier potential.

(a) List the main characteristics of PE decay.

- (b) Derive general expressions for decay energy Q_{PE} in PE decay using:
- (1) Nuclear rest energy method.
 - (2) Atomic rest energy method.
 - (3) Nuclear binding energy method.
- (c) Derive expressions for two-proton emission (2PE) decay in general and use them to calculate the decay energy $Q_{2\text{PE}}(^{45}_{26}\text{Fe})$ for 2PE decay of the iron-45 nucleus. Use the three methods available for Q value calculation and show that all three give the same end result. Show that single proton emission from Fe-45 nucleus is energetically forbidden.

SOLUTION:

(a) Proton emission (PE) decay is much less common than are β^+ and α decay and is not observed in naturally occurring radionuclides. In this type of decay the atomic number Z decreases by 1 and so does the atomic mass A



The main characteristics of PE decay are:

- (1) In PE decay a proton is ejected from the parent nucleus P and the parent nucleus sheds an orbital electron from its outermost shell to become a neutral daughter atom ${}^{A-1}_{Z-1}\text{D}$.
 - (2) The energetic proton ejected in PE decay slows down in moving through the absorber and captures an electron from its surroundings to become a neutral hydrogen atom ${}^1_1\text{H}$.
 - (3) Since N , the number of neutrons, does not change in proton emission decay, the parent P and daughter D have the same number of neutrons and are called isotones.
 - (4) For lighter, very proton-rich nuclei with an odd number of protons Z , proton emission decay is energetically possible and thus very likely to happen.
 - (5) For lighter, very proton-rich nuclei ($A \approx 50$) with an even number of protons Z , a simultaneous 2-proton emission may occur in situations where a sequential emission of two independent protons is energetically not possible.
 - (6) PE decay as a radioactive decay phenomenon was postulated in the early 1960s and discovered experimentally in the early 1980s in the category of single proton emission decay and in 2002 in the category of two-proton emission decay.
- (b) Like in other types of nuclear decay and for nuclear reactions in general, decay energy Q_{PE} (also called Q_{PE} value) can be determined by using: (1) Nuclear rest energies, (2) Atomic rest energies, and (3) Nuclear binding energies.

(1) *Nuclear rest energy method* is expressed as follows

$$Q_{\text{PE}} = \sum_{i,\text{before}} M_i c^2 - \sum_{i,\text{after}} M_i c^2 = \{M(\text{P}) - [M(\text{D}) + m_p]\}c^2, \quad (11.181)$$

suggesting that Q_{PE} value is determined by subtracting the sum of nuclear rest energies of reaction products (daughter nucleus D and ejected proton) $\sum_{i,\text{after}} M_i c^2$ after the reaction from the sum of nuclear rest energies of reactants (parent nucleus P) $\sum_{i,\text{before}} M_i c^2$ before the reaction. *Note:* M stands for nuclear mass.

(2) *Atomic rest energy method* is based on atomic rest energies and must account for all electrons participating in the PE decay, in addition to all nuclei

$$Q_{\text{PE}} = \sum_{i,\text{before}} \mathcal{M}_i c^2 - \sum_{i,\text{after}} \mathcal{M}_i c^2 = \{\mathcal{M}(\text{P}) - [\mathcal{M}(\text{D}) + \mathcal{M}({}_1^1\text{H})]\}c^2, \quad (11.182)$$

suggesting that Q_{PE} value is determined by subtracting the sum of atomic rest energies of reaction products (daughter atom D and ejected proton that becomes hydrogen atom H) $\sum_{i,\text{after}} \mathcal{M}_i c^2$ after the reaction from the sum of atomic rest energies of reactants (parent atom P) $\sum_{i,\text{before}} \mathcal{M}_i c^2$ before the reaction. *Note:* \mathcal{M} stands for atomic mass.

(3) *Binding energy method.* Q value for PE decay can also be determined with the help of nuclear binding energy E_B by subtracting the sum of nuclear binding energies of reactants (parent nucleus P) before the interaction $\sum_{i,\text{before}} E_B(i)$ from the sum of nuclear binding energies of reaction products (daughter nucleus D) after the interaction $\sum_{i,\text{after}} E_B(i)$, or

$$Q_{\text{PE}} = \sum_{i,\text{after}} E_B(i) - \sum_{i,\text{before}} E_B(i) = E_B(\text{D}) - E_B(\text{P}). \quad (11.183)$$

For PE decay to be feasible, Q_{PE} must be positive and this implies that:

- (1) As is evident from (11.181), the rest mass of the parent nucleus P must exceed the combined rest masses of the daughter nucleus D and the proton, i.e., $M(\text{P}) > M(\text{D}) + m_p$.
- (2) As is evident from (11.182), the rest mass of the parent atom P must exceed the combined rest masses of the daughter atom D and the hydrogen atom H, i.e., $\mathcal{M}(\text{P}) > \mathcal{M}(\text{D}) + \mathcal{M}({}_1^1\text{H})$.
- (3) As is evident from (11.183), the total binding energy of the daughter nucleus $E_B(\text{D})$ must exceed the total binding energy of the parent nucleus $E_B(\text{P})$, i.e., $E_B(\text{D}) > E_B(\text{P})$.

(c) In some very proton-rich nuclei, such as iron-45, single proton emission decay is energetically forbidden (Q value is negative) but it turns out that a simultaneous emission of two protons (2PE decay) is energetically possible because its Q value is positive. The three methods for 2-proton emission decay are expressed as follows:

(1) Nuclear rest energy method

$$\begin{aligned}
Q_{2\text{PE}}(^{45}_{26}\text{Fe}) &= \{M(\text{P}) - [M(\text{D}) + m_p]\}c^2 \\
&= \{M(^{45}_{26}\text{Fe}) - [M(^{43}_{24}\text{Cr}) + 2m_p]\}c^2 \\
&= \{41917.5085 \text{ MeV} - [40039.8468 \text{ MeV} + 2 \\
&\quad \times (938.2720 \text{ MeV})]\} \\
&= 1.118 \text{ MeV}.
\end{aligned} \tag{11.184}$$

(2) Atomic rest energy method

$$\begin{aligned}
Q_{2\text{PE}}(^{45}_{26}\text{Fe}) &= \{\mathcal{M}(\text{P}) - [\mathcal{M}(\text{D}) + 2\mathcal{M}(^1_1\text{H})]\}c^2 \\
&= \{\mathcal{M}(^{45}_{26}\text{Fe}) - [\mathcal{M}(^{43}_{24}\text{Cr}) + 2\mathcal{M}(^1_1\text{H})]\}c^2 \\
&= \{45.014560u - [42.997711u + 2 \times (1.007825u)]\} \\
&= (1.199 \times 10^{-3}u) \times (931.494028 \text{ MeV}/u) \\
&= 1.117 \text{ MeV}.
\end{aligned} \tag{11.185}$$

(3) Nuclear binding energy method

$$\begin{aligned}
Q_{2\text{PE}}(^{45}_{26}\text{Fe}) &= E_{\text{B}}(\text{D}) - E_{\text{B}}(\text{P}) = E_{\text{B}}(^{43}_{24}\text{Cr}) - E_{\text{B}}(^{45}_{26}\text{Fe}) \\
&= 330.42378 \text{ MeV} - 329.30608 \text{ MeV} \\
&= 1.118 \text{ MeV}.
\end{aligned} \tag{11.186}$$

The three methods for calculation of decay energy in 2PE decay of $^{45}_{26}\text{Fe}$ into $^{43}_{24}\text{Cr}$ give the same positive result (1.118 MeV) for $Q_{2\text{PE}}(^{45}_{26}\text{Fe})$, so we conclude that 2PE decay of $^{45}_{26}\text{Fe}$ is energetically feasible. However, the question of single PE decay still stands, so we now calculate the decay energy $Q_{\text{PE}}(^{45}_{26}\text{Fe})$ for PE decay of $^{45}_{26}\text{Fe}$ into manganese $^{45}_{25}\text{Mn}$ using (11.181), (11.182), and (11.183), respectively, as follows

$$\begin{aligned}
Q_{\text{PE}}(^{45}_{26}\text{Fe}) &= \{M(^{45}_{26}\text{Fe}) - [M(^{44}_{25}\text{Mn}) + m_p]\}c^2 \\
&= \{41917.5085 \text{ MeV} - [40979.3623 \text{ MeV} + 938.2713 \text{ MeV}]\} \\
&= -0125 \text{ MeV},
\end{aligned} \tag{11.187}$$

$$\begin{aligned}
Q_{\text{PE}}(^{45}_{26}\text{Fe}) &= \{\mathcal{M}(^{45}_{26}\text{Fe}) - [\mathcal{M}(^{44}_{25}\text{Mn}) + \mathcal{M}(^1_1\text{H})]\}c^2 \\
&= \{45.014560u - [44.006870u + 1.007825u]\} \\
&= (-1.35 \times 10^{-4}u) \times (931.494028 \text{ MeV}) \\
&= -0.1258 \text{ MeV}
\end{aligned} \tag{11.188}$$

and

$$\begin{aligned} Q_{\text{PE}}(^{45}_{26}\text{Fe}) &= E_{\text{B}}(^{44}_{25}\text{Mn}) - E_{\text{B}}(^{45}_{26}\text{Fe}) = 329.18028 \text{ MeV} - 329.30608 \text{ MeV} \\ &= -0.1258 \text{ MeV}. \end{aligned} \quad (11.189)$$

As expected, the three methods for calculation of Q_{PE} decay energy provide the same negative result ($Q_{\text{PE}} = -0.125 \text{ MeV} < 0$) showing that single PE decay of iron-45 is energetically forbidden; however, 2PE decay of iron-45 into chromium-43 is allowed, because its decay energy $Q_{2\text{PE}}$ is positive ($Q_{2\text{PE}} = 1.117 \text{ MeV} > 0$), as shown in (11.184), (11.185), and (11.186).

11.10.Q2

(238)

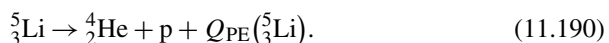
Proton emission (PE) decay is a relatively rare nuclear decay mode characterized by spontaneous emission of an energetic proton. Proton-rich artificially produced nuclei are susceptible to this type of radioactive decay that competes with β^+ decay. Two types of PE decay are known:

- (1) PE decay may occur from high-level excited states in daughter nucleus following β decay—this type of PE decay is called beta-delayed PE decay,
- (2) PE may occur from the ground state of very proton-rich nuclei—this type of PE decay is similar to the α decay tunneling process.

-
- (a) Determine decay energy $Q_{\text{PE}}(^5_3\text{Li})$ for proton emission (PE) decay of lithium-5 (^5_3Li) into helium-4 atom and free proton ejected from the parent nucleus. Use the three standard methods for calculation of the decay energy.
 - (b) For the proton emission decay of (a) determine kinetic energy of the proton (E_{K}_{p}) and recoil kinetic energy ($E_{\text{K}}_{\text{He-4}}$) of the He-4 daughter atom.

SOLUTION:

(a) Lithium-5 radionuclide undergoes the following radioactive decay in which an energetic proton is ejected from the nucleus and the parent nucleus transforms into a helium-4 daughter nucleus. The process is referred to as proton emission (PE) decay and is written as follows



Decay energy $Q_{\text{PE}}(^5_3\text{Li})$ will be calculated with three methods: (1) Nuclear rest energy method, (2) Atomic rest energy method, and (3) Nuclear binding energy method.

(1) *Nuclear rest energy method* with M standing for the nuclear rest mass

$$\begin{aligned} Q_{\text{PE}}({}^5_3\text{Li}) &= M({}^5_3\text{Li})c^2 - M({}^4_2\text{He})c^2 - m_{\text{p}}c^2 \\ &= 4.667.6182 \text{ MeV} - 3727.3791 \text{ MeV} - 938.2720 \text{ MeV} \\ &= 1.967 \text{ MeV}. \end{aligned} \quad (11.191)$$

(2) *Atomic rest energy method* with \mathcal{M} standing for the atomic rest mass

$$\begin{aligned} Q_{\text{PE}}({}^5_3\text{Li}) &= \mathcal{M}({}^5_3\text{Li}) - \mathcal{M}({}^4_2\text{He}) - \mathcal{M}({}^1_1\text{H}) \\ &= (5.012540u - 4.002603u - 1.007825u) \\ &= (1.112 \times 10^{-3}u) \times (931.494028 \text{ MeV}/u) \\ &= 1.967 \text{ MeV}. \end{aligned} \quad (11.192)$$

(3) *Binding energy method*

$$\begin{aligned} Q_{\text{PE}}({}^5_3\text{Li}) &= E_{\text{B}}({}^4_2\text{He})c^2 - E_{\text{B}}({}^5_3\text{Li})c^2 = 28.2957 \text{ MeV} - 26.3287 \text{ MeV} \\ &= 1.967 \text{ MeV}. \end{aligned} \quad (11.193)$$

(b) Decay energy $Q_{\text{PE}}({}^5_3\text{Li})$ calculated with three methods in (a) provides identical positive results, so a conclusion can be made that PE decay of lithium-5 into helium-4 is energetically allowed and its Q_{PE} decay energy is 1.967 MeV shared between the two decay products: ejected proton and recoil helium-4 daughter nucleus.

Now that we have the PE decay energy Q_{PE} , we concentrate on the calculation of kinetic energy of the two decay products produced in PE decay: the proton and the recoil daughter. In contrast to the situation with beta decays (β^- , β^+ , and electron capture), we should not expect the daughter nucleus in PE decay to acquire only a miniscule and negligible portion of the decay energy. This is so, because in beta decay the rest energy of the daughter atom is several orders of magnitude larger than that of the emitted beta particle and even more so for the neutrino. This significant difference in rest energy among the decay products results in an exceedingly small and essentially negligible energy transfer to the daughter atom, which means that the other decay products share the full amount of the decay energy.

In PE decay, on the other hand, the emitted proton's rest energy is comparable to that of the daughter atom, so that the two decay products share the decay energy Q_{PE} in inverse proportion to their rest energies and the recoil daughter picks up an appreciable amount of energy.

For decay of the parent nucleus at rest the proton and the daughter atom acquire vector momenta \mathbf{p}_{p} and \mathbf{p}_{D} , respectively, that are equal in magnitude but opposite in direction. Kinetic energies of the proton (E_{K}_{p}) and recoil daughter atom (E_{K}_{D}) are given classically as follows

$$(E_{\text{K}})_{\text{p}} = \frac{p^2}{2m_{\text{p}}} \quad \text{and} \quad (E_{\text{K}})_{\text{D}} = \frac{p^2}{2\mathcal{M}(\text{D})}, \quad (11.194)$$

where

- p is the magnitude of the momenta of the proton and daughter atom: $|\mathbf{p}_p| = |\mathbf{p}_D| = p$.
 m_p is the rest mass of the proton ($m_p = 938.2720 \text{ MeV}/c^2$).
 $M(D)$ is the rest mass of the daughter atom.

Decay energy Q_{PE} must be positive for PE decay to occur and is equal to the sum of kinetic energies $(E_K)_p$ and $(E_K)_D$ acquired by the emitted proton and recoil daughter atom, respectively

$$\begin{aligned} Q_{PE}(P) &= (E_K)_p + (E_K)_D = \frac{p^2}{2m_p} + \frac{p^2}{2M(D)} = \frac{p^2}{2} \left[\frac{1}{m_p} + \frac{1}{M(D)} \right] \\ &= \frac{p^2}{2m_p} \left[1 + \frac{m_p}{M(D)} \right] = \frac{p^2}{2M(D)} \left[\frac{M(D)}{m_p} + 1 \right]. \end{aligned} \quad (11.195)$$

Equation (11.195) can now be written as follows

$$Q_{PE}(P) = (E_K)_p \left[1 + \frac{m_p}{M(D)} \right] = (E_K)_D \left[\frac{M(D)}{m_p} + 1 \right], \quad (11.196)$$

yielding the following expressions for kinetic energies $(E_K)_p$ and $(E_K)_D$ of the emitted proton and the recoil daughter nucleus, respectively

$$(E_K)_p = Q_{PE}(P) \frac{1}{1 + \frac{m_p}{M(D)}} = Q_{PE}(P) \frac{M(D)}{M(D) + m_p} = Q_{PE}(P) \frac{M(D)c^2}{M(D)c^2 + m_p c^2} \quad (11.197)$$

and

$$(E_K)_D = Q_{PE}(P) \frac{1}{1 + \frac{M(D)}{m_p}} = Q_{PE}(P) \frac{m_p}{M(D) + m_p} = Q_{PE}(P) \frac{m_p c^2}{M(D)c^2 + m_p c^2}. \quad (11.198)$$

We now use (11.197) and (11.198) to determine the ejected proton kinetic energy $(E_K)_p$ and recoil daughter kinetic energy $(E_K)_D$ for our specific example of PE decay of ${}^5_3\text{Li}$ into ${}^4_2\text{He}$ and proton with decay energy Q_{PE} of 1.967 MeV.

(1) For ejected proton energy $(E_K)_p$ we get

$$\begin{aligned} (E_K)_p &= Q_{PE}({}^5_3\text{Li}) \frac{M({}^4_2\text{He})c^2}{M({}^4_2\text{He})c^2 + m_p c^2} \\ &= (1.967 \text{ MeV}) \\ &\quad \times \frac{(4.002603u) \times (931.494028 \text{ MeV}/u)}{(4.002603u) \times (931.494028 \text{ MeV}/u) + 938.272013 \text{ MeV}} \\ &= (1.967 \text{ MeV}) \times \frac{3728.400791}{4666.672804} = 1.572 \text{ MeV}. \end{aligned} \quad (11.199)$$

(2) Recoil kinetic energy $(E_K)_{\text{He-4}}$ of the helium-4 atom is

$$\begin{aligned}
 (E_K)_D &= Q_{\text{PE}}({}_3^5\text{Li}) \frac{m_p c^2}{M({}_2^4\text{He})c^2 + m_p c^2} \\
 &= (1.967 \text{ MeV}) \\
 &\quad \times \frac{(938.272013 \text{ MeV})}{(4.002603u) \times (931.494028 \text{ MeV}/u) + 938.272013 \text{ MeV}} \\
 &= (1.967 \text{ MeV}) \times \frac{938.272013}{4666.672804} \\
 &= 0.395 \text{ MeV}. \tag{11.200}
 \end{aligned}$$

In PE decay of lithium-5 into helium-4 and a proton, 79.9 % (1.572 MeV) of the decay energy Q_{PE} of 1.967 MeV is transferred to the ejected proton and 20.1 % (0.395 MeV) is transferred to the recoil helium-4 atom.

11.11 Neutron Emission Decay

11.11.Q1

(239)

Neutron emission (NE) decay from a neutron-rich nucleus is a competing process to β^- decay but is much less common than β^- decay and is not observed in naturally occurring radionuclides. In contrast to spontaneous fission that also produces neutrons, in neutron emission decay the atomic number Z remains the same but the atomic mass number A decreases by 1. Both the parent nucleus P and the daughter nucleus D are thus isotopes of the same nuclear species. The neutron emission decay relationship is written as follows:



- (a) Determine the general expressions for decay energy Q_{NE} for NE decay using (1) nuclear rest energy method, (2) atomic rest energy method, and (3) nuclear binding energy method.
- (b) Determine general expressions for kinetic energy $(E_K)_n$ of the ejected neutron and recoil kinetic energy $(E_K)_D$ of the daughter atom.
- (c) Using the general expressions for decay energy Q_{NE} derived in (a), calculate Q_{NE} for the following NE decay: ${}_{4}^{13}\text{Be} \rightarrow {}_{4}^{12}\text{Be} + \text{n} + Q_{\text{NE}}({}_{4}^{13}\text{Be})$. Show that the three methods in use for calculation of decay energy give the same results.

- (d) For the neutron emission (NE) decay of (c) use the expressions derived in (b) and determine kinetic energy $(E_K)_n$ of the ejected neutron and recoil kinetic energy $(E_K)_{\text{Be-12}}$ of the Be-12 daughter atom.

SOLUTION:

(a) Decay energy Q_{NE} of neutron emission (NE) decay appears as kinetic energy shared between the neutron ejected from the parent P nucleus and the recoil daughter D nucleus. It can be determined using three methods: (1) Nuclear rest energy method, (2) Atomic rest energy method, and (3) Nuclear binding energy method. All three methods must provide the same results and for NE decay to be energetically allowed Q_{NE} must be positive. Expressions for the three methods are written as follows (T5.7):

- (1) *Nuclear rest energy method* is expressed as follows with M standing for nuclear rest mass

$$Q_{\text{NE}}(\text{P}) = \sum_{i,\text{before}} M_i c^2 - \sum_{i,\text{after}} M_i c^2 = \{M(\text{P}) - [M(\text{D}) + m_n]\} c^2. \quad (11.202)$$

- (2) *Atomic rest energy method* is expressed as follows with \mathcal{M} standing for atomic rest mass

$$Q_{\text{NE}}(\text{P}) = \sum_{i,\text{before}} \mathcal{M}_i c^2 - \sum_{i,\text{after}} \mathcal{M}_i c^2 = \{\mathcal{M}(\text{P}) - [\mathcal{M}(\text{D}) + m_n]\} c^2. \quad (11.203)$$

- (3) *Nuclear binding energy method* is expressed as follows with E_B standing for the total nuclear binding energy

$$Q_{\text{NE}}(\text{P}) = \sum_{i,\text{after}} E_B(i) - \sum_{i,\text{before}} E_B(i) = E_B(\text{D}) - E_B(\text{P}). \quad (11.204)$$

Note: In method (1) and (2) the sum of rest energies of reaction products (daughter D and ejected neutron) after the NE decay is subtracted from parent P rest energy before the NE decay. In method (3) binding energy of parent nucleus before the NE decay is subtracted from the binding energy of the daughter after the NE decay.

(b) For NE decay with the parent nucleus at rest, the ejected neutron and the recoil daughter atom acquire vector momenta \mathbf{p}_n and \mathbf{p}_D , respectively, that are opposite in direction and equal in magnitude in order to satisfy the conservation of momentum principle. Conservation of total energy is satisfied with decay energy Q_{NE} being shared between the ejected neutron and recoil daughter atom.

Kinetic energies of the neutron $(E_K)_n$ and recoil daughter atom $(E_K)_D$ are given classically as follows

$$(E_K)_n = \frac{p^2}{2m_n} \quad \text{and} \quad (E_K)_D = \frac{p^2}{2\mathcal{M}(D)}, \quad (11.205)$$

where

p is the magnitude of the momenta of the neutron and daughter atom: $|\mathbf{p}_p| = |\mathbf{p}_D| = p$.

m_n is the rest mass of the proton ($m_n = 939.5654 \text{ MeV}/c^2$).

$\mathcal{M}(D)$ is the rest mass of the daughter atom.

Decay energy Q_{NE} must be positive for NE decay to occur and is equal to the sum of kinetic energies $(E_K)_n$ and $(E_K)_D$ acquired by the emitted proton and recoil daughter atom, respectively

$$\begin{aligned} Q_{NE}(P) &= (E_K)_n + (E_K)_D = \frac{p^2}{2m_n} + \frac{p^2}{2\mathcal{M}(D)} = \frac{p^2}{2} \left[\frac{1}{m_n} + \frac{1}{\mathcal{M}(D)} \right] \\ &= \frac{p^2}{2m_n} \left[1 + \frac{m_n}{\mathcal{M}(D)} \right] = \frac{p^2}{2\mathcal{M}(D)} \left[\frac{\mathcal{M}(D)}{m_n} + 1 \right]. \end{aligned} \quad (11.206)$$

Equation (11.206) can now be written as follows

$$Q_{NE}(P) = (E_K)_n \left[1 + \frac{m_n}{\mathcal{M}(D)} \right] = (E_K)_D \left[\frac{\mathcal{M}(D)}{m_n} + 1 \right], \quad (11.207)$$

yielding the following expressions for kinetic energies $(E_K)_n$ and $(E_K)_D$ of the emitted proton and the recoil daughter nucleus, respectively

$$(E_K)_n = Q_{NE}(P) \frac{1}{1 + \frac{m_n}{\mathcal{M}(D)}} = Q_{NE}(P) \frac{\mathcal{M}(D)}{\mathcal{M}(D) + m_n} = Q_{NE}(P) \frac{\mathcal{M}(D)c^2}{\mathcal{M}(D)c^2 + m_n c^2} \quad (11.208)$$

and

$$(E_K)_D = Q_{NE}(P) \frac{1}{1 + \frac{\mathcal{M}(D)}{m_n}} = Q_{NE}(P) \frac{m_n}{\mathcal{M}(D) + m_n} = Q_{NE}(P) \frac{m_n c^2}{\mathcal{M}(D)c^2 + m_n c^2}. \quad (11.209)$$

(c) Decay energy $Q_{NE}(^{13}_4\text{Be})$ for neutron emission decay of $^{13}_4\text{Be}$ will be calculated using three methods: (1) Nuclear rest energy method derived in (11.202), (2) Atomic rest energy method derived in (11.203), and (3) Nuclear binding energy method derived in (11.204).

(1) Nuclear rest energy method

$$\begin{aligned} Q_{NE}(^{13}_4\text{Be}) &= \{M(^{13}_4\text{Be}) - [M(^{12}_4\text{Be}) + m_n]\}c^2 \\ &= 12140.6243 \text{ MeV} - 11200.9611 \text{ MeV} - 9395654 \text{ MeV} \\ &= 0.0978 \text{ MeV}. \end{aligned} \quad (11.210)$$

(2) Atomic rest energy method

$$\begin{aligned}
 Q_{\text{NE}}(^{13}_4\text{Be}) &= \{ \mathcal{M}(^{13}_4\text{Be}) - [\mathcal{M}(^{12}_4\text{Be}) + m_n] \} c^2 \\
 &= (13.035691u - 12.026921u) - 939.5654 \text{ MeV} \\
 &= (1.00877u) \times (931.494028 \text{ MeV}/u) - 939.5654 \text{ MeV} \\
 &= 0.0978 \text{ MeV}. \tag{11.211}
 \end{aligned}$$

(3) Nuclear binding energy method

$$\begin{aligned}
 Q_{\text{NE}}(^{13}_4\text{Be}) &= E_{\text{B}}(^{12}_4\text{Be}) - E_{\text{B}}(^{13}_4\text{Be}) \\
 &= 68.64972 \text{ MeV} - 68.55187 \text{ MeV} \\
 &= 0.0979 \text{ MeV}. \tag{11.212}
 \end{aligned}$$

The three methods for calculation of decay energy in NE decay give the same positive result; therefore, one may conclude that NE decay of Be-13 is feasible. The decay energy is somewhat low, so that the kinetic energy of the ejected neutron and the recoil energy of the Be-12 daughter atom are also expected to be low and their exact values will be determined in (d).

(d) We now use (11.205) and (11.209) to determine the ejected neutron kinetic energy $(E_{\text{K}})_n$ and recoil daughter kinetic energy $(E_{\text{K}})_D$ for our specific example of NE decay of $^{13}_4\text{Be}$ into $^{12}_4\text{Be}$ and proton with decay energy Q_{NE} of 0.0978 MeV.

(1) For ejected neutron energy $(E_{\text{K}})_n$ we get

$$\begin{aligned}
 (E_{\text{K}})_p &= Q_{\text{PE}}(^{13}_4\text{Be}) \frac{\mathcal{M}(^{12}_4\text{Be})c^2}{\mathcal{M}(^{12}_4\text{Be})c^2 + m_n c^2} \\
 &= (0.0978 \text{ MeV}) \\
 &\quad \times \frac{(12.026921u) \times (931.494028 \text{ MeV}/u)}{(12.026921u) \times (931.494028 \text{ MeV}/u) + 939.565346 \text{ MeV}} \\
 &= (0.0978 \text{ MeV}) \times \frac{11203.00509}{12142.57043} = (0.0978 \text{ MeV}) \times 0.923 \\
 &= 0.0902 \text{ MeV}. \tag{11.213}
 \end{aligned}$$

(2) Recoil kinetic energy $(E_{\text{K}})_{\text{Be-12}}$ of the beryllium-12 atom is

$$\begin{aligned}
 (E_{\text{K}})_{\text{Be-12}} &= Q_{\text{PE}}(^{13}_4\text{Be}) \frac{m_n c^2}{\mathcal{M}(^{12}_4\text{Be})c^2 + m_n c^2} \\
 &= (0.0978 \text{ MeV}) \\
 &\quad \times \frac{(939.565346 \text{ MeV})}{(12.02692u) \times (931.494028 \text{ MeV}/u) + 939.565346 \text{ MeV}}
 \end{aligned}$$

$$\begin{aligned} &= (0.0978 \text{ MeV}) \times \frac{939.565346}{12142.5695} = (0.0978 \text{ MeV}) \times 0.077 \\ &= 0.0076 \text{ MeV}. \end{aligned} \quad (11.214)$$

In NE decay of beryllium-13 into beryllium-12 and a free neutron, 92.3 % (0.0902 MeV) of the decay energy Q_{NE} of 0.0978 MeV is transferred to the ejected neutron and 7.7 % (0.0076 MeV) is transferred to the recoil beryllium-12 atom.

11.12 Chart of Nuclides

11.12.Q1

(240)

Nuclear data for stable and radioactive nuclides are compiled in a graphic form referred to as the “Chart of Nuclides” drawn in such a way that each nuclide is assigned a unique pixel position in two-dimensional Cartesian diagram.

- (a) Provide names of at least four institutions or organizations that feature a *chart of nuclides* on their web site.
- (b) Answer the following basic questions on the chart of nuclides:
 - (1) Who is credited with developing the chart of nuclides and when?
 - (2) What information does a typical chart of nuclides feature?
 - (3) Roughly how many stable and radioactive nuclides are listed in a typical modern chart of nuclides?
 - (4) In chemistry and atomic physics there is an analog to the chart of nuclides. What is it called, who developed it, and when?
- (c) All known nuclides plotted on a typical chart of nuclides form an island on a map of nuclides. Sketch the “island of nuclides” in first quadrant of a Cartesian diagram and:
 - (1) On the map of nuclides label the abscissa and ordinate and indicate the cardinal directions (North, East, South, and West) with North pointing in the positive ordinate direction.
 - (2) Describe the shape and orientation of the “island of nuclides” on the map of nuclides.
 - (3) Discuss the shores of the island of nuclides and their relationship to “drip lines”.
 - (4) Explain the meaning of the mountain range on the “island of nuclides”.

- (d) Special features evident from the layout of the chart of nuclides:
- (1) Discuss “magic numbers” and the “curve of stability” on the island of nuclides.
 - (2) What do horizontal rows in the chart of nuclides represent?
 - (3) What do vertical columns in the chart of nuclides represent?
 - (4) What do diagonal lines in the ordinal direction SE \rightarrow NW on the island of nuclides represent?

SOLUTION:

(a) Some examples of a chart of nuclides available on the web:

- (1) Brookhaven National Laboratory—National Data Center: www.nndc.bnl.gov/chart/
- (2) International Atomic Energy Agency—Nuclear Data Services: www.nds.iaea.org/
- (3) Karlsruhe Nuclide Chart—European Atomic Energy Community: www.nucleonica.net/

(b) All known nuclides are uniquely characterized by their number of protons Z (atomic number) and their number of neutrons $N = A - Z$ where A is the number of nucleons (atomic mass number).

(1) Italian-American nuclear physicist Emilio Segrè was the first to suggest in the early 1940s the particular orderly presentation of all known nuclear species (stable nuclides and radioactive nuclides usually called radionuclides) in a chart of nuclides on a 2-dimensional Cartesian plot.

Each nuclide is characterized with its own unique combination of atomic number Z and neutron number N and allocated a square (pixel) on the chart of nuclides according to the N and Z values of the nuclide. To honor Segrè’s contribution to nuclear physics and his efforts on developing the nuclide chart the modern chart of nuclides is often referred to as the Segrè chart.

(2) In addition to the number of protons Z and number of neutrons N for a given nuclide, the **Segrè chart** usually indicates the possible radioactive decay paths for radionuclides and provides the following nuclear data:

- For *stable nuclides* it provides the atomic mass number A ; the nuclear mass in unified atomic mass units u ; the natural abundance; and, for example, cross sections for activation interactions.
- For *radionuclides* it provides the atomic mass number A , nuclear mass in unified atomic mass units u , radioactive half-life, and mode of decay.

(3) Currently there are 280 stable nuclides and close to 3500 natural and artificially produced radionuclides featured in a state-of-the-art Segrè chart.

(4) Recognizing periodicity in chemical behavior of then-known elements, Russian chemist Dmitry Mendeleev in 1869 organized the elements in a table of elements with rows and columns in order of increasing atomic weight. The rows and columns were organized such that they accounted for periodicity in chemical properties of elements by listing elements with similar chemical properties in the same column of the table. Mendeleev's table of elements eventually evolved into the modern Periodic Table of Elements in which each element, represented by a chemical symbol and its atomic number, is allocated a unique position in the table depending on its chemical and physical properties.

(c) Figure 11.7 shows a typical example of a condensed version of a modern Chart of Nuclides available from the European Atomic Energy Community in Karlsruhe, Germany. The chart includes all known nuclides from $Z = 1$ to $Z = 118$ and, in addition, it also shows regions of possible, but to date not yet discovered radionuclides. Pixels representing known, as well as unknown yet theoretically feasible nuclides, form a nuclear landscape in the shape of an "island of nuclides" in the sea of nuclear pixels ranging in Z from 0 to 120 and in N from 0 to ~ 180 , with the stable nuclides (shown with black pixels) forming the backbone (mountain range) in the central part of the island.

(1) For a given nuclear species, the number of neutrons $N = A - Z$ is plotted on the abscissa of the map of nuclides while Z is plotted on the ordinate axis. North on the map of nuclides is at the top of the map and South is at the bottom, East is on the right and West is on the left.

(2) The "**island of nuclides**" on the chart or map of nuclides is in the shape of an elongated island oriented from the South-West corner to the North-East corner on the map. The south shore of the island below the mountain ridge is occupied by known neutron-rich radionuclides and a vast "terra incognita" region formed by not yet discovered neutron-rich radionuclides (shown in dark grey color). The north shore of the island above the mountain ridge is occupied by known proton-rich radionuclides as well as by a small number of yet undiscovered proton-rich radionuclides. Very heavy nuclides that are prone to spontaneous fission (SF) occupy the NE tip of the island.

(3) The shores of the "island on nuclides" are delineated by the so-called drip lines beyond which nucleons are no longer bound to the nucleus. The neutron drip line (white line on the map) delineates the extent of the south shore, the proton drip line delineates the north shore, and the spontaneous fission drip line delineates the NE tip of the island.

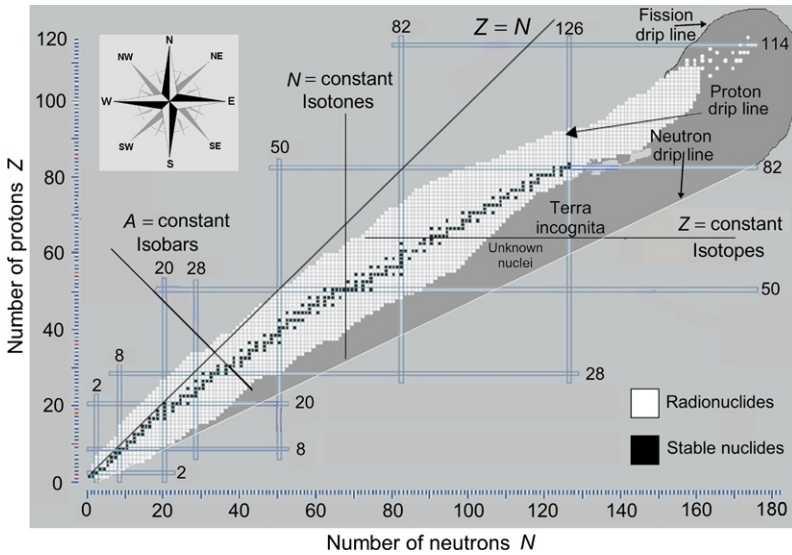


Fig. 11.7 Chart of Nuclides also known as the Segrè chart. Each known stable and radioactive nuclide is characterized by a unique combination of the number of protons Z and number of neutrons N , and assigned a pixel in a 2-dimensional chart displaying N on the abscissa axis and Z on the ordinate axis. Stable nuclides are shown by *dark pixel squares*, radioactive nuclides by *white pixel squares*. The ensemble of stable nuclides forms a “curve of stability”; neutron-rich radionuclides are below the curve of stability; proton-rich radionuclides are above it. Magic numbers for protons and neutrons are indicated as are lines of isotones, lines of isotopes, and lines of isobars

The actual position of the shore as delineated by the drip line, especially in the high Z region, is somewhat arbitrary and depends on various theories and a few sketchy experimental data. The position of the neutron and proton drip lines is governed by interplay in the nucleus between the nuclear strong attractive force in effect among all nucleons and the repulsive Coulomb force in effect among protons. The proton drip line is reached when the binding energy of the outermost proton in a nucleus becomes zero, and, similarly, the neutron drip line is reached when the binding energy of the outermost neutron becomes zero. Since the Coulomb force does not affect neutrons, the neutron drip line is much farther away from the “mountain range” of stable nuclides and the “terra incognita” region for neutron-rich radionuclides is much larger than that for proton-rich nuclides.

(4) Stable nuclides contain a balanced configuration of protons and neutrons because of a preference for pairing of nucleons. On the chart of nuclides they form the backbone or the mountain range of the “island of nuclides” (shown with black pixels in Fig. 11.7) and follow a curve of stability that is defined by an optimum number of protons and neutrons. The curve of stability follows $Z \approx N$ for low Z nuclides and then slowly transforms into $N \approx 1.5Z$ with increasing Z .

Below the curve of stability are neutron-rich radionuclides. Most of them undergo a nuclear transmutation by β^- decay but a few do so by direct neutron emission. Above the curve of stability are proton-rich radionuclides. Most of these undergo a nuclear transmutation by β^+ decay or electron capture but a few do so by direct emission of one proton or even two protons. All nuclides with $Z > 82$ are shown close to the NE tip of the “island of nuclides”. They undergo α decay or spontaneous fission and some may also undergo β decay.

(d) Special features of the Segrè chart of nuclides are noted as follows:

(1) In nature there are 280 nuclides that are considered stable with respect to radioactive decay. Some 60 % of these stable nuclei have an even number of protons and an even number of neutrons (even-even nuclei); some 20 % have an even-odd configuration and a further 20 % have an odd-even configuration. Only 4 stable nuclei are known to have an odd-odd proton / neutron configuration. A conclusion may thus be made that an even number of protons or even number of neutrons promotes stability of nuclear configurations.

When the number of protons is: 2, 8, 20, 28, 50, 82 or the number of neutrons is: 2, 8, 20, 28, 50, 82, 126 the nucleus is observed particularly stable and these numbers are referred to as *magic numbers*. Nuclei in which the number of protons as well as the number of neutrons is equal to a magic number belong to the most stable group of nuclei.

(2) Horizontal rows give the list of known isotopes ($Z = \text{const}$) for a given nuclear species. Stable nuclides are usually shown in black and other colors are used to designate neutron-rich versus proton-rich radionuclides.

(3) Vertical columns give the list of isotones ($N = \text{const}$) which are defined by nuclear species that have the same number of neutrons.

(4) Diagonal lines (in direction roughly perpendicular to the “curve of stability”) give the list of isobars for which $A = Z + N = \text{const}$ defined as nuclear species that contain the same number of nucleons.

11.12.Q2

(241)

The Chart of Nuclides also known as the Segrè chart summarizes the contemporary knowledge in nuclear physics and is available from many authors, institutions, publishers, commercial vendors, and standards laboratories. A typical example of the chart of nuclides is shown in Fig. 11.8, displaying a condensed version of the “Karlsruher Nuklidkarte” (Karlsruhe Chart of Nuclides) issued by the Joint Research Center of the European Commission in Karlsruhe, Germany. The 7th edition of the chart, issued in 2007, contained data on 280 stable nuclides, 2962 radionuclides in ground state, and 692 isomeric radionuclides as well as 8 radioactive decay modes.

- (a) Define stable nuclide, radionuclide in ground state, and isomeric radionuclide.
- (b) Discuss important features of nuclear stability.
- (c) Discuss the pertinent features of the Chart of Nuclides based on Fig. 11.8.

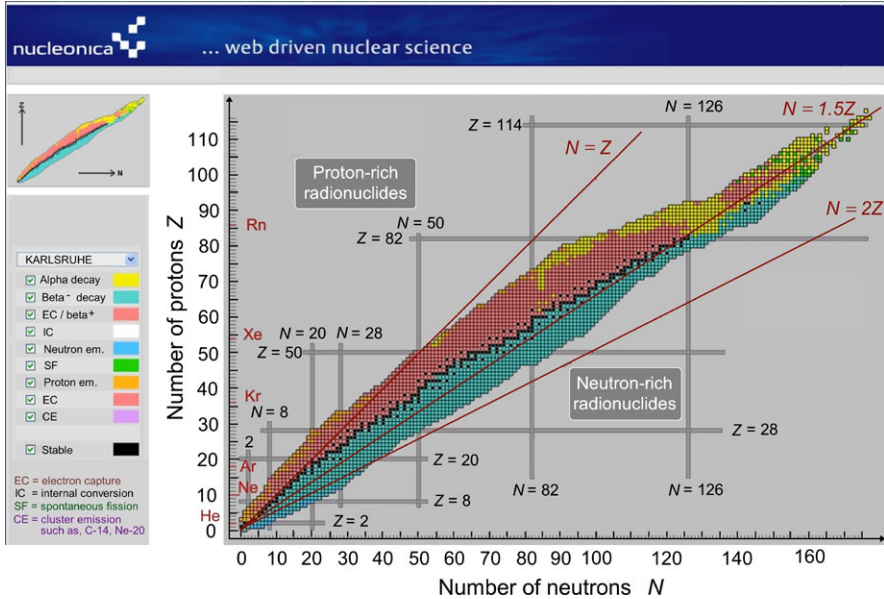


Fig. 11.8 Chart of the Nuclides also known as the Segrè chart. Each known stable and radioactive nuclide is characterized by its unique combination of the number of protons Z and number of neutrons N , and assigned a pixel in a 2-dimensional chart displaying Z on the ordinate axis and N on the abscissa axis. The stable nuclides are shown by *dark pixel squares*, radioactive nuclides by *colored pixel squares*. The plot of stable nuclides forms a curve of stability. The color code for nuclear decay is displayed on the left side-bar to the chart

SOLUTION:

(a) In terms of nuclear stability three categories of nuclides are known: (1) stable nuclide, (2) radioactive nuclide (radionuclide), and (3) isomer (metastable radionuclide).

(1) A *stable nuclide* contains nuclei that have zero probability of undergoing spontaneous nuclear decay. If a nuclide emits no radiation, it is not radioactive, and is assumed stable. If a nuclide emits radiation but has a half-life $t_{1/2}$ too long to be measured, it is also considered stable.

The number of known stable nuclides stands at 280, distributed over 80 elements with atomic number Z between 1 and 82. The number of stable isotopes for a given element varies between 1 for 26 elements up to 10 for tin ($Z = 50$), with 3.5 the mean number of isotopes per element. Two elements with $Z < 83$ (technetium: $Z = 43$ and promethium: $Z = 61$) have no stable isotope.

(2) A *radionuclide* contains unstable (radioactive) nuclei in ground state, decaying with a defined half-life $t_{1/2}$ into more stable nuclear species that may be stable or radioactive and differ from the original radioactive nucleus in atomic number Z and atomic mass number A . Various decay modes are available to an unstable nucleus to achieve a more stable configuration and they result in emission of photons or subatomic particles. Most common of these decay modes are: α decay, β^- decay, electron capture (EC), β^+ decay, and spontaneous fission (SF). Alpha and beta decays often leave the daughter nucleus in an excited state which essentially immediately decays directly or through other excited states into ground state emitting a gamma ray or internal conversion electron.

(3) *Isomeric or metastable radionuclide* contains unstable, excited nuclei decaying through gamma decay or internal conversion to the ground state of the same nuclei with a half-life $t_{1/2} > 10^{-9}$ s. Thus, isomeric nuclear transitions result in emission of gamma rays or internal conversion electrons. Unlike in decay modes of radionuclides in ground state, in decay of isomeric radionuclides, atomic number Z and atomic mass number A do not change and this sets the isomeric nuclides apart from radionuclides in the nuclear ground state.

Close to 700 isomeric or metastable radionuclides have been identified and the best known of these in medical physics is technetium-99m, the most widely used radionuclide for diagnostic imaging in nuclear medicine.

(b) Experiments have shown that the number of nucleons (protons and neutrons) the atomic nucleus contains affects the nuclear stability against decay. The general trend in binding energy per nucleon E_B/A provides the E_B/A maximum at around $A = 60$ and then drops for smaller and larger A . However, there are also considerable variations in stability of nuclei depending on the parity in the number of protons and neutrons forming a nucleus.

(1) The nucleus is held together by attractive strong force between the nucleons that must overcome the electrostatic repulsion between protons. Because of this repulsion the ratio Z/N decreases with increasing atomic number from $Z/N = 1$ for light (low Z) nuclei (1 proton for every neutron) to $Z/N \approx 0.64$ for heavy (high Z) nuclei (2 protons for every 3 neutrons).

(2) When the number of protons is: 2, 8, 20, 28, 50, 82 or the number of neutrons is: 2, 8, 20, 28, 50, 82, 126, the nucleus is observed particularly stable and in nuclear physics these numbers are referred to as *magic numbers*. Nuclei in which the number of protons as well as the number of neutrons is equal to a magic number are called “double magic” and belong to the most stable group of nuclei.

- (3) In nature there are 280 nuclides that are considered stable with respect to radioactive decay, all other nuclides (and there are over 3000 of them) are radioactive. Some 60 % (166) of these stable nuclides have an even number of protons and an even number of neutrons (even-even nuclei); some 20 % (57) have an even-odd configuration and a further 20 % (53) have an odd-even configuration. Only 4 stable nuclides are known to have an odd-odd proton–neutron configuration. A conclusion may thus be made that an even number of protons or even number of neutrons (pairing of nucleons) promotes the stability of nuclear configurations.
- (4) If the optimal equilibrium between protons and neutrons does not exist in a nucleus, the nucleus is unstable (radioactive) and decays with a specific decay constant into a more stable configuration that may also be unstable and decays further, forming a decay chain that eventually ends with a stable nuclide. Nine main processes or modes are available to unstable nuclei (radionuclides) to advance toward a more stable nuclear configuration; for a given radionuclide generally only one type or at most two types of decay process will occur.

(c) The Chart of Nuclides in Fig. 11.8 presents a condensed version of the whole chart and allows identification of its general features. Also shown are the magic numbers for protons and neutrons as well as the curve of nuclear stability that can be identified by following the landscape formed by stable nuclides shown with black pixel squares. Neutron-rich radionuclides are below the curve of stability and shown in green color, while proton-rich radionuclides are above the curve of stability and shown in orange color. The following features of the Chart of Nuclides are notable:

- (1) For a slight imbalance, radionuclides will decay by beta decay characterized by transformation of a proton into a neutron in β^+ decay and a transformation of a neutron into a proton in β^- decay.
- (2) For a large imbalance, the radionuclides will decay by emission of nucleons: α particles in α decay, protons in PE decay, and neutrons in NE decay.
- (3) For very large atomic mass number nuclides ($A > 230$) spontaneous fission, which competes with α decay, is also possible.
- (4) When radionuclide (Z, N) is below the curve of stability (i.e., is neutron-rich), the β^- decay and in extreme cases neutron emission are possible means to attain a more stable configuration. The resulting nucleus will be characterized by $(Z + 1, N - 1)$ for β^- decay and by $(Z, N - 1)$ for neutron emission decay. In β^- the atomic mass number A of the daughter is the same as that of the parent; in neutron emission decay A of the daughter decreases by 1.
- (5) When radionuclide (Z, N) is above the curve of stability (i.e., is proton-rich), the β^+ decay, electron capture or in extreme cases proton emission may be possible means to attain a more stable configuration. The resulting nucleus will be characterized by $(Z - 1, N + 1)$ for β^+ decay and electron capture, and by $(Z - 1, N)$ for proton emission decay. In β^+ decay and electron capture decay the atomic mass number A of the daughter nucleus is the same as that of the parent nucleus; in proton emission decay both Z and A decrease by 1.

- (6) Proton and neutron emission decay are much less common than α and β decays. The two nucleon emission decays are of no importance in medical physics and occur only in artificially produced radionuclides. The main characteristics of radionuclides that decay by proton or neutron emission are an extreme imbalance between the number of protons and the number of neutrons in their nuclei as well as very short half-lives.
- (7) In addition to β decay the radionuclides (Z, N) with $Z > 83$ may decay by α decay or spontaneous fission. In α decay the resulting nucleus is characterized by $(Z - 2, N - 2)$, in contrast to spontaneous fission where the resulting nuclei are much lighter than the parent nucleus.
- (8) In gamma decay and internal conversion decay the parent nucleus is excited and undergoes a de-excitation process by emitting a γ photon or a conversion electron, respectively. Both the parent nucleus and the daughter nucleus are characterized by (Z, N) , since the number of protons as well as the number of neutrons does not change in the decay process.

11.12.Q3

(242)

Most of the naturally occurring elements are mixtures of several stable isotopes, each isotope with its own relative natural abundance (also known as isotopic composition) w_i . For a given chemical element one stable isotope usually predominates; however, natural elements generally consist of atoms of same atomic number Z but of various different atomic mass numbers A as a result of different numbers of neutrons N . The mean atomic mass \bar{M} of a given natural element (also referred to as the *standard atomic weight* of the natural element) is determined as the weighted mean for all stable isotopes constituting the given element as follows

$$\bar{M} = \sum_i w_i \mathcal{M}_i \quad \text{and} \quad \sum_i w_i = 1, \quad (11.215)$$

where w_i is the relative weight (also called isotopic composition) of stable isotope i and \mathcal{M}_i is the atomic mass of stable isotope i constituting the given natural element.

- (a) Isotopic composition of a given natural element is not of much concern as far as chemical properties of the element are concerned. However, isotopes of the same element, despite having almost identical chemical properties, may differ significantly in nuclear properties. Briefly describe methods for separating a mixture of isotopes of a given element and compare the methods with those used for chemical separation of elements.

- (b) Determine the standard atomic weight \bar{M} of molybdenum from data on stable molybdenum isotopes available from the NIST (www.nist.gov/pml/data/comp.cfm).
- (c) Determine the standard atomic weight \bar{M} of lead from data on stable lead isotopes available from the NIST (www.nist.gov/pml/data/comp.cfm).

SOLUTION:

(a) Mixtures of chemical elements can in general be separated with chemical methods, however, mixtures of different isotopes of the same element are more difficult to separate because they generally do not differ in chemical properties and the separation must be based on more complex physical differences, such as atomic mass, rather than on chemical differences.

Isotope separation implies a physical separation of a specific isotope from a chemical element sample containing several isotopes of the same element. The motivation for isotope separation comes from the knowledge that isotopes of same element, despite having almost identical chemical properties, may differ significantly in nuclear properties.

The best-known and probably most important example of isotope separation is enrichment of natural uranium that contains 99.3 % of U-238 and 0.7 % of U-235. The uranium enrichment process increases the percent composition of U-235 in the sample from the natural level to a concentration of 1 % to 2 % in slightly enriched uranium, 3 % to 5 % in lowly enriched uranium to above 20 % in highly enriched uranium. The U-238 remaining in the sample after enrichment is known as depleted uranium and the separation of U-235 from U-238 is of importance because U-235 is fissile by thermal neutrons and U-238 is not.

(b) For molybdenum Mo with atomic number Z of 42, the NIST lists 7 stable isotopes (Mo-92, Mo-94, Mo-95, Mo-96, Mo-97, Mo-98, and Mo-100) and 26 radioactive isotopes ranging in atomic mass A from 83 to 115. The atomic mass \mathcal{M}_i and natural isotopic composition w_i for the 7 stable isotopes of molybdenum obtained from the NIST are listed in Table 11.5 that also shows that, accounting for the seven stable isotopes and their isotopic composition, the atomic weight (mean atomic mass) \bar{M} of natural molybdenum is 95.937.

(c) For lead Pb with atomic number Z of 82, the NIST lists 4 stable isotopes (Pb-204, Pb-206, Pb-207, and Pb-208) and 34 radioactive isotopes ranging in atomic mass A from 83 to 115. The atomic mass \mathcal{M}_i and natural isotopic composition w_i for the 4 stable isotopes of lead obtained from the NIST are listed in Table 11.6 that also shows that, accounting for the four stable isotopes and their isotopic composition, the atomic weight (mean atomic mass) \bar{M} of natural lead is 207.22.

Table 11.5 Atomic mass \mathcal{M}_i , isotopic composition w_i , and the product $w_i\mathcal{M}_i$ for the 7 stable isotopes of molybdenum

i	Stable isotope of molybdenum	Atomic mass \mathcal{M}_i	Isotopic composition w_i	$w_i\mathcal{M}_i$
1	Mo-92	91.9068114	0.1477	13.575
2	Mo-94	93.9050883	0.0923	8.667
3	Mo-95	94.9058421	0.1590	15.090
4	Mo-96	95.9046795	0.1668	15.997
5	Mo-97	96.9060215	0.0956	9.264
6	Mo-98	97.9054082	0.2419	23.683
7	Mo-100	99.9074776	0.0967	9.661
			$\sum_{i=1}^7 w_i = 1$	$\sum_{i=1}^7 w_i\mathcal{M}_i = 95.937$

Table 11.6 Atomic mass \mathcal{M}_i , isotopic composition w_i , and the product $w_i\mathcal{M}_i$ for the 4 stable isotopes of lead

i	Stable isotope of lead Pb	Atomic mass \mathcal{M}_i	Isotopic composition w_i	$w_i\mathcal{M}_i$
1	Pb-204	203.9730436	0.014	2.8556
2	Pb-206	205.9754653	0.241	49.6401
3	Pb-207	206.9758969	0.221	45.7417
4	Pb-208	207.9766521	0.524	108.9798
			$\sum_{i=1}^4 w_i = 1$	$\sum_{i=1}^4 w_i\mathcal{M}_i = 207.22$

11.12.Q4**(243)**

Atomic masses \mathcal{M} and nuclear masses M as well as the atomic rest energies $\mathcal{M}c^2$, nuclear rest energies Mc^2 , and nuclear binding energies E_B for all nuclides discussed in this book are provided in Appendix A and were determined from the atomic mass data compiled by the NIST and available from the NIST at: www.nist.gov/pml/data/comp.cfm.

(1) For a given nuclide listed in Appendix A, its nuclear rest energy Mc^2 was determined by ignoring the binding energy of atomic orbital electrons and subtracting the rest energy of all atomic orbital electrons ($Zm_e c^2$) from the atomic rest energy $\mathcal{M}(u)c^2$ as follows

$$Mc^2 = \mathcal{M}c^2 - Zm_e c^2 = \mathcal{M}(u) \times 931.494028 \text{ MeV/u} - Z \times 0.510999 \text{ MeV}. \quad (11.216)$$

(2) Nuclear binding energy E_B for a given nuclide listed in Appendix A is determined using the mass deficit equation (T1.25) which reads as follows

$$E_B = Zm_p c^2 + (A - Z)m_n c^2 - M c^2, \quad (11.217)$$

where the nuclear rest energy is determined with (11.216).

(3) For a given nuclide listed in Appendix A, binding energy per nucleon E_B/A is calculated by dividing (11.214) with the number of nucleons given by the atomic mass number A .

Using NIST atomic mass data for europium ($Z = 63$) determine:

- (a) Standard atomic weight of europium.
- (b) Atomic rest energy $\mathcal{M}c^2$, nuclear rest energy $M c^2$, nuclear binding energy E_B , and binding energy per nucleon E_B/A for europium-151.
- (c) Atomic rest energy $\mathcal{M}c^2$, nuclear rest energy $M c^2$, nuclear binding energy E_B , and binding energy per nucleon E_B/A for europium-153.
- (d) In (11.216) nuclear rest energy $M c^2$ is determined by subtracting the total rest energy of all atomic electrons $Zm_e c^2$ from the atomic rest energy $\mathcal{M}(u)c^2$. Binding energy $\sum_{i=1}^Z E_B(i)$ of the ensemble of atomic electrons to the atomic nucleus is ignored in (11.216) under the assumption that it is negligible in comparison to atomic and nuclear rest energies. Investigate the effect of electronic binding energy $\sum_{i=1}^Z E_B(i)$ on (11.216) and show that it can indeed be neglected in (11.216).

SOLUTION:

Nuclear data of Appendix A are based on atomic mass \mathcal{M} data available from the NIST and a summary of the calculation procedure is as follows

$$\mathcal{M} \xrightarrow{(1)} \mathcal{M}c^2 \xrightarrow{(2)} M c^2 \xrightarrow{(3)} E_B \xrightarrow{(4)} \frac{E_B}{A}$$

- (1) $\mathcal{M}c^2 = \mathcal{M}(u) \times 931.494028 \text{ MeV}$
- (2) $M c^2 = \mathcal{M}c^2 - Zm_e c^2 = \mathcal{M}c^2 - (0.5110 \text{ MeV})Z \quad (11.218)$
- (3) $E_B = Zm_p c^2 + (A - Z)m_n c^2 - M c^2 = \Delta M c^2$
- (4) $\frac{E_B}{A} = \frac{\Delta M c^2}{A},$

where $\Delta M c^2$ is the energy equivalent of the nuclear mass deficit $\Delta M = Zm_p + (A - Z)m_n - M$.

(a) The general expression for calculation of the standard atomic weight of an element is

$$\bar{M} = \sum_i w_i \mathcal{M}_i \quad \text{and} \quad \sum_i w_i = 1, \quad (11.219)$$

where w_i stands for the isotopic composition (weight) which is also available from the NIST.

According to the NIST europium has two stable isotopes: Eu-151 and Eu-153. Europium-151 has a relative weight of $w_{\text{Eu-151}} = 0.4781$ and atomic mass of $\mathcal{M}_{\text{Eu-151}} = 150.9198502$; Eu-153 has a relative weight of $w_{\text{Eu-153}} = 0.5219$ and atomic weight of $\mathcal{M}_{\text{Eu-153}} = 152.9212303$.

The standard atomic weight (mean atomic mass) is thus calculated as follows

$$\begin{aligned} \bar{M} &= \sum_i w_i \mathcal{M}_i = w_{\text{Eu-151}} \mathcal{M}_{\text{Eu-151}} + w_{\text{Eu-153}} \mathcal{M}_{\text{Eu-153}} \\ &= 0.4781 \times 150.9198502u + 0.5219 \times 152.921303u \\ &= 151.964u. \end{aligned} \quad (11.220)$$

(b) We now calculate atomic rest energy $\mathcal{M}c^2$, nuclear rest energy Mc^2 , nuclear binding energy E_B , and binding energy per nucleon E_B/A for Eu-152 based on $\mathcal{M}_{\text{Eu-151}} = 150.9198502$.

(1) Atomic rest energy $\mathcal{M}_{\text{Eu-151}}c^2$ of Eu-151 is calculated by multiplying the atomic rest mass in unified atomic mass units u with the energy equivalent of u which is $uc^2 = 931.494028 \text{ MeV}$

$$\mathcal{M}_{\text{Eu-151}}c^2 = (150.9198502u) \times (931.494028 \text{ MeV}/u) = 140\,580.9392 \text{ MeV}. \quad (11.221)$$

(2) Nuclear rest energy Mc^2 of Eu-151 is equal to atomic rest energy $\mathcal{M}c^2$ less rest energy of all atomic electrons $Zm_e c^2$

$$\begin{aligned} M_{\text{Eu-151}}c^2 &= \mathcal{M}_{\text{Eu-151}}c^2 - Zm_e c^2 = 140\,580.9392 \text{ MeV} - 63 \times (0.510\,999 \text{ MeV}) \\ &= 140\,580.9392 \text{ MeV} + 32.193 \text{ MeV} = 140\,548.7462 \text{ MeV}. \end{aligned} \quad (11.222)$$

(3) Nuclear binding energy E_B of Eu-151 is determined using the mass deficit equation (T1.25) as follows

$$\begin{aligned} E_B &= Zm_p c^2 + (A - Z)m_n c^2 - Mc^2 \\ &= 63 \times (938.272013 \text{ MeV}) + 88 \times (939.565346 \text{ MeV}) - (140\,548.7462 \text{ MeV}) \\ &= 59\,111.13682 \text{ MeV} + 82\,681.75045 \text{ MeV} - 140\,548.7462 \text{ MeV} \\ &= 1244.1411 \text{ MeV}. \end{aligned} \quad (11.223)$$

(4) Binding energy per nucleon E_B/A for Eu-151 is calculated by dividing (11.223) with the number of nucleons given by the atomic mass number A which for Eu-151 is 151 nucleons

$$\frac{E_B}{A} = \frac{1244.1411 \text{ MeV}}{151} = 8.2393 \text{ MeV.} \quad (11.224)$$

(c) For europium-153 we now apply the same process as in (b) and calculate atomic rest energy $\mathcal{M}c^2$, nuclear rest energy Mc^2 , nuclear binding energy E_B , and binding energy per nucleon E_B/A based on the NIST value for the rest mass in unified atomic mass units u $\mathcal{M}_{\text{Eu-153}} = 152.9212303$.

(1) Atomic rest energy $\mathcal{M}_{\text{Eu-153}}c^2$ is calculated by multiplying the atomic rest mass in unified atomic mass units u with the energy equivalent of u which is $uc^2 = 931.494028 \text{ MeV}$

$$\mathcal{M}_{\text{Eu-153}}c^2 = (152.9212303u) \times (931.494028 \text{ MeV}/u) = 142\,445.2128 \text{ MeV.} \quad (11.225)$$

(2) Nuclear rest energy Mc^2 of Eu-151 nucleus is equal to atomic rest energy $\mathcal{M}c^2$ less rest energy of all atomic electrons $Zm_e c^2$

$$\begin{aligned} M_{\text{Eu-153}}c^2 &= \mathcal{M}_{\text{Eu-153}}c^2 - Zm_e c^2 = 142\,445.2128 \text{ MeV} - 63 \times 0.510\,999 \text{ MeV} \\ &= 142\,445.2128 \text{ MeV} - 32.193 \text{ MeV} = 142\,413.0198 \text{ MeV.} \end{aligned} \quad (11.226)$$

(3) Nuclear binding energy E_B for Eu-153 is determined using the mass deficit equation (T1.25) as follows

$$\begin{aligned} E_B &= Zm_p c^2 + (A - Z)m_n c^2 - Mc^2 \\ &= 63 \times (938.272013 \text{ MeV}) + 90 \times (939.565346 \text{ MeV}) - (142445.2128 \text{ MeV}) \\ &= 59111.13682 \text{ MeV} + 84560.88114 \text{ MeV} - 142445.2128 \text{ MeV} \\ &= 1226.8052 \text{ MeV.} \end{aligned} \quad (11.227)$$

(4) Binding energy per nucleon E_B/A is calculated by dividing (11.227) with the number of nucleons given by the atomic mass number A which for Eu-151 is 151 nucleons

$$\frac{E_B}{A} = \frac{1226.8052 \text{ MeV}}{153} = 8.0183 \text{ MeV.} \quad (11.228)$$

(d) In (11.216) the nuclear rest energy Mc^2 is determined simply by subtracting $Zm_e c^2$, total rest energy of the ensemble of all atomic electrons, from the atomic rest energy $\mathcal{M}c^2$. Binding energy of orbital electrons $\sum_{i=1}^E E_B(i)$ to the atomic nucleus is neglected in (11.216) and in this section we investigate the validity of this approach.

To account for the electron binding energy we write (11.216) as follows

$$Mc^2 = \mathcal{M}c^2 - \left[Zm_e c^2 - \sum_{i=1}^Z E_B(i) \right], \quad (11.229)$$

where $\sum_{i=1}^Z E_B(i)$ is a sum of binding energies of individual electrons to the atomic nucleus ranging from 13.6 eV for hydrogen that has one orbital electron up to ~ 1 MeV for the heaviest elements with close to 100 orbital electrons, some of them in inner atomic shells (2 electrons in K shell, 8 electrons in L shell, etc.) that are very tightly bound to the nucleus. The total atomic binding energy $\sum_{i=1}^Z E_B(i)$ of all atomic electrons can, of course, be established by inspecting the atomic energy level diagram of a given atom and summing up binding energies of individual electrons. However, there is also an empirical expression available based on the Thomas-Fermi atomic model (T2.47) using an empirical constant as follows

$$\sum_{i=1}^Z E_B(i) \approx 15.73Z^{7/3}. \quad (11.230)$$

For europium ($Z = 63$) the empirical expression (11.230) yields total atomic binding energy $\sum_{i=1}^Z E_B(i)$ of 248 keV or 0.248 MeV while the sum of 63 electronic rest energies in (11.216) amounts to 32.2 MeV. This means that, instead of subtracting 32.2 MeV from atomic rest energy $\mathcal{M}c^2$ in (11.216), we should subtract (32.2 MeV $-$ 0.25 MeV = 31.95 MeV). Since the difference between accounting for and neglecting the total atomic binding energy is small and, moreover, since the total atomic binding energy in comparison to nuclear binding energy of ~ 8 MeV/nucleon is over 4 orders of magnitude smaller, it is customary and reasonable to neglect the total atomic binding energy in nuclear calculations unless one is interested in extreme precision.

11.13 Summary of Radioactive Decay Modes

11.13.Q1

(244)

Since Becquerel's discovery of natural radioactivity in 1896, radionuclides have found many important applications in science, industry, and medicine. In radiation medicine radionuclides are used for imaging in nuclear medicine, for radiotherapy in external beam radiotherapy as well as in brachytherapy, for blood irradiation in prevention of transfusion-associated graft versus host disease and for sterilization of medical supplies and equipment.

- (a) List at least 5 important characteristics of radionuclides used as radiation source for external beam radiotherapy.
- (b) List four radionuclides that out of close to 3000 known natural or artificial radionuclides were found suitable as source in external beam radiotherapy.
- (c) Calculate specific activity a for the four radionuclides potentially useful as teletherapy sources.

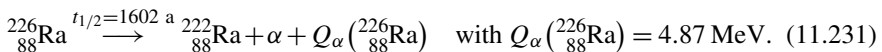
SOLUTION:

(a) The sought-after beams for use in external beam radiotherapy with a radioactive source are gamma rays that follow alpha or beta decay of a suitable radionuclide. The most important characteristics of gamma emitters used in external beam radiotherapy are:

- (1) Relatively *high gamma ray energy* to enable external beam radiotherapy in the megavoltage energy range.
- (2) Relatively *long half-life* to allow for relatively long (few years) duration of source usage. This minimizes the cost of periodic source replacements and machine downtime caused by source replacement.
- (3) *High specific activity* to minimize the source size for a given machine output. The smaller is the source size, the smaller is the geometric penumbra of the clinical beam.
- (4) *Large specific air-kerma rate constant* to maximize source output.
- (5) *As low cost* as possible for source manufacturing to minimize the cost of machine operation.
- (6) *Low safety hazard* to minimize the danger of malevolent usage.

(b) Out of close to 3000 natural and artificial radionuclides known, only four were identified as useful (radium-226, cobalt-60, and cesium-137) or potentially useful (europium-152) as source in external beam radiotherapy or in blood and food irradiators. And, even these four radionuclides do not meet to the same level all six source requirements listed in (a).

(1) **Radium-226** is an alpha emitter decaying with a half-life $t_{1/2}$ of 1602 years into radon-222 which in itself is radioactive and decays with a half-life $t_{1/2}$ of 3.824 days by alpha decay into polonium-218

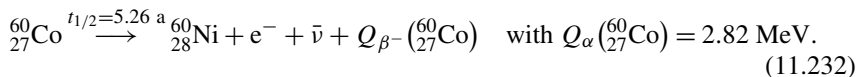


The radioactive progeny of the radium-226 radioactive decay series, when enclosed in a sealed radium source, undergo their own α or β decays accompanied by a spectrum of energetic γ rays that can be used in external beam radiotherapy.

Before the advent of cobalt-60 and cesium-137 teletherapy machines in 1950s all radionuclide based external beam radiotherapy machines made use of radium-226. They were called teleradium machines, contained up to 10 g of radium-226 ($\sim 10 \text{ Ci} = 370 \text{ TBq}$) and were very expensive because of the tedious radium-226 manufacturing process. They were also very inefficient because of the low specific activity of radium-226 and self-absorption of γ radiation in the source. Therefore, radium-226 appears on the list of radionuclide external beam sources largely because of its historical importance in early days of radioactivity studies; its use for external beam radiotherapy has been supplanted mainly by cobalt-60, less and less so by cesium-137, and possibly in the future by europium-152.

(2) **Cobalt-60** is β^- emitter that appeared on the teletherapy scene in the early 1950s when Canadian medical physicist Harold Johns developed a cobalt-60 teletherapy machine for use in cancer therapy. Since then, cobalt-60, produced by thermal neutron activation of stable cobalt-59 in a nuclear reactor, became the radionuclide source of choice for teletherapy machines. It has several characteristics that, in comparison with radium-226, make it much more suitable as source in teletherapy machines and its only relatively weak point is its half-life $t_{1/2}$ of 5.26 years which necessitates a source change every 5 to 10 years.

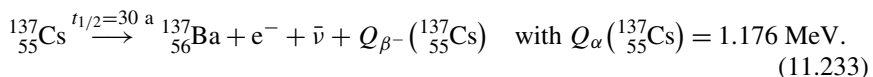
Cobalt-60 decays through β^- decay into nickel-60 as follows



The invention of the cobalt-60 teletherapy machine provided a tremendous boost in the quest for higher photon energies and placed the cobalt-60 machine into the forefront of radiotherapy for a number of years, mainly because it incorporated a radioactive source that very nicely met the essential requirements for radionuclide source enunciated in (a).

During the last 3 decades the linear accelerator, designed for radiotherapy and incorporating several new and exciting features not available from radionuclide sources, eclipsed the cobalt-60 teletherapy machine and became the machine of choice for radiotherapy of deep-seated tumors. However, because of its lower cost as well as simplicity in operation, the cobalt-60 teletherapy machine still serves an important purpose in developing countries.

(3) **Cesium-137** is one of only three radionuclides that have been used clinically to date for source in external beam radiotherapy. In comparison with cobalt-60, it does not satisfy the six requirements stated in (a) as well as does cobalt-60, except that it undergoes β^- decay into barium-137 with a half-life $t_{1/2}$ of 30 years compared to 5.26 years for cobalt



In the past cesium-137 has been used as source in external beam radiotherapy, as brachytherapy source, as well as a source for blood irradiators. During the last decade, its use for brachytherapy has been abandoned in favor of more practical

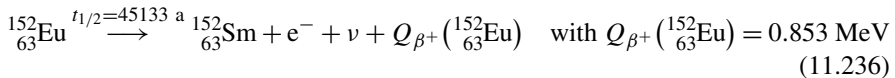
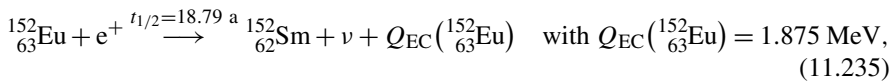
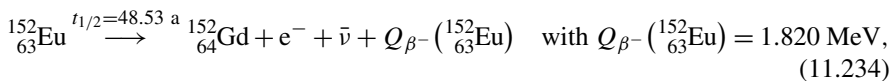
iridium-192 radionuclide, its use in teletherapy machines has been abandoned because of security concerns, and currently its use is limited to blood irradiators largely for practical reasons of long half-life (long-lasting machines) and lower γ ray energy that diminishes shielding requirements.

(4) Cobalt-60 meets the source criteria of (a) in all aspects quite well except for half-life $t_{1/2}$ which at 5.26 years is relatively short requiring costly source changes at higher than optimal frequency. In this regard, cesium-137 with $t_{1/2} = 30$ years is a much better source material, however, Cs-137 is also highly soluble in water and dispersible in air and thus poses a serious security problem that precludes its clinical use in modern teletherapy machines.

In mid 1990s reports appeared on a new source material, **Europium-152**, said to meet all source criteria as well or better than Co-60. For example, its half-life $t_{1/2}$ is 13.54 years, almost 3 times as long as that of Co-60, and, moreover, it can be produced in a nuclear reactor with thermal neutron activation about 10 times faster (few months) than Co-60 which takes several years making the source significantly cheaper.

Europium with atomic number $Z = 63$ is in the group of rare earth metals with two stable isotopes (Eu-151 and Eu-153) and 36 radioactive isotopes, most of them short-lived and ranging in atomic mass A from 130 to 167. In comparison with decay schemes of Co-60 and Cs-137, the decay scheme of Eu-152 is much more complex featuring 3 decay modes: β^- , electron capture, and β^+ , with branching fractions f_i : $f_{\beta^-} = 27.9\%$, $f_{EC} = 72.1\%$, and $f_{\beta^+} = 0.03\%$, respectively. The Eu-152 decay modes result in many γ ray photons originating from the daughters gadolinium-152 and samarium-152 and producing effective photon energy close to that of essentially mono-energetic Co-60. In addition, Eu-152 also produces β^- particles (electrons), β^+ particles (positrons), internal conversion electrons, Auger electrons, and characteristic x-ray photons and these additional emanations will be absorbed in source capsule of the Eu-152 source.

The decay modes of Eu-152 are as follows



where decay energies Q for the three decay modes: β^- , EC, and β^+ of Eu-152 were calculated using the standard expressions given by (T11.26), (T11.48), and (T11.39), respectively, and the partial half-lives $(t_{1/2})_i$ for individual decay i were determined based on branching fraction f_i for each given decay (T10.78). A summary of these calculations using appropriate data from Appendix A is as follows:

Half-life $t_{1/2}$ for decay of Eu-152 is 13.54 years and this is equivalent to the total decay constant λ

$$\lambda = \frac{\ln 2}{t_{1/2}} = \frac{\ln 2}{(13.54 \text{ a}) \times (365 \text{ d/a}) \times (24 \text{ h/d}) \times (3600 \text{ s/h})} = 1.623 \times 10^{-9} \text{ s}^{-1}, \quad (11.237)$$

that is the sum of three partial decay constants for the three decay modes of Eu-152

$$\begin{aligned} \lambda &= \sum_{i=1}^3 \lambda_i = \sum_{i=1}^3 f_i \lambda = \lambda_{\beta^-} + \lambda_{\text{EC}} + \lambda_{\beta^+} = f_{\beta^-} \lambda + f_{\text{EC}} \lambda + f_{\beta^+} \lambda \\ &= (f_{\beta^-} + f_{\text{EC}} + f_{\beta^+}) \lambda. \end{aligned} \quad (11.238)$$

(1) Beta minus (β^-) decay of europium-152 into gadolinium-152

$$\begin{aligned} Q_{\beta^-}({}^{152}_{63}\text{Eu}) &= [\mathcal{M}(Z, A) - \mathcal{M}(Z + 1, A)]c^2 = \mathcal{M}({}^{152}_{63}\text{Eu})c^2 - \mathcal{M}({}^{152}_{64}\text{Gd})c^2 \\ &= [151.921745u - 151.919791u]c^2 \\ &= (1.954 \times 10^{-3}u) \times (931.494028 \text{ MeV}/u) \\ &= 1.820 \text{ MeV}. \end{aligned} \quad (11.239)$$

(2) Electron capture (EC) decay of europium-152 into samarium-152

$$\begin{aligned} Q_{\text{EC}}({}^{152}_{63}\text{Eu}) &= [\mathcal{M}(Z, A) - \mathcal{M}(Z - 1, A)]c^2 = \mathcal{M}({}^{152}_{63}\text{Eu})c^2 - \mathcal{M}({}^{152}_{62}\text{Sm})c^2 \\ &= [151.921745u - 151.919732u]c^2 \\ &= (2.013 \times 10^{-3}u) \times (931.494028 \text{ MeV}/u) \\ &= 1.875 \text{ MeV}. \end{aligned} \quad (11.240)$$

(3) Beta plus (β^+) decay of europium-152 into samarium-152

$$\begin{aligned} Q_{\beta^+}({}^{152}_{63}\text{Eu}) &= [\mathcal{M}(Z, A) - \mathcal{M}(Z - 1, A) + 2m_e c^2]c^2 \\ &= \mathcal{M}({}^{152}_{63}\text{Eu})c^2 - \mathcal{M}({}^{152}_{64}\text{Gd})c^2 - 2m_e c^2 \\ &= [151.921745u - 151.919732u - 2 \times 5.4858 \times 10^{-4}u]c^2 \\ &= (0.916 \times 10^{-3}u) \times (931.494028 \text{ MeV}/u) \\ &= 0.853 \text{ MeV}. \end{aligned} \quad (11.241)$$

- (4) Decay constant λ_{β^-} and half-life $(t_{1/2})_{\beta^-}$ for beta minus decay of Eu-152 are as follows

$$\lambda_{\beta^-} = f_{\beta^-}\lambda = 0.279 \times (1.623 \times 10^{-9} \text{ s}^{-1}) = 4.528 \times 10^{-10} \text{ s}^{-1} \quad (11.242)$$

and

$$(t_{1/2})_{\beta^-} = \frac{\ln 2}{\lambda_{\beta^-}} = \frac{\ln 2}{(4.528 \times 10^{-10} \text{ s}^{-1})} = 1.531 \times 10^9 \text{ s} = 48.54 \text{ a.} \quad (11.243)$$

- (5) Decay constant λ_{EC} and half-life $(t_{1/2})_{\text{EC}}$ for electron capture decay of Eu-152 are

$$\lambda_{\text{EC}} = f_{\text{EC}}\lambda = 0.721 \times (1.623 \times 10^{-9} \text{ s}^{-1}) = 1.170 \times 10^{-9} \text{ s}^{-1} \quad (11.244)$$

and

$$(t_{1/2})_{\text{EC}} = \frac{\ln 2}{\lambda_{\text{EC}}} = \frac{\ln 2}{(1.170 \times 10^{-9} \text{ s}^{-1})} = 5.924 \times 10^8 \text{ s} = 18.79 \text{ a.} \quad (11.245)$$

- (6) Decay constant λ_{β^+} and half-life $(t_{1/2})_{\beta^+}$ for beta plus decay of Eu-152 are as follows

$$\lambda_{\beta^+} = f_{\beta^+}\lambda = 0.0003 \times (1.623 \times 10^{-9} \text{ s}^{-1}) = 4.869 \times 10^{-13} \text{ s}^{-1} \quad (11.246)$$

and

$$(t_{1/2})_{\beta^+} = \frac{\ln 2}{\lambda_{\beta^+}} = \frac{\ln 2}{(4.869 \times 10^{-13} \text{ s}^{-1})} = 1.424 \times 10^{12} \text{ s} = 45142 \text{ a.} \quad (11.247)$$

To verify the calculated partial decay constants λ_i and calculated half-lives $(t_{1/2})_i$ for the three decay modes of Eu-152 we write (11.238) as follows

$$\lambda = \frac{\ln 2}{t_{1/2}} = \sum_{i=1}^3 \lambda_i = (\ln 2) \sum_{i=1}^3 \frac{1}{(t_{1/2})_i} = (\ln 2) \left[\frac{1}{(t_{1/2})_{\beta^-}} + \frac{1}{(t_{1/2})_{\text{EC}}} + \frac{1}{(t_{1/2})_{\beta^+}} \right]. \quad (11.248)$$

From (11.248) we now get the following expression for the effective half-life $t_{1/2}$

for the combined effect of three modes of decay (β^- , EC, and β^+) of Europium-152

$$\begin{aligned} \frac{1}{t_{1/2}} &= \frac{1}{(t_{1/2})_{\beta^-}} + \frac{1}{(t_{1/2})_{\text{EC}}} + \frac{1}{(t_{1/2})_{\beta^+}} = \frac{1}{48.54 \text{ a}} + \frac{1}{18.79 \text{ a}} + \frac{1}{45142 \text{ a}} \\ &= 0.07384 \text{ a}^{-1}, \end{aligned} \quad (11.249)$$

from where it follows that $t_{1/2} = 13.54 \text{ a}$, as stated above in the discussion of suitability of Eu-152 as material for teletherapy machine source.

(c) Specific activity a of a radionuclide is defined as activity \mathcal{A} per unit mass m and is determined from the following expression

$$a = \frac{\mathcal{A}}{m} = \frac{\lambda N}{m} = \frac{\lambda N_A}{A} = \frac{(\ln 2) N_A}{t_{1/2} A}. \quad (11.250)$$

(1) Specific activity a of radium-226 is

$$\begin{aligned} a &= \frac{(\ln 2) N_A}{t_{1/2} A} = \frac{(\ln 2)}{(1602 \text{ a}) \times (365 \text{ d/a}) \times (24 \text{ h/d}) \times (3600 \text{ s/h})} \\ &\quad \times \frac{(6.022 \times 10^{23} \text{ mol}^{-1})}{(226 \text{ g} \cdot \text{mol}^{-1})} \\ &= 3.66 \times 10^{10} \text{ s}^{-1} \cdot \text{g}^{-1} = 36.6 \text{ TBq/g} = \frac{3.66 \times 10^{10} \text{ Bq/g}}{3.7 \times 10^{10} \text{ Bq/Ci}} \\ &= 0.989 \text{ Ci/g} \approx 1 \text{ Ci/g}. \end{aligned} \quad (11.251)$$

The old unit of activity, the curie (Ci), was initially defined as the activity of 1 g of radium-226 and given as $1 \text{ Ci} = 3.7 \times 10^{10} \text{ s}^{-1}$. The activity of 1 g of radium-226 was subsequently measured to be $3.665 \times 10^{10} \text{ s}^{-1}$; however, the definition of the curie was kept at $1 \text{ Ci} = 3.7 \times 10^{10} \text{ s}^{-1}$. The current activity of 1 g of radium-226 is thus 0.988 Ci or $3.665 \times 10^{10} \text{ Bq} = 36.65 \text{ TBq}$.

(2) Specific activity a of cobalt-60 is

$$\begin{aligned} a &= \frac{(\ln 2) N_A}{t_{1/2} A} = \frac{(\ln 2)}{(5.26 \text{ a}) \times (365 \text{ d/a}) \times (24 \text{ h/d}) \times (3600 \text{ s/h})} \\ &\quad \times \frac{(6.022 \times 10^{23} \text{ mol}^{-1})}{(60 \text{ g} \cdot \text{mol}^{-1})} \\ &= 4.194 \times 10^{13} \text{ s}^{-1} \cdot \text{g}^{-1} = 41940 \text{ TBq/g} \\ &= \frac{4.194 \times 10^{13} \text{ Bq/g}}{3.7 \times 10^{10} \text{ Bq/Ci}} = 1133 \text{ Ci/g}. \end{aligned} \quad (11.252)$$

Specific activity of cobalt-60 of 1133 Ci/g is the theoretical specific activity of carrier-free cobalt-60 source. This means that the source sample of cobalt-60 contains only cobalt-60 atoms. However, as a result of cobalt-60 production with neutron activation of cobalt-59 in a nuclear reactor, a practical commercial cobalt-60 source is not carrier free, rather, it contains a significant amount of cobalt-59 atoms remaining from the activation process as well as nickel-60 atoms from cobalt-60 decay during the activation process. Therefore, a practical commercial cobalt-60 teletherapy source activity does not exceed $\sim 300 \text{ Ci/g}$.

(3) Specific activity a of cesium-137 is

$$\begin{aligned}
 a &= \frac{(\ln 2) N_A}{t_{1/2} A} = \frac{(\ln 2)}{(30 \text{ a}) \times (365 \text{ d/a}) \times (24 \text{ h/d}) \times (3600 \text{ s/h})} \\
 &\quad \times \frac{(6.022 \times 10^{23} \text{ mol}^{-1})}{(137 \text{ g} \cdot \text{mol}^{-1})} \\
 &= 3.221 \times 10^{12} \text{ s}^{-1} \cdot \text{g}^{-1} = 3221 \text{ TBq/g} \\
 &= \frac{3.221 \times 10^{12} \text{ Bq/g}}{3.7 \times 10^{10} \text{ Bq/Ci}} = 87.04 \text{ Ci/g.} \quad (11.253)
 \end{aligned}$$

(4) Specific activity a of europium-152 is

$$\begin{aligned}
 a &= \frac{(\ln 2) N_A}{t_{1/2} A} = \frac{(\ln 2)}{(13.54 \text{ a}) \times (365 \text{ d/a}) \times (24 \text{ h/d}) \times (3600 \text{ s/h})} \\
 &\quad \times \frac{(6.022 \times 10^{23} \text{ mol}^{-1})}{(152 \text{ g} \cdot \text{mol}^{-1})} \\
 &= 6.431 \times 10^{12} \text{ s}^{-1} \cdot \text{g}^{-1} = 6431 \text{ TBq/g} \\
 &= \frac{6.431 \times 10^{12} \text{ Bq/g}}{3.7 \times 10^{10} \text{ Bq/Ci}} = 173.8 \text{ Ci/g.} \quad (11.254)
 \end{aligned}$$

Europium-152 source, similarly to cobalt-60 source, cannot be produced carrier-free with neutron activation of Eu-151 in a nuclear reactor. The practical activity is said to be around 150 Ci/g.

11.13.Q2

(245)

The chart of nuclides, also known as the Segrè chart, allocates to each known nuclide a pixel square uniquely defined by the nuclide's number of neutrons N plotted on the abscissa axis and number of protons Z plotted on the ordinate axis. For each nuclide entered into the chart, in addition to providing nuclear data, the chart also allows an investigation of possible nuclear decays as well as possible results of nuclear bombardment with various nuclear particles.

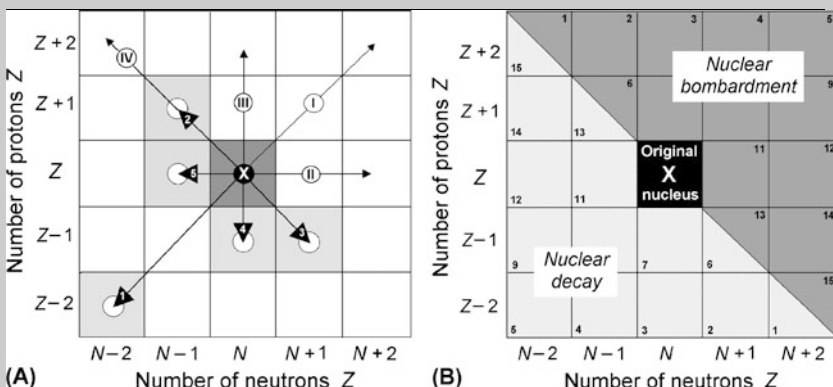


Fig. 11.9 A small section of the Chart of Nuclides centered about an original nucleus X with coordinates (N, Z). (A) Possible decay paths are indicated with numbered arrows and four special directions on the chart are labeled with roman numerals. (B) The small section of the Chart of Nuclides of (A) split into half along diagonal line. The upper half represents the region of nuclear bombardment; the lower half represents nuclear decay

- Figure 11.9(A) shows a small section of the Chart of Nuclides centered about the “original nucleus” X with coordinates (N, Z). Possible nuclear decay paths are indicated with arrows numbered from 1 to 5. For each arrow, identify and explain briefly the decay it represents and write appropriate equations to describe the decay as well as the associated decay energy (Q value). Note that an arrow may represent more than one decay mode.
- Four special directions (lines) are indicated in Fig. 11.9(A) with roman numerals I, II, III, and IV. Identify and explain briefly the special directions and explain their meaning.
- Figure 11.9(B) shows the small section of the Chart of Nuclides cut in half along the diagonal line IV. The upper half (dark grey pixels) represents the region of possible bombardment of nucleus X; the lower half (light grey pixels) represents the region of possible decay of nucleus X. The particles of interest in both regions are: β^- (electron), β^+ (positron), p (proton), n (neutron), d (deuteron), t (triton), helium-3 nucleus, and α particle (helium-4 nucleus). Place the particles of interest into appropriate pixel area using + sign in the nuclear bombardment region (absorption of particle) and - sign in the nuclear decay region (emission of particle).

SOLUTION:

(a) The decay paths of interest in connection with Fig. 11.9(A) can all be characterized with a defined, orderly, and reproducible change either in proton number Z or neutron number N or in both. Thus, gamma decay and internal conversion are excluded from this exercise because the two nuclear decays do not engender a change in either Z or N . Spontaneous fission is also excluded, because it is not linked with an orderly and reproducible change in Z or N . However, all the other standard decay modes are included and their effect on Fig. 11.9(A) will be investigated.

The decay modes to be considered are thus as follows: (1) alpha (α) decay, (2) beta minus (β^-) decay, (3) electron capture (EC) decay, (4) beta plus (β^+) decay, (5) proton emission (PE) decay, (6) two proton emission (2PE) decay, and (7) neutron emission (NE) decay.

Arrows of Fig. 11.9(A) are identified as follows (note: in equations below M stands for nuclear mass, \mathcal{M} for atomic mass, P for parent, and D for daughter):

(1) **Arrow #1** represents α decay that is characterized by the following changes in atomic number Z , neutron number N , and atomic mass number A : $Z \rightarrow Z - 2$, $N \rightarrow N - 2$, and $A \rightarrow A - 4$ to account for emission of an α particle (helium-4 nucleus) from the parent atom. The basic relationship for α decay is expressed as follows [see (T10.2)]

$${}^A_Z\text{P} \rightarrow {}^{A-4}_{Z-2}\text{D} + \alpha + Q_\alpha(\text{P}), \quad (11.255)$$

where $Q_\alpha(\text{P})$ is α decay energy (Q value) for parent P decaying into daughter D expressed by three possible methods (nuclear rest energy, atomic rest energy, or binding energy) as follows

$$\begin{aligned} Q_\alpha(\text{P}) &= \{M(\text{P}) - [M(\text{D}) + m_\alpha]\}c^2 = \{\mathcal{M}(\text{P}) - [\mathcal{M}(\text{D}) + \mathcal{M}({}^4_2\text{He})]\}c^2 \\ &= E_B(\text{D}) + E_B(\alpha) - E_B(\text{P}) = (E_K)_\alpha + (E_K)_\text{D}. \end{aligned} \quad (11.256)$$

(2) **Arrow #2** represents β^- decay characterized by A remaining the same, however, a neutron from the parent nucleus transforms into a proton, so that $Z \rightarrow Z + 1$ and $N \rightarrow N - 1$ resulting in $A = \text{const}$ and a β^- particle and an antineutrino are emitted. The basic relationship for β^- decay is expressed as follows [see (T10.15)]

$${}^A_Z\text{P} \rightarrow {}^A_{Z+1}\text{D} + e^- + \bar{\nu}_e + Q_{\beta^-}(\text{P}), \quad (11.257)$$

where $Q_{\beta^-}(\text{P})$ is β^- decay energy (Q value) for parent P decaying into daughter D expressed with the nuclear rest energy method or the atomic rest energy method as follows

$$\begin{aligned} Q_{\beta^-}(\text{P}) &= \{M(\text{P}) - [M(\text{D}) + m_e]\}c^2 = \{\mathcal{M}(\text{P}) - \mathcal{M}(\text{D})\}c^2 \\ &= (E_{\beta^-})_{\text{max}} + (E_K)_{\text{Dmax}} = (E_\beta)_{\text{max}} \left\{ 1 + \frac{m_e c^2 + \frac{1}{2}(E_\beta)_{\text{max}}}{M(\text{D})c^2} \right\}. \end{aligned} \quad (11.258)$$

(3a) **Arrow #3** represents electron capture (EC) decay in which the parent nucleus captures an orbital electron, a proton transforms into a neutron, and a neutrino is emitted. Thus, $Z \rightarrow Z - 1$, $N \rightarrow N + 1$, and A remains the same. The basic relationship for electron capture decay is given as [see (T10.17)]

$${}^A_Z\text{P} + e^- = {}^A_{Z-1}\text{D} + \nu_e + Q_{\text{EC}}(\text{P}), \quad (11.259)$$

where $Q_{\text{EC}}(\text{P})$ is EC decay energy (Q value) for parent P decaying into daughter D expressed with the nuclear rest energy method or with atomic rest energy method as follows

$$\begin{aligned} Q_{\text{EC}}(\text{P}) &= \{[M(\text{P}) + m_e] - M(\text{D})\}c^2 \\ &= \{M(\text{P}) - [M(\text{D}) - m_e]\}c^2 = \{\mathcal{M}(\text{P}) - \mathcal{M}(\text{D})\}c^2 = (E_{\text{K}})_{\text{D}} + E_{\nu_e}. \end{aligned} \quad (11.260)$$

(3b) **Arrow #3**, in addition to EC decay, also represents β^+ decay characterized by a proton from the parent nucleus transforming into a neutron accompanied by emission of a β^+ particle (positron) and a neutrino. Thus, $Z \rightarrow Z - 1$, $N \rightarrow N + 1$, and A remains the same. The basic relationship for β^+ decay is given as [see (T10.16)]

$${}^A_Z\text{P} \rightarrow {}^A_{Z-1}\text{D} + e^+ + \nu_e + Q_{\beta^+}(\text{P}), \quad (11.261)$$

where $Q_{\beta^+}(\text{P})$ is β^+ decay energy (Q value) for parent P decaying into daughter D expressed with the nuclear rest energy method or the atomic rest energy method as follows

$$\begin{aligned} Q_{\beta^+}(\text{P}) &= \{M(\text{P}) - [M(\text{D}) + m_e]\}c^2 = \{\mathcal{M}(\text{P}) - \mathcal{M}(\text{D}) + 2m_e\}c^2 \\ &= (E_{\beta^+})_{\text{max}} + (E_{\text{K}})_{\text{Dmax}} = (E_{\beta})_{\text{max}} \left\{ 1 + \frac{m_e c^2 + \frac{1}{2}(E_{\beta})_{\text{max}}}{M(\text{D})c^2} \right\}. \end{aligned} \quad (11.262)$$

(4a) **Arrow #4** represents proton emission (PE) decay in which parent nucleus emits a proton and the decay process is characterized by $Z \rightarrow Z - 1$, $N = \text{const}$, and $A \rightarrow A - 1$. The basic relationship for PE decay is given as follows

$${}^A_Z\text{P} \rightarrow {}^A_{Z-1}\text{D} + \text{p} + Q_{\text{PE}}(\text{P}), \quad (11.263)$$

where $Q_{\text{PE}}(\text{P})$ is proton emission decay energy (Q value) for parent P decaying into daughter D expressed with the nuclear rest energy method or atomic energy method as follows

$$\begin{aligned} Q_{\text{PE}}(\text{P}) &= \{M(\text{P}) - [M(\text{D}) + m_{\text{p}}]\}c^2 = \{\mathcal{M}(\text{P}) - [\mathcal{M}(\text{D}) + \mathcal{M}({}^1_1\text{H})]\}c^2 \\ &= E_{\text{B}}(\text{D}) - E_{\text{B}}(\text{P}) = (E_{\text{K}})_{\text{p}} + (E_{\text{K}})_{\text{D}}. \end{aligned} \quad (11.264)$$

(4b) **Arrow #4** extended vertically down from the $Z - 1$ pixel to the next pixel at $Z - 2$ [not shown in Fig. 11.9(A)] represents two-proton emission (2PE) decay in which the parent nucleus emits two protons and the decay process is characterized by $Z \rightarrow Z - 2$, $N = \text{const}$, and $A \rightarrow A - 2$. The basic relationships for 2PE decay are as follows

$${}^A_Z\text{P} \rightarrow {}^{A-2}_{Z-2}\text{D} + 2\text{p} + Q_{2\text{PE}}(\text{P}), \quad (11.265)$$

where $Q_{2\text{PE}}(\text{P})$ is decay energy for two-proton decay of parent P into daughter D expressed with the nuclear rest energy method or the atomic energy method as follows

$$\begin{aligned} Q_{2\text{PE}}(\text{P}) &= \{M(\text{P}) - [M(\text{D}) + 2m_{\text{p}}]\}c^2 = \{\mathcal{M}(\text{P}) - [\mathcal{M}(\text{D}) + 2\mathcal{M}({}^1_1\text{H})]\}c^2 \\ &= E_{\text{B}}(\text{D}) - E_{\text{B}}(\text{P}) = 2(E_{\text{K}})_{\text{p}} + (E_{\text{K}})_{\text{D}}. \end{aligned} \quad (11.266)$$

(5) **Arrow #5** represents neutron emission (NE) decay in which the parent nucleus emits a neutron and the decay process is characterized by $Z = \text{const}$, $N \rightarrow N - 1$, and $A \rightarrow A - 1$. The basic relationship for NE decay is

$${}^A_Z\text{P} \rightarrow {}^{A-1}_Z\text{D} + \text{n} + Q_{\text{NE}}(\text{P}), \quad (11.267)$$

where $Q_{\text{NE}}(\text{P})$ is decay energy (Q value) for parent P decay into daughter D through NE decay

$$\begin{aligned} Q_{\text{NE}}(\text{P}) &= \{M(\text{P}) - [M(\text{D}) + m_{\text{n}}]\}c^2 = \{\mathcal{M}(\text{P}) - [\mathcal{M}(\text{D}) + m_{\text{n}}]\}c^2 \\ &= E_{\text{B}}(\text{D}) - E_{\text{B}}(\text{P}) = (E_{\text{K}})_{\text{n}} + (E_{\text{K}})_{\text{D}}. \end{aligned} \quad (11.268)$$

The decay paths and decay expressions listed above are generic expressions and, of course, do not all hold in general. For a given nuclide, a particular decay can only happen if:

- (1) Nuclide is radioactive.
- (2) Decay energy Q_{decay} for a particular decay process is positive.

Figure 11.10 is a graphic answer to question in (a).

(b) As also indicated in Fig. 11.10, the four special lines through the parent nucleus, shown in Fig. 11.9(A), govern various nuclear decays and are named as follows:

- (1) Alpha decay line (I) governs α decay. In α decay parent P and daughter D are second nearest neighbors on the α decay line.
- (2) Isotope line (II) for $Z = \text{const}$ governs neutron emission decay. In NE decay parent P and daughter D are nearest neighbors on the isotope line.
- (3) Isotone line (III) for $N = \text{const}$ governs proton emission decay. In PE decay parent P and daughter D are nearest neighbors on the isotone line.

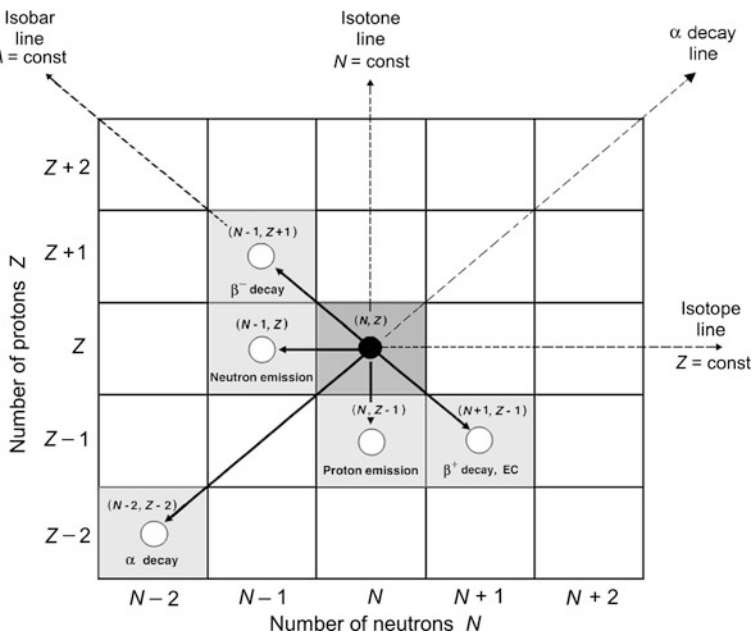


Fig. 11.10 Possible decay paths available in the Chart of Nuclides to a parent nuclide (N, Z) in its quest to attain a more stable configuration. Parent nucleus is shown by *solid black circle*, daughter nucleus is shown by *open circles*. Four special lines (α decay line, isotope line, isotone line, and isobar line) through the parent nucleus are also indicated

(4) Isobar line (IV) for $A = \text{const}$ governs β^- decay, electron capture, and β^+ decay. In β^- decay, electron capture, and β^+ decay parent P and daughter D are nearest neighbors on the isobar line.

(c) Figure 11.9(B) shows a small section of the Chart of Nuclides containing 25 pixels arranged in 5 rows and 5 columns with the nucleus of interest X at the center. The layout is split diagonally into two regions along the isobar line: the upper region (dark grey pixels) is the region of nuclear bombardment, the lower region (light grey pixels) is the region of nuclear decay. The same particles are of interest in both regions: β^- (electron), β^+ (positron), p (proton), n (neutron), d (deuteron), t (triton), ^3_2He (helium-3 nucleus), and α particle (helium-4 nucleus).

On the one hand, in the nuclear bombardment region these particles are projectiles entering the nucleus X and causing a nuclear reaction through first creating a composite nucleus Y*; on the other hand, in the nuclear decay region these particles are emitted from the nucleus in one of many possible decay modes.

For each of the above-listed particles we now find an appropriate pixel in the bombardment region and a corresponding pixel in the decay region. For example, for the α particle we look on the α -decay line and identify pixel #(+5) in the bombardment region and corresponding pixel #(-5) in the decay region. We then mark

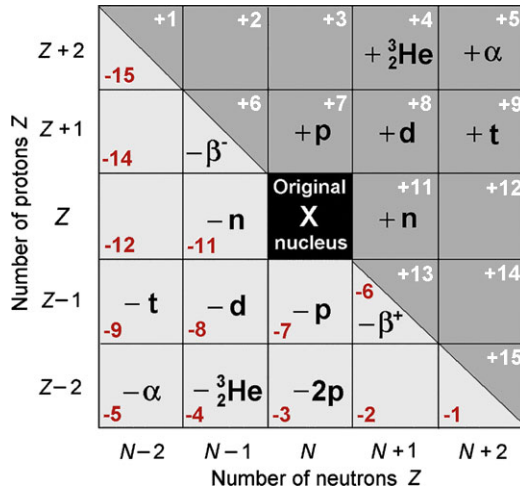


Fig. 11.11 Small section of the Chart of Nuclides containing 25 pixels arranged in 5 rows and 5 columns with the nucleus of interest X at the center. The layout is split diagonally into two regions along the isobar line: the upper region (*dark grey pixels*) is the region of nuclear bombardment, the lower region (*light grey pixels*) is the region of nuclear decay. The same particles are of interest in both nuclear regions: β^- (electron), β^+ (positron), p (proton), n (neutron), d (deuteron), t (triton), ${}^3_2\text{He}$ (helium-3 nucleus), and α particle (helium-4 nucleus)

pixel #(+5) with $+\alpha$ and pixel #(-5) with $-\alpha$, indicating, respectively, bombardment of target X with α particle (${}^A_Z\text{X} + \alpha \rightarrow {}^{A+4}_{Z+2}\text{Y}^*$) and decay of nuclide X with emission of α particle (${}^A_Z\text{X} \rightarrow {}^{A-4}_{Z-2}\text{Y} + \alpha$).

Following the approach that we took with the α particle with pixels +5 and -5, we identify pixels for the other listed particles and get the results shown in Fig. 11.11.

Chapter 12 consists of **26 problems** distributed over 10 sections devoted to practical and theoretical aspects of production of radionuclides that originated with the discovery of artificial radioactivity in 1934 credited to Frédéric Joliot and Irène Joliot-Curie. The vast majority of currently known radionuclides are man-made and artificially produced through a process of nuclear activation that uses bombardment of a stable nuclide with a suitable particle to induce a nuclear transformation of a stable parent into a radioactive daughter. Various particles or electromagnetic radiation generated by a variety of machines are used for the purpose of nuclear activation, most notably neutrons from nuclear fission reactors for neutron activation, protons from cyclotrons for proton activation, and high energy x-rays from high energy linear accelerators for photoactivation.

Section 12.1 addresses the origin of radioactive nuclides and touches upon the historical background on the discovery of natural and artificial radioactivity. Origin of radionuclides is covered by next two sections; naturally occurring in Sect. 12.2 and artificially produced in Sect. 12.3. The problem of radionuclides present in the environment is covered in Sect. 12.4.

The second part of this chapter deals with production of radionuclides, i.e., nuclear activation. Section 12.5 addresses general aspects of various types of nuclear activation and Sect. 12.6 addresses in detail the activation with thermal neutrons that is the most common type of nuclear activation. Three neutron activation models are studied: (1) Saturation model, (2) Depletion model, and (3) Parent depletion–daughter activation model.

Also addressed are problems dealing with nuclear fission induced by thermal neutrons. General aspects of neutron-induced fission are covered in Sect. 12.7 and Sect. 12.8 addresses the nuclear chain reaction covering the nuclear reactor and nuclear power generation. Problems in Sects. 12.9 and 12.10 concentrate on radionuclide generators and nuclear activation with heavy charged particle beams, respectively.

12.1 Origin of Radioactive Elements (Radionuclides)

12.1.Q1

(246)

According to their origin, radionuclides are placed into two general categories: (1) Naturally-occurring radionuclides and (2) Man-made (artificial) radionuclides.

- (a) Describe the experiments that lead to the discovery of: (1) Natural radioactivity and (2) Artificial or induced radioactivity. Also provide the names of physicists credited with the discoveries and the year of the discoveries.
- (b) Polonium-210, discovered in 1896 by Marie Skłodowska-Curie and Pierre Curie, was an important source of α particles during the first few decades of nuclear physics. Plot the decay scheme for polonium-210 and calculate: (1) Its specific activity, (2) Its α decay energy (Q value), (3) Kinetic energy $(E_K)_\alpha$ of the α particles it emits, (4) Power generated per gram of Po-210, and (5) Mass of radium-226 to produce the same rate of α particle emission as obtained from 1 mg of polonium-210.
- (c) Frédéric and Irène Joliot-Curie discovered artificial radioactivity using their strong polonium-210 source of α particles to bombard aluminum-27 nuclei triggering the following nuclear reaction (now referred to as the Joliot-Curie nuclear reaction)



Determine Q value for the Joliot-Curie nuclear reaction.

- (d) Calculate the threshold kinetic energy $(E_K)_{\text{thr}}$ of the Joliot-Curie nuclear reaction and show that kinetic energy $(E_K)_\alpha$ of polonium-210 α particles determined in (b) is sufficient to trigger the reaction.

SOLUTION:

(a) In this section we discuss the natural and artificial (induced) radioactivity. These two phenomena are but two steps in the 40-year long march of humanity from the basic understanding of the atomic nucleus to nuclear fission.

(1) Henri Becquerel discovered natural radioactivity in 1896 and received 50 % of the 1903 Nobel Prize in Physics for his discovery. The recipients of the other half of the Prize were Marie Skłodowska-Curie and Pierre Curie for their discovery of radium and polonium.

In the early 1896, soon after Röntgen's discovery of x rays, Becquerel decided to investigate a possible link between minerals that glow when exposed to light and

Röntgen's new rays, the x rays. Much of his work until that time involved studies of the phenomena of fluorescence and phosphorescence produced by uranium salts (potassium uranyl sulfate) which were recognized as efficient phosphors (fluorescing materials). His plan was to expose his fluorescing material to the sun and then place it and an object to be imaged onto a photographic plate, speculating that the photographic plate may show the image of the object and this would serve as proof that fluorescing materials emit x rays.

For several days the weather did not cooperate and Becquerel stored his uranium salt sample and the object in a drawer together with a photographic plate, waiting for a sunny day to carry out his experiment. When he finally removed the sample from the drawer, he noticed to his great surprise that the photographic plate was exposed and the object was clearly visible, despite his uranium salt not having been exposed to any sunlight. Several things became obvious to Becquerel:

- (i) Exposure of the plate was not caused by fluorescence or phosphorescence of the salt.
- (ii) Rays that produced exposure of the plate could not have been the recently discovered x rays.
- (iii) Uranium salt must be emitting the rays that cause the exposure of the photographic plate.

Becquerel's discovery of natural radioactivity, like Röntgen's discovery of x rays, is an example of momentous yet unexpected discoveries in science where a scientist, working on a mundane experiment, serendipitously finds stunning results and the pursuit of these results leads to completely new directions and new disciplines in science.

(2) Irène Joliot-Curie and Frédéric Joliot-Curie discovered artificial radioactivity in 1934 and in 1935 they received the Nobel Prize in Chemistry for their discovery that came on the heels of two other important discoveries in nuclear physics in 1932: namely, James Chadwick's discovery of the neutron and Carl Anderson's discovery of the positron. Both these discoveries played an important role in the discovery of induced radioactivity; however, it is reasonable to assume that Rutherford and his colleagues with their α particle scattering experiments on various metallic foils must have already dealt, albeit unknowingly, with induced radioactivity some 25 years earlier. Rutherford is also credited with the discovery of natural transmutation in 1919 when he irradiated nitrogen-14 nuclide with α particles and produced stable oxygen-17 nuclide and hydrogen

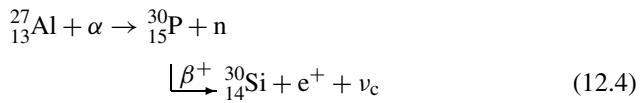


The idea of artificial (induced) radioactivity has been around for many years before the Joliot-Curie team actually carried out their definitive experiment in 1934 in which they irradiated an aluminum foil with α particles from a polonium source and noticed that the irradiated aluminum sample continued to eject ionizing particles

in large number long after the α particle irradiation was discontinued. The initial experiment is described as follows



and it resulted in a new, never seen before, isotope of phosphorus (${}_{15}^{30}\text{P}$) and free neutrons. However, in addition to the products of this reaction, the Joliot-Curies also observed energetic positrons emanating from the irradiated sample and they explained this phenomenon with β^+ decay of the phosphorus-30 nuclide that was produced in the initial reaction (12.3) and was undergoing its own decay with a half-life $t_{1/2}$ of about 3 minutes. One can thus consider ${}_{15}^{30}\text{P}$ an intermediate compound nucleus that is first created by irradiation of ${}_{13}^{27}\text{Al}$ with α particles and then decays through β^+ decay into ${}_{14}^{30}\text{Si}$, positron, and neutrino. The whole production process of induced radioactivity in ${}_{13}^{27}\text{Al}$ is thus given as follows



The discovery of induced radioactivity lead rapidly to production of new radionuclides for use in science, industry, biology, and medicine. During the past 80 years several thousand new nuclides have been produced and investigated, placing the discovery of induced radioactivity among the most important discoveries of the 20th century and making it an important step toward discovery of nuclear fission.

(b) Polonium-210 is a rare radionuclide with a half-life $t_{1/2} = 138.38$ d. It is produced naturally as a component of the uranium-238 / radium-226 decay chain but it can also be produced artificially in a nuclear reactor bombarding bismuth-209 with thermal neutrons to produce bismuth-210 which is also a component of the uranium-238 / radium-226 decay chain and decays to polonium-210 through β^+ decay with a half-life $t_{1/2}$ of 5 days.

As shown in Table 12.1, the uranium-238 / radium-226 decay chain consists of 14 radionuclides, 8 of these decay with α decay and 6 with β^+ decay. The decay scheme for the last element of the uranium-238 / radium-226 decay chain, polonium-210 decay into lead-206, is given in Fig. 12.1.

(1) Specific activity a of Po-210 is calculated as follows

$$\begin{aligned} a &= \frac{\mathcal{A}}{m} = \frac{\lambda N}{m} = \frac{\lambda N_{\text{A}}}{A} = \frac{(\ln 2) N_{\text{A}}}{t_{1/2} A} \\ &= \frac{(\ln 2) \times (6.022 \times 10^{23} \text{ mol}^{-1})}{(138.38 \text{ d}) \times (210 \text{ g}) \times (24 \text{ h/d}) \times (3600 \text{ s/h})} \\ &= 1.663 \times 10^{14} \text{ Bq/g} = 4493 \text{ Ci/g}. \end{aligned} \quad (12.5)$$

Table 12.1 Constituents of the uranium-238 / radium-226 decay chain

n	Symbol	Nuclide	Decay	Half-life $t_{1/2}$	Decay product
1	U-238	Uranium-238	Alpha	4.5×10^9 a	Thorium-234
2	Th-234	Thorium-234	Beta plus	24.1 d	Protactinium-234
3	Pa-234	Protactinium-234	Beta plus	1.17 min	Uranium-234
4	U-234	Uranium-234	Alpha	2.5×10^5 a	Thorium-230
5	Th-230	Thorium-230	Alpha	8×10^4 a	Radium-226
6	Ra-226	Radium-226	Alpha	1602 a	Radon-222
7	Rn-222	Radon-222	Alpha	3.82 d	Polonium-218
8	Po-218	Polonium-218	Alpha	3.1 min	Lead-214
9	Pb-214	Lead-214	Beta plus	27 min	Bismuth-214
10	Bi-214	Bismuth-214	Beta plus	19.7 min	Polonium-214
11	Po-214	Polonium-214	Alpha	1 μ s	Lead-210
12	Pb-210	Lead-210	Beta plus	22.3 a	Bismuth-210
13	Bi-210	Bismuth-210	Beta plus	5 d	Polonium-210
14	Po-210	Polonium-210	Alpha	138.4 d	Lead-206
15	Pb-206	Lead-206	none	STABLE	none

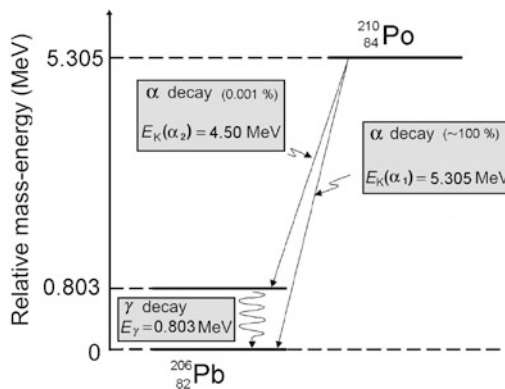


Fig. 12.1 Energy level diagram for the α decay of polonium-210 into stable lead-206. The relative rest energy levels for the ground states of the two nuclides are calculated from the respective atomic or nuclear rest energies given in Appendix A

(2) As discussed in detail in (T11.11), the decay energy for α decay of polonium-210 into stable lead-206 can be calculated with atomic rest energies, nuclear rest energies, or nuclear binding energies with data provided in Appendix A. In this example we will use nuclear rest energies as follows

$$\begin{aligned}
 Q_{\alpha}(^{210}_{84}\text{Po}) &= M(^{210}_{84}\text{Po})c^2 - [M(^{206}_{82}\text{Pb}) + m_{\alpha}]c^2 \\
 &= 195554.8682 \text{ MeV} - [191822.0820 \text{ MeV} + 3727.3791 \text{ MeV}] \\
 &= 5.41 \text{ MeV}.
 \end{aligned} \tag{12.6}$$

(3) Most of the decay energy Q_{α} goes to the emitted α particle as kinetic energy $(E_K)_{\alpha}$ and a very small amount to the lead-206 daughter nucleus, as a result of the large difference in mass between the α particle and the lead-206 nucleus. The two particles share the $Q_{\alpha}(^{210}_{84}\text{Po})$ in the inverse proportion to their mass. We thus have (T11.6)

$$(E_K)_{\alpha} = \frac{Q_{\alpha}(^{210}_{84}\text{Po})}{1 + \frac{m_{\alpha}}{M(^{206}_{82}\text{Pb})}} \approx \frac{5.41 \text{ MeV}}{1 + \frac{3727.3791}{191822.0820}} = \frac{5.41 \text{ MeV}}{1.0194} \approx 5.31 \text{ MeV}. \tag{12.7}$$

(4) Power P emitted by the polonium-210 nuclide per gram is determined from the specific activity a that gives the number of α decays per second multiplied by the kinetic energy carried by each α particle to get

$$\begin{aligned}
 P &= a \times (E_K)_{\alpha} \\
 &= (1.663 \times 10^{14} \text{ s}^{-1} \cdot \text{g}^{-1}) \times (5.31 \times 10^6 \text{ eV}) \times (1.6 \times 10^{-19} \text{ J/eV}) \\
 &= 141.0 \text{ J} \cdot \text{s}^{-1} \cdot \text{g}^{-1} = 141 \text{ W/g}.
 \end{aligned} \tag{12.8}$$

(5) Rate of α particle emission per unit mass of an α emitter is given by specific activity a expressed in units Bq/g giving the number of α decays per second. For radium-226 the specific activity a was defined as 1 Ci/g and subsequently refined to 0.988 Ci/g, i.e., 3.665×10^{10} Bq/g.

In (12.5) we calculated the specific activity of polonium-210 as 1.663×10^{14} Bq/g (4493 Ci/g) which means that 1.663×10^{11} α particles are produced per second in 1 mg sample of polonium-210. To obtain this rate of α particle emission from radium-226 we would need a radium-226 source with a mass of

$$m_{\text{Ra-226}} = \frac{1.663 \times 10^{11}}{3.665 \times 10^{10}} \text{ g} = 4.5 \text{ g}. \tag{12.9}$$

(c) Q value of the Joliot-Curie nuclear reaction $^{27}_{13}\text{Al} + \alpha = ^{30}_{15}\text{P} + \text{n}$ (12.1) can be determined with three methods: (1) Nuclear rest energy (Mc^2) method, (2) Atomic rest energy ($\mathcal{M}c^2$) method, and (3) Nuclear binding energy (E_B) method. All three methods should give the same result.

(1) In the *nuclear rest energy (Mc^2) method* Q value of the Joliot-Curie nuclear reaction is calculated as follows

$$\begin{aligned}
 Q(^{27}_{13}\text{Al}, \alpha) &= \sum_{i,\text{before}} M_i c^2 - \sum_{i,\text{after}} M_i c^2 \\
 &= [M(^{27}_{13}\text{Al})c^2 + m_{\alpha}c^2] - [M(^{30}_{15}\text{P})c^2 + m_{\text{n}}c^2]
 \end{aligned}$$

$$\begin{aligned}
&= [25126.4994 \text{ MeV} + 3727.3791 \text{ MeV}] \\
&\quad - [27916.9555 \text{ MeV} + 939.5654 \text{ MeV}] \\
&= -2.642 \text{ MeV}. \tag{12.10}
\end{aligned}$$

- (2) In the *atomic rest energy* ($\mathcal{M}c^2$) *method* Q value of the Joliot-Curie nuclear reaction is calculated as follows

$$\begin{aligned}
Q(^{27}_{13}\text{Al}, \alpha) &= \sum_{i, \text{after}} \mathcal{M}_i c^2 - \sum_{i, \text{before}} \mathcal{M}_i c^2 \\
&= [\mathcal{M}(^{27}_{13}\text{Al})c^2 + \mathcal{M}(^4_2\text{He})c^2] - [\mathcal{M}(^{30}_{15}\text{P})c^2 + m_n c^2] \\
&= [26.981539u + 4.002603u] - [29.978314u + 1.008664u] \\
&= (-2.836 \times 10^{-3}u) \times (931.494028 \text{ MeV}/u) \\
&= -2.642 \text{ MeV}. \tag{12.11}
\end{aligned}$$

- (3) In the *nuclear binding energy* (E_B) *method* Q value of the Joliot-Curie nuclear reaction is calculated as follows

$$\begin{aligned}
Q(^{27}_{13}\text{Al}, \alpha) &= \sum_{i, \text{after}} E_B(i) - \sum_{i, \text{before}} E_B(i) \\
&= E_B(^{30}_{15}\text{P})c^2 - [E_B(^{27}_{13}\text{Al}) + E_B(^4_2\text{He})] \\
&= [250.60489 \text{ MeV}] - [224.95161 \text{ MeV} + 28.29569 \text{ MeV}] \\
&= -2.642 \text{ MeV}. \tag{12.12}
\end{aligned}$$

As expected, the three methods for calculating Q value of the Joliot-Curie nuclear reaction (12.1) give the same result: -2.642 MeV . The negative value tells us that the reaction is endothermic, cannot occur spontaneously, and has a threshold energy that the α particle must meet or exceed in order to trigger the reaction.

(d) Two related methods are in use for calculation of threshold kinetic energy $(E_K)_{\text{thr}}$ of a projectile bombarding the target in an endothermic nuclear reaction ($Q < 0$); one is based on the relativistic invariant and the other on Q value of the nuclear reaction.

(1) The relativistic invariant is expressed as follows: $E^2 - p^2c^2|_{\text{before}} = E^2 - p^2c^2|_{\text{after}} = \text{inv}$, where E is the total energy of the system and p is the momentum of the system before and after the collision. Before the collision, the system consists of the projectile and the target and the invariant is expressed in the laboratory coordinate system, after the collision the system typically consists of two reaction products and the invariant is expressed in the center-of-mass coordinate system (T5.9).

The *relativistic invariant* for the Joliot-Curie nuclear reaction is given as

$$\begin{aligned} E^2 - p^2c^2 &= \left[M(^{27}_{13}\text{Al})c^2 + \sqrt{(m_\alpha c^2)^2 + p_\alpha^2 c^2} \right]^2 - p_\alpha^2 c^2 \\ &= \left[M(^{30}_{15}\text{P})c^2 + m_n c^2 \right]^2 - 0. \end{aligned} \quad (12.13)$$

Solving (12.13) for E_{thr} which is given as $E_{\text{thr}} = \sqrt{(m_\alpha c^2)^2 + p_\alpha^2 c^2}$ results in the following equation for the total threshold energy

$$E_{\text{thr}} = \frac{\{M(^{30}_{15}\text{P})c^2 + m_n c^2\}^2 - \{[M(^{27}_{13}\text{Al})c^2]^2 - (m_\alpha c^2)^2\}}{2M(^{27}_{13}\text{Al})c^2}. \quad (12.14)$$

Noting that total threshold energy E_{thr} can be expressed in terms of threshold kinetic energy $(E_K)_{\text{thr}}$ of the projectile (α particle) as $E_{\text{thr}} = (E_K)_{\text{thr}} + m_\alpha c^2$, we now get the following expression for $(E_K)_{\text{thr}}$

$$\begin{aligned} (E_K)_{\text{thr}} &= E_{\text{thr}} - m_\alpha c^2 = \frac{\{M(^{30}_{15}\text{P})c^2 + m_n c^2\}^2 - \{M(^{27}_{13}\text{Al})c^2 + m_\alpha c^2\}^2}{2M(^{27}_{13}\text{Al})c^2} \\ &= \frac{[27916.9555 + 939.5654]^2 - [25126.4994 + 3727.3791]^2}{2 \times 25126.4994} \text{ MeV} \\ &= \frac{152493.96}{50252.9988} \text{ MeV} = 3.035 \text{ MeV}. \end{aligned} \quad (12.15)$$

(2) Threshold kinetic energy $(E_K)_{\text{thr}}$ of the α particle is in terms of Q value given as (T5.15)

$$\begin{aligned} (E_K)_{\text{thr}} &\approx -Q \left(1 + \frac{m_\alpha c^2}{M(^{27}_{13}\text{Al})c^2} \right) = -(-2.642 \text{ MeV}) \times \left(1 + \frac{3727.3791}{25126.4994} \right) \\ &= (2.642 \text{ MeV}) \times 1.148 = 3.033 \text{ MeV}. \end{aligned} \quad (12.16)$$

Threshold kinetic energy $(E_K)_{\text{thr}}$ of the α particle is about 15 % larger than reaction Q value to satisfy the principle of conservation of total energy and momentum in the reaction. As shown in (b), kinetic energy of α particles emitted by Po-210 [$(E_K)_\alpha = 5.31 \text{ MeV}$] exceeds threshold kinetic energy of the Joliot-Curie reaction (12.1) [$(E_K)_{\text{thr}} = 3.03 \text{ MeV}$], attesting to the feasibility of the Joliot-Curie experiment that lead to discovery of artificial radioactivity.

12.2 Naturally Occurring Radionuclides

12.2.Q1

(247)

Naturally occurring radioactive elements (radionuclides) are almost exclusively members of one of four radioactive series that all begin with very heavy and long-lived parent that has a half-life of the order of the age of the Earth.

- (a) Give the standard categories and origin of naturally occurring radionuclides.
- (b) Prepare a table for the four naturally occurring radioactive series, filling out the following rows: (1) Name of series, (2) Parent radionuclide, (3) Atomic number Z , (4) Atomic mass number A , (5) Number of stages in chain, (6) Number of α decays in the chain, (7) Number of β decays in the chain, (8) Half-life (10^9 a), (9) Stable end product, (10) Found in nature? (11) Specific activity a in Bq/g, and (12) Specific activity a in Ci/g.
- (c) Carbon-14 is a cosmogenic radionuclide that can be used in dating of organic remains less than $\sim 60\,000$ years old. For carbon-14: (1) Discuss how it is produced. (2) Discuss the principles of carbon dating, and (3) Estimate the age of a small sample of papyrus for which a very accurate β counting technique determined a counting rate of 7.5 CPM (counts per minute) per gram.

SOLUTION:

(a) Naturally occurring radionuclides fall into 3 groups: primordial, secondary, and cosmogenic.

(1) *Primordial radionuclides* have existed since the formation of the Earth 4.6 billion years ago and are still present because of their very long half-life. Most primordial radionuclides are in the group of heavy elements, such as uranium-238 and thorium-232; however, a few examples of light primordial radionuclides are also known, such as potassium-40 ($t_{1/2} = 1.277 \times 10^9$ years).

(2) *Secondary radionuclides* are radionuclides derived from radioactive decay of primordial radionuclides. Since their half-lives are shorter than those of primordial radionuclides, they are still present only because of continuous replenishment through the decay of primordial radionuclides. Nuclides, be it stable or radioactive, produced through decay of a parent radionuclide are called *radiogenic nuclides*.

(3) *Cosmogenic radionuclides* have relatively short half-lives and are present in nature because cosmic rays are continuously forming them in the atmosphere.

Carbon-14 is the best-known radionuclide in this category. It decays with a half-life of 5730 years and is used for the so-called carbon dating of once-living objects, no older than some 60 000 years. Cosmic rays are energetic particles that originate from outer space and strike the Earth's atmosphere. The vast majority of cosmic rays ($\sim 87\%$) are protons, some 12% are alpha particles, and about 1% are electrons.

(b) The naturally occurring radioactive elements are almost exclusively members of one of four radioactive series that all begin with very heavy and long-lived primordial parents that have half-lives of the order of the age of the earth. The four naturally occurring series and their original parent radionuclide are named as follows:

- (1) *Thorium series* originates with thorium-232.
- (2) *Neptunium series* originates with neptunium-237.
- (3) *Uranium series* (also known as U-238 / radium-226 series) originates with uranium-238.
- (4) *Actinium series* originates with uranium-235.

The series begin with a specific parent nucleus that decays through several daughter products to reach a stable lead isotope in the thorium, actinium, and uranium series and stable bismuth-209 nuclide in the neptunium series. For each one of the four series most of the transitions toward the stable nuclides are α decays (6 to 8) interspersed with a few β decays.

The atomic mass numbers A for each member of the thorium series are multiples of 4 and, consequently, the thorium series is sometimes referred to as the $4n$ series. The atomic mass numbers of members of the neptunium series follow the rule $4n + 1$, the uranium series $4n + 2$, and the actinium series $4n + 3$. Therefore, these series are often referred to as the $4n + 1$, $4n + 2$, and $4n + 3$ series. Table 12.2 provides the basic characteristics of the four naturally occurring radioactive series (thorium, neptunium, uranium, and actinium).

(c) Atmospheric carbon contains three isotopes of carbon: stable carbon-12 (99%), stable carbon-13 ($\sim 1\%$), and radioactive carbon-14 continuously produced at a constant rate in the atmosphere by cosmic rays. Abundance of the carbon-14 isotope in atmospheric carbon is estimated at 1 ppt (1 part per trillion) and represents equilibrium between generation by cosmic rays and radioactive decay. This corresponds to about 600 billion of carbon-14 nuclei per mole of carbon (12 g) and is considered the equilibrium level of C-14. Thus, the ratio $^{14}\text{C}/^{12}\text{C} \approx 10^{-12}$.

(1) Carbon-14 is a relatively short-lived cosmogenic radionuclide decaying through β^- decay into nitrogen-14 with a half-life $t_{1/2}$ of 5730 years. It is produced in the upper Earth's atmosphere by nuclear reactions between free neutrons and nitrogen-14 nuclei in the following nuclear reaction: $^{14}_7\text{N} + n \rightarrow ^{14}_6\text{C} + p$. Free neutrons, required for this reaction, are produced in the upper atmosphere by cosmic rays (mainly protons) interacting with atmospheric molecules. Carbon-14 produced in the atmosphere through neutron interaction with nitrogen-14 immediately oxidizes

Table 12.2 Main characteristics of the four naturally occurring radioactive decay series

Name of series	Thorium	Neptunium	Uranium	Actinium
	$4n$	$4n + 1$	$4n + 2$	$4n + 3$
Parent radionuclide	Thorium-232	Neptunium-237	Uranium-238	Uranium-235
Atomic number Z	90	93	92	92
Atomic mass A	232	237	238	235
Number of stages	10	12	14	11
Number α decays	6	7	8	7
Number β decays	4	5	6	4
Half-life (10^9 a)	14.05	2.144×10^{-3}	4.47	0.704
Stable end product	$^{208}_{82}\text{Pb}$	$^{209}_{83}\text{Bi}$	$^{206}_{82}\text{Pb}$	$^{207}_{82}\text{Pb}$
Found in nature	YES	NO	YES	YES
Specific activity a	4060 Bq/g	2.66×10^7 Bq/g	12442 Bq/g	8×10^4 Bq/g
Specific activity a	0.11 $\mu\text{Ci/g}$	710 $\mu\text{Ci/g}$	0.34 $\mu\text{Ci/g}$	2.2 $\mu\text{Ci/g}$

(combines with oxygen) to form carbon dioxide and gets incorporated into living organic materials with the C-14/C-12 ratio that equals to the atmospheric ratio of 10^{-12} .

(2) Radiocarbon dating method was developed by Willard Libby at the University of Chicago and in 1960 he received the Nobel Prize in Chemistry for this work. The method is based on two premises. One premise assumes that radioactive C-14 is incorporated into living organisms by photosynthesis or ingestion of organic material with a C-14/C-12 ratio equal to atmospheric C-14/C-12 ratio; however, after organism's death the ratio gets progressively smaller with time because C-14 undergoes exponential radioactive decay and no longer gets replenished in dead organic material. The second premise assumes that the equilibrium ratio C-14/C-12 was constant for the past 60 000 years making the past 60 000 years the upper limit for the useful range in radiocarbon dating.

Assuming that the two premises are correct, a conclusion can be reached that for organic material the measured C-14/C-12 ratio in comparison with the equilibrium ratio of 10^{-12} can be used to estimate the age of the dead organic material.

(3) To establish the time period during which the C-14 nuclide has been decaying in the papyrus sample, we must first determine the equilibrium level of the ratio C-14/C-12 in CPM. In 1 g of carbon we have $\frac{1}{12}6.022 \times 10^{23}$ atoms and of these $\frac{1}{12}6.022 \times 10^{11}$ are C-14 atoms, since we know that $^{14}_6\text{C}/^{12}_6\text{C} \approx 10^{-12}$. The specific activity of 1 g of natural carbon is thus given as follows

$$a_{\text{C}} = \frac{(\ln 2)N_{\text{A}}}{(t_{1/2})_{\text{C-14}A}} = \frac{(\ln 2) \times (6.022 \times 10^{11})}{(5730 \text{ a}) \times (14 \text{ g}) \times (365 \text{ d/a}) \times (24 \text{ h/d}) \times (3600 \text{ s/h})}$$

$$= 0.165 \text{ s}^{-1} \cdot \text{g}^{-1} \quad (12.17)$$

or count rate C_0 in counts per minute $C_0 \sim 10$ CPM/g. Since the sample count rate is $C = 7.5$ CPM/g, we get the following result for the exponential decay of the organic papyrus sample

$$C(T) \approx C_0 e^{-\frac{(\ln 2)}{t_{1/2}} T} \quad \text{or} \quad T = -\frac{\ln(C/C_0)}{\ln 2} (t_{1/2})_{\text{C-14}} = -\frac{\ln 0.75}{\ln 2} \times (5730 \text{ a})$$

$$= 2380 \text{ a.} \quad (12.18)$$

Thus, the age of the papyrus sample is estimated as 2380 years.

12.3 Man-Made (Artificial) Radionuclides

12.3.Q1

(248)

Since Irène Joliot-Curie and Frédéric Joliot-Curie discovered artificial (induced) radioactivity in 1934 over 3000 different artificial radionuclides have been synthesized and investigated. Thus, the current list of known nuclides entered in a typical Chart of Nuclides (Segrè chart) contains some 280 stable nuclides and over 3500 radioactive nuclides (radionuclides).

- (a) Briefly discuss most common techniques and particles that are used in production of artificial radionuclides.
- (b) Many different names are used to designate nuclear reactions that produce artificial radionuclides. Discuss a few typical examples.
- (c) Briefly discuss the machines that are used in production of artificial radionuclides.
- (d) Compile as many terms as possible that are used for nuclear reactions of high-energy x rays interacting with target nuclei.

SOLUTION:

(a) Irène and Frédéric Joliot-Curie are credited with producing the first known artificial radionuclide, phosphorus-30, by irradiating an aluminum-27 foil with α particles from a polonium-210 source. Since then, several 1000 different artificial radionuclides have been produced and studied by using special techniques and machines, all based on the same basic principles enunciated by Joliot-Curies with their experiment in 1934.

The most common modern technique for producing artificial radionuclides is by inducing a nuclear reaction with a projectile bombarding a target (stable nuclide or long-lived radionuclide) and releasing two reaction products, one of them being the desired radionuclide and the other either a subatomic particle (most commonly neutron, proton, or α particle) or γ photon.

Various types of projectile are in use, such as:

- (1) *Thermal neutrons* typically inducing (n, γ) reaction and producing a radioactive isotope of the stable target (for example, ${}^{59}_{27}\text{Co} + n \rightarrow {}^{60}_{27}\text{Co} + \gamma$).
- (2) *Energetic heavy charged particles* typically inducing (p, n) reaction and producing a radionuclide different in atomic number Z from that of the target (for example, ${}^{18}_8\text{O} + p \rightarrow {}^{18}_9\text{F} + n$).
- (3) *High-energy x rays* most often inducing (γ, n) reaction and producing an isotope of the target with a lower atomic number Z than that of the target (for example, $d + \gamma \rightarrow p + n$, where d stands for deuteron).

(b) The lack of consistency in naming the various nuclear reactions associated with induced radioactivity can be attributed to several reasons, such as historical development of a technique, interest of the specific scientific community using a particular technique, and motivation for using a particular nuclear reaction.

- (1) When the objective of a particular bombardment of a target is purely scientific and focuses on the particular collision and on basic nuclear physics, then the nuclear reaction in relation to various types of projectile is referred to as **capture reaction**. Thus, (n, γ) stands for neutron capture, (p, n) for proton capture, and (γ, n) for photon capture.
- (2) When the ultimate goal of using nuclear bombardment of a target is to produce induced radioactivity in the target, then the technique is referred to as **nuclear activation**, with (n, γ) standing for neutron activation, (p, n) for proton activation, and (γ, n) for photon activation or photo-activation in short. During the past decades artificial radioactivity grew from a scientific curiosity into an important component of modern society, extremely useful for scientific, industrial, and medical purposes, but also controversial and potentially dangerous. Radionuclide sources produced under this category for scientific, industrial, and medical use have numerous applications in modern society and are of significant importance to medical physics in treatment of malignant disease with external beam radiotherapy and brachytherapy as well as for diagnostic imaging of disease in nuclear medicine.
- (3) When the ultimate goal of using the bombardment of a sample is an analysis of unknown sample's chemical composition, the techniques are referred to as **nuclear activation analysis**, with (n, γ) standing for neutron activation analysis, (p, n) for proton activation analysis, and (γ, n) for photon activation or photoactivation analysis in short.

The majority of activation analyses are carried out with neutron bombardment of a sample and the term activation analysis usually implies neutron activation analysis (NAA) with irradiation of the sample by thermal neutrons from a nuclear reactor. NAA is specific, highly sensitive, and can be applied to practically all elements of the periodic table of elements. Capture of a neutron in a nucleus of the sample results in formation of a new nucleus with the same atomic number Z as that of the original nucleus but with one more

neutron in the nucleus. This new isotope is usually radioactive and emits radiation through various possible nuclear decays. Most notable are γ rays that are emitted with unique and discrete energy levels, characteristic of a particular radionuclide emitting them. The γ ray spectrum is measured with γ ray spectroscopy and the results allow identification of elements present in the sample, since each nuclide in the chart of nuclides possesses its own characteristic γ ray imprint.

- (4) When the ultimate goal of a study is in-vivo body composition measurement using nuclear activation, the study is referred to as ***body composition activation analysis***. The technique is established well using neutron activation; however, attempts at using photoactivation for this purpose have been made in the past but so far have not attained any widespread use, most likely because, for this type of work, one requires a linac with energy of 25 MV or higher and these machines are not readily available in radiotherapy departments.

(c) Machines used in modern production of radionuclides are: (1) Nuclear reactors, (2) Heavy charged particle accelerators, (3) Radionuclide generators, and (4) High-energy electron linear accelerator.

- (1a) In *nuclear reactors* a high fluence of thermal neutrons is used to activate a stable nuclide to produce a neutron-rich radionuclide that typically decays through β^- decay with a given half-life $t_{1/2}$ and concurrently produces γ rays. Examples of neutron activation in a nuclear reactor of importance to medical physics and medicine are the production of sources for teletherapy machines (cobalt-60 and cesium-137), sources for brachytherapy procedures (e.g., iridium-192, gold-198), and radionuclides for nuclear medicine imaging (e.g., thallium-201, iodine-131).
- (1b) Another mode of induced radioactivity made possible with a nuclear reactor is induced fission of the reactor fuel triggered by neutrons. Most of the fission products produced in a reactor are radioactive, cover a wide range of atomic numbers and atomic abundances, and most are of no practical use. However, a few fission products can be separated by chemical means from all the other fission products present in the spent reactor fuel (for example, molybdenum-99) and they end up with much higher specific activity than that achievable with neutron activation. However, chemical separation of one fission radionuclide from the others is quite an elaborate procedure and often not possible for arbitrary radionuclides.
- (2) *Heavy charged particle accelerators* accelerate protons or heavier ions that bombard a target nuclide to produce a proton-rich radionuclide (often referred to as positron-emitting radionuclide) that typically decays through β^+ decay or electron capture and may or may not concurrently produce γ rays. Examples of proton-activated radionuclides of importance in medical physics and medicine (positron emission tomography—PET) are carbon-11, nitrogen-13, oxygen-15, fluorine-18, and rubidium-82.

- (3) *Radionuclide generator* contains a parent radionuclide that is usually produced in a nuclear reactor, has a relatively long half-life, and undergoes β^- decay into a daughter product that is used for nuclear medicine imaging and has a relatively short half-life. Several radionuclide generators are used to produce γ emitting radionuclides for imaging; however, the molybdenum-technetium (Mo-Tc) generator is by far the most common.
- (4) *High-energy electron linear accelerators* can be used to produce a bremsstrahlung photon spectrum with a high-energy component matching the giant resonance cross section for photonuclear reaction with a given target nucleus. This may trigger a photonuclear reaction (also called photodisintegration or phototransmutation) of the (γ, n) , (γ, p) , or (γ, α) type, resulting in a lighter isotope of the target nucleus in (γ, n) reaction or in a new nuclide in (γ, p) or (γ, α) reaction.

(d) In comparison to (n, γ) nuclear reaction normally described as neutron capture or neutron activation and (p, n) nuclear reaction normally described as proton capture and proton activation, many terms are used to describe high-energy photon interactions with target nuclei, such as: (1) Photonuclear reaction, (2) Photon capture, (3) Photodisintegration, (4) Photoactivation, and (5) Phototransmutation.

12.4 Radionuclides in the Environment

12.4.Q1

(249)

Over 60 radionuclides can be found in the environment and some of them pose a health hazard to humans.

- (a) Radionuclides that are found in the environment are grouped into four categories. List and briefly discuss the four categories. For each category give a few most notable examples.
- (b) Estimate the mean activity of modern carbon in organic material where carbon-14 decay is in equilibrium with cosmogenic production of C-14. The equilibrium ratio C-14/C-12 in organic material is 10^{-12} , that is, in organic carbon there is 1 carbon-14 atom per 10^{12} carbon-12 atoms. The half-life of carbon-14 is $t_{1/2} = 5730$ a. Compare your result calculated for natural carbon with that calculated for pure carbon-14.
- (c) Tritium is an important cosmogenic isotope of hydrogen undergoing β^- decay with a half-life $t_{1/2}$ of 12.3 years. Its concentration is expressed in tritium units (TU) where 1 TU corresponds to 1 tritium atom per 10^{18} hydrogen atoms. Determine the specific activity $a_{\text{H-3}}$ of tritium as well as the specific activity $a_{\text{H}_2\text{O}}$ of water in Bq/kg and Ci/kg containing 1 TU of tritium.

SOLUTION:

(a) Radionuclides are dispersed in varying concentrations over all components of the environment: soil, rock, water, air, upper atmosphere, etc., and they present varying levels of radiation hazard to humans. Based on their origin, radionuclides found in the environment are placed into the following four categories: (1) Primordial, (2) Secondary, (3) Cosmogenic, and (4) Anthropogenic.

(1) *Primordial nuclides* (stable or radioactive) are nuclides found on Earth that were formed by nuclear processes in stars and have existed in their current form already before the solar system was formed some 4.6×10^6 years ago. The number of these nuclides stands at 288 and of these, 34, called *primordial radionuclides*, have been found radioactive with long half-life $t_{1/2}$ exceeding 80×10^6 years (1.7 % of the age of the Earth). It is possible that of the 254 primordial nuclides that are considered stable today some are actually radioactive but their extremely long half-lives cannot be measured with currently available equipment. Two types of primordial radionuclides are known: those that head a radioactive decay chain or series and those that do not, since they decay directly into stable nuclides. There are over 20 radionuclides in the latter category; however, potassium-40 (amounting to a 0.012 % fraction of natural potassium $t_{1/2} = 1.3 \times 10^9$) is by far the most important source of background radiation for humans.

The other category of primordial radionuclides consists of three radioactive chain-forming radionuclides: uranium-238 (uranium series), uranium-235 (actinium series), and thorium-232 (thorium series), each one heading a chain that ends with a stable lead nuclide after a series of α and β^- decays some of which are also accompanied by γ decays.

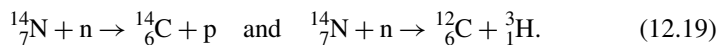
(2) In the category of *secondary radionuclides* we find radiogenic progeny of the three chain-forming primordial radionuclides. Often this category is considered part of the primordial category, however, the secondary radionuclides are clearly separated from the primordial ones. The secondary radionuclides have much shorter half-lives than the primordial radionuclides, thus, if they were around at the formation of the solar system, they would have definitely decayed by now. However, as members of one of the three primordial decay chains, they can exist in transient or secular equilibrium with long-lived parents and their numbers get replenished despite their short half-lives.

It is estimated that the naturally occurring radionuclides in the three primordial radioactive chains contribute about 50 % of the natural background external radiation and over 80 % of the natural background internal radiation. Radium-226 ($t_{1/2} = 1602$ s) and radon-222 ($t_{1/2} = 3.85$ d), members of the uranium decay series, are α emitters and are recognized as the most radiotoxic radionuclides contributing the major dose components from naturally occurring internal emitters. Radium-226 is chemically similar to calcium and concentrates in bone; radon-222 is in gaseous form and accumulates in the lung.

(3) *Cosmogenic radionuclides* are produced in the upper atmosphere where cosmic radiation (galactic and solar) through primary interactions with atmospheric molecules produces neutrons which in turn produce other radionuclides through neutron capture interactions with molecules of nitrogen, oxygen, argon, and other atmospheric gases. Radionuclides produced in the upper atmosphere are brought to the earth surface by rainwater and winds.

Cosmogenic radionuclides are not primordial since their half-lives are relatively short in comparison with the age of the solar system; however, cosmic radiation continuously replenishes the cosmogenic radionuclides establishing equilibrium between the cosmogenic production of a radionuclide and its radioactive decay.

The two most prevalent cosmogenic radionuclides are carbon-14 (C-14) with half-life $t_{1/2} = 5730$ years and tritium (H-3) with half-life $t_{1/2} = 12.3$ years. Both C-14 and H-3 are produced by neutron capture interaction between neutron and nitrogen-14 nucleus; C-14 by collision of a thermal neutron with N-14 and H-3 by collision of a fast neutron with N-14, as follows



Both C-14 and H-3 are β^- emitters and both react with atmospheric oxygen; C-14 is incorporated into carbon dioxide and H-3 into water, both gravitating toward the earth surface and contributing to background radiation in the environment. On the Earth's surface carbon-14 is incorporated into organic materials through photosynthesis and the standard food chain. The contribution of cosmogenic radionuclides to the environmental background equivalent dose is relatively small and not of concern from the radiation safety point of view.

(4) *Anthropogenic radionuclides* (i.e., man-made or artificial) have been released inadvertently or in controlled fashion into the environment during the 7 decades since the discovery of fission in 1938. This category of radionuclides consists of all radionuclides found in the environment that do not fit into one of the three natural categories listed above. Examples of inadvertent as well as controlled release of radioactivity into the environment are:

- (1) Atmospheric nuclear weapons tests (during 1940s–1960s) and use in Hiroshima and Nagasaki (1945).
- (2) Controlled release from nuclear power reactors.
- (3) Nuclear power reactor accidents, most notably Three Mile Island (USA—1979), Chernobyl (USSR—1986), and Fukushima (Japan—2011).
- (4) Controlled release from nuclear medicine tests and facilities.
- (5) Atmospheric burnout of satellites carrying radioactive sources.
- (6) Repository for spent nuclear reactor fuel and other high level nuclear waste.
- (7) Radioactive power generators in remote locations.

Most anthropogenic radionuclides are short-lived and do not pose much radiation hazard to humans. However, in this category there are also a few fission fragments, such as strontium-90 ($t_{1/2} = 28.1$ years) and cesium-137 ($t_{1/2} = 30$ years) that are

a serious threat to humans from a radiation safety point of view. Since radioactive iodine-129 and iodine-131 have the same physical properties as stable iodine, the two fission fragments produced from uncontrolled fission of uranium are of serious concern for humans because of iodine accumulation in the thyroid gland.

(b) Carbon-14 is a cosmogenic radionuclide continuously present in the environment because its radioactive decay with a half-life $t_{1/2} = 5730$ a is in equilibrium with its production in the upper atmosphere through thermal neutron interaction with nitrogen-14 stable nuclide. We first determine the specific activity a_{C-14} of carbon-14 and then calculate the specific activity a_C of natural carbon.

(1) Specific activity a_{C-14} of carbon-14 is calculated as follows

$$\begin{aligned} a_{C-14} &= \frac{\mathcal{A}_{C-14}}{m_{C-14}} = \frac{\lambda_{C-14} N_{C-14}}{m_{C-14}} = \frac{\lambda_{C-14} N_A}{A_{C-14}} = \frac{(\ln 2) N_A}{(t_{1/2})_{C-14} A_{C-14}} \\ &= \frac{(\ln 2) \times (6.022 \times 10^{23} \text{ mol}^{-1})}{(5730 \text{ a}) \times (14 \text{ g}) \times (365 \text{ d/a}) \times (24 \text{ h/d}) \times (3600 \text{ s/h})} \\ &= 0.165 \times 10^{12} \text{ s}^{-1} \cdot \text{g}^{-1} = 165 \text{ TBq/g} = \frac{0.165 \times 10^{12} \text{ Bq/g}}{3.7 \times 10^{10} \text{ Bq/Ci}} \\ &= 4.46 \text{ Ci/g}, \end{aligned} \quad (12.20)$$

where \mathcal{A}_{C-14} is the activity of carbon-14, m_{C-14} is the mass of carrier-free carbon-14, N_A is Avogadro number ($N_A = 6.022 \times 10^{23}$ atoms per mole), and $A_{C-14} = 14$ g is a mole of carbon-14.

(2) Now to the specific activity a_C of natural carbon in organic material that we calculate recalling that 1 g of natural carbon contains the following number of carbon atoms

$$n_C = \frac{N_C}{m_C} = \frac{1}{A} N_A = \frac{1}{(12 \text{ g/mol})} \times (6.022 \times 10^{23} \text{ atom/mol}) = 5.02 \times 10^{22} \text{ atom/g}. \quad (12.21)$$

Therefore in 1 g of natural carbon atoms in organic material the number n_{C-14} of carbon-14 atoms is given as $n_{C-14} = N_{C-14}/m_C = 5.02 \times 10^{22} \times 10^{-12} = 5.02 \times 10^{10}$ carbon-14 atoms, as a result of the equilibrium ratio C-14/C-12 = 10^{-12} .

This means that the specific activity of carbon in organic material can be expressed as

$$\begin{aligned} a_C &= \frac{\mathcal{A}_C}{m_C} = \frac{\lambda N_{C-14}}{m_C} = \frac{(\ln 2) N_{C-14}}{(t_{1/2})_{C-14} m_C} \\ &= \frac{(\ln 2) \times 5.02 \times 10^{10}}{(5730 \text{ a}) \times (1 \text{ g}) \times (365 \text{ d/a}) \times (24 \text{ h/d}) \times (3600 \text{ s/h})} \\ &= 0.193 \text{ s}^{-1}/\text{g} = 0.193 \text{ Bq/g} = 11.6 \text{ dpm} = \frac{0.193 \text{ Bq/g}}{3.7 \times 10^{10} \text{ Bq/Ci}} \\ &= 5.2 \text{ pCi/g}, \end{aligned} \quad (12.22)$$

where \mathcal{A}_C stands for activity of natural carbon, m_C mass of natural carbon, and dpm for number of decays per minute.

Comparing (12.20) with (12.22) we note that the specific activity a_{C-14} of C-14 exceeds the specific activity a_C of natural carbon almost by a factor of 10^{12} which is the ratio C-12/C-14.

(c) Specific activity a_{H-3} of carrier-free tritium is calculated as follows

$$\begin{aligned} a_{H-3} &= \frac{\mathcal{A}_{H-3}}{m_{H-3}} = \frac{\lambda_{H-3} N_{H-3}}{m_{H-3}} = \frac{(\ln 2) N_A}{(t_{1/2})_{H-3} A_{H-3}} \\ &= \frac{(\ln 2) \times (6.022 \times 10^{23} \text{ mol})}{(12.3 \text{ a}) \times (3.016 \text{ g}) \times (365 \text{ d/a}) \times (24 \text{ h/d}) \times (3600 \text{ s/h})} \\ &= 3.568 \times 10^{14} \text{ s}^{-1} \cdot \text{g}^{-1} = 3568 \text{ TBq/g} = \frac{3.568 \times 10^{14} \text{ Bq/g}}{3.7 \times 10^{10} \text{ Bq/Ci}} \\ &= 9643 \text{ Ci/g.} \end{aligned} \quad (12.23)$$

Specific activity a_{H_2O} of water containing 1 TU of tritium is determined as follows: 1 g of water contains $\frac{1}{18} \times 6.022 \times 10^{23}$ molecules of water or $\frac{2}{18} \times 6.022 \times 10^{23}$ hydrogen atoms. Since in 1 TU we have 1 tritium atom per 10^{18} hydrogen atoms, in 1 g of water we have $n_{TU} = \frac{2}{18} \times 6.022 \times 10^{23} \times 10^{-18} \text{ g}^{-1} = 6.69 \times 10^4 \text{ g}^{-1}$ atoms of tritium.

The specific activity a_{H_2O} of water with 1 TU of tritium is thus given

$$\begin{aligned} a_{H_2O} &= \frac{(\ln 2)}{(t_{1/2})_{H-3}} n_{TU} = \frac{(\ln 2) \times (6.69 \times 10^4 \text{ g}^{-1})}{(12.3 \text{ a}) \times (365 \text{ d/a}) \times (24 \text{ h/d}) \times (3600 \text{ s/h})} \\ &= 0.12 \text{ Bq/kg} = 3.2 \text{ pCi/kg.} \end{aligned} \quad (12.24)$$

12.5 General Aspects of Nuclear Activation

12.5.Q1

(250)

Several types of nuclear activation are known. Activation with thermal or fast neutrons is called neutron activation; activation with protons is proton activation; activation with high-energy photons is nuclear photoactivation. There are several common features that govern the physics behind the activation processes, such as cross section, target thickness, Q value, and threshold.

- (a) Cross section σ of a nuclear reaction is proportional to probability P of reaction occurrence, has units of area, and is defined as reaction rate divided by the incident particle fluence. Derive an expression for the probability P of an incident projectile to trigger a reaction in thin target and thick target. State all assumptions involved.
- (b) Define the reaction rate \dot{R} and derive its relationship with cross section σ for thin and thick targets.
- (c) An aluminum foil of thickness $x = 0.2$ mm is bombarded by neutrons in a nuclear reactor and the target gets activated through neutron capture reaction expressed by the following ${}_{13}^{27}\text{Al} + n \rightarrow {}_{13}^{28}\text{Al} + \gamma$. Calculate the number of neutrons captured per second by 1 cm^2 of the aluminum foil. Neutron capture cross section σ of aluminum is 2 mb, mass density ρ_{Al} of aluminum is 2.7 g/cm^3 , and the neutron fluence rate $\dot{\phi}$ in the nuclear reactor is $10^{13} \text{ cm}^{-2} \cdot \text{s}^{-1}$.
- (d) Estimate the probability that nuclear reactor-produced electronic antineutrino has an interaction with a proton when traversing the earth. Cross section for antineutrino interacting with a proton is 10^{-43} cm^2 , mean earth radius is $6.37 \times 10^8 \text{ cm}$, and mean mass density of the Earth is 5.52 g/cm^3 .

SOLUTION:

(a) Many ways have been devised for deriving and explaining nuclear reaction probability and reaction cross section.

(1) In a simplistic approach we might consider estimating the probability for a reaction between the incident particle and a target nucleus by treating the incident particles as points and the target nuclei as projecting an area πR^2 defined by the nuclear radius R . Any time an incident particle hits a nucleus, a reaction is assumed to happen; no reaction occurs when the particle misses the nucleus. This geometrical picture takes no account of the finite size of the incident particle nor does it consider the range of interaction forces that are in effect between the incident particle and the target nucleus. This approach is simple but suffers serious deficiencies.

(2) Rather than treating a geometrical cross sectional area πR^2 as a measure of interaction probability, we assign to the nucleus an effective area σ perpendicular to the incident beam such that a reaction occurs every time a bombarding particle hits any part of the effective disk area. This effective area is referred to as the reaction cross-section σ and is usually measured in barn, where $1 \text{ barn} = 1 \text{ b} = 10^{-24} \text{ cm}^2 = 10^{-28} \text{ m}^2$. Cross section σ is proportional to the reaction probability P . The range of reaction cross sections σ in nuclear physics varies from a low of 10^{-19} b to a high of 10^6 b , with the lower limit in effect for weak neutrino interactions with nuclei and the upper limit in effect for thermal neutron capture in certain nuclides.

Target of thickness x_0 projects an area S to the incident particle beam. The target contains N nuclei, each characterized with a reaction cross section σ . The density of target nuclei n^\square is equal to the atomic density (number of atoms per volume) and represents the number of nuclei N per volume \mathcal{V} of the target with $\mathcal{V} = Sx_0$. To determine the reaction rate R (number of nuclear reactions per unit time) we consider two target options with regard to target thickness x_0 : *thin targets* and *thick targets*.

(1) A *thin target* is thin enough so that no significant overlap between target nuclei occurs as the particle beam penetrates the target. This implies that negligible masking of target nuclei occurs in a thin target. The probability P for an incident particle to trigger a reaction in a thin target is the ratio of the effective area σN over the target area S

$$P = \frac{\sigma N}{S} = \frac{\sigma N x_0}{S x_0} = n^\square \sigma x_0, \quad (12.25)$$

where we used the definition of density of target nuclei given as $n^\square = N/\mathcal{V} = N/(Sx_0)$.

(2) In comparison with a thin target, a *thick target* has a thickness x_0 that engenders significant masking of target nuclei. In this case we assume that a thick target consists of a large number of thin targets. In each thin target layer of thickness dx the number of incident particles per unit area per unit time $\dot{\mathcal{N}}$ diminishes by $d\dot{\mathcal{N}}$ so that we can write $d\dot{\mathcal{N}}(x)$ as

$$-d\dot{\mathcal{N}}(x) = \dot{\mathcal{N}}(x)n^\square\sigma dx \quad (12.26)$$

or

$$\int_{\dot{\mathcal{N}}(x_0)}^{\dot{\mathcal{N}}(x)} \frac{d\dot{\mathcal{N}}(x)}{\dot{\mathcal{N}}(x)} = - \int_0^{x_0} n^\square\sigma dx, \quad (12.27)$$

where

$\dot{\mathcal{N}}_0$ is the number of particles per unit area per unit time striking the target.

$\dot{\mathcal{N}}(x_0)$ is the number of particles per unit area per unit time that traverse the thick target x_0 .

The solution to the simple integral equation (12.27) is an exponential function

$$\dot{\mathcal{N}}(x_0) = \dot{\mathcal{N}}_0 e^{-n^\square\sigma x_0} \quad (12.28)$$

and the number of incident particles \mathcal{N} that undergo a reaction in the thick target is expressed as the incident number of particles per unit area per unit time $\dot{\mathcal{N}}_0$ minus the number of particles $\dot{\mathcal{N}}(x_0)$ per unit area per unit time that traversed the thick target.

$$\dot{\mathcal{N}} = \dot{\mathcal{N}}_0 - \dot{\mathcal{N}}(x_0) = \dot{\mathcal{N}}_0(1 - e^{-n^\square\sigma x_0}). \quad (12.29)$$

(b) The reaction rate $\dot{\mathcal{R}}$ is the number of reactions per unit time and is a product of the reaction probability P and the number of incident particles per unit area per unit time

$$\dot{\mathcal{R}} = P\dot{\mathcal{N}}. \quad (12.30)$$

(1) If the number of incident particles per area per unit time (fluence rate) is $\dot{\mathcal{N}}_0 = \dot{\phi}$, then $\dot{\mathcal{R}}$, the number of reactions per unit area and unit time, for a thin target after incorporating (12.25) into (12.30) is given as follows

$$\dot{\mathcal{R}} = P\dot{\mathcal{N}}_0 = \dot{\mathcal{N}}_0 n^\square \sigma x_0. \quad (12.31)$$

(2) For a thick target the number of reactions per unit area per unit time $\dot{\mathcal{R}}$ is given by the number of incident particles \mathcal{N} that undergo a reaction in the target given in (12.89)

$$\dot{\mathcal{R}} = \dot{\mathcal{N}}_0 - \dot{\mathcal{N}}(x_0) = \dot{\mathcal{N}}_0 \{1 - e^{-n^\square \sigma x_0}\}. \quad (12.32)$$

Note that (12.32) transforms into (12.31) for small x_0 since $1 - e^{-n^\square \sigma x_0} \approx n^\square \sigma x_0$.

(c) To calculate the number of neutrons captured per cm^2 per second (activation rate) we will assume that we are dealing with a thin target and use (12.31) with cross section for neutron capture in aluminum $\sigma = 2 \text{ mb}$, target thickness $x_0 = 0.2 \text{ mm}$, neutron fluence $\dot{\mathcal{N}}_0 = \dot{\phi} = 10^{13} \text{ cm}^{-2} \cdot \text{s}^{-1}$, and number of aluminum nuclei per volume n_{Al}^\square determined as follows

$$\begin{aligned} n_{\text{Al}}^\square &= \frac{N_a}{V} = \rho \frac{N_a}{m} = \rho \frac{N_A}{A} = \frac{(2.7 \text{ g/cm}^3) \times (6.022 \times 10^{23} \text{ mol}^{-1})}{(27 \text{ g} \cdot \text{mol}^{-1})} \\ &= 6.022 \times 10^{22} \text{ cm}^{-3}. \end{aligned} \quad (12.33)$$

Probability P of neutron capture reaction to occur is given in (12.25) as

$$\begin{aligned} P &= n^\square \sigma x_0 = (6.022 \times 10^{22} \text{ cm}^{-3}) \times (2 \times 10^{-3} \times 10^{-24} \text{ cm}^2) \times (0.02 \text{ cm}) \\ &= 2.41 \times 10^{-6}. \end{aligned} \quad (12.34)$$

Reaction rate $\dot{\mathcal{R}}$ is the number of incident neutrons per cm^2 per second in (12.31) given as

$$\dot{\mathcal{R}} = P\dot{\mathcal{N}}_0 = (2.41 \times 10^{-6}) \times (10^{13} \text{ cm}^{-2} \cdot \text{s}^{-1}) = 2.41 \times 10^7. \quad (12.35)$$

Of 10^{13} neutrons incident on 1 cm^2 of the target each second, the number of neutrons captured is 2.41×10^7 or 1 captured neutron per $\sim 415\,000$ incident neutrons.

In the calculation above we assume that the target is a thin target. We now repeat the calculation assuming we are dealing with a thick target and use (12.32) to calculate the reaction rate, i.e., the number of captured neutrons per cm^2 per second

$$\begin{aligned}
\dot{\mathcal{R}} &= \dot{\mathcal{N}}_0 \{1 - e^{-n^\square \sigma x_0}\} \\
&= (10^{13} \text{ cm}^{-2} \cdot \text{s}^{-1}) \times \{1 - e^{-(6.022 \times 10^{22}) \times (2 \times 10^{-3} \times 10^{-24}) \times (2 \times 10^{-2})}\} \\
&= (10^{13} \text{ cm}^{-2} \cdot \text{s}^{-1}) \times \{1 - e^{-(2.41 \times 10^{-6})}\} \\
&\approx (10^{13} \text{ cm}^{-2} \cdot \text{s}^{-1}) \times \{1 - (1 + 2.41 \times 10^{-6})\} \\
&= 2.41 \times 10^7 \text{ cm}^{-2} \cdot \text{s}^{-1}.
\end{aligned} \tag{12.36}$$

Result (12.36) is identical to result (12.35) indicating that the target in this particular activation experiment can be considered a thin target and the simple equation (12.31) can be used for determination of the activation rate.

(d) Probability of antineutrino traversing Earth along the diameter of the earth being captured by a proton (capture cross section is estimates as $\sim 10^{-43} \text{ cm}^2$) is estimated using an assumption that the protons of the Earth represent a thin target to an antineutrino. We therefore use (12.25) with thin target thickness x_0 of earth diameter $2 \times (6.37 \times 10^8 \text{ cm}) = 12.74 \times 10^8 \text{ cm}$, cross section σ of 10^{-43} cm^2 , and calculate n^\square , the proton density, i.e., number of protons per cm^3 as follows

$$\begin{aligned}
n^\square &= \frac{N_p}{V} = \frac{\bar{\rho} N_p}{m} = \frac{\bar{\rho} N_A}{A} \left(\frac{A}{2} \right) \\
&= \frac{(5.52 \text{ g/cm}^3) \times (6.022 \times 10^{23} \text{ mol}^{-1})}{A (\text{g} \cdot \text{mol}^{-1})} \times \left(\frac{A}{2} \right) \\
&= 1.662 \times 10^{24} \text{ cm}^{-3},
\end{aligned} \tag{12.37}$$

where we assumed that the mean atomic weight of the Earth is around iron which means that the number of protons is approximately equal to the number of neutrons, so that number of protons in the mean nucleus of the Earth is $\sim A/2$.

Probability for antineutrino interaction with a proton is now given as

$$\begin{aligned}
P &= n^\square \sigma x_0 = (1.662 \times 10^{24} \text{ cm}^{-3}) \times (10^{-43} \text{ cm}^2) \times (12.74 \times 10^8 \text{ cm}) \\
&= 2.1 \times 10^{-10},
\end{aligned} \tag{12.38}$$

indicating that the neutrino interaction with a proton is very improbable.

12.6 Nuclear Activation with Neutrons

12.6.Q1

(251)

In practice the most commonly used nuclear activation process is triggered by thermal neutrons in a nuclear reactor, where a stable parent target nucleus P of thermal neutron cross section σ_P (in cm^2) upon bombardment with ther-

mal neutron fluence rate $\dot{\phi}$ (in $\text{cm}^{-2} \cdot \text{s}^{-1}$) is transformed into a radioactive daughter D that decays with a decay constant λ_D into a granddaughter G that may be stable or is radioactive



-
- (a) Discuss the initial and general conditions that apply to neutron activation process and state the general differential equation from which the activity $\mathcal{A}_D(t)$ of the daughter radionuclide D is derived for nuclear activation of the stable parent P. Define all parameters used in the derivation of $\mathcal{A}_D(t)$.
 - (b) Use the general expression for dN_D/dt described in (a) and derive $\mathcal{A}_D(t)$ valid for the saturation model of neutron activation.
 - (c) Use the general expression for dN_D/dt described in (a) and derive $\mathcal{A}_D(t)$ valid for the depletion model of neutron activation.
 - (d) Use the general expression for dN_D/dt described in (a) and derive $\mathcal{A}_D(t)$ valid for the parent depletion–daughter activation model of neutron activation.

SOLUTION:

(a) In artificial production of a radionuclide with thermal neutron activation the main objective is to produce activity $\mathcal{A}_D(t)$ in the activated daughter sample D which is an isotope of the stable parent nuclide P. The induced radioactivity $\mathcal{A}_D(t)$ depends on many factors, such as mass m and activation cross section σ_P of the parent sample, neutron fluence rate $\dot{\phi}$ in the reactor, as well as the decay constant λ_D and activation cross section σ_D of the daughter radionuclide. The daughter D nuclei are produced at a rate of $\sigma_P \dot{\phi} N_P(t)$ and they decay with a rate of $\lambda_D N_D(t)$. If the daughter D is affected by exposure to activation particles, one accounts for the daughter activation with the term $\sigma_D \dot{\phi} N_D(t)$. The number of daughter nuclei is $N_D(t)$ and the overall rate of change of the number of daughter nuclei is dN_D/dt obtained by combining the production rate of daughter nuclei $\sigma_P \dot{\phi} N_P(t)$ with the decay rate of daughter nuclei $\lambda_D N_D(t)$ and depletion of daughter nuclei through $\sigma_D \dot{\phi} N_D(t)$ to get the following differential equation for $dN_D(t)/dt$

$$\frac{dN_D(t)}{dt} = \sigma_P \dot{\phi} N_P(t) - \lambda_D N_D(t) - \sigma_D \dot{\phi} N_D(t), \quad (12.40)$$

where σ_P is the thermal neutron cross section of the parent nucleus, σ_D is the thermal neutron cross section of the daughter nucleus, $\dot{\phi}$ is the fluence rate of thermal neutrons, $N_P(t)$ is the number of parent P target nuclei, $N_D(t)$ is the number of daughter D nuclei and λ_D is the decay constant of the daughter nucleus related to its half-life $(t_{1/2})_D$ through $(t_{1/2})_D = (\ln 2)/\lambda_D$.

The solution to differential equation (12.40) for $N_D(t)$ is affected by several conditions, such as:

- (1) Initial conditions on the initial number $N_P(0)$ of parent nuclei at time $t = 0$ and initial number $N_D(0)$ of daughter nuclei at time $t = 0$.
- (2) General conditions on $N_P(t)$ during the activation process allowing two possibilities: (i) $N_P(t)$ is essentially constant with activation time t suggesting that $N_P(t)$ is not affected by activation of parent nuclei into daughter nuclei and (ii) $N_P(t)$ is diminishing with activation time t as a result of the activation of parent nuclei into daughter nuclei. The first [$N_P(t) = \text{const}$] option represents the saturation model of nuclear activation, while the second option represents the depletion model of nuclear activation.
- (3) General conditions on $N_D(t)$ during the activation process of the parent P. $N_D(t)$ grows through activation of parent P and diminishes during the activation process because of (i) daughter decay or (ii) daughter decay combined with daughter activation as a result of daughter exposure to neutrons. The saturation model or the depletion model of activation, listed in (2), cover the first option which assumes that the daughter is not affected by neutron exposure, while the second option which incorporates the daughter activation by neutron exposure represents the parent depletion–daughter activation model.

(b) For standard initial conditions $N_P(t = 0) = N_P(0)$ and $N_D(t = 0) = N_D(0) = 0$ as well as the general condition for the saturation model that (1) number of parent nuclei is constant, i.e., is so large that it is not affected by exposure to neutrons [$N_P(t) = N_P(0) = \text{const}$] and (2) daughter radionuclide is not affected by exposure to neutrons ($\sigma_D = 0$), the differential equation for dN_D/dt of (12.40) is written as

$$\frac{dN_D(t)}{dt} = \sigma_P \dot{\phi} N_P(0) - \lambda_D N_D(t) \quad (12.41)$$

or in integral form as

$$\int_0^{N_D(t)} \frac{d\{\sigma_P \dot{\phi} N_P(0) - \lambda_D N_D\}}{\sigma_P \dot{\phi} N_P(0) - \lambda_D N_D} = -\lambda_D \int_0^t dt. \quad (12.42)$$

The solution of the simple differential equation (12.42) is as follows

$$N_D(t) = \frac{\sigma_P \dot{\phi} N_P(0)}{\lambda_D} \{1 - e^{-\lambda_D t}\}. \quad (12.43)$$

Since the daughter activity $\mathcal{A}_D(t)$ equals to $\lambda_D N_D(t)$, we can write $\mathcal{A}_D(t)$ for the saturation model of neutron activation as (T12.13)

$$\mathcal{A}_D(t) = \sigma_P \dot{\phi} N_P(0) \{1 - e^{-\lambda_D t}\} = (\mathcal{A}_D)_{\text{sat}} \{1 - e^{-\lambda_D t}\}, \quad (12.44)$$

where we define $(\mathcal{A}_D)_{\text{sat}}$, the saturation daughter D activity that can be produced by bombardment of the parent P target with neutrons, as equal to $\sigma_P \dot{\phi} N_P(0)$.

The specific activity a of a radioactive source is defined as activity \mathcal{A} of the source per unit mass M of the source, i.e., $a = \mathcal{A}/M$. For the saturation model (12.44), we can thus express specific activity a as a function of activation time t as

$$a(t) = \frac{\mathcal{A}(t)}{M} = \frac{\sigma_P \dot{\phi} N_P(0)}{M} \{1 - e^{-\lambda_D t}\} = \frac{\sigma_P \dot{\phi} N_A}{A_P} \{1 - e^{-\lambda_D t}\} = a_{\text{sat}} \{1 - e^{-\lambda_D t}\}, \quad (12.45)$$

where we define a_{sat} as the saturation specific activity ($a_{\text{sat}} = \sigma_P \dot{\phi} N_A / A_P$) and we used the identity $N_P(0)/M = N_A / A_P$ with A_P the atomic weight of the parent nucleus and N_A the Avogadro number ($6.022 \times 10^{23} \text{ mol}^{-1}$).

(c) In the parent depletion model of neutron activation, one must account for the finite number of parent nuclei [$N_P(t) \neq \text{const}$]; however, an assumption is made that the daughter radionuclide is not affected by neutron exposure [$\sigma_P = 0$]. Equation (12.40) is for the depletion model stated as follows

$$\frac{dN_D(t)}{dt} = \sigma_P \dot{\phi} N_P(t) - \lambda_D N_D(t), \quad (12.46)$$

with $N_P(t)$ given as $N_P(t) = N_P(0)e^{-\sigma_P \dot{\phi} t}$, where $N_P(0)$ is the initial number of parent nuclei placed into the neutron fluence rate $\dot{\phi}$ at time $t = 0$.

The solution to (12.46), following the steps taken in the derivation of (T10.34) for the nuclear decay series $P \rightarrow D \rightarrow G$ and using the following initial conditions $N_P(t = 0) = N_P(0)$ and $N_D(t = 0) = N_D(0) = 0$ is given as follows (T12.21)

$$N_D(t) = N_P(0) \frac{\sigma_P \dot{\phi}}{\lambda_D - \sigma_P \dot{\phi}} [e^{-\sigma_P \dot{\phi} t} - e^{-\lambda_D t}]. \quad (12.47)$$

Recognizing that activity $\mathcal{A}_D(t) = \lambda_D N_D(t)$ we get the following expression for the growth in daughter activity $\mathcal{A}_D(t)$ with activation time t

$$\mathcal{A}_D(t) = \lambda_D N_D(t) = N_P(0) \frac{\lambda_D \sigma_P \dot{\phi}}{\lambda_D - \sigma_P \dot{\phi}} [e^{-\sigma_P \dot{\phi} t} - e^{-\lambda_D t}]. \quad (12.48)$$

Several interesting features are evident from (12.48), such as, for example:

- (1) Generally, in neutron activation $\sigma_P \dot{\phi} < \lambda_D$ resulting in dynamics similar to that referred to as transient equilibrium in nuclear decay series.
- (2) When $\sigma_P \dot{\phi} \ll \lambda_D$, we are dealing with a special case of transient equilibrium dynamics that in nuclear decay series is referred to as secular equilibrium dynamics. In this case, (12.48) simplifies to the expression derived above in (12.44) for the saturation model and is valid under the assumption that the fraction of nuclei transformed from parent to daughter in neutron activation is negligible in comparison to the initial number $N_P(0)$ of parent nuclei.
- (3) Equation (12.48) shows that, rather than reaching saturation at $t \rightarrow \infty$, the daughter activity $\mathcal{A}_D(t)$ is zero at $t = 0$ and, with increasing time from $t = 0$, first rises with t , reaches a maximum $(\mathcal{A}_D)_{\text{max}}$ at time $t = (t_{\text{max}})_D$, and then decreases as t increases further, until at $t = \infty$ it becomes zero again.

- (4) The time $(t_{\max})_D$ is determined by setting $(d\mathcal{A}_D/dt)_{t=(t_{\max})_D} = 0$ to get the following result

$$(t_{\max})_D = \frac{\ln \frac{\sigma_P \dot{\phi}}{\lambda_D}}{\sigma_P \dot{\phi} - \lambda_D} \equiv \frac{\ln \frac{\lambda_D}{\sigma_P \dot{\phi}}}{\lambda_D - \sigma_P \dot{\phi}}. \quad (12.49)$$

(d) Equation (12.40) describes the most general neutron activation process in which the parent P is exposed to neutrons and transforms into radioactive daughter D which decays with its own decay constant λ_D and, in addition, is affected by exposure to neutrons ($\sigma_D \neq 0$). The model that deals with this general nuclear activation process is referred to as the “parent depletion–daughter activation” model and can be described by a simple consolidation of the daughter decay term $[\lambda_D N_D(t)]$ and daughter activation term $[\sigma_D \dot{\phi} N_D(t)]$ into one term governed by a modified decay constant expressed as follows: $\lambda_D^* = \lambda_D + \sigma_D \dot{\phi}$, resulting in the following form of (12.40)

$$\frac{dN_D(t)}{dt} = \sigma_P \dot{\phi} N_P(t) - \lambda_D N_D(t) - \sigma_D \dot{\phi} N_D(t) = \sigma_P \dot{\phi} N_P(t) - \lambda_D^* N_D(t). \quad (12.50)$$

The solution to differential equation (12.50) is similar to that of (12.46) except that λ_D in (12.46) is replaced by a modified decay constant λ_D^* resulting in the following solution to (12.50)

$$N_D(t) = N_P(0) \frac{\sigma_P \dot{\phi}}{\lambda_D^* - \sigma_P \dot{\phi}} [e^{-\sigma_P \dot{\phi} t} - e^{-\lambda_D^* t}]. \quad (12.51)$$

The daughter activity $\mathcal{A}_D(t) = \lambda_D N_D(t)$ is in the depletion–activation model expressed as

$$\mathcal{A}_D(t) = N_P(0) \frac{\lambda_D \sigma_P \dot{\phi}}{\lambda_D^* - \sigma_P \dot{\phi}} [e^{-\sigma_P \dot{\phi} t} - e^{-\lambda_D^* t}] = \sigma_P \dot{\phi} N_P(0) \frac{\frac{\lambda_D}{\lambda_D^*}}{1 - \frac{\sigma_P \dot{\phi}}{\lambda_D^*}} [e^{-\sigma_P \dot{\phi} t} - e^{-\lambda_D^* t}]. \quad (12.52)$$

12.6.Q2

(252)

For better understanding of neutron activation processes we can express them in a general format by renormalizing the number of parent nuclei $N_P(t)$ and the number of daughter nuclei $N_D(t)$, defining a new parameter m , and new variables x , y_P , and y_D , similarly to the approach we took in Prob. 218 for radioactive decay series. The general parameters and variables for the saturation and depletion models of neutron activation are given as follows:

- (1) Parameter m , now called *activation factor* in parallel with the decay factor m of the radioactive decay series, is defined by the ratio: $m = \sigma_P \dot{\phi} / \lambda_D$,
- (2) Normalized activation time—variable x is defined as time normalized to half-life $(t_{1/2})_D$ of the daughter nucleus as follows: $x = mt / (t_{1/2})_D$,
- (3) Normalized number of parent nuclei y_P is defined as: $y_P = N_P(t) / N_P(0)$,
- (4) Normalized number of daughter nuclei y_D is given as: $y_D = \frac{\lambda_D N_D(t)}{\sigma_P \dot{\phi} N_P(0)} = \frac{\mathcal{A}_D(t)}{\sigma_P \dot{\phi} N_P(0)}$,

where σ_P is the cross section of the parent nucleus for neutron activation, $\dot{\phi}$ is the neutron fluence rate in the reactor, λ_D is the decay constant of the daughter nucleus, $N_P(0)$ is the initial number of parent nuclei, and $\mathcal{A}_D(t)$ is the activity of the daughter radionuclide.

- (a) Transform the equation that describes the number of parent nuclei $N_P(t)$ into a general format given by y_P as a function of variable x .
- (b) For the saturation model and depletion model of neutron activation transform the equation that describes the number of daughter nuclei $N_D(t)$ into a general format given by $z_D(x)$ for the saturation model and $y_D(x)$ for the depletion model as a function of dimensionless variable x and activation factor m .
- (c) For the depletion model and activation factor $m = 1$ use the l'Hôpital rule to obtain the general form of the daughter activity y_D derived in (b).
- (d) In the depletion model the characteristic time t_{\max} is defined as the time in which the daughter activity $\mathcal{A}_D(t)$ reaches its maximum value. Using the expression for y_D calculated in (b), determine the normalized time $(x_D)_{\max}$ at which $y_D(x)$ reaches its maximum for arbitrary positive activation factor m in the range $0 \leq m \leq \infty$ including $m = 1$.
- (e) Determine $(y_D)_{\max}$ as a function of activation factor m for all possible positive m in the range $0 \leq m \leq \infty$ including $m = 1$.
- (f) Evaluate the relationship between $(y_D)_{\max}$ and $(x_D)_{\max}$ for all possible positive m in the range $0 \leq m \leq \infty$ including $m = 1$.

SOLUTION:

The general variables x , y_P , y_D as well as the activation factor m are for neutron activation defined as follows

$$x = m \frac{t}{(t_{1/2})_D}; \quad (12.53)$$

$$y_P = \frac{N_P(t)}{N_P(0)}; \quad (12.54)$$

$$y_D = \frac{N_D(t)}{mN_P(0)} = \frac{\mathcal{A}_D(t)}{\sigma_P \dot{\phi} N_P(0)}; \quad (12.55)$$

$$m = \frac{\sigma_P \dot{\phi}}{\lambda_D}. \quad (12.56)$$

(a) The standard form for the number of parent nuclei $N_P(t)$, undergoing neutron activation in neutron fluence rate $\dot{\phi}$, is expressed by the following equation

$$N_P(t) = N_P(0)e^{-\sigma_P \dot{\phi} t}, \quad (12.57)$$

which, after incorporating (12.53), (12.54), and (12.56), takes up the following form (T12.27), giving the number of parent nuclei $N_P(t)$ normalized to the initial number of parent nuclei $N_P(0)$

$$y_P = \frac{N_P(t)}{N_P(0)} = e^{-\sigma_P \dot{\phi} t} = e^{-m\lambda_D t} = e^{-m \frac{t}{(t_{1/2})_D} \ln 2} = e^{-x \ln 2} = \frac{1}{2^x} \equiv 2^{-x}. \quad (12.58)$$

(b) The number of daughter nuclei $N_D(t)$ is proportional to the number of initial parent nuclei $N_P(t)$ but differs for the two neutron activation models, as derived in Prob. 251:

(1) For the saturation model given in (12.43) in Prob. 251 $N_D(t)$ and $\mathcal{A}_D(t)$ are

$$N_D(t) = \frac{\sigma_P \dot{\phi} N_P(0)}{\lambda_D} [1 - e^{-\lambda_D t}] \quad (12.59)$$

and

$$\mathcal{A}_D(t) = \lambda_D N_D(t) = \sigma_P \dot{\phi} N_P(0) [1 - e^{-\lambda_D t}] = \mathcal{A}_{\text{sat}} [1 - e^{-\lambda_D t}], \quad (12.60)$$

where \mathcal{A}_{sat} is the saturation activity defined as the product $\sigma_P \dot{\phi} N_P(0)$ and attained at time $t \rightarrow \infty$.

Combining (12.60) with (12.55) and (12.56) we now write the normalized daughter activity $z_D(x)$ for the saturation model as

$$\begin{aligned} z_D(x) &= \frac{N_D(t)}{mN_P(0)} = \frac{\lambda_D N_D(t)}{\sigma_P \dot{\phi} N_P(0)} = \frac{\mathcal{A}_D(t)}{\sigma_P \dot{\phi} N_P(0)} \\ &= 1 - e^{-\lambda_D t} = 1 - e^{-\frac{t \ln 2}{(t_{1/2})_D}} = 1 - e^{-\frac{x}{m} \ln 2} = 1 - \frac{1}{2^{x/m}}. \end{aligned} \quad (12.61)$$

(2) For the depletion model given in (12.47) in Prob. 251, $N_D(t)$ and $\mathcal{A}_D(t)$ are

$$N_D(t) = \frac{\sigma_P \dot{\phi} N_P(0)}{\lambda_D - \sigma_P \dot{\phi}} [e^{-\sigma_P \dot{\phi} t} - e^{-\lambda_D t}] \quad (12.62)$$

and

$$\mathcal{A}_D(t) = \lambda_D N_D(t) = \frac{\lambda_D \sigma_P \dot{\phi} N_P(0)}{\lambda_D - \sigma_P \dot{\phi}} [e^{-\sigma_P \dot{\phi} t} - e^{-\lambda_D t}]. \quad (12.63)$$

Combining (12.63) with (12.55) and (12.56) we now write the normalized daughter activity y_D for the depletion model as

$$\begin{aligned}
 y_D &= \frac{N_D(t)}{m N_P(0)} = \frac{\lambda_D N_D(t)}{\sigma_P \dot{\phi} N_P(0)} = \frac{\lambda_D}{\lambda_D - \sigma_P \dot{\phi}} \left[e^{-\sigma_P \dot{\phi} t} - e^{-\lambda_D t} \right] \\
 &= \frac{1}{1 - \frac{\sigma_P \dot{\phi}}{\lambda_D}} \left[e^{-\frac{\sigma_P \dot{\phi} \ln 2}{\lambda_D (t_{1/2})_D} t} - e^{-\frac{t \ln 2}{(t_{1/2})_D} \lambda} \right] \\
 &= \frac{1}{1 - m} \left[e^{-\frac{m t \ln 2}{(t_{1/2})_D}} - e^{-\frac{t \ln 2}{(t_{1/2})_D} \lambda} \right] = \frac{1}{1 - m} \left[e^{-x \ln 2} - e^{-\frac{x}{m} \ln 2} \right] \\
 &= \frac{1}{1 - m} \left[\frac{1}{2^x} - \frac{1}{2^{x/m}} \right]. \tag{12.64}
 \end{aligned}$$

(c) Equation (12.64) for normalized daughter activity y_D as a function of normalized time x is valid for all positive values of the activation factor m from 0 to ∞ with the exception of $m = 1$ for which y_D is not defined. However, since for $m = 1$ (12.64) gives $y_D = 0/0$, we can apply the l'Hôpital rule and determine the function that governs y_D at $m = 1$ as follows (T10.46)

$$y_D|_{m=1} = \lim_{m \rightarrow 1} \frac{\frac{d}{dm} \left[\frac{1}{2^x} - \frac{1}{2^{x/m}} \right]}{\frac{d}{dm} (1 - m)} = \lim_{m \rightarrow 1} \frac{-2^{-\frac{x}{m}} (\ln 2) \frac{x}{m^2}}{-1} = (\ln 2) \frac{x}{2^x}. \tag{12.65}$$

(d) Equation (12.64) of (b) gives the normalized daughter activity y_D [see (12.55)] as a function of normalized activation time x [see (12.53)] for $0 \leq m \leq \infty$ with the exception of $m = 1$ for which y_D is simplified and given by (12.65) in (c). Normalized daughter activities y_D of (12.64) and (12.65) are equal to zero for $x = 0$ (initial condition) and $x = \infty$ (when all nuclei of parent P and daughter D have decayed). This suggests that y_D (in conjunction with \mathcal{A}_D) passes through a maximum at a specified characteristic normalized time $(x_D)_{\max}$ between 0 and ∞ for all m except for $m = 1$. The characteristic time $(x_D)_{\max}$ can be determined as a function of activation factor m by setting $dy_D/dx|_{x=(x_D)_{\max}} = 0$ and solving for $(x_D)_{\max}$ as follows

$$\begin{aligned}
 \left. \frac{dy_D}{dx} \right|_{x=(x_D)_{\max}} &= \left. \frac{d}{dx} \left[\frac{1}{1 - m} \left(\frac{1}{2^x} - \frac{1}{2^{x/m}} \right) \right] \right|_{x=(x_D)_{\max}} \\
 &= \frac{1}{1 - m} \left[-2^{-x} \ln 2 + \frac{1}{m} 2^{-\frac{x}{m}} \ln 2 \right] \Big|_{x=(x_D)_{\max}} = 0. \tag{12.66}
 \end{aligned}$$

Solving (12.66) for $(x_D)_{\max}$ we now get

$$2^{-(x_D)_{\max}} = \frac{1}{m} 2^{-(x_D)_{\max}/m} \quad \text{or} \quad -(x_D)_{\max} \ln 2 = \ln \frac{1}{m} - \frac{(x_D)_{\max}}{m} \ln 2 \tag{12.67}$$

and finally

$$(x_D)_{\max} = \frac{m}{m - 1} \frac{\ln m}{\ln 2}. \tag{12.68}$$

For $m = 1$, (12.68) is not defined, however, since it gives $(x_D)_{\max} = 0/0$, we can apply the l'Hôpital rule to get $(x_D)_{\max}|_{m \rightarrow 1}$ as follows

$$(x_D)_{\max}|_{m \rightarrow 1} = \lim_{m \rightarrow 1} \frac{\frac{d(m \ln m)}{dm}}{\frac{d(m-1)}{dm} \ln 2} = \lim_{m \rightarrow 1} \frac{1 + \ln m}{\ln 2} = \frac{1}{\ln 2} = 1.4427. \quad (12.69)$$

Thus, $(x_D)_{\max}$ is calculated from (12.68) for any positive m except for $m = 1$ for which $(x_D)_{\max} = 1.44$, as determined in (12.69).

(e) The maximum daughter activity $(y_D)_{\max}$ can be determined by inserting $(x_D)_{\max}$ of (12.68) into y_D given by (12.64) as follows

$$\begin{aligned} (y_D)_{\max} &= y_D[(x_D)_{\max}] = \frac{1}{1-m} \left[\frac{1}{2^{(x_D)_{\max}}} - \frac{1}{2^{(x_D)_{\max}/m}} \right] \\ &= \frac{(1-m)^{-1}}{2^{(x_D)_{\max}}} \left[1 - \frac{1}{2^{[(x_D)_{\max}/m] - (x_D)_{\max}}} \right] \\ &= \frac{(1-m)^{-1}}{2^{(x_D)_{\max}}} \left[1 - \frac{1}{2^{(x_D)_{\max}[\frac{1-m}{m}]}} \right] = \frac{1}{1-m} F_1 [1 - F_2]. \end{aligned} \quad (12.70)$$

Components F_1 and F_2 of (12.70), after insertion of $(x_D)_{\max}$ given by (12.68) and using the following identity $e^z \ln 2 = e^{\ln 2^z} = 2^z$, yield the following expressions

$$F_1 = \frac{1}{2^{(x_D)_{\max}}} = \frac{1}{2^{\frac{m}{(1-m)} \frac{\ln m}{\ln 2}}} = 2^{\frac{m}{(1-m)} \frac{\ln m}{\ln 2}} = e^{\ln 2^{\frac{m}{(1-m)} \frac{\ln m}{\ln 2}}} = e^{\frac{m}{1-m} \ln m} \quad (12.71)$$

and

$$F_2 = \frac{1}{2^{(x_D)_{\max}[\frac{1-m}{m}]}} = \frac{1}{2^{\frac{m}{(m-1)} \frac{\ln m}{\ln 2} [\frac{1-m}{m}]}} = 2^{\frac{\ln m}{\ln 2}} = e^{\ln m} = m. \quad (12.72)$$

The maximum normalized daughter activity $(y_D)_{\max}$ of (12.70), after incorporating F_1 of (12.71) and F_2 of (12.72), can now be written as follows

$$(y_D)_{\max} = \frac{1}{1-m} F_1 [1 - F_2] = \frac{1}{1-m} e^{\frac{m}{1-m} \ln m} [1 - m] = e^{\frac{m}{1-m} \ln m}. \quad (12.73)$$

Since $(x_D)_{\max}$ not only defines the maximum in the normalized daughter activity $y_D(x)$ but also defines the point of ideal equilibrium where the $y_D(x)$ curve crosses over the $y_P(x)$ curve that is given in (12.58), we can state the following relationship

$$y_D[(x_D)_{\max}] = (y_D)_{\max} = y_P[(x_D)_{\max}], \quad (12.74)$$

suggesting a much simpler calculation of $y_D[(x_D)_{\max}]$ than that carried out in (12.70). In (12.58) we saw that $y_P(x)$ is given by a very simple expression as $y_P(x) = 2^{-x} = e^{-x \ln 2}$, allowing us to determine $y_D[(x_D)_{\max}]$ directly from (12.74) as follows

$$\begin{aligned}
 y_D[(x_D)_{\max}] &= (y_D)_{\max} = y_P[(x_D)_{\max}] = e^{-(x_D)_{\max} \ln 2} = e^{\frac{m}{1-m} \ln m} = e^{\ln m \frac{m}{1-m}} \\
 &= m^{\frac{m}{1-m}}.
 \end{aligned} \tag{12.75}$$

Equation (12.73) is valid for all positive m except for $m = 1$ in which case $(y_D)_{\max}$ can be determined by applying the l'Hôpital rule to (12.73) as follows

$$(y_D)_{\max}|_{m=1} = \lim_{m \rightarrow 1} \exp \frac{\frac{d(m \ln m)}{dm}}{\frac{d(1-m)}{dm}} = \lim_{m \rightarrow 1} \exp \frac{\ln m + 1}{-1} = e^{-1} = \frac{1}{e} = 0.368. \tag{12.76}$$

(f) It is easy to show that the relationship for positive m but $m \neq 1$ between $(y_D)_{\max}$ given by (12.73) and $(x_D)_{\max}$ given by (12.68) is a simple exponential expression

$$(y_D)_{\max} = e^{\frac{m}{1-m} \ln m} = e^{-\frac{m}{m-1} \ln m} = e^{-(\ln 2)(x_D)_{\max}} = 2^{-(x_D)_{\max}} = \frac{1}{2^{(x_D)_{\max}}}, \tag{12.77}$$

while for $m = 1$, $(y_D)_{\max} = 1/e = 0.368$, as shown in (12.76), and $(x_D)_{\max} = 1/\ln 2 = 1.4427$, as shown in (12.69).

12.6.Q3

(253)

The general parameters of the neutron activation process, such as activation factor m , normalized time x , normalized number of parent nuclei y_P , and normalized daughter activities z_D and y_D , are defined for the saturation model and depletion model of neutron activation in Prob. 252 and in Sect. T12.6.2.

- (a) For the saturation and depletion models of neutron activation and four activation factors m (0.2, 0.5, 1.0, and 5.0) calculate and plot on one graph $y_P(x)$, $z_D(x)$, and $y_D(x)$ against x for $0 \leq x \leq 3$ (in steps of x equal to 0.5). Plot data points for saturation model with open circles and connect them with dashed curves, those for depletion model with solid circles and connect them with solid curves.
- (b) For the curves plotted in (a) discuss the behavior of the saturation model curves in comparison with the depletion model curves for the same activation factor m .

- (c) For the saturation model curves and depletion model curves plotted in (a) calculate the initial slopes $dy_D/dx|_{x=0}$ and determine the radioactivation yield $Y_D = dy_D/dx|_{x=0}$.
- (d) For the four depletion model curves plotted in (a) determine x , y_P and y_D for points of ideal equilibrium. Summarize results for ideal equilibrium in tabular format.

SOLUTION:

Parameters of neutron activation are defined as follows (see Sect. T12.6.2):

- (1) Activation factor:

$$m = \frac{q_P \dot{\phi}}{\lambda_D} = \frac{(t_{1/2})_D \sigma_P \dot{\phi}}{\ln 2}. \quad (12.78)$$

- (2) Normalized activation time:

$$x = \frac{\sigma_P \dot{\phi}}{\ln 2} t = \frac{mt}{(t_{1/2})_D}. \quad (12.79)$$

- (3) Normalized number of parent nuclei:

$$y_P(x) = e^{-x \ln 2} = 2^{-x}. \quad (12.80)$$

- (4) Normalized daughter activity $y_D(x)$ according to saturation model of neutron activation:

$$z_D(x) = \frac{\mathcal{A}_D(t)}{\sigma_P \dot{\phi} N_P(0)} = 1 - e^{-\frac{x \ln 2}{m}} = 1 - 2^{-\frac{x}{m}}, \quad (12.81)$$

valid for all positive activation factors m .

- (5) Normalized daughter activity $y_D(x)$ according to depletion model of neutron activation

$$y_D(x) = \frac{1}{1-m} \left[e^{-x \ln 2} - e^{-\frac{x \ln 2}{m}} \right] = \frac{1}{1-m} \left[\frac{1}{2^x} - \frac{1}{2^{x/m}} \right], \quad (12.82)$$

valid for all positive activation factors m except for $m = 1$ for which $y_D(x)$ is simplified to read (T12.34)

$$y_D(x)|_{m=1} = \frac{x \ln 2}{2^x} = x e^{-x \ln 2} \ln 2. \quad (12.83)$$

In (12.78) through (12.83) σ_P is the neutron activation cross section of the parent nucleus, $\dot{\phi}$ is the neutron fluence rate in the nuclear reactor, λ_D is the decay constant of the daughter nucleus, and $(t_{1/2})_D$ is the half-life of the daughter radionuclide.

Table 12.3 Normalized daughter activities $z_D(x)$ for saturation model and $y_D(x)$ for depletion model for four values of activation factor m (0.2, 0.5, 1.0, and 5.0) in the range of normalized activation time x defined in (12.79) from $x = 0$ to $x = 3$ in steps of 0.5. Activity $z_D(x)$ for saturation model is calculated from (12.81) for all m , while $y_D(x)$ for all positive m except for $m = 1$ is calculated from (12.82) and $y_D(x)$ for $m = 1$ is calculated from (12.83). The number of parent nuclei $y_P(x)$ as a function of normalized activation time x is given for comparison

x	$y_P(x)$	Saturation model				Depletion model			
		$z_D(x)$				$y_D(x)$			
		$m = 0.2$	$m = 0.5$	$m = 1.0$	$m = 5.0$	$m = 0.2$	$m = 0.5$	$m = 1.0$	$m = 5.0$
0	1.0	0	0	0	0	0	0	0	0
0.5	0.707	0.823	0.00	0.293	0.067	0.663	0.414	0.245	0.058
1.0	0.500	0.969	0.750	0.500	0.129	0.586	0.500	0.347	0.093
1.5	0.354	0.994	0.875	0.646	0.188	0.435	0.457	0.368	0.115
2.0	0.250	0.999	0.938	0.750	0.242	0.311	0.375	0.347	0.127
2.5	0.177	1.0	0.969	0.823	0.293	0.221	0.291	0.306	0.133
3.0	0.125	1.0	0.984	0.875	0.340	0.156	0.219	0.260	0.134
∞	0	1.0	1.0	1.0	1.0	0	0	0	0

(a) The general physical quantities y_P , z_D , y_D of neutron activation were calculated using (12.80), (12.81), and (12.82), respectively, for four activation parameters m (0.2, 0.5, 1.0, and 5) in steps of 0.5 for normalized time x in the range $0 \leq x \leq 3$. Data points so calculated are listed in Table 12.3 and plotted in Fig. 12.2.

(1) The number of parent nuclei $y_P(x)$ is given by (12.80) and plotted in Fig. 12.2 with an exponentially diminishing curve in grey against x which is linearly proportional to σ_P and $\dot{\phi}$. The curve indicates that the depletion in the number of target nuclei is an exponential function of the form: $y_P(x) = e^{-x \ln 2}$.

(2) The normalized daughter activity $z_D(x)$ curves, calculated for the saturation model given by (12.81), for a given m grow exponentially from $z_D = 0$ at $x = 0$ to $z_D = 1$ at $x \rightarrow \infty$ and are shown by the four dashed curves in Fig. 12.2. In the saturation model we assume that the number of parent nuclei N_P is independent of activation time t , and this happens either by N_P being very large or activation factor m being very small.

(3) The depletion model is more realistic than the saturation model, since it also accounts for the depletion of the number of parent nuclei affecting the rate of production of daughter nuclei. This causes the normalized daughter activity $y_D(x)$ first to grow linearly with x from $x = 0$, then gradually reach a peak that is smaller than 1 attained in the saturation model, and then decrease toward zero for $x \rightarrow \infty$. The four dark solid curves in Fig. 12.2 represent normalized daughter activities $y_D(x)$ for four values of the activation factor m and given by (12.82) for $m \neq 1$ and (12.83) for $m = 1$.

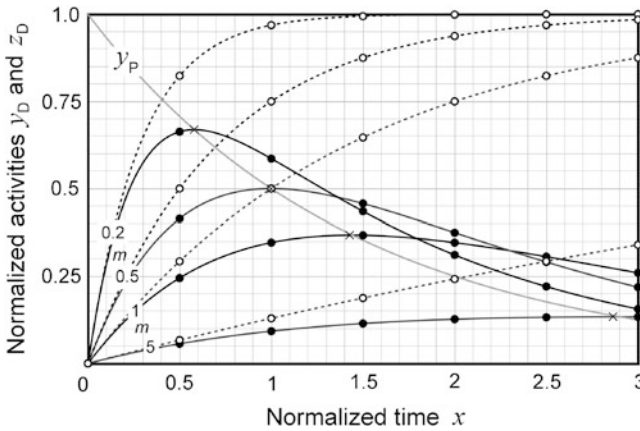


Fig. 12.2 Normalized daughter activities $z_D(x)$ for saturation model (dashed curves) and $y_D(x)$ for depletion model (heavy solid curves) as well as normalized number of parent nuclei $y_P(x)$ (light solid curve) against normalized activation time x

(b) In Fig. 12.2 we show a comparison of typical normalized activity curves for the saturation model (dashed) and depletion model (solid) of neutron activation. Based on the figure, the following conclusions can be reached:

(1) A comparison between the saturation model curve $z_D(x)$ and depletion model curve $y_D(x)$ for a given m shows a significant difference between the two curves. Activity curve $z_D(x)$ exponentially approaches saturation at $z_D(x) = 1.0$ for large x , while curve $y_D(x)$ reaches a peak $(y_D)_{\max}$ at $(x_D)_{\max}$ that is generally below $y_D(x) = 1$ and then decreases to $y_D(x) = 0$ as $x \rightarrow \infty$. The larger is m , the larger is the discrepancy between the two models and the smaller is $(y_D)_{\max}$ in comparison with $(z_D)_{\text{sat}} = 1$.

(2) In the saturation model the rate of production of daughter nuclei from the parent nuclei is balanced by the rate of decay of daughter nuclei and a perfect equilibrium between the two is reached in saturation. Since the number of parent nuclei suffers no depletion, the state of equilibrium continues to $x = \infty$.

(3) In the depletion model the number of parent nuclei decreases exponentially and this causes the daughter activity to grow at first, reach a peak, and then decrease to zero as $x \rightarrow \infty$, because of daughter decay as well as a diminishing number of parent nuclei being transformed into daughter nuclei. At $x = \infty$ we can assume that all parent nuclei have been transformed into daughter nuclei and all daughter nuclei have decayed, resulting in zero daughter activity.

(4) In practical neutron activation procedures the activation factor defined in (12.78) as $m = \sigma_P \dot{\phi} / \lambda_D$ is generally very small, justifying the use of the saturation model in studies of radioactivation dynamics. However, since m depends linearly on the

fluence rate $\dot{\phi}$, neutron activation processes with very high neutron fluence rates or relatively long activation times may invalidate the saturation model in favor of the depletion model.

(c) The radioactivation yield Y_D of daughter D is defined by the initial slope of the z_D or y_D versus x normalized activity curve:

(1) For the saturation model $z_D(x)$ is given by (12.81) and its initial slope $dz_D/dx|_{x=0}$ is given as

$$Y_D = \left. \frac{dz_D}{dx} \right|_{x=0} = \left. \frac{d}{dx} \left[1 - e^{-\frac{x \ln 2}{m}} \right] \right|_{x=0} = \left. \left[\frac{\ln 2}{m} e^{-\frac{x \ln 2}{m}} \right] \right|_{x=0} = \frac{\ln 2}{m}. \quad (12.84)$$

(2) For the depletion model $y_D(x)$ is given by (12.82) for $m \neq 1$ and by (12.83) for $m = 1$. For $m \neq 1$ the radioactivation yield is calculated from (12.82)

$$\begin{aligned} Y_D &= \left. \frac{dy_D}{dx} \right|_{x=0} = \frac{1}{1-m} \left. \frac{d}{dx} \left[e^{-x \ln 2} - e^{-\frac{x \ln 2}{m}} \right] \right|_{x=0} \\ &= \frac{1}{1-m} \left. \left[-\ln 2 e^{-x \ln 2} + \frac{\ln 2}{m} e^{-\frac{x \ln 2}{m}} \right] \right|_{x=0} = \frac{\ln 2}{m}, \end{aligned} \quad (12.85)$$

while for $m = 1$ it is calculated from (12.83)

$$Y_D = \left. \frac{dy_D}{dx} \right|_{x=0} = \left. \frac{d}{dx} [x e^{-x \ln 2} \ln 2] \right|_{x=0} = (\ln 2) [e^{-x \ln 2} - x \ln 2 e^{-x \ln 2}] \Big|_{x=0} = \ln 2. \quad (12.86)$$

As evident from (12.84), (12.85), and (12.82) the radioactivation yield Y_D of the daughter is equal to $(\ln 2)/m$ for both the saturation and the depletion models and for all activation factors m . This is also evident from Fig. 12.2 which shows that, for a given m , the initial slopes of daughter activity curves $z_D(x)$ and $y_D(x)$ at $x = 0$ are identical even though the two curves show completely different behavior as x increases from 0. Since Y_D is inversely proportional to m , we conclude that the larger is m , the shallower is the initial slope, the smaller is Y_D , the slower is the approach to saturation for $z_D(x)$ and the larger is $(x_D)_{\max}$, the normalized activation time, at which the peak in $y_D(x)$ occurs.

Results of radioactivation Y_D calculation for the four activation factors m (0.2, 0.5, 1.0, and 5.0) are as follows: $Y_D = (\ln 2)/m$ in general; $m = 0.2$, $Y_D = 3.47$; $m = 0.5$, $Y_D = 1.39$; $m = 1.0$, $Y_D = \ln 2 = 0.693$, and $m = 5$, $Y_D = 0.139$.

(d) The point of ideal equilibrium, as defined by Evans, is the point on $y_D(x)$ activity curve (for a given activation factor m and the depletion model) at which $y_D(x)$ exhibits its maximum value with coordinates $[(x_D)_{\max}, (y_D)_{\max}]$. One should note that this point occurs at the intersection of the y_D curve with the y_P curve, as indicated by points \times in Fig. 12.2.

(1) We now determine the general expression for $(x_D)_{\max}$ as a function of m by setting $dy_D/dx|_{x=(x_D)_{\max}} = 0$ for $y_D(x)$ of (12.82) and solving for $(x_D)_{\max}$ to get

$$\begin{aligned} \left. \frac{dy_D}{dx} \right|_{x=(x_D)_{\max}} &= \frac{1}{1-m} \left. \frac{d}{dx} \left[e^{-x \ln 2} - e^{-\frac{x \ln 2}{m}} \right] \right|_{x=(x_D)_{\max}} \\ &= \frac{\ln 2}{1-m} \left[-e^{-x \ln 2} + \frac{1}{m} e^{-\frac{x \ln 2}{m}} \right] \Big|_{x=(x_D)_{\max}} \\ &= \frac{\ln 2}{1-m} \left[-e^{-(x_D)_{\max} \ln 2} + \frac{1}{m} e^{-\frac{(x_D)_{\max} \ln 2}{m}} \right] = 0. \end{aligned} \quad (12.87)$$

Solving (12.87) for $(x_D)_{\max}$ results in the following expression for $(x_D)_{\max}$

$$(x_D)_{\max} = \frac{m}{m-1} \frac{\ln m}{\ln 2}, \quad (12.88)$$

valid for all positive m except for $m = 1$ for which (12.88) is not defined; however, since it gives $(x_D)_{\max} = 0/0$, we can apply the L'Hôpital rule to get $(x_D)_{\max}|_{m \rightarrow 1}$ as follows

$$(x_D)_{\max}|_{m \rightarrow 1} = \lim_{m \rightarrow 1} \frac{\frac{d(m \ln m)}{dm}}{\ln 2 \frac{d(m-1)}{dm}} = \lim_{m \rightarrow 1} \frac{1 + \ln m}{\ln 2} = \frac{1}{\ln 2} = 1.44. \quad (12.89)$$

(2) The maximum normalized activity $(y_D)_{\max}$ for a given activation factor m can be calculated simply by determining $y_P(x)$ of (12.80) at $x = (x_D)_{\max}$, recognizing that at the point of ideal equilibrium $y_P[(x_D)_{\max}] = y_D[(x_D)_{\max}]$. Of course, to determine $(y_D)_{\max}$ we can also insert (12.88) into $y_D(x)$ given by (12.82), but the calculation becomes much more cumbersome. The simpler approach thus gives

$$(y_D)_{\max} = y_D[(x_D)_{\max}] = y_P[(x_D)_{\max}] = e^{-(x_D)_{\max} \ln 2} = 2^{\left(\frac{m}{1-m}\right) \frac{\ln m}{\ln 2}} = e^{\frac{m \ln m}{1-m}}. \quad (12.90)$$

Equation (12.90) is valid for all positive m except for $m = 1$. We determine $(y_D)_{\max}$ for $m = 1$ by applying the L'Hôpital rule to (12.90) as follows

$$(y_D)_{\max}|_{m=1} = \lim_{m \rightarrow 1} e^{\frac{\frac{d}{dm}(m \ln m)}{\frac{d}{dm}(1-m)}} = \lim_{m \rightarrow 1} e^{\frac{\ln m + 1}{-1}} = e^{-1} = 0.368. \quad (12.91)$$

The two coordinates for points of ideal equilibrium $(x_D)_{\max}$ and $(y_D)_{\max}$ were for activation factors m of 0.2, 0.5, and 5.0 ($m \neq 1$) calculated using (12.88) and (12.90), respectively, and for $m = 1$ were given by (12.89) and (12.91), respectively. The summary of $(x_D)_{\max}$ and $(y_D)_{\max}$ results is presented in Table 12.4.

Table 12.4 Points of ideal equilibrium, as defined by Evans, with coordinates $(x_D)_{\max}$ and $(y_D)_{\max}$ calculated from (12.88) and (12.90), respectively, for $m \neq 1$. For $m = 1$ the two coordinates are given by (12.89) and (12.91), respectively

Activation factor m	0.2	0.5	1.0	5.0
$(x_D)_{\max} = \frac{m \ln m}{(m-1) \ln 2}$ for $m \neq 1$	0.581	1.000	$\frac{1}{\ln 2} = 1.443$	2.902
$(y_D)_{\max} = e^{\frac{m \ln m}{1-m}}$ for $m \neq 1$	0.669	0.500	$\frac{1}{e} = 0.368$	0.134

12.6.Q4

(254)

In discussions of neutron activation one usually assumes that the daughter radionuclide is not affected by the activation particles. However, there are situations in which this assumption does not hold and account must then be taken of the activation of the daughter radionuclide into a granddaughter nuclide. The model that deals with this type of activation is called the “parent depletion–daughter activation” model and this model too, similarly to the saturation and depletion models, can be written in compact format by introducing new parameters (see Sect. T12.6.5), in addition to the ones (x, m, y_P, y_D) used already in saturation and depletion models.

The standard parameters y_P and y_D of the saturation and depletion models are defined in Prob. 252 and the new parameters λ_D^* , ε^* , m^* , and y_D^* , used in conjunction with “depletion–activation” model are defined as follows:

$$\lambda_D^* = \lambda_D + \sigma_D \dot{\phi}, \quad \varepsilon^* = \frac{\lambda_D^*}{\lambda_D} = 1 + \frac{\sigma_D \dot{\phi}}{\lambda_D},$$

$$m^* = \frac{\sigma_P \dot{\phi}}{\lambda_D^*} = \frac{m}{\varepsilon^*}, \quad \text{and} \quad y_D^* = \frac{\mathcal{A}_D^*(t)}{\sigma_P \dot{\phi} N_P(0)},$$

where σ_P and σ_D are activation cross sections of parent P and daughter D nuclides, respectively, λ_D is the decay constant of the daughter, λ^* is the modified decay constant, $\dot{\phi}$ is the neutron fluence rate in the nuclear reactor, m is the activation factor, m^* is the modified activation factor, $\mathcal{A}_D^*(t)$ is the daughter radionuclide D activity, and $N_P(0)$ is the initial number of parent nuclei.

For the “parent depletion–daughter activation model”:

- (a) Transform the equation that describes the number of parent nuclei $N_P(t)$ into a general format given by y_P as a function of normalized time variable x .
- (b) Transform the equation that describes the activity of daughter nuclei $\mathcal{A}_D(t)$ of (d) in Prob. 251 into a general format given by $y_D^*(x)$ as a function of normalized time x and modified activation factor m^* .

- (c) Compare $y_D^*(x)$ calculated in (b) with $y_D(x)$ given for the depletion model in (b) of Prob. 252 and derive expressions for $(x_D^*)_{\max}$ and $(y_D^*)_{\max}$ as a function of m^* .

SOLUTION:

For the saturation and depletion models of neutron activation the general variables x , y_P , y_D as well as the activation factor m are defined as follows

$$x = m \frac{t}{(t_{1/2})_D}; \quad (12.92)$$

$$y_P = \frac{N_P(t)}{N_P(0)}; \quad (12.93)$$

$$y_D = \frac{N_D(t)}{mN_P(0)} = \frac{\mathcal{A}_D(t)}{\sigma_P \dot{\phi} N_P(0)}; \quad (12.94)$$

$$m = \frac{\sigma_P \dot{\phi}}{\lambda_D}. \quad (12.95)$$

In the “parent depletion–daughter activation model” we use the following additional parameters: λ_D^* , ε^* , and m^* as well as variable $y_D^*(x)$. The additional parameters are defined as follows

$$\lambda_D^* = \lambda_D + \sigma_D \dot{\phi}; \quad (12.96)$$

$$\varepsilon^* = \frac{\lambda_D^*}{\lambda_D} = 1 + \frac{\sigma_D \dot{\phi}}{\lambda_D}; \quad (12.97)$$

$$m^* = \frac{\sigma_P \dot{\phi}}{\lambda_D^*} = \frac{m}{\varepsilon^*}; \quad (12.98)$$

$$y_D^* = \frac{\mathcal{A}_D^*(t)}{\sigma_P \dot{\phi} N_P(0)}. \quad (12.99)$$

(a) The standard form for the number of parent nuclei $N_P(t)$, undergoing nuclear activation in particle fluence rate $\dot{\phi}$, is expressed by the following equation

$$N_P(t) = N_P(0)e^{-\sigma_P \dot{\phi} t}, \quad (12.100)$$

that, after incorporating (12.92), (12.93), and (12.95), takes up the following form giving the number of parent nuclei $N_P(t)$ normalized to the initial number of parent

nuclei $N_P(0)$ as

$$y_P = \frac{N_P(t)}{N_P(0)} = e^{-\sigma_P \dot{\phi} t} = e^{-m \lambda_D t} = e^{-m \frac{t}{(t/2)_D} \ln 2} = e^{-x \ln 2} = \frac{1}{2^x} \equiv 2^{-x}. \quad (12.101)$$

Equation (12.101) is valid in general irrespective of the activation model used, and is thus valid for the saturation, depletion, as well as depletion–activation model.

(b) The standard equation used for describing the depletion–activation model is in Prob. 251 [see (12.51)] expressed as (T12.47)

$$\frac{dN_D(t)}{dt} = \sigma_P \dot{\phi} N_P(t) - \lambda_D N_D(t) - \sigma_D \dot{\phi} N_D(t) = \sigma_P \dot{\phi} N_P(t) - \lambda_D^* N_D(t), \quad (12.102)$$

resulting in the following expression [Prob. 251, see (12.52)] for the daughter activity $\mathcal{A}_D^*(t)$

$$\mathcal{A}_D^*(t) = \lambda_D N_P(t) = \sigma_P \dot{\phi} N_P(0) \frac{\frac{\lambda_D}{\lambda_D^*}}{1 - \frac{\sigma_P \dot{\phi}}{\lambda_D^*}} [e^{-\sigma_P \dot{\phi} t} - e^{-\lambda_D^* t}], \quad (12.103)$$

where $\lambda_D^* = \lambda_D + \sigma_D \dot{\phi}$ is the modified decay constant for the daughter accounting for the radioactive daughter decay (through λ_D) as well as the daughter activation (through σ_D and $\dot{\phi}$).

Combining (12.103) with (12.96), (12.97), (12.98), and (12.99) as well as recalling that $\sigma_P \dot{\phi} t = x \ln 2$ and $\lambda_D^* t = (x/m^*) \ln 2$ we obtain the following expression (T12.57) for the normalized daughter activity y_D^*

$$y_D^*(x) = \frac{\mathcal{A}_D(t)}{\sigma_P \dot{\phi} N_P(0)} = \frac{1}{\varepsilon^*(1 - m^*)} [e^{-x \ln 2} - e^{-\frac{x}{m^*} \ln 2}] = \frac{1}{\varepsilon^*(1 - m^*)} \left[\frac{1}{2^x} - \frac{1}{2^{\frac{x}{m^*}}} \right]. \quad (12.104)$$

(c) Normalized daughter activity for the depletion model was determined in (12.64) of Prob. 252 as

$$\begin{aligned} y_D(x) &= \frac{N_D(t)}{m N_P(0)} = \frac{\lambda_D N_D(t)}{\sigma_P \dot{\phi} N_P(0)} = \frac{1}{1 - m} [e^{-x \ln 2} - e^{-\frac{x}{m} \ln 2}] \\ &= \frac{1}{1 - m} \left[\frac{1}{2^x} - \frac{1}{2^{x/m}} \right]. \end{aligned} \quad (12.105)$$

(1) A comparison of y_D^* given by (12.104) for the depletion–activation model with $y_D(x)$ given by (12.105) for the depletion model shows that the two expressions are similar except for the factor ε^* which is equal or larger than 1 ($\varepsilon^* \geq 1$) and depends on fluence rate $\dot{\phi}$. A closer look at expressions (12.104) and (12.105) shows that (12.105) of the depletion model actually follows from (12.104) of the depletion–activation model, since, for the depletion model, $\lambda_D^* = \lambda_D$ and $\varepsilon^* = 1$ as a result of

$\sigma_D = 0$. We conclude that the depletion model is a special case of the depletion–activation model when the activation cross section σ_D of the daughter nucleus is zero. Thus, we expect the behavior of $y_D^*(x)$ of the depletion–activation model to be similar to that of $y_D(x)$ of the depletion model: rise from 0 at $x = 0$ to reach a maximum $(y_D^*)_{\max}$ at $x = (x_D^*)_{\max}$, and then asymptotically decrease to 0 as $x \rightarrow \infty$.

(2) The characteristic normalized time $(x_D^*)_{\max}$ at which y_D^* exhibits its maximum $(y_D^*)_{\max}$ can be determined as a function of the activation factor m^* by setting $dy_D^*/dx|_{x=(x_D^*)_{\max}}$ and solving for $(x_D^*)_{\max}$ as follows

$$\begin{aligned} \frac{dy_D^*}{dx} \Big|_{x=(x_D^*)_{\max}} &= \frac{d}{dx} \left[\frac{1}{\varepsilon^*(1-m^*)} \left(\frac{1}{2^x} - \frac{1}{2^{x/m^*}} \right) \right] \Big|_{x=(x_D^*)_{\max}} \\ &= \frac{1}{\varepsilon^*(1-m^*)} \left[-2^{-x} \ln 2 + \frac{1}{m^*} 2^{-\frac{x}{m^*}} \ln 2 \right] \Big|_{x=(x_D^*)_{\max}} = 0. \end{aligned} \quad (12.106)$$

Solving (12.106) for $(x_D^*)_{\max}$ we now get

$$2^{-(x_D^*)_{\max}} = \frac{1}{m^*} 2^{-(x_D^*)_{\max}/m^*} \quad \text{or} \quad -(x_D^*)_{\max} \ln 2 = \ln \frac{1}{m^*} - \frac{(x_D^*)_{\max}}{m^*} \ln 2 \quad (12.107)$$

and finally the following expression for $(x_D^*)_{\max}$

$$(x_D^*)_{\max} = \frac{m^*}{(m^* - 1)} \frac{\ln m^*}{\ln 2}. \quad (12.108)$$

For $m^* = 1$ (12.108) is not defined; however, since it gives $(x_D^*)_{\max} = 0/0$, we can apply the l'Hôpital rule to get $(x_D^*)_{\max}|_{m^* \rightarrow 1}$ as follows

$$(x_D^*)_{\max} \Big|_{m^* \rightarrow 1} = \lim_{m^* \rightarrow 1} \frac{\frac{d(m^* \ln m^*)}{dm^*}}{\frac{d(m^* - 1)}{dm^*} \ln 2} = \lim_{m^* \rightarrow 1} \frac{1 + \ln m^*}{\ln 2} = \frac{1}{\ln 2} = 1.443. \quad (12.109)$$

Thus, $(x_D^*)_{\max}$ is given by (12.108) for any positive m^* except for $m^* = 1$ for which $(x_D^*)_{\max} = 1.443$, as determined in (12.109).

(3) The maximum daughter activity $(y_D^*)_{\max}$ can be determined by inserting $(x_D^*)_{\max}$ of (12.108) into $y_D^*(x)$ given by (12.104) as follows

$$\begin{aligned} (y_D^*)_{\max} &= y_D^*[(x_D^*)_{\max}] = \frac{1}{\varepsilon^*(1-m^*)} \left[\frac{1}{2^{(x_D^*)_{\max}}} - \frac{1}{2^{(x_D^*)_{\max}/m^*}} \right] \\ &= \frac{[\varepsilon^*(1-m^*)]^{-1}}{2^{(x_D^*)_{\max}}} \left[1 - \frac{1}{2^{[(x_D^*)_{\max}/m^*] - (x_D^*)_{\max}}} \right] \end{aligned}$$

$$\begin{aligned}
 &= \frac{[\varepsilon^*(1-m^*)]^{-1} \left[1 - \frac{1}{2^{(x_D^*)_{\max} \lfloor \frac{1-m^*}{m^*} \rfloor}} \right]}{2^{(x_D^*)_{\max}}} \\
 &= \frac{1}{\varepsilon^*(1-m^*)} F_1^* [1 - F_2^*].
 \end{aligned} \tag{12.110}$$

Components F_1^* and F_2^* of (12.110), after insertion of $(x_D^*)_{\max}$ given by (12.108) and using the following identity $e^{z \ln 2} = e^{\ln 2^z} = 2^z$, yield the following expressions

$$F_1^* = \frac{1}{2^{(x_D^*)_{\max}}} = \frac{1}{2^{\frac{m^*}{(m^*-1)} \frac{\ln m^*}{\ln 2}}} = 2^{\frac{m^*}{(1-m^*)} \frac{\ln m^*}{\ln 2}} = e^{\ln 2 \frac{m^*}{1-m^*} \frac{\ln m^*}{\ln 2}} = e^{\frac{m^*}{1-m^*} \ln m^*} \tag{12.111}$$

and

$$F_2^* = \frac{1}{2^{(x_D^*)_{\max} \lfloor \frac{1-m^*}{m^*} \rfloor}} = \frac{1}{2^{\frac{m^*}{(m^*-1)} \frac{\ln m^*}{\ln 2} \lfloor \frac{1-m^*}{m^*} \rfloor}} = 2^{\frac{\ln m^*}{\ln 2}} = e^{\ln m^*} = m^*. \tag{12.112}$$

The maximum normalized daughter activity $(y_D^*)_{\max}$ of (12.109) after incorporating F_1^* of (12.111) and F_2^* of (12.112) can now be written as follows

$$\begin{aligned}
 (y_D^*)_{\max} &= \frac{1}{\varepsilon^*(1-m^*)} F_1^* [1 - F_2^*] = \frac{1}{\varepsilon^*(1-m^*)} e^{\frac{m^*}{1-m^*} \ln m^*} [1 - m^*] \\
 &= \frac{1}{\varepsilon^*} e^{\frac{m^*}{1-m^*} \ln m^*} = \frac{1}{\varepsilon^*} (m^*)^{\frac{m^*}{1-m^*}}.
 \end{aligned} \tag{12.113}$$

12.6.Q5

(255)

In its most general form the “parent depletion–daughter activation model” (in short: “depletion–activation model”) describes the behavior of the normalized daughter activity with the following expression, as given in (12.104)

$$y_D(x) = \frac{1}{\varepsilon^*(1-m^*)} \left\{ \frac{1}{2^x} - \frac{1}{2^{x/m^*}} \right\} = \frac{1}{\varepsilon^*(1-m^*)} \{ e^{-x \ln 2} - e^{-(x/m^*) \ln 2} \}, \tag{12.114}$$

with parameters defined as follows: $y_D = \mathcal{A}_D(t)/[\sigma_P \dot{\varphi} N_P(0)]$; $x = m^* \lambda_D^* t / \ln 2$; $m = \sigma_P \dot{\varphi} / \lambda_D$; $\lambda_D^* = \lambda_D + \sigma_D \dot{\varphi}$; $\varepsilon^* = \lambda_D^* / \lambda_D$; $m^* = m / \varepsilon^*$.

Under special circumstances two simplifications of (12.114) are possible:

- (1) Daughter D is not affected by particle fluence rate $\dot{\phi}$, describing the so-called “depletion model” of nuclear activation and simplifying (12.114) to read [see (T12.28)]

$$y_D(x) = \frac{1}{(1-m)} \left\{ \frac{1}{2^x} - \frac{1}{2^{x/m}} \right\} = \frac{1}{(1-m)} \left\{ e^{-x \ln 2} - e^{-(x/m) \ln 2} \right\}. \quad (12.115)$$

- (2) The process of nuclear activation affects neither the number of parent nuclei which is very large [$N_P(t) = N_P(0) = \text{const}$] nor the daughter nuclei ($\sigma_D = 0$), describing the so-called “saturation model” of nuclear activation and simplifying (12.115) further to read [(T12.35)]

$$y_D(x) = \left\{ 1 - \frac{1}{2^{x/m}} \right\} = \left\{ 1 - e^{-(x/m) \ln 2} \right\}. \quad (12.116)$$

- (a) Elaborate on parameters of (12.114) and derive (12.115) and (12.116) from (12.114), clearly stating all assumptions and approximations made in the derivations.
- (b) Figure 12.3 plots normalized daughter activity y_D against normalized time x for various activation factors m in the range $m = 10^{-4}$ to $m = 10$. For each m two y_D curves are plotted: the dashed curve is for the saturation model (12.116), the solid curve is for the depletion model (12.115). Also plotted is the normalized number $y_P(x)$ of parent P nuclei. State an expression for y_P as a function of x for the saturation model and the depletion model. Based on Fig. 12.3 draw conclusions with regard to behavior of $y_D(x)$ for the two models and discuss the effect of the activation factor m on $y_D(x)$.
- (c) Equation (12.115) is not defined for $m = 1$. Determine an equation that replaces (12.115) in the limit as $m \rightarrow 1$.
- (d) The solid dots in Fig. 12.3 indicate maxima on depletion model curves. Derive expressions for $(x_D)_{\max}$ and $(y_D)_{\max}$ for a given positive activation factor m including $m = 1$. Compare $(y_D)_{\max}$ for depletion curves with $(y_D)_{\text{sat}}$ for saturation curves.

SOLUTION:

(a) Equation (12.114) represents the general form of the (parent) depletion–(daughter) activation model of the nuclear activation process in which parent P nuclei are transformed into daughter D nuclei, most often but not necessarily radioactive. The depletion–activation model of (12.114) accounts for the following factors that are effective during the activation process:

- (i) Activation of parent P nuclei through the activation cross section σ_P of the parent P nucleus.

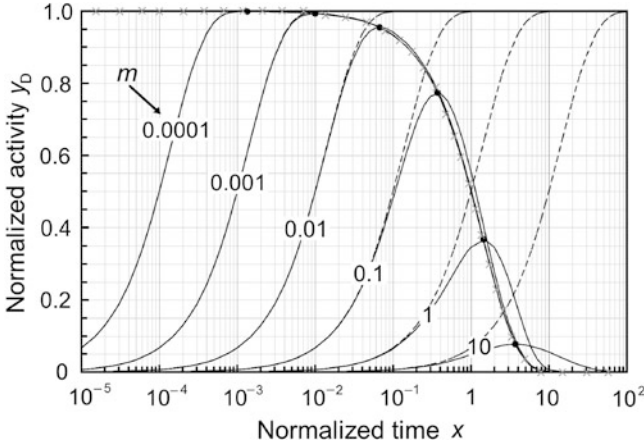


Fig. 12.3 Normalized daughter activity y_D against normalized time x for various activation factors m in the range $m = 10^{-4}$ to $m = 10$. For each m two y_D curves are plotted: the dashed curve for the saturation model (12.116), the solid curve for the depletion model (12.115). Also plotted is the normalized number y_P of parent P nuclei indicated with symbol \times

- (ii) Particle fluence rate $\dot{\phi}$.
- (iii) Depletion of parent nuclei through the initial number $N_P(0)$ of the parent nuclei.
- (iv) Decay of daughter nuclei through the decay constant λ_D and half-life $(t_{1/2})_D$ of the daughter D nucleus.
- (v) Activation of daughter D nuclei through the activation cross section σ_D of the daughter D nucleus.

Equation (12.114) gives the normalized activity y_D as a function of normalized activation time x and its parameters are defined as follows:

$$y_D = \mathcal{A}_D(t) / [\sigma_P \dot{\phi} N_P(0)] \text{ is the daughter activity } \mathcal{A}_D(t) \text{ normalized to } \sigma_P \dot{\phi} N_P(0). \tag{12.117}$$

$$x = m^* \lambda_D^* t / \ln 2 = m \lambda_D t / \ln 2 \text{ is the activation time } t \text{ normalized to } \frac{\ln 2}{m \lambda_D} = \frac{(t_{1/2})}{m}. \tag{12.118}$$

$$m = \sigma_P \dot{\phi} / \lambda_D \text{ is the activation factor defined by the quotient } q_P \dot{\phi} / \lambda_D. \tag{12.119}$$

$$\lambda_D^* = \lambda_D + \sigma_D \dot{\phi} \text{ is the decay constant } \lambda_D \text{ of the daughter D corrected for the loss of daughter D nuclei caused by activation of daughter D nuclei.} \tag{12.120}$$

$$\varepsilon^* = \lambda_D^* / \lambda_D \text{ is a parameter defined by the ratio between } \lambda_D^* \text{ and } \lambda_D. \tag{12.121}$$

$m^* = m/\varepsilon^* = m\lambda_D/\lambda_D^*$ is the activation factor m corrected for the loss of daughter D nuclei caused by activation of daughter D nuclei by activation particles. (12.122)

Equation (12.114) provides a general form for description of the nuclear activation process. Under special situations two approximations can be introduced to simplify (12.114):

(1) Depletion model evolves from the (parent) depletion–(daughter) activation model described by (12.114) under the condition that the daughter D nuclei are not affected by the activation particles, i.e., $\sigma_D = 0$. Parameters of (12.115) with $\sigma_D = 0$ are then given as follows

$$\lambda_D^* = \lambda_D + \sigma_D \dot{\phi} = \lambda_D; \quad \varepsilon^* = \frac{\lambda_D^*}{\lambda_D} = 1; \quad \text{and} \quad m^* = \frac{m}{\varepsilon^*} = m = \frac{\sigma_P \dot{\phi}}{\lambda_D}. \quad (12.123)$$

Insertion of (12.117) into (12.114) results in the following expression for $y_D(x)$

$$y_D(x) = \frac{1}{(1-m)} \left\{ \frac{1}{2^x} - \frac{1}{2^{x/m}} \right\} = \frac{1}{(1-m)} \{ e^{-x \ln 2} - e^{-(x/m) \ln 2} \}. \quad (12.124)$$

(2) Saturation model evolves from the depletion model (12.118) under the assumption that the number of parent nuclei $N_P(t)$ is very large, i.e., $N_P(t) = N_P(0) = \text{const}$ and therefore minimally affected by the activation process. This condition is satisfied when the activation factor $m = \sigma_P \dot{\phi} / \lambda_D \ll 1$ is very small (typically for $m \leq 10^{-3}$) which means that $\sigma_P \dot{\phi} \ll \lambda_D$. In this case (12.118) simplifies further to read

$$\begin{aligned} y_P &= \lim_{m \rightarrow 0} \left\{ \frac{1}{1-m} [e^{-x \ln 2} - e^{-(x/m) \ln 2}] \right\} = \lim_{m \rightarrow 0} \left\{ \frac{1}{1-m} [2^{-x} - 2^{-(x/m)}] \right\} \\ &= \lim_{m \rightarrow 0} \left\{ \frac{1}{1-m} [e^{-m \lambda_D t} - e^{-\lambda_D t}] \right\} = 1 - e^{-\lambda_D t} = 1 - e^{-(x/m) \ln 2} \\ &= 1 - 2^{-\frac{x}{m}}. \end{aligned} \quad (12.125)$$

(b) Figure 12.3 displays normalized daughter activity y_D against normalized time x for saturation model (12.116) of nuclear activation (dashed curves) and (parent) depletion model (12.115) of nuclear activation (solid curves) for activation factors m in the range $10^{-4} \leq m \leq 10$. Also shown (with symbols \times) is the normalized number y_P of parent nuclei given for both activation models as follows

$$y_P = \frac{N_P(t)}{N_P(0)} = e^{-\sigma_P \dot{\phi} t} = e^{-x \ln 2} = \frac{1}{2^x}. \quad (12.126)$$

Equation (12.126) exhibits pure exponential decay behavior with activation time t and is governed by the activation cross section σ_P usually in b (barn) where $1 \text{ b} = 10^{-24} \text{ cm}^2$ and particle fluence rate $\dot{\phi}$ in $\text{cm}^{-2} \cdot \text{s}^{-1}$.

A few notable features of (12.115) and (12.116) deduced from Fig. 12.3 are as follows:

- (1) In practical nuclear activation procedures the activation factor m defined in (12.119) as $m = \sigma_P \dot{\phi} / \lambda_D$ is positive but generally small, justifying the use of the saturation model in studies of radioactivation dynamics. However, since m depends linearly on the fluence rate $\dot{\phi}$, nuclear activation processes with very high fluence rates $\dot{\phi}$ or relatively long activation times x may invalidate the saturation model in favor of the depletion model.
- (2) For all m and both activation models $y_D(x) = 0$ for $x = 0$ and then increases with increasing x . For both models the initial slopes dy_D/dx of the $y_D(x)$ curves are the same for a given m . The initial slope is proportional to the radioactivation yield Y .
- (3) In the saturation model, $y_D(x)$ exponentially approaches its saturation value of $(y_D)_{\text{sat}} = 1$ and remains in saturation as $x \rightarrow \infty$. The larger is m , the shallower is the initial slope of the $y_D(x)$ curve and the slower is the approach to saturation.
- (4) In depletion model, $y_D(x)$ reaches a peak value $(y_D)_{\text{max}}$ at $x = (x_D)_{\text{max}}$, then decreases with increasing x and reverts back to 0 at $x \rightarrow \infty$. Peak value in $y_D(x)$ calculated for the depletion model is referred to as the point of ideal equilibrium and is equal to the saturation $(y_D)_{\text{max}} = (y_D)_{\text{sat}} = 1$ for small activation factor m (typically smaller than 10^{-3}) but decreases in magnitude as m increases. The larger is m , the larger is the discrepancy between the two models and the smaller is $(y_D)_{\text{max}}$ in comparison with $(y_D)_{\text{sat}} = 1$. Thus, $(y_D)_{\text{max}} = (y_D)_{\text{sat}} = 1$ for $m \leq 10^{-3}$; for $m > 10^{-3}$ parameter $(y_D)_{\text{max}}$ decreases with increasing m . For $m > 10^{-3}$ the depletion model rather than the saturation model should be used for determination of daughter activity.
- (5) For $m < 10^{-3}$ and $x \leq (x_D)_{\text{max}}$, the saturation model and the depletion model give identical results for $y_D(x)$ and attain a value of 1 at $x = (x_D)_{\text{max}}$. However, for $x > (x_D)_{\text{max}}$, y_D determined for the saturation model remains in saturation, while y_D determined for the depletion model decreases in harmony with y_P .
- (6) Similarly to the radioactive series decay, we can say that for all $0 < m < 1$, variables y_P and y_D are in transient equilibrium at $x \gg (x_D)_{\text{max}}$. For $m \geq 1$ no equilibrium between y_P and y_D exists at any x . Furthermore, for $m < 10^{-2}$, we can say that y_P and y_D are in a special form of transient equilibrium called secular equilibrium.

(c) Equation (12.115) given by the depletion model of nuclear activation for the normalized daughter activity y_D against normalized activation time x

$$y_D(x) = \frac{1}{(1-m)} \left\{ \frac{1}{2^x} - \frac{1}{2^{x/m}} \right\} = \frac{1}{(1-m)} \left\{ e^{-x \ln 2} - e^{-(x/m) \ln 2} \right\} \quad (12.127)$$

has physical meaning for all positive activation factors m except for $m = 1$ for which it yields an indeterminate form (0/0) that can be rendered determinate by applying the l'Hôpital rule on (12.115) as follows

$$\begin{aligned} y_D(x)|_{m=1} &= \lim_{m \rightarrow 1} \frac{\frac{d}{dm} \{e^{-x \ln 2} - e^{-\frac{x}{m} \ln 2}\}}{\frac{d}{dm} (1 - m)} = \lim_{m \rightarrow 1} \frac{-\frac{x}{m^2} (\ln 2) e^{-\frac{x}{m} \ln 2}}{-1} \\ &= x (\ln 2) e^{-x \ln 2} = (\ln 2) \frac{x}{2^x}. \end{aligned} \quad (12.128)$$

Thus, the solid curves, representing the depletion model in Fig. 12.3 for various positive activation factors m in the range between $m = 10^{-4}$ and $m = 10$, are plotted using (12.115) for all m except for $m = 1$. The curve for $m = 1$ is plotted using (12.128) and this curve, despite having no physical meaning, separates the parent-daughter equilibrium region characterized by $m < 1$ from the parent-daughter non-equilibrium region characterized by $m > 1$.

(d) The solid dots in Fig. 12.3 indicate points of ideal equilibrium on $y_D(x)$ curves for the depletion model and for all $m > 0$ occur at the intercept between $y_D(x)$ and $y_P(x)$ curves.

(1) The coordinate $(x_D)_{\max}$ of the point of ideal equilibrium for the depletion model (12.115) is determined by setting the first derivative dy_D/dx equal to 0 at $x = (x_D)_{\max}$ as follows

$$\begin{aligned} \left. \frac{dy_D}{dx} \right|_{x=(x_D)_{\max}} = 0 &= \frac{d}{dx} \left\{ \frac{1}{1-m} \left[e^{-x \ln 2} - e^{-\frac{x}{m} \ln 2} \right] \right\} \Bigg|_{x=(x_D)_{\max}} \\ &= \left\{ \frac{\ln 2}{1-m} \left[-e^{-x \ln 2} + \frac{1}{m} e^{-\frac{x}{m} \ln 2} \right] \right\} \Bigg|_{x=(x_D)_{\max}}. \end{aligned} \quad (12.129)$$

Inserting $x = (x_D)_{\max}$ into (12.129) and solving for $(x_D)_{\max}$ gives

$$(x_D)_{\max} \ln 2 = \ln m + \frac{(x_D)_{\max}}{m} \ln 2 \quad \text{or} \quad (x_D)_{\max} = \frac{m}{m-1} \frac{\ln m}{\ln 2}. \quad (12.130)$$

(2) The coordinate $(y_D)_{\max}$ of the point of ideal equilibrium can be determined by inserting (12.130) into (12.115) and finding $(y_D)_{\max}$. However, the calculation is cumbersome and a faster approach is to insert (12.130) into (12.126) which, in comparison with (12.115) is much simpler. Since for the point of ideal equilibrium $(y_D)_{\max} = y_D[(x_D)_{\max}] \equiv y_P[(x_D)_{\max}]$, we get $(y_D)_{\max}$ as follows

$$(y_D)_{\max} = y_D[(x_D)_{\max}] \equiv y_P[(x_D)_{\max}] = e^{-(x_D)_{\max} \ln 2} = e^{\frac{m}{1-m} \ln m}. \quad (12.131)$$

(3) Equations (12.130) and (12.131) are valid for all positive m with the exception of $m = 1$ for which they give 0/0. We now determine $(x_D)_{\max}|_{m=1}$ and $(y_D)_{\max}|_{m=1}$

by applying the l'Hôpital rule to get

$$(x_D)_{\max}|_{m \rightarrow 1} = \lim_{m \rightarrow 1} \frac{\frac{d(m \ln m)}{dm}}{(\ln 2) \frac{d(m-1)}{dm}} = \lim_{m \rightarrow 1} \frac{1 + \ln m}{\ln 2} = \frac{1}{\ln 2} = 1.44 \quad (12.132)$$

and

$$(y_D)_{\max}|_{m \rightarrow 1} = \lim_{m \rightarrow 1} e^{\frac{\frac{d(m \ln m)}{dm}}{d(1-m)}} = \lim_{m \rightarrow 1} e^{\frac{\ln m + 1}{-1}} = e^{-1} = 0.368. \quad (12.133)$$

(4) Parameter $(y_D)_{\max}$ of the depletion model of nuclear activation is the point of *ideal equilibrium* calculated from (12.131) for $m \neq 1$ and given as a constant equal to $1/e$ by (12.133) for $m = 1$. Parameter $(x_D)_{\max}$, in turn, depends on the activation factor m and is calculated from (12.130) for $m \neq 1$ and given as a constant $1/\ln 2$ by (12.132). From (12.133) we see that $(y_D)_{\max}$ is a simple exponential function of $(x_D)_{\max}$ and from (12.130) we note that $(x_D)_{\max}$ increases with an increasing m . We thus conclude that as m increases from zero, $(y_D)_{\max}$ decreases from 1.0, attains a value of $1/e = 0.368$ at $m = 1$, and then exponentially approaches 0 as $m \rightarrow \infty$. This is also shown by dots on the y_P curve in Fig. 12.3.

(5) Since $(\mathcal{A}_D)_{\text{sat}}$ is defined as $(\mathcal{A}_D)_{\text{sat}} = \sigma_P \dot{\phi} N_P(0)$ and $y_D(x) = (\mathcal{A}_D)_{\text{sat}} / [\sigma_P \dot{\phi} N_P(0)]$, we conclude that $(y_D)_{\text{sat}} = 1.0$.

(6) Since according to the depletion model of nuclear activation the normalized daughter activity $y_D(x)$ decreases with x for $x > (x_D)_{\max}$, it is obvious that in practice activation times beyond $(x_D)_{\max}$ are counter-productive and result in lower daughter activity that in optimal regions for $x < (x_D)_{\max}$.

12.6.Q6

(256)

Specific activity $(a_D)_{\text{theor}}$ of a radionuclide D is defined as activity \mathcal{A}_D per unit mass M_D of the radionuclide and is for a carrier-free radionuclide determined as follows

$$(a_D)_{\text{theor}} = \frac{\mathcal{A}_D}{M_D} = \frac{\lambda_D N}{M_D} = \frac{\lambda_D N_A}{A_D} = \frac{(\ln 2) N_A}{(t_{1/2})_D A_D}, \quad (12.134)$$

where λ_D , $(t_{1/2})_D$, and A_D are the decay constant, half-life, and atomic mass, respectively, of the radionuclide D and N_A is the Avogadro constant ($6.022 \times 10^{23} \text{ mol}^{-1}$).

- (a) Derive expressions for specific activity a_D of radionuclides produced in nuclear activation using: (1) saturation model of nuclear activation and (2) depletion model of nuclear activation. Discuss the dependence of a_D on activation time t and particle fluence rate $\dot{\phi}$. What is the maximum specific activity $(a_D)_{\max}$ achievable in nuclear activation using the saturation model and the depletion model?
- (b) Calculate the theoretical specific activity $(a_D)_{\text{theor}}$ given in (12.134) for the following radionuclides D of interest in medical physics: cobalt-60 (Co-60), molybdenum-99 (Mo-99), europium-152 (Eu-152), iridium-192 (Ir-192), and gold-198 (Au-198).
- (c) Determine the maximum specific activity $(a_D)_{\max}$ attainable in thermal neutron activation in a nuclear reactor with neutron fluence rate $\dot{\phi}$ of $5 \times 10^{11} \text{ cm}^{-2} \cdot \text{s}^{-1}$, $2 \times 10^{13} \text{ cm}^{-2} \cdot \text{s}^{-1}$, $3 \times 10^{14} \text{ cm}^{-2} \cdot \text{s}^{-1}$, and $1.2 \times 10^{16} \text{ cm}^{-2} \cdot \text{s}^{-1}$ for the daughter nuclei of (b). Use both the saturation model and the depletion model of nuclear activation and compare the results obtained with the two models.
- (d) Determine activation times $(t_{\max})_D$ required to attain maximum specific activities $(a_D)_{\max}$ of daughter D radionuclides of (b) and neutron fluence rates $\dot{\phi}$ of (c).

SOLUTION:

(a) The equation used for expressing nuclear activation with particle beams (T12.57) accounts for activation and depletion of parent P nuclei as well as for activation of daughter D nuclei. Activation of parent P and daughter D nuclei is governed by cross sections σ_P and σ_D , respectively; depletion of parent P nuclei is described by the difference between the number of parent P nuclei $N_P(t)$ at time t and the initial number $N_P(0)$ of parent nuclei P at time $t = 0$, where t stands for activation time.

Two approximations to the general activation equation [see (T12.57)] are in use:

- (1) The activation process affects neither the daughter nuclei ($\sigma_D = 0$) nor the number $N_P(t)$ of parent nuclei [$N_P(t) = N_P(0) = \text{constant}$] resulting in the so-called saturation model of nuclear activation. The initial number $N_P(0)$ of parent nuclei is assumed infinitely large and not affected by nuclear activation of parent P into daughter D.
- (2) The activation process does not affect the daughter nuclei ($\sigma_D = 0$); however, it affects the number $N_P(t)$ of parent nuclei [$N_P(0) > N_P(t) \neq \text{constant}$] resulting in the so-called depletion model of nuclear activation. $N_P(0)$ is finite and undergoes depletion during the nuclear activation process.

(1) **Saturation model:** The general equation for normalized daughter activity $y_D(x)$ as a function of normalized activation time x , with $x = m\lambda_D t / \ln 2 =$

$\sigma_P \dot{\phi} t / \ln 2$, is for the saturation model of nuclear activation expressed as [see (T12.35)]

$$y_D(x) = \frac{\mathcal{A}_D(t)}{\sigma_P \dot{\phi} N_P(0)} = \frac{\mathcal{A}_D(t)}{(\mathcal{A}_D)_{\text{sat}}} = 1 - e^{-\frac{x}{m} \ln 2}, \quad (12.135)$$

where

$(\mathcal{A}_D)_{\text{sat}}$ is the saturation activity of the daughter defined as $(\mathcal{A}_D)_{\text{sat}} = \sigma_P \dot{\phi} N_P(0)$.
 $\dot{\phi}$ is the particle fluence rate.
 m is the activation factor defined as $m = \sigma_P \dot{\phi} / \lambda_D$.

After insertion of (12.135) into (12.134) the specific activity a_D for the saturation model is given by the following expression

$$\begin{aligned} a_D &= \frac{\mathcal{A}_D(t)}{M_P} = \frac{(\mathcal{A}_D)_{\text{sat}} y_D(x)}{M_P} = \frac{(\mathcal{A}_D)_{\text{sat}}}{M_P} \left\{ 1 - e^{-\frac{x}{m} \ln 2} \right\} = \frac{\sigma_P \dot{\phi} N_P(0)}{M_P} \left\{ 1 - e^{-\frac{x}{m} \ln 2} \right\} \\ &= \frac{\sigma_P \dot{\phi} N_A}{A_P} \left\{ 1 - e^{-\frac{x}{m} \ln 2} \right\} = \frac{\sigma_P \dot{\phi} N_A}{A_P} \left\{ 1 - \frac{1}{2^{x/m}} \right\}, \end{aligned} \quad (12.136)$$

where we used the standard expression for $N_P(0)/M_P = N_A/A_P$ with M_P the initial mass of the parent P nuclide and A_P the atomic mass of the parent nuclide.

From (12.136) we note that the maximum activity $(a_D)_{\text{max}}$ for $x \rightarrow \infty$ is proportional to the particle fluence rate $\dot{\phi}$ and the proportionality constant is $(\sigma_P N_A / A_P)$

$$(a_D)_{\text{max}} = \frac{\sigma_P N_A}{A_P} \dot{\phi}. \quad (12.137)$$

The linear relationship between $(a_D)_{\text{max}}$ and $\dot{\phi}$ works fine at relatively low $\dot{\phi}$; however, at $\dot{\phi} \rightarrow \infty$, (12.137) suggests that $(a_D)_{\text{max}} \rightarrow \infty$ in contradiction with the theoretical specific activity $(a_D)_{\text{theor}}$ of (12.134) that is well defined, independent of $\dot{\phi}$, and finite for a given radionuclide.

(2) **Depletion model:** The general equation for normalized daughter activity $y_D(x)$ as a function of normalized activation time x , with $x = m \lambda_D t / \ln 2 = \sigma_P \dot{\phi} t / \ln 2$, is for the depletion model of nuclear activation expressed as [see (T12.33)]

$$y_D(x) = \frac{\mathcal{A}_D(t)}{\sigma_P \dot{\phi} N_P(0)} = \frac{1}{1-m} \left\{ e^{-x \ln 2} - e^{-\frac{x}{m} \ln 2} \right\} = \frac{1}{1-m} \left\{ \frac{1}{2^x} - \frac{1}{2^{x/m}} \right\}, \quad (12.138)$$

where m is the activation factor defined as $m = \sigma_P \dot{\phi} / \lambda_D$.

After insertion of (12.138) into (12.134) the specific activity a_D for the depletion model is given by the following

$$a_D = \frac{\mathcal{A}_D(t)}{M_P} = \frac{\sigma_P \dot{\phi} N_P(0) y_D(x)}{M_P} = \frac{\sigma_P \dot{\phi} N_A y_D(x)}{A_P} = \frac{\sigma_P \dot{\phi} N_A}{A_P(1-m)} \left\{ e^{-x \ln 2} - e^{-\frac{x}{m} \ln 2} \right\}, \quad (12.139)$$

where, as in (12.136), we used the relationship $N_P(0)/M_P = N_A/A_P$.

In contrast to (12.136) which exhibits $(a_D)_{\max}$ given by (12.137) at $x \rightarrow \infty$, (12.139) exhibits maximum specific activity $(a_D)_{\max}$ at the point of ideal equilibrium between y_P and y_D which occurs at $[(x_D)_{\max}, (y_D)_{\max}]$, as shown in (T12.29 through (T12.32)), while $\lim_{x \rightarrow \infty} (a_D)_{\max} = 0$.

The maximum specific activity $(a_D)_{\max}$ calculated for the depletion model is from (12.139) now written as follows

$$(a_D)_{\max} = \frac{\sigma_P \dot{\phi} N_A (y_D)_{\max}}{A_P} = \frac{\sigma_P N_A}{A_P} \dot{\phi} e^{\frac{m}{1-m} \ln m} = \frac{\sigma_P N_A}{A_P} \dot{\phi} \exp \left\{ -\frac{\frac{\sigma_P \dot{\phi}}{\lambda_D}}{\frac{\sigma_P \dot{\phi}}{\lambda_D} - 1} \ln \frac{\sigma_P \dot{\phi}}{\lambda_D} \right\}, \quad (12.140)$$

where we used the definition of $m = \sigma_P \dot{\phi} / \lambda_D$ and the expression for $(y_D)_{\max}$ derived in (12.131) of Prob. 255.

(b) Specific activity a_D of daughter radionuclide D produced in nuclear activation of parent nuclide P depends on various activation parameters, such as: activation cross section σ_P of the parent P nucleus, decay constant λ_D of the daughter D nucleus, activation particle fluence rate $\dot{\phi}$, and activation time t . For a given parent–daughter nuclear configuration, σ_P and λ_D are fixed, so that the specific activity a_D depends on $\dot{\phi}$ and t , as shown for the saturation model in (12.136) and for the depletion model in (12.139). However, as shown in Prob. 258, the maximum attainable specific activity $(a_D)_{\max}$ is limited by the theoretical specific activity $(a_D)_{\text{theor}}$ given in (12.134) which defines the upper limit of achievable specific activities in nuclear activation for a given parent–daughter configuration.

Theoretical specific activities $(a_D)_{\text{theor}}$ of various radionuclides of importance in medical physics (Co-60, Mo-99, Eu-152, Ir-192, and Au-198) are calculated with (12.134) as follows (thermal neutron cross sections σ_D are from the IAEA TRS Report #156)

- (1) Cobalt-60: $(t_{1/2})_{\text{Co-60}} = 5.26$ a, $A_{\text{Co-60}} = 59.93$ g/mol
Parent nucleus: cobalt-59, $\sigma_{\text{Co-59}} = 37.2$ b

$$\begin{aligned} (a_{\text{Co-60}})_{\text{theor}} &= \frac{(\ln 2) N_A}{(t_{1/2})_{\text{Co-60}} A_{\text{Co-60}}} \\ &= \frac{(\ln 2) \times (6.022 \times 10^{23} \text{ mol}^{-1})}{(5.26 \text{ a}) \times (365 \text{ d/a}) \times (24 \text{ h/d}) \times (3600 \text{ s/h}) \times (59.93 \text{ g} \cdot \text{mol}^{-1})} \\ &= 4.199 \times 10^{13} \text{ Bq/g} = 42.99 \text{ TBq/g} = \frac{4.199 \times 10^{13} \text{ Bq/g}}{3.7 \times 10^{10} \text{ Bq/Ci}} \\ &= 1.135 \times 10^3 \text{ Ci/g}. \end{aligned} \quad (12.141)$$

- (2) Molybdenum-99: $(t_{1/2})_{\text{Mo-99}} = 65.94 \text{ h}$, $A_{\text{Mo-99}} = 98.91 \text{ g/mol}$
 Parent nucleus: molybdenum-98, $\sigma_{\text{Mo-98}} = 0.13 \text{ b}$

$$\begin{aligned}
 (a_{\text{Mo-99}})_{\text{theor}} &= \frac{(\ln 2)N_A}{(t_{1/2})_{\text{Mo-99}}A_{\text{Mo-99}}} \\
 &= \frac{(\ln 2) \times (6.022 \times 10^{23} \text{ mol}^{-1})}{(65.94 \text{ h}) \times (3600 \text{ s/h}) \times (98.91 \text{ g} \cdot \text{mol}^{-1})} \\
 &= 1.778 \times 10^{16} \text{ Bq/g} = \frac{1.778 \times 10^{16} \text{ Bq/g}}{3.7 \times 10^{10} \text{ Bq/Ci}} \\
 &= 4.805 \times 10^5 \text{ Ci/g.} \tag{12.142}
 \end{aligned}$$

- (3) Europium-152: $(t_{1/2})_{\text{Eu-152}} = 13.54 \text{ a}$, $A_{\text{Eu-152}} = 151.92 \text{ g/mol}$
 Parent nucleus: europium-151, $\sigma_{\text{Eu-151}} = 5300 \text{ b}$

$$\begin{aligned}
 (a_{\text{Eu-152}})_{\text{theor}} &= \frac{(\ln 2)N_A}{(t_{1/2})_{\text{Eu-152}}A_{\text{Eu-152}}} \\
 &= \frac{(\ln 2) \times (6.022 \times 10^{23} \text{ mol}^{-1})}{(13.54 \text{ a}) \times (365 \text{ d/a}) \times (24 \text{ h/d}) \times (3600 \text{ s/h}) \times (151.92 \text{ g} \cdot \text{mol}^{-1})} \\
 &= 6.434 \times 10^{12} \text{ Bq/g} = 6.434 \text{ TBq/g} = \frac{6.434 \times 10^{12} \text{ Bq/g}}{3.7 \times 10^{10} \text{ Bq/Ci}} \\
 &= 1.739 \times 10^2 \text{ Ci/g.} \tag{12.143}
 \end{aligned}$$

- (4) Iridium-192: $(t_{1/2})_{\text{Ir-192}} = 73.8 \text{ d}$, $A_{\text{Mo-99}} = 98.91 \text{ g/mol}$
 Parent nucleus: iridium-191, $\sigma_{\text{Ir-191}} = 954 \text{ b}$

$$\begin{aligned}
 (a_{\text{Ir-192}})_{\text{theor}} &= \frac{(\ln 2)N_A}{(t_{1/2})_{\text{Ir-192}}A_{\text{Ir-192}}} \\
 &= \frac{(\ln 2) \times (6.022 \times 10^{23} \text{ mol}^{-1})}{(73.8 \text{ d}) \times (24 \text{ h/d}) \times (3600 \text{ s/h}) \times (191.96 \text{ g} \cdot \text{mol}^{-1})} \\
 &= 3.410 \times 10^{14} \text{ Bq/g} = 341 \text{ TBq/g} = \frac{3.410 \times 10^{14} \text{ Bq/g}}{3.7 \times 10^{10} \text{ Bq/Ci}} \\
 &= 9.217 \times 10^3 \text{ Ci/g.} \tag{12.144}
 \end{aligned}$$

- (5) Gold-198: $(t_{1/2})_{\text{Au-198}} = 64.68 \text{ h}$, $A_{\text{Au-198}} = 197.97 \text{ g/mol}$
 Parent nucleus: gold-197, $\sigma_{\text{Au-197}} = 98.8 \text{ b}$

$$\begin{aligned}
 (a_{\text{Au-198}})_{\text{theor}} &= \frac{(\ln 2)N_A}{(t_{1/2})_{\text{Au-198}}A_{\text{Au-198}}} \\
 &= \frac{(\ln 2) \times (6.022 \times 10^{23} \text{ mol}^{-1})}{(64.68 \text{ h}) \times (3600 \text{ s/h}) \times (197.97 \text{ g} \cdot \text{mol}^{-1})}
 \end{aligned}$$

$$\begin{aligned}
 &= 9.055 \times 10^{15} \text{ Bq/g} = \frac{9.055 \times 10^{15} \text{ Bq/g}}{3.7 \times 10^{10} \text{ Bq/Ci}} \\
 &= 2.447 \times 10^5 \text{ Ci/g.} \tag{12.145}
 \end{aligned}$$

(c) Maximum specific activities $(a_D)_{\max}$ of radionuclide D attainable in nuclear activation were derived in (a) and are given in (12.137) and (12.140) for the saturation model and the depletion model, respectively. We will now use these two expressions to determine $(a_D)_{\max}$ of (1) Co-60, (2) Mo-99, (3) Eu-152, (4) Ir-192, and (5) Au-198 for four neutron fluence rates: $5 \times 10^{11} \text{ cm}^{-2} \cdot \text{s}^{-1}$, $2 \times 10^{13} \text{ cm}^{-2} \cdot \text{s}^{-1}$, $3 \times 10^{14} \text{ cm}^{-2} \cdot \text{s}^{-1}$, and $1.2 \times 10^{16} \text{ cm}^{-2} \cdot \text{s}^{-1}$. Before embarking on calculation of $(a_D)_{\max}$, we summarize in Table 12.5 the relevant physical data, obtained from Appendix A or from the literature for the five radionuclides. Entries for $(a_D)_{\text{theor}}$ were determined in (b) with (12.134). In Table 12.6 we list activation factors m for the five radionuclides and four thermal neutron fluence $\dot{\phi}$ rates. It is evident that the range in $\dot{\phi}$ in nature is quite large in our example extending from about $\sim 2 \times 10^{-8}$ to $\sim 4 \times 10^4$. Entries for $(a_D)_{\text{theor}}$ were calculated in (b) with (12.134).

Results of $(a_D)_{\max}$ calculations are summarized for radionuclides cobalt-60, molybdenum-99, europium-152, iridium-192, and gold-198 in Table 12.7 for the saturation model determined with (12.137) and in Table 12.8 for the depletion model determined with (12.140). For a given radionuclide the maximum specific activity $(a_D)_{\max}$ in Table 12.7 is linearly proportional with $\dot{\phi}$ in the whole fluence rate range, while in Table 12.8 the maximum specific activity $(a_D)_{\max}$ is proportional to $\dot{\phi}$ at low $\dot{\phi}$ and saturates at $(a_D)_{\text{theor}}$ at high $\dot{\phi}$. Results displayed in Tables 12.7 and 12.8 are plotted in Fig. 12.4, for the saturation model with light solid lines and for the depletion model with heavy solid curves.

The practical range of thermal neutron fluence $\dot{\phi}$ in nuclear reactors ranges from $\sim 10^{11} \text{ cm}^{-2} \cdot \text{s}^{-1}$ to $\sim 10^{16} \text{ cm}^{-2} \cdot \text{s}^{-1}$. The range covered in Fig. 12.4 is an expanded practical range to illustrate the behavior of $(a_D)_{\max}$ that would be observed with saturation and depletion models if the practical fluence rate range were expanded to $\sim 10^{22} \text{ cm}^{-2} \cdot \text{s}^{-1}$. It is obvious that in the practical range of $\dot{\phi}$ activation of Mo-99 and to a large extent also of Au-198 can be adequately described by the saturation model of nuclear activation. Ir-192 and Co-60 follow the saturation model for $\dot{\phi} < \sim 10^{13} \text{ cm}^{-2} \cdot \text{s}^{-1}$ but above $10^{13} \text{ cm}^{-2} \cdot \text{s}^{-1}$ should be described with the depletion model. Eu-152 for all practical fluence rates $\dot{\phi}$ should be described with the depletion model.

(d) Activation time $(t_{\max})_D$ required to attain the maximum specific activity $(a_D)_{\max}$ of daughter D radionuclide at a given neutron fluence rate $\dot{\phi}$ is determined from the expression for $(x_D)_{\max}$ which gives the normalized time coordinate of the point of ideal parent-daughter equilibrium, derived in (12.88) of Prob. 253 and in (T12.29). The following relationship holds for $(x_D)_{\max}$ and $(t_{\max})_D$

$$(x_D)_{\max} = \frac{m}{m-1} \frac{\ln m}{\ln 2} = \frac{m\lambda_D(t_{\max})_D}{\ln 2} \quad \text{or} \quad (t_{\max})_D = \frac{(x_D)_{\max} \ln 2}{m\lambda_D} = \frac{\ln m}{(m-1)\lambda_D}, \tag{12.146}$$

Table 12.5 Parameters relevant in calculation of maximum attainable specific activity $(aD)_{\max}$ of Co-60, Mo-99, Eu-152, Ir-192, and Au-198 in activation with thermal neutrons

Daughter D	Co-60	Mo-99	Eu-152	Ir-192	Au-198
Atomic number	27	42	63	77	79
A_D (g/mol)	59.93	98.91	151.92	191.96	197.97
$(t_{1/2})_D$	5.26 a	65.94 h	13.54 a	73.8 d	64.48 h
λ_D (s^{-1})	4.179×10^{-9}	2.920×10^{-6}	1.623×10^{-9}	1.087×10^{-7}	2.986×10^{-6}
Parent P	Co-59	Mo-98	Eu-151	Ir-191	Au-197
Nuclear reaction	$^{59}_{27}\text{Co}(n, \gamma)^{60}_{27}\text{Co}$	$^{98}_{42}\text{Mo}(n, \gamma)^{99}_{42}\text{Mo}$	$^{151}_{63}\text{Eu}(n, \gamma)^{152}_{63}\text{Eu}$	$^{191}_{77}\text{Ir}(n, \gamma)^{192}_{77}\text{Ir}$	$^{197}_{79}\text{Au}(n, \gamma)^{198}_{79}\text{Au}$
A_P (g/mol)	58.93	97.91	150.92	190.96	196.97
σ_P (b)	37.2	0.13	5300	954	98.8
σ_P/λ_P ($\text{cm}^2 \cdot \text{s}$)	8.902×10^{-15}	4.452×10^{-20}	3.266×10^{-12}	8.776×10^{-15}	3.309×10^{-17}
$(aD)_{\text{theor}}$ (Ci/g)	1.135×10^3	4.805×10^5	1.739×10^2	9.217×10^3	2.447×10^5
λ_D/AD ($\frac{\text{mol}}{\text{g}}$)	6.973×10^{-11}	2.952×10^{-8}	1.068×10^{-11}	5.663×10^{-10}	1.508×10^{-8}

Table 12.6 Activation factor $m = \sigma_P \dot{\phi} / \lambda_D$ for various radionuclides of interest in medical physics and for four thermal neutron fluence rates $\dot{\phi}$: $5 \times 10^{11} \text{ cm}^{-2} \cdot \text{s}^{-1}$, $2 \times 10^{13} \text{ cm}^{-2} \cdot \text{s}^{-1}$, $3 \times 10^{14} \text{ cm}^{-2} \cdot \text{s}^{-1}$, and $1.2 \times 10^{16} \text{ cm}^{-2} \cdot \text{s}^{-1}$

Radionuclide	$\sigma_P / \lambda_D \text{ (cm}^2 \cdot \text{s)}$	Activation factor $m = \sigma_P \dot{\phi} / \lambda_D$			
		Thermal neutron fluence rate $\dot{\phi} \text{ (cm}^{-2} \cdot \text{s}^{-1})$			
		5×10^{11}	2×10^{13}	3×10^{14}	1.2×10^{16}
Cobalt-60	8.902×10^{-15}	4.5×10^{-3}	0.18	2.7	1.1×10^2
Molybdenum-99	4.452×10^{-20}	2.2×10^{-8}	8.9×10^{-7}	1.3×10^{-5}	5.3×10^{-4}
Europium-152	3.266×10^{-12}	1.7	65	9.8×10^2	3.9×10^4
Iridium-192	8.776×10^{-15}	4.4×10^{-3}	0.18	2.6	1.1×10^2
Gold-198	3.309×10^{-17}	3.3×10^{-5}	6.6×10^{-4}	9.9×10^{-3}	0.4

Table 12.7 Maximum attainable specific activities $(a_D)_{\max}$ in nuclear activation for five neutron activation reactions of importance in medical physics and for four neutron fluence rates $\dot{\phi}$ according to the *saturation model* of neutron activation given in (12.137). Specific activities are given in Ci/g

$\dot{\phi} \text{ (cm}^{-2} \cdot \text{s}^{-1})$	5×10^{11}	2×10^{13}	3×10^{14}	1.2×10^{16}
Cobalt-60	5.14	2.06×10^2	3.08×10^3	1.23×10^5
Molybdenum-99	1.08×10^{-2}	4.32×10^{-1}	6.48	2.59×10^2
Europium-152	2.86×10^2	1.14×10^4	1.72×10^5	6.86×10^6
Iridium-192	4.07×10	1.63×10^3	2.44×10^4	9.76×10^5
Gold-198	4.08	1.63×10^2	2.45×10^3	9.80×10^4

Table 12.8 Maximum attainable specific activities $(a_D)_{\max}$ in nuclear activation for five neutron activation reactions of importance in medical physics and for four neutron fluence rates $\dot{\phi}$ according to the *depletion model* of neutron activation given in (12.140). Specific activities are given in Ci/g

$\dot{\phi} \text{ (cm}^{-2} \cdot \text{s}^{-1})$	5×10^{11}	2×10^{13}	3×10^{14}	1.2×10^{16}
Cobalt-60	5.01	1.41×10^2	6.41×10^2	1.10×10^3
Molybdenum-99	1.08×10^{-2}	4.32×10^{-1}	6.48	2.58×10^2
Europium-152	8.07×10	1.64×10^2	1.74×10^2	1.75×10^2
Iridium-192	3.97×10	1.12×10^3	5.12×10^3	8.86×10^3
Gold-198	4.08	1.63×10^3	2.34×10^3	5.33×10^4

where m is the activation factor defined as $m = \sigma_P \dot{\phi} / \lambda_D$, σ_P is the activation cross section of the parent nuclide, and λ_D is the decay constant of the daughter radionuclide. Results of $(t_{\max})_D$ calculation using (12.146) are summarized in Table 12.9 and show that, for a given daughter radionuclide D, $(t_{\max})_D$ is roughly inversely proportional to the particle fluence rate $\dot{\phi}$. Thus, the higher is the thermal neutron fluence $\dot{\phi}$, the shorter is the activation time $(t_{\max})_D$ required to attain the maximum specific activity $(a_D)_{\max}$ for a given daughter D radionuclide.

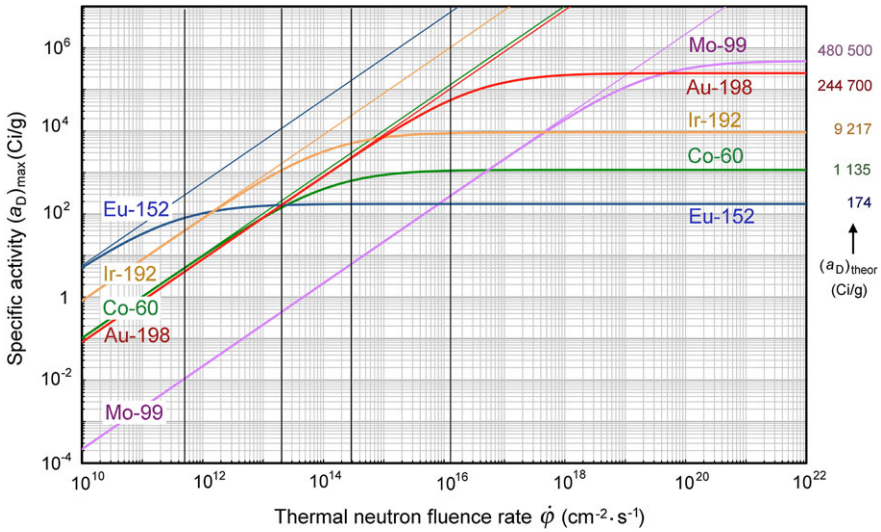


Fig. 12.4 Maximum attainable specific activity $(a_D)_{\max}$ against thermal neutron fluence rate $\dot{\phi}$ for saturation model of neutron activation according to (12.137) and for depletion model of neutron activation according to (12.139). The four heavy vertical lines represent the four fluence rates used in calculation of data for Tables 12.7 and 12.8. Data for saturation model saturate at $(a_D)_{\max} \rightarrow \infty$ as $\dot{\phi} \rightarrow \infty$, data for depletion model saturate at $(a_D)_{\max} \rightarrow (a_D)_{\text{theor}}$ as $\dot{\phi} \rightarrow \infty$

Table 12.9 Activation time $(t_{\max})_D$ required to attain the maximum specific activity $(a_D)_{\max}$ of daughter D radionuclide at a given neutron fluence rate $\dot{\phi}$ according to the depletion model of nuclear activation for five radionuclides of interest to medical physics. Data were calculated with (12.146) for photon fluence rates $\dot{\phi}$ of $5 \times 10^{11} \text{ cm}^{-2} \cdot \text{s}^{-1}$, $2 \times 10^{13} \text{ cm}^{-2} \cdot \text{s}^{-1}$, $3 \times 10^{14} \text{ cm}^{-2} \cdot \text{s}^{-1}$, and $1.2 \times 10^{16} \text{ cm}^{-2} \cdot \text{s}^{-1}$

Radionuclide	$(t_{1/2})_D$	Thermal neutron fluence rate $\dot{\phi}$ ($\text{cm}^{-2} \cdot \text{s}^{-1}$)			
		5×10^{11}	2×10^{13}	3×10^{14}	1.2×10^{16}
Cobalt-60	5.26 a	41.3 a	15.9 a	4.46 a	0.34 a
Molybdenum-99	65.9 h	69.8 h	55.2 h	44.5 h	29.9 h
Europium-152	13.53 a	15.1 a	1.27 a	0.14 a	0.005 a
Iridium-192	73.8 d	580.6 d	224.7 d	63.1 d	4.8 d
Gold-198	64.5 h	42.7 d	28.4 d	18.1 d	5.9 d

12.6.Q7

(257)

The depletion model of nuclear activation accounts for depletion in number N_P of parent P nuclei as a function of activation time t but assumes that the daughter D nuclei are not affected by the activation particles, resulting in $\sigma_D = 0$. As shown in Prob. 252 and (T12.31), the maximum normalized daughter activity $(y_D)_{\max}$ occurs at the point of ideal equilibrium and is for $m \neq 1$ expressed as

$$(y_D)_{\max} = \frac{(\mathcal{A}_D)_{\max}}{\sigma_P \dot{\phi} N_P(0)} = y_D[(x_D)_{\max}] = e^{-\frac{m}{1-m} \ln m}, \quad (12.147)$$

where m is the activation factor defined as $m = \sigma_P \dot{\phi} / \lambda_D$.

In contrast to the depletion model, the parent depletion–daughter activation model, as shown in Prob. 254, accounts for daughter activation ($\sigma_D \neq 0$) and the maximum normalized daughter activity $(y_D^*)_{\max}$ is expressed as follows

$$(y_D^*)_{\max} = \frac{(\mathcal{A}_D^*)_{\max}}{\sigma_P \dot{\phi} N_P(0)} = \frac{1}{\varepsilon^*} e^{-(x_D^*) \ln 2} = \frac{1}{\varepsilon^*} e^{-\frac{m^*}{1-m^*} \ln m^*}, \quad (12.148)$$

where m^* is the modified activation factor defined as $m^* = \sigma_P \dot{\phi} / \lambda_D^* = \sigma_P \dot{\phi} / (\lambda_D + \sigma_D \dot{\phi}) = m / \varepsilon^*$ and ε^* is a parameter defined as $\varepsilon^* = \lambda_D^* / \lambda_D = 1 + \sigma_D \dot{\phi} / \lambda_D$.

- (a) A typical example for parent depletion–daughter activation model is activation of iridium-191 into iridium-192 with the following relevant data: $\sigma_{\text{Ir-191}} = 954$ b, $\sigma_{\text{Ir-192}} = 1420$ b, $(t_{1/2})_{\text{Ir-192}} = 73.8$ d, and $\lambda_{\text{Ir-192}} = 1.087 \times 10^{-7} \text{ s}^{-1}$. Assume that a sample of Ir-191 undergoes neutron activation in a nuclear reactor with neutron fluence rate $\dot{\phi} = 10^{14} \text{ cm}^{-2} \cdot \text{s}^{-1}$ and calculate as well as plot (using steps of 0.5 in x for $0 \leq x \leq 5$) the following quantities: $y_{\text{Ir-191}}$ for saturation, depletion, and depletion activation models; $z_{\text{Ir-192}}$ for saturation model; $y_{\text{Ir-192}}$, $(x_{\text{Ir-192}})_{\max}$, and $(y_{\text{Ir-192}})_{\max}$ for depletion model; $y_{\text{Ir-192}}^*$, $(x_{\text{Ir-192}}^*)_{\max}$, and $(y_{\text{Ir-192}}^*)_{\max}$ for depletion–activation model.
- (b) In Prob. 256 the maximum attainable specific activity $(a_{\text{Ir-192}})_{\max}$ for neutron activation of iridium-191 was determined using the depletion model which ignores the activation cross section $\sigma_{\text{Ir-192}} = 1420$ b of the daughter Ir-192. Using the “parent depletion–daughter activation model” which accounts for daughter activation, calculate $(a_{\text{Ir-192}})_{\max}$ for four neutron fluence rates $\dot{\phi}$ (in $\text{cm}^{-2} \cdot \text{s}^{-1}$) of 5×10^{11} , 2×10^{13} , 1×10^{14} , 3×10^{14} , and 1.2×10^{16} . Also determine the normalized time $(x_{\text{Ir-192}}^*)_{\max}$ at which maximum specific activity occurs.
- (c) Compare $(a_{\text{Ir-192}})_{\max}$ calculated for the depletion–activation model in (b) with $(a_{\text{Ir-192}})_{\max}$ calculated for the depletion model in Prob. 256(c). Explain the difference in results.

SOLUTION:

(a) Parameters of the saturation model, depletion model, and the depletion-activation model applied to neutron activation of iridium-191 nuclide into iridium-192 radionuclide in a neutron fluence rate $\dot{\phi}$ of $10^{14} \text{ cm}^{-2} \cdot \text{s}^{-1}$ are determined as follows:

(1)

$$(t_{1/2})_{\text{D}} = (t_{1/2})_{\text{Ir-192}} = 73.8 \text{ d} = 6.376 \times 10^6 \text{ s}. \quad (12.149)$$

(2)

$$\lambda_{\text{D}} = \lambda_{\text{Ir-192}} = \frac{\ln 2}{(t_{1/2})_{\text{Ir-192}}} = \frac{\ln 2}{6.376 \times 10^6 \text{ s}} = 1.087 \times 10^{-7} \text{ s}^{-1}. \quad (12.150)$$

(3)

$$\sigma_{\text{P}} = \sigma_{\text{Ir-191}} = 954 \text{ b} = 954 \times 10^{-24} \text{ cm}^2. \quad (12.151)$$

(4)

$$\sigma_{\text{D}} = \sigma_{\text{Ir-192}} = 1420 \text{ b} = 1420 \times 10^{-24} \text{ cm}^2. \quad (12.152)$$

(5)

$$m = \frac{\sigma_{\text{P}} \dot{\phi}}{\lambda_{\text{D}}} = \frac{\sigma_{\text{Ir-191}} \dot{\phi}}{\lambda_{\text{Ir-192}}} = \frac{(954 \times 10^{-24} \text{ cm}^2) \times (10^{14} \text{ cm}^{-2} \cdot \text{s}^{-1})}{1.087 \times 10^{-7} \text{ s}^{-1}} = 0.878. \quad (12.153)$$

(6)

$$\lambda_{\text{D}}^* = \lambda_{\text{Ir-192}}^* = \lambda_{\text{Ir-192}} + \sigma_{\text{Ir-192}} \dot{\phi} = 2.507 \times 10^{-7} \text{ s}^{-1} \quad [\text{see (T12.48)}]. \quad (12.154)$$

(7)

$$\varepsilon^* = \frac{\lambda_{\text{D}}^*}{\lambda_{\text{D}}} = \frac{\lambda_{\text{Ir-192}}^*}{\lambda_{\text{Ir-192}}} = \frac{2.507 \times 10^{-7}}{1.087 \times 10^{-7}} = 2.306 \quad [\text{see T12.52}]. \quad (12.155)$$

(8)

$$m^* = \frac{\sigma_{\text{P}} \dot{\phi}}{\lambda_{\text{D}}^*} = \frac{\sigma_{\text{Ir-192}} \dot{\phi}}{\lambda_{\text{Ir-192}}^*} = \frac{m}{\varepsilon^*} = \frac{0.878}{2.306} = 0.381 \quad [\text{see T12.54}]. \quad (12.156)$$

(9)

$$\begin{aligned} (x_{\text{D}})_{\text{max}} &= (x_{\text{Ir-192}})_{\text{max}} = \frac{m \ln m}{(m-1) \ln 2} \\ &= \frac{0.878 \times \ln 0.878}{(0.878-1) \times \ln 2} = 1.351 \quad [\text{see Prob. 252 (12.68)}]. \end{aligned} \quad (12.157)$$

(10)

$$\begin{aligned} (x_D^*)_{\max} &= (x_{\text{Ir-192}}^*)_{\max} = \frac{m^* \ln m^*}{(m^* - 1) \ln 2} \\ &= \frac{0.381 \times \ln 0.381}{(0.381 - 1) \times \ln 2} = 0.857 \quad [\text{see Prob. 254 (12.108)}]. \end{aligned} \quad (12.158)$$

(11)

$$\begin{aligned} (y_D)_{\max} &= (y_{\text{Ir-192}})_{\max} = m^{\frac{m}{1-m}} = 0.878^{\frac{0.878}{1-0.878}} = 0.392 \\ &[\text{see Prob. 252 (12.73)}]. \end{aligned} \quad (12.159)$$

(12)

$$\begin{aligned} (y_D^*)_{\max} &= (y_{\text{Ir-192}}^*)_{\max} = \frac{1}{\varepsilon^*} (m^*)^{\frac{m^*}{1-m^*}} = \frac{0.381^{\frac{0.381}{1-0.381}}}{2.306} = 0.239 \\ &[\text{see Prob. 254 (12.110)}]. \end{aligned} \quad (12.160)$$

The normalized quantity $y_P(x)$ representing the number of parent nuclei $N_P(t)$ normalized to the initial number $N_P(0)$ of parent nuclei as a function of normalized time $x = mt/(t_{1/2})_D$ is the same for all three activation models and is given by (12.58) of Prob. 252 and (T12.27) as

$$y_P(x) = e^{-x \ln 2} = 2^{-x}. \quad (12.161)$$

The normalized daughter activity $y_D(x)$ defined as $y_D(x) = \mathcal{A}_D(t)/[\sigma_P \dot{\phi} N_P(0)]$ is calculated:

(i) for the saturation model with (12.61) of Prob. 252 expressed as

$$z_D(x) = \frac{\mathcal{A}_D(t)}{\sigma_P \dot{\phi} N_P(0)} = 1 - e^{-\frac{x}{m} \ln 2} = 1 - \frac{1}{2^{\frac{x}{m}}}, \quad (12.162)$$

(ii) for the depletion model with (12.64) of Prob. 252 expressed as

$$y_D(x) = \frac{\mathcal{A}_D(t)}{\sigma_P \dot{\phi} N_P(0)} = \frac{1}{1-m} \left\{ e^{-x \ln 2} - e^{-\frac{x}{m} \ln 2} \right\} = \frac{1}{1-m} \left\{ \frac{1}{2^x} - \frac{1}{2^{\frac{x}{m}}} \right\}, \quad (12.163)$$

(iii) for the depletion-activation model with (12.104) of Prob. 254 expressed as

$$\begin{aligned} y_D^*(x) &= \frac{\mathcal{A}_D(t)}{\sigma_P \dot{\phi} N_P(0)} = \frac{1}{\varepsilon^* (1-m^*)} \left\{ e^{-x \ln 2} - e^{-\frac{x}{m^*} \ln 2} \right\} \\ &= \frac{1}{\varepsilon^* (1-m^*)} \left\{ \frac{1}{2^x} - \frac{1}{2^{\frac{x}{m^*}}} \right\}. \end{aligned} \quad (12.164)$$

Table 12.10 Neutron activation of Ir-191 into Ir-192 in thermal neutron fluence rate $\dot{\phi}$ of $10^{14} \text{ cm}^{-2} \cdot \text{s}^{-1}$ listing: (i) normalized number $y_{\text{Ir-191}}$ of Ir-191 nuclei calculated with (12.161); (ii) normalized activity $z_{\text{Ir-192}}$ of Ir-192 calculated for saturation model with (12.162); (iii) normalized activity $y_{\text{Ir-192}}$ calculated for depletion model with (12.163); and (iv) normalized activity $y_{\text{Ir-192}}^*$ of Ir-192 calculated for depletion–activation model with (12.164)

x	$y_{\text{Ir-191}}$	$z_{\text{Ir-192}}$	$y_{\text{Ir-192}}$	$y_{\text{Ir-192}}^*$	x	$y_{\text{Ir-191}}$	$z_{\text{Ir-192}}$	$y_{\text{Ir-192}}$	$y_{\text{Ir-192}}^*$
0	1.000	0	0	0	3.0	0.125	0.906	0.257	0.085
0.5	0.707	0.326	0.273	0.213	3.5	0.088	0.937	0.207	0.061
1.0	0.500	0.546	0.376	0.237	4.0	0.063	0.958	0.164	0.043
1.5	0.354	0.694	0.390	0.202	4.5	0.044	0.971	0.127	0.031
2.0	0.250	0.794	0.359	0.157	5.0	0.031	0.981	0.098	0.022
2.5	0.177	0.861	0.310	0.116	5.5	0.022	0.987	0.074	0.015

Normalized number of parent nuclei $y_{\text{Ir-191}}$ as well as normalized daughter activities $z_{\text{Ir-192}}$ for the saturation model, $y_{\text{Ir-192}}$ for the depletion model, and $y_{\text{Ir-192}}^*$ for the depletion–activation model were calculated for normalized time x using (12.161), (12.162), (12.163), and (12.164), respectively, and the results are displayed in Table 12.10 and Fig. 12.5. Data were calculated for normalized time x in the range from $x = 0$ to $x = 5.5$ in increments of 0.5 and for neutron fluence rate $\dot{\phi}$ of $10^{14} \text{ cm}^{-2} \cdot \text{s}^{-1}$.

Several features of the data displayed in Fig. 12.5 are of note:

- (1) Plot of $y_{\text{Ir-191}}$ is the same for the three activation models.
- (2) Normalized activity of Ir-192 saturates at $z_{\text{Ir-192}} = 1$ at large x for the saturation model and displays a maximum for the depletion model and depletion–activation models.
- (3) Maximum in normalized activity of Ir-192 occurs at the point of ideal equilibrium at $(x_{\text{Ir-192}})_{\text{max}}$ for the depletion model, while for the depletion–activation model it occurs at $(x_{\text{Ir-192}}^*)_{\text{max}} < (x_{\text{Ir-192}})_{\text{max}}$.
- (4) Maximum $(y_{\text{Ir-192}})_{\text{max}}$ for the depletion model at the point of ideal equilibrium exceeds the maximum $(y_{\text{Ir-192}}^*)_{\text{max}}$ for the parent depletion–daughter activation model.

(b) The maximum specific activity $(a_{\text{D}}^*)_{\text{max}}$ for the depletion–activation model (T12.59) is determined from (12.164) and (12.160) using the following expression

$$\begin{aligned}
 (a_{\text{D}}^*)_{\text{max}} &= \frac{(\mathcal{A}_{\text{D}}^*)_{\text{max}}}{M_{\text{D}}} = \frac{\sigma_{\text{P}} \dot{\phi} N_{\text{P}}(0)}{M_{\text{D}}} (y_{\text{D}}^*)_{\text{max}} \approx \frac{\sigma_{\text{P}} \dot{\phi} N_{\text{A}}}{A_{\text{P}}} (y_{\text{D}}^*)_{\text{max}} \\
 &= \frac{\sigma_{\text{P}} N_{\text{A}}}{A_{\text{P}}} \frac{\dot{\phi}}{\varepsilon^*} (m^*)^{\frac{m^*}{1-m^*}}.
 \end{aligned} \tag{12.165}$$

Furthermore, the maximum in specific activity $(a_{\text{D}}^*)_{\text{max}}$ occurs at normalized time $(x_{\text{D}}^*)_{\text{max}}$ determined by setting $dy_{\text{D}}^*/dx|_{x=(x_{\text{D}}^*)_{\text{max}}} = 0$ at $x = (x_{\text{D}}^*)_{\text{max}}$ and solving for

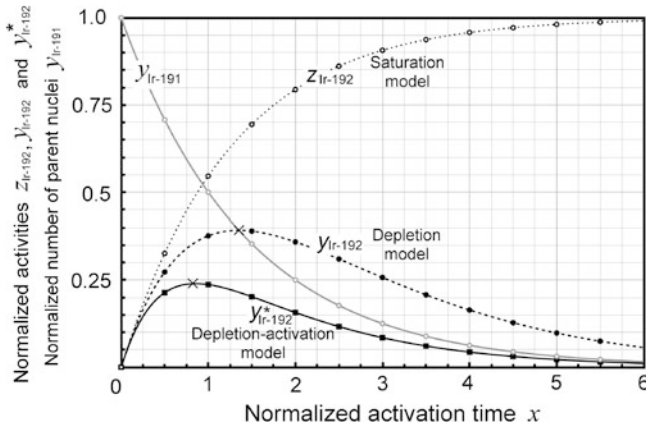


Fig. 12.5 (i) Normalized number $y_{\text{Ir-191}}$ of Ir-191 nuclei (*light solid curve*) calculated with (12.161); (ii) normalized activity $z_{\text{Ir-191}}$ of Ir-192 nuclei (*dotted curve*) calculated for saturation model with (12.162); (iii) normalized activity $y_{\text{Ir-192}}$ of Ir-192 nuclei (*dashed curve*) calculated for depletion model with (12.163); and (iv) normalized activity $y_{\text{Ir-191}}^*$ of Ir-192 nuclei (*heavy solid curve*) calculated for depletion–activation model with (12.164), all plotted against normalized activation time x for neutron activation of Ir-191 into Ir-192 in thermal neutron fluence rate $\dot{\phi}$ of $10^{14} \text{ cm}^{-2} \cdot \text{s}^{-1}$. Maxima in $y_{\text{Ir-192}}(x)$ and $y_{\text{Ir-192}}^*(x)$ are indicated with \times

$(x_{\text{D}}^*)_{\text{max}}$ to get the expression given in (12.158)

$$(x_{\text{D}}^*)_{\text{max}} = \frac{m^* \ln m^*}{(m^* - 1) \ln 2}. \tag{12.166}$$

We now use the parent depletion–daughter activation model to determine with (UU) the maximum attainable specific activity $(a_{\text{Ir-192}}^*)_{\text{max}}$ and with (12.166) the normalized activation time $(x_{\text{Ir-192}}^*)_{\text{max}}$ required to attain $(a_{\text{Ir-192}}^*)_{\text{max}}$ in neutron activation of parent P (Ir-191) into daughter D (Ir-192) for five thermal neutron fluence rates $\dot{\phi}$ in $(\text{cm}^{-2} \cdot \text{s}^{-1})$: 5×10^{11} , 2×10^{13} , 1×10^{14} , 3×10^{14} , and 1.2×10^{16} . In addition to basic parameters: parent thermal neutron cross section $\sigma_{\text{P}} = \sigma_{\text{Ir-191}} = 954 \text{ b}$, daughter thermal neutron cross section $\sigma_{\text{D}} = \sigma_{\text{Ir-192}} = 1420 \text{ b}$, and parent atomic mass $A_{\text{P}} = A_{\text{Ir-191}} = 190.96 \text{ g/mol}$, the other relevant parameters used in the calculations are listed in Table 12.11.

In Table 12.12 we list the maximum attainable specific activities $(a_{\text{Ir-192}})_{\text{max}}$ and $(a_{\text{Ir-192}}^*)_{\text{max}}$ as well as the associated normalized activation times $(x_{\text{Ir-192}})_{\text{max}}$ and $(x_{\text{Ir-192}}^*)_{\text{max}}$ for neutron activation of Ir-191 into Ir-192 with various neutron fluence rates $\dot{\phi}$ calculated for depletion and depletion–activation models, respectively. The data for the depletion model were determined in Prob. 256, data for the depletion–activation model were calculated with (12.165) and (12.166), respectively.

Several interesting conclusions, with regard to the maximum attainable specific activity and characteristic activation time can be reached based on information given in Table 12.12. We note that for all neutron fluence rates $\dot{\phi}$:

Table 12.11 Basic parameters of thermal neutron activation of Ir-191 into Ir-192 for the depletion model and the parent depletion–daughter activation model for various thermal neutron fluence rates $\dot{\phi}$

(1) $\dot{\phi}$ ($\text{cm}^{-2} \cdot \text{s}^{-1}$)	5×10^{11}	2×10^{13}	1×10^{14}	3×10^{14}	1.2×10^{16}
(2) $\lambda_{\text{Ir-192}}^*$	1.094×10^{-7}	1.371×10^{-7}	2.51×10^{-7}	5.347×10^{-7}	1.175×10^{-5}
(3) $\varepsilon^* = \lambda_{\text{Ir-192}}^*/\lambda_{\text{Ir-192}}$	1.007	1.261	2.310	4.919	157.8
(4) $m = \sigma_{\text{Ir-192}}\dot{\phi}/\lambda_{\text{P}}$	4.388×10^{-3}	1.755×10^{-1}	0.878	2.633	105.3
(5) $m^* = m/\varepsilon^*$	4.36×10^{-3}	1.39×10^{-1}	0.381	5.35×10^{-1}	6.68×10^{-1}

Table 12.12 Maximum attainable specific activities $(a_{\text{Ir-192}})_{\text{max}}$ and $(a_{\text{Ir-192}}^*)_{\text{max}}$ as well as the associated normalized activation times $(x_{\text{D}})_{\text{max}}$ and $(x_{\text{D}}^*)_{\text{max}}$ calculated for neutron activation of Ir-191 into Ir-192 using depletion and depletion–activation models, respectively

(1) $\dot{\phi}$ ($\text{cm}^{-2} \cdot \text{s}^{-1}$)	5×10^{11}	2×10^{13}	1×10^{14}	3×10^{14}	1.2×10^{16}
(2) $(x_{\text{Ir-192}})_{\text{max}}$	0.035	0.543	1.35	2.24	6.85
(3) $(x_{\text{Ir-192}}^*)_{\text{max}}$	0.0343	0.460	0.86	1.038	1.171
(4) $(x_{\text{Ir-192}})_{\text{max}}/(x_{\text{Ir-192}}^*)_{\text{max}}$	1.03	1.18	1.57	2.15	5.85
(5) $(x_{\text{Ir-192}})_{\text{max}} - (x_{\text{Ir-192}}^*)_{\text{max}}$	0.001	0.083	0.49	1.20	5.68
(6) $(a_{\text{Ir-192}})_{\text{max}}$ (Ci/g)	39.7	1120	3177	5120	8860
(7) $(a_{\text{Ir-192}}^*)_{\text{max}}$ (Ci/g)	39.24	932.5	1937	2402	2733
(7) $(a_{\text{Ir-192}})_{\text{max}}/(a_{\text{Ir-192}}^*)_{\text{max}}$	1.01	1.20	1.64	2.13	3.24
(8) $(a_{\text{Ir-192}})_{\text{max}} - (a_{\text{Ir-192}}^*)_{\text{max}}$	0.5	187	1240	2718	6127

- (1) Normalized characteristic activation time $(x_{\text{Ir-192}})_{\text{max}}$ for the depletion model exceeds $(x_{\text{Ir-192}}^*)_{\text{max}}$ for the depletion–activation model.
- (2) Ratio $(x_{\text{Ir-192}})_{\text{max}}/(x_{\text{Ir-192}}^*)_{\text{max}}$ increases from ~ 1 at low fluence rate $\dot{\phi} = 5 \times 10^{11} \text{ cm}^{-2} \cdot \text{s}^{-1}$ through ~ 1.6 at intermediate fluence rate $\dot{\phi} = 5 \times 10^{13} \text{ cm}^{-2} \cdot \text{s}^{-1}$ to ~ 6 at high fluence rate $\dot{\phi} = 1.2 \times 10^{16} \text{ cm}^{-2} \cdot \text{s}^{-1}$. Thus, the difference between $(x_{\text{Ir-192}})_{\text{max}}$ and $(x_{\text{Ir-192}}^*)_{\text{max}}$ increases with fluence rate $\dot{\phi}$.
- (3) Maximum attainable specific activity $(a_{\text{Ir-192}})_{\text{max}}$ for the depletion model exceeds $(a_{\text{Ir-192}}^*)_{\text{max}}$ for the depletion–activation model. This is explained by the loss of daughter D nuclei to nuclear activation that is ignored in the depletion model but is accounted for in the depletion–activation model.
- (4) Ratio $(a_{\text{Ir-192}})_{\text{max}}/(a_{\text{Ir-192}}^*)_{\text{max}}$ increases from ~ 1 at low fluence rate $\dot{\phi} = 5 \times 10^{11} \text{ cm}^{-2} \cdot \text{s}^{-1}$ through ~ 1.6 at intermediate fluence rate $\dot{\phi} = 5 \times 10^{13} \text{ cm}^{-2} \cdot \text{s}^{-1}$ to ~ 3.5 at high fluence rate $\dot{\phi} = 1.2 \times 10^{16} \text{ cm}^{-2} \cdot \text{s}^{-1}$. Thus, the difference between $(a_{\text{Ir-192}})_{\text{max}}$ and $(a_{\text{Ir-192}}^*)_{\text{max}}$ increases with fluence rate $\dot{\phi}$.

12.6.Q8

(258)

Three models are used for describing nuclear activation processes. Listed in order of increasing complexity they are: (1) Saturation model, (2) Depletion model, and (3) Depletion–activation model. The three models predict different expressions for normalized daughter D activity $y_D(x)$ as well as for the maximum daughter activity $(a_D)_{\max}$ attainable in nuclear activation. Expressions for $(a_D)_{\max}$ derived in Prob. 256 for the saturation and depletion models and in Prob. 257 for the depletion–activation model are, respectively, given as

$$(a_D)_{\max} = \frac{\sigma_P N_A}{A_P} \dot{\phi} \quad [\text{see (12.137) in Prob. 256}], \quad (12.167)$$

$$(a_D)_{\max} = \frac{\sigma_P N_A}{A_P} \dot{\phi} m^{\frac{m}{1-m}} \quad [\text{see (12.140) in Prob. 256}], \quad (12.168)$$

$$(a_D^*)_{\max} = \frac{\sigma_P N_A}{A_P} \frac{\dot{\phi}}{\epsilon^*} (m^*)^{\frac{m^*}{1-m^*}} \quad [\text{see (12.165) in Prob. 257}], \quad (12.169)$$

where m and m^* are activation factors defined as $m = \sigma_P \dot{\phi} / \lambda_D$ and $m^* = \sigma_P \dot{\phi} / (\lambda_D + \sigma_D \dot{\phi})$, respectively, with σ_P and σ_D the parent P and daughter D activation cross sections, respectively, $\dot{\phi}$ the fluence rate, and λ_D the daughter decay constant.

At first glance the three models seem to suggest that $(a_D)_{\max}$ is linearly proportional to $\dot{\phi}$, irrespective of the magnitude of $\dot{\phi}$, making $(a_D)_{\max}$ go to ∞ as $\dot{\phi} \rightarrow \infty$. This contradicts the standard relationship for specific activity $(a_D)_{\text{theor}}$ of a radionuclide D which states that $(a_D)_{\text{theor}}$ is finite and proportional to λ_D / A_D where λ_D and A_D are the decay constant and atomic mass of the radionuclide D and N_A , the Avogadro number, is the proportionality constant. The obvious conclusion is that $(a_D)_{\max}$ cannot exceed $(a_D)_{\text{theor}} = \lambda_D N_A / A_D$ irrespective of magnitude of $\dot{\phi}$.

-
- (a) Show that (12.168) for depletion model and (12.169) for depletion–activation model fulfill the condition $\lim_{\dot{\phi} \rightarrow \infty} (a_D)_{\max} \leq (a_D)_{\text{theor}}$ in contrast to (12.167) which predicts that, as $\dot{\phi} \rightarrow \infty$, $\lim_{\dot{\phi} \rightarrow \infty} (a_D)_{\max} = \infty$ producing a physically impossible result $(a_D)_{\max} \gg (a_D)_{\text{theor}}$.
- (b) Show that the ratio between $\lim_{\dot{\phi} \rightarrow \infty} (a_D^*)_{\max}$ for the depletion–activation model and $\lim_{\dot{\phi} \rightarrow \infty} (a_D)_{\max}$ for the depletion model is equal to a factor g^* that depends only on the parent–daughter cross section ratio $k^* = \sigma_P / \sigma_D$.
- (c) Calculate and plot the depletion–activation factor $g^*(k^*)$ against the parent–daughter cross section ratio k^* for k^* of 10^{-3} , 10^{-2} , 10^{-1} , 1, 10, 100, and 1000. Discuss a few notable properties of $g^*(k^*)$.

SOLUTION:

(a) Equations for the maximum attainable specific activity $(a_D)_{\max}$ given for the three nuclear activation models above depend linearly on the fluence rate $\dot{\phi}$ and for $\dot{\phi} \rightarrow \infty$ seemingly contradict the expression for $(a_D)_{\text{theor}}$ that predicts a definite and finite upper limit for $(a_D)_{\max}$. This apparent contradiction can be explained by evaluating the implicit dependence of activation factors m and m^* on $\dot{\phi}$.

- (1) The maximum specific activity $(a_D)_{\max}$ given in (12.167) for the saturation model of nuclear activation is proportional to fluence rate $\dot{\phi}$ and predicts clearly that, with increasing $\dot{\phi}$, $(a_D)_{\max}$ will eventually exceed $(a_D)_{\text{theor}} = \lambda_D N_A / A_P$ and, as $\dot{\phi} \rightarrow \infty$, $(a_D)_{\max} \rightarrow \infty$. Since $(a_D)_{\max}$ cannot exceed $(a_D)_{\text{theor}}$, we note that the validity of (12.167) is limited and some of its predictions cannot be trusted.
- (2) At first glance it seems that $(a_D)_{\max}$ given by (12.168) for the depletion model is, like (12.167) for the saturation model, proportional to $\dot{\phi}$ and therefore also exceeds the theoretical specific activity $(a_D)_{\text{theor}}$ for $\dot{\phi} \rightarrow \infty$. However, a closer look at $\lim_{\dot{\phi} \rightarrow \infty} (a_D)_{\max}$ for (12.168) produces a logical result, namely that the maximum daughter specific activity $(a_D)_{\max}$ derived from (12.168) does not exceed $(a_D)_{\text{theor}} = \lambda_D N_A / A_P$ even for $\dot{\phi} \rightarrow \infty$. Actually, in determining the limit of (12.168) for $\dot{\phi} \rightarrow \infty$, after introducing the definition of the activation factor $m = \sigma_P \dot{\phi} / \lambda_D$ into (12.168), we show in (12.170) that $\lim_{\dot{\phi} \rightarrow \infty} (a_D)_{\max} \approx (a_D)_{\text{theor}}$

$$\begin{aligned}
 \lim_{\dot{\phi} \rightarrow \infty} (a_D)_{\max} &= \frac{\sigma_P N_A}{A_P} \lim_{\dot{\phi} \rightarrow \infty} \left\{ \dot{\phi} m^{\frac{m}{1-m}} \right\} = \frac{\sigma_P N_A}{A_P} \lim_{\dot{\phi} \rightarrow \infty} \left\{ \dot{\phi} e^{\frac{m \ln m}{1-m}} \right\} \\
 &= \frac{\sigma_P N_A}{A_P} \lim_{\dot{\phi} \rightarrow \infty} \left\{ \dot{\phi} \exp \left[\frac{\frac{\sigma_P \dot{\phi}}{\lambda_D}}{1 - \frac{\sigma_P \dot{\phi}}{\lambda_D}} \ln \frac{\sigma_P \dot{\phi}}{\lambda_D} \right] \right\} \\
 &= \frac{\sigma_P N_A}{A_P} \lim_{\dot{\phi} \rightarrow \infty} \left\{ \dot{\phi} \exp \left[- \ln \frac{\sigma_P \dot{\phi}}{\lambda_D} \right] \right\} \\
 &= \frac{\sigma_P N_A}{A_P} \dot{\phi} \frac{\lambda_D}{\sigma_P \dot{\phi}} = \frac{\lambda_D N_A}{A_P} \approx (a_D)_{\text{theor}}. \tag{12.170}
 \end{aligned}$$

The result of (12.170) for $\dot{\phi} \rightarrow \infty$ is independent of particle fluence $\dot{\phi}$, irrespective of the magnitude of $\dot{\phi}$ and depends only on the decay constant λ_D of the daughter D radionuclide and the atomic mass A_P of the parent. Recognizing that $A_P \approx A_D$, at least for large atomic number activation targets, we can state that for depletion model of nuclear activation $\lambda_D N_A / A_P \approx (a_D)_{\text{theor}}$. Equation (12.170) shows that, according to the depletion model, $(a_D)_{\text{theor}}$ is the maximum specific activity $(a_D)_{\max}$ achievable in nuclear activation even with very high particle fluence rate $\dot{\phi}$.

- (3) It is also interesting to investigate $\lim(a_D)_{\max}$ of (12.168) for $\dot{\phi} \rightarrow 0$ yielding the following result

$$\begin{aligned} \lim_{\dot{\phi} \rightarrow 0} (a_D)_{\max} &= \lim_{m \rightarrow 0} (a_D)_{\max} = \lim_{m \rightarrow 0} \frac{m\lambda_D N_A}{A_P} e^{\frac{m}{1-m} \ln m} = \lim_{m \rightarrow 0} \frac{m\lambda_D N_A}{A_P} e^{\ln m^m} \\ &= \lim_{m \rightarrow 0} \frac{m\lambda_D N_A}{A_P} m^m = \frac{m\lambda_D N_A}{A_P} = \frac{\sigma_P N_A}{A_P} \dot{\phi}, \end{aligned} \quad (12.171)$$

where we note that $\lim_{m \rightarrow 0} m^m = 1$. The result of (12.171) for the depletion model at $\dot{\phi} \rightarrow 0$ is in perfect agreement with (12.167) obtained for the saturation model leading to the conclusion that for small particle fluence rate ($\dot{\phi} \rightarrow 0$) both the saturation model and the depletion model give identical result for $(a_D)_{\max}$ proportional to $\dot{\phi}$. However, as shown in (12.170) for $\dot{\phi} \rightarrow \infty$, the saturation model predicts the physically impossible result of $(a_D)_{\max} \rightarrow \infty$, while (12.170) for the depletion model predicts the logical result that $(a_D)_{\max}$ approaches $(a_D)_{\text{theor}}$.

- (4) We now evaluate $(a_D^*)_{\max}$ of (12.169) as $\dot{\phi} \rightarrow \infty$ for the depletion–activation model. Both m^* and ε^* , defined as

$$m^* = \frac{m}{\varepsilon^*} = \frac{\sigma_P \dot{\phi}}{\lambda_D + \sigma_D \dot{\phi}} \quad (12.172)$$

and

$$\varepsilon^* = \frac{\lambda_D^*}{\lambda_D} = \frac{\lambda_D + \sigma_D \dot{\phi}}{\lambda_D} = 1 + \frac{\sigma_D \dot{\phi}}{\lambda_D}, \quad (12.173)$$

respectively, depend on $\dot{\phi}$ and the limit of $(a_D^*)_{\max}$ as $\dot{\phi} \rightarrow \infty$ is determined as follows

$$\begin{aligned} \lim_{\dot{\phi} \rightarrow \infty} (a_D^*)_{\max} &= \frac{\sigma_P N_A}{A_P} \lim_{\dot{\phi} \rightarrow \infty} \left\{ \frac{\dot{\phi}}{\varepsilon^*} (m^*)^{\frac{m^*}{1-m^*}} \right\} = \frac{\sigma_P N_A}{A_P} \lim_{\dot{\phi} \rightarrow \infty} \left\{ \frac{\dot{\phi}}{\varepsilon^*} e^{\frac{m^* \ln m^*}{1-m^*}} \right\} \\ &= \frac{\sigma_P N_A}{A_P} \lim_{\dot{\phi} \rightarrow \infty} \left\{ \frac{\lambda_D \dot{\phi}}{\lambda_D + \sigma_D \dot{\phi}} \exp \left[\frac{\frac{\sigma_P \dot{\phi}}{\lambda_D + \sigma_D \dot{\phi}}}{1 - \frac{\sigma_P \dot{\phi}}{\lambda_D + \sigma_D \dot{\phi}}} \ln \frac{\sigma_P \dot{\phi}}{\lambda_D + \sigma_D \dot{\phi}} \right] \right\} \\ &= \frac{\sigma_P N_A}{A_P} \lim_{\dot{\phi} \rightarrow \infty} \left\{ \frac{\lambda_D}{\sigma_D} \exp \left[\frac{\frac{\sigma_P}{\sigma_D}}{1 - \frac{\sigma_P}{\sigma_D}} \ln \frac{\sigma_P}{\sigma_D} \right] \right\} \\ &\approx (a_D)_{\text{theor}} k^* e^{\frac{k^* \ln k^*}{1-k^*}}, \end{aligned} \quad (12.174)$$

where we define the parent–daughter cross section ratio σ_P/σ_D as k^* and we make the approximation $A_P \approx A_D$ to be able to use $\lambda_D N_A/A_P \approx (a_D)_{\text{theor}}$. The maximum attainable specific activity $(a_D^*)_{\max}$ as $\dot{\phi} \rightarrow \infty$ for depletion–activation model is according to (12.174) equal to $(a_D^*)_{\text{theor}}$ multiplied by a factor that depends on the parent–daughter cross section ratio k^* .

(b) The ratio between $\lim_{\dot{\varphi} \rightarrow \infty} (a_D^*)_{\max}$ of (12.174) for the depletion–activation model and $\lim_{\dot{\varphi} \rightarrow \infty} (a_D)_{\max}$ of (12.170) for the depletion model is expressed as a function of the parent–daughter cross section ratio $k^* = \sigma_P/\sigma_D$ as follows

$$\frac{\lim_{\dot{\varphi} \rightarrow \infty} (a_D^*)_{\max}}{\lim_{\dot{\varphi} \rightarrow \infty} (a_D)_{\max}} = k^* e^{\frac{k^* \ln k^*}{1-k^*}} = g^*(k^*), \tag{12.175}$$

where we introduce the depletion–activation factor $g^*(k^*)$ and define it as

$$g^*(k^*) = k^* e^{-\frac{k^* \ln k^*}{k^*-1}} = e^{-\frac{\ln k^*}{1-k^*}} = (k^*)^{\frac{1}{1-k^*}}. \tag{12.176}$$

The parent–daughter cross section ratio $k^* = \sigma_P/\sigma_D$ is always positive and ranges from $k^* = 0$ for $\sigma_P = 0$ through $k^* = 1$ for $\sigma_P = \sigma_D$ to $k^* = \infty$ for $\sigma_D = 0$. The depletion–activation factor $g^*(k^*)$, on the other hand, ranges from $g^*(k^*) = 0$ for $k^* = 0$ through $g^*(k^*) = 1/e$ for $k^* = 1$ to $g^*(k^*) = 1$ for $k^* = \infty$. The physical range of $g^*(k^*)$ is determined using the l’Hôpital rule as follows

$$g|_{k^* \rightarrow 0} = \lim_{k^* \rightarrow 0} (k^*)^{\frac{1}{1-k^*}} = \lim_{k^* \rightarrow 0} e^{\frac{\ln k^*}{1-k^*}} = \lim_{k^* \rightarrow 0} e^{\frac{\frac{d \ln k^*}{dk^*}}{\frac{d(1-k^*)}{dk^*}}} = \lim_{k^* \rightarrow 0} e^{\frac{\frac{1}{k^*}}{-1}} = e^{-\infty} = 0, \tag{12.177}$$

$$g|_{k^* \rightarrow 1} = \lim_{k^* \rightarrow 1} (k^*)^{\frac{1}{1-k^*}} = \lim_{k^* \rightarrow 1} e^{\frac{\ln k^*}{1-k^*}} = \lim_{k^* \rightarrow 1} e^{\frac{\frac{d \ln k^*}{dk^*}}{\frac{d(1-k^*)}{dk^*}}} = \lim_{k^* \rightarrow 1} e^{\frac{\frac{1}{k^*}}{-1}} = e^{-1} = \frac{1}{e} \tag{12.178}$$

and

$$\begin{aligned} g|_{k^* \rightarrow \infty} &= \lim_{k^* \rightarrow \infty} (k^*)^{\frac{1}{1-k^*}} = \lim_{k^* \rightarrow \infty} e^{\frac{\ln k^*}{1-k^*}} = \lim_{k^* \rightarrow \infty} e^{\frac{\frac{d \ln k^*}{dk^*}}{\frac{d(1-k^*)}{dk^*}}} \\ &= \lim_{k^* \rightarrow \infty} e^{\frac{\frac{1}{k^*}}{-1}} = e^0 = 1. \end{aligned} \tag{12.179}$$

Equation (12.170) shows that for the depletion model $(a_D)_{\max}$ cannot exceed $(a_D)_{\text{theor}}$ and (12.174) shows that for the depletion–activation model $(a_D)_{\max}$ cannot exceed $(a_D)_{\max}$ multiplied by $g^*(k^*)$. Since $g^*(k^*)$ is smaller than or equal to 1, we conclude that $(a_D)_{\max}$ for the depletion–activation model is generally smaller than $(a_D)_{\max}$ for the depletion model.

Table 12.13 Depletion–activation factor g^* for various values of the parent–daughter cross section ratio k^* in the range from 0.001 to 1000

$k^* = \frac{\sigma_P}{\sigma_D}$	0.001	0.01	0.1	1	10	100	1000
$g^* = (k^*)^{\frac{1}{1-k^*}}$	0.001	0.009	0.077	0.368	0.774	0.955	0.993

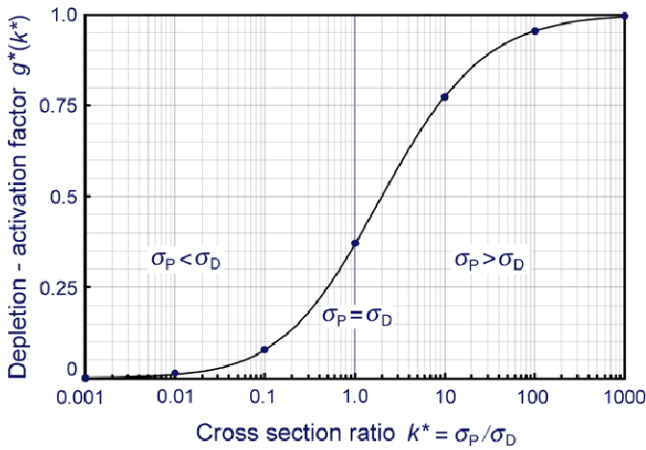


Fig. 12.6 Depletion–activation factor g^* against the parent–daughter cross section ratio k^* in the k^* range from 10^{-3} to 10^3 . In general, k^* ranges from 0 to ∞ while correspondingly g^* ranges from 0 to 1

(c) As shown in (12.177) the depletion–activation factor g^* depends on the parent–daughter cross section ratio k^* which has a physical range from 0 to ∞ . Table 12.13 and Fig. 12.6 display results of our calculation of g^* for several values of k^* in the range from 10^{-3} to 10^3 . Based on the g^* vs k^* plot we note the following characteristics of the depletion–activation factor g^* :

- (1) The range of g^* is from $g^* = 0$ for $k^* = 0$ ($\sigma_P = 0$) through $g^* = 1/e$ for $k^* = 1$ ($\sigma_P = \sigma_D$) to $g^* = 1$ for $k^* = \infty$ ($\sigma_D = 0$), as shown in (12.177), (12.178), and (12.179), respectively.
- (2) Since $(a_D^*)_{\max} \approx (a_D^*)_{\text{theor}} g^*$, as derived in (12.174), and the range of g^* is given as $0 \leq g^* \leq 1$, we conclude that $(a_D^*)_{\max} \leq (a_D^*)_{\text{theor}}$.
- (3) For $g^* = 0$, i.e., $\sigma_P = 0$, we get from (12.174) that $(a_D^*)_{\max} = 0$. This means that there is no parent activation and no production of radioactivity.
- (4) For $g^* = 1$, i.e., $\sigma_D = 0$, we get from (12.174) that $(a_D^*)_{\max} = (a_D)_{\text{theor}}$. This means that the daughter produced in activation does not get activated, so that the depletion model and the depletion–activation model give the same result for the maximum attainable daughter specific activity: $(a_D^*)_{\max} = (a_D)_{\max} = (a_D)_{\text{theor}} = \lambda_P N_A / A_D$.
- (5) For $\sigma_P < \sigma_D$, $k^* < 1$ and $0 < g^* < 1/e$.
- (6) For $\sigma_P = \sigma_D$, $k^* = 1$ and $g^* = 1/e$.
- (7) For $\sigma_P > \sigma_D$, $k^* > 1$ and $1/e < g^* < 1$.

12.6.Q9

(259)

To date, out of over 3500 known radionuclides only four (cesium-137, cobalt-60, europium-152, and radium-226) meet requirements for use in external beam radiotherapy and, of these, only cobalt-60 has gained widespread use as teletherapy source material. Cobalt-60 radionuclide is produced in a nuclear reactor through thermal neutron activation of stable cobalt-59.

A 10 g sample of cobalt-59 (atomic mass $M = 58.93$ g/mol) is irradiated with thermal neutrons in a nuclear reactor with thermal neutron fluence rate $\dot{\phi} = 1.2 \times 10^{13} \text{ cm}^{-2} \cdot \text{s}^{-1}$. Thermal neutron cross section $\sigma_{\text{Co-59}}$ of cobalt-59 is 37 b/atom and the half-life $(t_{1/2})_{\text{Co-60}}$ of cobalt-60 is 5.26 a, where a stands for year (annum).

- (a) Using the *saturation model* of neutron activation, discussed in Prob. 251 (12.44), calculate: (1) Saturation activity $(\mathcal{A}_{\text{Co-60}})_{\text{sat}}$, (2) Activity $\mathcal{A}_{\text{Co-60}}(t)$ against activation time t in steps of 1 year in the range $0 \leq t \leq 30$ a, and (3) Activation time t required for the sample activity $\mathcal{A}_{\text{Co-60}}(t)$ to reach 25 %, 50 %, 75 %, 90 %, and 100 % of saturation activity $(\mathcal{A}_{\text{Co-60}})_{\text{sat}}$.
- (b) Using the *depletion model* of neutron activation, discussed in Prob. 251 (12.48), calculate: (1) Activity $\mathcal{A}_{\text{Co-60}}(t)$ against activation time t in steps of 1 year in the range $0 \leq t \leq 30$ a, (2) Characteristic activation time $(t_{\text{max}})_{\text{Co-60}}$ required for the sample activity $\mathcal{A}_{\text{Co-60}}(t)$ to reach its maximum activity $(\mathcal{A}_{\text{Co-60}})_{\text{max}}$, (3) Maximum activity $(\mathcal{A}_{\text{Co-60}})_{\text{max}}$, and (4) Activation time t required for the sample activity $\mathcal{A}_{\text{Co-60}}(t)$ to reach fraction f of its maximum activity $(\mathcal{A}_{\text{Co-60}})_{\text{max}}$ for $f = 0.25, 0.50, 0.75, 0.90,$ and 1.00 .
- (c) Radioactivation yield Y_{D} of the daughter activation product is defined by the initial slope $d\mathcal{A}_{\text{D}}/dt$ of the $\mathcal{A}_{\text{D}}(t)$ curve at $t = 0$ (T12.14). Determine $Y_{\text{Co-60}}$ for the saturation model (T12.13) of (a) and the depletion model (T12.22) of (b).
- (d) On one graph plot the activity data of (a) for the saturation model with open circles and (b) for the depletion model with solid circles. On the saturation curve indicate the saturation activity $(\mathcal{A}_{\text{Co-60}})_{\text{sat}}$ and on the depletion curve indicate the maximum activity $(\mathcal{A}_{\text{Co-60}})_{\text{max}}$.

SOLUTION:

Recalling that half-life $(t_{1/2})_{\text{Co-60}} = 5.26$ a the decay constant of cobalt-60 is given as follows

$$\lambda_{\text{Co-60}} = \frac{\ln 2}{(t_{1/2})_{\text{Co-60}}} = \frac{\ln 2}{5.26 \text{ a}} = 0.1318 \text{ a}^{-1}$$

$$\begin{aligned}
 &= \frac{\ln 2}{(5.26 \text{ a}) \times (365 \text{ d/a}) \times (24 \text{ h/d}) \times (3600 \text{ s/h})} \\
 &= 4.179 \times 10^{-9} \text{ s}^{-1}.
 \end{aligned} \tag{12.180}$$

The product $\sigma_{\text{Co-59}}\dot{\phi}$ plays an important role in neutron activation theory and has, for our example that deals with cobalt-59 to cobalt-60 neutron activation in a nuclear reactor with thermal neutron fluence rate of $\dot{\phi} = 1.2 \times 10^{13} \text{ cm}^{-2} \cdot \text{s}^{-1}$, the following value

$$\begin{aligned}
 \sigma_{\text{Co-59}}\dot{\phi} &= (37 \times 10^{-24} \text{ cm}^2) \times (1.2 \times 10^{13} \text{ cm}^{-2} \cdot \text{s}^{-1}) = 4.44 \times 10^{-10} \text{ s}^{-1} \\
 &= 0.014 \text{ a}^{-1}.
 \end{aligned} \tag{12.181}$$

(a) Infinite number of parent nuclei: Saturation model

Activity $\mathcal{A}_{\text{Co-60}}(t)$ as a function of activation time t is in the saturation model expressed as follows (T12.13)

$$\mathcal{A}_{\text{Co-60}}(t) = \sigma_{\text{Co-59}}\dot{\phi}N_{\text{Co-59}}(0)[1 - e^{-\lambda_{\text{Co-60}}t}] = (\mathcal{A}_{\text{Co-60}})_{\text{sat}}[1 - e^{-\lambda_{\text{Co-60}}t}], \tag{12.182}$$

where the saturation activity $(\mathcal{A}_{\text{Co-60}})_{\text{sat}}$ is defined as

$$(\mathcal{A}_{\text{Co-60}})_{\text{sat}} = \sigma_{\text{Co-59}}\dot{\phi}N_{\text{Co-59}}(0), \tag{12.183}$$

with $N_{\text{Co-59}}(0)$ the initial number of Co-59 nuclei placed at activation time $t = 0$ into the nuclear reactor with thermal neutron fluence rate $\dot{\phi}$ of $1.2 \times 10^{13} \text{ cm}^{-2} \cdot \text{s}^{-1}$

$$N_{\text{Co-59}}(0) = \frac{N_{\text{A}}}{A}m = \frac{6.022 \times 10^{23} \text{ mol}^{-1}}{58.93 \text{ g} \cdot \text{mol}^{-1}} \times (10 \text{ g}) = 1.022 \times 10^{23}. \tag{12.184}$$

(1) After inserting (12.181) and (12.184) into (12.183), we now determine the saturation activity $(\mathcal{A}_{\text{Co-60}})_{\text{sat}}$ for our neutron activation example as follows

$$\begin{aligned}
 (\mathcal{A}_{\text{Co-60}})_{\text{sat}} &= \sigma_{\text{Co-59}}\dot{\phi}N_{\text{Co-59}}(0) = (4.44 \times 10^{-10} \text{ s}^{-1}) \times (1.022 \times 10^{23}) \\
 &= 4.537 \times 10^{13} \text{ s}^{-1} = 4.537 \times 10^{13} \text{ Bq} = \frac{4.537 \times 10^{13} \text{ Bq}}{3.7 \times 10^{10} \text{ Bq/Ci}} \\
 &= 1226.3 \text{ Ci}.
 \end{aligned} \tag{12.185}$$

(2) After inserting (12.185) into (12.182), the activity $\mathcal{A}_{\text{Co-60}}(t)$ of the sample as a function of activation time t is now given as

$$\begin{aligned}
 \mathcal{A}_{\text{Co-60}}(t) &= (\mathcal{A}_{\text{Co-60}})_{\text{sat}}[1 - e^{-\lambda_{\text{Co-60}}t}] \\
 &= (4.537 \times 10^{13} \text{ Bq}) \times [1 - e^{-(4.179 \times 10^{-9} \text{ s}^{-1})t}] \\
 &= (1226.3 \text{ Ci}) \times [1 - e^{-(0.1318 \text{ a}^{-1})t}].
 \end{aligned} \tag{12.186}$$

Table 12.14 Activity $\mathcal{A}_{\text{Co-60}}(t)$ of cobalt-60 for various activation times t in the range $0 \leq t \leq 30$ a (where a stands for year) calculated for the saturation model of neutron activation, as given in (12.186) under the following conditions: mass of cobalt-59 sample $m = 59$ g; neutron fluence rate $\dot{\phi} = 1.2 \times 10^{13} \text{ cm}^{-2} \cdot \text{s}^{-1}$

t (a)	$\mathcal{A}_{\text{Co-60}}(t)$	t (a)	$\mathcal{A}_{\text{Co-60}}(t)$	t (a)	$\mathcal{A}_{\text{Co-60}}(t)$	t (a)	$\mathcal{A}_{\text{Co-60}}(t)$
0	0	8	799.06	16	1077.45	24	1174.44
1	151.43	9	851.81	17	1095.83	25	1180.84
2	284.16	10	898.06	18	1111.94	26	1186.46
3	400.50	11	938.59	19	1126.06	27	1094.22
4	502.47	12	974.12	20	1138.44	28	1195.69
5	591.85	13	1005.26	21	1149.29	29	1199.47
6	670.20	14	1032.55	22	1158.80	30	1202.78
7	738.87	15	1056.48	23	1167.13	∞	1226.30

Table 12.15 Time t in years (a) and in cobalt-60 half-lives $(t_{1/2})_{\text{Co-60}} = 5.26$ a required for sample activity $\mathcal{A}_{\text{Co-60}}(t)$ to reach a given fraction $f_{\text{Co-60}} = \mathcal{A}_{\text{Co-60}}(t)/(\mathcal{A}_{\text{Co-60}})_{\text{sat}}$ of the saturation activity $(\mathcal{A}_{\text{Co-60}})_{\text{sat}}$

$f_{\text{Co-60}}$	0.25	0.50	0.75	0.90	1.00
$1 - f_{\text{Co-60}}$	0.75	0.50	0.25	0.10	0
t (a)	2.18	5.26	10.52	17.5	∞
$t [(t_{1/2})_{\text{Co-60}}]$	0.41	1.0	2.0	3.33	∞

Activities $\mathcal{A}_{\text{Co-60}}(t)$ of cobalt-60 calculated from (12.186) for the saturation model of neutron activation in steps of 1 year for activation times $0 \leq t \leq 30$ a are listed in Table 12.14.

(3) To estimate the activation time t during which a given activity fraction $f_{\text{Co-60}}$ of $(\mathcal{A}_{\text{Co-60}})_{\text{sat}}$ is attained we modify (12.182) as follows

$$\frac{\mathcal{A}_{\text{Co-60}}(t)}{(\mathcal{A}_{\text{Co-60}})_{\text{sat}}} = f_{\text{Co-60}} = 1 - e^{-\lambda_{\text{Co-60}}t}. \tag{12.187}$$

Solving (12.187) for activation time t gives

$$t = -\frac{-\ln(1 - f_{\text{Co-60}})}{\lambda_{\text{Co-60}}} = \frac{\ln \frac{1}{1 - f_{\text{Co-60}}}}{\lambda_{\text{Co-60}}}. \tag{12.188}$$

Results of (12.188) for activity fractions $\lambda_{\text{Co-60}}$ of 0.25, 0.50, 0.75, 0.90, and 1.0 are given in Table 12.15.

(b) Finite number of parent nuclei: Depletion model

Activity $\mathcal{A}_{\text{Co-60}}(t)$ as a function of activation time t is in the depletion model expressed as follows (T12.22)

$$\begin{aligned}\mathcal{A}_{\text{Co-60}}(t) &= (\sigma_{\text{Co-59}}\dot{\phi})N_{\text{Co-59}}(0)\frac{\lambda_{\text{Co-60}}}{\lambda_{\text{Co-60}} - \sigma_{\text{Co-59}}\dot{\phi}}\left[e^{-\sigma_{\text{Co-59}}\dot{\phi}t} - e^{-\lambda_{\text{Co-60}}t}\right] \\ &= \mathcal{A}_0\left[e^{-\sigma_{\text{Co-59}}\dot{\phi}t} - e^{-\lambda_{\text{Co-60}}t}\right],\end{aligned}\quad (12.189)$$

where \mathcal{A}_D is a parameter of the depletion model, dependent on neutron cross section $\sigma_{\text{Co-59}}$ of the Co-59 nucleus, neutron fluence rate $\dot{\phi}$ in the reactor, and the initial number $N_{\text{Co-59}}(0)$ of Co-59 nuclei placed into the reactor, as well as the decay constant $\lambda_{\text{Co-60}}$. Parameter \mathcal{A}_0 of (12.189) is fortuitously related to the saturation activity $(\mathcal{A}_{\text{Co-60}})_{\text{sat}}$ of the saturation model given in (12.185) and is for our neutron activation example given as follows

$$\begin{aligned}\mathcal{A}_0 &= (\sigma_{\text{Co-59}}\dot{\phi})N_{\text{Co-59}}(0)\frac{\lambda_{\text{Co-60}}}{\lambda_{\text{Co-60}} - \sigma_{\text{Co-59}}\dot{\phi}} = (\mathcal{A}_{\text{Co-60}})_{\text{sat}}\frac{\lambda_{\text{Co-60}}}{(\lambda_{\text{Co-60}} - \sigma_{\text{Co-59}}\dot{\phi})} \\ &= (4.537 \times 10^{13} \text{ s}^{-1}) \times \frac{(4.179 \times 10^{-9} \text{ s}^{-1})}{(4.179 \times 10^{-9} \text{ s}^{-1} - 0.444 \times 10^{-9} \text{ s}^{-1})} \\ &= 5.076 \times 10^{13} \text{ s}^{-1} = 50.76 \text{ TBq} = \frac{5.076 \times 10^{13} \text{ Bq}}{3.7 \times 10^{10} \text{ Bq/Ci}} \\ &= 1372.19 \text{ Ci}.\end{aligned}\quad (12.190)$$

(1) Following the depletion model of neutron activation, after inserting (12.180), (12.181), and (12.190) into (12.188), the activity $\mathcal{A}_{\text{Co-60}}(t)$ as a function of activation time t is expressed as

$$\begin{aligned}\mathcal{A}_{\text{Co-60}}(t) &= \mathcal{A}_0\left[e^{-\sigma_{\text{Co-59}}\dot{\phi}t} - e^{-\lambda_{\text{Co-60}}t}\right] \\ &= (1372.19 \text{ Ci}) \times \left[e^{-(0.014 \text{ a}^{-1})t} - e^{-0.132 \text{ a}^{-1}t}\right] \\ &= (5.077 \times 10^{13} \text{ Bq}) \times \left[e^{-(0.444 \times 10^{-9} \text{ s}^{-1})t} - e^{-4.179 \times 10^{-9} \text{ s}^{-1}t}\right].\end{aligned}\quad (12.191)$$

(2) For the depletion model, the activity $\mathcal{A}_{\text{Co-60}}$ is 0 at activation time $t = 0$, rises with t until it reaches a maximum $(\mathcal{A}_{\text{Co-60}})_{\text{max}}$ at characteristic activation time $t = (t_{\text{Co-60}})_{\text{max}}$, then it decreases with t and asymptotically approaches 0 at $t \rightarrow \infty$. The characteristic activation time $(t_{\text{max}})_{\text{Co-60}}$, at which activity maximum $(\mathcal{A}_{\text{Co-60}})_{\text{max}}$ occurs, is given by the following expression (T12.24), determined from setting to zero the derivative of (12.191) with respect to activation time t . For our specific example the characteristic time $(t_{\text{max}})_{\text{Co-60}}$ is given as

$$(t_{\text{max}})_{\text{Co-60}} = \frac{\ln \frac{\lambda_{\text{Co-60}}}{\sigma_{\text{Co-59}}\dot{\phi}}}{\lambda_{\text{Co-60}} - \sigma_{\text{Co-59}}\dot{\phi}} = \frac{\ln \frac{4.179 \times 10^{-9} \text{ s}^{-1}}{0.444 \times 10^{-9} \text{ s}^{-1}}}{4.179 \times 10^{-9} \text{ s}^{-1} - 0.444 \times 10^{-9} \text{ s}^{-1}}$$

$$= 6.003 \times 10^8 \text{ s} = 19.03 \text{ a.} \quad (12.192)$$

(3) The maximum activity $(\mathcal{A}_{\text{Co-60}})_{\text{max}}$ is calculated by inserting $(t_{\text{max}})_{\text{Co-60}}$ determined in (12.192) into (12.191) to get

$$\begin{aligned} (\mathcal{A}_{\text{Co-60}})_{\text{max}} &= \mathcal{A}_{\text{Co-60}}[(t_{\text{max}})_{\text{Co-60}}] = \mathcal{A}_0 \left[e^{-(\sigma_{\text{Co-59}} \dot{\psi}) \times (t_{\text{max}})_{\text{Co-60}}} - e^{-\lambda_{\text{Co-60}} \times (t_{\text{max}})_{\text{Co-60}}} \right] \\ &= (1372.19 \text{ Ci}) \times \left[e^{-(0.444 \times 10^{-9} \text{ s}^{-1}) \times (6.003 \times 10^8 \text{ s})} \right. \\ &\quad \left. - e^{-(4.179 \times 10^{-9} \text{ s}^{-1}) \times (6.003 \times 10^8 \text{ s})} \right] \\ &= (1372.19 \text{ Ci}) \times [e^{-0.2665} - e^{-2.509}] \\ &= (1372.19 \text{ Ci}) \times [0.766 - 0.081] \\ &= (1372.19 \text{ Ci}) \times 0.685 = 940 \text{ Ci} = (940 \text{ Ci}) \times (3.7 \times 10^{10} \text{ Bq/Ci}) \\ &= 3.478 \times 10^{13} \text{ Bq.} \end{aligned} \quad (12.193)$$

It is interesting to note that, for our specific example, the saturation activity $(\mathcal{A}_{\text{Co-60}})_{\text{sat}}$ is 1226.3 Ci, as determined with the saturation model, while the maximum activity $(\mathcal{A}_{\text{Co-60}})_{\text{max}}$ is 940 Ci, as determined with the depletion model.

Activities $\mathcal{A}_{\text{Co-60}}(t)$ of cobalt-60 calculated from (12.191) for the depletion model of neutron activation in steps of 1 year for activation times $0 \leq t \leq 30$ are listed in Table 12.16.

(4) The activation time t , required for cobalt-60 activity $\mathcal{A}_{\text{Co-60}}(t)$ to reach a fraction f of its maximum value $(\mathcal{A}_{\text{Co-60}})_{\text{max}}$, is determined by inserting $f(\mathcal{A}_{\text{Co-60}})_{\text{max}} = (940 \text{ Ci}) \times f$ into (12.191) and solving for activation time t . The result is a transcendental equation of the form

$$\mathcal{A}_{\text{Co-60}}(t) = (1372.19 \text{ Ci}) \times [e^{-(0.014 \text{ a}^{-1})t} - e^{-(0.132 \text{ a}^{-1})t}] = (940 \text{ Ci}) \times f \quad (12.194)$$

or

$$e^{-(0.014 \text{ a}^{-1})t} = e^{-(0.132 \text{ a}^{-1})t} + 0.685f. \quad (12.195)$$

The transcendental equation (12.195) can be solved graphically for activation time t by plotting on the same graph the left side function $y_1(t) = e^{-(0.014 \text{ a}^{-1})t}$ of (12.195) separately from the right side function $y_2(t) = e^{-(0.132 \text{ a}^{-1})t} + 0.685f$ of (12.195) and determining the intercept of the two functions as the solution of (12.195).

A plot of the two functions y_1 and y_2 is shown in Fig. 12.7 for five values of fraction f : 0.25, 0.50, 0.75, 0.90, and 1.0. For a given f the intercept between functions y_1 and y_2 provides the solution to the transcendental equation (12.195). For all f (except for $f = 1$) the two functions y_1 and y_2 exhibit two intercepts, one ($t_{f\text{-asc}}$) for the ascending portion of the activity $\mathcal{A}_{\text{Co-60}}(t)$ curve and another ($t_{f\text{-denc}}$) for the descending portion of the $\mathcal{A}_{\text{Co-60}}(t)$ curve. For $f = 1$ there is only

Table 12.16 Activity $\mathcal{A}_{\text{Co-60}}(t)$ of cobalt-60 for various activation times t in the range $0 \leq t \leq 30$ a (where a stands for year) calculated for the depletion model of neutron activation, as given in (12.190) under the following conditions: mass of cobalt-59 sample $m = 59$ g; neutron fluence rate $\dot{\phi} = 1.2 \times 10^{13} \text{ cm}^{-2} \cdot \text{s}^{-1}$

t (a)	$\mathcal{A}_{\text{Co-60}}(t)$	t (a)	$\mathcal{A}_{\text{Co-60}}(t)$	t (a)	$\mathcal{A}_{\text{Co-60}}(t)$	t (a)	$\mathcal{A}_{\text{Co-60}}(t)$
0	0	8	749.49	16	930.78	24	922.85
1	150.61	9	791.46	17	936.07	25	916.36
2	280.50	10	826.36	18	939.02	26	909.17
3	392.26	11	855.11	19	939.96	27	901.40
4	488.16	12	878.48	20	939.16	28	893.13
5	570.20	13	897.16	21	936.85	29	884.45
6	640.12	14	911.77	22	933.24	30	875.43
7	699.43	15	922.82	23	928.52	∞	0

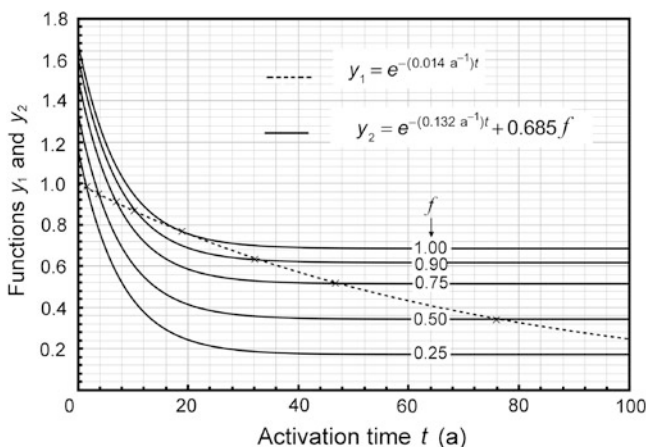


Fig. 12.7 Graphical solution to transcendental equation (QQ) provided by the intercept of two functions: $y_1 = e^{-(0.014 \text{ a}^{-1})t}$ (shown dashed) and $y_2 = e^{-(0.132 \text{ a}^{-1})t} + 0.685f$ (shown with solid curves for five values of fraction $f = \mathcal{A}_{\text{Co-60}}(t)/(\mathcal{A}_{\text{Co-60}})_{\text{max}}$). Intercepts between functions y_1 and y_2 are indicated by \times . For all values of f except for $f = 1$ functions y_1 and y_2 exhibit two intercepts; for $f = 1$ there is only one intercept occurring at the maximum of the activity $\mathcal{A}_{\text{Co-60}}(t)$ curve

one intercept between y_1 and y_2 and it occurs at the maximum of the $\mathcal{A}_{\text{Co-60}}(t)$ curve at the characteristic activation time $(t_{\text{max}})_{\text{Co-60}}$, given in (12.192).

Activation times t_f required for the cobalt sample to reach a given fraction f of the maximum activity $(\mathcal{A}_{\text{Co-60}})_{\text{max}}$ are given in Table 12.17 for 5 selected values of f (0.25, 0.50, 0.75, 0.90, and 1.0). In practice, for obvious reasons, one would only be interested in activation time $t_{f-\text{asc}}$ to reach a desired activity fraction f .

Table 12.17 Activation times $t_{f\text{-asc}}$ and $t_{f\text{-desc}}$ on the ascending and descending portions, respectively, of the activity $\mathcal{A}_{\text{Co-60}}(t)$ curve for five values of fraction f : 0.25, 0.50, 0.75, 0.90, and 1.0. The f fraction is defined as $f = \mathcal{A}_{\text{Co-60}}(t)/(\mathcal{A}_{\text{Co-60}})_{\text{max}}$ with $(\mathcal{A}_{\text{Co-60}})_{\text{max}} = 940$ Ci for our example of cobalt-59 to cobalt-60 neutron activation and its analysis using the depletion model

f	0.25	0.50	0.75	0.90	1.00
$f \times (\mathcal{A}_{\text{Co-60}})_{\text{max}}$ (Ci)	235	470	705	846	940
$t_{f\text{-asc}}$ (a)	1.63	3.80	7.09	10.66	19.03
$t_{f\text{-desc}}$ (a)	126.04	76.53	47.35	33.13	19.03

(c) Radioactivation yield $Y_{\text{Co-60}} = d\mathcal{A}_{\text{Co-60}}/dt|_{t=0}$ is calculated as follows:

(1) For the saturation model (12.186) gives the following expression for $\mathcal{A}_{\text{Co-60}}(t)$

$$\begin{aligned}\mathcal{A}_{\text{Co-60}}(t) &= (4.537 \times 10^{13} \text{ Bq}) \times [1 - e^{-(4.179 \times 10^{-9} \text{ s}^{-1})t}] \\ &= (1226.3 \text{ Ci}) \times [1 - e^{-(0.1318 \text{ a}^{-1})t}]\end{aligned}\quad (12.196)$$

and the radioactivation yield $Y_{\text{Co-60}} = d\mathcal{A}_{\text{Co-60}}/dt|_{t=0}$ is then determined as follows

$$\begin{aligned}Y_{\text{Co-60}} &= \left. \frac{d\mathcal{A}_{\text{Co-60}}}{dt} \right|_{t=0} = (4.537 \times 10^{13} \text{ s}^{-1}) \times (4.179 \times 10^{-9} \text{ s}^{-1}) \\ &= 1.9 \times 10^5 \text{ s}^{-2}.\end{aligned}\quad (12.197)$$

(2) For the depletion model (12.101) gives the following expression for $\mathcal{A}_{\text{Co-60}}(t)$

$$\mathcal{A}_{\text{Co-60}}(t) = (5.077 \times 10^{13} \text{ Bq}) \times [e^{-(0.444 \times 10^{-9} \text{ s}^{-1})t} - e^{-(4.179 \times 10^{-9} \text{ s}^{-1})t}]\quad (12.198)$$

and the radioactivation yield $Y_{\text{Co-60}} = d\mathcal{A}_{\text{Co-60}}/dt|_{t=0}$ is then determined as follows

$$\begin{aligned}Y_{\text{Co-60}} &= \left. \frac{d\mathcal{A}_{\text{Co-60}}}{dt} \right|_{t=0} \\ &= (5.077 \times 10^{13} \text{ Bq}) \times [-0.444 \times 10^{-9} \text{ s}^{-1} + 4.179 \times 10^{-9} \text{ s}^{-1}] \\ &= (5.077 \times 10^{13} \text{ Bq}) \times (3.735 \times 10^{-9}) \\ &= 1.9 \times 10^5 \text{ s}^{-2}.\end{aligned}\quad (12.199)$$

As expected, both activation models give identical results for the radioactivation yield $Y_{\text{Co-60}}$ as a result of identical initial ($t = 0$) slopes of $\mathcal{A}_{\text{Co-60}}(t)$ curves plotted against activation time t .

(d) Figure 12.8 plots the cobalt-60 activity $\mathcal{A}_{\text{Co-60}}(t)$ against activation time t for our example of neutron activation of a 10 g sample of cobalt-59 into cobalt-60 in a nuclear reactor with thermal neutron fluence $\dot{\phi}$ of $1.2 \times 10^{13} \text{ cm}^{-2} \cdot \text{s}^{-1}$. $\mathcal{A}_{\text{Co-60}}(t)$ is

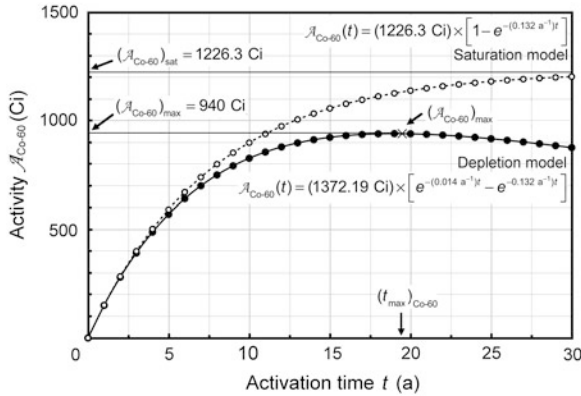


Fig. 12.8 Cobalt-60 activity $\mathcal{A}_{\text{Co-60}}(t)$ against activation time t for neutron activation of a 10 g sample of cobalt-59 into cobalt-60 in a nuclear reactor with thermal neutron fluence $\dot{\phi}$ of $1.2 \times 10^{13} \text{ cm}^{-2} \cdot \text{s}^{-1}$. *Dashed curve* plots $\mathcal{A}_{\text{Co-60}}(t)$ determined with the saturation model of neutron activation expressed with (12.186); *solid curve* plots $\mathcal{A}_{\text{Co-60}}(t)$ determined with the depletion model of neutron activation expressed with (12.191). The saturation model curve saturates at $(\mathcal{A}_{\text{Co-60}})_{\text{sat}} = 1226.3 \text{ Ci}$ for $t \rightarrow \infty$; the depletion model curve attains a broad maximum $(\mathcal{A}_{\text{Co-60}})_{\text{max}} = 940 \text{ Ci}$ at $(t_{\text{max}})_{\text{Co-60}} = 19.03 \text{ a}$

shown with dashed curve for the saturation model (12.186) and with solid curve for the depletion model (12.191). Both curves exhibit the same initial slope at $t = 0$ (i.e., same radioactivation yield $Y_{\text{Co-60}} = 1.9 \times 10^5 \text{ s}^{-2}$); however, with increasing activation time t the curves diverge and the saturation model curve increases exponentially and saturates at $(\mathcal{A}_{\text{Co-60}})_{\text{sat}} = 1226.3 \text{ Ci}$ for $t \rightarrow \infty$, while the depletion model curve attains a broad maximum $(\mathcal{A}_{\text{Co-60}})_{\text{max}} = 940 \text{ Ci}$ at $(t_{\text{max}})_{\text{Co-60}} = 19.03 \text{ a}$ and then gradually drops to 0 as $t \rightarrow \infty$.

12.6.Q10

(260)

Production of cobalt-60 (Co-60) radionuclide from cobalt-59 (Co-59) nuclide is usually treated like a simple parent P–daughter D–granddaughter G nuclear series, whereby the natural parent Co-59 nuclide is activated with thermal neutrons (activation cross section $\sigma_P = 37 \text{ b}$) in a nuclear reactor into daughter radionuclide Co-60 that subsequently decays through β^- nuclear decay with a half-life $t_{1/2} = 5.26 \text{ a}$ into the granddaughter nuclide nickel-60 (Ni-60) [see Fig. 12.9(A)].

However, a closer look at the activation and decay diagrams of Co-60 nuclide shows that the activation process is significantly more complex, as shown schematically in Fig. 12.9(B). Activation of Co-59 actually has two possible branches:

Branch (1) leads directly to ground state of Co-60 with $\sigma_{P1} = f_1^P \sigma_P = 17$ b and $f_1^P = 17/37 = 0.46$ Branch (2) leads to a metastable state of Co-60m with $\sigma_{P2} = f_2^P \sigma_P = 20$ b and $f_2^P = 20/37 = 0.54$.

The Co-60 daughter D1 radionuclide has two possible avenues open for transformation:

- (1) To decay through β^- decay into Ni-60 with $t_{1/2} = 5.26$ a.
- (2) To become activated by thermal neutrons into Co-61 with $\sigma_{D1} = 2$ b.

The Co-60m daughter D2 radionuclide has 3 avenues open for transformation:

- (1) To become activated by thermal neutrons into Co-61m with $\sigma_{D2} = 58$ b.
- (2) To decay with $t_{1/2} = 10.5$ m through γ decay into Co-60 (branching ratio $f_\gamma^{D2} = 0.998$).
- (3) To decay with $t_{1/2} = 10.5$ m through β^- decay into Ni-60 (branching ratio $f_{\beta^-}^{D2} = 0.002$).

-
- (a) Write and solve the differential equation governing the change dN_D/dt in the number of daughter D (Co-60) nuclei for the activation–decay series (A) of Fig. 12.9. Express the activity $\mathcal{A}_D(t)$ of daughter D (Co-60) against t for the following initial conditions at $t = 0$: initial number of parent P nuclei is $N_P(0)$; initial number of daughter nuclei $N_D(t = 0) = 0$.
 - (b) Write and solve the differential equation governing the change dN_{D1}/dt in the number of daughter D1 (Co-60) nuclei for the activation–decay series (B) of Fig. 12.9. Express the activity $\mathcal{A}_D(t)$ of daughter D (Co-60) against t for the following initial conditions at $t = 0$: initial number of parent P nuclei is $N_P(0)$; initial number of daughter nuclei $N_D(t = 0) = 0$.
 - (c) A pure 10 g Co-59 target is placed into a nuclear reactor with thermal neutron fluence rate $\dot{\phi} = 5 \times 10^{14} \text{ cm}^2 \cdot \text{s}^{-1}$. Calculate the activity of Co-60 against time t in steps of 2 years from 0 to 10 years based on expressions derived in (a) and (b) above for nuclear activation–decay schemes (A) and (B) of Fig. 12.9. Superimpose your calculated results on the graph presented in Fig. 12.10.

SOLUTION:

- (a) The differential equation for change dN_D/dt in the number of daughter D (Co-60) nuclei for nuclear activation–decay series of Fig. 12.9(A) is given as follows, recognizing that dN_D/dt is governed by two terms describing:

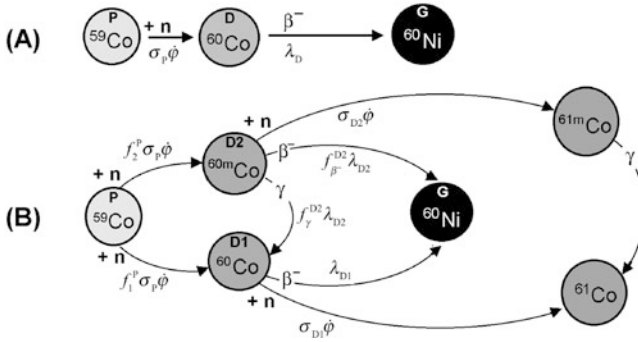


Fig. 12.9 Nuclear activation–decay series in production of cobalt-60 through neutron activation of cobalt-59. Decay series (A) depicts the simplified model, decay series (B) depicts the actual activation–decay scheme

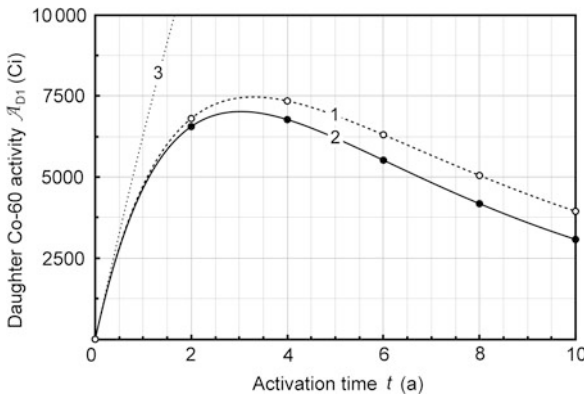


Fig. 12.10 Activity of cobalt-60 daughter against activation time t for neutron activation of cobalt-59 of mass $m = 10$ g in a nuclear reactor with neutron fluence rate $\dot{\phi} = 5 \times 10^{14} \text{ cm}^{-2} \cdot \text{s}^{-1}$. Curve (1) is for simplified nuclear activation–decay series (A) of Fig. 12.9, curve (2) for the actual nuclear activation–decay series shown as series (B) in Fig. 12.9. Curve (3) is added for comparison and represents daughter activity calculated for series (A) and the saturation model of nuclear activation that ignores the decay of cobalt-60 radionuclide during the activation process

- (1) Production rate of daughter D (Co-60) through neutron activation of parent P (Co-59), expressed as $+\sigma_P \dot{\phi} N_P(0)e^{-\sigma_P \dot{\phi} t}$,
- (2) Loss of daughter D (Co-60) through β^- decay of daughter D (Co-60) into granddaugther G (Ni-60), expressed as $-\lambda_D N_D(t)$,

resulting in the following expression for dN_D/dt

$$\frac{dN_D}{dt} = \sigma_P \dot{\phi} N_P(0)e^{-\sigma_P \dot{\phi} t} - \lambda_D N_D(t). \tag{12.200}$$

Equation (12.200) is a first order differential equation of the form

$$\frac{d\eta(t)}{dt} + p(t)\eta(t) = q(t), \quad (12.201)$$

with the following solution

$$\eta(t) = \frac{\int u(t)q(t) dt + C}{u(t)}, \quad (12.202)$$

where C is a constant and the function $u(t)$ is defined as

$$u(t) = e^{\int p(t) dt}. \quad (12.203)$$

After rearranging (12.200) to match the format of (12.201), we get the following values for parameters of (12.201): $p(t) = \lambda_D$, $u(t) = e^{\lambda_D t}$, and $q(t) = \sigma_P \dot{\phi} N_P(0) e^{-\sigma_P \dot{\phi} t}$. Inserting these parameters into (12.202) we get the following expression for $N_D(t)$

$$N_D(t) = \frac{\sigma_P \dot{\phi} N_P(0)}{\lambda_D - \sigma_P \dot{\phi}} e^{-\sigma_P \dot{\phi} t} + C e^{-\lambda_D t}. \quad (12.204)$$

To determine constant C we apply the initial condition $N_D(t = 0) = 0$ to get

$$C = -\frac{\sigma_P \dot{\phi} N_P(0)}{\lambda_D - \sigma_P \dot{\phi}} \quad (12.205)$$

and, after inserting (12.205) into (12.204), we get the following well-known solutions for the number of daughter D (Co-60) nuclei (T10.34)

$$N_D(t) = \frac{\sigma_P \dot{\phi} N_P(0)}{\lambda_D - \sigma_P \dot{\phi}} [e^{-\sigma_P \dot{\phi} t} - e^{-\lambda_D t}] \quad (12.206)$$

and the daughter D (Co-60) activity $\mathcal{A}_D(t) = \lambda_D N_D(t)$ is expressed as follows (T10.35)

$$\mathcal{A}_D(t) = \frac{\lambda_D \sigma_P \dot{\phi} N_P(0)}{\lambda_D - \sigma_P \dot{\phi}} [e^{-\sigma_P \dot{\phi} t} - e^{-\lambda_D t}]. \quad (12.207)$$

(b) The differential equation for change dN_{D1}/dt in the number of daughter D1 (Co-60) nuclei for nuclear activation–decay series depicted in Fig. 12.9(B) is given as follows, recognizing that dN_{D1}/dt is governed by four terms describing:

- (1) Production rate of daughter D1 (Co-60) through neutron activation of parent P (Co-59), expressed as $+f_1^P \sigma_P \dot{\phi} N_P(0) e^{-\sigma_P \dot{\phi} t}$,
- (2) Production rate of daughter D1 (Co-60) through γ decay of daughter D2 (Co-60m), expressed as $+f_\gamma^{D2} \lambda_{D2} N_{D2}(t)$,
- (3) Loss of daughter D1 (Co-60) through activation of daughter D1 (Co-60) into Co-61, expressed as $-\sigma_{D1} \dot{\phi} N_{D1}(t)$,

- (4) Loss of daughter D1 (Co-60) through β^- decay of daughter D2 (Co-60) into grand-daughter G (Ni-60), expressed as $-\lambda_{D1} N_{D1}(t)$,

resulting in the following expression for dN_{D1}/dt

$$\frac{dN_{D1}}{dt} = f_1^P \sigma_P \dot{\phi} N_P(0) e^{-\sigma_P \dot{\phi} t} + f_\gamma^{D2} \lambda_{D2} N_{D2}(t) - \lambda_{D1}^* N_{D1}(t), \quad (12.208)$$

where λ_{D1}^* is a modified decay constant linking into one constant the β^- decay and neutron activation of D1 expressed as

$$\lambda_{D1}^* = \lambda_{D1} + \sigma_{D1} \dot{\phi}, \quad (12.209)$$

with λ_{D1} the decay constant of daughter D1, σ_{D1} the neutron activation cross section of daughter D1, and $\dot{\phi}$ the neutron fluence rate.

To solve (12.208) we will need to know the number of daughter D2 (Co-60m) nuclei $N_{D2}(t)$ appearing in (12.208). Therefore, we now set up a differential equation that describes the change dN_{D2}/dt in the number N_{D2} that is, as shown in Fig. 12.9(B), governed by 4 terms:

- (1) Production rate of daughter D2 (Co-60m) through activation of parent P (Co-59), expressed as: $+f_2^P \sigma_P \dot{\phi} N_P(0) e^{-\sigma_P \dot{\phi} t}$,
- (2) Loss of daughter D2 (Co-60m) through neutron activation of daughter D2 (Co-60m) into Co-61m, expressed as $-\sigma_{D2} \dot{\phi} N_{D2}(t)$,
- (3) Loss of daughter D2 (Co-60m) through β^- decay into granddaughter G (Ni-60), expressed as $-f_{\beta^-}^{D2} \lambda_{D2} N_{D2}(t)$,
- (4) Loss of daughter D2 (Co-60m) through isomeric γ decay into daughter D1 (Co-60), expressed as $-f_\gamma^{D2} \lambda_{D2} N_{D2}(t)$.

The change dN_{D2}/dt in the number of daughter D2 nuclei is thus expressed as follows

$$\begin{aligned} \frac{dN_{D2}}{dt} &= f_2^P \sigma_P \dot{\phi} N_P(0) e^{-\sigma_P \dot{\phi} t} - [\sigma_{D2} \dot{\phi} + f_{\beta^-}^{D2} \lambda_{D2} + f_\gamma^{D2} \lambda_{D2}] N_{D2}(t) \\ &= f_2^P \sigma_P \dot{\phi} N_P(0) e^{-\sigma_P \dot{\phi} t} - \lambda_{D2}^* N_{D2}(t), \end{aligned} \quad (12.210)$$

where λ_{D2}^* is a modified decay constant linking into one constant the β^- decay, isomeric γ decay, and neutron activation of daughter D2 expressed as

$$\lambda_{D2}^* = \sigma_{D2} \dot{\phi} + f_{\beta^-}^{D2} \lambda_{D2} + f_\gamma^{D2} \lambda_{D2} = \sigma_{D2} \dot{\phi} + \lambda_{D2}, \quad (12.211)$$

with σ_{D2} the neutron activation cross section of daughter D2 and λ_{D2} the decay constant of D2.

Rearranging (12.210) to match the format of (12.201) we get the following values for the parameters of (12.201): $p(t) = \lambda_{D2}^*$, $u(t) = e^{\lambda_{D2}^* t}$, and $q(t) = f_2^P \sigma_P \dot{\phi} N_P(0) e^{-\sigma_P \dot{\phi} t}$. Inserting these parameters into (12.202) we get the following expression for $N_{D2}(t)$

$$N_{D2}(t) = \frac{\int e^{\lambda_{D2}^* t} f_2^P \sigma_P \dot{\phi} N_P(0) e^{-\sigma_P \dot{\phi} t} dt + C}{e^{\lambda_{D2}^* t}}$$

$$\begin{aligned}
 &= f_2^P \sigma_P \dot{\phi} N_P(0) e^{-\lambda_{D2}^* t} \int e^{(\lambda_{D2}^* - \sigma_P \dot{\phi})t} dt + C e^{-\lambda_{D2}^* t} \\
 &= \frac{f_2^P \sigma_P \dot{\phi} N_P(0)}{\lambda_{D2}^* - \sigma_P \dot{\phi}} e^{-\sigma_P \dot{\phi} t} + C e^{-\lambda_{D2}^* t}. \tag{12.212}
 \end{aligned}$$

We now use the initial condition $N_{D2}(t = 0) = 0$ and get from (12.212) the constant C

$$C = -\frac{f_2^P \sigma_P \dot{\phi} N_P(0)}{\lambda_{D2}^* - \sigma_P \dot{\phi}}. \tag{12.213}$$

After inserting (12.213) into (12.212) we get the number $N_{D2}(t)$ of daughter D2 (Co-60m) nuclei as follows

$$N_{D2}(t) = \frac{f_2^P \sigma_P \dot{\phi} N_P(0)}{\lambda_{D2}^* - \sigma_P \dot{\phi}} \{e^{-\sigma_P \dot{\phi} t} - e^{-\lambda_{D2}^* t}\}. \tag{12.214}$$

Inserting (12.214) into (12.208) and rearranging the terms to match with (12.201), we now obtain the following differential equation for the change dN_{D1}/dt in number of daughter nuclei D1 (Co-60)

$$\begin{aligned}
 &\frac{dN_{D1}(t)}{dt} + \lambda_{D1}^* N_{D1}(t) \\
 &= f_1^P \sigma_P \dot{\phi} N_P(0) e^{-\sigma_P \dot{\phi} t} + \frac{f_\gamma^{D2} \lambda_{D2} f_2^P \sigma_P \dot{\phi} N_P(0)}{\lambda_{D2}^* - \sigma_P \dot{\phi}} \{e^{-\sigma_P \dot{\phi} t} - e^{-\lambda_{D2}^* t}\}, \tag{12.215}
 \end{aligned}$$

similar to (12.200) and (12.208), another first order differential equation that upon comparison with (12.201) yields the following values for the parameters of (12.201)

$$\begin{aligned}
 p(t) &= \lambda_{D1}^*, \quad u(t) = e^{\lambda_{D1}^* t}, \quad \text{and} \\
 q(t) &= f_1^P \sigma_P \dot{\phi} N_P(0) e^{-\sigma_P \dot{\phi} t} + \frac{f_\gamma^{D2} \lambda_{D2} f_2^P \sigma_P \dot{\phi} N_P(0)}{\lambda_{D2}^* - \sigma_P \dot{\phi}} \{e^{-\sigma_P \dot{\phi} t} - e^{-\lambda_{D2}^* t}\}. \tag{12.216}
 \end{aligned}$$

Inserting parameters of (12.216) into (12.202) we get the following expression for $N_{D1}(t)$

$$\begin{aligned}
 N_{D1}(t) &= \frac{\int e^{\lambda_{D1}^* t} \{f_1^P \sigma_P \dot{\phi} N_P(0) e^{-\sigma_P \dot{\phi} t} + \frac{f_\gamma^{D2} \lambda_{D2} f_2^P \sigma_P \dot{\phi} N_P(0)}{\lambda_{D2}^* - \sigma_P \dot{\phi}} \{e^{-\sigma_P \dot{\phi} t} - e^{-\lambda_{D2}^* t}\}\} dt + C}{e^{\lambda_{D1}^* t}} \\
 &= \frac{\{f_1^P \sigma_P \dot{\phi} N_P(0) + \frac{f_\gamma^{D2} \lambda_{D2} f_2^P \sigma_P \dot{\phi} N_P(0)}{\lambda_{D2}^* - \sigma_P \dot{\phi}}\} \int e^{(\lambda_{D1}^* - \sigma_P \dot{\phi})t} dt}{e^{\lambda_{D1}^* t}}
 \end{aligned}$$

$$\begin{aligned}
& - \frac{\frac{f_{\gamma}^{D2} \lambda_{D2} f_2^P \sigma_P \dot{\varphi} N_P(0)}{\lambda_{D2}^* - \sigma_P \dot{\varphi}} \int e^{(\lambda_{D1}^* - \lambda_{D2}^*)t} dt}{e^{\lambda_{D1}^* t}} + C e^{-\lambda_{D1}^* t} \\
& = \frac{f_1^P \sigma_P \dot{\varphi} N_P(0) + \frac{f_{\gamma}^{D2} \lambda_{D2} f_2^P \sigma_P \dot{\varphi} N_P(0)}{\lambda_{D2}^* - \sigma_P \dot{\varphi}}}{\lambda_{D1}^* - \sigma_P \dot{\varphi}} e^{-\sigma_P \dot{\varphi} t} \\
& - \frac{f_{\gamma}^{D2} \lambda_{D2} f_2^P \sigma_P \dot{\varphi} N_P(0)}{(\lambda_{D2}^* - \sigma_P \dot{\varphi})(\lambda_{D1}^* - \lambda_{D2}^*)} e^{-\lambda_{D2}^* t} + C e^{-\lambda_{D1}^* t}. \tag{12.217}
\end{aligned}$$

To determine the constant C we use the initial condition $N_{D1}(t=0) = 0$ to get

$$C = \frac{f_{\gamma}^{D2} \lambda_{D2} f_2^P \sigma_P \dot{\varphi} N_P(0)}{(\lambda_{D2}^* - \sigma_P \dot{\varphi})(\lambda_{D1}^* - \lambda_{D2}^*)} - \frac{f_1^P \sigma_P \dot{\varphi} N_P(0) + \frac{f_{\gamma}^{D2} \lambda_{D2} f_2^P \sigma_P \dot{\varphi} N_P(0)}{\lambda_{D2}^* - \sigma_P \dot{\varphi}}}{\lambda_{D1}^* - \sigma_P \dot{\varphi}}. \tag{12.218}$$

Substituting (12.218) into (12.217) we get the following expression for the number $N_{D1}(t)$ of daughter D1 (Co-60) nuclei for nuclear activation–decay series depicted in Fig. 12.9(B)

$$\begin{aligned}
N_{D1}(t) & = \frac{f_1^P \sigma_P \dot{\varphi} N_P(0) + \frac{f_{\gamma}^{D2} \lambda_{D2} f_2^P \sigma_P \dot{\varphi} N_P(0)}{\lambda_{D2}^* - \sigma_P \dot{\varphi}}}{\lambda_{D1}^* - \sigma_P \dot{\varphi}} \{e^{-\sigma_P \dot{\varphi} t} - e^{-\lambda_{D1}^* t}\} \\
& - \frac{f_{\gamma}^{D2} \lambda_{D2} f_2^P \sigma_P \dot{\varphi} N_P(0)}{(\lambda_{D2}^* - \sigma_P \dot{\varphi})(\lambda_{D1}^* - \lambda_{D2}^*)} \{e^{-\lambda_{D2}^* t} - e^{-\lambda_{D1}^* t}\}. \tag{12.219}
\end{aligned}$$

Activity $\mathcal{A}_{D1}(t)$ of daughter D1 (Co-60) is determined by multiplying (12.219) with the decay constant λ_{D1} resulting in the following

$$\begin{aligned}
\mathcal{A}_{D1}(t) & = \lambda_{D1} N_{D1}(t) \\
& = \frac{\lambda_{D1} f_1^P \sigma_P \dot{\varphi} N_P(0) + \frac{\lambda_{D1} f_{\gamma}^{D2} \lambda_{D2} f_2^P \sigma_P \dot{\varphi} N_P(0)}{\lambda_{D2}^* - \sigma_P \dot{\varphi}}}{\lambda_{D1}^* - \sigma_P \dot{\varphi}} \{e^{-\sigma_P \dot{\varphi} t} - e^{-\lambda_{D1}^* t}\} \\
& - \frac{\lambda_{D1} f_{\gamma}^{D2} \lambda_{D2} f_2^P \sigma_P \dot{\varphi} N_P(0)}{(\lambda_{D2}^* - \sigma_P \dot{\varphi})(\lambda_{D1}^* - \lambda_{D2}^*)} \{e^{-\lambda_{D2}^* t} - e^{-\lambda_{D1}^* t}\}. \tag{12.220}
\end{aligned}$$

Daughter D1 (Co-60) activity of (12.220) appears quite complicated, however, we can rearrange its terms to get an expression consisting of a simple term in the form of (12.207) for the activation–decay series depicted in Fig. 12.9(A) multiplied by a correction factor F_{corr} to account for the increased complexity of the activation–decay series depicted in Fig. 12.9(B). Equation (12.220) thus reads

$$\mathcal{A}_{D1}(t) = \frac{\lambda_{D1} f_1^P \sigma_P \dot{\varphi} N_P(0)}{\lambda_{D1}^* - \sigma_P \dot{\varphi}} [e^{-\sigma_P \dot{\varphi} t} - e^{-\lambda_{D1}^* t}] \left\{ 1 + \frac{f_2^P \lambda_{D2}}{f_1^P \lambda_{D1}} \frac{f_{\gamma}^{D2}}{\lambda_{D2}^* - \sigma_P \dot{\varphi}} \right\}$$

Table 12.18 Relevant parameters for use in (12.207) with mass of Co-59 sample $m_{\text{Co-59}} = 10$ g and neutron fluence rate $\dot{\phi} = 5 \times 10^{14} \text{ cm}^2 \cdot \text{s}^{-1}$

σ_P	$37 \times 10^{-24} \text{ cm}^2$
$\lambda_D = \ln(2)/(t_{1/2})_{\text{Co-60}}$	$\ln(2)/5.26 \text{ a} = 4.179 \times 10^{-9} \text{ s}^{-1}$
$\dot{\phi}$	$5 \times 10^{14} \text{ cm}^{-2} \text{ s}^{-1}$
$N_P(0) = mN_A/A$	$(10 \text{ g}) \times (6.022 \times 10^{23} \text{ atom/mol}) / (59 \text{ g/mol}) = 1.021 \times 10^{23} \text{ atom}$
$\sigma_P \dot{\phi}$	$(37 \times 10^{-24} \text{ cm}^2) \times (5 \times 10^{14} \text{ cm}^{-2} \text{ s}^{-1}) = 1.85 \times 10^{-8} \text{ s}^{-1}$
$\lambda_D \sigma_P \dot{\phi} N_P(0)$	$(4.179 \times 10^{-9} \text{ s}^{-1}) \times (1.85 \times 10^{-8} \text{ s}^{-1}) \times (1.021 \times 10^{23} \text{ atom}) = 7.890 \times 10^6 \text{ s}^{-2}$
$\lambda_D - \sigma_P \dot{\phi}$	$4.179 \times 10^{-9} \text{ s}^{-1} - 1.85 \times 10^{-8} \text{ s}^{-1} = -1.432 \times 10^{-8} \text{ s}^{-1}$

$$\begin{aligned}
 & - \frac{f_2^P f_\gamma^{D2} \lambda_{D2} (\lambda_{D1}^* - \sigma_P \dot{\phi})}{(\lambda_{D2}^* - \sigma_P \dot{\phi}) (\lambda_{D1}^* - \lambda_{D2}^*)} \frac{(e^{-\lambda_{D2}^* t} - e^{-\lambda_{D1}^* t})}{(e^{-\sigma_P \dot{\phi} t} - e^{-\lambda_{D1}^* t})} \Big\} \\
 & = \frac{\lambda_{D1} f_1^P \sigma_P \dot{\phi} N_P(0)}{\lambda_{D1}^* - \sigma_P \dot{\phi}} \left[e^{-\sigma_P \dot{\phi} t} - e^{-\lambda_{D1}^* t} \right] \times F_{\text{corr}}. \quad (12.221)
 \end{aligned}$$

Comparing the two activation–decay series (A) and (B) of Fig. 12.9 we note that series (B) transforms into series (A) for the following special values of parameters: $f_1^P = 1$, $f_2^P = 0$, $\lambda_{D1} = \lambda_D$, and $\sigma_{D1} = 0$. Inserting these values into (12.221) we indeed get (12.207) from (12.221) for the activity of the daughter Co-60 in neutron activation of Co-59 since $\lambda_{D1}^* = \lambda_{D1} = \lambda_D$ and $F_{\text{corr}} = 1$.

(c) We now investigate the specific Co-60 activation–decay example for a Co-59 sample (mass $m_{\text{Co-59}} = 10$ g and neutron fluence rate $\dot{\phi} = 5 \times 10^{14} \text{ cm}^2 \cdot \text{s}^{-1}$) and calculate the daughter D1 activity first with (12.207) for the activation–decay series (A) of Fig. 12.9 and then with (12.221) for the activation–decay series (B) of Fig. 12.9.

(1) *Nuclear activation–decay series* (A) of Fig. 12.9. The relevant parameters for use of (12.207), summarized in Table 12.18, result in the following expression for activity $\mathcal{A}_D(t)$ of daughter D (Co-60) as a function of activation time t

$$\begin{aligned}
 \mathcal{A}_D(t) &= \frac{7.890 \times 10^6 \text{ s}^{-2}}{-1.432 \times 10^{-8} \text{ s}^{-1}} \times \left\{ e^{-(1.850 \times 10^{-8} \text{ s}^{-1})t} - e^{-(4.179 \times 10^{-9} \text{ s}^{-1})t} \right\} \\
 &= (5.509 \times 10^{14} \text{ Bq}) \times \left\{ e^{-(4.179 \times 10^{-9} \text{ s}^{-1})t} - e^{-(1.850 \times 10^{-8} \text{ s}^{-1})t} \right\} \\
 &= (14890 \text{ Ci}) \times \left\{ e^{-(4.179 \times 10^{-9} \text{ s}^{-1})t} - e^{-(1.850 \times 10^{-8} \text{ s}^{-1})t} \right\}. \quad (12.222)
 \end{aligned}$$

Using (12.222) with activation times t from 0 to 10 years in steps of 2 years yields activities $\mathcal{A}_D(t)$ summarized in Table 12.19. The data presented in Table 12.19 are also plotted as data points in Fig. 12.10 on curve (1).

Table 12.19 Activity $\mathcal{A}_D(t)$ of daughter D (Co-60) calculated from (12.222) for mass of Co-59 sample $m_{\text{Co-59}} = 10 \text{ g}$ and neutron fluence rate $\dot{\phi} = 5 \times 10^{14} \text{ cm}^2 \cdot \text{s}^{-1}$ for activation times t between 0 and 10 years in steps of 2 years. These data points are superimposed on curve (1) in Fig. 12.10

t (years)	$e^{-(1.850 \times 10^{-8} \text{ s}^{-1})t}$	$e^{-(4.179 \times 10^{-9} \text{ s}^{-1})t}$	$\mathcal{A}_D(t)$ (Ci)
0	1.000	1.000	0
2	0.311	0.768	6804
4	0.097	0.590	7346
6	0.030	0.454	6304
8	0.009	0.348	5049
10	0.003	0.268	3943

Table 12.20 Relevant parameters for use in (12.221) with mass of Co-59 sample $m_{\text{Co-59}} = 10 \text{ g}$ and neutron fluence rate $\dot{\phi} = 5 \times 10^{14} \text{ cm}^2 \cdot \text{s}^{-1}$

σ_P	$37 \times 10^{-24} \text{ cm}^2$
σ_{D1}	$2 \text{ b} = 2 \times 10^{-24} \text{ cm}^2$
σ_{D2}	$58 \text{ b} = 58 \times 10^{-24} \text{ cm}^2$
f_1^P	0.46
f_2^P	0.54
f_γ^{D2}	0.998
$\lambda_{D1} = \ln(2)/(t_{1/2})_{\text{Co-60}}$	$\ln(2)/(5.29 \text{ a}) = 4.179 \times 10^{-9} \text{ s}^{-1}$
$\lambda_{D2} = \ln(2)/(t_{1/2})_{\text{Co-60m}}$	$\ln(2)/(10.5 \text{ m}) = 1.1 \times 10^{-3} \text{ s}^{-1}$
$\dot{\phi}$	$5 \times 10^{14} \text{ cm}^{-2} \text{ s}^{-1}$
$\sigma_P \dot{\phi}$	$(37 \times 10^{-24} \text{ cm}^2) \times (5 \times 10^{14} \text{ cm}^{-2} \text{ s}^{-1}) = 1.85 \times 10^{-8} \text{ s}^{-1}$
$\sigma_{D1} \dot{\phi}$	$(2 \times 10^{-24} \text{ cm}^2) \times (5 \times 10^{14} \text{ cm}^{-2} \text{ s}^{-1}) = 1.00 \times 10^{-9} \text{ s}^{-1}$
$\sigma_{D2} \dot{\phi}$	$(58 \times 10^{-24} \text{ cm}^2) \times (5 \times 10^{14} \text{ cm}^{-2} \text{ s}^{-1}) = 2.90 \times 10^{-8} \text{ s}^{-1}$
$\lambda_{D1}^* = \lambda_{D1} + \sigma_{D1} \dot{\phi}$	$(4.179 \times 10^{-9} \text{ s}^{-1}) + (1.00 \times 10^{-9} \text{ s}^{-1}) = 5.179 \times 10^{-9} \text{ s}^{-1}$
$\lambda_{D2}^* = \lambda_{D2} + \sigma_{D2} \dot{\phi}$	$(1.1 \times 10^{-3} \text{ s}^{-1}) + (2.90 \times 10^{-8} \text{ s}^{-1}) \approx 1.1 \times 10^{-3} \text{ s}^{-1}$
$N_P(0) = m N_A / A$	$(10 \text{ g}) \times (6.022 \times 10^{23} \text{ mol}^{-1}) / (59 \text{ g/mol}) = 1.021 \times 10^{23} \text{ atom}$
$\lambda_{D1}^* - \sigma_P \dot{\phi}$	$5.179 \times 10^{-9} \text{ s}^{-1} - 1.85 \times 10^{-8} \text{ s}^{-1} = -1.332 \times 10^{-8} \text{ s}^{-1}$
$\lambda_{D2}^* - \sigma_P \dot{\phi}$	$1.1 \times 10^{-3} \text{ s}^{-1} - 1.85 \times 10^{-8} \text{ s}^{-1} \approx 1.1 \times 10^{-3} \text{ s}^{-1}$
$\lambda_{D1}^* - \lambda_{D2}^*$	$5.179 \times 10^{-9} \text{ s}^{-1} - 1.1 \times 10^{-3} \text{ s}^{-1} \approx -1.1 \times 10^{-3} \text{ s}^{-1}$
$\lambda_{D1} f_1^P \sigma_P \dot{\phi} N_P(0)$	$(4.179 \times 10^{-9} \text{ s}^{-1}) \times (0.46) \times (1.85 \times 10^{-8} \text{ s}^{-1}) \times (1.021 \times 10^{23} \text{ atom}) = 3.63 \times 10^5 \text{ s}^{-2}$
$\lambda_{D1} f_\gamma^{D2} \lambda_{D2} f_2^P \sigma_P \dot{\phi} N_P(0)$	$(4.179 \times 10^{-9} \text{ s}^{-1}) \times (0.998) \times (1.1 \times 10^{-3} \text{ s}^{-1}) \times (0.54) \times (1.85 \times 10^{-8} \text{ s}^{-1}) \times (1.021 \times 10^{23} \text{ atom}) = 4.678 \times 10^3 \text{ s}^{-3}$

Table 12.21 Activity $\mathcal{A}_D(t)$ of daughter D1 (Co-60) calculated from (12.223) for mass of Co-59 sample $m_{\text{Co-59}} = 10 \text{ g}$ and neutron fluence rate $\dot{\phi} = 5 \times 10^{14} \text{ cm}^2 \cdot \text{s}^{-1}$ for activation times t between 0 and 10 years in steps of 2 years. Data points listed in this table are superimposed onto curve (2) in Fig. 12.10

t (years)	$e^{-(1.850 \times 10^{-8} \text{ s}^{-1})t}$	$e^{-(5.179 \times 10^{-9} \text{ s}^{-1})t}$	$e^{-(1.1 \times 10^{-3} \text{ s}^{-1})t}$	$\mathcal{A}_{D1}(t)$ (Ci)
0	1.000	1.000	1.000	0
2	0.311	0.721	0	6556
4	0.097	0.520	0	6771
6	0.030	0.375	0	5520
8	0.009	0.271	0	4179
10	0.003	0.195	0	3076

(2) *Nuclear activation–decay series* (B) of Fig. 12.9. The relevant parameters for use with (12.207), summarized in Table 12.20, result in the following expression for activity $\mathcal{A}_{D1}(t)$ of daughter D1 (Co-60) as a function of activation time t

$$\begin{aligned}
 \mathcal{A}_{D1}(t) &= \frac{3.63 \times 10^5 \text{ s}^{-2} + \frac{4.678 \times 10^3 \text{ s}^{-3}}{1.1 \times 10^{-3} \text{ s}^{-1}}}{-1.332 \times 10^{-8} \text{ s}^{-1}} \left\{ e^{-(1.85 \times 10^{-8} \text{ s}^{-1})t} - e^{-(5.179 \times 10^{-9} \text{ s}^{-1})t} \right\} \\
 &\quad - \frac{4.678 \times 10^3 \text{ s}^{-3}}{(1.1 \times 10^{-3} \text{ s}^{-1}) \times (-1.1 \times 10^{-3} \text{ s}^{-1})} \\
 &\quad \times \left\{ e^{-(1.1 \times 10^{-3} \text{ s}^{-1})t} - e^{-(5.179 \times 10^{-9} \text{ s}^{-1})t} \right\} \\
 &= (15990 \text{ Ci}) \times \left\{ e^{-(5.179 \times 10^{-9} \text{ s}^{-1})t} - e^{-(1.85 \times 10^{-8} \text{ s}^{-1})t} \right\} \\
 &\quad + (0.1044 \text{ Ci}) \times \left\{ e^{-(1.1 \times 10^{-3} \text{ s}^{-1})t} - e^{-(5.179 \times 10^{-9} \text{ s}^{-1})t} \right\}. \quad (12.223)
 \end{aligned}$$

Using (12.223) with activation times t from 0 to 10 years in steps of 2 years yields activities $\mathcal{A}_{D1}(t)$ summarized in Table 12.21. The data presented in Table 12.21 are also plotted as data points in Fig. 12.10 on curve (2).

12.6.Q11

(261)

A 10 g cobalt-59 (Co-59) sample is placed in a nuclear reactor with a neutron fluence rate $\dot{\phi}$ of $5 \times 10^{14} \text{ cm}^2 \cdot \text{s}^{-1}$.

- (a) Calculate the activity $\mathcal{A}_{\text{Co-60}}(t)$ of the Co-60 daughter against activation time t in steps of 2 years from 0 to 10 years as well as the maximum

activity $(\mathcal{A}_{\text{Co-60}})_{\text{max}}$ and time $(t_{\text{max}})_{\text{Co-60}}$ at which it is attained using three nuclear activation models:

- (1) Saturation model.
- (2) Parent depletion model.
- (3) Parent depletion–daughter activation model.

The neutron activation cross sections for the parent Co-59 nucleus and for the daughter Co-60 nucleus are $\sigma_{\text{P}} = 37 \times 10^{-24} \text{ cm}^2 = 37 \text{ b}$ and $\sigma_{\text{D}} = 2 \times 10^{-24} \text{ cm}^2 = 2 \text{ b}$, respectively, and the half-life of Co-60 is $(t_{1/2})_{\text{Co-60}} = 5.26 \text{ a}$. Compare the results of $(\mathcal{A}_{\text{Co-60}})_{\text{max}}$ and $(t_{\text{max}})_{\text{Co-60}}$ with a summary in tabular form for the three activation models.

- (b) Compare the activities of Co-60 calculated in (a) to the activities in Table 12.21 calculated using the complex activation scheme presented in Prob. 260.
- (c) Plot activities of Co-60 calculated in (a) and indicate parameters $(\mathcal{A}_{\text{Co-60}})_{\text{max}}$ and $(t_{\text{max}})_{\text{Co-60}}$ for the 3 models.

SOLUTION:

- (a) In nuclear activation four effects contribute to activity $\mathcal{A}_{\text{D}}(t)$ of the daughter:
 - (i) Production of the daughter through parent activation,
 - (ii) Depletion of the parent,
 - (iii) Decay of the daughter, and
 - (iv) Activation of the daughter.

Many levels of complexity are available for description of cobalt-60 activity in nuclear activation of cobalt-59 ranging from a simple saturation model all the way to accounting for the two branches available for Co-59 activation, shown schematically in Fig. 12.9 (Prob. 260). In this problem we compare $\mathcal{A}_{\text{Co-60}}(t)$ for the three simplest models assuming that Co-60 is produced from Co-59 through only one branch rather than two and that the cross section $\sigma_{\text{Co-59}}$ for neutron activation of Co-59 is equal to 37 b which is the sum of cross sections of the two branches. In reality, Co-60 is produced (i) directly through one branch with a cross section of 17 b and (ii) through an intermediate step of metastable Co-60m with a cross section of 20 b. The metastable Co-60m has a very short half-life and, for simplicity, one usually assumes that Co-60 is produced only through the direct branch with a cross section of 37 b.

- (1) **Saturation model:** In the saturation model, parent depletion and daughter activation are ignored during the activation process and the activity of the daughter $\mathcal{A}_{\text{D}}(t)$ as a function of activation time t is

$$\mathcal{A}_{\text{D}}(t) = \sigma_{\text{P}} \dot{\phi} N_{\text{P}}(0) [1 - e^{-\lambda_{\text{D}} t}], \quad (12.224)$$

Table 12.22 Relevant parameters for use of the saturation model (12.224) in neutron activation of Co-59 with mass $m_{\text{Co-59}} = 10 \text{ g}$ in a reactor with neutron fluence rate $\dot{\phi} = 5 \times 10^{14} \text{ cm}^2 \cdot \text{s}^{-1}$

$\sigma_{\text{Co-59}}$	$37 \times 10^{-24} \text{ cm}^2$
$\lambda_{\text{Co-60}} = \ln 2 / (t_{1/2})_{\text{Co-60}}$	$\ln(2) / 5.26 \text{ a} = 4.179 \times 10^{-9} \text{ s}^{-1}$
$\dot{\phi}$	$5 \times 10^{14} \text{ cm}^{-2} \text{ s}^{-1}$
$N_{\text{Co-59}}(0) = mN_A / A$	$(10 \text{ g}) \times (6.022 \times 10^{23} \text{ mol}^{-1}) / (59 \text{ g} \cdot \text{mol}^{-1}) = 1.021 \times 10^{23} \text{ (atoms)}$
$\sigma_{\text{Co-59}} \dot{\phi}$	$(37 \times 10^{-24} \text{ cm}^2) \times (5 \times 10^{14} \text{ cm}^{-2} \text{ s}^{-1}) = 1.85 \times 10^{-8} \text{ s}^{-1}$
$\sigma_{\text{Co-59}} \dot{\phi} N_{\text{Co-59}}(0)$	$(1.85 \times 10^{-8} \text{ s}^{-1}) \times (1.021 \times 10^{23}) = 1.889 \times 10^{15} \text{ s}^{-1}$

Table 12.23 Activity $\mathcal{A}_{\text{Co-60}}(t)$ of daughter Co-60 calculated from the saturation model (12.225) for mass of Co-59 sample $m_{\text{Co-59}} = 10 \text{ g}$ and neutron fluence rate $\dot{\phi} = 5 \times 10^{14} \text{ cm}^2 \cdot \text{s}^{-1}$ for activation times t between 0 and 10 years in steps of 2 years. Data are also plotted as curve (1) in Fig. 12.11

t (years)	$e^{-(4.179 \times 10^{-9} \text{ s}^{-1})t}$	$\mathcal{A}_{\text{Co-60}}(t)$ (Ci)
0	1.000	0
2	0.768	11824
4	0.590	20908
6	0.454	27888
8	0.348	33250
10	0.268	37371
∞	0	51054

where $N_P(0)$ is the number of parent nuclei at time $t = 0$ and $\lambda_D = \ln 2 / (t_{1/2})_D$ is the decay constant of the daughter.

The relevant parameters for use of (12.224) in Co-59 nuclear activation are summarized in Table 12.22 and result in the following expression for activity $\mathcal{A}_{\text{Co-60}}(t)$ of the Co-60 daughter as a function of activation time t

$$\begin{aligned}
 \mathcal{A}_{\text{Co-60}}(t) &= \sigma_{\text{Co-59}} \dot{\phi} N_{\text{Co-59}}(0) [1 - e^{-\lambda_{\text{Co-60}} t}] \\
 &= (1.889 \times 10^{15} \text{ Bq}) \times [1 - e^{-(4.179 \times 10^{-9} \text{ s}^{-1})t}] \\
 &= \frac{1.889 \times 10^{15} \text{ Bq}}{3.7 \times 10^{10} \text{ Bq/Ci}} [1 - e^{-(4.179 \times 10^{-9} \text{ s}^{-1})t}] \\
 &= (51054 \text{ Ci}) \times [1 - e^{-(4.179 \times 10^{-9} \text{ s}^{-1})t}]. \quad (12.225)
 \end{aligned}$$

The use of (12.225) with activation times t from 0 to 10 years in steps of 2 years yields Co-60 activities $\mathcal{A}_{\text{Co-60}}(t)$ that are summarized in Table 12.23 and plotted as curve (1) with open square data points in Fig. 12.11.

For the saturation model, the maximum daughter activity $(\mathcal{A}_{\text{Co-60}})_{\text{max}}$ occurs at the saturation activity $(\mathcal{A}_{\text{Co-60}})_{\text{sat}} = \sigma_{\text{Co-59}} \dot{\phi} N_{\text{Co-59}}(0)$ that is attained at activation time $t \rightarrow \infty$. Thus, for the mass of Co-59 sample $m_{\text{Co-59}} = 10 \text{ g}$ and neutron fluence

Table 12.24 Relevant parameters for use of the parent depletion model (12.227) in activation of a Co-59 sample with mass $m_{\text{Co-59}} = 10 \text{ g}$ and neutron fluence rate $\dot{\phi} = 5 \times 10^{14} \text{ cm}^2 \cdot \text{s}^{-1}$

$\sigma_{\text{Co-59}}$	$37 \times 10^{-24} \text{ cm}^2$
$\lambda_{\text{Co-60}} = \ln 2 / (t_{1/2})_{\text{Co-60}}$	$\ln(2) / 5.26 \text{ a} = 4.179 \times 10^{-9} \text{ s}^{-1} = 0.4179 \times 10^{-8} \text{ s}^{-1}$
$\dot{\phi}$	$5 \times 10^{14} \text{ cm}^{-2} \text{ s}^{-1}$
$N_{\text{Co-59}}(0) = m N_A / A$	$(10 \text{ g}) \times (6.022 \times 10^{23} \text{ mol}^{-1}) / (59 \text{ g} \cdot \text{mol}^{-1}) = 1.021 \times 10^{23} \text{ (atoms)}$
$\sigma_{\text{Co-59}} \dot{\phi}$	$(37 \times 10^{-24} \text{ cm}^2) \times (5 \times 10^{14} \text{ cm}^{-2} \text{ s}^{-1}) = 1.85 \times 10^{-8} \text{ s}^{-1}$
$\lambda_{\text{Co-60}} \sigma_{\text{Co-59}} \dot{\phi} N_{\text{Co-59}}(0)$	$(4.179 \times 10^{-9} \text{ s}^{-1}) \times (1.85 \times 10^{-8} \text{ s}^{-1}) \times (1.021 \times 10^{23}) = 7.890 \times 10^6 \text{ s}^{-2}$
$\lambda_{\text{Co-60}} - \sigma_{\text{Co-59}} \dot{\phi}$	$0.4179 \times 10^{-8} \text{ s}^{-1} - 1.85 \times 10^{-8} \text{ s}^{-1} = -1.432 \times 10^{-8} \text{ s}^{-1}$

$$\text{rate } \dot{\phi} = 5 \times 10^{14} \text{ cm}^2 \cdot \text{s}^{-1}$$

$$(\mathcal{A}_{\text{Co-60}})_{\text{max}} = (\mathcal{A}_{\text{Co-60}})_{\text{sat}} = \sigma_{\text{Co-59}} \dot{\phi} N_{\text{Co-59}}(0) = 1.889 \times 10^{15} \text{ Bq} = 51054 \text{ Ci.} \quad (12.226)$$

(2) **Parent depletion model:** In the parent depletion model, the activity of the daughter $\mathcal{A}_{\text{D}}(t)$ as a function of activation time t takes into account the depletion of parent nuclei during the activation process but ignores the loss of daughter nuclei as a result of neutron activation. The daughter activity $\mathcal{A}_{\text{D}}(t)$ is in general expressed as follows

$$\mathcal{A}_{\text{D}}(t) = \frac{\lambda_{\text{D}} \sigma_{\text{P}} \dot{\phi} N_{\text{P}}(0)}{\lambda_{\text{D}} - \sigma_{\text{P}} \dot{\phi}} [e^{-\sigma_{\text{P}} \dot{\phi} t} - e^{-\lambda_{\text{D}} t}]. \quad (12.227)$$

The relevant parameters for describing the Co-60 activity $\mathcal{A}_{\text{Co-60}}(t)$ with the parent depletion model in nuclear activation of Co-59 are summarized in Table 12.24 and result in the following expression for activity $\mathcal{A}_{\text{Co-60}}(t)$ as a function of activation time t

$$\begin{aligned} \mathcal{A}_{\text{D}}(t) &= \frac{7.890 \times 10^6 \text{ s}^{-2}}{-1.432 \times 10^{-8} \text{ s}^{-1}} \times [e^{-(1.850 \times 10^{-8} \text{ s}^{-1})t} - e^{-(4.179 \times 10^{-9} \text{ s}^{-1})t}] \\ &= (5.510 \times 10^{14} \text{ Bq}) \times [e^{-(4.179 \times 10^{-9} \text{ s}^{-1})t} - e^{-(1.850 \times 10^{-8} \text{ s}^{-1})t}] \\ &= (14891 \text{ Ci}) \times [e^{-(4.179 \times 10^{-9} \text{ s}^{-1})t} - e^{-(1.850 \times 10^{-8} \text{ s}^{-1})t}]. \quad (12.228) \end{aligned}$$

The use of (12.228) with activation times t from 0 to 10 years in steps of 2 years yields Co-60 activities $\mathcal{A}_{\text{Co-60}}(t)$ that are summarized in Table 12.25 and plotted with open circle data points in Fig. 12.11 as curve (2).

As evident from curve (2) of Fig. 12.11, in parent depletion model the daughter activity $\mathcal{A}_{\text{D}}(t)$ is zero at activation time $t = 0$, and with increasing t reaches a maximum $(\mathcal{A}_{\text{D}})_{\text{max}}$ at $t = (t_{\text{max}})_{\text{D}}$ and then drops as t increases further until at $t = \infty$ it becomes zero again. The maximum daughter activity $(\mathcal{A}_{\text{D}})_{\text{max}}$ is attained

Table 12.25 Activity $\mathcal{A}_D(t)$ of daughter Co-60 calculated from (12.228) for mass of Co-59 sample $m_{\text{Co-59}} = 10$ g and neutron fluence rate $\dot{\phi} = 5 \times 10^{14} \text{ cm}^2 \cdot \text{s}^{-1}$ for activation times t between 0 and 10 years in steps of 2 years. Data are also plotted in Fig. 12.11 as curve (2)

t (years)	$e^{-(1.850 \times 10^{-8} \text{ s}^{-1})t}$	$e^{-(4.179 \times 10^{-9} \text{ s}^{-1})t}$	$A_{\text{Co-60}}(t)$ (Ci)
0	1.000	1.000	0
2	0.311	0.768	6804
4	0.097	0.590	7346
6	0.030	0.454	6304
8	0.009	0.348	5049
10	0.003	0.268	3943
∞	0	0	0

at a characteristic time $(t_{\text{max}})_D$ given by

$$(t_{\text{max}})_D = \frac{\ln \frac{\sigma_P \dot{\phi}}{\lambda_D}}{\sigma_P \dot{\phi} - \lambda_D}. \quad (12.229)$$

For a neutron fluence rate $\dot{\phi} = 5 \times 10^{14} \text{ cm}^2 \cdot \text{s}^{-1}$, Co-59 parent nuclei, and Co-60 daughter nuclei the characteristic time $(t_{\text{max}})_{\text{Co-60}}$ is calculated as follows

$$\begin{aligned} (t_{\text{max}})_{\text{Co-60}} &= \frac{\ln \frac{\sigma_{\text{Co-59}} \dot{\phi}}{\lambda_{\text{Co-60}}}}{\sigma_{\text{Co-59}} \dot{\phi} - \lambda_{\text{Co-60}}} = \frac{\ln \frac{1.85 \times 10^{-8} \text{ s}^{-1}}{4.179 \times 10^{-9} \text{ s}^{-1}}}{1.85 \times 10^{-8} \text{ s}^{-1} - 0.4179 \times 10^{-9} \text{ s}^{-1}} \\ &= 1.039 \times 10^8 \text{ s} = 3.29 \text{ a}. \end{aligned} \quad (12.230)$$

To determine the maximum activity of Co-60 $(\mathcal{A}_{\text{Co-60}})_{\text{max}}$ at activation time $(t_{\text{max}})_{\text{Co-60}}$ given in (12.230) for Co-59 sample mass $m_{\text{Co-59}} = 10$ g and neutron fluence rate $\dot{\phi} = 5 \times 10^{14} \text{ cm}^2 \cdot \text{s}^{-1}$ we insert (12.230) into (12.228) and get

$$\begin{aligned} (\mathcal{A}_{\text{max}})_{\text{Co-60}} &= \mathcal{A}_{\text{Co-60}}[(t_{\text{max}})_{\text{Co-60}}] \\ &= \frac{\lambda_{\text{Co-60}} \sigma_{\text{Co-59}} \dot{\phi} N_{\text{Co-59}}(0)}{\lambda_{\text{Co-60}} - \sigma_{\text{Co-59}} \dot{\phi}} \left[e^{-\sigma_{\text{Co-59}} \dot{\phi} \times (t_{\text{max}})_{\text{Co-60}}} - e^{-\lambda_{\text{Co-60}} \times (t_{\text{max}})_{\text{Co-60}}} \right] \\ &= \frac{7.890 \times 10^6 \text{ s}^{-2}}{-1.432 \times 10^{-8} \text{ s}^{-1}} \times \left[e^{-(4.179 \times 10^{-9} \text{ s}^{-1}) \times (1.039 \times 10^8 \text{ s}^{-1})} \right. \\ &\quad \left. - e^{-(1.850 \times 10^{-8} \text{ s}^{-1}) \times (1.039 \times 10^8 \text{ s}^{-1})} \right] \\ &= (5.510 \times 10^{14} \text{ Bq}) \times (0.6478 - 0.1463) \\ &= (14891 \text{ Ci}) \times 0.5015 = 7468 \text{ Ci}. \end{aligned} \quad (12.231)$$

(3) Parent depletion–daughter activation model: In the parent deletion–daughter activation model, the activity of the daughter $\mathcal{A}_D(t)$ as a function of activation time t taking into account depletion of parent nuclei during activation as well as loss of

Table 12.26 Relevant parameters for use of (12.232) with mass of Co-59 sample $m_{\text{Co-59}} = 10 \text{ g}$ and neutron fluence rate $\dot{\phi} = 5 \times 10^{14} \text{ cm}^2 \cdot \text{s}^{-1}$

$\sigma_{\text{Co-59}}$	$37 \text{ b} = 37 \times 10^{-24} \text{ cm}^2$
$\sigma_{\text{Co-60}}$	$2 \text{ b} = 2 \times 10^{-24} \text{ cm}^2$
$\lambda_{\text{Co-60}} = \ln 2 / (t_{1/2})_{\text{Co-60}}$	$\ln 2 / 5.26 \text{ a} = 4.179 \times 10^{-9} \text{ s}^{-1}$
$\dot{\phi}$	$5 \times 10^{14} \text{ cm}^{-2} \cdot \text{s}^{-1}$
$N_{\text{Co-59}}(0) = mN_A / A$	$(10 \text{ g}) \times (6.022 \times 10^{23} \text{ mol}^{-1}) / (59 \text{ g} \cdot \text{mol}^{-1}) = 1.021 \times 10^{23} \text{ (atoms)}$
$\sigma_{\text{Co-59}}\dot{\phi}$	$(37 \times 10^{-24} \text{ cm}^2) \times (5 \times 10^{14} \text{ cm}^{-2} \cdot \text{s}^{-1}) = 1.85 \times 10^{-8} \text{ s}^{-1}$
$\sigma_{\text{Co-60}}\dot{\phi}$	$(2 \times 10^{-24} \text{ cm}^2) \times (5 \times 10^{14} \text{ cm}^{-2} \cdot \text{s}^{-1}) = 1 \times 10^{-9} \text{ s}^{-1}$
$\lambda_{\text{Co-60}}^* = \lambda_{\text{Co-60}} + \sigma_{\text{Co-60}}\dot{\phi}$	$(4.179 \times 10^{-9} \text{ s}^{-1}) + (1 \times 10^{-9} \text{ s}^{-1}) = 5.179 \times 10^{-9} \text{ s}^{-1}$
$\lambda_{\text{Co-60}}\sigma_{\text{Co-59}}\dot{\phi}N_{\text{Co-59}}(0)$	$(4.179 \times 10^{-9} \text{ s}^{-1}) \times (1.85 \times 10^{-8} \text{ s}^{-1}) \times (1.021 \times 10^{23}) = 7.890 \times 10^6 \text{ s}^{-2}$
$\lambda_{\text{Co-60}}^* - \sigma_{\text{Co-59}}\dot{\phi}$	$0.5179 \times 10^{-8} \text{ s}^{-1} - 1.85 \times 10^{-8} \text{ s}^{-1} = -1.332 \times 10^{-8} \text{ s}^{-1}$

daughter nuclei because of neutron activation is given by

$$\mathcal{A}_{\text{D}}(t) = \frac{\lambda_{\text{D}}\sigma_{\text{P}}\dot{\phi}N_{\text{P}}(0)}{\lambda_{\text{D}}^* - \sigma_{\text{P}}\dot{\phi}} [e^{-\sigma_{\text{P}}\dot{\phi}t} - e^{-\lambda_{\text{D}}^*t}], \quad (12.232)$$

where $\lambda_{\text{D}}^* = \lambda_{\text{D}} + \sigma_{\text{D}}\dot{\phi}$ is a modified decay constant accounting for daughter decay as well as for daughter activation.

The relevant parameters for describing the Co-60 activity $\mathcal{A}_{\text{Co-60}}(t)$ with the parent depletion–daughter activation model in nuclear activation of Co-59 are summarized in Table 12.26 and result in the following expression for activity $\mathcal{A}_{\text{Co-60}}(t)$ as a function of time t

$$\begin{aligned} \mathcal{A}_{\text{Co-60}}(t) &= \frac{\lambda_{\text{Co-60}}\sigma_{\text{Co-59}}\dot{\phi}N_{\text{Co-59}}(0)}{\lambda_{\text{Co-60}}^* - \sigma_{\text{Co-59}}\dot{\phi}} [e^{-\sigma_{\text{Co-59}}\dot{\phi}t} - e^{-\lambda_{\text{Co-60}}^*t}] \\ &= \frac{7.890 \times 10^6 \text{ s}^{-2}}{-1.332 \times 10^{-8} \text{ s}^{-1}} \times [e^{-(1.850 \times 10^{-8} \text{ s}^{-1})t} - e^{-(5.179 \times 10^{-9} \text{ s}^{-1})t}] \\ &= (5.923 \times 10^{14} \text{ Bq}) \times [e^{-(0.5179 \times 10^{-8} \text{ s}^{-1})t} - e^{-(1.850 \times 10^{-8} \text{ s}^{-1})t}] \\ &= (16008 \text{ Ci}) \times [e^{-(5.179 \times 10^{-9} \text{ s}^{-1})t} - e^{-(1.850 \times 10^{-8} \text{ s}^{-1})t}]. \end{aligned} \quad (12.233)$$

The use of (12.233) with activation times t from 0 to 10 years in steps of 2 years yields Co-60 activities $\mathcal{A}_{\text{Co-60}}(t)$ that are summarized in Table 12.27 and plotted as curve (3) with solid circle data points in Fig. 12.11.

For the parent depletion–daughter activation model, the maximum daughter activity $(\mathcal{A}_{\text{D}}^*)_{\text{max}}$ is attained at a characteristic time $(t_{\text{max}}^*)_{\text{D}}$ given by

$$(t_{\text{max}}^*)_{\text{D}} = \frac{\ln \frac{\sigma_{\text{P}}\dot{\phi}}{\lambda_{\text{D}}^*}}{\sigma_{\text{P}}\dot{\phi} - \lambda_{\text{D}}^*}, \quad (12.234)$$

Table 12.27 Activity $\mathcal{A}_D(t)$ of daughter Co-60 calculated from (12.233) for mass of Co-59 sample $m_{\text{Co-59}} = 10$ g and neutron fluence rate $\dot{\phi} = 5 \times 10^{14} \text{ cm}^2 \cdot \text{s}^{-1}$ for activation times t between 0 and 10 years in steps of 2 years. The data are also plotted as solid circle data points in Fig. 12.11

t (years)	$e^{-(1.850 \times 10^{-8} \text{ s}^{-1})t}$	$e^{-(5.179 \times 10^{-9} \text{ s}^{-1})t}$	$\mathcal{A}_D(t)$ (Ci)
0	1.000	1.000	0
2	0.311	0.721	6563
4	0.097	0.520	6778
6	0.030	0.375	5526
8	0.009	0.270	4184
10	0.003	0.195	3080

which is of same form as (12.229) for parent depletion model except that λ_D is replaced by λ_D^* .

For neutron fluence rate $\dot{\phi}$ of $5 \times 10^{14} \text{ cm}^2 \cdot \text{s}^{-1}$, Co-59 parent, and Co-60 daughter the characteristic time $(t_{\text{max}}^*)_D$ at maximum activity $(\mathcal{A}_{\text{Co-60}}^*)_{\text{max}}$ of the Co-60 daughter for the parent depletion–daughter activation model is calculated as

$$\begin{aligned} (t_{\text{max}}^*)_{\text{Co-60}} &= \frac{\ln \frac{\sigma_{\text{Co-59}} \dot{\phi}}{\lambda_{\text{Co-60}}^*}}{\sigma_{\text{Co-59}} \dot{\phi} - \lambda_{\text{Co-60}}^*} = \frac{\ln \frac{1.85 \times 10^{-8} \text{ s}^{-1}}{5.179 \times 10^{-9} \text{ s}^{-1}}}{1.85 \times 10^{-8} \text{ s}^{-1} - 0.5179 \times 10^{-8} \text{ s}^{-1}} \\ &= \frac{1.273}{1.332 \times 10^{-8} \text{ s}^{-1}} = 9.557 \times 10^7 \text{ s} = 3.03 \text{ a.} \end{aligned} \quad (12.235)$$

To determine the maximum activity $(\mathcal{A}_{\text{Co-60}}^*)_{\text{max}}$ attained during neutron activation in the Co-59 sample of mass $m_{\text{Co-59}} = 10$ g and with neutron fluence rate $\dot{\phi} = 5 \times 10^{14} \text{ cm}^2 \cdot \text{s}^{-1}$ we insert (12.235) into (12.233) and get

$$\begin{aligned} (\mathcal{A}_{\text{Co-60}}^*)_{\text{max}} &= \mathcal{A}_{\text{Co-60}}[(t_{\text{max}}^*)_{\text{Co-60}}] \\ &= \frac{\lambda_{\text{Co-60}} \sigma_{\text{Co-59}} \dot{\phi} N_{\text{Co-59}}(0)}{\lambda_{\text{Co-60}}^* - \sigma_{\text{Co-59}} \dot{\phi}} \left[e^{-(\sigma_{\text{Co-59}} \dot{\phi}) \times (t_{\text{max}}^*)_{\text{Co-60}}} \right. \\ &\quad \left. - e^{-(\lambda_{\text{Co-60}}^*) \times (t_{\text{max}}^*)_{\text{Co-60}}} \right] \\ &= (16008 \text{ Ci}) \times \left[e^{-(5.179 \times 10^{-9} \text{ s}^{-1}) \times (9.557 \times 10^7 \text{ s})} \right. \\ &\quad \left. - e^{-(1.850 \times 10^{-8} \text{ s}^{-1}) \times (9.557 \times 10^7 \text{ s})} \right] \\ &= 7027 \text{ Ci.} \end{aligned} \quad (12.236)$$

Table 12.28 presents the maximum Co-60 activity $(\mathcal{A}_{\text{Co-60}}^*)_{\text{max}}$ as well as characteristic times $(t_{\text{max}})_{\text{Co-60}}$ at which the maximum activity $(\mathcal{A}_{\text{Co-60}}^*)_{\text{max}}$ of Co-60 occurs in neutron activation of a 10 g sample of Co-59 in a nuclear reactor with neutron fluence rate $\dot{\phi}$ of $5 \times 10^{14} \text{ cm}^2 \cdot \text{s}^{-1}$ as predicted by three activation models: (1) saturation, (2) parent depletion, and (3) parent depletion–daughter activation.

Table 12.28 Maximum activity $(\mathcal{A}_{\text{Co-60}})_{\text{max}}$ and characteristic time $(t_{\text{max}})_{\text{Co-60}}$ for the neutron activation of 10 g sample of Co-59 in reactor with neutron fluence rate $\dot{\phi}$ of $5 \times 10^{14} \text{ cm}^{-2} \cdot \text{s}^{-1}$ for three activation models: (1) Saturation, (2) Parent depletion, and (3) Parent depletion–daughter activation

Activation model	Maximum activity $(\mathcal{A}_{\text{Co-60}})_{\text{max}}$ (Ci)	Characteristic time $(t_{\text{max}})_{\text{Co-60}}$ (a)
Saturation	51054	∞
Parent depletion	7468	3.29
Parent depletion–daughter activation	7027	3.03

Table 12.29 Activity $\mathcal{A}_{\text{Co-60}}(t)$ of daughter Co-60 calculated using (1) saturation model, (2) parent depletion model, (3) parent depletion–daughter activation model, and (4) complex model of Prob. 260 for mass of Co-59 sample $m_{\text{Co-59}} = 10 \text{ g}$ and reactor neutron fluence rate $\dot{\phi} = 5 \times 10^{14} \text{ cm}^2 \cdot \text{s}^{-1}$ for activation times t between 0 and 10 years in steps of 2 years

t (years)	Activity $\mathcal{A}_{\text{Co-60}}(t)$ of daughter Co-60			
	Saturation	Parent depletion	Parent depletion–daughter activation	Complex model
	(1)	(2)	(3)	(4)
0	0	0	0	0
2	11824	6804	6563	6556
4	20908	7346	6778	6771
6	27888	6304	5526	5520
8	33250	5049	4184	4179
10	37371	3943	3080	3076
∞	51054	0	0	0

It is obvious that the saturation model grossly over-predicts $(\mathcal{A}_{\text{Co-60}})_{\text{max}}$ in comparison to the other two models because $\sigma_{\text{Co-59}}\dot{\phi}$ and $\lambda_{\text{Co-60}}$ are of the same order of magnitude and the saturation model is valid only when $\sigma_P\dot{\phi} \ll \lambda_{\text{Co-60}}$.

(b) Activities $\mathcal{A}_{\text{Co-60}}(t)$ of Co-60 calculated using the saturation model (12.226), the parent depletion model (12.228), the parent depletion–daughter activation (12.232) model, and the complex model presented in Prob. 262 for a Co-59 sample of mass $m_{\text{Co-59}} = 10 \text{ g}$ irradiated with neutron fluence rate $\dot{\phi} = 5 \times 10^{14} \text{ cm}^2 \cdot \text{s}^{-1}$ for activation times t between 0 and 10 years in steps of 2 years are for comparison purposes listed in Table 12.29. The four models are listed in order of increasing complexity, the complex model accounting for all possible avenues and effects that affect the production of Co-60 through neutron activation of Co-59. This suggests the choice of model (4) as the gold standard to which the other models can be compared. Several observations can now be made about the four activation models based on Table 12.29:

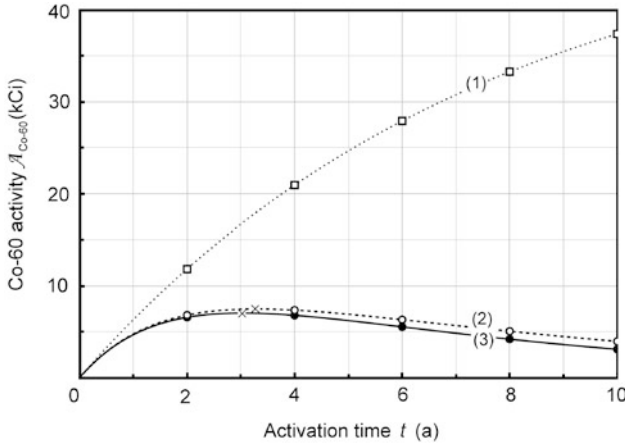


Fig. 12.11 Activity of cobalt-60 daughter against activation time t for neutron activation of a cobalt-59 sample of mass $m = 10$ g in a nuclear reactor with neutron fluence rate $\dot{\phi} = 5 \times 10^{14} \text{ cm}^{-2} \cdot \text{s}^{-1}$. *Open square points* (\square) represent data calculated from (12.225) for the saturation model (1), *open circle points* (\circ) represent data calculated from (12.228) for the parent depletion model (2), and *solid circle points* (\bullet) represent data calculated from (12.233) for the parent depletion–daughter activation model (3). Maxima in activity for the parent depletion model and for the parent depletion–daughter activation model are designated by (\times)

- (i) In comparison with the complex model the other three models all overestimate the activity of Co-60 for all activation times.
- (ii) All four models exhibit the same initial slope (radiation yield); however, with increasing activation time t they exhibit their own behavior against time t . Saturation model saturates for $t \rightarrow \infty$ at very high and unrealistic saturation activity $\mathcal{A}_{\text{sat}}(\infty) = 51054 \text{ Ci}$; the other three models reach a peak at $(\mathcal{A}_{\text{Co-60}})_{\text{max}}$ around 7000 Ci and then approach zero as $t \rightarrow \infty$.
- (iii) In comparison with the complex model, activities calculated for the saturation model are significantly higher; for the parent depletion model are up to 30 % higher; and for the parent depletion–daughter activation model are essentially identical. This suggests that the parent depletion–daughter activation model, despite ignoring the intermediate branch of the Co-59 activation process, is an excellent and significantly better replacement for the more complicated and cumbersome complex model studied in Prob. 262.

(c) Activities $\mathcal{A}_{\text{Co-60}}(t)$ of Co-60 calculated in (a) and presented in Table 12.28 for (1) saturation model, (2) parent depletion model, and (3) parent depletion–daughter activation model are plotted in Fig. 12.11. The data calculated for the complex activation model in Prob. 262 are not shown separately in the figure but we note that they are essentially identical with the data presented in curve (3) for the parent depletion–daughter activation model. Conclusions reached in (b) based on Table 12.29 are substantiated by diagrams of Fig. 12.11.

12.6.Q11

(262)

Gold-198 seeds or grains are used for permanent interstitial brachytherapy procedures. Gold-198 is produced in nuclear reactors by activation of pure gold-197 seeds (parent nuclei) with thermal neutrons. Neutron activation cross section σ_P for the parent nuclei is 98.7 barns. Gold seeds are activated in the reactor to achieve a specific activity a of approximately 2600 TBq/g (70 Ci/g). Gold-198 is β^- emitter, decaying with a half-life $t_{1/2}$ of 2.7 days into 3 states (2 excited states and ground state) of mercury-198. Gamma rays associated with gold-198 decay actually come from the de-excitation of the mercury-198 nuclide that instantaneously follows the β^- decay of gold-198.

- (a) Assuming that the saturation model is adequate for describing the growth of gold-198 activity during activation with thermal neutrons, state an equation that describes the growth in specific activity of gold-198 during activation in a reactor with a constant neutron fluence rate $\dot{\phi} = 4 \times 10^{13} \text{ cm}^{-2} \cdot \text{s}^{-1}$.
- (b) Determine the maximum attainable specific activity (saturation specific activity) a_{sat} for the gold seed in this reactor.
- (c) Plot the specific activity $a(t)$ given in (a) from time $t = 0$ to $t = 300$ h.
- (d) Calculate activation time t required to obtain specific activity a of gold-198 equal to: (1) 70 Ci/g, (2) half of saturation specific activity a_{sat} determined in (b), and (3) 95 % of saturation specific activity a_{sat} determined in (b).
- (e) Estimate the fraction of depleted parent nuclei for the activation times determined in (d) and justify the use of the saturation activation model in production of gold-198 seeds.
- (f) Define the radioactivation yield Y_D in general and calculate it for the gold-197 activation into gold-198 in a nuclear reactor with neutron fluence $\dot{\phi}$ of $4 \times 10^{13} \text{ cm}^{-2} \cdot \text{s}^{-1}$.

SOLUTION:

(a) Specific activity a of a radioactive source is defined as activity \mathcal{A} of the source per unit mass M of the source, i.e., $a = \mathcal{A}/M$. For the saturation model, we can thus express specific activity a against activation time t as (T12.13)

$$a(t) = \frac{\mathcal{A}(t)}{M} = \frac{\sigma_P \dot{\phi} N_P(0)}{M} \{1 - e^{-\lambda_D t}\} = \frac{\sigma_P \dot{\phi} N_P}{A_P} \{1 - e^{-\lambda_D t}\} = a_{\text{sat}} \{1 - e^{-\lambda_D t}\}, \quad (12.237)$$

where we define a_{sat} as the saturation specific activity ($a_{\text{sat}} = \sigma_P \dot{\phi} N_A / A_P$) and we used the identity $N_P(0)/M = N_A / A_P$ with A_P the atomic weight of the parent nucleus and N_A is the Avogadro number ($6.022 \times 10^{23} \text{ mol}^{-1}$).

For our specific case of gold-198 produced by activation of stable gold-197 with thermal neutron ($\dot{\varphi} = 4 \times 10^{13} \text{ cm}^{-2} \cdot \text{s}^{-1}$) in a nuclear reactor, the growth of specific activity $a(t)$ of gold-198 seed is, based on (12.237), given as

$$\begin{aligned} a(t) &= \frac{\sigma_{\text{Au-197}} \dot{\varphi} N_{\text{A}}}{A_{\text{Au-197}}} \left\{ 1 - e^{-\frac{(\ln 2)t}{t_{1/2}}} \right\} \\ &= \frac{(98.7 \times 10^{-24} \text{ cm}^2) \times (4 \times 10^{13} \text{ cm}^{-2} \cdot \text{s}^{-1}) \times (6.022 \times 10^{23} \text{ mol}^{-1})}{(197 \text{ g} \cdot \text{mol}^{-1})} \\ &\quad \times \left\{ 1 - e^{-(0.0107 \text{ h})t} \right\} \\ &= (1.21 \times 10^{13} \text{ Bq} \cdot \text{g}^{-1}) \times \left\{ 1 - e^{-(0.0107 \text{ h}^{-1})t} \right\} = (326.2 \text{ Ci/g}) \\ &\quad \times \left\{ 1 - e^{-(0.0107 \text{ h}^{-1})t} \right\}, \end{aligned} \quad (12.238)$$

where we made use of the conversion: $1 \text{ s}^{-1} = 1 \text{ Bq} = (3.7 \times 10^{10})^{-1} \text{ Ci}$ and calculated the decay constant of the daughter nucleus λ_{D} as

$$\lambda_{\text{D}} = \frac{\ln 2}{(t_{1/2})_{\text{D}}} = \frac{\ln 2}{(2.7 \text{ d}) \times (24 \text{ h/d})} = 0.0107 \text{ h}^{-1} = 2.972 \times 10^{-6} \text{ s}^{-1}. \quad (12.239)$$

(b) Under the assumption that the saturation model adequately describes the growth of gold-198 specific activity for thermal neutron activation of gold-197, the maximum attainable specific activity (saturation value) is determined using (12.238) with time $t = \infty$ or we use our definition of a_{sat} that we introduced with (12.237)

$$\begin{aligned} a_{\text{sat}} &= \frac{\sigma_{\text{P}} \dot{\varphi} N_{\text{A}}}{A_{\text{P}}} \\ &= \frac{(98.7 \times 10^{-24} \text{ cm}^2) \times (4 \times 10^{13} \text{ cm}^{-2} \cdot \text{s}^{-1}) \times (6.022 \times 10^{23} \text{ mol}^{-1})}{(197 \text{ g} \cdot \text{mol}^{-1})} \\ &= \lim_{t \rightarrow \infty} a = \lim_{t \rightarrow \infty} \frac{\sigma_{\text{Au-197}} \dot{\varphi} N_{\text{A}}}{A_{\text{Au-197}}} \left\{ 1 - e^{-\lambda_{\text{D}} t} \right\} \\ &= (326.2 \text{ Ci/g}) \times \lim_{t \rightarrow \infty} \left\{ 1 - e^{-(0.0107 \text{ h}^{-1})t} \right\} \\ &= 326.2 \text{ Ci/g} = 1.21 \times 10^{13} \text{ Bq/g}. \end{aligned} \quad (12.240)$$

(c) In preparation to plot the specific activity $a(t)$ for the first 300 hours of the activation process of gold-197 into gold-198 we use (12.238) to calculate the specific activity $a(t)$ from time $t = 0$ to time $t = 300 \text{ h}$ in steps of 50 hours and show the results in Table 12.30 and Fig. 12.12.

(d) In this section we determine activation times t under various conditions using (12.238) solved for the specific time t as follows

$$\frac{a(t)}{a_{\text{sat}}} = \left\{ 1 - e^{-\lambda_{\text{D}} t} \right\} \quad \text{or} \quad t = -\frac{1}{\lambda_{\text{D}}} \left\{ 1 - \frac{a(t)}{a_{\text{sat}}} \right\}. \quad (12.241)$$

Table 12.30 Growth of gold-198 specific activity during the first 300 hours of thermal neutron activation of gold-197 in nuclear reactor with neutron fluence rate $\dot{\phi} = 4 \times 10^{13} \text{ cm}^{-2} \cdot \text{s}^{-1}$

Time t (h)	$(0.0107 \text{ h}^{-1})t$	$1 - e^{-(0.0107 \text{ h}^{-1})t}$	$a(t) = (326.2 \text{ Ci/g}) \times \{1 - e^{-(0.0107 \text{ h}^{-1})t}\}$
0	0.000	0.000	0.0
50	0.535	0.414	135.1
100	1.070	0.657	214.3
150	1.605	0.799	260.6
200	2.140	0.882	287.8
250	2.675	0.931	303.7
300	3.210	0.960	313.3
∞	∞	1.0	326.2

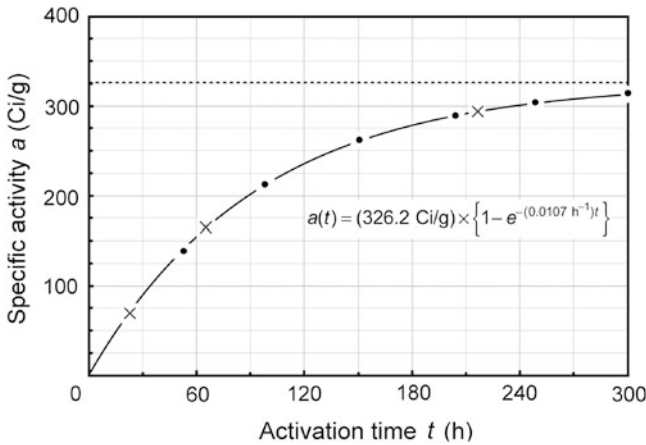


Fig. 12.12 Specific activity $a(t)$ against activation time t for activation of gold-197 into gold-198 $[(t_{1/2})_D = (t_{1/2})_{\text{Au-198}} = 2.7 \text{ d}]$ with thermal neutrons in a nuclear reactor with fluence rate $\dot{\phi}$ of $4 \times 10^{13} \text{ cm}^{-2} \cdot \text{s}^{-1}$. Cross section $\sigma_p = \sigma_{\text{Au-197}}$ for thermal neutron activation of gold-197 is 98.7 b; data points calculated with (12.238) are shown with solid circles, specific activities calculated in (d) are shown with symbol \times

- (1) Time t_1 required for the specific activity $a(t_1) = a_1$ of the Au-197/Au-198 gold seed to reach 70 Ci/g.

$$\begin{aligned}
 t_1 &= -\frac{1}{\lambda_D} \ln \left\{ 1 - \frac{a(t_1)}{a_{\text{sat}}} \right\} = -\frac{1}{0.0107 \text{ h}^{-1}} \ln \left\{ 1 - \frac{70 \text{ Ci/g}}{326.2 \text{ Ci/g}} \right\} \\
 &= 22.6 \text{ h} = 0.94 \text{ d}.
 \end{aligned}
 \tag{12.242}$$

- (2) Time t_2 required for specific activity a_2 of the Au-197/Au-198 gold seed to reach 50 % of the saturation specific activity a_{sat} determined in (b) as $a_{\text{sat}} =$

326.2 Ci/g; i.e., $a_2 = 163.1$ Ci/g.

$$\begin{aligned} t_2 &= -\frac{1}{\lambda_D} \ln \left\{ 1 - \frac{a(t_2)}{a_{\text{sat}}} \right\} = -\frac{1}{0.0107 \text{ h}^{-1}} \ln \left\{ 1 - \frac{163.1 \text{ Ci/g}}{326.2 \text{ Ci/g}} \right\} \\ &= \frac{\ln 2}{0.0107 \text{ h}^{-1}} \\ &= \frac{1}{\lambda_D} = (t_{1/2})_{\text{Au-198}} = 2.7 \text{ d} = 64.8 \text{ h}. \end{aligned} \quad (12.243)$$

In the saturation neutron activation model where an assumption is made that the number of parent nuclei is infinite, 50 % of saturation specific activity is attained in an activation time t that is equal to the half-life $(t_{1/2})_D$ of the daughter nucleus. In the case of Au-197 \rightarrow Au-198 activation, a specific activity equal to 50 % of the saturation specific activity is reached at an activation time t equal to the half-life $(t_{1/2})_{\text{Au-198}} = 2.7$ d of the daughter Au-198 nucleus.

- (3) Time t_3 required for specific activity a_3 of the Au-197/Au-198 gold seed to reach 95 % of the saturation specific activity a_{sat} determined in (b) as $a_{\text{sat}} = 326.2$ Ci/g, i.e., $a_3 = 309.9$ Ci/g.

$$\begin{aligned} t_3 &= -\frac{1}{\lambda_D} \ln \left\{ 1 - \frac{a(t_3)}{a_{\text{sat}}} \right\} = -\frac{1}{0.0107 \text{ h}^{-1}} \ln \left\{ 1 - \frac{309.9 \text{ Ci/g}}{326.2 \text{ Ci/g}} \right\} \\ &= \frac{\ln(1 - 0.95)}{0.0107 \text{ h}^{-1}} = 280.0 \text{ h}. \end{aligned} \quad (12.244)$$

(e) The depletion of parent nuclei during activation is described with the following relationship

$$N_P(t) = N_P(0)e^{-\sigma\phi t}, \quad (12.245)$$

where $N_P(0)$ is the initial number of parent nuclei at time $t = 0$ and $N_P(t)$ is the number of parent nuclei at time t . The fraction of depleted parent nuclei f_{dep} after activation time t is defined as the ratio

$$f_{\text{dep}} = \frac{N_P(0) - N_P(t)}{N_P(0)} = 1 - \frac{N_P(t)}{N_P(0)} = 1 - e^{-\sigma\phi t}. \quad (12.246)$$

Therefore, the fractions $(f_{\text{dep}})_1$, $(f_{\text{dep}})_2$, and $(f_{\text{dep}})_3$ of depleted gold-197 nuclei after activation times determined in (d) as (1) $t_1 = 22.6$ h, (2) $t_2 = 64.8$ h, and (3) $t_3 = 280.0$ h, respectively, in a nuclear reactor with a neutron fluence rate $\dot{\phi} = 4 \times 10^{13} \text{ cm}^{-2} \cdot \text{s}^{-1}$ are from (12.246) given as

$$(f_{\text{dep}})_1 = 1 - e^{-(98.7 \times 10^{-24} \text{ cm}^2) \times (4 \times 10^{13} \text{ cm}^{-2} \cdot \text{s}^{-1}) \times (22.6 \text{ h}) \times (3600 \text{ s/h})} \approx 3.2 \times 10^{-4}, \quad (12.247)$$

$$(f_{\text{dep}})_2 = 1 - e^{-(98.7 \times 10^{-24} \text{ cm}^2) \times (4 \times 10^{13} \text{ cm}^{-2} \cdot \text{s}^{-1}) \times (64.8 \text{ h}) \times (3600 \text{ s/h})} \approx 9.2 \times 10^{-4}, \quad (12.248)$$

$$(f_{\text{dep}})_3 = 1 - e^{-(98.7 \times 10^{-24} \text{ cm}^2) \times (4 \times 10^{13} \text{ cm}^{-2} \cdot \text{s}^{-1}) \times (280 \text{ h}) \times (3600 \text{ s/h})} \approx 4 \times 10^{-3}. \quad (12.249)$$

Equations (12.247), (12.248), and (12.249) show that the fraction of depleted gold-197 nuclei during activation in a reactor with a neutron fluence rate of $\dot{\phi} = 4 \times 10^{13} \text{ cm}^{-2} \cdot \text{s}^{-1}$ is small and can be neglected so as to be able to use the saturation activation model. For example, as shown in (PP), even at 95 % of the saturation specific activity of gold-198, the depletion of gold-197 nuclei is less than 0.5 % of the initial value, and at smaller fractions of saturation specific activity, the depletion is even less pronounced.

(f) Specific activity $a_D(t)$ of the daughter nuclide D given in (12.237) exhibits a simple exponential growth behavior and its initial slope at $t = 0$ is defined as the radio-activation yield Y_D of the daughter nuclide produced in the radioactivation process. Y_D represents the initial rate of formation of the new daughter activity that depends upon the irradiation conditions as well as the decay constant λ_D of the daughter

$$Y_D = \frac{da_D(t)}{dt} = \lim_{t \rightarrow 0} \sigma_P \dot{\phi} \frac{N_A}{A} \lambda_D e^{-\lambda_D t} = \sigma_P \dot{\phi} \frac{N_A}{A} \lambda_D = a_{\text{sat}} \lambda_D. \quad (12.250)$$

Radioactivation yield Y_D for the specific case of gold-197 radioactivation into gold-198 in nuclear reactor with neutron fluence rate $\dot{\phi}$ of $4 \times 10^{13} \text{ cm}^{-2} \cdot \text{s}^{-1}$ is calculated as follows

$$\begin{aligned} Y_{\text{Au-198}} &= \sigma_{\text{Au-197}} \dot{\phi} \frac{N_A}{A} \lambda_{\text{Au-198}} = a_{\text{sat}} \lambda_{\text{Au-198}} \\ &= (2.972 \times 10^{-6} \text{ s}^{-1}) \times (1.21 \times 10^{13} \text{ s}^{-1} \cdot \text{g}^{-1}) = 3.6 \times 10^7 \text{ s}^{-2} \cdot \text{g}^{-1}, \end{aligned} \quad (12.251)$$

where the saturation specific activity a_{sat} was determined in (12.239) and the decay constant $\lambda_{\text{Au-198}}$ of gold-198 was determined in (12.238).

12.6.Q13

(263)

The most common type of nuclear reaction is that in which two nuclei interact and produce one or more reaction products. The reaction is called binary and one of the two reactants is the projectile (usually a moving particle or photon) and the other is the target (usually a stationary nucleus). Nuclear reaction between a neutron n and atomic nucleus ${}^A_Z\text{X}$ is an example of a typical binary interaction, most commonly resulting in emission of a γ ray photon or emission of a proton. The reaction is called neutron capture or neutron activation.

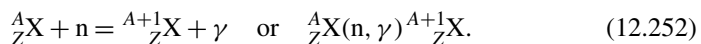
- (a) What, if any, is the difference between the terms “neutron capture” and “neutron activation”? Describe the important features of the (n, γ) reaction and the (n, p) reaction.
- (b) List and briefly describe 4 neutron capture (neutron activation) reactions of importance to medical physics. For each activation product discuss the isotopic purity and specific activity of the resulting radiation source.
- (c) For each neutron activation daughter D listed in (b) prepare a table containing the following
- (1) Parent nuclide P.
 - (2) Neutron capture cross section σ_P .
 - (3) Neutron capture reaction ${}^A_Z\text{P}(n, \gamma) {}^{A+1}_Z\text{P}$.
 - (4) Daughter nuclide D.
 - (5) Half-life. $(t_{1/2})_D$.
 - (6) Decay constant λ_D .
 - (7) Decay mode of daughter D.
 - (8) Theoretical specific activity $(a_D)_{\text{theor}}$.
 - (9) Practical specific activity $(a_D)_{\text{pract}}$.

SOLUTION:

(a) As far as the nuclear reaction between a neutron (projectile) n and parent nucleus (target) ${}^A_Z\text{X}$ is concerned, there is no essential difference between the terms “neutron capture” and “neutron activation”. Both terms describe the same reaction and its outcome, that is, activation of the target nucleus through capture of the neutron projectile. However, the choice between the two names that are used for the nuclear reaction triggered by the neutron depends on the reaction outcome. When our interest is the fate of the neutron projectile, we call the reaction neutron capture and when our interest is in the production of radioactive daughter product, we call the reaction neutron activation.

The (n, γ) and (n, p) nuclear reactions are the two most common types of neutron capture reaction:

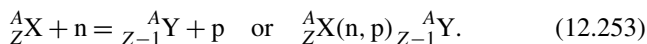
- (1) The (n, γ) reaction results in neutron capture and emission of one or more γ rays. The schematic representation of the nuclear reaction is as follows



In the (n, γ) reaction the target nucleus ${}^A_Z\text{X}$ captures a neutron and is converted into an excited nucleus ${}^{A+1}_Z\text{X}^*$ that undergoes an immediate de-excitation to its ground state ${}^{A+1}_Z\text{X}$ through emission of a γ ray or several γ rays if the

transition to ground state goes through intermediate excited states. Note that the parent nucleus A_ZX and the daughter nucleus ${}^{A+1}_ZX$ are isotopes of the same chemical element. The ${}^{A+1}_ZX$ nucleus is neutron rich as well as unstable (radioactive) and decays with a given half-life through β^- decay into a more stable configuration.

- (2) The (n, p) reaction results in neutron capture and emission of a proton and is schematically represented as follows



The (n, p) reaction produces a new nucleus ${}^{A-1}_{Z-1}Y$ that is an isobar of the target nucleus A_ZX . The target nucleus captures the neutron projectile and promptly ejects a proton to become converted into a new nucleus ${}^{A-1}_{Z-1}Y$. Note that nuclei A_ZX and ${}^{A-1}_{Z-1}Y$ do not represent the same chemical element; however, they possess the same atomic mass number A which means that they are isobars.

- (b) The four neutron activation processes of importance to medical physics are:
- (1) Production of cobalt-60 radionuclide for use in cobalt-60 sealed sources for external beam radiotherapy.
 - (2) Production of iridium-192 radionuclide for use in iridium-192 sealed sources for high dose rate (HDR) remote afterloading brachytherapy.
 - (3) Production of molybdenum-99 radionuclide for use in generating technetium-99m radionuclide with radionuclide generators for nuclear medicine imaging.
 - (4) Production of lithium-7 radionuclide in boron neutron capture therapy.

(1) **Cobalt-60** is the most widely used radionuclide source in teletherapy machines for external beam radiotherapy and is the radionuclide of choice in Gamma units used for stereotactic radiosurgery. It has also been used in blood irradiators as well as in remote afterloading machines for brachytherapy.

Cobalt-60 is produced in a nuclear reactor by irradiating stable cobalt-59 with thermal neutrons [${}^{59}\text{Co}(n, \gamma){}^{60}\text{Co}$] and it decays through beta minus decay with a half-life $(t_{1/2})_{\text{Co-60}}$ of 5.26 years into excited nickel-60, in each Co-60 nuclear disintegration, emitting a beta particle (electron) and two gamma ray photons (1.17 MeV and 1.33 MeV). The beta particle comes from the beta minus decay of cobalt-60; the two gamma rays originate from the gamma decay of excited nickel-60 into ground state of nickel-60. Since the two gamma rays originating from the gamma decay of nickel-60 follow instantaneously the beta minus nuclear decay of cobalt-60 into excited nickel-60, it is customary to refer to these gamma rays as cobalt-60 gamma rays even though they are actually produced in the gamma decay of nickel-60.

As shown in Probs. 260 and 261 (see Figs. 12.9 and 12.11), the actual nuclear activation / decay scheme of Co-60 is significantly more complicated than the simplified, yet adequate for practical purposes, scheme normally invoked in the discussion of Co-60 activation and decay.

The theoretical specific activity ($a_{\text{Co-60}}$) of cobalt-60 is calculated under the assumption that the radioactive nuclide contains only the daughter nuclei, i.e., the source is carrier-free

$$\begin{aligned}
 (a_{\text{Co-60}})_{\text{theor}} &= \frac{A_{\text{Co-60}}}{m} = \frac{\lambda_{\text{Co-60}} N_{\text{Co-60}}}{m} = \frac{(\ln 2) N_A}{(t_{1/2})_{\text{Co-60}} A_{\text{Co-60}}} \\
 &= \frac{(\ln 2) \times (6.022 \times 10^{23} \text{ mol}^{-1})}{(5.26 \text{ a}) \times (365 \text{ d/a}) \times (24 \text{ h/d}) \times (3600 \text{ s/h}) \times (60 \text{ g} \cdot \text{mol}^{-1})} \\
 &= 4.194 \times 10^{13} \text{ s}^{-1}/\text{g} = 41.94 \text{ TBq/g} = \frac{41.94 \times 10^{12} \text{ Bq} \cdot \text{g}^{-1}}{3.7 \times 10^{10} \text{ Bq/Ci}} \\
 &= 1133.5 \text{ Ci/g.} \tag{12.254}
 \end{aligned}$$

In practice, manufacturing a cobalt-60 carrier-free source would be very difficult because cobalt-60 is produced through neutron activation in a nuclear reactor and at the end of the relatively lengthy activation process (few months to few years) the cobalt-60 radionuclide is found in a mixture consisting of:

- (i) Cobalt-60 nuclei produced by neutron capture in cobalt-59.
- (ii) Remaining cobalt-59 parent nuclei that escaped activation.
- (iii) Nickel-60 nuclei that were produced in beta minus decay of some of cobalt-60 nuclei during the activation process.

Typical activity of a cobalt source for external beam radiotherapy is of the order of 10^4 Ci (370 TBq). A Gamma Unit contains about 200 cobalt sources at ~ 30 Ci each for a total activity of some 6000 Ci per machine.

Because of the difficulty in physical separation of Co-60 from the mixture, a cobalt-60 teletherapy source is not carrier-free; rather, it contains a mixture of Co-59, Co-60, and Ni-60. The highest practical specific activity of a cobalt-60 source amounts to about 300 Ci/g or about 25 % of the theoretical specific activity of Co-60 given in (12.254). Obviously, the higher is the specific activity of a teletherapy source, the smaller is the source diameter, the closer comes the source to point source geometry, and the smaller is the geometrical beam penumbra.

(2) **Iridium-192** is the most widely used radionuclide source in remote afterloading machines for brachytherapy. It is produced in a nuclear reactor by irradiating with thermal neutrons natural iridium samples consisting of Ir-191 (natural abundance of 37.3 %) and Ir-193 (natural abundance of 62.7 %). Both isotopes in natural iridium are stable with cross sections σ_P of 954 b and 100 b, respectively.

Irradiation with thermal neutrons of Ir-191 results in Ir-192 [$^{191}\text{Ir}(n, \gamma)^{192}\text{Ir}$], irradiation of Ir-193 results in Ir-194 [$^{193}\text{Ir}(n, \gamma)^{194}\text{Ir}$]. Both Ir-192 and Ir-194 are radioactive isotopes of iridium with half-lives of 73.8 days and 19.3 hours, respectively. Iridium-194 produced in natural iridium by neutron activation has a much shorter half-life than Ir-192 and it decays to stable platinum-194 within a few days, thereby not affecting the radiation emanating from an Ir-192 source.

Similarly to the cobalt-60 source, an iridium-192 source is not carrier-free because of the difficulty involved in separation of Ir-192 from the sample mixture that is even more complicated than that of a cobalt source. After the activation process, the iridium-192 source contains:

- (i) Remaining Ir-191.
- (ii) Osmium-192 (Os-192) and platinum-192 (Pt-192), both daughters of Ir-192 that was produced and decayed during the activation process through β^- decay into Pt-192 or through electron capture into Os-192.
- (iii) Ir-193 remaining from the activation process or produced by neutron activation of Ir-192.
- (iv) Ir-194 produced through neutron activation of Ir-193.
- (v) Daughter products of Ir-194 decay.

Clearly, the practical specific activity of an iridium-192 source is lower than the theoretical specific activity of Ir-192 calculated as follows

$$\begin{aligned}
 (a_{\text{Ir-192}})_{\text{theor}} &= \frac{A_{\text{Ir-192}}}{m} = \frac{\lambda_{\text{Ir-192}} N_{\text{Ir-192}}}{m} = \frac{(\ln 2) N_A}{(t_{1/2})_{\text{Ir-192}} A_{\text{Ir-192}}} \\
 &= \frac{(\ln 2) \times (6.022 \times 10^{23} \text{ mol}^{-1})}{(73.8 \text{ d}) \times (24 \text{ h/d}) \times (3600 \text{ s/h}) \times (192 \text{ g} \cdot \text{mol}^{-1})} \\
 &= 3.410 \times 10^{14} \text{ s}^{-1}/\text{g} = 341 \text{ TBq/g} = \frac{341 \times 10^{12} \text{ Bq} \cdot \text{g}^{-1}}{3.7 \times 10^{10} \text{ Bq/Ci}} \\
 &= 9216 \text{ Ci/g}. \tag{12.255}
 \end{aligned}$$

Production of iridium-192 radionuclide suffers the additional complication of the activation product Ir-192 being affected by neutron irradiation and undergoing its own activation with a cross section $\sigma_{\text{Ir-192}}$ of 1420 b. During the activation process this results in depletion of Ir-192 not only because of its radioactive decay but also because of its activation into Ir-193. This suggests that, instead of the standard depletion model of nuclear activation, one should use the parent depletion–daughter activation model which offers a better approximation to the production of the Ir-192 daughter radionuclide and accounts for the loss in daughter nuclei not only because of the decay of the radioactive daughter but also because of the neutron activation of the daughter.

Typical Ir-192 source activity for use in HDR brachytherapy is 10 Ci (0.37 TBq) and the practical specific activity of the brachytherapy source is up to ~ 600 Ci/g, compared to the theoretical specific activity of Ir-192 given in (12.255) as 9216 Ci/g.

(3) **Molybdenum-99** (Mo-99) is a radionuclide of importance to medical physics, since it serves as parent nucleus for production of technetium-99m (Tc-99m) in radionuclide ^{99}Mo – $^{99\text{m}}\text{Tc}$ generators. These generators are devices that allow extraction of Tc-99m radionuclide of high specific activity from a radioactive mixture produced by Mo-99 beta minus decay into Tc-99m.

Technetium-99m (Tc-99m) is the most widely used radionuclide in nuclear medicine, being used in some 80 % of all clinical nuclear imaging tests. It emits 140.5 keV gamma rays with a physical half-life of 6.02 hours and thus possesses properties that make it very suitable for nuclear clinical imaging, providing high quality images combined with relatively low patient radiation dose.

Two techniques are in use for commercial production of Mo-99, both using thermal neutrons from a nuclear reactor to irradiate suitably prepared targets. The prevalent technique for Mo-99 production uses the fission process in highly enriched uranium-235 (HEU) targets and the less common technique uses neutron capture in enriched Mo-98 targets. The two reactions are expressed as follows: (1) Fission— $^{235}\text{U}(n, f)^{99}\text{Mo}$ and (2) Neutron activation— $^{98}\text{Mo}(n, \gamma)^{99}\text{Mo}$.

While each technique has its advantages and disadvantages over the other technique, fission compared to neutron activation produces Mo-99 with a significantly higher specific activity, as a result of its more than two orders of magnitude larger cross section for Mo-99 production (37 b against 0.13 b). The main drawback of fission is that it produces a high level of nuclear waste in comparison with neutron activation of Mo-98 which produces minimal nuclear waste. In addition to Mo-99, fission of U-235 produces a large number of other fission products and three of them are also of importance in medical physics: iodine-131 and xenon-133 both used in nuclear imaging and cesium-137 used as radiation source, mainly in blood irradiators but was in the past also used as source for external beam radiotherapy.

Theoretical specific activity $a_{\text{Mo-99}}$ of Mo-99 is determined as follows

$$\begin{aligned}
 (a_{\text{Mo-99}})_{\text{theor}} &= \frac{\mathcal{A}_{\text{Mo-99}}}{m} = \frac{\lambda_{\text{Mo-99}} N_{\text{Mo-99}}}{m} = \frac{(\ln 2) N_{\text{A}}}{(t_{1/2})_{\text{Mo-99}} A_{\text{Mo-99}}} \\
 &= \frac{(\ln 2) \times (6.022 \times 10^{23} \text{ mol}^{-1})}{(66 \text{ h}) \times (3600 \text{ s/h}) \times (99 \text{ g} \cdot \text{mol}^{-1})} = 1.775 \times 10^{16} \text{ s}^{-1}/\text{g} \\
 &= 1.775 \times 10^4 \text{ TBq/g} = \frac{1.775 \times 10^{16} \text{ Bq} \cdot \text{g}^{-1}}{3.7 \times 10^{10} \text{ Bq/Ci}} \\
 &= 4.797 \times 10^5 \text{ Ci/g}. \tag{12.256}
 \end{aligned}$$

The thermal neutron cross section for fission of U-235 is 600 b and the fission yield of Mo-99 in a U-235 target is about 6 %, suggesting a fission cross section for Mo-99 of 37 b. The neutron activation cross section of Mo-98 is about 300 times smaller at about 0.13 b. The practical specific activity of fission-produced Mo-99 with 90 % HEU can exceed 5000 Ci/g, while the practical specific activity of Mo-99 produced with neutron activation of Mo-98 is of the order of 1 Ci/g, clearly much lower than that of fission-produced Mo-99. Of course, practical specific activities for both the fission- as well as activation-produced Mo-99 are much lower than the theoretical specific activities calculated in (12.256) assuming a carrier-free Mo-99 radionuclide.

Table 12.31 Several important parameters of four nuclides of interest in medical physics: cobalt-60 used as sealed radiation source for external beam radiotherapy, iridium-192 used as sealed radiation source for high dose rate brachytherapy, molybdenum-99 used for generating technetium-99m for nuclear imaging, and lithium-7 produced as the daughter nuclide in boron neutron capture therapy

(1) Parent nuclide P	Cobalt-59 (Co-59)	Iridium-191 (Ir-191)	Molybdenum-99 (Mo-99)	Boron-10 (B-10)
(2) Neutron capture cross section σ_p	37.2	954	0.13	3840
(3) Neutron capture reaction ${}^A_Z\text{P}(n, \gamma) {}^{A+1}_Z\text{P}$	${}^{59}_{27}\text{Co}(n, \gamma) {}^{60}_{27}\text{Co}$	${}^{191}_{77}\text{Ir}(n, \gamma) {}^{192}_{77}\text{Ir}$	${}^{98}_{42}\text{Mo}(n, \gamma) {}^{99}_{42}\text{Mo}$	${}^{10}_5\text{B}(n, \alpha) {}^7_3\text{Li}$
(4) Daughter nuclide D	Cobalt-60 (Co-60)	Iridium-192 (Ir-192)	Molybdenum-98 (Mo-99)	Lithium-7 (Li-7)
(5) Half-life $(t_{1/2})_D = \frac{\ln 2}{\lambda_D}$	5.26 a	73.8 d	66 h	Stable
(6) Decay constant $\lambda_D(\text{s}^{-1}) = (\ln 2)/(t_{1/2})_D$	4.179×10^{-9}	1.087×10^{-7}	2.917×10^{-6}	N/A
(7) Decay mode of daughter (granddaughter in bracket)	$\beta^- ({}^{60}_{28}\text{Ni})$	$\beta^- ({}^{192}_{78}\text{Pt})$ and EC (${}^{192}_{76}\text{Os}$)	$\beta^- ({}^{99m}_{43}\text{Tc})$	N/A
(8) Theoretical specific activity $(a_D)_{\text{theor}}$	1.133×10^3	9.215×10^3	4.797×10^5	N/A
(9) Practical specific activity $(a_D)_{\text{pract}}$	~ 300	~ 500	~ 1	N/A

Notes: EC = electron capture; N/A = not applicable; A = atomic mass number; Z = atomic number

(4) **Boron** neutron capture therapy (BNCT) is another example of the use of neutron capture for medical purpose. In contrast to the three other examples discussed above (Co-59, Ir-191, and Mo-98) where neutron activation is used to manufacture radionuclides (Co-60, Ir-192, and Mo-99, respectively) for use in medicine, BNCT represents an example in which thermal neutrons are used directly in clinical work. A thermal neutron beam from a nuclear reactor is made to irradiate tissue previously loaded with boron-10 radionuclide to produce, in tissue, energetic heavy charged particles (${}^7_3\text{Li}$ and α) through the following neutron capture nuclear reaction



Q value for the neutron capture reaction (12.257) of 2.79 MeV can be calculated with data available in Appendix A using the rest energy method or the binding energy method (see Prob. 207). The Li-7 ion and the α particle produced in the neutron capture reaction share Q value energy in the inverse proportion of their rest

masses, so that they acquire kinetic energy of the order of 1 MeV each. This kinetic energy gives them a range of about 10 μm in tissue that is of the order of a typical cell diameter. By virtue of their relatively large masses and large kinetic energy both reaction products are densely ionizing (high LET) particles that can produce significant radiation damage on the cellular level during their short travel through tissue. In addition, the cellular damage produced by these densely ionizing particles depends much less on the presence of oxygen than is the case with standard sparsely ionizing beams, such as x rays, gamma rays, and electrons.

(c) In (b) we list four neutron activation (capture) nuclear reactions for the following daughter nuclides of interest to medical physics: cobalt-60, iridium-192, molybdenum-99, and lithium-7. Several important parameters of these daughter nuclides and their parent nuclides are listed in Table 12.31.

12.7 Nuclear Fission Induced by Neutron Bombardment

12.7.Q1

(264)

When neutrons bombard certain heavy nuclei (atomic number $Z \geq 92$), rather than undergoing capture, i.e., inducing nuclear activation, the neutrons may induce a process called nuclear fission in which the target nucleus breaks up into two daughter nuclei of lighter mass. The fission process is accompanied with production of several fast neutrons and γ rays.

-
- (a) Define the following terms that are part of the nomenclature describing nuclear fission:
- (1) Thermal neutron vs. fast neutron.
 - (2) Prompt neutron vs. delayed neutron.
 - (3) Fission reaction vs. fusion reaction.
 - (4) Fission: spontaneous vs. neutron-induced.
 - (5) Fissionable vs. fissile nucleus.
 - (6) Fertile nuclide vs. fissile nuclide.
 - (7) Fission: fragment vs. product.
 - (8) Uranium ore vs. uranium tailings.
 - (9) Enriched vs. depleted uranium.
 - (10) Fissile radionuclide: naturally-occurring vs. artificially produced.
- (b) Estimate energy release per fission of U-235 induced by a thermal neutron. Determine the fraction of U-235 mass converted into energy in U-235 fission induced by thermal neutrons. Relevant data are available in Appendix A.

- (c) Use the result of (b) to estimate energy release from 1 g of U-235 undergoing fission induced by thermal neutrons and compare the result to energy-equivalent of 1 g of U-235.
- (d) Assume that a nuclear reactor consumes 1 g of U-235 per day. Estimate the power of the reactor and the number of fissions per second required for sustaining such power output.

SOLUTION:

(a) The nomenclature used in the physics of fission is defined as follows:

(1) **Thermal neutron vs. fast neutron.** Neutrons belong to the category of indirectly ionizing radiation, transferring energy to absorbing medium through an intermediate step in which energy is transferred to a charged particle (proton or heavier nuclei) first and then transferred from the charged particle to the absorbing medium in the second step. In terms of their kinetic energy E_K , free neutrons (also referred to as extra-nuclear neutrons) are classified into several categories; of these, the best-known categories are thermal neutron and fast neutron, both types also of interest in medical physics with thermal neutrons used in boron neutron capture therapy (BNCT) and fast neutrons used in external beam radiotherapy and brachytherapy.

Thermal neutron is defined as a free neutron in equilibrium with its environment. When a thermal neutron propagates through an absorber at room temperature, its kinetic energy is thus of the order of 0.025 eV, corresponding to a speed of ~ 2000 m/s and deBroglie wavelength of ~ 2 Å. Note that at room temperature (~ 300 K) thermal energy kT , where k is the Boltzmann constant (8.6173×10^{-5} eV/K), is equal to $\sim (1/40)$ eV = 0.025 eV.

Fast neutron is defined as a free neutron with kinetic energy E_K exceeding 0.1 MeV. Neutrons produced in fission have kinetic energy E_K of the order of a few MeV. Fission cross section of a given absorber has a strong dependence on neutron kinetic energy. For example, uranium-235 has a large fission cross section for a thermal neutron and a much smaller cross section for a fast neutron.

(2) **Prompt neutron vs. delayed neutron.** Prompt neutron is a neutron emitted within 10^{-14} s of the fission process in which also fission fragments are released. Delayed neutron is a neutron emitted after the fission event as a result of β^- decays of the fission fragments that follow the fission process. In β^- decay the daughter nucleus is normally left in an excited state and it attains the ground state through γ decay. However, the daughter nucleus may be left in such highly excited state that neutron emission decay may become possible whereby the daughter releases an energetic free neutron. The neutron emission is delayed by the β^- decay half-life of the parent fission product.

The vast majority (>99 %) of fission-emitted neutrons are of the prompt variety and less than 1 % are delayed neutrons. The mean kinetic energy of delayed neutrons

is ~ 500 keV as compared to 2 MeV for prompt neutrons. In terms of numbers and energy the delayed neutrons are of little importance, however, they play an important role in controlling the nuclear chain reaction in nuclear reactors.

(3) **Fission nuclear reaction vs. fusion nuclear reaction.** Nuclear fission is a nuclear process in which a heavy nucleus breaks up into smaller components, typically consisting of two lighter nuclei, several neutrons, and gamma rays, all carrying a relatively large amount of energy. Fission occurs either spontaneously as a type of radioactive decay called spontaneous fission (SF) or is induced by bombarding a suitable (fissionable) nucleus with a neutron resulting in a nuclear reaction referred to as neutron-induced fission. Fusion, on the other hand, is described as a nuclear reaction in which two light nuclei overcome their mutual Coulomb repulsion and fuse into a heavier nucleus. In fission and fusion a relatively large amount of energy is released as a result of higher binding energy per nucleon in daughter products compared to parent products.

(4) **Spontaneous fission vs. neutron-induced fission.** Fission only occurs in very heavy nuclei with atomic number Z of 92 or higher. Two types of fission are known: spontaneous and neutron induced. In spontaneous fission (SF) a heavy nucleus disintegrates spontaneously by splitting into two nearly equal fission fragments and emitting 2 to 4 neutrons. G.N. Flerov and K.A. Petržak are credited with discovery of SF nuclear decay in 1940 noticing that uranium-238, in addition to α decay, may undergo spontaneous nuclear break up.

Neutron-induced fission is characterized by an interaction between a free neutron and a heavy nucleus. The neutron enters the nucleus and is captured by the nucleus; however, instead of producing a heavier radionuclide through a process referred to as neutron activation (neutron capture). The neutron causes an imbalance in the nucleus, leading the parent nucleus to break apart into two lighter radioactive nuclei with concurrent emission of γ rays and several neutrons.

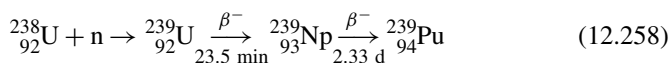
Otto Hahn and Friedrich Strassmann in 1938 carried out experiments that lead to the discovery of uranium's ability to break apart (fission) under the influence of neutron bombardment. L. Meitner and O. Frisch in 1939 offered physical explanation of the nuclear fission process and coined the term "fission". In 1942 E. Fermi and L. Szilárd postulated neutron multiplication and chain reaction in uranium and offered experimental proof of it in 1942.

(5) **Fissionable nucleus vs. fissile nucleus.** Heavy nuclei that can undergo induced fission when struck by a neutron are in general referred to as fissionable nuclei. Fissile nucleus is a narrower term referring to a nucleus undergoing fission with thermal neutrons. For example, uranium-238 is a fissionable nuclide because it can undergo fission with fast neutrons; however, it is not fissile, since thermal neutrons cannot induce fission in it. On the other hand, uranium-235 is a fissionable nuclide in general terms but is also called fissile, since it fissions with thermal neutrons.

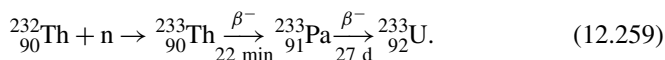
Often fissile nuclides are defined alternatively as those nuclides that are not only fissionable but also through fission produce a sufficient number of neutrons to be

able to sustain a nuclear chain reaction. Fissionable nuclides, on the other hand, are then those that can be made to undergo fission but do not produce a large enough number of neutrons to sustain a chain reaction. Under this definition, uranium-235 is fissile because it can sustain a nuclear chain reaction, while uranium-238 is fissionable yet not fissile because it cannot sustain a nuclear chain reaction.

(6) **Fertile nuclide vs. fissile nuclide.** Nuclides that do not undergo fission themselves when bombarded with thermal neutrons but transform into a fissile nuclide through neutron activation followed by two β^- decay processes are referred to as fertile nuclides. Best known examples of fertile nuclide are U-238 and thorium-232 (Th-232) which, through exposure to fast neutrons in a nuclear reactor followed by two relatively short-half-life β^- decays, transform into fissile plutonium-239 (Pu-239) and uranium-233 (U-233), respectively, as follows



and



Plutonium-239 (${}^{239}\text{Pu}$) is artificially produced from fertile uranium-238 bombarded with neutrons to get uranium-239 through neutron activation. Uranium-239 undergoes β^- decay with a half-life of 23.5 minutes into neptunium-239 that, in turn, undergoes β^- decay with a half-life of 2.33 days into fissile plutonium-239.

Uranium-233 (${}^{233}\text{U}$) is artificially produced from thorium-232 bombarded with neutrons to get thorium-233 through neutron activation. Thorium-233 undergoes β^- decay with a half-life of 22 minutes into protactinium-233 that, in turn, undergoes β^- decay with a half-life of 27 days into fissile uranium-233.

(7) **Fission fragment vs. fission product (by-product).** Fission fragment is the common name for nuclei directly produced in nuclear fission. The mass distribution of the fragments depends on the atomic mass of the fissionable nucleus and on the kinetic energy of the neutron projectile. Any combination of lighter nuclei is possible for fission fragments as long as the fission process honors the conservation of atomic number Z and mass number A .

Nuclei formed in fission as fission fragments range in atomic number from 30 to 64 and in atomic mass from 60 to about 150. At low excitation energy (thermal neutron) the fissile nucleus undergoes fission that results in an asymmetric distribution of fission fragments with daughter nuclei clustering around atomic mass numbers A of 95 and 140, while in fission triggered by fast neutrons the mass distribution of fission fragments is close to symmetric.

The fission fragments are highly unstable because they usually contain an excessive number of neutrons, i.e., are neutron-rich; consequently they undergo a series of nuclear decays until a stable configuration of nucleons is reached. Fission fragments

along with their nuclear decay progeny are referred to as nuclear fission product or fission by-product.

(8) **Uranium ore vs. uranium tailings.** Uranium ore is described as uranium-bearing mineral that contains a sufficiently high concentration of uranium to make extraction of uranium economically profitable. Primary uranium ores are uraninite and pitchblende, both naturally occurring uranium oxides. Uranium is extracted from uranium-bearing minerals at uranium processing plants.

Uranium tailings are a type of long-lived, low-level radioactive waste generated during processing of uranium ore to extract uranium. Tailings are deposited in large mounds in the vicinity of mills where uranium ore is processed. They contain many radioactive contaminants, the most important being radium-226 which decays into radon-222, making the tailings a radiation health hazard for the general public.

(9) **Enriched uranium vs. depleted uranium.** Uranium (U) is one of the three natural elements contributing to terrestrial radioactivity; the other two are thorium (Th) and potassium (K). The natural composition of uranium is 92.27 % of U-238 that is fissionable, 0.72 % of U-235 that is fissile, and ~0.01 % of U-234.

Since U-235 is the fissile component of uranium and most power reactors and even more so, atomic weapons, require a higher concentration of U-235, isotope separation methods have been developed for enhancing the percentage of U-235 in uranium samples. These methods are referred to as *uranium enrichment* and uranium so produced is called enriched uranium. Several grades of enriched uranium are known and in increasing percentage of U-235 they are:

- (i) Slightly enriched uranium (0.9 % to 2 % of U-235).
- (ii) Low enriched uranium (2 % to 20 % of U-235).
- (iii) Reactor grade U (3 % to 5 % of U-235).
- (v) Highly enriched U (above 20 % of U-235).
- (vi) Weapons grade U (above 85 % of U-235).

Uranium enrichment process leaves behind a large amount of uranium that is depleted of U-235 and referred to as depleted uranium when it contains less than 0.3 % of U-235. Thus, depleted uranium is a waste product in the manufacture of fuel for nuclear reactors and weapons grade uranium. It has many civilian and military applications mainly because of its high physical density (19.1 g/cm³), however, it also presents both a chemical and radiological hazard to general public.

(10) **Naturally occurring fissile radionuclide vs. artificially produced fissile radionuclide.** Many heavy nuclides are fissionable, however, only three fissile nuclides that can undergo thermal neutron induced fission are known: uranium-235 appears in nature and two (plutonium-239 and uranium-233) are produced artificially from fertile nuclides (U-238 and Th-232, respectively).

(b) Uranium-235 is the only naturally occurring fissile nuclide. In fission induced by a thermal neutron, the U-235 nucleus breaks up into two smaller nuclei (one with

atomic mass A of about 95 and the other with $A \approx 140$) as well as 2 to 6 neutrons (2.5 neutrons per fission on average):

- (1) Binding energy per nucleon E_B/A before fission of U-235 is $E_B^{U-235}/A = 7.6$ MeV/nucleon.
- (2) Binding energy per nucleon E_B/A after fission for each of the two fission fragments (FF) is $E_B^{FF}/A \approx 8.45$ MeV/nucleon.
- (3) Energy per nucleon released per fission of U-235 is estimated as

$$\begin{aligned}\Delta E/A &= E_B^{\text{after}}/A - E_B^{\text{before}}/A = E_B^{FF}/A - E_B^{U-235}/A \\ &\approx 8.45 \text{ MeV/nucleon} - 7.6 \text{ MeV/nucleon} \\ &= 0.85 \text{ MeV/nucleon.}\end{aligned}\tag{12.260}$$

Since the U-235 nucleus has 235 nucleons (92 protons + 143 neutrons), we estimate the total energy release per fission of U-235 as

$$\Delta E = A(\Delta E/A) = (235 \text{ nucleon}) \times 0.85 \text{ MeV/nucleon} \approx 200 \text{ MeV/fission.}\tag{12.261}$$

Nuclear rest energy of U-235 nucleus is $M_{U-235}c^2 = 218894.9987$ MeV. Therefore, fraction of U-235 mass converted into energy in nuclear fission of U-235 is $\sim 190/218895 = 0.0009 \approx 0.1\%$

(c) Energy release in fission of 1 g of U-235.

We first determine the number of U-235 atoms in 1 g of U-235 and then multiply this number with 200 MeV per fission to obtain the energy release per 1 g of U-235:

- (1) One mole of U-235 is 235.04 g of U-235 and by definition it contains Avogadro number of atoms of U-235 ($N_A = 6.022 \times 10^{23} \text{ mol}^{-1}$).
Therefore, in 1 g of U-235 there are $N_A/235$ atoms, i.e., 2.562×10^{21} atoms of U-235.
- (2) Energy release per fission of 1 g of U-235 is now given as

$$\begin{aligned}&\sim (2.562 \times 10^{21}) \times (200 \text{ MeV}) \\ &= 5.124 \times 10^{29} \text{ eV} \\ &= (5.124 \times 10^{29} \text{ eV}) \times (1.6 \times 10^{-19} \text{ J/eV}) = 8.21 \times 10^{10} \text{ J} \\ &= 8.21 \times 10^7 \text{ kJ.}\end{aligned}\tag{12.262}$$

(3) Energy equivalent of 1 g of U-235 is given as

$$\begin{aligned}mc^2 &= (1 \text{ g}) \times (3 \times 10^8 \text{ m/s})^2 = 9 \times 10^{16} \times 10^{-3} \text{ kg} \cdot \text{m}^2 \cdot \text{s}^{-2} \\ &= 9 \times 10^{13} \text{ J} = \frac{9 \times 10^{13} \text{ J}}{1.6 \times 10^{-19} \text{ J/eV}} = 5.6 \times 10^{32} \text{ eV.}\end{aligned}\tag{12.263}$$

This again, like in (b), shows that in fission of U-235 approximately 0.1 % of the total mass of U-235 is transformed into energy $[(8.2 \times 10^{10} \text{ J}) / (9 \times 10^{13} \text{ J}) \approx 0.001]$.

(d) Consumption of 1 g of U-235 per day implies an operating power of

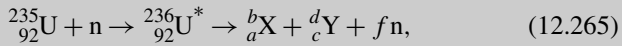
$$\frac{8.2 \times 10^{10} \text{ J}}{\text{d}} = \frac{8.2 \times 10^{10} \text{ J}}{24 \times 3600 \text{ s}} \approx 9.5 \times 10^5 \text{ W} \approx 1 \text{ MW}. \quad (12.264)$$

If a nuclear reactor consumes 1 g of U-235 per day, i.e., operates at ~ 1 MW of power, it means that 2.562×10^{21} fissions occur per day or $(2.562 \times 10^{21}) / (24 \times 3600) \approx 3 \times 10^{16}$ fissions occur per second. This corresponds to $\sim 3 \times 10^{10}$ fissions per watt of power per gram of U-235.

12.7.Q2

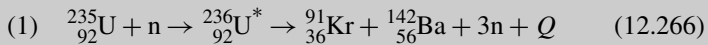
(265)

The general equation for fission of uranium-235 (U-235) is expressed as follows

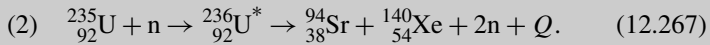


where parent nucleus ${}_{92}^{235}\text{U}$ has been penetrated by a thermal neutron n to produce a compound nucleus ${}_{92}^{236}\text{U}^*$ that is unstable and breaks up by the fission process into two unstable nuclei (fission fragments) ${}_a^b\text{X}$ and $_c^d\text{Y}$ as well as several (f) fast neutrons.

- (a) Discuss the rules governing a , b , c , d , and f of (12.265) and sketch the yield of fission fragments in fission of U-235.
- (b) Two examples of U-235 fission with thermal neutron are given in (12.266) and (12.267) as



and



Determine the energy released in the fission processes (12.266) and (12.267) using two methods: (i) Rest energy method and (ii) Binding energy method. Both methods should give same result for a given fission reaction. Appropriate data are available in Appendix A.

- (c) It is generally assumed that in U-235 fission with thermal neutrons energy of ~ 200 MeV is released. Prepare a block diagram and partition the energy of 200 MeV in absolute terms and as percentage of 200 MeV over all events that (i) accompany or (ii) follow the fission process.

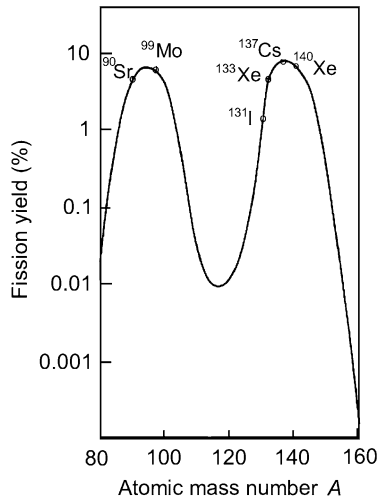


Fig. 12.13 Yield of fission fragments against atomic mass number A for uranium-235 bombarded with thermal neutrons

SOLUTION:

(a) A uranium-235 nucleus undergoing fission does not break up into two equal fragments; rather, it breaks up into several fast neutrons and two unequal fragments of which, in comparison with 50 % of the U-235 nuclear mass, one is significantly lighter and the other significantly heavier. In a given fission event any combination of fission fragments is possible as long as the fission process honors the conservation of atomic number Z and atomic mass number A . This means that in (12.265) the following rules apply: $a + c = 92$ and $b + d + f = 236$, with f the number of neutrons produced in fission that can vary between 2 to 6 with mean value of 2.4.

Nuclei formed in fission as fission fragments range in Z from 30 to 64 and in A from 60 to 150 and over 100 nuclides of 35 different elements have been identified as fission fragments of U-235 fission. As shown in Fig. 12.13, fission fragments have an asymmetrical yield distribution with daughter nuclei clustering around $A = 95$ and $A = 140$ with much higher probability than around $A = 118$ which would give a symmetrical distribution of fission yield.

All fission fragments are by virtue of their synthesis neutron-rich and therefore unstable (radioactive). They progress to nuclear stability by a succession of β^- decays forming chains of isobars, accompanied by beta particles and antineutrinos. Two of the fission-generated isobar chains are well known in medical physics, one with $A = 99$ (molybdenum-99) and the other with $A = 140$ (xenon-140), each occurring in about 6 % of all U-235 fissions. Distributions of fission yields for the other two fissile nuclides (uranium-233 and plutonium-239) are similar to that shown for U-235 in Fig. 12.13.

(b) In the calculation of fission Q value (energy released in fission) of (12.266) and (12.267) we note that the fission is induced by a thermal neutron which, as the name implies, has negligible kinetic energy of the order of 0.025 eV. In the calculation of Q value for the fission reaction we can therefore assume that the two reactants (projectile: neutron and target: U-235 nucleus) are both at rest before the reaction.

Two simple methods are in use for determining Q value of a typical fission nuclear reaction [(T5.7) and (T5.8)]:

Rest energy method: Q value is determined by subtracting the sum of nuclear rest energies of reaction products (fission fragments and free neutrons released) after the reaction $\sum_{i,\text{after}} M_i c^2$ from the sum of nuclear rest energies of reactants (projectile: thermal neutron and target: fissile nucleus) before the reaction $\sum_{i,\text{before}} M_i c^2$, or

$$Q = \sum_{i,\text{before}} M_i c^2 - \sum_{i,\text{after}} M_i c^2. \quad (12.268)$$

Binding energy method: Q value is determined by subtracting the sum of nuclear binding energies of reactants (thermal neutron and fissile target) before the reaction $\sum_{i,\text{before}} E_B(i)$ from the sum of nuclear binding energies of reaction products (fission fragments) after the reaction $\sum_{i,\text{after}} E_B(i)$, or

$$Q = \sum_{i,\text{after}} E_B(i) - \sum_{i,\text{before}} E_B(i). \quad (12.269)$$

We now determine Q value for fission reactions (12.266) and (12.267) using (12.268) and (12.269) for both reactions.

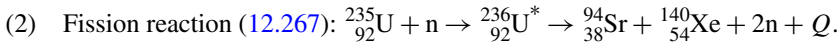
(1) Fission reaction (12.266): ${}^{235}_{92}\text{U} + \text{n} \rightarrow {}^{236}_{92}\text{U}^* \rightarrow {}^{91}_{36}\text{Kr} + {}^{142}_{56}\text{Ba} + 3\text{n} + Q$.

Rest energy method:

$$\begin{aligned} Q &= \sum_{i,\text{before}} M_i c^2 - \sum_{i,\text{after}} M_i c^2 \\ &= \{M({}^{235}_{92}\text{U})c^2 + m_n c^2\} - \{M({}^{91}_{36}\text{Kr})c^2 + M({}^{142}_{56}\text{Ba})c^2 + 3m_n c^2\} \\ &= [218894.9987 + 939.5654] \\ &\quad - [132165.7134 + 84676.2556 + 2818.6962] \text{ MeV} \\ &= [219834.5641 - 219660.6652] \text{ MeV} = 173.9 \text{ MeV}. \end{aligned} \quad (12.270)$$

Binding energy method:

$$\begin{aligned} Q &= \sum_{i,\text{after}} E_B(i) - \sum_{i,\text{before}} E_B(i) = \{E_B({}^{91}_{36}\text{Kr}) + E_B({}^{142}_{56}\text{Ba})\} - \{E_B({}^{235}_{92}\text{U}) + 0\} \\ &= \{777.6357 \text{ MeV} + 1180.1387 \text{ MeV}\} - \{1783.8710 \text{ MeV} + 0\} = 173.9 \text{ MeV}. \end{aligned} \quad (12.271)$$



Rest energy method:

$$\begin{aligned}
 Q &= \sum_{i,\text{before}} M_i c^2 - \sum_{i,\text{after}} M_i c^2 \\
 &= \{M({}_{92}^{235}\text{U})c^2 + m_n c^2\} - \{M({}_{38}^{94}\text{Sr})c^2 + M({}_{54}^{140}\text{Xe})c^2 + 2m_n c^2\} \\
 &= [\{218894.9987 + 939.5654\} \\
 &\quad - \{87462.1839 + 130308.7287 + 1879.1308\}] \text{ MeV} \\
 &= [219834.5641 - 219650.0434] \text{ MeV} = 184.5 \text{ MeV}. \quad (12.272)
 \end{aligned}$$

Binding energy method:

$$\begin{aligned}
 Q &= \left\{ \sum_{i,\text{after}} E_B(i) \right\} - \left\{ \sum_{i,\text{before}} E_B(i) \right\} \\
 &= \{E_B({}_{38}^{94}\text{Sr}) + E_B({}_{54}^{140}\text{Xe})\} - \{E_B({}_{92}^{235}\text{U}) + 0\} \\
 &= \{807.8150 \text{ MeV} + 1160.7287 \text{ MeV}\} - \{1783.8710 \text{ MeV} + 0\} \\
 &= 184.6 \text{ MeV}. \quad (12.272)
 \end{aligned}$$

Since we can get similar results for any of the numerous known fission reactions, we can make three conclusions regarding the fission Q value:

- (1) Q value of a fission reaction induced by thermal neutron in a fissile material is positive and this means that fission reactions are exothermic, release a significant amount of energy, and, to run, require no threshold energy.
- (2) The two methods available for calculation of Q value (rest energy method and binding energy method) give identical results for a given fission reaction.
- (3) Equations (12.266) and (12.267) are two examples of typical U-235 fission reaction but they give different Q values: (12.266) gives 173.9 MeV and (12.267) gives 184.5 MeV. This illustrates the well-known fact about fission reactions, namely, that there are large variations in energies released in fission even for the same fissile nuclide.

(c) Energy released per fission event is of great theoretical and practical interest. Because of the large variations in various possible fission events for a given fissile material, only mean values for the various physical parameters are usually given. For example, some notable parameters of U-235 fission are as follows:

- (1) The number of prompt neutrons produced ranges from 2 to 8 with the mean value of 2.5.
- (2) Kinetic energies of prompt neutrons ranges from 0.5 MeV to 4 MeV with mean at 2 MeV.

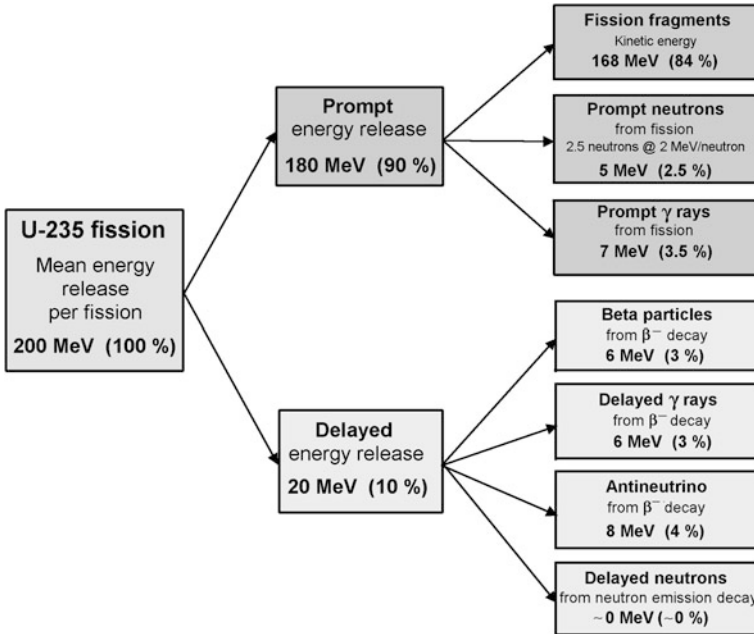


Fig. 12.14 Partition of mean energy release of 200 MeV in fission of U-235 by thermal neutrons. Energy release is divided into two main components: prompt energy release (180 MeV) and delayed energy release (20 MeV)

- (3) The mean total energy release is assumed to be 200 MeV. It consists of 180 MeV (90 %) for prompt energy release and 20 MeV (10 %) for delayed energy release.
- (4) The prompt energy release consists of 180 MeV (90 %) of 168 MeV (84 %) for kinetic energy of fission fragments, 5 MeV (2.5 %) for kinetic energy of prompt neutrons (2.5 neutrons at 2 MeV/neutron), and 7 MeV (3.5 %) as prompt γ ray energy.
- (5) The delayed energy release of 20 MeV (10 %) is caused by the β^- decay of neutron-rich fission fragments and consists of 6 MeV (3 %) for beta particles, 6 MeV (3 %) for antineutrinos, and 6 MeV for delayed γ rays, all three from the β^- decay of fission fragments.
- (6) Delayed neutrons also originate from β^- when the daughter nucleus is so highly excited that it undergoes neutron emission decay rather than the standard γ decay. However, the number and energy of delayed neutrons are small, so that they are ignored in stating the mean fission energy partition.

Points (1) through (6) above are illustrated in Fig. 12.14 indicating that:

Prompt energy release has 3 components:

- (i) Kinetic energy of fission fragments (168 MeV).
- (ii) Kinetic energy of prompt neutrons (5 MeV).

(iii) Energy of prompt gamma rays.

Delayed energy release is attributed to the beta minus decay of the neutron-rich fission fragments and has 4 components:

- (i) Kinetic energy of beta particles (6 MeV).
- (ii) Delayed gamma rays (6 MeV).
- (iii) Antineutrino energy (8 MeV).
- (iv) Energy of delayed neutrons which is essentially negligible.

12.8 Nuclear Chain Reaction

12.8.Q1

(266)

Chain reaction is defined as reaction resulting in products that on the average cause one or more reactions of the same type as the original reaction and the process continues for several generations forming a chain of reactions. While chemical chain reactions are possible, the best known chain reactions occur in nuclear physics in connection with nuclear fission where they are referred to as nuclear chain reactions.

- (a) Define the following terms that form the nomenclature describing nuclear reactors:
- (1) Chemical reaction vs. nuclear reaction.
 - (2) Controlled nuclear fission chain reaction vs. uncontrolled fission chain reaction.
 - (3) Critical mass vs. subcritical mass and super-critical mass.
 - (4) Moderator of nuclear reactor vs. control rod of nuclear reactor.
 - (5) Advantages and disadvantages of nuclear power.
 - (6) Commissioning of nuclear reactor vs. decommissioning of nuclear reactor.
- (b) For a nuclear reactor core: (1) List principal components and (2) Draw its block diagram.
- (c) List and briefly describe three nuclear reactor accidents from around the world that had a serious negative effect on development of fission-based nuclear power generation.

SOLUTION:

(a) The nomenclature used in reactor physics is defined as follows:

(1) **Chemical reaction vs. nuclear reaction.** The two types of reaction have many similarities and are defined in similar fashion. For example, both types of reaction

can be either spontaneous (exothermic) requiring no energy input and releasing energy or they can be induced (endothermic) requiring energy input and characterized by an energy threshold. Moreover, components initially involved in a reaction are called reactants, while the components resulting from a reaction are called reaction products.

The main difference between chemical and nuclear reaction is that a chemical reaction deals with orbital electrons of outer atomic shells (valence electron) with binding energy of the order of a few eV, while a nuclear reaction deals with nucleons (proton and neutron) residing in atomic nucleus with binding energy of the order of a few MeV. Thus, the potential for energy release in a nuclear reaction is several orders of magnitude larger than that in a chemical reaction.

For example, this is of great significance in power generation, where nuclear energy released in fission of 1 g of uranium-235 is equivalent to energy release generated by burning 3 tons of high-grade coal.

(2) **Controlled nuclear fission chain reaction vs. uncontrolled fission chain reaction.** In a nuclear chain reaction, a neutron starts a fission reaction and at least one neutron that can start a new fission reaction is produced in the initial reaction as well as in all subsequent generations.

The most important characteristic of nuclear chain reactions is that the reactions are self-sustaining. For example, in fission of uranium-235 nucleus on average 2.5 neutrons are produced along with the two daughter fission fragments. These new neutrons can induce additional fission in the uranium-235 absorber and in principle a self-sustaining chain reaction becomes possible.

An uncontrolled fission chain reaction is defined as a chain reaction in which the number of neutrons available for inducing fission is growing from one generation to the next, such as, for example, in an atomic bomb. A controlled fission chain reaction, on the other hand, is a chain reaction in which the number of neutrons available for inducing fission in the next generation is maintained in a nuclear reactor by the so-called control rods at a level that keeps the reaction rate constant, i.e., controlled.

(3) **Critical mass vs. subcritical mass and super-critical mass.** Any nuclear chain reaction can be described by a parameter called effective neutron multiplication factor (also known as fission reproduction factor) k , defined as the number of neutrons from a given fission in a given generation that can cause fission in the next generation. Generally, the factor k is smaller than the actual number of fission-generated neutrons because some of the neutrons generated either escape the system or undergo non-fission reactions. The value of k determines the fate of a chain reaction as follows:

For $k < 1$, the system cannot sustain a chain reaction, the fission power diminishes with time, and the mass of the fissile material is classified as *sub-critical*.

For $k = 1$, every fission event causes a new fission on average. This leads to a constant fission power level, a steady-state chain reaction, and the fissile mass is classified as *critical*. The critical mass is defined as the smallest amount of fissile

material able to sustain a nuclear chain reaction. Nuclear power plants operate in this mode. The critical mass of a fissile material depends upon its nuclear fission cross section, density, enrichment, shape, and temperature. For a given fissile material, the shape with minimal critical mass is spherical, since a sphere requires the minimum surface area per mass.

For $k > 1$, every fission event causes an increase in number of subsequent fissions leading to a runaway chain reaction described as *super-critical*. Nuclear weapons operate in this mode.

(4) **Moderator vs. control rod in nuclear reactor.** Fission cross section of fissile materials (U-235, Pu-239, and U-233) is inversely proportional to neutron velocity, therefore, a thermal neutron has a much higher fission cross section than a fast neutron. On the other hand, nuclear fission results in fast neutrons with kinetic energy of a few MeV rather than thermal neutrons, so, in order to sustain a chain reaction, the fast neutrons produced in fission must be slowed down to thermal energy. In a nuclear reactor the neutron moderator is a medium that reduces the speed of fast neutrons produced in fission reactions and transforms them into thermal neutrons to sustain the chain reaction. This process is called neutron thermalization or slowing down.

Materials commonly used as reactor moderators are: ordinary water, heavy water, or solid graphite and the slowing down of neutrons is caused by inelastic and elastic collisions between the neutron and nuclei of the moderator. Since neutron is relatively light, the most efficient energy transfer in a collision with moderator nucleus will be, when the mass of the nucleus is of the order of the neutron mass. Protium in ordinary water, deuterium in heavy water and carbon in solid graphite are therefore the most efficient moderator materials.

The role of reactor control rods is to absorb a large number of neutrons that are produced in fission. Therefore, the rod contains elements that have a large cross section for absorption of neutrons and are not fissionable. Boron-10 and cadmium-113 are most common materials used for neutron absorption in reactor control rods. The rods are used to maintain a desired fission reaction rate and also to shut down the nuclear reactor.

(5) **Advantages and disadvantages of nuclear power.** Since its inception six decades ago, nuclear power has been the most controversial of large-scale electric power technologies. On the one hand, it has a significant advantage over fossil fuel based electric power generation, since a claim can be made that, during its operation, it does not produce greenhouse gases nor does it produce acid rain and cause global warming. On the other hand, it has a serious side effect, because it produces radioactive waste in spent fuel, some of it very long-lived, that will be bothersome and hazardous to humans and environment for many generations to come.

Another issue with fission-based nuclear power is the inherent safety of nuclear technology. In principle, fission reactors are extremely safe and well protected with safety features of multiple redundancies; however, history has shown that reactors are not completely fail safe and the world has already seen several serious accidental

partial or complete reactor core meltdowns with drastic consequences for humans and environment.

There clearly is a need for replacing the fossil fuel based electric power generation, and fission based nuclear power largely, but not completely, meets the requirements. The nagging problems of potential for serious accidents, disposal of radioactive waste, and decommissioning of old and contaminated nuclear power plants are three aspects of the fission based nuclear power cycle that have not been satisfactorily solved to date and have fueled the debate on whether or not to use nuclear power. With rapid advancement in nuclear technology, be it fission or fusion based, there is hope that in the future humanity will succeed in developing efficient, clean, safe, and environmentally friendly nuclear technology and silence the current debate on merits of nuclear power.

(6) **Commissioning and decommissioning of nuclear reactors** are two very important components of a nuclear power plant life cycle; commissioning is carried out just before the beginning of commercial operation of a nuclear power plant, decommissioning after the end of commercial use. According to the International Atomic Energy Agency (IAEA) from Vienna, Austria there are currently close to 450 nuclear power plants in operation around the world and some 140 nuclear plants have already been shut down after reaching their design life. Since the projected life of a nuclear power plant is 40 years to 50 years and the first nuclear power plants were opened in the 1950s, the number of nuclear power plants reaching obsolescence is rapidly increasing.

Commissioning is carried out by the owner institution and involves verification and testing of all systems, structures, equipment, and procedures to be used during commercial operation of the plant under routine as well as emergency conditions. The commissioning process must be approved by the national licensing agency and should be sufficiently extensive to allow institutional operators to become familiar with the proposed plant operation and functioning of all systems and equipment.

Testing of the nuclear reactor is the most important component of the commissioning process. It should cover the following aspects:

- (i) Fuel loading and pre-criticality test of equipment performance,
- (ii) Making the reactor critical,
- (iii) Testing all aspects of power generation,
- (iv) Carrying out extensive radiation survey of the entire plant in normal power generation mode,
- (v) Testing emergency shut-down procedures.

During the commissioning it should be established that, for use of the operators, clear and detailed instruction manuals are available and understood by the operators and that the manuals cover all procedures, systems and equipment both under routine and emergency conditions.

Results of all tests carried out under the commissioning process should be documented clearly and extensively and submitted to the national body that will issue the operating license for the commercial use of the plant.

As some “nuclear” countries are opting out of nuclear power as a result of a few, yet catastrophic, nuclear power accidents and as the first batch of nuclear power plants installed in 1950s and 1960s is becoming obsolete, decommissioning of nuclear power plants is rapidly becoming an important issue for governments and societies around the world.

The term “decommissioning” involves all steps involved in dealing with end-of-life closure of nuclear facilities such as nuclear power plants. In comparison with decommissioning processes of other major industrial installations, the decommissioning of nuclear installations is the most complicated and controversial, since it deals mainly with issues related to radioactive contamination of the nuclear power plant and the safe disposal of the contaminated material to bring the plant area back to an unrestricted level or to a partially restricted level.

Three protocols have been used for decommissioning of nuclear power plants; however, experience with the process is still scarce because of the relatively low number of obsolete nuclear power plants to date. All three protocols prescribe removal of the spent nuclear fuel from the reactor for disposal at a suitable government approved radioactive dump. In all other aspects the three protocols differ significantly from each other. Decommissioning is clearly an expensive proposition, costing about 15 % to 20 % of capital cost of a new nuclear power plant installation; however, it must be taken seriously, irrespective of the cost. The three protocols are:

- (i) *Immediate dismantling* involves immediate separation of radioactive debris from non-radioactive debris and removal of both to appropriate and approved sites.
- (ii) *Deferred dismantling* postpones dismantling for a long period of time to allow the short-lived contamination to decay, but it postpones the actual dismantling to future generations.
- (iii) *Entombment* involves placement of the reactor building into a concrete envelope (sarcophagus).

Routine operation of nuclear power plants actually does not produce much radioactive waste on an annual basis; however, decommissioning of a nuclear power plant produces a significant amount of radioactive waste, some of it to remain radioactive for many generations as well as centuries to come. It is imperative that this is taken into account in design of new nuclear power plants to make the eventual decommissioning efficient and to minimize the expense and amount of radioactive waste produced.

(b) Principal components of a nuclear reactor core are (see Fig. 12.15)

- (1) Fuel elements containing fissile fission material, such as uranium-233, uranium-235, or plutonium-239.
- (2) Control rods (containing neutron absorber such as boron or cadmium) for control of mean neutron generation factor k .
- (3) Moderator (e.g., water, heavy water, or solid graphite) to slow down fission-produced fast neutrons to thermal neutron velocity.

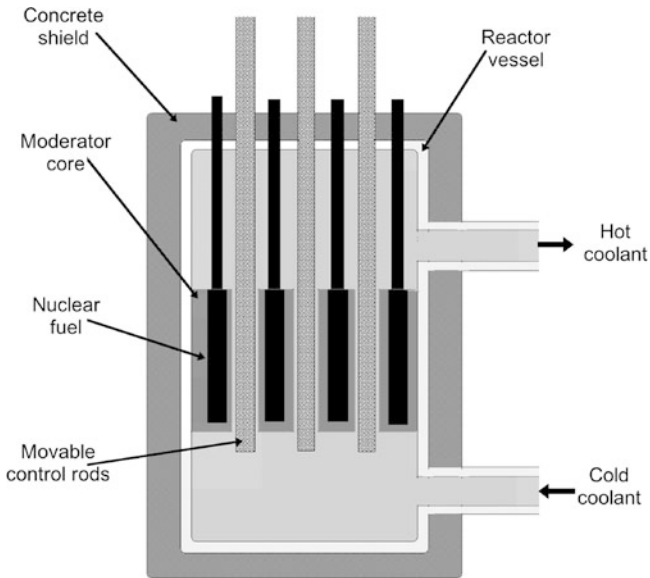


Fig. 12.15 Schematic diagram of nuclear reactor core highlighting the four main components: (fuel elements, (2) Control rods, (3) Moderator, and (4) Coolant

(4) Coolant (usually water) to maintain a stable temperature in the reactor core.

(c) Major accidents in nuclear power plants are rare but they do happen occasionally, and when they do, the consequences can be very serious. In 1989 the International Atomic Energy Agency (IAEA) introduced the International Nuclear and Radiological Event Scale (INES) as a tool for promptly communicating to the public in consistent terms the safety significance of reported nuclear and radiological incidents (lower levels) and accidents (upper levels). The INES scale has 7 levels ranging from 0 (no safety significance) in steps of 1 to level 7 (major accident).

The following three nuclear power plant accidents stand out as the worst accidents in the history of fission-based nuclear power: (1) Three Mile Island (TMI), USA, (2) Chernobyl, Ukraine (former Soviet Union), and (3) Fukushima Daiichi, Japan. Each one of these accidents highlights how a succession of mundane and well controllable malfunctions can escalate a relatively simple incident into a major catastrophe.

(1) **Three Mile Island (TMI) accident of 1979** is a perfect example on how a minor malfunction in a secondary non-nuclear system can, with bad luck, bad design, and improper action by personnel, escalate into a major disaster. The TMI accident was caused by a minor problem in the secondary cooling system that caused the temperature as well as pressure to rise in the primary cooling system and resulted in an automatic reactor shut down. The pressure relief valve controlled excessive pressure in the primary cooling system (as per design); however, the valve, after the

pressure problem was rectified, remained stuck in the open position and continued to drain the coolant from the primary cooling circuit, yet neither the safety interlocks nor the operators noticed the malfunction. The reactor core was left without adequate cooling, the residual decay heat was not properly removed from the reactor core, and a portion of the core with fuel rods melted.

Adequate water-cooling of the reactor core was eventually restored but the reactor core sustained such severe damage that its repair and continued operation were not feasible. On the positive side, the containment building housing the reactor prevented any serious radiation leak and no physical or radiological injuries to personnel or general public were reported. The contamination cleanup was very costly and took about 14 years to complete. Currently, the reactor is permanently shut down and all radioactive waste including the reactor fuel and the damaged core were shipped to an off-site government storage facility. The reactor site is still monitored and the reactor building is slated for decommissioning in 2014.

The TMI accident was the first in a series of serious nuclear accidents involving reactor meltdown. It brought about much more stringent reactor safety regulations and seriously dampened the enthusiasm for new fission based nuclear power plants around the world.

(2) **Chornobyl nuclear accident of 1986** turned out to be the worst industrial accident of all time. It had such far-reaching consequences that the term accident does not adequately characterize it; far more appropriate terms to describe it are “calamity”, “disaster”, or “catastrophe”, because it affected so many people, contaminated such vast areas of the world, cost an enormous amount of money to mitigate, and hastened the demise of a world power, the Soviet Union.

In the mid 1980s the Chornobyl nuclear power plant housed four nuclear reactors of Soviet design using slightly enriched uranium (2 %) oxide for the fissile fuel but it also had several design flaws that proved fateful. For example, a design quirk produced a temporary increase in reactor power output when control rods were inserted into the reactor core. Under certain conditions this could cause severe core overheating. The moderator used by the reactor was made of graphite, a known moderator material but potentially dangerous because, in overheating, its carbon constituent can catch fire. Moreover, the reactor itself was used not only for power generation but also for production of plutonium-239 for military purposes. This required special cranes for rapid exchange of fuel rods thereby precluding construction of a containment building that, for prevention of radioactive escape of fission products in core meltdown, is an essential and standard component of a nuclear power plant.

The disaster started during a rather mundane experiment to verify the reactor's behavior when operated under emergency power. To avoid being hindered by reactor shut down triggered by safety circuits, the operators by-passed them and lifted the control rods from the reactor core. This caused a significant increase in fission rate and surge in power which in turn increased the temperature of the reactor to over 2000 C, melted the fuel rods, and produced such high steam pressure in the water cooling circuit that the top of the reactor was blown off. Next, carbon of the graphite moderator ignited scattering large amounts of radioactivity, such as iodine-131, cesium-137, and strontium-90, from the melted fuel rods into the atmosphere.

Investigations of the disaster have shown that the disaster was completely self-inflicted and resulted from several bad decisions on the part of reactor operators as well as some design problems with the reactor. If the safety circuits were not disabled, they would manage the reactor overheating and bring it under control. However, without the safety interlocks, the operators were too slow in lowering the control rods to prevent the core meltdown and, once the meltdown got started, there was no way to stop it.

The consequences of the disaster were enormous. Some 30 workers died during the first few days of the accident and several dozen workers perished as result of radiation poisoning during subsequent weeks. Radioactive fallout was spread over the northern hemisphere, neighboring cities of Pripyat (pop. 50 000) and Chornobyl (pop. 12 500) were made inhabitable, about 350 000 people from the vicinity of the reactor were resettled, and a permanent 30 km radius exclusion zone around the reactor was established.

Health effects on millions of people who received excessive radiation doses are difficult to quantify. It is clear, however, that health effects on millions of people living in the former Soviet Union as well as eastern, central, and northern Europe were not negligible and not all of them manifested themselves to date.

The demolished reactor building and the remnants of the reactor were entombed into a concrete envelope (sarcophagus) that, unfortunately, only 25 years later is already crumbling. This means that soon a new entombment will need to be carried out, again at enormous cost that Ukraine, now the new country owning the problem, will not be able to finance alone.

Note: The nuclear power plant accident occurred in Soviet Union and was originally known as the “Chernobyl” accident; however, since Chornobyl is now located in Ukraine, it seems more appropriate to use Ukrainian spelling “Chornobyl” rather than the Russian spelling “Chernobyl”.

(3) **Fukushima nuclear disaster of 2011** is an example of natural forces playing havoc with well-constructed nuclear power reactors. The Fukushima Daiichi nuclear power plant is located on the west coast of the largest Japanese island of Honshu, some 300 km north of Tokyo. It consisted of six boiling water nuclear power reactors designed by General Electric, each protected by its own containment building constructed to withstand the most severe earthquake on record in Japan. A sea wall, able to withstand tsunami waves of up to 5.5 m in height, was built to protect the plant, since it is located on the seacoast and under sea-level earthquakes tend to cause tsunamis with waves that travel rapidly across the sea and can become very high when reaching coastal shallow waters.

An enormous earthquake hit the Honshu island of Japan in March of 2011. Its epicenter was about 200 km off the coast of the Fukushima Daiichi nuclear power plant and its magnitude read 9 on the Richter scale. At the time of the earthquake, three of the six reactors were in operation and all three shut down automatically and orderly as a result of signals from the seismic reactor protection detectors. Structurally all six reactors withstood the earthquake well; however, all external electrical power to the plant was lost and emergency diesel generators began to provide the

necessary AC power to emergency services used mainly for cooling of the reactors. One hour after the main tremor the situation in the plant was under control; however, serious problems arose when the tsunami waves started arriving at the doorstep of the power plant.

The tsunami waves were enormous exceeding the 5.5 m high protective wall of the power plant by a factor of 3. They overwhelmed the site, flooded the emergency diesel generators rendering them inoperable, and disabled the reactor core cooling used to remove the decay heat. Reactor core temperatures increased past tolerance levels, fuel rods became damaged generating contamination radioactivity as well as hydrogen through oxidation of overheated zirconium fuel rod cladding, and containment pressures increased drastically. Core meltdown occurred in several reactors; however, the extent of the damage is not known yet. Several explosions, most likely caused by build up of hydrogen have damaged the containment domes causing escape of radioactivity into the environment, mainly iodine-131, cesium-137, and strontium-90.

Three fire engines were used to pump sea water into the reactor cooling pools and eventually the situation was brought under control, but not before a large amount of radioactivity was released from the plant and contaminated the immediate vicinity of the plant. Some radioactive contamination from the damaged reactors escaped into the sea.

In contrast with the Chornobyl accident that spewed radioactivity all over Europe, most of the radioactivity that escaped from the Fukushima plant was dispersed over the Pacific ocean, making the health consequences less of a concern than did Chornobyl. Consequences of the Fukushima disaster were not as severe as those of Chornobyl; however, on the INES scale the disaster, like that of Chornobyl, is rated as level 7, because in the Fukushima power plant there were six nuclear reactor that were more or less affected by problems with reactor core cooling.

12.8.Q2

(267)

Boron-10 and cadmium-113 are used in control rods of nuclear reactors to maintain controlled chain reaction and to shut down the reactor. The respective nuclear reactions are: $^{10}_5\text{B}(n, \alpha)^7_5\text{Li}$ and $^{113}_{48}\text{Cd}(n, \gamma)^{114}_{48}\text{Cd}$.

- (a) Determine Q value for the $^{10}_5\text{B}(n, \alpha)^7_5\text{Li}$ neutron capture nuclear reaction. Use and compare three methods for Q value calculation: (1) Atomic rest energy method, (2) Nuclear rest energy method, and (3) Nuclear binding energy method. All required atomic and nuclear data are provided in Appendix A.

- (b) For ${}^{10}_5\text{B}(n, \alpha){}^7_3\text{Li}$ neutron capture nuclear reaction determine kinetic energy $(E_K)_\alpha$ of the α particle and recoil kinetic energy $(E_K)_{\text{Li-7}}$ of the Li-7 nucleus.
- (c) Determine Q value for the ${}^{113}_{48}\text{Cd}(n, \gamma){}^{114}_{48}\text{Cd}$ neutron capture nuclear reaction. Use and compare three methods for Q value calculation: (1) Atomic rest mass method, (2) Nuclear rest energy method, and (3) Nuclear binding energy method. All required atomic and nuclear data are provided in Appendix A.
- (d) For ${}^{113}_{48}\text{Cd}(n, \gamma){}^{114}_{48}\text{Cd}$ neutron capture nuclear reaction determine energy E_γ of the γ ray photon and recoil kinetic energy $(E_K)_{\text{Cd-114}}$ of the Cd-114 nucleus.

SOLUTION:

Reaction energy or Q value of a nuclear reaction can be calculated with three methods and all three are expected to give the same result for a given nuclear reaction. The three methods are:

- (1) Atomic rest energy method (T5.7).
- (2) Nuclear rest energy method (T5.7).
- (3) Nuclear binding energy method (T5.8).

We note the following general points related to the two neutron capture reactions:

- (i) Neutrons in the two nuclear reactions of this problem are thermal neutrons. In our calculations we can thus assume that their kinetic energy $E_K^n \approx 0$ is negligible and that the two target nuclei (boron-10 and cadmium-113) are initially at rest.
- (ii) Total momentum before the nuclear reaction is zero causing the momenta of reaction products after the reaction to be opposite in direction and equal in magnitude.
- (iii) Principles of total energy conservation and momentum conservation are used in the calculation of nuclear reaction Q value as well as energy and momentum of the reaction products.

(a) Q value of the ${}^{10}_5\text{B}(n, \alpha){}^7_3\text{Li}$ neutron capture nuclear reaction is determined as follows:

- (1) Atomic rest energy \mathcal{M} method:

$$\begin{aligned}
 Q &= \{\mathcal{M}({}^{10}_5\text{B})c^2 + m_n c^2\} - \{\mathcal{M}({}^7_3\text{Li})c^2 + \mathcal{M}({}^4_2\text{He})c^2\} \\
 &= \{(10.012937 \text{ u}) + (1.008665 \text{ u})\}c^2 - \{(7.016004 \text{ u}) + (4.002603 \text{ u})\}c^2 \\
 &= \{11.021602 - 11.018607\} \times (931.494028 \text{ MeV}) = 2.79 \text{ MeV}. \quad (12.273)
 \end{aligned}$$

(2) Nuclear rest energy M method:

$$\begin{aligned} Q &= \{M({}^{10}_5\text{B})c^2 + m_n c^2\} - \{M({}^7_3\text{Li})c^2 + m_\alpha c^2\} \\ &= \{9324.4360 \text{ MeV} + 939.5654 \text{ MeV}\} \\ &\quad - \{6533.8328 \text{ MeV} + 3727.3788 \text{ MeV}\} \\ &= \{10264.0014 \text{ MeV} - 10261.2116 \text{ MeV}\} = 2.79 \text{ MeV}. \end{aligned} \quad (12.274)$$

(3) Binding energy E_B method:

$$\begin{aligned} Q &= \{E_B({}^7_3\text{Li}) + E_B({}^4_2\text{He})\} - \{E_B({}^{10}_5\text{B})c^2 + 0\} \\ &= \{39.2446 \text{ MeV} + 28.2959 \text{ MeV}\} - \{64.7508 \text{ MeV}\} = 2.79 \text{ MeV}. \end{aligned} \quad (12.275)$$

The three methods used in determination of Q value provide identical results, as expected. *Note* that in the atomic rest energy method of (12.273) we use the atomic rest mass \mathcal{M} of the helium-4 atom (α particle neutralized by two electrons) to account for all orbital electrons involved in the reaction, while in (12.274) we use the nuclear rest mass M of the α particle. In (12.275) the thermal neutron is free and thus has no binding energy.

(b) To determine for the nuclear reaction ${}^{10}_5\text{B}(n, \alpha){}^7_3\text{Li}$ kinetic energy $(E_K)_\alpha$ of the α particle ejected in the nuclear reaction and recoil energy $(E_K)_{\text{Pb-218}}$ $(E_K)_{\text{Li-7}}$ of the lithium-7 reaction product we use the principles of: (1) total energy conservation and (2) momentum conservation. The two conservation principles are for the nuclear reaction expressed as follows:

(1) For total energy conservation (T5.6) we recognize that kinetic energies in α decay are relatively small allowing us to use classical mechanics for expression of energy conservation

$$Q = (E_K)_\alpha + (E_K)_{\text{Li-7}} = \frac{p_\alpha^2}{2m_\alpha} + \frac{p_{\text{Li-7}}^2}{2\mathcal{M}_{\text{Li-7}}}. \quad (12.276)$$

(2) For momentum conservation we note that momentum before the nuclear reaction is zero causing the two momenta \mathbf{p}_α and $\mathbf{p}_{\text{Li-7}}$ after the nuclear reaction to be opposite in direction and equal in magnitude

$$0 = \mathbf{p}_\alpha + \mathbf{p}_{\text{Li-7}} \quad (12.277)$$

or

$$|\mathbf{p}_\alpha| \equiv p_\alpha = \sqrt{2m_\alpha(E_K)_\alpha} = |\mathbf{p}_{\text{Li-7}}| \equiv p_{\text{Li-7}} = \sqrt{2\mathcal{M}_{\text{Li-7}}(E_K)_{\text{Li-7}}}, \quad (12.278)$$

where

- p_α is the magnitude of α particle momentum.
 $p_{\text{Li-7}}$ is the magnitude of the lithium-7 atomic recoil momentum.
 m_α is the rest mass of the α particle.
 $\mathcal{M}_{\text{Li-7}}$ is the rest mass of the lithium-7 atom

$$\mathcal{M}_{\text{Li-7}}c^2 = (7.016004 \text{ u}) \times (931.494024 \text{ MeV/u}) = 6535.3658 \text{ MeV}.$$

Using (12.276) we can now express the conservation of energy as

$$Q = (E_K)_\alpha + (E_K)_{\text{Li-7}} = \frac{p_\alpha^2}{2m_\alpha} + \frac{p_{\text{Li-7}}^2}{2\mathcal{M}_{\text{Li-7}}} = \frac{p_\alpha^2}{2} \left[\frac{1}{m_\alpha} + \frac{1}{\mathcal{M}_{\text{Li-7}}} \right] \quad (12.279)$$

from where it follows that

$$p_\alpha^2 = p_{\text{Li-7}}^2 = 2Q \left[\frac{1}{m_\alpha} + \frac{1}{\mathcal{M}_{\text{Li-7}}} \right]^{-1}. \quad (12.280)$$

Inserting (12.280) into (12.279) we now get the following expressions for $(E_K)_\alpha$ and $(E_K)_{\text{Li-7}}$

$$(E_K)_\alpha = \frac{p_\alpha^2}{2m_\alpha} = \frac{Q}{m_\alpha} \left[\frac{1}{m_\alpha} + \frac{1}{\mathcal{M}_{\text{Li-7}}} \right]^{-1} = \frac{Q}{\left[1 + \frac{m_\alpha}{\mathcal{M}_{\text{Li-7}}} \right]} \quad (12.281)$$

$$\begin{aligned}
 &= \frac{2.79 \text{ MeV}}{\left\{ 1 + \frac{3727.3791 \text{ MeV}}{(7.016004 \text{ u}) \times (931.494028 \text{ MeV/u})} \right\}} = \frac{2.79 \text{ MeV}}{1.5703} \\
 &= 1.78 \text{ MeV}
 \end{aligned} \quad (12.282)$$

and

$$\begin{aligned}
 (E_K)_{\text{Li-7}} &= \frac{p_{\text{Li-7}}^2}{2\mathcal{M}_{\text{Li-7}}} = \frac{Q}{\mathcal{M}_{\text{Li-7}}} \left[\frac{1}{m_\alpha} + \frac{1}{\mathcal{M}_{\text{Li-7}}} \right]^{-1} = \frac{Q}{\left[1 + \frac{\mathcal{M}_{\text{Li-7}}}{m_\alpha} \right]} \\
 &= \frac{2.79 \text{ MeV}}{\left\{ 1 + \frac{7.016004 \text{ u} \times (931.494028 \text{ MeV/u})}{3727.3791 \text{ MeV}} \right\}} = \frac{2.79 \text{ MeV}}{2.7533} = 1.01 \text{ MeV}.
 \end{aligned} \quad (12.283)$$

(c) Q value of the ${}^{113}_{48}\text{Cd}(n, \gamma){}^{114}_{48}\text{Cd}$ neutron capture nuclear reaction is determined as follows:

(1) Atomic rest energy \mathcal{M} method:

$$\begin{aligned}
 Q &= \{ \mathcal{M}({}^{113}_{48}\text{Cd})c^2 + m_n c^2 \} - \{ \mathcal{M}({}^{114}_{48}\text{Cd})c^2 + 0 \} \\
 &= \{ (112.904402 \text{ u}) + (1.008665 \text{ u}) \} c^2 - \{ (113.903359 \text{ u}) \} c^2 \\
 &= \{ 113.913067 - 113.903359 \} \times (931.494028 \text{ MeV}) = 9.04294 \text{ MeV}.
 \end{aligned} \quad (12.284)$$

(2) Nuclear rest energy M method:

$$\begin{aligned} Q &= \{M({}_{48}^{113}\text{Cd})c^2 + m_n c^2\} - \{M({}_{48}^{114}\text{Cd})c^2 + 0\} \\ &= \{105145.2523 \text{ MeV} + 939.5654 \text{ MeV}\} - \{106075.7748 \text{ MeV}\} \\ &= \{106084.8177 \text{ MeV} - 106075.7748 \text{ MeV}\} = 9.0429 \text{ MeV}. \end{aligned} \quad (12.285)$$

(3) Binding energy E_B method:

$$\begin{aligned} Q &= \{E_B({}_{48}^{114}\text{Cd}) + 0\} - \{E_B({}_{48}^{113}\text{Cd})c^2 + 0\} \\ &= 972.5984 \text{ MeV} - 963.5555 \text{ MeV} = 9.0429 \text{ MeV}. \end{aligned} \quad (12.286)$$

(d) To determine for the nuclear reaction ${}_{48}^{113}\text{Cd}(n, \gamma){}_{48}^{114}\text{Cd}$ energy E_γ of the γ ray ejected in the nuclear reaction and recoil energy $(E_K)_{\text{Cd-114}}$ of the cadmium-114 reaction product we use the principles of:

- (1) Conservation of total energy.
- (2) Conservation of momentum.

The two conservation principles are for the nuclear reaction expressed as:

(1) Total energy conservation (T5.6) is expressed as follows

$$Q = E_\gamma + (E_K)_{\text{Cd-114}} = E_\gamma + \frac{p_{\text{Cd-114}}^2}{2M_{\text{Cd-114}}}. \quad (12.287)$$

(2) For momentum conservation we note that momentum before the nuclear reaction is zero causing the two momenta \mathbf{p}_γ and $\mathbf{p}_{\text{Cd-114}}$ after the nuclear reaction to be opposite in direction and equal in magnitude

$$\mathbf{0} = \mathbf{p}_\gamma + \mathbf{p}_{\text{Cd-114}} \quad (12.288)$$

or

$$|\mathbf{p}_\gamma| \equiv p_\gamma = \frac{E_\gamma}{c} = |\mathbf{p}_{\text{Cd-114}}| \equiv p_{\text{Cd-114}} = \sqrt{2M_{\text{Cd-114}}(E_K)_{\text{Cd-114}}}, \quad (12.289)$$

where

- p_γ is the magnitude of γ photon momentum.
 $p_{\text{Cd-114}}$ is the magnitude of the cadmium-114 atomic recoil momentum.
 $M_{\text{Cd-114}}$ is the rest mass of the cadmium-114 atom. Note: in the calculation we use atomic mass rather than nuclear mass, since the whole atom rather than just the nucleus recoils after the reaction. $M_{\text{Cd-114}}c^2 = (113.903359 \text{ u}) \times (931.494024 \text{ MeV/u}) = 106100.2987 \text{ MeV}$.

Inserting (12.289) in the form of $p_{\text{Cd-114}} = E_\gamma/c$ into (12.287) we obtain a quadratic equation for photon energy E_γ

$$\frac{E_\gamma^2}{2\mathcal{M}_{\text{Cd-114}}c^2} + E_\gamma - Q = 0, \quad (12.290)$$

with the following physically relevant solution

$$\begin{aligned} E_\gamma &= \mathcal{M}_{\text{Cd-114}}c^2 \left\{ \sqrt{1 + \frac{2Q}{\mathcal{M}_{\text{Cd-114}}c^2}} - 1 \right\} \\ &= (106100.2987 \text{ MeV}) \times \left\{ \sqrt{1 + \frac{2 \times (9.0429 \text{ MeV})}{106100.2987 \text{ MeV}}} - 1 \right\} \\ &= 9.0425 \text{ MeV}. \end{aligned} \quad (12.291)$$

Recoil energy $(E_K)_{\text{Cd-114}}$ of the cadmium-114 atom is from (12.276) given as the difference between Q value of 9.0429 MeV and photon energy $E_\gamma = 9.0425$ MeV of (12.291). The recoil energy of the cadmium-114 atom is thus given as

$$(E_K)_{\text{Cd-114}} = Q - E_\gamma = 9.0429 \text{ MeV} - 9.0425 \text{ MeV} = 0.0004 \text{ MeV} = 400 \text{ eV}. \quad (12.292)$$

As shown in (12.291) and (12.292), the photon carries away most of the energy released by the nuclear reaction ${}^{113}_{48}\text{Cd}(n, \gamma) {}^{114}_{48}\text{Cd}$. Only a minute, essentially negligible, fraction (0.004 %) is given to the cadmium-114 recoil atom.

12.9 Production of Radionuclides with Radionuclide Generator

12.9.Q1

(268)

Used in some 80 % of all nuclear medicine imaging tests, technetium-99m (Tc-99m) is the most widely used radionuclide for imaging in nuclear medicine. Its parent nucleus is molybdenum-99 (Mo-99) which decays into Tc-99m through β^- decay with a half-life of 2.75 days (66 hours). Technetium-99m is an isomeric (metastable) radionuclide emitting 140 keV gamma rays with a physical half-life of 6.01 hours. It provides sufficiently high-energy γ rays for clinical imaging and has a half-life long enough for investigation of metabolic processes, yet short enough so as not to deliver an excessive total body dose to the patient.

The relatively short 6-hour half-life of Tc-99m makes the logistics of source production, delivery, and storage problematic.

A method to circumvent the transportation and delivery problem was developed in 1950s at the Brookhaven National Laboratory in Upton, NY, whereby a supplier, rather than shipping the Tc-99m radionuclide, ships the longer-lived parent radionuclide Mo-99 in a device referred to as radionuclide generator and Tc-99m is extracted from the generator when it is actually needed.

Two techniques, both based on nuclear reactor technology, are used for producing the parent radionuclide Mo-99 used in Tc-99m generators for on-site generation of the Tc-99m radionuclide. One technique is based on neutron activation of stable nuclide Mo-98 to produce the daughter radionuclide Mo-99 through the neutron capture reaction ${}_{42}^{98}\text{Mo}(n, \gamma){}_{42}^{99}\text{Mo}$. The second, more common, technique uses fission of enriched uranium-235 to produce Mo-99 as one of the many fission fragments in the U-235 target bombarded with thermal neutrons.

- (a) Describe the targets used in production of Mo-99 with:
- (1) Neutron activation of Mo-98 technique.
 - (2) Fission of uranium-235 technique.
- (b) Discuss post-production processing of targets in the two Mo-99 production techniques.
- (c) Find the appropriate model for describing the growth of the Mo-99 radionuclide when either Mo-98 or U-235 target is bombarded with thermal neutrons in a nuclear reactor. Calculate the maximum achievable specific activities of Mo-99 produced from pure natural molybdenum target and pure natural uranium target in a nuclear reactor with a fluence rate $\dot{\phi} = 5 \times 10^{13} \text{ cm}^{-2} \cdot \text{s}^{-1}$. Most of the appropriate data can be found in Appendix A; however, the additional information provided in Table 12.32 may be useful.
- (d) Express the specific activity $a_{\text{Mo-99}}(t)$ against time t for the two Mo-99 production techniques of target activation in a nuclear reactor. For pure natural molybdenum target as well as for natural uranium target calculate and plot at least 10 points ranging in specific activity $a_{\text{Mo-99}}(t)$ from 0 to $0.98 (a_{\text{Mo-99}})_{\text{max}}$.

SOLUTION:

(a) Both techniques currently used in production of Mo-99 radionuclide rely on thermal neutron irradiation of appropriate targets in a nuclear reactor; however, each technique is based on its own specific physical process and uses its own specific target: (1) neutron activation technique uses thermal neutron capture in Mo-98 parent

Table 12.32 Some atomic and nuclear properties of molybdenum-98 and uranium-235 that may be of use in answering questions related to the production of molybdenum-99 for use in molybdenum–technetium radionuclide generators

Parent P nuclide	Molybdenum-98 (Mo-98)	Uranium-235 (U-235)
Natural abundance w_P (%)	24.13	0.72
Cross section σ_P (b)	0.13 (neutron activation)	587 (nuclear fission)
Daughter D radionuclide	Mo-99	Mo-99
Branching ratio f_{Mo-99} (%)	100	6.1

nuclide to produce Mo-99 daughter radionuclide and (2) nuclear fission technique uses nuclear fission of uranium-235 radionuclide and extracts Mo-99 from the family of fission fragments produced in the U-235 target.

(1) **Neutron activation of Mo-98 into Mo-99 (neutron activation target)** The most common target for neutron activation of Mo-98 into Mo-99 is molybdenum trioxide (MoO_3) without any Mo-98 enrichment. Molybdenum has 7 natural stable isotopes with Mo-98 (abundance 24.13 %) the most abundant natural molybdenum isotope. Enrichment of Mo-98 in molybdenum target can produce up to a 4-fold increase in specific activity of the molybdenum target; however, in comparison with the enrichment process, irradiation with neutrons of larger targets is more economical.

In addition to Mo-98 two other natural isotopes in molybdenum target also get activated: Mo-92 into Mo-93 and Mo-100 into Mo-101. However, both Mo-93 and Mo-101 have relatively short half-lives (6.9 h and 14.6 min, respectively) in comparison with Mo-99 half-life of 66 h, so that the two radioisotopes do not contribute appreciably to the radioactivity of the molybdenum neutron activation product. On the other hand, chemical impurities in molybdenum targets should be removed prior to neutron activation to maximize the radionuclidic purity of the Mo-99 product for use in nuclear medicine imaging.

(2) **Fission of uranium-235 for Mo-99 production (nuclear fission target)** Currently, most of the Mo-99 radionuclide used in Mo/Tc radionuclide generators is produced by bombarding a U-235 target with thermal neutron causing a nuclear fission reaction which results in U-235 fission. About 6.1 % of fission reactions produce Mo-99 nuclei either through direct fission or through subsequent decay of nuclear fission fragments. Targets used in production of Mo-99 are usually made of highly enriched uranium (HEU) to maximize the yield of Mo-99. The abundance of U-235 in natural uranium is 0.7 % compared to 99.3 % for U-238 and an HEU target contains U-235 in excess of 90 %, making the transportation and use of these targets problematic because of the possibility of use of these targets for military purposes. Targets come in the form of fuel plates containing an aluminum-uranium alloy or in the form of uranium oxide thin films coated inside a stainless steel tube.

(b) Post-irradiation processing in production of Mo-99.

(1) **Neutron activation of Mo-98 into Mo-99** Target processing in which chemical impurities are removed to minimize the production of undesirable radionuclides is mainly done prior to target bombardment with neutrons. After bombardment the radionuclidic purity of the Mo-99 target product is verified by measuring activities of radionuclides other than Mo-99 and its daughter Tc-99m to ensure that they are at maximum acceptable levels or below.

(2) **Fission of uranium-235 in Mo-99 production (fission targets)** Processing of fission targets post irradiation allows production of high purity and high specific activity of Mo-99 radionuclide. Processing must be carried out rapidly after irradiation to minimize the loss of Mo-99 to natural radioactive decay.

The processing is carried out in hot cells where chemicals are added to dissolve the target. For targets containing aluminum, alkaline dissolution is used in a sodium hydroxide solution (NaOH) whereas acidic dissolution is used for uranium oxide based targets.

(c) Maximum attainable specific activity $(a_{\text{Mo-99}})_{\text{max}}$ for the two targets: (1) Mo-98 target undergoing thermal neutron activation into Mo-99 and (2) U-235 target undergoing neutron fission producing Mo-99 as one of the fission fragments.

To calculate the maximum attainable specific activity $(a_{\text{Mo-99}})_{\text{max}}$ for the two targets (Mo-98 and U-235) we need to determine which of the available mathematical models for nuclear activation best describes the growth of the Mo-99 activity in the target. As shown in Prob. 251, three nuclear activation models are available in general: saturation model, depletion model, and depletion-activation model. Since the choice of which model to use depends largely on the activation factor $m = \sigma_P \dot{\phi} / \lambda_D$ for the given nuclear target (note: for $m < 10^{-3}$ the simple saturation model of nuclear activation can be used for describing the growth of the daughter activity), we first determine m for the two target nuclides.

(1) For the Mo-98 target, the neutron activation cross section of the parent nucleus Mo-98 is $\sigma_{\text{Mo-98}} = 0.13 \text{ b}$ ($1 \text{ b} = 1 \text{ barn} = 10^{-24} \text{ cm}^2$) and when the molybdenum target is placed in a neutron fluence rate $\dot{\phi} = 5 \times 10^{13} \text{ cm}^2 \cdot \text{s}^{-1}$ the activation factor m is given as follows

$$\begin{aligned} m &= \frac{\sigma_{\text{Mo-98}} \dot{\phi}}{\lambda_{\text{Mo-98}}} = \frac{(0.13 \times 10^{-24} \text{ cm}^2) \times (5 \times 10^{13} \text{ cm}^{-2} \cdot \text{s}^{-1})}{2.92 \times 10^{-6} \text{ s}^{-1}} \\ &= 2.23 \times 10^{-6} \ll 0.001. \end{aligned} \quad (12.293)$$

(2) For the uranium target, only 6.1 % of all fission processes of the parent nuclei U-235 produce Mo-99. The production of Mo-99 in this case is governed by the an effective cross section $(\sigma_{\text{U-235}})_{\text{eff}}$ that is the product of the general fission cross section of the parent U-235 nuclide and the yield $f_{\text{Mo-99}} = 0.061$ of the daughter Mo-99 nuclide. The effective activation cross section $(\sigma_{\text{U-235}})_{\text{eff}}$ is thus as follows

$$(\sigma_{\text{U-235}})_{\text{eff}} = f_{\text{Mo-99}} \sigma_{\text{U-235}} = 0.061 \times (587 \text{ b}) = 35.8 \text{ b}. \quad (12.294)$$

For U-235 target placed in a neutron fluence rate $\dot{\phi} = 5 \times 10^{13} \text{ cm}^2 \cdot \text{s}^{-1}$ the activation factor m is

$$\begin{aligned} m &= \frac{(\sigma_{\text{U-235}})_{\text{eff}} \dot{\phi}}{\lambda_{\text{Mo-99}}} = \frac{(35.8 \times 10^{-24} \text{ cm}^2) \times (5 \times 10^{13} \text{ cm}^{-2} \cdot \text{s}^{-1})}{2.92 \times 10^{-6} \text{ s}^{-1}} \\ &= 6.14 \times 10^{-4} < 0.001. \end{aligned} \quad (12.295)$$

We conclude from (12.293) and (12.295) that the simple saturation model may be used to describe the growth of Mo-99 activity for both activation processes, since $m < 0.001$ for both processes. The general expression for the daughter activity $\mathcal{A}_{\text{D}}(t)$ is, according to the saturation model of nuclear activation, given as follows (T.12.23)

$$\mathcal{A}_{\text{D}}(t) = \mathcal{A}_{\text{sat}} [1 - e^{-\lambda_{\text{D}} t}] = \sigma_{\text{P}} \dot{\phi} N_{\text{P}}(0) [1 - e^{-\lambda_{\text{D}} t}], \quad (12.296)$$

where \mathcal{A}_{sat} is the saturation activity, $N_{\text{P}}(0)$ is the initial number of parent P nuclei, λ_{D} is the decay constant of daughter D, and σ_{P} is the cross section for thermal neutron interaction with the parent P atom, be it neutron activation of a molybdenum (Mo-98) target or nuclear fission of an uranium (U-235) target.

Using (12.296) we now write the specific activity of the Mo-99 daughter radionuclide as

$$\begin{aligned} a_{\text{Mo-99}}(t) &= \frac{\mathcal{A}_{\text{Mo-99}}}{m_{\text{P}}} = \frac{\sigma_{\text{P}} \dot{\phi} N_{\text{P}}(0)}{m_{\text{P}}} [1 - e^{-\lambda_{\text{Mo-99}} t}] \\ &\approx \frac{\sigma_{\text{P}} \dot{\phi} N_{\text{A}}}{A_{\text{P}}} [1 - e^{-\lambda_{\text{Mo-99}} t}] = (a_{\text{Mo-99}})_{\text{max}} [1 - e^{-\lambda_{\text{Mo-99}} t}], \end{aligned} \quad (12.297)$$

where m_{P} stands for the mass of the parent nuclide and N_{A} is the Avogadro number. We use the \approx sign in (12.297) because we are determining the specific activity of Mo-99 that is not carrier-free, rather, it is mixed together with all natural isotopes of either molybdenum in a molybdenum target or uranium in a uranium target. In (12.297) we then use for A_{P} the atomic weights for natural molybdenum ($A_{\text{Mo}} = 95.962 \text{ g/mol}$) and natural uranium ($A_{\text{U}} = 238.0289 \text{ g/mol}$), respectively, but we also account for the fraction by weight w_{P} of the particular parent isotope and for the branching ratio, as shown in the calculation of the maximum specific activity $(a_{\text{Mo-99}})_{\text{max}}$ below.

The maximum specific activities of the Mo-99 radionuclide are from (12.297) given as follows:

(1) For a pure natural molybdenum target

$$\begin{aligned} (a_{\text{Mo-99}})_{\text{max}} &= w_{\text{Mo-98}} \frac{\sigma_{\text{Mo-98}} \dot{\phi} N_{\text{A}}}{A_{\text{Mo}}} \\ &= 0.2413 \times (0.13 \times 10^{-24} \text{ cm}^2) \times (5 \times 10^{13} \text{ cm}^{-2} \cdot \text{s}^{-1}) \end{aligned}$$

$$\begin{aligned}
 & \times \frac{(6.022 \times 10^{23} \text{ mol}^{-1})}{95.96 \text{ g} \cdot \text{mol}^{-1}} \\
 & = 9.84 \times 10^9 \text{ Bq/g} = \frac{9.84 \times 10^9 \text{ Bq/g}}{3.7 \times 10^{10} \text{ Bq/Ci}} \\
 & \approx 0.27 \text{ Ci/g}, \tag{12.298}
 \end{aligned}$$

where $w_{\text{Mo-98}}$ accounts for the fraction by weight of the Mo-98 isotope in natural molybdenum (24.13 %) from which the Mo-99 radionuclide is produced through neutron activation in nuclear reactor.

(2) For a natural uranium target

$$\begin{aligned}
 (a_{\text{Mo-99}})_{\text{max}} & = w_{\text{U-235}} (\sigma_{\text{U-235}})_{\text{eff}} \dot{\phi} \frac{N_{\text{A}}}{A_{\text{U}}} \\
 & = 0.0072 \times (35.8 \times 10^{-24} \text{ cm}^2) \times (5 \times 10^{13} \text{ cm}^{-2} \cdot \text{s}^{-1}) \\
 & \quad \times \frac{6.022 \times 10^{23} \text{ mol}}{238.03 \text{ g/mol}} \\
 & = 3.26 \times 10^{10} \text{ Bq/g} = \frac{3.26 \times 10^{10} \text{ Bq/g}}{3.7 \times 10^{10} \text{ Bq/Ci}} \\
 & \approx 0.9 \text{ Ci/g}, \tag{12.299}
 \end{aligned}$$

where $w_{\text{U-235}}$ accounts for the fraction by weight of U-235 in natural uranium (0.72 %) from which the Mo-99 radionuclide is produced through the fission reaction of thermal neutrons on uranium target. The effective cross section $(\sigma_{\text{U-235}})_{\text{eff}}$ is defined in (12.294).

Comparing (12.299) and (12.298) we note that the maximum attainable specific activity of Mo-99 from a natural uranium target is about 3.3 times larger than that from a natural molybdenum target. Significantly higher specific activities through fission are achievable when instead of natural uranium target a highly enriched uranium target with $f_{\text{U-235}} > 0.95$ is used providing a two orders of magnitude increase in specific activity. Moreover, the chemical separation of Mo-99 from all other fission products in the U-235 fission target also increases the specific activity of the Mo-99 activation product. Therefore, for practical reasons most of the Mo-99 radionuclide produced in nuclear reactors for use in radionuclide generators around the world is produced through enriched uranium targets. The main drawbacks of this approach are the security concerns related to manufacturing, transportation, and use of highly enriched (nuclear weapons grade) uranium as well as the associated production of radioactive nuclear waste.

(d) Combining (12.297) and (12.298) or (12.299) we express the growth of specific activity $a_{\text{Mo-99}}(t)$ as:

(1) For a pure natural molybdenum target

$$\begin{aligned}
 a_{\text{Mo-99}}(t) &= (a_{\text{Mo-99}})_{\text{max}} [1 - e^{-\lambda_{\text{Mo-99}}t}] \\
 &= (0.27 \text{ Ci/g}) \times [1 - e^{-(0.0105 \text{ h}^{-1})t}].
 \end{aligned}
 \tag{12.300}$$

(2) For a pure natural uranium target

$$\begin{aligned}
 a_{\text{Mo-99}}(t) &= (a_{\text{Mo-99}})_{\text{max}} [1 - e^{-\lambda_{\text{Mo-99}}t}] \\
 &= (0.9 \text{ Ci/g}) \times [1 - e^{-(0.0105 \text{ h}^{-1})t}].
 \end{aligned}
 \tag{12.301}$$

According to (12.300) and (12.301) the maximum specific activity $(a_{\text{Mo-99}})_{\text{max}}$ is attained at time $t = \infty$ in the two types of target. However, we can find a reasonable activation time frame by determining at what time t is the specific activity equal to say 98 % of $(a_{\text{Mo-99}})_{\text{max}}$. Solving

$$\frac{a_{\text{Mo-99}}(t_{0.98})}{(a_{\text{Mo-99}})_{\text{max}}} = 0.98 = [1 - e^{-(0.0105 \text{ h}^{-1})t_{0.98}}]
 \tag{12.302}$$

for $t_{0.98}$ we get $t_{0.98} = 505 \text{ h}$. We thus choose a time scale from 0 to 600 hours and use (12.300) and (12.301) to calculate the growth of Mo-99 specific activity $a_{\text{Mo-99}}(t)$ in steps of 50 hours from 0 to 550 hours. The results of the calculation are shown in Table 12.33 and plotted in Fig. 12.16 for pure molybdenum and pure uranium targets.

Table 12.33 Specific activity $a_{\text{Mo-99}}(t)$ against activation time t calculated for natural molybdenum target from (12.300) and for natural uranium target from (12.301) for activation times between 0 and 600 h in steps of 50 h

(1)	Activation time (h)	0	50	100	150	200	250	300
(2)	Molybdenum target	0.0	0.110	0.176	0.214	0.237	0.250	0.258
(3)	Uranium target	0.0	0.368	0.585	0.714	0.790	0.835	0.861
(1)	Activation time (h)	350	400	450	500	550	600	∞
(2)	Molybdenum target	0.263	0.266	0.268	0.269	0.269	0.270	0.270
(3)	Uranium target	0.877	0.887	0.892	0.895	0.897	0.898	0.9

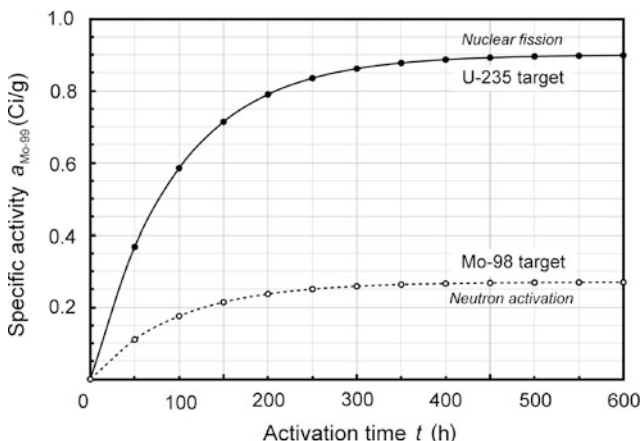


Fig. 12.16 Specific activity $a_{\text{Mo-99}}(t)$ against activation time t for molybdenum-99 radionuclide produced by nuclear activation of natural molybdenum target (*dashed curve and open circle data points*) and thermal neutron fission of natural uranium target (*solid curve and solid circle data points*)

12.9.Q2

(269)

Some 40 million nuclear medicine imaging procedures are carried out around the world every year and about 80 % of these rely on technetium-99m (Tc-99m) radionuclide as radiation source. The Tc-99m radionuclide is derived from radionuclide generators based on molybdenum-99 (Mo-99) as the longer-lived parent radionuclide in the generator. Currently, Mo-99 used in generators is produced by neutron bombardment of suitable targets in nuclear reactors.

Two types of target are used in Mo-99 production: (1) Natural molybdenum target relying on neutron activation of Mo-98 into Mo-99 and (2) Highly enriched uranium-235 (HEU) target relying on fission of U-235 which in about 6.1 % of fissions results in Mo-99 radionuclide.

- Briefly discuss the advantages and disadvantages of each of the two current Mo-99 production techniques, both based on nuclear reactor.
- Some of the concerns with regard to the HEU based Mo-99 production technique are so serious that much effort is spent on trying to develop a less controversial technique. State the major concerns with the HEU technique and briefly describe a few alternative techniques that may prove practical for large scale Mo-99 production in the future.
- Prepare a table listing at least 5 possible techniques for Mo-99 radionuclide production based on particle accelerators. For each technique prepare the following table columns:

- (1) Type of particle accelerator.
- (2) Projectile used in nuclear reaction for production of Mo-99 radionuclide.
- (3) Accelerator target for generating the required projectile.
- (4) Target used in nuclear reaction to produce the Mo-99 radionuclide.
- (5) Nuclear reaction with which Mo-99 radionuclide is produced.

SOLUTION:

(a) Of the two nuclear reactor based Mo-99 production techniques, the HEU fission technique, in comparison with Mo-98 neutron activation technique, is by far the prevalent technique, mainly because it provides Mo-99 with a significantly higher specific activity. Another advantage of the uranium fission technique is that, concurrently with Mo-99, it produces other fission products, such as iodine-131, that can be used in nuclear medicine.

However, the U-235 fission technique is characterized by two serious disadvantages in comparison with the Mo-98 neutron activation technique: (1) Security issue related to the use of highly enriched (weapons grade) uranium-235 for non-military purposes and (2) Production of radioactive waste. We note that Mo-98 activation, in contrast to HEU fission, is not associated with any extraordinary security concerns nor does it produce any radioactive waste.

Both techniques are reactor based, so that as far as the Mo-99 supply chain is concerned both techniques suffer similar problems. There are only a few nuclear reactors around the world (all of them of advanced age and close to end-of-life) that have additional facilities required for production of Mo-99 radionuclide using HEU targets. Therefore, migration of Mo-99 production from nuclear reactors to other non-reactor based techniques is a long-term goal that to date has been discussed at great lengths but has not yet been realized.

(b) The most serious concern with regard to the production of Mo-99 with the HEU fission technique is that the process involves the use of weapons-grade HEU, presenting a significant security risk related to nuclear proliferation stemming from production, transport, and use of HEU for non-military purpose. This leads to increased pressure to discontinue civilian use of HEU in favor of much safer natural uranium or, preferably, depleted uranium as target material for Mo-99 production in nuclear reactors.

Of course, migration from HEU to depleted uranium would only alleviate the HEU security problem while the problem of aging nuclear reactors and production of radioactive waste in the form of fission fragments would still be present.

Radioactive waste generated in Mo-99 production is of concern since Mo-99 appears in HEU target as fission fragment characterized with a branching ratio of only 6.1 %. Most often, all other fragments produced in the target are discarded as

radioactive waste, highlighting the question of disposal and storage of long-lived radioactive waste for generations to come.

The security issue related to HEU targets as well as problems with radioactive waste and aging nuclear reactors are stimulating serious proposals for devising Mo-99 production techniques based on particle accelerators rather than on nuclear reactors. Most of these techniques have been known for years; however, developing them for large-scale clinical Mo-99 production is neither simple nor inexpensive.

Several promising nuclear reactions are under consideration. Electron accelerators as well as proton and heavier ion machines have been considered as possible alternative means for Mo-99 production, but no concrete practical solutions have been developed to date.

Some of these innovative techniques, aimed at dispensing with use of HEU targets, are as follows:

- (1) *High-power electron linear accelerators (linacs)* producing bremsstrahlung x-ray beams in bremsstrahlung targets can be considered as potential source of high intensity photon beam used either in: (i) photonuclear (photodisintegration) reaction on Mo-100 through the reaction $^{100}_{42}\text{Mo}(\gamma, n)^{99}_{42}\text{Mo}$ or (ii) photo-fission reaction on uranium-238.

Both the photodisintegration and photo-fission techniques are feasible but require very high intensity x-ray beams that are not yet readily available. Moreover, the electron accelerator, be it a high-energy linac or a microtron, must produce a photon beam spectrum with peak energy exceeding the threshold for (i) photonuclear reaction and (ii) photo-fission, respectively.

The Mo-99 branching ratio in photo-fission of U-238 is about 6 % just like in regular neutron triggered U-235 fission; however, the cross section of photo-fission in contrast to regular fission is over two orders of magnitude lower, requiring very high intensity photon beams. The major advantage of photo-fission is that it bypasses the need for nuclear reactor and that it is based on readily available U-238 (in natural uranium or in depleted uranium). Thus, no highly enriched U-235 would be required, but the problem of production and disposal of radioactive waste in the form of fission products would remain.

- (2) *Proton accelerators* generating protons that bombard high atomic number targets to produce neutrons can be used as source of neutrons for (i) neutron activation of Mo-98 targets or (ii) nuclear fission of U-235 targets, similar to the current nuclear reactor based Mo-99 production techniques. This would solve the problem with aging nuclear reactors; however, it would not alleviate the problem of nuclear waste produced in U-235 targets.
- (3) *Deuteron accelerators* generating deuterons striking a low atomic number target (tritium or carbon) to produce fast neutrons could be used to bombard enriched Mo-100 targets with fast neutrons to trigger the following neutron activation reaction: $^{100}_{42}\text{Mo}(n, 2n)^{99}_{42}\text{Mo}$. Advantage of this technique would be that production of radioactive waste would be very small.
- (4) Another possibility under consideration for Mo-99 production is bombardment of zirconium-96 (Zr-96) target with energetic α particles obtained by

accelerating ${}^4_2\text{He}$ nuclei (α particles) in an accelerator. While α particle accelerators are available, it is not clear whether or not they can provide sufficiently high currents to enable an efficient production of Mo-99 through the nuclear reaction ${}^{96}_{40}\text{Zr}(\alpha, n){}^{99}_{42}\text{Mo}$. Of course, the α particle kinetic energy must exceed the threshold kinetic energy of the nuclear reaction (see Prob. 270).

- (5) Also considered is direct production of Tc-99m based on nuclear reaction ${}^{100}_{42}\text{Mo}(p, 2n){}^{99\text{m}}_{42}\text{Tc}$ triggered with *protons from a cyclotron* bombarding a Mo-100 target. This approach would bypass the intermediate step of Mo-99 production that is used in all currently employed or investigated options for Tc-99m production.

This direct solution is feasible, however, since Tc-99m would be produced directly rather than through the intermediate Mo-99 step, the short Tc-99m half-life would preclude the shipping of Tc-99m to sites remote from the cyclotron. Thus, the user would have to produce Tc-99m on-site and only a few medical centers around the world would be capable of implementing this approach because of the large cost involved in purchasing and operating a cyclotron just for the purpose of Tc-99m production. We should note, however, that this approach has the added attraction of not producing radioactive waste associated with reactor based nuclear fission in uranium targets as well as with linac based photo-fission in uranium targets. Moreover, around the world there already is a hospital-installed base of cyclotrons for producing fluorine-18 radionuclide for positron emission studies. Many of these machines could be used for production of Tc-99m in the future.

(c) The techniques for Mo-99 production, discussed in (b), are summarized in Table 12.34. In contrast to the two current techniques for Mo-99 production both based on nuclear reactors, Table 12.34 presents 6 possible techniques using a variety of reaction targets (Mo-98, Mo-100, U-235, and Zr-96) as well as four different particle accelerators:

- (1) Two techniques use high energy electron linear accelerators (linacs) to produce high energy x rays which are used to induce: (1) photodisintegration [(γ, n) reaction] of a Mo-100 target into Mo-99 radionuclide and (2) photo-fission of U-238 target producing fission fragment Mo-99 among many other fission fragments.
- (2) Two techniques use proton accelerators to produce neutrons which can be used to induce: (1) neutron activation in a Mo-98 target or (2) nuclear fission in a U-235 target. The two techniques are similar to the currently used reactor based techniques except that neutron projectiles originate in a particle accelerator rather than in a nuclear reactor. Like in a nuclear reactor, the result of neutron bombardment of Mo-98 or U-235 targets results in production of the Mo-99 radionuclide and uranium targets produce radioactive waste that must be dealt with appropriately.
- (3) The fifth technique uses neutrons produced in a deuteron accelerator and bombards a Mo-100 target to produce Mo-99 through a $(n, 2n)$ nuclear reaction.
- (4) The sixth technique uses energetic α particles from a particle accelerator to bombard Zr-96 to produce the Mo-99 radionuclide.

Table 12.34 Six potential techniques for production of Mo-99 based on particle accelerators: (i) Two techniques are based on high-energy electron linac producing high-energy x-ray photons for photodisintegration of Mo-100 and for photo-fission of U-238. (ii) Two techniques are based on proton accelerator producing neutrons for neutron activation of Mo-98 and nuclear fission of U-235. (iii) One technique is based on deuteron accelerator producing fast neutrons for neutron activation of Mo-100. (iv) One technique is based on α particle accelerator producing α particles to trigger nuclear reaction ${}_{40}^{96}\text{Zr}(\alpha, n){}_{42}^{99}\text{Mo}$

(1)	(2)	(3)	(4)	(5)
Type of accelerator	Accelerator target	Projectile produced	Target for nuclear reaction	Nuclear reaction
(1) Electron accelerator	Bremsstrahlung target	X-ray photon	Mo-100	Photodisintegration ${}_{42}^{100}\text{Mo}(\gamma, n){}_{42}^{99}\text{Mo}$
(2)			U-238	Photo-fission ${}_{92}^{238}\text{U}(\gamma, f){}_{42}^{99}\text{Mo}$
(3) Proton accelerator	High atomic number target (Pb, W, U, etc.)	Neutron	Mo-98	Neutron activation ${}_{42}^{98}\text{Mo}(n, \gamma){}_{42}^{99}\text{Mo}$
(4)			U-235	Nuclear fission ${}_{92}^{235}\text{U}(n, f){}_{42}^{99}\text{U}$
(5) Deuteron accelerator	Tritium or carbon target	Fast neutron	Mo-100	Neutron activation ${}_{42}^{100}\text{Mo}(n, 2n){}_{42}^{99}\text{Mn}$
(6) Alpha particle accelerator	–	–	Zr-96	Nuclear reaction ${}_{40}^{96}\text{Zr}(\alpha, n){}_{42}^{99}\text{Mo}$

12.9.Q3

(270)

Several nuclear reactions, all endothermic and based on particle accelerators, are investigated for possible use in large-scale production of molybdenum-99 (Mo-99) radionuclide for radionuclide Tc-99m generators [e.g., ${}_{42}^{100}\text{Mo}(\gamma, n){}_{42}^{99}\text{Mo}$ and ${}_{40}^{96}\text{Zr}(\alpha, n){}_{42}^{99}\text{Mo}$] or for direct production of Tc-99m radionuclide [e.g., ${}_{42}^{100}\text{Mo}(p, 2n){}_{42}^{99m}\text{Tc}$].

- Define Q value of a nuclear reaction and its relationship with threshold energy E_{thr} of the nuclear reaction. Describe the various methods used in calculation of Q value and E_{thr} .
- Calculate Q value and threshold photon energy $(E_{\gamma}^{\text{PN}})_{\text{thr}}$ for photodisintegration of Mo-100, i.e., for photonuclear reaction ${}_{42}^{100}\text{Mo}(\gamma, n){}_{42}^{99}\text{Mo}$, investigated for use in production of the Mo-99 radionuclide, serving as source of Tc-99m radionuclide in radionuclide generators. Provide a schematic diagram for the photodisintegration process.
- Calculate Q value and threshold kinetic energy $(E_{\alpha}^{\alpha})_{\text{thr}}$ of the α particle projectile for the nuclear reaction ${}_{40}^{96}\text{Zr}(\alpha, n){}_{42}^{99}\text{Mo}$ investigated for use in production of the Mo-99 radionuclide.

- (d) Calculate Q value and threshold kinetic energy $(E_K^p)_{\text{thr}}$ of the proton projectile for the nuclear reaction $^{100}_{42}\text{Mo}(p, 2n)^{99\text{m}}_{43}\text{Tc}$ investigated for clinical use in direct production of the Tc-99m radionuclide.
- (e) Another possible nuclear reaction for use in Mo-99 production is neutron activation of Mo-100 through the nuclear reaction $^{100}_{42}\text{Mo}(n, 2n)^{99}_{42}\text{Mo}$. Calculate Q value for the reaction and determine the type of neutron to be used for the activation process.

SOLUTION:

(a) Q value of a nuclear reaction is defined as the difference between $\sum_{i,\text{before}} M_i c^2$, the sum of rest energies $M_i c^2$ of reactants (typically, the projectile and target) before the reaction and $\sum_{i,\text{after}} M_i c^2$, the sum of rest energies of reaction products after the reaction. In short, Q value with the rest energy method is determined as follows

$$Q = \sum_{i,\text{before}} M_i c^2 - \sum_{i,\text{after}} M_i c^2. \quad (12.303)$$

Alternatively, Q value of a nuclear reaction is defined as the difference between $\sum_{i,\text{after}} E_B(i)$, the sum of binding energies $E_B(i)$ of reaction products after the reaction and $\sum_{i,\text{before}} E_B(i)$, the sum of binding energies of reactants (typically, the projectile and target) before the reaction. In short, Q value with the binding energy method is given as

$$Q = \sum_{i,\text{after}} E_B(i) - \sum_{i,\text{before}} E_B(i). \quad (12.304)$$

Thus, two methods are in use for determining a nuclear reaction Q value: (1) rest energy method and (2) binding energy method, and both methods should provide identical result. Each nuclear reaction possesses a characteristic Q value that can be either positive ($Q > 0$), zero ($Q = 0$), or negative ($Q < 0$).

For $Q > 0$, the nuclear reaction is called exothermic (or exoergic) and results in release of energy.

For $Q = 0$, the nuclear reaction is termed elastic and no energy is released or absorbed.

For $Q < 0$, the nuclear reaction is called endothermic (or endoergic) and, to take place, it requires an energy transfer from the projectile to the target.

An exothermic reaction can proceed spontaneously; an endothermic reaction, on the other hand, cannot take place unless the projectile has a kinetic energy exceeding a minimum energy referred to as threshold energy E_{thr} . In general, threshold kinetic energy $(E_K)_{\text{thr}}$ is related to Q value by the following expression (T5.15)

$$(E_K)_{\text{thr}} = -Q \left[1 + \frac{m_{\text{projectile}} c^2}{M_{\text{target}} c^2} \right], \quad (12.305)$$

where $m_{\text{projectile}}$ and M_{target} are rest masses of the projectile and target, respectively. As a result of photon rest mass m_γ being zero, we note that threshold energy $(E_\gamma^{\text{PN}})_{\text{thr}}$ for a photonuclear reaction in which a photon plays the role of projectile is equal to $-Q$ or we can say that the absolute value of Q is equal to threshold energy, i.e., $(E_\gamma^{\text{PN}})_{\text{thr}} = |Q|$.

Alternatively, threshold kinetic energy $(E_K)_{\text{thr}}$ of an endothermic nuclear reaction (or minimum energy that a projectile must possess in order to trigger an endothermic nuclear reaction) can be derived using the relativistic invariant $E^2 - p^2c^2 = \text{inv}$ (T5.9) to get the following expression (T5.13)

$$(E_K)_{\text{thr}} = \frac{[\sum_{i,\text{after}} M_i c^2]^2 - [M_{\text{target}} c^2 + m_{\text{projectile}} c^2]^2}{2M_{\text{target}} c^2}, \quad (12.306)$$

where $\sum_{i,\text{after}} M_i c^2$ stands for a sum of rest energies of reaction products after the nuclear reaction. Note that (12.305) is derived from (12.306) making an assumption that $Q \ll M_{\text{target}} c^2$.

(b) We now determine Q value of the ${}^{100}_{42}\text{Mo}(\gamma, n){}^{99}_{42}\text{Mo}$ photonuclear reaction, first using the rest energy method of (12.303) and then the binding energy method of (12.304):

(1) *Rest energy method:*

$$\begin{aligned} Q &= \sum_{i,\text{before}} M_i c^2 - \sum_{i,\text{after}} M_i c^2 = [0 + M({}^{100}_{42}\text{Mo})c^2] - [M({}^{99}_{42}\text{Mo})c^2 + m_n c^2] \\ &= [0 + 93041.7604 \text{ MeV}] - [92110.4849 \text{ MeV} + 939.5654 \text{ MeV}] \\ &= [93041.7604 \text{ MeV}] - [93050.0503 \text{ MeV}] = -8.29 \text{ MeV}. \end{aligned} \quad (12.307)$$

(2) *Binding energy method:*

$$\begin{aligned} Q &= \sum_{i,\text{after}} E_B(i) - \sum_{i,\text{before}} E_B(i) = [E_B({}^{99}_{42}\text{Mo}) + 0] - [0 + E_B({}^{100}_{42}\text{Mo})] \\ &= [852.1677 \text{ MeV}] - [860.4575 \text{ MeV}] = -8.29 \text{ MeV}. \end{aligned} \quad (12.308)$$

Components i of the photonuclear reaction are defined in Fig. 12.17 and the parameters $M_i c^2$ of (12.307) and $E_B(i)$ of (12.308) are listed in Appendix A. As evident from (12.307) and (12.308), the two methods for calculation of Q value of photonuclear reaction ${}^{100}_{42}\text{Mo}(\gamma, n){}^{99}_{42}\text{Mo}$ yield identical results of -8.29 MeV . A negative Q value indicates that the reaction is endothermic, which means that the reaction cannot run spontaneously, rather, energy must be supplied for reaction to occur. Usually energy for endothermic reactions is supplied in the form of kinetic energy of the projectile when the projectile is a particle. In the case of photonuclear reactions the photon plays the role of projectile and energy is supplied in the form of photon energy $h\nu$.

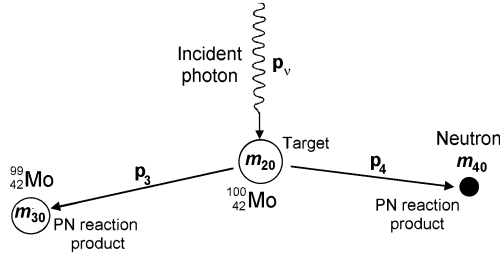


Fig. 12.17 Schematic diagram of the photonuclear (PN) reaction $^{100}_{42}\text{Mo}(\gamma, n)^{99}_{42}\text{Mo}$. A high-energy bremsstrahlung photon, generated by a high-energy electron striking a linac target, plays the role of the projectile, while a molybdenum-100 (Mo-100) nucleus is the nuclear reaction target. Mo-99 and a free neutron are reaction products

Threshold energy $(E_{\gamma}^{\text{PN}})_{\text{thr}}$ of 8.29 MeV for the $^{100}_{42}\text{Mo}(\gamma, n)^{99}_{42}\text{Mo}$ photonuclear reaction is relatively high and to get a photon spectrum with such a high maximum energy requires a high-energy electron accelerator that generates high-energy bremsstrahlung x rays through bombarding a suitable thick target with electrons of kinetic energy exceeding 8.29 MeV. The electron linac also should produce a high intensity bremsstrahlung beam, because the cross section for the photonuclear reaction is relatively small.

(c) Q value of nuclear reaction $^{96}_{40}\text{Zr}(\alpha, n)^{99}_{42}\text{Mo}$ is determined using: (1) rest energy method of (12.303) and (2) binding energy method of (12.304):

(1) *Rest energy method:*

$$\begin{aligned}
 Q &= \sum_{i, \text{after}} M_i c^2 - \sum_{i, \text{before}} M_i c^2 = [m_{\alpha} c^2 + M(^{96}_{40}\text{Zr})c^2] - [M(^{99}_{42}\text{Mo})c^2 + m_n c^2] \\
 &= [3727.3788 \text{ MeV} + 89317.5477 \text{ MeV}] \\
 &\quad - [92110.4849 \text{ MeV} + 939.5654 \text{ MeV}] \\
 &= [93044.9265 \text{ MeV}] - [93050.0503 \text{ MeV}] = -5.1238 \text{ MeV}. \quad (12.309)
 \end{aligned}$$

(2) *Binding energy method:*

$$\begin{aligned}
 Q &= \sum_{i, \text{after}} E_B(i) - \sum_{i, \text{before}} E_B(i) = [E_B(^{99}_{42}\text{Mo}) + 0] - [E_B(\alpha) + E_B(^{96}_{40}\text{Zr})] \\
 &= [852.1677 \text{ MeV}] - [828.9953 \text{ MeV} + 28.2959 \text{ MeV}] \\
 &= [852.1677 \text{ MeV}] - [857.2912 \text{ MeV}] = -5.1235 \text{ MeV}. \quad (12.310)
 \end{aligned}$$

Since Q value is negative, the nuclear reaction is endothermic and is triggered by energy supplied in the form of kinetic energy of the α particle projectile. Minimum energy $(E_K^{\alpha})_{\text{thr}}$ to trigger the reaction is referred to as threshold energy and is

from (12.305) calculated as

$$\begin{aligned}(E_K^\alpha)_{\text{thr}} &= -Q \left[1 + \frac{m_\alpha c^2}{M(^{100}_{42}\text{Mo})c^2} \right] = -(-5.1238 \text{ MeV}) \left[1 + \frac{3727.3788}{89317.5439} \right] \\ &= (5.1238 \text{ MeV}) \times 1.0417 = 5.34 \text{ MeV.}\end{aligned}\quad (12.311)$$

We can also calculate threshold energy of the α particle projectile directly from (12.306) as follows

$$\begin{aligned}(E_K^\alpha)_{\text{thr}} &= \frac{[M(^{99}_{42}\text{Mo})c^2 + m_n c^2]^2 - [m_\alpha c^2 + M(^{96}_{40}\text{Zr})c^2]^2}{2M(^{96}_{40}\text{Zr})c^2} \\ &= \frac{\{[92110.4849 + 939.5654]^2 - [3727.3788 + 89317.5477]^2\} (\text{MeV})^2}{2 \times (89317.5477 \text{ MeV})} \\ &= \frac{8658311861 - 8657358347}{178635.0954} \text{ MeV} = 5.34 \text{ MeV.}\end{aligned}\quad (12.312)$$

As expected, (12.311) and (12.312) give identical result, confirming 5.34 MeV as threshold kinetic energy ($E_K^\alpha)_{\text{thr}}$ that a α particle must exceed to trigger the nuclear reaction $^{96}_{40}\text{Zr}(\alpha, n)^{99}_{42}\text{Mo}$.

(d) Q value of nuclear reaction $^{100}_{42}\text{Mo}(p, 2n)^{99m}_{43}\text{Tc}$ is determined using: (1) rest energy method of (12.303) and (2) binding energy method of (12.304):

(1) *Rest energy method:*

$$\begin{aligned}Q &= \sum_{i,\text{before}} M_i c^2 - \sum_{i,\text{after}} M_i c^2 = [m_p c^2 + M(^{100}_{42}\text{Mo})c^2] - [M(^{99m}_{43}\text{Tc})c^2 + m_n c^2] \\ &= [938.2720 + 93041.7604] (\text{MeV}) - [92108.6129 + 2 \times 939.5654] (\text{MeV}) \\ &= [93980.0324 \text{ MeV}] - [93987.7437 \text{ MeV}] = -7.7113 \text{ MeV.}\end{aligned}\quad (12.313)$$

(2) *Binding energy method:*

$$\begin{aligned}Q &= \sum_{i,\text{after}} E_B(i) - \sum_{i,\text{before}} E_B(i) = [E_B(^{99m}_{43}\text{Tc}) + 0] - [E_B(^{100}_{42}\text{Mo}) + 0] \\ &= [852.7430 \text{ MeV}] - [860.4575 \text{ MeV}] = -7.7145 \text{ MeV.}\end{aligned}\quad (12.314)$$

Since Q value is negative, the nuclear reaction is endothermic and is triggered by energy supplied in the form of kinetic energy of the proton projectile. Both the rest energy method and the binding energy method give almost identical results with an average Q value of -7.7129 MeV. Minimum energy ($E_K^p)_{\text{thr}}$ to trigger the reaction is referred to as threshold energy and is from (12.305) calculated as

$$(E_K^p)_{\text{thr}} = -Q \left[1 + \frac{m_p c^2}{M(^{100}_{42}\text{Mo})c^2} \right] = -(-7.7129 \text{ MeV}) \left[1 + \frac{938.2720}{93041.7604} \right]$$

$$= (7.7129 \text{ MeV}) \times 1.010 = 7.79 \text{ MeV}. \quad (12.315)$$

We can also calculate threshold energy of the proton projectile $(E_K^p)_{\text{thr}}$ directly from (12.316)

$$\begin{aligned} (E_K^p)_{\text{thr}} &= \frac{[M(^{99m}_{42}\text{Tc})c^2 + 2m_n c^2]^2 - [m_p c^2 + M(^{100}_{42}\text{Mo})c^2]^2}{2M(^{100}_{42}\text{Mo})c^2} \\ &= \frac{\{[92108.6129 + 2 \times 939.5654]^2 - [938.2720 + 93041.7604]^2\} (\text{MeV})^2}{2 \times (93041.7604 \text{ MeV})} \\ &= \frac{8833695966 - 8832246490}{186083.5208} \text{ MeV} = 7.79 \text{ MeV}. \end{aligned} \quad (12.316)$$

As expected, (12.314) and (12.316) give identical result, confirming 7.79 MeV as threshold kinetic energy $(E_K^p)_{\text{thr}}$ that a proton must exceed to trigger the nuclear reaction $^{100}_{42}\text{Mo}(p, 2n)^{99m}_{43}\text{Tc}$.

(e) Q value of neutron activation reaction $^{100}_{42}\text{Mo}(n, 2n)^{99}_{42}\text{Mo}$ calculated with: (1) the rest energy method of (12.303) and (2) the binding energy method of (12.304) is obtained as follows

(1) *Rest energy method:*

$$\begin{aligned} Q &= \sum_{i, \text{before}} M_i c^2 - \sum_{i, \text{after}} M_i c^2 = [m_n c^2 + M(^{100}_{42}\text{Mo})c^2] - [M(^{99}_{42}\text{Mo})c^2 + 2m_n c^2] \\ &= [939.5645 + 93041.7604] (\text{MeV}) - [92110.4849 + 2 \times 939.5654] (\text{MeV}) \\ &= [93981.3258 \text{ MeV}] - [93989.6157 \text{ MeV}] = -8.29 \text{ MeV}. \end{aligned} \quad (12.317)$$

(2) *Binding energy method:*

$$\begin{aligned} Q &= \sum_{i, \text{after}} E_B(i) - \sum_{i, \text{before}} E_B(i) = [E_B(^{99}_{42}\text{Mo}) + 0] - [E_B(^{100}_{42}\text{Mo})] \\ &= [852.1677 \text{ MeV}] - [860.4575 \text{ MeV}] = -8.29 \text{ MeV}. \end{aligned} \quad (12.318)$$

Since Q value is negative, the neutron activation reaction is endothermic and is triggered by energy supplied in the form of kinetic energy of the neutron projectile. This means that thermal neutrons cannot be used to trigger this nuclear reaction; however, fast neutrons with kinetic energy exceeding threshold kinetic energy will be suitable. We now use (12.305) to determine the threshold kinetic energy $(E_K^n)_{\text{thr}}$ that a fast neutron must possess to be able to trigger the nuclear reaction

$$\begin{aligned} (E_K^n)_{\text{thr}} &= -Q \left[1 + \frac{m_n c^2}{M(^{100}_{42}\text{Mo})c^2} \right] = -(-8.29 \text{ MeV}) \left[1 + \frac{939.5654}{93041.7604} \right] \\ &= (8.29 \text{ MeV}) \times 1.010 = 8.37 \text{ MeV}. \end{aligned} \quad (12.319)$$

We can also calculate threshold energy of the neutron projectile (E_K^n)_{thr} directly from (12.306)

$$\begin{aligned} (E_K^n)_{\text{thr}} &= \frac{[M({}_{42}^{99}\text{Mo})c^2 + 2m_n c^2]^2 - [m_n c^2 + M({}_{42}^{100}\text{Mo})c^2]^2}{2M({}_{42}^{100}\text{Mo})c^2} \\ &= \frac{\{[92110.4849 + 2 \times 939.5654]^2 - [939.5654 + 93041.7604]^2\} (\text{MeV})^2}{2 \times (93041.7604 \text{ MeV})} \\ &= \frac{8834047859 - 8832489599}{186083.5208} \text{ MeV} = 8.37 \text{ MeV}. \end{aligned} \quad (12.320)$$

Both (12.319) and (12.320) give the same result, confirming that threshold kinetic energy the neutron projectile in neutron activation reaction ${}_{42}^{100}\text{Mo}(n, 2n){}_{42}^{99}\text{Mo}$ must possess is 8.37 MeV and suggesting that fast neutrons from a machine accelerating deuterons that bombard a light nuclear target, such as tritium or carbon, may be suitable for this purpose.

12.10 Nuclear Activation with Protons and Heavier Charged Particles

12.10.Q1

(271)

Radionuclides produced in cyclotron with charged particle activation are positron emitters used in positron emission tomography (PET) scanners for diagnostic imaging. PET scanning is considered a non-invasive imaging technique that provides a functional image of organs and tissues, in contrast to CT scanning and MRI scanning that provide anatomic images of organs and tissues. Carbon-11, a positron emitter decaying through β^+ decay with a half-life $t_{1/2}$ of 20.4 minutes into boron-11, is the most stable artificial radioisotope of carbon and is one of four common positron emitters used in medicine for imaging with PET scanners.

A cyclotron operating at 40 μA and generating a 15 MeV proton beam is used to produce carbon-11 radionuclide through nuclear activation of a gaseous nitrogen-14 pressurized target. The principal nuclear activation reaction for production of carbon-11 is



- (a) Calculate the nuclear reaction energy Q for activation reaction (12.321). The appropriate rest energies and nuclear binding energies of components of (12.321) are provided in Appendix A. Use the three known methods for calculation of Q value (nuclear rest energy, atomic rest energy, and nuclear binding energy) and show that they give the same result.
- (b) Calculate threshold kinetic energy $(E_K)_{\text{thr}}^p$ of the proton for the proton activation reaction (12.321) assuming that the target parent nucleus (nitrogen-14) is initially at rest.
- (c) Determine the effective gaseous nitrogen-14 activation target thickness x_{eff} for the incident 15 MeV proton beam, if the pressure of the gas is 15 atm and its temperature is 20 °C. The density of nitrogen gas at STP (0 °C and 1 atm) is $\rho_{\text{STP}} = 1.251 \times 10^{-3} \text{ g/cm}^3$.
- (d) If the activity of the daughter is 3.52 Ci after an activation time $t = (t_{1/2})_{11\text{C}}$, calculate the mean activation cross section $\bar{\sigma}_p$ in the (12.321) activation reaction for the incident proton beam of kinetic energy $(E_K)_0^p$.

SOLUTION:

(a) Nuclear reaction energy Q , also known as reaction Q value for a nuclear reaction, provides the energy release or energy absorption during the nuclear reaction. We will determine Q value of the activation reaction (12.321) with the following three methods:

(1) *Nuclear rest energy method:* The sum of nuclear rest energies of the reaction products (i.e., total nuclear rest energy after reaction) is subtracted from the sum of nuclear rest energies of the reactants (i.e., total nuclear rest energy before reaction)

$$\begin{aligned}
 Q &= \left\{ \sum_i M_i c^2 \right\}_{\text{before}} - \left\{ \sum_i M_i c^2 \right\}_{\text{after}} \\
 &= \{M({}^{14}_7\text{N})c^2 + m_p c^2\} - \{M({}^{11}_6\text{C})c^2 + m_\alpha c^2\} \\
 &= \{13040.2028 + 938.2720\} \text{ (MeV)} - \{10254.0186 + 3727.3791\} \text{ (MeV)} \\
 &= -2.92 \text{ MeV}. \tag{12.322}
 \end{aligned}$$

(2) *Atomic rest energy method:* The sum of atomic rest energies of the reaction products (i.e., total atomic rest energy after reaction) is subtracted from the sum of atomic rest energies of the reactants (i.e., total atomic rest energy before reaction)

$$Q = \left\{ \sum_i M_i c^2 \right\}_{\text{before}} - \left\{ \sum_i M_i c^2 \right\}_{\text{after}}$$

$$\begin{aligned}
&= \{ \mathcal{M}({}^{14}_7\text{N})c^2 + \mathcal{M}({}^1_1\text{H})c^2 \} - \{ \mathcal{M}({}^{11}_6\text{C})c^2 + \mathcal{M}({}^4_2\text{He})c^2 \} \\
&= \{ 14.003074u + 1.007825u \} - \{ 11.011434u + 4.002603u \} \\
&= -(3.138 \times 10^{-3}u) \times (931.494028 \text{ MeV}/u) = -2.92 \text{ MeV}. \quad (12.323)
\end{aligned}$$

(3) *Binding energy method*: The sum of nuclear binding energies of the reactants (i.e., total binding energy before reaction) is subtracted from the sum of nuclear binding energies of reaction products (i.e., total binding energy after reaction)

$$\begin{aligned}
Q &= \left\{ \sum_i (E_B)_i \right\}_{\text{after}} - \left\{ \sum_i (E_B)_i \right\}_{\text{before}} = \{ E_B({}^{11}_6\text{C}) + E_B({}^4_2\text{He}) \} - \{ E_B({}^{14}_7\text{N}) + 0 \} \\
&= 73.4402 \text{ MeV} + 28.2957 \text{ MeV} - (104.6587 \text{ MeV} + 0 \text{ MeV}) \\
&= -2.92 \text{ MeV}. \quad (12.324)
\end{aligned}$$

As expected, the three calculation methods of Q value (activation energy) give the same result equal to -2.92 MeV , indicating that the activation reaction is endothermic (endoergic) and that for the activation to happen, the proton must have a certain minimum kinetic energy called the threshold kinetic energy $(E_K)_{\text{thr}}^p$ that will be determined in (b).

(b) An exothermic reaction can occur spontaneously; an endothermic reaction cannot take place unless the projectile possesses total energy E exceeding the reaction threshold energy E_{thr} . This means that the projectile must possess kinetic energy exceeding threshold kinetic energy $(E_K)_{\text{thr}}$ that can be determined from the relativistic invariant

$$j = E^2 - p^2c^2 = \text{inv}, \quad (12.325)$$

where E stands for the total energy before the collision and total energy after the collision and p is the total momentum before collision and total momentum after the collision.

The invariant for conditions before the collision is written in laboratory coordinate system, the invariant for conditions after the collision is written in the center-of-mass coordinate system. For a general endothermic nuclear reaction $A(a, b)B$, where a is the projectile and A is the target, the relativistic invariant is given as follows

$$j_{\text{before}} = \left(\sqrt{m_a^2c^4 + p_a^2c^2} + m_Ac^2 \right)^2 - p_a^2c^2 = j_{\text{after}} = (m_Bc^2 + m_b c^2)^2 - 0. \quad (12.326)$$

Solving (12.326) for $E_{\text{thr}}^a = \sqrt{m_a^2c^4 + p_a^2c^2}$, with p_a the total momentum before interaction, results in the following expression for the total threshold energy E_{thr}^a (T5.12) of the nuclear reaction

$$E_{\text{thr}}^a = \frac{(m_Bc^2 + m_b c^2)^2 - (m_a^2c^4 + m_A^2c^4)}{2m_Ac^2}. \quad (12.327)$$

Noting that $E_{\text{thr}}^a = (E_K)_{\text{thr}}^a + m_a c^2$, where $(E_K)_{\text{thr}}^a$ is the threshold kinetic energy of the projectile, we get the following expression for $(E_K)_{\text{thj}}^a$ (T5.13)

$$(E_K)_{\text{thr}}^a = \frac{(m_B c^2 + m_b c^2)^2 - (m_a c^2 + m_A c^2)^2}{2m_B c^2}. \quad (12.328)$$

The threshold kinetic energy $(E_K)_{\text{thr}}^a$ of the projectile given in (12.328) may now be written in terms of nuclear reaction Q value. First, we note that from the definition of Q value (T5.5) we can write the following expression linking Q value with rest masses of the projectile m_a , target m_A , and reaction products m_B and m_b

$$(m_B c^2 + m_b c^2)^2 = (m_a c^2 + m_A c^2)^2 + Q^2 - 2Q(m_a c^2 + m_A c^2). \quad (12.329)$$

Inserting the relationship (12.329) into (12.328) we obtain the following expression for $(E_K)_{\text{thr}}^a$ (T5.15)

$$(E_K)_{\text{thr}}^a = -Q \left[\frac{m_a c^2 + m_A c^2}{m_A c^2} - \frac{Q}{2m_A c^2} \right] \approx -Q \left(1 + \frac{m_a}{m_A} \right), \quad (12.330)$$

where, since $Q \ll m_A c^2$, we can ignore the $Q/2m_A c^2$ term in (12.330).

In (12.330) the threshold kinetic energy $(E_K)_{\text{thr}}^a$ of the projectile exceeds the $|Q|$ value by a relatively small amount to account for conservation of both energy and momentum in the collision.

We now use (12.327), (12.328), and (12.330) to calculate total threshold energy E_{thr}^p and threshold kinetic energy $(E_K)_{\text{thr}}^p$ of the incident proton in the proton activation reaction $^{14}\text{N} + p \rightarrow ^{11}\text{C} + \alpha$ given in (12.321).

(1) Threshold energy E_{thr}^p of the proton using (12.327) is expressed as

$$\begin{aligned} E_{\text{thr}}^p &= \frac{\{M(^{11}_6\text{C})c^2 + m_\alpha c^2\}^2 - \{[M(^{14}_7\text{N})]^2 c^4 + m_p^2 c^4\}}{2M(^{14}_7\text{N})c^2} \\ &= \frac{\{10254.0186 + 3727.3791\}^2 - \{[938.2720]^2 + [13040.2028]^2\}}{2 \times (13040.2028)} \text{ MeV} \\ &= 941.4055 \text{ MeV} \end{aligned} \quad (12.331)$$

resulting in threshold kinetic energy of $941.4055 \text{ MeV} - 938.2720 \text{ MeV} = 3.1335 \text{ MeV}$.

(2) Threshold energy E_{thr}^p of the proton using (12.328)

$$\begin{aligned} E_{\text{thr}}^p &= \frac{\{M(^{11}_6\text{C})c^2 + m_\alpha c^2\}^2 - \{M(^{14}_7\text{N})c^2 + m_p^2 c^4\}^2}{2M(^{14}_7\text{N})c^2} \\ &= \frac{\{10254.0186 + 3727.3791\}^2 - \{938.2720 + 13040.2028\}^2}{2 \times (13040.2028)} \text{ MeV} \\ &= 941.4055 \text{ MeV}. \end{aligned} \quad (12.332)$$

(3) Threshold kinetic energy $(E_K)_{\text{thr}}^{\text{p}}$ of the proton using (12.330)

$$\begin{aligned} (E_K)_{\text{thr}}^{\text{p}} &\approx -Q \left(1 + \frac{m_{\text{p}}c^2}{M({}^{14}\text{N})c^2} \right) = -(-2.92 \text{ MeV}) \left(1 + \frac{938.2720}{13040.2028} \right) \\ &= 3.130 \text{ MeV}. \end{aligned} \quad (12.333)$$

From (12.331), (12.332), and (12.333) we note that the calculated threshold results are consistent, since

$$(E_K)_{\text{thr}}^{\text{p}} = E_{\text{thr}}^{\text{p}} - m_{\text{p}}c^2 \approx -Q \left(1 + \frac{m_{\text{p}}c^2}{M({}^{14}\text{N})c^2} \right) = 3.13 \text{ MeV}. \quad (12.334)$$

In (a) we determined the activation energy $|Q| = 2.92 \text{ MeV}$ (12.322) for activation reaction (12.321) and in (12.334) we determined that the threshold proton kinetic energy $(E_K)_{\text{thr}}^{\text{p}} = 3.13 \text{ MeV}$ that is $\sim 7\%$ higher than $|Q|$ to account for the recoil kinetic energy of the target.

(c) Cyclotron targets are most commonly of the thick target variety, resulting in complete beam absorption in the target material. As the proton beam penetrates the target, its energy decreases as a result of Coulomb interactions with the orbital electrons of the target. Nuclear activation can only be produced in the target in layers where kinetic energy of protons is greater than or equal to the threshold kinetic energy of the projectile for the nuclear reaction to occur. We refer to this target thickness as the effective activation target thickness x_{eff} for a given incident kinetic energy $(E_K)_0^{\text{p}}$ and determine it using the continuous-slowing-down-approximation range R_{CSDA} as follows

$$x_{\text{eff}} = \frac{R_{\text{CSDA}}[(E_K)_0^{\text{p}}] - R_{\text{CSDA}}[(E_K)_{\text{thr}}^{\text{p}}]}{\rho}, \quad (12.335)$$

where ρ is the mass density of the target and we accounted for threshold kinetic energy $(E_K)_{\text{thr}}^{\text{p}}$ of the proton by subtracting the proton CSDA range $R_{\text{CSDA}}[(E_K)_{\text{thr}}^{\text{p}}]$ for the threshold kinetic energy from the proton range $R_{\text{CSDA}}[(E_K)_0^{\text{p}}]$ for the incident proton kinetic energy $(E_K)_0^{\text{p}}$.

The nitrogen-14 target of our example is pressurized to $P = 15$ and ran at a temperature $T = 20 \text{ }^\circ\text{C}$, resulting in the following target density ρ determined from the ideal gas formula

$$\begin{aligned} \rho(T, P) &= \rho_{\text{NTP}} \times \frac{273.2 \text{ K}}{T} \times \frac{P}{(101.325 \text{ kPa})} \\ &= (1.251 \times 10^{-3} \text{ g/cm}^3) \times \frac{273.2}{293.2} \times \frac{15}{1} = 1.748 \times 10^{-2} \text{ g/cm}^3. \end{aligned} \quad (12.336)$$

Looking up data for the proton CSDA range R_{CSDA} in nitrogen-14 from the NIST database (shown in Fig. 12.18) and using the density ρ calculated in (12.336), we get the following result for the required effective nitrogen target thickness x_{eff}

$$\begin{aligned} x_{\text{eff}} &= \frac{R_{\text{CSDA}}[(E_{\text{K}})_{0}^{\text{p}} = 15 \text{ MeV}] - R_{\text{CSDA}}[(E_{\text{K}})_{\text{thr}}^{\text{p}} - 3.13 \text{ MeV}]}{\rho} \\ &= \frac{0.2870 \text{ g/cm}^2 - 0.0184 \text{ g/cm}^2}{1.748 \times 10^{-2} \text{ g/cm}^3} = 15.37 \text{ cm}, \end{aligned} \quad (12.337)$$

where we used 15 MeV for the incident proton energy $(E_{\text{K}})_{0}^{\text{p}}$ and 3.13 MeV for threshold proton energy $(E_{\text{K}})_{\text{thr}}^{\text{p}}$, as determined in (12.334). *Note:* Proton data in the NIST table (physics.nist.gov/PhysRefData/Star/Text/PSTAR.html) are given for density at temperature of 20 °C and pressure of 101.325 kPa (1 atm).

(d) Discussions presented for neutron activation could in principle be generalized to charged particle activation; however, the following points should be considered:

- (1) In neutron activation the target is immersed in a sea of thermal neutrons and the neutron fluence is constant. In charged particle activation, beam attenuation in thick targets that are routinely used in production of medical positron-emitting radionuclides complicates matters considerably. In the thick target the particle beam is completely stopped in the target or, at least, it is degraded in energy to a level below the threshold energy.
- (2) As the charged particles traversing a thick target lose energy through Coulomb interactions with orbital electrons of the target, the activation yield is affected, since the cross section for activation depends on charged particle energy.
- (3) The specific activities produced by charged particle activation are several orders of magnitude lower than those produced in neutron activation, so that in general parent nuclide depletion is not of concern in charged particle activation.

Charged particle activation is illustrated in Fig. 12.19. The charged particle beam is striking a target of cross sectional area A and activation takes place in the target from the surface to effective depth x_{eff} . Since the saturation model can be used to describe charged particle activation, we express the growth of activity $d\mathcal{A}(t)$ in a slab thickness of dx as

$$d\mathcal{A}(t) = \sigma_{\text{p}}(E_{\text{K}})\dot{\phi}(1 - e^{-\lambda_{\text{D}}t}) dN_{\text{p}}(0), \quad (12.338)$$

where $\sigma_{\text{p}}(E_{\text{K}})$ is the activation cross section at proton kinetic energy E_{K} and $dN_{\text{p}}(0)$ is the number of parent nuclei in the slab thickness dx .

For a beam current I the particle fluence rate $\dot{\phi}$ is given as

$$\dot{\phi} = \frac{I}{qA}, \quad (12.339)$$

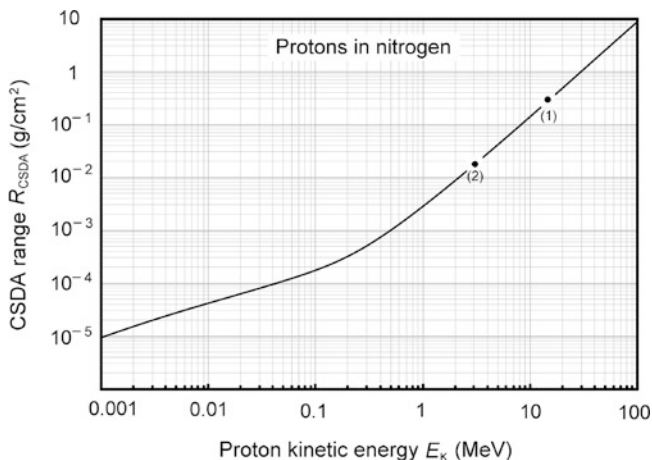


Fig. 12.18 CSDA range of protons against incident kinetic energy $(E_K)_0^p$ in nitrogen. Data are from the NIST. Point (1) is for incident proton kinetic energy of 15 MeV, point (2) is for threshold kinetic energy of 3.13 keV applicable to activation reaction $^{14}\text{N} + p \rightarrow ^{11}\text{C} + \alpha$ (12.321)

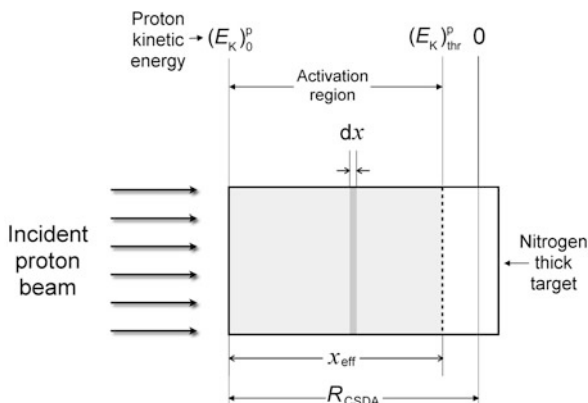


Fig. 12.19 Schematic diagram of thick target used in charged particle activation. Activation region, ranging from the target surface where proton kinetic energy equals to incident proton kinetic energy $(E_K)_0^p = 15$ MeV down to proton kinetic energy $(E_K)_{\text{thr}}^p = 3.13$ MeV that is the threshold energy for the activation reaction $^{14}\text{N} + p \rightarrow ^{11}\text{C} + \alpha$ (12.321), is shown in grey color. Effective depth x_{eff} in the thick target is the depth (measured in the direction of the incident proton beam) at which the proton energy drops to the threshold kinetic energy for the activation reaction

where q is the charge of the incident charged particle and A is the cross sectional area of the beam. $dN_p(0)$ can be expressed in terms of the density n^\square of the target nuclei (number of target nuclei per volume) as

$$dN_p(0) = n^\square A dx. \tag{12.340}$$

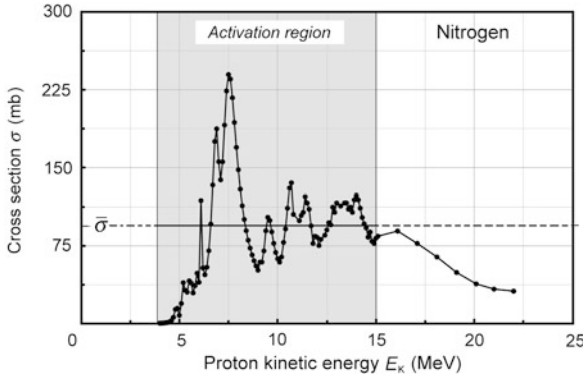


Fig. 12.20 Cross section σ_{N-14} against proton kinetic energy E_K for proton capture in nitrogen-14. The activation region for the activation reaction $^{14}\text{N} + p \rightarrow ^{11}\text{C} + \alpha$ is shown in grey color and ranges from the incident proton kinetic energy of $(E_K)_0^p = 15$ MeV down to threshold kinetic energy of $(E_K)_{\text{thr}}^p = 3.13$ MeV. Data are from the National Nuclear Data Center, Brookhaven National Laboratory, New York, USA at www.nndc.bnl.gov/

Upon inserting (12.339) and (12.340) into (12.338) we get the following expression

$$d\mathcal{A}(t) = n \frac{I}{q} (1 - e^{-\lambda_D t}) \sigma_P(E_K) dx. \tag{12.341}$$

The total daughter activity is obtained by integrating (12.341) as follows

$$\mathcal{A}(t) = \int_0^{x_{\text{eff}}} d\mathcal{A}(t) = n \frac{I}{q} (1 - e^{-\lambda_D t}) \int_0^{x_{\text{eff}}} \sigma_P(E_K) dx. \tag{12.342}$$

The second integral in (12.341) can be expressed as

$$\int_0^{x_{\text{eff}}} \sigma_P(E_K) dx = \int_{(E_K)_0^p}^{(E_K)_{\text{thr}}^p} \sigma_P(E_K) \frac{dx}{dE_K} dE_K = \int_{(E_K)_0^p}^{(E_K)_{\text{thr}}^p} \frac{\sigma_P(E_K)}{\rho S_{\text{col}}(E_K)} dE_K, \tag{12.343}$$

where $S_{\text{col}}(E_K)$ is the collision stopping power for the charged particles. As shown in Fig. 12.20 for our example of proton activation of nitrogen-14 with protons of kinetic energy of 15 MeV, the activation cross section $\sigma_P(E_K)$ is a complex function of the particle kinetic energy and (12.343) can be calculated by numerical methods. To simplify matters we express (12.343) as a product of thickness x_{eff} and a mean activation cross section $\bar{\sigma}_P$ to obtain the following simplified expression for (12.344)

$$\mathcal{A}(t) = n \frac{I}{q} \bar{\sigma}_P x_{\text{eff}} (1 - e^{-\lambda_D t}) = n \frac{I}{q} \bar{\sigma}_P x_{\text{eff}} \left(1 - e^{-\frac{(\ln 2)t}{(t_{1/2})_D}} \right), \tag{12.344}$$

where we used the standard relationship between decay constant λ_D and half-life $(t_{1/2})_D$ for the activation product (daughter D) $\lambda_D = (\ln 2)/(t_{1/2})_D$.

After solving (12.344) for $\bar{\sigma}_p$ we get

$$\bar{\sigma}_p = \frac{\mathcal{A}(t)q}{n^{\square} I x_{\text{eff}} [1 - e^{-\frac{\ln(2)}{(t_{1/2})^D} t}]}. \quad (12.345)$$

For the problem at hand, the nuclear density n^{\square} for the nitrogen-14 target is calculated as

$$n^{\square} = \rho \frac{N_A}{A} = (1.748 \times 10^{-2} \text{ g/cm}^3) \times \frac{(6.022 \times 10^{23} \text{ mol}^{-1})}{(14 \text{ g} \cdot \text{mol}^{-1})} = 7.459 \times 10^{20} \text{ cm}^{-3} \quad (12.346)$$

and (12.345) gives the following result for the mean activation cross section $\bar{\sigma}_{\text{N-14}}$ of nitrogen-14 with the following input data: $x_{\text{eff}} = 15.37 \text{ cm}$, as determined in (12.337); activation time $t = (t_{1/2})_{\text{C-11}} = 20.4 \text{ min}$; activity $\mathcal{A}(t)$ at activation time t is $3.52 \text{ Ci} = 1.30 \times 10^{11} \text{ Bq}$; proton charge $q = 1.602 \times 10^{-19} \text{ C}$; and the proton beam current $I = 4 \times 10^{-5} \text{ A}$

$$\begin{aligned} \bar{\sigma}_{\text{N-14}} &= \frac{\mathcal{A}(t)q}{n^{\square} I x_{\text{max}} [1 - e^{-\frac{\ln(2)}{(t_{1/2})^D} t}]} \\ &= \frac{(1.30 \times 10^{11} \text{ s}^{-1}) \times (1.602 \times 10^{-19} \text{ A} \cdot \text{s})}{(7.459 \times 10^{20} \text{ cm}^{-3}) \times (4 \times 10^{-5} \text{ A}) \times (15.49 \text{ cm}) \times 0.5} \\ &= 9.09 \times 10^{-26} \text{ cm}^2 = 90.9 \text{ mbarn}. \end{aligned} \quad (12.347)$$

Chapter 13 consists of **17 problems** distributed over 11 sections and dealing with theoretical and practical aspects of uniform waveguides and acceleration waveguides used in linear accelerators (linacs) for acceleration of electrons in generation of clinical x-ray and electron beams. Because of their versatility and compact design, clinical linacs are currently the most widely used radiation source for external beam radiotherapy in the developed world. They represent a significant technological advancement over x-ray machines and cobalt-60 teletherapy machines that were used for routine radiotherapy in the past before the advent of linacs.

Section 13.1 covers general aspects of transmission of energy and communication signals through three types of waveguide: electromagnetic (EM), optical, and acoustic. Boundary conditions governing propagation microwaves in an EM waveguide are covered in Sect. 13.2 and Sect. 13.3 addresses the partial differential equations that are used for describing the propagation of microwaves through a uniform EM rectangular or circular transmission waveguide. Electric and magnetic fields present in an EM waveguide are described in Sect. 13.4 and Sect. 13.5 deals with general conditions that must be met for particle acceleration.

The second half of the chapter starts with the dispersion relationship for a uniform EM waveguide covered by problems in Sect. 13.6. Section 13.7 deals with the transverse magnetic (TM)₀₁ mode that is the mode that is used for particle acceleration in acceleration waveguides. Relationships between the phase velocity of the RF wave and the particle velocity is studied in Sect. 13.8, while Sect. 13.9 concentrates on the relationship between group velocity of the RF wave and the velocity of energy flow in a uniform waveguide.

The chapter concludes with Sect. 13.10 that deals with theoretical and practical aspects of acceleration waveguides and Sect. 13.11 that concentrates on the capture condition applied to acceleration waveguides.

13.1 Microwave Propagation in Uniform Waveguide

13.1.Q1

(272)

Theory of waveguide is a highly specialized subject in communication engineering; however, it also plays an important role in the science of medical physics. This is so because the most sophisticated and most prevalent modern high-technology machine, the linear accelerator (linac), used in radiotherapy is based on a specially designed waveguide called acceleration waveguide. Therefore, a medical physicist who calibrates the output and all other operating parameters of a clinical linac must understand the basic theory behind the waveguide, since an acceleration waveguide is the linac component that enables the acceleration of electrons to relativistic energies required for production of clinical x-ray and electron beams with a linac.

- (a) Define a waveguide and briefly describe its basic characteristics.
- (b) List and briefly discuss at least three domains that make use of waveguide. Prepare a table listing the three domains and for each domain state the waveguide core material as well as the waveguide wall material.
- (c) Define the propagation mode of a waveguide and cutoff frequency of a waveguide.
- (d) Define the dispersion relationship for an EM waveguide.
- (e) Define phase velocity v_{ph} and group velocity v_{gr} for an EM wave propagating through a waveguide.

SOLUTION:

(a) Transmission of energy and communication signals carried by waves is very important in modern technology and is studied extensively in communication engineering. A given frequency range generally requires a specifically designed “medium” (transmission line) for optimal transmission of waves in that frequency range. For example, ordinary electrical cables are used for carrying low frequency alternating current (AC), but these cannot be used for transmission of higher frequency radio-signals and microwaves. The problem with transmission of high frequency waves through regular cable arises because power loss in the form of emitted radiation and wave reflection at discontinuities in the cable prevent efficient transmission. Therefore, high frequency waves must be transmitted through other means, such as coaxial cables, strip lines, optical fibers, and waveguides, the choice depending on frequency and type of wave as well as the material used for wave transmission.

Waveguide is a special transmission line used in transmission of a variety of waves of appropriate frequency, such as microwaves, acoustic waves, and optical

signals. Some design characteristics of waveguides for these different domains are the same or similar for all applications and others are specific to a particular area.

Characteristics common to waveguides in all domains can be summarized as follows:

- (1) Waveguides are shaped in the form of a tube with a cylindrical or rectangular cross section.
- (2) In a waveguide waves propagate in the direction of the central axis of the tube and under ideal conditions no power is lost.
- (3) Waveguide tube is filled with vacuum or with medium in which the wave is propagated; waveguide wall guides the waves along the central axis of the tube and contains the waves.
- (4) The diameter of the waveguide tube in cylindrical cross section and the longer side of the rectangle in rectangular waveguide tube cross section are of the order of the wavelength of the wave transmitted through the waveguide.
- (5) Properties of waves in a waveguide depend on initial conditions and boundary conditions.
- (6) Because of the boundary conditions there are only a limited number of frequencies that can propagate in the waveguide.

(b) Three most common domains of waveguide use are in transmission of: (1) electromagnetic (EM) waves, (2) optical waves, and (3) acoustic (sound) waves. In addition to the common characteristics discussed in **(a)**, waveguide types have their own specific characteristics that depend on their physical characteristics and boundary conditions. A summary of main characteristics of the three domains of waveguides: electromagnetic, optical, and acoustic is presented in Table 13.1.

- (1) **Electromagnetic waveguides** have the tube walls made of a conductor most often copper and the inside of the tube is either evacuated or filled with a dielectric gas such as sulfur-hexafluoride SF_6 under pressure exceeding atmospheric pressure. EM waves striking a conductor are fully reflected by the conductor; they do not pass through a conductor. The boundary conditions are such that electric field at the boundary with a conductor is perpendicular to the boundary, while the magnetic field is parallel to it. EM waveguides are excellent in transmission of microwaves in the frequency range between ~ 300 MHz and ~ 30 GHz.

There are numerous examples of EM waveguide use in modern life, such as: (i) in radar technology where waveguides transfer RF power from the source to antenna and back, (ii) in microwave oven where EM waveguide is used to deliver RF from the magnetron source to the cooking chamber, and (iii) in medical linear accelerator employing two types of waveguide: transmission waveguide for transmitting microwave power from the power source to the acceleration waveguide that is used for accelerating electrons to the high energies used in radiotherapy.

- (2) **Optical waveguides** are usually referred to as fiber optic cables or light pipes and the waveguide consists of a fiber cable made of a high-purity transparent dielectric material such as glass or plastic as core material, coated with a

Table 13.1 Three domains of waveguides: electromagnetic, optical, and acoustic

Wave type	Waveguide core: transmitting medium	Waveguide wall
Electromagnetic (EM)	Vacuum or dielectric gas	Conductor (copper)
Optical	Transparent glass or plastic	“Cladding layer”
Acoustic (sound)	Air or wire	Rigid solid wall

“cladding” layer of lower refractive index than that of the core and providing total internal light reflection inside the core. Light and optical signals are very efficiently transmitted through a fiber optic cable for very long distances and with minimal loss of signal. Examples of optical waveguide use in medicine are bronchoscope, endoscope, and laparoscope in various diagnostic procedures.

- (3) **Acoustic waveguides** consist either of a rigid tube filled with some medium, such as air that allows propagation of sound waves, or is simply a wire used to transmit ultrasonic waves. In medicine acoustic waveguides are used in many areas from the simple yet very important stethoscope to transmission of ultrasound for diagnostic and therapeutic purpose, such as in ultrasonic angioplasty in treatment of heart disease or in interstitial and intracavitary hyperthermia in treatment of cancer.

(c) Waveguides act as high-pass filter, meaning that they pass frequencies exceeding a certain lowest frequency called the cutoff frequency ω_c and they attenuate frequencies below the cutoff frequency. The cutoff frequency ω_c thus defines the high pass filter properties of the waveguide.

- (1) Frequencies that can propagate through a waveguide for a given boundary condition form a transmission mode of the waveguide.
- (2) The lowest frequency of a given mode that can propagate through a waveguide is called the cutoff frequency ω_c for the given mode of the waveguide.
- (3) The mode with the lowest cutoff frequency is called the basic mode of the waveguide and its cutoff frequency is defined as the cutoff frequency ω_c of the waveguide.
- (4) For a given frequency ω of an EM wave to be transmitted, a waveguide is chosen whose dimensions are such that ω exceeds ω_c of the waveguide’s basic mode but is smaller than ω_c of all other modes. This ensures that the basic mode is the only mode of propagation through the waveguide.

(d) Dispersion relationship (ω, k_g) for an EM waveguide relates the frequency ω of an EM wave and waveguide wave number (propagation coefficient) k_g . It is derived from the Maxwell equations for a uniform waveguide and is given by the

following hyperbolic equation

$$\omega = \sqrt{\omega_c^2 + c^2 k_g^2}. \quad (13.1)$$

(e) Propagation of an EM wave through a waveguide is characterized by two types of velocity: phase velocity v_{ph} and group velocity v_{gr} , both following from the dispersion relationship as

$$v_{\text{ph}} = \frac{\omega}{k_g} = \frac{c}{\sqrt{1 - \frac{\omega_c^2}{\omega^2}}} \quad (13.2)$$

and

$$v_{\text{gr}} = \frac{d\omega}{dk_g} = c\sqrt{1 - \frac{\omega_c^2}{\omega^2}}. \quad (13.3)$$

From (13.2) and (13.3) we note that since $\omega \geq \omega_c$, the phase velocity $v_{\text{ph}} \geq c$ and the group velocity that is defined as the velocity of energy transmission in the waveguide $v_{\text{gr}} \leq c$.

13.2 Boundary Conditions

13.2.Q1

(273)

Propagation of electromagnetic (EM) waves inside conducting tubes (waveguides) that are either evacuated or filled with a non-conducting dielectric medium is described with the help of Maxwell equations and appropriate boundary conditions. The boundary conditions can be derived from Maxwell equations and depend on the waveguide geometry as well as the electric and magnetic properties of waveguide materials.

- (a) For a given medium define the permittivity ε and permeability μ .
- (b) For vacuum state its permittivity (electric constant) ε_0 and permeability (magnetic constant) μ_0 .
- (c) For a given medium define its relative permittivity ε_r and relative permeability μ_r .
- (d) Discuss the effect of boundary conditions on propagation of EM waves.
- (e) Consider a boundary between two dielectric media: medium 1 is characterized by permittivity ε_1 and permeability μ_1 and medium 2 is characterized by permittivity ε_2 and permeability μ_2 . Derive the general boundary condition on electric field \mathcal{E} from appropriate Maxwell equation in the differential form.

- (f) Consider a boundary between two dielectric media: medium 1 is characterized by permittivity ϵ_1 and permeability μ_1 and medium 2 is characterized by permittivity ϵ_2 and permeability μ_2 . Derive the general boundary condition on magnetic field \mathcal{B} from appropriate Maxwell equation in the differential form.
- (g) Assume that medium 1 in (e) and (f) is vacuum and medium 2 is a perfect conductor. Determine the boundary conditions on electric field \mathcal{E} and magnetic field \mathcal{B} .

SOLUTION:

(a) Permittivity ϵ of a given material is a measure for how the polarization of the material is affected by the application of an external electric field.

Permeability μ of a given material is a measure for how the magnetization of a given material is affected by the application of an external magnetic field.

(b) Permittivity ϵ_0 of vacuum, also called the *electric constant* and permittivity of free space, is a physical constant equal to $\epsilon_0 = 8.85 \times 10^{-12} \text{ (A} \cdot \text{s)/(V} \cdot \text{m)}$ and determined from the following expression $\epsilon_0 = 1/(c^2\mu_0)$, where c is the speed of light in vacuum ($\sim 3 \times 10^8 \text{ m/s}$) and μ_0 is the magnetic constant defined as $4\pi \times 10^7 \text{ (V} \cdot \text{s)/(A} \cdot \text{m)}$.

Permeability μ_0 of vacuum, also called the *magnetic constant* and permeability of free space, is a physical constant defined as $4\pi \times 10^7 \text{ (V} \cdot \text{s)/(A} \cdot \text{m)}$.

(c) Relative electric permittivity ϵ_r of a given material is defined as the ratio of permittivity ϵ of the material divided by the electric constant ϵ_0 , i.e., $\epsilon_r = \epsilon/\epsilon_0$.

Relative magnetic permeability μ_r of a given material is defined as the ratio of permeability μ of the material divided by the magnetic constant μ_0 , i.e., $\mu_r = \mu/\mu_0$.

(d) Electromagnetic waves in free space are not subject to any restrictions on allowed frequencies; however, in the presence of boundaries, only certain frequencies and wavelengths are allowed for EM waves in a bound region, such as a waveguide. Boundaries between media of different electric and magnetic properties impose conditions on electric and magnetic fields at boundaries as well as on EM waves in bound regions. These constraints are referred to as boundary conditions and can be derived from Maxwell equations in the differential form in conjunction with Stokes and Gauss theorems to obtain Maxwell equations in the integral form.

In studies of the behavior of electric field \mathcal{E} and magnetic field \mathcal{B} it is customary to decompose each of these vectors into two orthogonal components: normal components \mathcal{E}_n and \mathcal{B}_n that are perpendicular to the boundary between media 1 and 2 and tangential components \mathcal{E}_t and \mathcal{B}_t that are in the plane of the boundary. For the two media 1 and 2 we thus have the following components: \mathcal{E}_{n1} , \mathcal{E}_{t1} , \mathcal{E}_{n2} , and \mathcal{E}_{t2} lying in the plane of vectors \mathcal{E}_1 and \mathcal{E}_2 for the electric field and \mathcal{B}_{n1} , \mathcal{B}_{t1} , \mathcal{B}_{n2} , and \mathcal{B}_{t2} lying in the plane of vectors \mathcal{B}_1 and \mathcal{B}_2 for the magnetic field.

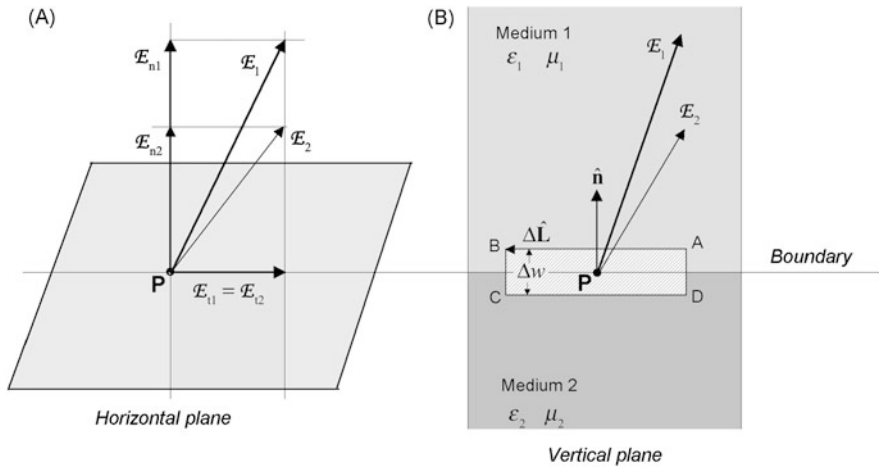


Fig. 13.1 Boundary condition on electric field \mathcal{E} at the boundary between two dielectric media: medium 1 with permittivity ϵ_1 and medium 2 with permittivity ϵ_2 . (A) shows the horizontal plane forming the boundary between the two media. It also shows the two electric field vectors \mathcal{E}_1 and \mathcal{E}_2 in the vertical plane decomposed into transverse components \mathcal{E}_{t1} and \mathcal{E}_{t2} and normal components \mathcal{E}_{n1} and \mathcal{E}_{n2} . The two transverse components are equal. (B) shows the method used for evaluation of the closed loop integral of (13.5)

(e) Boundary condition on electric field \mathcal{E} at a boundary between medium 1 and medium 2 is derived from the following Maxwell equation (T1.138) in the differential form

$$\nabla \cdot \mathcal{E} = -\frac{\partial \mathcal{B}}{\partial t}. \tag{13.4}$$

After applying Stokes theorem (T1.135) on Maxwell equation (13.4), we get the Maxwell–Faraday equation [Maxwell equation (13.4) in integral form]

$$\iint_A \nabla \cdot \mathcal{E} \, dA = \oint_\ell \mathcal{E} \cdot d\mathbf{L} = -\frac{d}{dt} \iint_A \mathcal{B} \cdot d\mathbf{A} = -\frac{d\phi_{\text{mag}}}{dt}, \tag{13.5}$$

stating that the line integral of \mathcal{E} around loop ℓ is equal to the rate of change of the magnetic flux ϕ_{mag} through area A defined by loop ℓ .

Consider a rectangular contour (loop) ℓ of width Δw and length ΔL embedded into the two media and straddling the boundary between the two media, as shown in Fig. 13.1. In the limit as $\Delta w \rightarrow 0$, the magnetic flux crossing the loop decreases to 0, so that the line integral becomes

$$\oint \mathcal{E} \cdot d\mathbf{L} = \int_A^B \mathcal{E}_1 \cdot d\mathbf{L} + \int_C^D \mathcal{E}_2 \cdot d\mathbf{L} = 0. \tag{13.6}$$

For small ΔL (13.6) can be simplified to read

$$\mathcal{E}_1 \cdot \Delta \mathbf{L} + \mathcal{E}_2 \cdot (-\Delta \mathbf{L}) = 0, \tag{13.7}$$

yielding the following result for the boundary condition on tangential components \mathcal{E}_{t1} and \mathcal{E}_{t2} of the electric field in medium 1 and medium 2

$$\mathcal{E}_{t1}\Delta L - \mathcal{E}_{t2}\Delta L = 0 \quad \text{or} \quad \mathcal{E}_{t1} = \mathcal{E}_{t2} \quad (13.8)$$

and showing that the tangential component \mathcal{E}_t of the electric field \mathbf{E} is continuous on the boundary between two dielectric media with different permittivity ε and permeability μ . We can also state that on either side of the boundary between two dielectric media the tangential components of the electric field \mathbf{E} are equal. The boundary condition (13.8) in scalar form can be expressed in vector form as follows

$$\hat{\mathbf{n}} \times (\mathbf{E}_1 - \mathbf{E}_2) = 0, \quad (13.9)$$

where $\hat{\mathbf{n}}$ is a unit vector perpendicular to the contour at the point of interest.

(f) Boundary condition on magnetic field \mathbf{B} at a boundary between medium 1 and medium 2 is derived from the following Maxwell equation (T1.137) in the differential form

$$\nabla \cdot \mathbf{B} = 0. \quad (13.10)$$

After applying the Gauss theorem (T1.134) on Maxwell equation (13.6), we get the Maxwell–Faraday equation [Maxwell equation (13.6) in integral form]

$$\iiint_V \nabla \cdot \mathbf{B} \, d\mathcal{V} = \oiint_A \mathbf{B} \cdot d\mathbf{A} = 0. \quad (13.11)$$

Consider a thin cylinder of height Δh and mantle area of ΔA_3 and two sides of areas ΔA_1 and ΔA_2 where $\Delta A_1 = \Delta A_2 \gg \Delta A_3$. The cylinder straddles the boundary between the two media 1 and 2, as shown in Fig. 13.2.

The closed surface integral of (13.11) can now be expressed as follows

$$\begin{aligned} \oiint_A \mathbf{B} \cdot d\mathbf{A} &= \iint_{A_1} \mathbf{B} \cdot d\mathbf{A} + \iint_{A_2} \mathbf{B} \cdot d\mathbf{A} + \iint_{A_3} \mathbf{B} \cdot d\mathbf{A} \\ &= \iint_{A_1} \mathbf{B} \cdot \hat{\mathbf{n}} \, dA + \iint_{A_2} \mathbf{B} \cdot \hat{\mathbf{n}} \, dA + \iint_{A_3} \mathbf{B} \cdot \hat{\mathbf{n}} \, dA = 0, \end{aligned} \quad (13.12)$$

where the last term of (13.12) results from the limit as the cylinder height $\Delta h \rightarrow 0$ and mantle area $A_3 \rightarrow 0$. Furthermore, if each end of the cylinder is of small area ΔA with opposing unit vectors that are both perpendicular to the boundary, we can write (13.12) as

$$\mathcal{B}_{n1}\Delta A - \mathcal{B}_{n2}\Delta A = 0 \quad \text{or} \quad \mathcal{B}_{n1} = \mathcal{B}_{n2}. \quad (13.13)$$

Thus, the normal component \mathcal{B}_n of the magnetic field \mathbf{B} is continuous on the boundary between two dielectric media. We can also state that on either side of the boundary between two dielectric media the normal components of the magnetic

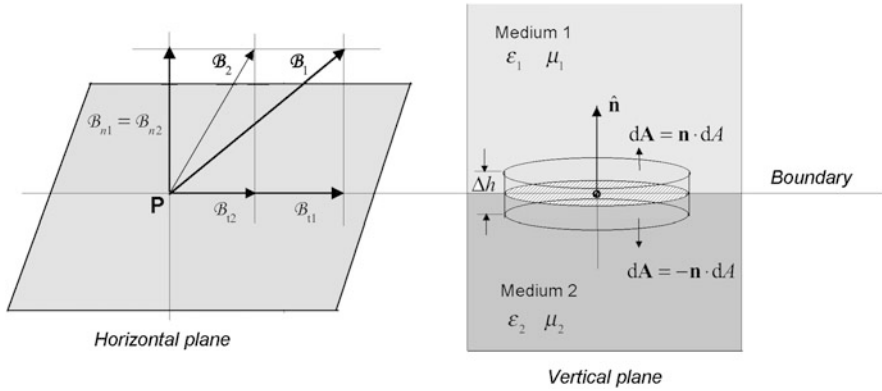


Fig. 13.2 Boundary condition on magnetic field \mathcal{B} at the boundary between two dielectric media: medium 1 with permeability μ_1 and medium 2 with permeability μ_2 . (A) shows the horizontal plane forming the boundary between the two media. It also shows the two magnetic field vectors \mathcal{B}_1 and \mathcal{B}_2 in the vertical plane decomposed into transverse components \mathcal{B}_{t1} and \mathcal{B}_{t2} and normal components \mathcal{B}_{n1} and \mathcal{B}_{n2} . The two normal components are equal. (B) shows the method used in calculation of the closed surface integral of (13.12)

field \mathcal{B} are equal. The boundary condition (13.13) in scalar form can be expressed in vector form as follows

$$\hat{\mathbf{n}} \cdot (\mathcal{B}_1 - \mathcal{B}_2) = 0, \tag{13.14}$$

where $\hat{\mathbf{n}}$ is a unit vector perpendicular to the contour at the point of interest.

(g) The general EM boundary conditions on electric field \mathcal{E} and magnetic field \mathcal{B} at a boundary between two dielectric media 1 and 2 can be expressed in scalar notation and vector notation as follows:

- (1) Tangential component \mathcal{E}_t of \mathcal{E} is continuous across the boundary, i.e., the same on each side of the boundary

$$\mathcal{E}_{t1} = \mathcal{E}_{t2} \quad \text{or} \quad (\mathcal{E}_1 - \mathcal{E}_2) \times \hat{\mathbf{n}} = 0. \tag{13.15}$$

- (2) Normal component \mathcal{B}_n of \mathcal{B} is continuous across the boundary, i.e., the same on each side of the boundary

$$\mathcal{B}_{n1} = \mathcal{B}_{n2} \quad \text{or} \quad (\mathcal{B}_1 - \mathcal{B}_2) \cdot \hat{\mathbf{n}} = 0. \tag{13.16}$$

Boundary conditions on electric field \mathcal{E} and magnetic field \mathcal{B} at a boundary between a dielectric non-conducting medium 1 and perfect conductor (medium 2) follows from (13.15) and (13.16) recognizing that inside a perfect conductor there is no electric field and no magnetic field, because the charges inside the conductor are assumed to be so mobile that they move instantly in response to changes in the fields to generate appropriate surface charges and surface currents to produce zero electric and magnetic fields inside the conductor.

For a boundary between dielectric medium 1 and perfect conductor [medium 2: $\mathcal{E}_{t2} = 0$ and $\mathcal{B}_{n2} = 0$] we conclude from (13.15) and (13.16) that:

- (1) $\mathcal{E}_{t1} = 0$, since in general $\mathcal{E}_{t1} = \mathcal{E}_{t2}$, therefore \mathcal{E}_{t1} must be zero, if $\mathcal{E}_{t2} = 0$. Thus, there is no tangential component of electric field on the dielectric side of the dielectric–conductor boundary and the normal component of the electric field coincides with the electric field. The electric field lines are always perpendicular to the boundary. The boundary condition for electric field in the dielectric material is from (13.15) given as $\mathcal{E}_1 \times \hat{\mathbf{n}}|_S = 0$.
- (2) $\mathcal{B}_{n1} = 0$, since in general $\mathcal{B}_{n1} = \mathcal{B}_{n2}$, therefore \mathcal{B}_{n1} must be zero, if $\mathcal{B}_{n2} = 0$. Thus, there is no normal component of the magnetic field on the dielectric side of the dielectric–conductor boundary and the tangential component of the magnetic field coincides with the magnetic field. The magnetic field lines are parallel to the boundary. The boundary condition for magnetic field in the dielectric material is from (13.16) given as $\mathcal{B}_1 \cdot \hat{\mathbf{n}}|_S = 0$.

13.3 Differential Wave Equation

13.3.Q1

(274)

Electromagnetic (EM) waveguide is a device used for propagation of EM waves in the radiofrequency (microwave) domain from source to user. Two types of EM waveguide are in use: (1) Uniform waveguide used for transmission of RF power and (2) Accelerating waveguide used for acceleration of elementary particles in linear accelerators (linacs). The behavior of the uniform and accelerating waveguide is described with the 3-dimensional partial differential wave equation for the electric field \mathcal{E} and magnetic field \mathcal{B} in conjunction with appropriate boundary conditions on \mathcal{E} and \mathcal{B} .

- (a) Briefly summarize the main characteristics of a uniform EM waveguide and sketch the geometry used in design and study of EM waveguides.
- (b) Briefly describe how waveguides are analyzed theoretically and state the boundary conditions on \mathcal{E}_z and \mathcal{B}_z at the boundary between the waveguide core and waveguide wall.
- (c) From appropriate Maxwell equations derive the wave equations for electric field \mathcal{E} for an EM waveguide with copper wall and evacuated core.
- (d) From appropriate Maxwell equations derive the wave equations for magnetic field \mathcal{B} for an EM waveguide with copper wall and evacuated core.

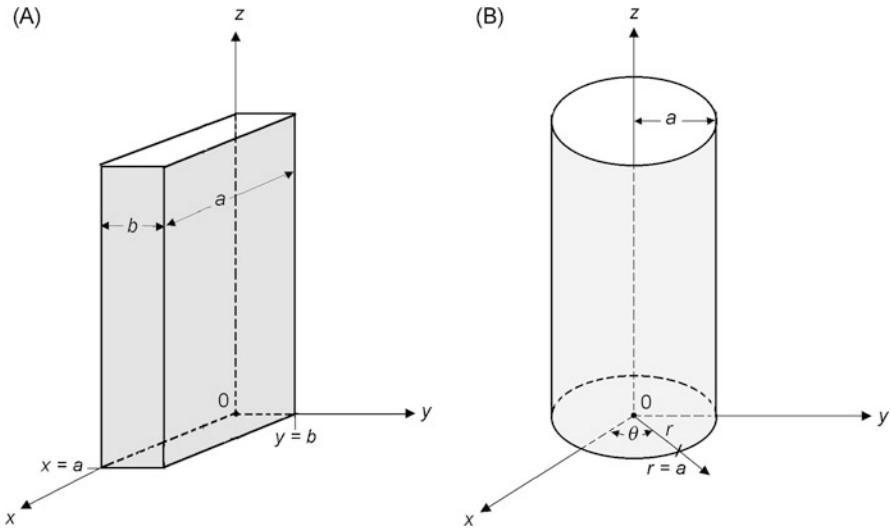


Fig. 13.3 Geometry used in study of uniform EM waveguides: (A) rectangular waveguide with sides a and b and (B) circular waveguide with radius a . Waveguide wall is made of conducting material (copper), waveguide core is evacuated or filled with pressurized dielectric gas

SOLUTION:

(a) Electromagnetic (EM) uniform waveguide is a hollow metallic pipe used for transmission of microwaves from the source of microwave power (magnetron or klystron) to user (transmitting antenna in radar installations, cooking chamber in microwave ovens, accelerating waveguide in particle linacs, etc.). The main characteristics of a uniform waveguide are:

- (1) The cross sectional profile of a uniform waveguide is most commonly rectangular (with longer side a and shorter side b) or circular (with radius a) and, as the name implies, uniform (i.e., the cross sectional profile is smooth and does not change along the axis of the waveguide). Figure 13.3 shows the geometry used for rectangular waveguides in (A) and circular waveguides in (B). It is assumed that the axis of the waveguide tube is oriented in the direction of the z -axis of the Cartesian coordinate system for rectangular waveguides and cylindrical coordinate system for circular waveguides.
- (2) Walls of uniform waveguides are made of a conducting medium, such as copper; core of the uniform waveguide is either evacuated or more commonly filled with pressurized (~ 2 atm) dielectric gas, such as sulfur hexafluoride (SF_6).
- (3) The cross sectional dimensions of a typical uniform EM waveguide are of the order of the wavelength of the RF waves that the waveguide transmits.
- (4) Radiofrequency waves propagate in a uniform waveguide with phase velocity v_{ph} that exceeds the speed of light c in vacuum and with group velocity v_{gr}

that is between 0 and c . Since v_{gr} is generally less than c , uniform waveguides can be used for transmission of radiofrequency power but cannot be used for acceleration of charged particles in linear accelerators (linacs).

- (5) EM waveguides function as a high pass filter. This means that to propagate in a given waveguide the RF frequency must exceed a certain minimum frequency referred to as the cutoff frequency of the waveguide. Waveguides also function as wideband devices and are used for transmission of RF power or communication signals.

(b) Waveguides are analyzed by solving the wave equations for the electric field \mathcal{E} and magnetic field \mathcal{B} in the core of the waveguide in conjunction with boundary conditions that account for waveguide wall and core materials as well as waveguide geometry. The wave equations are partial differential equations of the second order derived from Maxwell equations. They have multiple solutions or modes, each mode categorized by its minimum frequency, called cutoff frequency that can be transmitted through the waveguide.

The general boundary conditions for EM waveguides with perfect copper conductor wall and dielectric (non-conducting) core are written in vector form as follows: $\mathcal{E} \times \hat{\mathbf{n}}|_S = 0$ and $\mathcal{B} \cdot \hat{\mathbf{n}}|_S = 0$, with S representing the boundary surface between the conductor and dielectric of the waveguide and $\hat{\mathbf{n}}$ the unit vector normal to surface S . Thus, just inside the waveguide core only normal component of \mathcal{E} and tangential component of \mathcal{B} can exist and moreover, inside the perfect conductor there are no electric and magnetic fields.

In scalar form we express the boundary conditions as: $\mathcal{E}_{\text{tang}}|_S = 0$ and $\mathcal{B}_{\text{norm}}|_S = 0$, where $\mathcal{E}_{\text{tang}}|_S$ and $\mathcal{B}_{\text{norm}}|_S$ are the tangential component of \mathcal{E} and normal component of \mathcal{B} , respectively, at the boundary surface. Furthermore, $\mathcal{E}_{\text{tang}}|_S$, the tangential component of \mathcal{E} , is actually given as $\mathcal{E}_z|_S$ and $\mathcal{B}_{\text{norm}}|_S$, the normal component of \mathcal{B} , is given as $(\partial \mathcal{B}_z / \partial n)|_S$. The general boundary conditions on \mathcal{E} and \mathcal{B} can thus be summarized as follows

$$\mathcal{E} \times \hat{\mathbf{n}}|_S = 0 \quad \text{or} \quad \mathcal{E}_{\text{tang}}|_S = 0 \quad \text{or} \quad \mathcal{E}_z|_S = 0 \quad (13.17)$$

and

$$\mathcal{B} \cdot \hat{\mathbf{n}}|_S = 0 \quad \text{or} \quad \mathcal{B}_{\text{norm}}|_S = 0 \quad \text{or} \quad \left. \frac{\partial \mathcal{B}_z}{\partial n} \right|_S = 0. \quad (13.18)$$

The boundary conditions imposed on \mathcal{E}_z and \mathcal{B}_z differ from one another and in general cannot be satisfied simultaneously. Therefore, the transverse fields inside a uniform waveguide are divided into two distinct modes: transverse magnetic (TM) and transverse electric (TE) with the following characteristics:

- (1) In the TM mode, the magnetic field \mathcal{B}_z in the direction of propagation is zero everywhere and the boundary condition on \mathcal{E}_z is given by (13.17).
- (2) In the TE mode, the electric field \mathcal{E}_z in the direction of propagation is zero everywhere and the boundary condition on \mathcal{B}_z is given by (13.18).

(c) The propagation of microwaves through a uniform EM waveguide is governed by four Maxwell equations and appropriate boundary conditions. The four Maxwell equations for electric field \mathcal{E} and magnetic field \mathcal{B} (in general differential form on the left and in differential form suitable for use with waveguides on the right, accounting for absence of charges and currents resulting in charge density in vacuum $\rho = 0$ and current density in vacuum $\mathbf{j} = 0$) are given as follows:

- (1) Maxwell–Gauss equation (also known as Gauss law of electricity)

$$\nabla \cdot \mathcal{E} = \frac{\rho}{\varepsilon_0}; \quad (13.19)$$

$$\nabla \cdot \mathcal{E} = 0. \quad (13.20)$$

- (2) Maxwell–Gauss law (also known as Gauss law of magnetism)

$$\nabla \cdot \mathcal{B} = 0; \quad (13.21)$$

$$\nabla \cdot \mathcal{B} = 0. \quad (13.22)$$

- (3) Maxwell–Faraday equation (also known as Faraday law of induction)

$$\nabla \times \mathcal{E} = -\frac{\partial \mathcal{B}}{\partial t}; \quad (13.23)$$

$$\nabla \times \mathcal{E} = -\frac{\partial \mathcal{B}}{\partial t}. \quad (13.24)$$

- (4) Maxwell–Ampère equation (also known as Ampère circuital law)

$$\nabla \times \mathcal{B} = \mu_0 \mathbf{j} + \frac{1}{c^2} \frac{\partial \mathcal{E}}{\partial t}; \quad (13.25)$$

$$\nabla \times \mathcal{B} = \frac{1}{c^2} \frac{\partial \mathcal{E}}{\partial t}. \quad (13.26)$$

Applying the curl vector operator ($\nabla \times$) on (13.24) and using the vector identity

$$\nabla \times \nabla \times \mathbf{A} = \nabla \nabla \cdot \mathbf{A} - \nabla^2 \mathbf{A}, \quad (13.27)$$

where

\mathbf{A} is an arbitrary vector function,

∇ is the gradient vector operator often labeled as *grad*,

$\nabla \cdot$ is the divergence vector operator often labeled as *div*,

∇^2 is the vector Laplacian operator where $\nabla^2 \equiv \Delta = \nabla \cdot \nabla \equiv \text{div grad}$,

results in the following expression linking electric field vector \mathcal{E} and magnetic field vector \mathcal{B}

$$\nabla \times \nabla \times \mathcal{E} = \nabla \nabla \cdot \mathcal{E} - \nabla^2 \mathcal{E} = -\frac{\partial}{\partial t} \nabla \times \mathcal{B}, \quad (13.28)$$

which, after inserting (13.20) and (13.26), evolves into a 3-dimensional linear partial differential wave equation of the second order in four variables (3 spatial and 1 temporal) for the electric field vector \mathcal{E}

$$\nabla^2 \mathcal{E} = \frac{1}{c^2} \frac{\partial^2 \mathcal{E}}{\partial t^2}. \quad (13.29)$$

(d) Applying the curl vector operator ($\nabla \times$) on (13.26) and using the vector identity (13.27) results in the following expression linking magnetic field vector \mathcal{B} and electric field vector \mathcal{E}

$$\nabla \times \nabla \times \mathcal{B} = \nabla \nabla \cdot \mathcal{B} - \nabla^2 \mathcal{B} = -\frac{\partial}{\partial t} \nabla \times \mathcal{E}, \quad (13.30)$$

which, after inserting (13.22) and (13.24), evolves into a 3-dimensional partial differential wave equation of the second order in four variables (3 spatial and 1 temporal) for the magnetic field vector \mathcal{B}

$$\nabla^2 \mathcal{B} = \frac{1}{c^2} \frac{\partial^2 \mathcal{B}}{\partial t^2}. \quad (13.31)$$

13.3.Q2

(275)

Electric field \mathcal{E} and magnetic field \mathcal{B} in a uniform EM waveguide are described with wave equations

$$\nabla^2 \mathcal{E} = \frac{1}{c^2} \frac{\partial^2 \mathcal{E}}{\partial x^2} \quad (13.32)$$

and

$$\nabla^2 \mathcal{B} = \frac{1}{c^2} \frac{\partial^2 \mathcal{B}}{\partial x^2} \quad (13.33)$$

in conjunction with appropriate boundary conditions.

Consider a rectangular uniform EM waveguide oriented along the z axis of the Cartesian coordinate system, while the long side a of the rectangular cross section is oriented along the x axis and the short side b along the y axis, as shown on the sketch in Fig. 13.4.

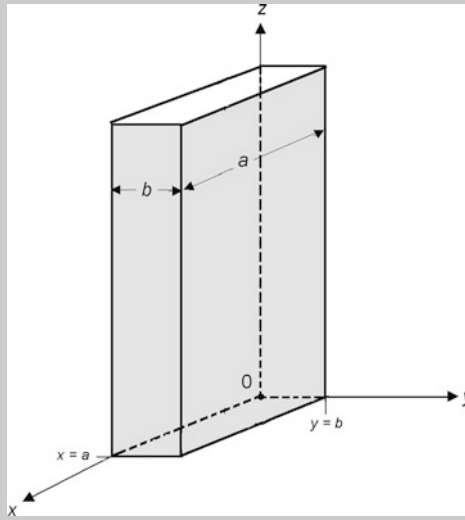


Fig. 13.4 Geometry for the rectangular uniform EM waveguide with sides a and b with $a > b$

- (a) Specify the boundary conditions on the tangential electric field component $\mathcal{E}_{\text{tang}}|_S$ and on the normal magnetic field component $\mathcal{B}_{\text{norm}}|_S$ for the rectangular uniform EM waveguide.
- (b) Using boundary conditions derived in (a), solve wave equations (13.32) and (13.33) for the z components \mathcal{E}_z and \mathcal{B}_z of the electric field \mathcal{E} and magnetic field \mathcal{B} , respectively, for propagation of microwaves in the positive z direction of the rectangular uniform EM waveguide.
- (c) Introduce the special modes of EM fields propagating in uniform EM waveguides.
- (d) Briefly discuss the validity of the assumption that electric and magnetic fields that propagate through the core of a uniform EM waveguide vanish at the boundary between the waveguide core and conducting wall.

SOLUTION:

(a) Solutions to wave equations (13.32) and (13.33) depend on boundary conditions and, in general, uniform EM waveguides are governed by boundary conditions on the tangential component of electric field \mathcal{E} and normal component of magnetic field \mathcal{B} , respectively as

$$\mathcal{E} \times \hat{\mathbf{n}}|_S = \mathcal{E}_{\text{tang}}|_S = 0 \quad \text{and} \quad \mathcal{B} \cdot \hat{\mathbf{n}}|_S = \mathcal{B}_{\text{norm}}|_S = 0. \quad (13.34)$$

For a rectangular waveguide of sides a and b boundary conditions (13.34) can be expressed as follows:

- (1) Dirichlet-type boundary conditions on tangential component of electric field:
 $\mathcal{E}_{\text{tang}}|_S = 0$

$$\mathcal{E}_z|_{x=0} = \mathcal{E}_z|_{x=a} = 0 \quad \text{and} \quad \mathcal{E}_z|_{y=0} = \mathcal{E}_z|_{y=b} = 0. \quad (13.35)$$

- (2) Neumann-type boundary condition on normal component of magnetic field:
 $\mathcal{B}_{\text{norm}}|_S = 0$

$$\left. \frac{\partial \mathcal{B}_z}{\partial x} \right|_{x=0} = \left. \frac{\partial \mathcal{B}_z}{\partial x} \right|_{x=a} = 0 \quad \text{and} \quad \left. \frac{\partial \mathcal{B}_z}{\partial y} \right|_{y=0} = \left. \frac{\partial \mathcal{B}_z}{\partial y} \right|_{y=b} = 0. \quad (13.36)$$

(b) Since the problem deals with a rectangular waveguide, we will seek solutions to wave equations (13.32) and (13.33) in the Cartesian coordinate system. The electric field \mathcal{E} of (13.32) has three components and each component is a function of spatial coordinates x , y , and z as well as of the temporal coordinate t

$$\mathcal{E} = [\mathcal{E}_x(x, y, z, t), \mathcal{E}_y(x, y, z, t), \mathcal{E}_z(x, y, z, t)]. \quad (13.37)$$

Similarly, the magnetic field \mathcal{B} of (13.33) has three components and each of them depends on spatial coordinates x , y , and z as well as of the temporal coordinate t

$$\mathcal{B} = [\mathcal{B}_x(x, y, z, t), \mathcal{B}_y(x, y, z, t), \mathcal{B}_z(x, y, z, t)]. \quad (13.38)$$

Wave equations (13.32) for \mathcal{E} and (13.33) for \mathcal{B} contain the vector Laplacian operator ∇^2 which, when applied to an arbitrary vector field \mathbf{A} (such as \mathcal{E} and \mathcal{B}) with components A_x , A_y , and A_z , generates another vector field. In Cartesian coordinates the generated vector field is equal to the vector field of the scalar Laplacian operator applied to the individual components of the vector field.

Expressed in Cartesian coordinates, (13.32) and (13.33) are given in the following format

$$\nabla^2 \mathbf{A} \equiv \begin{pmatrix} \frac{\partial^2 A_x}{\partial x^2} + \frac{\partial^2 A_x}{\partial y^2} + \frac{\partial^2 A_x}{\partial z^2} \\ \frac{\partial^2 A_y}{\partial x^2} + \frac{\partial^2 A_y}{\partial y^2} + \frac{\partial^2 A_y}{\partial z^2} \\ \frac{\partial^2 A_z}{\partial x^2} + \frac{\partial^2 A_z}{\partial y^2} + \frac{\partial^2 A_z}{\partial z^2} \end{pmatrix} = \frac{1}{c^2} \frac{\partial^2 \mathbf{A}}{\partial t^2} \equiv \frac{1}{c^2} \begin{pmatrix} \frac{\partial^2 A_x}{\partial t^2} \\ \frac{\partial^2 A_y}{\partial t^2} \\ \frac{\partial^2 A_z}{\partial t^2} \end{pmatrix}, \quad (13.39)$$

clearly showing that the three components of \mathbf{A} which stands for \mathcal{E} or \mathcal{B} can be obtained by applying the scalar Laplacian operator on the individual components and for each component (A_x , A_y , and A_z) we get the wave equation of the

form

$$\nabla^2 \eta = \frac{\partial^2 \eta}{\partial x^2} + \frac{\partial^2 \eta}{\partial y^2} + \frac{\partial^2 \eta}{\partial z^2} = \frac{1}{c^2} \frac{\partial^2 \eta}{\partial t^2}, \quad (13.40)$$

where η stands for components of the electric field \mathcal{E} (\mathcal{E}_x , \mathcal{E}_y , and \mathcal{E}_z) as well as components of magnetic field \mathcal{B} (\mathcal{B}_x , \mathcal{B}_y , and \mathcal{B}_z) and all components are a function of spatial coordinates x , y , and z as well as of the temporal coordinate t . In waveguide theory finding the \mathcal{E}_z and \mathcal{B}_z components of \mathcal{E} and \mathcal{B} , respectively, is of main interest, since the waveguide axis is parallel to the z axis of the Cartesian coordinate system and the RF wave is propagating as a plane wave in the z direction.

Conditions imposed on $\eta(x, y, z, t)$ fall into two categories:

- (1) Those involving spatial coordinates x , y , and z and governed by boundary conditions given in (13.35) for Dirichlet-type boundary conditions and in (13.36) for Neumann-type boundary conditions.
- (2) Those involving the temporal coordinate t and governed by initial conditions.

The most common approach to solving the 3-dimensional wave equation (13.40) is to apply the method of separation of variables. This method usually provides a solution to a partial differential equation in the form of an infinite series, such as a Fourier series, for example. We first separate out the time factor by defining $\eta(x, y, z, t)$ as a product of two functions: ϕ and T

$$\eta(x, y, z, t) = \phi(x, y, z)T(t), \quad (13.41)$$

where ϕ is a function of spatial coordinates x , y , and z only and T is a function of time t only.

Inserting (13.41) into (13.40) and dividing by $\phi(x, y, z)T(t)$ gives

$$\frac{\nabla^2 \phi}{\phi} \equiv \frac{1}{c^2} \frac{1}{T} \frac{\partial^2 T}{\partial t^2}, \quad (13.42)$$

with the left hand side of (13.42) depending on spatial coordinates x , y , and z only, and the right hand side depending on time t only. If this equality is to hold for all x , y , z and t , it is evident that each side must be equal to a constant. This constant is identical for both sides and usually referred to as the separation constant Λ . From (13.42) we thus get two equations

$$\nabla^2 \phi = \Lambda \phi \quad (13.43)$$

and

$$\frac{\partial^2 T}{\partial t^2} = \Lambda c^2 T. \quad (13.44)$$

Equation (13.43) is referred to as the Helmholtz partial differential equation representing an eigenvalue problem in three dimensions with ϕ the eigenfunction, Λ the

eigenvalue, and ∇^2 the scalar Laplacian operator in Cartesian coordinates. The Helmholtz equation (13.43) results in three different types of solution depending on the value of the separation constant Λ :

- (1) For $\Lambda > 0$ the solutions are exponential functions.
- (2) For $\Lambda = 0$ the solution is a linear function.
- (3) For $\Lambda < 0$ the solutions are trigonometric functions.

The Dirichlet boundary condition of (13.35) can be satisfied only for $\Lambda < 0$ and this will result in trigonometric solutions for function η . We now concentrate on finding solutions to the wave equation and set $\Lambda = -k^2$ to satisfy the usual periodicity requirement. Parameter k is called the *free space wave number* and is related to angular frequency ω through the standard relationship

$$k = \frac{\omega}{c}, \quad (13.45)$$

with c the speed of light in vacuum. Incorporating $\Lambda = -k^2$ into (13.43) and (13.44) yields the following equations for $\phi(x, y, z)$ and $T(t)$, respectively

$$\nabla^2 \phi + k^2 \phi = 0 \quad (13.46)$$

and

$$\frac{\partial^2 T}{\partial t^2} + k^2 c^2 T = \frac{\partial^2 T}{\partial t^2} + \omega^2 T = 0. \quad (13.47)$$

The solutions for $T(t)$ in (13.47) are either trigonometric or exponential but we reject the latter on physical grounds. Instead of using real trigonometric functions we express $T(t)$ as

$$T(t) \propto e^{-i\omega t}, \quad (13.48)$$

and assume that ω may be either positive or negative.

For the Helmholtz equation, given in (13.43), we again use the method of separation of variables and express $\phi(x, y, z)$ as a product of three functions: $X(x)$, $Y(y)$, and $Z(z)$ to get

$$\phi(x, y, z) = X(x)Y(y)Z(z), \quad (13.49)$$

insert (13.49) into (13.46), divide the result by $X(x)Y(y)Z(z)$, and get

$$\frac{1}{X} \frac{\partial^2 X}{\partial x^2} + \frac{1}{Y} \frac{\partial^2 Y}{\partial y^2} + \frac{1}{Z} \frac{\partial^2 Z}{\partial z^2} + k^2 = 0. \quad (13.50)$$

Since in our waveguide geometry the RF wave is propagating in the positive z direction as a plane wave, we rewrite (13.50) as

$$-\frac{1}{X} \frac{\partial^2 X}{\partial x^2} - \frac{1}{Y} \frac{\partial^2 Y}{\partial y^2} = \frac{1}{Z} \frac{\partial^2 Z}{\partial z^2} + k^2 \quad (13.51)$$

and note that the left hand side of (13.51) is a function of x and y only and the right hand side is a function of z only. This can hold only when the two sides are equal to a constant that we designate as γ^2 . The right hand side of (13.51) now gives

$$\frac{1}{Z} \frac{\partial^2 Z}{\partial z^2} + k^2 = \gamma^2 \quad \text{or} \quad \frac{\partial^2 Z}{\partial z^2} + k_z^2 Z = 0, \quad (13.52)$$

and results in the following trigonometric solution for propagation in the positive z direction

$$Z(z) \propto e^{ik_z z}, \quad (13.53)$$

where k_z is referred to as waveguide wave number or propagation coefficient and defined as

$$k_z^2 = k^2 - \gamma^2 \quad \text{or} \quad \gamma^2 = k^2 - k_z^2. \quad (13.54)$$

We now address the left hand side of (13.51) that, after insertion of (13.52), reads

$$\frac{1}{X} \frac{\partial^2 X}{\partial x^2} + \frac{1}{Y} \frac{\partial^2 Y}{\partial y^2} + (k^2 - k_z^2) = 0. \quad (13.55)$$

Equation (13.55) can be separated into the following two Helmholtz equations

$$\frac{\partial^2 X}{\partial x^2} + k_x^2 X = 0 \quad \text{and} \quad \frac{\partial^2 Y}{\partial y^2} + k_y^2 Y = 0 \quad (13.56)$$

with the provision that

$$k_x^2 + k_y^2 = k^2 - k_z^2 \quad \text{or} \quad k_x^2 + k_y^2 + k_z^2 = k^2 = \frac{\omega^2}{c^2}. \quad (13.57)$$

Equation (13.57) is called the *dispersion relationship* linking the RF frequency ω with the propagation coefficient k_z in a rectangular uniform EM waveguide. This relationship is of importance in waveguide theory, since it defines the propagation coefficient k_z for a given frequency ω and a given mode. Moreover, it enables the determination of RF frequencies that can propagate through a given waveguide as well as phase and group velocities of RF waves based on boundary conditions and waveguide geometry.

Solutions to (13.56) depend on the boundary conditions which are, for \mathcal{E} and \mathcal{B} in a rectangular waveguide of sides a and b and based on (13.35) and (13.36) of (a), respectively, given as follows

- (1) Dirichlet boundary conditions on tangential component of electric field:

$$\mathcal{E}_x|_{x=0} = \mathcal{E}_z|_{x=a} = 0 \quad \text{and} \quad \mathcal{E}_z|_{y=0} = \mathcal{E}_x|_{y=b} = 0, \quad (13.58)$$

resulting in the following solutions for $X(x)$ and $Y(y)$

$$X(x) = \sin k_x x = \sin \frac{m\pi}{a} x \quad \text{and} \quad Y(y) = \sin k_y y = \sin \frac{n\pi}{b} y, \quad (13.59)$$

since from the boundary conditions (13.58) it follows that $k_x = m\pi/a$ and $k_y = n\pi/b$, where m and n are integers.

- (2) Neumann-type boundary condition on normal component of magnetic field:
 $\mathbf{B} \cdot \hat{\mathbf{n}}|_S = 0$

$$\left. \frac{\partial \mathcal{B}_z}{\partial x} \right|_{x=0} = \left. \frac{\partial \mathcal{B}_z}{\partial x} \right|_{x=a} = 0 \quad \text{and} \quad \left. \frac{\partial \mathcal{B}_z}{\partial y} \right|_{y=0} = \left. \frac{\partial \mathcal{B}_z}{\partial y} \right|_{y=b} = 0, \quad (13.60)$$

resulting in the following solutions for $X(x)$ and $Y(y)$

$$X(x) = \cos k_x x = \cos \frac{m\pi}{a} x \quad \text{and} \quad Y(y) = \cos k_y y = \cos \frac{n\pi}{b} y, \quad (13.61)$$

since from the boundary conditions (13.60) it follows that $k_x = m\pi/a$ and $k_y = n\pi/b$, where m and n are integers.

According to the boundary conditions (13.60) and (13.60) for a rectangular uniform EM waveguide, the following points can be made on tangential \mathcal{E} and normal \mathcal{B} components:

- (1) Tangential component of the electric field \mathcal{E} must vanish at all boundaries of the waveguide which means that \mathcal{E}_z must be zero for all times t and for all z at $x = 0$ and $x = a$ as well as at $y = 0$ and $y = b$.
- (2) Normal component of the magnetic field \mathcal{B} must vanish at all boundaries of the waveguide which means that $\partial \mathcal{B}_z / \partial x$ must be zero for all times t and for all z at $x = 0$ and $x = a$. In addition, it means that $\partial \mathcal{B}_z / \partial y$ must be zero for all t and for all z at $y = 0$ and $y = b$.

The general solution for \mathcal{E}_z , based on (13.48), (13.53), and (13.60), can now be expressed as superposition of all modes

$$\mathcal{E}_z(x, y, z, t) = T(t)Z(z)X(x)Y(y) = \sum_{m=0}^{\infty} \sum_{n=0}^{\infty} A_{mn} \sin \frac{m\pi x}{a} \sin \frac{n\pi y}{b} e^{i(k_z z - \omega_{mn} t)} \quad (13.62)$$

while the general solution for \mathcal{B}_z , based on (13.48), (13.53), and (13.61), as superposition of all modes is given as

$$\mathcal{B}_z(x, y, z, t) = T(t)Z(z)X(x)Y(y) = \sum_{m=0}^{\infty} \sum_{n=0}^{\infty} B_{mn} \cos \frac{m\pi x}{a} \cos \frac{n\pi y}{b} e^{i(k_z z - \omega_{mn} t)}. \quad (13.63)$$

- (c) The boundary conditions on \mathcal{E} and \mathcal{B} in EM waveguides are dissimilar, therefore, in general, they cannot be satisfied simultaneously and this results in two distinct modes of EM fields in the waveguide:

- (1) Transverse electric (TE) mode for which $\mathcal{E}_z = 0$ everywhere and the boundary condition is $\partial \mathcal{B}_z / \partial x|_{x=0} = \partial \mathcal{B}_z / \partial x|_{x=a} = \partial \mathcal{B}_z / \partial y|_{y=0} = \partial \mathcal{B}_z / \partial y|_{y=b} = 0$.
- (2) Transverse magnetic (TM) mode for which $\mathcal{B}_z = 0$ everywhere and the boundary condition is $E_z|_{x=0} = E_z|_{x=a} = E_z|_{y=0} = E_z|_{y=b} = 0$.
- (3) In addition to TE and TM modes another mode is known, the so-called TEM mode (transverse electromagnetic mode) for which both \mathcal{E}_z and \mathcal{B}_z components are zero everywhere. However, it turns out that this mode cannot propagate in a regular EM waveguide, since two distinct conducting surfaces (for example, a coaxial cable) are required for propagation of the TEM mode.

(d) As an EM wave strikes an ideal conductor characterized by infinite conductivity, the wave is completely reflected; however, in practice the current density j_s on the surface of the conductor does not drop to zero instantaneously; rather, it drops exponentially with depth d of penetration into the conductor, i.e., as $j = j_s e^{-d/\delta}$. This phenomenon is referred to as the *skin effect* and skin depth δ , defined as the depth at which the current density drops to $1/e$ ($\sim 36.8\%$) of the surface value, is inversely proportional to the square root of the EM frequency ν and permeability μ of the conductor.

The skin effect is of importance in microwave transmission with waveguides and also plays a role in AC power transmission at 50 Hz or 60 Hz. For example, according to Jackson, at 50 Hz skin depth in copper is ~ 1 cm, while at 1000 MHz it drops four orders of magnitude to ~ 1 μm , justifying the assumption of zero electric and magnetic fields in the wall of a EM waveguide used in microwave power transmission.

13.3.Q3

(276)

Electric field \mathcal{E} and magnetic field \mathcal{B} in a uniform EM waveguide are described with wave equation

$$\nabla^2 \mathcal{E} = \frac{1}{c^2} \frac{\partial^2 \mathcal{E}}{\partial t^2} \quad (13.64)$$

and

$$\nabla^2 \mathcal{B} = \frac{1}{c^2} \frac{\partial^2 \mathcal{B}}{\partial t^2} \quad (13.65)$$

in conjunction with appropriate boundary conditions.

Consider a circular uniform EM waveguide of radius a oriented along the z axis of the cylindrical coordinate system, as shown on the sketch in Fig. 13.5.

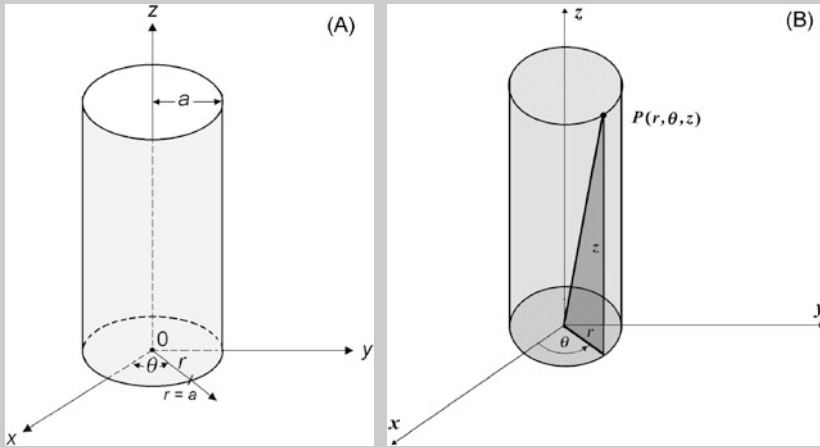


Fig. 13.5 (A) Geometry for the circular uniform EM waveguide of radius a and centered along z axis of a cylindrical coordinate system; (B) Relationship between Cartesian coordinate system (x, y, z) and cylindrical coordinate system (r, θ, z)

- (a) Specify the boundary conditions on the tangential electric field component $\mathcal{E}_{\text{tang}}|_S$ and on the normal magnetic field component $\mathcal{B}_{\text{norm}}|_S$ for the circular uniform EM waveguide.
- (b) Using boundary conditions derived in (a), solve wave equations (13.64) and (13.65) for the z components \mathcal{E}_z and \mathcal{B}_z of the electric field \mathcal{E} and magnetic field \mathcal{B} , respectively, for propagation of microwaves in the positive z direction of the rectangular uniform EM waveguide.
- (c) Using boundary conditions derived in (a) and general solutions derived for \mathcal{E}_z and \mathcal{B}_z in (b), determine expressions for \mathcal{E}_z in the lowest TM mode and \mathcal{B}_z in the lowest TE mode.

SOLUTION:

(a) Solutions to wave equations (13.64) and (13.65) depend on boundary conditions and, in general, uniform EM waveguides are governed by boundary conditions on the tangential component of electric field \mathcal{E} and normal component of magnetic field \mathcal{B} , respectively, as

$$\mathcal{E} \times \hat{\mathbf{n}}|_S = \mathcal{E}_{\text{tang}}|_S = 0 \quad \text{and} \quad \mathcal{B} \cdot \hat{\mathbf{n}}|_S = \mathcal{B}_{\text{norm}}|_S = 0. \tag{13.66}$$

For a circular waveguide of radius a boundary conditions (13.66) can be expressed as follows

- (1) Dirichlet-type boundary condition on tangential component of electric field:
 $\mathcal{E}_{\text{tang}}|_S = 0$

$$\mathcal{E}_z|_S = 0 \quad \text{or} \quad \mathcal{E}_z|_{r=a} = 0. \quad (13.67)$$

- (2) Neumann-type boundary condition on normal component of magnetic field:
 $\mathcal{B}_{\text{norm}}|_S = 0$

$$\left. \frac{d\mathcal{B}_z}{dn} \right|_S = 0 \quad \text{or} \quad \left. \frac{d\mathcal{B}_z}{dr} \right|_{r=a} = 0. \quad (13.68)$$

(b) Since the problem deals with a circular waveguide, we will seek solutions to wave equations (13.64) and (13.65) in the cylindrical coordinate system, as indicated in Fig. 13.5(A). The standard relationship between the Cartesian and cylindrical coordinate system with a common z axis is presented in Fig. 13.5(B) and is given as

$$x = r \cos \theta, \quad y = r \sin \theta, \quad \text{and} \quad z = z. \quad (13.69)$$

The electric field \mathcal{E} of (13.64) has three components in cylindrical coordinates and each component is a function of spatial coordinates r , θ , and z as well as of the temporal coordinate t

$$\mathcal{E} = [\mathcal{E}_r(r, \theta, z, t), \mathcal{E}_\theta(r, \theta, z, t), \mathcal{E}_z(r, \theta, z, t)]. \quad (13.70)$$

Similarly, the magnetic field \mathcal{B} of (13.65) has three components in cylindrical coordinates and each of them depends on spatial coordinates r , θ , and z as well as the temporal coordinate t

$$\mathcal{B} = [\mathcal{B}_r(r, \theta, z, t), \mathcal{B}_\theta(r, \theta, z, t), \mathcal{B}_z(r, \theta, z, t)]. \quad (13.71)$$

Wave equations (13.64) for \mathcal{E} and (13.65) for \mathcal{B} contain the vector Laplacian operator ∇^2 which, when applied to an arbitrary vector field \mathbf{A} (such as \mathcal{E} and \mathcal{B}) with components A_r , A_θ , and A_z , generates another vector field. The generated vector field is equal to the vector field of the scalar Laplacian operator applied to the individual components of the vector field.

Expressed in cylindrical coordinates, (13.64) and (13.65) are given in the following format

$$\nabla^2 \mathbf{A} = \begin{vmatrix} \frac{\partial^2 A_r}{\partial r^2} + \frac{1}{r} \frac{\partial A_r}{\partial r} + \frac{1}{r^2} \frac{\partial^2 A_r}{\partial^2 \theta^2} + \frac{\partial^2 A_r}{\partial z^2} - \frac{2}{r^2} \frac{\partial A_\theta}{\partial \theta} - \frac{A_r}{r^2} \\ \frac{\partial^2 A_\theta}{\partial r^2} + \frac{1}{r} \frac{\partial A_\theta}{\partial r} + \frac{1}{r^2} \frac{\partial^2 A_\theta}{\partial^2 \theta^2} + \frac{\partial^2 A_\theta}{\partial z^2} + \frac{2}{r^2} \frac{\partial A_r}{\partial \theta} - \frac{A_\theta}{r^2} \\ \frac{\partial^2 A_z}{\partial r^2} + \frac{1}{r} \frac{\partial A_z}{\partial r} + \frac{1}{r^2} \frac{\partial^2 A_z}{\partial^2 \theta^2} + \frac{\partial^2 A_z}{\partial z^2} + 0 + 0 \end{vmatrix} = \frac{1}{c^2} \frac{\partial^2 \mathbf{A}}{\partial t^2} = \frac{1}{c^2} \begin{vmatrix} \frac{\partial^2 A_r}{\partial r^2} \\ \frac{\partial^2 A_\theta}{\partial r^2} \\ \frac{\partial^2 A_z}{\partial r^2} \end{vmatrix}. \quad (13.72)$$

As evident from (13.72), the individual relationships for the r and θ components of vector field \mathbf{A} are quite complicated; however, the relationship for the z component of \mathbf{A} retains the original form of the wave equation, expressed by the scalar

Laplacian operator in the cylindrical coordinate system as

$$\frac{\partial^2 A_z}{\partial r^2} + \frac{1}{r} \frac{\partial A_z}{\partial r} + \frac{1}{r^2} \frac{\partial^2 A_z}{\partial \theta^2} + \frac{\partial^2 A_z}{\partial z^2} \equiv \frac{1}{r} \frac{\partial}{\partial r} \left(r \frac{\partial A_z}{\partial r} \right) + \frac{1}{r^2} \frac{\partial^2 A_z}{\partial \theta^2} + \frac{\partial^2 A_z}{\partial z^2} = \frac{1}{c^2} \frac{\partial^2 A_z}{\partial t^2}. \quad (13.73)$$

Using the scalar Laplacian operator in cylindrical coordinates of (13.73), we now express the wave equations for \mathcal{E}_z and \mathcal{B}_z as follows

$$\nabla^2 \mathcal{E}_z \equiv \frac{\partial^2 \mathcal{E}_z}{\partial r^2} + \frac{1}{r} \frac{\partial \mathcal{E}_z}{\partial r} + \frac{1}{r^2} \frac{\partial^2 \mathcal{E}_z}{\partial \theta^2} + \frac{\partial^2 \mathcal{E}_z}{\partial z^2} = \frac{1}{c^2} \frac{\partial^2 \mathcal{E}_z}{\partial t^2} \quad (13.74)$$

and

$$\nabla^2 \mathcal{B}_z \equiv \frac{\partial^2 \mathcal{B}_z}{\partial r^2} + \frac{1}{r} \frac{\partial \mathcal{B}_z}{\partial r} + \frac{1}{r^2} \frac{\partial^2 \mathcal{B}_z}{\partial \theta^2} + \frac{\partial^2 \mathcal{B}_z}{\partial z^2} = \frac{1}{c^2} \frac{\partial^2 \mathcal{B}_z}{\partial t^2}. \quad (13.75)$$

Equations (13.74) and (13.75) for \mathcal{E}_z and \mathcal{B}_z , respectively, are known as 3-dimensional wave equations in cylindrical coordinates; they are linear partial differential equations of the second order in four variables (three spatial variables: r , θ , and z , and one temporal variable: t) with constant coefficients. The two equations have identical form and can in general be written as follows

$$\nabla^2 \eta \equiv \frac{1}{r} \frac{\partial}{\partial r} \left(r \frac{\partial \eta}{\partial r} \right) + \frac{1}{r^2} \frac{\partial^2 \eta}{\partial \theta^2} + \frac{\partial^2 \eta}{\partial z^2} = \frac{\partial^2 \eta}{\partial r^2} + \frac{1}{r} \frac{\partial \eta}{\partial r} + \frac{1}{r^2} \frac{\partial^2 \eta}{\partial \theta^2} + \frac{\partial^2 \eta}{\partial z^2} = \frac{1}{c^2} \frac{\partial^2 \eta}{\partial t^2}, \quad (13.76)$$

with η a function of r , θ , z , and t representing both $\mathcal{E}_z(r, \theta, z, t)$ and $\mathcal{B}_z(r, \theta, z, t)$.

The conditions imposed on $\eta(r, \theta, z, t)$ fall into two categories:

- (1) Those involving spatial coordinates r , θ , and z and governed by boundary conditions, given in (13.67) for Dirichlet-type boundary condition and in (13.68) for Neumann-type boundary condition.
- (2) Those involving the temporal coordinate t and governed by initial conditions.

The most common approach to solving the 3-dimensional wave equation (13.76) is to apply the method of separation of variables. This method usually provides a solution to a partial differential equation in the form of an infinite series, such as a Fourier series, for example. We first separate out the time factor by defining $\eta(r, \theta, z, t)$ as a product of two functions: ϕ and T

$$\eta(r, \theta, z, t) = \phi(r, \theta, z)T(t), \quad (13.77)$$

where ϕ is a function of spatial coordinates r , θ , and z only and T is a function of time t only.

Inserting (13.77) into (13.76) and dividing by $\phi(r, \theta, z)T(t)$ gives

$$\frac{\nabla^2 \phi}{\phi} \equiv \frac{1}{c^2} \frac{1}{T} \frac{\partial^2 T}{\partial t^2}, \quad (13.78)$$

with the left hand side of (13.78) depending on spatial coordinates r , θ , and z only, and the right hand side depending on time t only. If (13.78) is to hold for all r , θ , z ,

and t , it is evident that each side must be equal to a constant. This constant is identical for both sides of (13.78) and usually referred to as the separation constant Λ . From (13.78) we thus get two equations

$$\nabla^2 \phi = \Lambda \phi \quad (13.79)$$

and

$$\frac{\partial^2 T}{\partial t^2} = \Lambda c^2 T. \quad (13.80)$$

Equation (13.79) is referred to as the Helmholtz partial differential equation representing an eigenvalue problem in three dimensions with ϕ the eigenfunction, Λ the eigenvalue, and ∇^2 the scalar Laplacian operator in cylindrical coordinates [see (13.76)]. The Helmholtz equation (13.79) results in three different types of solution, depending on the value of the separation constant Λ :

- (1) For $\Lambda > 0$ the solutions are exponential functions.
- (2) For $\Lambda = 0$ the solution is a linear function.
- (3) For $\Lambda < 0$ the solutions are trigonometric functions.

The Dirichlet boundary condition of (13.67) can be satisfied only for $\Lambda < 0$ and this will result in trigonometric solutions for function η . We now concentrate on finding solutions to the wave equation and set $\Lambda = -k^2$ to satisfy the usual periodicity requirement. Parameter k is called the *free space wave number* or free space propagation coefficient and is related to angular frequency ω through the standard relationship

$$k = \frac{\omega}{c}, \quad (13.81)$$

with c the speed of light in vacuum. Incorporating $\Lambda = -k^2$ into (13.79) and (13.80) yields the following equations for $\phi(r, \theta, z)$ and $T(t)$, respectively

$$\nabla^2 \phi = k^2 \phi = 0 \quad (13.82)$$

and

$$\frac{\partial^2 T}{\partial t^2} + k^2 c^2 T = \frac{\partial^2 T}{\partial t^2} + \omega^2 T = 0. \quad (13.83)$$

The solutions for $T(t)$ of (13.83) are either trigonometric or exponential functions but we reject the latter on physical grounds. Instead of using real trigonometric functions we express $T(t)$ as

$$T(t) \propto e^{-i\omega t}, \quad (13.84)$$

and assume that ω may be either positive or negative.

For the Helmholtz equation, given in (13.82), we again use the method of separation of variables and express $\phi(r, \theta, z)$ as a product of three functions: $R(r)$, $\Theta(\theta)$, and $Z(z)$ to get

$$\phi(r, \theta, z) = R(r)\Theta(\theta)Z(z). \quad (13.85)$$

We now insert (13.85) into (13.82), divide the result by $R(r)\Theta(\theta)Z(z)$, and get the following

$$\frac{1}{R} \frac{\partial^2 R}{\partial r^2} + \frac{1}{rR} \frac{\partial R}{\partial r} + \frac{1}{r^2} \frac{1}{\Theta} \frac{\partial^2 \Theta}{\partial \theta^2} + \frac{1}{Z} \frac{\partial^2 Z}{\partial z^2} + k^2 = 0. \quad (13.86)$$

Since in our waveguide geometry the RF wave is propagating in the positive z direction as a plane wave, we rewrite (13.86) as

$$-\left[\frac{1}{R} \frac{\partial^2 R}{\partial r^2} + \frac{1}{rR} \frac{\partial R}{\partial r} + \frac{1}{r^2} \frac{1}{\Theta} \frac{\partial^2 \Theta}{\partial \theta^2} \right] = \frac{1}{Z} \frac{\partial^2 Z}{\partial z^2} + k^2 \quad (13.87)$$

and note that the left hand side of (13.87) is a function of r and θ only and the right hand side of (13.87) is a function of z only. This can hold only when the two sides are equal to a constant that we designate as γ_n^2 . The right hand side of (13.87) now gives

$$\frac{1}{Z} \frac{\partial^2 Z}{\partial z^2} + k^2 = \gamma_n^2 \quad \text{or} \quad \frac{1}{Z} \frac{\partial^2 Z}{\partial z^2} + k_g^2 = 0, \quad (13.88)$$

and results in the following trigonometric solution for propagation in the positive z direction

$$Z(z) \propto e^{ik_g z}, \quad (13.89)$$

where k_g is referred to as the *waveguide wave number* or waveguide propagation coefficient and defined as

$$k_g^2 = k^2 - \gamma_n^2. \quad (13.90)$$

Equation (13.90) is a general form of the dispersion relationship for uniform circular EM waveguide dependent on constant γ_n . Once γ_n is determined through boundary conditions on z components \mathcal{E}_z and \mathcal{B}_z of the electric field \mathcal{E} and magnetic field \mathcal{B} , the dispersion relationship is expressed in the form $\omega = f(k_g)$ and used in calculation of cutoff frequency ω_c , phase velocity v_{ph} and group velocity v_{gr} for a given transmission mode.

We now address the left hand side of (13.87) which, after insertion of (13.88), reads

$$-\left[\frac{r^2}{R} \frac{\partial^2 R}{\partial r^2} + \frac{r}{R} \frac{\partial R}{\partial r} + \gamma_n^2 r^2 \right] = \frac{1}{\Theta} \frac{\partial^2 \Theta}{\partial \theta^2}. \quad (13.91)$$

The left hand side of (13.91) depends on r alone and the right hand side on θ alone and again, as seen above, this can hold in general if both sides are equal to a constant that must be negative to provide physically relevant solutions. We therefore set the constant equal to $-m^2$ and get the following expression for the right hand side of (13.91)

$$\frac{\partial^2 \Theta}{\partial \theta^2} + m^2 \Theta = 0 \quad (m = 0, 1, 2, 3, \dots). \quad (13.92)$$

Equation (13.92) has the following standard general trigonometric solution leading to trigonometric or complex exponential functions that serve as eigenfunctions

$$\Theta(\theta) = A \cos m\theta + B \sin m\theta. \quad (13.93)$$

Inserting (13.92) into (13.91) and multiplying the result with R/r^2 gives the following expression for $R(r)$

$$\frac{\partial^2 R}{\partial r^2} + \frac{1}{r} \frac{\partial R}{\partial r} + \left(\gamma_n^2 - \frac{m^2}{r^2} \right) R = 0, \quad (13.94)$$

representing the Bessel differential equation of order m or an eigenvalue equation with eigenvalue γ_n^2 when boundary conditions are imposed on $R(r)$. The physical conditions imposed on \mathcal{E}_z and \mathcal{B}_z , and thus on $R(r)$ as well, stipulate that:

- (1) $R(r)$ must be finite at $r = 0$.
- (2) $R(r = a)$ must satisfy either the Dirichlet boundary condition $R(r)|_{r=a} = 0$ of (13.67) or the Neumann boundary condition $dR/dr|_{r=a} = 0$ of (13.68).

The general solution to the Bessel equation (13.94) of order m consists of cylindrical functions; among these, given for non-negative integer values of m , the best known are the Bessel functions of the first kind $J_m(\gamma_n r)$ and Bessel functions of the second kind $N_m(\gamma_n r)$ (also known as Neumann functions). A few important features of $J_m(x)$ and $N_m(x)$ are apparent:

- (1) With increasing x , functions $J_m(x)$ and $N_m(x)$ oscillate about zero with a slowly diminishing amplitude and a decrease in separation between successive roots (zeros).
- (2) The two Bessel functions $J_m(x)$ and $N_m(x)$ possess an infinite number of roots, usually designated as x_{mn} and defined as those values of x at which the Bessel functions cross zero, i.e., where $J_m(x) = 0$ or $N_m(x) = 0$.
- (3) For $x = 0$, the Bessel functions of the first kind are finite; for integer $m > 0$ all Bessel functions of the first kind are equal to zero, i.e., $J_{m>0}(x)|_{x=0} = 0$ and for $m = 0$ the zero order Bessel function of the first kind equals to 1, i.e., $J_0(x)|_{x=0} = 1$.
- (4) For $x = 0$, the Bessel functions of the second kind (Neumann functions) exhibit a singularity, i.e., $\lim_{x \rightarrow 0} N_m(x) = -\infty$.

The general solution to the Bessel differential equation (13.94) is given as

$$R(r) = C J_m(\gamma_n r) + D N_m(\gamma_n r), \quad (13.95)$$

where C and D are coefficients determined from the initial conditions. Since the Neumann functions are singular at $r = 0$, to obtain a physically relevant solution to (13.94) we set $D = 0$ in (13.95) to get the following general solution for $R(r)$

$$R(r) = C J_m(\gamma_n r). \quad (13.96)$$

Combining solutions for $R(r)$, $\Theta(\theta)$, $Z(z)$, and $T(t)$ given in (13.96), (13.94), (13.89), and (13.84), respectively, we get the following general solution of the wave equation (13.76) for $\eta(r, \theta, z, t)$ representing the electric field component \mathcal{E}_z and the magnetic field component \mathcal{B}_z . The general solution is written in the form of a double series with A_{mn} and B_{mn} that can be determined with the help of initial conditions

$$\begin{aligned}\eta(r, \theta, z, t) &= R(r)\Theta(\theta)Z(z)T(t) \\ &= \sum_{m=0}^{\infty} \sum_{n=1}^{\infty} J_m(\gamma_n r) \{A_{mn} \cos m\theta + B_{mn} \sin m\theta\} e^{+i(k_g z - \omega t)} \\ &= \sum_{m=0}^{\infty} \sum_{n=1}^{\infty} J_m(\gamma_n r) \{A_{mn} \cos m\theta + B_{mn} \sin m\theta\} e^{+i\varphi}. \quad (13.97)\end{aligned}$$

In (13.97) m is the order of the Bessel function, n the rank order number of the given root of the Bessel function, and $(k_g z - \omega_{mn} t)$ is usually referred to as the *phase of the wave* φ . Each pair of integers (m, n) corresponds to a particular characteristic mode of RF propagation through the uniform waveguide. The general solution (13.97) to the wave equation (13.76) is given as a linear superposition of all allowed modes for $m = 0, 1, 2, \dots$ and $n = 1, 2, 3, \dots$. The value of γ_n is determined using the boundary condition (13.67) for electric field \mathcal{E} or (13.68) for magnetic field \mathcal{B} in conjunction with the general solution (13.97) for \mathcal{E}_z or \mathcal{B}_z .

(c) The z components of the electric field \mathcal{E} and magnetic field \mathcal{B} are written, respectively, in general form as double series with both \mathcal{E}_z and \mathcal{B}_z different from zero

$$\mathcal{E}_z(r, \theta, z, t) = \sum_{m=0}^{\infty} \sum_{n=1}^{\infty} J_m(\gamma_n r) [A_{mn} \cos m\theta + B_{mn} \sin m\theta] e^{i(k_g z - \omega t)} \quad (13.98)$$

and

$$\mathcal{B}_z(r, \theta, z, t) = \sum_{m=0}^{\infty} \sum_{n=1}^{\infty} J_m(\gamma_n r) [C_{mn} \cos m\theta + D_{mn} \sin m\theta] e^{i(k_g z - \omega t)}, \quad (13.99)$$

where A_{mn} , B_{mn} , C_{mn} , and D_{mn} are coefficients that can be determined from initial conditions. On the other hand, parameter γ_n in the argument of the Bessel function of (13.98) and (13.99) is determined from the boundary conditions on \mathcal{E}_z and \mathcal{B}_z . Since these are generally different, they cannot be applied simultaneously and the fields are split into two special categories: transverse magnetic (TM) modes and transverse electric (TE) modes, characterized as follows:

- (1) For the TM_{mn} modes, $\mathcal{B}_z = 0$ everywhere in the waveguide core and \mathcal{E}_z is governed by the Dirichlet-type boundary condition $\mathcal{E}_z|_{r=a} = 0$ which specifies that $\mathcal{E}_z = 0$ at the boundary between waveguide core and conducting wall of

Table 13.2 Zeros (roots) of Bessel functions (x_{mn} : left side of table) and first derivative of Bessel functions (y_{mn} : right side of table) for order m of Bessel function in the range from 0 to 3 and rank order number n of the roots from 1 to 3. The lowest values of z for $J_m(z)$ and for $dJ_m(z)/dz$ are shown in bold face

x_{mn} for $J_m(z) = 0$			y_{mn} for $dJ_m(z)/dz = 0$				
	$n = 1$	$n = 2$	$n = 3$		$n = 1$	$n = 2$	$n = 3$
$m = 0$	2.405	5.520	8.654	$m = 0$	0	3.832	7.016
$m = 1$	3.832	7.016	10.174	$m = 1$	1.841	5.331	8.536
$m = 2$	5.136	8.417	11.620	$m = 2$	3.054	6.706	9.970
$m = 3$	6.380	9.761	13.015	$m = 3$	4.201	8.015	11.346

the waveguide. The $\mathcal{E}_z|_{r=a} = 0$ boundary condition results in the following solution for γ_n of (13.98)

$$\mathcal{E}_z|_{r=a} = J_m(\gamma_n r)|_{r=a} = J_m(\gamma_n a) = 0 \rightarrow \gamma_n = \frac{x_{mn}}{a}, \quad (13.100)$$

where x_{mn} is the n -th zero (root) of the m -th order Bessel function. Roots of Bessel functions for $0 \leq m \leq 2$ and $1 \leq n \leq 3$ are listed in Table 13.2. The lowest TM_{mn} mode will be for $m = 0$ and $n = 1$, giving the following expression for \mathcal{E}_z

$$\mathcal{E}_z(r, \theta, z, t) = \mathcal{E}_{z0} J_0\left(\frac{x_{01}}{a} r\right) e^{i\varphi} = \mathcal{E}_{z0} J_0\left(\frac{2.405}{a} r\right) e^{i\varphi} \quad (13.101)$$

where \mathcal{E}_{z0} is the electric field amplitude, φ is the phase of the wave, and $x_{01} = 2.405$ is the first zero (root) of the $J_0(z)$ Bessel function, as found in standard tables of Bessel functions and listed in Table 13.2.

- (2) For the TE_{mn} modes, $\mathcal{E}_z = 0$ everywhere in the waveguide core and \mathcal{B}_z is governed by the Neumann-type boundary condition $d\mathcal{B}_z/dr|_{r=a} = 0$, that results in the following solution for γ_n of (13.99)

$$\left. \frac{d\mathcal{B}_z}{dr} \right|_{r=a} = \left. \frac{dJ_m(\gamma_n r)}{dr} \right|_{r=a} = \frac{dJ_m(\gamma_n a)}{dr} = 0 \rightarrow \gamma_n = \frac{y_{mn}}{a}, \quad (13.102)$$

where y_{mn} is the n -th zero (root) of the first derivative of the m -th order Bessel function. Roots of the first derivative of Bessel functions for $0 \leq m \leq 3$ and $1 \leq n \leq 3$ are listed in Table 13.2.

As shown in Table 13.2, the lowest non-trivial TE_{mn} mode will be for $m = 1$ and $n = 1$, resulting in the following expression for \mathcal{B}_z

$$\mathcal{B}_z(r, \theta, z, t) = \mathcal{B}_{z0} J_1\left(\frac{y_{11}}{a} r\right) e^{i\varphi} = \mathcal{B}_{z0} J_1\left(\frac{1.841}{a} r\right) e^{i\varphi}, \quad (13.103)$$

where \mathcal{B}_{z0} is the magnetic field amplitude, φ is the phase of the wave, and $y_{11} = 1.841$ is the first zero (root) of the derivative of the $J_1(z)$ Bessel function, as found in standard tables of Bessel functions and listed in Table 13.2.

13.4 Electric and Magnetic Fields in Uniform Waveguides

13.4.Q1

(277)

Two types of waveguide are used for transmission of microwave power and signals: rectangular and circular. Waveguides are usually oriented with their central axes parallel to the z axis of the Cartesian coordinate system for rectangular waveguides and cylindrical coordinate system for circular waveguides. The z components \mathcal{E}_z and \mathcal{B}_z of electric field \mathcal{E} and magnetic field \mathcal{B} , respectively, are for rectangular waveguides in general given as follows

$$\begin{aligned}\mathcal{E}_z(x, y, z, t) &= \sum_{m=0}^{\infty} \sum_{n=0}^{\infty} A_{mn} \sin k_x x \sin k_y y e^{i(k_z z - \omega t)} \\ &= \sum_{m=0}^{\infty} \sum_{n=0}^{\infty} A_{mn} \sin \frac{m\pi x}{a} \sin \frac{n\pi y}{b} e^{i\varphi}\end{aligned}\quad (13.104)$$

and

$$\begin{aligned}\mathcal{B}_z(x, y, z, t) &= \sum_{m=0}^{\infty} \sum_{n=0}^{\infty} B_{mn} \cos k_x x \cos k_y y e^{i(k_z z - \omega t)} \\ &= \sum_{m=0}^{\infty} \sum_{n=0}^{\infty} B_{mn} \cos \frac{m\pi x}{a} \cos \frac{n\pi y}{b} e^{i\varphi},\end{aligned}\quad (13.105)$$

where A_{mn} and B_{mn} are constants that can be determined from initial conditions, $\varphi = k_z z - \omega t$ is the phase of the RF wave, and k_x , k_y , and k_z are the waveguide wave numbers or propagation coefficients with k_x and k_y determined from boundary conditions.

-
- (a) For a uniform rectangular EM waveguide of cross section sides a and b where $a > b$:
- (1) Explain how components \mathcal{E}_z and \mathcal{B}_z of electric field \mathcal{E} and magnetic field \mathcal{B} , respectively, are determined.
 - (2) Explain how other components of \mathcal{E} and \mathcal{B} are determined once \mathcal{E}_z and \mathcal{B}_z are known.
- (b) Show that for a uniform rectangular EM waveguide the transverse components \mathcal{E}_x and \mathcal{E}_y of the electric field \mathcal{E} as well as the transverse components \mathcal{B}_x and \mathcal{B}_y of the magnetic field \mathcal{B} can be determined directly from known axial components \mathcal{E}_z and \mathcal{B}_z of electric field \mathcal{E} and magnetic field \mathcal{B} , respectively.

- (c) For a uniform rectangular EM waveguide determine the transverse fields \mathcal{E}_x , \mathcal{E}_y , \mathcal{B}_x and \mathcal{B}_y for: (1) TM modes, (2) TE modes, and (3) TEM modes. In your calculations assume that axial components \mathcal{E}_z and \mathcal{B}_z are known and use the general expressions from (b).
- (d) For a uniform rectangular EM waveguide determine all components of electric field \mathcal{E} and magnetic field \mathcal{B} for the lowest (dominant): (1) transverse electric (TE) mode and (2) transverse magnetic (TM) mode. The rectangular cross section of the waveguide core has sides a and b with $a > b$.

SOLUTION:

(a) Electric field \mathcal{E} and magnetic field \mathcal{B} in the core of a uniform EM waveguide are vectors with three components, each component depending on three spatial coordinates and one temporal coordinate. For a rectangular EM waveguide the components of \mathcal{E} and \mathcal{B} are:

$$\mathcal{E} = [\mathcal{E}_x(x, y, z, t), \mathcal{E}_y(x, y, z, t), \mathcal{E}_z(x, y, z, t)] \quad (13.106)$$

and

$$\mathcal{B} = [\mathcal{B}_x(x, y, z, t), \mathcal{B}_y(x, y, z, t), \mathcal{B}_z(x, y, z, t)]. \quad (13.107)$$

- (1) Components \mathcal{E}_z and \mathcal{B}_z are determined from wave equations for \mathcal{E}_z and \mathcal{B}_z given as

$$\nabla^2 \mathcal{E}_z = \frac{1}{c^2} \frac{\partial^2 \mathcal{E}_z}{\partial^2 t^2} \quad (13.108)$$

and

$$\nabla^2 \mathcal{B}_z = \frac{1}{c^2} \frac{\partial^2 \mathcal{B}_z}{\partial^2 t^2}, \quad (13.109)$$

where c is the speed of light in vacuum and ∇^2 is the scalar Laplacian operator expressed in Cartesian coordinates for rectangular waveguide as follows

$$\nabla^2 = \frac{\partial^2}{\partial x^2} + \frac{\partial^2}{\partial y^2} + \frac{\partial^2}{\partial z^2}. \quad (13.110)$$

Wave equations (13.108) and (13.109) are linear partial differential equations of the second order in four variables (3 spatial and one temporal) with constant coefficients. The most common method for solving the wave equations is the method of separation of variables leading to solutions for the z components \mathcal{E}_z and \mathcal{B}_z of the electric field \mathcal{E} and magnetic field \mathcal{B} , respectively, in the core of the waveguide.

- (2) Once \mathcal{E}_z and \mathcal{B}_z are known, the other components of \mathcal{E} and \mathcal{B} are determined from Maxwell equations for free space expressed as follows

$$\nabla \cdot \mathcal{E} = 0; \quad (13.111)$$

$$\nabla \cdot \mathcal{B} = 0; \quad (13.112)$$

$$\nabla \times \mathcal{E} = -\frac{\partial \mathcal{B}}{\partial t}; \quad (13.113)$$

$$\nabla \times \mathcal{B} = \frac{1}{c^2} \frac{\partial \mathcal{E}}{\partial t}, \quad (13.114)$$

with $(\nabla \cdot)$ the divergence and $(\nabla \times)$ the curl on vectors \mathcal{E} and \mathcal{B} . It is also useful to note that from (13.104) and (13.105) the following expressions apply for derivatives: $\partial/\partial z = ik_z$ and $\partial/\partial t = -i\omega$ with k_z the waveguide propagation coefficient parallel to the central axis of the waveguide and ω the angular frequency of the EM wave in contrast to $k = \omega/c$ that is defined as the free space propagation coefficient.

- (b) We start the derivation of components \mathcal{E}_x , \mathcal{E}_y , \mathcal{B}_x , and \mathcal{B}_y with (13.111) and (13.112) for rectangular EM waveguide and express the two equations in Cartesian coordinates as follows

$$\nabla \cdot \mathcal{E} = \frac{\partial \mathcal{E}_x}{\partial x} + \frac{\partial \mathcal{E}_y}{\partial y} + \frac{\partial \mathcal{E}_z}{\partial z} = \frac{\partial \mathcal{E}_x}{\partial x} + \frac{\partial \mathcal{E}_y}{\partial y} + ik_z \mathcal{E}_z = 0 \quad (13.115)$$

and

$$\nabla \cdot \mathcal{B} = \frac{\partial \mathcal{B}_x}{\partial x} + \frac{\partial \mathcal{B}_y}{\partial y} + \frac{\partial \mathcal{B}_z}{\partial z} = \frac{\partial \mathcal{B}_x}{\partial x} + \frac{\partial \mathcal{B}_y}{\partial y} + ik_z \mathcal{B}_z = 0 \quad (13.116)$$

and then express (13.113) and (13.114) in Cartesian coordinates as

$$\nabla \times \mathcal{E} = \begin{vmatrix} \hat{\mathbf{i}} & \hat{\mathbf{j}} & \hat{\mathbf{k}} \\ \frac{\partial}{\partial x} & \frac{\partial}{\partial y} & \frac{\partial}{\partial z} \\ \mathcal{E}_x & \mathcal{E}_y & \mathcal{E}_z \end{vmatrix} = -\frac{\partial}{\partial t} \begin{vmatrix} \mathcal{B}_x \hat{\mathbf{i}} \\ \mathcal{B}_y \hat{\mathbf{j}} \\ \mathcal{B}_z \hat{\mathbf{k}} \end{vmatrix} = i\omega \begin{vmatrix} \mathcal{B}_x \hat{\mathbf{i}} \\ \mathcal{B}_y \hat{\mathbf{j}} \\ \mathcal{B}_z \hat{\mathbf{k}} \end{vmatrix} \quad (13.117)$$

and

$$\nabla \times \mathcal{B} = \begin{vmatrix} \hat{\mathbf{i}} & \hat{\mathbf{j}} & \hat{\mathbf{k}} \\ \frac{\partial}{\partial x} & \frac{\partial}{\partial y} & \frac{\partial}{\partial z} \\ \mathcal{B}_x & \mathcal{B}_y & \mathcal{B}_z \end{vmatrix} = \frac{1}{c^2} \frac{\partial}{\partial t} \begin{vmatrix} \mathcal{E}_x \hat{\mathbf{i}} \\ \mathcal{E}_y \hat{\mathbf{j}} \\ \mathcal{E}_z \hat{\mathbf{k}} \end{vmatrix} = -\frac{i\omega}{c^2} \begin{vmatrix} \mathcal{E}_x \hat{\mathbf{i}} \\ \mathcal{E}_y \hat{\mathbf{j}} \\ \mathcal{E}_z \hat{\mathbf{k}} \end{vmatrix} \quad (13.118)$$

where $\hat{\mathbf{i}}$, $\hat{\mathbf{j}}$, and $\hat{\mathbf{k}}$ are the standard unit vectors along x , y , and z axes of the Cartesian coordinate system. Equations (13.117) and (13.118) have the following components of the curl operator [Note: (13.119), (13.120), and (13.121) follow from (13.117); (13.122), (13.123), and (13.129) follow from (13.118)]

$$\frac{\partial \mathcal{E}_z}{\partial y} - \frac{\partial \mathcal{E}_y}{\partial z} = i\omega \mathcal{B}_x = \frac{\partial \mathcal{E}_z}{\partial y} - ik_z \mathcal{E}_y \quad \text{or} \quad \mathcal{B}_x = -\frac{i}{\omega} \frac{\partial \mathcal{E}_z}{\partial y} - \frac{k_z}{\omega} \mathcal{E}_y, \quad (13.119)$$

$$\frac{\partial \mathcal{E}_x}{\partial z} - \frac{\partial \mathcal{E}_z}{\partial x} = i\omega \mathcal{B}_y = ik_z \mathcal{E}_x - \frac{\partial \mathcal{E}_z}{\partial x} \quad \text{or} \quad \mathcal{B}_y = +\frac{i}{\omega} \frac{\partial \mathcal{E}_z}{\partial x} + \frac{k_z}{\omega} \mathcal{E}_x, \quad (13.120)$$

$$\frac{\partial \mathcal{E}_y}{\partial x} - \frac{\partial \mathcal{E}_x}{\partial y} = i\omega \mathcal{B}_z \quad \text{or} \quad \mathcal{B}_z = \frac{i}{\omega} \left[-\frac{\partial \mathcal{E}_y}{\partial x} + \frac{\partial \mathcal{E}_x}{\partial y} \right], \quad (13.121)$$

$$\frac{\partial \mathcal{B}_z}{\partial y} - \frac{\partial \mathcal{B}_y}{\partial z} = -\frac{i\omega}{c^2} \mathcal{E}_x = \frac{\partial \mathcal{B}_z}{\partial y} - ik_z \mathcal{B}_y \quad \text{or} \quad \mathcal{E}_x = \frac{ic^2}{\omega} \frac{\partial \mathcal{B}_z}{\partial y} + \frac{k_z c^2}{\omega} \mathcal{B}_y, \quad (13.122)$$

$$\frac{\partial \mathcal{B}_x}{\partial z} - \frac{\partial \mathcal{B}_z}{\partial x} = -\frac{i\omega}{c^2} \mathcal{E}_y = ik_z \mathcal{B}_x - \frac{\partial \mathcal{B}_z}{\partial x} \quad \text{or} \quad (13.123)$$

$$\mathcal{E}_y = -\frac{k_z c^2}{\omega} \mathcal{B}_x - \frac{ic^2}{\omega} \frac{\partial \mathcal{B}_z}{\partial x},$$

$$\frac{\partial \mathcal{B}_y}{\partial x} - \frac{\partial \mathcal{B}_x}{\partial y} = -\frac{i\omega}{c^2} \mathcal{E}_z \quad \text{or} \quad \mathcal{E}_z = \frac{ic^2}{\omega} \left[-\frac{\partial \mathcal{B}_y}{\partial x} - \frac{\partial \mathcal{B}_x}{\partial y} \right]. \quad (13.124)$$

Pairing up appropriate equations in the group from (13.119) to (13.124), we can now determine components \mathcal{E}_x , \mathcal{E}_y , \mathcal{B}_x , and \mathcal{B}_y as follows:

- (1) Inserting \mathcal{B}_y of (13.120) into (13.122) gives the following expression for component \mathcal{E}_x

$$\mathcal{E}_x = i \left[\frac{k_z c^2}{\omega^2} \frac{\partial \mathcal{E}_z}{\partial x} + \frac{c^2}{\omega} \frac{\partial \mathcal{B}_z}{\partial y} \right] \left(1 - \frac{k_z^2 c^2}{\omega^2} \right)^{-1} = \frac{i}{\gamma^2} \left[k_z \frac{\partial \mathcal{E}_z}{\partial x} + \omega \frac{\partial \mathcal{B}_z}{\partial y} \right]. \quad (13.125)$$

- (2) Inserting \mathcal{B}_x of (13.119) into (13.123) gives the following expression for component \mathcal{E}_y

$$\mathcal{E}_y = i \left[-\frac{c^2}{\omega} \frac{\partial \mathcal{B}_z}{\partial x} + \frac{k_z c^2}{\omega^2} \frac{\partial \mathcal{E}_z}{\partial y} \right] \left(1 - \frac{k_z^2 c^2}{\omega^2} \right)^{-1} = \frac{i}{\gamma^2} \left[-\omega \frac{\partial \mathcal{B}_z}{\partial x} + k_z \frac{\partial \mathcal{E}_z}{\partial y} \right]. \quad (13.126)$$

- (3) Inserting \mathcal{E}_y of (13.123) into (13.119) gives the following expression for component \mathcal{B}_x

$$\mathcal{B}_x = i \left[\frac{k_z c^2}{\omega^2} \frac{\partial \mathcal{B}_z}{\partial x} - \frac{1}{\omega} \frac{\partial \mathcal{E}_z}{\partial y} \right] \left(1 - \frac{k_z^2 c^2}{\omega^2} \right)^{-1} = \frac{i}{\gamma^2} \left[k_z \frac{\partial \mathcal{B}_z}{\partial x} - \frac{\omega}{c^2} \frac{\partial \mathcal{E}_z}{\partial y} \right]. \quad (13.127)$$

- (4) Inserting \mathcal{E}_x of (13.122) into (13.120) gives the following expression for component \mathcal{B}_y

$$\mathcal{B}_y = i \left[\frac{1}{\omega} \frac{\partial \mathcal{E}_z}{\partial x} + \frac{k_z c^2}{\omega^2} \frac{\partial \mathcal{B}_z}{\partial y} \right] \left(1 - \frac{k_z^2 c^2}{\omega^2} \right)^{-1} = \frac{i}{\gamma^2} \left[\frac{\omega}{c^2} \frac{\partial \mathcal{E}_z}{\partial x} + k_z \frac{\partial \mathcal{B}_z}{\partial y} \right]. \quad (13.128)$$

with $\gamma^2 = k^2 - k_z^2$ and $\omega = kc$ where c is the speed of light in vacuum and k is the free space propagation coefficient. Equations (13.125) through (13.128) show that the transverse components \mathcal{E}_x , \mathcal{E}_y , \mathcal{B}_x , and \mathcal{B}_y can be determined with relative ease directly from known axial components \mathcal{E}_z and \mathcal{B}_z .

(c) Equations (13.125) through (13.128) give general expressions for transverse components \mathcal{E}_x , \mathcal{E}_y , \mathcal{B}_x , and \mathcal{B}_y as a function of axial components \mathcal{E}_z and \mathcal{B}_z for a uniform rectangular EM waveguide. We now determine the transverse components for the three special modes: (1) TM where $\mathcal{B}_z = 0$ everywhere, (2) TE where $\mathcal{E}_z = 0$, and (3) TEM where $\mathcal{B}_z = \mathcal{E}_z = 0$ everywhere. The three special modes are characterized as follows:

- (1) TM modes: $\mathcal{B}_z = 0$ everywhere inside the waveguide core and the transverse components \mathcal{E}_x , \mathcal{E}_y , \mathcal{B}_x , and \mathcal{B}_y are given as follows

$$\mathcal{E}_x = \frac{ik_z}{\gamma^2} \frac{\partial \mathcal{E}_z}{\partial x}, \quad \mathcal{E}_y = \frac{ik_z}{\gamma^2} \frac{\partial \mathcal{E}_z}{\partial y}, \quad \mathcal{B}_x = -\frac{i}{\gamma^2} \frac{\omega}{c^2} \frac{\partial \mathcal{E}_z}{\partial y}, \quad \mathcal{B}_y = \frac{i}{\gamma^2} \frac{\omega}{c^2} \frac{\partial \mathcal{E}_z}{\partial x}. \quad (13.129)$$

- (2) TE modes: $\mathcal{E}_z = 0$ everywhere inside the waveguide core and the transverse components \mathcal{E}_x , \mathcal{E}_y , \mathcal{B}_x , and \mathcal{B}_y are given as follows

$$\mathcal{E}_x = \frac{i\omega}{\gamma^2} \frac{\partial \mathcal{B}_z}{\partial y}, \quad \mathcal{E}_y = -\frac{i\omega}{\gamma^2} \frac{\partial \mathcal{B}_z}{\partial x}, \quad \mathcal{B}_x = \frac{ik_z}{\gamma^2} \frac{\partial \mathcal{B}_z}{\partial x}, \quad \mathcal{B}_y = \frac{ik_z}{\gamma^2} \frac{\partial \mathcal{B}_z}{\partial y}. \quad (13.130)$$

- (3) TEM mode: Both $\mathcal{E}_z = 0$ and $\mathcal{B}_z = 0$ everywhere and (13.125) through (13.128) show that all transverse components \mathcal{E}_x , \mathcal{E}_y , \mathcal{B}_x , and \mathcal{B}_y are also equal to zero.

(d) Components of lowest (dominant) TE and TM modes in a uniform rectangular EM waveguide with $a > b$ are determined as follows:

The general expressions for z components \mathcal{E}_z and \mathcal{B}_z of electric field $\boldsymbol{\mathcal{E}}$ and magnetic field $\boldsymbol{\mathcal{B}}$, respectively, are determined from appropriate wave equations (see Prob. 277) and given in (13.104) and (13.105), respectively, while the general expressions for the other four components \mathcal{E}_x , \mathcal{E}_y , \mathcal{B}_x , and \mathcal{B}_y were derived in (b). We now use these expressions to determine the electric and magnetic field components for the dominant TE and TM modes, recalling that parameter γ is for rectangular EM waveguide given as

$$\gamma^2 = k^2 - k_z^2 = k_x^2 + k_y^2 = \left(\frac{m\pi}{a}\right)^2 + \left(\frac{n\pi}{b}\right)^2, \quad (13.131)$$

where k is the free space wave number related to microwave angular frequency ω through $k = \omega/c$ and k_x , k_y , and k_z are waveguide propagation constants, the first two determined from boundary conditions and k_z the wave number for the plane wave propagating unhindered along the axis of the waveguide.

- (1) *Transverse electric (TE) modes* are characterized by $\mathcal{E}_z = 0$ everywhere in the waveguide core and the dominant (lowest) TE mode occurs for $m = 1$ and $n = 0$ (note: $\cos 0^\circ = 1$). Inserting $m = 1$ and $n = 0$ into (13.131) we get the following

expression for parameter γ^2

$$\gamma^2 = \left(\frac{m\pi}{a}\right)^2 + \left(\frac{n\pi}{b}\right)^2 = \frac{\pi^2}{a^2}. \quad (13.132)$$

- (i) Magnetic field component \mathcal{B}_z for the dominant TE mode is now from (13.105) given as

$$\mathcal{B}_z = \mathcal{B}_{10} \cos\left(\frac{\pi x}{a}\right) e^{i\varphi}. \quad (13.133)$$

- (ii) Electric field component \mathcal{E}_x of (13.125) is zero because $\partial\mathcal{E}_z/\partial x = 0$ and $\partial\mathcal{B}_z/\partial y = 0$.
 (iii) Electric field component \mathcal{E}_y is determined from (13.126) using $\mathcal{E}_z = 0$, \mathcal{B}_z from (13.132), $\partial\mathcal{E}_z/\partial y = 0$, and γ^2 from (13.132) as follows

$$\mathcal{E}_y = -i \frac{\omega}{\gamma^2} \frac{\partial\mathcal{B}_z}{\partial x} = i \frac{\pi\omega}{\gamma^2 a} \mathcal{B}_{10} \sin\left(\frac{\pi x}{a}\right) e^{i\varphi} = i \frac{\omega a}{\pi} \mathcal{B}_{10} \sin\left(\frac{\pi x}{a}\right) e^{i\varphi}. \quad (13.134)$$

- (iv) Magnetic field component \mathcal{B}_x is determined from (13.127) using $\mathcal{E}_z = 0$, \mathcal{B}_z from (13.132), $\partial\mathcal{E}_z/\partial y = 0$, and γ^2 from (13.132) as follows

$$\mathcal{B}_x = i \frac{k_z}{\gamma^2} \frac{\partial\mathcal{B}_z}{\partial x} = -i \frac{\pi k_z}{\gamma^2 a} \mathcal{B}_{10} \sin\left(\frac{\pi x}{a}\right) e^{i\varphi} = -i \frac{k_z a}{\pi} \mathcal{B}_{10} \sin\left(\frac{\pi x}{a}\right) e^{i\varphi}. \quad (13.135)$$

- (v) Magnetic field component \mathcal{B}_y of (13.128) is zero because $\partial\mathcal{E}_z/\partial x = 0$ and $\partial\mathcal{B}_z/\partial y = 0$.

(2) *Transverse magnetic (TM) modes* are characterized by $\mathcal{B}_z = 0$ everywhere in the waveguide core and the dominant (lowest) TM mode occurs for $m = 1$ and $n = 1$ (note: $\sin 0^\circ = 0$). Inserting $m = 1$ and $n = 1$ into (13.131) we get the following expression for parameter γ^2

$$\gamma^2 = \left(\frac{m\pi}{a}\right)^2 + \left(\frac{n\pi}{b}\right)^2 = \pi^2 \left(\frac{1}{a^2} + \frac{1}{b^2}\right). \quad (13.136)$$

- (i) The electric field component \mathcal{E}_z for the dominant TM mode is now from (13.104) given as

$$\mathcal{E}_z = \mathcal{E}_{11} \sin\left(\frac{\pi x}{a}\right) \sin\left(\frac{\pi y}{b}\right) e^{i\varphi}. \quad (13.137)$$

- (ii) The electric field component \mathcal{E}_x is determined from (13.125) using $\mathcal{B}_z = 0$, \mathcal{E}_z from (13.137), $\partial\mathcal{B}_z/\partial y = 0$, and γ^2 from (13.136) as follows

$$\begin{aligned}\mathcal{E}_x &= i \frac{k_z}{\gamma^2} \frac{\partial \mathcal{E}_z}{\partial x} = i \frac{\pi k_z}{\gamma^2 a} \mathcal{E}_{11} \cos\left(\frac{\pi x}{a}\right) \sin\left(\frac{\pi y}{b}\right) e^{i\varphi} \\ &= i \frac{k_z}{\pi\left(\frac{1}{a} + \frac{a}{b^2}\right)} \mathcal{B}_{11} \cos\left(\frac{\pi x}{a}\right) \sin\left(\frac{\pi y}{b}\right) e^{i\varphi}.\end{aligned}\quad (13.138)$$

- (iii) The electric field component \mathcal{E}_y is determined from (13.126) using $\mathcal{B}_z = 0$, \mathcal{E}_z from (13.137), $\partial\mathcal{B}_z/\partial x = 0$, and γ^2 from (13.136) as follows

$$\begin{aligned}\mathcal{E}_y &= i \frac{k_z}{\gamma^2} \frac{\partial \mathcal{E}_z}{\partial y} = i \frac{\pi k_z}{\gamma^2 b} \mathcal{E}_{11} \sin\left(\frac{\pi x}{a}\right) \cos\left(\frac{\pi y}{b}\right) e^{i\varphi} \\ &= i \frac{k_z}{\pi\left(\frac{b}{a^2} + \frac{1}{b}\right)} \mathcal{B}_{11} \sin\left(\frac{\pi x}{a}\right) \cos\left(\frac{\pi y}{b}\right) e^{i\varphi}.\end{aligned}\quad (13.139)$$

- (iv) The magnetic field component \mathcal{B}_x is determined from (13.127) using $\mathcal{B}_z = 0$, \mathcal{E}_z from (13.137), $\partial\mathcal{B}_z/\partial x = 0$, and γ^2 from (13.136) as follows

$$\begin{aligned}\mathcal{B}_x &= -i \frac{\omega}{\gamma^2 c^2} \frac{\partial \mathcal{E}_z}{\partial y} = -i \frac{\pi \omega}{\gamma^2 c^2 b} \mathcal{E}_{11} \sin\left(\frac{\pi x}{a}\right) \cos\left(\frac{\pi y}{b}\right) e^{i\varphi} \\ &= -i \frac{\pi \omega}{\pi\left(\frac{b}{a^2} + \frac{1}{b}\right)} \mathcal{E}_{11} \sin\left(\frac{\pi x}{a}\right) \cos\left(\frac{\pi y}{b}\right) e^{i\varphi}.\end{aligned}\quad (13.140)$$

- (v) The magnetic field component \mathcal{B}_y is determined from (13.128) using $\mathcal{B}_z = 0$, \mathcal{E}_z from (13.137), $\partial\mathcal{B}_z/\partial y = 0$, and γ^2 from (13.136) as follows

$$\begin{aligned}\mathcal{B}_y &= i \frac{\omega}{\gamma^2 c^2} \frac{\partial \mathcal{E}_z}{\partial x} = i \frac{\pi \omega}{\gamma^2 c^2 a} \mathcal{E}_{11} \cos\left(\frac{\pi x}{a}\right) \sin\left(\frac{\pi y}{b}\right) e^{i\varphi} \\ &= i \frac{\omega}{\pi c^2\left(\frac{1}{a} + \frac{a}{b^2}\right)} \mathcal{E}_{11} \cos\left(\frac{\pi x}{a}\right) \sin\left(\frac{\pi y}{b}\right) e^{i\varphi}.\end{aligned}\quad (13.141)$$

13.5 General Conditions for Particle Acceleration

13.5.Q1

(278)

Particle accelerators have played an invaluable role in science, industry, and medicine since Röntgen's discovery of x rays in 1895. They are also perfect example of translational research that is characterized with translation of novel scientific advances to industry and medicine for the benefit of humanity.

Many particle accelerators have been developed during the past 100 years and most of them have proven useful in imaging and/or therapy of disease with ionizing radiation.

- (a) List and briefly discuss at least 3 basic physical conditions for particle acceleration that must be met in a particle accelerator irrespective of accelerator design.
- (b) In addition to the general conditions presented in (a) list and briefly discuss at least 3 additional conditions that electric field used in acceleration of electrons in a linear accelerator (linac) must meet.
- (c) Briefly discuss the difference between a uniform circular EM waveguide used in transmission of microwave power and an accelerator EM waveguide used for electron acceleration in a linear accelerator.

SOLUTION:

(a) Three general conditions that must be met for particle acceleration in an accelerator are:

(1) *Particle to be accelerated must be charged.* Charge, either positive or negative, is the most important attribute that a particle to be accelerated must possess. It is impossible to accelerate neutral particles in an accelerator, yet, accelerators that produce neutral particles are quite common in science, industry, and medicine, such as for example, (i) X-ray machines, (ii) Linear accelerators producing high-energy x rays, (iii) Neutron generators, and (iv) Cyclotrons producing neutrons. However, in all these machines, neutral particles (x-ray photons and neutrons) are not accelerated in the machine; rather, they are produced in a suitable target by charged particles that are accelerated in the machine and made to strike the target after they have been accelerated to the desired kinetic energy.

X rays are produced in the target by energetic electrons that strike the target and undergo bremsstrahlung interactions with the nuclei of the target. Neutrons, on the other hand, are produced in nuclear reactions between heavy charged particles, such as deuterons striking a tritium target in a neutron generator and protons or deuterons striking a beryllium-9 target in a cyclotron.

(2) In an accelerator *particles are accelerated with an electric field* according to the following convention: Electric field used for particle acceleration must be oriented in the direction of propagation for positively charged particles and in direction opposite to direction of propagation for negatively charged particles.

Depending on the type of electric field used in particle acceleration, accelerators are divided into two major categories: (i) Electrostatic accelerators employ electrostatic fields and (ii) Cyclic accelerators use electromagnetic (EM) fields of a given, well-defined frequency.

In an electrostatic accelerator the particles are accelerated by applying an electrostatic field using a constant potential that fixes the magnitude of the final kinetic energy of the charged particle accelerated in the machine. Since the electrostatic fields \mathcal{E} are conservative ($\nabla \times \mathcal{E} = \mathbf{0}$), final kinetic energy that a charged particle can attain in an electrostatic machine depends only on the potential difference existing in the machine between the source of charged particles and the exit point on the machine. Kinetic energy that an electrostatic accelerator can produce is limited to few MeV by electrical discharges that occur between the high voltage terminal and the grounded components of the machine.

Electric fields used in cyclic accelerators are variable, non-conservative ($\nabla \times \mathcal{E} \neq \mathbf{0}$), and associated with a variable magnetic field. This results in some closed paths along which the kinetic energy gained by the particle differs from zero. If the charged particle follows such a closed path many times over, it gains a small amount of energy in each passage and, after a large number of passes through the same path, attains a high kinetic energy that exceeds significantly the maximum potential difference existing in the machine. The final kinetic energy of the accelerated charged particle is thus equal to the relatively small energy gain acquired by the charged particle in each passage through the closed path multiplied by the number of passes made by the charged particle.

Kinetic energy attained in cyclic accelerators can be very large and depends more on machine design and available funding than on any practical problems unlike the discharge that limits the maximum kinetic energy in electrostatic machines. Best known examples of electrostatic machine are: x-ray machine, neutron generator, and Van de Graaff accelerator. In the group of cyclic accelerator we have linear accelerator (linac), betatron, microtron, cyclotron, and synchrotron.

(3) *The charged particle must be accelerated in high vacuum.* Acceleration of charged particles in accelerators can only happen in evacuated structures to avoid deleterious collisions between the accelerated particles and the medium in which the particles propagate. These collisions would result in loss of particle kinetic energy through inelastic collisions with nuclei of the medium or in change in direction through elastic scattering between the accelerated particle and nuclei of the medium. Both effects would adversely affect the accelerating process and are avoided by accelerating the particles in evacuated chambers. Typical vacuum in accelerating structures is of the order of 10^{-7} torr.

(b) Four specific conditions for acceleration of electrons in linear accelerators (linacs) are all related to the radiofrequency mode used for electron acceleration that must:

(1) *Possess a phase velocity v_{ph} that matches the velocity of the accelerated particle v_{part} .* Since particles cannot exceed the speed of light c in vacuum, the condition $v_{part} \simeq v_{ph}$ means that the phase velocity v_{ph} of RF waves used in particle acceleration should not exceed the speed of light c .

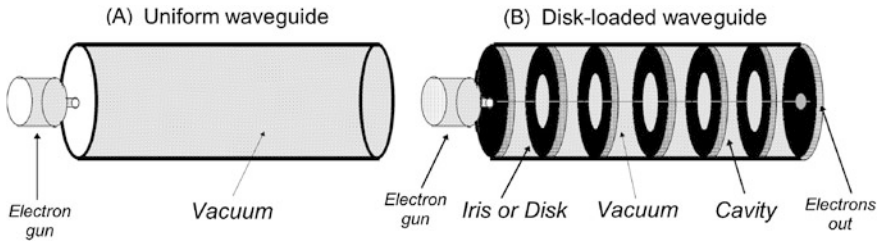


Fig. 13.6 Schematic diagram of EM waveguide. (A) Uniform (transmission) waveguide and (B) disk-loaded (acceleration) waveguide. The section of the waveguide between two successive irises in an acceleration waveguide is called a waveguide cavity. The electron gun serves as source of electrons to be accelerated in the waveguide

(2) Provide a finite, non-zero value for the z component \mathcal{E}_z of the electric field \mathcal{E} at $r = 0$, so as to enable electron acceleration along the central axis of the circular waveguide used for acceleration.

(3) Satisfy the Dirichlet boundary condition $\mathcal{E}_z = 0$ at $r = a$ on the boundary between the evacuated core and wall of the waveguide to enable particle acceleration along the central axis of the circular waveguide.

(4) Produce $\mathcal{B}_z = 0$ everywhere in the core of the EM waveguide to prevent interference of axial magnetic field on the propagation of the accelerated electrons along the central axis of the waveguide.

(c) EM waveguides used for transmission of microwave power or signals have either rectangular or circular cross section and are either evacuated or filled with a pressurized dielectric gas. They are called uniform waveguide because their cross sections do not vary with the z coordinate along the central axis of the waveguide.

Waveguides used for particle acceleration in linear accelerators, on the other hand, are called acceleration waveguide. They are always evacuated and have a circular cross section that is not uniform; rather, it varies with the z coordinate and consists of a circular, uniform waveguide, periodically loaded with irises or disks, as shown schematically in Fig. 13.6.

Out of necessity, an acceleration waveguide is much more complicated than a uniform waveguide. While in principle one could contemplate using a uniform waveguide for charged particle acceleration, a closer look at the properties of a uniform waveguide reveals that RF waves propagate in a uniform waveguide with a phase velocity v_{ph} that exceeds the speed of light c in vacuum. Since the particle velocity v_{part} cannot exceed c and v_{ph} exceeds c the requirement for $v_{\text{part}} = v_{\text{ph}}$ cannot be met and this automatically excludes a uniform waveguide from charged particle acceleration. However, the $v_{\text{part}} = v_{\text{ph}}$ requirement can be met in a waveguide by lowering the RF phase velocity to c and this can be achieved by loading a uniform waveguide with periodic perturbations in the form of irises that effectively decrease the uniform waveguide phase velocity to a level that the accelerated charged particle can follow.

13.6 Dispersion Relationship

13.6.Q1

(279)

Wave properties of photons and matter, such as wavelength λ , wave vector k , frequency ν , angular frequency ω , phase velocity v_{ph} , group velocity v_{gr} , speed of light c , and index of refraction n , are connected through various simple relationships. These are usually summarized with the so-called dispersion relationship, expressed in the format of ω against k .

In addition to playing an important role in condensed matter physics, optics, and acoustics dispersion is also relevant to propagation of microwaves through uniform as well as accelerating electromagnetic (EM) waveguides. Uniform EM waveguides are: (i) rectangular or circular in cross section, (ii) evacuated or filled with pressurized dielectric gas, and (iii) governed by geometric boundary conditions that are either of the Dirichlet-type or the Neumann-type.

Consider a rectangular uniform EM waveguide oriented along the z axis of the Cartesian coordinate system, while the long side a of the rectangular cross section is oriented along the x axis and the short side b along the y axis.

- (a) State and briefly discuss the dispersion relationship for a plane electromagnetic (EM) wave in vacuum.
- (b) For an evacuated rectangular uniform EM waveguide sketch a diagram with the waveguide in Cartesian coordinate system and summarize the derivation of the dispersion (ω, k_z) relationship starting with the wave equation for electric field \mathcal{E} and magnetic field \mathcal{B} .
- (c) For an evacuated rectangular uniform EM waveguide derive: (1) Cutoff frequency ω_c for a given RF mode, (2) Phase velocity v_{ph} , and (3) Group velocity v_{gr} .
- (d) For uniform rectangular EM waveguide: (1) Sketch the dispersion (ω, k_z) relationship. For an arbitrary point on the dispersion curve indicate how to determine phase velocity v_{ph} and group velocity v_{gr} . (2) Sketch the normalized phase velocity v_{ph}/c and group velocity v_{gr}/c against ω/ω_c for $0 \leq \omega/\omega_c \leq 5$.
- (e) Determine: (1) Lowest TM_{mn} cutoff frequency for the TM_{mn} mode where $\mathcal{B}_z = 0$ everywhere and $\mathcal{E}_z|_{x=0,a} = \mathcal{E}_z|_{y=0,b} = 0$, (2) Lowest TE_{mn} cutoff frequency for the TE_{mn} mode where $\mathcal{E}_z = 0$ everywhere and $\partial\mathcal{B}_z/\partial z|_{x=0,a} = \partial\mathcal{B}_z/\partial z|_{y=0,b} = 0$, (3) Ratio between the lowest cutoff frequency for TM modes and lowest cutoff frequency for TE modes, and (4) Cutoff frequency ω_c of the waveguide.

SOLUTION:

(a) Dispersion relationship for a plane EM wave in vacuum is derived from the basic relationship $v = c/\lambda$ for photons in vacuum without any constraints imposed by either boundary conditions or interaction with media. Multiplication of both sides of $v = c/\lambda$ with 2π results in the following simple (ω, k) dispersion relationship

$$2\pi v = \frac{2\pi}{\lambda} c \quad \text{or} \quad \omega = ck, \quad (13.142)$$

since $2\pi v = \omega$ and $2\pi/\lambda = k$. The dispersion relationship (13.142) states that angular frequency ω of a photon is proportional to its wave number k with speed of light c in vacuum the proportionality constant.

From (13.142) it follows that the phase velocity v_{ph} , defined as the ratio ω/k , is equal to speed of light c in vacuum and so is the group velocity v_{gr} , defined as $d\omega/dk$. Thus, for a plane EM wave in vacuum, we have both v_{ph} and v_{gr} equal to a constant, the speed of light c in vacuum.

$$v_{\text{ph}} = \frac{\omega}{k} = c \quad \text{and} \quad v_{\text{gr}} = \frac{d\omega}{dk} = c. \quad (13.143)$$

(b) Dispersion (ω, k_z) relationship, cutoff frequency ω_c , phase velocity v_{ph} , and group velocity v_{gr} for a uniform rectangular EM waveguide are derived from the wave equations for the z components of the electric field \mathcal{E} and magnetic field \mathcal{B} in conjunction with boundary conditions on the tangential component of \mathcal{E} and normal component of \mathcal{B} in a rectangular uniform EM waveguide. The wave equations for \mathcal{E} and \mathcal{B} are derived from Maxwell equations in vacuum [see (T13.13) and (T13.16), respectively and Prob. 274].

The wave equations for \mathcal{E}_z and \mathcal{B}_z are given as 3-dimensional linear partial differential equation of the second order in four variables (3 spatial and one temporal) in the following form

$$\nabla^2 \eta(x, y, z, t) = \frac{1}{c^2} \frac{\partial^2 \eta(x, y, z, t)}{\partial t^2}, \quad (13.144)$$

where $\eta(x, y, z, t)$ stands for $\mathcal{E}_z(x, y, z, t)$ and $\mathcal{B}_z(x, y, z, t)$ components of \mathcal{E} and \mathcal{B} , respectively.

The \mathcal{E}_z and \mathcal{B}_z components are the important solutions obtained from wave equations (13.144). The other components (\mathcal{E}_x , \mathcal{E}_y , \mathcal{B}_x , and \mathcal{B}_y) are determined using \mathcal{E}_z and \mathcal{B}_z solutions of (13.144) in conjunction with the four Maxwell equations for free space (see Prob. 277).

The most common approach to solving the wave equation (13.144) for $\eta(x, y, z, t)$ is to apply the method of separation of variables. The method was described in detail in Prob. 276 and here only the important points will be summarized:

- (1) First, the time factor is isolated by defining $\eta(x, y, z, t)$ as a product of two functions: $[\phi(x, y, z, t)$ and $T(t)]$ and inserting the product into (13.144) to get

$$\frac{\nabla^2 \phi}{\phi} = \frac{1}{c^2} \frac{\partial^2 T}{\partial t^2} = -k^2, \quad (13.145)$$

where k^2 is a positive constant and k is called the free space wave number or free space propagation coefficient. The solution for $T(t)$ is $T(t) \propto e^{-i\omega t}$ where $\omega = ck$ with ω the angular frequency of the RF wave.

- (2) Next, function $\phi(x, y, z)$ is defined as product of three functions $\phi(x, y, z) = X(x)Y(y)Z(z)$ and we now express the Helmholtz equation of (13.145) as

$$-\frac{1}{X} \frac{\partial^2 X}{\partial x^2} - \frac{1}{Y} \frac{\partial^2 Y}{\partial y^2} = \frac{1}{Z} \frac{\partial^2 Z}{\partial z^2} + k^2 = \gamma^2. \quad (13.146)$$

From the right hand side of (13.146) we get the following Helmholtz equation for $Z(z)$

$$\frac{\partial^2 Z}{\partial z^2} + k_z^2 Z = 0, \quad (13.147)$$

with solution for $Z(z)$ given as $Z(z) \propto e^{ik_z z}$, where γ^2 is a constant and k_z is the waveguide wave number or waveguide propagation coefficient defined as $k_z^2 = k^2 - \gamma^2$ for plane wave propagation along the z axis of the Cartesian coordinate system.

- (3) The left side of (13.146) now reads

$$\frac{1}{X} \frac{\partial^2 X}{\partial x^2} + \frac{1}{Y} \frac{\partial^2 Y}{\partial y^2} + \gamma^2 = \frac{1}{X} \frac{\partial^2 X}{\partial x^2} + \frac{1}{Y} \frac{\partial^2 Y}{\partial y^2} + (k^2 - k_z^2) = 0 \quad (13.148)$$

and can be separated into two Helmholtz equations given as follows

$$\frac{\partial^2 X}{\partial x^2} + k_x^2 X = 0 \quad \text{and} \quad \frac{\partial^2 Y}{\partial y^2} + k_y^2 Y = 0, \quad (13.149)$$

with the provision that

$$k_x^2 + k_y^2 = k^2 - k_z^2 = \gamma^2 \quad \text{or} \quad k_x^2 + k_y^2 + k_z^2 = k^2 = \frac{\omega^2}{c^2}. \quad (13.150)$$

Equation (13.150) is the so-called dispersion relationship (ω, k_z) linking the RF frequency ω with the propagation coefficient k_z in an evacuated uniform EM waveguide. The dispersion relationship (13.150) is of importance in waveguide theory, since it defines the propagation coefficient k_z for a given frequency ω and a given mode of the RF wave. Moreover, it enables determination of RF frequencies that can propagate through a given waveguide as well as the cutoff frequency ω_c , phase velocity v_{ph} , and group velocity v_{gr} of RF waves, based on boundary conditions and waveguide geometry.

- (4) Solutions to the two equations in (13.149) as well as coefficients k_x and k_y are determined from the boundary conditions that are, for \mathcal{E} and \mathcal{B} in a rectangular waveguide of sides a and b , respectively, given as follows:

- (i) The general *Dirichlet boundary condition* on the tangential component of electric field $\mathcal{E}_t|_S = 0$ is for a rectangular uniform EM waveguide expressed as

$$\mathcal{E}_z|_{x=0} = \mathcal{E}_z|_{x=a} = 0 \quad \text{and} \quad \mathcal{E}_z|_{y=0} = \mathcal{E}_z|_{y=b} = 0, \quad (13.151)$$

resulting in the following solutions for $X(x)$ and $Y(y)$

$$X(x) = \sin k_x x = \sin \frac{m\pi}{a} x \quad \text{and} \quad Y(y) = \sin k_y y = \sin \frac{n\pi}{b} y, \quad (13.152)$$

since from the boundary conditions (13.151) it follows that $k_x = \frac{m\pi}{a}$ and $k_y = \frac{n\pi}{b}$, where m and n are integers ranging from 1 to ∞ where the lowest value is 1 rather than 0 to avoid nontrivial solutions.

- (ii) The general *Neumann-type boundary condition* on normal component of magnetic field $\mathcal{B} \cdot \hat{\mathbf{n}}|_S = 0$ is for a rectangular uniform EM waveguide expressed as

$$\left. \frac{\partial \mathcal{B}_z}{\partial x} \right|_{x=0} = \left. \frac{\partial \mathcal{B}_z}{\partial x} \right|_{x=a} = 0 \quad \text{and} \quad \left. \frac{\partial \mathcal{B}_z}{\partial y} \right|_{y=0} = \left. \frac{\partial \mathcal{B}_z}{\partial y} \right|_{y=b} = 0, \quad (13.153)$$

resulting in the following solutions for $X(x)$ and $Y(y)$

$$X(x) = \cos k_x x = \cos \frac{m\pi}{a} x \quad \text{and} \quad Y(y) = \cos k_y y = \cos \frac{n\pi}{b} y, \quad (13.154)$$

since from the boundary conditions (13.153) it follows that $k_x = \frac{m\pi}{a}$ and $k_y = \frac{n\pi}{b}$, where m and n are integers ranging from 0 to ∞ .

- (5) We now take a closer look at the dispersion relationship (13.150), insert the expressions for $k_x = m\pi/a$ and $k_y = n\pi/b$ from (13.152) and (13.154) into (13.150), and obtain the following dispersion relationship for an evacuated

rectangular uniform EM waveguide

$$k_z = \sqrt{1 - \frac{\omega^2}{c^2} - k_x^2 - k_y^2} = \frac{1}{c} \sqrt{\omega^2 c^2 (k_x^2 + k_y^2)} = \frac{1}{c} \sqrt{\omega^2 - \pi^2 c^2 \left[\frac{m^2}{a^2} + \frac{n^2}{b^2} \right]}, \quad (13.155)$$

where the two integers m and n specify the mode of transverse electric and magnetic fields in a waveguide; however, they do not uniquely specify the frequency, since boundaries are in effect only in transverse directions x and y but not in the longitudinal direction of wave propagation along the z axis.

(c) Cutoff frequency ω_c , phase velocity v_{ph} , and group velocity v_{gr} for RF waves propagating in a given rectangular uniform EM waveguide are determined as follows:

- (1) *Cutoff frequency ω_c for a given RF mode.* From (13.155) we note that for an RF wave to propagate without attenuation, the propagation constant k_z must be real. Thus, ω^2/c^2 must exceed $k_x^2 + k_y^2 = \pi[(m/a)^2 + (n/b)^2]$, i.e.,

$$\frac{\omega}{c} > \pi \sqrt{\frac{m^2}{a^2} + \frac{n^2}{b^2}} \quad (13.156)$$

and, as a consequence, each mn mode of a waveguide is associated with a minimum frequency, called *cutoff frequency* $(\omega_c)_{mn}$ of the mn mode and defined as

$$(\omega_c)_{mn} = c \sqrt{\left(\frac{m\pi}{a}\right)^2 + \left(\frac{n\pi}{b}\right)^2}. \quad (13.157)$$

Inserting (13.157) into (13.155), we now get the following equation for the propagation coefficient k_z

$$k_z = \sqrt{\frac{\omega^2}{c^2} - k_x^2 - k_y^2} = \frac{1}{c} \sqrt{\omega^2 - \pi^2 c^2 \left[\frac{m^2}{a^2} + \frac{n^2}{b^2} \right]} = \frac{1}{c} \sqrt{\omega^2 - (\omega_c)_{mn}^2}. \quad (13.158)$$

Equation (13.158) can also be expressed in the canonical form of a hyperbola given as

$$\frac{\omega^2}{(\omega_c)_{mn}^2} - \frac{c^2}{(\omega_c)_{mn}^2} k_z^2 = 1, \quad (13.159)$$

where the cutoff frequency $(\omega_c)_{mn}^2$ is the distance between the center C and apex A of the hyperbola. However, in contrast to (13.158) and (13.159), the dispersion relationship for an EM waveguide is most often presented as

$$\omega^2 = (\omega_c)_{mn}^2 + c^2 k_z^2 \quad \text{or} \quad \omega = \pm \sqrt{(\omega_c)_{mn}^2 + c^2 k_z^2}. \quad (13.160)$$

- (2) *Phase velocity* v_{ph} for a rectangular waveguide is defined as the ratio ω/k_z and represents the speed with which one would need to travel along the waveguide axis in order to stay in phase with the RF wave

$$\begin{aligned} v_{\text{ph}} &= \frac{\omega}{k_z} = \frac{c\sqrt{k_x^2 + k_y^2 + k_z^2}}{k_z} = \frac{c\sqrt{k_z^2 + (\frac{m\pi}{a})^2 + (\frac{n\pi}{b})^2}}{k_z} \\ &= \frac{c\omega}{\sqrt{\omega^2 - (\omega_c)_{mn}^2}} = \frac{c}{\sqrt{1 - \frac{(\omega_c)_{mn}^2}{\omega^2}}}. \end{aligned} \quad (13.161)$$

From (13.161) we note that $v_{\text{ph}} \geq c$ and that the dynamic range for the phase velocity v_{ph} is from c for $\omega \rightarrow \infty$ to ∞ for $\omega \rightarrow (\omega_c)_{mn}$, i.e., $c \leq v_{\text{ph}} \leq \infty$. Thus, phase velocity v_{ph} of an RF wave in a rectangular uniform waveguide always exceeds the speed of light c in vacuum and approaches c as $\omega \rightarrow \infty$.

- (3) *Group velocity* v_{gr} is the speed of propagation of energy and information along the waveguide and is defined as $d\omega/dk_z$

$$\begin{aligned} v_{\text{gr}} &= \frac{d\omega}{dk_z} = \frac{ck_z}{\sqrt{k_x^2 + k_y^2 + k_z^2}} = \frac{ck_z}{\sqrt{k_z^2 + (\frac{m\pi}{a})^2 + (\frac{n\pi}{b})^2}} \\ &= \frac{c\sqrt{\omega^2 - (\omega_c)_{mn}^2}}{\omega} = c\sqrt{1 - \frac{(\omega_c)_{mn}^2}{\omega^2}}. \end{aligned} \quad (13.162)$$

From (13.162) we note that $v_{\text{gr}} \leq c$ and that the dynamic range of the group velocity is from 0 for $\omega \rightarrow (\omega_c)_{mn}$ to c for $\omega \rightarrow \infty$, i.e., $0 \leq v_{\text{gr}} \leq c$. Thus, group velocity v_{gr} , which represents the velocity of energy and signal propagation in uniform rectangular EM waveguide, is always less than the speed of light c in vacuum and approaches c as $\omega \rightarrow \infty$.

(d) Figure 13.7 shows a sketch of the hyperbolic dispersion relationship (ω, k_z) with k_z plotted on the abscissa axis and ω on the ordinate axis for a uniform rectangular EM waveguide. The asymptotes to the hyperbola form an angle of $\arctan c$ with the k_z axis. For an arbitrary point P on the hyperbola one can determine the phase velocity v_{ph} and group velocity v_{gr} as follows:

- (1) *Phase velocity* v_{ph} : Connect point P with the origin O of the coordinate system (note: point O corresponds to center C of the dispersion hyperbola). The angle between the \overline{PO} line and the $+k_z$ abscissa axis is labeled as α_{ph} and the tangent of this angle is the phase velocity

$$v_{\text{ph}} = \tan \alpha_{\text{ph}} = \frac{\omega}{k_z}. \quad (13.163)$$

- (2) *Group velocity* v_{gr} : Draw a tangent to dispersion curve at point P. The angle between the tangential line through point P and the k_z axis is labeled as α_{gr}

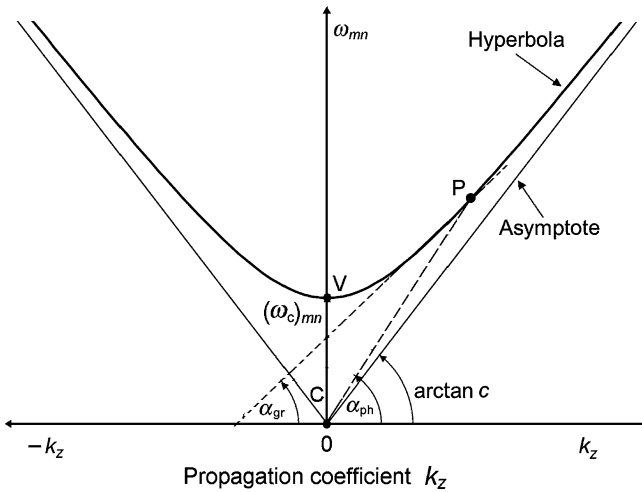


Fig. 13.7 Sketch of the dispersion hyperbolic relationship (13.160) with A the vertex and C the center of the hyperbola

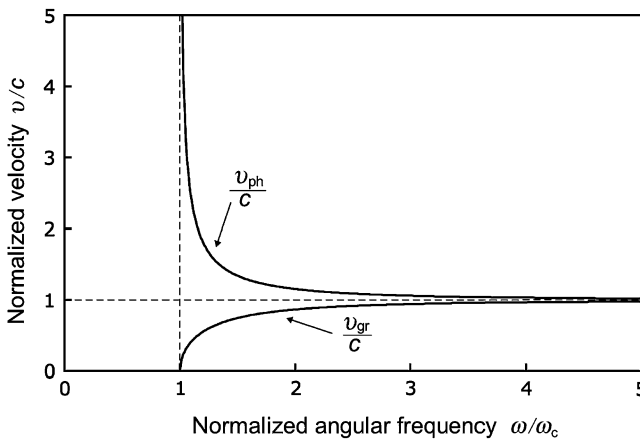


Fig. 13.8 Sketch of phase velocity v_{ph} and v_{gr} , both normalized to speed of light c in vacuum and plotted against frequency ω normalized to the cutoff frequency ω_c for a uniform rectangular EM waveguide

and the trigonometric tangent of this angle is equal to group velocity

$$v_{gr} = \tan \alpha_{gr} = \frac{d\omega}{dk_z}. \tag{13.164}$$

Figure 13.8 shows a sketch of phase velocity v_{ph} [see (13.161)] and group velocity v_{gr} [see (13.162)] both normalized to speed of light c in vacuum and plotted against frequency ω normalized to cutoff frequency ω_c .

13.6.Q2

(280)

Electromagnetic (EM) waveguides are hollow structures with metallic walls and central core that is either evacuated or filled with pressurized dielectric gas. It is mainly used for transmission of microwave power and signals; however, with some structural modifications, it can also be used for acceleration of charged particles. The cross section of EM waveguides is either rectangular with core sides a and b where $a > b$ or circular with core radius a .

- (a) For a uniform **rectangular** evacuated EM waveguide:
- (1) State the dispersion relationship (ω, k_z) for a given mode mn .
 - (2) State the general cutoff frequency $(\omega_c)_{mn}$ for a given mode mn .
 - (3) For the TM_{mn} mode where $\mathcal{B}_z = 0$ everywhere and $\mathcal{E}_z|_{x=0,a} = \mathcal{E}_z|_{y=0,b} = 0$ determine the lowest cutoff frequency $(\omega_c)_{mn}$ as well as the z component \mathcal{E}_z of the electric field \mathcal{E} .
 - (4) For the TE_{mn} mode where $\mathcal{E}_z = 0$ everywhere and $\partial\mathcal{B}_z/\partial z|_{x=0,a} = \partial\mathcal{B}_z/\partial z|_{y=0,b} = 0$ determine the lowest cutoff frequency $(\omega_c)_{mn}$ as well as the z component \mathcal{B}_z of the magnetic field \mathcal{B} .
 - (5) Determine the ratio between the lowest TM cutoff frequency and the lowest TE cutoff frequency.
 - (6) Determine the cutoff frequency ω_c of the waveguide.
- (b) A uniform rectangular evacuated EM waveguide is used for transmission of microwave power. The longer side a of the rectangular cross section of the waveguide core is 8.05 cm, the shorter side b is 3.26 cm. For the waveguide determine: (1) the 5 lowest cutoff frequencies of the TE_{mn} modes, (2) the 5 lowest cutoff frequencies of TM_{mn} modes, and (3) the 5 lowest modes (either TE or TM) that will be allowed to propagate in the waveguide.
- (c) The waveguide of (b) is used for transmission of microwave power in the S microwave band at $\nu = 2856$ MHz. State the modes of the 2856 MHz microwave input that will be allowed to propagate in the EM waveguide.
- (d) Determine the phase velocity v_{ph} and group velocity v_{gr} of the 2856 MHz microwaves propagating in the waveguide of (b).

SOLUTION:

- (a) Parameters of uniform rectangular evacuated EM waveguide (see Prob. 279):

- (1) *Dispersion relationship* (ω, k_z) for a given mode mn is expressed as follows

$$\omega^2 = (\omega_c)_{mn}^2 + c^2 k_z^2, \quad (13.165)$$

where ω_{mn} is the microwave angular frequency, $(\omega_c)_{mn}$ is the cutoff frequency, and k_z is the propagation coefficient.

(2) In general as well as for special transverse magnetic (TM) and transverse electric (TE) modes the *cutoff frequency* $(\omega_c)_{mn}$ for a given mode mn is expressed as

$$(\omega_c)_{mn} = c\sqrt{k_x^2 + k_y^2} = \pi c\sqrt{\left(\frac{m}{a}\right)^2 + \left(\frac{n}{b}\right)^2}. \quad (13.166)$$

(3) *Lowest cutoff frequency* $(\omega_c^{\text{TM}})_{mn}$ for TM_{mn} modes. The TM_{mn} modes are: (i) characterized by $\mathcal{B}_{z=0}$ everywhere in the core of the waveguide and (ii) governed by the Dirichlet-type boundary condition on the boundary between the core and wall of the waveguide, i.e., $\mathcal{E}_z|_{x=0,a} = \mathcal{E}_z|_{y=0,b} = 0$. The TM_{mn} solution of the wave equation for \mathcal{E}_z accounting for the Dirichlet-type boundary condition is

$$\mathcal{E}_z(x, y, z, t) = \sum_m \sum_n (\mathcal{E}_{z0})_{mn} \sin \frac{m\pi}{a}x \sin \frac{n\pi}{b}y e^{i(k_z z - \omega t)}, \quad (13.167)$$

with $(\mathcal{E}_{z0})_{mn}$ the amplitude of the TM wave. Based on (13.166) and (13.167) we note that the lowest non-trivial TM mode will be characterized by $m = 1$ and $n = 1$ to give the following cutoff frequency $(\omega_c^{\text{TM}})_{11}$

$$(\omega_c^{\text{TM}})_{11} = \pi c\sqrt{\frac{1}{a^2} + \frac{1}{b^2}} = \frac{\pi c}{a}\sqrt{1 + \left(\frac{a}{b}\right)^2} \quad (13.168)$$

and z component \mathcal{E}_z of the electric field \mathcal{E}

$$\mathcal{E}_z(x, y, z, t) = (\mathcal{E}_{z0})_{11} \sin \frac{\pi}{a}x \cos \frac{\pi}{b}y e^{i(k_z z - \omega t)}. \quad (13.169)$$

(4) *Lowest cutoff frequency* $(\omega_c^{\text{TE}})_{mn}$ for TE_{mn} modes. The TE_{mn} modes are (i) characterized by $\mathcal{E}_z = 0$ everywhere in the core of the waveguide and (ii) governed by the Neumann-type boundary condition on the boundary between the core and wall of the waveguide, i.e., $d\mathcal{B}_z/dz|_{x=0,a} = d\mathcal{B}_z/dz|_{y=0,b} = 0$. The TE_{mn} solution of the wave equation for \mathcal{B}_z accounting for the Neumann-type boundary condition is

$$\mathcal{B}_z(x, y, z, t) = \sum_m \sum_n (\mathcal{B}_{z0})_{mn} \cos \frac{m\pi}{a}x \cos \frac{n\pi}{b}y e^{i(k_z z - \omega t)}, \quad (13.170)$$

with $(\mathcal{B}_{z0})_{mn}$ the amplitude of the TE wave.

Based on (13.166) and (13.167) we note that the lowest non-trivial TE mode for $a > b$ will be characterized by $m = 1$ and $n = 0$ to give the following cutoff frequency $(\omega_c^{\text{TE}})_{10}$

$$(\omega_c^{\text{TE}})_{10} = \pi c\sqrt{\frac{1}{a^2}} = \frac{\pi c}{a} \quad (13.171)$$

and z component \mathcal{B}_z of the magnetic field \mathcal{B}

$$\mathcal{B}_z(x, y, z, t) = (\mathcal{B}_{z0})_{10} \cos \frac{\pi}{a} x e^{i(k_z z - \omega t)}. \quad (13.172)$$

(5) Using (13.168) and (13.169), the ratio between the lowest cutoff frequency $(\omega_c^{\text{TM}})_{11}$ for the TM modes and the lowest cutoff frequency $(\omega_c^{\text{TE}})_{10}$ for the TE modes is given as

$$\frac{(\omega_c^{\text{TM}})_{11}}{(\omega_c^{\text{TE}})_{10}} = \sqrt{1 + \left(\frac{a}{b}\right)^2}. \quad (13.173)$$

Since $a > b$, we note that $(\omega_c^{\text{TM}})_{11} > (\omega_c^{\text{TE}})_{10}$ and this tells us that the lowest cutoff frequency for all modes in the rectangular waveguide is the TE_{10} mode.

(6) *Cutoff frequency* ω_c for a given waveguide is defined as the cutoff frequency of the lowest mode mn that can propagate through a waveguide. Thus, the TE_{10} is the mode with the lowest cutoff frequency of all modes in a uniform rectangular EM waveguide and therefore the cutoff frequency for rectangular waveguides is from (13.166) given as $(\omega_c^{\text{TE}})_{10} = \pi c/a$. Note that the cutoff frequency of a rectangular waveguide is inversely proportional to a , the long side of the rectangular waveguide cross section but does not depend on b , the short side of the rectangular waveguide cross section.

Waveguide for transmission of a given radiofrequency (RF) are usually designed such that, at the given RF, the only mode they transmit is the TE_{10} mode. This means that the cutoff frequencies of all TM modes as well as the cutoff frequencies of all TE modes above the TE_{10} mode exceed the given RF.

(b) The general dispersion equation used for the determination of the cutoff frequency $(\nu_c)_{mn}$ of the mn mode in a rectangular EM waveguide is given as

$$(\nu_c)_{mn} = \frac{1}{2\pi} (\omega_c)_{mn} = \frac{c}{2} \sqrt{\left(\frac{m}{a}\right)^2 + \left(\frac{n}{b}\right)^2}. \quad (13.174)$$

The same equation (13.174) is used for the special TM_{mn} and TE_{mn} modes; however, we must recognize the lower limits on m and n for each of the special modes as a result of the boundary conditions. As shown in (a), the lower limits on m and n are as follows: for TM_{mn} modes $m \geq 1$ and $n \geq 1$, while for TE_{mn} $m \geq 1$ and $n \geq 0$ or $m \geq 0$ and $n \geq 1$.

We now use (13.175) to determine the cutoff frequencies for a set of TE_{mn} and TM_{mn} modes for various values of m and n starting with the lowest allowed values. The results are shown in Table 13.3. We also rank the TE_{mn} and TE_{mn} modes for the first five cutoff frequencies starting with the lowest value.

According to Table 13.3:

Table 13.3 Set of cutoff frequencies for TE_{mn} modes and TM_{mn} modes to determine the 5 lowest cutoff frequencies $(\nu_c^{TE})_{mn}$ for TE_{mn} modes and 5 lowest cutoff frequencies $(\nu_c^{TM})_{mn}$ for TM_{mn} modes in a uniform rectangular EM waveguide with longer side $a = 8.05$ cm and shorter side $b = 3.26$ cm. The lowest TE mode and lowest TM mode are shown in bold

(1) TE_{mn} cutoff frequencies $(\nu_c^{TE})_{mn}$ (MHz)				(2) TM_{mn} cutoff frequencies $(\nu_c^{TM})_{mn}$ (MHz)			
m	n	$(\nu_c^{TE})_{mn}$	Rank	m	n	$(\nu_c^{TM})_{mn}$	Rank
1	0	1863	(1)	1	1	4964	(1)
0	1	4600	(3)	1	2	9389	(5)
1	1	4964	(4)	2	1	5921	(2)
1	2	9389		2	2	9928	
1	3	13929		2	3	14298	
2	0	3726	(2)	3	1	7240	(3)
2	1	5921		3	2	10767	
2	2	9928		3	3	14575	
2	3	14298		4	1	8759	(4)
3	0	5590	(5)				
3	1	7240					
3	2	10767					

- (1) Five lowest cutoff frequencies $(\nu_c^{TE})_{mn}$ for TE_{mn} modes are: TE_{10} (1863 MHz), TE_{20} (3726 MHz), TE_{01} (4600 MHz), TE_{11} (4964 MHz), TE_{30} (5590 MHz).
- (2) Five lowest cutoff frequencies for the TM_{mn} modes are: TM_{11} (4964 MHz), TM_{21} (5921 MHz), TM_{31} (7240 MHz), TM_{41} (8759 MHz), TM_{12} (9389 MHz).
- (3) Combined order of 5 lowest special modes in the waveguide is as follows: TE_{10} (1863 MHz), TE_{20} (3726 MHz), TE_{01} (4600 MHz), TM_{11} (4964 MHz), TE_{11} (4964 MHz).

(c) The input microwaves to be transmitted through the waveguide have a frequency $\nu = 2856$ MHz that is below the lowest TM_{11} mode cutoff, but is above the waveguide cutoff of 1863 MHz (lowest cutoff for TE_{mn} modes). Since the second lowest cutoff for TE_{mn} modes is at 3736 MHz (TM_{20}) exceeding 2856 MHz, the input microwaves can propagate only with the TE_{10} mode. This “single mode operation” reflects the standard approach to design of transmission waveguides where the cross sectional dimensions are chosen such that they allow only one mode and all the other modes are excluded.

(d) As derived in Prob. 279 [(13.161) and (13.162)], the phase velocity ν_{ph} and group velocity ν_{gr} of microwaves propagating in a uniform rectangular EM waveguide with angular frequency ω or frequency ν are, respectively, expressed as

$$\nu_{ph} = \frac{c}{\sqrt{1 - \frac{(\omega_c)_{mn}^2}{\omega^2}}} = \frac{c}{\sqrt{1 - \frac{(\nu_c)_{mn}^2}{\nu^2}}} \tag{13.175}$$

and

$$v_{\text{ph}} = c \sqrt{1 - \frac{(\omega_c)_{mn}^2}{\omega^2}} = c \sqrt{1 - \frac{(v_c)_{mn}^2}{v^2}}. \quad (13.176)$$

As shown in **(b)**, microwaves of frequency $\nu = 2856$ MHz propagate through rectangular EM waveguide ($a = 8.05$ cm and $b = 3.26$ cm) in only one mode (transverse electric TE_{10} mode) for which the cutoff frequency is $(v_c^{\text{TE}})_{10} = 1863$ MHz, as shown in Table 13.6.

(1) Phase velocity v_{ph} is calculated using (13.175) as follows

$$\begin{aligned} v_{\text{ph}} &= \frac{c}{\sqrt{1 - \frac{(\omega_c)_{mn}^2}{\omega^2}}} = \frac{c}{\sqrt{1 - \frac{(v_c)_{mn}^2}{v^2}}} = \frac{c}{\sqrt{1 - \left(\frac{1863}{2856}\right)^2}} \\ &= 1.32c = 3.96 \times 10^8 \text{ m/s} > c. \end{aligned} \quad (13.177)$$

(2) Group velocity v_{gr} is calculated using (13.176) as

$$\begin{aligned} v_{\text{ph}} &= c \sqrt{1 - \frac{(\omega_c)_{mn}^2}{\omega^2}} = c \sqrt{1 - \frac{(v_c)_{mn}^2}{v^2}} = c \sqrt{1 - \left(\frac{1863}{2856}\right)^2} \\ &= 0.76c = 2.27 \times 10^8 \text{ m/s} < c. \end{aligned} \quad (13.178)$$

13.6.Q3

(281)

The theory of uniform circular electromagnetic (EM) waveguides relies on solutions to wave equations and boundary conditions in cylindrical coordinates as well as Bessel functions and first derivative of Bessel functions.

(a) For a uniform **circular** evacuated EM waveguide of core radius a :

- (1) State the general dispersion relationship for a uniform circular EM waveguide.
- (2) State the general cutoff frequency $(\omega_c)_{mn}$ for a given mode mn .
- (3) For the TM_{mn} mode where $\mathcal{B}_z = 0$ everywhere and $\mathcal{E}_z|_{r=a} = 0$ determine the lowest cutoff frequency $(\omega_c^{\text{TM}})_{mn}$.
- (4) For the TE_{mn} mode where $\mathcal{E}_z = 0$ everywhere and $\partial \mathcal{B}_z / \partial r|_{r=a} = 0$ determine the lowest cutoff frequency $(\omega_c^{\text{TE}})_{mn}$.
- (5) Determine the ratio between the lowest TM cutoff frequency and the lowest TE cutoff frequency.
- (6) Derive an expression for the cutoff frequency ω_c of a circular EM waveguide.

- (b) Figure 13.9 displays five Bessel functions $J_m(z)$ for $0 \leq m \leq 4$ and $0 \leq z \leq 10$. Use the diagram to determine all zeros (roots) of: (1) Bessel functions displayed and (2) First derivatives of the Bessel functions displayed. Mark the zeros on the diagram using solid circles for zeros of Bessel functions and open circles for zeros of the first derivative of the Bessel functions. Identify the zeros on the diagram using x_{mn} for the zeros of Bessel functions and y_{mn} for zeros of the first derivative of Bessel functions.
- (c) A uniform circular evacuated EM waveguide with core radius $a = 1.05$ cm is used for transmission of microwave power. For the waveguide determine:
- (1) Five lowest cutoff frequencies $(\nu_c^{\text{TM}})_{mn}$ for TM_{mn} modes.
 - (2) Five lowest cutoff frequencies $(\nu_c^{\text{TE}})_{mn}$ for TE_{mn} modes.
 - (3) Five lowest cutoff frequencies $(\nu_c)_{mn}$ for the circular EM waveguide.
 - (4) Cutoff frequency ν_c for the circular EM waveguide.
- (d) Assume that the circular EM waveguide of (c) is used for transmission of microwave power in the X band at $\nu = 10^4 \times 10^4$ MHz. Determine the TE_{mn} and TM_{mn} modes that are allowed to propagate through the waveguide.
- (e) Determine: (1) phase velocity ν_{ph} and (2) group velocity ν_{gr} of 10^4 MHz microwaves propagating in the uniform circular EM waveguide of (c).

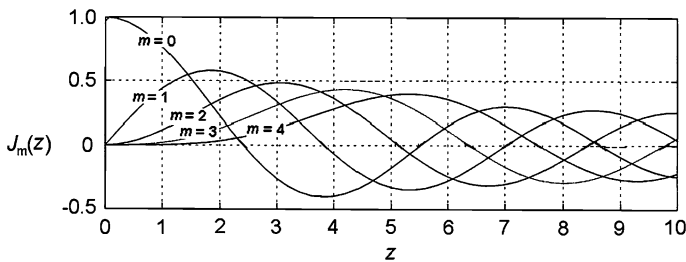


Fig. 13.9 Bessel functions $J_m(z)$ with m the order of Bessel function and z the argument of Bessel function for $0 \leq m \leq 4$ and $0 \leq z \leq 10$

SOLUTION:

(a) Parameters of uniform **circular** evacuated EM waveguide (see Prob. 276):

(1) *Dispersion relationship* for a uniform circular EM waveguide is in general form written as

$$\gamma_n^2 = k^2 - k_g^2, \quad (13.179)$$

where k is the free space wave number ($k = \omega/c$), k_g is the wave number or propagation coefficient of the circular waveguide, and γ_n is a constant determined from \mathcal{E}_z and \mathcal{B}_z solutions to wave equations in conjunction with the boundary conditions on \mathcal{E}_z and \mathcal{B}_z for a circular EM waveguide.

The z components \mathcal{E}_z and \mathcal{B}_z of the electric field \mathcal{E} and magnetic field \mathcal{B} are written, respectively, in general form as a double series

$$\mathcal{E}_z(x, \theta, z, t) = \sum_{m=0}^{\infty} \sum_{n=1}^{\infty} J_m(\gamma_n r) [A_{mn} \cos m\theta + B_{mn} \sin m\theta] e^{i(k_g z - \omega t)} \quad (13.180)$$

and

$$\mathcal{B}_z(x, \theta, z, t) = \sum_{m=0}^{\infty} \sum_{n=1}^{\infty} J_m(\gamma_n r) [C_{mn} \cos m\theta + D_{mn} \sin m\theta] e^{i(k_g z - \omega t)}, \quad (13.181)$$

where A_{mn} , B_{mn} , C_{mn} , and D_{mn} are constants that can be determined from initial conditions. Parameter γ_n in the argument of the Bessel function $J_m(\gamma_n r)$ in (13.180) and (13.181) is determined from the boundary conditions on \mathcal{E}_z and \mathcal{B}_z . Since these are generally different, they cannot be applied simultaneously and the two fields are split into two special categories or modes [transverse magnetic (TM) and transverse electric (TE)], characterized as follows:

- (i) For the TM_{mn} modes, $\mathcal{B}_z = 0$ everywhere in the waveguide core and \mathcal{E}_z is governed by the Dirichlet-type boundary condition $\mathcal{E}_z|_{r=a} = 0$ which specifies that $\mathcal{E}_z = 0$ at the boundary between the waveguide core and the conducting wall of the waveguide. The $\mathcal{E}_z|_{r=a} = 0$ boundary condition results in the following solution for γ_n of (13.180)

$$\mathcal{E}_z|_{r=a} = J_m(\gamma_n r)|_{r=a} = J_m(\gamma_n a) = 0 \quad \text{resulting in} \quad \gamma_n = \frac{x_{mn}}{a}, \quad (13.182)$$

where x_{mn} is the n -th zero (root) of the m -th order Bessel function of the first kind (J_m). Insertion of (13.182) into (13.179) results in the following expression for the TM_{mn} dispersion relationship in the form of $\omega = f(k_g)$

$$\omega^2 = c^2 \left(\frac{x_{mn}}{a} \right)^2 + c^2 k_g^2 = (\omega_c^{\text{TM}})_{mn}^2 + c^2 k_g^2 \quad \text{or} \quad \omega = \sqrt{(\omega_c^{\text{TM}})_{mn}^2 + c^2 k_g^2}, \quad (13.183)$$

where $(\omega_c^{\text{TM}})_{mn} = cx_{mn}/a$ is the cutoff frequency for TM_{mn} modes at $k_g = 0$.

- (ii) For the TE_{mn} modes, $\mathcal{E}_z = 0$ everywhere in the waveguide core and \mathcal{B}_z is governed by the Neumann-type boundary condition $d\mathcal{B}_z/dr|_{r=a} = 0$ that results in the following solution for γ_n of (13.181)

$$\left. \frac{d\mathcal{B}_z}{dr} \right|_{r=a} = \left. \frac{dJ_m(\gamma_n r)}{dr} \right|_{r=a} = \frac{dJ_m(\gamma_n a)}{dr} = 0 \quad \text{resulting in} \quad \gamma_n = \frac{y_{mn}}{a}, \quad (13.184)$$

where y_{mn} is the n -th zero (root) of the first derivative of the m -th order Bessel function of the first kind. Insertion of (13.184) into (13.179) results in the following expression for the TE_{mn} dispersion relationship in the form of $\omega = f(k_g)$

$$\omega^2 = c^2 \left(\frac{y_{mn}}{a} \right)^2 + c^2 k_g^2 = (\omega_c^{\text{TE}})_{mn}^2 + c^2 k_g^2 \quad \text{or} \quad \omega = \sqrt{(\omega_c^{\text{TE}})_{mn}^2 + c^2 k_g^2}, \quad (13.185)$$

where $(\omega_c^{\text{TE}})_{mn} = cy_{mn}/a$ is the cutoff frequency for TE_{mn} modes at $k_g = 0$.

(2) *Cutoff frequency* $(\omega_c)_{mn}$ is the lowest frequency with which a mode mn can propagate through an EM waveguide. All frequencies exceeding $(\omega_c)_{mn}$ can propagate through the waveguide without attenuation; frequencies below $(\omega_c)_{mn}$ are attenuated and cannot propagate through the waveguide.

- (i) Cutoff frequency $(\omega_c^{\text{TM}})_{mn}$ for given transverse magnetic (TM) mode mn is from (13.183) for $k_g = 0$ expressed as

$$(\omega_c^{\text{TM}})_{mn} = c \frac{x_{mn}}{a}, \quad (13.186)$$

where x_{mn} is the n -th zero (root) of the m -th order Bessel function (J_m).

- (ii) Cutoff frequency $(\omega_c^{\text{TE}})_{mn}$ for given transverse electric (TE) mode mn is from (13.185) for $k_g = 0$ expressed as

$$(\omega_c^{\text{TE}})_{mn} = c \frac{y_{mn}}{a}, \quad (13.187)$$

where y_{mn} is the n -th zero (root) of the first derivative of the m -th order Bessel function.

- (3) *Lowest cutoff frequency* $(\omega_c^{\text{TM}})_{mn}$ for TM_{mn} modes. The lowest TM_{mn} mode will occur for $m = 0$ and $n = 1$, giving the following expressions for \mathcal{E}_z of (13.180)

$$\mathcal{E}_z(r, \theta, z, t) = \mathcal{E}_{z0} J_0 \left(\frac{x_{01}}{a} r \right) e^{i\varphi} = \mathcal{E}_{z0} J_0 \left(\frac{2.405}{a} r \right) e^{i\varphi} \quad (13.188)$$

and for $(\omega_c^{\text{TM}})_{mn}$ of (13.186)

$$(\omega_c^{\text{TM}})_{01} = c \frac{x_{01}}{a} = c \frac{2.405}{a}, \quad (13.189)$$

where \mathcal{E}_{z0} is the electric field amplitude, φ is the phase of the wave, $x_{01} = 2.405$ is the first zero (root) of the zeroth order Bessel function of the first kind [$J_0(z)$], c is the speed of light in vacuum, and a is the radius of the uniform circular evacuated EM waveguide.

(4) *Lowest cutoff frequency* $(\omega_c^{\text{TE}})_{mn}$ for TE_{mn} modes. The lowest TE_{mn} mode will be for $m = 1$ and $n = 1$, giving the following expression for \mathcal{B}_z of (13.181)

$$\mathcal{B}_z(r, \theta, z, t) = \mathcal{B}_{z0} J_1\left(\frac{y_{11}}{a} r\right) e^{i\varphi} = \mathcal{B}_{z0} J_1\left(\frac{1.841}{a} r\right) e^{i\varphi} \quad (13.190)$$

and for $(\omega_c^{\text{TE}})_{mn}$ of (13.187)

$$(\omega_c^{\text{TE}})_{11} = c \frac{y_{11}}{a} = c \frac{1.841}{a}, \quad (13.191)$$

where \mathcal{B}_{z0} is the magnetic field amplitude, φ is the phase of the wave, and $y_{11} = 1.841$ is the first zero (root) of the derivative of the $J_1(z)$ Bessel function of the first kind.

(5) Using (13.189) and (13.191), the ratio between the lowest cutoff frequency $(\omega_c^{\text{TM}})_{01}$ for TM modes and the lowest cutoff frequency $(\omega_c^{\text{TE}})_{11}$ for TE modes is given as

$$\frac{(\omega_c^{\text{TM}})_{01}}{(\omega_c^{\text{TE}})_{11}} = \frac{2.405}{1.841} = 1.306. \quad (13.192)$$

(6) *Cutoff frequency* ω_c for a given waveguide is defined as the cutoff frequency of the lowest mode mn that can propagate through a waveguide. Thus, the TE_{11} is the mode with the lowest cutoff frequency of all modes in a uniform circular EM waveguide and therefore the cutoff frequency for circular waveguides is from (13.191) given as $\omega_c = 1.841c/a$. Note that the cutoff frequency of a circular EM waveguide is inversely proportional to radius a of the waveguide core.

Circular waveguides for transmission of a given radiofrequency (RF) are usually designed such that, at the given RF, the only mode they transmit is the TE_{11} mode. This means that the cutoff frequencies of all TM modes as well as the cutoff frequencies of all TE modes with the exception of the TE_{11} mode exceed the frequency of the given RF.

Circular waveguides used for particle acceleration are loaded with disks (irises) and designed such that, in addition to the TE_{11} mode, they also transmit the TM_{01} mode to enable particle acceleration.

(b) Figure 13.10 displays five Bessel functions $J_m(z)$ for $0 \leq m \leq 4$ and z in the range from 0 to 10. Superimposed onto the diagram are zeros (roots) x_{mn} of the five Bessel functions as well as zeros (roots) y_{mn} of the first derivatives of the five Bessel functions.

Roots x_{mn} of a Bessel function $J_m(z)$ occur at points where the Bessel curve crosses the abscissa (z) axis with m designating the order of the Bessel function and n designating the rank of a given root starting with $n = 1$ for the first non-trivial root as z increases from 0 to ∞ .

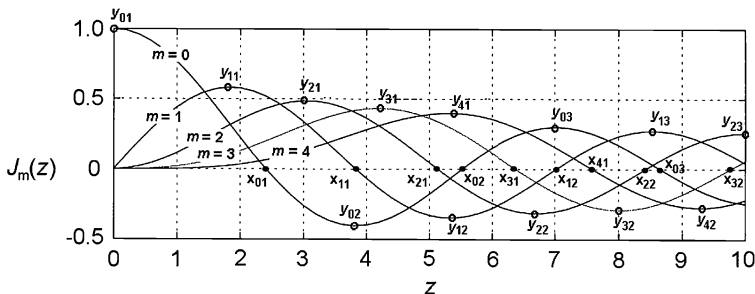


Fig. 13.10 Bessel functions $J_m(z)$ with m the order of Bessel function and z the argument of Bessel function for $0 \leq z \leq 10$ and $0 \leq m \leq 4$. Superimposed on the Bessel curves are the zeros (roots) x_{mn} (shown with solid circles) of Bessel function $J_m(z)$ as well as y_{mn} (shown with open circles) of the first derivative $dJ_m(z)/dz$ of Bessel function $J_m(z)$

Table 13.4 Zeros (roots) of Bessel functions (x_{mn} —left side of table) and zeros of first derivative of Bessel functions (y_{mn} —right side of table) for order m of Bessel function $J_m(z)$ in the range from 0 to 4 and rank order number n of the roots from 1 to 3. Data were obtained to two significant figures from Fig. 13.10

x_{mn} for $J_m(z) = 0$	y_{mn} for $dJ_m(z)/dz = 0$						
	$n = 1$	$n = 2$	$n = 3$				
$m = 0$	2.4	5.5	8.7	$m = 0$	0	3.8	7.0
$m = 1$	3.8	7.0	—	$m = 1$	1.8	5.3	8.5
$m = 2$	5.1	8.4	—	$m = 2$	3.1	6.7	10
$m = 3$	6.4	9.8	—	$m = 3$	4.2	8.2	—
$m = 4$	7.6	—	—	$m = 4$	5.3	9.3	—

Roots y_{mn} of the first derivative $dJ_m(z)/dz$ of Bessel function $J_m(z)$ occur at points where $J_m(z)$ exhibits a local maximum or minimum, i.e., where the tangent on the Bessel curve becomes horizontal. In y_{mn} parameter m again is the order of the Bessel function and n is the rank of the root starting with $n = 1$ for the root with the lowest z value.

Roots x_{mn} of y_{mn} and $J_m(z)$ and $dJ_m(z)/dz$, respectively, for $0 \leq m \leq 4$ and $0 \leq z \leq 10$ estimated to two significant figures from the five curves of Fig. 13.10 are listed in Table 13.4 for use in (c) in calculation of cutoff frequencies $(v_c^{TM})_{mn}$ and $(v_c^{TE})_{mn}$ of uniform circular EM waveguides.

(c) Cutoff frequencies $(v_c^{TM})_{mn}$ and $(v_c^{TE})_{mn}$ for the TM_{mn} and TE_{mn} modes, respectively, in a uniform circular EM waveguide of core radius a were calculated from the following expressions derived from (13.186) and (13.187), respectively

$$(v_c^{TM})_{mn} = \frac{1}{2\pi} (v_c^{TM})_{mn} = \frac{c}{2\pi a} x_{mn} = \xi_a x_{mn} \tag{13.193}$$

Table 13.5 TM and TE cutoff frequencies $(v_c^{TM})_{mn}$ and $(v_c^{TE})_{mn}$ for a uniform circular EM waveguide with a core radius of 1.05 cm

TM cutoff frequencies $(v_c^{TM})_{mn}$						TE cutoff frequencies $(v_c^{TE})_{mn}$					
<i>m</i>	<i>n</i>	Notation	<i>x_{mn}</i>	$(v_c^{TM})_{mn}$	Rank	<i>m</i>	<i>n</i>	Notation	<i>x_{mn}</i>	$(v_c^{TE})_{mn}$	Rank
0	1	<i>x</i> ₀₁	2.4	10920	(1)	0	1	<i>y</i> ₀₁	0	0	(0)
0	2	<i>x</i> ₀₂	5.5	25025	(4)	0	2	<i>y</i> ₀₂	3.8	17290	(3)
0	3	<i>x</i> ₀₃	8.7	39585	(9)	0	3	<i>y</i> ₀₃	7.0	31850	(8)
1	1	<i>x</i> ₁₁	3.8	17290	(2)	1	1	<i>y</i> ₁₁	1.8	8190	(1)
1	2	<i>x</i> ₁₂	7.0	31850	(6)	1	2	<i>y</i> ₁₂	5.4	24570	(6)
1	3	<i>x</i> ₁₃	10.2	46410	(11)	1	3	<i>y</i> ₁₃	8.5	38675	(10)
2	1	<i>x</i> ₂₁	5.1	23205	(3)	2	1	<i>y</i> ₂₁	3.1	14105	(2)
2	2	<i>x</i> ₂₂	8.4	38220	(8)	2	2	<i>y</i> ₂₂	6.7	30485	(7)
3	1	<i>x</i> ₃₁	6.4	29120	(5)	2	3	<i>y</i> ₂₃	10	45500	(12)
3	2	<i>x</i> ₃₂	9.8	44590	(10)	3	1	<i>y</i> ₃₁	4.2	19110	(4)
4	1	<i>x</i> ₄₁	7.6	34580	(7)	3	2	<i>y</i> ₃₂	8.0	36400	(9)
						4	1	<i>y</i> ₄₁	5.3	24115	(5)
						4	2	<i>y</i> ₄₂	9.3	42315	(11)

and

$$(v_c^{TE})_{mn} = \frac{1}{2\pi} (v_c^{TE})_{mn} = \frac{c}{2\pi a} y_{mn} = \xi_a y_{mn}, \tag{13.194}$$

where *x_{mn}* is the *n*-th zero (root) of the *m*-th order Bessel function and *y_{mn}* is the *n*-th zero of the first derivative of the *m*-th order Bessel function, and $\xi_a = c/(2\pi a)$ is a constant used in calculation of TM and TE cutoff frequencies in an evacuated waveguide of radius *a*.

Before embarking on calculation of cutoff frequencies using (13.193) and (13.194) we determine the waveguide constant ξ_a for use in (13.193) to determine TM cutoff frequencies $(v_c^{TM})_{mn}$ and in (13.194) to determine TE cutoff frequencies $(v_c^{TE})_{mn}$

$$\xi_a = \frac{c}{2\pi a} = \frac{3 \times 10^8 \text{ m/s}}{2\pi \times (1.05 \times 10^{-2} \text{ m})} = 4.55 \times 10^9 \text{ Hz} = 4550 \text{ MHz}. \tag{13.195}$$

Next we calculate a set of low-level TM cutoff frequencies using (13.193) in conjunction with (13.195) and *x_{mn}* data of Table 13.4 and a set of TE cutoff frequencies using (13.194) in conjunction with (13.195) and *y_{mn}* data of Table 13.4. Results of TM and TE cutoff frequencies calculated for a uniform circular EM waveguide with core radius of 1.05 cm are presented in Table 13.5.

According to Table 13.5:

- (1) Five lowest cutoff frequencies $(v_c^{TM})_{mn}$ for *TM_{mn}* modes are: *TM*₀₁ (10920 MHz), *TM*₁₁ (17290 MHz), *TM*₂₁ (23205 MHz), *TM*₀₂ (25025 MHz), and *TM*₃₁ (29120 MHz).

- (2) Five lowest cutoff frequencies $(\nu_c^{\text{TE}})_{mn}$ for TE_{mn} modes are: TE_{11} (8190 MHz), TE_{21} (14105 MHz), TE_{02} (17290 MHz), TE_{31} (19110 MHz), and TE_{41} (24115 MHz).
- (3) Combined order of 5 lowest special modes in the waveguide is as follows: TE_{11} (8190 MHz), TM_{01} (10920 MHz), TE_{21} (14105 MHz), TM_{11} (17290 MHz), and TE_{01} (17290 MHz).
- (4) The cutoff frequency $\omega_c = 2\pi\nu_c$ of the waveguide is given by the lowest cutoff frequency of the two special modes (TM and TE) propagating through the waveguide. For the circular EM waveguide in this problem, the lowest cutoff frequency occurs for the TE_{11} mode with $(\nu_c^{\text{TE}})_{11} = 8190$ MHz and we conclude that the cutoff frequency ν_c of the waveguide is 8190 MHz.

(d) The input microwaves to be transmitted through the circular waveguide have a frequency $\nu = 10^4$ MHz in the X band microwave frequency range. This frequency is below the lowest TM cutoff frequency of $(\nu_c^{\text{TM}})_{01} = 10920$ MHz which means that no TM modes can propagate in this EM waveguide. Of the TE modes only the TE_{11} can propagate, since its cutoff frequency of 8190 MHz is below the input microwave frequency of 10^4 MHz. Thus, the circular EM waveguide with a radius of 1.05 cm allows propagation of 10^4 MHz microwaves only in one mode, the TE_{11} mode with a cutoff frequency $(\nu_c^{\text{TE}})_{11} = 8190$ MHz. This is another example of waveguide design that allows only a single mode operation.

(e) The phase velocity v_{ph} and group velocity v_{gr} of microwaves propagating in a uniform circular EM waveguide with angular frequency ω or frequency ν are calculated from the dispersion relationship (ω, k_g) given in (13.184) as follows

$$\omega = \sqrt{(\omega_c)_{mn}^2 + c^2 k_g^2} \quad \text{or} \quad k_g = \frac{1}{c} \sqrt{\omega^2 - (\omega_c)_{mn}^2}, \quad (13.196)$$

where $(\omega_c)_{mn} = 2\pi(\nu_c)_{mn}$ is the cutoff frequency of mode mn propagating through the circular EM waveguide and k_g is the propagation coefficient of the waveguide.

(1) In general, the phase velocity v_{ph} is defined as the ratio between ω of the propagating wave and the associated k_g of the waveguide

$$v_{\text{ph}} = \frac{\omega}{k_g} = \frac{c\omega}{\sqrt{\omega^2 - (\omega_c)_{mn}^2}} = \frac{c}{\sqrt{1 - \frac{(\omega_c)_{mn}^2}{\omega^2}}} = \frac{c}{\sqrt{1 - \frac{(\nu_c)_{mn}^2}{\nu^2}}}. \quad (13.197)$$

In (d) we established that in a circular EM waveguide with core radius $a = 1.05$ cm microwaves with frequency $\nu = 10^4$ MHz in the X microwave band can only propagate in a TE_{11} mode that has a cutoff frequency $(\nu_c^{\text{TE}})_{11} = 8190$ MHz. Therefore, the phase velocity v_{ph} of 10000 MHz microwaves propagating in this waveguide is from (13.197) calculated as follows

$$v_{\text{ph}} = \frac{c}{\sqrt{1 - \frac{(\nu_c^{\text{TE}})_{11}^2}{\nu^2}}} = \frac{c}{\sqrt{1 - \left(\frac{8190}{10000}\right)^2}} = 1.74c = 5.5 \times 10^8 \text{ m/s} > c. \quad (13.198)$$

(2) Group velocity v_{gr} is in general defined as the derivative $d\omega/dk_g$

$$\begin{aligned} v_{gr} &= \frac{d\omega}{dk_g} = \frac{d}{dk_g} \left(\sqrt{(\omega_c)_{mn}^2 + c^2 k_g^2} \right) = \frac{2c^2 k_g}{2\sqrt{(\omega_c)_{mn}^2 + c^2 k_g^2}} = c \frac{\sqrt{\omega^2 - (\omega_c)_{mn}^2}}{\omega} \\ &= c \sqrt{1 - \frac{(\omega_c)_{mn}^2}{\omega^2}} = c \sqrt{1 - \frac{(v_c)_{mn}^2}{v^2}}. \end{aligned} \quad (13.199)$$

For the cutoff frequency $v_c = (v_c^{TE})_{11} = 8190$ MHz and microwave frequency of 10^4 Hz propagating through a circular EM waveguide of radius $a = 1.05$ cm the group velocity v_{gr} is from (13.199) calculated as

$$v_{gr} = c \sqrt{1 - \frac{(v_c^{TE})_{11}^2}{v^2}} = c \sqrt{1 - \left(\frac{8190}{10000} \right)^2} = 0.57c = 1.72 \times 10^8 \text{ m/s} < c. \quad (13.200)$$

13.7 Transverse Magnetic TM_{01} Mode

13.7.Q1

(282)

Electromagnetic (EM) waveguides are used for transmission of microwave power and signals as well as for charged particle acceleration in linear accelerators (linacs).

- (a) Briefly describe at least five notable differences between EM waveguides used for:
- (1) Transmission of microwave power and signals in a transmission waveguide.
 - (2) Acceleration of charged particles in an acceleration waveguide of a linac.
- (b) For a uniform circular evacuated EM waveguide:
- (1) State z components \mathcal{E}_z and \mathcal{B}_z of electric field \mathcal{E} and magnetic field \mathcal{B} , respectively.
 - (2) Explain how components \mathcal{E}_z and \mathcal{B}_z are determined.
 - (3) Explain how the other four components (\mathcal{E}_r , \mathcal{E}_θ , \mathcal{B}_r , and \mathcal{B}_θ) of \mathcal{E} and \mathcal{B} are determined once \mathcal{E}_z and \mathcal{B}_z are known.
- (c) Show that for a uniform circular evacuated EM waveguide the transverse components \mathcal{E}_r and \mathcal{E}_θ of the electric field \mathcal{E} as well as the transverse components \mathcal{B}_r and \mathcal{B}_θ of the magnetic field \mathcal{B} can be determined

directly from known axial components \mathcal{E}_z and \mathcal{B}_z of electric field \mathcal{E} and magnetic field \mathcal{B} , respectively.

- (d) For a uniform circular evacuated EM waveguide determine the transverse fields \mathcal{E}_r , \mathcal{E}_θ , \mathcal{B}_r , and \mathcal{B}_θ for:
- (1) Transverse magnetic (TM) modes ($\mathcal{B}_z = 0$ everywhere).
 - (2) Transverse electric (TE) modes ($\mathcal{E}_z = 0$ everywhere).
 - (3) Transverse electromagnetic (TEM) modes ($\mathcal{E}_z = 0$ and $\mathcal{B}_z = 0$ everywhere).
- (e) For a uniform circular evacuated EM waveguide determine all components of electric field \mathcal{E} and magnetic field \mathcal{B} for the lowest (dominant): (1) transverse magnetic (TM) mode and (2) transverse electric (TE) mode. The radius of the circular waveguide core is a .

SOLUTION:

(a) The basic principles behind transmission EM waveguides and acceleration EM waveguides are the same; however, there are several notable differences between the two types of waveguide with respect to: (1) Design, (2) Cross section, (3) Operating mode, (4) Core material, and (5) Microwave phase velocity. Summary of notable differences is provided in Table 13.6.

(1) *Design.* Transmission waveguides are uniform in cross section meaning that their cross section does not change along the direction of RF propagation. Acceleration waveguides, on the other hand, are non-uniform meaning that their cross section varies periodically along the direction of RF propagation. They are loaded with disks that define distinct cavities in the acceleration waveguide and cause partial reflection of the RF wave in order to slow down the phase velocity below the speed of light in vacuum.

(2) *Cross section.* Transmission waveguide most often has a rectangular cross section with sides a and b where $a > b$, while the cross section of accelerator waveguide is circular with basic core radius a and disk radius b where $a > b$. In addition to rectangular transmission waveguides, it is possible to have circular transmission EM waveguides; however, all acceleration waveguides are circular.

(3) *Operating mode.* Transmission waveguides are usually designed such that only the lowest (dominant) transverse microwave mode can propagate through the waveguide. This is the transverse electric TE_{11} mode characterized by $m = 1$ and $n = 1$. Particle acceleration, on the other hand, is carried out with the lowest (dominant) transverse magnetic (TM_{01}) mode characterized by $m = 0$ and $n = 1$, since this is the lowest special mode with \mathcal{E}_z oriented in the direction of particle motion; a necessary condition for charged particle acceleration.

Table 13.6 Summary of notable differences between transmission and acceleration EM waveguides

Characteristic feature	Transmission EM waveguide	Acceleration EM waveguide
Design	Uniform	Non-uniform (disk-loaded)
Cross section	Rectangular (circular possible)	Circular only
Operating special mode	Transverse electric TE ₁₀	Transverse magnetic TM ₀₁
Core medium	Dielectric gas or vacuum	Vacuum only
RF phase velocity v_{ph}	$v_{ph} > c$	$v_{ph} \lesssim c$

(4) *Core medium.* Transmission waveguides are usually filled with a pressurized dielectric gas, however, it is also possible to transmit microwaves in evacuated transmission waveguides; acceleration waveguides are always evacuated.

(5) *Phase velocity.* In transmission waveguides the phase velocity v_{ph} of the RF wave exceeds the speed of light c in vacuum ($v_{ph} > c$); acceleration waveguides, on the other hand, are designed such that v_{ph} is slowed down to slightly below c in order to allow the charged particle to follow the RF wave.

(b) Electric field \mathcal{E} and magnetic field \mathcal{B} in the core of a uniform circular evacuated EM waveguide are vectors with three components, each component depending on three spatial coordinates and one temporal coordinate

$$\mathcal{E} = [\mathcal{E}_r(r, \theta, z, t), \mathcal{E}_\theta(r, \theta, z, t), \mathcal{E}_z(r, \theta, z, t)] \quad \text{and}$$

$$\mathcal{B} = [\mathcal{B}_r(r, \theta, z, t), \mathcal{B}_\theta(r, \theta, z, t), \mathcal{B}_z(r, \theta, z, t)].$$

(1) The \mathcal{E}_z and \mathcal{B}_z components of \mathcal{E} and \mathcal{B} for a uniform evacuated circular EM waveguide are given by the following expressions

$$\mathcal{E}_z(x, \theta, z, t) = \sum_{m=0}^{\infty} \sum_{n=0}^{\infty} J_m(\gamma_n r) [A_{mn} \cos m\theta + B_{mn} \sin m\theta] e^{i\varphi} \quad (13.201)$$

and

$$\mathcal{B}_z(x, \theta, z, t) = \sum_{m=0}^{\infty} \sum_{n=0}^{\infty} J_m(\gamma_n r) [C_{mn} \cos m\theta + D_{mn} \sin m\theta] e^{i\varphi}, \quad (13.202)$$

where γ_n is a parameter determined from boundary conditions and related to free space wave number k and waveguide wave number (waveguide propagation coefficient) k_g as $\gamma_n^2 = k^2 - k_g^2$, $\varphi = k_g z - \omega t$ is the phase of the RF wave, and A_{mn} , B_{mn} , C_{mn} , and D_{mn} are coefficients that are determined from initial conditions.

(2) Components \mathcal{E}_z and \mathcal{B}_z are determined from wave equations for \mathcal{E}_z and \mathcal{B}_z

$$\nabla^2 \mathcal{E}_z = \frac{1}{c^2} \frac{\partial^2 \mathcal{E}_z}{\partial t^2} \quad (13.203)$$

and

$$\nabla^2 \mathcal{B}_z = \frac{1}{c^2} \frac{\partial^2 \mathcal{B}_z}{\partial t^2} \quad (13.204)$$

where c is the speed of light in vacuum and ∇^2 is the scalar Laplacian operator expressed in cylindrical coordinates for circular EM waveguide as follows

$$\nabla^2 = \frac{\partial^2}{\partial r^2} + \frac{1}{r} \frac{\partial}{\partial r} + \frac{1}{r^2} \frac{\partial^2}{\partial \theta^2} + \frac{\partial^2}{\partial z^2}. \quad (13.205)$$

Wave equations (13.203) and (13.204) are linear partial differential equations of the second order in four variables (3 spatial and one temporal) with constant coefficients. The most common method for solving the two wave equations is the method of separation of variables leading to solutions for the z components \mathcal{E}_z and \mathcal{B}_z of the electric field \mathcal{E} and magnetic field \mathcal{B} in the core of the waveguide.

(3) Once \mathcal{E}_z and \mathcal{B}_z are known, the other components of \mathcal{E} and \mathcal{B} in an evacuated circular EM waveguide are determined from Maxwell equations for free space expressed as follows

$$\nabla \cdot \mathcal{E} = 0, \quad (13.206)$$

$$\nabla \cdot \mathcal{B} = 0, \quad (13.207)$$

$$\nabla \times \mathcal{E} = -\frac{\partial \mathcal{B}}{\partial t}, \quad (13.208)$$

$$\nabla \times \mathcal{B} = \frac{1}{c^2} \frac{\partial \mathcal{E}}{\partial t} \quad (13.209)$$

with $(\nabla \cdot)$ the divergence and $(\nabla \times)$ the curl on vectors \mathcal{E} and \mathcal{B} .

(c) We start the derivation of components \mathcal{E}_r , \mathcal{E}_θ , \mathcal{B}_r , and \mathcal{B}_θ for circular EM waveguide with Maxwell equations (13.206) and (13.207) as $\nabla \cdot \mathcal{E} = 0$ and $\nabla \cdot \mathcal{B} = 0$, respectively, and express them in cylindrical coordinates as follows

$$\nabla \cdot \mathcal{E} = \frac{1}{r} \frac{\partial}{\partial r}(r\mathcal{E}_r) + \frac{1}{r} \frac{\partial \mathcal{E}_\theta}{\partial \theta} + \frac{\partial \mathcal{E}_z}{\partial z} = \frac{1}{r} \frac{\partial}{\partial r}(r\mathcal{E}_r) + \frac{1}{r} \frac{\partial \mathcal{E}_\theta}{\partial \theta} + ik_z \mathcal{E}_z = 0 \quad (13.210)$$

and

$$\nabla \cdot \mathcal{B} = \frac{1}{r} \frac{\partial}{\partial r}(r\mathcal{B}_r) + \frac{1}{r} \frac{\partial \mathcal{B}_\theta}{\partial \theta} + \frac{\partial \mathcal{B}_z}{\partial z} = \frac{1}{r} \frac{\partial}{\partial r}(r\mathcal{B}_r) + \frac{1}{r} \frac{\partial \mathcal{B}_\theta}{\partial \theta} + ik_z \mathcal{B}_z = 0. \quad (13.211)$$

Next, we express (13.208) and (13.209), respectively, in cylindrical coordinates as

$$\begin{aligned} \nabla \times \mathcal{E} = \text{curl } \mathcal{E} \text{ rot } \mathcal{E} &= \begin{vmatrix} \hat{\mathbf{r}} & \hat{\boldsymbol{\theta}} & \hat{\mathbf{z}} \\ \frac{\partial}{\partial r} & \frac{\partial}{\partial \theta} & \frac{\partial}{\partial z} \\ \mathcal{E}_r & r\mathcal{E}_\theta & \mathcal{E}_z \end{vmatrix} = -\frac{\partial}{\partial t} \begin{vmatrix} \mathcal{B}_r \hat{\mathbf{r}} \\ \mathcal{B}_\theta \hat{\boldsymbol{\theta}} \\ \mathcal{B}_z \hat{\mathbf{z}} \end{vmatrix} = i\omega \begin{vmatrix} \mathcal{B}_r \hat{\mathbf{r}} \\ \mathcal{B}_\theta \hat{\boldsymbol{\theta}} \\ \mathcal{B}_z \hat{\mathbf{z}} \end{vmatrix} \\ &= \left[\frac{1}{r} \frac{\partial \mathcal{E}_z}{\partial \theta} - \frac{\partial \mathcal{E}_\theta}{\partial z} \right] \hat{\mathbf{r}} + \left[\frac{\partial \mathcal{E}_r}{\partial z} - \frac{\partial \mathcal{E}_z}{\partial r} \right] \hat{\boldsymbol{\theta}} + \frac{1}{r} \left[\frac{\partial(r\mathcal{E}_\theta)}{\partial r} - \frac{\partial \mathcal{E}_r}{\partial \theta} \right] \hat{\mathbf{z}} \quad (13.212) \end{aligned}$$

and

$$\begin{aligned}\nabla \times \mathcal{B} &= \text{curl } \mathcal{B} \text{ rot } \mathcal{B} = \begin{vmatrix} \hat{\mathbf{r}} & \hat{\boldsymbol{\theta}} & \hat{\mathbf{z}} \\ \frac{\partial}{\partial r} & \frac{\partial}{\partial \theta} & \frac{\partial}{\partial z} \\ \mathcal{B}_r & r\mathcal{B}_\theta & \mathcal{B}_z \end{vmatrix} = \frac{1}{c^2} \frac{\partial}{\partial t} \begin{vmatrix} \mathcal{E}_r \hat{\mathbf{r}} \\ \mathcal{E}_\theta \hat{\boldsymbol{\theta}} \\ \mathcal{E}_z \hat{\mathbf{z}} \end{vmatrix} = -\frac{i\omega}{c^2} \begin{vmatrix} \mathcal{E}_r \hat{\mathbf{r}} \\ \mathcal{E}_\theta \hat{\boldsymbol{\theta}} \\ \mathcal{E}_z \hat{\mathbf{z}} \end{vmatrix} \\ &= \left[\frac{1}{r} \frac{\partial \mathcal{B}_z}{\partial \theta} - \frac{\partial \mathcal{B}_\theta}{\partial z} \right] \hat{\mathbf{r}} + \left[\frac{\partial \mathcal{B}_r}{\partial z} - \frac{\partial \mathcal{B}_z}{\partial r} \right] \hat{\boldsymbol{\theta}} + \frac{1}{r} \left[\frac{\partial(r\mathcal{B}_\theta)}{\partial r} - \frac{\partial \mathcal{B}_r}{\partial \theta} \right] \hat{\mathbf{z}}, \quad (13.213)\end{aligned}$$

where $\hat{\mathbf{r}}$, $\hat{\boldsymbol{\theta}}$, and $\hat{\mathbf{z}}$ are the standard unit vectors in the cylindrical coordinate system. Equations (13.212) and (13.213) have the following components of the curl operator [Note: (13.214), (13.215), and (13.216) follow from (13.212); (13.217), (13.218), and (13.219) from (13.213)]

$$\frac{1}{r} \frac{\partial \mathcal{E}_z}{\partial \theta} - \frac{\partial \mathcal{E}_\theta}{\partial z} = i\omega \mathcal{B}_r = \frac{1}{r} \frac{\partial \mathcal{E}_z}{\partial \theta} - ik_z \mathcal{E}_\theta \quad \text{or} \quad \mathcal{B}_r = -\frac{i}{\omega r} \frac{\partial \mathcal{E}_z}{\partial \theta} - \frac{k_g}{\omega} \mathcal{E}_\theta, \quad (13.214)$$

$$\frac{\partial \mathcal{E}_z}{\partial z} - \frac{\partial \mathcal{E}_r}{\partial r} = i\omega \mathcal{B}_\theta = ik_g \mathcal{E}_r - \frac{\partial \mathcal{E}_z}{\partial r} \quad \text{or} \quad \mathcal{B}_\theta = \frac{k_g}{\omega} \mathcal{E}_r + \frac{i}{\omega} \frac{\partial \mathcal{E}_z}{\partial r}, \quad (13.215)$$

$$\frac{1}{r} \left[\frac{\partial(r\mathcal{E}_\theta)}{\partial r} - \frac{\partial \mathcal{E}_r}{\partial \theta} \right] = i\omega \mathcal{B}_z \quad \text{or} \quad \mathcal{B}_z = \frac{i}{\omega r} \left[-\frac{\partial(r\mathcal{E}_\theta)}{\partial r} + \frac{\partial \mathcal{E}_r}{\partial \theta} \right], \quad (13.216)$$

$$\frac{1}{r} \frac{\partial \mathcal{B}_z}{\partial \theta} - \frac{\partial \mathcal{B}_\theta}{\partial z} = -\frac{i\omega}{c^2} \mathcal{E}_r = \frac{1}{r} \frac{\partial \mathcal{B}_z}{\partial \theta} - ik_g \mathcal{B}_\theta \quad \text{or} \quad (13.217)$$

$$\mathcal{E}_r = \frac{ic^2}{\omega r} \frac{\partial \mathcal{B}_z}{\partial \theta} + \frac{k_g c^2}{\omega} \mathcal{B}_\theta,$$

$$\frac{\partial \mathcal{B}_r}{\partial z} - \frac{\partial \mathcal{B}_z}{\partial r} = -\frac{i\omega}{c^2} \mathcal{E}_\theta = ik_g \mathcal{B}_r - \frac{\partial \mathcal{B}_z}{\partial r} \quad \text{or} \quad \mathcal{E}_\theta = -\frac{k_g c^2}{\omega} \mathcal{B}_r - \frac{ic^2}{\omega} \frac{\partial \mathcal{B}_z}{\partial r}, \quad (13.218)$$

$$\frac{1}{r} \frac{\partial(r\mathcal{B}_\theta)}{\partial r} - \frac{\partial \mathcal{B}_r}{\partial \theta} = -\frac{i\omega}{c^2} \mathcal{E}_z \quad \text{or} \quad \mathcal{E}_z = \frac{ic^2}{\omega} \left[\frac{\partial \mathcal{B}_\theta}{\partial r} - \frac{\partial \mathcal{B}_r}{\partial \theta} \right]. \quad (13.219)$$

Pairing up appropriate equations in the group from (13.214) to (13.219), we can now determine components \mathcal{E}_r , \mathcal{E}_θ , \mathcal{B}_r , and \mathcal{B}_θ as follows:

- (1) Inserting \mathcal{B}_θ of (13.215) into (13.217) gives the following expression for component \mathcal{E}_r

$$\mathcal{E}_r = i \left[\frac{k_g c^2}{\omega^2} \frac{\partial \mathcal{E}_z}{\partial r} + \frac{c^2}{\omega r} \frac{\partial \mathcal{B}_z}{\partial \theta} \right] \left(1 - \frac{k_g^2 c^2}{\omega^2} \right)^{-1} = \frac{i}{\gamma_n^2} \left[k_g \frac{\partial \mathcal{E}_z}{\partial r} + \frac{\omega}{r} \frac{\partial \mathcal{B}_z}{\partial \theta} \right]. \quad (13.220)$$

- (2) Inserting \mathcal{B}_r of (13.214) into (13.218) gives the following expression for component \mathcal{E}_θ

$$\mathcal{E}_\theta = i \left[-\frac{c^2}{\omega} \frac{\partial \mathcal{B}_z}{\partial r} + \frac{k_g c^2}{\omega^2 r} \frac{\partial \mathcal{E}_z}{\partial \theta} \right] \left(1 - \frac{k_g^2 c^2}{\omega^2} \right)^{-1} = \frac{i}{\gamma_n^2} \left[-\omega \frac{\partial \mathcal{B}_z}{\partial r} + \frac{k_g}{r} \frac{\partial \mathcal{E}_z}{\partial \theta} \right]. \quad (13.221)$$

- (3) Inserting \mathcal{E}_θ of (13.218) into (13.214) gives the following expression for component \mathcal{B}_r

$$\mathcal{B}_r = i \left[\frac{k_g c^2}{\omega^2} \frac{\partial \mathcal{B}_z}{\partial r} - \frac{1}{\omega r} \frac{\partial \mathcal{E}_z}{\partial \theta} \right] \left(1 - \frac{k_g^2 c^2}{\omega^2} \right)^{-1} = \frac{i}{\gamma_n^2} \left[k_g \frac{\partial \mathcal{B}_z}{\partial r} + \frac{\omega}{c^2 r} \frac{\partial \mathcal{E}_z}{\partial \theta} \right]. \quad (13.222)$$

- (4) Inserting \mathcal{E}_r of (13.217) into (13.215) gives the following expression for component \mathcal{B}_θ

$$\mathcal{B}_\theta = i \left[\frac{1}{\omega} \frac{\partial \mathcal{E}_z}{\partial r} + \frac{k_g c^2}{\omega^2 r} \frac{\partial \mathcal{B}_z}{\partial \theta} \right] \left(1 - \frac{k_g^2 c^2}{\omega^2} \right)^{-1} = \frac{i}{\gamma_n^2} \left[\frac{\omega}{c^2} \frac{\partial \mathcal{E}_z}{\partial r} + \frac{k_g}{r} \frac{\partial \mathcal{B}_z}{\partial \theta} \right]. \quad (13.223)$$

with $\gamma_n^2 = k^2 - k_g^2$ and $\gamma = kc$ where k is the free space propagation coefficient. Equations (TT) through (13.223) show that the transverse components \mathcal{E}_r , \mathcal{E}_θ , \mathcal{B}_r , and \mathcal{B}_θ can be determined with relative ease using Maxwell equations for free space in conjunction with known axial components \mathcal{E}_z and \mathcal{B}_z that are determined from appropriate wave equations (13.203) and (13.204), respectively.

(d) Equations (13.220) through (13.223) give general expressions for transverse components \mathcal{E}_r , \mathcal{E}_θ , \mathcal{B}_r , and \mathcal{B}_θ as a function of axial components \mathcal{E}_z and \mathcal{B}_z for a uniform circular EM waveguide. We now determine the transverse components for the three special modes: transverse magnetic (TM), transverse electric (TE), and transverse electromagnetic (TEM) that are characterized as follows:

- (1) TM modes: $\mathcal{B}_z = 0$ everywhere inside the waveguide core and the Dirichlet-type boundary condition $\mathcal{E}_z|_{r=a} = 0$ applies to \mathcal{E}_z at the boundary between the waveguide core and waveguide wall resulting in the following expression for γ_n

$$\gamma_n = \frac{x_{mn}}{a}, \quad (13.224)$$

where x_{mn} is the n -th zero of the m -th order Bessel function.

The transverse components \mathcal{E}_r , \mathcal{E}_θ , \mathcal{B}_r , and \mathcal{B}_θ are now from (13.220) through (13.223) simplified as follows, recognizing that $\partial \mathcal{B}_z / \partial r = \partial \mathcal{B}_z / \partial \theta = 0$, since for TM modes $\mathcal{B}_z = 0$ everywhere inside the waveguide core

$$\mathcal{E}_r = \frac{ik_g}{\gamma_n^2} \frac{\partial \mathcal{E}_z}{\partial r}, \quad (13.225)$$

$$\mathcal{E}_\theta = \frac{ik_g}{\gamma_n^2 r} \frac{\partial \mathcal{E}_z}{\partial \theta}, \quad (13.226)$$

$$\mathcal{B}_r = \frac{i\omega}{\gamma_n^2 c^2 r} \frac{\partial \mathcal{E}_z}{\partial \theta}, \quad (13.227)$$

$$\mathcal{B}_\theta = \frac{i\omega}{\gamma_n^2 c^2} \frac{\partial \mathcal{E}_z}{\partial r}. \quad (13.228)$$

(2) TE modes: $\mathcal{E}_z = 0$ everywhere inside the waveguide core and the Neumann-type boundary condition $\partial \mathcal{B}_z / \partial r|_{r=a} = 0$ applies to $\partial \mathcal{B}_z / \partial r$ at the boundary between the waveguide core and waveguide wall resulting in the following expression for γ_n

$$\gamma_n = \frac{y_{mn}}{a}, \quad (13.229)$$

where y_{mn} is the n -th zero of the first derivative of the m -th order Bessel function.

The transverse components \mathcal{E}_r , \mathcal{E}_θ , \mathcal{B}_r , and \mathcal{B}_θ are now from (13.220) through (13.223) given as follows, recognizing that $\partial \mathcal{E}_z / \partial r = \partial \mathcal{E}_z / \partial \theta = 0$, since $\mathcal{E}_z = 0$ everywhere in the waveguide core

$$\mathcal{E}_r = \frac{i\omega}{\gamma_n^2 r} \frac{\partial \mathcal{B}_z}{\partial \theta}, \quad (13.230)$$

$$\mathcal{E}_\theta = -\frac{i\omega}{\gamma_n^2} \frac{\partial \mathcal{B}_z}{\partial r}, \quad (13.231)$$

$$\mathcal{B}_r = \frac{ik_g}{\gamma_n^2} \frac{\partial \mathcal{B}_z}{\partial r}, \quad (13.232)$$

$$\mathcal{B}_\theta = \frac{ik_g}{\gamma_n^2 r} \frac{\partial \mathcal{B}_z}{\partial \theta}. \quad (13.233)$$

(3) TEM mode: Both $\mathcal{E}_z = 0$ and $\mathcal{B}_z = 0$ everywhere and (13.220) through (13.223) show that all transverse components \mathcal{E}_r , \mathcal{E}_θ , \mathcal{B}_r , and \mathcal{B}_θ are also equal to zero. We conclude that TEM modes cannot propagate through uniform circular EM waveguides.

(e) Components of lowest (dominant) TM and TE modes in a uniform evacuated circular EM waveguide with radius a are determined using the following steps:

The general expressions for z components \mathcal{E}_z and \mathcal{B}_z of electric field \mathcal{E} and magnetic field \mathcal{B} , respectively, given in (13.201) and (13.202), respectively, are used here to determine \mathcal{E}_z and \mathcal{B}_z for the dominant TM and TE modes, respectively. Expressions for the other four components \mathcal{E}_r , \mathcal{E}_θ , \mathcal{B}_r , and \mathcal{B}_θ for the special modes were derived in (d). We now use these expressions to determine the electric and magnetic field components for the dominant TM and TE modes.

(1) *Transverse magnetic (TM) modes* are characterized by $\mathcal{B}_z = 0$ everywhere in the waveguide core and the dominant (lowest) TM mode occurs for $m = 0$ and $n = 1$, resulting in the following expression for parameter γ_n from (13.224)

$$\gamma_n = \frac{x_{01}}{a} = \frac{2.405}{a}. \quad (13.234)$$

- (i) The electric field component \mathcal{E}_z for the dominant TM_{01} mode is now from (13.201) given as

$$\mathcal{E}_z = \mathcal{E}_{01} J_0(\gamma_1 r) e^{i\varphi} = \mathcal{E}_{01} J_0\left(\frac{x_{01}}{a} r\right) e^{i\varphi} = \mathcal{E}_{01} J_0\left(\frac{2.405}{a} r\right) e^{i\varphi}. \quad (13.235)$$

- (ii) The magnetic field component $\mathcal{B}_z = 0$ everywhere in the waveguide core for TM modes.
 (iii) The electric field component \mathcal{E}_r is determined from (aa) using $\mathcal{B}_z = 0$, \mathcal{E}_z from (13.235), and γ_n from (13.234) for $m = 0$ and $n = 1$ to get the following result

$$\begin{aligned} \mathcal{E}_r &= i \frac{k_g}{\gamma_1^2} \frac{\partial \mathcal{E}_z}{\partial r} = i \frac{k_g}{\gamma_n^2} \frac{\partial}{\partial r} \left[\mathcal{E}_{01} J_0\left(\frac{x_{01}}{a} r\right) e^{i\varphi} \right] = -i \frac{k_g}{\gamma_n^2} \frac{x_{01}}{a} \mathcal{E}_{01} J_1\left(\frac{x_{01}}{a} r\right) e^{i\varphi} \\ &= -i \frac{k_g a}{x_{01}} \mathcal{E}_{01} J_1\left(\frac{x_{01}}{a} r\right) e^{i\varphi} = -i \frac{k_g a}{2.405} \mathcal{E}_{01} J_1\left(\frac{2.405}{a} r\right) e^{i\varphi}, \end{aligned} \quad (13.236)$$

where we used $x_{01} = 2.405$ and the following recursive relationship for Bessel function $J_m(x) \frac{dJ_m(x)}{dx} = -J_{m+1}(x) + \frac{m}{x} J_m(x)$ resulting in $\frac{dJ_0(x)}{dx} = -J_1(x)$ or $\frac{d}{dr} J_0\left(\frac{x_{01}}{a} r\right) = -\frac{x_{01}}{a} J_1\left(\frac{x_{01}}{a} r\right)$.

- (iv) The electric field component \mathcal{E}_θ of (13.226) is zero because $\partial \mathcal{E}_z / \partial \theta = 0$

$$\mathcal{E}_\theta = i \frac{k_g}{\gamma_n^2 r} \frac{\partial \mathcal{E}_z}{\partial \theta} = 0. \quad (13.237)$$

- (v) The magnetic field component \mathcal{B}_r of (13.227) is zero because $\partial \mathcal{E}_z / \partial \theta = 0$

$$\mathcal{B}_r = i \frac{\omega}{\gamma_n^2 c^2} \frac{\partial \mathcal{E}_z}{\partial \theta} = 0. \quad (13.238)$$

- (vi) The magnetic field component \mathcal{B}_θ for the dominant TM_{01} mode is determined from (13.228) using $\mathcal{B}_z = 0$, \mathcal{E}_z from (13.235), and γ_n from (13.234) for $m = 0$ and $n = 1$ as follows

$$\begin{aligned} \mathcal{B}_\theta &= i \frac{\omega}{\gamma_n^2 c^2} \frac{\partial \mathcal{E}_z}{\partial r} = i \frac{\omega}{\gamma_n^2 c^2} \frac{\partial}{\partial r} \left[\mathcal{E}_{01} J_0\left(\frac{x_{01}}{a} r\right) e^{i\varphi} \right] \\ &= -i \frac{\omega x_{01}}{\gamma_n^2 c^2 a} \mathcal{E}_{01} J_1\left(\frac{x_{01}}{a} r\right) e^{i\varphi} = -i \frac{\omega a}{c^2 x_{01}} \mathcal{E}_{01} J_1\left(\frac{x_{01}}{a} r\right) e^{i\varphi} \\ &= -i \frac{\omega a}{2.405 c^2} \mathcal{E}_{01} J_1\left(\frac{2.405}{a} r\right) e^{i\varphi}, \end{aligned} \quad (13.239)$$

where we used again $\frac{d}{dr} J_0\left(\frac{x_{01}}{a} r\right) = -\frac{x_{01}}{a} J_1\left(\frac{x_{01}}{a} r\right)$.

- (2) *Transverse electric (TE) modes* are characterized by $\mathcal{E}_z = 0$ everywhere in the waveguide core and the dominant (lowest) TE mode occurs for $m = 1$ and $n = 1$,

resulting in the following expression for parameter γ_n from (13.229)

$$\gamma_n = \frac{y_{11}}{a} = \frac{1.841}{a}. \quad (13.240)$$

- (i) The magnetic field component \mathcal{B}_z for the dominant TE₁₁ mode is from (13.202) given as

$$\mathcal{B}_z = \mathcal{B}_{11} J_0(\gamma_1 r) e^{i\varphi} = \mathcal{B}_{11} J_0\left(\frac{y_{11}}{a} r\right) e^{i\varphi} = \mathcal{B}_{11} J_0\left(\frac{1.841}{a} r\right) e^{i\varphi}. \quad (13.241)$$

- (ii) The electric field component $\mathcal{E}_z = 0$ everywhere in the waveguide core for TE modes.
 (iii) The electric field component \mathcal{E}_r of (13.230) is zero because $\partial \mathcal{B}_z / \partial \theta = 0$

$$\mathcal{E}_r = i \frac{\omega}{\gamma_n^2 r} \frac{\partial \mathcal{B}_z}{\partial \theta} = 0. \quad (13.242)$$

- (iv) The electric field component \mathcal{E}_θ for the dominant TE₁₁ mode is determined from (13.231) using $\mathcal{E}_z = 0$, \mathcal{B}_z from (13.241), and γ_n from (13.240) for $m = 1$ and $n = 1$ as follows

$$\begin{aligned} \mathcal{E}_\theta &= -i \frac{\omega}{\gamma_n^2} \frac{\partial \mathcal{B}_z}{\partial r} = -i \frac{\omega}{\gamma_n^2} \frac{\partial}{\partial r} \left[\mathcal{B}_{11} J_0\left(\frac{y_{11}}{a} r\right) e^{i\varphi} \right] = i \frac{\omega y_{11}}{\gamma_n^2 a} \mathcal{B}_{11} J_1\left(\frac{y_{11}}{a} r\right) e^{i\varphi} \\ &= i \frac{\omega a}{y_{01}} \mathcal{B}_{01} J_1\left(\frac{y_{11}}{a} r\right) e^{i\varphi} = i \frac{\omega a}{1.841 c^2} \mathcal{B}_{11} J_1\left(\frac{1.841}{a} r\right) e^{i\varphi}, \end{aligned} \quad (13.243)$$

where we used $y_{11} = 1.841$ and the following recursive relationship for Bessel function $J_m(x)$

$$\begin{aligned} \frac{dJ_m(x)}{dx} &= -J_{m+1}(x) + \frac{m}{x} J_m(x) \quad \text{that results in} \quad \frac{dJ_0(x)}{dx} = -J_1(x) \quad \text{or} \\ \frac{d}{dr} J_0\left(\frac{y_{11}}{a} r\right) &= -\frac{y_{11}}{a} J_1\left(\frac{y_{11}}{a} r\right). \end{aligned}$$

- (v) The magnetic field component \mathcal{B}_r for the dominant TE₁₁ mode is determined from (13.232) using $\mathcal{E}_z = 0$, \mathcal{B}_z from (13.241), and γ_n from (13.240) for $m = 1$ and $n = 1$ as follows

$$\begin{aligned} \mathcal{B}_r &= i \frac{k_g}{\gamma_n^2} \frac{\partial \mathcal{B}_z}{\partial r} = i \frac{k_g}{\gamma_n^2} \frac{\partial}{\partial r} \left[\mathcal{B}_{11} J_0\left(\frac{y_{11}}{a} r\right) e^{i\varphi} \right] = -i \frac{k_g y_{11}}{\gamma_n^2 a} \mathcal{B}_{11} J_1\left(\frac{y_{11}}{a} r\right) e^{i\varphi} \\ &= -i \frac{k_g a}{y_{11}} \mathcal{B}_{11} J_1\left(\frac{y_{11}}{a} r\right) e^{i\varphi} = -i \frac{k_g a}{1.841} \mathcal{B}_{11} J_1\left(\frac{1.841}{a} r\right) e^{i\varphi}, \end{aligned} \quad (13.244)$$

where we used again $\frac{d}{dr} J_0\left(\frac{y_{11}}{a} r\right) = -\frac{y_{11}}{a} J_1\left(\frac{y_{11}}{a} r\right)$.

(vi) The magnetic field component \mathcal{B}_θ of (13.233) is zero because $\partial\mathcal{B}_z/\partial\theta = 0$

$$\mathcal{B}_\theta = i \frac{k_g}{\gamma_n^2 r} \frac{\partial\mathcal{B}_z}{\partial\theta} = 0. \quad (13.245)$$

13.8 Acceleration Waveguide Compared to Transmission Waveguide

13.8.Q1

(283)

The theory of waveguides used for charged particle acceleration in linear accelerators (linacs) is very complex and relies on many approximations and empirical relationships. However, the acceleration waveguide theory is based solidly on the theory of uniform circular EM waveguides that is well understood, relatively simple, and governs the transmission of microwaves in waveguides. Therefore, each acceleration waveguide has an equivalent circular transmission waveguide that provides a rough guidance for determination of parameters governing electron acceleration in acceleration waveguides.

- (a) Microwaves used for acceleration of electrons in standard clinical linacs used for radiotherapy are produced in an RF driver that operates at a frequency ν of 2856 MHz. For microwaves of $\nu = 2856$ MHz and a uniform circular EM waveguide equivalent to an acceleration waveguide of core radius $a = 5.25$ cm state or calculate:
- (1) Wavelength λ and wave number k .
 - (2) Special RF mode used for electron acceleration in acceleration waveguide.
 - (3) Cutoff frequency ν_c for the special RF mode used for electron acceleration.
 - (4) Cutoff frequency ν_c of the acceleration waveguide with core radius $a = 5.25$ cm.
 - (5) Parameter γ_n of the equivalent transmission waveguide for the special mode used for electron acceleration of (2).
 - (6) Parameter γ_n of equivalent transmission waveguide for the dominant special mode.
 - (7) Wave number (waveguide propagation coefficient) k_g for the special mode used for electron acceleration of (2).

- (b) Assume that 2856 MHz microwaves used for electron acceleration in an acceleration waveguide of radius $a = 5.25$ cm are propagating through an equivalent uniform EM waveguide. For the uniform circular EM waveguide of radius 5.25 cm calculate and plot:
- (1) Dispersion relationship (ω vs k_g).
 - (2) Point P on the ω vs k_g dispersion curve.
 - (3) Phase velocity v_{ph} at point P.
 - (4) Group velocity v_{gr} at point P.
- (c) Show that for particle acceleration with microwaves in a waveguide the particle velocity v_{part} must be approximately equal to the phase velocity v_{ph} of the microwaves that are used for particle acceleration in the waveguide.
- (d) Explain why uniform EM waveguides are not suitable for charged particle acceleration.

SOLUTION:

(a) In this problem, the acceleration waveguide has a core radius a of 5.25 cm. Its equivalent uniform waveguide also has a core radius of 5.25 cm and, despite being significantly simpler, provides several useful basic parameters of the acceleration waveguide.

(1) Wavelength λ and wave number k for microwaves with frequency $\nu = 2856$ MHz or angular frequency $\omega = 2\pi\nu = 2\pi \times (2856 \text{ MHz}) = 17936 \text{ MHz}$

$$\lambda = \frac{c}{\nu} = \frac{3 \times 10^8 \text{ m} \cdot \text{s}^{-1}}{2.856 \times 10^9 \text{ s}^{-1}} = 0.105 \text{ m} = 10.5 \text{ cm} \quad (13.246)$$

and

$$k = \frac{2\pi}{\lambda} = \frac{2\pi\nu}{c} = \frac{\omega}{c} = \frac{2\pi}{0.105 \text{ m}} 59.8 \text{ m}^{-1}, \quad (13.247)$$

where c is the speed of light in vacuum (3×10^8 m/s).

(2) *Electron acceleration* is carried out in an acceleration waveguide with microwaves of $\nu = 2856$ MHz ($\lambda = 10.5$ cm) propagating in the transverse magnetic (TM₀₁) special mode with $m = 0$ and $n = 1$. This mode has several useful features for charged particle acceleration, such as: (i) Z component of magnetic field \mathcal{B}_z is zero everywhere in the waveguide core, (ii) $\mathcal{E}_z \neq 0$ on the central axis of the waveguide enabling particle acceleration along waveguide z axis, and (iii) $\mathcal{E}_z|_{r=a} = 0$ at the boundary between the waveguide core and waveguide wall at $r = a$ (Dirichlet-type boundary condition).

(3) *Cutoff frequency* (ν_c^{TM}) for the TM_{01} special mode used for electron acceleration is the same for both the acceleration waveguide and its equivalent uniform waveguide and calculated as

$$\begin{aligned} (\nu_c^{\text{TM}})_{01} &= \frac{(\omega_c^{\text{TM}})_{01}}{2\pi} = \frac{c}{2\pi} \frac{x_{01}}{a} = \frac{(3 \times 10^8 \text{ m} \cdot \text{s}^{-1}) \times 2.405}{2\pi \times (5.25 \times 10^{-2} \text{ m})} \\ &= 2.188 \times 10^9 \text{ s}^{-1} = 2188 \text{ MHz}, \end{aligned} \quad (13.248)$$

or

$$(\omega_c^{\text{TM}})_{01} = c \frac{x_{01}}{a} = 2\pi (\nu_c^{\text{TM}})_{01} = 2\pi \times (2188 \text{ MHz}) = 13741 \text{ MHz}, \quad (13.249)$$

where $x_{01} = 2.405$ is the first zero (root) of the Bessel function of zero order (see Prob. 281).

(4) *The cutoff frequency* ν_c of the waveguide is by definition equal to the cutoff frequency of the dominant (lowest) special mode propagating through the waveguide. For a uniform circular EM waveguide the dominant mode is the TE_{11} mode and its cutoff frequency $(\nu_c^{\text{TE}})_{11}$ is defined as the waveguide cutoff frequency ν_c and determined from

$$\begin{aligned} (\nu_c^{\text{TE}})_{11} &= \frac{(\omega_c^{\text{TE}})_{11}}{2\pi} = \frac{c}{2\pi} \frac{y_{11}}{a} = \frac{(3 \times 10^8 \text{ m} \cdot \text{s}^{-1}) \times 1.841}{2\pi \times (5.25 \times 10^{-2} \text{ m})} \\ &= 1.675 \times 10^9 \text{ s}^{-1} = 1675 \text{ MHz}, \end{aligned} \quad (13.250)$$

or

$$(\omega_c^{\text{TE}})_{11} = 2\pi (\nu_c^{\text{TE}})_{11} = 2\pi \times (1675 \text{ MHz}) = 10519 \text{ MHz}, \quad (13.251)$$

where $y_{01} = 1.841$ is the first zero (root) of the first derivative of the Bessel function of zero order (see Prob. 281). Note that the dominant mode in the circular waveguide (TE_{11}) cannot be used for particle acceleration because in the TE_{mn} special modes $\mathcal{E}_z = 0$ everywhere in the waveguide core and $\mathcal{E}_z \neq 0$ is required for charged particle acceleration.

(5) *Parameter* γ_n for the TM_{01} mode and microwaves of frequency $\nu = 2856 \text{ MHz}$

$$\gamma_n = \frac{x_{01}}{a} = \frac{2.405}{5.25 \times 10^{-2} \text{ m}} = 45.8 \text{ m}^{-1}. \quad (13.252)$$

(6) The dominant mode in the waveguide is the TE_{11} mode and the *parameter* γ_n for this mode is given as follows

$$\gamma_n = \frac{y_{11}}{a} = \frac{1.841}{5.25 \times 10^{-2} \text{ m}} = 35.1 \text{ m}^{-1}. \quad (13.253)$$

(7) *Waveguide propagation coefficient* k_g for 2856 MHz microwaves and TM_{01} special mode

$$k_g = \sqrt{k^2 - \gamma_n^2} = \sqrt{(59.8 \text{ m})^2 - (45.8 \text{ m})^2} = 38.5 \text{ m}^{-1}. \quad (13.254)$$

(b) The *basic dispersion relationship* for TM_{mn} modes in uniform circular EM waveguides is

$$\gamma_n^2 = \left(\frac{x_{mn}}{a}\right)^2 = \frac{(\omega_c^{\text{TM}})_{mn}^2}{c^2} k^2 - k_g^2 = \frac{\omega^2}{c^2} - k_g^2, \quad (13.255)$$

while for TE_{mn} modes it is given as

$$\gamma_n^2 = \left(\frac{y_{mn}}{a}\right)^2 = \frac{(\omega_c^{\text{TE}})_{mn}^2}{c^2} k^2 - k_g^2 = \frac{\omega^2}{c^2} - k_g^2, \quad (13.256)$$

where x_{mn} is the n -th zero (root) of the m -th order Bessel function and y_{mn} is the n -th zero of the first derivative of the m -th order Bessel function. $(\omega_c^{\text{TM}})_{mn}^2$ and $(\omega_c^{\text{TE}})_{mn}^2$ are cutoff angular frequencies for microwaves propagating through the uniform waveguide in TM_{mn} and TE_{mn} special modes, respectively.

(1) After rearranging the terms in (13.256) we get the standard form of the general *dispersion relationship for TM_{mn} modes* in circular EM waveguide of radius $a = 5.25 \text{ cm}$

$$\omega^2 = (\omega_c^{\text{TM}})_{mn}^2 + c^2 k_g^2 \quad \text{or} \quad \omega = \sqrt{(\omega_c^{\text{TM}})_{mn}^2 + c^2 k_g^2} \quad (13.257)$$

that, for the TM_{01} mode with $(\omega_c^{\text{TM}})_{01} = 2\pi(\nu_c^{\text{TM}})_{01}$ from (13.249), is written as

$$\omega = \sqrt{(\omega_c^{\text{TM}})_{01}^2 + c^2 k_g^2} = \sqrt{(1.3741 \times 10^{10} \text{ Hz})^2 + (3 \times 10^8 \text{ m} \cdot \text{s}^{-1})^2 \times k_g^2}. \quad (13.258)$$

A plot of (13.258) in the k_g range from 0 to $\pm 120 \text{ m}^{-1}$ corresponding to ω range from 0 to 45 GHz is shown in Fig. 13.11. The shape of the (13.258) curve shows a hyperbola whose vertex V is the cutoff angular frequency $(\omega_c^{\text{TM}})_{01} = 1.374 \text{ GHz}$ and whose center C is at the origin of the (k_g, ω) Cartesian coordinate system.

- (2) Also shown in Fig. 13.11 is point P representing the $(k_g = 38.5 \text{ m}^{-1}, \omega = 17.936 \text{ GHz})$ point on the diagram corresponding to propagation of $\nu = 2856 \text{ MHz}$ microwaves through the uniform waveguide in the TM_{01} mode.
- (3) Phase velocity ν_{ph} at point P is calculated from the basic definition

$$\nu_{\text{ph}} = \frac{\omega}{k_g} = \frac{1.7936 \times 10^{10} \text{ s}^{-1}}{38.5 \text{ m}^{-1}} = 4.66 \times 10^8 \text{ m/s} \quad (13.259)$$

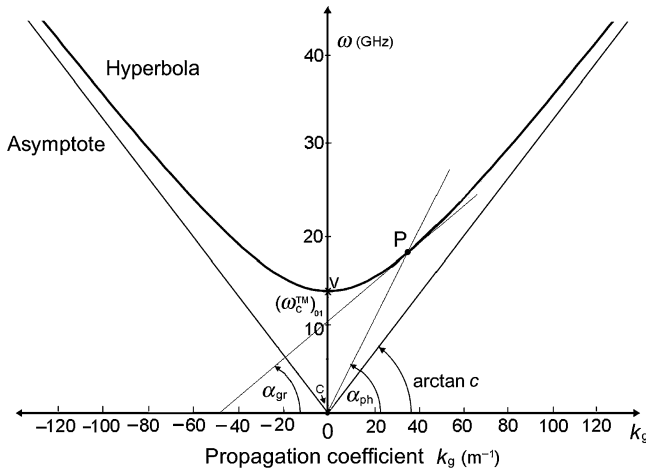


Fig. 13.11 Hyperbolic dispersion diagram of (13.257) for a uniform circular EM waveguide with radius a of 5.25 cm. Point P indicates the (ω, k_g) position on the dispersion hyperbola for microwaves with $\nu = 2856$ MHz propagating through the waveguide. The asymptotes of the dispersion hyperbola form an angle of $\arctan c$ with the abscissa (k_g) axis. The two faint lines through point P define angles α_{ph} and α_{gr} that can be used for graphical determination of the phase velocity v_{ph} and group velocity v_{gr} , respectively

or from the dispersion relationship (13.257) as

$$v_{ph} = \frac{c}{\sqrt{1 - \left[\frac{(\omega_c^{TM})_{01}}{\omega}\right]^2}} = \frac{c}{\sqrt{1 - \left[\frac{13741}{17936}\right]^2}} = \frac{c}{\sqrt{0.413}}$$

$$= 1.56c = 4.67 \times 10^8 \text{ m/s} > c \tag{13.260}$$

or graphically from the graph of Fig. 13.11 recalling that $v_{ph} = \tan \alpha_{ph}$.

- (4) Group velocity v_{ph} at point P is calculated from the dispersion relationship as follows

$$v_{gr} = \frac{d\omega}{dk_g} c \sqrt{1 - \left[\frac{(\omega_c^{TM})_{01}}{\omega}\right]^2} = c \sqrt{1 - \left[\frac{13741}{17936}\right]^2}$$

$$= 0.642c = 1.93 \times 10^8 \text{ m/s} < c \tag{13.261}$$

or graphically from the graph of Fig. 13.11 recalling that $v_{gr} = \tan \alpha_{gr}$.

- (c) The phase φ of the radiofrequency wave propagating in the $+z$ direction that coincides with the central axis of a uniform circular waveguide is expressed as follows

$$\varphi = k_g z - \omega t, \tag{13.262}$$

where ω is the angular frequency of the RF wave and k_g is the waveguide wave number or propagation coefficient.

The angular frequency ω of the RF wave as seen by a stationary observer ($z = \text{const}$) is given by

$$\left| \frac{d\varphi}{dt} \right| = \left| \frac{d}{dt}(k_g z - \omega t) \right| = \omega. \quad (13.263)$$

The angular frequency ω' of the RF wave as seen by an observer (or accelerated charged particle) traveling with the RF wave is calculated as follows

$$\frac{d\varphi}{dt'} = \omega' = \frac{d}{dt'}(k_g z - \omega t) = k_g \frac{dz}{dt'} - \omega \frac{dt}{dt'} = k_g \frac{dz}{dt} \frac{dt}{dt'} - \omega \frac{dt}{dt'} = (k_g v_{\text{part}} - \omega) \frac{dt}{dt'}, \quad (13.264)$$

where t' is the time measured in the reference frame of the moving observer and the particle velocity v_{part} is defined as $v_{\text{part}} = dz/dt$ where t is the time measured by stationary observer.

Since dt/dt' is the Lorentz factor γ in relativistic physics and the phase velocity v_{ph} of the RF wave is defined as $v_{\text{ph}} = \omega/k_g$, we can write (13.264) as

$$\omega' = \frac{dt}{dt'}(k_g v_{\text{part}} - \omega) = \gamma(k_g v_{\text{part}} - \omega) = \gamma\omega \left(\frac{v_{\text{part}}}{v_{\text{ph}}} - 1 \right). \quad (13.265)$$

Equation (13.265) is known as the relativistic Doppler effect. We note from (13.265) that, for the accelerated charged particle to continuously see an accelerating field with a constant phase along the central axis of the waveguide, the angular frequency ω' in the reference frame of the charged particle must be zero or at least small. The $\omega' = 0$ condition is met when in (13.265) we set $v_{\text{part}}/v_{\text{ph}} = 1$ or $v_{\text{part}} = v_{\text{ph}}$. Based on this, one concludes that a necessary condition for particle acceleration with electromagnetic fields in the microwave radiofrequency region is that the particle velocity v_{part} must be approximately equal to the phase velocity v_{ph} of microwaves used for particle acceleration.

(d) Several conclusions can be reached based on the discussion in sections **(a)**, **(b)**, and **(c)**:

(1) In **(c)** we showed that, for charged particle acceleration with microwaves, the accelerated charged particle should see a constant RF phase φ during the acceleration process. This condition is fulfilled when the velocity v_{part} of the accelerated particle is equal to the phase velocity v_{ph} of the RF wave used in particle acceleration.

(2) In **(b)** we showed that in a uniform waveguide the phase velocity v_{ph} of a typical RF wave used in particle acceleration ($\nu = 2856$ MHz) exceeds the speed of light c in vacuum. Since this is true for all uniform EM waveguides in general and since no particle can travel faster than c in vacuum, it is obvious that uniform waveguides,

propagating RF waves with v_{ph} exceeding c , cannot be used for charged particle acceleration.

(3) The necessary condition for charged particle acceleration with microwaves is that particle velocity v_{part} is equal to the RF phase velocity v_{ph} . Since v_{ph} in uniform EM waveguides exceeds c and particle velocity cannot exceed c , it is obvious that means must be used to decrease v_{ph} of uniform waveguides below c , if RF waves are to be used for particle acceleration. This is what was done when acceleration EM waveguide was developed from uniform circular EM waveguide by loading the latter with disks or irises that slow down the phase velocity of the RF wave to slightly below c enabling the accelerated charged particle to follow the accelerating RF field.

(4) We also note from (a) that the special waveguide mode that fulfills the condition of having electric field in the direction of circular waveguide central axis is the TM_{01} transverse magnetic mode in contrast with the dominant mode of the circular waveguide that is the TE_{11} transverse electric mode that cannot be used for particle acceleration but is very suitable for transmission of microwave power and signals.

13.9 Relationship Between Velocity of Energy Flow and Group Velocity in Uniform Waveguide

13.9.Q1

(284)

During the past three decades linear accelerator (linac) grew from a sophisticated and expensive alternative machine for megavoltage radiotherapy into the most widely used high technology machine in modern cancer treatment with ionizing radiation. In contrast to cobalt teletherapy machines that are based on radionuclide cobalt-60 gamma source, a linac uses microwave power to accelerate electrons to megavoltage kinetic energy. Three conditions must be met for charged particle acceleration with microwave power in an electromagnetic (EM) waveguide:

- (i) An electric field component oriented in, or opposite to, the direction of the waveguide axis must be present in the waveguide ($\mathcal{E}_z \neq 0$ on the waveguide axis at $r = 0$).
 - (ii) The velocity v_{part} of the accelerated charged particle should match the phase velocity v_{ph} of microwaves used in the acceleration process ($v_{\text{part}} = v_{\text{ph}}$).
 - (iii) The phase velocity v_{ph} of the radiofrequency wave used in electron acceleration must not exceed the speed of light c in vacuum ($v_{\text{ph}} < c$).
-

- (a) Briefly discuss how condition (i) above is satisfied in acceleration of electrons in an EM waveguide of a linac.
- (b) Briefly discuss why condition (ii) is important for charged particle acceleration with microwave fields.
- (c) Briefly discuss how condition (iii) above is fulfilled in acceleration of electrons in an acceleration waveguide of a linac.
- (d) Determine the relationship between velocity v_{en} of energy flow and group velocity v_{gr} of microwaves propagating through a uniform circular EM waveguide in the transverse magnetic TM_{01} mode.

SOLUTION:

(a) In a uniform circular EM waveguide of core radius a , condition (i) is satisfied in the simplest manner by the transverse magnetic TM_{01} special mode propagating through a uniform EM waveguide. This mode is the dominant TM_{mn} mode; however, it is not the dominant mode of the waveguide. This distinction belongs to the transverse electric TE_{11} mode that has the lowest cutoff frequency of all modes propagating through the waveguide, but does not have a non-zero electric field component \mathcal{E}_z in the direction of the waveguide axis. Therefore, the TE_{11} mode cannot be considered for electron acceleration; however, it is used for efficient transmission of microwave power and signals, while the TM_{01} mode is a candidate for use in electron acceleration with radiofrequency (RF) waves, because it fulfills condition (i) above.

The transverse magnetic TM_{01} mode fulfills condition (i) and is characterized by the following attributes:

- (1) Magnetic field component \mathcal{B}_z is zero everywhere in the waveguide core (only the transverse component \mathcal{B}_θ is present in the core; \mathcal{B}_r is also zero).
- (2) In contrast to the TE_{11} mode where $\mathcal{E}_z = 0$ everywhere in the core of the waveguide, in the TM_{01} mode a non-zero electric field component \mathcal{E}_z is present on the central axis of the waveguide, thereby satisfying condition (i) for particle acceleration.
- (3) The \mathcal{E}_z component of the electric field \mathcal{E} is governed by the Dirichlet-type boundary condition $\mathcal{E}_z|_{r=a} = 0$ at the $r = a$ boundary between the evacuated waveguide core and the conductive waveguide wall.

(b) Condition (ii) results from the requirement that the accelerated charged particle must continuously see an accelerating electric field in the direction of propagation along the central axis of the acceleration waveguide. This means that the phase φ of the \mathcal{E}_z component of the electric field \mathcal{E} must remain constant; that is, the angular frequency ω' of the RF wave as measured by an observer traveling with the accelerated particle should be zero or at least very small. The $\omega' = 0$ condition is fulfilled when the velocity v_{part} of the accelerated particle is equal to the phase velocity v_{ph} of the RF wave used in particle acceleration (see Prob. 283).

(c) Condition (i) is fulfilled by the TM_{01} special mode propagating through a uniform circular EM waveguide and condition (ii) simply states that $v_{\text{part}} = v_{\text{ph}}$. However, condition (iii) requires that $v_{\text{ph}} \lesssim c$ and this immediately excludes the potential use of a uniform waveguide for charged particle acceleration, because the phase velocity v_{ph} of microwaves propagating in a uniform EM waveguide always exceeds c and approaches c only for $\omega \rightarrow \infty$.

Since particle velocity cannot be increased above c , the condition $v_{\text{part}} = v_{\text{ph}}$ can be met only by decreasing the phase velocity of the RF wave in the waveguide below c . This entails adding a periodic perturbation into a uniform waveguide of core radius a in the form of disks or irises with circular holes of radius b in the center. At these obstacles RF waves suffer partial reflection and this effectively reduces v_{ph} of the RF wave propagating through the waveguide. With an appropriate choice of disk separation and radii a and b where $b \ll a$, wave reflections at the disks can push v_{ph} down to a level where $v_{\text{ph}} \lesssim c$, making particle acceleration physically possible.

In contrast to uniform circular EM waveguides (also called transmission EM waveguides) circular EM waveguides suitable for particle acceleration are called acceleration waveguides or disk-loaded waveguides. They are more complicated than uniform waveguides; however, many parameters of acceleration waveguides are similar to those of uniform waveguides of the same radius a , so that data measured for transmission waveguides are routinely used to approximate parameters of acceleration waveguides.

(d) The velocity v_{en} of energy flow in a waveguide will be determined from the general relationship

$$\bar{P} = W_{\text{tot}} v_{\text{en}} \quad \text{or} \quad v_{\text{en}} = \frac{\bar{P}}{W_{\text{tot}}}, \quad (13.266)$$

where

\bar{P} is the mean power flowing through a transverse cross section A of the waveguide.

W_{tot} is the total EM energy stored per unit length in the waveguide.

Mean power \bar{P} is related to the Poynting vector \mathbf{S} that represents energy flow with dimensions of energy/(area \times time) or power/area. Mean power \bar{P} is thus determined by integrating the Poynting vector \mathbf{S} over the transverse cross section \mathbf{A} of the waveguide

$$\bar{P} = \iint_A \bar{\mathbf{S}} \, d\mathbf{A} = \frac{1}{2\mu_0} \text{Re} \iint_A \mathbf{E} \times \mathbf{B}^* \, d\mathbf{A} = \frac{1}{2\mu_0} \text{Re} \iint_A \mathcal{E}_T \mathcal{B}_T^* \, dA, \quad (13.267)$$

where \mathbf{E} and \mathbf{B} are the electric and magnetic field, respectively, and \mathcal{E}_T and \mathcal{B}_T are the transverse components (perpendicular to direction of propagation as well as to one another) of \mathbf{E} and \mathbf{B} , respectively. The factor of $\frac{1}{2}$ in (13.267) arises from the time average over one complete period, Re stands for “real part”, and the asterisk (*) indicates complex conjugate.

The time average of stored energy W_{tot} per unit length of the waveguide has two components: electric W_{el} and magnetic W_{mag} given as follows

$$W_{\text{el}} = \frac{1}{4} \varepsilon_0 \iint_A \mathcal{E}_T \mathcal{E}_T^* dA \quad (13.268)$$

and

$$W_{\text{mag}} = \frac{1}{4\mu_0} \iint_A \mathcal{B}_T \mathcal{B}_T^* dA, \quad (13.269)$$

the extra factor of $\frac{1}{2}$ in (13.268) and (13.269) arises from the time average over one complete period, and ε_0 and μ_0 are the electric and magnetic constant, respectively.

The stored energy per unit length of the waveguide W_{tot} is given as the sum of the two components: W_{el} and W_{mag}

$$W_{\text{tot}} = W_{\text{el}} + W_{\text{mag}} = \frac{1}{4} \varepsilon_0 \iint_A \mathcal{E}_T \mathcal{E}_T^* dA + \frac{1}{4\mu_0} \iint_A \mathcal{B}_T \mathcal{B}_T^* dA = \frac{1}{2\mu_0} \iint_A \mathcal{B}_T \mathcal{B}_T^* dA, \quad (13.270)$$

where in the last term of (13.270) we simplified the expression for W_{tot} recognizing that the two components W_{el} and W_{mag} are equal giving $W_{\text{tot}} = 2W_{\text{mag}}$.

Inserting (12.267) and (13.270) into (13.265) results in the following general expression for the velocity of energy flow in a uniform EM waveguide

$$v_{\text{en}} = \frac{\bar{P}}{W_{\text{tot}}} = \frac{\frac{1}{2\mu_0} \text{Re} \iint_A \mathcal{E}_T \mathcal{B}_T^* dA}{\frac{1}{2\mu_0} \iint_A \mathcal{B}_T \mathcal{B}_T^* dA}. \quad (13.271)$$

We now use the general expression (13.271) to calculate the velocity of energy flow for the transverse magnetic TM_{01} mode of microwaves propagating in a uniform circular EM waveguide of radius a . The TM_{01} mode is the dominant TM_{mn} mode in a circular EM waveguide and is characterized by:

- (i) $\mathcal{B}_z = 0$ everywhere in the waveguide core.
- (ii) Dirichlet-type boundary condition $\mathcal{E}_z|_{r=a} = 0$.
- (iii) Non-zero z component of electric field ($\mathcal{E}_z \neq 0$) on the axis of the waveguide and as such under appropriate circumstances can be used for charged particle acceleration.

In general, the \mathcal{E}_z and \mathcal{B}_z components of \mathcal{E} and \mathcal{B} are determined from wave equations and the remaining components (\mathcal{E}_r , \mathcal{E}_θ , \mathcal{B}_r , and \mathcal{B}_θ) of \mathcal{E} and \mathcal{B} are determined from Maxwell equations. In Prob. 282(e) we derived the following expressions for the z components as well as the transverse components of \mathcal{E} and \mathcal{B} of the TM_{01} mode in a uniform circular EM waveguide of radius a

$$\mathcal{E}_r = -ik_g \left(\frac{a}{x_{01}} \right) \mathcal{E}_{01} J_1 \left(\frac{x_{01}}{a} r \right) e^{i\varphi}, \quad (13.272)$$

$$\mathcal{E}_\theta = 0, \quad (13.273)$$

$$\mathcal{E}_z = \mathcal{E}_{01} J_0\left(\frac{x_{01}}{a}r\right) e^{i\varphi}, \quad (13.274)$$

$$\mathcal{B}_r = 0, \quad (13.275)$$

$$\mathcal{B}_\theta = -i \frac{\omega}{c^2} \left(\frac{a}{x_{01}}\right) \mathcal{E}_{01} J_1\left(\frac{x_{01}}{a}r\right) e^{i\varphi}, \quad (13.276)$$

$$\mathcal{B}_z = 0. \quad (13.277)$$

For the TM_{01} mode the mean power \bar{P} of (13.267) and energy stored per unit distance W_{tot} of (13.271) are calculated as follows

$$\begin{aligned} \bar{P} &= \frac{1}{2\mu_0} \text{Re} \iint_A \mathcal{E}_T \mathcal{B}_T^* dA = \frac{1}{2\mu_0} \int_0^a \int_0^{2\pi} \mathcal{E}_r \mathcal{B}_\theta^* r dr d\theta \\ &= \frac{\pi}{\mu_0} \int_0^a \left\{ (-i) k_g \left(\frac{a}{x_{01}}\right) \mathcal{E}_{01} J_1\left(\frac{x_{01}}{a}r\right) e^{i\varphi} \right\} \\ &\quad \times \left\{ (+i) \frac{\omega}{c^2} \left(\frac{a}{x_{01}}\right) \mathcal{E}_{01} J_1\left(\frac{x_{01}}{a}r\right) e^{-i\varphi} \right\} r dr \\ &= \frac{\pi k_g \omega}{\mu_0 c^2} \left(\frac{a}{x_{01}}\right)^2 \mathcal{E}_{01}^2 \int_0^a J_1^2\left(\frac{x_{01}}{a}r\right) r dr \end{aligned} \quad (13.278)$$

and

$$\begin{aligned} W_{\text{tot}} &= \frac{1}{2\mu_0} \iint_A \mathcal{B}_T \mathcal{E}_T^* dA = \frac{1}{2\mu_0} \int_0^a \int_0^{2\pi} \mathcal{B}_\theta \mathcal{E}_r^* r dr d\theta \\ &= \frac{\pi}{\mu_0} \int_0^a \left\{ (-i) \frac{\omega}{c^2} \left(\frac{a}{x_{01}}\right) \mathcal{E}_{01} J_1\left(\frac{x_{01}}{a}r\right) e^{i\varphi} \right\} \\ &\quad \times \left\{ i \frac{\omega}{c^2} \left(\frac{a}{x_{01}}\right) \mathcal{E}_{01} J_1\left(\frac{x_{01}}{a}r\right) e^{-i\varphi} \right\} r dr \\ &= \frac{\pi \omega^2}{\mu_0 c^4} \left(\frac{a}{x_{01}}\right)^2 \mathcal{E}_{01}^2 \int_0^a J_1^2\left(\frac{x_{01}}{a}r\right) r dr. \end{aligned} \quad (13.279)$$

After inserting (13.278) and (13.279) into (13.266) we get, for the TM_{01} mode, the following expression for the velocity v_{en} of energy flow in a uniform circular EM waveguide of radius a

$$v_{\text{en}} = \frac{\bar{P}}{W_{\text{tot}}} = \frac{\frac{\pi k_g \omega}{\mu_0 c^2} \left(\frac{a}{x_{01}}\right)^2 \mathcal{E}_{01}^2 \int_0^a J_1^2\left(\frac{x_{01}}{a}r\right) r dr}{\frac{\pi \omega^2}{\mu_0 c^4} \left(\frac{a}{x_{01}}\right)^2 \mathcal{E}_{01}^2 \int_0^a J_1^2\left(\frac{x_{01}}{a}r\right) r dr} = \frac{k_g c^2}{\omega}. \quad (13.280)$$

Several observations are now possible after a closer look at the result $v_{\text{en}} = \frac{k_g c^2}{\omega}$:

- (1) Since by definition $v_{\text{ph}} = \frac{\omega}{k_{\text{g}}}$ and $v_{\text{ph}} \geq c$, we note that $v_{\text{en}} = \frac{c^2}{v_{\text{ph}}} \leq c$.
- (2) Since $v_{\text{ph}} v_{\text{gr}} = c^2$, we note from (13.280) that $v_{\text{en}} = v_{\text{gr}}$.
- (3) Since $k_{\text{g}} = \frac{\sqrt{\omega^2 - \omega_{\text{c}}^2}}{c}$, we note that $v_{\text{en}} = c \sqrt{1 - \frac{\omega_{\text{c}}^2}{\omega^2}} = v_{\text{gr}}$.

Thus, the velocity v_{en} of energy flow through the waveguide is equal to the group velocity v_{gr} of microwave propagation in the waveguide.

13.9.Q2**(285)**

A microwave travelling in a uniform EM waveguide can be characterized by its frequency ν , angular frequency $\omega = 2\pi\nu$, wavelength λ_{g} , propagation coefficient $k_{\text{g}} = 2\pi/\lambda_{\text{g}}$, energy $h\nu = hc/\lambda_{\text{g}}$, phase velocity $v_{\text{ph}} = \omega/k_{\text{g}}$, group velocity $v_{\text{gr}} = d\omega/dk_{\text{g}}$, as well as associated electric field \mathcal{E} and magnetic field \mathcal{B} , each field with three spatial components and one temporal component. In general, the \mathcal{E}_z and \mathcal{B}_z components of \mathcal{E} and \mathcal{B} are determined from wave equations and the remaining components are determined from Maxwell equations.

For a uniform rectangular EM waveguide with cross sectional sides a and b where $a > b$ determine the velocity of energy flow v_{en} for microwaves traveling through the waveguide in the transverse electric (TE_{mn}) mode and show that v_{en} equals the group velocity v_{gr} of the microwave. Determine v_{en} using the following intermediate steps:

- Determine the x , y , and z components of the electric field \mathcal{E} and magnetic field \mathcal{B} .
- Calculate the time averaged Poynting vector $\bar{\mathbf{S}}$ for the microwave described in (a).
- Calculate the mean energy density ρ_{en} for the microwave described in (a).
- Integrate $\bar{\mathbf{S}}$ of (b) over the waveguide cross section to get the mean power \bar{P} flowing through a transverse cross section A of the waveguide.
- Integrate ρ_{en} of (c) over the cross section A of the waveguide to get the total energy W_{tot} stored per unit length in the waveguide.
- The ratio between \bar{P} of (d) and W_{tot} of (e) is by definition equal to v_{en} of energy flow in the waveguide core. Determine this ratio and show that v_{en} equals to the group velocity v_{gr} of microwaves propagating in the TE_{mn} mode through the waveguide.

SOLUTION:

(a) As shown in Prob. 277, components \mathcal{E}_z and \mathcal{B}_z of the electric and magnetic fields \mathcal{E} and \mathcal{B} , respectively, are determined from wave equations for \mathcal{E}_z and \mathcal{B}_z . For TE_{mn} modes ($\mathcal{E}_z = 0$) everywhere in the waveguide core) propagating in a uniform

rectangular EM waveguide the results for \mathcal{E}_z and \mathcal{B}_z are as follows

$$\mathcal{E}_z(x, y, z, t) = 0 \quad \text{and} \quad \mathcal{B}_z(x, y, z, t) = \mathcal{B}_0 \cos\left(\frac{m\pi}{a}x\right) \cos\left(\frac{n\pi}{b}y\right) e^{i\varphi}, \quad (13.281)$$

where m and n are integers, and $\varphi = k_z z - \omega t$ is the phase of the microwave. When deriving the other components for the electric and magnetic fields (\mathcal{E}_x , \mathcal{E}_y , \mathcal{B}_x and \mathcal{B}_y) we will need derivatives $\partial\mathcal{B}_z/\partial x$ and $\partial\mathcal{B}_z/\partial y$, so we state them here

$$\frac{\partial\mathcal{B}_z}{\partial x} = -\frac{m\pi}{a}\mathcal{B}_0 \sin\left(\frac{m\pi}{a}x\right) \cos\left(\frac{n\pi}{b}y\right) e^{i\varphi} \quad (13.282)$$

and

$$\frac{\partial\mathcal{B}_z}{\partial y} = -\frac{n\pi}{b}\mathcal{B}_0 \cos\left(\frac{m\pi}{a}x\right) \sin\left(\frac{n\pi}{b}y\right) e^{i\varphi}. \quad (13.283)$$

In (13.130) it was shown that components \mathcal{E}_x and \mathcal{E}_y as well as \mathcal{B}_x and \mathcal{B}_y can be expressed simply as function of axial components and for special modes (TE and TM) the situation is even simpler with transverse components for TE modes expressed as a function of \mathcal{B}_z and for TM modes as a function of \mathcal{E}_z . For the TE_{mn} modes we thus have the following expressions for components \mathcal{E}_x , \mathcal{E}_y , \mathcal{B}_x , and \mathcal{B}_y derived from Maxwell equations

$$\mathcal{E}_x = \frac{i\omega}{\gamma^2} \frac{\partial\mathcal{B}_z}{\partial y} = -\frac{i\omega}{\gamma^2} \frac{n\pi}{b} \mathcal{B}_0 \cos\left(\frac{m\pi}{a}x\right) \sin\left(\frac{n\pi}{b}y\right) e^{i\varphi}, \quad (13.284)$$

$$\mathcal{E}_y = -\frac{i\omega}{\gamma^2} \frac{\partial\mathcal{B}_z}{\partial x} = \frac{i\omega}{\gamma^2} \frac{m\pi}{a} \mathcal{B}_0 \sin\left(\frac{m\pi}{a}x\right) \cos\left(\frac{n\pi}{b}y\right) e^{i\varphi}, \quad (13.285)$$

$$\mathcal{B}_x = \frac{ik_z}{\gamma^2} \frac{\partial\mathcal{B}_z}{\partial x} = -\frac{ik_z}{\gamma^2} \frac{m\pi}{a} \mathcal{B}_0 \sin\left(\frac{m\pi}{a}x\right) \cos\left(\frac{n\pi}{b}y\right) e^{i\varphi} \quad (13.286)$$

and

$$\mathcal{B}_y = \frac{ik_z}{\gamma^2} \frac{\partial\mathcal{B}_z}{\partial y} = -\frac{ik_z}{\gamma^2} \frac{n\pi}{b} \mathcal{B}_0 \cos\left(\frac{m\pi}{a}x\right) \sin\left(\frac{n\pi}{b}y\right) e^{i\varphi}, \quad (13.287)$$

where parameter γ is defined as

$$\gamma^2 = k^2 - k_z^2 = \frac{\omega^2}{c^2} - k_z^2 = \left(\frac{m\pi}{a}\right)^2 + \left(\frac{n\pi}{b}\right)^2 = \frac{\omega_c^2}{c^2} \quad (13.288)$$

with ω_c the cutoff frequency for the uniform rectangular EM waveguide and TE_{mn} mode.

(b) The Poynting vector \mathbf{S} is in general defined as the energy flow per unit time (power) per unit area A and is given by the vector product $\mathbf{S} = \mathbf{E} \times \mathbf{B} / \mu_0$, where μ_0 is the magnetic constant. For periodic sinusoidal electromagnetic (EM) fields of

more interest is the mean Poynting vector $\bar{\mathbf{S}}$ averaged over time and determined by treating the electric and magnetic field vectors \mathcal{E} and \mathcal{B} as complex vectors to get

$$\bar{\mathbf{S}} = \frac{1}{2\mu_0} \mathcal{E} \times \mathcal{B}^*, \quad (13.289)$$

with \mathcal{B}^* the complex conjugate of \mathcal{B} and the factor $1/2$ arising from the time average of the sinusoidal function over one time period.

In matrix format we now express the mean Poynting vector $\bar{\mathbf{S}}$ as

$$\bar{\mathbf{S}} = \frac{1}{2\mu_0} \begin{bmatrix} \hat{\mathbf{i}} & \hat{\mathbf{j}} & \hat{\mathbf{k}} \\ \mathcal{E}_x & \mathcal{E}_y & \mathcal{E}_z \\ \mathcal{B}_x^* & \mathcal{B}_y^* & \mathcal{B}_z^* \end{bmatrix} = (\mathcal{E}_y \mathcal{B}_z^* - \mathcal{E}_z \mathcal{B}_y^*) \hat{\mathbf{i}} - (\mathcal{E}_x \mathcal{B}_z^* - \mathcal{E}_z \mathcal{B}_x^*) \hat{\mathbf{j}} + (\mathcal{E}_x \mathcal{B}_y^* - \mathcal{E}_y \mathcal{B}_x^*) \hat{\mathbf{k}}, \quad (13.290)$$

resulting in the following expressions for components \bar{S}_x , \bar{S}_y , and \bar{S}_z of the Poynting vector \mathbf{S}

$$\begin{aligned} \bar{S}_x &= \frac{1}{2\mu_0} (\mathcal{E}_y \mathcal{B}_z^* - \mathcal{E}_z \mathcal{B}_y^*) \\ &= \frac{i\omega \mathcal{B}_0^2}{2\mu_0 \gamma^4} \left(\frac{m\pi}{a} \right) \sin\left(\frac{m\pi}{a} x \right) \cos\left(\frac{m\pi}{a} x \right) \cos^2\left(\frac{n\pi}{b} y \right), \end{aligned} \quad (13.291)$$

$$\begin{aligned} \bar{S}_y &= \frac{1}{2\mu_0} (\mathcal{E}_z \mathcal{B}_x^* - \mathcal{E}_x \mathcal{B}_z^*) \\ &= \frac{i\omega \mathcal{B}_0^2}{2\mu_0 \gamma^4} \left(\frac{n\pi}{b} \right) \cos^2\left(\frac{m\pi}{a} x \right) \sin\left(\frac{n\pi}{b} y \right) \cos\left(\frac{n\pi}{b} y \right) \end{aligned} \quad (13.292)$$

and

$$\begin{aligned} \bar{S}_z &= \frac{1}{2\mu_0} (\mathcal{E}_x \mathcal{B}_y^* - \mathcal{E}_y \mathcal{B}_x^*) \\ &= \frac{\omega k \mathcal{B}_0^2}{2\mu_0 \gamma^4} \left[\left(\frac{n\pi}{b} \right)^2 \cos^2\left(\frac{m\pi}{a} x \right) \sin^2\left(\frac{n\pi}{b} y \right) \right. \\ &\quad \left. + \left(\frac{m\pi}{a} \right)^2 \sin^2\left(\frac{m\pi}{a} x \right) \cos^2\left(\frac{n\pi}{b} y \right) \right]. \end{aligned} \quad (13.293)$$

(c) Mean energy density $\bar{\rho}_{\text{en}}$ for the microwave is given by (*note*: the extra factor $\frac{1}{2}$ again accounts for average over time period)

$$\begin{aligned} \bar{\rho}_{\text{en}} &= \frac{1}{4} \left(\epsilon_0 \mathcal{E} \cdot \mathcal{E}^* + \frac{1}{\mu} \mathcal{B} \cdot \mathcal{B}^* \right) \\ &= \frac{\epsilon_0}{4} (\mathcal{E}_x \cdot \mathcal{E}_x^* + \mathcal{E}_y \cdot \mathcal{E}_y^* + \mathcal{E}_z \cdot \mathcal{E}_z^*) + \frac{1}{4\mu_0} (\mathcal{B}_x \cdot \mathcal{B}_x^* + \mathcal{B}_y \cdot \mathcal{B}_y^* + \mathcal{B}_z \cdot \mathcal{B}_z^*) \end{aligned}$$

$$\begin{aligned}
&= \frac{\varepsilon_0 \omega^2 \mathcal{B}_0^2}{4\gamma^4} \left\{ \left(\frac{n\pi}{b} \right)^2 \cos^2 \left(\frac{m\pi}{a} x \right) \sin^2 \left(\frac{n\pi}{b} y \right) \right. \\
&\quad \left. + \left(\frac{m\pi}{a} \right)^2 \sin^2 \left(\frac{m\pi}{a} x \right) \cos^2 \left(\frac{n\pi}{b} y \right) \right\} \\
&\quad + \frac{1}{4\mu_0} \left\{ \frac{k_z^2 \mathcal{B}_0^2}{\gamma^4} \left[\left(\frac{m\pi}{a} \right)^2 \sin^2 \left(\frac{m\pi}{a} x \right) \cos^2 \left(\frac{n\pi}{b} y \right) \right. \right. \\
&\quad \left. \left. + \left(\frac{n\pi}{b} \right)^2 \cos^2 \left(\frac{m\pi}{a} x \right) \sin^2 \left(\frac{n\pi}{b} y \right) \right] \right. \\
&\quad \left. + \mathcal{B}_0^2 \cos^2 \left(\frac{m\pi}{a} x \right) \cos^2 \left(\frac{n\pi}{b} y \right) \right\}. \tag{13.294}
\end{aligned}$$

(d) Mean power \bar{P} flowing through a transverse cross section \mathbf{A} of the waveguide core is given by an integral of the axial component of the mean Poynting vector \mathbf{S} over \mathbf{A}

$$\bar{P} = \int \bar{\mathbf{S}} \cdot d\mathbf{A} = \int_0^a \int_0^b \bar{S}_z dx dy = \frac{\omega k_z \mathcal{B}_0^2 ab}{8\mu_0 \gamma^4} \left[\left(\frac{n\pi}{b} \right)^2 + \left(\frac{m\pi}{a} \right)^2 \right], \tag{13.295}$$

where we used the following definite integrals

$$\int_0^a \sin^2 \left(\frac{m\pi}{a} x \right) dx = \int_0^a \cos^2 \left(\frac{m\pi}{a} x \right) dx = \frac{a}{2} \tag{13.296}$$

and

$$\int_0^b \sin^2 \left(\frac{n\pi}{b} y \right) dy = \int_0^b \cos^2 \left(\frac{n\pi}{b} y \right) dy = \frac{b}{2}. \tag{13.297}$$

Recalling the identity (13.288), the mean power \bar{P} flowing through cross section A given in (13.295) simplifies to read

$$\bar{P} = \frac{\omega k_z \mathcal{B}_0^2 ab}{8\mu_0 \gamma^4} \left[\left(\frac{n\pi}{b} \right)^2 + \left(\frac{m\pi}{a} \right)^2 \right] = \frac{\omega k_z \mathcal{B}_0^2 ab}{8\mu_0 \omega_c^2}. \tag{13.298}$$

(e) The time average of total stored energy W_{tot} per unit length of waveguide core is given by the integral of mean energy density ρ_{en} over the cross section of the waveguide core A

$$W_{\text{tot}} = \int_A \bar{\rho}_{\text{en}} dA = \int_0^a \int_0^b \bar{\rho}_{\text{en}} dx dy. \tag{13.299}$$

Integrating (13.294) in conjunction with (13.288) and the well-known identity $c^2 = (\varepsilon_0\mu_0)^{-1}$ we obtain

$$\begin{aligned}
 W_{\text{tot}} &= \int_A \bar{\rho}_{\text{en}} dA = \int_0^a \int_0^b \bar{\rho}_{\text{en}} dx dy \\
 &= \frac{\varepsilon_0\omega^2 \mathcal{B}_0^2 ab}{16\gamma^4} \left\{ \left(\frac{n\pi}{b}\right)^2 + \left(\frac{m\pi}{a}\right)^2 \right\} + \frac{\mathcal{B}_0^2 ab}{16\mu_0} \left\{ \frac{k_z^2}{\gamma^4} \left[\left(\frac{m\pi}{a}\right)^2 + \left(\frac{n\pi}{b}\right)^2 \right] + 1 \right\} \\
 &= \frac{\varepsilon_0\omega^2 c^2 \mathcal{B}_0^2 ab}{16\omega_c^2} + \frac{\mathcal{B}_0^2 ab}{16\mu_0} \left\{ \frac{c^2 k_z^2}{\omega_c^2} + 1 \right\} \\
 &= \frac{\omega^2 \mathcal{B}_0^2 ab}{16\mu_0\omega_c^2} + \frac{\omega^2 \mathcal{B}_0^2 ab}{16\mu_0\omega_c^2} = \frac{\omega^2 \mathcal{B}_0^2 ab}{8\mu_0\omega_c^2}. \tag{13.300}
 \end{aligned}$$

(f) The velocity v_{en} of energy propagation in the waveguide core is determined from the ratio between \bar{P} of (13.298) and W_{tot} of (13.300)

$$v_{\text{en}} = \frac{\int_0^a \int_0^b \bar{S}_z dx dy}{\int_0^a \int_0^b \bar{\rho}_{\text{en}} dx dy} = \frac{\frac{\omega k c^2 \mathcal{B}_0^2 ab}{8\mu_0\omega_c^2}}{\frac{\omega^2 \mathcal{B}_0^2 ab}{8\mu_0\omega_c^2}} = \frac{k_z c^2}{\omega}. \tag{13.301}$$

Several observations are now possible after a closer look at the result $v_{\text{en}} = k_z c^2 / \omega$ of (13.301). We note that (13.301) obtained for a rectangular uniform waveguide is identical to (13.280) obtained for a cylindrical uniform waveguide. Therefore, the same conclusions we reached in Prob. 284 for cylindrical waveguide will apply to a rectangular waveguide of interest in this problem. The following points can be made:

- (1) Since by definition $v_{\text{ph}} = \omega/k_g$ and $v_{\text{ph}} \geq c$, we note that $v_{\text{en}} = c^2/v_{\text{ph}} \leq c$.
- (2) Since $v_{\text{ph}} v_{\text{gr}} = c^2$, we note from (13.301) that $v_{\text{en}} = v_{\text{gr}}$.
- (3) Since $k_{\text{gr}} = \sqrt{\omega^2 - \omega_c^2}/c$, we note that $v_{\text{en}} = c\sqrt{1 - \omega_c^2/\omega^2} = v_{\text{gr}}$.

Thus, the velocity v_{en} of energy flow through the waveguide is equal to the group velocity v_{gr} of microwave propagation in the waveguide.

13.10 Disk-Loaded Waveguide

13.10.Q1

(286)

Uniform electromagnetic (EM) waveguides (also called transmission EM waveguides) are suitable for transmission of microwave power and signals and they also meet several, but not all, requirements for charged particle acceleration. It turns out, however, that with certain modifications, uniform EM

waveguides can be transformed into waveguides suitable for particle acceleration and, to distinguish them from uniform waveguides, they are then referred to as disk-loaded EM waveguides or acceleration EM waveguides.

-
- (a) Briefly discuss the differences between a transmission EM waveguide and an acceleration EM waveguide.
 - (b) Draw schematic diagrams of a transmission EM waveguide and an acceleration EM waveguide.
 - (c) Draw the dispersion diagram for a typical acceleration EM waveguide and its equivalent uniform EM waveguide.
 - (d) Briefly state and explain the salient features of an acceleration EM waveguide.

SOLUTION:

(a) Both types of waveguide: (i) uniform (transmission) waveguide and (ii) accelerating (disk-loaded) waveguide are used for transmission of microwave power; however, in design and purpose there are significant differences between the two waveguide types, such as:

- (1) Transmission waveguide is much simpler in design than acceleration waveguide.
- (2) Transverse cross section of transmission waveguide is either rectangular or circular, while cross section of acceleration waveguide is always circular.
- (3) Core of transmission waveguide is either evacuated or filled with pressurized dielectric gas, that of acceleration waveguide is always evacuated.
- (4) Transmission waveguide is essentially a pipe of uniform cross section (rectangular or circular); acceleration waveguide is a cylinder loaded with periodic perturbations in the form of disks (irises) that create partitions in the waveguide tube and define sections called cavity in the waveguide.
- (5) The phase velocity v_{ph} of microwaves propagating in a transmission waveguide exceeds the speed of light c in vacuum making charged particle acceleration impossible; the phase velocity of microwaves propagating in acceleration waveguide is slightly less than c to allow charged particle acceleration. The role of disks in acceleration waveguide is to decrease the phase velocity v_{ph} of a uniform waveguide, where for practical microwave frequencies it always exceeds the speed of light c in vacuum, to a level below c to allow charged particle acceleration.
- (6) It is clear that the transmission (uniform) waveguide and the acceleration (disk-loaded) waveguide are related, since the latter slowly evolved from the former. One may state that in view of this relationship each disk-loaded waveguide can be approximated with a uniform waveguide and we can refer to it as an equivalent, yet much simpler, waveguide. This equivalent waveguide has the same core radius as the accelerator waveguide but cannot be used for

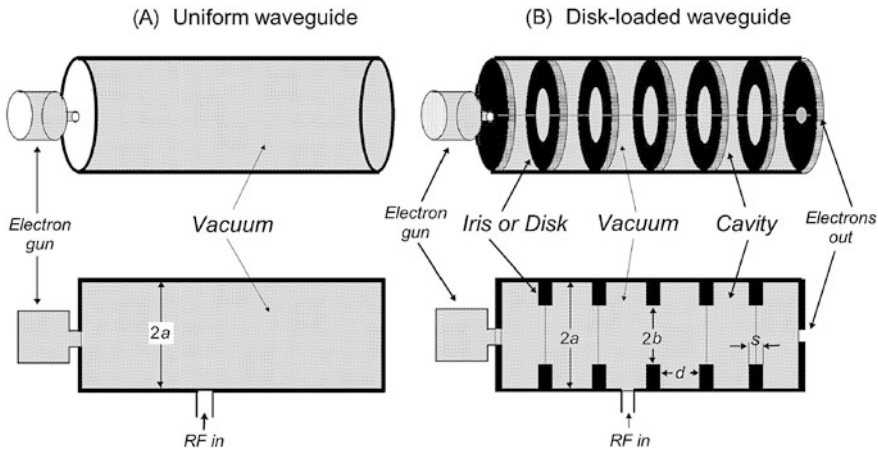


Fig. 13.12 Schematic diagram of (A) uniform (transmission) waveguide and (B) disk-loaded (acceleration) waveguide both of core radius a . One may say that the uniform waveguide serves as the equivalent waveguide to the accelerator waveguide

charged particle acceleration (recall that $v_{ph} > c$ in uniform waveguide and for particle acceleration we must have $v_{part} \approx v_{ph}$); however, the equivalent uniform waveguide can serve as a simple pathway toward determination of the basic parameters of the acceleration waveguide.

(b) Figure 13.12 shows schematic diagrams of a uniform (transmission) circular EM waveguide of core radius a and of a disk-loaded (acceleration) EM waveguide of core radius a , radius b of circular hole at the center of the disk, disk-separation (cavity height) d , and disk thickness s .

(c) Figure 13.13 shows the dispersion (ω, k_g) diagrams for an acceleration waveguide (solid curves) and for its equivalent uniform waveguide (dotted curve). The uniform waveguide curve is a hyperbola with only one cutoff frequency ω_c and its pass band ranges in frequency from $\omega = \omega_c$ to $\omega = \infty$, while its stop band has frequencies from $\omega = 0$ to $\omega = \omega_c$. The acceleration waveguide features an infinite number of pass bands and stop bands, but only the lowest pass band for $\omega_{c1} < \omega < \omega_{c2}$ in the transverse magnetic TM mode can be used for charged particle acceleration. The lowest cutoff frequency ω_{c1} of the acceleration waveguide in the TM mode is equal to the cutoff frequency ω_c of the equivalent uniform waveguide.

(d) Figure 13.13 depicts dispersion (ω, k_g) diagrams for an acceleration (disk-loaded) waveguide (solid curves) and its equivalent (same core radius a) transmission (uniform) waveguide (dotted curve). The dispersion diagram for the equivalent uniform waveguide is a simple hyperbola with its vertex defining the cutoff frequency ω_c and the center of the hyperbola coinciding with the origin of the Cartesian (k_g, ω) coordinate system.

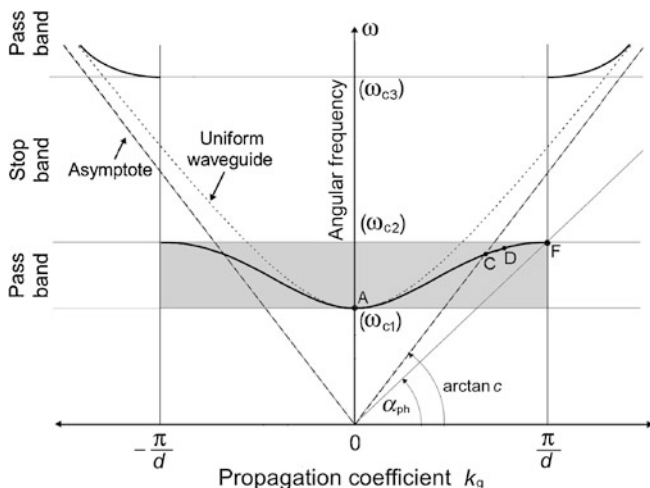


Fig. 13.13 Dispersion diagram (ω, k_g) for a disk-loaded (acceleration) EM waveguide. For comparison the dispersion diagram for an equivalent (same core radius a) uniform circular EM waveguide is shown in the background with the *dotted curve* and its asymptotes are plotted with *dashed straight lines*. The first Brillouin zone for $(\omega_{c1}^{TM})_{01} \leq \omega \leq (\omega_{c2}^{TM})_{01}$ and $-\pi/d \leq k_g \leq \pi/d$ is shown in *grey color*. Electron acceleration is carried out with k_g and ω in the first Brillouin zone for special transverse magnetic mode TM_{mn} for $m = 0$ and $n = 1$

The dispersion diagram for the acceleration waveguide is considerably more complicated than that of its equivalent uniform waveguide. It features an infinite number of pass bands and stop bands that are limited by cutoff frequencies ω_{cN} and Brillouin zones limited by distinct wavenumbers k_g in increments of π/d with d the separation between two successive disks in the waveguide, as shown in Fig. 13.12.

Brillouin zones play an important role in many types of periodic structures in physics and engineering, such as, for example, models governing x-ray, neutron, and electron wave propagation in crystals where the crystal lattice represents a typical periodic structure. The dispersion diagram (E, k) for a crystal can be plotted in the form of energy E against wave number k for: (i) a free electron resulting in a dispersion diagram (E, k) similar to the dispersion diagram (ω, k_g) for a uniform waveguide and (ii) for an electron in a monoatomic linear lattice of lattice constant d , resulting in a dispersion diagram (E, k) similar to the dispersion diagram (ω, k_g) for a disk-loaded EM waveguide.

Charged particle acceleration is carried out only in the first Brillouin zone in the k_g range extending from $-\pi/d$ to π/d and in the TM_{01} mode with the cutoff angular frequency $(\omega_{c1}^{TM})_{01}$ that is identical to the cutoff frequency $(\omega_c^{TM})_{01}$ of the equivalent uniform (transmission) waveguide.

As an RF wave propagates through a disk-loaded waveguide, it is partially reflected at each disk, the reflected fraction depending on the relative magnitudes of the wavelength λ_g and the perturbation parameter $(a - b)$ with a the radius of the uniform waveguide and b the radius of the disk opening, as shown in Fig. 13.12. When radius b is comparable to a , i.e. $a - b \ll a$, the perturbation caused by the

disks is small, the reflection of the radiofrequency wave at the disk is negligible, and the disk-loaded waveguide behaves much like uniform waveguide with radius a .

In general, when $\lambda_g \gg (a - b)$, corresponding to $k_g \ll (a - b)$, the fraction of wave reflection at disks is small. The dispersion relationship of the disk-loaded waveguide then tends to that of a uniform waveguide and the cut-off frequency ω_c at $k_g = 0$ of the disk-loaded waveguide is identical to that of a uniform waveguide. However, with increasing k_g , corresponding to a decreasing λ_g since $k_g = 2\pi/\lambda_g$, the fraction of the reflected wave at each disk steadily increases, and so does the interference between the incident and reflected wave, until at $\lambda_g = 2d$ or $k_g = \pi/d$ purely stationary waves are setup in each cavity defined by the disk separation d . In this case, the cavities are in resonance, only stationary waves are present in the cavities, and there is no energy propagation possible from one cavity to another. This implies that the group velocity v_{gr} at point F of Fig. 13.13 is zero ($v_{gr} = 0$) and the tangent to the $(\omega - k_g)$ dispersion relationship at $k_g = \pi/d$ must be horizontal, in contrast to the uniform waveguide where the tangent to the dispersion relationship is horizontal only at $k_g = 0$, and then with an increasing k_g its slope steadily rises to its limit of c as $k_g \rightarrow \infty$.

For both the uniform as well as the disk-loaded waveguide the group velocity v_{gr} is zero at the cutoff frequency corresponding to the propagation coefficient $k_g = 0$ (point A in Fig. 13.13). As k_g increases from 0, the group velocity for uniform waveguide steadily increases until at $k_g = \infty$ it reaches a value of c . For a disk-loaded waveguide, on the other hand, with k_g increasing from zero, v_{gr} first increases, reaches a maximum smaller than c , and then decreases until at $k_g = \pi/d$ it reverts to $v_{gr} = 0$.

The dispersion curve for a disk-loaded waveguide thus deviates from that of a uniform waveguide and, as shown in Fig. 13.13, exhibits discontinuities at $k_g = n\pi/d$, with n an integer. The discontinuities in frequency ω separate regions of ω that can pass through the disk-loaded waveguide (pass bands) from regions of ω that cannot pass (stop bands). Two such bands are shown in Fig. 13.13: a pass band for frequencies ω between (ω_{c1}) and (ω_{c2}) in light grey color, and a stop band for frequencies between (ω_{c2}) and (ω_{c3}) . The region between $k = -\pi/d$ and $k = +\pi/d$ is called the first Brillouin zone and energy E versus wave number k diagram is called the Brillouin diagram.

A closer look at the disk-loaded dispersion relationship curve of Fig. 13.13 shows the following features:

- (1) For angular frequencies ω in the range $(\omega_{c1}) \leq \omega \leq (\omega_{c2})$ in the first pass band (also called the first Brillouin zone) frequencies in the region between points C and F on the dispersion plot have a phase velocity v_{ph} smaller than or equal to c as a result of $\alpha_{ph} \leq \arctan c$. Loading the uniform waveguide with disks thus decreases the phase velocity below c for certain angular frequencies ω , opening the possibility for electron acceleration with radiofrequency microwaves.
- (2) Frequency (ω_{c2}) clearly has a phase velocity v_{ph} which is smaller than c ; yet, the frequency (ω_{c2}) would not be suitable for electron acceleration despite $v_{ph} < c$ because, simultaneously, at frequency (ω_{c2}) , the group velocity of the

wave is zero ($v_{gr} = 0$; tangent to dispersion curve at point F is horizontal). Since the velocity v_{en} of energy flow in a waveguide equals to group velocity v_{gr} of microwaves propagating in the waveguide, it is obvious that for $v_{gr} = v_{en} = 0$ energy transfer from the microwave to the accelerated electrons is not impossible and thus points such as point F will not be suitable for acceleration despite satisfying the necessary (but not sufficient) condition $v_{ph} < c$.

- (3) However, there are frequencies in the frequency pass band between (ω_{c1}) and (ω_{c2}) , such as angular frequency ω for point D on the dispersion plot in Fig. 13.13, for which $v_{ph} \lesssim c$ and at the same time $v_{gr} > 0$, and these frequencies are suitable for electron acceleration.
- (4) In practice, frequencies which give v_{ph} smaller than yet close to c , i.e., $v_{ph} \lesssim c$, are used for electron acceleration in disk-loaded waveguides. The group velocities for these frequencies between points C and D on the dispersion curve of Fig. 13.13 are non-zero but nonetheless very low, so that for a typical accelerating waveguide the phase velocity is about two orders of magnitude larger than the group velocity ($v_{ph}/v_{gr} \approx 100$).

13.11 Capture Condition

13.11.Q1

(287)

Several conditions must be met for particle acceleration with microwaves in an acceleration waveguide of a linear accelerator (linac). Some of these conditions are general and valid for all particle accelerators, others are specific to linear accelerators only.

- (a) State and briefly explain at least three conditions for particle acceleration that are common to all accelerators.
- (b) State and briefly explain at least three conditions for particle acceleration that are specific to particle acceleration in acceleration waveguide of a linac.
- (c) Derive the capture condition for particle acceleration with microwaves in an acceleration waveguide of a linac.
- (d) Determine the limits for the minimum electric field amplitude $(E_{z0})_{min}$ of the capture condition as $\beta_0 \rightarrow 0$ and $\beta_0 \rightarrow 1$ and explain the results.
- (e) Sketch the minimum electric field amplitude $(E_{z0})_{min}$ against electron injection velocity β_0 for the capture condition and microwaves of frequency $\nu = 2856$ MHz in an acceleration waveguide of a clinical linac.

SOLUTION:

- (a) Three general conditions for particle acceleration in any type of particle accelerator are:

(1) Particle to be accelerated must be charged. All particles generated by accelerators are accelerated by electric fields, be it electrostatic fields in electrostatic accelerators or electromagnetic fields in cyclic accelerators. Particles with positive charge move in the direction of electric field, negatively charged particles move in direction opposite to the electric field. Neutral particles cannot be accelerated with electric fields.

(2) Electric field used for particle acceleration must be oriented in the direction of propagation of the charged particle for positively charged particles and in direction opposite to propagation for negatively charged particles.. In a particle accelerator the trajectory of the accelerated particle is: (i) linear, (ii) circular, or (iii) in the shape of racetrack.

- (i) Linear trajectory is found in x-ray tube, neutron generator, Van de Graaff generator, and linear accelerator.
- (ii) Circular trajectory is found in betatron, cyclotron, and microtron.
- (iii) Racetrack trajectory is used in microtron and synchrotron.

(3) Particle must be accelerated in vacuum rather than in a dielectric material to avoid deleterious collisions between the accelerated particle and atoms of the medium in which the accelerated particle is traveling.

(b) Three conditions that must be met for acceleration of electrons in an acceleration electromagnetic (EM) waveguide of a linear accelerator (linac).

(1) The radiofrequency (RF) mode to be used for electron acceleration in an EM waveguide must provide a finite, non-zero value electric field component \mathcal{E}_{z0} at $r = 0$ to enable the electron acceleration along the central axis of the waveguide. Of the three special modes of relevance to RF propagation:

- (i) Transverse electric (TE_{mn}) mode for which $\mathcal{E}_z = 0$ everywhere in waveguide core,
- (ii) Transverse magnetic (TM_{mn}) mode for which $\mathcal{B}_z = 0$ everywhere in the waveguide core,
- (iii) Transverse electromagnetic (TEM_{mn}) mode for which $\mathcal{E}_z = \mathcal{B}_z = 0$,

only two modes (TE and TM) can propagate in an EM waveguide, and only one (TM) of these two modes produces non-zero electric field along the central axis of the waveguide, i.e., $\mathcal{E}_z|_{r=a} \neq 0$. Thus, TM_{mn} modes are used for electron acceleration and, of all possible m and n values, the lowest ones are used for electron acceleration ($m = 0$ and $n = 1$). Of all possible angular frequencies ω , the angular frequency used for acceleration must be in the first Brillouin zone between cutoff frequencies ω_{c1} and ω_{c2} and of such magnitude that produces a phase velocity v_{ph} less than and approximately equal to speed of light c in vacuum and a group velocity v_{gr} larger than zero.

While TM_{mn} modes can propagate in a uniform EM waveguide, the phase velocity v_{ph} in a uniform waveguide exceeds c making uniform waveguides unsuitable

for charged particle acceleration. To achieve $v_{\text{ph}} \leq c$ one uses a uniform waveguide modified with periodic perturbations (disks or irises) that effectively decrease v_{ph} to a level below c and this type of waveguide is referred to as disk-loaded or acceleration waveguide.

(2) To allow the RF wave to accelerate electrons the phase velocity v_{ph} of the RF wave must be equal to the particle velocity v_{part} . Thus, the electron generated by the electron gun must be injected into the acceleration waveguide with a certain velocity v_{part} [corresponding to a certain kinetic energy $(E_K)_{\text{inj}}$] that matches the phase velocity of the RF wave. Since: (i) the accelerated particle velocity cannot exceed c and (ii) v_{part} must be matched with v_{ph} , it becomes obvious that v_{ph} of the RF wave used for particle acceleration in an acceleration waveguide should be equal or less than c , i.e., $v_{\text{ph}} \leq c$.

(3) Condition (2) states that for electron acceleration with RF fields $v_{\text{part}} \approx v_{\text{ph}}$; however, the electron is injected into the acceleration waveguide with a relatively low velocity v_{part} [that is with relatively low kinetic energy $(E_K)_{\text{inj}}$] that is substantially smaller than c and is then accelerated in the waveguide to final relativistic kinetic energy corresponding to final velocity $\sim c$. Thus, the condition $v_{\text{part}} \approx v_{\text{ph}}$ cannot be fulfilled easily at the entrance side of the waveguide.

There are two possible solutions to this problem: one is to lower the phase velocity of the RF wave v_{ph} on the electron gun side of the acceleration waveguide to obtain $v_{\text{inj}} \approx v_{\text{ph}}$ and then gradually increase the phase velocity v_{ph} toward c as the accelerated charged particle gains kinetic energy. This approach is referred to as velocity modulation of the RF wave.

The other solution is to provide sufficiently large amplitude of the electric field \mathcal{E}_z for the wave to capture the electron at the entrance to the accelerating waveguide despite its relatively low injection velocity v_0 that is significantly smaller than the phase velocity v_{ph} of the RF wave.

Of the two options, the first one is more difficult as it involves modulation of the phase velocity v_{ph} by using non-uniform cavities in the entrance section of the acceleration waveguide and uniform cavities farther down the waveguide. Early linac designs contained many cavities with varying inner diameter, aperture radius, and axial spacing; more recently, only a few cavities were used for this purpose, and currently, a single half-cavity provides the phase modulation. The improved understanding of velocity modulation has resulted in a substantial lowering of the required gun injection voltage from historical levels of above 100 kV to current levels of around 25 kV.

The second approach to $v_0 < v_{\text{ph}} \approx 0$ is based on the calculation of the minimum amplitude of the electric field $[(\mathcal{E}_z)_0]_{\text{min}}$ that still allows the RF wave to capture the electron injected with a relatively low velocity v_{inj} from the electron gun into the acceleration waveguide. The larger is $[(\mathcal{E}_z)_0]_{\text{min}}$ in the waveguide the lower is the required injection velocity or injection kinetic energy of the electron entering the waveguide. The relationship between $[(\mathcal{E}_z)_0]_{\text{min}}$ and v_0 is referred to as the capture condition for an acceleration EM waveguide and must be satisfied for the acceleration to proceed.

(c) The **capture condition** is derived from the relativistic equation of motion of the electron in the electric field with the help of two simplifying assumptions:

(1) RF wave propagates through the acceleration waveguide with a phase velocity v_{ph} approximately equal to c (i.e., $v_{\text{ph}} \approx c$).

(2) Electric field \mathcal{E}_z is in the direction of propagation and has a sinusoidal behavior in time, such that

$$\mathcal{E}_z = (\mathcal{E}_z)_0 \sin \varphi, \quad (13.302)$$

with $(\mathcal{E}_z)_0$ the amplitude of the electric field and φ the phase angle between the wave and the electron, given as:

$$\varphi = k_g z - \omega t, \quad (13.303)$$

where

ω is the angular frequency of the wave.

k_g is the waveguide wave number or propagation coefficient.

z is the coordinate along the waveguide axis.

The rate of change d/dt of phase φ with time t is from (BB) given as

$$\frac{d\varphi}{dt} = k_g \frac{dz}{dt} - \omega = k_g v_{\text{part}} - \omega = \frac{2\pi}{\lambda_g} (\beta - 1) \quad (13.304)$$

with $v_{\text{ph}} \approx c$ [assumption (1) above], $k_g = 2\pi/\lambda_g$ where λ_g is the RF wavelength, and $\beta = v_{\text{part}}/c$ is the electron velocity v_{part} normalized to speed of light c in vacuum. The relativistic equation of motion for the electron moving in the electric field \mathcal{E}_z may be written as

$$F = \frac{dp}{dt} = \frac{d}{dt} m(v)v = \frac{d}{dt} \frac{m_e \beta c}{(1 - \beta^2)^{1/2}} = e\mathcal{E} = e(\mathcal{E}_z)_0 \sin \varphi, \quad (13.305)$$

with

F force exerted on the electron by the electric field \mathcal{E}_z .

p electron momentum.

$m(v)$ mass of the electron at velocity v .

m_e electron rest mass (0.511 MeV).

Equations (13.304) and (13.305) are now simplified as follows

$$\frac{d\varphi}{dt} = a(\beta - 1) \quad (13.306)$$

and

$$\frac{d}{dt} \frac{\beta}{(1 - \beta^2)^{1/2}} = b \sin \varphi, \quad (13.307)$$

respectively, introducing parameters a and b defined as $a = 2\pi c/\lambda_g$ and $b = e(E_z)_0/(m_e c)$.

Introducing a new variable $\cos \alpha = \beta$ into (13.306) and (13.307) we get, respectively,

$$\frac{d\varphi}{dt} \equiv \frac{d\varphi}{d\alpha} \frac{d\alpha}{dt} = a(\cos \alpha - 1) \quad \text{or} \quad \frac{d\alpha}{dt} = a(\cos \alpha - 1) \frac{d\alpha}{d\varphi} \quad (13.308)$$

and

$$\frac{d \cos \alpha}{dt \sin \alpha} \equiv \frac{d}{dt} \cot \alpha \equiv \frac{d \cot \alpha}{d\alpha} \frac{d\alpha}{dt} \equiv \frac{1}{\sin^2 \alpha} \frac{d\alpha}{dt} = b \sin \alpha \quad \text{or} \quad \frac{d\alpha}{dt} = -b \sin^2 \alpha \sin \varphi. \quad (13.309)$$

After equating the two expressions above for $d\alpha/dt$, rearranging terms, and integrating over φ from initial φ_0 to φ and over α from initial α_0 to α , we get

$$\begin{aligned} -\frac{b}{a} \int_{\varphi_0}^{\varphi} \sin \varphi \, d\varphi &= \int_{\alpha_0}^{\alpha} \frac{\cos \alpha - 1}{\sin^2 \alpha} \, d\alpha \equiv \int_{\alpha_0}^{\alpha} \frac{\cos \alpha}{\sin^2 \alpha} \, d\alpha - \int_{\alpha_0}^{\alpha} \frac{d\alpha}{\sin^2 \alpha} \\ &\equiv \int_{\alpha_0}^{\alpha} \frac{d(\sin \alpha)}{\sin^2 \alpha} - \int_{\alpha_0}^{\alpha} \frac{d\alpha}{\sin^2 \alpha}, \end{aligned} \quad (13.310)$$

that results in

$$\begin{aligned} \frac{b}{a} [\cos \varphi - \cos \varphi_0] &= \left[-\frac{1}{\sin \alpha} + \cot \alpha \right]_{\alpha_0}^{\alpha} \equiv \left[\frac{\cos \alpha - 1}{\sin \alpha} \right]_{\alpha_0}^{\alpha} \\ &\equiv \left[-\frac{\sqrt{1 - \cos \alpha} \sqrt{1 - \cos \alpha}}{\sqrt{1 - \cos \alpha} \sqrt{1 + \cos \alpha}} \right]_{\alpha_0}^{\alpha} \\ &\equiv \left(\frac{1 - \cos \alpha_0}{1 + \cos \alpha_0} \right)^{1/2} - \left(\frac{1 - \cos \alpha}{1 + \cos \alpha} \right)^{1/2}. \end{aligned} \quad (13.311)$$

After inserting $\cos \alpha = \beta$ and $\cos \alpha_0 = \beta_0$, and recognizing that at the end of the acceleration process $\beta \approx 1$, we obtain

$$\cos \varphi - \cos \varphi_0 = \frac{a}{b} \left(\frac{1 - \beta_0}{1 + \beta_0} \right)^{1/2} = \frac{2\pi}{\lambda_g} \frac{m_e c^2}{e(E_z)_0} \left(\frac{1 - \beta_0}{1 + \beta_0} \right)^{1/2}, \quad (13.312)$$

where $\beta_0 = v_0/c$ with v_0 the initial (injection) velocity of the electron injected into the accelerating waveguide from the electron gun. Since the left-hand side of (13.312) cannot exceed 2, we obtain the following relationship for the capture condition

$$(\mathcal{E}_z)_0 \geq \frac{\pi m_e c^2}{\lambda_g e} \sqrt{\frac{1 - \beta_0}{1 + \beta_0}} = \frac{K}{\lambda_g} \sqrt{\frac{1 - \beta_0}{1 + \beta_0}}, \quad (13.313)$$

where $K = \pi m_e c^2 / e = 1.605 \text{ MV}$ is the capture constant of the electron in a disk-loaded acceleration waveguide. The minimum amplitude of the electric field $[(\mathcal{E}_z)_0]_{\min}$ is thus expressed as follows

$$[(\mathcal{E}_z)_0]_{\min} = \frac{K}{\lambda_g} \sqrt{\frac{1 - \beta_0}{1 + \beta_0}}. \quad (13.314)$$

Equation (13.314) is referred to as the capture condition and must be satisfied, if an electron entering the acceleration waveguide from the electron gun with initial velocity v_0 is to be captured by the radiofrequency wave that has a phase velocity close to c .

The well known relativistic relationship between the electron initial (injection) velocity β_0 and the electron initial kinetic energy $(E_K)_0$ is given as follows [see (T2.7)]

$$\beta_0 = \sqrt{1 - \frac{1}{(1 + \frac{(E_K)_0}{m_e c^2})^2}}, \quad (13.315)$$

allowing us to estimate $[(\mathcal{E}_z)_0]_{\min}$, the minimum amplitude of the radiofrequency field, for typical gun injection voltage potentials in the range from 20 keV to 100 keV.

(d) The capture condition (13.314), relating (i) minimum amplitude $[(\mathcal{E}_z)_0]_{\min}$ of electric field required to capture an electron injected into an acceleration EM waveguide and (ii) velocity β_0 of an electron injected into the waveguide from the electron gun, is given in (13.293). The range covered by the capture condition extends from 0 to 1 for normalized velocity β and the limiting values of $[(\mathcal{E}_z)_0]_{\min}$ are given as follows:

(1) The upper limit of $[(\mathcal{E}_z)_0]_{\min}$ is attained when $\beta_0 \rightarrow 0$ corresponding to $v_0 = 0$

$$\lim_{\beta_0 \rightarrow 0} [(\mathcal{E}_z)_0]_{\min} = \lim_{\beta_0 \rightarrow 0} \frac{K}{\lambda_g} \sqrt{\frac{1 - \beta_0}{1 + \beta_0}} = \frac{K}{\lambda_g} = \frac{1.605 \text{ MV}}{\lambda_g}, \quad (13.316)$$

indicating that microwaves with an electric field amplitude $(\mathcal{E}_z)_0 > 1.605 \text{ MV} / \lambda_g$ would be able to catch stationary or low kinetic energy free electrons and accelerate them to speed of light c without any velocity modulation.

The $\beta_0 \rightarrow 0$ limit, of course, begs the question on whether or not this is feasible in practice. Standard clinical linacs operate at a microwave frequency ν of 2856 MHz corresponding to microwave wavelength $\lambda_g = 10.5 \text{ cm}$ and a limit in (13.316) of $1.53 \times 10^7 \text{ V/m}$. For miniature waveguides used in specialized equipment, such as CyberKnife and Tomotherapy, the operating frequency ν is 10^4 MHz corresponding to $\lambda_g = 3 \text{ cm}$ and a limit in (13.316) of $5.35 \times 10^7 \text{ V/m}$. Currently, microwaves of

Table 13.7 Minimum electric field amplitude $[(\mathcal{E}_z)_0]_{\min}$ against initial electron velocity β_0 for the capture condition and microwave frequency of $\nu = 2856$ MHz

$\beta_0 = v_0/c$	0	0.2	0.4	0.6	0.8	1.0
$[(\mathcal{E}_z)_0]_{\min}$ (MV/m)	15.3	12.5	10.0	7.65	5.1	0

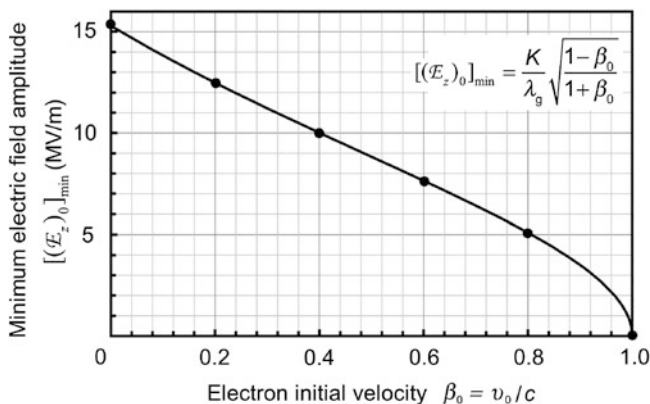


Fig. 13.14 Sketch of minimum electric field amplitude $[(\mathcal{E}_z)_0]_{\min}$ against initial electron velocity β_0 for the capture condition and microwave frequency of $\nu = 2856$ MHz. The *solid circle data points* are taken from Table 13.7

electric field amplitudes exceeding 10^7 V/m are about an order of magnitude larger than the levels available from commercial microwave power sources (klystrons and magnetrons). However, during the past four decades of commercial development of clinical linacs, the electron gun potentials have been steadily dropping from about 150 kV to about 25 kV as a result of steady improvement in design of microwave power sources.

(2) The lower limit of $[(\mathcal{E}_z)_0]_{\min}$ is attained when $\beta_0 \rightarrow 1$ corresponding to $v_0 = c$

$$\lim_{\beta_0 \rightarrow 1} [(\mathcal{E}_z)_0]_{\min} = \lim_{\beta_0 \rightarrow 1} \frac{K}{\lambda_g} \sqrt{\frac{1 - \beta_0}{1 + \beta_0}} = 0. \quad (13.317)$$

This limit is obviously trivial, since once the electron travels with velocity c there is no need for a further acceleration, at least not in the range of clinically relevant electron kinetic energies.

(e) A sketch of $[(\mathcal{E}_z)_0]_{\min}$ against β_0 for microwave frequency of $\nu = 2856$ MHz ($\lambda_g = 10.5$ cm) is prepared by using the capture condition of (13.314) and calculating several points of $[(\mathcal{E}_z)_0]_{\min} = f(\beta_0)$ for $0 \leq \beta_0 \leq 1$ in β_0 increments of 0.2. Results of the calculation are shown in Table 13.7 and Fig. 13.14 noting that the upper ($\beta_0 \rightarrow 0$) and lower ($\beta_0 \rightarrow 1$) limits in $(\mathcal{E}_z)_0$ that were discussed in (d) are also included in the table.

13.11.Q2

(288)

In a clinical linear accelerator electrons are generated by an electron gun and injected into the acceleration waveguide with a relatively low kinetic energy $(E_K)_0$ between 20 keV and 150 keV (depending on the gun design). At the end of the acceleration process the electrons exit the acceleration waveguide with kinetic energy E_K between 4 MeV and 25 MeV (depending on waveguide design). Most modern waveguides do not use phase velocity modulation for capturing electrons injected from the gun into the acceleration waveguide; rather, they rely on the capture condition and employ sufficiently high electric field amplitude \mathcal{E}_z of the accelerating radio-frequency (RF) fields to capture the injected electrons and accelerate them to the desired final kinetic energy.

- (a) Calculate the minimum injection kinetic energy $[(E_K)_0]_{\min}$ of electrons in an acceleration waveguide with constant phase velocity v_{ph} , electric field amplitude $(\mathcal{E}_z)_0 = 8 \times 10^6$ V/m, and microwave frequency $\nu = 2856$ MHz.
- (b) Express the capture condition in the form $[(\mathcal{E}_z)_0]_{\min}$ as a function of the injected electron kinetic energy $(E_K)_0$ and:
- (1) Prepare a table listing $[(\mathcal{E}_z)_0]_{\min}$ of the capture condition (see Prob. 287) for microwaves of frequency $\nu = 2856$ MHz and the following kinetic energies $(E_K)_0$ in MeV of an electron injected into the acceleration waveguide: 0.01, 0.1, 1, 10, and 100.
 - (2) Determine two limits of interest on $[(\mathcal{E}_z)_0]_{\min}$ for $(E_K)_0 \rightarrow 0$ and $(E_K)_0 \rightarrow \infty$.
 - (3) Plot the tabulated data as solid circle data points on a graph of $[(\mathcal{E}_z)_0]_{\min}$ against $(E_K)_0$ with $[(\mathcal{E}_z)_0]_{\min}$ on the ordinate axis (linear scale) and $(E_K)_0$ on the abscissa axis (logarithmic scale). Also plot on the graph with an open circle the result of the $[(E_K)_0]_{\min}$ calculation carried out in (a).
- (c) Calculate the minimum electric field amplitude $[(\mathcal{E}_z)_0]_{\min}$ required for an electron acceleration waveguide operated with constant phase velocity v_{ph} , final electron kinetic energy of 6 MeV, electron injection kinetic energy $(E_K)_0$ of 20 keV, and microwave frequency $\nu = 10^4$ MHz.
- (d) Comment on the dependence of the minimum electric field amplitude $[(\mathcal{E}_z)_0]_{\min}$ on: (1) wavelength λ_g and frequency ν of microwaves used for acceleration of electrons with no velocity modulation and (2) velocity β_0 and kinetic energy $(E_K)_0$ of electrons injected into the acceleration waveguide for acceleration without velocity modulation of microwaves.

SOLUTION:

(a) The minimum injection kinetic energy $(E_K)_{\min}$ is calculated from the capture condition (13.314) expressed in Prob. 287 as follows

$$[(\mathcal{E}_z)_0]_{\min} = \frac{K}{\lambda_g} \sqrt{\frac{1 - \beta_0}{1 + \beta_0}}, \quad (13.318)$$

where

$[(\mathcal{E}_z)_0]_{\min}$ is the minimum microwave electric field amplitude required for capturing an electron injected into the acceleration waveguide with initial normalized velocity β_0 .

K is the capture constant of the electron $K = \pi m_e c^2 / e = 1.605 \text{ MV}$.

λ_g is the wavelength of the microwaves used for electron acceleration in the waveguide.

β_0 is the normalized initial (injection) velocity of the electron injected into the waveguide.

In this problem, $(\mathcal{E}_z)_0$ in (13.318) is known ($8 \times 10^6 \text{ V/m}$) and we are looking first for the minimum required normalized velocity $(\beta_0)_{\min}$ and then for minimum required kinetic energy $(E_K)_{\min}$ that satisfies (13.318) for the given electric field amplitude $(\mathcal{E}_z)_0$. We write (13.318) as

$$(\mathcal{E}_z)_0 = \frac{K}{\lambda_g} \sqrt{\frac{1 - (\beta_0)_{\min}}{1 + (\beta_0)_{\min}}} \quad \text{or} \quad \left[\frac{\lambda_g}{K} (\mathcal{E}_z)_0 \right]^2 \equiv \kappa^2 = \frac{1 - (\beta_0)_{\min}}{1 + (\beta_0)_{\min}}, \quad (13.319)$$

where we introduce a new constant κ for the problem at hand

$$\kappa = \frac{\lambda_g (\mathcal{E}_z)_0}{K} = \frac{c (\mathcal{E}_z)_0}{v K} = \frac{(3 \times 10^8 \text{ m/s}) \times (8 \times 10^6 \text{ V/m})}{(2856 \times 10^6 \text{ s}^{-1}) \times (1.605 \times 10^6 \text{ V})} = 0.524. \quad (13.320)$$

Solving (13.319) for $(\beta_0)_{\min}$ we get

$$(\beta_0)_{\min} = \frac{1 - \kappa^2}{1 + \kappa^2} = \frac{1 - 0.524^2}{1 + 0.524^2} = 0.569 \quad (13.321)$$

for the minimum normalized velocity $(\beta_0)_{\min}$ of an electron injected into the acceleration waveguide in which the accelerating microwave electric field amplitude $(\mathcal{E}_z)_0$ is 8 MV/m .

A $(\beta_0)_{\min}$ of 0.569 corresponds to the following minimum kinetic energy $(E_K)_{\min}$ of the electron injected into the acceleration waveguide

$$\begin{aligned} (E_K)_{\min} &= m_e c^2 \left(\frac{1}{\sqrt{1 - (\beta_0)_{\min}^2}} \right) = (0.511 \text{ MeV}) \times \left(\frac{1}{\sqrt{1 - 0.569^2}} - 1 \right) \\ &= 0.110 \text{ MeV}. \end{aligned} \quad (13.322)$$

Thus, the minimum required kinetic energy $(E_K)_{\min}$ that an electron must possess to be captured by microwaves of frequency $\nu = 2856$ MHz and electric field amplitude $(\mathcal{E}_z)_0 = 8$ MV/m upon its injection from the electron gun into the acceleration waveguide is 110 keV.

(b) The minimum electric field amplitudes $[(\mathcal{E}_z)_0]_{\min}$ of $\nu = 2856$ MHz microwaves that are just high enough to capture electrons of a given kinetic energy $(E_K)_0$ injected into an acceleration waveguide are determined using the capture condition (T13.110) expressed in the form $[(\mathcal{E}_z)_0]_{\min}$ as a function of $(E_K)_0$ rather than β_0 .

The modification of the capture condition from the β_0 to $(E_K)_0$ dependence is simple, since β_0 and $(E_K)_0$ are related through the following relativistic expressions (T2.7)

$$(E_K)_0 = m_e c^2 \left[\frac{1}{\sqrt{1 - (\beta_0)^2}} - 1 \right] \quad \text{or} \quad \beta_0 = \sqrt{1 - \frac{1}{\left[1 + \frac{(E_K)_0}{m_e c^2}\right]^2}}, \quad (13.323)$$

where $m_e c^2$ is the rest energy of the electron (0.511 MeV).

Insertion of (13.323) into the capture condition (13.318) results in the following expression for the capture condition

$$[(\mathcal{E}_z)_0]_{\min} = \frac{K}{\lambda_g} \sqrt{\frac{1 - \sqrt{1 - \frac{1}{\left[1 + \frac{(E_K)_0}{m_e c^2}\right]^2}}}{1 + \sqrt{1 - \frac{1}{\left[1 + \frac{(E_K)_0}{m_e c^2}\right]^2}}}}. \quad (13.324)$$

- (1) Equation (13.324) was used to calculate $[(\mathcal{E}_z)_0]_{\min}$ as a function of $(E_K)_0$ data presented in Table 13.8 and shown with solid circles in Fig. 13.15. The limit of $[(\mathcal{E}_z)_0]_{\min}$ for $(E_K)_0 \rightarrow 0$ is K/λ_g and the limit of $[(\mathcal{E}_z)_0]_{\min}$ for $(E_K)_0 \rightarrow \infty$ is 0.
- (2) The two limits of (13.324) for $(E_K)_0 \rightarrow 0$ and $(E_K)_0 \rightarrow \infty$ corresponding to limits $\beta_0 \rightarrow 0$ and $\beta_0 \rightarrow 1$, respectively, are

$$\begin{aligned} \lim_{(E_K)_0 \rightarrow 0} [(\mathcal{E}_z)_0]_{\min} &= \lim_{\beta_0 \rightarrow 0} [(\mathcal{E}_z)_0]_{\min} = \lim_{\nu_0 \rightarrow 0} [(\mathcal{E}_z)_0]_{\min} \\ &= \frac{K}{\lambda_g} = \frac{1.605 \times 10^6 \text{ V}}{10.5 \times 10^{-2} \text{ m}} = 15.3 \text{ MV/m} \end{aligned} \quad (13.325)$$

and

$$\lim_{(E_K)_0 \rightarrow \infty} [(\mathcal{E}_z)_0]_{\min} = \lim_{\beta_0 \rightarrow \infty} [(\mathcal{E}_z)_0]_{\min} = \lim_{\nu_0 \rightarrow \infty} [(\mathcal{E}_z)_0]_{\min} = 0. \quad (13.326)$$

- (3) The data of Table 13.8 for 2856 MHz microwaves are plotted in Fig. 13.15 with solid circles on a semi-logarithmic plot of the form $(\mathcal{E}_z)_0$ on the ordinate (linear scale: y axis) against $(E_K)_0$ on the abscissa (logarithmic scale: x

Table 13.8 Minimum electric field amplitude $[(\mathcal{E}_z)_0]_{\min}$ of $\nu = 2856$ MHz microwaves against kinetic energy $(E_K)_0$ calculated using (13.324) for various incident kinetic energies $(E_K)_0$ of electrons injected into an acceleration waveguide

$(E_K)_0$ (MeV)	0	0.001	0.01	0.1	1.0	10	100	∞
$[(\mathcal{E}_z)_0]_{\min}$ (MV/m)	15.3	14.4	12.6	8.26	2.66	0.38	0.004	0

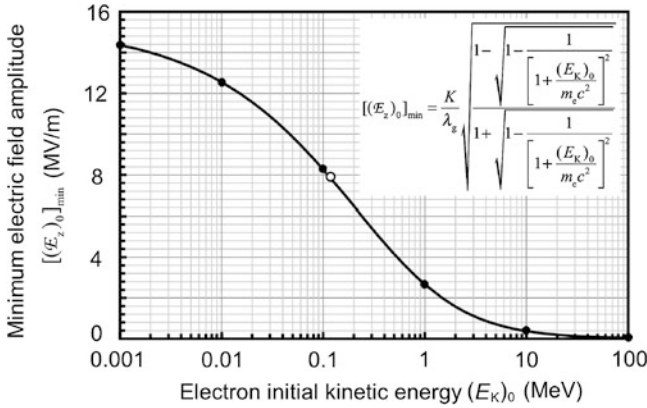


Fig. 13.15 Minimum electric field amplitude $[(\mathcal{E}_z)_0]_{\min}$ of $\nu = 2856$ MHz microwaves plotted against kinetic energy $(E_K)_0$ of electrons injected into an acceleration waveguide for the capture condition (13.324). Solid circles represent data presented in Table 13.8; the open circle represents the electron injection kinetic energy calculated in (a) for $[(\mathcal{E}_z)_0]_{\min} = 8$ MV/m

axis). The open circle on the graph represents the result of the $(E_K)_0$ calculation for $[(\mathcal{E}_z)_0]_{\min} = 8 \times 10$ MV/m.

(c) The minimum electric field amplitude $[(\mathcal{E}_z)_0]_{\min}$ of $\nu = 10^4$ MHz ($\lambda_g = 3$ cm) microwaves that is just high enough to capture electrons of kinetic energy $(E_K)_0 = 25$ keV = 0.025 MeV injected into a miniature acceleration waveguide is determined using the capture condition (13.324) as follows

$$\begin{aligned}
 [(\mathcal{E}_z)_0]_{\min} &= \frac{K}{\lambda_g} \sqrt{\frac{1 - \sqrt{1 - \frac{1}{[1 + \frac{(E_K)_0}{m_e c^2}]^2}}}{1 + \sqrt{1 - \frac{1}{[1 + \frac{(E_K)_0}{m_e c^2}]^2}}}} \\
 &= \frac{1.605 \times 10^6 \text{ V}}{3 \times 10^{-2} \text{ m}} \times \sqrt{\frac{1 - \sqrt{1 - \frac{1}{[1 + \frac{20 \times 10^3}{0.511 \times 10^6}]^2}}}{1 + \sqrt{1 - \frac{1}{[1 + \frac{20 \times 10^3}{0.511 \times 10^6}]^2}}}
 \end{aligned}$$

$$\begin{aligned}
&= \left[53.5 \times 10^6 \frac{\text{V}}{\text{m}} \right] \times \sqrt{\frac{1 - 0.272}{1 + 0.272}} \\
&= \left[53.5 \times 10^6 \frac{\text{V}}{\text{m}} \right] \times 0.757 = 40 \text{ MV/m}. \quad (13.327)
\end{aligned}$$

(d) As seen from the capture condition (13.318) and the modified capture condition (13.324), the minimum electric field amplitude $[(\mathcal{E}_z)_0]_{\min}$ is inversely proportional to microwave wavelength λ_g or proportional to microwave frequency ν since $\nu = c/\lambda_g$. Thus, for the same electron injection velocity β_0 or same injection kinetic energy $(E_K)_0$ the minimum electric field amplitude $[(\mathcal{E}_z)_0]_{\min}$ increases with microwave frequency ν . This means that a miniature waveguide operated in the X band at 10^4 MHz ($\lambda_g = 3$ cm) has by factor of $10.5/3 = 3.5$ larger $[(\mathcal{E}_z)_0]_{\min}$ than a standard linac acceleration waveguide operating in the S band at a frequency of $\nu = 2856$ MHz corresponding to a wavelength of $\lambda_g = 10.5$ cm.

As also seen from the capture condition of (13.318) and modified capture condition of (13.324), for a given microwave wavelength λ_g or frequency ν , the maximum in $[(\mathcal{E}_z)_0]_{\min} = K/\lambda_g$ occurs as $\beta_0 \rightarrow 0$ corresponding to $(E_K)_0 \rightarrow 0$. Furthermore, as β_0 [i.e., $(E_K)_0$] increase from zero, $[(\mathcal{E}_z)_0]_{\min}$ decreases from K/λ_g and approaches zero as $\beta_0 \rightarrow 1$ corresponding to $(E_K)_0 \rightarrow \infty$.

Chapter 14 consists of **12 problems** spread over 6 sections that deal with practical aspects of particle accelerators in medicine. Many types of particle accelerators were built for nuclear physics and particle physics research and most of them have also found some use in medicine, mainly but not solely for treatment of cancer. Two categories of particle accelerator are known: electrostatic and cyclic.

The best-known examples of electrostatic accelerator are the x-ray tube and the neutron generator. Three types of x-ray tube (Crookes tube, Coolidge tube, field emission carbon nanotube) are covered in this chapter. Cyclic accelerators are divided into two categories: linear and circular. Many types of circular accelerator have been designed for research purposes and most are also used in medicine, such as betatron, microtron, cyclotron, and synchrotron.

Of all cyclic accelerators, the linear accelerator (linac) is by far the most important and most widely used accelerator in medicine because of its versatility and compact design. Modern radiotherapy achieved its successes as a result of the advances that were introduced during the past few years in the linear accelerator technology and computerization, making the dose delivery extremely sophisticated and heavily dependent on skills of the radiotherapy team consisting of radiation oncologist, medical physicist, radiation dosimetrist, and treatment technologist.

Section 14.1 concentrates on basic characteristics of particle accelerators and Sect. 14.2 deals with practical use of x rays. Practical considerations in production of x rays are covered in Sect. 14.3, while Sect. 14.4 consists of several problems on traditional sources of x rays. Section 14.5 concentrates on circular accelerators and covers the betatron, microtron, yclotron, synchrotron, and synchrotron light source; all machines that have been or are used in medicine. The chapter concludes with a large section covering various practical issues related to linear accelerators (linacs) used in radiotherapy for generation of megavoltage xray and electron beams.

14.1 Basic Characteristics of Particle Accelerators

14.1.Q1

(289)

Numerous types of accelerator have been built for basic research in nuclear physics and high-energy physics and most of them have been adapted for at least some limited use in radiotherapy.

-
- (a) State the three basic physical conditions that must be met for particle acceleration in an accelerator.
 - (b) State the two major classes of particle accelerator and briefly explain the main characteristics of each class.
 - (c) Provide a table that lists: (i) Most important accelerators in physics, (ii) Their inventor, if known, (iii) Year of invention, (iv) Particles accelerated by the accelerator, (v) Is or was the particular accelerator used in radiotherapy?
 - (d) Summarize the list of most important accelerators in physics in a classification diagram format.

SOLUTION:

(a) Irrespective of the accelerator type, three basic physical conditions must be met for particle acceleration:

- (1) Particle to be accelerated must be charged (either positively or negatively).
- (2) The accelerator must provide electric field for particle acceleration.
- (3) The electric field used for particle acceleration must be provided in the direction of particle motion.

The various types of particle accelerators differ in the way they produce the accelerating electric field and in how the field acts on the charged particles to be accelerated in the machine.

(b) As far as the accelerating electric field is concerned, there are two main classes of accelerator: (1) electrostatic and (2) cyclic.

(1) In *electrostatic accelerators* the particles are accelerated by applying an electrostatic electric field through a voltage difference, constant in time, whose value fixes the value of the final kinetic energy of the accelerated particle. Since the electrostatic fields are conservative, the kinetic energy that the particle can gain depends only on the point of departure and point of arrival and, hence, cannot be larger than the potential energy corresponding to the maximum voltage drop existing in the machine. Kinetic energy that an electrostatic accelerator can reach is limited by the

Table 14.1 Some characteristics of most important particle accelerators in physics

Electrostatic accelerators	Inventor(s)	Year of invention	Particles accelerated	Used in radiotherapy
X-ray machine	William Crookes William Coolidge	~1872 1913	Electrons	YES
Neutron generator	–	–	Deuteron	YES
Van de Graaff generator	Van de Graaff	1929	Electrons Protons	YES
Cockroft-Walton generator	John D. Cockroft Ernest T.S. Walton	1932	Protons	No
Cyclic accelerators				
Linear accelerator	–	–	Electrons Protons	YES
Betatron	Donald Kerst	1940	Electrons	YES
Microtron	Vladimir Veksler	1950	Electrons	YES
Cyclotron	Leo Szilard Ernest Lawrence	1932	Protons Heavier ions	YES
Synchrocyclotron	Edwin McMillan	1952	Protons Heavier ions	NO
Synchrotron	Vladimir Veksler Edwin McMillan	~1944	Electrons Protons	YES

discharges that occur between the high voltage terminal and the walls of the accelerator chamber when the voltage drop exceeds a certain critical value (typically 1 MV).

(2) The electric fields used in *cyclic accelerators* are variable and non-conservative, associated with a variable magnetic field and resulting in some close paths along which the kinetic energy gained by the particle differs from zero. If the particle is made to follow such a closed path many times over, one obtains a process of gradual acceleration that is not limited to the maximum voltage drop existing in the accelerator. Thus, the final kinetic energy of the particle is obtained by submitting the charged particle to the same, relatively small, potential difference a large number of times, each cycle adding a small amount of energy to total kinetic energy of the particle.

Cyclic accelerators fall into two main categories: *linear* and *circular*, depending on particle's trajectory during the acceleration. In a linear accelerator the particle undergoes rectilinear motion, while in a circular accelerator the particle's trajectory is circular. All cyclic accelerators except for the linear accelerator fall into the category of circular accelerator.

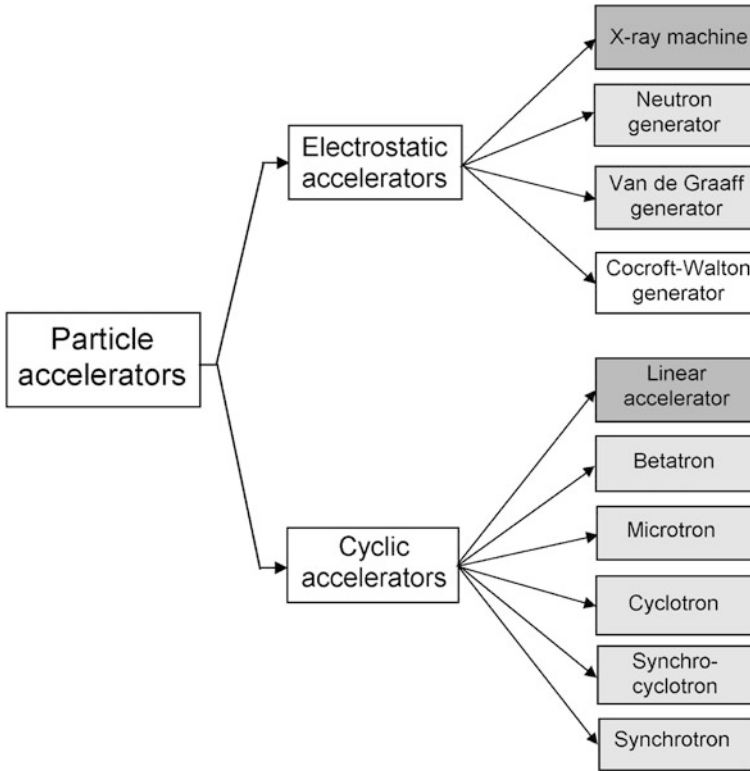


Fig. 14.1 Classification diagram of particle accelerators of importance in physics and medical physics. Accelerators used in medicine in addition to physics are shown with *grey* background; the two most common machines (x-ray machine and linear accelerator) are shown in *darker grey* color

Examples of electrostatic accelerators used in medicine are: superficial and orthovoltage x-ray machines and neutron generators. In the past, Van de Graaff accelerators have been used for megavoltage radiotherapy, however, their use was discontinued with the advent of first the betatron and then the linear accelerator. For medical use, the best-known example of a cyclic accelerator is the linear accelerator (linac); all other examples fall into the circular accelerator category and are the microtron, betatron, cyclotron, and synchrotron.

(c) A list of most important particle accelerators in physics is given in Table 14.1.

(d) Charged particle accelerators are divided into two main categories: electrostatic and cyclic and each of the two categories is subdivided further into several distinct subgroups depending on the specific technique they use for particle acceleration. The classification diagram for most important particle accelerators is given in Fig. 14.1.

14.2 Practical Use of X Rays

14.2.Q1

(290)

The serendipitous discovery of x rays by Röntgen in 1895 ushered in the era of modern physics and spawned two new medical specialties and a new physics specialty.

- (a) Name and briefly describe the three new specialties resulting from the discovery of x rays.
- (b) Two other radiation physics discoveries soon after Röntgen's discovery of x rays in 1895 also made a significant contribution to science in general and medicine in particular. Name and briefly discuss the two discoveries.
- (c) X rays are not only used in science and medicine, they are also heavily used in industry and in many other aspects of modern life. List and briefly discuss at least five areas of x ray use in industry and modern life.
- (d) Three areas of x-ray physics: (1) x-ray crystallography, (2) x-ray spectroscopy, and (3) x-ray astronomy became scientific specialties in their own right. Briefly discuss the three scientific specialties.

SOLUTION:

(a) The usefulness of x rays for medical applications in diagnosis and treatment of human disease became apparent within a few weeks after Wilhelm Röntgen's discovery of x rays in 1895. First came the use of x rays for imaging of diseased organs, for locating foreign objects imbedded in tissues (gun shot wounds) and for identifying broken bones, eventually leading to the medical specialty of diagnostic radiology.

Concurrently with the development of the x-ray imaging modality, attempts were made to use x rays for treatment of disease, eventually leading to the medical specialty of radiotherapy, also called therapeutic radiology or radiation oncology.

From their early beginnings both diagnostic radiology as well as radiation oncology relied heavily on physicists for routine use of radiation and for developments of new techniques and equipment. The involvement of physicists in the two new medical specialties eventually lead to a specialty of physics referred to as medical physics. During the past two decades medical physics has undergone a tremendous evolution, progressing from a branch of applied science on the fringes of physics into an important mainstream discipline that can now be placed on equal footing with other more traditional branches of physics such as nuclear physics, particle physics, and condensed matter physics.

Initially, most technological advances in medical use of ionizing radiation were related to:

- (1) Improvements in efficient x-ray beam delivery.
- (2) Development of analog imaging techniques.
- (3) Optimization of image quality with concurrent minimization of delivered dose.
- (4) Increase in beam energies for radiotherapy.

During the past two decades, on the other hand, most developments in radiation medicine were related to integration of computers in imaging, development of digital diagnostic imaging techniques, and incorporation of computers into therapeutic dose delivery with high-energy linear accelerators. Radiation dosimetry and treatment planning have also undergone tremendous advances in recent years: from development of new absolute and relative dosimetry techniques to improved theoretical understanding of basic radiation interactions with human tissues, and to the introduction of Monte Carlo techniques in the determination of dose distributions resulting from penetration of ionizing radiation into tissue.

(b) Two physics discoveries, important not only for modern physics but also for radiation medicine, followed soon after Röntgen's discovery of x rays. In 1896 Henri Becquerel discovered natural radioactivity; the discovery eventually leading to the physics specialties of nuclear physics and high-energy physics and a subspecialty of diagnostic radiology referred to as nuclear medicine. In 1898 Marie Skłodowska-Curie and Pierre Curie discovered radium and the discovery led to applications of sealed radionuclides in treatment of malignant disease referred to as brachytherapy.

(c) X rays for industrial use are produced by x-ray machines, linear accelerators (also called linacs), and betatrons, depending on the x-ray energy required. Superficial and orthovoltage x rays originate in x-ray machines, x-rays in the megavoltage range of energies are produced by linear accelerators and betatrons. Industrial use of x rays covers a wide variety of purposes dealing with safety and quality assurance issues, such as:

- (1) Inspection of luggage, shoes, mail, cargo containers, etc.
- (2) Nondestructive testing and inspection of welds, cast metals, parts of automobiles and airplanes, iron reinforcement bars, cracks and pipes inside concrete structures.
- (3) Food irradiators for sterilization and pest control.
- (4) Ionizing radiation based sterilizers of surgical equipment and blood irradiators.
- (5) Small animal irradiators for radiobiological experiments.

(d) In addition to stimulating new specialties in medicine and physics, as mentioned in **(a)**, and to some extent in industry, as mentioned in **(c)**, x rays also enabled new developments in physics, chemistry, and astronomy, such as: (1) x-ray crystallography, (2) x-ray spectroscopy, and (3) x-ray astronomy.

(1) **X-ray crystallography** is a study of crystal structures through the use of x-ray diffraction techniques. X rays are very suitable for this purpose because their wavelength in the 10 keV to 100 keV energy range is of the order of typical crystalline lattice separations. An x-ray beam striking a crystalline lattice is scattered by the spatial distribution of atomic electrons and the imaged diffraction pattern provides information on the atomic or molecular structure of the crystalline sample.

In 1912 Max von Laue established the wave nature of x rays and predicted that crystals exhibit diffraction phenomena. Soon thereafter, William H. Bragg and William L. Bragg analyzed the crystalline structure of sodium chloride, derived the Bragg relationship $2d \sin \phi = m\lambda$ linking the lattice spacing d with x-ray wavelength λ , and laid the foundation for x-ray crystallography. The crystal lattice of a sample acts as a diffraction grating and the interaction of x rays with the atomic electrons creates a diffraction pattern which is related, through a Fourier transform, to the electron spectral distribution in the sample under investigation.

Instrumentation for x-ray diffraction studies consists of a mono-energetic x-ray source, a device to hold and rotate the crystal, and a detector suitable for measuring the positions and intensities of the diffraction pattern. Mono-energetic x rays are obtained by special filtration of x rays produced either by an x-ray tube or from an electron synchrotron storage ring. The basic principles of modern x-ray crystallography are essentially the same as those enunciated almost 100 years ago by von Laue and the Braggs; however, the technique received a tremendous boost by incorporation of computer technology after the 1970s, increasing significantly the accuracy and speed of the technique.

(2) **X-ray spectroscopy** is an analytical technique for determination of elemental composition of solid or liquid samples in many fields, such as material science, environmental science, geology, biology, forensic science, and archaeometry (archaeological science). The technique is divided into three related categories: the most common of them is the x-ray absorption spectrometry (also called x-ray fluorescence spectrometry), and the other two are x-ray photoelectron spectrometry and Auger spectrometry. All three techniques rely on creation of vacancies in atomic shells of the various elements in the sample under study as well as on an analysis of the effects that accompany the creation of vacancies (e.g., emission of photoelectron, emission of characteristic line spectrum, and emission of Auger electron). Like other practical emission spectroscopic methods, x-ray spectroscopy consists of three steps:

- (i) *Excitation of atoms in the sample* to produce fluorescence emission lines (or photoelectrons or Auger electrons) characteristic of the elements in the sample.
- (ii) *Measurement of intensity and energy of the emitted characteristic lines* (or electrons).
- (iii) *Conversion of measured data to concentration or mass* with the nanogram range reached with standard spectrometers.

While x-ray spectroscopy was initially used to further the understanding of x-ray absorption and emission spectra from various elements, its role now is reversed and

it is used as a non-destructive analytical tool for the purpose of chemical analysis of samples of unknown composition.

(3) **X-ray astronomy** is a relatively new branch of astronomy dealing with the study of x-ray emission from celestial objects, such as neutron stars, pulsars, and black holes. The specialty was born in 1962 when Italian-American astronomer *Riccardo Giacconi* discovered a cosmic x-ray source in the form of a compact star located in the constellation of Scorpius. For this discovery Giacconi received the 2002 Nobel Prize in Physics.

Since the x-rays emitted by celestial objects have relatively low energies of the order of a few kiloelectron volts, they cannot penetrate through the Earth's atmosphere to reach the surface of the Earth. Thus, to study these celestial rays, detectors must be taken above the Earth's atmosphere. Methods used to achieve this involve mounting x-ray detectors on rockets, balloons, or satellites. The x-ray detectors used for this purpose are either special charge-coupled devices (CCDs) or microcalorimeters.

14.3 Practical Considerations in Production of X Rays

14.3.Q1

(291)

In principle, all charged particles can emit radiation under certain conditions. In practice, however, the choice of charged particles that can produce measurable amounts of radiation of interest in medical physics, medicine, and industry is limited to light charged particles (electrons and positrons). It is well known that light charged particles interacting with an absorber (target) emit characteristic radiation and bremsstrahlung photons. However, it is less known that, when light charged particles interact with a target, other types of radiation may also be produced, depending on specific conditions related to the particle interaction with the target atoms.

Below we list 8 possible interactions between electrons and positrons with their environment that may result in emission of some sort of radiation. For each interaction state the name of inter-action and type of radiation emitted followed by a brief description of the interaction.

- (a) Rapid deceleration of energetic electrons striking an absorber (target).
- (b) Direct interaction between high-energy electron and nucleus
- (c) Deceleration of electrons in a retarding potential in vacuum.
- (d) Deceleration of electrons in patients irradiated with photon or electron beams.
- (e) Acceleration of electrons in a linac waveguide.

- (f) Curved motion of electrons in circular accelerators.
- (g) Deceleration of positrons in positron emission tomography (PET).
- (h) Atomic polarization effects when electrons move through transparent dielectric absorber.

SOLUTION:**(a) Rapid deceleration of energetic electrons striking an absorber (target).**

As energetic electrons strike an absorber (target) they penetrate the target and may experience various Coulomb-type interactions with atoms of the target. These interactions are either elastic or inelastic collisions between the incident electrons with either orbital electrons of the target or nuclei of the target. Of the four types of Coulomb interactions, inelastic collisions between incident electron and orbital electrons result in the so-called characteristic (fluorescence) x rays and inelastic collisions between incident electron and nucleus of the target result in the so-called bremsstrahlung x rays. Energy of a characteristic x-ray photon is equal to the orbital energy transition that produced the photon and this energy is characteristic of the target atom, hence the name “characteristic radiation”. Energy of bremsstrahlung photon depends on the kinetic energy of the incident electron and the strength of the Coulomb interaction between the incident electron and the nucleus.

Thus, the x-ray spectrum produced by electrons striking a target has a continuous bremsstrahlung component ranging from 0 to kinetic energy of incident electrons and superimposed on this continuous spectrum are several discrete spectral lines characteristic of the target material.

The photon spectra used in medicine for diagnosis of disease typically range from 50 kVp to 150 kVp, while x-ray spectra used in radiotherapy for treatment of disease fall into three somewhat arbitrarily defined ranges: superficial x rays from 50 kVp to 80 kVp and orthovoltage x rays from 80 kVp to 350 kVp, both types generated by x-ray machines, as well as megavoltage x rays from 4 MV to 25 MV, generated mainly by linear accelerators and less commonly by microtrons and betatrons.

(b) Direct interaction between high-energy electron and nucleus. Many types of interaction are available to energetic electrons as they penetrate a target and interact elastically or in-elastically with orbital electrons and nuclei of the target atoms. Most of these interactions are of the Coulomb type and the inelastic interactions with orbital electrons are followed by characteristic x rays, while inelastic interactions with nuclei are accompanied by bremsstrahlung x rays, as discussed in (a).

In addition to these effects, the incident electrons may also undergo direct nuclear interaction with target nuclei and precipitate emission of neutron or proton through nuclear reactions labeled as: (e, n), (e, p), and (e, np) accompanied by transmutation of the target nucleus from stable to radioactive or from highly radioactive to less radioactive or even stable. Transition from stable to radioactive state is of concern in activation of linac components in high-energy radiotherapy, while transition from

radioactive to more stable configuration is of great interest in the possible decontamination of highly radioactive waste.

The bremsstrahlung photons produced in electron–nucleus inelastic collision may also have a nuclear interaction with target nuclei of the type (γ, n) , (γ, p) , and (γ, np) , similar to direct electron interactions with target nuclei of the type (e, n) , (e, p) , and (e, np) , discussed above. These photon interactions have similar outcomes as the electron–nucleus interactions and are called photonuclear reaction or photodisintegration. In addition to these, photons may also trigger fission reactions in heavy nuclei and this type of interaction is referred to as the photofission reaction (γ, f) . Thus, direct electron–nucleus interactions and reactions between electron-generated bremsstrahlung photon and nucleus have essentially identical outcomes; however, the cross sections for photonuclear reaction are significantly larger than those for associated direct electron–nucleus reactions.

(c) Deceleration of electrons in a retarding potential in vacuum. Deceleration of electrons in a retarding potential results in microwave radiation in contrast to deceleration of light charged particles in solid targets that produces bremsstrahlung x rays. Deceleration of electrons in a retarding potential is used in magnetrons and klystrons that serve as sources of radiofrequency power and amplifiers of radiofrequency power, respectively, for particle acceleration in linear accelerator (linac), microtron, and synchrotron.

(d) Deceleration of electrons released or produced in patients irradiated with photon beams. When high-energy photon beams are used in patient irradiation, photons interact with atoms of the irradiated tissue and, in these interactions, energetic electrons (in photoelectric effect, Compton effect, pair production) and positrons (in pair production) are set in motion in tissue. As the energetic electrons and positrons travel through tissue, they experience standard Coulomb interactions with tissue atoms and in some of these interactions bremsstrahlung photons are produced. These photons carry their energy out of the irradiated volume and contribute to the unwanted total body dose that the patient receives during the treatment of localized disease.

(e) Acceleration of electrons in a linac waveguide. The electron is injected into a linac waveguide with a typical kinetic energy of 25 keV that it receives in the electron gun. In the waveguide the electron is then accelerated from 25 keV up to the nominal energy of the linac which is of the order of several MeV or even larger in research linacs. According to Larmor relationship a charged particle accelerated or decelerated will lose part of its kinetic energy in the form of photons. Thus, at least in principle, an electron following a rectilinear motion in a linac waveguide should emit some bremsstrahlung radiation during its acceleration process. It turns out, however, that the emission of this unwanted radiation is minimal and is accounted for when the total leakage radiation produced by a clinical linac is measured.

(f) Motion of electrons in circular accelerators such as betatron, microtron, and synchrotron as well as storage ring implies curved motion of charged particles in transverse magnetic field resulting in circular paths and constant acceleration.

According to Larmor relationship, this results in emission of radiation that is called synchrotron radiation or “magnetic bremsstrahlung” and is typically of lower energy than standard bremsstrahlung. In comparison with synchrotron radiation, the accelerations in production of standard bremsstrahlung are random and also much stronger.

On the one hand, in circular electron accelerators the synchrotron radiation is an unwanted result of the electron acceleration process in circular paths and, on the other hand, storage rings may be designed such that they generate synchrotron radiation for use in science and medicine.

(g) Deceleration of positrons (slowing down before annihilation) in positron emission tomography (PET) imaging studies of human organs results in unwanted stray radiation through the bremsstrahlung process between the positron and nuclei of tissue atoms. In a clinical PET test a positron-emitting radionuclide is administered to the patient by injection or inhalation. The radionuclide circulates through the bloodstream to reach a particular organ. The positrons emitted by the radionuclide have a relatively short range in tissue but most of them lose all of their kinetic energy either through collisions with orbital electrons of tissue atoms (collision loss) or nuclei of tissue atoms (radiation loss). The positron eventually annihilates with an orbital electron of a tissue atom and two annihilation quanta used for PET imaging are emitted.

(h) Atomic polarization effects when electrons move through a transparent dielectric absorber with a uniform velocity that exceeds the speed of light in the dielectric absorber result in visible light referred to as Čerenkov radiation. The efficiency for production of Čerenkov radiation is several orders of magnitude lower than the efficiency for bremsstrahlung production.

The emitted Čerenkov radiation does not come directly from the charged particle. Rather, the emission of Čerenkov radiation involves a large number of atoms of the transparent dielectric medium that become polarized by the fast charged particle moving with uniform velocity through the medium. The orbital electrons of the polarized atoms are accelerated by the fields of the charged particle and emit radiation coherently along the surface of a forward directed cone centered on the charged particle direction of motion.

14.4 Traditional Sources of X Rays

14.4.Q1

(292)

William Crookes is one of the prominent scientists of the 19th century, best known for his invention in the early 1870s of the “cathode ray” tube, now referred to as the Crookes tube. Crookes tubes were used in experimental

physics for almost 50 years and are a precursor to modern vacuum tubes and cathode ray TV tubes.

-
- (a) Describe the basic principles of the Crookes tube.
 - (b) Describe the difference between the Crookes tube and Crookes x-ray tube.
 - (c) List and briefly describe at least 3 of the many seminal physics experiments that were carried out with Crookes tubes at the end of 19th century and the beginning of 20th century.

SOLUTION:

(a) **Crookes tube** is an electric discharge tube consisting of a sealed glass envelope that is evacuated to an air pressure between 0.005 Pa (4×10^{-5} torr) and 0.1 Pa (7.5×10^{-4} torr) and incorporates two electrodes (cathode and anode) connected to an external high voltage DC power supply. During the first three decades after the invention of the Crookes tube, many important experiments were carried out with the tube, and physicists soon established that the positively charged anode attracted unknown rays (referred to as “cathode rays”) originating in the cathode. Physicists were studying the cathode rays of Crookes tubes for many years but the understanding of their exact nature eluded them until Joseph J. Thomson in 1897 established that they were a new species of particle, negatively charged, and with mass of the order of 1800 times smaller than that of the hydrogen ion. Thomson called the new particle electron and succeeded in measuring the ratio between its charge and mass.

The basic principles of Crookes tube are now understood as follows: When high voltage is applied to the tube, electric discharge in the rarefied residual air inside the tube ionizes some air molecules. Positive ions move in the electric field toward the negatively charged cathode and create more ions through collisions with air molecules. As positive ions strike the negatively charged cold cathode, electrons are released from the cathode, move toward the anode in the electric field that is present between the cathode and the anode, and strike the anode. In contrast to a hot cathode that is based on thermionic electron emission, a cold cathode of a Crookes tube emits electrons upon impact by positive ions.

(b) **Crookes x-ray tube.** There is no essential difference in design between the Crookes tube and the Crookes x-ray tube. Both terms refer to the so-called “cathode ray” tube that Crookes developed in 1870s for investigation of electrical conductivity of gases at low pressure. However, after Röntgen’s discovery of x rays, it became apparent that a Crookes tube produced not only “cathode rays” but also a “new kind of ray” that became called x ray, so the description of the Crookes apparatus was expanded to encompass the “new kind of ray” and became known as Crookes x-ray tube.

(c) Of the many discoveries that originated through experimental work based on Crookes tube, three that seem the most important and were recognized with Nobel Prize in Physics are:

- (1) *Discovery of x rays* by Wilhelm K. Röntgen in 1895 (Nobel Prize in Physics—1901).
- (2) *Discovery of electron* by Joseph J. Thomson in 1897 (Nobel Prize in Physics—1906).
- (3) *Oil-drop experiment* and determination of electron mass by Robert A. Millikan in 1913 (Nobel Prize in Physics—1923).

(1) **Discovery of x rays.** In November 1895 Wilhelm K. Röntgen, a German physicist working at the University of Würzburg, discovered serendipitously that a Crookes tube, in addition to “cathode rays”, generated a new kind of ray which penetrated the tube housing and behaved in a very peculiar fashion outside the tube. For example, the rays were inducing fluorescence in platinocyanide crystals stored on a shelf across the laboratory. They were also capable of exposing photographic film and had the ability to penetrate opaque objects including hands, feet, and other parts of the human body. Röntgen named the unknown radiation x rays and soon thereafter the “new kind of rays” were introduced in medicine for diagnostic purposes. Röntgen’s discovery ushered in the era of modern physics and revolutionized medicine by spawning three new specialties: diagnostic imaging and radiotherapy as specialties of medicine as well as medical physics as a specialty of physics. For his discovery Röntgen received many honors and awards that culminated in his receiving the inaugural Nobel Prize in Physics in 1901.

The exact nature of x rays remained a mystery for a number of years until in 1912 Max von Laue, a German physicist, showed with a crystal diffraction experiment that x rays were electromagnetic radiation similar to visible light but of much smaller wavelength. Subsequently it became apparent that when the “cathode ray” electrons strike the anode (target), they undergo interactions with orbital electrons and nuclei of the target and some of these interactions result in characteristic and bremsstrahlung photons, respectively, that form the x-ray spectrum.

(2) **Discovery of electron.** In 1897 Joseph J. Thomson, a British physicist from the Cavendish Laboratory of Cambridge University, proposed that “cathode rays” observed in Crookes tubes were actually very small constituents of atoms and called them negatively charged particles or corpuscles. This was a very bold speculation at a time when atom was considered the smallest building block of matter and, as such, indivisible. Further experiments have shown that Thomson’s speculation was correct and the negatively charged corpuscles forming cathode rays were accepted as building blocks of all atoms and were called electron. However, Thomson’s hypothesis that electrons were the only building blocks of atoms was proven wrong with the subsequent discovery of proton and neutron as additional constituents of the atom.

Thomson could not measure directly the mass m_e and charge e of the electron; however, he succeeded in determining their ratio, the specific charge of the electron

e/m_e , by measuring the deflection of electron trajectories in electric field \mathcal{E} and magnetic field \mathcal{B} both applied to a modified Crookes tube perpendicularly to the electron trajectory. Thomson's experiment consisted of 3 stages:

- (i) First he proved that, at sufficiently low air pressure in the Crookes tube, the electric field \mathcal{E} and magnetic field \mathcal{B} affected the trajectory of electrons in the tube.
- (ii) Next, he balanced the electric force $F_E = e\mathcal{E}$ and magnetic force $F_B = e\nu\mathcal{B}$ to achieve zero deflection of the electron trajectory with non-zero electric and magnetic fields. From $F_E = F_B$ and the known \mathcal{E} and \mathcal{B} he determined the velocity ν of the electrons in the tube as $\nu = \mathcal{E}/\mathcal{B}$.
- (iii) Then, he turned off the magnetic field, measured the deflection of the electron trajectory as a result of electric field \mathcal{E} , and from the measured deflection and known velocity of the electrons determined the specific charge of the electron e/m_e as $\sim 1.7 \times 10^{11}$ C/kg.

The measured specific charge of the electron of $e/m_e \approx 1.7 \times 10^{11}$ C/kg was several orders of magnitude larger than the then largest known specific charge of positive hydrogen ion (now known as proton) of $e/m_{H^+} \approx 10^8$ C/kg. The ratio of 1700 between the two specific charges could be explained either by much larger charge of the electron than hydrogen ion or by a much smaller mass of the electron compared to mass of the hydrogen ion. Thomson was convinced that the difference was caused by the much smaller mass of the electron compared to hydrogen ion, and it later turned out that his reasoning was correct. Thomson received the 1906 Nobel Prize in Physics "*in recognition of the great merits of his theoretical and experimental investigations on the conduction of electricity by gases*". The currently accepted value for the specific charge of the electron is $e/m_e \approx 1.759 \times 10^{11}$ C/kg, indicating that Thomson's result of $\sim 1.7 \times 10^{11}$ C/kg was quite reasonable if one considers the type of equipment in use for physics measurements more than a century ago.

(3) **Determination of electron charge e .** In 1909 Robert A. Millikan, an American physicist, carried out at the University of Chicago his now-famous oil-drop experiment with which he determined the charge of the electron and proved experimentally the quantization of electric charge. Millikan's experimental apparatus was simple and consisted of two chambers (upper and lower) connected with a small hole. An oil droplet atomizer was connected to the upper chamber and the hole allowed some small oil droplets to fall from the upper chamber into the lower chamber equipped with two electrodes connected to a variable DC power supply. The movement of oil droplets in the lower chamber was traced with a microscope used to establish the droplet speed and size.

Charge was applied to droplets randomly through irradiation of the air in the lower chamber using a Crookes x-ray tube. X rays ionized the air producing positive ions and electrons. Free electrons produced by ionizing radiation in air do not move freely in air, rather, they attach themselves to molecules of oxygen to form negative ions. The presence of oil droplets in ionized air also allowed free electrons to attach themselves to oil drops, changing some oil droplets from neutral to charged state.

Oil droplets were observed with the microscope and once a given oil droplet was identified the electrode potential was varied until the droplet stopped falling and was suspended in mid air. This indicated that the vertical electric force eE balanced perfectly the pull of gravity on the droplet, i.e., its weight mg . Droplets that did not acquire any electrons would not be affected by the electric field and would continue to drop; droplets that acquired more than one electron charge would require a lower electric potential to achieve suspension with no motion in air.

After numerous experiments Millikan determined that the electron charge e (elementary charge of electricity) was $e = 1.59 \times 10^{-19}$ C which is within 1 % of the value $e = 1.602 \times 10^{-19}$ C accepted today. He also noticed that there was variation in measured charge on oil droplets; however, the measured charge was always $e = 1.59 \times 10^{-19}$ C or an integer multiple of this number. This means that electric charge in nature is quantized and its lowest value is $e = 1.59 \times 10^{-19}$ C. Millikan received the Nobel Prize in Physics in 1923 “for his work on the elementary charge of electricity and on the photoelectric effect”.

14.4.Q2**(293)**

A typical x-ray system used in science, medicine, or industry consists of five major components: (1) X-ray tube, (2) X-ray generator, (3) Control console, (4) Object under study, and (5) Image receptor.

- (a) Briefly describe the role of the five basic components of an x-ray system.
- (b) Draw a basic schematic diagram of an x-ray tube and briefly describe its major components.
- (c) Discuss the three x-ray tube designs that have been in use for x-ray production with x-ray tubes since Röntgen discovered x rays in 1895.
- (d) Prepare a table listing the following entries for the three x-ray tube designs: (1) X-ray tube type, (2) Cathode type (cold or hot cathode), (3) Electron ejection process from the cathode, (4) Air pressure in the x-ray tube, (5) Relative x-ray output, (6) Time of introduction and period of clinical use.
- (e) The anode of an x-ray tube is also called target. Briefly describe the main characteristics of a typical x-ray target.

SOLUTION:

(a) The basic components of an x-ray system are: (1) X-ray tube, (2) X-ray generator, (3) Control console, (4) Imaged object, and (5) Image receptor.

(1) **X-ray tube** serves as the source of x rays that are produced in the tube by relatively high energy electrons striking the tube anode, also called the x-ray target.

The electrons are generated in the tube cathode and accelerated toward the target by the electrostatic field between the tube anode and the tube cathode. In the x-ray target, electrons suffer rapid deceleration and through interactions with target atoms produce x-ray photons: characteristic x-ray photons in electron–orbital electron interactions and bremsstrahlung x-ray photons in electron–nucleus interactions.

(2) **X-ray generator** (also referred to as high-voltage power supply) provides current at DC high voltage used for acceleration of electrons in the x-ray tube, thereby controlling the quantity and characteristics of x rays that the x-ray tube emits. X-ray equipment requires an adjustable high voltage ranging from ~ 50 kV to ~ 150 kV for standard x-ray procedures. Some special procedures are carried out with voltage below or above this range.

The DC high voltage in an x-ray machine is usually produced from a low voltage AC power grid by first increasing the AC voltage with a step-up transformer and then applying a rectifier circuit to obtain DC high voltage. Several methods are used for DC rectification and the objective of these is to deliver DC voltage with as small voltage variation (also called ripple) as possible. Typically, an increased sophistication in circuitry of an x-ray generator increases its cost but decreases its output voltage ripple and brings the output voltage closer to perfect DC potential. The high frequency x-ray generator currently represents the state-of-the-art choice in diagnostic x-ray systems for delivery of optimal DC potential.

(3) **Control console** is used to select the operating parameters of the x-ray generator, such as mode of operation, kilovoltage, tube current, and exposure time. These parameters in turn control the quantity and quality of the x-ray beam used for imaging of the object.

(4) **Imaged object** under study can be a patient or an inanimate object undergoing a diagnostic test intended to provide nondestructive testing of interior organs or structures. Thus, from a technical perspective the imaged object becomes part of the x-ray system. The acquisition of the desired information depends heavily on the characteristics of the imaged object and appropriate choice of parameters to be used in the imaging study. One should note that only a small fraction of energy expended to produce the x rays will be carried by the x rays, as most of the energy goes into heat that must be dissipated from the target. Furthermore, most of the energy carried by the x rays is actually absorbed by the imaged object and only a small fraction is transmitted through the object and carried to the image receptor to form the latent image.

(5) **Image receptor** is a series of devices that convert into visible image the radiographic information contained by the x-ray beam emanating from the imaged object. Various devices have been developed as image receptors during the more than 100 years of x-ray imaging:

- (i) The most common image receptor in the past during the era of analog conventional radiography has been radiographic film combined with special screens

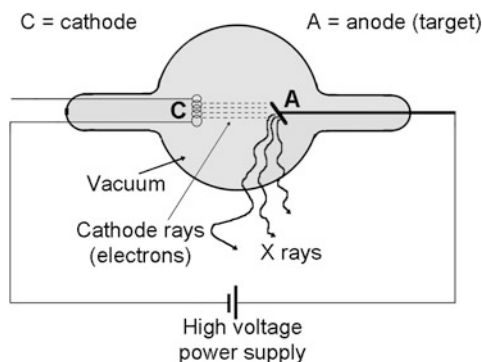


Fig. 14.2 Schematic diagram of a typical x-ray tube and its main components

and a film developer. Upon exposure of the imaged object, film stored the latent image that was subsequently rendered visible through chemical development of the exposed film in a film developer.

- (ii) In the current era of digital imaging there are two options: computed radiography and digital radiography.

In computed radiography the image receptor is the digital imaging cassette that stores the latent image on a special reusable plate coated with photostimulable phosphor (barium fluorohalide). For readout, the plate is transferred to a laser reader that scans the latent image with red light and renders it visible in blue light that is captured by a photodetector and converted to a digital signal for viewing.

In digital radiography the latent x-ray image is captured with a flat panel detector containing a photoconductor that absorbs x rays in an amorphous selenium material and converts the latent image into digital signal.

(b) In Fig. 14.2 we show a schematic diagram of a simple x-ray tube with “cathode rays” (electrons) emanating from the cathode and accelerated toward the anode (target). The electrons strike the anode and lose some of their kinetic energy (typically only 1 % or less) in the form of x rays. The high voltage power supply establishes the DC potential between the cathode and the anode. The x-ray tube is evacuated, however, the residual pressure in the tube depends on the tube design.

(c) Three x-ray tube designs have been in use since 1895 when Röntgen discovered that cathode rays in Crookes cathode ray tube produce x rays in striking the tube anode. Basic components of x-ray tubes shown in Fig. 14.2 are the same for all x-ray tubes used to date; however, the three designs differ in their method for electron generation in the cathode, with two designs using a cold cathode and one a hot cathode. The three designs are: (1) Crookes x-ray tube—using cold cathode bombardment with positive air molecules to eject electrons from the cold cathode, (2) Coolidge x-ray tube—using thermionic emission of electrons from the hot cathode, and (3) Carbon nanotube (CNT) x-ray tube—using field emission for electron ejection from the cold cathode.

(1) **Crookes x-ray tube** is a Crookes cathode ray tube used for production of x rays. It is an electric discharge tube invented by British chemist/physicist William Crookes in the early 1870s. It consists of a sealed glass tube which is evacuated to an air pressure between 0.005 Pa and 0.1 Pa (4×10^{-5} tor and 7.5×10^{-4} tor) and incorporates two electrodes (cathode and anode) connected to an external DC power supply. When high voltage is applied to the tube, electric discharge in the rarefied air inside the tube ionizes some air molecules. Positive ions move in the electric field toward the cathode and create more ions through collisions with air molecules. As positive ions strike the cathode, electrons (cathode rays) are released from the cathode, move toward the anode in the electric field that is present between the cathode and the anode, and strike the anode. Investigating “cathode rays”, Röntgen in 1895 serendipitously discovered x rays as rays emanating from the anode bombarded with “cathode rays”.

For the first two decades after 1895, x-ray tubes used for clinical work were of the Crookes tube type; simple in design but suffering from severe practical problems related to the magnitude and reliability of the x-ray output. Low x-ray output combined with large fluctuations in x-ray output and difficulties in controlling the output were the main drawbacks of Crookes x-ray tubes.

(2) **Coolidge x-ray tube**. In 1913 William Coolidge, an American physicist, introduced a new x-ray tube design based on a hot cathode which significantly improved the reliability and performance of clinical x-ray tubes. Almost 100 years later, Coolidge’s hot cathode idea still provides the basis for design of modern x-ray tubes.

The hot cathode consists of a filament made of a high melting point metal, typically tungsten (melting point 3422 °C) or a tungsten based alloy, heated to a relatively high temperature to serve as source of electrons. The hot cathode emits electrons thermionically (see Sect. 1.27) in contrast to the cold cathode of the Crookes x-ray tube in which positive air ions striking the cathode trigger the generation of electrons. Another important difference between the Coolidge tube and the Crookes tube is that the Coolidge tube operates under high vacuum of the order of 10^{-4} Pa to prevent collisions between electrons and molecules of air and also to prevent filament deterioration because of oxidation.

The main advantages of the Coolidge x-ray tube are its stability and its design feature that allows the external control of the x-ray output. The hotter is the filament, the larger is the number of emitted electrons. The filament is heated with electric current; increasing the filament current increases the filament temperature and this in turn results in an increase in number of thermionically emitted electrons. This number of emitted electrons is proportional to the number of electrons accelerated toward the anode (tube current) and this in turn is proportional to the number of x rays produced in the anode (x-ray output). Increasing the high voltage potential between the anode and the cathode increases the kinetic energy of the electrons striking the target (anode) and this increases the energy of the emitted x rays.

(3) **Carbon nanotube based x-ray tube**. The Coolidge hot cathode improved significantly the x-ray tube performance, however, hot cathodes have some draw-

backs, so that for decades, concurrently with improvements in hot cathode technology, search was on for alternative, more practical, and cheaper source of electrons preferably based on cold cathode design.

Field emission (see Sect. 1.28.2), which allows emission of electrons from the surface of a solid under the influence of a strong electric field, seems an excellent candidate for a practical and efficient cold cathode design. Attempts in this direction have been made for decades; however, the use of extremely small metal tips to achieve the large local electric field always resulted in electrodes that were unreliable, relatively inefficient, and not durable enough for routine x-ray tube operation.

During the past decade, a new generation of carbon based material called carbon nanotube (CNT) has been developed in nanotechnology laboratories and showed great promise for use as cold cathode-type electron source. Carbon nanotubes are ordered molecular structures formed by carbon, yet different from the two well-known carbon forms: graphite and diamond. They are molecular scale tubes with typical diameter of a few nanometers and a height of up to a few millimeters. The tubes have remarkable electronic properties and special physical characteristics that make them of great academic as well as potential commercial interest. They are extremely strong, yet flexible as well as light and thus hold promise for aerospace applications. Depending on their structure, they can behave like metal with conductivity higher than copper or like semiconductor potentially useful in design of nanoscale electronic devices. CNTs are mechanically, chemically, and thermally extremely robust and, since they also form atomically very sharp tips, they are also very efficient field emission materials for use as cold cathode electron source in x-ray tubes.

Miniature x-ray tubes using CNT cold cathode design are already commercially available. They generate electrons at room temperature and provide controllable as well as stable output currents and respectable life of the cathode. They can be used for “electronic brachytherapy” in medicine where they replace sealed radionuclide sources as well as in space exploration for performing remote mineralogical analyses on solid bodies of the solar system. Use of cold cathode for high power x-ray tubes in medicine and industry, however, if it happens, is far in the future, since the technology of CNT production is still in a rudimentary stage and field emission cold cathodes are currently no match for the standard Coolidge hot cathode x-ray tube design.

(d) Table 14.2 lists the main characteristics of the three main types of x-ray tube categorized according to cathode design: Crookes x-ray tube, Coolidge x-ray tube, and Carbon nanotube (CNT) x-ray tube. However, Crookes x-ray tubes are no longer in use and CNT x-ray tubes are not ready yet for mainstream use. This means that Crookes tubes are on the list because of their historical significance and CNT x-ray tubes are on the list because of their potential for practical use in the future. Currently, the vast majority of x-ray tubes used in medicine and industry are of Coolidge type design using a hot cathode.

Table 14.2 lists the following entries: (1) X-ray tube type, (2) Cathode type (cold or hot), (3) Electron ejection process, (4) Air pressure in x-ray tube, (5) Relative x-ray output, and (6) Period of clinical use.

Table 14.2 Main characteristics of x-ray tubes: Crookes x-ray tube, Coolidge x-ray tube, and carbon nanotube (CNT) x-ray tube

(1)	X-ray tube type	Crookes x-ray tube	Coolidge x-ray tube	CNT x-ray tube
(2)	Cathode type	COLD	HOT	COLD
(3)	Electron ejection	Cathode bombardment with positive ions	Thermionic emission	Field emission in strong electric field
(4)	Air pressure	Intermediate vacuum 0.005 Pa to 0.1 Pa	High vacuum $\sim 10^{-4}$ Pa	Intermediate vacuum $\sim 10^{-4}$ Pa
(5)	Relative x-ray output	LOW and erratic; depends on air pressure inside tube	HIGH, variable and steady; depends on cathode temperature	LOW; depends on CNT design
(6)	Clinical use period	1895 to ~ 1920	1913 to present	Relatively new design

(e) Electrons generated by the cathode bombard the target (anode) of an x-ray tube and a minute fraction of the electron's kinetic energy (typically 1 % or less) is transformed into x rays (characteristic radiation and bremsstrahlung) and the rest into heat. The anode thus has three functions in an x-ray tube: (1) to define the positive potential in the x-ray tube, (2) to produce x rays, and (3) to dissipate the heat.

The anode material must have a high melting point to be able to withstand the high operating temperature and a relatively high atomic number for adequate x-ray production. Most common target materials for x-ray tubes are tungsten (wolfram) with atomic number $Z = 74$ and melting point of 3422°C and molybdenum with $Z = 42$ and melting point of 2617°C . Tungsten is used in x-ray tubes operating above 50 kV and molybdenum in x-ray tubes below 50 kV.

The two most important practical attributes of x-ray targets for imaging or radiotherapy are:

- (1) Small focal spot (as close as possible to “point source”) to minimize beam penumbra. A smaller beam penumbra results in sharper image in x-ray imaging and in better dose distribution in radiotherapy.
- (2) Relatively large beam output (large electron fluence striking the target) to minimize exposure time. Short exposure time in imaging as well as radiotherapy minimizes potential for patient or organ motion during x-ray exposure.

A “point source” and short exposure time, of course, are mutually exclusive, since, in the limit, they imply a concentration of infinite electron fluence on zero area focal spot, a situation that cannot be supported in practice. Many practical ways for spreading the electrons striking the target over a large area of the target and still keeping the appearance of a small focal spot have been introduced into x-ray tube design, such as so-called line focus and rotating anode.

In (d) we saw that x-ray tubes may be classified according to cathode design into three categories: however, since essentially all x-ray tubes currently used in medicine or industry are of Coolidge type design, the classification according to

cathode design is only of historical significance. For practical purposes, modern x-ray tubes are classified according to anode (target) design into imaging x-ray tubes and radiotherapy x-ray tubes. Targets of imaging tubes fulfill more stringent focal size requirements and have smaller focal spots than therapy x-ray tubes. On the other hand, in comparison with imaging tubes, targets of therapy tubes are simpler in design, have larger focal spots, and must withstand 10 times as high mean energy input but only 10 % of instantaneous energy input.

14.5 Circular Accelerators

14.5.Q1

(294)

With the exception of the linear accelerator, all cyclic particle accelerators used in science, industry, and medicine fall into the category of circular accelerators. Common to all circular accelerators is the circular motion of accelerated particles with either a constant radius or increasing radius.

- (a) Five types of circular cyclic particle accelerator have found use in medicine. List the five machines and briefly explain the purpose of their application in medicine.
- (b) Prepare a table for the five machines listed in (a) with the following entries:
- | | |
|-----------------------------------|--|
| (1) Name of particle accelerator. | (2) Inventor of the machine. |
| (3) Year of invention. | (4) Particles accelerated. |
| (5) Frequency of operation. | (6) Magnetic field used
(static or variable). |
| (7) Particle trajectory. | (8) Radius of orbit
(constant or increasing). |
- (c) Draw a schematic diagram for each of the five machines listed in (a).

SOLUTION:

(a) The five cyclic particle accelerators that accelerate charged particles in circular or spiral orbits and were found useful in medicine are: (1) Betatron, (2) Cyclotron, (3) Microtron, (4) Synchrotron, and (5) Storage ring. The machines differ significantly in design and mode of operation; however, in all five machines the charged particles are accelerated by an appropriate electric field oriented in the direction of particle motion and are kept in curved orbits by a strong static magnetic field.

(1) **Betatron** was developed in 1940 by Donald Kerst at the University of Illinois in Urbana-Champlain as a cyclic electron accelerator for basic nuclear physics re-

search; however, its potential for use in radiotherapy for treatment of deep-seated malignant tumors was realized soon thereafter.

In 1950s and 1960s, before the advent of clinical linear accelerators (linacs), betatrons played an important role in megavoltage radiotherapy with photon energies above that of 1.25 MeV cobalt-60 gamma rays. At that time betatron provided the only practical means for production of clinical megavoltage photon beams in the range from 10 MV to 25 MV and for production of clinical electron beams in the energy range from 4 MeV to 30 MeV.

The rapid development of clinical linacs after 1970 made the betatron use in radiotherapy obsolete, because of the numerous advantages of clinical linacs over betatrons. Today, betatrons are no longer used in radiotherapy; however, they continue to be used for industrial radiography at relatively low photon energy of 25 MV and for high-energy physics research at electron kinetic energy up to 350 MeV.

(2) **Cyclotron** was developed by Ernest O. Lawrence in 1932 at the University of California in Berkeley for acceleration of positive or negative ions to kinetic energy of a few MeV. Initially the cyclotron was used for basic nuclear physics research and subsequently also became used in medicine for:

- (i) Production of radionuclides, such as molybdenum-99 that is used in radionuclide generator for generation of technetium-99m, for nuclear medicine tests.
- (ii) Production of proton and neutron beams for radiotherapy treatment of cancer patients.
- (iii) Production of positron emitting radionuclides, such as fluorine-18, for use in positron emission tomography (PET) imaging.

(3) **Microtron** is a cyclic electron accelerator producing electrons in the energy range from 5 MeV to 50 MeV. Vladimir Veksler proposed the microtron concept in 1944 and the first prototype machine was built at the National Research Council of Canada in 1947.

Despite the early development of microtrons for scientific purposes, their translation into medical environment was much slower and less successful than that of clinical linacs. Microtron has some significant advantages over a clinical linac, such as more compact design, smaller focal spot, and smaller electron beam energy spread, yet clinical linac is by far the prevalent machine used for megavoltage radiotherapy around the world. It seems that clinical linacs had a head start during 1960s and microtrons with their clinical appearance in mid 1970s have never been able to catch up. In terms of beam characteristics for the same nominal beam energy clinical beams from microtrons and linacs are essentially the same.

(4) **Synchrotron** is a cyclic particle accelerator used for acceleration of electrons and heavy charged particles such as protons and heavier ions to relativistic energies. American physicist Edwin M. McMillan at the University of California in Berkeley built the first electron synchrotron in 1945 but Russian physicist Vladimir Veksler published the principles of the machine independently before. Marcus L.E. Oliphant from Birmingham, UK designed and built the first proton synchrotron in 1952.

Synchrotron is a complex and expensive accelerator, so its potential for use in medicine is limited. In the past, it has been used as source of protons and heavier charged particles for radiotherapy and recently has been considered for production of molybdenum-99 (Mo-99) radionuclide in manufacturing of technetium-99m radionuclide generators for nuclear medicine studies. Currently, most of Mo-99 is produced by nuclear reactors; however, this avenue has some serious practical drawbacks and synchrotron is considered as a possible replacement of nuclear reactors in Mo-99 production.

(5) **Storage ring** also called **synchrotron light source** is a synchrotron cyclic accelerator modified for use in storing charged particles of a given kinetic energy for the purpose of applying the radiation emitted by the charged particles for basic research and medical purposes. It is well known that a charged particle moving on a curved path or orbit is constantly accelerated and loses part of its kinetic energy in the form of radiation according to the Larmor law (T4.18). The radiation so emitted by relativistic charged particles moving in circular trajectories is called synchrotron radiation (SR) or “magnetic bremsstrahlung”. SR radiation is extracted from storage rings through special ports referred to as beam-lines.

The unique properties of SR beams, such as their very large intensity, small angular beam divergence, vertical collimation, a broad band of energies, and ease of rendering them monochromatic, make SR an attractive imaging tool for new imaging studies. Of course, because of cost, synchrotrons and storage rings are of limited availability around the world, so medical use of SR is not expected to become widespread. However, one can assume that the most sophisticated and unique SR

Table 14.3 Basic physical parameters of the five types of cyclic accelerators used in medicine. The table lists only cyclic accelerators in which particles move in circular or spiral orbits

(1)	Circular accelerator	Betatron	Cyclotron	Microtron	Synchrotron	Storage ring
(2)	Inventor	Donald W. Kerst	Ernest O. Lawrence	Vladimir Veksler	Edwin M. McMillan	–
(3)	Year of invention	1940	1932	1944	1945	–
(4)	Particle(s) accelerated	Electron	Proton or heavier ion	Electron	Electron or proton or ion	Electron or proton or ion
(5)	Operational frequency	60 Hz to 180 Hz	10 MHz to 30 MHz	3 GHz or 10 GHz	e: few 100 MHz p: MHz	e: few 100 MHz p: MHz
(6)	Magnetic field	Variable	Static	Static	Variable	Variable
(7)	Particle trajectory	Circle	Spiral	Spiral	Circle	Circle
(8)	Radius of orbit	Const	Increases with energy	Increases with energy	Const	Const

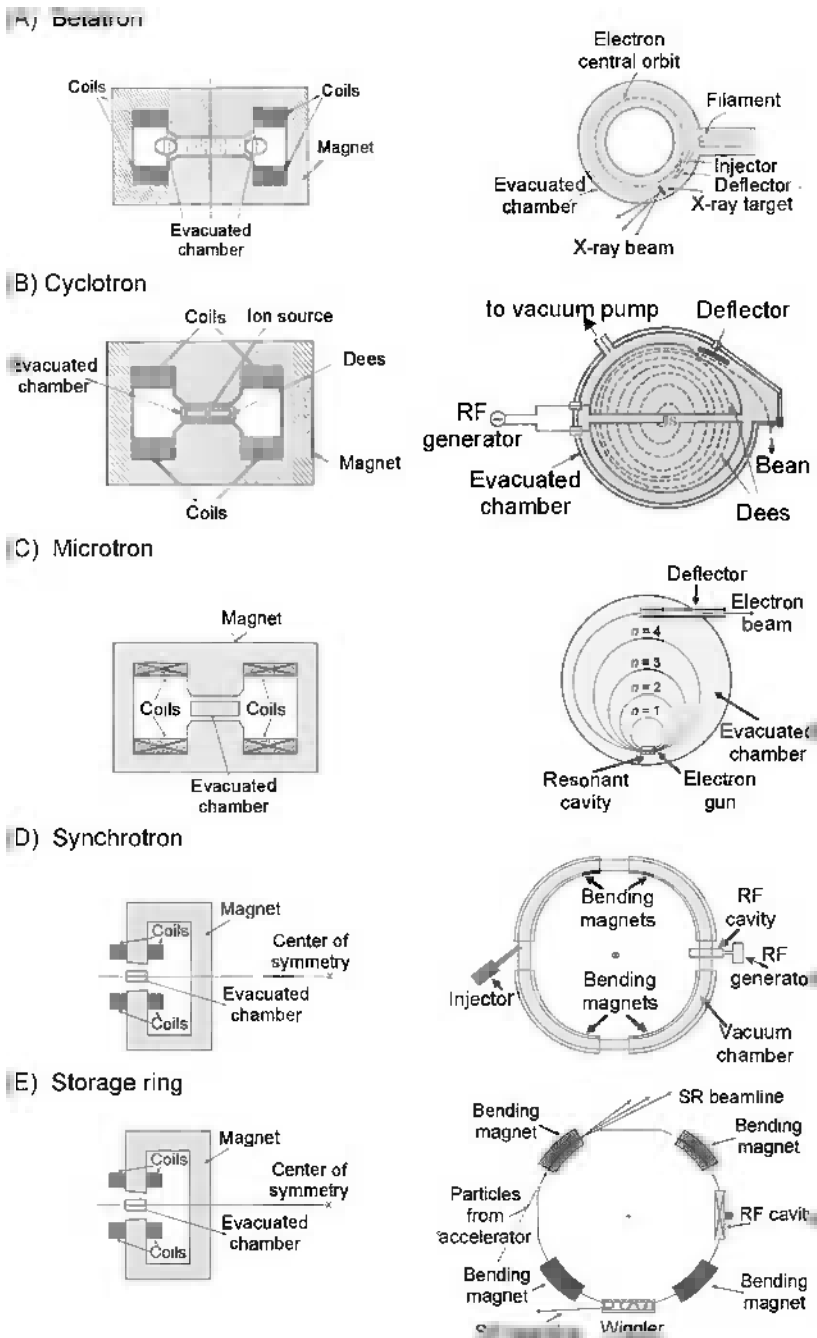


Fig. 14.3 Schematic diagrams of various cyclic accelerators used in medicine: (A) Betatron, (B) Cyclotron, (C) Microtron, (D) Synchrotron, and (E) Storage ring (synchrotron light source)

techniques will become available around the world on national scale, similar to the situation with heavy ion synchrotrons for use in radiotherapy that are becoming available on centralized national basis.

Medical use of SR is rapidly expanding with studies of medical use of SR concentrated in two broad areas: imaging and radiotherapy, for example, in multiple-energy computed tomography and microbeam radiotherapy, respectively. Most imaging studies are done on cardiovascular imaging and coronary angiography, mammography in breast cancer, bronchography, and bone disease.

In radiotherapy the use of the concept of microbeam radiotherapy (MRT) developed at the Brookhaven National Laboratory is studied using strips of multiple, parallel, narrow SR microbeams (width: $\sim 50 \mu\text{m}$; height: few millimeters) with energy between 50 keV and 150 keV. The separation between microbeams is of the order of 100 μm . The rationale behind microbeam radiotherapy is that endothelial cells that are destroyed by high radiation dose within the microbeam will regenerate from endothelial cells populating the contiguous strips between microbeams. Obviously, MRT would be difficult to incorporate on standard radiotherapy equipment.

Medical investigation of SR is concentrated on areas not already covered by standard imaging and radiotherapy techniques. The motivation obviously is to open new modalities for imaging and therapy of disease by employing the unique characteristics of SR, rather than simply moving standard imaging and therapy techniques onto significantly more expensive storage rings.

(b) Table 14.3 lists the basic physical parameters of the five cyclic particle accelerators that have found use in medicine: (1) Betatron, (2) Cyclotron, (3) Microtron, (4) Synchrotron, and (5) Storage ring.

(c) Figure 14.3 shows schematic diagrams for 5 cyclic accelerators used in medicine: (A) Betatron, (B) Cyclotron, (C) Microtron, (D) Synchrotron, and (E) Storage ring.

14.5.Q2

(296)

The ultimate limiting factor in the quest for maximum practical attainable particle energy in particle accelerator (ignoring escalating cost) is the radiation loss that the particle experiences during the acceleration process. The radiation loss by accelerated charged particle is in classical physics expressed by the Larmor equation (14.1) and in relativistic physics by the Liénard equation (14.2) as follows

$$P = \frac{dE}{dt} = \frac{q^2}{6\pi\epsilon_0 c^3} \dot{\mathbf{v}}^2 = \frac{q^2}{6\pi\epsilon_0 c^3} \left(\frac{d\mathbf{v}}{dt} \right)^2 = \frac{q^2}{6\pi\epsilon_0 m^2 c^3} \left(\frac{d\mathbf{p}}{dt} \right) \left(\frac{d\mathbf{p}}{dt} \right) \quad (14.1)$$

and

$$P = \frac{dE}{dt} = \frac{q^2 \gamma^6}{6\pi \epsilon_0 c^3} \left[\dot{\mathbf{v}}^2 - \frac{(\mathbf{v} \times \dot{\mathbf{v}})^2}{c^2} \right], \quad (14.2)$$

where P is the power emitted by a particle of charge q accelerated with acceleration $\mathbf{a} = \dot{\mathbf{v}}$ and γ is the Lorentz factor $(1 - \beta^2)^{-1/2} = E/E_0$ with E and E_0 the charged particle total energy and rest energy, respectively, and β the velocity normalized to speed of light c in vacuum.

- (a) Calculate the ratio f_P of power P radiated to power dE/dt supplied by external sources for an electron accelerated in a linear accelerator (linac) waveguide. Assume that typical energy gain for an electron accelerated in a linac waveguide is ~ 10 MeV/m.
- (b) Since synchrotron radiation is usually produced in circular machines, the corresponding energy loss per full turn (revolution) in an important parameter. Derive an expression for energy E_{rad} radiated per revolution for an electron accelerated in a synchrotron accelerator.
- (c) Assume that typical energy gain per revolution of an electron accelerated in a synchrotron with radius $R = 1$ m and nominal energy of 300 MeV is ~ 5 keV per turn. Determine the fractional energy loss per revolution f_E , i.e., ratio of radiation energy loss per revolution to energy gain per revolution.
- (d) For synchrotron radiation plot the energy E_{rad} radiated per revolution against the nominal energy E of the synchrotron in the range $1 \text{ MeV} \leq E \leq 10^5 \text{ MeV}$ for circular trajectories with radii R of 1 m, 10 m, 100 m, and 1000 m.
- (e) According to the Larmor law a charged particle undergoing acceleration or deceleration emits part of its kinetic energy in the form of radiation. For electron and proton compare emission of radiation in: (1) Bremsstrahlung radiation loss in traversing a target and (2) Synchrotron radiation loss in synchrotron or storage ring.

SOLUTION:

(a) Electrons, even in low energy 4 MV linacs used in radiotherapy, are already relativistic and become ultra-relativistic at the extremely high energies used in large research linacs. Therefore, we use the Liénard relationship of (14.2) in our calculation of energy loss in a linac waveguide and simplify it by accounting for co-linearity of vectors \mathbf{v} and $\mathbf{a} = \dot{\mathbf{v}}$. Under the condition $\mathbf{v} \parallel \dot{\mathbf{v}}$ we note that $\mathbf{v} \times \dot{\mathbf{v}} = \mathbf{0}$. The Liénard equation for rectilinear acceleration of an electron in a linac is then given by an expression similar in form to the classical Larmor equation (14.1) except for the Lorentz γ factor to sixth power which seems to point to a drastic increase in

radiation loss when particle velocity v approaches c resulting in $\gamma \rightarrow \infty$

$$P = \frac{dE}{dt} = \frac{q^2 \gamma^6}{6\pi \epsilon_0 c^3} \dot{v}^2. \quad (14.3)$$

Next, we express the product of the cube of the Lorentz factor γ^3 and electron acceleration $a = \dot{v}$ of (14.3) as a function of dp/dt starting with the general relativistic relationship

$$p = mv = \gamma m_e v \quad (14.4)$$

and

$$\begin{aligned} \frac{dp}{dt} &= \frac{d}{dt}(\gamma m_e v) = \gamma m_e \dot{v} + \dot{\gamma} m_e v = \gamma m_e \dot{v} + \left(\frac{\gamma^3 v}{c^2} \dot{v} \right) m_e v = \gamma m_e \dot{v} (1 + \gamma^2 \beta^2) \\ &= \gamma^3 m_e \dot{v}, \end{aligned} \quad (14.5)$$

where

m is the relativistic mass of the accelerated electron ($m = \gamma m_e$).

m_e is the electron rest mass ($m_e = 0.5110 \text{ MeV}/c^2$).

γ is the Lorentz factor given as $\gamma = (1 - \beta^2)^{-1/2}$ with $\beta = v/c$ and v the electron velocity.

\dot{v} is the electron acceleration.

In the derivation of (14.5) we used the following two relationships

$$\dot{\gamma} = \frac{1}{(1 - \frac{v^2}{c^2})^{3/2}} \frac{v}{c^2} \dot{v} \quad (14.6)$$

and

$$1 + \gamma^2 \beta^2 = 1 + \frac{\beta^2}{1 - \beta^2} = \frac{1 - \beta^2 + \beta^2}{1 - \beta^2} = \gamma^2. \quad (14.7)$$

After inserting (14.5) in the form $\gamma^3 \dot{v} = (1/m_e)(dp/dt)$ into (14.3), we now get the following expression for the radiation loss of an electron accelerated rectilinearly in a linac waveguide

$$P = \frac{dE}{dt} = \frac{e^2 (\gamma^3 \dot{v})^2}{6\pi \epsilon_0 c^3} = \frac{e^2}{6\pi \epsilon_0 m_e^2 c^3} \left(\frac{dp}{dt} \right)^2 = \frac{e^2}{6\pi \epsilon_0 m_e^2 c^3} \left(\frac{dE}{dx} \right)^2, \quad (14.8)$$

where we used the relationship $dp/dt = dE/dx$. This relationship follows from general physics relationships $dp/dt = d(mv)/dt = F = dE/dx$ indicating that dp/dt , the rate of change of electron momentum, is equal to dE/dx , the change in total energy of the particle per unit distance. Equation (14.8) shows that in one-dimensional linear acceleration of electron accelerated in a waveguide the radiated power P does not depend on electron total energy E or momentum p but depends on external force F provided by the electric field in the waveguide.

Fraction f_P of radiated power P to input power dE/dt is from (14.8) given as

$$\begin{aligned} f_P &= \frac{P}{dE/dt} = \frac{e^2}{6\pi\epsilon_0 m_e^2 c^3} \frac{(\frac{dE}{dx})(\frac{dE}{dx})}{(\frac{dE}{dt})} = \frac{2}{3} \left(\frac{e^2}{4\pi\epsilon_0 m_e c^2} \right) \frac{1}{m_e c^2 \beta} \left(\frac{dE}{dx} \right) \\ &= \frac{2r_e}{3m_e c^2 \beta} \left(\frac{de}{dx} \right), \end{aligned} \quad (14.9)$$

where r_e is a constant called classical radius of the electron (2.818 fm) and β is the electron velocity v normalized to the speed of light in vacuum.

For a typical linac we have $dE/dt \approx 10$ MeV/m and $\beta \approx 1$, so that (14.9) gives the following fractional radiation loss f_E for an electron accelerated in a linac waveguide

$$f_P = \frac{2r_e}{3m_e c^2} \left(\frac{dE}{dx} \right) = \frac{2 \times (2.818 \times 10^{-15} \text{ m})}{3 \times (0.511 \text{ MeV})} \times (10 \text{ MeV/m}) \approx 3.7 \times 10^{-14}. \quad (14.10)$$

As shown by (14.10), the radiation loss experienced by an electron accelerated in a linac waveguide is extremely small and therefore negligible. This holds even more for heavier charged particles such as a proton because of the inverse proportionality of radiation loss with the rest mass of the accelerated particle [see (d)].

(b) To determine radiation loss of an electron accelerated in a synchrotron accelerator or of an electron in a holding pattern in a storage ring we again use the Liénard relativistic equation (14.3) and note that, in a synchrotron, acceleration $\mathbf{a} = \dot{\mathbf{v}}$ is always perpendicular to velocity \mathbf{v} and this results in another significant simplification of (14.3)

$$\begin{aligned} P &= \frac{dE}{dt} = \frac{e^2 \gamma^6}{6\pi\epsilon_0 c^3} = \left[\dot{v}^2 - \frac{(\mathbf{v} \times \dot{\mathbf{v}})^2}{c^2} \right] \\ &= \frac{e^2 \gamma^6}{6\pi\epsilon_0 c^3} \left[\dot{v}^2 - \frac{v^2 \dot{v}^2}{c^2} \right] = \frac{e^2 \gamma^6 \dot{v}^2}{6\pi\epsilon_0 c^3} (1 - \beta^2) = \frac{e^2 \gamma^4 v^4}{6\pi\epsilon_0 c^3 R^2} \\ &= \frac{c e^2 \gamma^4 \beta^4}{6\pi\epsilon_0 R^2}, \end{aligned} \quad (14.11)$$

where we used $1 - \beta^2 = 1/\gamma^2$ and for circular motion $\dot{v} = v^2/R$.

Radiation loss ΔE in one complete revolution of a highly relativistic electron ($\beta \rightarrow 1$) is calculated by first determining the duration τ of one revolution as

$$\tau = \frac{2\pi R}{v} \approx \frac{2\pi R}{c}, \quad (14.12)$$

where R is the radius of the electron circular trajectory in a synchrotron and we used $v \rightarrow c$ for relativistic electron. Radiation loss E_{SR} in the form of synchrotron radiation (SR) per one revolution is now given as

$$\begin{aligned}
 E_{\text{SR}} &= P\tau = \frac{ce^2\gamma^4\beta^4}{6\pi\epsilon_0R^2} \frac{2\pi R}{c} = \frac{e^2\gamma^4}{3\epsilon_0R} = \frac{e^2}{3\epsilon_0R} \left(\frac{E}{m_e c^2}\right)^4 \\
 &= \frac{e^2}{3\epsilon_0(m_e c^2)^4} \frac{E^4}{R} = \left\{ 8.85 \times 10^{-8} \frac{\text{eV} \cdot \text{m}}{(\text{MeV})^4} \right\} \frac{E^4}{R}. \quad (14.13)
 \end{aligned}$$

The radiation loss per revolution of an electron accelerated in a synchrotron or stored in a storage ring is calculated from (14.13), showing that the radiation emitted is proportional to the fourth power of nominal electron energy E and inversely proportional to the radius R of the electron orbit. The proportionality constant is $8.85 \times 10^{-8} \text{ eV} \cdot \text{m} \cdot (\text{MeV})^{-4}$.

(c) For an electron synchrotron of radius $R = 1 \text{ m}$ and nominal energy $E = 300 \text{ MeV}$, and energy gain $E_{\text{gain}} = 5 \text{ keV}$ per revolution we determine the electron energy loss E_{SR} per revolution in the form of synchrotron radiation from (14.3) as follows

$$\begin{aligned}
 E_{\text{SR}} &= \left\{ 8.85 \times 10^{-8} \frac{\text{eV} \cdot \text{m}}{(\text{MeV})^4} \right\} \frac{E^4}{R} = \left\{ 8.85 \times 10^{-8} \frac{\text{eV} \cdot \text{m}}{(\text{MeV})^4} \right\} \times \frac{(300 \text{ MeV})^4}{(1 \text{ m})} \\
 &\approx 0.7 \text{ keV}. \quad (14.14)
 \end{aligned}$$

Fractional energy loss per revolution f_E is given by the ratio $f_E = E_{\text{SR}}/E_{\text{gain}}$ to get

$$f_E = \frac{E_{\text{SR}}}{E_{\text{gain}}} = \frac{0.7}{5} = 0.14, \quad (14.15)$$

obviously of significant magnitude in comparison with the fractional power loss of electrons in a linear accelerator, determined in (a).

(d) In Fig. 14.4 we plot (14.13) on a log-log scale the energy lost in the form of synchrotron radiation E_{SR} in eV against nominal synchrotron energy E in the range from $E = 1 \text{ MeV}$ to $E = 10^5 \text{ MeV}$ for four synchrotron radii: 1 m, 10 m, 100 m, and 1000 m. Since we are dealing with a power function, the resulting graph comprises four parallel lines, one for each of the four synchrotron radii. The solid data point on the $R = 1 \text{ m}$ plot indicates the result of the calculation presented in (14.14) of (c).

(e) According to the Larmor law stated in (14.1) a charged particle undergoing acceleration or deceleration emits a portion of its kinetic energy in the form of electromagnetic radiation, be it as bremsstrahlung photons or as synchrotron radiation depending on the force acting on the charged particle.

(1) **Emission of bremsstrahlung radiation** by charged particle traversing a target. The Larmor equation (14.1) states that the rate of bremsstrahlung energy loss dE_B/dt is proportional to $|\dot{v}|^2$ where $|\dot{v}|$, the acceleration of charged particle of mass m_0 and charge ze passing through a target of atomic number Z , is in turn proportional to zEe^2/m_0 by virtue of the Coulomb force $F_{\text{Coul}} = (zZe^2)/(4\pi\epsilon_0r^2)$

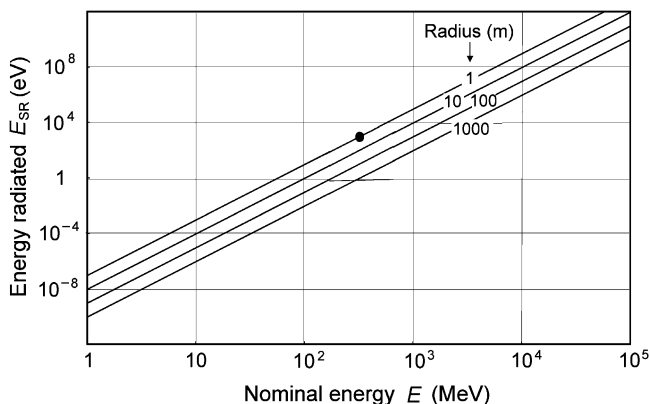


Fig. 14.4 Energy E_{SR} lost in the form of synchrotron radiation (SR) per revolution in a synchrotron accelerator or in an electron storage ring against nominal synchrotron energy E in the range from $E = 1$ MeV to $E = 10^5$ MeV for four synchrotron radii: 1 m, 10 m, 100 m, and 1000 m. The *solid data point* on the $R = 1$ m plot indicates the result of the calculation presented in (14.14) of (c) predicting that, in a synchrotron accelerator with a radius of 1 m, energy lost in the form of synchrotron radiation in one revolution amounts to $E_{SR} = 0.7$ keV

in effect between the charged particle and absorber nuclei. *Note:* r is the distance between the two charges—nucleus and charged particle).

Bremsstrahlung loss is thus inversely proportional to m_0^2 , the square of the mass of the accelerated charged particle traversing the absorber target. As a consequence of this dependence on mass, the bremsstrahlung loss of electron and positron is significantly larger than the loss experienced by a proton, α particle, or heavier ion. Therefore, radiation stopping power is only considered for electrons and positrons and deemed negligible for heavier charged particles. To put an order of magnitude on the bremsstrahlung power ratio $P_B(\text{electron})/P_B(\text{proton})$ at the same kinetic energy of the electron and proton, we simply take the square of the ratio of rest masses of the two charged particles to get

$$\frac{P_B(\text{electron})}{P_B(\text{proton})} = \frac{m_p^2}{m_e^2} = \frac{938.3^2}{0.511^2} = 1836^2 \approx 3.4 \times 10^6. \quad (14.16)$$

The result of (14.16) shows that an electron is about 3.4×10^6 times more efficient than proton in production of bremsstrahlung.

(2) **Emission of synchrotron radiation** by charged particle moving in magnetic field of a synchrotron or storage ring. The Liénard equation (14.11) states that the rate of energy loss dE_{SR}/dt in emission of synchrotron radiation is proportional to $\gamma^4 \dot{\mathbf{v}}^2$, where $\dot{\mathbf{v}}$ is the charged particle acceleration ($\dot{\mathbf{v}} = \dot{v}^2/R$) and γ is the particle Lorentz factor given as $\gamma = E/E_0$ with E and E_0 the charged particle total energy and rest energy, respectively.

Since $E_0 = m_0 c^2$, we note that the synchrotron radiation loss dE_{SR}/dt is inversely proportional to m_0^4 , the fourth power of the rest mass of the accelerated

charged particle. As a consequence of this dependence on mass, the synchrotron radiation loss of electron and positron is significantly larger than that experienced by a proton for the same radius of curvature R of the trajectory and same particle energy E . To put an order of magnitude on the synchrotron radiation power ratio $P_{\text{SR}}(\text{electron})/P_{\text{SR}}(\text{proton})$ at the same total energy E of the two particles and the same radius R of their circular trajectory, we simply take the fourth power of the ratio of rest masses of the two particles to get

$$\frac{P_{\text{SR}}(\text{electron})}{P_{\text{SR}}(\text{proton})} = \frac{m_{\text{p}}^4}{m_{\text{e}}^4} = \frac{938.3^4}{0.511^4} = 1836^4 \approx 1.14 \times 10^{13}. \quad (14.17)$$

The result of (14.17) shows that an electron is 1.14×10^{13} times more efficient than proton in production of synchrotron radiation.

14.5.Q3

(296)

In a cyclotron the particles are accelerated along a spiral trajectory guided inside two evacuated half-cylindrical electrodes (referred to as dees because of their D-shape form) by a uniform magnetic field that is produced between the pole pieces of a large magnet. A radiofrequency (RF) voltage with a constant frequency is applied between the two electrodes and the charged particle is accelerated while crossing the gap between the two electrodes.

The operation of a cyclotron is possible if the time required for the particles to describe each semicircle in a dee is constant and if the angular frequency ω of the RF generator is such that the transit time inside one of the two dees is equal to half period of field oscillation. In standard cyclotron operation the Lorentz force F_{L} keeping the particle in circular orbit is equal to the centripetal force

$$F_{\text{L}} = qvB = \frac{mv^2}{r}, \quad (14.18)$$

where q is the charge of the accelerated particle, v is the velocity of the particle, B is the magnetic field used for keeping the charged particle in circular orbit inside the dees, m is the mass of the charged particle, and r is the radius of particle orbit during one revolution.

Assuming the validity of classical mechanics ($m = \text{constant}$), (14.18) can be solved for the angular frequency $\omega = v/r$ and for radius r to get the following expressions for ω and r

$$\omega = \omega_{\text{cyc}} = \frac{2\pi}{T} = 2\pi v_{\text{cyc}} = \frac{qB}{m_0} \quad (14.19)$$

and

$$r = \frac{m_0 v}{q \mathcal{B}} = \frac{\sqrt{2m_0 E_K}}{q \mathcal{B}}, \quad (14.20)$$

where q is the charge of the particle and E_K is its kinetic energy.

A cyclotron with radius $R = 1.34$ m of the dees, a magnetic field $\mathcal{B} = 0.45$ Vs/m², and a potential difference $\Delta V = 150$ kV between the two dees is used to accelerate protons. Mass of proton is $m_p = 938.3$ MeV/ c^2 and charge of proton $q = e = 1.602 \times 10^{-19}$ A · s. Determine:

- Maximum achievable kinetic energy $(E_K)_{\max}$ for protons accelerated from rest.
- Angular frequency (also called angular cyclotron frequency) ω_{cyc} and cyclotron frequency ν_{cyc} of the RF generator.
- Time required to accelerate a proton from rest to the maximum energy determined in (a).
- Maximum achievable kinetic energy $(E_K)_{\max}$ and cyclotron frequency ω_{cyc} of the RF generator if the cyclotron is used to accelerate alpha particles. Mass of alpha particle is $m_\alpha = 3727.4$ MeV/ c^2 and charge of alpha particle $q = 2e = 3.204 \times 10^{-19}$ A · s.
- Time required for accelerating α particle from rest to maximum energy determined in (d).
- Relativistic form of (14.19) and (14.20) for relativistic particles.

SOLUTION:

(a) The final kinetic energy $(E_K)_{\max}$ of a particle accelerated in a cyclotron depends on the radius of R of the dees, charge q and rest energy $m_0 c^2$ of the charged particle, and magnetic field \mathcal{B} holding the charged particle in a circular orbit. The velocity v of the particle during the last acceleration across the gap between the dees is from (14.20) given as

$$v = \frac{q \mathcal{B} R}{m_0}, \quad (14.21)$$

resulting in the following expression for final kinetic energy $(E_K)_{\max}$

$$E_K = \frac{m_0 v^2}{2} = \frac{R^2 q^2 \mathcal{B}^2}{2m_0}. \quad (14.22)$$

For $R = 1.34$ m and $\mathcal{B} = 0.45$ Vs/m² the maximum kinetic energy of an accelerated proton is

$$(E_K)_{\max} = \frac{R^2 q^2 \mathcal{B}^2}{2m_0} = \frac{(1.34 \text{ m})^2 \times e^2 \times (0.45 \text{ V} \cdot \text{s} \cdot \text{m}^{-2})^2 \times (3 \times 10^8 \text{ m} \cdot \text{s}^{-1})^2}{2 \times (938.3 \times 10^6 \text{ eV})}$$

$$\begin{aligned}
 &= \frac{(1.34)^2 \times (0.45)^2 \times (3 \times 10^8)^2 \text{ eV}}{2 \times (938.3 \times 10^6)} = 17.4 \times 10^6 \text{ eV} \\
 &= 17.4 \text{ MeV}. \tag{14.23}
 \end{aligned}$$

(b) Angular frequency ω_{cyc} of the RF generator is given in (14.19). For cyclotron with a magnetic field $\mathcal{B} = 0.45 \text{ Vs/m}^2$ used for acceleration of protons we get

$$\begin{aligned}
 \omega_{\text{cyc}} &= \frac{q\mathcal{B}}{m_0} = \frac{e \times (0.45 \text{ V} \cdot \text{s} \cdot \text{m}^{-2}) \times (3 \times 10^8 \text{ m} \cdot \text{s}^{-1})^2}{(938.3 \times 10^6 \text{ eV})} = 4.31 \times 10^7 \text{ s}^{-1} \\
 &= 43.2 \text{ MHz}. \tag{14.24}
 \end{aligned}$$

(c) Protons, while inside the cyclotron, follow a spiral trajectory. After crossing the gap between the two electrodes, the protons follow a semicircular orbit with a radius defined by (14.20). If N is the number of crossings the proton makes between the two electrodes and ΔE_K is the kinetic energy gained by protons in a single crossing, protons must cross the electrodes $N = E_K/\Delta E_K$ times to reach kinetic energy of E_K .

For protons accelerated in a cyclotron with a potential difference of $\Delta V = 150 \text{ kV}$ kinetic energy ΔE_K gained after a single crossing of the gap between electrodes is

$$\Delta E_K = q\Delta V = e \times (150 \text{ kV}) = 150 \text{ keV}. \tag{14.25}$$

For $\Delta E_K = 150 \text{ keV}$ the number of electrode crossings N required for protons to reach a kinetic energy $(E_K)_{\text{max}} = 17.4 \text{ MeV}$ is

$$N = \frac{(E_K)_{\text{max}}}{\Delta E_K} = \frac{17.4 \text{ MeV}}{150 \text{ keV}} \approx 116. \tag{14.26}$$

Since the protons follow a semicircular path between two consecutive crossings each the number of semicircle paths is $N - 1$. Thus, the time T required for protons to gain energy $(E_K)_{\text{max}} = 17.4 \text{ MeV}$ is

$$T = \frac{\pi \times (N - 1)}{\omega_{\text{cyc}}} = \frac{\pi \times 115}{4.31 \times 10^7 \text{ s}^{-1}} \approx 8.4 \text{ } \mu\text{s}. \tag{14.27}$$

(d) The maximum achievable kinetic energy $(E_K)_{\text{max}}$ of the alpha particle when accelerated using a cyclotron with $R = 1.34 \text{ m}$ and $\mathcal{B} = 0.45 \text{ Vs/m}^2$ is determined using (14.22) with $m_\alpha = 3727.4 \text{ MeV}/c^2$ and $q = 3.204 \times 10^{-19} \text{ A} \cdot \text{s}$. Thus,

$$\begin{aligned}
 (E_K)_{\text{max}} &= \frac{R^2 q^2 \mathcal{B}^2}{2m_0} = \frac{(1.34 \text{ m})^2 \times (2e)^2 \times (0.45 \text{ V} \cdot \text{s} \cdot \text{m}^{-2})^2 \times (3 \times 10^8 \text{ m} \cdot \text{s}^{-1})}{2 \times (3727.4 \times 10^6 \text{ eV}/c^2)} \\
 &= \frac{(1.34)^2 \times 4 \times (0.45)^2 \times (9 \times 10^{16})}{2 \times (3727.4 \times 10^6)} = 17.6 \times 10^6 \text{ eV} = 17.6 \text{ MeV}. \tag{14.28}
 \end{aligned}$$

Note: Maximum kinetic energy $(E_K)_{\text{max}}$ of proton and alpha particle accelerated in a cyclotron of same dee radius R of and same magnetic field \mathcal{B} are essentially

identical as a result of the ratio $q_p/(m_p c^2)$ for the proton being essentially equal to the ratio $q_\alpha/(m_\alpha c^2)$ for the alpha particle.

Angular frequency ω_{cyc} of the RF generator for alpha particles accelerated in cyclotron with dee radius $R = 1.34$ m and magnetic field $\mathcal{B} = 0.45$ Vs/m² is calculated from (14.19) as

$$\begin{aligned}\omega_{\text{cyc}} &= \frac{q\mathcal{B}}{m_0} = \frac{(2e) \times (0.45 \text{ V} \cdot \text{s} \cdot \text{m}^{-2}) \times (3 \times 10^8 \text{ m} \cdot \text{s}^{-1})^2}{(3727.4 \times 10^6 \text{ eV})} = 2.17 \times 10^7 \text{ s}^{-1} \\ &= 21.7 \text{ MHz.}\end{aligned}\quad (14.29)$$

(e) Kinetic energy gained by alpha particle in a single crossing of an electrode gap of $\Delta V = 150$ kV is

$$\Delta E_K = q\Delta V = 2e \times (150 \text{ kV}) = 300 \text{ keV}, \quad (14.30)$$

and to reach a kinetic energy of $(E_K)_{\text{max}} = 17.6$ MeV from rest, the number of times the alpha particles must cross the electrode gap is

$$N = \frac{(E_K)_{\text{max}}}{\Delta E_K} = \frac{17.6 \text{ MeV}}{150 \text{ keV}} \approx 59. \quad (14.31)$$

Time required to accelerate an α particle from rest to maximum energy $(E_K)_{\text{max}}$ of 17.6 MeV is calculated from (14.27) with $N = 59$ and $\omega_{\text{cyc}} = 21.7$ MHz

$$T = \frac{\pi \times (N - 1)}{\omega_{\text{cyc}}} = \frac{\pi \times 58}{2.17 \times 10^7 \text{ s}^{-1}} \approx 8.4 \text{ } \mu\text{s}. \quad (14.32)$$

(f) Equations (14.19) and (14.20) for cyclotron frequency ω_{cyc} and radius r , respectively, are valid for classical physics where an assumption is made that particle mass m_0 is constant and kinetic energy is given as $E_K = \frac{1}{2}m_0v^2$ irrespective of particle velocity v . To get corresponding equations for relativistic particles we replace m_0 of (14.19) and (14.20) with relativistic mass $m = \gamma m_0$ where γ is the Lorentz factor $\gamma = (1 - \beta^2)^{-1/2}$ and $\beta = v/c$ to get (see Prob. 35)

$$\omega_{\text{cyc}} = \frac{q\mathcal{B}}{\gamma m_0} \quad (14.33)$$

and

$$r = \frac{\gamma m_0 v}{q\mathcal{B}} = \frac{p}{q\mathcal{B}} = \frac{E_K \sqrt{1 + \frac{2m_0 c^2}{E_K}}}{q\mathcal{B}c} \quad \text{or} \quad r = \frac{\gamma m_0 v}{q\mathcal{B}} = \frac{\gamma m_0 c^2 \beta}{q\mathcal{B}c} = \frac{E\beta}{q\mathcal{B}c}, \quad (14.34)$$

where

m_0 is particle rest mass.

p is particle momentum [$p = mv = \gamma m_0 \beta c$].

E_K is particle kinetic energy [$E_K = E - E_0 = (\gamma - 1)E_0 = (\gamma - 1)m_0 c^2$].

E is particle total energy [$E = E_K + E_0 = \gamma E_0 = \gamma m_0 c^2$].

E_0 is particle rest energy [$E_0 = m_0 c^2$].

14.6 Clinical Linear Accelerator

14.6.Q1

(297)

During the past two decades medical linear accelerator (linac) has become the most common and most versatile machine in treatment of cancer with ionizing radiation. In contrast to linacs used for high-energy physics research, medical linacs are compact machines mounted isocentrically so as to allow practical radiation treatment aiming the radiation beam toward the patient from various directions to concentrate the radiation dose in the tumor and spare healthy tissues as much as possible.

- (a) Provide a historical perspective on the development of high technology radiotherapy machines.
- (b) Briefly discuss the general features of a typical modern multipurpose medical linac.
- (c) List and discuss briefly the advantages and disadvantages of linacs over cobalt-60 teletherapy machines in megavoltage radiotherapy.
- (d) List and briefly discuss the advantages and disadvantages of linacs over betatrons in megavoltage radiotherapy.
- (e) During the past 50 years medical linacs have gone through five distinct generations. List and briefly discuss the features introduced in each new generation of medical linacs.

SOLUTION:

(a) Soon after their invention, essentially all new high technology machines developed for physics research have been translated into medicine for imaging or treatment of disease. The trend started within weeks of Röntgen's discovery of x rays in 1895 with the Crookes x-ray tube becoming an important medical tool and spawning two new medical specialties: diagnostic radiology and radiotherapy as well as a new physics specialty: medical physics. Soon thereafter came the Coolidge x-ray tube (1913), Van de Graaff generator (1929), proton cyclotron (1932), betatron (1940), microtron (1944), synchrotron (1945), and linear accelerator (early 1950s). All these machines were first introduced in physics research and soon thereafter applied in medicine for imaging or radiotherapy.

The first machine designed and built directly for radiotherapy without prior use in nuclear physics was the cobalt-60 teletherapy machine. Developed in Canada in the early 1950s by medical physicist Harold E. Johns, the cobalt-60 machine became the first truly practical and widely available megavoltage cancer therapy machine in the world. It incorporates a cobalt-60 source artificially produced with neutron activation of natural cobalt in a nuclear reactor. The cobalt-60 radionuclide

is characterized with features suitable for use in external beam radiotherapy, such as high gamma ray energy (~ 1.25 MeV) for better beam penetration into tissue, relatively long half-life (5.26 years) to avoid frequent need for source replacement, and high specific activity to minimize the source size.

Another notable direct development for medical use was the GammaKnife machine that Swedish neurosurgeon Lars Leksell introduced in 1968 for use in stereotactic radiosurgery, a sophisticated specialized radiotherapy technique for irradiation of brain lesions. The machine incorporated close to 200 miniature cobalt-60 sources, each source with activity of about 30 Ci (1.11 TBq) producing a small radiation beam aimed toward the isocenter of the machine. Even today the modern version of the GammaKnife is a popular neurosurgical tool around the world; however, during the past two decades the radiosurgical technique became readily available on modern medical linacs as well as on specialized linacs such as the CyberKnife.

During the late 1950s and throughout the 1960s the cobalt teletherapy machine was the workhorse machine in radiotherapy departments and high-energy radiotherapy with megavoltage beams of effective energy above 8 MeV was carried out at that time with betatrons in a few specialized centers around the world. However, since betatrons provided less than an optimal option for megavoltage radiotherapy, a significant effort was made by several manufacturers of specialized medical equipment toward developing a compact and practical isocentric low energy linac (4 MV and 6 MV) to compete with cobalt machines as well as a 25 MV linac to provide a better option than betatron for high-energy radiotherapy.

The development of a practical clinical linac took some time, but in the early 1970s several low-energy (4 MV and 6 MV) linacs as well as high-energy (25 MV) linacs became commercially available and started to serve as replacement machines for cobalt machines and betatrons. By the late 1980s, cobalt-60 machines became almost extinct in the developed world and betatrons were no longer used for cancer therapy. Since then, linacs have undergone tremendous technological development through 5 generations; each generation introducing significant improvements over the previous one. It is now impossible to imagine modern radiotherapy without access to a state-of-the-art fifth generation clinical linear accelerator.

(b) The main characteristics of a multipurpose medical linac are as follows:

(1) Medical linacs are cyclic electron accelerators that accelerate electrons to kinetic energy in the range between 4 MeV and 25 MeV using non-conservative microwave radiofrequency (RF) fields.

(2) Most standard medical linacs operate in the S-band microwave frequency range at 2856 MHz (wavelength $\lambda \approx 10.5$ cm); some special purpose medical linacs (for example, CyberKnife and Tomotherapy machine) operate with a miniature waveguide in the X-band microwave frequency range at $\sim 10^4$ MHz (wavelength $\lambda \approx 3$ cm).

(3) In a linac, the electrons, produced in an “electron gun”, are accelerated following straight trajectories in special, evacuated, disk-loaded structures called acceleration waveguides. Electrons follow a linear path through the same, relatively low,

potential difference several times, each time gaining a defined increment in kinetic energy, until they exit the acceleration waveguide in the form of a pulsed electron pencil beam.

(4) The electron pencil beam, upon exiting the acceleration waveguide, enters the “clinical beam forming system” that generates the clinical beam from the pencil electron beam. Two types of clinical beams (either x rays or electrons) are usually available from a medical linac; both types are characterized by various clinically-relevant characteristics, such as effective energy, field size, dose rate, depth dose distribution in water, flatness, symmetry, etc.

(5) Typical multipurpose medical linac is isocentrically-mounted with a source-axis distance (SAD) of 100 cm, producing either a flat and symmetric clinical x-ray beam with variable field sizes up to $40 \times 40 \text{ cm}^2$ at the linac isocenter or a flat and symmetric clinical electron beam with field sizes up to $25 \times 25 \text{ cm}^2$ at a source-skin distance (SSD) of 100 cm.

(6) Typical multipurpose medical linac produces two x-ray energies (6 MV and 18 MV) and 5 to 6 electron energies (in MeV: 4, 6, 9, 12, 15, and 18) with a dose rate at the isocenter of $\sim 100 \text{ cGy/min}$ to $\sim 500 \text{ cGy/min}$. Optional high dose rates exceeding 1000 cGy/min are available for use in specialized radiotherapy treatments such as total body irradiation, stereotactic radiosurgery, and total skin electron irradiation.

(7) Two independent transmission ionization chambers continuously monitor the parameters of the clinical beam, such as flatness, symmetry, output, and delivered dose. The ionization chambers turn the machine off either when the preset dose at the dose reference point in the patient has been delivered or before, for patient safety, if any deviation of beam parameters from preset tolerance levels have occurred.

(8) Modern multipurpose linacs are equipped to deliver, in addition to traditional radiotherapy beams and treatment plans, a series of modern radiotherapy techniques, such as intensity modulated radiotherapy (IMRT), intensity modulated arc therapy (IMAT), image guided radiotherapy (IGRT), and adaptive radiotherapy (ART). They also can deliver a series of specialized radiotherapy techniques, such as total body irradiation (TBI) with x-ray beams, total skin electron irradiation (TSEI), electron arc therapy, and stereotactic external beam irradiation.

(c) During the past two decades linac eclipsed the cobalt-60 teletherapy machine and became the most widely used radiation-producing machine in modern radiotherapy. In comparison with a cobalt-60 teletherapy machine, advantages of a typical modern linac are:

- (1) Higher photon beam energy resulting in better skin sparing effect and more effective beam penetration into tissue.
- (2) Electron beams for treatment of superficial lesions.

- (3) X-ray mode with two beam energies (6 MV and 18 MV) and electron mode with 5 or 6 electron beam energies in the range from 6 MeV to 22 MeV.
- (4) Higher output dose rate resulting in shorter treatment time.
- (5) Beam intensity modulation for IMRT treatment.
- (6) No highly radioactive source replacement is required.
- (7) No high activity radionuclide with associated security and decommissioning issues is present.

Despite the significant technological and practical advantages of linacs over cobalt machines, the latter still occupy an important place in the radiotherapy armamentarium, mainly because of significantly lower capital, installation, maintenance, and operation costs in comparison with linacs. Manufacturers of cobalt machines were slow in incorporating the many new features that are not necessarily unique to linacs, such as large source-axis distance, high output, dynamic wedge, independent jaws, and a multileaf collimator. With these features slowly moving onto modern cobalt machines, one can expect that, in the developing world, the cobalt-60 teletherapy machines, owing to their relatively low cost, simplicity of design, ease of operation, and relatively inexpensive maintenance and calibration cost, are likely to play an important role in cancer therapy for the foreseeable future.

(d) Betatron provided a relatively inexpensive option for access to high-energy radiotherapy during 1950s and 1960s; however, it had several serious inherent drawbacks that made its use in radiotherapy obsolete immediately after clinical linacs became available in the early 1970s. The main clinical disadvantages of betatron in comparison to linac are as follows:

- (1) Significantly lower beam output resulting in long and inconvenient treatment times.
- (2) Relatively small field sizes (as a result of flattening the low-output beam) limiting the treatment fields required for radiotherapy.
- (3) Very noisy operation when beam is turned on, resulting in an uncomfortable treatment procedure for the patient.
- (4) Design incorporating the bulky magnet used for electron acceleration and for keeping the electron in circular motion does not lend itself to isocentric mounting thereby presenting a severe obstacle to efficient radiotherapy treatment.

As far as advantages of betatron over linac are concerned, two come to mind:

- (1) The bremsstrahlung x-ray beam is produced in a betatron by a thin target and in a linac by a thick target. This means that, for electrons of same kinetic energy striking the target, the betatron x-ray beam is inherently more penetrating than a linac x-ray beam; however, this discrepancy is not very pronounced and can be mitigated by using in a linac a low atomic number Z thick target (e.g., copper) and a low Z flattening filter.
- (2) Betatron for the same nominal beam energy, costing only about 50 % of the cost of a linac, is significantly cheaper than a linac; however, the difference in

cost does not outweigh the disadvantages that the use of a betatron entails in a clinical setting. Difference in cost notwithstanding, as soon as high-energy clinical linacs became commercially available, they immediately replaced betatrons as the machine of choice for high-energy radiotherapy.

(e) During the past 50 years, medical linacs have gone through five distinct generations, making the contemporary machines extremely sophisticated in comparison with machines of the 1960s. Each generation introduced the following new features:

- (1) *Low energy photons (4–8 MV):*
straight-through beam; fixed flattening filter; external wedges; symmetric jaws; single transmission ionization chamber; isocentric mounting.
- (2) *Medium energy photons (10–15 MV) and electrons:*
bent beam; movable target and flattening filter; scattering foils; dual transmission ionization chamber; electron cones (applicators).
- (3) *High energy photons (18–25 MV) and electrons:*
dual photon energy and multiple electron energies; achromatic bending magnet; dual scattering foils or scanned electron pencil beam; motorized wedge; asymmetric or independent collimator jaws.
- (4) *High energy photons and electrons:*
computer-controlled operation; dynamic wedge; electronic portal imaging device; multileaf collimator (MLC).
- (5) *High energy photons and electrons:*
photon beam intensity modulation with multileaf collimator; full dynamic conformal dose delivery with intensity modulated beams produced with a multileaf collimator; on-board imaging for use in adaptive radiotherapy.

14.6.Q2**(298)**

Various types of linacs are available for clinical use. Some provide x rays only in the low megavoltage range (4 MV or 6 MV), others provide both x rays and electrons at various megavoltage energies. Some medical linacs are highly specialized and use miniature waveguides to achieve their specialized aims. A typical modern high-energy linac provides two photon energies (e.g., 6 MV and 18 MV) and several electron energies in the range from 4 MeV to 22 MeV.

- (a) Draw a schematic diagram of a typical modern S band medical linac and identify its main components.
- (b) Beam-forming components of medical linacs are usually grouped into six systems. List and briefly discuss each of the six systems.

- (c) The treatment head of a medical linac contains several components that contribute to the production, shaping, localizing, and monitoring of clinical x-ray beams. List (in the direction of the pencil electron beam exiting the accelerating waveguide) and briefly discuss the important components found in a typical head of a modern medical linac and used in *production of clinical x-ray beam*.
- (d) Treatment head of a medical linac contains several components that contribute to the production, shaping, localizing, and monitoring of clinical electron beams. List (in the direction of the pencil electron beam exiting the accelerating waveguide) and briefly discuss the important components found in a typical head of a modern medical linac and used in *production of clinical electron beams*.
- (e) Draw a schematic diagram of a typical high-energy linac head indicating the important components that are used in production of: (A) clinical x-ray beams and (B) clinical electron beams.

SOLUTION:

(a) A **schematic diagram** of a typical modern S-band medical linac is shown in Fig. 14.5. Also shown are the connections and relationships among the various linac components. The diagram provides a general layout of the important linac components; however, there are significant variations from one commercial machine to another, depending on the final electron beam kinetic energy as well as on the particular design used by the manufacturer. The length of the accelerating waveguide depends on the final electron kinetic energy, and ranges from ~ 30 cm at 4 MeV to ~ 150 cm at 25 MeV. It is reasonable to assume that all clinical linacs will have a schematic diagram similar to the one shown in Fig. 14.5.

The process of producing a clinical x-ray beam or a clinical electron beam out of the electron pencil beam generated by an electron linac is quite sophisticated. It incorporates 50 years of basic research, clinical experience, and technological development all merged into producing a clinical beam with the goal of providing an efficient and optimal treatment of patients who suffer life-threatening, mainly malignant, disease that can be treated with ionizing radiation.

(b) **Beam-forming components** of medical linacs are as follows:

- (1) *Injection system.*
- (2) *RF power generation system.*
- (3) *Accelerating waveguide.*
- (4) *Auxiliary system.*
- (5) *Beam transport system.*
- (6) *Beam collimation and beam monitoring system.*

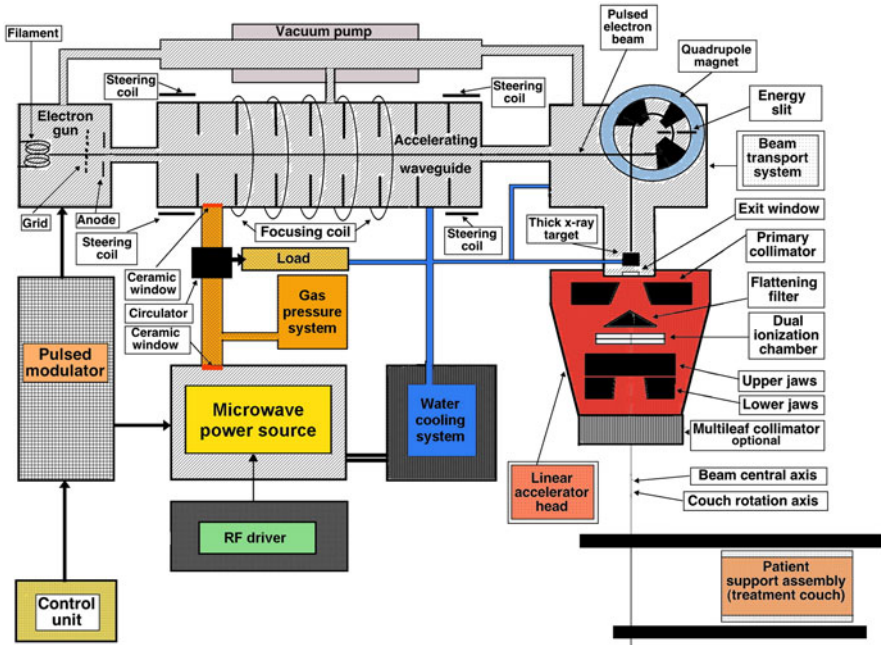


Fig. 14.5 Schematic diagram of a medical linear accelerator (linac) depicting the major components that are involved in the production of clinical radiation beams for use in treatment of disease

(1) *Injection system* is the source of electrons, essentially a simple electrostatic accelerator called an electron gun. Two types of electron gun are in use: diode type and triode type, both containing a heated cathode (at a negative potential of the order of -25 kV) and a perforated grounded anode. In addition, triode type gun also incorporates a grid placed between the cathode and the anode. Electrons are thermionically emitted from the heated cathode, focused into a pencil beam and accelerated toward the perforated anode through which they drift into the accelerating waveguide.

(2) *Radiofrequency (RF) power generating system* produces the high power microwave radiation used for electron acceleration in the accelerating waveguide and consists of two components: the RF power source and the pulsed modulator. The RF power source is either a magnetron or a klystron in conjunction with a low power RF oscillator (RF driver). Both devices use electron acceleration and deceleration in vacuum for production of the high power RF fields. The pulsed modulator produces the high voltage, high current, short duration pulses required by the RF power source and the electron injection system for electron acceleration in the linac.

(3) Electrons are accelerated in the *acceleration waveguide* by means of an energy transfer from the pulsed high power RF field that is set up in the acceleration waveguide and produced by the RF power generator. The accelerating waveguide is in principle obtained from a circular uniform waveguide by adding a series of

disks (irises) with circular holes at the center, positioned at equal distances along the tube. These disks divide the acceleration waveguide into a series of cylindrical cavities that form the basic structure of the accelerating waveguide of a linac.

(4) *Auxiliary system* of a linac consists of several basic systems that are not directly involved with electron acceleration, yet they make the acceleration possible and the linac viable for clinical operation. These systems are: the vacuum-pumping system, water-cooling system, air-pressure system, and shielding against leakage radiation.

(5) *Electron beam transport system* brings the pulsed high-energy electron pencil beam from the acceleration waveguide onto the target in the x-ray therapy mode and onto the scattering foil in the electron therapy mode.

(6) *Beam monitoring system* and *beam collimation system* forms an essential system in a medical linac ensuring that radiation dose as well as radiation field may be delivered to the patient as prescribed, with a high numerical and spatial accuracy.

(c) **Production of clinical x-ray beam** in the x-ray therapy mode. Electrons, originating in the electron gun, are accelerated in the accelerating waveguide to the desired kinetic energy and then brought, in the form of a pulsed pencil beam, through the beam transport system into the linac treatment head, where the clinical x-ray beams are formed. The important components used in clinical x-ray beam production are (listed in the direction of the accelerated electron pencil beam):

- (1) Bremsstrahlung target (retractable).
- (2) Beryllium exit window.
- (3) Primary collimator.
- (4) Flattening filter (retractable).
- (5) Dose monitoring system.
- (6) Upper adjustable and independent collimator jaws.
- (7) Lower adjustable and independent collimator jaws.
- (8) Multileaf collimator (completely open).

(1) *Bremsstrahlung target (retractable)*. As the electron pencil beam of kinetic energy E_K strikes the thick target (with a typical focal spot of 2 mm diameter) electrons are rapidly decelerated and lose part of their kinetic energy in the form of bremsstrahlung x rays through inelastic interactions with target nuclei. The x-ray beam thus produced has a continuous spectral distribution with photon energies ranging from 0 up to E_K . The intensity of the x-ray beam produced in the target is mainly forward peaked and a flattening filter is used to flatten the beam and make it suitable for clinical application. In low energy linacs that do not have a clinical electron therapy option the bremsstrahlung target is not retractable and is usually permanently imbedded into the accelerating waveguide. In linacs that also offer

electron beam therapy mode the bremsstrahlung target is retractable and in clinical electron therapy mode moves away from the path of the electron pencil beam to allow production of a clinical electron beam.

(2) *Beryllium exit window* separates from the atmospheric pressure the evacuated linac components ($\sim 10^{-6}$ tor) that produce and transport the electron pencil beam.

(3) *Primary collimator* defines the maximum circular field available from the linac. This maximum field size is typically of the order of 30 cm diameter at 100 cm from the target.

(4) *Flattening filter* produces a flat x-ray beam out of the forward peaked beam generated in the bremsstrahlung thick target. Typical profile of an unflattened beam produced in a bremsstrahlung target measured at 100 cm from the target exhibits a peak (100 %) on the beam central axis and drops to ~ 30 % at the edge of the maximum field defined by the primary collimator. Thus, to flatten this raw (unflattened) beam profile, the intensity on the central beam axis must be diminished from 100 % down to ~ 30 %. All other points on the raw intensity profile must also be diminished to read as close as possible to the same absolute intensity measured at the edge of the maximum field, and this is achieved with a flattening filter that is usually designed empirically in the form of a cone centered on the beam central axis.

(5) *Dose monitoring system* of a medical linac is based on two independent transmission ionization chambers permanently imbedded into the linac clinical x-ray and electron beams. The chambers are used to monitor the beam output (patient dose) continuously during patient treatment. In addition to dose monitoring, the chambers are also used for monitoring the radial and transverse flatness of the radiation beam as well as its symmetry and energy.

For patient safety, the linac dosimetry system usually consists of two separately sealed ionization chambers with completely independent biasing power supplies and read out electrometers. If the primary chamber fails during patient treatment, the secondary chamber will terminate the irradiation, usually after an additional dose of only a few % above the prescribed dose has been delivered. For added patient safety linacs are also equipped with backup timers in addition to two ionization chambers. In the event of simultaneous failure of both the primary as well as the secondary ionization chamber, the linac timer will shut the machine down with a minimal overdose delivered to the patient.

(6) and (7) Upper adjustable and independent collimator jaws together with the lower adjustable and independent collimator jaws form the *secondary collimator system* of a clinical linac. The jaws are adjustable to project square and rectangular fields of dimensions from 0×0 up to 40×40 cm² at the linac isocenter that is 100 cm from the bremsstrahlung target. Since the jaws are independent, asymmetric square and rectangular fields are also possible.

(8) *Multileaf collimator* (MLC). The MLC is a relatively new addition to modern linac dose delivery technology. In principle, the idea behind an MLC is simple: MLC allows production of irregularly shaped radiation fields with much accuracy as well as efficiency and is based on an array of narrow collimator leaf pairs, each leaf controlled with its own miniature motor. The building of a reliable MLC system presents a substantial technological challenge and current models incorporate up to 160 leaves (80 pairs) covering radiation fields up to $40 \times 40 \text{ cm}^2$ and requiring 160 individually computer-controlled motors and control circuits.

Note: A typical modern high-energy linac offers two clinical x-ray beams: low megavoltage energy at 6 MV and high energy at $\sim 18 \text{ MV}$. In order to obtain an optimized clinical beam, linac employs a separate target—flattening filter combination for each beam energy.

(d) Production of clinical electron beam in the electron beam therapy mode. Megavoltage electron beams in the energy range from 4 MeV to 22 MeV represent an important treatment modality in modern radiotherapy, often providing a unique option in treatment of superficial tumors. Like clinical x-ray beams, clinical electron beams are also produced in the head of the modern medical linac, starting with the electron pencil beam of desired kinetic energy (Note: the pencil electron beam current used to produce the same dose rate at depth of dose maximum in the patient is approximately two to three orders of magnitude lower in the clinical electron beam mode compared to the clinical photon beam mode).

While clinical x-ray beams are produced with an appropriate target—flattening filter combination and collimated to desired field shape using the primary, secondary, and multileaf collimators, clinical electron beams are most commonly produced with scattering foils and collimated with electron cones. The important components used in clinical electron beam production (listed in the direction of the accelerated electron pencil beam) are:

- (1) _____
- (2) Beryllium exit window.
- (3) Primary collimator.
- (4) Scattering foil, also called scattering filter (retracted in the clinical x-ray therapy mode).
- (5) Two independent transmission ionization chambers.
- (6) Upper adjustable and independent collimator jaws.
- (7) Lower adjustable and independent collimator jaws.
- (8) Multileaf collimator (fully opened in the clinical electron therapy mode).
- (9) Electron cone (also called electron applicator).

(1) *Bremsstrahlung target* used for production of clinical x-ray beam is in production of clinical electron beam retracted from the pencil beam.

(2) *Beryllium exit window* separates the evacuated linac components ($\sim 10^{-6}$ tor) from the atmospheric pressure. It is strong to withstand the pressure difference between vacuum and atmospheric pressure, yet very thin to transmit the electron pencil

beam from the vacuum into atmospheric pressure. It is made of low atomic number material ($Z = 4$) to produce as little bremsstrahlung contamination of the electron beam as possible.

(3) *Primary collimator* affects the unflattened photon beam produced in the bremsstrahlung target in the clinical x-ray therapy mode. It has no effect on the pencil electron beam in the clinical electron therapy mode.

(4) *Scattering foils*. The scattering of the electron pencil beam over the relatively large area used in electron beam radiotherapy (up to $30 \times 30 \text{ cm}^2$ at linac isocenter) is achieved by placing one or more thin foils of high atomic number material (e.g., lead) into the pencil beam at the level of the flattening filter used in the x-ray therapy mode. Another option for producing large electron fields, albeit much more complex and therefore seldom used, is pencil beam magnetic scanning. The technique is implemented with two computer-controlled magnets that deflect the electron pencil beam in two orthogonal planes, thereby scanning the pencil beam across the clinical treatment field.

(5) Dose monitoring system is the same for the clinical x-ray therapy mode and the clinical electron therapy mode, discussed in (c).

(6) and (7) Because of the significant scattering of electrons in air compared to photon scattering in air the *secondary collimator system* cannot be used for defining the field size in clinical electron beams. Therefore, the secondary collimation system plays only a secondary role in electron beam therapy unlike the situation with clinical x-ray beams where the clinical beam is formed with three collimator types: primary, secondary, and MLC.

Radiation field for clinical electron beams is determined with the electron beam cones rather than with the upper and lower jaws of the secondary collimator and the MLC. However, for a given electron cone size, the MLC is placed into a completely open position and the upper and lower jaws must be set to a position prescribed for a particular electron cone, so as to reproduce the electron scattering conditions and keep the electron beam flatness optimal.

(8) *Multileaf collimator* plays no role in clinical electron therapy mode and must be placed into fully open position in the clinical electron therapy mode.

(9) *Electron cones* are used to define the desired clinical electron beam field size. The scattering of electrons in air makes the use of photon collimators that are placed relatively far (typically 40 cm to 50 cm) from the patient impossible and the collimation for electron beams must be placed close to the patient, typically a few centimeters from the patient surface. This is achieved with electron cones that define the electron beam field size and must be removed when clinical x-ray beam therapy mode is used.

(e) Figure 14.6 depicts a **typical linac head** employed in production of (A) clinical x-ray beams and (B) clinical electron beams.

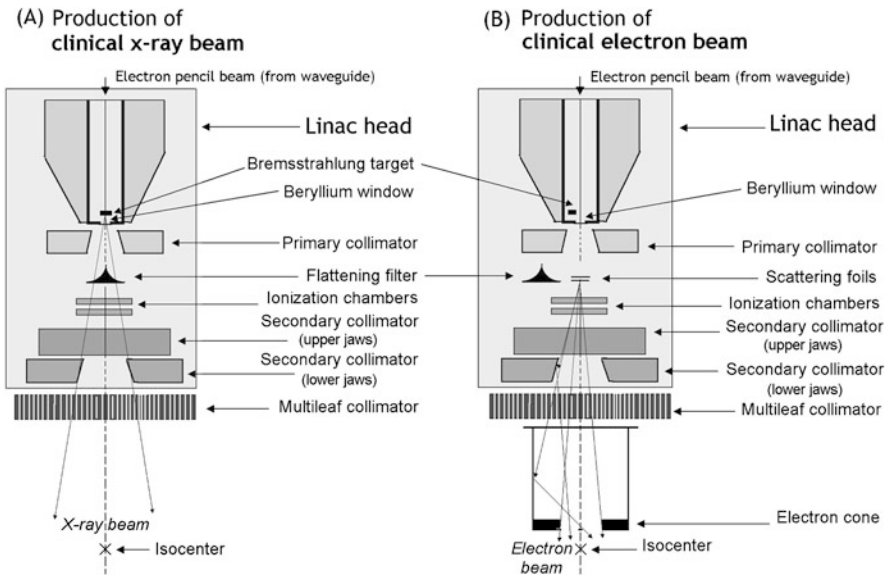


Fig. 14.6 Schematic representation of a typical medical linac head with **(A)** depicting the important components briefly described in **(c)** for production of clinical x-ray beams and **(B)** depicting the important components briefly described in **(d)** for production of clinical electron beams

14.6.Q3

(299)

Except for constant potential x-ray machines, all particle accelerators operate in some sort of pulsed operation. In linear accelerator (linac) the major components including the source of radiofrequency (RF system), electron gun (injection system), acceleration of electrons in the accelerating wave guide (acceleration system), and production of bremsstrahlung x rays in the linac bremsstrahlung target in the clinical x-ray mode or arrival of electrons at the scattering foils in the clinical electron mode operate in a pulsed mode with a relatively low duty cycle.

A medical 18 MV linac operates at a pulse repetition rate (rep rate) $\rho = 100 \text{ s}^{-1} = 100 \text{ pps}$, duty cycle $\delta = 2 \times 10^{-4}$, and a peak current $I_p = 120 \text{ mA}$. A thick bremsstrahlung target is used for x-ray production and the cathode of the electron gun (triode type) is operated at -25 kV . The linac runs in the S-band frequency range at $\nu = 2856 \text{ MHz}$.

- (a) Define the duty cycle δ and pulse repetition rate ρ .
- (b) Calculate the period T of the pulsed operation of the linac.
- (c) Calculate the pulse width τ of the linac.

- (d) Calculate the mean pencil beam current \bar{I} of the linac.
- (e) Calculate the charge q_τ deposited per pulse in the thick target of the linac.
- (f) Calculate the charge $q_{t=1\text{ s}}$ deposited per second in the thick linac bremsstrahlung target.
- (g) Calculate the power P_{pulse} deposited per pulse in the thick linac bremsstrahlung target.
- (h) Calculate the mean power \bar{P} deposited in the thick bremsstrahlung target of the linac.
- (i) Sketch the linac pulse sequence and identify its main parameters of the linac above: (1) Pulse width τ , (2) Period T , (3) Peak current I_P , and (4) Mean current \bar{I} .
- (j) Calculate the power P_X deposited in the target (anode) of a typical constant potential x-ray tube used for radiotherapy at anode voltage $U_a = 100\text{ kV}$ and tube current $I = 50\text{ mA}$. Compare your result for the x-ray tube with the mean power \bar{P}_L deposited onto a linac target calculated in (g). Explain the difference.
- (k) Define thick and thin targets in linac x-ray production.
- (l) Briefly describe the main steps in the pulsed operation of a medical linac. Indicate these steps for the linac on the graph plotted in (h).

SOLUTION:

(a) In telecommunications and electronics the duty cycle δ is defined as the fraction of time during which a particular periodic system is in active state or

$$\delta = \frac{\tau}{T}, \quad (14.35)$$

where τ is the duration of the active pulse and T is the period of the periodic operation. The pulse repetition rate ρ (in short, “rep rate”) is defined as the number of pulses per unit time.

(b) Period T of pulsed operation for linac

$$T = \frac{1}{\rho} = \frac{1}{100\text{ s}^{-1}} = 10^{-2}\text{ s} = 10^4\text{ }\mu\text{s}. \quad (14.36)$$

(c) Pulse width τ for linac^(*)

$$\tau = \delta \cdot T = (2 \times 10^{-4}) \times (10^{-2}\text{ s}) = 2 \times 10^{-6}\text{ s} = 2\text{ }\mu\text{s}. \quad (14.37)$$

(d) Mean pencil beam current \bar{I} in the accelerating waveguide

$$\bar{I} = \delta \cdot I_P = (2 \times 10^{-4}) \times (120 \times 10^{-3}\text{ A}) = 2.4 \times 10^{-5}\text{ A} = 24\text{ }\mu\text{A}. \quad (14.38)$$

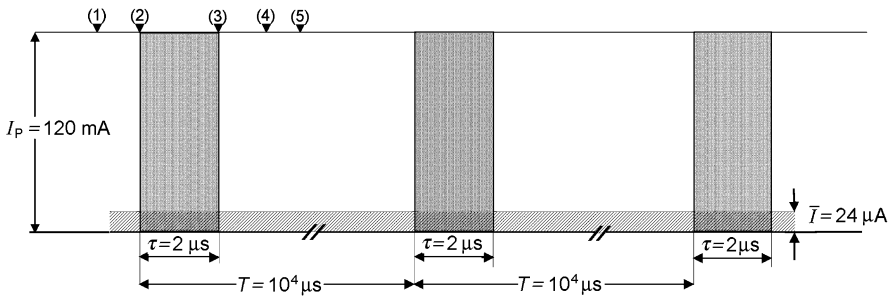


Fig. 14.7 Pulse sequence for electrons arriving at the bremsstrahlung target. Numbers (1) through (5) refer to main steps of linac pulse sequence listed in (l)

(e) Charge q_τ deposited per pulse in the thick bremsstrahlung target

$$q_\tau = I_p \cdot \tau = (120 \times 10^{-3} \text{ A}) \times (2 \times 10^{-6} \text{ s}) = 2.4 \times 10^{-7} \text{ As} = 0.24 \mu\text{C} = 240 \text{ nC}. \quad (14.39)$$

(f) Charge $q_{t=1 \text{ s}}$ deposited per $t = 1 \text{ s}$ in the x-ray target

$$q_{t=1 \text{ s}} = \bar{I} \cdot t = (2.4 \times 10^{-5} \text{ A}) \times (1 \text{ s}) = 2.4 \times 10^{-5} \text{ As} = 24 \mu\text{C}. \quad (14.40)$$

(g) Power P_τ deposited per pulse in the thick bremsstrahlung target (instantaneous power):

$$P_\tau = I_p U = (120 \times 10^{-3} \text{ A}) \times (18 \times 10^6 \text{ V}) = 2.16 \times 10^6 \text{ W} = 2.16 \text{ MW}. \quad (14.41)$$

(h) Mean power \bar{P} deposited in the thick bremsstrahlung target

$$\bar{P} = \bar{I} \cdot U = (2.4 \times 10^{-5} \text{ A}) \times (18 \times 10^6 \text{ V}) = 432 \text{ W} = 0.432 \text{ kW}. \quad (14.42)$$

Note: Cathode potential of -25 kV is irrelevant in the calculation of power per pulse P_τ and the mean power \bar{P} ; the important quantity in power calculation is the kinetic energy $E_K = 18 \text{ MeV}$ of the electron striking the bremsstrahlung target, implying a potential U of 18 MV .

(i) Sketch of the linac pulse sequence based on linac data given above is summarized in Fig. 14.7. Parameters calculated for the specific medical linac data of this problem are as follows: period $T = 10^4 \mu\text{s}$, pulse width $\tau = 2 \mu\text{s}$, mean pencil beam current $\bar{I} = 24 \mu\text{A}$, charge deposited per pulse $q_\tau = 240 \text{ nC}$, charge deposited per 1 second $q_{t=1 \text{ s}} = 240 \mu\text{C}$, power deposited per pulse $P_\tau = 2.16 \text{ MW}$, and mean power $\bar{P} = 432 \text{ W}$.

(j) Power P_X deposited in the target (anode) of the x-ray tube:

$$P_X = I_a U = (50 \text{ mA}) \times (100 \text{ kV}) = 5000 \text{ W} = 5 \text{ kW}. \quad (14.43)$$

In **(h)** we show that for a typical medical linac the mean power \bar{P} deposited in its thick bremsstrahlung target by an electron pencil beam with kinetic energy E_K of 18 MeV is ~ 432 W. On the other hand, in (14.43) we show that for a typical therapy x-ray machine the power deposited in its x-ray target (anode) by an electron pencil beam with kinetic energy E_K of 100 keV is ~ 5000 W. A comparison of the two power values shows that the power deposited into a linac target is more than an order of magnitude lower than that deposited into an x-ray target. We Note: the calculated power depositions are normalized to roughly the same output for both machines, amounting to about 100 cGy/min at a distance of 100 cm from the target.

The two calculations confirm that efficiency for bremsstrahlung production increases with kinetic energy E_K of the incident electron in addition to also depending on the atomic number Z of the target. It is well known that in x-ray tubes operating in the diagnostic energy range of the order of 100 kV (referred to as the orthovoltage range in radiotherapy) the efficiency of x-ray production is of the order of 1 %. This means that only 1 % of the incident electron's kinetic energy E_K goes into x-ray production and 99 % is transformed into heat that must be somehow dissipated so as not to damage the target (anode). Thus the heat that must be dissipated amounts to almost 100 times the energy transformed into x rays and this is not a simple task, as shown by the complicated design of cooling methods applied to commercial x-ray tubes.

In megavoltage radiotherapy, on the other hand, as a result of the relatively high kinetic energy E_K of electrons striking the bremsstrahlung target (from 4 MeV to 25 MeV), the efficiency for x-ray production at ~ 10 % is much higher than in orthovoltage x-ray tubes where the efficiency is below 1 %. Thus, since the ratio between cooling power and x-ray power is only a factor of 10 for linacs rather than 100 for x-ray tubes, the cooling of linac targets is less of a concern than the cooling of targets in x-ray tubes.

Efficiency for x-ray production also depends on the atomic number of the bremsstrahlung target. For the same kinetic energy E_K of the incident electron, the higher is the atomic number Z of the target, the larger is the intensity of the emitted bremsstrahlung. However, we must note that here we are talking about the emitted intensity integrated over the 4π geometry around the target. In the first approximation we can state that the integrated intensity of the emitted bremsstrahlung is proportional to Z^2 for a thin target and is approximately linearly proportional to Z for a thick target.

(k) For a given incident kinetic energy $(E_K)_0$ a thin target is a target whose thickness is much less than the range of electrons of kinetic energy $(E_K)_0$ in the target material. A thick target, on the other hand, is defined as a target with thickness of the order of the range of electrons of kinetic energy E_K in the target material.

The effective energy of the thin target photon spectrum is higher than that of a thick target because in a thin target incident electrons of kinetic energy $(E_K)_0$ produce all bremsstrahlung photons while bremsstrahlung photons produced in a thick target are produced by electrons ranging in kinetic energy from incident kinetic energy $(E_K)_0$ all the way down to zero.

(I) *Typical* medical linac pulsed operation sequence proceeds as follows (the 5 steps are indicated on the pulse sequence diagram of Fig. 14.7 for the specific data for the medical linac of this problem):

- (1) Control unit turns ON the RF power in the RF system. It takes of the order of $1 \mu\text{s}$ to fill the acceleration waveguide with RF power and produce a field required for acceleration of electrons.
- (2) Electron gun is then turned ON, electrons are injected into the acceleration waveguide for a few microseconds and accelerated toward the bremsstrahlung target.
- (3) Electron gun is turned OFF and injection of electrons into the acceleration waveguide is stopped.
- (4) RF system is switched OFF, the acceleration waveguide is completely de-excited in about $1 \mu\text{s}$ through dumping the residual energy into a dissipative load.
- (5) System is ready for the next cycle that will start after a time interval $T - \tau - (\sim 1 \mu\text{s})$.

14.6.Q4

(300)

Medical linear accelerators (linacs) vary in design from one manufacturer to another; however, all medical linacs contain the same basic systems and components and apply similar techniques to produce clinical x-ray beams and clinical electron beams.

Figure 14.8 depicts a schematic diagram of a medical linac with systems as well as a major and minor components identified only with white or black numbers.

- (a) Identify the numbered systems, major components, and minor components. For each entry write a short note explaining the role the system or component plays in the linac operation.
- (b) Answer the following short questions on the linac represented in Fig. 14.8.
 - (1) What type of linac does the diagram most likely represent and why?
 - (2) What clinical mode does the diagram represent and why?
 - (3) What type of electron gun does the diagram show? Explain.
 - (4) What type of RF generator does the diagram show? Explain.
- (c) Give the order of magnitude for the following parameters of a typical medical linac:
 - (1) Peak pencil beam current.

- (2) Mean pencil beam current for clinical x-ray mode.
- (3) Mean beam current for clinical electron mode.
- (4) Duty cycle and pulse repetition rate.
- (5) Peak modulator current and peak voltage.
- (6) Radiofrequency of operation for standard linac and miniature linac.
- (7) Beam current pulse width.

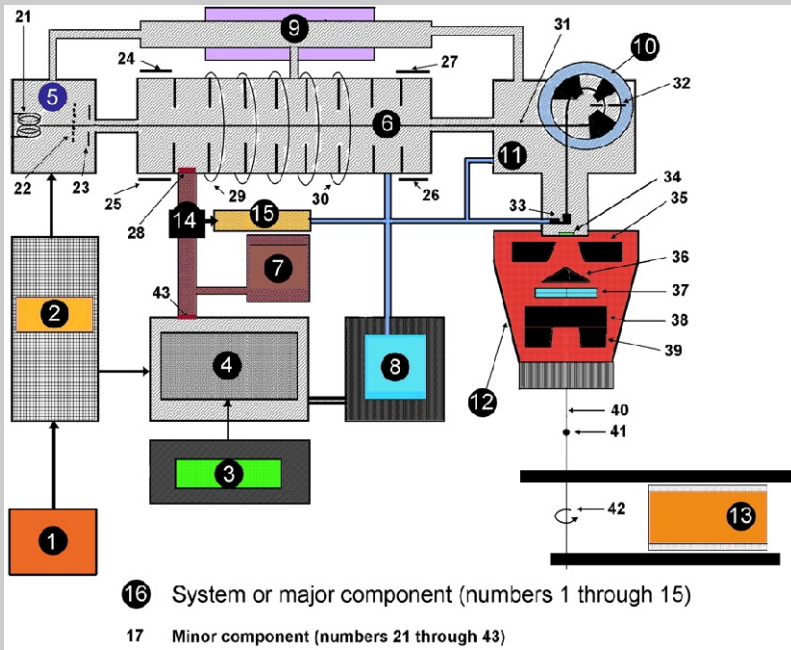


Fig. 14.8 Schematic diagram of a typical medical linear accelerator (linac)

SOLUTION:

(a) MAJOR SYSTEMS AND COMPONENTS of a medical linac are as follows:

(1) **Control unit** forms part of the control console located in the control area of a medical linac installation immediately outside the shielded treatment room. The control unit usually has two major components: machine control unit and treatment control unit, both integrated and handled by a computer. Based on the information that was entered on the treatment control unit, the machine control unit sends the appropriate trigger pulses to the beam forming system of the linac, sets the desired dose rate, controls the pulsed operation of the beam forming system, and terminates the production of radiation once the preset dose has been attained.

(2) **Pulsed modulator** generates the high current (~ 100 A), high voltage (~ 100 V) and short duration (few μs) pulses required to run the RF power generating system (4) and the electron gun (5). The main components of a pulsed modulator are: (i) three-phase full wave rectifier, (ii) pulse-forming network (PFN), (iii) hydrogen thyratron, (iv) pulse transformer, and (v) pulse repetition frequency generator.

(3) **RF driver** is a low power microwave oscillator providing low power RF input to a klystron tube for amplification and subsequent use for electron acceleration in accelerating waveguide.

(4) **RF power generation system** is the source of RF fields that are used in the accelerating waveguide (6) for accelerating electrons by means of energy transfer from the high power RF fields set up in the accelerating waveguide by microwave radiation. These fields are generated either by a magnetron that serves as source and amplifier of RF power or by a klystron which uses low power RF from a microwave oscillator (RF driver) and amplifies it into high power RF field. Both magnetron and klystron are devices that rely on electron deceleration in vacuum for production of the high power RF fields required for electron acceleration in the accelerating waveguide.

(5) **Electron gun** serves as the electron injection system producing low energy electrons and injecting them into the accelerating waveguide. The electron gun is a simple electrostatic electron accelerator, thermionically releasing electrons from a heated cathode and accelerating them toward the anode. Two types of electron gun are in use: (i) diode-type gun has only two electrodes: cathode and anode and (ii) triode-type gun has a grid electrode in addition to cathode and anode. In a diode gun the pulsed electron injection into the accelerating waveguide is controlled with pulsed cathode voltage while in a triode gun the pulsed emission of electrons is controlled with appropriate grid potential. Typical gun voltage on both gun types is -25 kV on the cathode with a grounded anode. The gun on this diagram is a triode-type gun, since it incorporates a grid.

(6) **Acceleration waveguide** provides the mechanism for electron acceleration in a linac. It is a hollow evacuated ($\sim 10^{-6}$ tor) copper cylinder loaded with periodic copper disks (irises) with a hole in the center. The disks divide the waveguide into a series of cylindrical cavities that form the basic structure of the acceleration waveguide in a linac. The role of the cavities is: (i) to slow down the phase velocity of the microwaves in the waveguide to allow electrons to follow the wave during the acceleration process, (ii) to couple and distribute microwave power between adjacent cavities, and (iii) to provide a suitable electric field pattern for acceleration of electrons.

Two types of acceleration waveguide have been developed for acceleration of electrons: travelling wave structure and standing wave structure. In the travelling wave structure the microwaves enter the waveguide on the gun side and propagate

toward the high-energy end of the waveguide where they are either absorbed without any reflection or exit the waveguide to be absorbed in a resistive load of fed back to the input end of the accelerating structure. In the standing wave structure, each end of the acceleration waveguide is terminated with a conducting disk to reflect the microwave power with a $\pi/2$ phase change, resulting in a buildup of standing waves in the waveguide.

Most medical linacs operate in the S band frequency range at 2856 MHz where typical accelerating cavities are about 10 cm in diameter and 2.5 cm to 5 cm in length. Typical energy gain in the acceleration waveguide is about 1 MeV per cavity. The length of the acceleration waveguide depends on the final electron kinetic energy and the type of waveguide (travelling type is about twice as long as the standing waveguide for the same final energy) and ranges from ~ 30 cm at 4 MeV (standing wave) to ~ 150 cm at 10 MeV (travelling wave).

(7) **Gas pressure system** is filled with a dielectric gas used to pressurize the uniform waveguides that transfer the microwave power from the RF power generation system into the accelerating waveguide. While accelerating waveguides must be evacuated for acceleration of electrons, uniform waveguides that are used for efficient transmission of microwave power can do so either in vacuum or at elevated dielectric gas pressure. Since keeping high vacuum in a uniform waveguide is much more difficult than keeping elevated gas pressure, it is standard procedure to fill the microwave transmission lines (uniform waveguides) with a suitable dielectric gas at elevated pressure. Most common gas used for this purpose is sulfur-hexafluoride (SF_6) at double the atmospheric pressure.

(8) **Water-cooling system** uses cooling water circulating through a heat exchanger for cooling of linac components that heat up during the use of the linac. These are: (i) RF power generating system, (ii) Circulator and RF load, (iii) Pulse transformer in the modulator, (iv) Accelerating waveguide, (v) Bending magnets in the beam transport system, and (vi) Bremsstrahlung target when linac operates in the clinical x-ray mode.

(9) **Vacuum system** incorporating an ion pump to maintain high operating vacuum in all linac systems transmitting electrons in the electron acceleration process: (i) injection system, (ii) electron acceleration system, and (iii) electron beam transport system. The ion pump operates as a cold cathode discharge tube and provides the high vacuum required for unimpeded motion of the electron pencil beam from the electron gun through the accelerating waveguide and beam transport system toward the bremsstrahlung target in clinical x-ray mode or exit window in clinical electron mode.

(10) **Quadrupole bending magnet** provides 270° bending of the pulsed electron pencil beam and this is the most common of several possible approaches to electron beam bending in medical linacs exceeding 6 MeV in the final kinetic energy of the electron. The 270° bending system is achromatic and provides electrons with a long

exposure to the magnetic field. It also refocuses the electron spectral spread and directional spread, and provides a small focal spot provided that the bremsstrahlung target is placed into the bending magnet focus. One drawback of the 270° bending magnet compared to a 90° bending magnet is that the 270° bending magnet is significantly bulkier, requiring more space and an increase in the height of the linac isocenter.

(11) **Electron beam transport system** is used to transfer the pulsed electron pencil beam from the high-energy end of the accelerating waveguide to the bremsstrahlung target where x rays are produced or to the beryllium exit window where electron pencil beam exits the vacuum and proceeds in air toward the electron beam scattering foil.

(12) **Linac head** contains all components that are used to produce clinical x-ray beams and clinical electron beams for radiotherapy, such as bremsstrahlung target and flattening filter, electron scattering foils, three types of collimator: primary, secondary (upper and lower jaws, and multi-leaf), dual ionization chambers, and a few auxiliary devices, such as field size readout, field defining light, and range finder helping in patient set up in preparation for radiation treatment.

(13) **Motorized patient support assembly** (“treatment couch” in short) is used to bring the patient into proper position for radiation treatment using three translational motions (height, transverse, and longitudinal) as well as rotational motion about the vertical central beam axis.

(14) **Circulator** (also called isolator) is an important component in transmission of microwave power from the RF generator to the accelerating waveguide. It is a three-port passive device with peculiar RF transmission properties that can be illustrated as follows: RF entering at port 1 exits at port 2; RF entering at port 2 exits at port 3; and RF entering at port 3 exits at port 1. Thus, connecting RF power from the RF power generator to port 1, connecting port 2 to accelerating waveguide, and connecting port 3 to a microwave load (15) will transmit RF power without impediment from the RF generator to the accelerating waveguide but will send the RF power reflected from the accelerating waveguide directly into the RF load where it will be fully absorbed. Since the cathodes of magnetrons and klystrons are very sensitive to reflected RF power, we note that the circulator protects the RF generator from adverse effects of the RF power reflected from the accelerating waveguide.

(15) **RF load** is connected to the circulator to absorb the RF power reflected from the accelerating waveguide thereby protecting the RF power source from damage that would be inflicted by reflected RF power. It is made of ferrite, a special ceramic mixed with iron to give it magnetic properties useful in absorbing the RF power. To dissipate the absorbed RF power the circulator is also connected to the water-cooling system (8).

MINOR COMPONENTS of a clinical linac are as follows:

(21) **Heated cathode** is a component of the diode-type and triode-type electron gun. It is made of tungsten and heated to a high temperature for thermionic emission of electrons. Typical voltage on the cathode is at -25 kV, pulsed in diode-type electron guns and held at constant potential in triode-type electron guns.

(22) **Grid** is the extra electrode of the triode-type electron gun. The flow of electrons in this type of gun is controlled with voltage difference between the cathode (-25 kV) and the grid ($\pm \sim 200$ V) with respect to the cathode). When the grid is more negative than the cathode, no electron current is flowing; when the grid is less negative than the cathode, the electron current is flowing.

(23) **Anode** of the diode-type and triode-type electron gun is perforated so that electrons generated by the cathode can pass through on their way into the accelerating waveguide. The anode is kept at ground potential.

(24) **Steering coil** keeps the accelerated electron pencil beam as close as possible to the axis of the cylindrical accelerating waveguide and steer the beam toward the opening which connects the accelerating waveguide with the with the beam transport system or directly onto the bremsstrahlung target in low-energy straight-through linacs.

(25), (26), and (27) **Steering coil**: see (24).

(28) **Ceramic window** separates the evacuated accelerating waveguide from the pressurized RF transmission waveguide. The window is transparent to microwaves and made of strong dielectric materials, such as ceramic or quartz, to withstand the pressure difference of ~ 200 kPa.

(29) **Focusing coil** is used for focusing the accelerated electron pencil beam in order to minimize the beam divergence and cross section. The beam divergence results from a small radial component of the electric field in the accelerating waveguide as well as from the repulsion among electrons in the pencil beam. Focusing solenoid coils are coaxial with the accelerating waveguide.

(30) **Focusing coil**: see (29).

(31) **Pulsed electron pencil beam** originates in the heated cathode of the electron gun, is accelerated in the accelerating waveguide, and enters the beam transport system.

(32) **Energy slits** are placed into the bending magnet to remove from the pencil beam the electrons that are not within ± 5 % of the nominal electron beam energy. The bending magnet separates electrons according to their energy by bending more energetic electrons less and less energetic electrons more than electrons with nominal energy. Energy slits pass electrons with energy within the ± 5 % window of

nominal energy and absorb electrons with higher and lower energy. The electrons that do not pass through the window, of course, create unwanted bremsstrahlung radiation in their interaction with the energy slit and contribute to the leakage radiation produced by the linac.

(33) **Removable bremsstrahlung thick target** is used to produce clinical bremsstrahlung x rays from the electron pencil beam. To ensure that no electrons can traverse the bremsstrahlung target, the target thickness must be about 10 % larger than the range of electrons in the target material for kinetic energy equal to nominal kinetic energy of pencil beam electrons. It is made of (i) as low as practically possible atomic number material for optimum x-ray production in the forward direction and (ii) as high mass density as possible to minimize the required target thickness. It turns out that copper is a material that meets reasonably well both the low atomic number ($Z = 29$) requirement and the high density ($\rho = 8.9 \text{ g/cm}^3$) requirement and is now commonly used as target material in high energy clinical linacs.

(34) **Beryllium exit window** is traversed by the electron pencil beam as it exits the evacuated beam transport system on its way to the scattering foils and it is also traversed by the forward-peaked bremsstrahlung x-ray beam before it passes through the flattening filter. To affect as little as possible both the electron pencil beam as well as the bremsstrahlung x-ray beam, the exit window is made of beryllium that is a metal with the lowest atomic number ($Z = 4$) and excellent strength. At first glance one may speculate that, with the low Z of 4, beryllium would also be an excellent bremsstrahlung target material; however, beryllium has a low mass density of 1.85 g/cm^3 and this excludes it from candidacy for bremsstrahlung target.

(35) **Primary collimator** defines the maximum circular x-ray field size available from the linac. The radius of this field is of the order of 30 cm at 100 cm from the bremsstrahlung target.

(36) **Flattening filter** is used to produce a flat clinical beam from the primary forward-peaked x-ray beam generated in the bremsstrahlung target. The choice of material for flattening filter as far as atomic number Z is concerned is, similar to bremsstrahlung targets, as low as possible. The problem again is the density of the material because low Z materials usually also have low mass density and in order to conserve space in the linac head one wishes to have a flattening filter of high mass density to minimize its height. Copper again seems to be a good compromise between the two contradictory requirements.

(37) **Dose monitoring system** of a medical linac is based on two independent transmission ionization chambers permanently imbedded into the linac clinical x-ray and electron beams. To avoid fluctuations in measuring signal with ambient temperature, pressure, and humidity the two ionization chambers are also usually permanently sealed with a given mass of air as the sensitive dose-measuring material. For patient safety two ionization chambers are used, so that if the primary

chamber fails to turn the beam off, the secondary chamber will do so with minimal delay to ensure that the patient is not significantly overexposed to radiation.

(38) **Secondary collimator—adjustable upper jaws** consist of two independent jaws that define radiation field widths from 0 to 40 cm at 100 cm from the bremsstrahlung target. Note: the combination of the upper and lower set of jaws that are perpendicular to each other defines the secondary collimator system and produces radiation fields from 0×0 to 40×40 cm² at 100 cm from the bremsstrahlung target.

(39) **Secondary collimator—adjustable lower jaws** consist of two independent jaws that define radiation field lengths from 0 to 40 cm at 100 cm from the bremsstrahlung target. Note: the combination of the upper and lower set of jaws that are perpendicular to each other defines the secondary collimator system and produces radiation fields from 0×0 to 40×40 cm² at 100 cm from the bremsstrahlung target.

(40) **Central axis** of clinical x-ray beams as well as clinical electron beams. This line also defines the rotation axis of the linac head.

(41) **Linac isocenter** is a point in the linac treatment room at which three axes defined for an *ideal* clinical linac intersect. The three axes are: (i) Gantry rotation axis, (ii) Collimator rotation axis coinciding with the clinical beam central axis (for x-ray beams as well as for electron beams), and (iii) Couch rotation axis. Moreover, the mechanical isocenter as well as the radiation isocenter are expected to coincide.

The practical clinical situation is much more complicated, since it is impossible to manufacture, install, and maintain a clinical linac with an infinitesimally small isocenter point. In addition, the mechanical and radiation isocenter do not necessarily agree. Generally, the three axes do not intersect for all possible orientations of the linac gantry, collimator, and couch because of the excessive weight of linac components; rather, the three axes define a sphere in space that the three axes intersect for all possible positions of the gantry, collimator, and couch. For general radiotherapy the diameter of this sphere must be smaller than 2 mm and the center-of-mass of this sphere is defined as the radiation isocenter. This stringent specification is difficult to attain and even its verification is not a trivial process.

(42) **Couch rotation axis** defines the vertical axis in space about which the couch (patient support assembly) rotates. For the linac gantry pointing vertically down or vertically up, the couch rotation axis should coincide with the collimator rotation axis as well as with the central axes of clinical x-ray beams and clinical electron beams.

(43) **Ceramic window**: separates the klystron from the pressurized waveguide; see (28).

(b) Figure 14.8 depicts a schematic diagram of a typical medical linac and allows us to answer the four questions as follows:

(1) Clinical linac depicted in Fig. 14.8 is most likely a linac providing two clinical x-ray energies as well as several clinical electron beam energies in the range from 4 MeV to 20 MeV. We reach this conclusion based on the following features evident on the schematic diagram:

- (i) The electron pencil beam is transferred from the acceleration waveguide to the bremsstrahlung target through a beam transport system. This feature is used in high-energy linacs; “straight-through” low-energy linacs (4 MV and 6 MV) are much simpler (and therefore cheaper) incorporating a permanently embedded thick target at the high-energy end of the acceleration waveguide without employing a beam transport system with bending magnet and energy slits and without offering a clinical electron beam mode.
- (ii) The diagram shows two thick bremsstrahlung targets (33) with the thicker target in the beam. We thus conclude that the linac is a high-energy machine providing two clinical x-ray energies, most likely at low energy of 6 MV and at high energy around 18 MV.
- (iii) Since the bremsstrahlung targets are movable, we assume that an electron clinical mode is also available on the linac. In electron beam mode both the target and flattening filter are moved out of pencil beam’s path and a scattering foil is placed into the pencil electron beam to produce a clinically useful large field electron beam.

(2) Of the two possible clinical modes the diagram represents the clinical x-ray mode, since it shows a bremsstrahlung target in the path of the pulsed electron pencil beam and it also shows a flattening filter on the central axis of the clinical beam.

(3) Of the two possible electron gun types (diode and triode) the diagram shows a triode gun that incorporates a grid electrode for control of the flow of electrons from the heated cathode to the grounded perforated anode.

(4) Of the two possible RF generator types (magnetron and klystron) the diagram shows a klystron type RF generator, since it incorporates an RF driver indicating that the generator has a separate RF source (RF driver) that sends a low-power signal for amplification by the klystron.

(c) Order of magnitude for selected clinical linac parameters:

- (1) Peak pencil beam current for clinical x-ray mode: $I_p \approx 50 \text{ mA}$.
- (2) Mean pencil beam current for clinical x-ray mode: $\bar{I}_X \approx 50 \text{ }\mu\text{A}$.
- (3) Mean beam current for clinical electron mode: $\bar{I}_e \approx 0.01 \bar{I}_X$.
- (4) Duty cycle and pulse repetition rate: $\delta \approx 10^{-3}$ and $\rho = 100 \text{ s}^{-1} = 100 \text{ pps}$, respectively.

-
- (5) Peak modulator current and voltage: $I_{P,\text{mod}} \approx 100$ A and $U_{P,\text{mod}} \approx 100$ kV, respectively.
 - (6) Radiofrequency of operation: standard linac at 2856 MHz, miniature linac at $\sim 10^4$ MHz.
 - (7) Beam current pulse width: $\tau \approx 2$ μs .

Main Attributes of Nuclides Presented in This Book

A

Data given in Table A.1 can be used to determine the various decay energies for the specific radioactive decay examples as well as for the nuclear activation examples presented in this book. M stands for nuclear rest mass; \mathcal{M} stands for atomic rest mass. The data were obtained as follows:

- (1) Data for atomic masses \mathcal{M} were obtained from the NIST and are given in unified atomic mass units u.
- (2) Rest mass of the proton m_p , neutron m_n , electron m_e , and of the unified atomic mass unit u are as follows:

$$m_u = 1.672621637 \times 10^{-27} \text{ kg} = 1.007276467 \text{ u} = 938.272013 \text{ MeV}/c^2 \quad (\text{A.1})$$

$$m_n = 1.674927211 \times 10^{-27} \text{ kg} = 1.008664916 \text{ u} = 939.565346 \text{ MeV}/c^2 \quad (\text{A.2})$$

$$m_e = 9.109382215 \times 10^{-31} \text{ kg} = 5.485799094 \times 10^{-4} \text{ u} \\ = 0.510998910 \text{ MeV}/c^2 \quad (\text{A.3})$$

$$1 \text{ u} = 1.660538782 \times 10^{-27} \text{ kg} = 931.494028 \text{ MeV}/c^2 \quad (\text{A.4})$$

- (3) For a given nuclide, its nuclear rest energy was determined by subtracting the rest energy of all atomic orbital electrons \mathcal{M} from the atomic rest energy $\mathcal{M}(u)c^2$ as follows

$$Mc^2 = \mathcal{M}(u)c^2 - Zm_e c^2 = \mathcal{M}(u) \times 931.494028 \text{ MeV}/u - Z \times 0.510999 \text{ MeV} \quad (\text{A.5})$$

The binding energy of orbital electrons to the nucleus is ignored in (A.5).

- (4) The nuclear binding energy E_B for a given nuclide was determined using the mass deficit equation given in (T1.25) to get

$$E_B = Zm_p c^2 + (A - Z)m_n c^2 - Mc^2 \quad (\text{A.6})$$

with Mc^2 given in (A.5) and the rest energy of proton, neutron, and electron given in (A.1), (A.2), and (A.3) respectively.

- (5) For a given nuclide the binding energy per nucleon E_B/A is calculated by dividing the binding energy E_B of (A.6) with the number of nucleons equal to the atomic mass number A of a given nuclide.

Table A.1 Main attributes of nuclides presented in this book (in the entry for half-life: a = year, d = day, h = hour, min = minute, s = second)

Element and its nuclides	Z	A	Atomic mass \mathcal{M} (u)	Nuclear rest energy Mc^2 (MeV)	Binding energy E_B (MeV)	$\frac{E_B}{\text{nucleon}}$ ($\frac{\text{MeV}}{\text{nucleon}}$)	Half-life $t_{1/2}$	
Hydrogen	H	1	1	1.007825	938.2720	–	–	Stable
Deuterium	D	1	2	2.014102	1875.6130	2.2244	1.1122	Stable
Tritium	T	1	3	3.016049	2808.9206	8.4821	2.8274	12.3 a
Helium	He	2	3	3.016029	2808.3910	7.7184	2.5728	Stable
	He	2	4	4.002603	3727.3788	28.2959	7.0740	Stable
	He	2	5	5.012220	4667.8310	27.4091	5.4818	8×10^{-22} s
	He	2	6	6.018889	5605.5372	29.2682	4.8780	0.801 s
Lithium	Li	3	5	5.012540	4667.6181	26.3287	5.2657	10^{-21} s
	Li	3	6	6.015123	5601.5182	31.9939	5.3323	Stable
	Li	3	7	7.016004	6533.8328	39.2446	5.6064	Stable
Beryllium	Be	4	7	7.016929	6534.1835	37.6006	5.3715	53 d
	Be	4	8	8.005305	7454.8498	56.4996	7.0625	8.19×10^{-17} s
	Be	4	9	9.012182	8392.7497	58.1651	6.4628	Stable
	Be	4	12	12.026921	11200.9611	68.6497	5.7208	21.49 ms
	Be	4	13	13.035691	12140.6243	68.5518	5.2732	2.7×10^{-21} s
Boron	B	5	9	9.013329	8393.3071	56.3143	6.2571	8.5×10^{-19} s
	B	5	10	10.012937	9324.4360	64.7508	6.4751	Stable
	B	5	11	11.009305	10252.5469	76.2053	6.9278	Stable
Carbon	C	6	11	11.011434	10254.0190	73.4398	6.6763	20.33 min
	C	6	12	12.000000	11174.8623	92.1618	7.6802	Stable
	C	6	13	13.003355	12109.4815	97.1080	7.4698	Stable
	C	6	14	14.003242	13040.8703	105.2845	7.5203	5730 a
Nitrogen	N	7	13	13.005739	12111.1912	94.1050	7.2388	10 min
	N	7	14	14.003074	13040.2028	104.6587	7.4756	Stable
	N	7	15	15.000109	13968.9350	115.4919	7.6995	Stable
	N	7	17	17.008450	15839.6935	123.8646	7.2862	4.173 s
Oxygen	O	8	15	15.003066	13971.1784	111.9551	7.4637	122.24 s
	O	8	16	15.994915	14895.0798	127.6191	7.9762	Stable
	O	8	17	16.999132	15830.5023	131.7624	7.7507	Stable
	O	8	18	17.999160	16762.0221	139.8075	7.7671	Stable
Fluorine	F	9	18	18.000938	16763.1673	137.3690	7.6316	1.83 h
	F	9	19	18.998403	17692.3009	147.8013	7.7790	Stable
Neon	Ne	10	20	19.992440	18617.7285	160.6451	8.0323	Stable
Aluminum	Al	13	27	26.981539	25126.4995	224.9516	8.3315	Stable
Phosphorus	P	15	30	29.978314	27916.9555	250.6049	8.3535	2.498 min
Chromium	Cr	24	43	42.997710	40039.8461	330.4238	7.6843	21 ms

Table A.1 (Continued)

Element and its nuclides		Z	A	Atomic mass \mathcal{M} (u)	Nuclear rest energy Mc^2 (MeV)	Binding energy E_B (MeV)	$\frac{E_B}{\text{nucleon}}$ ($\frac{\text{MeV}}{\text{nucleon}}$)	Half-life $t_{1/2}$
Manganese	Mn	25	44	44.006870	40979.3616	329.1803	7.4814	0.1 μ s
	Mn	25	45	44.994513	41899.3452	348.7621	7.7503	70 ns
Iron	Fe	26	45	45.014560	41917.5078	329.3061	7.3179	0.35 μ s
Cobalt	Co	27	57	56.936291	53022.0207	498.2859	8.7419	271.736 d
	Co	27	59	58.933200	54882.1269	517.3085	8.7679	Stable
	Co	27	60	59.933822	55814.2003	524.8005	8.7467	5.26 a
Nickel	Ni	28	60	59.930791	55810.8659	526.8415	8.7807	Stable
	Ni	28	63	62.929669	58604.3058	552.0998	8.7635	100.17 a
Krypton	Kr	36	82	81.913484	76283.5252	714.2732	8.7106	Stable
	Kr	36	89	88.917632	82807.8494	766.9094	8.6170	3.15 min
	Kr	36	91	90.923451	84676.2538	777.6357	8.5454	8.57 min
	Kr	36	92	91.926156	85610.2731	783.1817	8.5129	1.84 s
	Kr	36	94	93.934363	87480.9176	791.6680	8.4220	210 ms
Rubidium	Rb	37	82	81.918209	76287.4155	709.0895	8.6474	1.2575 min
	Rb	37	90	89.914802	83736.1973	776.8335	8.6315	2.633 min
	Rb	37	96	95.934270	89343.2988	807.1242	8.4075	203 ms
Strontium	Sr	38	90	89.907738	83729.1065	782.6310	8.6959	28.808 a
	Sr	38	94	93.915361	87462.1839	807.8150	8.5938	1.255 min
Zirconium	Zr	40	96	95.908273	89317.5477	828.9953	8.6354	Stable
Molybdenum	Mo	42	95	94.905842	88382.7670	821.6240	8.6487	Stable
	Mo	42	98	97.905408	91176.8409	846.2430	8.6351	Stable
	Mo	42	99	98.907711	92110.4849	852.1677	8.6078	65.92 h
	Mo	42	100	99.907478	93041.7604	860.4575	8.6046	Stable
Technetium	Tc	43	99	98.906255	92108.6129	852.7430	8.6136	2.11×10^5 a
Cadmium	Cd	48	113	112.904402	105145.2523	963.5555	8.5270	Stable
	Cd	48	114	113.903359	106075.7748	972.5984	8.5316	Stable
Iodine	I	53	125	124.904210	116320.4427	1056.6789	8.4534	59.407 d
	I	53	127	126.904473	118183.6758	1072.5765	8.4455	Stable
	I	53	131	130.906125	121911.1907	1103.3230	8.4223	8.02 h
Xenon	Xe	54	131	130.905082	121909.7082	1103.5122	8.4238	Stable
	Xe	54	140	139.921641	130308.7287	1160.7287	8.2909	13.6 s
Cesium	Cs	55	137	136.907084	127500.0262	1149.2929	8.3890	30.2 a
	Cs	55	138	137.911017	128435.1888	1153.7002	8.3602	33.42 min
	Cs	55	142	141.924299	132173.5374	1173.6131	8.2649	1.689 s
Barium	Ba	56	137	136.905821	127498.3387	1149.6870	8.3919	Stable
	Ba	56	139	138.908841	129364.1457	1163.0154	8.3670	1.3861h
	Ba	56	141	140.914412	131232.3218	1173.9700	8.3260	18.27 min
	Ba	56	142	141.916454	132165.7185	1180.1387	8.3108	10.6 min
	Ba	56	144	143.922951	134034.7607	1190.2273	8.2655	11.5 s

Table A.1 (Continued)

Element and its nuclides	Z	A	Atomic mass \mathcal{M} (u)	Nuclear rest energy Mc^2 (MeV)	Binding energy E_B (MeV)	$\frac{E_B}{\text{nucleon}}$ ($\frac{\text{MeV}}{\text{nucleon}}$)	Half-life $t_{1/2}$
Lanthanum La	57	139	138.906353	129361.3169	1164.5508	8.3781	Stable
Samarium Sm	62	152	151.919732	141480.6412	1253.1048	8.2441	Stable
Europium Eu	63	151	150.919850	140548.7460	1244.1412	8.2393	$\geq 1.7 \times 10^{18}$ a
	63	152	151.921745	141482.0053	1250.4474	8.2266	13.54 a
	63	153	152.921230	142413.0196	1258.9984	8.2287	Stable
Gadolinium Gd	64	152	151.919791	141479.6741	1251.4852	8.2335	1.08×10^{14} a
Osmium Os	76	192	191.961479	178772.1354	1526.1178	7.9485	Stable
Iridium Ir	77	191	190.960591	177839.3032	1518.0913	7.9481	Stable
	77	192	191.962602	178772.6704	1524.2894	7.9390	73.8 d
	77	193	192.962924	179704.4644	1532.0607	7.9381	Stable
Platinum Pt	78	192	191.961035	178770.6998	1524.9667	7.9425	Stable
Gold Au	79	197	196.966552	183432.7980	1559.4019	7.9157	Stable
	79	198	197.968242	184365.8743	1565.8975	7.9090	2.695 d
Thallium Tl	81	208	207.982019	193692.6254	1632.2134	7.8472	3.05 min
Lead Pb	82	205	204.974482	190890.6040	1614.2387	7.8743	1.73×10^7 a
	82	206	205.974465	191822.0821	1622.3258	7.8754	Stable
	82	207	206.975881	192754.8952	1629.0781	7.8699	Stable
	82	208	207.976636	193687.0925	1636.4462	7.8675	Stable
	82	212	211.991898	197413.9072	1667.8998	7.8675	Stable
Bismuth Bi	83	209	208.980383	194621.5658	1640.2449	7.8481	Stable
	83	212	211.991286	197426.2120	1654.3017	7.8033	1.01 h
Polonium Po	84	210	209.982873	195554.8683	1645.2144	7.8344	15.6 min
	84	211	210.986653	196489.8918	1649.7632	7.8188	0.516 s
	84	216	216.001915	201161.5783	1675.9036	7.7588	0.145 s
	84	218	218.008973	203031.1325	1685.4730	7.7315	3.167 min
Radon Rn	86	220	220.011394	204895.3622	1697.7946	7.7172	0.9267 min
	86	222	222.017578	206764.1021	1708.1781	7.6945	3.8 d
Radium Ra	88	224	224.020212	208628.5302	1720.3014	7.6799	3.657 d
	88	226	226.025403	210496.3452	1731.6097	7.6620	1602 a
	88	228	228.031070	212364.6211	1742.4720	7.6424	5.739 a
Actinium Ac	89	228	228.031021	212364.0642	1741.7356	7.6392	6.139 h
Thorium Th	90	228	228.028741	212361.4305	1743.0760	7.6451	1.91286 a
	90	232	232.038050	216096.0679	1766.6924	7.6151	1.4×10^{16} a
Uranium U	92	233	233.039628	217028.0099	1771.7291	7.6040	1.6×10^6 a
	92	235	235.043923	218894.9987	1783.8710	7.5909	0.7×10^9 a
	92	236	236.045568	219828.0342	1790.4086	7.5865	2.3×10^7 a
	92	238	238.050783	221695.8708	1801.6949	7.5701	4.5×10^9 a
	92	239	239.054288	222630.6297	1806.5013	7.5586	23.5 min
	92	240	240.056592	223564.2793	1812.4250	7.5518	14.11 h

Table A.1 (Continued)

Element and its nuclides		Z	A	Atomic mass \mathcal{M} (u)	Nuclear rest energy Mc^2 (MeV)	Binding energy E_B (MeV)	$\frac{E_B}{\text{nucleon}}$ ($\frac{\text{MeV}}{\text{nucleon}}$)	Half-life $t_{1/2}$
Neptunium	Np	93	239	239.052913	222628.8379	1806.9998	7.5607	2.35 d
Plutonium	Pu	94	239	239.052157	222627.6227	1806.9217	7.5603	24×10^3 a
	Pu	94	240	240.053814	223560.6690	1813.4486	7.5560	6567.1 a
	Pu	94	244	244.064204	227296.3238	1836.0554	7.5248	7.93×10^7 a
Curium	Cm	96	248	248.072349	231028.8557	1859.1901	7.4967	0.35×10^6 a
Californium	Cf	98	252	252.081626	234762.4513	1881.2693	7.4654	2.65 a
	Cf	98	256	256.093440	238499.4321	1902.5499	7.4318	12.3 min
Fermium	Fm	100	256	256.091767	238496.8517	1902.5436	7.4318	158 min

A

a	year (annum)
a	acceleration; radius of atom; center to vertex distance for a hyperbola; specific activity; year (annum)
a_{eff}	effective specific activity
a_{H}	radius of hydrogen atom
a_{max}	maximum specific activity
a_{SF}	specific activity for spontaneous fission decay
a_{TF}	Thomas-Fermi atomic radius
a_{theor}	theoretical specific activity
a_0	Bohr radius (0.5292 Å)
a_{α}	specific activity for alpha decay
A	ampère (SI unit of current)
\mathbf{A}	vector function
A	atomic mass number; number of nucleons in atomic nucleus
Å	angstrom (unit of length or distance: 10^{-10} m)
A_{R}	Richardson constant in thermionic emission
$A_2(z)$	spatial spread of electron beam
A	activity
A_{D}	daughter activity
A_{P}	parent activity
A_{sat}	saturation activity
\mathcal{A}_{SF}	activity for spontaneous fission decay

B

b	barn (unit of area: 10^{-24} cm ²)
B	boron atom
b	impact parameter
b_{max}	maximum impact parameter
b_{min}	minimum impact parameter
B_{col}	atomic stopping number in collision stopping power
B	build-up factor in broad beam attenuation
\mathcal{B}	magnetic field

B_{rad}	parameter in radiation stopping power
Bq	becquerel (SI unit of activity)
$B(x)$	build-up factor in broad beam attenuation
C	
c	speed of light in vacuum (3×10^8 m/s)
c_n	speed of light in medium
C	coulomb (unit of electric charge); carbon atom
C	constant, shell correction constant
C_f	form factor constant
C_0	collision stopping power constant ($0.3071 \text{ MeV cm}^2/\text{mol}$)
C_n	Bateman constants in Bateman equations
Ci	curie (old unit of activity: $3.7 \times 10^{10} \text{ s}^{-1} = 3.7 \times 10^{10} \text{ Bq}$)
C_K	K-shell correction for stopping power
C_M	nuclear mass correction factor
C_R	recoil correction factor in Čerenkov radiation
C_v	electric field correction factor
$C_{\alpha-N}$	constant in α particle scattering
C_λ	Wien displacement constant in wavelength domain ($2.898 \times 10^{-3} \text{ m K}$)
C_ν	Wien displacement constant in frequency domain ($5.880 \times 10^{10} \text{ s}^{-1}/\text{K}$)
D	
d	day, deuteron
d	distance; spacing; diameter
D	daughter nucleus
D	dose
$D_{\alpha-N}$	distance of closest approach (between α particle and nucleus)
D_{eff}	effective characteristic scattering distance
$D_{\alpha-N}$	effective characteristic scattering distance of closest approach between α particle and nucleus
D_{e-a}	effective characteristic scattering distance between electron and atom
D_{e-e}	effective characteristic scattering distance between the electron and orbital electron
D_{e-N}	effective characteristic scattering distance between electron and nucleus
D_{ex}	exit dose
D_s	surface dose
E	
e	electron charge ($1.6 \times 10^{-19} \text{ C}$)
e	electron

e^-	electron
e^+	positron
eV	electron volt (unit of energy: 1.6×10^{-19} J)
$e\phi$	work function
E	energy
\mathcal{E}	electric field
E_{ab}	energy absorbed
\bar{E}_{ab}	mean energy absorbed
E_B	binding energy
$E_B(K)$	binding energy of K shell electron
E_{col}	energy lost through collisions
E_{Coul}	Coulomb barrier energy
E_i	initial total energy of charged particle
\mathcal{E}_{in}	electric field for incident radiation
E_K	kinetic energy
E'_K	kinetic energy of scattered (recoil) particle
$(E_K)_0$	initial kinetic energy of charged particle
$(E_K)_{crit}$	critical kinetic energy
$(E_K)_D$	recoil kinetic energy of daughter
$(E_K)_f$	final kinetic energy
$(E_K)_i$	initial kinetic energy
$(E_K)_{IC}$	kinetic energy of conversion electron
$(E_K)_{max}$	maximum kinetic energy
$(E_K)_n$	kinetic energy of incident neutron
$(E_K)_{thr}$	threshold kinetic energy
E_n	allowed energy state (eigenvalue)
E_0	rest energy, incident energy
\mathcal{E}_{out}	electric field for scattered radiation
E_p	barrier potential
E_R	Rydberg energy
E_{rad}	energy radiated by charged particle
E_{SR}	radiation loss per revolution in synchrotron
E_{thr}	threshold energy
E_{thr}^{PN}	threshold photon energy of photonuclear interaction
E_{tr}	energy transferred
\bar{E}_{tr}	average (mean) energy transferred
$(\mathcal{E}_z)_0$	amplitude of electric field in uniform waveguide
E_ν	photon energy; energy of neutrino
E'_ν	scattered photon energy
\bar{E}_{tr}^{PP}	mean energy transferred from photons to charged particles in pair production
\bar{E}_{tr}^C	mean energy transferred from photons to electrons in Compton effect
\bar{E}_{tr}^{PE}	mean energy transferred from photons to electrons in photoelectric effect (photoeffect)

E_β	energy of beta particle
$(E_\beta)_{\max}$	maximum total energy of electron or positron in β decay
E_γ	energy of gamma photon
$(E_\gamma)_{\text{thr}}$	threshold energy for pair production

F

f	function; theoretical activity fraction; branching fraction in radioactive decay
fm	femtometer (10^{-15} m)
\bar{f}_{ab}	total mean energy absorption fraction
\bar{f}_{C}	mean fraction of energy transferred from photons to electrons in Compton effect
$(\bar{f}_{\text{C}})_{\max}$	maximum energy transfer fraction in Compton effect
f_{E}	Rydberg energy correction factor for finite nuclear mass
f_i	fraction of decay constant, branching ratio
f_{n}	fraction of spontaneous fission (SF) decay competing with α decay
\bar{f}_{n}	mean number of neutrons produced by each spontaneous fission decay
f_{P}	ratio of power radiated to power supplied
\bar{f}_{PE}	mean fraction of energy transferred from photon to electrons in photoelectric effect
\bar{f}_{PP}	mean fraction of energy transferred from photons to charged particles in pair production
f_{r}	Bohr radius correction factor for finite nuclear mass
\bar{f}_{R}	mean energy transfer fraction in Rayleigh scattering
f_{recoil}	nuclear recoil correction factor
f_{spin}	spin correction factor
f_{v}	Bohr velocity correction factor for finite nuclear mass
\bar{f}_{tr}	total mean energy transfer fraction
$f(x)$	function of independent variable x
$f(\beta)$	velocity function
F	force
F	fluorine atom
F_{coul}	Coulomb force
$F(K)$	form factor
$F(x, Z)$	atomic form factor
$F(x, \text{H})$	atomic form factor of hydrogen
F_{KN}	Klein-Nishina form factor
F_{L}	Lorentz force
F_{n}	neutron kerma factor
F^+	stopping power function for positrons
F^-	stopping power function for electrons

G

g	gram (unit of mass: 10^{-3} kg)
\bar{g}	mean radiation fraction
\bar{g}_A	mean in-flight radiation fraction
\bar{g}_B	mean bremsstrahlung fraction
\bar{g}_i	mean impulse ionization fraction
G	granddaughter nucleus
G	Newtonian gravitational constant
Gy	gray (SI unit of kerma and dose: 1 J/kg)

H

h	Planck constant (6.626×10^{-34} J s); hour
H	hydrogen atom
H	equivalent dose; Hamiltonian operator
Hz	unit of frequency (s^{-1})
H_μ	muonic hydrogen
\bar{H}	antihydrogen
^1H	protium (hydrogen atom with one proton and one electron)
\hbar	reduced Planck constant ($h/2\pi$)

I

I	iodine atom
I	electric current; mean ionization/excitation potential; beam intensity; radiation intensity
I_0	initial photon beam intensity

J

j	current density; quantum number in spin-orbit interaction; specific ionization
J	joule (SI unit of energy)
$J(x)$	Bessel function (of first kind)

K

k	wave number, free space wave number, Boltzmann constant (0.8617×10^{-4} eV K^{-1}); effective neutron multiplication factor in fission chain reaction
k_g	wave guide wave number (propagation coefficient)
kg	kilogram (SI unit of mass)
$k(K_\alpha)$	wave number for K_α transition
kVp	kilovolt peak (in x-ray tubes)
k^*	ratio σ_P/σ_D in neutron activation
\mathbf{k}_i	initial wave vector
\mathbf{k}_j	final wave vector

K	$n = 1$ allowed shell (orbit) in an atom; Kelvin temperature
K	kerma; capture constant for electron in disk-loaded waveguide
K_{col}	collision kerma
K_{rad}	radiation kerma
K_{α}	characteristic electronic transition from L shell to K shell
L	
l	length
L	$n = 2$ allowed shell (orbit) in an atom
L	angular momentum; restricted stopping power
L	angular momentum vector; distance vector
ℓ	orbital quantum number; distance; path length
M	
m	meter (SI unit of length or distance)
m	mass; magnetic quantum number; decay factor in parent-daughter-granddaughter decay; activation factor in nuclear activation; integer in Bragg relationship; mean number of elastic scattering interactions of neutron in moderator
m_e	electron rest mass ($0.5110 \text{ MeV}/c^2$)
m_{e^-}	electron rest mass ($0.5110 \text{ MeV}/c^2$)
m_{e^+}	positron rest mass ($0.5110 \text{ MeV}/c^2$)
m_{ℓ}	magnetic quantum number
m_n	neutron rest mass ($939.6 \text{ MeV}/c^2$)
m_0	rest mass of particle
m_p	proton rest mass ($938.3 \text{ MeV}/c^2$)
m_{α}	rest mass of α particle
$m(v)$	relativistic mass m at velocity v
m^*	modified activation factor
M	$n = 3$ allowed shell (orbit) in an atom
\mathbf{M}_{if}	matrix element
M	mass of heavy nucleus
MeV	mega electronvolt (unit of energy: 10^6 eV)
MHz	megahertz (unit of frequency: 10^6 Hz)
Mu	muonium
MU	monitor unit (in linacs)
MV	megavoltage (in linacs)
$M(Z, A)$	nuclear mass in atomic mass units
$\mathcal{M}(Z, A)$	atomic mass in atomic mass units
N	
n	neutron
nm	nanometer (unit of length or distance: 10^{-9} m)
n	principal quantum number

n^{\square}	number of atoms per volume
N	$n = 4$ allowed shell (orbit) in an atom; nitrogen; number of neutrons in nucleus
NPP	nuclear pair production
$N(x)$	Neumann function (Bessel function of second kind)
N	number of radioactive nuclei; number of experiments in central limit theorem; number of mono-energetic electrons in medium
\mathcal{N}	number of photons
N_a	number of atoms
N_A	Avogadro number (6.022×10^{23} atom/mol)
N_e	number of electrons per volume; electron density
N_t/m	number of specific nuclei per unit mass of tissue
O	
O	oxygen
OER	oxygen enhancement ratio
P	
p	proton
p	momentum
p_e	electron momentum
p_ν	photon momentum
\mathbf{p}_i	initial particle momentum vector
\mathbf{p}_f	final particle momentum vector
P	parent nucleus phosphorus atom
P	power; probability
Pa	Pascal (SI unit of pressure)
PE	photoelectric
P_j	probability for photoelectric effect, if it occurs, to occur in the j subshell
PP	pair production
$P(x)$	probability density function
$P(\epsilon, Z)$	pair production function
Ps	positronium
P_K	fraction of photoelectric interactions that occur in the K-shell
P_{Ruth}	probability of Rutherford scattering
Q	
q	charge
\underline{Q}	charge; nuclear reaction energy; Q value
\bar{Q}	expectation (mean) value of physical quantity Q
$[Q]$	operator associated with the physical quantity Q
Q_{EC}	decay energy (Q value) for electron capture
Q_{IC}	decay energy (Q value) for internal conversion

Q_α	decay energy (Q value) for alpha decay
Q_β	decay energy (Q value) for beta decay
R	
r	radius vector; separation between two interacting particles
rad	old unit of absorbed dose (100 erg/g); radian
rem	old unit of equivalent dose
r_e	classical electron radius (2.818 fm)
r_n	radius of the n -th allowed Bohr orbit
\bar{r}	average electron radius
R	Rayleigh scattering; roentgen (unit of exposure: 2.58×10^{-4} C/kg _{air})
RBE	relative biological effectiveness
R	radial wave function; radius (of nucleus); reaction rate; distance of closest approach
\bar{R}	mean range
R_{CSDA}	continuous slowing down approximation range
R_{H}	Rydberg constant for hydrogen (109678 cm^{-1})
R_{max}	maximum penetration depth
R_0	nuclear radius constant (1.25 fm)
$R_{\alpha-N}$	distance between the α particle and nucleus in a non-direct hit collision
R_∞	Rydberg constant assuming an infinite nuclear mass (109737 cm^{-1})
R_{50}	depth of the 50 % percentage depth dose in water for electron beam
S	
s	second (unit of time)
s	spin quantum number
sr	steradian
S	mass stopping power
S	Poynting vector
\bar{S}	mean total mass stopping power
S_{col}	mass collision stopping power
\bar{S}_{col}	mean collision stopping power
S_{in}	Poynting vector of incident radiation
\bar{S}_{in}	mean Poynting vector of incident radiation
S_{out}	Poynting vector of scattered radiation
\bar{S}_{out}	mean Poynting vector of scattered radiation
S_{rad}	mass radiation stopping power
S_{tot}	total mass stopping power
Sv	sievert (SI unit of equivalent dose)
$S(x, Z)$	incoherent scattering function
T	
t	triton
t	time; thickness of absorber in mass scattering power

t_{\max}	characteristic time in nuclear decay series or nuclear activation
$t_{1/2}$	half-life
$(t_{1/2})_{\text{eff}}$	effective half-life
T	temperature; linear scattering power; temporal function; period of linac pulse; barrier transmission factor
T_{α}	Gamow potential barrier transmission factor
T/ρ	mass scattering power
Torr	old unit of pressure (1 Torr \approx 1 mm Hg)
TE	transverse electric mode
TM	transverse magnetic mode
TP	triplet production

U

u	unified atomic mass constant (931.5 MeV/ c^2)
u	particle velocity after collision; EM field density
U	uranium atom
U	applied potential
U_C	Coulomb potential energy
$U(z)$	barrier potential

V

v	velocity
v_{thr}	threshold velocity in Čerenkov effect
v_{en}	velocity of energy flow
v_{gr}	group velocity
v_n	velocity of electron in n -th allowed orbit
v_{part}	particle velocity
v_{ph}	phase velocity
v_{α}	velocity of α particle
V	volt (unit of potential difference)
V	volume; potential energy
$V_{\text{TF}}(r)$	Thomas-Fermi potential
V_{FNS}	potential energy for finite nuclear size
V_{Yuk}	Yukawa potential
\mathcal{V}	volume

W

w_C	relative weight of Compton interaction
w_{PE}	relative weight of photoelectric interaction
w_{PP}	relative weight of pair production interaction
w_R	radiation weighting factor; relative weight of Rayleigh interaction
w_C	relative weight of Compton effect
w_{PE}	relative weight of photoelectric effect
w_{PP}	relative weight of pair production

W	transmitted particle in weak interaction; tungsten (wolfram) atom
W_{el}	electric energy stored per unit length
W_{if}	transition (reaction) rate
W_{mag}	magnetic energy stored per unit length
X	
x	momentum transfer variable ($x = \sin(\theta/2)/\lambda$); normalized time $x = t/t_{1/2}$; horizontal axis (abscissa) in Cartesian coordinate system; coordinate in Cartesian coordinate system; time normalized to half-life of parent nuclide
x_{f}	particle final position
x_{mn}	zero of Bessel function
x_{i}	particle initial position
x_0	target thickness
\bar{x}	mean free path
$(x_{\text{D}})_{\text{max}}$	maximum normalized characteristic time of the daughter
$x_{1/10}$	tenth value layer
$x_{1/2}$	half-value layer
$\frac{A}{Z}\text{X}$	nucleus with symbol X, atomic mass number A, and atomic number Z
X	exposure
X_0	target thickness; radiation length
$\bar{X}_{\text{PE}}(j)$	mean fluorescence emission energy
Y	
y	vertical axis (ordinate) in Cartesian coordinate system; coordinate in 3-dimensional Cartesian coordinate system
y_{mn}	zero of first derivative of Bessel function
Y	radiation yield; activation yield
y_{p}	activity normalized to initial parent activity in nuclear series decay; normalized parent activity
$(y_{\text{D}})_{\text{max}}$	maximum normalized daughter activity
Y_{D}	radioactivation yield of the daughter
$Y[(E_{\text{K}})_0, Z]$	radiation yield
Z	
z	atomic number of the projectile; depth in phantom; axis in 3-dimensional Cartesian coordinate system (aplicate axis)
z_{max}	depth of dose maximum
Z	atomic number; number of protons in atomic nucleus; number of electrons in atom
Z_{eff}	effective atomic number
Z^0	transmitted particle in weak interaction

Greek Letter Symbols



α

- α fine structure constant (1/137); ratio σ_P/σ_D ; nucleus of helium atom (alpha particle)
 α_{IC} internal conversion factor

β

- β normalized particle velocity (v/c)
 β^+ beta plus particle (positron)
 β^- beta minus particle (electron)
 β_0 incident energy of electron entering waveguide

γ

- γ photon originating in a nuclear transition; ratio of total to rest energy of a particle; ratio of total to rest mass of a particle; Lorentz factor

δ

- δ polarization (density effect) correction for stopping power; delta particle (electron)
 Δ energy threshold for restricted stopping power

ϵ

- ϵ eccentricity of hyperbola; normalized photon energy; Planck energy
 ϵ^* ratio λ_D^*/λ_D
 ϵ_0 electric constant (8.85×10^{-12} A s/(V m)); electric permittivity of vacuum

θ

- θ scattering angle for a single scattering event; scattering angle of photon; scattering angle of projectile in projectile/target collision;
 θ_{cer} Čerenkov characteristic angle
 θ_{max} characteristic angle in bremsstrahlung production; maximum scattering angle

θ_{\min}	minimum scattering angle
θ_R	characteristic angle for Rayleigh scattering
Θ	scattering angle for multiple scattering
$\overline{\theta^2}$	mean square of scattering angle
$\bar{\theta}^2$	square of mean scattering angle
$\sqrt{\overline{\Theta^2}}$	root mean square scattering angle
η	
η	pair production parameter; maximum energy transfer fraction in nuclear collision; energy boundary between hard and soft collision; fluorescence efficiency
$\eta(E_K)$	energy transfer fraction
η_β	correction factor for β decay
κ	
κ	linear attenuation coefficient for pair production
${}_a\kappa$	atomic attenuation coefficient for pair production
κ/ρ	mass attenuation coefficient for pair production
λ	
λ	wavelength; separation constant; decay constant; de Broglie wavelength of particle
λ_C	Compton wavelength
$(\lambda)_c$	cut-off wavelength in uniform wave guide
λ_D	decay constant of daughter nuclide
λ_D^*	modified decay constant
λ_{\min}	Duane-Hunt short wavelength cut-off
λ_P	decay constant of parent nuclide
Λ	separation constant; mean free path of neutrons
μ	
μ	linear attenuation coefficient; reduced mass
μ_{ab}	linear energy absorption coefficient
μ_{eff}	effective attenuation coefficient
μ_H	reduced mass of hydrogen atom
μ_m	mass attenuation coefficient
μ_0	magnetic constant ($4\pi \times 10^{-7}$ Vs/(Am)); magnetic permeability of vacuum
μ_{tr}	linear energy transfer coefficient
μ/ρ	mass attenuation coefficient
(μ_{ab}/ρ)	mass energy absorption coefficient
(μ_{tr}/ρ)	mass energy transfer coefficient
${}_a\mu$	atomic attenuation coefficient

$e\mu$	electronic attenuation coefficient
μm	unit of length or distance (10^{-6} m)
ν	
ν	frequency
ν_{eq}	photon frequency at which the atomic cross sections for Rayleigh scattering and Compton scattering are equal
ν_e	electronic neutrino
ν_{cyc}	cyclotron frequency
ν_{orb}	orbital frequency
ν_{trans}	transition frequency
ν_{μ}	muonic neutrino
ξ	
ξ	ratio between daughter and parent nuclide activities at time t ; Thomas-Fermi atomic radius constant; absorption edge parameter in photoelectric effect
π	
π	pi meson (pion)
π^+	positive pi meson (pion)
π^-	negative pi meson (pion)
\prod_i	product of components i
ρ	
ρ	mass density; energy density
$\rho(E_f)$	density of final states
σ	
σ	cross section; linear attenuation coefficient; standard deviation
σ_{rad}	cross section for emission of bremsstrahlung
σ_{C}	Compton linear cross section (attenuation coefficient)
$\sigma_{\text{C}}^{\text{KN}}$	Klein-Nishina cross section for Compton effect
$a\sigma_{\text{C}}$	atomic attenuation coefficient (cross section) for Compton effect
$a\sigma_{\text{R}}$	atomic attenuation coefficient (cross section) for Rayleigh scattering
$a\sigma_{\text{Th}}$	atomic attenuation coefficient (cross section) for Thomson scattering
$e\sigma_{\text{Th}}$	Thomson electronic attenuation coefficient
$e\sigma_{\text{C}}$	electronic attenuation coefficient for Compton effect
σ_{D}	daughter cross section in particle radioactivation
σ_{P}	parent cross section in particle radioactivation
σ_{PN}	cross section for photonuclear interaction
σ_{Mott}	cross section for Mott scattering
σ_{R}	Rayleigh cross section (linear attenuation coefficient)

σ_{Ruth}	cross section for Rutherford scattering
σ_{Th}	Thomson cross section (linear attenuation coefficient)
${}_a\sigma$	atomic cross section (in cm^2/atom)
${}_e\sigma$	electronic cross section (in $\text{cm}^2/\text{electron}$)
Σ	macroscopic cross section of absorbing medium for neutrons
\sum_i	sum of components i
τ	
τ	linear attenuation coefficient for photoelectric effect; normalized electron kinetic energy; mean (average) life; pulse width in linac pulse
${}_a\tau$	atomic attenuation coefficient for photoelectric effect
τ/ρ	mass attenuation coefficient for photoelectric effect
ϕ	
ϕ	angle between radius vector and axis of symmetry on a hyperbola; recoil angle of the target in projectile/target collision; neutron recoil angle in elastic scattering on nucleus; recoil angle of the electron in Compton scattering
φ	particle fluence
$\dot{\varphi}$	particle fluence rate
χ	
χ	homogeneity factor; energy independent momentum transfer function
ψ	
ψ	wavefunction (eigenfunction) depending on spatial coordinates; energy fluence; polarization angle
Ψ	wavefunction depending on spatial and temporal coordinates
ω	
ω	fluorescence yield; angular frequency
ω_c	cutoff angular frequency of waveguide
ω_{cyc}	cyclotron frequency
ω_{K}	fluorescence yield for K-shell transition
Ω	solid angle

(1) **Atomic Weights and Isotopic Compositions**

Web Database Developers: *J.S. Coursey, D.J. Schwab, J.J. Tsai, and R.A. Dragoset*

Atomic weights are available for elements 1 through 112, 114, and 116, and isotopic compositions or abundances are given where appropriate.

<http://www.nist.gov/pml/data/comp.cfm>

(2) **Bibliography of Photon Attenuation Measurements**

Data compiler: *J.H. Hubbell*; Web Database Developers: *J.S. Coursey, J. Hwang, and D.S. Zucker*

This bibliography contains papers (1907–1995) reporting absolute measurements of photon (XUV, x-ray, gamma-ray, bremsstrahlung) total interaction cross sections or attenuation coefficients for the elements and some compounds used in a variety of medical, industrial, defense, and scientific applications. The energy range covered is from 10 eV to 13.5 GeV.

http://www.nist.gov/pml/data/photon_cs/index.cfm

(3) **Elemental Data Index and Periodic Table of Elements**

Web Database Developers: *M.A. Zucker, A.R. Kishore, R. Sukumar, and R.A. Dragoset*

Elemental Data Index provides access to the holdings of NIST Physics Laboratory online data organized by element. It is intended to simplify the process of retrieving online scientific data for a specific element.

<http://www.nist.gov/pml/data/edi.cfm>

(4) **Fundamental Physical Constants**

The NIST Reference on Constants, Units, and Uncertainty.

www.physics.nist.gov/cuu/constants/

(5) **Ground Levels and Ionization Energies for the Neutral Atoms**

W.C. Martin, A. Musgrove, S. Kotochigova, and J.E. Sansonetti

This table gives the principal ionization energies (in eV) for the neutral atoms from hydrogen ($Z = 1$) through rutherfordium ($Z = 104$). The spectroscopy notations for the electron configurations and term names for the ground levels are also included.

http://www.nist.gov/pml/data/ion_energy.cfm

(6) International System of Units (SI)

The NIST Reference on Constants, Units, and Uncertainty

The SI system of units is founded on seven SI base units for seven base quantities that are assumed to be mutually independent. The SI base units as well as many examples of derived units are given.

www.physics.nist.gov/cuu/Units/units.html

(7) Periodic Table: Atomic Properties of the Elements

R.A. Dragoset, A. Musgrove, C.W. Clark, and W.C. Martin

A periodic table, containing NIST critically evaluated data on atomic properties of the elements was designed as a NIST handout for use at exhibitions and trade shows. The publication of the handout coincided with NIST's centennial celebration in 2001. One side of the handout (shown below) is available online in two formats (PDF & TIFF), and is suitable for high-resolution color printing for desk or wall-chart display. [The other side of the handout (available only in the PDF files) contains historical information.

<http://www.nist.gov/pml/data/periodic.cfm>

(8) Photon Cross Sections Database: XCOM

M.J. Berger, J.H. Hubbell, S.M. Seltzer, J.S. Coursey, and D.S. Zucker

A web database is provided which can be used to calculate photon cross sections for scattering, photoelectric absorption and pair production, as well as total attenuation coefficients, for any element, compound or mixture $Z \leq 100$ at energies from 1 keV to 100 GeV.

www.physics.nist.gov/PhysRefData/Xcom/Text/XCOM.html

(9) Stopping-Power and Range Tables for Electrons, Protons, and Helium Ions

M.J. Berger, J.S. Coursey, and M.A. Zucker

The databases ESTAR, PSTAR, and ASTAR calculate stopping-power and range tables for electrons, protons, or helium ions, according to methods described in ICRU Reports 37 and 49. Stopping-power and range tables can be calculated for electrons in any user-specified material and for protons and helium ions in 74 materials.

<http://www.nist.gov/pml/data/star/index.cfm>

(10) **Tables of X-Ray Mass Attenuation Coefficients and Mass Energy-Absorption Coefficients from 1 keV to 20 MeV for Elements $Z = 1$ to 92 and 48 Additional Substances of Dosimetric Interest**

J.H. Hubbell and S.M. Seltzer

Tables and graphs of the photon mass attenuation coefficient μ/ρ and the mass energy-absorption coefficient μ_{en}/ρ are presented for all elements from $Z = 1$ to $Z = 92$, and for 48 compounds and mixtures of radiological interest.

<http://www.nist.gov/pml/data/xraycoef/index.cfm>

(11) **X-Ray Form Factor, Attenuation, and Scattering Tables**

C.T. Chantler, K. Olsen, R.A. Dragoset, A.R. Kishore, S.A. Kotochigova, and D.S. Zucker

Detailed Tabulation of Atomic Form Factors, Photoelectric Absorption and Scattering Cross Section, and Mass Attenuation Coefficients for Z from 1 to 92. The primary interactions of x-rays with isolated atoms from $Z = 1$ (hydrogen) to $Z = 92$ (uranium) are described and computed within a self-consistent Dirac-Hartree-Fock framework. The results are provided over the energy range from either 1 eV or 10 eV to 433 keV, depending on the atom. Self-consistent values of the f_1 and f_2 components of the atomic scattering factors are tabulated, together with the photoelectric attenuation coefficient τ/ρ and the K-shell component τ_K/ρ , the scattering attenuation coefficient σ/ρ (coh + inc), the mass attenuation coefficient μ/ρ , and the linear attenuation coefficient μ , as functions of energy and wavelength.

<http://www.nist.gov/pml/data/ffast/index.cfm>

(12) **X-ray Transition Energies**

R.D. Deslattes, E.G. Kessler Jr., P. Indelicato, L. de Billy, E. Lindroth, J. Anton, J.S. Coursey, D.J. Schwab, K. Olsen, and R.A. Dragoset

This X-ray transition table provides the energies and wavelengths for the K and L transitions connecting energy levels having principal quantum numbers $n = 1, 2, 3,$ and 4 . The elements covered include $Z = 10$, neon to $Z = 100$, fermium. There are two unique features of this database: (1) all experimental values are on a scale consistent with the International System of measurement (the SI) and the numerical values are determined using constants from the Recommended Values of the Fundamental Physical Constants: 1998 and (2) accurate theoretical estimates are included for all transitions.

<http://www.nist.gov/pml/data/xraytrans/index.cfm>

(13) Fundamental Physical Constants*CODATA*

CODATA, the Committee on Data for Science and Technology, is an interdisciplinary scientific committee of the International Council for Science (ICSU), which works to improve the quality, reliability, management and accessibility of data of importance to all fields of science and technology. The CODATA committee was established in 1966 with its secretariat housed at 51, Boulevard de Montmorency, 75016 Paris, France. It provides scientists and engineers with access to international data activities for increased awareness, direct cooperation and new knowledge. The committee was established to promote and encourage, on a world-wide basis, the compilation, evaluation, and dissemination of reliable numerical data of importance to science and technology.

www.codata.org

(14) Nuclear Energy Agency Data Bank*Organisation for Economic Cooperation and Development (OECD)*

The nuclear energy agency data bank of the Organization for Economic Cooperation and Development (OECD) maintains a nuclear database containing general information, evaluated nuclear reaction data, format manuals, preprocessed reaction data, atomic masses, and computer codes.

www.nea.fr/html/databank/

(15) Mathematica*Wolfram MathWorld*

Wolfram MathWorld™ is web's most extensive mathematical resource, provided as a free service to the world's mathematics and internet communities as part of a commitment to education and educational outreach by Wolfram Research, makers of Mathematica, an extensive technical and scientific software. Assembled during the past decade by Eric W. Weisstein, MathWorld emerged as a nexus of mathematical information in mathematics and educational communities. The technology behind MathWorld is heavily based on Mathematica created by Stephen Wolfram.

mathworld.wolfram.com

(16) Nuclear Data*National Nuclear Data Center*

National Nuclear Data Center (NNDC) of the *Brookhaven National Laboratory* (BNL) in the USA developed a software product (NuDat 2) that allows users to search and plot nuclear structure and nuclear decay data interactively. The program provides an interface between web users and several databases containing nuclear structure, nuclear decay and some neutron-induced nuclear reaction information. Using NuDat 2, it is possible to search

for nuclear level properties (energy, half-life, spin-parity), gamma-ray information (energy, intensity, multipolarity, coincidences), radiation information following nuclear decay (energy, intensity, dose), and neutron-induced reaction data from the BNL-325 book (thermal cross section and resonance integral). The information provided by NuDat 2 can be seen in tables, level schemes and an interactive chart of nuclei.

www.nndc.bnl.gov

(17) Nucleonica

European Commission: Joint Research Centre

Nucleonica is a new nuclear science web portal from the European Commission's Joint Research Centre. The portal provides a customizable, integrated environment and collaboration platform for the nuclear sciences using the latest internet "Web 2.0" dynamic technology. It is aimed at professionals, academics and students working with radionuclides in fields as diverse as the life sciences, the earth sciences, and the more traditional disciplines such as nuclear power, health physics and radiation protection, nuclear and radiochemistry, and astrophysics. It is also used as a knowledge management tool to preserve nuclear knowledge built up over many decades by creating modern web-based versions of so-called legacy computer codes. Nucleonica also publishes and distributes the *Karlsruhe Nuklidkarte* (Karlsruhe Chart of the Nuclides).

www.nucleonica.net

Bibliography

1. F.H. Attix, *Introduction to Radiological Physics and Radiation Dosimetry* (Wiley, New York, 1986)
2. V. Balashov, *Interaction of Particles and Radiation with Matter* (Springer, Berlin, 1997)
3. British Journal of Radiology, Suppl. 25, *Central Axis Depth Dose Data for Use in Radiotherapy* (British Institute of Radiology, London, 1996)
4. E. Butkov, *Mathematical Physics* (Addison-Wesley, Reading, 1968)
5. J.R. Cameron, J.G. Skofronick, R.M. Grant, *The Physics of the Body*, 2nd edn. (Medical Physics Publishing, Madison, 1999)
6. S.R. Cherry, J.A. Sorenson, M.E. Phelps, *Physics in Nuclear Medicine*, 3rd edn. (Saunders, Philadelphia, 2003)
7. R. Eisberg, R. Resnick, *Quantum Physics of Atoms, Molecules, Solids, Nuclei and Particles* (Wiley, New York, 1985)
8. R.D. Evans, *The Atomic Nucleus* (Krieger, Malabar, 1955)
9. H. Goldstein, C.P. Poole, J.L. Safco, *Classical Mechanics*, 3rd edn. (Addison Wesley, Boston, 2001)
10. J. Hale, *The Fundamentals of Radiological Science* (Thomas, Springfield, 1974)
11. W. Heitler, *The Quantum Theory of Radiation*, 3rd edn. (Dover Publications, New York, 1984)
12. W. Hendee, G.S. Ibbott, *Radiation Therapy Physics* (Mosby, St. Louis, 1996)
13. W.R. Hendee, E.R. Ritenour, *Medical Imaging Physics*, 4th edn. (Wiley, New York, 2002)
14. International Commission on Radiation Units and Measurements (ICRU), Electron beams with energies between 1 and 50 MeV. ICRU Report 35 (ICRU, Bethesda, MD, USA), 1984
15. International Commission on Radiation Units and Measurements (ICRU), Stopping powers for electrons and positrons. ICRU Report 37 (ICRU, Bethesda, MD, USA), 1984
16. J.D. Jackson, *Classical Electrodynamics*, 3rd edn. (Wiley, New York, 1999)
17. H.E. Johns, J.R. Cunningham, *The Physics of Radiology*, 4th edn. (Thomas, Springfield, 1984)
18. F. Khan, *The Physics of Radiation Therapy*, 3rd edn. (Williams & Wilkins, Baltimore, 2003)
19. S.C. Klevenhagen, *Physics and Dosimetry of Therapy Electron Beams* (Medical Physics Publishing, Madison, 1993)
20. K.S. Krane, *Modern Physics* (Wiley, New York, 1996)
21. D.R. Lide, *CRC Handbook of Chemistry and Physics*, 93th edn. (CRC Press, Boca Raton, 2012)
22. P. Marmier, E. Sheldon, *Physics of Nuclei and Particles* (Academic Press, New York, 1970)
23. P. Metcalfe, T. Kron, P. Hoban, *The Physics of Radiotherapy X Rays from Linear Accelerators*, 2nd edn. (Medical Physics Publishing, Madison, 2007)
24. E. Persico, E. Ferrari, S.E. Segre, *Principles of Particle Accelerators* (W.A. Benjamin, New York, 1968)
25. E.B. Podgoršak (ed.), *Radiation Oncology Physics: A Handbook for Teachers and Students* (International Atomic Energy Agency, Vienna, 2005)
26. E.B. Podgoršak, *Radiation Physics for Medical Physicists*, 2nd edn. (Springer, Berlin, 2010)

27. J.W. Rohlf, *Modern Physics from α to Z_0* (Wiley, New York, 1994)
28. R.A. Seaway, C.J. Moses, C.A. Moyer, *Modern Physics* (Saunders College Publishing, Philadelphia, 1989)
29. P. Sprawls, *Physical Principles of Medical Imaging* (Medical Physics Publishing, Madison, 1995)
30. R.L. Sproull, *Modern Physics: The Quantum Physics of Atoms, Solids, and Nuclei* (Krieger, Malabar, 1990)
31. J.E. Turner, *Atoms, Radiation, and Radiation Protection*, 3rd edn. (Wiley, New York, 2007)
32. J. Van Dyk (ed.), *The Modern Technology of Radiation Oncology* (Medical Physics Publishing, Madison, 1999)

Index

Symbols

α alpha decay, 685
 α decay, 748
 α particle accelerator, 924
 α particle scattering, 697
 β^+ , 748
 β particle energy spectra, 705
 β^- decay, 862
 β^+ decay, 727
 β^- beta decay, 685
 β emission spectrum, 703
 γ decay, 738
 γ photon, 740
 γ ray spectroscopy, 800

A

Absorption, 601
Absorption edge, 476, 481
Absorption parameter, 476
Absorption spectrum, 213
Accelerating electric field, 1042
Accelerating waveguide, 950, 951, 1086
Acceleration EM waveguide, 1024
Acceleration of electron, 942
Acceleration waveguide, 49, 942, 979, 999, 1008, 1015, 1028, 1030, 1077, 1081, 1092
Acceleration waveguide theory, 1008
Accelerator EM waveguide, 977
Accelerator-based neutron generator, 624
Acoustic waveguide, 944
Acoustic waves, 942
Actinide series, 632
Actinium series, 796, 802
Activation cross section, 938
Activation factor, 814, 819, 824, 841, 843, 849
Activation of iridium-191, 843
Activation of linac components, 1049
Activation of the daughter, 871
Activation reaction, 932
Activation time, 856, 879
Activity, 21, 638, 642
Activity of parent (Mo-99), 655
Activity of the daughter, 647, 649
Activity of the parent, 649
Activity ratio, 667
Adaptive radiotherapy (ART), 1077
Air-pressure system, 1082
Alpha decay, 694, 696, 737
Alpha decay line, 784
Alpha decay of radium-226, 101
Alpha decay tunneling, 98
Alpha particle, 18, 287, 360, 697
Alpha particle scattering, 120
Amorphous selenium, 1057
Ampère circuital law, 953
Ampère law, 108
Analog imaging techniques, 1046
Anatomic image, 931
Angular distribution of α particles, 122
Angular momentum, 311
Angular momentum of electron, 184
Annihilation, 727, 1051
Annihilation photon, 555
Annihilation quantum, 20, 496, 570, 576, 718, 727, 1051
Anthropogenic radionuclide, 803
Antihydrogen, 190, 203
Antineutrino, 705, 806
Arrhenius diagram, 93, 106
Arrhenius-type graph, 93
Artificial or induced radioactivity, 788, 798
Artificial radioactivity, 638, 788
Artificial radionuclide, 774
Atmospheric carbon, 796
Atomic attenuation coefficient, 388, 390, 394, 516, 532, 539, 559
Atomic cross section for Thomson scattering, 408
Atomic energy level, 187, 188, 210
Atomic energy level diagram, 181, 195, 197, 201, 202, 210, 213

- Atomic energy level diagram for hydrogen atom, 207
- Atomic energy level diagram for tungsten, 233, 240
- Atomic energy levels of lead, 211
- Atomic form factor, 442, 449, 459
- Atomic form factor of hydrogen, 442, 445
- Atomic mass, 30
- Atomic mass data, 769
- Atomic orbital electron, 695
- Atomic polarization effects, 1049, 1051
- Atomic radius, 33, 208, 222
- Atomic rest energy, 932
- Atomic rest energy $M_{\text{Eu-151}}c^2$ of Eu-151, 771
- Atomic rest energy method, 697, 700, 715, 719, 721, 749, 752, 792, 909
- Atomic shell vacancy, 226
- Atomic stopping number, 315, 320, 324
- Atomic structure, 24
- Atomic volume, 208
- Attenuation coefficient at absorption edge, 478
- Attenuation of collimated neutron beam, 587
- Attenuation of the neutron beam, 583
- Auger effect, 228
- Auger electron, 17, 226, 235, 237, 241, 380, 465, 520, 521, 556, 703, 704
- Auger spectrometry, 1047
- Average (mean) lifetime, 640
- B**
- Backscattering, 410, 413
- Bakelite, 548
- Balmer, 214
- Balmer line, 194, 196
- Balmer photon, 195
- Barrier penetration, 98
- Barrier transmission coefficient, 102, 105
- Basic Einstein relationship, 55
- Basic physical quantities, 10
- Bateman constants, 675
- Bateman equation, 671, 675
- Beam collimation system, 1082
- Beam monitoring system, 1082
- Beam quality, 379
- Beam quality indices, 381
- Beam quality specification, 381
- Beam-forming component, 1079
- Beam-forming components of medical linac, 1080
- Becquerel (Bq), 638
- Bell curve, 113
- Beryllium exit window, 1083, 1096
- Beryllium-9 target, 628
- Bessel differential equation, 967
- Bessel function, 991, 992
- Bessel functions of the first kind, 967
- Beta decay, 694, 703, 737
- Beta decay category, 703
- Beta minus decay, 694, 704, 708
- Beta minus decay of Ir-192, 734
- Beta particle, 17, 753
- Beta plus (β^+) decay, 694, 704, 717
- Beta-delayed PE decay, 752
- Betatron, 257, 380, 382, 978, 1029, 1044, 1046, 1049, 1050, 1061, 1075
- Bethe equation, 314, 323, 332
- Bhabha scattering, 118
- Binary radiotherapy modality, 621
- Binding effects of electrons, 448
- Binding energy corrections, 449
- Binding energy method, 273, 276, 499, 503, 504, 508, 622, 624, 629, 898, 927
- Binding energy of the electron, 181, 183, 465
- Binding energy per nucleon, 28, 30, 712, 770
- Binding energy per nucleon for Eu-151, 772
- Biological marker, 717
- Bipartition angle, 475
- Bismuth-212, 685
- Blackbody emission, 41
- Blackbody radiation, 36, 37
- Blood irradiator, 738
- Blood sugar concentration, 26
- Blue shift, 68
- Body composition activation analysis, 800
- Bohr atom, 184, 188, 199, 201, 212
- Bohr atomic model, 179
- Bohr atomic theory, 215
- Bohr orbit, 201
- Bohr postulate, 187
- Bohr radius, 87, 169, 209, 223, 449
- Bohr radius constant, 4, 104, 187, 201, 443
- Bohr theory, 190, 203, 216
- Bohr theory for hydrogen atom, 189
- Bohr theory of one-electron atom, 184
- Bohr theory of one-electron atoms, 219
- Boltzmann constant, 94
- Born approximation, 168, 481
- Born screening angle, 168, 174
- Boron, 889
- Boron neutron capture therapy, 582, 621, 885
- Boron-10, 621, 909
- Boron-11, 931
- Boundary condition, 943, 945, 950, 954, 961
- Boundary condition on electric field, 947
- Boundary condition on magnetic field, 948
- Brachytherapy, 582, 708, 731, 738, 799, 800, 879, 885, 891, 1046
- Brackett, 214

- Bragg additivity rule, 317
 Bragg angle, 76
 Bragg diffraction, 75, 89
 Bragg law, 88
 Bragg peak, 327
 Bragg reflection, 76, 77
 Bragg relationship, 1047
 Branching decay, 685
 Branching fraction, 632, 685
 Bremsstrahlung, 210, 249, 352, 566, 568, 574, 928, 1048, 1049, 1053, 1056, 1060, 1069, 1078, 1086
 Bremsstrahlung beam, 384
 Bremsstrahlung characteristic angle, 250
 Bremsstrahlung cross section, 307
 Bremsstrahlung intensity, 250
 Bremsstrahlung loss, 171, 1070
 Bremsstrahlung photon, 380
 Bremsstrahlung production, 242, 254
 Bremsstrahlung radiation, 246, 350, 377
 Bremsstrahlung radiation loss, 1066
 Bremsstrahlung spectrum, 380
 Bremsstrahlung target, 1082
 Bremsstrahlung x ray, 20, 377
 Brillouin diagram, 1027
 Brillouin zone, 1026
 Broad beam geometry, 398
 Broglie wavelength, 77
 Brookhaven National Laboratory, 760, 938, 1065
 Buildup factor, 398
- C**
- Cadmium-113, 909
 Californium, 632
 Cancer diagnosis, 718
 Capture condition, 1028, 1031, 1035
 Capture constant of the electron, 1033
 Capture reaction, 799
 Carbon, 562, 903
 Carbon dating, 795
 Carbon dioxide, 797
 Carbon ion, 360
 Carbon nanotube, 1057
 Carbon-11, 718, 721, 800, 931
 Carbon-14, 795, 796, 801
 Carrier-free radionuclide, 834
 Categories of nuclear decay, 694
 Cathode ray, 1053, 1058
 Center C of the hyperbola, 129
 Center-of-Mass (CM) frame, 281
 Center-of-mass coordinate system, 630
 Center-of-mass system, 490
 Central axis, 1097
 Central potential, 442
 Ceramic window, 1095
 Čerenkov angle, 259, 262
 Čerenkov radiation, 258, 262, 1051
 Cesium-137, 712, 737, 742, 775, 854
 Chadwick nuclear reaction, 274
 Chain reaction, 892, 901
 Characteristic activation time, 857
 Characteristic angle, 168, 169, 248, 254
 Characteristic bremsstrahlung angle, 254
 Characteristic energy, 269
 Characteristic (fluorescence) photon, 235, 465, 520
 Characteristic (fluorescence) radiation, 226
 Characteristic (fluorescence) x rays, 20
 Characteristic line, 216
 Characteristic normalized time, 827
 Characteristic photons, 210
 Characteristic radiation, 241, 1048, 1060
 Characteristic scattering distance, 165
 Characteristic scattering distance for electron–atom scattering, 168
 Characteristic scattering distance for Moller scattering, 167
 Characteristic scattering distance for Mott scattering, 167
 Characteristic scattering distance for Rutherford scattering, 167
 Characteristic time, 647, 649, 651, 655, 656, 663, 877
 Characteristic x ray, 380, 408, 703, 1049
 Characteristic x-ray lines, 216, 218
 Characteristic x-ray photons, 1056
 Charge distribution of nuclei, 119
 Charged particle activation, 931, 936
 Charged particle Coulomb interaction, 227
 Chart of nuclides, 759, 763, 780, 798
 Chemical reaction, 901
 Chemical separation of elements, 767
 Chernobyl, Ukraine, 906
 Circular accelerator, 1044, 1049, 1061
 Circular electron accelerator, 1051
 Circular uniform EM waveguide, 962
 Circular waveguide, 951, 962
 Circulator, 1094
 Classical electron radius, 4
 Classical Larmor expression, 179, 246
 Classical particle, 66
 Classical radius of the electron, 172
 Classification diagram of particle accelerators, 1044
 Classification of radiation, 14
 Clinical beam, 1077
 Clinical beam forming system, 1077

- Clinical electron beam, 1080, 1090
 Clinical linac, 942
 Clinical linear accelerator, 1035, 1075
 Clinical neutron beam, 628
 Clinical x-ray beam, 1080, 1090
 Co-60 activation–decay, 868
 Coaxial cable, 942
 Cobalt teletherapy machine, 1014
 Cobalt-60, 712, 737, 775, 835, 837, 854, 885
 Cobalt-60 gamma source, 1014
 Cobalt-60 teletherapy machine, 6, 382, 738, 1075
 Coincidence detection, 718
 Cold cathode, 1052, 1057
 Cold neutron, 582
 Collector plate, 220
 Collision loss, 350, 380, 1051
 Collision stopping power, 314, 319, 938
 Collision stopping power constant, 315, 320, 332
 Collision stopping power of water for proton, 321
 Commissioning of nuclear reactor, 901
 Complementarity principle, 88
 Complete x-ray spectrum, 381
 Composite decay curve, 682
 Compound nucleus, 790, 896
 Compton atomic attenuation coefficient, 535
 Compton atomic cross section, 534
 Compton cross section, 481
 Compton differential atomic cross section, 449
 Compton effect, 395, 419, 429, 431, 436, 513, 520, 523, 540, 544, 557, 562, 1050
 Compton electronic cross section, 441, 448, 534
 Compton electronic energy transfer cross section, 441
 Compton equation, 408
 Compton graph, 439, 528, 542, 547, 560, 564
 Compton interaction, 562
 Compton Klein-Nishina coefficient, 535
 Compton mean energy transfer fraction, 547
 Compton recoil electron, 17
 Compton scattering, 155, 227, 409, 416, 438, 516, 526, 532, 553, 568, 576
 Compton scattering theory, 445
 Compton wavelength, 4, 261, 408
 Compton wavelength of electron, 410
 Compton wavelength of proton, 410
 Compton wavelength shift equation, 259
 Computed radiography, 1057
 Conditions for particle acceleration, 976
 Conservation of angular momentum, 130, 144, 311
 Conservation of atomic number, 897
 Conservation of charge, 488
 Conservation of energy, 120, 153, 204, 260, 269, 276, 281, 289, 409, 472, 494, 514, 699, 729
 Conservation of energy in Compton effect, 425
 Conservation of kinetic energy, 271, 289, 593
 Conservation of momentum, 153, 260, 268, 270, 281, 284, 288, 430, 435, 488, 495, 497, 593, 729, 740, 913
 Conservation of total energy, 259, 284, 430, 435, 475, 487, 496, 794, 913
 Constant potential x-ray tube, 1087
 Constituents of nuclides, 24
 Control console, 1055
 Control rod, 901, 909
 Control unit, 1090, 1091
 Conversion electron, 741
 Coolant, 906
 Coolidge tubes, 106
 Coolidge x-ray tube, 1057, 1075
 Core of transmission waveguide, 1024
 Corpuscular nature, 88
 Correction factor, 189
 Correction factor for β decay, 708
 Cosmic neutron, 582
 Cosmic ray, 796
 Cosmic x-ray source, 1048
 Cosmogenic isotope of hydrogen, 801
 Cosmogenic production of C-14, 801
 Cosmogenic radionuclide, 795, 803
 Coster-Kronig electron, 17, 226, 237
 Coulomb barrier, 100, 279
 Coulomb barrier constant, 280
 Coulomb barrier energy, 277
 Coulomb collision, 311, 380
 Coulomb elastic scattering, 165
 Coulomb electric field, 300
 Coulomb electrostatic attraction, 178
 Coulomb force, 129, 178, 279, 311
 Coulomb interaction, 118, 119, 301, 309, 310, 377, 437, 555, 582, 935, 936, 1049, 1050
 Coulomb law, 243
 Coulomb nuclear excitation, 303
 Coulomb point-source potential, 168
 Coulomb potential, 99, 120
 Coulomb potential energy, 100
 Coulomb scattering, 118, 140, 166
 Coulomb shielding, 149
 Count rate, 798
 Critical kinetic energy, 343, 347
 Critical mass, 901
 Crookes tube, 1051

- Crookes x-ray tube, 1052, 1075
 Cross section, 388, 390, 601
 Cross section for neutrons, 606
 Cross section of a nuclear reaction, 805
 Cross sections for Rutherford scattering, 145
 Crystal diffraction experiment, 1053
 CSDA range, 356, 360, 935
 Curie (Ci), 639
 Curl vector operator, 954
 Curve of stability, 760, 766
 Cutoff angle, 149, 171
 Cutoff frequency, 952, 980, 984, 987, 994, 1008, 1010
 Cutoff frequency of the waveguide, 942, 980, 987
 CyberKnife, 1076
 Cyclic accelerator, 256, 978, 1043
 Cyclic electron accelerator, 1076
 Cyclic particle accelerator, 1061, 1062
 Cyclotron, 628, 718, 924, 931, 978, 1029, 1044, 1061, 1071, 1075
 Cyclotron angular frequency, 64
 Cyclotron frequency, 1072, 1074
 Cyclotron target, 935
- D**
- D-d reaction, 624
 D-t fusion, 624
 Dating of organic, 795
 Daughter D, 642, 646
 Daughter nucleus D, 640
 Davisson-Germer experiment, 74, 75
 De Broglie particle-wave hypothesis, 81
 De Broglie wavelength, 69, 74, 76, 77, 79, 83, 119
 De Broglie wavelength for electron, 79
 Decay constant, 633, 639, 640, 642, 663, 682, 685
 Decay constant of U-238, 747
 Decay energy, 694, 700
 Decay energy of neutron, 710
 Decay energy Q_α , 792
 Decay energy $Q_\alpha(P)$, 697
 Decay energy Q_β , 704
 Decay energy Q_{β^+} , 719, 721, 733
 Decay energy Q_{β^+} (Q value of decay), 717
 Decay energy Q_{β^-} , 708, 712, 714, 732
 Decay energy Q_γ , 738
 Decay energy Q_{decay} , 732
 Decay energy Q_{EC} , 727, 733
 Decay energy Q_{IC} , 742
 Decay energy Q_{NE} , 755
 Decay energy Q_{PE} , 749
 Decay energy $Q_{\text{PE}}(^5_3\text{Li})$, 752
 Decay factor, 663, 667, 814
 Decay of the daughter, 871
 Decay paths available in the Chart of Nuclides, 785
 Decay rate of U-238, 747
 Decay scheme for polonium-210, 788
 Decay scheme of cesium-137, 742
 Decay scheme of radon-222, 700
 Decay series: P \rightarrow D \rightarrow G, 659
 Decommissioning of nuclear reactor, 901
 Decontamination of highly radioactive waste, 1050
 Deferred dismantling, 905
 Delayed energy release, 900
 Delayed neutron, 890, 900
 Delta ray electron, 17
 Delta ray electron threshold energy, 372
 Density correction, 314
 Density effect parameter, 336
 Depleted uranium, 768, 894, 922
 Depletion model, 811, 814, 818, 820, 835, 843, 844, 849, 854
 Depletion model of neutron activation, 810
 Depletion of the parent, 871
 Depletion-activation factor, 849, 852
 Depletion-activation model, 828, 844, 849
 Depth dose distribution, 385
 Depth of dose maximum, 583
 Derived physical constants, 4
 Determination of electron charge, 1054
 Deuterium, 18, 190, 191, 194, 203, 903
 Deuteron, 18, 319, 322, 324, 325, 360, 585, 628, 630
 Deuteron accelerator, 923
 Deuteron-triton, 624
 Diagnostic energy range, 381
 Diagnostic radiology, 1045
 Diagram for lead, 210
 Dielectric medium, 945
 Differential Klein-Nishina electronic cross section, 415
 Differential scattering cross section, 402
 Differential wave equation, 950
 Diffraction grating, 88, 214
 Diffraction pattern, 75, 1047
 Diffraction phenomena, 1047
 Digital imaging, 1057
 Digital imaging cassette, 1057
 Digital radiography, 1057
 Dipolar transitions, 229
 Direct-hit collision, 121, 131, 144, 312
 Direct-hit elastic collision, 135
 Directly ionizing radiation, 17, 18
 Dirichlet boundary condition, 967, 979, 983

- Dirichlet-type boundary condition, 956, 963, 1015
- Discovery of electron, 1053
- Discovery of induced radioactivity, 790
- Discovery of natural transmutation, 789
- Discovery of radium and polonium, 788
- Discovery of the electron, 122
- Discovery of the neutron, 789
- Discovery of the positron, 789
- Discovery of x rays, 976, 1045, 1052
- Discrete characteristic photon, 704
- Disintegration (decay) energy, 695
- Disk-loaded dispersion relationship, 1027
- Disk-loaded waveguide, 1023, 1027
- Dispersion diagram, 1025
- Dispersion relationship, 966, 980, 987, 991, 1009, 1011
- Dispersion relationship for an EM waveguide, 942
- Distance of closest approach, 100, 103, 120, 131, 134, 137, 140, 143, 146, 149
- Distribution of ejection angles, 472
- Divergence vector operator, 953
- Doppler equation, 67
- Doppler shifts, 67
- Dose, 21, 601, 611
- Dose build-up, 583
- Dose deposition by neutrons, 612
- Dose deposition in water, 21
- Dose monitoring system, 1083, 1096
- Doubly ionized lithium, 197
- Drip line, 759, 761
- Duane-Hunt law, 377, 380
- Duty cycle, 1086
- E**
- Eccentricity of the hyperbola, 129, 137, 141
- Eccentricity of the hyperbolic trajectory, 131
- Effective activation target thickness, 935
- Effective half-life, 633
- Effective linear attenuation coefficient, 398
- Effective mass of a two-body system, 190
- Effective threshold energy, 277
- Efficiency for x-ray production, 1089
- Eigenfunction, 81, 957, 965
- Eigenvalue, 958, 965
- Eigenvalue equation, 967
- Eigenvalue problem, 965
- Ejection angle of the photoelectron, 472
- Elastic collision, 290, 294, 377, 490, 614
- Elastic scattering, 119, 301, 589, 598
- Elastic scattering interaction, 598
- Elastic scattering of neutron, 583, 592
- Electric field amplitude, 1033
- Electric field correction factor, 243
- Electromagnetic (EM) force, 11
- Electromagnetic (EM) waveguide, 950, 987, 999, 1014
- Electromagnetic force constant, 12
- Electromagnetic radiation pressure, 111
- Electromagnetic spectrum, 41
- Electromagnetic waveguide, 943
- Electromagnetic waves in free space, 946
- Electron, 695, 1052
- Electron acceleration, 1009
- Electron accelerator, 923
- Electron affinity, 208
- Electron arc therapy, 1077
- Electron beam transport system, 1082, 1094
- Electron capture, 227, 704, 727
- Electron capture (EC) decay, 694
- Electron charge, 89
- Electron cones, 1085
- Electron configuration of atoms, 208
- Electron density, 320
- Electron gun, 1030, 1035, 1076, 1086, 1090, 1092
- Electron in ground state of hydrogen, 443
- Electron injection velocity, 1028
- Electron momentum, 65
- Electron orbital velocity, 187, 188
- Electron-atom, 165
- Electron-nucleus scattering, 153
- Electron-positron pair, 483, 486
- Electronegativity, 208
- Electronic antineutrino, 695
- Electronic attenuation coefficient, 516
- Electronic binding effects, 449
- Electronic brachytherapy, 1059
- Electronic Compton attenuation coefficient, 519
- Electronic configuration of tungsten, 231
- Electronic cross section for Thomson scattering, 402
- Electronic neutrino, 695
- Electronic pair production, 483, 516, 553, 557, 574
- Electronic transition, 194, 218, 226, 555
- Electronic transitions to K shell in lead, 211
- Electronic triplet production attenuation coefficient, 519
- Electronic vacancy, 226, 235, 554
- Electrostatic accelerator, 978, 1042
- EM waveguide, 961, 992, 1001
- Emission of bremsstrahlung radiation, 1069
- Emission of synchrotron radiation, 1070
- Emission spectrum, 213

- Endothermic nuclear reaction, 275, 500, 631, 793
- Endothermic reaction, 272, 490, 926, 933
- Energetic heavy charged particle, 799
- Energy absorbed, 571, 578
- Energy level diagram, 180
- Energy level diagram for tungsten, 238
- Energy loss per unit path length, 304
- Energy quantization, 34, 41
- Energy radiated from the annihilation in flight, 486
- Energy released per fission, 899
- Energy slits, 1095
- Energy transfer, 152
- Energy transfer fraction, 270, 289, 595
- Energy transfer from charged particle to medium, 300
- Energy transfer from energetic heavy charged particles (CP) to a medium, 309
- Energy transferred, 577
- Enriched deuterium, 191
- Enriched uranium, 894
- Enrichment of natural uranium, 768
- Entombment, 905
- Equilibria in parent-daughter activities, 666
- Equivalent circular transmission waveguide, 1008
- Equivalent dose, 21
- Equivalent incident kinetic energy, 360
- Equivalent one-body problem, 190
- Equivalent uniform waveguide, 1025
- Error function, 115
- Europium-152, 712, 835, 838, 854
- Excited hydrogen atom, 195
- Excited states, 180
- Exothermic reaction, 272, 490, 926, 933
- Expectation value, 85
- Expectation value of particle position, 86
- Exponential laws of radioactivity, 638
- Exposure, 21
- Exposure time, 1060
- External beam radiotherapy, 582, 708, 738, 774, 799, 854, 885
- Extreme relativistic case, 494
- Extreme relativistic region, 78
- F**
- Fano corrections, 314
- Fano shell correction, 316
- Far field component of the electric field, 246
- Faraday law of induction, 108, 953
- Fast neutron, 582, 630, 890, 896
- Fast neutron beam, 583
- Fast neutron from d-t reaction, 582
- Fast neutron region, 612
- FDG, 718
- Fertile nuclide, 890
- Field contraction, 243
- Field emission, 106, 107, 1057
- Field expansion, 243
- Filament, 1058
- Fine structure constant, 4
- Finite mass of the nucleus, 190
- Finite nuclear mass, 187, 188, 197
- Finite size of the nucleus, 184
- First Brillouin zone, 1026
- First derivative of Bessel functions, 991
- First excited state of mercury atom, 220
- First pass band, 1027
- Fissile nucleus, 890
- Fissile radionuclide, 890
- Fission, 29, 30, 589, 592, 602, 632, 638, 888, 890, 896, 1050
- Fission fragment, 893, 896
- Fission of U-235, 921
- Fission of uranium-235, 896
- Fission product, 800, 891, 893
- Fission product nuclei, 695
- Fission Q value, 898
- Fission reaction, 597
- Fission-based nuclear power, 903
- Fissionable nucleus, 892
- Flattening filter, 383, 1079, 1083, 1096
- Fluorescence, 789
- Fluorescence yield, 226, 235
- Fluorescing material, 789
- Fluorine-18, 718, 721, 800
- Focal spot, 1060
- Focusing coil, 1095
- Food irradiator, 1046
- Forces in nature, 11
- Form factor constant, 444
- Forward scattering, 413
- Forward transformation, 43
- Fowler-Nordheim equation, 106
- Fractional energy transfer, 268
- Franck-Hertz apparatus, 220
- Franck-Hertz experiment, 219
- Free electron, 83, 404, 406, 429, 450, 465
- Free (extra-nuclear) neutron, 583
- Free neutron, 796
- Free particle, 81
- Free space propagation coefficient, 965, 982
- Free space wave number, 958, 965, 974, 982
- Fuel elements, 905
- Fuel loading, 904
- Fukushima Daiichi, Japan, 906
- Full-width-at-half-maximum (FWHM), 115

- Functional image, 931
 Fundamental force, 11
 Fundamental forces in nature, 11
 Fundamental particles, 13
 Fusion, 29, 30, 624, 890
- G**
- Gamma decay, 694, 737
 Gamma emission, 651
 Gamma emission (GE) decay, 694
 Gamma emitter, 737
 Gamma ray, 20, 738, 774
 Gamma ray photon, 708
 GammaKnife, 6, 1076
 Gamow formula, 103
 Gamow potential barrier, 102
 Gas pressure system, 1093
 Gauss law for electricity, 108, 953
 Gauss law for magnetism, 108
 Gauss law of magnetism, 953
 Gauss-Ostrogradski divergence theorem, 108
 Gaussian distribution, 112, 122
 Geiger-Marsden scattering experiment, 122
 General EM boundary conditions, 949
 General form of daughter activity, 663
 Generator, 718
 Glucose metabolism, 718
 Gold-198, 835, 838
 Gold-198 seeds, 879
 Gradient vector operator, 953
 Granddaughter G, 646
 Granddaughter radionuclide Tc-99, 651
 Graphs of vector momenta, 473
 Gravitational force, 11
 Gravitational force constant, 12
 Grid, 1095
 Ground state energy level, 180
 Ground state energy of the hydrogen atom, 200
 Ground state of Co-60, 862
 Ground state of hydrogen, 178
 Ground state of mercury atom, 220
 Ground state wave function of hydrogen, 445
 Group velocity, 942, 951, 980, 985, 987, 992, 1009, 1019, 1027
 Group velocity in uniform waveguide, 1014
- H**
- Hadron, 582
 Half value layer, 539
 Half-life, 640, 642, 682
 Half-life for SF decay of U-238, 747
 Half-life of Mo-99, 655
 Half-value layer (HVL), 382, 388, 391, 395
 Hard collision stopping power, 304
- Hard collisions, 304, 365
 Hard electron-electron collision, 574
 Hard or direct collision, 301
 Hartree approximation, 212, 216, 744
 Hartree radius, 209
 Hartree theory of multi-electron atoms, 215
 Head-on collision, 100, 103, 120, 121, 134, 146, 149, 594
 Head-on (direct) elastic collision, 283
 Head-on (direct hit) elastic collision, 293
 Head-on elastic collision, 282, 284, 293
 Heated cathode, 1095
 Heated filament, 376
 Heavy charged particle, 17, 300
 Heavy charged particle accelerator, 800
 Heavy hydrogen, 191
 Heavy water, 191
 Heisenberg uncertainty principle, 87, 168
 Heliocentric Copernican planetary system, 33
 Helion, 18
 Helium-4, 752
 Helmholtz equation, 958, 982
 Helmholtz partial differential equation, 965
 Heterogeneous photon beam, 393
 HEU fission technique, 922
 HEU for non-military purpose, 922
 High gamma ray energy, 774
 High pass filter, 952
 High specific activity, 774
 High Z targets, 378
 High-energy electron accelerator, 928
 High-energy electron linear accelerators, 800
 High-energy linac, 1079
 High-energy radiotherapy, 1049
 High-energy x ray, 799
 Highly enriched uranium, 768
 Highly enriched uranium-235 (HEU) target, 921
 Hollow circles, 238
 Hot cathode, 1057
 Hubbell's method, 445
 Humphreys, 214
 Hydrogen, 194, 195, 201, 213, 442, 445, 606
 Hydrogen atom, 87, 178, 187, 195, 199, 223, 268
 Hydrogen atom in ground state, 206, 223
 Hydrogen ground state wave function, 222
 Hyperbolic trajectory, 140, 144
- I**
- IC decay, 742
 IC electron, 742
 Ideal equilibrium, 819, 824, 833, 843
 Image guided radiotherapy (IGRT), 1077

Image quality, 1046
 Image receptor, 1055
 Imaging in nuclear medicine, 914
 Imaging physics, 21
 Imaging x-ray tube, 1061
 Immediate dismantling, 905
 Impact parameter, 128, 131, 132, 137, 140, 144, 168, 301, 312
 In-flight annihilation, 302, 486, 494, 496, 555, 566, 575
 In-vivo body composition measurement, 800
 Incoherent scattering, 455
 Incoherent scattering function, 442, 445, 449
 Incoherent scattering function of hydrogen, 445
 Independently decaying radionuclides in a sample, 682
 Indirectly ionizing photon radiation, 20
 Indirectly ionizing radiation, 18, 19, 582, 585
 Indistinguishable colliding particles, 370
 Induced fission, 800
 Inelastic collision, 269, 301, 304, 377
 Inelastic scattering, 409, 589, 592
 Inertial frame, 45
 Infinite mass of the nucleus, 187
 Infinite nuclear mass, 188
 Initial condition, 943, 964
 Injection system, 1081, 1086
 Intense neutron emitter, 632
 Intensity modulated arc therapy (IMAT), 1077
 Intensity modulated radiotherapy (IMRT), 1077
 Intensity of bremsstrahlung, 245
 Intensity of bremsstrahlung radiation, 248
 Interaction mechanism, 567, 573
 Interaction probability, 806
 Intermediate charged particles, 300
 Intermediate compound nucleus, 272
 Internal conversion electron, 17, 737, 741
 Internal conversion factor, 742
 Internal conversion (IC), 227, 704, 737, 741
 Internal conversion (IC) decay, 694
 International Atomic Energy Agency, 760, 904
 International nuclear and radiological event scale (INES), 906
 Invariant, 275, 490, 630, 793, 933
 Invariant for the Joliot-Curie nuclear reaction, 794
 Inverse Chadwick reaction, 275
 Inverse Compton effect, 409, 434
 Inverse Compton scattering, 431
 Inverse Galilean transformation, 283
 Inverse Lorentz transformation, 44, 285
 Inverse square law, 583

Inverse transformation, 43
 Iodine-131, 712, 800
 Ionic radius, 209
 Ionization chamber, 1077
 Ionization potential, 180
 Ionization potential of atom, 208
 Ionization potential of mercury atom, 220
 Ionization stopping power, 304
 Ionizing radiation, 16, 21, 398, 1014, 1046
 Iridium source, 731
 Iridium-192, 731, 737, 835, 838, 886
 Island of nuclides, 759
 Isobar, 763
 Isobar line, 785
 Isocenter, 1077
 Isomer, 740, 764
 Isomeric radionuclide, 764
 Isomeric transition, 739
 Isotone, 763
 Isotone line, 784
 Isotope, 763, 767
 Isotope line, 784
 Isotope separation, 768
 Isotopic composition, 767
 IUPAC notation, 215, 237, 240
 IUPAC x-ray notation, 229

J

Johns, HE and Cunningham, JR, 368, 372, 549

K

K absorption edge, 211, 522
 K shell, 183
 K shell binding energy, 212
 K shell electron, 744
 K shell of tungsten, 235
 K shell vacancy, 233
 K-shell absorption edge, 481
 K-shell binding energy, 468, 476, 560
 K-shell electron, 474
 K-shell electron in lead, 468
 K-shell vacancy migration, 241
 Karlsruhe Chart of Nuclides, 763
 Karlsruhe Nuclide Chart, 760
 Karlsruher Nuklidkarte, 763
 Kepler-Newton planetary model, 178
 Kerma, 21, 601, 603, 606, 611, 619
 Kerma factor, 605
 Kinetic energy method, 273
 Kinetic energy of the scattered electron, 156, 158, 161, 162
 Klein-Gordon equation, 82
 Klein-Nishina coefficients, 534

Klein-Nishina differential atomic cross section, 449
 Klein-Nishina differential electronic cross section, 419, 424
 Klein-Nishina electronic Compton energy transfer coefficient, 440
 Klein-Nishina form factor, 415, 449
 Klein-Nishina (KN) equations, 424, 448, 449
 Klein-Nishina total electronic cross section, 438
 Klystron, 951, 1034, 1050

L

Laboratory coordinate system, 630
 Laplacian operator, 956, 963, 971, 1002
 Large specific air-kerma rate constant, 774
 Larmor equation, 1065
 Larmor law, 178, 1063
 Larmor relationship, 246, 256, 257, 1050
 Latent image, 1057
 Leakage radiation, 386, 1050
 Least squares fit to measured data, 391, 642
 Least squares theory, 218
 Length contraction, 46, 49
 Liénard equation, 1065
 Light charged particle, 17, 300, 306, 1048
 Linac, 800, 1079
 Linac head, 1080, 1094
 Linac isocenter, 1097
 Linear accelerator, 376, 383, 738, 979, 1046, 1049, 1061, 1090
 Linear accelerator (linac), 49, 54, 942, 950, 977, 978, 999, 1008, 1014, 1028, 1044, 1050, 1066, 1075, 1086
 Linear attenuation coefficient, 388, 390, 394, 516, 532
 Linear attenuation coefficient for pair production, 484
 Linear energy absorption coefficient, 394
 Linear energy transfer coefficient, 394
 Linear partial differential equation of the second order, 981, 1002
 Linear stopping power, 304, 327
 Lithium borate, 25
 Lithium-5, 752
 Long half-life, 774
 Loosely bound electron, 467
 Lorentz contraction, 242
 Lorentz factor, 44, 47, 51, 52, 54, 56, 59, 61, 66, 67, 70, 84, 249, 251, 257, 290, 1066, 1074
 Lorentz field expansion, 244
 Lorentz force, 61, 64, 1071
 Lorentz transformation, 43, 44, 46, 69

Low cost, 774
 Low safety hazard, 774
 Low Z target, 378, 385
 Lowest cutoff frequency, 987, 994
 Lowest Lyman-type emission line, 203
 Lowest TE_{mn} cutoff frequency, 980
 Lowest TM_{mn} cutoff frequency, 980
 Lucite, 318
 Lyman, 214
 Lyman series of muonic hydrogen, 201
 Lyman spectral series, 200

M

Macroscopic cross section, 585, 604
 Macroscopic cross section of hydrogen, 607
 Macroscopic cross section of oxygen, 607
 Magic number, 760, 765
 Magnetic bremsstrahlung, 256, 1063
 Magnetron, 951, 1034, 1050
 Major accidents in nuclear power plants, 906
 Major modes of radioactive decay, 694
 Making the reactor critical, 904
 Man-made (artificial) radionuclide, 788
 Manganese, 533
 Map of nuclides, 759
 Mass attenuation coefficient, 388, 390, 394, 476, 516, 523, 524, 532, 534, 539, 548, 559
 Mass collision stopping power, 305, 323, 327, 330, 332, 335, 340, 344, 348, 350, 364, 375
 Mass defect, 28
 Mass deficit, 28
 Mass energy absorption coefficient, 394, 532, 534, 538, 539, 548, 559
 Mass energy transfer, 440
 Mass energy transfer coefficient, 394, 532, 534, 538, 539, 548, 559, 605
 Mass radiation stopping power, 305, 306, 344, 348, 350
 Mass scattering power, 174
 Mass stopping power, 303, 304, 319
 Massless particle, 52
 Materialization, 483, 486
 Maximum activity, 858
 Maximum attainable specific activity, 842, 848, 850, 879, 917
 Maximum Čerenkov angle, 262
 Maximum cutoff angle, 169
 Maximum daughter activity, 849
 Maximum energy transfer, 284, 290
 Maximum energy transfer fraction, 288, 290, 293, 595
 Maximum momentum transfer, 284, 313

- Maximum scattering angle, 151, 174, 440
Maximum specific activity, 835, 843, 846
Maximum specific ionization, 327
Maxwell equations, 88, 107, 945, 950, 1002, 1019
Mean atomic mass, 26, 767
Mean bremsstrahlung fraction, 561, 566
Mean energy absorbed, 538, 539, 548, 562
Mean energy absorbed in carbon, 566
Mean energy absorbed in lead absorber, 532
Mean energy density, 1019
Mean energy radiated, 548
Mean energy required to produce an ion pair, 327
Mean energy transfer for individual effect i , 530
Mean energy transfer fraction, 438, 520, 527, 544, 559, 592, 596, 612, 614
Mean energy transfer fraction for Compton effect, 536
Mean energy transfer fraction for Compton scattering, 534
Mean energy transfer fraction for individual effect i , 530
Mean energy transfer fraction for pair production, 534, 536
Mean energy transfer fraction for photoelectric effect, 534, 535, 546
Mean energy transfer fraction for Rayleigh scattering, 534, 536
Mean energy transfer fraction in Compton effect, 528
Mean energy transfer fraction in photoelectric effect, 528
Mean energy transfer fraction in Rayleigh scattering, 528
Mean energy transfer in pair production, 484
Mean energy transferred, 562, 605, 614
Mean energy transferred to charged particles, 537, 539
Mean energy transferred to electrons, 559
Mean fluorescence emission energies, 521
Mean free path (MFP), 388, 393, 395
Mean free path of neutron, 585
Mean in-flight annihilation fraction, 561, 566
Mean ionization/excitation potential, 312, 324, 344, 368
Mean ionization/excitation potential of water, 320
Mean lifetime, 642
Mean lifetime of the pion, 48
Mean mass collision stopping power, 364
Mean molecular mass, 27
Mean number of elastic collisions, 600
Mean Poynting vector, 110, 111
Mean radiation fraction, 533, 561, 566
Mean rate of energy loss, 173
Mean rest energy, 26
Mean square scattering angle, 149, 174
Mean stopping power, 363
Mean transfer fraction for Compton effect, 564
Mean weighted energy transfer fraction for individual effect i , 530
Measurement of blood glucose, 26
Medical linac, 1075, 1077, 1079, 1090, 1093
Medical physics, 1045
Megavoltage photon beam, 583
Megavoltage radiotherapy, 1014, 1044, 1075, 1089
Megavoltage radiotherapy energy range, 381
Megavoltage x rays, 1049
Megavoltage x-ray machines, 383
Metastable decay, 708
Metastable excited state, 704
Metastable state, 739
Metastable state of Co-60m, 862
Microbeam radiotherapy, 1065
Microscopic neutron cross section, 585
Microtron, 923, 978, 1029, 1044, 1049, 1050, 1061, 1075
Microwave power source, 1034
Microwave power transmission, 961
Microwaves, 942
Miniature waveguide, 1033, 1076
Miniature x-ray tube, 1059
Minimum Čerenkov angle, 262
Minimum cutoff angle, 168
Minimum electric field amplitude, 1034, 1035
Minimum excitation potential, 180
Minimum injection kinetic energy, 1035
Minimum scattering angle, 151, 168, 174
Mo-99 production, 924
Mode of radiation, 21
Moderation, 597
Moderator, 597
Moderator of nuclear reactor, 901
Modified activation factor, 824, 843
Modified decay constant, 813, 824, 865
Modulation of the phase velocity, 1030
Molecular imaging, 718
Molière scattering, 118
Møller scattering, 118, 165
Molybdenum, 768, 1060
Molybdenum target, 921
Molybdenum-99, 651, 737, 800, 835, 838, 887, 914, 925
Molybdenum-technetium (Mo-Tc) generator, 801

- Momentum, 82
 Momentum conservation, 193, 467, 701, 910
 Momentum of the emitted photon, 181
 Momentum of the incident electron, 156
 Momentum of the scattered electron, 158
 Momentum transfer, 128, 152, 310
 Momentum transfer in coherent photon scattering, 455
 Momentum transfer variable, 442, 445, 449, 456, 459
 Mono-energetic gamma source, 393
 Mono-energetic x rays, 1047
 Mono-energetic x-ray source, 1047
 Monochromatic neutrons, 75
 Monte Carlo technique, 1046
 Moseley equation, 216
 Moseley law, 215
 Motorized patient support assembly, 1094
 Mott elastic scattering, 161
 Mott scattering, 118, 152, 165
 Multi-electron atom, 212, 216
 Multileaf collimator (MLC), 1079, 1084
 Multiple Compton scattering, 410
 Multiple Rutherford interactions, 124
 Multiple scattering, 149
 Muon, 188
 Muonic atom, 201
 Muonic hydrogen, 188, 190, 203
 Muonic hydrogen atom, 201
 Muonic transition, 202
 Muonium, 189, 190, 203
- N**
- Narrow beam geometry, 390, 398
 Narrow photon beam, 539
 Natural radioactivity, 638, 696, 788, 1046
 Naturally occurring radionuclides, 698, 788, 795
 NE decay, 755
 Negative pions, 300
 Neon ion, 360
 Neptunium series, 796
 Neptunium-237, 797
 Net energy transferred, 571, 577
 Neumann boundary condition, 967
 Neumann functions, 967
 Neumann-type boundary condition, 956, 963, 983
 Neutrino, 705, 727, 753, 790
 Neutron, 695
 Neutron absorption, 602
 Neutron activation, 602, 731, 805, 810, 813, 818, 824, 883, 888, 915, 936
 Neutron activation analysis, 632, 799
 Neutron activation cross section, 819
 Neutron activation of cobalt-59, 863
 Neutron activation of Ir-191, 846
 Neutron activation of Mo-98, 915, 921
 Neutron activation target, 916
 Neutron bombardment, 799, 890
 Neutron capture, 583, 589, 592, 602, 612, 615, 621, 806, 883, 884, 909
 Neutron decay, 711
 Neutron dosimetry, 582, 611
 Neutron drip line, 761
 Neutron elastic scattering, 592
 Neutron emission (NE) decay, 694, 755, 891
 Neutron emitting radionuclide, 624
 Neutron factor, 634, 746
 Neutron fluence, 585, 601, 606
 Neutron fluence rate, 585
 Neutron flux density, 585
 Neutron generator, 978, 1029
 Neutron interaction, 601
 Neutron kerma factor, 605
 Neutron kerma factor of water, 610
 Neutron multiplication, 892
 Neutron radiography, 632
 Neutron scattering, 595, 601
 Neutron slowing down process, 598
 Neutron source, 591
 Neutron yield, 624
 Neutron yield of U-238, 748
 Neutron-induced fission, 892
 Neutron-rich, 694
 Neutron-rich nucleus, 755
 Neutron-rich radioactive nucleus, 704
 Neutron-rich radionuclide, 761
 New kind of ray, 1052
 Newton second law in relativistic form, 61
 Nitrogen-13, 718, 721, 800
 Nominal accelerating potential (NAP), 382
 Non-elastic scattering, 589
 Non-relativistic electron, 74
 Non-uniform cavities, 1030
 Normal probability distribution, 112
 Normalization constant, 85
 Normalized activation time, 814, 819
 Normalized daughter activity, 819
 Normalized number of daughter nuclei, 814
 Normalized number of parent nuclei, 814, 819
 Nuclear activation, 799, 805, 829, 835, 849, 871, 890
 Nuclear activation analysis, 799
 Nuclear activation with proton, 931
 Nuclear activation-decay series in production of cobalt-60, 863
 Nuclear binding energy, 30, 755, 770, 932

- Nuclear binding energy method, 698, 700, 749, 752, 792, 909
 Nuclear binding energy of Eu-151, 771
 Nuclear chain reaction, 892, 901
 Nuclear Compton effect, 409, 513
 Nuclear Compton scattering, 513
 Nuclear de-excitation energy, 741
 Nuclear decay, 731
 Nuclear decay mode, 694
 Nuclear disintegration, 639
 Nuclear fission, 499, 788, 890
 Nuclear fission reactor, 591
 Nuclear fission target, 916
 Nuclear force, 589
 Nuclear imaging, 708
 Nuclear medicine, 799, 914, 1046
 Nuclear medicine imaging, 582, 738, 800, 885
 Nuclear models, 31
 Nuclear pair production, 395, 483, 516, 520, 532, 540, 544, 553, 557, 570
 Nuclear photoelectric effect, 499
 Nuclear potential barrier, 104
 Nuclear power, 903
 Nuclear power accident, 905
 Nuclear power plant, 904
 Nuclear probe, 119
 Nuclear radius, 33, 77, 119, 120
 Nuclear radius constant, 99, 174
 Nuclear reaction, 277, 490, 500, 503, 611, 615, 628, 719, 883, 901, 1049
 Nuclear reactor, 16, 597, 624, 731, 799, 800, 806, 809, 824, 835, 843, 854, 870, 879, 891, 892, 901, 915, 921
 Nuclear reactor core, 905
 Nuclear recoil correction factor, 158
 Nuclear rest energy, 30, 932
 Nuclear rest energy method, 698, 700, 715, 719, 721, 749, 752, 753, 755, 792, 909
 Nuclear rest energy of Eu-151, 771
 Nuclear stability, 696
 Nuclear structure, 27
 Nuclear transformation, 639, 694, 697
 Nuclear transmutation, 639
 Nucleon emission decay, 767
 Nuclide Tc-99, 662
 Numerical integration, 352, 357
 Numerical summation, 352
- O**
- Oil-drop experiment, 1053
 One-electron atom, 179, 184, 190, 194, 199, 203, 216
 One-electron structure, 183
 Open circles, 785
- Operating license, 904
 Optical fiber, 942
 Optical prism, 214
 Optical signals, 943
 Optical waveguide, 943
 Opting out of nuclear power, 905
 Orbital electron radius, 188
 Orbital shell vacancies, 704
 Organic carbon, 801
 Origin of radiation, 20
 Orthovoltage x rays, 1049
 Orthovoltage x-ray machine, 1044
 Osmium-192, 731
 Outer focus of the hyperbola, 129, 138
 Oxygen, 606
 Oxygen-15, 718, 721, 800
- P**
- Pair production, 476, 486, 494, 526, 562, 564, 570, 1050
 Pairing of nucleons, 766
 Parameters of pair production, 487
 Parent depletion model, 871
 Parent depletion–daughter activation, 824, 843
 Parent depletion–daughter activation model, 811, 828, 871
 Parent depletion–daughter activation model of neutron activation, 810
 Parent nucleus P, 640
 Parent P, 646
 Partial decay constant, 633, 685, 748
 Partial differential equations of the second order, 952
 Partial differential wave equation, 950
 Particle, 695
 Particle acceleration, 1042, 1050
 Particle accelerator, 591, 925, 976
 Particle counter, 145, 147
 Particle scattering, 128, 148
 Particle-wave duality, 69, 76
 Particles released in nuclear decays, 695
 Partition of energy, 740
 Paschen, 214
 Pass band, 1026
 PE decay, 752
 Penetration of the nucleus, 301
 Percentage depth dose (PDD), 22, 382
 Periodic table of elements, 182, 208, 215, 761
 Permeability, 945
 Permittivity, 945
 PET imaging, 717, 718
 PET scanning, 726
 Pfund, 214
 Phase modulation, 1030

- Phase of the wave, 968
Phase velocity, 942, 951, 979, 980, 985, 987, 992, 1009, 1024
Phase velocity modulation, 1035
Phosphorescence, 789
Phosphorus-30, 798
Photo-fission, 499, 923
Photoactivation, 799, 801
Photocathode, 92
Photodetector, 1057
Photodisintegration, 395, 499, 512, 557, 801, 923, 925
Photoelectric atomic cross section, 480
Photoelectric effect, 206, 227, 395, 465, 476, 516, 520, 523, 524, 532, 535, 540, 544, 553, 557, 562, 576, 1050
Photoelectric experiment, 89
Photoelectric linear attenuation coefficient, 483
Photoelectric mass attenuation coefficient, 476, 483
Photoelectric (PE) interaction, 468, 471
Photoelectric work function, 92, 94
Photoelectron, 17, 89, 91, 206, 240, 468, 471, 479, 521, 570
Photoelectron current, 90
Photographic plate, 214, 789
Photon beam attenuation, 390
Photon beam spectrum, 923
Photon capture, 801
Photon energy, 40
Photon energy fluence, 606
Photon momentum, 41, 182
Photon rest energy, 182
Photon wavelength, 40
Photoneutron source, 592
Photonuclear decay, 503
Photonuclear (PN) reaction, 395, 499, 503, 507, 512, 553, 557, 592, 801, 925
Phototransmutation, 801
Planck constant, 90
Planck law, 36, 37, 77, 182, 210
Planck-Einstein quantum hypothesis, 80, 81
Platinum-192, 731
Plutonium-239, 893
Point source, 1060
Polarization angle, 403
Polarization vector, 403
Polonium, 638
Polonium-210, 788, 798
Polonium-212, 685
Polonium-218, 700
Positron, 570, 575, 585, 695, 721, 790
Positron annihilation, 227, 486, 555, 570
Positron emission, 727
Positron emission tomography, 6, 717, 800, 1049, 1051
Positron emitter, 931
Positron emitting radionuclide, 717, 718
Positronium, 188, 190, 199
Positronium reduced mass, 200
Potassium-40, 802
Potential barrier, 106, 697
Potential barrier wall, 101
Potential energy, 107
Potential energy operator, 80
Power generation mode, 904
Poynting theorem, 110
Poynting vector, 110, 245, 402, 1016, 1019
Practical specific activity, 884
Pre-criticality, 904
Primary atomic shell vacancy, 226
Primary collimator, 1083, 1085, 1096
Primordial nuclides, 802
Primordial radionuclides, 795
Principal quantum number, 212
Principle of complementarity, 88
Probability distribution, 112
Probability for Auger effect, 229, 235
Probability for photoelectric effect, 521
Probability of neutron capture reaction, 808
Probability of the photoelectric effect, 476
Production of a radionuclide, 810
Production of artificial radionuclide, 798
Production of bremsstrahlung, 555
Production of clinical electron beam, 1080
Production of clinical x-ray beam, 1080
Production of cobalt-60, 861, 885
Production of iridium-192, 885
Production of lithium-7, 885
Production of molybdenum-99, 885, 925
Production of positron emitting radionuclides, 1062
Production of radionuclides, 1062
Production of the daughter, 871
Production of x rays, 1048
Projected life of a nuclear power plant, 904
Prompt energy release, 900
Prompt neutron, 890
Propagation coefficient, 959
Propagation mode of a waveguide, 942
Protium, 18, 33, 190, 191, 194, 903
Proton, 18, 628, 630, 632, 695
Proton accelerator, 923
Proton activation, 805
Proton drip line, 761
Proton emission (PE) decay, 694, 748, 752
Proton momentum, 65
Proton rich, 694

- Proton to neutron transformation, 727
 Proton-activated radionuclide, 800
 Proton-rich nucleus, 719
 Proton-rich nuclide, 748
 Proton-rich radioactive nucleus, 704
 Proton-rich radionuclide, 718, 728, 761
 Pulse repetition rate, 1086
 Pulse sequence, 1087
 Pulsed electron pencil beam, 1095
 Pulsed modulator, 1092
 Pulsed operation, 1086
- Q**
- Q_{PE} decay energy, 753
 Quadrupole bending magnet, 1093
 Quantization, 34
 Quantization of angular momentum, 187
 Quantization of atomic energy levels, 219
 Quantum operators, 82
 Quantum physics, 88
 Quantum uncertainty, 85
 Quantum uncertainty in position, 86
 Q value, 272, 277, 500, 612, 615, 621, 624, 628, 629, 635, 793, 889, 932
 Q value calculation, 909
 Q value for decay, 708, 721
 Q value for EC decay, 727
 Q value for PE decay, 750
 Q value for the Joliot-Curie nuclear reaction, 788
 Q value of α decay, 697
 Q value of a nuclear reaction, 925
 Q value of radioactive decay, 694
 Q value of the Joliot-Curie nuclear reaction, 792
- R**
- Radiation dosimetry, 1046
 Radiation fraction, 539
 Radiation length, 171, 174
 Radiation loss, 350, 568, 570, 574, 1051, 1065, 1067
 Radiation measurement, 20
 Radiation oncology, 1045
 Radiation pressure, 112
 Radiation source, 712, 731, 774, 921
 Radiation stopping power, 304, 306, 308, 319, 357
 Radiation survey, 904
 Radiation yield, 350, 365
 Radioactivation dynamics, 832
 Radioactivation yield, 819, 832, 854, 879
 Radioactive contamination, 905
 Radioactive decay, 639, 640, 646, 694, 703, 727, 746, 766
 Radioactive decay chain, 671
 Radioactive decay modes, 773
 Radioactive decay series, 646, 675, 813
 Radioactive neutron source, 592
 Radioactive nuclear decay, 694
 Radioactive series, 655
 Radioactive transformation, 646
 Radioactive waste, 922
 Radioactivity, 638
 Radiocarbon dating, 797
 Radiofrequency (RF) mode, 1029
 Radiofrequency (RF) power generating system, 1081
 Radiofrequency wave, 951
 Radiogenic progeny, 802
 Radiographic film, 1056
 Radionuclide, 798
 Radionuclide generator, 915
 Radionuclide in ground state, 764
 Radionuclide Mo-99, 662
 Radionuclide Mo-99 decay, 655
 Radionuclide P, 642
 Radionuclide sources, 582, 799
 Radionuclide Tc-99m, 655, 662
 Radionuclide Tc-99m generator, 925
 Radiotherapy, 891, 1042, 1060, 1062, 1065, 1075, 1077, 1087
 Radiotherapy physics, 21
 Radiotherapy x-ray tube, 1061
 Radium, 638, 1046
 Radium-226, 700, 737, 774, 802, 854
 Radius, 189
 Radius of Bohr orbit, 184
 Radius of hydrogen atom, 223
 Radius of orbit, 187
 Radius of the gold nucleus, 120
 Radon-222, 700, 737, 802
 Range of charged particle, 356
 Rate of energy loss, 304
 Ratio of "tissue-phantom ratios" (TPR_{20,10}), 382
 Rayleigh (coherent) scattering, 441
 Rayleigh differential atomic cross section, 459
 Rayleigh scattering, 395, 456, 476, 516, 520, 523, 525, 532, 535, 540, 544, 553, 557, 577
 Rayleigh-Jeans law, 35
 Reaction rate, 806
 Reaction rate of neutron, 585
 Reaction threshold, 507
 Recoil angle of the target, 270
 Recoil (Compton) electron kinetic energy, 155

Recoil correction factor, 162
 Recoil energy, 132
 Recoil energy of the gold nucleus, 157
 Recoil kinetic energy of the nucleus, 162
 Recoil momentum, 132
 Recoil momentum of the nucleus, 157
 Recoil nucleus kinetic energy, 155
 Recombination process, 204
 Rectangular EM waveguide, 991
 Rectangular uniform EM waveguide, 954
 Rectangular waveguide, 951, 956
 Rectilinear acceleration, 1066
 Recurrence equation, 598
 Red shift, 68
 Reduced de Broglie wavelength, 78
 Reduced mass, 186, 190, 199, 203
 Reduced mass of hydrogen, 199
 Relative permeability, 945
 Relative permittivity, 945
 Relative weight for individual effect i , 530
 Relative weight of photon interaction i , 527
 Relativistic acceleration, 64
 Relativistic Doppler effect, 1013
 Relativistic electron, 75
 Relativistic expression for total energy, 182
 Relativistic force, 61
 Relativistic invariant, 933
 Relativistic invariant method, 499, 503, 504, 508
 Relativistic Larmor expression, 246
 Relativistic Larmor relationship, 249
 Relativistic mass, 46, 52, 56
 Relativistic momentum, 58
 Relativistic particle, 66
 Relativistic particle momentum, 257
 Relativistic relations, 50
 Removable bremsstrahlung thick target, 1096
 Removal of the spent nuclear fuel, 905
 Rest energy, 53
 Rest energy method, 273, 276, 499, 503, 504, 508, 622, 624, 629, 635, 898, 927
 Rest mass, 46, 56
 Restricted collision stopping power, 367
 Restricted stopping power, 373
 Retarding potential, 89, 91
 RF driver, 1008, 1092
 RF load, 1094
 RF power generation system, 1092
 RF system, 1090
 Richardson constant, 93, 94, 106
 Richardson-Dushman equation, 93, 94, 106
 Root-mean-square atomic radius, 223
 Root-mean-square radius, 209
 Root-mean-square scattering angle, 151, 174

Roots of a Bessel function, 995
 Rubidium-82, 718, 721, 800
 Rules used in scientific publishing, 7
 Rutherford atomic model, 127
 Rutherford cross-section, 149
 Rutherford differential cross section, 124
 Rutherford elastic scattering, 137
 Rutherford model, 127
 Rutherford nuclear model, 126
 Rutherford nuclear model of the atom, 122
 Rutherford scattering, 118, 132, 134, 143, 145, 149, 158, 165, 310
 Rutherford-Bohr atom, 89, 192
 Rutherford-Bohr atomic model, 33, 178, 185, 213, 215, 697
 Rutherford-Bohr model, 219
 Rutherford-Bohr theory, 178
 Rydberg constant, 4, 198
 Rydberg constant for hydrogen, 199
 Rydberg constant of positronium, 200
 Rydberg energy, 4, 187, 201, 204, 216, 219

S

S band, 1076, 1093
 Safe disposal of the contaminated material, 905
 Saturation model, 811, 814, 818, 820, 829, 835, 844, 849, 854, 871, 879, 936
 Saturation model of neutron activation, 810
 Saturation specific activity, 879
 Scattered photon energy fraction, 429, 436
 Scattering, 601
 Scattering angle, 128, 140, 403, 408
 Scattering angle of the projectile, 270
 Scattering experiment, 145, 148
 Scattering foil, 1085
 Schematic diagram for decay, 720
 Schematic diagram for thermionic emission, 107
 Schematic diagram of a Coulomb collision, 311
 Schematic diagram of a medical linear accelerator (linac), 1081
 Schematic diagram of a photoneuclear reaction, 500
 Schematic diagram of a two-particle collision, 273
 Schematic diagram of an elastic collision, 593
 Schematic diagram of an x-ray tube, 1055
 Schematic diagram of EM waveguide, 979
 Schematic diagram of the collision, 270
 Schematic diagram of the Compton photoneuclear reaction, 514

- Schematic diagram of the photoelectric effect, 465
- Schematic diagram of the photonuclear reaction, 506
- Schematic diagram of the positron in-flight annihilation process, 499
- Schematic diagram of Thomson scattering, 404
- Schematic diagrams of various cyclic accelerators, 1064
- Schematic representation of a typical medical linac head, 1086
- Schematic representation of the scattering process, 288
- Schematic representation of the Schottky barrier, 96
- Schödinger equation, 82
- Schottky barrier, 95
- Schottky effect, 95, 98, 106
- Schottky equation, 95
- Schrödinger equation, 83, 443
- Schrödinger wave equation, 80
- Screening constant, 212, 218
- Secondary charged particle, 582
- Secondary collimator, 1097
- Secondary collimator system, 1083
- Secondary radionuclide, 795, 802
- Secular equilibrium, 669, 802, 812, 832
- Segrè chart, 763, 780, 798
- Sensitive scattering area, 146
- Separation constant, 965
- Separation distance, 99
- Separation of variables, 958, 965
- Shell correction, 314
- Shell vacancy, 554, 557
- Shielding against leakage radiation, 1082
- Short-range force, 11
- Side scattering, 413, 433
- Simple Monte Carlo history, 567, 573
- Single scattering, 149
- Singly ionized helium ion, 204
- Sketch of the dispersion hyperbolic relationship, 986
- Sketch of the incoherent scattering function, 448
- Sketch of the linac pulse sequence, 1088
- Skin depth, 961
- Skin effect, 961
- Soft collision stopping power, 304
- Soft collisions, 304
- Soft or distant collision, 301
- Soft tissue elemental composition, 611
- Solid black circle, 785
- Solid circle, 238
- Solid curves, 237
- Source diameter, 886
- Source of microwave power, 951
- Source of x rays, 376, 1055
- Source-skin distance, 1077
- Spallation, 589, 592, 602
- Spatial wave function, 83
- Special modes of EM fields, 955
- Special relativity, 52, 82
- Special theory of relativity, 43
- Specific activity, 634, 638, 712, 795, 834, 879, 920
- Specific activity of cesium-137, 780
- Specific activity of cobalt-60, 779
- Specific activity of europium-152, 780
- Specific activity of radium-226, 779
- Specific activity of U-238, 747
- Specific charge of positive hydrogen ion, 1054
- Specific charge of the electron, 1053
- Specific ionization, 326
- Spectral distribution, 391
- Spectral energy density, 35, 37
- Spectroscopic notation, 229
- Spectrum of hydrogen, 213
- Spontaneous fission, 632, 634, 699, 746, 761, 892
- Spontaneous fission drip line, 761
- Spontaneous fission neutron source, 592
- Spontaneous fission (SF), 694, 748
- Spontaneous nuclear decay, 639
- Spontaneous radioactive decay, 696
- Stable isotopes of lead, 769
- Stable nuclear configuration, 766
- Stable nuclide, 764, 798
- Standard atomic weight, 767
- Standard atomic weight of europium, 770
- Standard molecular weight, 27
- Standard Newton second law, 61
- Steering coil, 1095
- Stereotactic external beam irradiation, 1077
- Stereotactic radiosurgery, 1076, 1077
- Stokes-Kelvin curl theorem, 108
- Stop band, 1026
- Stopping material, 343, 347
- Stopping medium, 323
- Stopping power, 303, 347
- Stopping power constant for light CP, 335
- Stopping power data of lead, 351
- Stopping power function of electron, 336
- Stopping power functions, 340
- Storage of long-lived radioactive waste, 923
- Storage ring, 256, 1047, 1050, 1063, 1066
- Strip line, 942
- Strong force, 11
- Strong interaction, 582

- Subcritical mass, 901
 Super Coster-Kronig electron, 226, 237
 Super-critical mass, 901
 Superficial x rays, 1049
 Surface photoelectric experiment, 89, 91
 Synchrotron, 257, 978, 1029, 1044, 1050, 1061, 1075
 Synchrotron light source, 1063
 Synchrotron radiation, 20, 256, 257, 1063, 1066, 1069
 Synchrotron radiation loss, 1066
- T**
- Target cooling, 381
 Target thickness, 932
 TE mode, 952, 962, 971, 989
 TE₁₁ mode, 1015
 Technetium generators, 738
 Technetium-99m, 651, 914, 921
 Teleradium machine, 775
 Teletherapy machine, 775, 800
 Teletherapy source, 774, 854, 886
 TEM modes, 971
 Tenth-value layer (TVL), 388, 395
 Terra incognita, 761
 Thallium-208, 685
 Theoretical specific activity, 835, 837, 884, 886, 888
 Theory of waveguide, 942, 1008
 Therapeutic radiology, 1045
 Thermal neutron, 76, 582, 615, 799, 890, 896, 910
 Thermal neutron cross section, 621, 810
 Thermal neutron region, 612
 Thermalization, 597, 903
 Thermion, 17
 Thermionic electron emission, 1052
 Thermionic emission, 92, 94, 106, 107, 1057, 1095
 Thermionic work function, 93
 Thermionically, 220
 Thermoluminescence dosimetry (TLD), 25
 Thick target, 377, 807, 936, 1083
 Thick target bremsstrahlung, 378, 384
 Thick tungsten target, 383
 Thin target, 377, 807, 1087
 Thin tungsten target, 383
 Thomas-Fermi atomic model, 168, 773
 Thomas-Fermi atomic radius, 169
 Thomas-Fermi radius, 209
 Thompson scattering, 415
 Thomson atomic model, 697
 Thomson classical cross section, 4
 Thomson classical scattering, 403
 Thomson classical theory, 408
 Thomson differential cross section, 449
 Thomson differential electronic cross section, 459
 Thomson differential scattering cross section, 417
 Thomson electronic cross section, 441, 481
 Thomson low energy limit, 535
 Thomson model, 126
 Thomson model of the atom, 126
 Thomson "plum pudding" model, 126
 Thomson "plum pudding" model of the atom, 122
 Thomson scattering, 395, 450, 451
 Thomson total atomic cross section, 406
 Thorium series, 796, 802
 Thorium-232, 797, 802
 Three Mile Island (TMI), USA, 906
 Threshold energy, 275, 624, 630
 Threshold energy for electronic pair production, 490
 Threshold energy for nuclear pair production, 490
 Threshold energy for the PN reaction, 499
 Threshold energy for triplet production, 440
 Threshold energy of a photonuclear reaction, 504
 Threshold for nuclear pair production, 483
 Threshold for PN reaction, 508
 Threshold for the photonuclear reaction, 502
 Threshold kinetic energy, 275, 277, 490, 629, 631, 793, 926, 932
 Threshold kinetic energy of projectile, 493
 Threshold total energy, 490
 Tightly bound electron, 467, 478
 Time dilation, 46
 Time of collapse, 200
 Time of collapse of the Bohr orbit, 199
 Time of orbit collapse, 179
 TM mode, 952, 962, 971
 TM₀₁ mode, 1015
 Tomotherapy, 1076
 Total body dose to the patient, 914
 Total body irradiation, 1077
 Total decay constant, 685
 Total decay constant of U-238, 748
 Total energy, 53, 54, 56, 82
 Total energy conservation, 466, 701, 910
 Total energy level of the electron in orbit, 187
 Total mass stopping power, 305, 350, 365
 Total mean energy absorption fraction, 532
 Total mean energy transfer fraction, 534, 537, 539
 Total skin electron irradiation, 1077

- Total stopping power, 319
 Transcendental equation, 858
 Transient equilibrium, 669, 812, 832
 Translational research, 976
 Transmission coefficient, 102
 Transmission EM waveguides, 1016
 Transmission ionization chamber, 1077
 Transmission line, 942
 Transmission of high frequency waves, 942
 Transmission of microwave power, 970, 979, 987, 999, 1023
 Transmission of microwaves, 951
 Transmission of RF power, 950, 952
 Transmission waveguide, 999, 1008
 Transmitting antenna, 951
 Transmutation, 1049
 Transuranic element, 632
 Transverse electric (TE), 961
 Transverse electric (TE) mode, 968, 1000
 Transverse electromagnetic mode, 961
 Transverse electromagnetic (TEM) mode, 1000
 Transverse magnetic (TM) mode, 961, 968, 1000, 1025
 Treatment head, 1080
 Treatment planning, 1046
 Triode-type electron gun, 1095
 Triplet production, 227, 438, 483, 516, 520, 532, 540, 544, 557, 574
 Tritium, 18, 190, 801
 Tritium unit, 801
 Triton, 18, 360
 Tumor control probability (TCP), 621
 Tungsten, 1058, 1060
 Tunneling, 101, 752
 Tunneling of alpha particles, 101
 Tunneling of particles, 697
 Two-body problem, 190
 Two-particle elastic collision, 592
 Two-proton emission (2PE) decay, 749
 Two-quantum annihilation of the positron, 494
 Type of radiation, 21
 Typical linac head, 1085
- U**
- U-235 fission, 896
 Ultra-cold neutron, 582
 Ultra-relativistic electron, 432, 438
 Uncertainty in momentum, 87
 Uncertainty principle, 87
 Uncontrolled fission, 901
 Uniform circular electromagnetic (EM) waveguide, 991
 Uniform circular EM waveguide, 966, 977, 1008, 1015
 Uniform electromagnetic (EM) waveguide, 1023
 Uniform EM waveguide, 954, 961, 980, 1009, 1019
 Uniform rectangular EM waveguide, 970, 1019
 Uniform waveguide, 942, 950, 968
 Unit of activity, 638
 Unit of neutron fluence, 586
 Unit of neutron fluence rate, 586
 Unit of specific activity, 638
 Units of momentum, 60
 Unpolarized beam, 403
 Unrestricted collision stopping power, 371
 Unrestricted mass collision stopping power, 373
 Unrestricted stopping power, 368
 Uranium, 700
 Uranium ore, 894
 Uranium series, 796, 802
 Uranium tailings, 894
 Uranium-233, 893
 Uranium-235, 797, 802, 894
 Uranium-238, 746, 797, 802
 Uranium-238 / radium-226 decay chain, 790
- V**
- Vacancies in absorber atom, 520
 Vacancy, 240
 Vacuum system, 1093
 Vacuum-pumping system, 1082
 Value, 490
 Value of decay, 704
 Van de Graaff accelerator, 978, 1044
 Van de Graaff generator, 1029, 1075
 Van der Waals radius, 209
 Vector diagrams for PE interaction, 471, 474
 Vector function, 953
 Vector identity, 954
 Vector Laplacian operator, 953
 Velocity, 189
 Velocity function, 332
 Velocity modulation of the RF wave, 1030
 Velocity of energy flow, 1014, 1019
 Vertex of the hyperbola, 143
 Vertex of the hyperbolic trajectory, 130
 Volume element, 567, 573
 Voxel, 567, 573
- W**
- Water phantom, 567, 573
 Water-cooling system, 1082, 1093

- Wave equation, 44, 88, 950, 955, 961, 971, 981, 1002
- Wave equation for the free electron, 83
- Wave function, 80, 83, 85, 223
- Wave guide, 376
- Wave nature, 88
- Wave number, 83, 197
- Wave vector, 111
- Waveguide, 49, 942, 945, 961, 990, 1019, 1048, 1050, 1066
- Waveguide core, 995, 1000
- Waveguide core material, 942
- Waveguide geometry, 945
- Waveguide propagation coefficient, 966, 1011
- Waveguide wall material, 942
- Waveguide wave number, 959, 966
- Wavelength shift, 410
- Weak force, 11
- Weapons-grade HEU, 922
- Weizsäcker binding energy, 31
- White spectrum, 215
- Wien displacement constant, 39
- Wien displacement law, 37
- Work function, 37, 89, 91, 92, 94, 106
- X**
- X band microwave frequency, 998
- X-band, 1076
- X-ray absorption spectrometry, 1047
- X-ray astronomy, 1045
- X-ray crystallography, 1045
- X-ray fluorescence spectrometry, 1047
- X-ray generator, 1055
- X-ray imaging, 1060
- X-ray intensity spectra, 377
- X-ray machine, 376, 978, 1046, 1049, 1086
- X-ray photoelectron spectrometry, 1047
- X-ray production, 379, 1087
- X-ray spectroscopy, 1045
- X-ray spectrum, 1049
- X-ray system, 1055
- X-ray target, 376, 379, 383
- X-ray tube, 1029, 1055, 1057
- X-ray yield, 379, 380
- Y**
- Young experiment, 88
- Z**
- Zero (root) of the Bessel function, 969, 1010